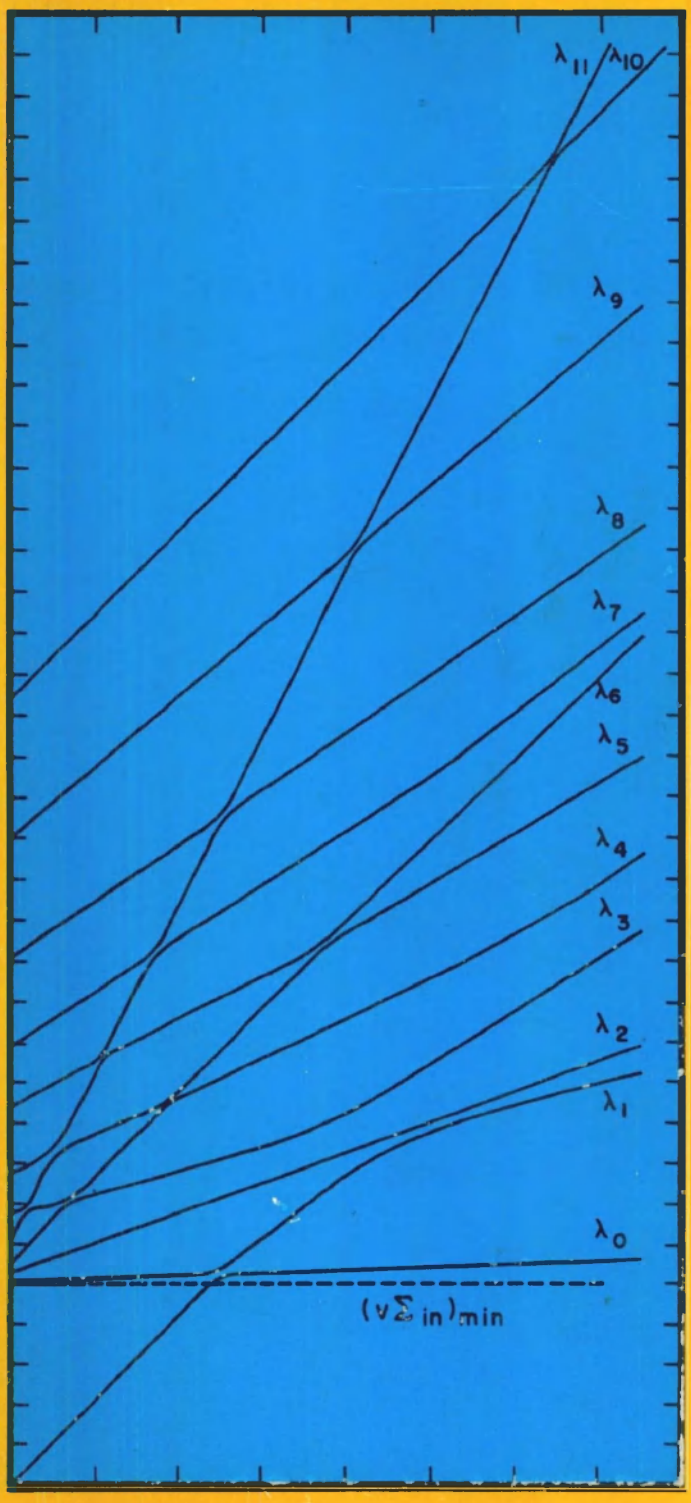


Vol. II

PULSED NEUTRON RESEARCH

Proceedings of a Symposium, Karlsruhe, 10-14 May 1965

INTERNATIONAL ATOMIC ENERGY AGENCY, VIENNA, 1965

PULSED NEUTRON RESEARCH

VOL. II

The following States are Members of the International Atomic Energy Agency:

AFGHANISTAN
ALBANIA
ALGERIA
ARGENTINA
AUSTRALIA
AUSTRIA
BELGIUM
BOLIVIA
BRAZIL
BULGARIA
BURMA
BYELORUSSIAN SOVIET SOCIALIST REPUBLIC
CAMBODIA
CAMEROON
CANADA
CEYLON
CHILE
CHINA
COLOMBIA
CONGO, DEMOCRATIC REPUBLIC OF
COSTA RICA
CUBA
CYPRUS
CZECHOSLOVAK SOCIALIST REPUBLIC
DENMARK
DOMINICAN REPUBLIC
ECUADOR
EL SALVADOR
ETHIOPIA
FINLAND
FRANCE
FEDERAL REPUBLIC OF GERMANY
GABON
GHANA
GREECE
GUATEMALA
HAITI
HOLY SEE
HONDURAS
HUNGARY
ICELAND
INDIA
INDONESIA
IRAN
IRAQ
ISRAEL
ITALY
IVORY COAST
JAPAN
KENYA
REPUBLIC OF KOREA
KUWAIT
LEBANON
LIBERIA
LIBYA
LUXEMBOURG
MADAGASCAR
MALI
MEXICO
MONACO
MOROCCO
NETHERLANDS
NEW ZEALAND
NICARAGUA
NIGERIA
NORWAY
PAKISTAN
PARAGUAY
PERU
PHILIPPINES
POLAND
PORTUGAL
ROMANIA
SAUDI ARABIA
SENEGAL
SOUTH AFRICA
SPAIN
SUDAN
SWEDEN
SWITZERLAND
SYRIA
THAILAND
TUNISIA
TURKEY
UKRAINIAN SOVIET SOCIALIST REPUBLIC
UNION OF SOVIET SOCIALIST REPUBLICS
UNITED ARAB REPUBLIC
UNITED KINGDOM OF GREAT BRITAIN AND NORTHERN IRELAND
UNITED STATES OF AMERICA
URUGUAY
VENEZUELA
VIET-NAM
YUGOSLAVIA

The Agency's Statute was approved on 23 October 1956 by the Conference on the Statute of the IAEA held at United Nations Headquarters, New York; it entered into force on 29 July 1957. The Headquarters of the Agency are situated in Vienna. Its principal objective is "to accelerate and enlarge the contribution of atomic energy to peace, health and prosperity throughout the world".

Printed by the IAEA in Austria
October 1965

PROCEEDINGS SERIES

PULSED NEUTRON RESEARCH

PROCEEDINGS OF THE SYMPOSIUM ON
PULSED NEUTRON RESEARCH
HELD BY THE
INTERNATIONAL ATOMIC ENERGY AGENCY
AT KARLSRUHE, 10-14 MAY 1965

In two volumes

VOL.II

INTERNATIONAL ATOMIC ENERGY AGENCY
VIENNA, 1965

Symposium on Pulsed Neutron Research, Karlsruhe, 10-14 May 1965.
Proceedings ... held by the International Atomic Energy Agency, Vienna, the Agency, 1965.
2 vols. (IAEA Proceedings series)

621.039.512
539.125.5

PULSED NEUTRON RESEARCH
IAEA, VIENNA, 1965
STI/PUB/104

FOREWORD

In recent years there has been growing interest in transient, as opposed to static, techniques of neutron and reactor physics investigation. Perhaps the most notable example of the newer transient techniques is the pulsed neutron source method which has been applied to various studies of the detailed interaction of neutrons with non-multiplying as well as multiplying media.

More than 230 scientists from 22 countries and 3 international organizations participated in this IAEA Symposium held at the Kernforschungszentrum Karlsruhe, at the invitation of the Government of the Federal Republic of Germany. Although there have been previous meetings concerned with pulsed neutron measurements (notably at Berkeley in 1958 and at Brookhaven in 1962), this was the first international meeting on pulsed neutron research in which working scientists from all parts of the world participated.

This Symposium has provided not only new and significant pulsed neutron data, but also, what is equally important, fresh viewpoints of interpretation pointing toward useful directions for future pulsed neutron investigation. The general opinion of participants at Karlsruhe was that the potential value of pulsed neutron studies, on fast systems particularly, has scarcely been tapped and that much greater effort in this direction can be expected in the coming years.

EDITORIAL NOTE

The papers and discussions incorporated in the proceedings published by the International Atomic Energy Agency are edited by the Agency's editorial staff to the extent considered necessary for the reader's assistance. The views expressed and the general style adopted remain, however, the responsibility of the named authors or participants.

For the sake of speed of publication the present Proceedings have been printed by composition typing and photo-offset lithography. Within the limitations imposed by this method, every effort has been made to maintain a high editorial standard; in particular, the units and symbols employed are to the fullest practicable extent those standardized or recommended by the competent international scientific bodies.

The affiliations of authors are those given at the time of nomination.

The use in these Proceedings of particular designations of countries or territories does not imply any judgement by the Agency as to the legal status of such countries or territories, of their authorities and institutions or of the delimitation of their boundaries.

The mention of specific companies or of their products or brand-names does not imply any endorsement or recommendation on the part of the International Atomic Energy Agency.

CONTENTS OF VOL. II

THERMAL MULTIPLYING SYSTEMS (Session IV)

Survey of pulsed neutron source methods for multiplying media (SM-62/58) 3
E. Garelis (United States of America)

An experimental study of the ($k\beta/\ell$) pulsed neutron source technique in light water assemblies (SM-62/68) 25
P. Meyer (United States of America)

Discussion 47

Modified pulsed source techniques (SM-62/48) 49
T. Gozani (Israel)
P. Demarmels, T. Hurlimann and H. Winkler (Switzerland)

Reactivity measurement by the pulsed neutron method (SM-62/46) .. 63
S.A. Scott (Israel)

Discussion 76

Interpretation of pulsed source experiments (SM-62/71) 77
C.A. Preskitt and E.A. Nephew (United States of America)

The measurement of reactivity in multi-region subcritical systems by the pulsed neutron technique (SM-62/25) 97
J. Sherwin and J.H. Leng (United Kingdom)

Pulsed-source experiments with multiplying and non-multiplying heavy water systems (SM-62/92) 119
E. Utzinger, W. Heer and H.R. Lutz (Switzerland)

Pulsed neutron measurements on a heavy water power reactor (MZFR) at zero energy (SM-62/6) 137
G. Bronner, W.-H. Dio and G. Schlosser (Federal Republic of Germany)

Étude des milieux multiplicateurs homogènes à l'aide de sources pulsées de neutrons (SM-62/83) 157
J.G. Bruna, J.P. Brunet, J. Buchet, M. Houelle et H. Tellier (France)

Discussion 179

The common belgonucleaire-CEN programme for the survey study of UO_2-PuO_2-H_2O lattices by the pulsed neutron technique (SM-62/13) 181
J. Debrue, F. Motte, R. Delrue, E. Fossoul, M. Stiévenart and G. Tavernier (Belgium)

Study of solid-moderated enriched uranium epithermal systems by the pulsed neutron technique (SM-62/57) 193
J.R. Morton III (United States of America)

Étude de réseaux à pas variable uranium-eau légère par des mesures cinétiques et stationnaires (SM-62/94) 219
P.H. Gavin (Suisse)

Pulsed neutron studies of BeO-natural uranium lattices (SM-62/41) . 231
B. V. Joshi, V.R. Nargundkar and K. Subbarao (India)
Discussion 239
Subcriticality determination on a reflected graphite system by the pulsed neutron method (SM-62/18) 241
K. Sumita and Y. Kaneko (Japan)
Étalonnage de barres de contrôle dans les réseaux uranium-naturel graphite (SM-62/82) 261
S. Fuster, M. Sagot, A. Tarabella et H. Tellier (France)
Far subcriticality measurements by the pulsed neutron technique (SM-62/50) 281
M. Petrović (Yugoslavia)
Определение параметра β/ℓ графито-водяного реактора нулевой мощности "АННА" при помощи импульсного источника нейтронов (SM-62/102) 287
С. Хващевски и К. Дыбовски (Польша)
Pulsed neutron reactivity measurements in the near-critical state (SM-62/16) 299
K. Einfeld, H. Hennies, G. Memmert and W. Ullrich (Federal Republic of Germany)
Discussion 313

FAST NEUTRON SYSTEMS (Session V)

Pulsed neutron experiments on fast and intermediate systems (SM-62/88) 317
F. Storrer (EURATOM)
Discussion 335
Mesures par neutrons pulsés sur des assemblages critiques (SM-62/84) 337
R. Compte, J. Massieux et M. Roche (France)
Discussion 355
Determination of neutron lifetimes and reactivities in the fast critical FR-0 assembly (SM-62/29) 357
A. Bergström, B. Brunfelter and J. Kockum (Sweden)
Fast-reactor physics parameters from a pulsed source (SM-62/56).. 373
W. Y. Kato, H.H. Meister, G. W. Main, J.L. Russell, Jr., and K.L. Crosbie (United States of America)
Discussion 396
SUAK, a fast subcritical facility for pulsed neutron measurements (SM-62/2) 399
H. Borgwaldt, M. Küchle, F. Mitzel and E. Wattecamps (Federal Republic of Germany)
Discussion 415
Some measurements of fast reactor spectra by the time-of-flight technique using a pulsed neutron source (SM-62/27) 417
W. J. Paterson, W.B. McCormick and J. W. Weale (United Kingdom)
Discussion 433

Measurements of fast neutron spectra in reactor materials (SM-62/23) 435
D.B. Gayther and P.D. Goode (United Kingdom)
Discussion 443
Determination of neutron spectra in bulk media by time-of-flight (SM-62/61) 445
J.L. Russell, Jr., J.R. Beyster, J.R. Brown, K.L. Crosbie, G.K. Houghton, A.E. Profio and G.D. Trimble (United States of America)
Discussion 459
Theoretical considerations concerning the pulsation of fast subcritical assemblies (SM-62/12) 461
M. Stiévenart (Belgium)
Contribution to the theory of pulsed and modulated experiments on fast neutron multiplying media (SM-62/86) 479
M. Cadilhac, P. Govaerts, P. Hammer, M. Moore, B. Nicolaenko and F. Storrer (EURATOM)
Discussion 491
Contribution to the study of fast neutron non-multiplying assemblies by the pulsed neutron technique (SM-62/14) 493
G. Deconninck, P. d'Oultremont and M. Stiévenart (Belgium)
Discussion 408
The pulsed neutron technique applied to fast non-multiplying assemblies (SM-62/74) 511
L.E. Beghian and S. Wilensky (United States of America)
Discussion 525

PULSED REACTORS AND NEUTRON SOURCES (Session VI)

Fast burst reactors in the United States of America (SM-62/53) 529
T.F. Wimett (United States of America)
Discussion 552
The pulsed fast reactor as a source for pulsed neutron experiments (SM-62/34) 553
V. Raievski, W. Kley, R. Haas, J. Larrimore, T. Asaoka, K. Giegerich, R. Misenta, J. Randles, G. Riccobono, H. Rief, F. Sciuto, H. Wundt (EURATOM), G. Tavernier, J. van Dievoet, J. van Miegroet (Belgium), and H. Hildenbrand, H.R. Schwarz (Federal Republic of Germany)
Discussion 570
The transient characteristics of a new pulse research reactor (SM-62/69) 575
J. MacPhee and R.F. Lumb (United States of America)
Discussion 587
Two compact, high-intensity pulsed neutron sources (SM-62/4) 589
W. Eyrich and A. Schmidt (Federal Republic of Germany)
Discussion 607
The generation of neutron pulses and modulated neutron fluxes with sealed-off neutron tubes (SM-62/9) 609
C.W. Elenga and O. Reifenschweiler (Netherlands)
Discussion 622

High-output neutron generating tubes for reactivity measurements (SM-62/28) 623
P.D. Lomer, J.E. Bounden, J.D.L.H. Wood and W.J. Barnes (United Kingdom)
Système à fréquence et largeur d'impulsions ajustables permettant la pulsation et la modulation de milieux multipliants sous-critiques à neutrons rapides (SM-62/85) 635
M. Duquesne, R. Gerbier, F. Lyon et A. Schmitt (France)
Discussion 652
General Discussion 653

RELATED TECHNIQUES (Session VII)

Techniques closely related to pulsed neutron research (SM-62/76) ... 657
R.E. Uhrig (United States of America)
Discussion 697
Excitation of neutron waves by modulated and pulsed sources (SM-62/77) 701
R.B. Perez and R.S. Booth (United States of America)
Discussion 725
Comparative study of several types of pulsed and modulated experiments on fast multiplying media (SM-62/87) 729
M. Cadilhac, P. Govaerts, P. Hammer, M. Moore, B. Nicolaenko and F. Storrer (EURATOM)
Measurements of the prompt neutron decay constant of the VERA reactor using the pulsed source method (SM-62/26) 759
J.W. Weale, W.J. Paterson, H. Goodfellow and M.H. McTaggart (United Kingdom)
Mesures au moyen d'une source pulsée et modulée dans un réacteur (SM-62/38) 775
W. Rotter (Belgique)
Discussion 795
Pulsed source and noise measurements on the STARK reactor at Karlsruhe (SM-62/3) 799
M. Edelmann, G. Kussmaul, H. Meister, D. Stegemann and W. Väth (Federal Republic of Germany)
Pulsed neutron source and reactor noise studies of plutonium systems (SM-62/60) 825
S.R. Bierman and E.D. Clayton (United States of America)
A simple cross-correlation method for the study of the neutron pulse transfer function in media using a statistically pulsed neutron source (SM-62/33) 849
R. Haas, W. Matthes and B. Weckermann (EURATOM)
Discussion 861
Theory of pulsed neutron experiments in highly heterogeneous multiplying media (SM-62/8) 863
S.E. Corno (Italy)
Discussion 882

SUMMARY (Session VIII)

Summary of the symposium on pulsed neutron research (SM-62/97) . 885
M. Nelkin (United States of America)
Discussion 895

Chairmen of Sessions and Secretariat of the Symposium 899

List of Participants 901

Author Index 915

THERMAL MULTIPLYING SYSTEMS

(Session IV)

SURVEY OF PULSED NEUTRON SOURCE METHODS FOR MULTIPLYING MEDIA

E. GARELIS
GENERAL ELECTRIC COMPANY, VALLECITOS ATOMIC LABORATORY,
PLEASANTON, CALIF., UNITED STATES OF AMERICA

Abstract — Résumé — Аннотация — Resumen

SURVEY OF PULSED NEUTRON SOURCE METHODS FOR MULTIPLYING MEDIA. In recent years there have existed two schools of thought on the most effective manner of obtaining measurements of the shutdown reactivity using pulsed neutron generators; these are (i) the conventional pulsed neutron source measurements with a repetitively pulsed source and (ii) methods based on a pseudo-random impulse response technique using cross-correlation between input and output. In both techniques the pertinent information obtained is identical, i.e. ideally both methods serve to determine the response function.

The development of pulsed neutron source techniques on thermal systems for the purpose of reactivity measurements is traced from the early efforts of Sjöstrand to the recent ($k\beta/\ell$) method. In the usual pulsed neutron source method, the Green's function of the subcritical assembly, the reactor response to a delta function source of neutrons, is the sought-after property. The exponential decay, $\exp(-\alpha t)$, of the Green's function yields a spatially independent prompt neutron decay constant. The methods by which the reactivity is derived from the α-measurement, e.g. the α-delayed critical measurement and the recent ($k\beta/\ell$) method, are discussed. The fundamental modal treatments are examined in the light of the theory of the pulsed neutron source techniques as developed for the ($k\beta/\ell$) model.

The implications of the pulsed neutron source theory to obtain precise decay constants and suitable data for the analysis of pulsed systems are considered. Experimental work is reviewed that shows the advantages as well as the limitations of the ($k\beta/\ell$) technique.

The use of pseudo-random impulse response methods with cross-correlation between the input and output for the determination of the Green's function of a multiplying assembly is also discussed. It is shown that the information obtained by the pseudo-random method is identical to that obtained from the repetitively pulsed method. Thus, this makes it possible to apply the methods developed for the repetitive to that of the pseudo-random technique.

MÉTHODES DES NEUTRONS PULSÉS POUR L'ÉTUDE DES MILIEUX MULTIPLICATEURS. Depuis quelques années, il existe deux opinions sur la manière la plus efficace de mesurer la réactivité d'arrêt au moyen de générateurs de neutrons pulsés, savoir: a) les mesures classiques au moyen d'une source pulsée à répétition; b) des méthodes qui sont fondées sur la réponse à des impulsions pseudo-aléatoires et utilisent une corrélation entre l'entrée et la sortie. Dans les deux cas, les renseignements pertinents que l'on obtient sont identiques, en d'autres termes, idéalement les deux méthodes servent à déterminer la fonction de réponse.

L'auteur retrace l'évolution des méthodes de mesure de la réactivité fondées sur les sources pulsées dans les systèmes à neutrons thermiques, depuis les premières tentatives de Sjöstrand jusqu'à la récente méthode de ($k\beta/\ell$). Dans la méthode habituelle, la fonction de Green relative à l'assemblage sous-critique – la réponse du réacteur à une source de neutrons à fonction delta – constitue la propriété recherchée. La décroissance exponentielle, $\exp(-\alpha t)$, de la fonction de Green donne une constante de décroissance des neutrons instantanés indépendante du lieu. L'auteur examine les méthodes permettant de déduire la réactivité de la mesure de α, par exemple, la mesure de α à l'état critique retardé et la récente méthode de ($k\beta/\ell$). Il étudie notamment les traitements du mode fondamental à la lumière de la théorie des méthodes des neutrons pulsés, telles qu'elle a été mise au point pour le modèle ($k\beta/\ell$).

L'auteur examine les incidences de la théorie des neutrons pulsés en vue d'obtenir des constantes de décroissance précises et les données voulues pour l'analyse des systèmes pulsés. Il passe en revue les travaux expérimentaux qui font ressortir à la fois les avantages et les limitations de la technique de ($k\beta/\ell$).

Il discute en outre l'emploi des méthodes qui sont fondées sur la réponse à des impulsions pseudo-aléatoires et utilisent une corrélation entre l'entrée et la sortie, pour la détermination de la fonction de Green

d'un milieu multiplicateur. Il montre que les renseignements obtenus par ces méthodes sont identiques à ceux fournis par les méthodes de la source pulsée à répétition, ce qui permet d'appliquer aux premières les procédés qui ont été mis au point pour les secondes.

ОБЗОР МЕТОДОВ С ИСПОЛЬЗОВАНИЕМ ИСТОЧНИКОВ ИМПУЛЬСНЫХ НЕЙТРОНОВ ДЛЯ РАЗМНОЖАЮЩЕЙ СРЕДЫ. В последние годы существовали два направления в области эффективных способов получения измерений остаточной реактивности с использованием генераторов импульсных нейтронов: 1) обычные измерения с источником импульсных нейтронов при непрерывном пульсирующем источнике и 2) методы, основанные на псевдослучайном ответе импульса с использованием соотношения между входом и выходом. В обоих случаях получаемая информация идентична, т.е. оба направления идеально служат определению ответной функции.

Разработка методов с источником импульсных нейтронов на тепловых системах в целях измерения реактивности прослеживается от первоначальных попыток Сьестрэнда до недавнего метода ($к\beta/\ell$). При обычном методе с источником импульсных нейтронов функция подкритической сборки Грина, ответ реактора на дельта-функцию источника нейтронов, представляет собой поиск свойств. Экспоненциальный распад, эксп ($-\alpha t$), функции Грина дает пространственно независимую постоянную распада мгновенных нейтронов. Обсуждаются методы, с помощью которых выводится реактивность из альфа-измерения, например измерение запаздывающей критической альфа и последний метод ($к\beta/\ell$). Изучаются основные виды обработки модели в свете теории с источником импульсных нейтронов, которые разработаны для модели ($к\beta/\ell$).

Рассматриваются осложнения, связанные с теорией источника импульсных нейтронов для получения точных постоянных распада и соответствующих данных для анализа импульсных систем. Рассматривается экспериментальная работа, которая показывает преимущества, а также недостатки метода ($к\beta/\ell$).

Обсуждается также использование метода псевдослучайного ответа импульса с корреляцией между входом и выходом для определения функции Грина на размножающей сборке. Показано, что информация, полученная псевдослучайным методом, является идентичной той, которая получена в результате повторного импульсного метода. Таким образом, это делает возможным применять методику, разработанную для повторения метода псевдо-случайности.

ESTUDIO PANORAMICO DE LOS METODOS DE EMPLEO DE FUENTES DE NEUTRONS PULSADOS EN MEDIOS MULTIPLICADORES. En los últimos años ha habido dos tendencias principales acerca de la manera más eficaz de medir la reactividad de parada, empleando fuentes de neutrones pulsados: la primera preconizaba el empleo de métodos tradicionales de medición con fuentes neutrónicas reiteradamente pulsadas, y la segunda propugnaba la aplicación de métodos basados en una técnica seudoaleatoria de respuesta a los impulsos, utilizando una correlación entre los datos de entrada y los de salida. La información obtenida con una y otra técnica es la misma; en teoría, ambos métodos sirven para determinar la función de respuesta.

Se reseña el desarrollo de las técnicas de empleo de fuentes de neutrones pulsados aplicadas a sistemas térmicos con miras a medir la reactividad, desde los primeros intentos de Sjostrand hasta el reciente método ($k\beta/\ell$). Con el método usual de empleo de estas fuentes, la propiedad que se procura determinar es la función de Green del conjunto subcrítico empleado, es decir, la respuesta del reactor a una fuente de neutrones de función delta. El decrecimiento exponencial ($e^{-\alpha t}$) de la función de Green proporciona una constante de decrecimiento de los neutrones instantáneos que es independiente del espacio. El autor examina los métodos para obtener el valor de la reactividad partiendo de la medida de α, como por ejemplo el método de la medición de la criticidad por neutrones retardados α y el reciente método ($k\beta/\ell$). Seguidamente examina el tratamiento del modo fundamental teniendo en cuenta la base teórica de las técnicas de empleo de fuentes de neutrones pulsados que se han perfeccionado para el modelo ($k\beta/\ell$).

Se exponen las repercusiones de la teoría de la fuente de neutrones pulsados en lo que se refiere a la obtención de valores exactos de la constante de decrecimiento y de datos adecuados para el análisis de los sistemas pulsados. También se examina la labor experimental realizada y se ponen de manifiesto tanto las ventajas como las limitaciones de la técnica ($k\beta/\ell$).

El autor estudia también los métodos seudoaleatorios de respuesta a los impulsos, que utilizan una correlación entre los datos de entrada y los de salida para determinar la función de Green de un conjunto multiplicador, y pone de manifiesto que la información obtenida con el método seudoaleatorio es idéntica a la conseguida por el método de la pulsación reiterada. Por consiguiente, los métodos desarrollados para la técnica de la pulsación reiterada se pueden aplicar a la técnica seudoaleatoria.

1. INTRODUCTION

In the classic paper by SJÖSTRAND [1] on pulsed measurements in subcritical reactors, Sjöstrand indicated that it was Von Dardel who suggested the use of a pulsed neutron source to study reactivities and neutron lifetimes of subcritical assemblies. Sjöstrand derived a relation for the reactivity of a subcritical assembly by considering the prompt and delayed multiplication of a pulsed source; a preliminary account of his work was given at the 1955 Geneva Conference [2]. Also at the same conference, SHAPIRO [3] reported on the prompt decay measurements of Antonov et al. These measurements were made on a uranium-graphite assembly using a pulsed neutron source. In an early review paper BECKURTS [4] gives a summary of the pulsed neutron methods as applied to reactor physics research including thermalization measurements. This paper will concentrate on the pulsed neutron methods for reactivity measurements in thermal systems.

In the usual pulsed neutron experiments for the determination of the subcriticality of an assembly, the assembly is repetitively pulsed with short bursts of neutrons and the resulting time profile of the neutron density is measured with an appropriate detector and recorded with a time analyser. The pulsing is continued until adequate counting statistics are obtained and an accurate representation of the time decay profile can be obtained. The pulse rate R should be small compared to the prompt decay constant to allow the prompt neutron density to decay before the next neutron burst. Since the neutron burst approximates a delta function source, the reactor response is essentially the Green's function for the reactor. A typical response curve is shown in Fig. 1.

The Green's function, the impulse response function, of an assembly is also obtained by a technique using a pseudo-random input with cross correlation between the input and resulting output. These methods were first adopted by communication workers in the field of information transmission; the cross correlation methods are described in detail by LEE [5]. The pseudo-random methods are identical in principle to noise measurement methods. A detailed study comparing the pseudo-random method with noise measurements and allied measurements is given by VALAT and STERN [6].

The exponential decay, $\exp(-\alpha t)$, of the Green's function yields the prompt decay constant of the fundamental spatial mode. This measurement lends itself to a direct comparison to a calculated quantity using multigroup methods, i.e. the prompt eigenvalue calculation. In part, this fact has provided an impetus for the α-measurement. An examination of the usual reactor kinetics equations [7] gives an expression for α, the prompt decay constant. For the case where α is large compared to the decay constants of the delayed neutron precursors, α is given by

$$\alpha = [1 - k(1-\beta)]/\ell \qquad (1)$$

where k is the effective multiplication constant, β the delayed fraction and ℓ the effective prompt neutron lifetime.

From a theoretical and experimental point of view, the decay constant of the fundamental mode has an advantage in that it is a unique parameter of

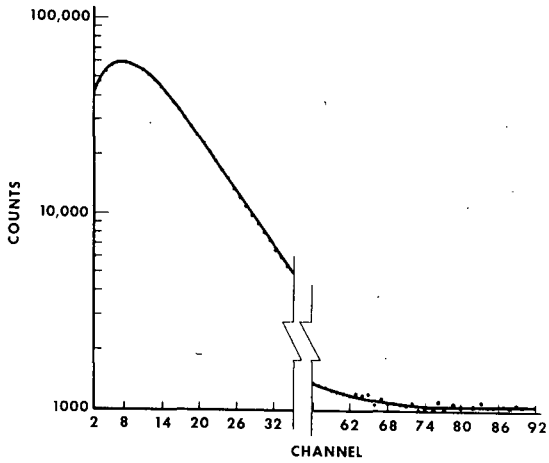


Fig. 1

A typical response curve
(3 wt. % UO_2 stainless steel clad H_2O moderator with 50 ppm B^{10})

$\alpha \sim 1300\ s^{-1} \sim 7$ dollars
R = 50 pulses per second; 45 000 pulses
Channel width = 80 μs; 127 channels

the assembly; however, from a safety point of view, merely knowing the decay constant leaves a great deal unsaid. In particular, it is desirable to have some measure of how far the system is removed from prompt critical, i.e. the reactivity expressed in units of β. Designating α at delayed critical as α_c, then the ratio of (α/α_c) would be a measure of how far the system is removed from prompt critical and hence the quantity

$$(\alpha/\alpha_c) - 1$$

gives a measure from delayed critical. This method of expressing reactivity was introduced by SIMMONS and KING [8]. In general, the determination of α_c is ambiguous since the subcritical reactor with prompt decay constant α can be made critical in many different ways, e.g. changing enrichment, increasing water height, removing control, etc. Each critical configuration will be a different assembly and hence will have a different value of α_c. A thorough discussion of the reactivity concept is given by GOZANI [9].

The recent $(k\beta/\ell)$ technique by GARELIS and RUSSELL [10] for pulsed neutron measurements gives the reactivity directly in units of β as does the method of Sjöstrand. In the $(k\beta/\ell)$ technique, the parameter $(k\beta/\ell)$ is determined using the complete response curve of the pulsed source and the theory is based on a bare monoenergetic diffusion theory model. In the analysis all spatial modes are taken into account as opposed to the fundamental modal treatment of the early method by Sjöstrand. Recent measurements by General Atomic [11, 12] and by the Vallecitos Atomic Laboratory [13] indicate that the $(k\beta/\ell)$ technique gives useful information for bare assemblies

and for close-to-critical measurements (within several dollars). Using the fundamental equation for the $(k\beta/\ell)$ technique, CORNGOLD [14] was able to show that the method is only valid for the bare monoenergetic diffusion theory model.

Using the results obtained from the pulsed neutron theory, it has been possible to outline experimental procedures so as to make it possible to obtain more precise pulsed neutron measurements [15]. Also within the framework of the $(k\beta/\ell)$ technique it has been shown that both the pseudo-random impulse response methods and pulsed neutron methods yield the same information providing the proper procedures are used in carrying out the experiments.

II. THE $(k\beta/\ell)$ TECHNIQUE

It is perhaps constructive to discuss the development of some of the pertinent equations of the $(k\beta/\ell)$ technique, leaving the bulk of the details to the previously published material [10, 15]. The theory of the $(k\beta/\ell)$ technique is based on a bare, one-group diffusion theory model with m-delayed precursors. Consider the time-dependent neutron density $N(\vec{r}, \vec{r}';t)$ at some point $\vec{r}$ at time t as a result of a unit repetitive pulsed source pulsed at the rate of R pulses per second at point $\vec{r}'$. The equations are given by

$$-(M^2/\ell_o)\nabla^2 N + [1-k_o(1-\beta)](N/\ell_o) + \partial N/\partial t - \sum_{i=1}^{m} \lambda_i C_i = S(\vec{r}, \vec{r}';t) \tag{2}$$

$$\partial C_i/\partial t + \lambda_i C_i = k_o \beta_i (N/\ell_o), \quad i = 1, 2, \ldots, m \tag{3}$$

$$S(\vec{r}, \vec{r}';t) = \delta(\vec{r}-\vec{r}') \sum_j \delta(t-j/R) \quad , \tag{4}$$

where M^2 represents the migration area, $k_o(\ell_o)$ the infinite multiplication constant (lifetime), C_i the i-th delayed precursor concentration, and $\beta = \Sigma\beta_i$ the total delayed fraction. It should be noted that it is tacitly assumed that the source strength of each burst is constant; this is not necessary and this point is considered later. The usual procedure is used in solving the above; that is, the precursor concentration is eliminated in the Laplace transformed equations and the density is expanded in terms of the eigenfunctions

$$N(\vec{r}, \vec{r}';t) = \sum A_n(t)\psi_n(\vec{r}) \tag{5}$$

where

$$\nabla^2\psi_n + B_n^2\psi_n = 0 \tag{6}$$

and ψ_n vanishes on the boundary of the assembly. Following the procedure

as given in [10], the quasi-equilibrium neutron density is found to be given by

$$N(\vec{r},\vec{r}';t) = \sum_{n=1}^{\infty}\left[e^{-\alpha_n \tau} + R/(\alpha_n \rho_n)\right]\psi_n(\vec{r})\psi_n(\vec{r}') \tag{7}$$

where $0 < \tau < 1/R$ represents the cycle time,

$$\alpha_n = [1-k_n(1-\beta)]/\ell_n \tag{8}$$

$$\rho_n = (1-k_n)/(k_n\beta) \tag{9}$$

and

$$k_n = k_o/(1+M^2B_n^2) \text{ and } \ell_n = \ell_o/(1+M^2B_n^2). \tag{10}$$

The derivation assumes $\lambda_i \ll R \ll \alpha_n$. The restriction of $R \gg \lambda_i$ assures a constant delayed background. This restriction means that the assembly is pulsed at such a rate that the delayed precursors do not decay and hence a constant delayed contribution results. Quantitatively the delayed contribution is constant to the second order in (λ/R), i.e. $0(\lambda/R)^2$. The largest precursor decay constant, which in turn represents the shortest lived precursor, is about 3 s^{-1} so that pulse rates large as compared to 3 are necessary for a constant delayed neutron contribution. For assemblies that are about a dollar subcritical the quasi-equilibrium condition will be attained by pulsing the assembly long compared to the longest lived precursor, the 55-s precursor. For close-to-critical assemblies the time required is considerably longer.

Several observations regarding the resulting quasi-equilibrium neutron density in Eq. (7) are perhaps in order. The delayed contribution is proportional to the pulse rate R; the faster the assembly is pulsed, the larger the delayed contribution relative to the prompt contribution. Also, the delay tail is inversely proportional to $(\alpha_n \rho_n)$ and hence approximately inversely proportional to the square of the reactivity.

The total neutron density as given in Eq. (7) is decomposed into prompt and delayed contributions by writing

$$N = N_p(\tau) + N_d \tag{11}$$

and identifying the above with their terms in Eq. (7) gives

$$N_p(\tau) = \sum e^{-\alpha_n \tau}\psi_n(\vec{r})\psi_n(\vec{r}') \tag{12}$$

$$N_d = \sum [R/(\alpha_n \rho_n)]\psi_n(\vec{r})\psi_n(\vec{r}'). \tag{13}$$

We now consider the following integral

$$I_1 = \int_0^{1/R} N_p(\tau)d\tau \tag{14}$$

and since $\alpha_n \gg R$, we can write

$$I_1 = \int_0^{\infty} N_p(\tau)d\tau = \sum (1/\alpha_n)\psi_n(\vec{r})\,\psi_n(\vec{r}') \,. \tag{15}$$

Similarly, consider

$$I_2 = \int_0^{\infty} N_p\,[\exp(k_1\beta/\ell_1)\,\tau]d\tau \tag{16}$$

where we have again made the assumption that the top limit of $1/R$ can be replaced by infinity. When Eq. (12) and the explicit definition of α_n are used, Eq. (16) becomes

$$I_2 = \sum \psi_n(\vec{r})\,\psi_n(\vec{r}') \int_0^{\infty} \exp[-\tau(1-k_n)/\ell_n]d\tau \,. \tag{17}$$

Note that Eq. (17) follows, since the ratio of (k_1/ℓ_1) is modally independent and hence the term $(k_n\beta/\ell_n)$ can be inserted through the summation sign. More specifically

$$(k_n/\ell_n) = [k_o(NLP)_n]/[\ell_o(NLP)_n] \tag{18}$$

where $(NLP)_n$ is equal to the non-leakage probability for the n-th spatial mode, $(1+M^2B_n^2)^{-1}$, and hence (k/ℓ) is modally independent. Carrying out the integration as indicated in Eq. (17) gives

$$I_2 = \sum \psi_n(\vec{r})\,\psi_n(\vec{r}')[\ell_n/(1-k_n)] \,. \tag{19}$$

Subtracting I_1 from I_2 and comparing the result with Eq. (13) yields

$$\int_0^{\infty} N_p \exp[(k\beta/\ell)\tau]d\tau - \int_0^{\infty} N_p d\tau = N_d/R \,. \tag{20}$$

Equation (20) is the desired result. If the experimentally determined prompt and delayed distributions are used, the parameter $(k\beta/\ell)$ can be determined by an iterative calculation. A simple code [16] has been written to perform this calculation.

It should be pointed out that an important requirement of the method is the determination of the prompt density from the total density. This is accomplished by pulsing at a rate such that $R \gg \lambda$ so that a constant delayed distribution results. In practice, it appears that for a core that is about one dollar subcritical, R = 10 pulses per second is sufficiently fast to give a constant delayed distribution. This criterion becomes difficult to meet when the assembly is very close to critical. For example, in Eq.(17) the replacement of the top limit of $1/R$ by infinity requires that

$$\alpha_1 - (k\beta/\ell) \gg R, \tag{21}$$

a condition that does not appear to be compatible with $R \gg \lambda$ when α approaches its value at delayed critical, (β/ℓ). In this case it can be argued that at near delayed critical the m-delayed groups can be replaced by a single delayed group with an average precursor decay constant. This average decay constant has a value of about 0.1 s^{-1} so that a pulse rate of one burst per second satisfies the criterion of $R \gg \lambda$ and also satisfies Eq.(21). For the higher spatial modes the delayed roots of the inhour equation rapidly approach their asymptotic values, that of the decay constants, and hence the single delayed group approximation is no longer valid. However, for the near-critical case the effect of the higher modes is presumably small and hence a fundamental modal treatment would be a valid approximation.

A. Corngold's formulation

CORNGOLD [14] has examined the $(k\beta/\ell)$ theory and was able to show that the technique is only rigorously valid for a bare one-group diffusion theory model. In the study of the general velocity-dependent case, Corngold was able to show some interesting limiting cases. In this paper an outline of the formalism as developed by Corngold is given. It should be noted that this treatment is exact and no restrictions or approximations are made on the nuclear parameters, whereas in the $(k\beta/\ell)$ development [10] certain approximations were made regarding the magnitude of the roots of the inhour equation.

Based on a one-pulse experiment, [see section II-C], Eq.(20) becomes

$$\int_0^\infty N_p(\tau) e^{-s\tau} d\tau = \int_0^\infty N dt \tag{22}$$

where s represents $-(k\beta/\ell)$. Corngold interpreted Eq.(22) in terms of the Laplace transforms; i.e. the left-hand side is equal to the Laplace transform of the prompt density, $\tilde{N}_p(s)$, and the right-hand side represents the Laplace transform of the total neutron density with the transform variable set equal to zero, $\tilde{N}(s=0)$. If the detector response function, $D(\vec{r}, v)$, is accounted for, the $(k\beta/\ell)$ technique, as defined by Eq.(22), yields

$$\{D, \tilde{N}_p(s)\} = \{D, \tilde{N}(s=0)\} \tag{23}$$

where the brackets represent the scalar product,

$$\{f, g\} = \int d\vec{v}\, d\vec{r}\, fg . \tag{24}$$

In essence, therefore, we seek a value of s such that Eq.(23) holds.

The neutron and precursor equations for m-delayed groups are given by

$$\left(\frac{\partial}{\partial t} - K\right)N = \sum \lambda_i f_i C_i + S \tag{25}$$

$$\left(\frac{\partial}{\partial t} + \lambda_i\right)C_i = \beta_i \Delta N, \quad i = 1, 2, \ldots, m , \tag{26}$$

where K represents the prompt neutron operator (in either diffusion or transport theory), Δ represents an integral operator for the fission source term,

$$\Delta N = \int d\vec{v}\, \nu\nu q_f(\vec{r}, v) N(\vec{r}, \vec{v}, t), \tag{27}$$

f_i represents the energy distribution of the delayed precursors and the remaining symbols have their usual meaning. Taking the Laplace transform of Eqs.(25) and (26) and eliminating the precursor concentration yields

$$\tilde{N}(s) = \left[(s-K) - \sum_{i=1}^{m} \frac{\lambda_i f_i \beta_i}{s+\lambda_i} \right]^{-1} \tilde{S} . \tag{28}$$

When β_i is set equal to 0 in Eq.(28), the prompt density is given by

$$\tilde{N}_p(s) = (s-K)^{-1}\, \tilde{S} , \tag{29}$$

so that if Eq.(28) with s = 0 is used, Eq.(23) becomes

$$\{D, (K-s)^{-1}\tilde{S}\} = \{D, (K+\Delta_d)^{-1}\tilde{S}\} , \tag{30}$$

where for convenience we have set

$$\Delta_d = \sum f_i \beta_i \Delta . \tag{31}$$

Equation (30) is the basic equation as derived by Corngold and represents the starting point for his investigation. In particular, he makes the observation that for the equation to hold for an arbitrary source and detector function, s must be equal to a constant and equal to the operator Δ_d. The operator Δ_d is equal to a constant only in the case of monoenergetic diffusion theory and is given by

$$s = -\beta\nu v\sigma_f \tag{32}$$

which is equivalent to $s = -(k\beta/\ell)$. Furthermore, Corngold also notes that the $(k\beta/\ell)$ technique holds point by point, i.e.

$$s = -\beta\nu v\sigma_f(\vec{r}). \tag{33}$$

This then shows the precise limitation of the $(k\beta/\ell)$ technique.

B. Eigenfunction expansion problem

B. Eigenfunction expansion problem

Using an eigenfunction expansion method [17], it has been incorrectly shown that the $(k\beta/\ell)$ method is valid for the bare monoenergetic transport theory model. The difficulty was, as pointed out by Corngold, that the eigenfunctions were incomplete with respect to the space in angle. In the paper dealing with the eigenfunction expansion, the angular flux was expanded thusly

$$N(\vec{r}, \vec{\Omega}, t) = \sum B_s(t)\, \psi_s(\vec{r}, \vec{\Omega}) , \tag{34}$$

where the $\psi_s(\vec{r}, \vec{\Omega})$ are defined as the reactivity eigenfunctions as given by COHEN [18].

To understand the completeness problem it is perhaps somewhat simpler to consider an energy-dependent diffusion theory model rather than the monoenergetic transport theory case. In this case, for a bare assembly, the reactivity eigenfunctions would be given by

$$(L + B_n^2)\psi_n(v) = (1/k_n)g(v)\int_0^\infty \nu\sigma_f(v')\psi_n(v')dv' , \tag{35}$$

where L is a velocity-dependent operator, B_n^2 the buckling, k_n the eigenvalue and g(v) is the speed distribution of the fission neutrons. Now solving the above for $\psi_n(v)$ and multiplying the resulting expression by $\nu\sigma_f(v)$ and integrating gives

$$k_n = \int_0^\infty dv'\nu\sigma_f(v')(L + B_n^2)^{-1}g(v') . \tag{36}$$

For each value of B_n^2 there is only one value of k_n since g(v) is a specified function of the speed. If $\psi_n(v)$ were complete with respect to the speed, then there would exist a sequence of k_n for each value of B_n^2. If this were the case, it would then be possible to assign an arbitrary energy distribution for any given spatial mode. This argument was pointed out by Corngold.

C. *Pulsing techniques*

An essential part of the experimental technique is the determination of an equilibrium pulse. A simple procedure has been developed [15] that assures the experimenter of an equilibrium pulse regardless of the non-uniformity of the pulsed neutron source. This procedure can be best understood by considering the analysis of a single burst of neutrons in an assembly. It can be shown that if a core is pulsed with a single burst of neutrons and the time analyser (TA) set at a given repetition rate R, then the sum of all contributions recorded in the TA will correspond to the quasi-equilibrium neutron distribution as obtained for a repetitively pulsed core with a uniform source (equal number of neutrons per burst). This is illustrated in Fig. 2.

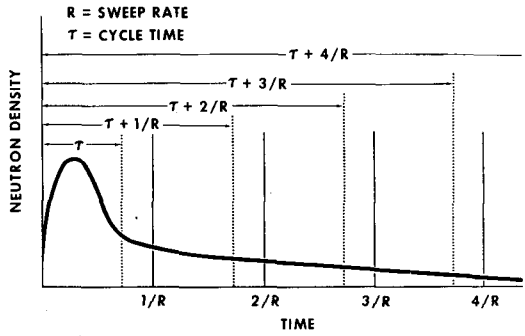


Fig. 2

A single pulse analysis

Now, since the neutron diffusion equations are linear, other individual pulses can be superimposed to have the net result of a repetitively pulsed core. Therefore, the pulses need not be of uniform strength providing the TA continues to record after the pulsing stops. Note that the recording starts with the first pulse. The TA should be allowed to record the data after the pulsing stops for times long compared to the 55-s precursor. It is a straightforward calculation [15] to consider the more general problem of the effect of starting the TA after the pulsing has commenced.

Before this work, it was believed that the pulsed neutron source had to be uniform to attain the quasi-equilibrium state. This observation is significant in both the usual α-measurement and in the $(k\beta/\ell)$ technique. For example, in the α-measurement the procedure is to fit the count rate time profile to an exponential, after removing the background, to determine the fundamental decay constant. Since the above pulsing technique gives a known delayed background, a constant, by ensuring the quasi-equilibrium state, the analysis for the α-determination is on a firmer basis. Also, in the $(k\beta/\ell)$ technique, the need for a precise knowledge of the delayed tail is crucial if meaningful results are to be obtained. In the general case the shape of the delayed tail cannot be readily calculated except where $R \gg \lambda$.

Most of the commercially available sealed pulsed neutron source tubes are designed to be used at a maximum of 10 bursts per second. Effectively, a tube may be pulsed at virtually any pulse rate by using the above pulsing

technique. For example, to simulate a pulse rate of R = 25 bursts per second, the tube is operated at R = 5 and the TA is set to make five complete sweeps for each burst.

The problem of obtaining a known delayed background to obtain a precise α-measurement has been considered by using calculational techniques. For example, in the case of a heavy water or graphite moderated system it is difficult to have the pulse rate R such that $\lambda \ll R \ll \alpha$, especially for close-to-critical systems. For example, in a heavy water system KÜCHLE [19] applied a time-dependent background correction to an α-measurement. Küchle used the time-dependent fundamental mode calculation of FRAUDE [20]. Fraude found an expression for the density of the form

$$n(t) \sim e^{-\alpha t} F(t,\rho) ,$$

where $F(t, \rho)$ is a term that is calculated assuming a monoenergetic diffusion theory model with delayed precursors. In this case a fit to the pulsed data, assuming $F(t, \rho) = 1$, gives an error of about 5% in the reactivity. Küchle finds that with the correction for the delayed neutrons a good exponential fit results.

SASTRE and WEINSTOCK [21] considered the identical problem for a uranium-graphite system. In this case the delayed contribution was calculated with an iterative technique. In this experiment the assembly was pulsed repetitively once every three minutes. At this rate, all but the longest lived precursor decay and the mode of pulsing can be considered as a single pulse problem. In both experiments it would have been interesting to determine whether or not a constant delayed neutron contribution could have been obtained.

III. OTHER PULSED NEUTRON METHODS

A. Method of Sjöstrand

SJÖSTRAND [1, 2] considered the case where the reactor is excited by a sequence of uniform rectangular pulses. The pulse rate was assumed to be large compared to the decay constants of the precursors and the pulse length larger than $(1/\alpha)$. In this fashion an equilibrium distribution results with a constant delay tail. Sjöstrand considered the resulting areas under the prompt and total neutron distribution as the prompt and total multiplication, respectively. If the area under the prompt distribution is designated as A_1, then

$$A_1 = S_0/[1-k(1-\beta)] \tag{37}$$

and if A_2 is the area under the delayed distribution, then

$$A_1 + A_2 = S_0/(1-k) , \tag{38}$$

where S_0 is proportional to the source. Combining Eqs. (37) and (38) gives

$$A_1/A_2 = (1-k)/(k\beta), \tag{39}$$

the reactivity in dollars; that is, the ratio of the prompt multiplication to the delayed multiplication gives the reactivity directly in units of β. Note that this is a fundamental modal treatment and that this expression follows directly from Eq.(7) for a single spatial mode. Sjöstrand applied correction factors in an attempt to account for the effects of the higher spatial modes. The method depends upon the condition that the prompt and delayed contributions can be separately determined. A number of measurements by this technique were made on a heavy water system.

B. Method of Simmons and King

SIMMONS and KING [8] considered reactivity measurements by comparing the ratio of the prompt decay constant, α to the decay constant at delayed critical (see the discussion in the Introduction). According to the definition of α, $\alpha_c = (\beta/\ell)$ and if the ratio of (β/ℓ) is not appreciably different for the subcritical reactor, then

$$\rho = (\alpha/\alpha_c) - 1 \tag{40}$$

and if Eq.(1) is employed, the above becomes

$$\rho = (1-k)/\beta \text{ for } 1-\beta \cong 1. \tag{41}$$

In practice α_c is measured by making close-to-critical α-measurements in conjunction with asymptotic period measurements. These measurements coupled with the inhour equation give an estimate of α_c. In water assemblies a simple extrapolation of α versus water height measurements gives a value of α_c. In some cases α_c is determined by pulsing a critical reactor [12].

Arguments have been advanced that (β/ℓ) does not remain constant and hence the above does not hold. In addition, it is argued that this method is a fundamental modal treatment and that the higher spatial modes are neglected. However, based on a bare monoenergetic diffusion theory model, this method is identical to the $(k\beta/\ell)$ method. For example, at delayed critical $\alpha_c = (k\beta/\ell)$ with $k = 1$. Now for a bare system the ratio of (k/ℓ) is a constant and therefore

$$\alpha_c = (\beta/\ell)_{\text{critical}} = (k\beta/\ell)_{\text{non-critical}} \tag{42}$$

providing the assembly is made critical merely by increasing its size. The reasoning above is identical to that used in the $(k\beta/\ell)$ method, see Eq.(18). In practice the two methods do not give identical results unless the assemblies are near critical, see the results of BROWN et al. [12].

C. Method of Gozani

To circumvent the modal contamination problem of Sjöstrand, GOZANI [22] considered the equilibrium response of a repetitively pulsed reactor

pulsed at the rate of R pulses per second for times $\tau > \tau_w$, where τ_w is a so-called waiting time and $\tau_w < 1/R$. For his analysis Gozani considered a reactor pulsed with a sequence of rectangular neutron pulses of width d seconds with the pulse rate chosen so that a constant delayed tail results, $R \gg \lambda$. Following Sjöstrand, Gozani assumed that the reactor response can be separated into a prompt part and a constant delayed tail,

$$N(\tau) = N_p(\tau) + N_d . \tag{43}$$

Gozani reasoned that for τ_w of order $1/\alpha$ where α is the prompt fundamental mode decay constant, the contribution of the higher spatial modes to the neutron density following a pulse of neutrons will be negligible and hence a fundamental modal treatment will suffice.

Proceeding on this basis, Gozani then shows that the reactivity is given by

$$\rho = Rd(e^{\alpha d}-1)N^{-1}{}_p(\tau_w)e^{\alpha\tau_w}/N_d , \tag{44}$$

where the exponential term in the brackets results from the finite pulse width. If a narrow pulse, $\alpha d \ll 1$, is assumed, then the above becomes

$$\rho = RN_p(\tau_w)e^{\alpha\tau_w}/(\alpha N_d) . \tag{45}$$

Note that the above equation follows precisely from Eq. (7) for a single mode. The product $N_p(\tau_w)$ exp $(\alpha\tau_w)$ is equal to the normalization, $\psi_1(\vec{r})\psi_1(\vec{r}')$, that is, the value of the prompt distribution for the fundamental mode when extrapolated to zero time. This normalization can be obtained by extrapolating the die-away curve for the fundamental mode back to zero time and subtracting the constant delayed contribution. For example, for a single mode Eq. (13) gives

$$\rho = R\psi_1(\vec{r})\psi_1(\vec{r}')/(\alpha N_d) , \tag{46}$$

which is equivalent to Eq. (45) above.

IV. EXPERIMENTAL MEASUREMENTS

The recent pulsed neutron measurements carried out by the Vallecitos Atomic Laboratory on low-enriched uranium oxide water-moderated and reflected assemblies are, in part, summarized in a series of quarterly reports [13]. These measurements were made to examine the limitations of the $(k\beta/\ell)$ method as applied to pulsed neutron source measurements, and to examine the prediction of the pulsing techniques as described earlier. It was found that for assemblies that are close to critical, within several dollars, the value of $(k\beta/\ell)$ obtained was independent of the relative source-to-detector location and hence the method gives a unique measurement. As the assemblies become more subcritical, the measured value of $(k\beta/\ell)$ shows a stronger source-to-detector position dependence. The bulk of these

measurements was carried out by Meyer and is reported at this Symposium in considerable detail [23].

A series of pulsed neutron measurements was carried out on unreflected, uranium, water-moderated systems by BROWN et al. [11, 12] of General Atomic for the express purpose of examining the $(k\beta/\ell)$ technique. The assembly, a rectangular parallelepiped approximately 18 in × 18 in × 8 in, consisted of uranium aluminium fuel plates spaced with narrow water gaps. A series of measurements was made from critical to 30 dollars subcritical with $(k\beta/\ell)$ varying from 232 at critical down to 190 s^{-1}. The reactivity was decreased by removing fuel. The measurements using $(k\beta/\ell)$ and α-delayed critical were compared. The agreement in reactivity is within 5% down to 4 dollars subcritical. It will be recalled that for a bare one-group diffusion theory model both methods should give identical results. The variation in $(k\beta/\ell)$ as a function of subcriticality gives an indication of the difference in the two methods for real systems. At reactivities beyond 4 dollars the difference in α_c and $(k\beta/\ell)$ becomes significant and hence the difference in the reactivities between the two methods becomes significant.

To demonstrate the condition that the $(k\beta/\ell)$ method accounts for all spatial modes, Brown et al. pulsed the assembly using three different detector positions. The experimental data is shown in Fig. 3 for the three

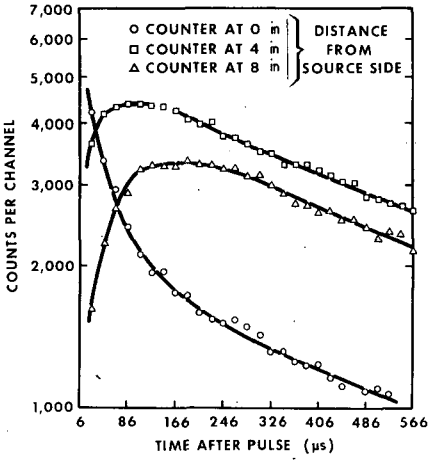


Fig. 3

Response curves for different detector positions
(BROWN et al. [12])

detector locations. The values of $(k\beta/\ell)$ were found to be 222, 222, and 225 for the counters located at 0, 4 and 8 in from the source side, respectively. Note that the three detector positions give widely different appearing response curves, indicating that the modal content of each is considerably different. Also to be noted is that all three curves have the same asymptotic slope, the same fundamental prompt decay constant. The numerical values of $(k\beta/\ell)$ appear to be within experimental error; this experiment provides a graphic illustration of the ability of the method to account for all of the spatial modes.

At the other extreme, as opposed to a bare core, RUSSELL et al. [24] considered a highly subcritical core reflected on only one side. The purpose of the experiment was to impose a drastic test on the validity of the $(k\beta/\ell)$ technique for a reflected assembly. Varying the detector from the reflector to various positions in the core gave varying values of $(k\beta/\ell)$ ranging from a maximum of about 200 to 100 s^{-1}. The cores varied from about 30 to 100 dollars subcritical. The same type of variation, except to a lesser degree, was noted by MEYER [23].

The α-measurement has the particular advantage that it yields itself to a direct comparison with a calculated value, i.e. the prompt eigenvalue calculation. This allows the designers to have a check point on their cross-sections by calculating a directly measurable quantity. This avoids all of the ambiguity associated with reactivity measurements. An extensive series of α-measurements with calculated comparisons was carried out by BACH [25, 26] and his associates at the Knolls Atomic Power Laboratory on a bare and reflected polyethylene-moderated uranium assembly. As a check on the validity of their α-measurements a series of experiments was carried out with a 1/v poison (boric acid) added to the assembly. If a uniform addition of the 1/v absorber is assumed throughout the assembly, a linear variation of the decay constant should result.

MEISTER [27] carried out a series of α-measurements for a subcritical, natural uranium, heavy water assembly. The assembly was sufficiently subcritical, $\alpha \sim 200$ s^{-1}, so that it could be pulsed at a rate of 10 pulses per second to yield a constant delayed distribution. In close-to-critical measurements, the delayed distribution becomes more of a problem, cf. the effort of KÜCHLE [19]. Measurements showing the approach of the density to the fundamental mode following a burst are given. The time-dependent decay constants are analysed for several of the spatial harmonics.

In a control rod study programme at the Vallecitos Atomic Laboratory, MEYER and BALLOWE [28] carried out several α-measurements on a large number of diverse absorber materials in a number of different cores. The fuel consisted of 1.3, 3.00, and fully enriched uranium with light and heavy water, organic, and graphite moderators. In a companion study, KEAR and RUDERMAN [29] considered various calculational models, in order to make a comparison with the measured values. Some additional measurements have been reported by PETERSEN et al. [30] of the Laboratory. KOLAR and KLOVERSTROM [31] have also reported some α- measurements on control rod worths in a bare graphite, fully enriched uranium assembly. HENRY et al. [32] and SILVER et al. [33] made control rod worth measurements on the Oak Ridge Bulk Shielding reactor.

ALBRECHT et al. [34] reported some α-measurements for a plutonium-polystyrene assembly. Both pulsed neutron and random noise analysis measurements were compared.

A number of prompt decay measurements was reported by SAGOT et al. [35] on the various thermal critical assemblies at Saclay. OGURA et al. [36] carried out some measurements on a subcritical, light water moderated, low-enriched uranium oxide assembly.

V. PSEUDO-RANDOM METHODS

In the pseudo-random impulse response method, the assembly is subjected to a binary pseudo-random neutron source and the cross correlation of the output with the input yields the Greens function for the assembly. The binary pseudo-random input source is a periodic sequence whose auto-correlation function approximates a periodic sequence of delta functions. These methods have the inherent advantage that extraneous uncorrelated noise signals do not contribute to the Greens function since the extraneous signal and the input are uncorrelated. The statistical analysis of the errors associated with the cross correlation method have been investigated by STERN et al. [37], STERN [38] and VALAT [39].

In both techniques, the repetitive pulsing and the pseudo-random, the final information obtained is identical. A pseudo-random input with a period of $1/R$ seconds is equivalent to repetitively pulsing an assembly at R times per second [40]. With this equivalence established it is then possible to apply the pulsing theory and the $(k\beta/\ell)$ technique directly to the data obtained from the pseudo-random methods.

To show this correspondence between the two methods we consider an assembly that can be completely characterized by its Greens function $g(t,t')$, where the position and velocity variables are suppressed. The generation of the pseudo-random function is described by ROE [41] and others, see for example [42, 43]. Following Roe, we introduce a function $f(t)$ that can be represented by a binary periodic sequence that takes on values of either plus or minus one,

$$f(t) = +1 \text{ or } -1 \quad n\Delta t \le t \le (n+1)\,\Delta t, \quad n \text{ integer} \tag{47}$$

and

$$f(t+\nu\Delta t) = f(t). \tag{48}$$

In addition, $f(t)$ has the average value of $1/\nu$,

$$(1/\nu\Delta t)\int_0^{\nu\Delta t} f(t)dt = (1/\nu), \tag{49}$$

and its auto-correlation function approximates a sequence of delta functions,

$$(1/\nu\Delta t)\int_0^{\nu\Delta t} f(t)f(t+\tau)dt = \sum_{n=-\infty}^{\infty} \delta(\tau - n\nu\Delta t) - (1/\nu)\,. \tag{50}$$

Consider an assembly that is pulsed with an external source where the source can be represented by a pseudo-random sequence,

$$\tilde{f}(t) = 1 + f(t)\,, \tag{51}$$

where the source $\bar{f}(t)$ represents a source that is either on or off. The output of the assembly, n(t), is given by

$$n(t) = \int_0^t g(z, 0)\bar{f}(t-z)dz \tag{52}$$

since $g(z, 0) = 0$ for $z < 0$ and $\bar{f}(t) = 0$ for $t < 0$. The cross correlation of the "biased" input f(t) with the output is given by

$$\phi_{fn}(\tau) = (1/\nu\Delta t)\int_0^{N\nu\Delta t} f(t-\tau)n(t)dt \tag{53}$$

where the cross correlation is carried out over N whole cycles. Using Eq. (52) in (53) and changing orders of integration and using the approximation as given in Eq. (50) with (49) gives

$$\phi_{fn}(\tau) = \int_0^{N\nu\Delta t} dz g(z, 0)(1/\nu\Delta t)\int_{z-\tau}^{-\tau} f(x)\bar{f}(x+\tau-z)dx$$

$$+ N \sum_{n=-N+1}^{0} g(\tau, n\nu\Delta t), \quad 0 < \tau < \nu\Delta t. \tag{54}$$

The first term on the right-hand side of the above represents a correction and cannot be evaluated explicitly since the integration does not extend over an integral number of periods. Since $g(z, 0)$ is proportional to a sum of negative exponentials for subcritical assemblies, it can be shown [40] that the integral term in Eq. (54) does not increase with N and hence the integral term can be made as small as necessary relative to the term containing the sum. Therefore, for sufficiently large values of N, Eq. (54) becomes

$$\phi_{fn}(\tau) = N \sum_{n=-N+1}^{0} g(\tau, n\nu\Delta t) \text{ as } N \to \infty. \tag{55}$$

For an assembly not too close to critical and for values of $N\nu\Delta t$ long compared to the half-life of the 55-s precursor, the above will represent the response to an equilibrium pulse. The procedure to obtain an equilibrium pulse using the pseudo-random techniques is now clear. The assembly is pulsed with a pseudo-random signal sufficiently long to obtain an equilibrium pulse shape. The experiment is then repeated: if no change results then the time was sufficiently long to make the correction term as expressed in Eq. (54) negligible. Using the above methods it should then be possible to obtain data equivalent to the repetitive pulsing method and hence α-

measurements can be made with the proper correction for the delayed contribution. It should perhaps be pointed out that the condition that the autocorrelation function does not give a zero contribution between the peaks is exactly compensated by the condition that the input neutron source must be either on or off.

One of the first series of measurements using the pseudo-random technique was carried out by BALCOMB et al. [44] on a fully enriched bare uranium assembly and on the Kiwi reactor, an experimental rocket prototype reactor. The measurements were carried out by varying the reactivity of the assembly in a pre-programmed pseudo-random fashion by injecting a slug of plastic into the core. RAJAGOPAL [45] carried out measurements on the cross correlation of the random variation of an absorber and the reactor output to obtain the impulse response function. In the experiments by Balcomb et al. and Rajagopal, it was possible to vary the reactivity since the assemblies were critical.

Recognizing the need to consider subcritical systems, STERN et al. [37] considered the use of a neutron source modulated in a pseudo-random off-on manner, since the variation of an absorber in a subcritical system will not produce a measurable neutron output. They also recognized that the pseudo-random variation of a neutron source has the advantage over a pulsed source in that the duty cycle of the source in the former case is 50%, whereas in the pulsed source method it is in the order of a fraction of a per cent. This is an advantage since good counting statistics can be obtained in a relatively short time as compared to the pulsed method. The neutron source is controlled by a shift register with feedback which produces the pseudo-random signal input. The cross correlation is carried out in a series of scalars which are controlled by the shift registers. STERN and VALAT [46] reported on some preliminary measurements that were carried out at Saclay on the RUBEOLE and ULYSSE critical assemblies.

UHRIG [47, 48] reported on a series of measurements in light and heavy water moderated, natural uranium assemblies. The neutron generators were controlled by the method as described by STERN et al. [37]. The neutron output was recorded on magnetic tape and the correlations were then carried out on an off-line computer.

VI. CONCLUSIONS

The usefulness of the $(k\beta/\ell)$ technique for the interpretation of the reactivity of bare systems and for close-to-critical reflected systems appears to have merit. In particular, an α-delayed critical, (β/ℓ), measurement can be made with relative ease merely by making a single pulsed measurement near critical and interpreting $(k\beta/\ell)$ as (β/ℓ) since $k \sim 1$. This has the obvious advantage of making the measurement on a subcritical assembly rather than on a critical one. All of the methods used to determine reactivity share a common problem in that all the methods require a precise knowledge of the delayed neutron contribution. In this respect the $(k\beta/\ell)$ technique provides a quantitative mechanism for obtaining this background. A knowledge of the background is essential for the precise determination of a prompt decay constant. The latter is especially important for a near critical as-

sembly where the delayed background can be an appreciable fraction of the total neutron density, e.g., for the measurement of (β/ℓ).

The feasibility of determining precise prompt decay constants introduces the possibility of considering an experiment which gives a macroscopic measure of the spectrum of an assembly by measuring the overall fission ratios. Basically, the method depends upon the differences in the yields of the various delayed neutron precursors. The reactivity and period measurements of an assembly are related through the inhour equation which in turn depends upon the properties of the delayed neutrons. In the case of an assembly containing more than one fissionable isotope, the total delayed fraction will depend upon the fission fraction in each isotope. Using the $(k\beta/\ell)$ technique, the reactivity ρ in units of β along with an asymptotic period is determined at several points in the neighbourhood of criticality. Using these values with the assumed values of the decay constants and yields of the delayed precursors, a simple least squares fit can be used to determine the fission fraction. The success of the method depends upon the accuracy with which the pulsed neutron source parameters α and $(k\beta/\ell)$ and the asymptotic period can be determined. In principle it should be possible to obtain any desired degree of accuracy merely by obtaining sufficiently large counting statistics.

The future efforts of investigating the theory of pulsed neutron methods should be extended to reflected and to energy-dependent models or both. This, of course, means the study of the general time-dependent neutron diffusion equation, a formidable undertaking. However, with the aid of judicious approximations some inroads may be accomplished on selected problems.

ACKNOWLEDGEMENT

This effort was sponsored under the auspices of the United States Atomic Energy Commission Contract No. AT(04-3)-189 Project Agreement 26, and the support received is gratefully acknowledged.

REFERENCES

[1] SJÖSTRAND, N. G., Ark. Fys. 11 (1957) 233.
[2] SJÖSTRAND, N. G., Proc. UN Int. Conf. PUAE 5 (1956) 52.
[3] SHAPIRO, F. L., Proc. UN Int. Conf. PUAE 5 (1956) 87.
[4] BECKURTS, K. H., Nucl. Instrum. Meth. 11 (1961) 144.
[5] LEE, Y. W., Statistical Theory of Communication, John Wiley and Sons, Inc., N. Y. (1960).
[6] VALAT, J. and STERN, T. E., Analysis of the accuracy of certain methods used for measuring very low reactivities, CEA Rpt 2229 (1964).
[7] GLASSTONE, S. and EDLUND, M. C., The Elements of Nuclear Reactor Theory X D. Van Nostrand Co., Inc., N. Y. (1952).
[8] SIMMONS, B. E. and KING, J. S., Nucl. Sci. Engng 3 (1958) 595.
[9] GOZANI, T., Nukleonik 5 (1963) 55.
[10] GARELIS, E. and RUSSELL, Jr., J. L., Nucl. Sci. Engng 16 (1963) 263.
[11] BROWN, J. R., YOUNG, J. C., BEYSTER, J. R., HOUSTON, D. H. and MOWRY, W. R., Trans. Amer. nucl. Soc. 6 (1963) 284.

[12] BROWN, J. R., YOUNG, J. C., BEYSTER, J. R., HOUSTON, D. H., MOWRY, W. R. and RUSSELL, Jr., J. L., Measurements of subcritical reactivity using a pulsed-neutron source, General Atomic Rpt 4838 (1964).

[13] MEYER, P. and GARELIS, E., Development of pulsed neutron applications to power reactor start-up procedures, 9th Quarterly and Summary Rpt GEAP-4644 (1964). See also the other Quarterlies as referenced in the above document.

[14] CORNGOLD, N., Trans. Amer. nucl. Soc. 7 (1964) 282 and CORNGOLD, N., On the analysis of pulsed, multiplying systems, General Atomic Rpt 5405 (1964).

[15] GARELIS, E., Nucl. Sci. Engng 18 (1964) 242.

[16] GARELIS, E. and MEYER, P., Development of pulsed neutron application to power reactor start-up procedures, 7th and 8th Quarterly Rpt, GEAP-4606 (1964).

[17] GARELIS, E., Nucl. Sci. Engng 19 (1964) 131.

[18] COHEN, E. R., Proc. 2nd UN Int. Conf. PUAE 11 (1958) 302.

[19] KÜCHLE, M., in Exponential and Critical Experiments II IAEA, Vienna (1964) 575.

[20] FRAUDE, A., Nukleonik 4 (1962) 84.

[21] SASTRE, C. and WEINSTOCK, E. V., Nucl. Sci. Engng 20 (1964) 359.

[22] GOZANI, T., Nukleonik 4 (1962) 348.

[23] MEYER, P., "An experimental study of the (kβ/ℓ) pulsed neutron source technique in light water assemblies", these Proceedings II.

[24] RUSSELL, Jr., J. L., BROWN, J. C. and YOUNG, J. C., Trans. Am. nucl. Soc. 7 (1964) 71.

[25] BACH, D. R., BUNCH, S. I., CERBONE, R. J. and SLOVACEK, R. E., Nucl. Sci. Engng 11 (1961) 199.

[26] BACH, D. R., BISTLINE, J. A., BUNCH, S. I., CERBONE, R. J., FEINER, F., SKOLNIK, W. and SLOVACEK, R. E., in Exponential and Critical Experiments II IAEA, Vienna (1964) 391.

[27] MEISTER, H., Reactor Sci. Tech. 17 (1963) 97.

[28] MEYER, P. and BALLOWE, W. C., An experimental parametric study of the effects of control rods on the prompt neutron decay constant in multiplying media, Rpt GEAP-4019 (1962).

[29] KEAR, G. H. and RUDERMAN, M. H., An analysis of methods in control rod theory and comparisons with experiment, Rpt GEAP 3937 (1962).

[30] PETERSEN, G. T., ALINE, P. G. and McWHORTER, R. J., in Exponential and Critical Experiments II IAEA, Vienna (1964) 209.

[31] KOLAR, O. C. and KLOVERSTROM, F. A., Nucl. Sci. Engng 10 (1961) 45.

[32] HENRY, K. M., JOHNSON, E. B., PEREZ BELLES, R., DE SAUSSURE, G. and SILVER, E. G., Trans. Amer. nucl. Soc. 2 (1959) 28.

[33] SILVER, E. G., DE SAUSSURE, G., HENRY, K. M., JOHNSON, E. B., KINGTON, J. D. and BELLES, R. P., Trans. Amer. nucl. Soc. 3 (1960) 278.

[34] ALBRECHT, R. W., BIERMAN, S. R. and GARLID, K. L., Trans. Amer. nucl. Soc. 7 (1964) 47.

[35] SAGOT, M., TELLIER, H., JACQUEMART, R. and KREMSER, J., in Exponential and Critical Experiments III IAEA, Vienna (1964) 163.

[36] OGURA, S., HAYATA, K., SUGENO, M., KONDO, T., MUKAE, M. and NAGANUMA, O., in Exponential and Critical Experiments II (1964) 43.

[37] STERN, T. E., BLAQUIERE, A. and VALAT, J., Rector Sci. Tech. 16 (1962) 499.

[38] STERN, T. E., in Noise Analysis in Nuclear Systems, AEC Symposium Series No. 4 (UHRIG, R. E., Co-ordinator) US Dept. of Commerce, Wash. D. C. (1964) 203.

[39] VALAT, J., in Noise Analysis in Nuclear Systems, US Dept. of Commerce, Wash. D. C. (1964) 219.

[40] GARELIS, E., submitted for publication to Nucl. Sci. Engng (1965).

[41] ROE, G. M., Pseudo-random sequences for the determination of system response characteristics: sampled data systems, G. E. Res. Lab. 63-RL-3341 E (1963).

[42] PETERSON, W. W., Error correcting codes, M. I. T. Press, Cambridge, Mass. (1961).

[43] CORRAN, E. R. and CUMMINS, J. D., Binary codes with impulse auto correlation function for dynamic experiments, U. K. A. E. A. Rpt AEEW-R 210 (1962).

[44] BALCOMB, J. D., DEMUTH, H. B. and GYFTOPOULUS, E. P., Nucl. Sci. Engng 11 (1961) 159.

[45] RAJAGOPAL, V., Nucl. Sci. Engng 12 (1962) 218.

[46] STERN, T. E. and VALAT, J., in Reactor Kinetics and Control, AEC Symposium Series No. 2 (WEAVER, L. E., Co-ordinator) US Dept. of Commerce, Wash., D. C. (1964) 27.

[47] UHRIG, R. E., in Noise Analysis in Nuclear Systems, AEC Symposium Series No. 4 (UHRIG, R. E., Coordinator) US Dept. of Commerce, Wash. D. C., (1964) 251.

[48] UHRIG, R. E., in Exponential and Critical Experiments III IAEA, Vienna (1964) 239.

AN EXPERIMENTAL STUDY OF THE ($k\beta/\ell$) PULSED NEUTRON SOURCE TECHNIQUE IN LIGHT WATER ASSEMBLIES

P. MEYER
GENERAL ELECTRIC COMPANY,
VALLECITOS ATOMIC LABORATORY,
PLEASANTON, CALIF., UNITED STATES OF AMERICA

Abstract — Résumé — Аннотация — Resumen

AN EXPERIMENTAL STUDY OF THE ($k\beta/\ell$) PULSED NEUTRON SOURCE TECHNIQUE IN LIGHT WATER ASSEMBLIES. A new pulsed neutron model and experimental technique have been investigated in light water reflected cores with special emphasis on application in large central station power reactors. The pulsed neutron source method is based upon a bare, monoenergetic diffusion theory model. It uses the complete neutron density versus time profile of a pulsed assembly to obtain the parameters α and ($k\beta/\ell$) from a single measurement. The distinguishing feature of this method is that all spatial modes are taken into account, as opposed to the usual fundamental mode treatment. A new pulsing method that simplifies the experiments to obtain reliable data for both the α and ($k\beta/\ell$) measurement has also been experimentally verified.

The results of a test programme performed in the Vallecitos Thermal Critical Assembly to investigate the range of validity of the ($k\beta/\ell$) model in various lattices are discussed. The dependence of ($k\beta/\ell$) upon the relative source and detector position over a large range of subcriticality is shown. It has been established that the new technique eliminates the need for a separate α-delayed critical, (β/ℓ) determination, a measurement which, particularly in large power reactors, is at best difficult and expensive to perform. The experimental results indicate that the ($k\beta/\ell$) theory yields meaningful results for reasonably small reflected cores down to at least 3.5 dollars subcritical. In large cores the reflector problem is minimized since the importance of the reflector is decreased and reasonable results can be expected at even lower subcriticalities. This is confirmed by experiments which were carried out in a 150 MW(t) boiling water reactor before and after full power operation, and the 12.5 MW(t) Vallecitos Experimental Superheat Reactor at room and design temperatures and design pressure. Both of these facilities exhibited the multi-core effect that is found in large power reactor cores and an interpretation of these pulsed measurements is made possible by the proper placement of pulsed source and detectors.

ÉTUDE EXPÉRIMENTALE DE LA MÉTHODE ($k\beta/\ell$) DES NEUTRONS PULSÉS DANS LES ASSEMBLAGES A L'EAU ORDINAIRE. De nouveaux modèle et méthode expérimentale des neutrons pulsés ont été étudiés dans des assemblages à l'eau ordinaire, avec réflecteur, l'attention étant plus spécialement portée sur leur application aux réacteurs de grande puissance des centrales nucléaires. La nouvelle méthode est fondée sur un modèle théorique de diffusion monoénergétique sans réflecteur. Elle utilise la courbe complète du nombre volumique de neutrons en fonction du temps dans un assemblage pulsé pour obtenir, à l'aide d'une seule mesure, les paramètres α et ($k\beta/\ell$). Cette méthode présente la caractéristique particulière de tenir compte de tous les modes spatiaux, alors que l'on s'en tient habituellement au mode fondamental. On a également soumis à une vérification expérimentale un nouveau procédé de production des bouffées qui simplifie les conditions expérimentales requises pour obtenir des valeurs numériques sûres en vue de mesurer α et ($k\beta/\ell$).

Les auteurs discutent les résultats d'un programme exécuté avec l'assemblage critique de Vallecitos pour étudier dans quelles limites le modèle ($k\beta/\ell$) peut être utilisé dans différents réseaux. Ils montrent que ($k\beta/\ell$) dépend de la position relative de la source et du détecteur pour un grand nombre d'états sous-critiques. Il a été établi que la nouvelle méthode supprime la nécessité de déterminer séparément α pour l'état critique retardé et (β/ℓ), détermination qui, notamment dans les grands réacteurs de puissance, est pour le moins difficile et coûteuse. Les résultats expérimentaux montrent que le modèle ($k\beta/\ell$) donne des résultats satisfaisants pour les cœurs relativement petits, avec réflecteur, au moins jusqu'à une sous-criticité de 3,5 dollars. Dans les grands cœurs, le réflecteur pose un problème moindre puisque son importance diminue et l'on peut obtenir

des résultats satisfaisants même lorsque la sous-criticité atteint des valeurs plus basses. Cela a été confirmé par des expériences effectuées dans un réacteur à eau bouillante de 150 MW(t) avant et après fonctionnement à pleine puissance, ainsi que dans le réacteur expérimental de 12,5 MW(t) à surchauffe de Vallecitos aux températures ambiante et théorique et à la pression théorique. Ces deux installations ont permis d'observer l'effet dû aux diverses régions, que l'on rencontre dans les cœurs des grands réacteurs de puissance. Il est possible d'interpréter les mesures à l'aide des sources pulsées en positionnant convenablement la source et les détecteurs.

ОПЫТНОЕ ИЗУЧЕНИЕ МЕТОДА ИСТОЧНИКА ПУЛЬСИРУЮЩИХ НЕЙТРОНОВ ($k\beta/\ell$) В СБОРКАХ С ОБЫЧНОЙ ВОДОЙ. Новая модель пульсирующих нейтронов и опытные методы подвергались исследованиям в активных зонах с отражателем из легкой воды, причем особый упор был сделан на применение в крупных энергетических реакторах центральных станций. Метод источника пульсирующих нейтронов основывается на теоретической модели моноэнергетического рассеяния без отражателя. В нем используется полная нейтронная плотность по отношению к сечению по времени пульсирующей сборки с тем, чтобы получить параметры и ($k\beta/\ell$) с одного измерения. Отличительной особенностью этого метода является то, что все пространственные модели принимаются в расчет как противопоставляемые обычному основному состоянию обработки. Новый пульсирующий метод, который упрощает опытные потребности для получения относительных данных как по измерению α, так и ($k\beta/\ell$), точно так же разнообразился в опытном порядке.

Обсуждаются результаты опытной программы, проведенной на термокритической сборке Валеситоса для исследования степени пригодности модели ($k\beta/\ell$) в различных решетках. Показывается зависимость ($k\beta/\ell$) от относительного источника и положения детектора при сверхбольших подкритичностях. Было установлено, что новый метод устраняет необходимость отдельного измерения запаздывающей критичности α, определения (β,ℓ), измерения, которое в особенности в крупных энергетических реакторах является наиболее трудным и дорогостоящим делом. Опытные результаты указывают на то, что теория ($k\beta/\ell$) дает многообещающие результаты для вполне подходящего занижения небольших активных зон с отражателем почти до 3,5 долларов подкритичности. В крупных активных зонах проблема отражателя уменьшается, поскольку значимость рефлектора уменьшается и вполне подходящие результаты можно ожидать даже при более низких подкритичностях. Это подтверждается экспериментами, которые проводились в реакторе с кипящей водой мощностью 150 мгвт до и после освоения полной эксплуатационной мощности и в опытном реакторе с перегревом в Валлеситос мощностью 12,5 мгвт при комнатных и проектных температурах и проектном давлении. Обе эти установки демонстрируют эффект множественности активных зон, который был найден в активных зонах крупных энергетических реакторов, и толкование этих пульсирующих измерений стало возможным благодаря соответствующему размещению пульсирующего источника и детекторов.

ESTUDIO EXPERIMENTAL DE LA TECNICA DE NEUTRONES PULSADOS ($k\beta/\ell$) EN CONJUNTOS DE AGUA LIGERA. El autor ha investigado un nuevo modelo de neutrones pulsados y una técnica experimental para su empleo en cuerpos de agua ligera con reflector, estudiando sobre todo su empleo en los reactores de gran potencia de las centrales nucleares. El nuevo método se basa en un modelo teórico de difusión monoenergética sin reflector. Para obtener los parámetros α y ($k\beta/\ell$) con una sola medición, se utiliza la curva completa de la densidad neutrónica en función del tiempo en un conjunto pulsado. Una característica de este método es que se tienen en cuenta todos los modos espaciales, cosa que no sucede con los métodos corrientes que se suelen guiar por el modo fundamental. Se ha comprobado también experimentalmente un nuevo método de pulsación que simplifica los requisitos experimentales necesarios para obtener valores numéricos seguros para la medición de α y ($k\beta/\ell$).

Los autores discuten los resultados de un programa desarrollado con el conjunto térmico crítico de Vallecitos para investigar los límites de empleo del modelo ($k\beta/\ell$) en distintos reticulados. Se indica que ($k\beta/\ell$) depende de la posición relativa de la fuente y del detector para una amplia gama de estados subcríticos. La nueva técnica elimina la necesidad de determinar por separado el valor α para el estado crítico retardado y el cociente (β/ℓ), medición que suele ser difícil y costosa en especial en los grandes reactores de potencia. Los resultados experimentales ponen de manifiesto que el modelo ($k\beta/\ell$) da buenos resultados para cuerpos relativamente pequeños y con reflector, al menos hasta un valor subcrítico de 3,5 dólares. En cuerpos de grandes dimensiones, el problema planteado por el reflector es relativamente pequeño puesto que este componente pierde importancia y se pueden obtener resultados satisfactorios incluso cuando los valores subcríticos son más bajos. Esto se ha confirmado con los experimentos efectuados en un reactor de agua hir-

viente de 150 MW(t) antes y después de su funcionamiento a plena potencia, así como con el reactor experimental de sobrecalentamiento (de 12,5 MW(t)) de Vallecitos, a la temperatura ambiente así como a la temperatura y presión previstos en el proyecto. Ambas instalaciones han permitido observar el efecto debido a las diversas regiones, efecto que se manifiesta en el cuerpo de los reactores de gran potencia; las mediciones hechas con fuentes pulsadas pueden interpretarse colocando en el lugar adecuado la fuente y los detectores.

1. INTRODUCTION

As an outgrowth of pulsed neutron work [1, 2] carried out previously at Vallecitos, there has been a continuing effort to improve existing analytical models and experimental techniques. In the course of this work, an improved theoretical model was proposed by GARELIS and RUSSEL [3] and is discussed at this Symposium in a paper by GARELIS [4]. The method determines the parameter $(k\beta/\ell)$ from the complete response curve of a repetitively pulsed assembly. Using this value of $(k\beta/\ell)$ with the prompt decay constant α obtained from the same measurement, the reactivity can be determined in units of β. The assembly is pulsed at the rate of R pulses per second such that $\lambda \ll R \ll \alpha$, where λ is the shortest lived precursor decay constant. This method of pulsing enables one to separate the total density $n(\tau)$ into a time-dependent prompt distribution $n_p(\tau)$ and a constant delayed contribution n_d; that is,

$$n(\tau) = n_p(\tau) + n_d .$$

The condition $R \gg \lambda$ assures a constant delayed contribution. Without a known constant background it would be necessary to determine the complete time-dependent delayed distribution in order to separate the individual components. This is indeed a difficult problem to carry out with a reasonable amount of precision.

From the neutron density versus time profile the integrals

$$I_1 = \int_0^\infty n_p dt \quad \text{and} \quad I_2 = \int_0^\infty n_p [\exp(k\beta/\ell)\tau]\, d\tau$$

are obtained which satisfy the equation

$$R(I_2 - I_1) = n_d .$$

When the above is employed, a simple iterative calculation [10] gives the parameter $(k\beta/\ell)$.

An essential part of the experimental technique is the determination of an equilibrium pulse. A procedure has been developed [5] which assures the experimenter of an equilibrium pulse regardless of the uniformity of the pulsed source. The precise knowledge of the delayed tail is crucial for the determination of $(k\beta/\ell)$. In addition, a known delayed tail is also necessary to arrive at a reliable exponential fit for the determination of α, especially in close-to-critical measurements where the tail represents a large fraction of the total density.

2. EXPERIMENTAL TECHNIQUES AND APPARATUS

The apparatus required to carry out experiments of this type is relatively simple and all components are commercially available. A pulsed neutron generator capable of producing short bursts of neutrons and a neutron detection system with an appropriate time analyser is needed. It may be helpful to discuss some of the requirements which must be placed on the individual components.

2.1. Neutron generators

The pulse generators are usually of the (D, T) type, because of the positive Q-value of this reaction, requiring rather low ion energies. The particular choice usually depends upon the assembly and the purpose of the measurements to be carried out, see for example the review paper by BECKURTS [6]. A power reactor will require from 10^8 to 10^9 neutrons per burst because of its physical size and existing large neutron and gamma background. This is particularly true for measurements to be made after power operation. A source strength of 10^6 neutrons per burst will usually suffice in the average size thermal assembly. Some aspects of the problems involved in experiments in high gamma fields have been discussed in detail in previous work [7, 8, 9].

For most of this work a Kaman Pulsatron Model 810 was used. This accelerator, a sealed tube device, was packaged together with its high voltage transformer in a stainless steel container (see Fig. 1).

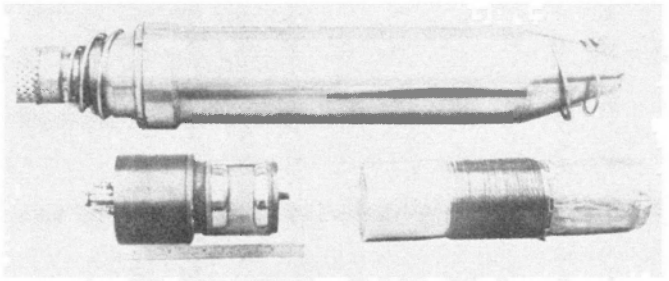


Fig. 1

Pulsed neutron source assembly

2.2. Neutron detection system

The counting efficiency of the detectors must be rather high to gather sufficient statistics for the delayed neutron contribution. This applies, in particular, to measurements in highly subcritical configurations. This high counting efficiency, however, also gives rise to large count rates in the peak channels in close-to-critical measurements. Consequently, an appropriately short dead-time must be maintained to prevent count losses from exceeding the usual first order corrections.

The two neutron detectors which have been used are 1- and 2-in diameter General Electric U^{235} fission counters with a 5% carbon dioxide and 95% argon gas mixture at a total pressure of 1 atm. Carbon dioxide was chosen for its higher ion mobility as compared to that of the customary methane. The electron collection time of these counters is 0.04 μs and the efficiency is rated at 1.2 and 0.2 counts/nv, for the 2- and 1-in chambers, respectively.

The precision with which the neutron density versus time profile can be obtained depends in part upon the number of channels available in the time analyser; for most measurements 256 channels are adequate. A Technical Measurement Corporation CN 110 computer unit with a Model 212 plug-in logic unit is currently used, providing 256 channels with channel widths varying from 10 to 2560 μs and a memory storage capacity of 2^{20} counts per channel.

3. MEASUREMENTS

An extensive series of experiments was performed in the Vallecitos Thermal Critical Assembly (TCA). Measurements were carried out on reflected light water moderated, slightly enriched uranium oxide lattices in various geometries. Experiments were also carried out on the Humbolt Bay Power Reactor at Eureka, California, which are summarized in some earlier reports [10, 11]. Additional experiments were conducted in the Vallecitos Experimental Superheat Reactor (EVESR).

3.1. Small core measurements

In the TCA four different basic configurations were considered: (i) uniform pitch lattices, 3% enriched fuel, (ii) clumped lattice, 3% enriched fuel, (iii) uniform two-region core; consisting of 1.3% and 3% enriched fuel, and (iv) boron poisoned uniform and clumped lattices. The fuel rods were $\frac{1}{2}$-in diameter rods approximately 4 ft in length placed on a square pitch of 0.8 in.

In most measurements, the source and detectors were placed in the reflector near the core-reflector boundary at half core height. Initially the critical water height was established for the basic array. Pulsed neutron measurements were then conducted at reduced water heights and in smaller lattices at a constant water height. In some cases two separate detectors were used simultaneously in different locations. Before any source pulsing was started, stable neutron flux conditions were verified by observing the reactor flux monitors. In this stable condition, the extraneous reactor background was determined by sweeping the time analyser without pulsing the source. This background must be subtracted from the total background accumulated in the pulsed measurement to obtain the true source-induced delayed contribution, n_d, used to calculate $(k\beta/\ell)$. Pulsing was then started and data accumulation began simultaneously. Pulse repetition rates R were chosen by the condition $\lambda \ll R \ll \alpha$ and also by practical considerations which take into account the time required for one sweep, i.e. 256 Δt where Δt is the channel width. To reduce actual counting time losses, R was selected so that 1/R, the pulsing period, was only slightly greater

than 256 Δt, the time per sweep. Whenever this pulse rate R was beyond the capability of the neutron generator, a simple pulse rate divider was used to overcome this limitation [5]. The divider reduced the actual burst rate of the neutron source while maintaining the desired sweep rate of the time analyser. The effective pulse rate R to be used for the $(k\beta/\ell)$ calculation is then the sweep rate of the time analyser. To avoid the background from obscuring the prompt contribution, care must be exercised whenever the burst rate is lower than the sweep rate. After the source pulsing is stopped, sweeping of the time analyser is continued until the neutron flux dies down to the original flux level before pulsing. This procedure is necessary to assure that all delayed neutrons produced during the experiment are properly counted.

The parameter $(k\beta/\ell)$ when measured near critical was also compared with a value obtained from a reactor period measurement. Using the inhour equation, the reactivity is calculated in the usual manner. From this and the measured prompt decay constant, α, $(k\beta/\ell)$ is given by

$$(k\beta/\ell) = \alpha/(\rho + 1),$$

where ρ is in units of β.

To demonstrate the effect of pulse rates on the measured value of $(k\beta/\ell)$ some experiments were made on an assembly at approximately one dollar subcritical. Figure 2 is a plot of $(k\beta/\ell)$ versus pulse rate R. It shows clearly a sharp levelling off at $R \sim 10$ pulses per second. In near-critical measurements of thermal systems a repetition rate of 10 per second cannot be maintained. One reason for this is that alpha is relatively small and hence correspondingly long times are required for the prompts to decay into

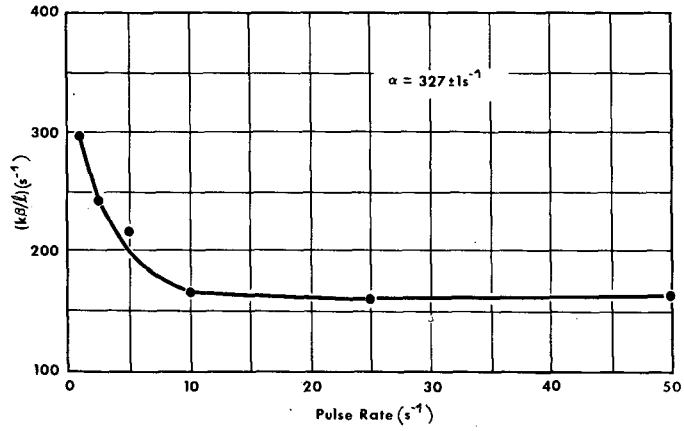


Fig. 2

Effect of pulse rate on $(k\beta/\ell)$ calculation

the background. Therefore, the channel width must also be correspondingly large to cover the complete decay profile. This gives rise to sweep times which can be larger than 1/R for large values of R. In addition, the delayed

contribution n_d depends directly upon R, while n_p does not. Large pulse rates thus cause an undue build-up of the delayed contribution which increases the statistical uncertainty in the prompt part and lowers the precision in alpha. It can be reasoned [3, 4] that in close-to-critical systems, the delayed precursors may be replaced by a mean precursor with $\lambda \sim 0.1\ s^{-1}$. This permits an equilibrium pulse to be obtained at lower pulse rates. Some measurements in only slightly subcritical arrays, (5 to 20 cents) appear to support this line of reasoning.

3.1.1. Uniform lattice measurements

The results of the uniform lattice measurements are given in Tables I, II and III. Table I gives the results of a series of measurements which were performed to exhibit a $(k\beta/\ell)$ dependence, if any, upon core size and pulse repetition rates. Measurements started with a 21×23 critical array down to a highly subcritical 12×12 array. In the 21×23 lattice, $(k\beta/\ell)$ was also obtained at different water heights. The following observations are significant. For the 21×23 array it is apparent that $(k\beta/\ell)$ decreases slightly as the reactivity is increased by lowering the water height. Further, it should be noted that $(k\beta/\ell)$ for Run 3123-F agrees with the measurement of α_c as obtained by a period measurement. In the 18×23 array, different burst and sweep rates were applied at a constant water height. For this array note that $(k\beta/\ell)$ is essentially identical at two different effective repetition rates with three different burst rates. In Run 3135, the generator was set at a burst rate of 12.5 pulses per second and the sweep rate at twice the burst rate to give an effective pulse rate of R = 25 and this value of $(k\beta/\ell)$ is in agreement with the values obtained by pulsing the assembly at the rate of 10 and 25 pulses per second.

Table II contains the results of a series of measurements on the close-to-critical array to investigate the detector position dependence of $(k\beta/\ell)$. This core was a 21×23 array with four elements removed from the centre to allow for the placement of the detector in the centre of the core. One observes that the agreement is very good, the centre location giving the highest value of $(k\beta/\ell)$. The variation in α is well within 2%. The assembly was about a dollar subcritical. To investigate the position dependence further, a smaller core was constructed.

In Table III results are given for an 18×18 array, again with four elements removed from the centre. In this case, the array is about 10 to 15 dollars subcritical and there appears to be a significant amount of detector position dependence. Note that, as in the case of the 21×23 array, the largest value of $(k\beta/\ell)$ is obtained in the centre. The alpha values measured all fall within about 2%; the range is from 1808 to 1839 s^{-1}. This is excellent agreement. Again note the agreement between runs 3173-F2 and 3173-2F2 with variations in burst and sweep rates.

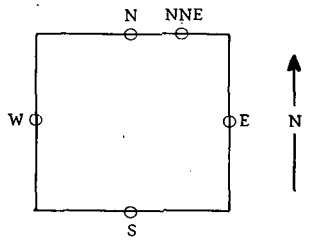
3.1.2. Clumped lattice

In power reactors, clumped lattices are used rather than uniform lattices. This spacing is necessary for control rods, cooling channels, etc.

TABLE I

UNIFORM LATTICE, 3% FUEL, $(k\beta/\ell)$ VERSUS CORE SIZE

Source and detector located 47 cm above bottom fuel plane.



Run	Lattice	Water height (cm)	Position		Pulse rate (pps)		α (s^{-1})	$(k\beta/\ell)$ (s^{-1})	$k(\beta = 0.0072)$
			PNS	Detector	Sweeps	Bursts			
3123-F	21×23	90.27	N	S	5	5	194 ± 1	185[a]	0.9997
3158	21×23	85.00	W	E	10	10	271 ± 2	183	0.9965
3158-2	21×23	81.00	W	E	20	20	346 ± 1	179	0.9933
3158-3	21×23	77.00	W	E	25	25	435 ± 1	178	0.9897
3135	18×23	90.50	S	N	25	12.5	772 ± 8	171	0.9753
3135-2	18×23	90.50	S	N	10	10	760 ± 2	171	0.9759
3135-3	18×23	90.50	S	N	25	25	766 ± 2	164	0.9743
3159	20×20	90.50	W	N	25	25	845 ± 3	156	0.9691
3160	18×18	90.50	S	N	25	25	1573 ± 4	149	0.9357
3161	16×16	90.50	W	N	50	50	2464 ± 6	107	0.8634
3162	14×14	90.50	S	NNE	25	25	3057 ± 22	108	0.8355
3163	12×12	90.50	W	NNE	75	75	3770 ± 22	73	0.7338

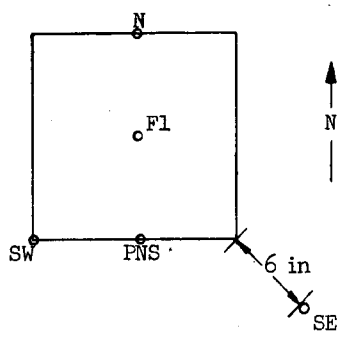
[a] (β/ℓ) obtained from two period measurements at this moderator height was found to be identical to this value.

TABLE II

UNIFORM LATTICE, 21×23 ARRAY, 3% FUEL

Critical water height = 107.57 cm
Actual water height = 95.00 cm

A 304-SS tube, 1.50 O.D. × 0.049 wall, closed at the bottom to prevent water from entering,, extended throughout the core along the vertical axis; 4 fuel rods were removed. Source and detector located 47 cm from bottom fuel plane.



Run	Detector position	Pulse rate (pps)		α (s^{-1})	(kβ/ℓ) (s^{-1})	k(β=0.0072)
		Sweeps	Bursts			
3206-4F1	F1	10	10	338±1	187	0.9942
3207-1F2	F2-N	10	10	340±2	186	0.9941
3206-3F2	F2-SW	10	10	335±2	183	0.9941
3208-2F2	F2-SE	10	10	335±1	176	0.9935

In this series of experiments a basic uniform array of 23×35 was set up and then every sixth row and column was removed, thus creating water gaps and a basic array of 4×6 bundles each consisting of a 5×5 sub-array. The results are given in Table IV and for the most part are self-evident. In this series there appears to be no detector position dependence even though the assembly is about 3.5 dollars subcritical. Note again the variation in sweep and burst rates. In one run, Run 3130, the detector was covered with 0.020 in of cadmium. There appears to be no significant difference in the results. This would seem to indicate that the measurements are somewhat energy independent. These experiments also demonstrate the reproducibility of the individual measurements.

3.1.3. Multi-region cores

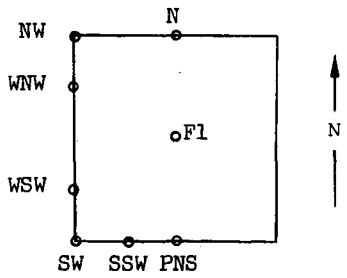
Two multi-region cores were constructed both with 1.3 and 3.0% fuel. The core configurations and results are given in Tables V and VI. Again the purpose of these measurements is to show the detector position dependence of $(k\beta/\ell)$. Both cores were close to critical, about 60 cents subcritical, consequently very little position dependence is evident. In previous mea-

TABLE III

UNIFORM LATTICE, 18×18 ARRAY, 3% FUEL

Water height = 90.50 cm

A 304-SS tube, 1.50 O.D. × 0.049 wall, closed at the bottom to prevent water from entering, extended throughout the core along the vertical axis; 4 fuel rods were removed. Source and detector located 47 cm from bottom fuel plane.



Run	Detector position	Pulse rate (pps)		α (s^{-1})	($k\beta/\ell$) (s^{-1})	$k(\beta = 0.0072)$
		Sweeps	Bursts			
3173-F1	F1	25	25	1817 ± 10	162	0.9313
3170-F2	N	25	25	1839 ± 6	139	0.9191
3171-F2	NW	25	25	1813 ± 10	133	0.9166
3172-F2	WNW	25	25	1826 ± 12	137	0.9186
3173-F2	WSW	25	25	1808 ± 12	130	0.9149
3173-2F2	WSW	50	25	1829 ± 9	129	0.9133
3174-F2	SW	50	25	1823 ± 16	113	0.9021
3175-F2	SSW	50	25	1816 ± 5	119	0.9071

surements [2], α-delayed critical was measured for the 1.3% fuel and found to be 130 s^{-1} as compared to 185 s^{-1} for the 3.0% fuel. Comparing Tables V and VI, it is noted that as the proportion of the 1.3% fuel is increased, the ($k\beta/\ell$) decreases as might be expected from their respective values. The agreement in the α-measurement is again very good.

3.1.4. Boric acid experiments

An indirect test of the ($k\beta/\ell$) technique to highly subcritical assemblies may be obtained by pulsing cores containing a dissolved 1/v poison (boron) in the moderator [7]. The experiment is interpreted as follows: since ($k\beta/\ell$) is modally independent, it can be represented by ($k_0\beta/\ell_0$) where the zero subscript refers to properties of the infinite medium case. Using the

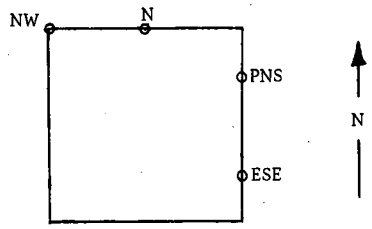
TABLE IV

CLUMPED LATTICE, 4×6 BUNDLES, 3% FUEL

Water height = 132.00 cm

Bundle: 5×5 elements

Source and detector located 47 cm above bottom fuel plane.



Run	Detector position	Pulse rate (pps)		α (s^{-1})	(kβ/ℓ) (s^{-1})	k(β = 0.0072)
		Sweeps	Bursts			
3126	N	10	10	509 ± 1	118	0.9766
3126-2	N	10	10	510 ± 1	116	0.9762
3132-2	N	25	12.5	508 ± 5	116	0.9763
3132-3	N	5	5	504 ± 4	119	0.9773
3130[a]	N	10	10	510 ± 4	115	0.9760
3128	NW	10	10	502 ± 2	115	0.9763
3128-2	NW	10	10	506 ± 2	114	0.9759
3129	ESE	10	10	501 ± 2	119	0.9774
3129-2	ESE	10	10	507 ± 2	119	0.9771

[a] Detector cadmium covered, 0.020 in.

four factor formula to represent the infinite multiplication factor k_0 by $\eta f(p, \epsilon \sim 1)$ yields

$$k_0 = \nu\sigma_f/\sigma_a \quad \text{and} \quad \ell_0 = 1/\nu\sigma_a$$

and hence

$$(k\beta/\ell) = \beta\,\nu(\sigma_f v)$$

where v is the average neutron velocity and the remaining symbols have their usual meaning. The ratio $(k\beta/\ell)$ depends on the non-1/v dependence of

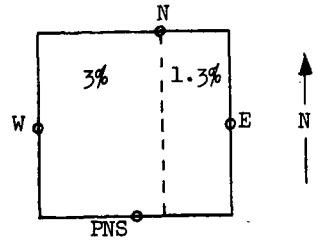
TABLE V

UNIFORM LATTICE, MULTI-REGION, 1.3% AND 3% FUEL

Critical water height = 92.93 cm

Array: 1.3% Fuel - 6x23
3% Fuel - 17x23

Source and detector located 47 cm above bottom fuel plane.



Run	Detector position	Water height (cm)	Pulse rate (pps)		α (s^{-1})	(kβ/ℓ) (s^{-1})	k(β = 0.0072)
			Sweeps	Bursts			
3137	N	92.20	5	5	183 ± 2	174	0.9996
3138	N	85.00	10	10	291 ± 1	179	0.9955
3139	E	85.00	10	10	290 ± 1	176	0.9954
3140	W	85.00	10	10	295 ± 1	179	0.9954

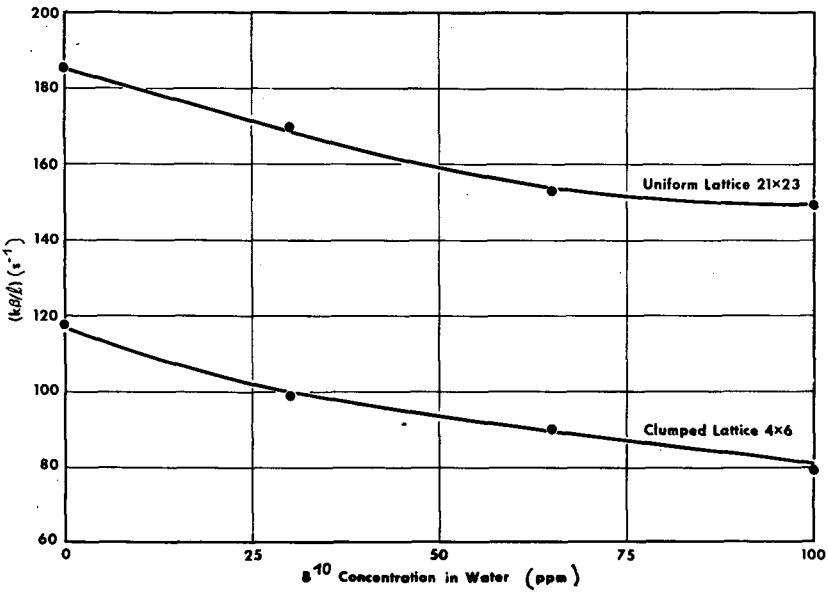


Fig. 3

(kβ/ℓ) versus boron calculation

the fuel fission cross-section and the fuel disadvantage factor. For a U^{235} system, σ_f varies approximately as 1/v and in the range 0 to 100 ppm of B^{10} there should be less than a 1% change in the flux.

Reagent grade natural boric acid H_3BO_3, (J. T. Baker, Cat. No. 0084) was dissolved in the moderator to give boron-10 concentrations of 30, 65 and 100 ppm of water. The measurements were made on the uniform and clumped lattices. The results are given in Tables VII and VIII, respectively. For the uniform lattice, Table VII, α varies from 194 for the clean core up to 2370 for 100 ppm of B^{10} while the $(k\beta/\ell)$ varies from 185 to 146. As the boric acid concentration increases in the moderator (and reflector) the importance of the reflector should tend to diminish and hence the cores should approach the properties of a bare core. A plot of $(k\beta/\ell)$ versus the boron concentration as shown in Fig. 3 shows that indeed $(k\beta/\ell)$ tends to flatten out as the poison concentration increases.

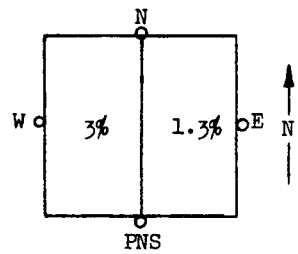
TABLE VI

UNIFORM LATTICE, MULTI-REGION, 1.3% AND 3% FUEL

Critical water height = 100.75 cm

Array: 1.3% Fuel - 13×23
3% Fuel - 14×23

Source and detector located 47 cm above bottom fuel plane.



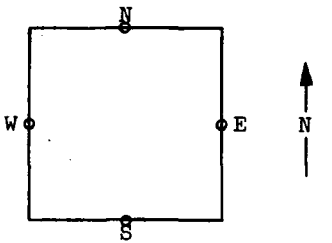
Run	Detector position	Water height (cm)	Pulse rate (pps)		α (s^{-1})	$(k\beta/\ell)$ (s^{-1})	$k(\beta=0.0072)$
			Sweeps	Bursts			
3143-3	W	100.00	5	5	174 ± 3	166	0.9997
3144	N	90.50	10	10	295 ± 2	167	0.9945
3145	E	90.50	10	10	290 ± 1	164	0.9945
3143	W	90.50	10	10	292 ± 1	170	0.9949
3144-2	N	85.00	10	10	373 ± 1	165	0.9910
3145-2	E	85.00	10	10	373 ± 1	162	0.9907
3143-2	W	85.00	10	10	375 ± 1	172	0.9915

TABLE VII

UNIFORM LATTICE, 21×23 ARRAY, 3% FUEL, (kβ/ℓ) VERSUS BORON-10 CONCENTRATION

Critical water height = 91.16 cm
Actual water height = 90.50 cm

Source and detector located 47 cm above bottom fuel plane.



Run	Position		Pulse rate (pps)		B^{10} (ppm)	α (s^{-1})	k(β/ℓ) (s^{-1})	k (β = 0.0072)
	PNS	Detector	Sweeps	Bursts				
3123-F[a]	N	S	5	5	0	194 ± 1	185	0.9997
3147	W	E	25	25	30	807 ± 2	169	0.9735
3147-3	S	E	25	25	30	815 ± 5	171	0.9736
3147-4	W	E	25	25	30	810 ± 2	169	0.9735
3152	S	E	25	25	65	1591 ± 6	152	0.9361
3152-2	S	E	25	25	65	1595 ± 3	153	0.9365
3152-3	S	E	25	25	65	1608 ± 3	154	0.9364
3152-4	W	E	50	50	65	1596 ± 8	155	0.9374
3154	W	E	50	50	100	2339 ± 15	152	0.9064
3155	S	E	25	25	100	2370 ± 3	146	0.9014

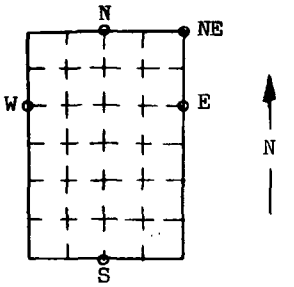
[a] Water height for this run was 90.27 cm

TABLE VIII

CLUMPED LATTICE, 3% FUEL, (kβ/ℓ) VERSUS BORON-10 CONCENTRATION

Array: 6×4 bundles @ 5×5 elements.
Actual water height = 132.00 cm

Source and detector located 47 cm above bottom fuel plane.



Run	Position		Pulse rate (pps)		B^{10} (ppm)	α (s^{-1})	(kβ/ℓ) (s^{-1})	k (β = 0.0072)
	PNS	Detector	Sweeps	Bursts				
3126	NE	N	10	10	0	509 ± 1	118	0.9766
3132-2	NE	N	25	12.5	0	508 ± 5	116	0.9763
3132-3	NE	N	5	5	0	504 ± 4	119	0.9773
3148	S	E	25	25	30	1238 ± 12	97	0.9218
3149	W	E	50	50	30	1275 ± 13	103	0.9239
3149-2	S	E	50	25	30	1238 ± 24	96	0.9215
3150	S	E	50	25	65	2256 ± 9	90	0.8526
3156	S	E	25	25	100	3239 ± 25	83	0.7860
3157	S	E	25	25	100	3203 ± 27	74	0.7663

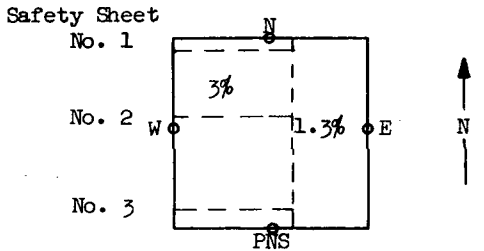
TABLE IX

MULTI-REGION CORE, $(k\beta/\ell)$ VERSUS CONTROL BLADE WORTH

Critical water height = 92.44 cm
Actual water height = 92.20 cm

Array: 1.3 Fuel - 6 × 23
3% Fuel - 17 × 23

Source and detector located 47 cm above bottom fuel plane.



Run	Position		Safety sheet inserted	Pulse rate (pps)		α (s^{-1})	$(k\beta/\ell)$ (s^{-1})	k (β = 0.0072)
	PNS	Detector		Sweeps	Bursts			
3137	S	N	None	5	5	183 ± 2	174[a]	0.9996
3139-2	S	E	No. 3	10	10	512 ± 2	173	0.9861
3140-2	S	W	No. 3	10	10	513 ± 2	176	0.9864
3139-3	S	E	No. 2 & 3	25	12.5	1494 ± 9	139	0.9342
3140-3	S	W	No. 2 & 3	25	12.5	1410 ± 6	144	0.9406
3139-4	S	E	No. 1, 2, & 3	25	12.5	1835 ± 10	134	0.9164

[a] (β/ℓ) obtained from a period measurement was 173 s^{-1}.

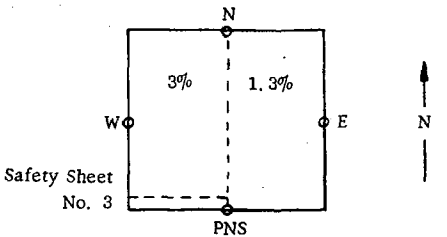
TABLE X

MULTI-REGION CORE, (kβ/ℓ) VERSUS POSITION

Critical water height = 100.75 cm
Actual water height = 100.75 cm

Array: 1.3% Fuel - 13×23
3% Fuel - 14×23

Source and detector located 47 cm above bottom fuel plane.



Run	Position		Safety sheet inserted	Pulse rate (pps)		α (s^{-1})	(kβ/ℓ) (s^{-1})	k (β = 0.0072)
	PNS	Detector		Sweeps	Bursts			
3143-3[a]	S	W	None	5	5	174 ± 3	167[b]	0.9997
3143-4	S	W	No. 3	10	10	400 ± 1	167	0.9900
3144-3	S	N	No. 3	25	12.5	403 ± 2	164	0.9896
3144-4	S	N	No. 3	25	25	403 ± 1	164	0.9896
3145-3	S	E	No. 3	25	12.5	399 ± 1	161	0.9895
3145-4	S	E	No. 3	25	25	402 ± 4	161	0.9893

[a] Water height for this run was 100.00 cm.

[b] (β/ℓ) from period measurement was 166 s^{-1}.

3.1.5. Control blade measurements

Several measurements were made to investigate the detector position dependence of control rod worth measurements in different lattices. These measurements were made in multi-region cores of 1.3 and 3.0% fuel and in a clumped lattice assembly. The control sheets consisted of a 0.020-in boral slab sandwiched between two sheets of 35 mil aluminium approximately 12 in wide. Table IX gives the results of $(k\beta/\ell)$ in a multi-region core as a function of the number of control blades and detector position. For the particular arrays chosen, the worth of a blade is independent of detector position within experimental error. Note that $(k\beta/\ell)$ decreases with an increasing number of control blades.

Table X considers a different assembly with only one control blade and again investigates the dependence of $(k\beta/\ell)$ and α on the detector position. It can be seen that for this case there appears to be very little, if any, position dependence. Note again in Tables IX and X that the burst and sweep rates differed from one measurement to another and yet give the same results. It is of interest to note the reproducibility of individual measurements of α and $(k\beta/\ell)$.

3.2. Pulsed measurements in large cores

To demonstrate the feasibility of pulsed neutron experiments in large irradiated reactor cores some measurements were made in the Pacific Gas and Electric Humboldt Bay Reactor (150 MW(t)) before and after full power operation. Results of this work have been reported elsewhere [12]. Additional measurements were performed in the ESADA Vallecitos Experimental Superheat Reactor (EVESR) to obtain physics information for the start-up test programme which could not be effectively determined by critical tests. The EVESR has several unique nuclear design features such as flooding-unflooding reactivity effects, and a strong positive temperature effect at room temperature which the pulsed neutron measurements were especially helpful in determining. To our knowledge these are the first pulsed neutron measurements to be conducted with a reactor at design temperature (540°F) and pressure (1000 lb/in^2). The measurements provided control rod worth, flooding reactivity effects, temperature effects, and fuel bundle worth. A considerable effort was required as part of the EVESR programme to design and build some special hardware to permit accessibility of the source and detector to the reactor core, since provisions for this type of measurement were not made in the basic reactor design. Results of these measurements and their discussion are available elsewhere [10, 11]. One case of particular interest is discussed below.

Two relatively large regions of different shut down were obtained by selective control rod withdrawal; the outer region fully shut down by eight peripheral control crosses and the inner region partially shut down as shown in Fig. 4. The plot shows clearly the prompt decay constants associated with each of the two regions. The steeper slope represents the outer region where the detector was located and this slope appeared from estimates to be relatively unaffected by central control withdrawal indicating decoupling

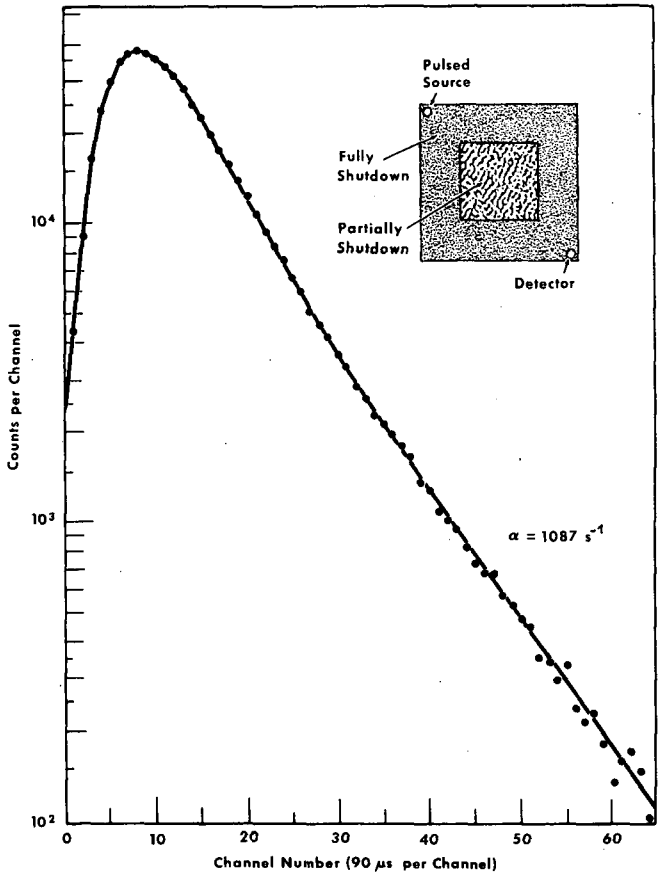


Fig. 4

EVESR core, two regions

of the two regions. Regardless of which region the detector was placed in, the lowest decay constant could always be obtained. The values of (kβ/ℓ), on the other hand, differed from region to region.

4. CONCLUSIONS

From the extensive series of measurements that were made on reflected assemblies it is reasonable to conclude that the (kβ/ℓ) technique is valid for assemblies that are about 3 to 4 dollars subcritical. This implies that the method gives a unique value; that is, there is no source-detector position dependence of (kβ/ℓ). Based upon the uniform 18×18 array, Table III, it can be said that there is a definite position dependence in (kβ/ℓ). This array is more than 10 dollars subcritical. However, for the 21×23 array, Table II there is no position dependence for this assembly which is about a dollar

subcritical. The results shown in Table IV suggest that the method is applicable to an assembly that is about 3.50 dollars subcritical. Indications are that the method may be valid for assemblies that exceed 3.50 dollars; however, the lower limit of the validity lies somewhere between 4 and 10 dollars subcritical. For measurements in this range it is recommended that the position dependence be investigated. The lower limit may be extended somewhat further for control rod measurements. It is not clear that the effect of the subcriticality achieved by fuel removal has the same effect on the measurement as that of inserting a control rod. Bare core measurements have been performed by another Laboratory [13] and no position dependence was observed in their experiments. From these measurements it appears that bare core experiments present no difficulties.

From the results presented in this report and from other measurements [10], it can be concluded that the $(k\beta/\ell)$ measurement makes an α-delayed critical measurement unnecessary. An α-delayed critical determination usually implies a period measurement which in turn means that the reactor has to be made critical. In power reactors and especially in developmental reactors, this can be very time consuming and hence an expensive procedure. Essentially, the $(k\beta/\ell)$ technique reduces the number of measurements and is particularly useful in systems that do not permit a standard α-delayed critical measurement.

Another significant feature of the experimental programme was to demonstrate the pulsing technique previously described [4]. For an ordinary α-measurement, this pulsing technique gives the experimenter a tool to obtain a flat delayed neutron background so that the prompt decay constant can be determined. In addition, for the $(k\beta/\ell)$ measurement, the technique eliminates the need for a uniform source strength, a requirement which in practice cannot be met. It also extends the usefulness of most commercially available pulsed neutron generators which have a rather low burst rate capability.

It is perhaps worthwhile to discuss some of the difficulties in applying these techniques to large cores. It is evident, for example, that the "large core" properties were not exhibited in the small experimental assemblies investigated, whereas the Humboldt Bay (150 MW(t)) and the Vallecitos Experimental Superheat Reactor (12.5 MW(t)) experiments clearly exhibited decoupled properties. That is, more than one alpha was observed depending upon the detector position. It is also clear that the decoupled cores may yield a different value of $(k\beta/\ell)$ for each region. This behaviour of decoupled cores has been recognized for some time [14]. Nevertheless, the most reactive core zone can be identified by the proper placement of detectors, i.e. a detector for each decoupled region.

In the case of large power reactors it is clear that the reflector problem is minimized since the importance of the reflector decreases as the size of the reactor increases. It is concluded that with proper care and attention to the detector placement, useful information can be obtained. Furthermore, the $(k\beta/\ell)$ technique is particularly useful in the measurement of the fundamental reactor parameters that need to be obtained during the loading procedures. Good measurements can readily be obtained during the initial start-up since the cores are clean and hence have only a negligible extraneous gamma background.

The pulsed neutron method suggested by SIMMONS and KING [15] to predict reactivities assumes that the ratio of (β/ℓ) remains unchanged for a subcritical assembly as compared to that of the critical one. The $(k\beta/\ell)$ technique makes no such assumption. In all the measurements made to date the value of $(k\beta/\ell)$ decreased whenever a given assembly was made more subcritical. It should therefore be recognized that the technique of Simmons and King normally underestimates the shut down.

In general, it can be said that only minor changes, depending upon the reactor to be measured, have to be made on commercially available pulsed neutron equipment. Although all the measurements reported were performed on thermal reactors, there appears to be no reason why these methods cannot also be applied to fast systems, utilizing slightly different pulsed sources, neutron detectors, and time analysers.

ACKNOWLEDGEMENTS

This work was performed under the auspices of the United States Atomic Energy Commission. Helpful criticism by E. Garelis and G. T. Petersen in the preparation of this paper is gratefully acknowledged.

REFERENCES

[1] KEAR, G. and RUDERMAN, M. H., An analysis of methods in control rod theory and comparisons with experiment, AEC Res. and Dev. Rpt GEAP-3937, (May 1962).

[2] MEYER, P. and BALLOWE, W. C., An experimental parametric study of the effects of control rods on the prompt neutron decay constants in multiplying media, AEC Res. and Dev. Rpt GEAP-4019 (April 1962).

[3] GARELIS, E. and RUSSELL, J. L., Nucl. Sci. Engng 16 (1963) 263-70.

[4] GARELIS, E., "Survey of pulsed neutron source methods for multiplying media", these Proceedings II.

[5] GARELIS, E., Nucl Sci. Engng 18 (1964) 242-45.

[6] BECKURTS, K. H., Nucl. Instrum. Meth. 11 (1961) 144.

[7] GARELIS, E. and MEYER, P., Development of pulsed neutron application to power reactor start-up procedures - 4th Quarterly Progress Report, AEC Res. Dev. Rpt, 1 Jan. - 31 March 1963, Rpt GEAP-4217.

[8] GARELIS, E. and MEYER, P., Development of pulsed neutron application to power reactor start-up procedures - 5th Quarterly Progress Report, AEC Res. Dev. Rpt, 1 April - 30 June 1963, Rpt GEAP-4305.

[9] GARELIS, E. and MEYER, P., Development of pulsed neutron application to power reactor start-up procedures - 6th Quarterly Progress Report, AEC Res. Dev. Rpt, 1 July - 30 Sep. 1963, Rpt GEAP-4388.

[10] GARELIS, E. and MEYER, P., Development of pulsed neutron application to power reactor start-up procedures - 7th and 8th Quarterly Progress Report, AEC Res. Dev. Rpt, 1 Oct. - 31 March 1963, Rpt GEAP-4606.

[11] MEYER, P. and GARELIS, E., Development of pulsed neutron application to power reactor start-up procedures - 9th Quarterly and Summary Report, AEC Res. Dev. Rpt, 1 April - 30 June 1964, Rpt GEAP-4644.

[12] MEYER, P., Trans. Amer. nucl. Soc. 6 (1963) 287.

[13] BROWN, J. R., YOUNG, J. C., BEYSTER, J. R., HUSTON, D. H. and MOWRY, W. R., Trans. Amer. nucl. Soc. 6 (1963) 284-85.

[14] BRUGGE, R. O. and BARTU, A. S., Trans. Amer. nucl. Soc. 3 (1960) 100.

[15] SIMMONS, B. E. and KING, J. S., Nucl. Sci. Engng 3 (1958) 595.

BIBLIOGRAPHY

CORNGOLD, N., On the analysis of pulsed multiplying systems, General Atomic Rpt 5405 (1964).
PATERSON, W.J. and WEALE, J.W., "Pulsed source methods in fast reactor physics", Proc. 3rd UN Int. Conf. PUAE, 1964.

DISCUSSION

(on the foregoing two papers)

S. CHWASZCZEWSKI: Dr. Meyer's paper discusses variations in $(k\beta/\ell)$ as a function of source and detector location for assemblies in which boron poisoning and water level were varied. Were any measurements made of the dependence of $(k\beta/\ell)$ on detector and source location in the reactor when a negative reactivity of about -10 $ was introduced by means of the control rods?

P. MEYER: Yes, we have made $(k\beta/\ell)$ measurements in control-rod poisoned systems, with large as well as small geometries. A few measurements are reported in this paper, but I would also refer you to some of the references quoted therein.

N.G. SJÖSTRAND: I found Dr. Garelis' survey most interesting. It would seem that there are still some uncertainties in our interpretation, especially as regards the effect of harmonic modes. It might be possible to overcome some of the difficulties by means of a suitable experimental arrangement. One possibility might be to have a number of detectors distributed in the reactor, make a simultaneous time analysis and in this way integrate over the whole neutron population in the reactor.

E. GARELIS: An experiment of this sort has, in fact, already been considered by Dr. Becker and Dr. Quisenberry of KAPL (Knolls Atomic Power Laboratory); it was reported at the recent Arizona Conference on Reactor Kinetics. These two scientists measured the reactivity for several detector locations and, rather than average the different values, applied a space-dependent correction factor. This correction factor brought the values into line with the measured centre value. In a General Atomic report Dr. Noel Corngold has also discussed the theoretical problem of averaging data from a number of detectors.

C.A. PRESKITT: Have any measurements been made in graphite-moderated reactors with the $(k\beta/\ell)$ method? I imagine that the space dependence would be much greater in this case.

P. MEYER: I believe that Dr. Fuster from Saclay, who is presenting a paper at this Symposium*, has made some $(k\beta/\ell)$ measurements in a large graphite system.

R. PEREZ: I should like to draw attention to the fact that the one-point reactor kinetic equations are not correct even in cases where an asymptotic behaviour has been achieved. Let me illustrate this by imagining that we wish to compute the decay constant by some variational technique. We can use as trial function the fluxes (real and adjoint) obtained by solution of multigroup equations in which the time derivatives $\partial/\partial t$ are replaced by $\alpha\,(s^{-1})$. Obviously, it is possible to derive a "one-point" reactor equation in which reactivity, as well as β and ℓ, will be functions of the decay constant itself. Hence the interpretation of reactivity in a pulsed experiment will be ambiguous. I think that one should endeavour to interpret pulsed-neutron experiments by direct computation of the eigenvalue α.

---

* FUSTER, S., SAGOT, M., TARABELLA, A. and TELLIER, H., paper (SM-62/82), these Proceedings II.

E. GARELIS: I agree.

M.N. MOORE: If it is assumed that the kinetics are determined by a single constant parameter k, then even though we might treat the neutron density as a function of space and time, i.e. a field, we have still employed a point model for the reactivity. What these experiments show is that the reactivity must also depend upon space and the possibility of such space dependence must be included in the kinetics.

E. GARELIS: In our method we do not assume a point kinetic model. All spatial modes are taken into account. We have, however, assumed a bare reactor in our development. The bare-core experiment of General Atomic shows that all modes are taken into account.

J. SHERWIN: Measurements with this technique have been carried out at Windscale on the HERO graphite-moderated reactor and it has been found that the method is good at 1% subcritical, having no spatial dependence. At lower subcritical states, i.e. 4% subcritical, the method proved to be spatially dependent.

In addition to making this comment, could I perhaps also ask Dr. Meyer whether the $(k\beta/\ell)$ measurements were checked against other methods of measuring reactivity?

P. MEYER: No, we have not done so in this system, except with values obtained by period measurements. We have, however, made comparisons with calibrated control rods in another assembly, down to -6 $ I believe, and the agreement was good.

MODIFIED PULSED SOURCE TECHNIQUES

T. GOZANI
ATOMIC ENERGY COMMISSION,
TEL AVIV, ISRAEL

AND

P. DEMARMELS, T. HÜRLIMANN AND H. WINKLER
SWISS FEDERAL INSTITUTE FOR REACTOR RESEARCH,
WÜRENLINGEN, SWITZERLAND

Abstract — Résumé — Аннотация — Resumen

MODIFIED PULSED SOURCE TECHNIQUES. The modified pulsed source techniques of Gozani and of Garelis and Russell were checked experimentally at the swimming pool reactor SAPHIR. These methods are characterized by the simultaneous experimental determination of negative reactivity and generation time. Both quantities obtained by these methods are in units of dollar (i. e. β_{eff}) and therefore are independent of arbitrary theoretical definitions.

Measurements were carried out for several subcritical states. Various proposed correction terms were scrutinized experimentally. The effects of the finite width of the neutron pulses were investigated. Measurements were carried out for a variety of delayed neutron states at the beginning and end of the experiment. All corrected reactivity values agreed well within their statistical errors.

Systematic errors caused by spatial harmonics were studied by varying the position of the detector. It is shown that in the presence of positive harmonics (normally close to the source) the evaluation procedure proposed by Gozani generally gave results slightly below the correct reactivity values, whereas the procedure proposed by Garelis and Russell resulted in slightly larger ones. For negative harmonics the situation is reversed. Thus, the two methods may be used to bracket the correct values of reactivity and generation time. The reactivity of a state near -10$ was measured in this manner with a precision of 2%.

MÉTHODE DES SOURCES PULSÉES MODIFIÉES. Les méthodes des sources pulsées modifiées par Gozani et par Garelis et Russell ont été contrôlées expérimentalement dans le réacteur à piscine SAPHIR. Une caractéristique de ces méthodes est qu'elles permettent de déterminer simultanément l'antiréactivité et le temps de génération du système à l'étude. Dans l'un comme dans l'autre cas, les quantités obtenues s'expriment en dollars (c'est-à-dire β_{eff}) et sont donc indépendantes des définitions théoriques arbitraires.

Les auteurs ont fait des mesures sur plusieurs états sous-critiques. Ils ont etudié expérimentalement la valeur de diverses corrections envisagées. Ils ont examiné l'effet de la largeur finie des bouffées de neutron. An début et à la fin de l'expérience, ils ont fait des mesures sur divers états des neutrons retardés. Toutes les valeurs de la réactivité corrigées concordaient fort bien dans les limites de leurs erreurs statistiques.

Les auteurs ont étudié les erreurs systématiques résultant des harmoniques du lieu en faisant varier la position du détecteur. Ils montrent qu'en présence d'harmoniques positives (normalement proches de la source), la méthode d'évaluation proposée par Gozani donne habituellement des résultats légèrement inférieurs aux valeurs correctes de la réactivité et celle de Garelis et Russell des valeurs un peu supérieures. Pour ce qui est des harmoniques négatives, c'est l'inverse qui est vrai. Ainsi, les deux méthodes peuvent être utilisées pour cerner les valeurs correctes de la réactivité et du temps de génération. On a pu ainsi mesurer avec une précision de 2% la réactivité d'un état voisin de -10$.

ОБ УСОВЕРШЕНСТВОВАННОМ МЕТОДЕ С ИМПУЛЬСНЫМ ИСТОЧНИКОМ. Усовершенствованные методы с импульсными источниками Гозани и Гарелиса, а также Рассела проверяли экспериментально на реакторе бассейнового типа "Сапфир". Эти методы характеризуются одновременным экспериментальным определением отрицательной реактивности и продолжительности времени генерации исследуемой системы. Оба количества, полученные

этими методами, выражаются в долларах (т.е. β-эффективное) и поэтому зависят от произвольных теоретических определений.

Производились измерения для нескольких подкритичных состояний. Различные коррективы тщательно исследовались экспериментальным путем. Например, исследовался эффект изменения широты импульса и скорость повторения импульсов. Измерения для различных состояний запаздывающих нейтронов проводились в начале и в конце эксперимента. Все скорректированные величины реактивности хорошо согласуются в пределах их статистических ошибок.

Систематические ошибки, вызванные пространственной гармоникой, изучаются путем изменения положения детектора. Показывается ,что при наличии положительной гармоники (обычно близко к источнику) процедура оценки, предложенная Гозани, в общем дает результаты несколько ниже правильных величин реактивности, тогда как процедура, предложенная Гарелисом и Расселом, дает в конечном счете несколько завышенные величины. Для отрицательной гармоники наступает противоположное положение. Таким образом, для охвата правильных величин реактивности и продолжительности генерации можно использовать два метода. Реактивность состояния, близкого к -10 долларам, измерялась, таким образом, с точностью до 2%.

OBSERVACIONES SOBRE LA TECNICA MODIFICADA DE LA FUENTE DE NEUTRONES PULSADOS. Los autores han comprobado experimentalmente con el reactor de tipo piscina SAPHIR, la validez de las técnicas modificadas de la fuente de neutrones pulsados debidas a Gozani y a Garelis y Russell. Estos métodos se caracterizan porque la determinación experimental simultánea del tiempo de generación y de valores negativos de la reactividad en el sistema estudiado. Por estos métodos ambas magnitudes se obtienen expresadas en«dólares»(es decir, en β_{ef}), siendo, por lo tanto, independientes de definiciones teóricas de carácter arbitrario.

Los autores han realizado medidas de varios estados subcríticos y examinan experimentalmente diversas correcciones propuestas. Investigan los efectos de la anchura finita de los impulsos de neutrones. También realizan mediciones para diversos estados de los neutrones retardados al principio y al final del experimento. Todos los valores de la reactividad corregidos concuerdan satisfactoriamente dentro del margen de error estadístico correspondiente.

Los autores estudian los errores sistemáticos debidos a armónicos espaciales, modificando para ello la posición del detector. Demuestran que en presencia de armónicos positivos (por lo general próximos a la fuente) el método de evaluación propuesto por Gozani suele dar resultados ligeramente inferiores a los valores correctos de la reactividad, mientras que el método propuesto por Garelis y Russell proporciona resultados ligeramente superiores. Con los armónicos negativos sucede lo contrario. Se tiene así la posibilidad de emplear ambos métodos a fin de abarcar en los resultados los valores correctos de la reactividad y del tiempo de generación. De esta forma se ha medido, con una precisión del 2%, la reactividad de un estado próxima a -10 dólares.

1. INTRODUCTION

Two modifications of the normal pulsed source technique (e.g. [1-7]) have been proposed in recent years, the first one in 1962 by GOZANI [8] and the second one in 1963 by GARELIS and RUSSELL [9][1]. The modifications essentially consist in combining the measured prompt and delayed neutron populations by a functional relationship in addition to the usual determination of the prompt decay constant.

The relationship of the populations and the decay constant yield the two global parameters of the reactor: reactivity and generation time, both divided by the effective delayed neutron fraction (β_{eff}).

[1] The first method proposed by GOZANI [8] is called, for the sake of brevity, the GO-version. The second method proposed by GARELIS and RUSSELL [9] is designated as the Gr-version.

The main difference between the usual pulsed source technique and the modified techniques consists in including the delayed neutron tail as a physical quantity instead of disregarding it as a mere background in the same manner as the constant reactor background which is independent of the pulsed source.

In the normal pulsed source technique the generation time is determined for the critical reactor. This quantity is usually assumed to be constant, or it is corrected by simple [5], often insufficient procedures for the subcritical state under investigation. The reactivity calculated from this generation time and the prompt decay constant is affected by the error inherent in the generation time. The modified methods are free from such an assumption.

An extensive series of measurements was carried out at the Swiss swimming pool reactor SAPHIR. The main purpose was to check carefully all theoretical aspects developed in connection with these modified techniques (see [10]).

The use of neutron bursts with finite width, which improves counting statistics, is shown to yield correct results, such as delta bursts. Measurements under various delayed neutron states, for example, before or after delayed neutron equilibrium is reached, were carried out. They gave consistent results if made according to appropriate experimental procedures or if corrected theoretically.

The major advantage of the pulsed source technique is the possibility to exclude the influence of prompt harmonics. This is still maintained in the modified versions; however a relatively small amount of systematic error caused by harmonics is introduced from the delayed neutrons. It is shown that the two modified versions behave in an opposite manner in the presence of harmonics: When the contribution from harmonics is predominantly positive, e.g. by measuring close to the source, the GO-version gives results slightly lower than the proper value, whereas the GR-version gives slightly higher values. In the presence of predominant negative harmonics the situation is reversed. This property is used to bracket the correct values of the reactivity and the generation time within narrow limits.

2. THEORY

2.1. General

The theory of the modified pulsed source techniques has been developed in detail in Ref. [10]. The main assumptions, approximations and their implications on the experimental results are re-stated here.

The basic assumption pertaining to the modified pulsed source is that the delayed neutron spatial distributions or the delayed neutron eigenfunctions are identical in shape with the persisting prompt eigenfunction (i.e. the fundamental prompt kinetic eigenfunction, see [11] and [12]). This assumption is generally valid except for some rare cases, such as small reactive cores heavily reflected by D_2O or Be. Even in these cases there are places far from interfaces and boundaries where all fundamental eigenfunctions coincide rather well.

The persisting prompt eigenfunction is the basic function from which the reactivity ρ, the generation time Λ and the effective fraction of delayed neutrons $\beta_{i,eff}$ are computed. This is an essential point to be recalled when theory and experiments are compared. The corresponding quantities belonging to higher modes are calculated with the higher prompt eigenfunction.

The quantities ρ, Λ and $\beta_{i,eff}$ are not uniquely defined quantities because of the various possibilities of weighting functions, e.g. static, kinetic or dynamic [11, 13]. However, if they are divided by $\beta_{eff}\,(=\sum_{i=1}^{l}\beta_{i,eff})$, the ambiguity disappears.

The reactivity (now in dollar units), the generation time (now the reduced generation time [13]) and the relative effective fractional yields become independent of weighting functions. The various theoretical interpretations, which involve the weighting, affect only the dollar unit (i.e. β_{eff}).

2.2. Rectangular pulsed source

In general, pulsed source equipments supply neutron bursts of finite, variable width d in the form of a rectangular wave of period T. Applying the point reactor kinetic equations with l delayed neutron groups, summing the neutron density from the first source pulse up to the last (the M-th) pulse, separating into a prompt and a delayed population and assuming

$$M|\gamma_0|T \gg 1,\ |\gamma_j|T \ll 1 \qquad j = 1, 2, \ldots\ldots l,$$

one obtains with rather high accuracy (see [10]):

$$N_{pr}(\theta) = M\Lambda^* J\left(\frac{A_0}{-\gamma_0}\right)\left[(1-e^{\gamma_0\theta}) + \left(\frac{e^{-\gamma_0 d}-1}{e^{-\gamma_0 T}-1}\right)e^{\gamma_0\theta}\right] \quad \text{for } 0 \leqslant \theta \leqslant d \tag{1}$$

$$N_{pr}(\theta) = M\Lambda^* J\left(\frac{A_0}{-\gamma_0}\right)\left(\frac{e^{-\gamma_0 d}-1}{1-e^{\gamma_0 T}}\right)e^{\gamma_0\theta} \qquad \text{for } d \leqslant \theta \leqslant T \tag{2}$$

$$N_d(\theta) = M\Lambda^* J\frac{d}{T}\left[1+\left(\frac{T}{2}-\theta\right)\frac{\bar{\lambda}|\rho|}{1+|\rho|} - D(MT,\rho)\right]\sum_{j=1}^{l}\left(\frac{A_j}{-\gamma_j}\right), \tag{3}$$

where

N_{pr}, N_d = prompt and delayed neutron population, respectively
J = source intensity
θ = multichannel time (channel number)

The γ_j's are solutions of the inhour equation

$$\rho = \gamma_j\left(\Lambda^* + \sum_{i=1}^{l}\frac{b_i}{\gamma_j+\lambda_i}\right) \tag{4}$$

In subcritical systems all γ_j's are negative.

$$A_j^{-1} = \Lambda^* + \sum_{i=1}^{1} \frac{b_i \lambda_i}{(\gamma_j + \lambda_i)^2}, \tag{5}$$

where

ρ = reactivity in dollar units
Λ^* = reduced generation time
b_i, λ_i = delayed neutron constants
$\bar{\lambda} = \sum_{i=1}^{1} b_i \lambda_i, \quad \bar{\lambda}^2 = \sum_{i=1}^{1} b_i \lambda_i^2.$

Assuming

$$|\gamma_0| >> |\gamma_j| \qquad j = 1, 2, \ldots 1,$$

one finds the following approximations:

$$|\gamma_0| \cong \frac{1+|\rho|}{\Lambda^*} + \left[\frac{\bar{\lambda}}{1+|\rho|} + \frac{\bar{\lambda}^2 \Lambda^*}{(1+|\rho|)^2}\right] = \text{prompt decay constant} \tag{6}$$

$$\frac{A_0}{-\gamma_0} \cong \frac{1}{1+|\rho|} \frac{1}{\left[1 + \frac{2\bar{\lambda}\Lambda^*}{(1+|\rho|)^2}\right]} \tag{7}$$

$$\sum_{j=1}^{1} \frac{A_j}{-\gamma_j} \cong \frac{1}{|\rho|(1+|\rho|)} \left[1 + \frac{2\bar{\lambda}\Lambda^*|\rho|}{(1+|\rho|)^2}\right] \tag{8}$$

The expression

$$D(MT, \rho) = \frac{|\rho|(1+|\rho|)}{MT} \sum_{j=1}^{1} \frac{A_j}{\gamma_j^2} \left(1 - e^{\gamma_j MT}\right) \tag{9}$$

describes the amount by which the delayed neutron population is lower owing to the fact that the data accumulation starts with the very first neutron pulse. For most practical cases, i.e. $MT \geqslant 600$ s and $|\rho| > 0.4$ \$, Eq. (9) may be approximated by (delayed groups of U^{235}, $\Lambda^* = 0.01$ s)

$$D \cong \frac{1}{MT} \frac{1+|\rho|}{|\rho|} \left(\Lambda^* + \sum_{i=1}^{6} \frac{b_i}{\lambda_i}\right) = \frac{13.1 \text{ s}}{MT} \frac{1+|\rho|}{|\rho|} \tag{10}$$

2.3. Reactivity evaluation

The usual evaluation procedure is to fit an exponential function to the experimental $N_{pr}(\theta)$ from a certain time θ_1 on. After θ_1 the spatial prompt

harmonics are assumed to be negligible. The least-squares fit furnishes the persisting prompt decay constant γ_0, and the initial prompt amplitude $N_{pr}(0)$:

$$N_{pr}(0) = N_{pr}(\theta)\, e^{-\gamma_0 \theta} . \tag{11}$$

This initial amplitude is not directly measured but has to be found by extrapolation backwards, because of the presence of harmonics and the finiteness of the neutron pulse. The delayed neutron population $N_d(\theta)$ is measured from the tail of the accumulated neutron density which follows the neutron pulses in a time region $\theta \gg 1/\gamma_0$. The subtraction of the constant reactor background from the tail therefore yields $N_d(\theta)$.
From Eqs.(2) and (3) one thus obtains

$$|\rho| = \frac{C_d(\theta)}{\left(1+\frac{2\bar{\lambda}}{|\gamma_0|}\right)} \frac{d}{T} \frac{1-e^{|\gamma_0|T}}{e^{|\gamma_0|d}-1} \frac{N_{pr}(0)}{N_d(\theta)}, \quad \text{(GO-version)} \tag{12}$$

where $C_d(\theta)$, is the delayed correction factor

$$C_d(\theta) = 1+\left(\frac{T}{2}-\theta\right)\frac{\bar{\lambda}|\rho|}{1+|\rho|} - D(MT,\rho) . \tag{13}$$

The dependence of $C_d(\theta)$ on ρ is usually very weak. Hence iteration is hardly necessary. An iteration procedure may be required when measuring close-to-critical states (see [10], Appendix 2).

With $N_{pr}(\theta)$, γ_0 and $N_d(\theta)$, another functional relationship may be constructed which furnishes g, the inverse of the generation time, by iteration:

$$C_g \int_0^\infty N_{pr}(\theta) e^{g\theta}\, d\theta - \int_0^\infty N_{pr}(\theta) d\theta = \frac{1}{C_d} T N_d(\theta) , \tag{14}$$

where

$$C_g = \frac{gd}{e^{gd}-1}\left[1+\frac{2\bar{\lambda}}{|\gamma_0|(1+|\rho|)} - \frac{g}{|\gamma_0|}\left(e^{\gamma_0 T} + \frac{1-e^{(\gamma_0+g)d}}{e^{gd}-1}\,\frac{e^{\gamma_0(d+T)}}{1-e^{\gamma_0 T}}\right)\right] \cong \frac{gd}{e^{gd}-1} \tag{15}$$

Equation (14) may be considered as an extension of the GR-method [9] to finite pulse width.

A simpler method to evaluate reactivity uses the ratio of the integrated densities of the prompt and delayed neutrons:

$$|\rho_a| = \frac{\int_0^T N_{pr}(\theta) d\theta}{T N_d(\theta)/C_d(\theta)} \frac{1}{\left(1+\frac{2\bar{\lambda}}{|\gamma_0|}\right)} . \tag{16}$$

This formula is only correct when the prompt harmonics, in addition to the delayed, are absent. This is entirely equivalent to the measurement of reactivity by the source jerk technique ("Amplitude method" [12]). Such a method supplemented by measurements of γ_0, was used by SJÖSTRAND [14] for control rod calibration.

2.4. The systematic error from spatial harmonics

Probably the most difficult problems in reactivity measurements of far subcritical states stem from the presence of harmonics. Harmonics are generally defined as the deviation of the actual neutron distribution from the persisting distribution, when both distributions are appropriately normalized. The deviation of the prompt neutron distribution from its persisting (or fundamental) eigenfunction is called prompt harmonics. The deviation of the delayed neutron distribution from the same persisting prompt eigenfunction is called the delayed harmonics.

The higher prompt harmonics are characterized by large negative decay constants. Hence during the neutron pulse they are rapidly built up, and more important, after the end of the neutron pulse they swiftly decay. So unless a neutron detector is placed in an extremely unfavourable position, e.g. close to the source, the persisting mode will predominate after a certain time θ_1, which is of the order of a few $1/|\gamma_0|$. On this basis one may assume that the prompt persisting eigenvalue γ_0, and the extrapolated initial amplitude $N_{pr}(0)$ can be measured accurately, free of harmonic effect in most practical cases.

The clusters of the delayed neutron eigenvalues [11] of the higher modes hardly depend on the mode. Therefore the amount of delayed harmonics does not actually vary with time. However, since all delayed thermal neutrons belong to the second or to later generations of the source neutrons, they assume a distribution similar to the persisting one.

When the actual measured quantities $N_{pr}(0,\vec{x})$, $N_d(\theta,\vec{x})$ and γ_0 are substituted into Eq. (13), one obtains (for details see [10]):

$$|\rho'| = \frac{|\rho|}{1+H_d} \tag{17}$$

H_d characterizes the delayed neutron harmonics and may be approximated by

$$H_d \cong \sum_{q=2}^{\infty} \frac{W_q(\vec{x},\vec{x}_0)}{W_1(\vec{x},\vec{x}_0)} \frac{|\rho_1|(1+|\rho_1|)}{|\rho_q|(1+|\rho_q|)} \tag{18}$$

$W_q(\vec{x},\vec{x}_0)$ is the statistical weight factor depending on the kinetic eigenfunctions n_q and their adjoints n_q^+ at the positions of the detector $(\vec{x})$ and the source $(\vec{x}_0)$, respectively. The index $q = 1$ designates the persisting mode.

When the same substitution is introduced in Eq. (14), the GR-method becomes (see [10]):

$$C_g \int_0^\infty N_{pr}(\theta, \vec{x}) e^{g\theta} d\theta = \left[\int_0^\infty N_{pr}(\theta, \vec{x}) d\theta + T N_d(\theta, \vec{x}) / C_d \right] [1 - H_g] , \qquad (19)$$

where

$$H_g(\vec{x}, \vec{x}_0) \cong \sum_{q=1}^{\infty} W_q \frac{g - g_q}{g_q} \frac{1}{\rho_q^2} \Big/ \sum_{q=2}^{\infty} W_q \frac{1}{|\rho_q|} \qquad (20)$$

The reactivity $|\rho_a|$ obtained by Eq.(16) is very sensitive to the content of harmonics

$$|\rho_a'| \cong |\rho_a| \frac{1 + H_{pr}}{1 + H_d} \qquad (21)$$

H_{pr} originates from the prompt harmonics and is defined by

$$H_{pr}(\vec{x}, \vec{x}_0) = \sum_{q=2}^{\infty} \frac{W_q}{W_1} \left(\frac{1 + |\rho_1|}{1 + |\rho_q|} \right) \qquad (22)$$

Since the reactivity $|\rho_q|$ increases very rapidly with the increase of the modal index q, $H_d \ll H_{pr}$. In regions of strong harmonics H_{pr} and H_d will have the same sign. Therefore the following situation is met (Eq.18):

$$\begin{array}{ll} \text{Positive harmonics predominate:} & |\rho'|_{GO} \lesssim |\rho| \\ \text{Negative harmonics predominate:} & |\rho'|_{GO} \gtrsim |\rho| \end{array} \qquad (23)$$

The harmonic term H_g (Eq.20) is caused by the deviation of the modal generation time Λ_q^* from that of the persisting mode λ^*: $\lambda_q^*/\lambda^* = g/g_q \neq 1$. The assumption made in the original paper [9] was $g = g_q$, which is only correct in the simple model of one-group theory on bare systems. In complicated systems this assumption can be completely wrong [12]. This is also demonstrated in the experimental part of the present paper. The harmonic term H_g is positive when positive harmonics predominate. Therefore the iterated g will be smaller than the true value and the reactivity calculated by means of the inhour equation will be larger. This leads to a situation which is the reverse of Eq.(23). Thus the correct reactivity value can be bracketed between the two measurable limits.

$$\begin{array}{ll} \text{Positive harmonics predominate:} & |\rho'|_{GO} < |\rho| < |\rho|_{GR} \\ \text{Negative harmonics predominate:} & |\rho'|_{GO} > |\rho| > |\rho|_{GR} \end{array} \qquad (24)$$

3. EXPERIMENTAL SET-UP

The experiments have been performed at the swimming pool reactor SAPHIR of the Swiss Federal Institute for Reactor Research in Würenlingen. The core configuration is shown in Fig.1.

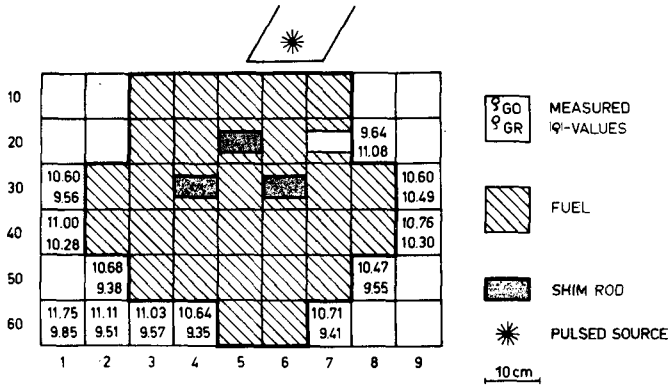


Fig. 1

Core configuration and measured reactivity values

The pulsed source equipment used in the experiments was the TNC neutron generator model 9001 [15], slightly changed to increase the ratio of neutron output during and after the pulse to 10^5. The neutrons were detected by a fission chamber with fast preamplifier [16] and recorded by a TMC 256 multichannel analyser with the pulsed source plug-in unit. The detector could be placed at the various positions around the core.

4. RESULTS

4.1. Low subcritical state ($\rho \approx -0.65$ \$)

The validity, applicability and the precision of the modified pulsed source techniques have been demonstrated by measuring reactor states in the domain of $-1\ \$ \leqslant \rho \leqslant 0$, where the harmonic contamination remains moderate. Measurements were carried out in different positions around the core. Reactivity values determined at position 62 in three measurements are given in Table I. They show agreement between ρ_{GO} and ρ_{GR} within the statistical error, although negative harmonics are present as is indicated by the low value of $\rho_a = -0.579\ \$$.

4.2. Measurements with various delayed neutron states

Data accumulation may be started and stopped at different values of the time-dependent delayed neutron population. Whenever the delayed states at the beginning and at the end of a measurement are different and not in equilibrium, the term D (Eq. 10) has to be employed to introduce the necessary corrections into the formulae of the modified pulsed source techniques.

Several measurements were carried out at $\rho = -0.83\ \$$ under various conditions. Measuring only during a time when the delayed neutrons are in their constant equilibrium state, or starting data accumulation with the first pulse, varying pulse intensity at will and stopping only after all de-

TABLE I

RESULTS OF MEASUREMENTS IN REACTOR POSITION 62 OF THE -0.65 $ STATE

Measured number	$-\rho_{GO}$ ($)	$-\rho_{GR}$ ($)	Λ^*_{GO} (ms)	Λ^*_{GR} (ms)
1023	0.6414 ± 0.0045	0.6390 ± 0.0094	8.340 ± 0.039	8.328 ± 0.046
1024	0.6413 ± 0.0061	0.6448 ± 0.0124	8.365 ± 0.052	8.385 ± 0.063
1025	0.6430 ± 0.0059	0.6429 ± 0.0110	8.316 ± 0.047	8.316 ± 0.056

layed neutrons have decayed, both correspond to D = 0 and give exactly the same ρ- and Λ^*-values. The data from these measurements also agree with data obtained by starting the recording with the first pulse and stopping at any time during pulsing. In this case the correction term D has to be applied. The last procedure proved to be the most satisfactory from the practical point of view. The statistical accuracy is good because of high signal-to-background ratio. Little or no time is lost to achieve the initial delayed state and the correction by D is very simple.

4.3. The effect of harmonics

Many reactivity measurements were carried out in the far subcritical state of -10 $ at the various positions around the reactor core. The main objective was to get better insight into the effect of harmonics on the evaluated reactivity and to find ways to minimize it.

The prompt decay constant, γ_0, and the initial extrapolated prompt amplitude, $N_{pr}(0)$, can be determined without harmonics contamination in most practical cases. The γ_0-value was actually found to be independent of measuring position.

The data were analysed according to the GO-version (Eq. 12), GR-version (Eq. 14) and the normal amplitude method (Eq. 16). Results are summarized in Table II. The statistical accuracy is quite good. Most results have uncertainties less than 2%. It must be remembered, however, that these errors are not purely from statistics but to some extent reflect the elimination of the harmonics effect in γ_0 and N_{pr} by the selection of an appropriate channel interval. Also listed in Table II are the average values

$$\bar{\rho} = (\rho_{GO} + \rho_{GR})/2, \text{ and } \bar{\lambda}^* = (\lambda^*_{GO} + \lambda^*_{GR})/2 \tag{25}$$

as well as a harmonics index H, defined by

$$H = (\rho_a - \bar{\rho})/\bar{\rho} \tag{26}$$

The effect of the harmonics on the two versions of the modified pulsed

TABLE II

RESULTS FOR THE -10 $ STATE

Meas. pos.	$-\rho_{GO}$ ($)	$-\rho_{GR}$ ($)	$-\bar{\rho}$ ($)	$-\rho_a$ ($)	H	λ^*_{GO} (ms)	λ^*_{GR} (ms)	$\bar{\lambda}^*$ (ms)
31	10.60	9.56	10.08	7.95	-0.210	9.85	8.96	9.41
41	11.00	10.28	10.64	7.70	-0.278	10.26	9.21	9.74
52	10.68	9.38	10.03	7.22	-0.281	9.26	8.82	9.04
61	11.75	9.85	10.80	7.08	-0.344	10.98	9.34	10.16
62	11.11	9.51	10.31	6.94	-0.327	10.88	9.25	10.07
63	11.03	9.57	10.30	6.94	-0.327	10.31	9.06	9.69
64	10.64	9.38	10.00	7.00	-0.300	9.82	8.73	9.28
67	10.71	9.41	10.06	7.32	-0.271	10.09	8.97	9.53
58	10.47	9.55	10.01	8.17	-0.184	9.82	9.36	9.59
49	10.76	10.33	10.53	9.51	-0.097	10.11	9.71	9.91
39	10.60	10.49	10.55	10.81	+0.025	9.88	9.80	9.84
28	9.64	11.08	10.36	14.36	+0.386	9.03	10.25	9.64

source is illustrated in Fig. 1. The reactivity values obtained according to Eqs. (12) and (14) are specified in their pertinent measuring positions.

With the aid of Table II and Fig. 1 it is seen that at most measuring positions the harmonics content is negative, except close to the source. In the transition region (at position 39) the harmonics contribution almost vanishes and both methods give the correct reduced generation time and reactivity value

$$\bar{\Lambda}^* = 9.84 \pm 0.08 \text{ ms}, \quad \bar{\rho} = -10.55 \pm 0.1 \text{ \$}.$$

In the region of negative harmonics the GO-method gives too large values (cf. Eq. (17)), whereas the GR-version, in general, yields smaller values (cf. Eq. (19)). The strong attenuation of harmonics achieved by the modified techniques may be seen by comparing the columns ρ_{GO} and ρ_{GR} with ρ_a in Table II.

4.4. The effect of the finite pulse width

The use of finite neutron pulses is important from the experimental point of view. It permits a large number of neutrons per pulse to be introduced into the reactor, even if the source intensity is relatively small.

The basic Eqs. (12) and (14) fully take into account finite rectangular pulses. The ability of these expressions to handle extreme cases with very wide pulses (e.g. $|\gamma_0|d \approx 1$) was confirmed experimentally. Table III shows results obtained in position 28 for some pulse widths. The last column $\delta\rho_{GR}/\rho_{GR}$ gives the error in the GR-method, if the finiteness of the pulse is disregarded, i.e. if C_g (Eq. (15)) is set equal to unity. In this connection it is worthwhile noticing that C_g is slightly influenced by harmonics (see [10]). Therefore large corrections for the finite width increase somewhat the effect of the spatial harmonics in the GR-method.

TABLE III

EFFECT OF PULSE WIDTH

d (μs)	$-\gamma_0$ (s^{-1})	$-\rho_{GO}$ (\$)	$-\rho_{GR}$ (\$)	$-\delta\rho_{GR}/\rho_{GR}$ (d-correction)
80	1177.9	9.61	10.83	0.041
80	1177.7	9.79	11.30	0.042
330	1177.4	9.60	11.05	0.165
330	1180.6	9.59	10.94	0.164
330	1177.1	9.26	11.18	0.164
1030	1176.7	9.69	11.19	0.567

5. CONCLUSIONS

The two modifications of the usual pulsed source technique, proposed by GOZANI [8] and by GARELIS and RUSSELL [9] have been thoroughly discussed from the theoretical and experimental point of view. The methods were scrutinized under normal and various extraordinary conditions. All results were consistent if the measurements were carried out appropriately and evaluated along the lines mentioned in this paper.

From the large amount of material accumulated in our series of measurements the following additional conclusions may be drawn:

(a) The statistical precision of reactivity and generation time, attained in a rather short measuring time, is very satisfactory; for $|\rho| \leqslant 2$ \$, better than 1% and for $\rho \approx -6$ \$, approximately 2%.

(b) The use of wide neutron pulses ($|\gamma_0|d \approx 0.5$) and short pulsing periods ($|\gamma_0|T < 4$) is recommended when the source intensity is weak.

(c) It is not necessary to wait with the measurement until the delayed neutrons have attained their equilibrium state. It is recommended to start data accumulation with the first pulse. The correction term $D(MT, \rho)$ is usually small and may be calculated with the simple approximation proposed in the text (Eq.(10)).

(d) The two modifications of the pulsed source technique achieve a strong reduction of the prompt harmonics. However a relatively small amount of systematic error is still inherent in both methods. In the GO-version it is caused by pure delayed harmonics, whereas in the GR-version it is the delayed harmonics weighted with the deviation of the modal generation time from the persisting one.

(e) For far subcritical states where high harmonics contamination constitutes the main problem, the following procedure is recommended: Measure in a number of places in the system. Analyse the data according to the GO-version, the GR-version and the amplitude method. Find a position where the contribution from harmonics is negligible. When no such position can be found, the reactivity value is bracketed between ρ_{GO} and ρ_{GR}. A good guess of the proper value is given by the average $\bar{\rho} = \frac{1}{2}(\rho_{GO} + \rho_{GR})$.

(f) It should be noted that ρ_{GO} and Λ^*_{GO} can be calculated in a straightforward manner. In principle no computer is needed. However ρ_{GR}, or rather Λ^*_{GR}, is implicitly given in an integral equation which is not solved by hand.

REFERENCES

[1] SIMONS, B.E. and KING, J.S., Nucl. Sci. Engng 3 (1958) 595.
[2] BENGSTON, J., Proc. 2nd UN Int. Conf. PUAE 12 (1958) 63.
[3] BECKURTS, K.H., Nucl. Instrum. Meth. 11 (1961) 144.
[4] BACH, D.R. et al., Nucl. Sci. Engng 11 (1961) 199.
[5] DE SAUSSURE, G. et al., Nucl. Sci. Engng 9 (1961) 291.
[6] KOLAR, D.C. and KLOVERSTROM, F.A., Nucl. Sci. Engng 10 (1961) 45.
[7] INTERNATIONAL ATOMIC ENERGY AGENCY, Exponential and Critical Experiments (3 vols.) IAEA, Vienna (1964).

[8] GOZANI, T., Nukleonik 4 (1962) 348.
[9] GARELIS, E. and RUSSELL, J.L., Jr., Nucl. Sci. Engng 16 (1963) 263.
[10] GOZANI, T., EIR-Bericht Nr. 79 (1965).
[11] GOZANI, T., Nukleonik 5 (1963) 55.
[12] GOZANI, T., EIR-Bericht Nr. 28 (1962).
[13] LEWINS, J., Nucl. Sci. Engng 9 (1961) 399.
[14] SJÖSTRAND, N.G., Ark. Fys. 11 (1956) 233.
[15] PRUD'HOME, J.T., Texas Nuclear Corporation Neutron Generators (1962).
[16] BEHRINGER, K., Internal EIR-Rpt. TM-PH 105 (1962).

REACTIVITY MEASUREMENT BY THE PULSED NEUTRON METHOD

S. A. SCOTT
TECHNION, ISRAEL INSTITUTE OF TECHNOLOGY,
HAIFA, ISRAEL

Abstract — Résumé — Аннотация — Resumen

REACTIVITY MEASUREMENT BY THE PULSED NEUTRON METHOD. An extensive series of subcritical reactivity measurements has been carried out with the IRR-1 swimming pool reactor, to test the applicability of the pulsed neutron method to a fully reflected core heavily contaminated with fission products. A Kaman pulsed neutron source was located on the grid plate, and up to 11$ negative reactivity was obtained by completely inserting the control rods, both singly and in groups.

Each subcritical reactivity level was determined by the pulsed neutron technique and compared to stable period and rod drop measurements. The pulsed neutron data was analysed in three ways:

(1) The prompt neutron decay period α was determined at each reactivity level, including the value α_0 at delayed critical. The reactivity in $ is then given by $\alpha = \alpha_0 (1+\$)$ where $\alpha_0 = k/\ell^*$. A correction is applied to account for the dependence on reactivity of the reduced prompt neutron average lifetime ℓ^*.

(2) The method of Garelis and Russell. It is shown that serious errors are introduced by this method of analysis if the prompt neutron density reaches the constant background level before the arrival of the following pulse. The effect is particularly important in situations close to delayed critical. A suitable correction term is developed and applied to the analysis.

(3) On the assumption that only the fundamental harmonic term is present, the Garelis and Russell form of analysis is simplified to $\$ = AR/D\alpha$ where A/D is the saturated prompt-to-delayed neutron ratio during the pulse.

A detailed evaluation of these forms of analysis is presented, and the experimental results are compared with those obtained by the "conventional" techniques of stable period and rod drop. Finally a composite form of analysis is recommended, in which the improved Garelis and Russell method is used to obtain α_0, which is then used in the decay period method for reactivity measurements.

MESURE DE LA RÉACTIVITÉ PAR LA MÉTHODE DES NEUTRONS PULSÉS. Une longue série de mesures de la réactivité sous-critique a été effectuée à l'aide du réacteur piscine IRR-I en vue de déterminer si la méthode des neutrons pulsés est applicable à un cœur entièrement réfléchi et fortement contaminé par des produits de fission. Une source de neutrons pulsés Kaman étant placée sur la plaque de base, on a obtenu des valeurs de l'antiréactivité allant jusqu'à 11$ en insérant à fond les barres de commande, soit individuellement, soit en groupes.

Chaque niveau de réactivité sous-critique a été déterminé par la méthode des neutrons pulsés et comparé aux résultats des méthodes de la période constante et de la chute des barres. Les données fournies par la méthode des neutrons pulsés ont été analysées de trois façons suivantes:

1. La constante de décroissance des neutrons instantanés α a été déterminée pour chaque niveau de réactivité, y compris la valeur α_0 à l'état critique retardé. La réactivité en $ est alors donnée par $\alpha = \alpha_0(1+\$)$, où $\alpha_0 = k/\ell^*$. On applique un facteur de correction pour tenir compte de la variation de la durée de vie moyenne des neutrons instantanés ℓ^* en fonction de la réactivité.

2. Méthode de Garelis et Russell. L'auteur montre que cette méthode d'analyse donne lieu à des erreurs graves si le nombre volumique des neutrons instantanés atteint le niveau de bruit de fond constant avant l'arrivée de la bouffée suivante. L'effet est particulièrement important dans des états voisins de l'état critique retardé. Il a mis au point un facteur de correction approprié qu'il applique dans l'analyse.

3. En admettant que seul le terme harmonique fondamental est présent, la forme d'analyse de Garelis et Russell se ramène à $\$ = AR/D\alpha$, où A/D est le rapport entre les neutrons instantanés saturés et les neutrons retardés pendant la bouffée.

L'auteur présente une évaluation détaillée de ces formes d'analyse et compare les résultats de l'ex-

périence à ceux qui ont été obtenus par les techniques «classiques» de la période constante et de la chute des barres. Il recommande enfin la forme d'analyse suivante qui met à profit plusieurs méthodes: on se sert de la méthode améliorée de Garelis et Russell pour obtenir α_0, puis on utilise α_0 dans la méthode de la période de décroissance pour faire les mesures de réactivité.

ИЗМЕРЕНИЕ РЕАКТИВНОСТИ С ПОМОЩЬЮ МЕТОДА ИМПУЛЬСНЫХ НЕЙТРОНОВ. На реакторе бассейнового типа IRR-I была проведена большая серия измерений подкритической реактивности, чтобы определить возможность применения метода импульсных нейтронов для активной зоны с полным отражателем, сильно загрязненной продуктами деления. Камановский источник импульсных нейтронов поместили на решетчатой пластинке, и отрицательная реактивность величиной до 11 долларов была получена в результате полного введения регулирующих стержней. Стержни вводились как поодиночке, так и группами.

Каждая подкритическая реактивность была определена с помощью метода импульсных нейтронов и сопоставлена с результатами измерений во время устойчивого периода и сброса стержня. Данные по импульсным нейтронам анализировались тремя путями:

1. Период распада мгновенных нейтронов α был определен при каждой реактивности, включая значение α_0 при запаздывающей критичности. Затем реактивность в долларах выражалась как $\alpha = \alpha_0 (1 + \$)$, где $\alpha_0 = k/\ell^*$. Для учета зависимости сокращенного среднего времени жизни мгновенных нейтронов ℓ^* от реактивности была внесена поправка.

2. Метод Гарелиса и Рассела. Показано, что этот метод анализа связан с серьезными ошибками, если плотность мгновенных нейтронов достигает уровня постоянного фона до образования следующего импульса. Это происходит при условиях, близких к запаздывающей критичности, и при больших подкритических реактивностях, когда скорость пульсирования R является низкой. Разработан и применяется для этого анализа поправочный член.

3. Исходя из предположения, что имеется только член фундаментальной гармоники, форма анализа Гарелиса и Рассела упрощена до $\$ = AR/D\alpha$, где A/D - отношение насыщенных мгновенных нейтронов к запаздывающим в течение импульса.

Дается подробная оценка этих видов анализа, и экспериментальные результаты сравниваются с результатами, полученными с помощью "обычных" методов устойчивого периода и сброса стержней. И, наконец, рекомендуется составная форма анализа, при которой используется усовершенствованный метод Гарелиса и Рассела для получения α_0, которое затем используется для измерений реактивности по методу периода распада.

MEDICIONES DE LA REACTIVIDAD POR EL METODO DE LOS NEUTRONES PULSADOS. En el reactor IRR-I de tipo piscina se han hecho numerosas mediciones de la reactividad para el estado subcrítico, a fin de estudiar la posibilidad de aplicar el método de los neutrones pulsados a un cuerpo de reactor totalmente rodeado de reflector y fuertemente contaminado con productos de fisión. Para ello se colocó una fuente Kaman de neutrones pulsados en la rejilla, y se obtuvieron valores negativos de la reactividad de hasta 11 dólares introduciendo completamente las barras de control, tanto una a una como en grupos.

Cada uno de los valores de la reactividad para el estado subcrítico se determinó empleando la técnica de los neutrones pulsados, y se compararon los resultados con las mediciones efectuadas por los métodos de período estable y de descenso de las barras. Los datos obtenidos con neutrones pulsados se sometieron a un triple análisis:

1. Se determinó el período α de decrecimiento de los neutrones instantáneos para cada valor de la reactividad, incluido el valor α_0 correspondiente a los neutrones retardados. En este caso, la criticidad expresada en «dólares» viene dada por $\alpha = \alpha_0 (1 + \$)$, en donde $\alpha_0 = k/\ell^*$. Para tener en cuenta la variación en función de la reactividad de la menor vida media ℓ^* de los neutrones inmediatos, se introdujo la oportuna corrección.

2. Se demostró que el método de análisis de Garelis y Russell origina graves errores cuando la densidad de los neutrones instantáneos alcanza el nivel de fondo constante antes de la llegada del impulso siguiente. El efecto es particularmente importante cuando está próxima a alcanzarse la criticidad por neutrones retardados. También en este caso se aplicó al análisis un término de corrección apropiado previamente calculado.

3. Se simplificó el método de análisis de Garelis y Russell partiendo del supuesto de que sólo se halla presente el término correspondiente al armónico fundamental. La fórmula queda reducida a $\$ = AR/D\alpha$, en la cual A/D es la razón de saturación, durante el impulso, de los neutrones instantáneos a los retardados.

El autor evalúa detenidamente estos procedimientos de análisis y compara los resultados experimentales con los obtenidos por las técnicas «tradicionales» de período estable y de descenso de las barras. Por último,

recomienda una modalidad combinada de análisis que utiliza el método perfeccionado de Garelis y Russell para obtener el valor α_0, el cual se emplea seguidamente para medir la reactividad con el método del período de decrecimiento.

1. INTRODUCTION

The measurement of subcritical reactivity by the pulsed neutron technique has been investigated under a wide variety of conditions, ranging from cold, clean, unreflected assemblies with simple geometry [1-3] to reactor cores having none of these desirable properties [4, 5]. The purpose of most of these experiments has been the investigation of the pulsed neutron technique itself, its accuracy, its range of validity and the importance of its theoretical shortcomings.

The present work was undertaken with the rather different purpose of investigating the practical application of pulsed neutron measurements to the everyday problems encountered in the operation of research reactors. This is the preliminary stage in a long-term project aimed at the development of a reactivity meter capable of monitoring subcritical operations, such as fuel handling, control rod replacement and movement of in-core experimental apparatus. Such a meter should use a simple neutron source which does not require reactor down-time for its insertion or removal. The use of inexpensive detection and electronic equipment is desirable, and subcritical reactivity values should be provided in a minimum time and with the use of a minimum number of source pulses. High accuracy is not necessary and reactivity measurements with an error of several per cent would probably be sufficient for most purposes.

2. THE EXPERIMENTAL ARRANGEMENT

The measurements were made using the IRR-1 swimming pool reactor [6]. A pulsed neutron source of the sealed tube, pulse transformer type was used (Kaman NT-60-8), inserted in a watertight aluminium tube located on the reactor grid plate. The neutron detection system comprised a sensitive fission chamber, also in a long aluminium tube resting on the grid plate, followed by fairly standard amplifiers, discriminator and a multichannel pulse analyser. The overall dead-time was 0.2 μs. Data output was by printer, punched tape and strip-chart recorder.

Preliminary measurements showed that the effect of transient harmonic neutron distributions could be reduced by locating both the source and the detector symmetrically with respect to the core. The final arrangement is shown in Fig. 1. The source was level with the centre of the fuel elements, while the height of the detector was adjusted to reduce gamma-ray pile-up to an acceptable level.

The reactor has been operated since June 1960 at power levels up to 2.5 MW, and fuel burn-up values of about 15% had been reached at the time of the present work. Consequently the fuel was heavily contaminated with fission products, and gamma-ray dose rates in excess of 10^5 rad/h were measured close to the fuel elements. Apart from causing serious concern

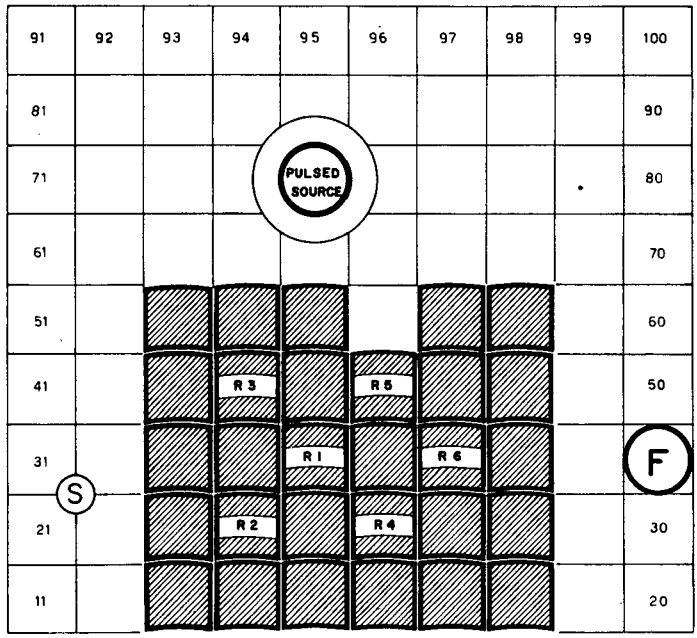


Fig. 1

Core configuration PQ-1

S - Start-up source
F - Fission chamber

about radiation damage in the pulsed neutron source, such high dose rates give rise to a high photoneutron source contribution which effectively prevents experimental work at delayed critical. Approach-to-critical curves are not straight, even close to delayed critical, and extrapolation from them leads to inaccurate results. Near critical an intense pulsed neutron source is required to give results significantly above the background level and the delayed neutron contribution cannot be determined with good accuracy.

3. THE PULSED NEUTRON SOURCE METHOD (PS)

This method of measuring reactivity is based upon the simple expression [4] relating the prompt neutron fundamental decay constant α to the reduced reactivity ρ^*:

$$\alpha = \alpha_0(1-\rho^*) = \alpha_0(1+\$) \tag{1}$$

Here $\alpha_0 = k/l^* = 1/\Lambda^*$ where l^* and Λ^* are the reduced prompt neutron average lifetime and reduced generation time respectively. To account for the dependence of l^* on reactivity, we assume the simple relationship

$$l^* = l_c^*(1+\epsilon\,\$) \simeq \Lambda^*(1+\epsilon'\,\$) \tag{2}$$

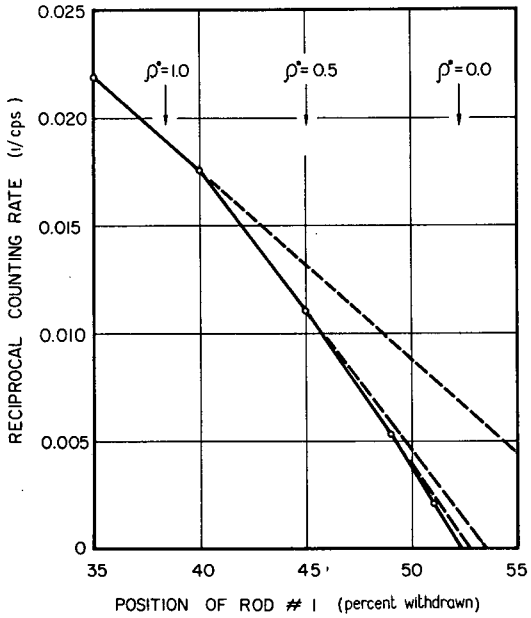


Fig. 2

Approach to critical
Rods 2 to 6 fully withdrawn

where ϵ and ϵ' are constants. (To be precise, $\epsilon' = \epsilon k + \beta\bar{\gamma}$). In principle, reactivity values can be obtained from experimental measurements of α, although this implies calculating the value of ϵ and determining l_c^* by a measurement of α at delayed critical.

A simple core arrangement was obtained by withdrawing all the control rods except rod No. 1. This was then withdrawn in stages to permit a standard approach-to-critical measurement. The effect of the intense photoneutron source contribution is apparent in Fig. 2. In addition to the reciprocal counting rate measurements, a pulsed neutron run was made at each position of the control rod. The source was operated at a repetition rate of 1 pulse per second, with each run comprising a few hundred pulses. Subsequent analysis gave the prompt neutron decay constant α, and Fig. 3 shows how extrapolation was used to determine the value $\alpha_0 = \alpha_c$ at delayed critical. The result obtained, $\alpha_c = 114 \pm 3\ s^{-1}$, corresponds to a prompt neutron mean-life $l_c^* = 8.77 \pm 0.23$ ms.

A series of reactivity measurements was carried out over a range of 11 \$. For the sake of simplicity and to facilitate direct comparison with rod-drop measurements, the various subcritical reactivity values were obtained by fully inserting one or more of the control rods. In each case, after equilibrium had been reached, a pulsed neutron measurement was made using up to 1000 source pulses at a rate of 1 pulse per second. The experimentally determined values of α are plotted in Fig. 4 as a function of the reactivity in dollars obtained from stable-period measurements. The results indicate a value of $\epsilon' \simeq 0.010$, which is in poor agreement with de Saussure's

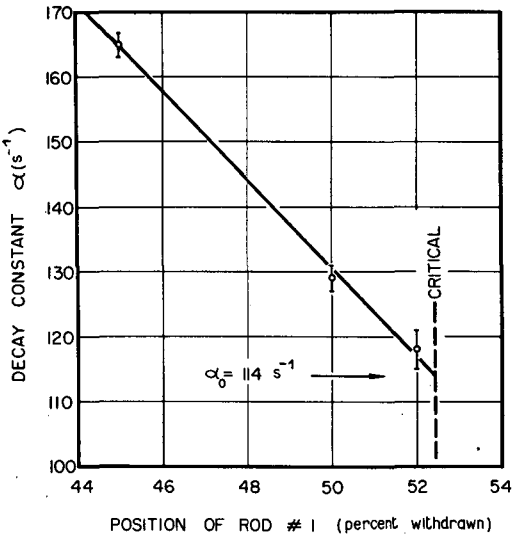


Fig. 3

Determination of α_0
Delayed critical rod position determined from approach-to-critical

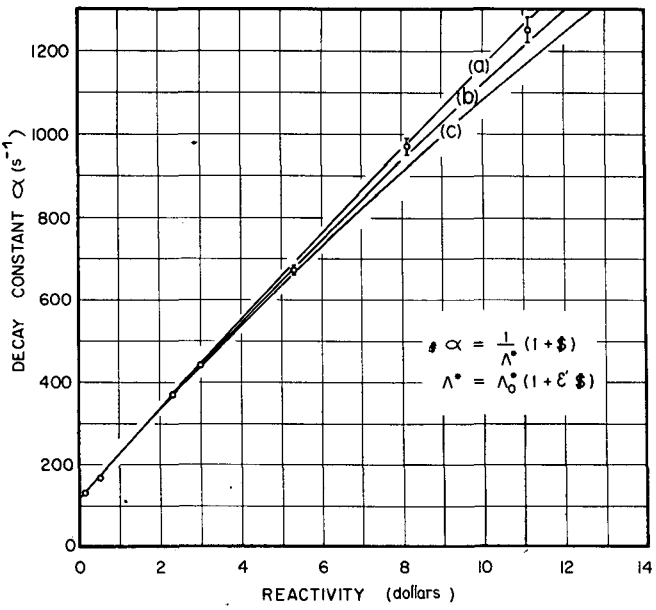


Fig. 4

Determination of ϵ'
Reactivity values obtained from stable-period measurements
(a) $\epsilon' = 0.008$ (b) $\epsilon' = 0.012$ (c) $\epsilon' = 0.016$

calculated value of $\epsilon' = 0.016$ for the BSR lattice [4], whose core design and mean-life ($l_c^* = 8.9$ ms) are similar to those of the IRR-1. However, it is entirely possible that a systematic error is introduced by summing stable-period reactivity measurements, leading to an erroneous value for ϵ'. Consequently it can only be concluded that, up to about 11 $ subcritical, a value of $\epsilon' \simeq 0.010$ (and hence $\epsilon \simeq 0.002$, assuming $\beta\overline{\gamma} = 0.008$) is required to obtain pulsed neutron reactivity measurements with an accuracy comparable to that obtained by summing stable-period measurements.

Data analysis was performed by the general least squares programme ANALYSER [7], using an exponential series as the fitting function. All runs were analysed by a three parameter fit, and Fig. 5 shows the general form of a decay curve and its analysed components. Data were progressively rejected from the beginning and end of the decay curve to check for the adequacy of a three parameter fit, and it was found that at large values of reactivity an additional harmonic term had to be included.

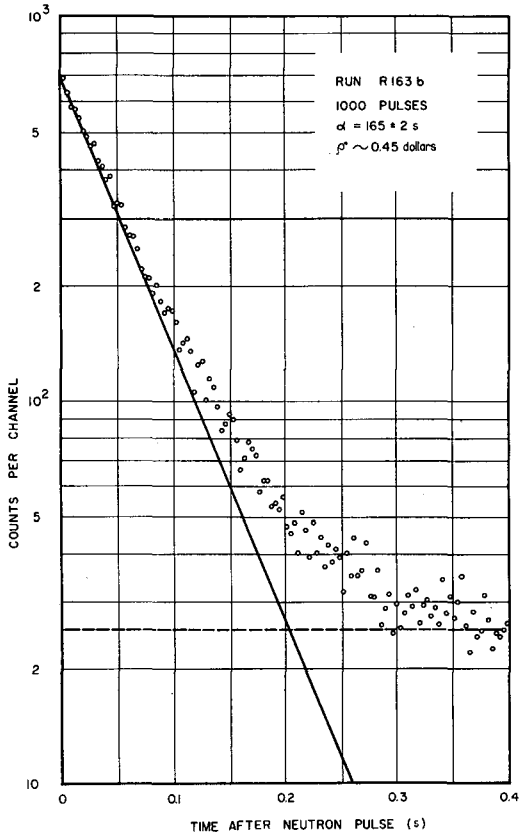


Fig. 5

Pulsed neutron decay curve
The analysed exponential and background components are indicated

Near critical the effect of the delayed neutron component was appreciable. Figure 6 shows a series of three parameter fits with progressive leading data rejection. Data obtained before the delayed neutron level had built up to its saturation value show no effect, but with data obtained after saturation the influence of the delayed neutron component is clear.

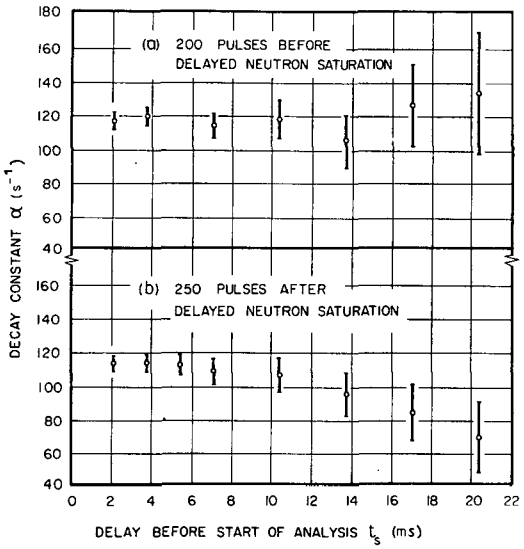


Fig. 6

The effect of the delayed neutron level on the computed value of α

4. THE GARELIS-RUSSELL METHOD (GR)

This method, originally proposed by GARELIS and RUSSELL [8], is also known as the $k\beta/l$ method. Analysis of a pulsed neutron decay curve yields a prompt neutron component $N_p(t)$ and an effectively constant term comprising the delayed neutron equilibrium level D and a component B resulting from source multiplication. The value of D is determined implicitly by measuring B before operating the pulsed neutron source.

Instead of making measurements at or near critical, the value of α_0 is found which satisfies the equation

$$\int_0^\infty N_p(t)(e^{\alpha_0 t}-1)dt = \frac{D}{R}, \qquad (3)$$

where R is the neutron source pulsing rate. In practice the integral is replaced by the summation of the prompt neutron component n_i in each of J channels of width W seconds. Consequently the integral is replaced by a sum over m mean-lives (that is, up to time $t_m = m/\alpha$) and we have

$$S_m = \sum_{i=1}^{J} n_i(e^{\alpha_0 t} - 1) = \frac{DK_m}{WR} \qquad (4)$$

The correction factor K_m, included to account for the prompt neutron component after t_m [9], is given by

$$K_m = \frac{S_m}{S_\infty} = 1 - e^{-m}\,(re^{m/r} - r + 1)\,, \qquad (5)$$

where $r = \alpha/\alpha_0$ and the reasonable assumption has been made that $N_p(t)$ is a simple exponential function after t_m. The value of t_m is chosen to be rather less than the time at which $N_p = B+D$, since beyond this no meaningful information can be obtained about N_p. Consequently the correction term is of greatest importance when B+D is relatively large, such as for measurements near delayed critical.

In the present work, photoneutron production gives rise to a large value of B, while D is relatively small owing to the low pulsing rate. As a result accurate measurements of D were possible only near delayed critical. An example of the computational technique is shown in Fig. 7. After the normal data analysis has yielded values of α and D, the value of S_m/K_m is computed for a range of values of α_0. The resultant curve intersects the value of D/WR at the correct value for α_0. The result is seen to be insensitive to the chosen value of m, and the final error is a result of the large uncertainty in the computed value of D (caused by large B) and the error in the value of the decay constant α, (in this case, $\alpha = 129 \pm 2\ s^{-1}$).

5. THE SIMPLIFIED PULSED SOURCE METHOD (SPS)

In general the prompt neutron component N_p will consist of a fundamental term and harmonic terms. However, by careful positioning of source and detector, and for certain control rod configurations the harmonic terms will be negligible. Under these circumstances $N_p = A\,e^{-\alpha t}$, which may be used together with Eq. (1) to simplify Eq. (3) to the form

$$\$ = AR/D\alpha\ . \qquad (6)$$

Similar expressions have been derived by GOZANI [10] for a source pulse of finite length, and more recently by CORNGOLD [11] for the case of a single harmonic mode. The simple relationship of Eq. (6) is of particular interest for use as the basis for a simple form of on-line reactivity meter, since the value of α_0 is not required.

6. OTHER TECHNIQUES

As far as possible the pulsed neutron results were compared with stable-period (SP) and rod-drop (RD) measurements. The stable-period reactivity values were obtained by summing appropriate sections of the control rod

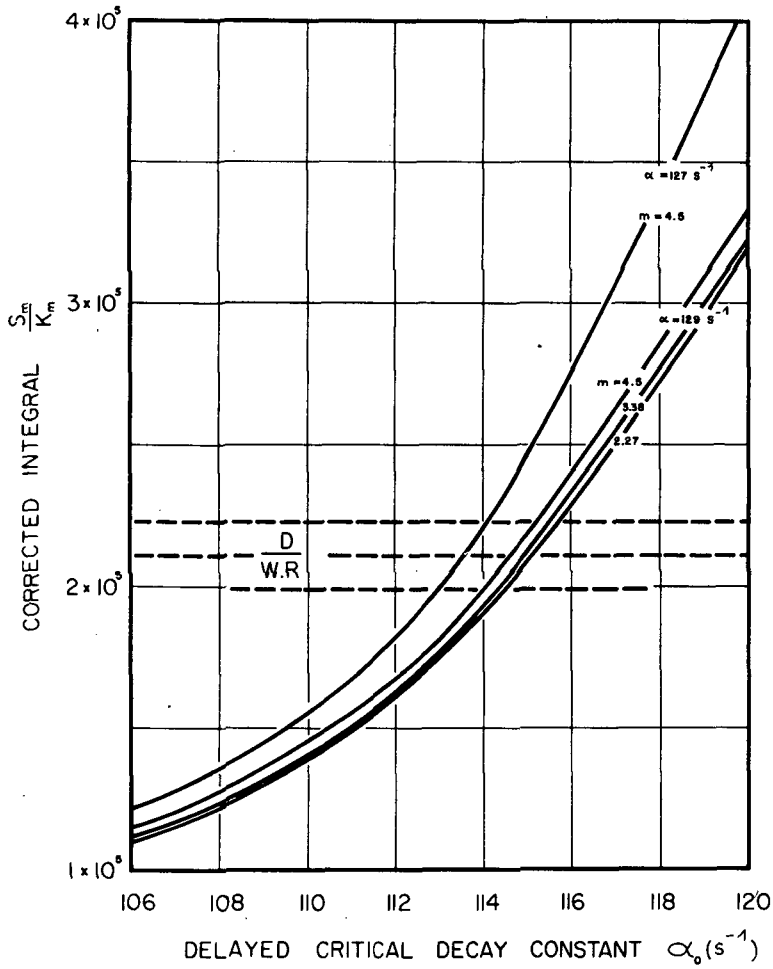


Fig. 7

Determination of α_0 by the kβ/l method

calibration curves. These curves were obtained by the usual method of measuring stable periods for small positive reactivity values followed by control rod balancing to return to delayed critical.

Each subcritical core arrangement was obtained by dropping the required rod or rods from a critical situation, and the neutron decay was recorded on a multichannel analyser set to 1 second per channel. Two types of analysis were used. The first, (RD1) was the integral-count method of HOGAN [12], in which the rod value is given in dollars [13] by

$$\$ = \frac{\frac{1}{k}\sum a_i/\lambda_i}{\int_0^\infty \frac{n(t)dt}{n_0}} \simeq \frac{12.75\, n_0}{\int_0^\infty n(t)\, dt} \qquad (7)$$

The second type of analysis (RD2) is based on a solution of the kinetics equations by an iterative method [14], yielding a set of theoretical "decay curves" with which the experimental decay may be compared. Figure 8 shows some examples of both theoretical curves and experimental results.

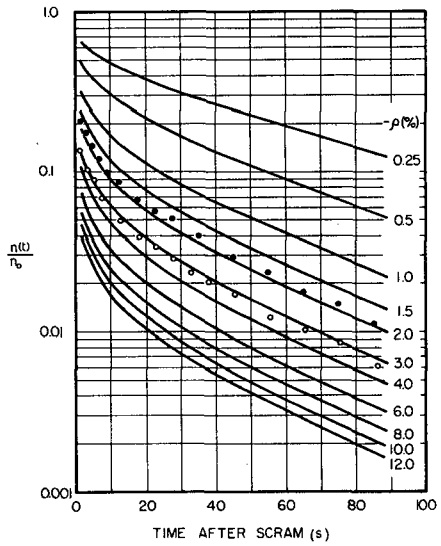


Fig. 8

The rod-drop technique

— Calculated curves (IA-820)
• Experimental results, Rod No. 2, $\rho = -0.0185$
0 Experimental results, Rods. Nos. 2+3, $\rho = -0.0320$

7. RESULTS AND CONCLUSIONS

The experimentally determined reactivity values are compared in Table I. While good agreement is shown between the stable-period (SP) and pulsed-source (PS) techniques, it should be remembered that the method used to determine ϵ was effectively a normalization of these results. The rod-drop (RD) results are in general agreement with the other techniques, although some discrepancies are apparent. The estimated errors are considerably smaller than the scatter of the results, especially in the case of the RD1 method.

It is to be expected that the measured reactivity of a group of rods will be equal to or slightly less than the sum of their individual values. While a difference is indeed suggested by some of the RD results, it is far from conclusive.

From the results shown in Table I it is concluded that even with a low cost pulsed neutron source, operating at a low pulsing rate in a reactor heavily contaminated with fission products, reactivity can be measured up to at least 11 $ with an accuracy of about 5%, using less than 1000 source

TABLE I

COMPARISON OF EXPERIMENTAL RESULTS

Rods inserted	Reactivity in dollars SP	PS	RD1	RD2
2	2.97	2.93 ± 0.15	2.88 ± 0.03	2.63 ± 0.07
3	2.31	2.29 ± 0.09	2.11 ± 0.02	2.28 ± 0.07
2,3	5.28	5.12 ± 0.20	5.05 ± 0.06	4.53 ± 0.10
Sum 2+3	5.28	5.22 ± 0.18	4.99 ± 0.04	4.91 ± 0.10
4,5	8.13	8.1 ± 0.4	6.7 ± 0.1	7.8 ± 0.2
2,4,5	11.10	11.0 ± 0.6	11.6 ± 0.3	10.6 ± 0.5
Sum 2+4+5	11.10	11.0 ± 0.4	9.6 ± 0.1	10.4 ± 0.2

pulses for each measurement. Under the same conditions the Garelis-Russell method (GR) can be used to obtain α_0 at reactivity values up to about 1 $ subcritical. Unfortunately the highly desirable procedure of using the GR-method to determine α_0 over a wide reactivity range, leading to values of l^* and hence ϵ, is not practicable under these conditions. It should, however, be possible to determine ϵ in this way by using a source with a higher pulsing rate, preferably in a clean reactor core.

The results of the simplified pulsed source method (SPS) are shown in Table II. Again the reactivity range was limited, but it is seen that the method is in good agreement with the SP and PS methods. This suggests that a reactivity meter can probably be developed using the very simple form of Eq.(6), hence avoiding the complications implicit in a measurement of α_0.

TABLE II

THE SIMPLIFIED PULSED SOURCE METHOD

Position of rod No. 1 (%)	Reactivity in dollars SP	PS	SPS
45	0.52	0.45 ± 0.04	0.61 ± 0.07
50	0.15	0.13 ± 0.03	0.125 ± 0.007

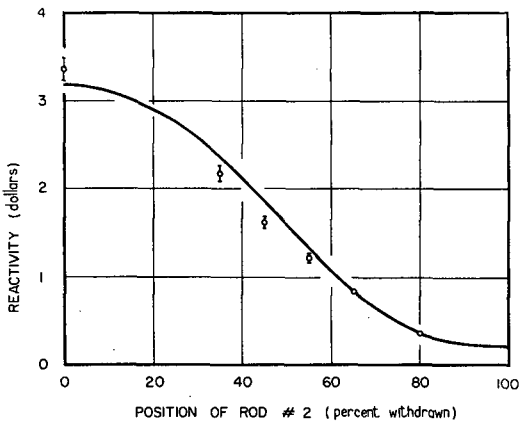


Fig. 9

Withdrawal of a control rod

Figure 9 shows an example of the type of measurement which can be carried out using the simple equipment and under the adverse conditions described in the present work. Control rod No. 2 was withdrawn from the core, the operation being monitored by a series of pulsed neutron measurements. Up to 1000 source pulses were used in each case. Reactivity values were calculated by the PS method, and the value $\epsilon = 0.002$ was used. However, for measurements of this type sufficient accuracy would be obtained by neglecting the dependence of l^* on reactivity.

ACKNOWLEDGEMENTS

It is a pleasure to acknowledge many helpful discussions with Dr. J.R. Wolberg and the assistance of Dr. G. Ben David and the IRR-1 operating crew.

REFERENCES

[1] KOLAR, O.C. and KLOVERSTROM, F.A., Nucl. Sci. Engng 10 (1961) 45-52.
[2] BACH, D.R., BUNCH, S.I., CERBONE, R.J. and SLOVACEK, R.E., Nucl. Sci. Engng 11 (1961) 199-210.
[3] BROWN, J.R., Rpt. GA 4838 (1964).
[4] DE SAUSSURE, G., HENRY, K. and PEREZ-BELLES, R., Nucl. Sci. Engng 9 (1961) 291-98.
[5] MEYER, P., Trans. Amer. nucl. Soc. 6 (1963) 287.
[6] KAHAN, R.S., Rpt. IA 680 (1961).
[7] SCOTT, S.A., Rpt. TNSD 104 (1965).
[8] GARELIS, E. and RUSSELL, J.L., Nucl. Sci. Engng 16 (1963) 263-70.
[9] SCOTT, S.A. and WOLBERG, J.R., Trans. Amer. nucl. Soc. (1965).
[10] GOZANI, T., Nukleonik 4 (1962) 348-49.
[11] CORNGOLD, N., Trans. Amer. nucl. Soc. 7 (1964) 282.
[12] HOGAN, W.S., Nucl. Sci. Engng 8 (1960) 518-22.
[13] KEEPIN, G.R., Physics of Nuclear Kinetics, Addison and Wesley, N.Y. (1965) 245.
[14] ROTHENSTEIN, W., Rpt. IA-820 (1963).

DISCUSSION

S. CHWASZCZEWSKI: The rod-reactivity measurement data quoted in your paper strike me as being somewhat unusual. The sum of the reactivities of the individual rods is generally higher than the reactivity of the rods inserted into the reactor together. A screening effect ought to be involved here.

S. SCOTT: That is true. We did in fact try to measure the difference in reactivity obtained when two rods are inserted together and then separately. However, no significant difference was found greater than experimental errors of a few per cent.

J. RUSSELL: I think you will find that if two rods are close together there is liable to be a negative screening effect, whereas rods placed further apart at an optimum position may have a positive screening effect. This effect is, of course, a result of shifting the neutron flux.

INTERPRETATION OF PULSED SOURCE EXPERIMENTS *

C. A. PRESKITT AND E. A. NEPHEW
OAK RIDGE NATIONAL LABORATORY,
OAK RIDGE, TENN., UNITED STATES OF AMERICA

Abstract — Résumé — Аннотация — Resumen

INTERPRETATION OF PULSED SOURCE EXPERIMENTS. Pulsed neutron experiments performed during reactor commissioning programmes constitute important examples in which non-separable transients play an important role. Subcritical states studied with partial core loadings are generally highly reflected, for example, and suffer gross flux distortions upon insertion of control rods.

We have developed methods for theoretically simulating the response of non-uniform reactors to pulsed sources and have applied these to a wide range of typical experimental conditions anticipated during the commissioning programme of the Experimental Gas-Cooled Reactor (EGCR). The space-dependent kinetics equations are solved for two to six neutron groups and one to six delayed neutron precursors by a semi-analytical method which is based entirely on the application of matrix techniques.

Two classes of experiments have been examined, involving respectively the prompt transient and the total transient. In the first class we consider the common prompt decay experiment and the $(\bar{\beta}/\bar{\Lambda})$ technique, and in the second the source-jerk experiment. Theoretical simulations of these have been used to study the effects of higher modes and other factors affecting their interpretation.

We have found that space-dependent effects are greatly suppressed in many important cases in experiments performed with 14-MeV source neutrons. Furthermore, for the source-jerk experiments, a relationship has been derived involving the volume integration of experimental measurements which provides an exact expression for the reactivity including the effects of all modes.

INTERPRÉTATION DES EXPÉRIENCES A L'AIDE DE SOURCES PULSÉES. Les expériences à l'aide de neutrons pulsés faites dans le cadre des opérations de mise en service d'un réacteur fournissent des exemples importants de cas où des états transitoires non séparables jouent un rôle dominant. Ainsi des états sous-critiques étudiés avec des charges partielles sont en général fortement réfléchis, le flux subissant des distorsions excessives au moment de l'introduction des barres de commande.

Les auteurs ont élaboré des méthodes permettant de simuler en théorie la réponse des réacteurs hétérogènes à des sources pulsées et les ont appliquées dans un grand nombre de conditions d'expérience caractéristiques prévues au cours de la mise en service du réacteur expérimental refroidi par un gaz (EGCR). Ils ont résolu les équations de la cinétique qui sont fonction de l'espace, pour deux à six groupes de neutrons et un à six précurseurs de neutrons retardés, par une méthode semi-analytique qui est entièrement fondée sur l'application de méthodes matricielles.

Les auteurs ont analysé deux catégories d'expériences portant respectivement sur les états transitoires associés aux neutrons instantanés et les états transitoires associés à tous les neutrons (instantanés et retardés). Dans la première catégorie, ils ont étudié l'expérience habituelle de décroissance des neutrons instantanés et la méthode $(\bar{\beta}/\bar{\Lambda})$ et, dans la deuxième catégorie, l'expérience qui consiste à retirer brusquement la source. Ils ont utilisé des simulations théoriques de ces expériences pour étudier les effets des modes supérieurs et d'autres facteurs affectant leur interprétation.

Les auteurs ont constaté que, dans beaucoup de cas importants, les effets variables dans l'espace sont en grande partie supprimés lorsque les expériences s'effectuent à l'aide de neutrons de 14 MeV. En outre, pour l'expérience consistant à retirer brusquement la source, ils ont établi une relation, fondée sur l'intégration en volume des mesures expérimentales, qui fournit une expression exacte de la réactivité, y compris les effets de tous les modes.

* Research sponsored by the United States Atomic Energy Commission under contract with the Union Carbide Corporation.

ИНТЕРПРЕТАЦИЯ ЭКСПЕРИМЕНТОВ С ИСТОЧНИКАМИ ИМПУЛЬСНЫХ НЕЙТРОНОВ. Эксперименты с импульсными нейтронами, выполненные по программе пуска реакторов в эксплуатацию, представляют собой важный пример, в котором основную роль играют неразделяемые переходные процессы. Например, подкритические состояния, изученные на основе частичных загрузок активных зон, в целом в значительной степени отражаются, и при введении в них регулирующих стержней имеют место значительные искажения потоков.

Разработаны методы, теоретически отвечающие неоднородным реакторам в отношении источников импульсных нейтронов, которые применены в широком диапазоне типичных экспериментальных условий, приемлемых в ходе осуществления программы пуска в эксплуатацию экспериментального реактора с газовым охлаждением (EGCR) Кинетические уравнения, зависящие от пространства, решаются для двух-шести групп нейтронов и одного – шести предшественников запаздывающих нейтронов с помощью полуаналитического метода, который полностью основан на применении матричных методов.

Изучены два класса экспериментов, затрагивающих соответственно мгновенный переход и полный переходный процесс. В первом классе рассматривается общий эксперимент мгновенного распада и метод (β/Λ), а во втором - эксперимент с резким перемещением источника. Теоретическое моделирование этих экспериментов использовалось для изучения эффектов высоких видов и других факторов, затрагивающих их интерпретацию.

Установлено, что эффекты, зависящие от пространства, в значительной степени подавляются во многих важных случаях при экспериментах, проводимых с источником нейтронов 14 Мэв. Более того, для эксперимента с резким перемещением источника было выведено соотношение, связанное с объемной интеграцией экспериментальных измерений, которое дает точное выражение для величины реактивности, в том числе и эффектов всех видов.

INTERPRETACION DE EXPERIMENTOS CON FUENTES DE NEUTRONES PULSADOS. Los experimentos hechos con neutrones pulsados en el curso de un programa de puesta en servicio de un reactor constituyen un claro ejemplo en el que los fenómenos transitorios no separables desempeñan un papel primordial. Así, los estados subcríticos que se han estudiado con cargas parciales suelen experimentar una reflexión considerable, registrándose además fuertes distorsiones del flujo al introducirse las barras de control.

Los autores han ideado métodos para simular teóricamente la respuesta de reactores heterogéneos a las fuentes de neutrones pulsados, y los han aplicado en una gama de condiciones experimentales características previstas durante la ejecución del programa de puesta en servicio del reactor experimental refrigerado con las (EGCR). Las ecuaciones cinéticas en función del espacio se resuelven para dos a seis grupos de neutrones y para distinto número de precursores de neutrones retardados – de uno a seis –, empleando un método semianalítico basado enteramente en la aplicación de técnicas matriciales.

Los autores examinan dos tipos de experimentos que entrañan, respectivamente, fenómenos transitorios asociados a los neutrones instantáneos y fenómenos transitorios totales. Dentro del primer grupo, han estudiado el experimento corriente de decrecimiento instantáneo y la técnica de $(\overline{\beta}/\overline{\Lambda})$, y dentro del segundo, el experimento de extracción súbita de la fuente, recurriendo a la simulación teórica de estos experimentos para estudiar los efectos de los armónicos superiores y otros factores que intervienen en su interpretación.

Han comprobado que, en muchos casos importantes, los efetos espaciales quedan eliminados en gran parte cuando los experimentos se realizan con neutrones emitidos por una fuente de 14 MeV. Además, en el caso del experimento de extracción súbita de la fuente, han establecido una relación en la que interviene la integración en volumen de los resultados de las mediciones experimentales y que proporciona una expresión exacta de la reactividad, incluidos los efectos de todos los modos.

1. INTRODUCTION

The studies discussed here have been performed as an aid in the planning of pulsed source experiments as part of the commissioning programme for the Experimental Gas-Cooled Reactor (EGCR) [1]. The studies have been aimed primarily at the theoretical simulation of planned experiments, in order to optimize the experimental conditions. Representative data may thus be generated for precisely known conditions and may be studied to anticipate difficulties of interpretation.

In this paper, we outline a matrix formulation which has been very successfully applied to a wide range of transient and static problems and then present the results of studies in which this method has been applied to simulate the common prompt decay experiment, the (β/Λ) or $(k\beta/\ell)$ technique, and the source-jerk experiment. Other formulations are possible, including the complete space-time iteration and numerical integration of the equations. We feel that the approach presented here better fills an important need for flexibility, however, and allows for easy manipulation of the results for performing subsidiary calculations and applying a variety of boundary conditions.

2. REVIEW OF MATHEMATICAL FORMALISM

In discussing reactor transients, the usual operator-vector form of the reactor kinetics equations is very effective in simplifying the mechanics of manipulating the equations. This approach leads naturally to a matrix formulation which is classical to other areas of mathematical physics, but which has not been extensively applied to reactor problems. Such an approach has been used by GARABEDIAN and his co-workers for a number of linear problems [2-4] and recently has been extended to the solution of certain non-linear problems [5].

For the problems to be discussed here it is convenient to write the reactor equations in the form

$$[L + (1 - \beta_T)f_p M]\,\phi + f_d \lambda C + S = v^{-1}\frac{\partial \phi}{\partial t} \tag{1}$$

and

$$\beta M \phi - \lambda C = \frac{\partial C}{\partial t}\,. \tag{2}$$

The symbols ϕ, C, and S refer to time-dependent vectors that are defined in a space whose co-ordinates in general represent position, direction and energy, and the remaining symbols refer to time-independent operators that transform vectors in this space. For example, L is a net loss operator that causes absorption and transfer of neutrons between different points of the phase space; M is a fission-source operator; and f_d and f_p are spectrum operators for delayed and prompt neutrons. The scalar β_T is the total number of delayed-neutron precursors formed per fission. Without further elaboration, it is sufficient to point out that the operations implied by Eqs. (1) and (2) may be understood by considering the operators to be matrices of operators and considering the terms in the sense of matrix products. Since the form of the operators is not specified, Eqs. (1) and (2) may be considered to be exact, and approximations are introduced only if, for example, diffusion theory or a P_ℓ approximation is employed in specifying the form of the operators.

If the vectors in Eqs. (1) and (2) are represented by expansions in terms of the functions W_ν which are solutions to Helmholtz's equation,

$$\nabla^2 W_\nu + B^2_\nu W_\nu = 0 \ , \tag{3}$$

the mathematics of the problem may be cast into the form of matrix equations in the multi-dimensional vector space defined by the W_ν as base vectors. The fluxes and precursor densities are then vectors represented by their time-dependent projections on the base vectors,

$$T_\nu(t) = (W_\nu, \phi(t)) \ , \tag{4}$$

and operators in Eqs. (1) and (2) are represented by time-independent matrices describing transformations of the base vectors,

$$L_{\mu\nu} = (W_\mu, LW_\nu) \ . \tag{5}$$

In computational terms typical matrices are illustrated by the forms

$$\Sigma_{\mu\nu} = \int W_\mu \Sigma W_\nu \ d\underline{r} \ d\underline{\Omega} \tag{6a}$$

and

$$(\nabla \cdot D\nabla)_{\mu\nu} = \int W_\mu \nabla \cdot D\nabla W_\nu \ d\underline{r} \ d\underline{\Omega} \tag{6b}$$

In practice the cross-sections will be region-wise constant and the above matrices may be computed analytically by summing region integrals involving only the functions W_ν. The formulae for these matrix elements are presented in Ref. [6] for cylindrical, spherical, and symmetrical and non-symmetrical slab geometries. Other details of the treatment may also be found in this reference.

3. EXPERIMENTS INVOLVING THE PROMPT TRANSIENT

It is convenient to make a distinction between transients involving principally the prompt fission neutrons and those in which the delayed neutron precursors exhibit a substantial time dependence.

In the first case we find it useful to reduce Eqs. (1) and (2) to a single matrix equation. This is accomplished by defining a composite vector,

$$\Phi = \begin{pmatrix} \Psi \\ C \end{pmatrix} \ , \tag{7}$$

and composite matrices

$$A' = \begin{pmatrix} L + (1 - \beta_T) f_p M & f_d \lambda \\ \beta M & -\lambda \end{pmatrix} \tag{8}$$

and

$$V = \begin{pmatrix} v & 0 \\ 0 & I \end{pmatrix} . \tag{9}$$

In terms of these, Eqs. (1) and (2) become

$$A\Phi + VS = \frac{\partial \Phi}{\partial t} , \tag{10}$$

where

$$A = VA' . \tag{11}$$

Equation (10) is a matrix equation with no explicit space dependence and represents a set of ordinary first-order linear differential equations in time only.

We may resort to several standard matrix techniques [6, 7] in solving Eq. (10), but the most useful for application to pulsing experiments is written in terms of the eigenvectors and eigenvalues of the matrix A. If these are defined by the equation

$$AX_\alpha = \omega_\alpha X_\alpha , \tag{12}$$

it is a straightforward matter to show that the solution to Eq. (10) may be written as

$$\Phi = - A^{-1}VS + \sum_\alpha C_\alpha X_\alpha e^{\omega_\alpha t} . \tag{13}$$

The constants C_α are determined by initial conditions and are obtained by applying vector matching conditions for each time at which the source is switched either on or off. If we select the initial condition $\Phi(0) = 0$, then Eq. (13) yields the result

$$\sum_\alpha C_\alpha(1)\ \omega_\alpha X_\alpha = VS , \tag{14}$$

where $C_\alpha(1)$ represents the set of C_α for the first source-on interval. The $C_\alpha(1)$ are easily obtained by solving Eq. (14) as a matrix equation, and the C_α for succeeding intervals may be shown to satisfy the following recursion relationship,

$$C_\alpha(n) = (-1)^{n-1}\ C_\alpha(1) + C_\alpha(n-1)\ e^{\omega_\alpha \Delta t_{n-1}} . \tag{15}$$

In Eq. (15) the source is assumed to be present during each odd-numbered interval. If all ω_α are negative, then the above recursion may be summed to obtain the results

$$C_\alpha^{on}(\infty) = C_\alpha(1)\ \frac{1 - e^{\omega_\alpha \Delta t_2}}{1 - e^{\omega_\alpha / R}} \tag{16}$$

and

$$C_\alpha^{off}(\infty) = - C_\alpha(1) \frac{1 - e^{\omega_\alpha \Delta t_1}}{1 - e^{\omega_\alpha / R}} \quad . \tag{17}$$

A uniform pulsing sequence has been assumed in which the source is on for a period Δt_1 and off for a period Δt_2, the repetition rate, R, being $1/(\Delta t_1 + \Delta t_2)$.

In presenting the above formulation we have attempted to emphasize the inherent simplicity of an entirely matrix approach. This emphasis is made not because it is basically new, but rather because the approach has been found to be highly flexible and easily adaptable to the reasonably exact treatment of a wide range of transient problems. This will be demonstrated in this section by studies of the usual prompt period and the β/Λ, (or $k\beta/\ell$) methods and in the following section by studies of the source-jerk experiment. Once standardized routines are available for generating the necessary matrix elements and for extracting eigenvectors and eigenvalues, a wide range of otherwise tedious operations may be reduced to simple matrix and vector manipulations.

All pulsing experiments studied for the EGCR are amply handled with about ten terms in the vector expansions, two neutron groups, and one delayed neutron precursor.* The generalized vector, Eq. (7), then has 30 components and the matrix A has 30 eigenvalues and corresponding eigenvectors. Ten of these eigenvalues lie near minus the precursor decay constant and are referred to as "delayed" modes. Ten others are the usual "prompt" modes, and the remaining ten are related to generation times and neutron multiplication during the slowing-down process. On the IBM-7090 computer a typical problem of the above size requires about 5 min of computing time to find all eigenvalues and eigenvectors and an additional minute to generate the transient fluxes for a prescribed pulsing sequence.

As an aid in selecting and planning pulsing experiments to be done during the commissioning programme of the Experimental Gas-Cooled Reactor (EGCR) we have studied a wide range of configurations to determine the nature of the transients and the means for interpreting them. The EGCR is a graphite-moderated heterogeneous reactor with fuel elements placed on an 8-in square lattice pitch. The fuel element consists of a cluster of seven rods of UO_2, enriched to 2.46%, and clad in stainless steel. A full core loading consists of 234 channels, but since the system may be made critical with a loading of $\sim$46 channels, a number of planned pulsing experiments involve highly reflected assemblies. It has been of special interest, then, to study the effect of the thick reflector on the average neutron generation time $\bar{\Lambda}$ and the effective delayed neutron yield, $\bar{\beta}$.

As a matter of convention we will always deal with Λ and β as defined in terms of the static reactivity, ρ_s [8, 9], which by definition is an eigenvalue of the equation

* The method has been applied, however, with up to six neutron groups and up to six delayed neutron precursors.

$$[L + (1 - \rho_s)\, f_s M]\, \varphi_s = 0 \,, \tag{18}$$

where, in terms of the operators in Eqs. (1) and (2), we have

$$f_s = (1 - \beta_T)\, f_p + f_d \beta \,. \tag{19}$$

In terms of ρ_s the inhour equation is written

$$\rho_s = \omega \left[\bar{\Lambda} + \sum_i \frac{\bar{\beta}_i}{\lambda_i + \omega} \right] , \tag{20}$$

where

$$\bar{\Lambda} = \frac{(\phi_s^+,\ v^{-1}\phi)}{(f_s^+ \phi_s^+,\ M\phi)} \,, \tag{21}$$

and

$$\sum_i \bar{\beta}_i = \bar{\beta} = \frac{(f_d^+ \phi_s^+,\ \beta M \phi)}{(f_s^+ \phi_s^+,\ M\phi)} \,. \tag{22}$$

If first-order perturbation theory is assumed to apply, that is assuming $\phi = \phi_s$, then $\bar{\Lambda}$ and $\bar{\beta}$ are equal respectively to the changes in ρ_s associated with a poison addition equal to $1/v$ and with the removal of the delayed neutrons [10, 11]. In highly reflected systems, however, we have found that the transient neutron distributions show a significant dependence on the period, with the result that first-order perturbation theory is a poor approximation in computing the neutron generation time. This is illustrated by studies we have made of the expected initial approach-to-criticality for the EGCR. For loadings from 20 channels up to the critical loading of ~46 channels we have computed the generation time by evaluating Eq. (21) using both the transient flux vector and the static flux vector. The result is illustrated in Fig. 1. It may be seen that the static approximation becomes progressively poorer as the prompt decay constant increases. This is to be expected, of course, and results from the distortion of the static distribution by the long neutron storage time in the reflector. The distortion characteristic of these cases is illustrated in Fig. 2 for a 30 channel loading. This distortion can become quite pronounced even for normal reflector thicknesses if the period is sufficiently short, as may be seen from the result for a full core loading with all control rods inserted shown in Fig. 3.

A number of other cases have been studied and are presented in Table I. Without exception the generation time increases as the systems studied here are made more subcritical. Of particular interest are the cases in which control rods are inserted into cores of fixed size.

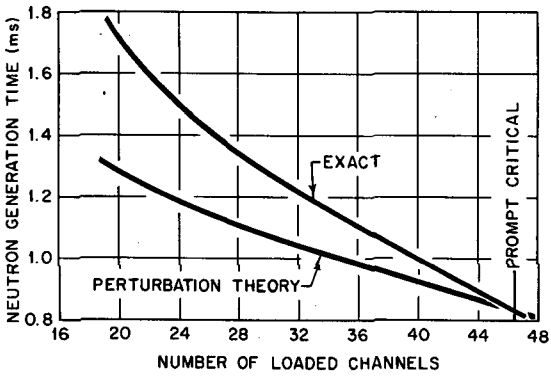


Fig. 1

Variation of neutron generation time during the approach to the minimum critical core

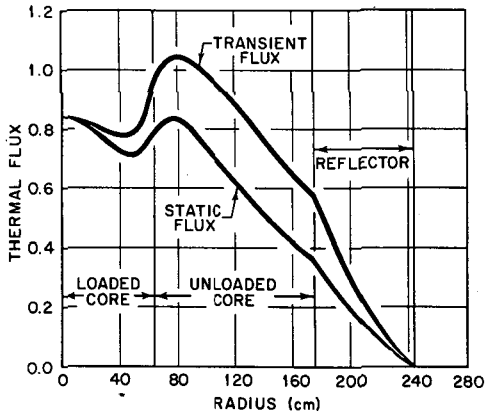


Fig. 2

Comparison of fundamental prompt and static modes in the 30 channel core

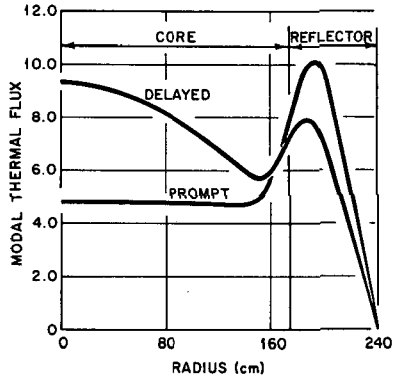


Fig. 3

Comparison of fundamental prompt and delayed modes in the full core with all control rods inserted

TABLE I

KINETICS PARAMETERS FOR PULSING EXPERIMENTS IN APPROACH TO CRITICAL FOR EGCR

Number of loaded channels	Number of control rods inserted	ρ_s	ω (s^{-1})	$\bar{\Lambda}$ (ms)	$\bar{\beta}/\beta$	$\bar{\beta}/\bar{\Lambda}$ (s^{-1})
20	None	- 0.1313	- 80.5	1.717	1.0530	4.029
30	None	- 0.0657	- 56.6	1.281	1.0444	5.357
40	None	- 0.0166	- 23.4	1.000	1.0374	6.816
44	None	- 0.0097	- 17.9	0.925	1.0341	7.345
44	1	- 0.0814	- 68.7	1.285	1.0352	5.292
44	4	- 0.1677	- 129.1	1.352	1.0418	5.062

The variations of the effective delayed neutron yields β are considerably less pronounced than those of the neutron generation time. For the quantity β, in fact, we have found that the first-order perturbation theory is essentially exact. Using this approximation, that is by computing the change in ρ_s resulting from the removal of the delayed neutrons, we obtain the results presented in Table I. The accuracy of this approximation has been checked by evaluating Eq. (22) for the 20 channel loading using the transient flux vector. The value $\bar{\beta}/\beta = 1.0539$ obtained by this method verifies the accuracy of the approximation even for this reasonably extreme case.

The low sensitivity of β to flux distortion by the transient is to be expected from the examination of Eq. (22) and has been pointed out by several authors [9, 11, 12]. It is apparent from Eq. (22) that $\bar{\beta}$ will be sensitive to distortions in the flux spectrum at source energies, but in contrast with Λ is independent of the neutron distribution in the reflector.

Before proceeding to other types of experiments it is instructive to examine certain properties of modes higher than the fundamental. With six delayed neutron precursors it is well known that the galaxy of modes group into clusters of seven, not including those mentioned previously which are associated with the slowing-down process, and that each cluster is associated with a different value of the reactivity appearing in Eq. (20). It has been speculated that the neutron spatial distributions are nearly the same for all modes of a given cluster and that successive clusters may be distinguished by counting the number of zeros of the distributions [13]. We have found that these properties can be ascribed to the modes of simple systems only and are largely inapplicable to the prompt modes of highly reflected systems. The six delayed modes of a cluster are found to be quite similar to the static neutron distribution since these modes represent reasonably slow transients, the decay constants being nearly equal to the six values of λ_i for the precursors. The remaining mode may appear quite differently, however, as already illustrated in Figs. 2 and 3. Regarding the number of zeros in the distributions for higher-order clusters we have

found the situation to be rather complex. Within a given cluster the number of zeros in the thermal neutron distributions appears to be the same for all modes, but the positions of the zeros of the prompt mode may be quite different from those of the delayed modes. The epithermal neutron distributions, on the other hand, may contain a number of zeros quite unrelated to that of the thermal distribution. These properties are illustrated by the distributions presented in Fig. 4, which represent a 90-channel loading of

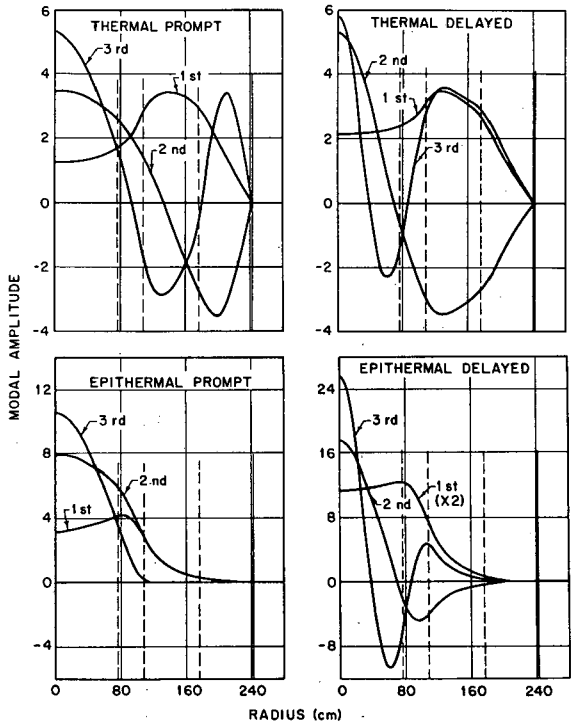


Fig. 4

Modal flux distributions in the 90 channel core with five central control rods inserted

the EGCR with the central five control rods fully inserted. The central zone, which contains 45 channels, is thus highly subcritical and this is surrounded by 45 additional loaded channels, 144 empty channels and a solid reflector. The calculations presented here include two neutron groups and one delayed neutron precursor with an effective decay constant taken to be $\lambda = 0.08\ s^{-1}$.

A typical pulsing experiment has been simulated for this loading, with a pulse length of either 10 ms or 50 μs and a repetition rate of 2 s^{-1}. The modal reactivities, decay constants, certain of the generation times, and modal amplitudes during the decay are presented in Table II for the first three clusters of modes.

A great amount of useful information may be obtained from a simulation such as that presented here for the 90 channel loading. The large difference in shape between the prompt and delayed modes is immediately apparent

TABLE II

KINETICS PARAMETERS FOR PULSING EXPERIMENT IN 90 CHANNEL CORE WITH FIVE CENTRAL CONTROL RODS INSERTED
$R = 2\ s^{-1}$, $\lambda = 0.08\ s^{-1}$

Mode	ρ_s	ω (s^{-1})	$\bar{\Lambda}$ (ms)	C ($n/cm^2\ s$)	
				$\Delta t_1 = 10$ ms	$\Delta t_1 = 50\ \mu s$
1st prompt	- 0.09394	- 90.492	0.9634	1.00	1.000
1st delayed		- 0.074625		2.573×10^{-3}	1.662×10^{-3}
2nd prompt	- 0.80771	- 543.93	1.4725	0.373	1.342
2nd delayed		- 0.079336		4.280×10^{-5}	2.762×10^{-5}
3rd prompt	- 2.89122	- 936.77	3.0791	0.192	1.183
3rd delayed		- 0.079813		7.510×10^{-7}	4.849×10^{-7}

from Fig. 4, for example. The zero of the second prompt mode occurs at nearly the peak of the second delayed mode, and these cannot both be eliminated by the selection of detector or source positions. The maximum ratio of fundamental prompt to fundamental delayed modes occurs at the zero of the second prompt mode, however, and this would thus appear to be a good selection for the detector position. The advantage of long pulses for this experiment is apparent from the results presented in Table II. With a 50-μs pulse width we have $\omega \Delta t_1 \ll 1$ for the prompt modes and their relative amplitudes are then proportional to their decay constants ω. With $\Delta t_1 = 10$ ms, on the other hand, all prompt modes except the fundamental have reached their saturated amplitude and a more favourable modal balance is achieved. Further increases in pulse length, of course, will begin to saturate the fundamental prompt mode and will only contribute to the delayed mode amplitudes.

The value of theoretical simulation of experiments is well illustrated by a study of the $(\bar{\beta}/\bar{\Lambda})$ technique for complicated configurations. In the context of a one-group model for a uniform bare reactor it has been shown [14, 15] that $\bar{\beta}/\bar{\Lambda}$ may be obtained from the condition

$$I_2 - I_1 = \frac{N_d}{R}\ , \tag{23}$$

where

$$I_2 = \int_0^{1/R} N_p e^{(\bar{\beta}/\bar{\Lambda})t}\, dt \tag{24}$$

and

$$I_1 = \int_0^{1/R} N_p\, dt\ , \tag{25}$$

with N_d and N_p being the delayed and prompt components of the total transient, and R, as before, the pulse repetition rate.

Certain conditions for the validity of Eq. (23) have been pointed out previously [13-16] and may be summarized as follows:

(1) β/Λ must be the same for all modes.

(2) All modes of a given cluster must have the same spatial distribution.

(3) $R \gg \lambda_i$, λ_i = precursor decay constants.

(4) $R \ll -\omega_o$, ω_o = decay constant of fundamental prompt mode.

It should be pointed out in addition, however, that important limitations result from the assumption in the treatment that $S(x,t) = S_o\delta(x)\delta(t)$ and that condition four above should actually be written $R \ll -(\omega_o + \beta/\Lambda)$. Since $-\omega_o \to \bar{\beta}/\bar{\Lambda}$ as $\rho \to 0$, the latter requirement is inconsistent with condition three and precludes the possibility of applying Eq. (23) to nearly critical systems. Regarding the delta function source, two points should be made. If condition two above is violated, then departures of the source from $\delta(x)$ will affect the ratio of N_p to N_d and Eq. (23) will not apply. Also, if S departs from $\delta(t)$ then, again, N_p/N_d will be changed, as may be seen from Eq. (17), and again Eq. (23) will not apply. For the modified condition four, with pulses of width Δt_1 and $R = 1/(\Delta t_1 + \Delta t_2)$, it can be shown that Eq. (23) is correct for a mode with prompt decay constant ω if written

$$I_2 - I_1 = N_d \Delta t_2 \left[\frac{e^{\omega \Delta t_1} - 1}{\omega \Delta t_1} \right] \left[1 + \frac{\rho - \bar{\beta}}{\bar{\beta}} e^{(\rho/\bar{\Lambda})\Delta t_2} \right] . \qquad (26)$$

The first correction factor in Eq. (26) accounts for changes in N_p/N_d arising from saturation effects in prompt modes when long pulses are used. The second arises if $-(\omega + \beta/\Lambda)$ is not large compared to the repetition rate, that is, if the system is near critical. A possible conflict of requirements thus arises concerning the optimum pulse length. By using a pulse length $\Delta t_1 \sim 1/\omega_o$ we may make a significant reduction in the amplitudes of higher prompt modes relative to the fundamental prompt mode, but a serious correction would then arise due to the saturation of this mode. We have found by theoretical simulation of this experiment, however, that the effects of higher prompt modes are largely unimportant for systems like the EGCR, even with very short pulses. The contribution of successive prompt modes to the term $I_2 - I_1$ falls approximately as $(1/\omega)^2$ and the higher delayed modes are observed to be excited to low amplitudes only. In many important cases, however, condition two above is badly violated and the experiment has a gross space dependence if interpreted in terms of Eqs. (23) or (26). If calculations of the modal distributions are performed then corrections may be applied for the apparent space dependence of $\bar{\beta}/\bar{\Lambda}$, or alternatively, the experiment may be performed with several detectors and analysed in a manner similar to that presented for the source-jerk experiment in the following section.

The degree of space dependence possible is illustrated in Fig. 5 for the case of the 90 channel core described above. In this case almost no effect is present owing to the higher modes and the space dependence is caused by different spatial distributions for the fundamental prompt and delayed modes.

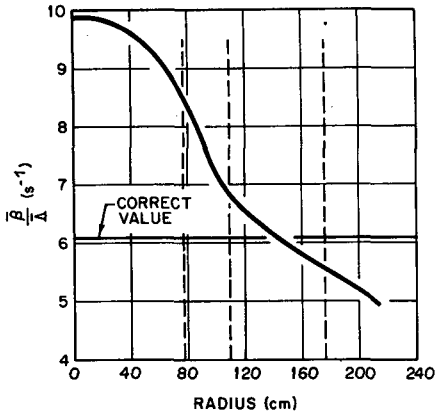


Fig. 5

Apparent space dependence of $\bar{\beta}/\Lambda$ for a single detector placed at various positions in the 90 channel core

4. EXPERIMENTS INVOLVING THE TOTAL TRANSIENT

Although the $(\bar{\beta}/\Lambda)$ technique may be considered to involve the total transient, that is, both the prompt and delayed transients, this technique is designed to minimize the magnitude of the delayed transient and we have considered it in the previous section. A better example is provided by the source-jerk experiment first described by SCHMID [17]. It should be noted, however, that the interpretation of the experiment discussed here is different from that presented in Refs. [13 and 18] under the same name.

In the source-jerk experiment, we consider that the system has reached a steady state for some initial extraneous source vector S_o. At $t = 0$, a fixed source is removed and the extraneous source vector becomes S, which for the usual case will be a source resulting from spontaneous fission or (γ, n) and (γ, f) reactions caused by fission-product decay gamma rays. Three vectors are defined, with reference to the formalism established in section 2,

$$\psi(t_o) = \int_o^{t_o} \phi(t)\, dt \,, \tag{27}$$

$$R(t_o) = \int_o^{t_o} \lambda C(t)\, dt \,, \tag{28}$$

and

$$N(t_o) = \int_o^{t_o} S(t)\, dt \,. \tag{29}$$

Equations (1) and (2) are integrated from $t = 0$ to $t = t_o$, and $R(t_o)$, $C(0)$, and

$C(t_o)$ are eliminated by assuming steady states to exist at $t = 0$ and $t = t_o$. The result is

$$[L + f_s M]\,\psi(t_o) = -\,[f_d \lambda^{-1}\beta M + v^{-1}]\,[\phi(0) - \phi(t_o)] - N(t_o)\ , \qquad (30)$$

which includes the static spectrum operator defined by Eq. (19).

Equation (30) is the basic relationship that is satisfied by the measurable quantities, namely $\psi(t_o)$, $\phi(0)$, and $\phi(t_o)$, but does not within itself relate these to the reactivity of the system. The absence of any reference to reactivity results from the fact that the reactivity is a separately definable quantity. It is a global parameter for the reactor that is a particular average over the system with an arbitrary weighting function (see, for example, the papers by GROSS and MARABLE [8] and by GOZANI [9]). Although it is not necessarily the most meaningful, only the static reactivity defined by Eq. (18) is considered here because it is the most familiar in reactor calculations.

For any real operator A an adjoint operator A^+ can be defined that satisfies the relations

$$(X, AY) = (A^+X, Y) = (Y, A^+X)\ , \qquad (31)$$

where X and Y are two vectors defined in the same space as A. By defining such adjoints for the operators in Eq. (18), this equation may be written in the equivalent form

$$[L' + (1 - \rho_s)M^+ f_s^+]\,\phi_s^+ = 0\ , \qquad (32)$$

where ϕ_s^+ will be called the static adjoint vector.

At $t = t_o$ a static condition is assumed in the system so that

$$[L + f_s M]\,\phi(t_o) + S = 0\ , \qquad (33)$$

with which, by integrating from $t = 0$ to $t = t_o$, we obtain

$$[L + f_s M]t_o\,\phi(t_o) + N(t_o) = 0\ . \qquad (34)$$

Taking the scalar products of ϕ_s^+ with Eq. (34), $t_o\,\phi(t_o)$ with Eq. (32) and subtracting the resulting equations gives

$$(\phi_s^+, N[t_o]) = -\,\rho_s\ t_o(\phi_s^+, f_s M\phi[t_o])\ , \qquad (35)$$

where use has been made of Eq. (31).

Returning to Eq. (30), we take the scalar products of ϕ_s^+ with this equation and $\psi(t_o)$ with Eq. (32) and subtract the resulting equations. After making use of Eqs. (31) and (35), one obtains for the solution of ρ_s

$$\rho_s = -\,\frac{(f_s^+\phi_s^+, M[\phi(0) - \phi(t_o)])}{(f_s^+\phi_s^+, M[\psi(t_o) - t_o\phi(t_o)])}\,(\beta_T\bar{\Lambda}_c + \bar{\Lambda}_n)\ , \qquad (36)$$

where

$$\overline{\Lambda}_c = \frac{1}{\beta_T} \frac{(f_d^+\phi_s^+, \lambda^{-1}\beta M[\phi(0) - \phi(t_o)])}{(f_s^+\phi_s^+, M[\phi(0) - \phi(t_o)])} , \tag{37}$$

and

$$\overline{\Lambda}_n = \frac{(\phi_s^+, v^{-1}[\phi(0) - \phi(t_o)])}{(f_s^+\phi_s^+, M[\phi(0) - \phi(t_o)])} . \tag{38}$$

Equation (36) has been obtained using a completely general form of the reactor equations, and since no assumptions have been made concerning the form of the operators in these equations it follows that Eq. (36) is an exact relationship. It constitutes only a formal identity, however, unless its terms may be evaluated for a practical experiment.

The significance of the quantities Λ_c and Λ_n may easily be seen by reference to previous relationships. If the system is in a steady state, then $\lambda^{-1}\beta M\phi$ is a vector that represents the precursor concentration, as may easily be seen from Eq. (2). Likewise, $\beta_T M\phi$ is a vector representing the precursor production rate. The quantity Λ_c is thus the average precursor generation time with the weights explicitly displayed in Eq. (37). In a similar manner, it may be seen that Λ_n is an average neutron generation time.

In perhaps more familiar terms Λ_c may be related to the effective delayed neutron yields. It is not difficult to show that

$$\overline{\Lambda}_c = \frac{1}{\beta_T} \sum_i \frac{\overline{\beta}_i}{\lambda_i} , \tag{39}$$

where the $\overline{\beta}_i$ are averages analogous to Eq. (22), but with ϕ replaced by $\phi(0) - \phi(t_o)$.

It is important to note several properties of Eq. (36) that affect its evaluation in any practical experiment. It may be observed that the appropriate quantities to measure are $M\phi$ and $M\psi$. For a uniform fuel composition, these can be measured exactly with a fission chamber but only approximately with a BF_3 chamber. The difference between these two measurements, of course, will depend on the difference between the thermal and epithermal flux distribution and on the amount of epithermal fission. In principle, $f_s^+\phi_s^+$ may also be measured, since it is proportional to the reactivity change caused by a lump of fissionable material. This measurement is probably only practical, however, for a critical state. The crucial items in the analysis of this experiment are the number of detectors necessary and the accuracy required for the weighting function. Both of these are fixed by the difference between $M\phi$ and $M\psi$, since, if these have identical shapes, the ratio of averages will be independent of the weight.

To simulate the problems of analysing source-jerk experiments with the above approach we have applied the matrix formulation described earlier to the solution of the above equations. Equations (30) and (32) are solved to obtain $\psi(\infty)$ and ϕ_s^+, and Eq. (33) is solved with $S = S_o$ to obtain $\phi(0)$. Equations (36), (37) and (38) are then evaluated to obtain ρ_s, $\bar{\Lambda}_c$ and $\bar{\Lambda}_n$ respectively. The calculation is done with six neutron groups and six delayed-neutron precursors. The selection of neutron group structure was made to distinguish between prompt and delayed source neutrons, in order to obtain realistic values for $\bar{\Lambda}_c$ (or β_i), as described above.

In obtaining the solutions necessary for the evaluation of Eq. (36), the spatial dependence of the functions $M\phi(0)$ and $M\psi$ is computed and the results that would be obtained with different types of detectors located at various positions in the core are studied. Of particular importance, of course, is the sensitivity of Eq. (36) to the number, type and position of detectors whose counting data are used to perform the indicated integrals. The fully loaded EGCR with one atmosphere of air pressure and all control rods inserted is a typical case of interest. For this reactor, $\rho_s = -0.1226$.

For cylindrical geometry, the reactivity is expressed principally in terms of the functions of $rf_s^+\phi_s^+M\phi(0)$ and $rf_s^+\phi_s^+M\psi(t_o)$, which are shown in Fig. 6. These spatial distributions are the basic functions to be determined from the experimental measurements, and the ratio of areas under these curves is the multiplier in Eq. (36) that expresses the reactivity in terms of the quantity $(\beta_T\bar{\Lambda}_c + \bar{\Lambda}_n)$, which, presumably, is known.

The significance of the static reactivity as an average for the core is emphasized by Fig. 7, in which the apparent reactivity is compared with the actual reactivity when the experiment is done with a single detector placed

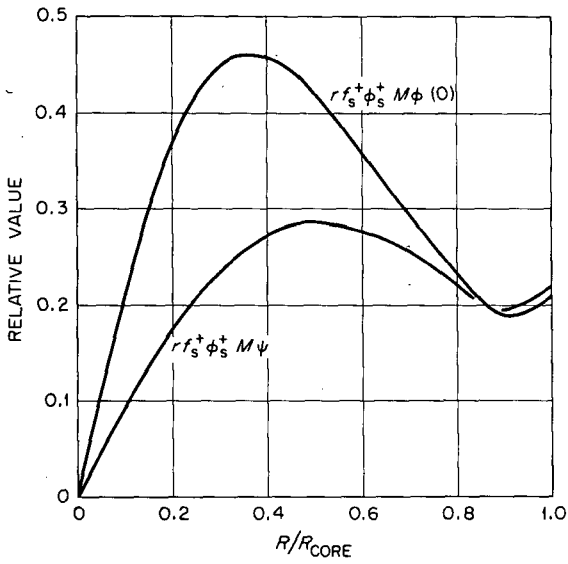


Fig. 6

Spatial variation of the weighted initial source and the weighted integrated source in the full core with all control rods inserted

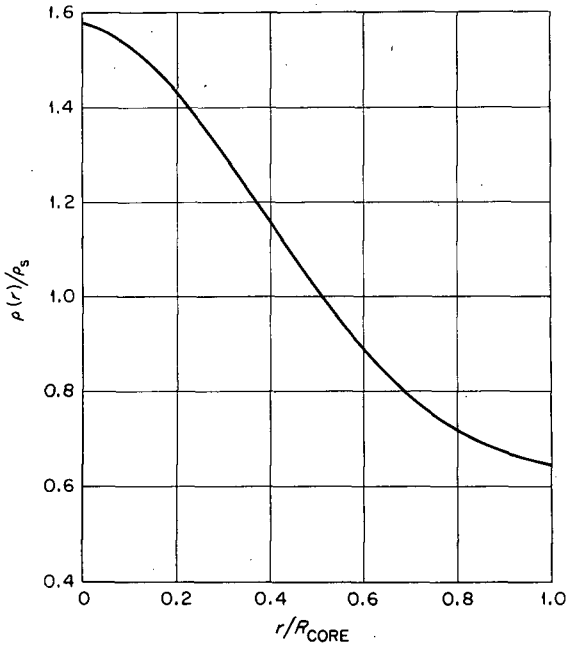


Fig. 7

Comparison of the true reactivity and the apparent reactivity from a single detector placed at various positions in the full core with all control rods inserted

at various positions within the core. For this case it is apparent that the reactivity could be determined exactly from a single detector placed at a radius of 0.51 times the core radius. For other detector positions this figure gives a spatially dependent correction factor that would have to be applied to the data from a single detector.

The effect on the experiment of the number and placement of detectors may be determined from a study of Fig. 6. For example, with three detectors placed at 0.2, 0.4 and 1.0 times the core radius and assuming a linear variation between detectors, the resulting integrals give $\rho = -0.1274$, which is in error by 4%. If an additional detector is placed at 0.8 times the core radius, we obtain $\rho = -0.1233$, and the error is reduced to 0.5%. On the basis of this example it appears that an accurate value of the reactivity may be obtained with relatively few detectors.

For the case studied here we obtain, $\Lambda_n = 0.4592$ ms, $\beta_T \Lambda_c = 0.08397\ s^{-1}$, and $\bar{\Lambda}_c / \Lambda_c = 1.0113$. The term in Eq. (36) involving the neutron generation time thus represents an 0.5% contribution to the reactivity, and the distinction between β_i and $\bar{\beta}_i$ introduces a 1% effect on the reactivity. Also, for this case, the reactivity obtained from measurements made with 1/v detectors differs by only 0.1% from that obtained with fission chambers.

The conditions under which this experiment may be space-independent are extremely complex, since this requires that $\psi(t_o)$ be proportional to $\phi(0)$ in the multiplying region, and it appears that this condition can never be rigorously fulfilled. Even if the reactor is excited to a flux distribution

TABLE III

EFFECT OF HIGH SOURCE ENERGY ON SPACE DEPENDENCE OF SOURCE-JERK REACTIVITY

r/R_{core}	Case description					
	30 channels, no control rods, 1 atm $\rho_s = -0.0704$		90 channels, five control rods, 1 atm $\rho_s = -0.0939$		Full core, all control rods, 1 atm $\rho_s = -0.1226$	
	τ (cm^2)		τ (cm^2)		τ (cm^2)	
	0	700	0	700	0	700
0.0	-0.0777	-0.0699	-0.1899	-0.1216	-0.2955	-0.1937
0.2	-0.0765	-0.0703	-0.1600	-0.1172	-0.2021	-0.1754
0.4	-0.0734	-0.0702	-0.1158	-0.1070	-0.1310	-0.1413
0.6	-0.0700	-0.0702	-0.0913	-0.0952	-0.0969	-0.1095
0.8	-0.0677	-0.0705	-0.0790	-0.0872	-0.0781	-0.0883
1.0	-0.0668	-0.0711	-0.0753	-0.0841	-0.0704	-0.0794

containing only a single transient mode, the precursor densities will be in improper balance with the neutron density for the mode and a significant space dependence will develop. Even if the experiment were possible in a critical reactor we can show from Eq. (30) that space-dependent terms persist which relate to the difference in energy spectrum of the prompt and delayed neutrons. In practical cases this latter difference may only be formal, however, and the experiment approaches space independence for near-critical systems.

An important improvement results for the space dependence in some cases if the experiment is performed with 14-MeV source neutrons rather than with the lower energy Po-Be sources commonly used for the measurement [19]. This results from the significant suppression of higher modes brought about by the diffusion of the external source neutrons into an extended spatial distribution. The neutron age in graphite for source neutrons originating at 14 MeV has been computed using the continuous slowing-down model with the data given in Ref. [20]. At the median fission source energy of 1.6 MeV the age of 14-MeV source neutrons is 532 cm^2 for a graphite density of 1.7 g/cm^3. The corresponding figure for Po-Be neutrons is 127 cm^2. In a typical gas-cooled reactor this will be increased by $\sim 35\%$ due to the presence of voids, with the result that the age of 14-MeV source neutrons will normally be ~ 700 cm^2.

If age theory is applied to the slowing-down problem between 14-MeV and fission source energies, then for a finite uniform medium it is not dif-

ficult to show that an initial source vector with elements S_ν^o is replaced by a vector with elements given by

$$S_\nu = S_\nu^o \, e^{-B_\nu^2 \tau} , \qquad (40)$$

where the B_ν^2 are the usual bucklings which are eigenvalues of Eq. (3). The marked effect of this diffusion, into an extended source is illustrated in Table III for several loadings. As would be expected, the space dependence is greatly suppressed when the extended source overlaps the entire loading, and the effect decreases as the size of the loading increases.

REFERENCES

[1] Experimental gas-cooled reactor final hazards summary report I, USAEC Rpt ORO-568 (10 Oct. 1962).

[2] GARABEDIAN, H.L. and THOMAS, D.H., An analytic approach to two-dimensional reactor theory, Nucl. Sci. Engng 14 (1962) 266-71.

[3] GARABEDIAN, H.L. and LEFFERT, C.B., A time-dependent analysis of spatial flux distributions, Nucl. Sci. Engng 6 1 (1959) 26-32.

[4] GARABEDIAN, H.L. and FODERARO, A., A new method for the solution of group diffusion equations, Nucl. Sci. Engng 8 1 (1960) 44-52.

[5] GARABEDIAN, H.L. and LYNCH, R.E., Nonlinear reactor kinetics, Nucl. Sci. Engng 21 4 (1965) 550-69.

[6] PRESKITT, C.A. and NEPHEW, E.A., Transients induced by pulsed neutron sources in multiregion reactors, USAEC Rpt ORNL-TM-993, Oak Ridge National Lab. (Jan. 1965).

[7] CODDINGTON, E.A. and LEVINSON, N., Theory of Ordinary Differential Equations, McGraw-Hill Book Co., Inc., N.Y. (1955).

[8] GROSS, E.E. and MARABLE, J.H., Static and dynamic multiplication factors and their relation to the inhour equation, Nucl. Sci. Engng 7 4 (1960) 281-91.

[9] GOZANI, T., The concept of reactivity and its application to kinetic measurements, Nucleonik 5 2 (1963) 55.

[10] HENRY, A.F., Computation of parameters appearing in the reactor kinetics equations, USAEC Rpt WAPD-142 (Dec. 1955).

[11] HENRY, A.F., Application of reactor kinetics to the analysis of experiments, Nucl. Sci. Engng 3 (1958) 52.

[12] LEWINS, J., The use of the generation time in reactor kinetics, Nucl. Sci. Engng 7 2 (1960) 122.

[13] HENRY, A.F., The application of inhour modes to the description of non-separable reactor transients, Nucl. Sci. Engng 20 (1964) 338-51.

[14] GARELIS, E. and RUSSELL, J.L., Jr., Theory of pulsed neutron source measurements, Nucl. Sci. Engng 16 (1963) 263-70.

[15] GARELIS, E., Theory of pulsing techniques, Nucl. Sci. Engng 18 2 (1964) 242.

[16] WALLACE, S.K., A note on the analysis of pulsed neutron shutdown measurements, Nucl. Sci. Engng 21 1 (1965) 116.

[17] SCHMID, P., Absolute reactivity measurement from transient behavior of a subcritical nuclear reactor, RAG-Bericht Nr. 1 (June 1957).

[18] JANKOWSKI, F.J., KLEIN, D. and MILLER, T.M., Calibration of control rods, Nucl. Sci. Engng 2 (1957) 288-302.

[19] PRESKITT, C.A., Solutions to the age equation in finite systems with an application to pulsed source experiments, USAEC Rpt ORNL-TM-765, Oak Ridge National Lab. (13 Dec. 1963).

[20] JOANOU, G.D., GOODJOHN, A.J. and WIKNER, N.F., Legendre expansion coefficients for the angular distribution of elastically scattered neutrons and fast-neutron cross sections for beryllium, deuterium, carbon, oxygen, zirconium, lead, and bismuth, USAEC Rpt GA-2156 (15 May 1961).

THE MEASUREMENT OF REACTIVITY IN MULTI-REGION SUBCRITICAL SYSTEMS BY THE PULSED NEUTRON TECHNIQUE

J. SHERWIN AND J.H. LENG
UNITED KINGDOM ATOMIC ENERGY AUTHORITY,
WINDSCALE WORKS, CUMBERLAND, UNITED KINGDOM

Abstract — Résumé — Аннотация — Resumen

THE MEASUREMENT OF REACTIVITY IN MULTIREGION SUBCRITICAL SYSTEMS BY THE PULSED NEUTRON TECHNIQUE. The prompt decay of a thermalized burst of neutrons in a multiregion subcritical system is examined using a two-group diffusion theory. It is shown that a relationship can be established between the prompt decay constant of the fundamental mode and the effective multiplication factor of the system in terms of two parameters, defined, for the purposes of this paper, as the reactor response coefficient and the prompt decay correction and which depend to a large extent on the spatial flux patterns within the system.

For the uniform bare system, the response coefficient can be identified with the mean neutron lifetime in the system; for a multiregion system it represents a compound of the lifetimes in each region weighted by perturbation type integrals. The second parameter, the decay correction, can have no physical meaning in that it arises from an attempt to relate the two scales of reactivity involved; that is the scale using the prompt decay constant and the scale derived using the effective multiplication factor.

The properties of these parameters are examined here with reference to an enriched uranium graphite-moderated reactor consisting of uniform core and reflector and it is shown that the two parameters are not uniquely defined by the reactivity of the system but depend on the method chosen to make the system subcritical.

Two sets of measurements are treated by the theory. In one, the Windscale Advanced Gas-Cooled Reactor was shut down by a uniform poison. In the other the reactivity of a core in the zero-energy reactor HERO was varied by altering the loaded radius. The neutron pulse measurements are all shown to be in good agreement with more conventional methods of reactivity determination. Some discussion of the experimental techniques and the difficulties encountered in the graphite-moderated systems is presented.

MESURE DE LA RÉACTIVITÉ DANS LES SYSTÈMES SOUS-CRITIQUES A PLUSIEURS RÉGIONS PAR LA MÉTHODE DES NEUTRONS PULSES. Les auteurs étudient la décroissance des neutrons instantanés d'une bouffée thermalisée de neutrons dans un système sous-critique à plusieurs régions, au moyen d'une théorie de diffusion à deux groupes. Ils montrent qu'on peut établir un rapport entre la constante de décroissance du mode fondamental des neutrons instantanés et le facteur de multiplication effectif du système en fonction de deux paramètres qui ont été définis, aux fins du présent mémoire, comme le coefficient de réponse du réacteur et le facteur de correction pour la décroissance des neutrons instantanés et qui dépendent dans une large mesure des structures de flux spatiales à l'intérieur du système.

Pour le système uniforme sans réflecteur, le coefficient de réponse peut être considéré comme étant identique à la durée de vie moyenne des neutrons dans le système; pour un système à plusieurs régions, c'est une moyenne des durées de vie dans toutes les régions pondérées par des intégrales du type à perturbation. Le deuxième paramètre – le facteur de correction pour la décroissance – ne peut avoir aucune signification physique, en ce sens qu'il ressort d'une tentative faite pour établir une relation entre les deux échelles de réactivité, savoir l'échelle que l'on obtient en utilisant la constante de décroissance des neutrons instantanés et celle que l'on obtient en utilisant le facteur de multiplication effectif.

Les auteurs étudient les propriétés de ces paramètres en se référant à un réacteur à uranium enrichi ralenti au graphite, qui se compose d'un cœur uniforme et d'un réflecteur; ils montrent que les deux paramètres ne sont pas définis uniquement par la réactivité du système, mais dépendent de la méthode choisie pour rendre le système sous-critique.

Deux séries de mesures sont traitées d'une manière théorique. Dans l'une, le réacteur à gaz poussé de Windscale a été arrêté par un poison uniforme. Dans l'autre, on a fait varier la réactivité d'un cœur du

réacteur HERO de puissance zéro en modifiant le rayon de la charge. Les auteurs montrent que toutes les mesures faites au moyen des neutrons pulsés sont en bon accord avec les résultats des méthodes classiques de détermination de la réactivité. Ils discutent les méthodes expérimentales utilisées et les difficultés rencontrées dans les systèmes ralentis au graphite.

ИЗМЕРЕНИЕ РЕАКТИВНОСТИ В МНОГОЗОННЫХ ПОДКРИТИЧЕСКИХ СИСТЕМАХ МЕТОДОМ ИМПУЛЬСНЫХ НЕЙТРОНОВ. Мгновенный распад термализованной вспышки нейтронов в многозонной подкритической системе изучался с помощью двухгрупповой теории диффузии. Показывается, что можно установить связь между постоянной мгновенного распада основного состояния и коэффициентом эффективного размножения системы в рамках двух определенных параметров для целей публикуемого доклада в качестве коэффициента чувствительности реактора и поправки на мгновенный распад, которые зависят в большой степени от пространственного размещения потоков в системе.

При однородной системе без отражателя коэффициент чувствительности можно установить при определении среднего периода жизни нейтрона в системе, для многозонной системы такой коэффициент представляет собой сочетание периодов жизни в каждой зоне, усложненных интегралами возмущения. Второй параметр, поправка на распад может не иметь физического смысла в связи с тем, что она появляется при попытке установить связь между двумя соответствующими масштабами реактивности, то-есть масштабом при определении которого используется постоянная мгновенного распада, и масштабом, выводимым с использованием коэффициента эффективного размножения.

Изучаются свойства этих параметров с упором на реактор с обогащенным ураном и графитовым замедлителем, состоящий из однородной активной зоны и отражателя, и показывается, что эти два параметра не определяются однозначно размером реактивности системы, а зависят от избранного метода доведения системы до состояния подкритичности.

Оба вида измерений рассматриваются в теории. В одном случае усовершенствованный реактор с газовым охлаждением в Уиндскейле был остановлен в результате равномерного отравления. В другом случае реактивность активной зоны в реакторе нулевой мощности HERO изменялась путем изменения радиуса загрузки. Результаты измерений импульсов нейтронов хорошо согласуются с результатами определения реактивности более обычными методами. Проводится некоторое обсуждение экспериментальных методов и трудностей, возникающих при использовании систем с графитовым замедлителем.

MEDICIONES DE LA REACTIVIDAD EN SISTEMAS SUBCRITICOS DE VARIAS REGIONES MEDIANTE LA TECNICA DE LOS NEUTRONES PULSADOS. Los autores estudian el decrecimiento inmediato de una ráfaga de neutrones termalizados en un sistema subcrítico de varias regiones, empleando una teoría de difusión de dos grupos. Demuestran que es posible establecer una relación entre la constante de decrecimiento inmediato del modo fundamental y el factor de multiplicación efectiva del sistema eligiendo dos parámetros que, para los fines de la presente memoria se definen como el coeficiente de respuesta del reactor y como la corrección del decrecimiento inmediato, los cuales dependen en gran medida de la distribución espacial del flujo en el interior del sistema.

En el caso de un sistema uniforme desprovisto de reflector, el coeficiente de respuesta puede identificarse con la vida media de los neutrones en el sistema; en el caso de un sistema de varias regiones, ese coeficiente representa una combinación de la vida media de los neutrones en cada región, ponderada por integrales del tipo de perturbación. En cuanto al segundo parámetro – la corrección del decrecimiento –, puede carecer de significado material en el sentido de que deriva de un intento de relacionar las dos escalas de reactividad que intervienen en el problema, es decir, la escala obtenida con la constante de decrecimiento inmediato y la escala obtenida empleando el factor de multiplicación efectiva.

Los autores examinan las propiedades de estos parámetros en el caso de un reactor de uranio enriquecido moderado con grafito y constituido por un cuerpo y un reflector uniformes, y ponen de manifiesto que los dos parámetros no quedan definidos únicamente por la reactividad del sistema, sino que dependen del método elegido para hacer que el sistema resulte subcrítico.

Los autores tratan por métodos teóricos dos conjuntos de mediciones. Uno de ellos se obtuvo en el reactor avanzado de Windscale, refigerado con gas, cuyo funcionamiento se interrumpió deliberadamente por un envenenamiento uniforme. En el segundo caso se hizo variar la reactividad del cuerpo del reactor «HERO» de potencia nula modificando el radio de la zona cargada. Todas las mediciones de los impulsos neutrónicos concuerdan satisfactoriamente con las obtenidas por otros métodos más clásicos de determinación de la reactividad. Por último, los autores examinan las técnicas experimentales y las dificultades encontradas en los sistemas moderados con grafito.

1. INTRODUCTION

During the past few years increasing use has been made of the pulsed neutron source technique for the measurement of reactor parameters by means of subcritical facilities. The applications of this technique fall conveniently into two classes; (a) near-critical facilities (~5%) [1] for the measurement of worths of absorbers and fuel elements, and (b) well subcritical systems, where by varying the system dimensions, information about the slowing-down model and lattice parameters can be found [2, 3].

The experiments have, in general, all been concerned with either bare systems, or reflected systems in which the core dimensions are large enough for the system to be considered bare. Under these circumstances the neutron flux within the system can be considered to be everywhere separable in space and energy [4] the spatial part being in the form of solutions of the wave equation. This leads at once to a simple single parametric expression for the time dependence of a thermalized burst of neutrons introduced into the system, the validity of which, within the limits of the mathematical model, does not depend on the degree to which the system is subcritical. Physically this is because the fundamental distribution following a burst of neutrons is determined solely by the boundary of the system, assuming that the extrapolation distance at the boundary is small or independent of neutron energy. For the case of a multi-region system, however, the form of the fundamental depends on the degree to which the system is subcritical and hence any simple relationship connecting the decay of the fundamental and the reactivity of the system will be only of an approximate nature in the same way that perturbation theory is an approximation.

The problem of the prompt decay in a subcritical multi-region system has been considered here using the two-group diffusion theory. The method employed is to expand the fundamental distribution of the decaying transient in terms of the distributions used in defining the conventional reactivity scale. It is found that in order to relate the prompt decay constant of the fundamental to the effective multiplication of the system, it is necessary to introduce two parameters, both of which depend on the spatial flux patterns within the system. It will be shown that some physical meaning can be attached to one of these parameters but that the other arises from the attempt to relate one scale of reactivity to a different one and can have no physical significance. Because of the complicated form of these parameters it has not been possible to predict their properties in general. This paper therefore considers the simplest multi-region system: that of a uniform cylindrical core and reflector corresponding roughly to the WAGR (Windscale Advanced Gas-cooled Reactor) type of lattice [5]. Estimates are given of the changes induced in these parameters following variations in core geometry and the insertion of single control absorbers. The latter sections of the paper apply the theoretical model developed here to measurements taken on the WAGR and HERO reactors [5]. Some discussion is presented of the experimental techniques and difficulties encountered in graphite-moderated systems.

2. THEORY

2.1. Decay of flux following a burst of neutrons

In pulsed neutron measurements, a burst of high energy neutrons is injected into a subcritical system and the resultant thermal flux transient is followed using a time analyser. The width of the initial burst is normally small compared to the time taken for the transient to end, and can be considered as occurring instantaneously. Physically, no thermal neutrons will be available for counting until the initial burst is thermalized; in the two-group formalism, however, it is assumed that the thermal neutrons start appearing with the burst. Thus the solution of the problem, in terms of a two-group theory, will involve two parameters, one describing the slowing down of the initial burst, and the second describing the decay of the thermal flux. It is this latter parameter which is measured and which will be shown to depend on the reactivity of the system. In the analysis the effect of delayed neutrons is ignored since, for the time scales involved, the delayed neutrons may be considered as part of the background. The reproduction constant k used here will therefore differ by a factor $(1-\beta)$ from the value normally used in quasi-stationary diffusion theory.

Consider the time-dependent equations [4] for a subcritical system in which the lattice parameters are functions of position. In particular the multiplication constant is taken as k within the core and zero elsewhere. It is assumed that the system is excited by an instantaneous source at time $t = 0$.

$$\operatorname{div} D_F \operatorname{grad} F - \Sigma_F F + \frac{k}{p}\Sigma_N N = \frac{1}{S_F}\frac{\partial F}{\partial t} \tag{1}$$

$$\operatorname{div} D_N \operatorname{grad} N - \Sigma_N N + p\,\Sigma_F F = \frac{1}{S_N}\frac{\partial N}{\partial t} \tag{2}$$

$$\text{for } t > 0 .$$

F and N refer to the fast and thermal fluxes respectively, the other symbols follow normal usage. S_F and S_N are the group velocities.

It should be emphasized that the parameters used in Eqs. (1) and (2) are functions of position and therefore the equations hold over all regions. By separating the fluxes into spatial- and time-dependent parts the functions F and N can be expressed in terms of the eigenfunctions f_n and g_n defined by the equations.

$$\operatorname{div} D_F \operatorname{grad} f_n - \Sigma_F f_n + \frac{k}{p}\Sigma_N g_n = \frac{\lambda_n}{S_F} f_n \tag{3}$$

$$\operatorname{div} D_N \operatorname{grad} g_n - \Sigma_N g_n + p\,\Sigma_F f_n = \frac{\lambda_n}{S_N} g_n \tag{4}$$

where

$$F = \sum_n^{\infty} A_n f_n \exp(\lambda_n t); \qquad N = \sum_n^{\infty} A_n g_n \exp(\lambda_n t) \tag{5}$$

The coefficients A_n depend on the position within the assembly of the source of neutrons and can be obtained using the orthogonality relations between the f and g functions. For a subcritical system, the decay constant λ_n will be negative, the smallest value $|\lambda|$ corresponding to the fundamental of Eqs. (3) and (4). Some time after the burst of neutrons therefore, the decay of the thermal flux within the system will be essentially that of the fundamental. In principle, Eqs. (3) and (4) could be solved for the lattice parameters in terms of the experimentally determined decay constants λ in the same way as mentioned in section 1. (b). However, for the use on near-critical systems it is more convenient to relate λ to the reactivity of the system, where by reactivity we mean the quantity ρ defined such that $(1-\rho)$ is the quantity by which the ν-value of the fissile isotope must be multiplied to make the system just critical. We will also define $(1-\rho)$ as $(1/k_{eff})$. An important feature of Eqs. (3) and (4), when describing the decay of the fundamental, is that only for $\lambda = 0$, that is at prompt critical, will the flux distribution be the same as the critical distribution, and for non-zero values of λ the distribution will differ from that at critical.

Consider the eigenfunctions U and V defined by the static Eqs. (6) and (7).

$$\operatorname{div} D_F \operatorname{grad} U_i - \Sigma_F U_i + \mu_i \frac{k}{p} \Sigma_N V_i = 0 \tag{6}$$

$$\operatorname{div} D_N \operatorname{grad} V_i - \Sigma_N V_i + p \Sigma_F U_i = 0 . \tag{7}$$

Here μ_i is the eigenvalue for the equations. In the case of the lowest eigenvalue μ, Eqs. (6) and (7) are those associated with reactivity calculations, μ being defined as $1/k_{eff}$.

For each eigenvalue and corresponding eigenvector we can define an adjoint vector such that there is some orthogonality relationship between each set of eigenvectors and the corresponding adjoints. It is usual [4] on physical grounds to assume that the vectors and adjoints each form a complete set in the reactor. Consequently we can expand the fundamental solutions in terms of these eigenfunctions and their adjoints.

Expanding f and g, corresponding to the fundamental solutions of Eqs. (3) and (4) in terms of U_i and V_i, we have

$$f = \sum_i^{\infty} C_i U_i \quad \text{and} \quad g = \sum_i^{\infty} E_i V_i . \tag{8}$$

Substituting from Eq. (8) into Eqs. (3) and (4) using Eqs. (6) and (7), we obtain

$$\sum^{\infty} [(E_i - \mu_i C_i)\Sigma_N \frac{k}{p} V_i - \frac{\lambda}{S_F} C_i U_i] = 0 \tag{9}$$

$$\sum^{\infty} [(C_i - E_i)p\Sigma_F U_i - \frac{\lambda}{S_N} E_i V_i] = 0 . \tag{10}$$

Equations (9) and (10) can be simplified by using the adjoint functions U* and V* defined by transposing the diffusion matrix of Eqs. (6) and (7), since it can be shown that the V and U*, and U and V* functions are orthogonal in that

$$\int_{CR} \frac{k}{p} \Sigma_N V_i U_j^* \, dr^3 = 0 \quad \text{for } i \neq j,$$

where i and j refer to two particular solutions of Eqs. (9) and (10), and

$$\int_{CR} p \Sigma_F U_i V_j^* dr^3 = 0 \quad \text{for } i \neq j$$

CR denotes integration over the volume of core and reflector.

In the case of a two-zone system, where k = 0 in the reflector the first identity becomes

$$\int_C V_i U_j^* \, dr^3 = 0 \quad \text{for } i \neq j$$

Thus multiplying Eq. (9) by U_1^* and Eq. (10) by V_1^*, the fundamental solutions of the adjoint equations, and integrating Eq. (9) over the core and Eq. (10) over the core and reflector regions gives

$$[E_1 - \mu C_1] I_3 - \lambda C_1 I_4 - \lambda \sum \int_{CR} C_i \frac{U_i U_1^*}{S_F} \, dr^3 = 0$$

and

$$[C_1 - E_1] I_2 - \lambda E_1 I_1 - \lambda \sum' \int_{CR} E_i \frac{V_i V_1^*}{S_N} dr^3 = 0,$$

where

$$I_1 = \int_{CR} \frac{V_1 V_1^*}{S_N} \, dr^3; \qquad I_4 = \int_{CR} \frac{U_1 U_1^*}{S_F} \, dr^3$$

$$I_2 = \int_{CR} p \Sigma_F U_1 V_1^* \, dr^3; \qquad I_3 = \int_{CR} \frac{k}{p} \Sigma_N V_1 \, U_1^* \, dr^3$$

are the perturbation integrals and Σ' represents summation over all but the first term of the series.

2.2. Prompt decay correction

Elimination of C_1 and E_1 gives a quadratic in λ, namely

$$\lambda^2 + \lambda\left[\frac{I_2}{I_1} + \mu\frac{I_3}{I_4}\right] + \frac{I_2 I_3}{I_1 I_4}[\mu - (1+\alpha_i)] = 0, \tag{11}$$

where α_i is composed of functions involving the summation over all but the first term of the series.

This parameter will be defined, for the purpose of this note, as the prompt decay correction and is given by

$$\alpha_i = \frac{I_1 I_4}{I_2 I_3}\left[\lambda^2 \sum{}' \frac{C_i}{C_1}\frac{I_4'}{I_4} \sum{}' \frac{E_i'}{E_1}\frac{I_1'}{I_1} - \frac{\lambda I_3}{I_4}\sum{}' \frac{E_i}{C_1}\frac{I_1'}{I_1} - \frac{\lambda I_2}{I_1}\sum{}' \frac{C_i}{E_1}\frac{I_4'}{I_4}\right] \tag{11a}$$

where for example

$$I_4' = \int_{CR} \frac{U_i U_1^*}{S_F}\, dr^3.$$

Equation (11) has two roots, one describing the slowing down of the initial burst, the other describing the decay of the thermal flux. If terms of the order

$$2[\mu - (1+\alpha_i)]^2 / (\mu I_1/I_2 + I_4/I_3)^3 (I_2 I_3/I_1 I_4)$$

are ignored, the decay of thermal flux has the form

$$-\lambda = \frac{I_3 I_2}{I_1 I_4}\frac{(\mu - (1+\alpha_i))}{[I_2/I_1 + \mu I_3/I_4]}. \tag{12}$$

Within the framework of the two-group diffusion solution, this expression describes the decay of the thermal flux for any degree of subcriticality; however, for its practical application, the term α_i must be ignored, since to evaluate it requires a knowledge of the degree of subcriticality and of the detailed flux distributions. The term α_i may therefore be considered as the error introduced by assuming the subcritical neutron distributions to be the same as the critical distribution and the point at which α_i becomes significant to mark the breakdown of the relationship between λ and the reactivity of the systems.

2.3. Effect of delayed neutrons

The analysis used in the preceding sections ignored the contribution of delayed neutrons to the decay scheme since the time scale involved in a measurement of λ is small compared to that of production of delayed neutrons. The multiplying constant k used here differs therefore from that used in steady state calculations, k_∞, since k refers only to the prompt neutrons.

Similarly $1/\mu$ is the effective multiplication of the system for prompt neutrons; $k_{eff} = 1$ refers to prompt critical. To reconcile the two definitions it is necessary to replace k by $k(1-\beta)$ and μ by $\mu/(1-\beta)$ in Eq. (12); μ then refers to effective multiplication of the system relative to delayed critical.

Equation (12) becomes with these modifications

$$-\lambda = \frac{I_3 I_2}{I_1 I_4}(1-\beta)\frac{[(\mu/1-\beta)-(1+\alpha_i)]}{[I_2/I_1 + \mu I_3/I_4]} \tag{12a}$$

where $(1-\beta)$ is assumed constant over all regions.

2.4. Reduction to one-dimensional case

In the case of cylindrical geometry in which the system is axially uniform and diffusion is anisotropic, Eqs. (1) and (2) are modified to introduce streaming terms and the cross-section terms modified to

$$(\Sigma_F + \gamma^2 D_{FZ}) \quad \text{and} \quad (\Sigma_N + \gamma^2 D_{MZ}),$$

where γ^2 is the axial buckling. These changes effect only the values of the perturbation integrals.

2.5. Choice of boundary conditions

The solutions of Eqs. (3) and (4), and (6) and (7) require the specification of the appropriate boundary conditions at the core reflector boundaries. If Eqs. (6) and (7) are solved using Westcott values for the lattice parameters to find U and V then, in order that continuity be obeyed, it is necessary to introduce a factor $\sqrt{T}$. That is $U\sqrt{T}$ and $V\sqrt{T}$ are taken as continuous over the boundary.

As a result, if U_1 and V_1 are derived using the Westcott convention, the orthogonality conditions stated previously become

$$\int_{CR} \frac{k}{p} \Sigma_N V_i U_j^* \sqrt{T}\, dr^3 = 0$$

$$\int_{CR} p \Sigma_F U_i V_j^* \sqrt{T}\, dr^3 = 0 \qquad \text{for } i \neq j$$

2.6. Decay in a bare system

For a bare system, the functions U and V are proportional, consequently α_i is everywhere zero. For this case Eq. (12a) can be further simplified since here

$$\frac{I_4}{I_3} = \frac{\mu}{(1+B^2L_S^2)\Sigma_F S_F}; \qquad \frac{I_2}{I_1} = (1+B^2L^2)\Sigma_N S_N$$

$$\mu k_\infty = (1+B^2L^2)(1+B^2L_S^2).$$

Substitution gives

$$-\lambda = \frac{1}{\ell}\left[1 - k_{eff}(1-\beta)\right] \tag{12b}$$

where ℓ, normally defined as the mean lifetime, is given by the expression:

$$\ell = \frac{1}{(1+B^2L^2)\Sigma_N S_N} + \frac{1}{(1+B^2L_S^2)\Sigma_F S_F}$$

2.7. Prompt decay in reflected system

It is to be expected that the relationship given in Eq. (12b) will hold for large reactors where the core dimensions are very large compared to the reflector savings. For a smaller reactor, however, such as the WAGR where the reflector forms an appreciable part of the reactor it will be shown below that to relate the prompt decay to the effective multiplication of the system, it is necessary to define two parameters, both of which depend not only on the core and reflector lattice constants but also on the detailed flux pattern within the reflector.

Thus if we define R as the reactor response coefficient, where R is given by

$$R = \left[k_{eff}\frac{I_4}{I_3} + \frac{I_1}{I_2}\right]$$

then Eq. (12a) may be re-arranged in the form

$$-\lambda = \frac{1}{R}\left[1 - k_{eff}(1-\beta)(1+\alpha_i)\right], \tag{12c}$$

where α_i is the prompt decay correction defined in section 2.2.

Comparison of Eq. (12c) with Eq. (12a) indicates that with R defined in this way, the relation between the prompt decay and the effective multiplication of the system is identical except for the term $(1+\alpha_i)$; consequently Eq. (12c) may be considered to be a more general form of Eq. (12b) and ℓ to be the value of R in a bare system. It will be shown later that α_i is appreciable only when the system is well subcritical; hence for near critical systems the prompt decay may be assumed to be related to the effective multiplication of the system by an equation of the form of Eq. (12b). An examination of the following sections will indicate under what circumstances this approximation is justified.

3. DEPENDENCE OF R AND α_i ON REACTOR SIZE AND LATTICE

A detailed examination of the forms of R and α_i indicates that little can be specified in general about the behaviour of these two parameters when the lattice and size of the core varies. This is because the main contribution to R, for the sizes concerned here, comes from the I_1/I_2 term. Hence the

TABLE I

CASES CONSIDERED

Case	Core type	Central absorber	Core radius (cm)
A	small	none	varied from 81
B	small	single	varied from 97
C	small	several	fixed 81
D	small	several	fixed 75
E	large	none	varied from 155
F	large	several	fixed 155
G	large	several	fixed 130
H	larger	none	varied from 205

core and reflector lattice constants have, in the main, only an indirect effect on R. Similarly α_i is composed in the main of cross-product terms involving the first and higher eigenfunctions and of the prompt decay constant.

To gain insight into how R and α_i vary in graphite-moderated reactors, a number of systems have been examined solving Eqs. (3) and (4) directly

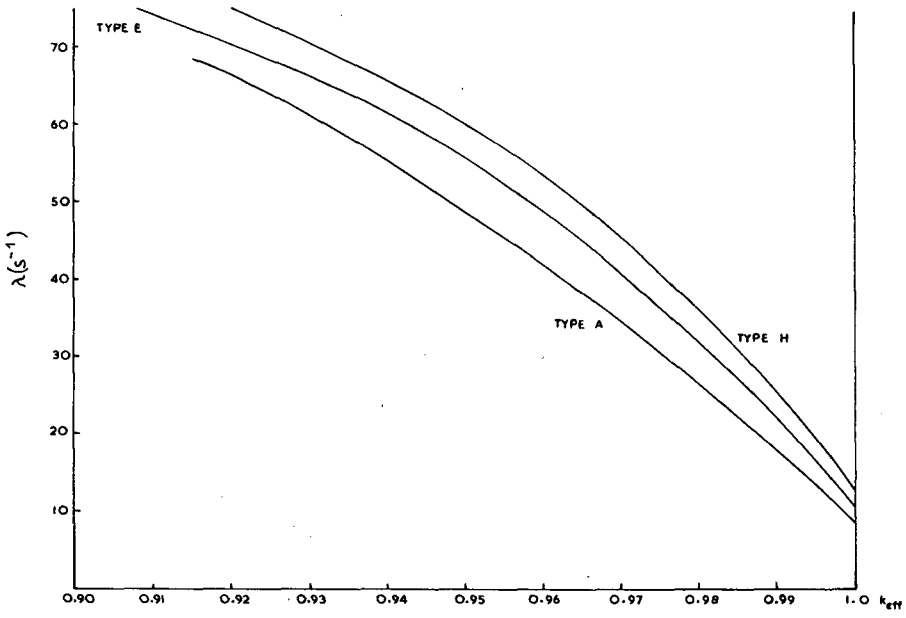


Fig. 1

Prompt decay constant versus effective multiplication for cases A, E and H

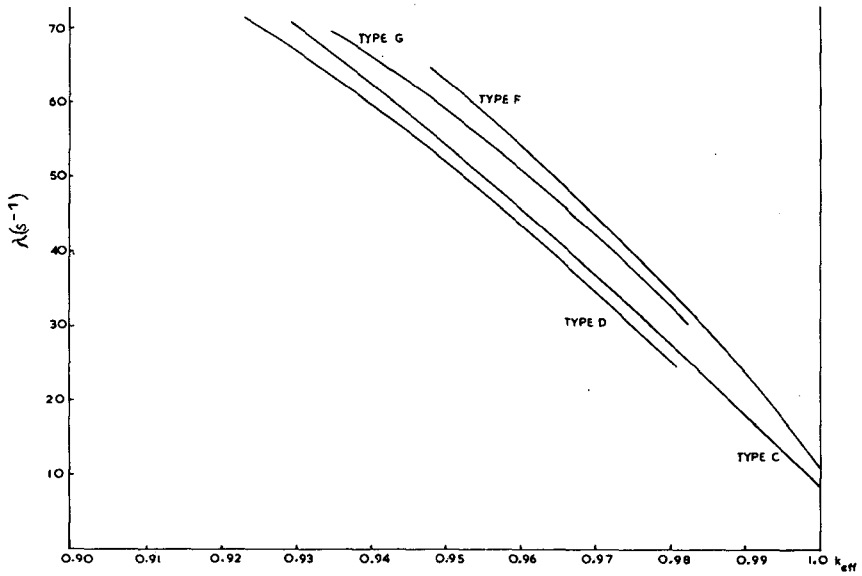


Fig. 2

Prompt decay constant versus effective multiplication for cases C, D, F and G

for λ and Eqs. (6) and (7) to obtain the corresponding values of k_{eff} and the perturbation integrals.

Figures 1 and 2 give typical curves of λ versus the effective multiplication constant for the systems considered in Table I. The difference between the cases considered in the two graphs is that for Fig. 1, variations in k_{eff} are produced by varying the core radius whilst for Fig. 2, the radius is fixed and the variations in k_{eff} are produced by the insertion of different central absorbers. From the obviously different forms of comparable cases it can be seen that not only is the variation of λ with k_{eff} affected by the radius of the system, but also is dependent on the way in which a change in k_{eff} is produced. It is concluded therefore that λ is not uniquely defined by the effective multiplication of the system and its value at delayed critical.

4. DISCUSSION OF RESULTS

4.1. Variation of reactor response coefficient

As mentioned previously, the value of R, for the systems considered here, depends mainly on the magnitude of the ratio I_1/I_2, the values of the core and reflector lattice constants affecting R only indirectly through their influence on the flux patterns within the system. Consequently for these systems it is to be expected that the greatest change in R will arise from variations in the core radius, since the values of the perturbation integrals will be most sensitive to changes at the core-reflector boundary. This is borne out in Fig. 3, where R is plotted against core radius for several types

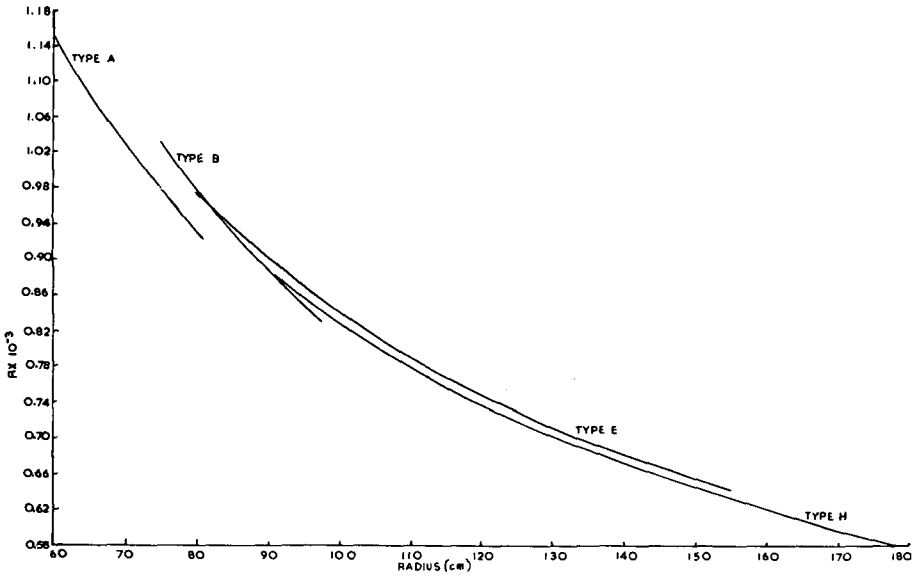


Fig. 3

Variation of reactor response coefficient with core radius

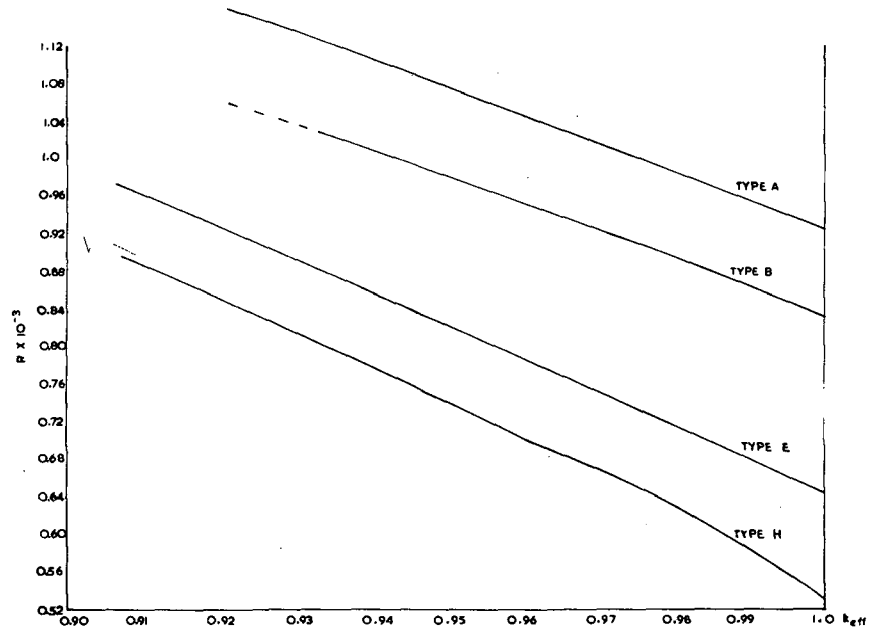


Fig. 4

Variation of reactor response coefficient with k_{eff} of system

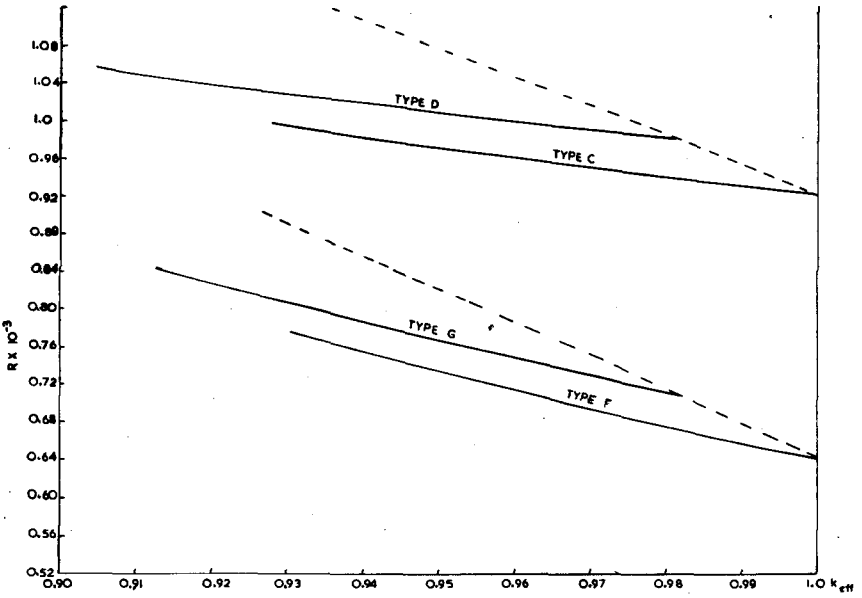


Fig. 5

Variation of reactor response coefficient with k_{eff} of system

of system, including a small system with central control rod and Figs. 4 and 5, where R is plotted against k_{eff}. Figure 4 shows the change in R corresponding to a change in k_{eff} produced by varying the core radius, whilst Fig. 5 shows the change in R corresponding to a change in k_{eff} produced by different central absorbers in cores of fixed radius. Finally in Table II, the change in R is given appropriate to a 10% change in lattice parameter for both the small and larger cores.

TABLE II

APPROXIMATE SENSITIVITY OF R TO LATTICE CONSTANTS

Type of core	Core constants*							Reflector constants*				
	k	N	F	D_{FR}	D_{NR}	p	T	N	F	D_{FR}	D_{NR}	Radius *core*
small A	0	+7	+3	-2	-1	+4	+2	+3	-2	-0.6	+1	+8
larger H	0	+10	+1	-1	-0.5	+3	+5	+1	-1	+0.3	+1	+7

* Figures in columns give % change in R for two core sizes corresponding to a 10% decrease in the lattice constant heading the column, other constants remaining unchanged.

The properties of the parameter R as indicated by the Figs. 3, 4, and 5 and Table II can be summarized briefly as follows:

(a) R varies almost linearly with the k_{eff} of the system to at least $k_{eff} = 0.90$.

(b) The rate at which R varies with the k_{eff} of the system depends strongly on the manner in which the change in k_{eff} is introduced. This is because of the way the ratio of the perturbation integrals I_1/I_2 varies with k_{eff}. These integrals are influenced most strongly by changes which take place in the spatial flux distributions at the core-reflector interface. Consequently absorbers placed near the centre of the core will not produce the same effect on R as absorbers placed in the core or reflector near to the interface or changes in the core radius and it is thus necessary to calculate the variation of R for all particular cores considered.

(c) Uniform changes of the lattice constants produce changes in R as shown in Table II. In general the thermal cross-sections of the core and reflector have the most effect on R. This is to be expected since in an infinite and uniform system the lifetime of neutrons in the system is proportional to the mean free path. The changes in R are given corresponding to two core sizes, types A and H. These verify that in a small core, the reflector is more important than for the larger core.

(d) In small systems where the reflector dimensions are comparable with those of the core, the value of R is determined mainly by the properties of the reflector. Conversely, in very large systems such as Calder the effect of the reflector can be assumed to be negligible. Thus for reactors within these two limits, such as the full-sized WAGR, the value of R depends on both the core and reflector properties.

(e) The value of R can only reasonably be measured at delayed critical, since here for most systems α_i can be assumed negligible and yet the delayed neutron background will remain reasonably constant. Any attempt to measure R at subcritical states will require an estimate of the prompt decay correction α_i.

4.2. Variation of prompt decay correction

A discussion as to the meaning of the parameter α_i defined here as the prompt decay correction is conceptually difficult since it arises from the difference between the two different reactivity scales which are being compared, that is between the scale using the prompt decay constant which is a physically observable quantity and the scale derived using the effective multiplication factor. It is obvious from a comparison of Eqs. (3), (4) and (6), (7) that at prompt critical the two scales are equivalent with $\lambda = 0$ and $\mu = 1/(1-\beta)$. Consequently near delayed critical we may assume that for most systems $\alpha_i = 0$; however, what is not obvious is how α_i varies with the lattice constants and with k_{eff} for the system, and under what circumstances it may be ignored without serious error being introduced. In principle, determination of α_i is feasible since the various constants such as E_i and C_i can be obtained using the orthogonality relationships for the U and V functions. This however requires a detailed knowledge of the spatial variations of the fundamental functions f and g, and of the eigenfunctions of U and V and

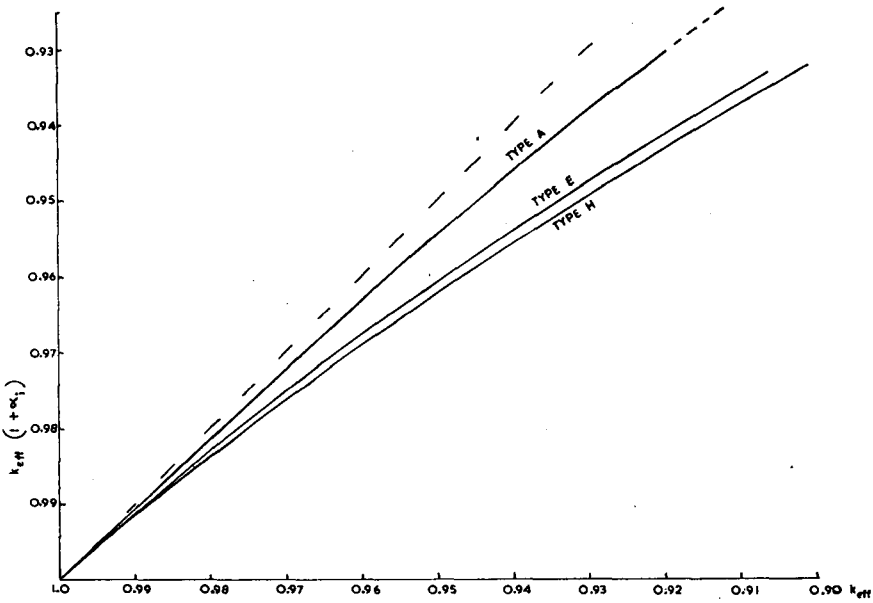


Fig. 6

Variation of $k_{eff}(1+\alpha_i)$ with k_{eff} for cases A, E and H

their adjoints. Under most circumstances this is not possible so that estimates of α_i must depend completely on a theoretical estimate. Fortunately as already noted α_i is small near critical so that under these circumstances only a relatively inaccurate estimate is required.

Estimates of the prompt decay correction have been formed by substituting the calculated values of λ etc., into Eq. (12c). It is found that α_i is small near to critical and increases rapidly as the degree of subcriticality increases, the rate of increase depending on the size of the system. This is shown in Fig. 6 in which $k_{eff}(1+\alpha_i)$ is plotted against k_{eff} for systems of types A, E, and H. Since it is to be expected that for very large systems α_i will vanish, there must be some system at which the correction for a given k_{eff} becomes a maximum. In Fig. 7 the variation of λ with $\sqrt{\alpha_i}$ is plotted for types A, E and H. The evidence from Figs. 6 and 7 would tend to suggest that this system would correspond roughly to the fully loaded Windscale AGR.

4.3. Required accuracy of α_i and R

Any relationship such as Eq. (12c), is of use only if it can assess the reactivity of a system with a reasonable accuracy. The parameters R and α_i noted here are in fact derived quantities depending to a fair degree on the geometry and lattice constants of the system. It is true that spot values of R can be found by pulsing at delayed critical. However, as Figs. 3 and 5 show, the value of R depends not only on the size but also on the operation

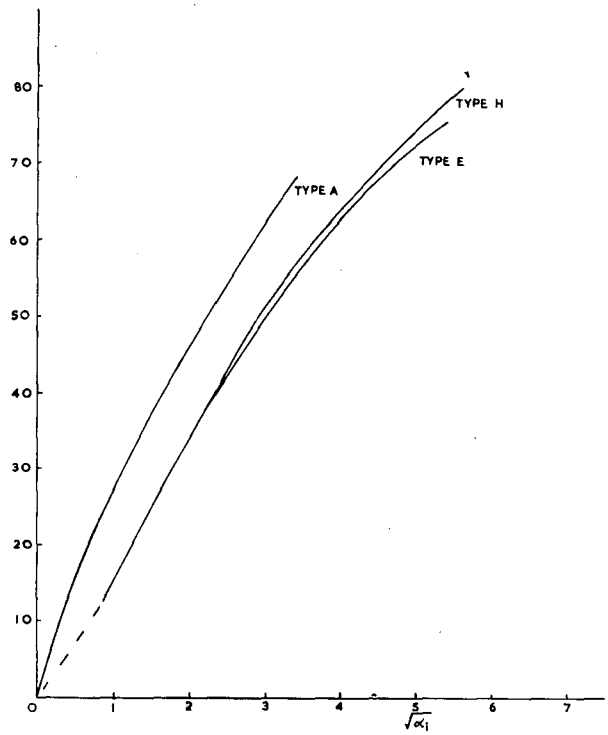


Fig. 7

λ versus $\sqrt{\alpha_i}$ for systems type A, E and H

used to produce the change in reactivity. It is instructive therefore to estimate the accuracy obtainable in a reactivity measurement assuming that α_i can be estimated to within 25% and R to within 10%. Table III gives the estimates of the resultant error in reactivity as a function of reactivity. The estimates are applicable to all the three core sizes considered here, the increased error in α_i for the larger cores being offset by the decrease in the error in R.

TABLE III

ERROR IN REACTIVITY CAUSED BY 25% ERROR IN α_i AND 10% ERROR IN R

k_{eff}	0.99	0.97	0.95	0.93	0.91
Reactivity (% Δk/k)	1.01	3.09	5.26	7.53	9.89
Error in reactivity (% Δk/k)	0.2	0.4	0.6	0.8	1.1

The results quoted in Table III tend to overestimate the error at small reactivities since it is reasonable to assume that R could be specified to less than 10% near to critical. It is therefore fair to assume that the reactivity of a system, or changes in that system can be measured to about 10% in reactivity provided calculations for the reactor response coefficient R and prompt decay correction α_i are undertaken for the particular system in question.

5. EXPERIMENTAL ARRANGEMENT

Measurements were made during the commissioning of the WAGR and further measurements were done as part of the experimental programme on the HERO reactor. These are both graphite-moderated reactors with fuel channels on a triangular lattice. The two reactors have similar cores; however WAGR is power producing while HERO is zero energy [5]. For the WAGR experiments, the neutron pulses were produced using the pulsatron G tube developed by SERL (Services Electronics Research Lab.) of Baldock [6]. The design of the tube requires that the EHT transformer producing the accelerating voltage be mounted next to the tube. This meant that because of the confined space available, a small heavily rated transformer had to be used. This was found liable to break down in the insulation. For the HERO experiments a more recent development, the K-tube, was used. This dispenses with the in-core transformer and uses a more robust one located outside the reactor core.

The output from BF_3 neutron counters positioned within the core was fed into a 16-channel time analyser [7] to record the neutron flux decay. Timing pulses to trigger the electronic units synchronously with the time analyser were provided by a built-in crystal oscillator. A special feature of the equipment is that counts arriving during the switching period from one channel to another are not lost but are delayed and accumulated in the next channel.

6. EXPERIMENTAL TECHNIQUES

One advantage claimed for the pulsed source method over other methods of measuring subcritical reactivity is that the measurement is independent of the positions within the reactor of the source and detectors. The experience on HERO would suggest that whilst this is true for systems far from critical, near to critical every effort should be made to minimize the effect of harmonics. The difficulty is that near to critical it is extremely difficult to separate the fundamental mode from the higher harmonics when analysing the transient unless the source and detector have been specially positioned. For the measurements quoted here therefore, the source and detector positions were chosen to minimize this higher harmonics contribution as much as possible. For the WAGR the pulsatron tube was located at the core mid-height in an experimental loop tube halfway along the core radius. Four boron trifluoride detectors located at approximately halfway along the core radius and at 1/3, 1/2, 2/3 and 9/10 the core height were

used to detect the neutron pulses. Since the output from the pulsed neutron source ($\sim 10^6$ n/s) was rather less than that from the 10-c Po-Be reactor source, the experiments were carried out with the latter removed from the reactor.

For most of the experiments in the HERO reactor the axial leakage is less than the radial leakage. As a result higher harmonics in the axial direction are more readily excited than those in the radial direction. Consequently two closely matched boron trifluoride proportional counters were located at 1/3 and 2/3 the extrapolated height of the reactor and the common output fed into the time analyser through a known dead-time unit. This arrangement minimized contributions from the first and second axial harmonics. Ideally the detectors would also be placed at the zero of the first radial harmonic and with the neutron tube at the core mid-height in the centre of the reactor. However, because of engineering considerations it was not possible to locate the tube at the core mid-height anywhere in the fuel region and it was placed just outside the fuel region in the reflector. The detectors (because of their smaller physical size) could be placed in the fuel region and were placed near the centre of the reactor. The time analyser enables the period of decay following a simple neutron pulse to be split up into sixteen consecutive time intervals, the counts recorded in each time interval during consecutive pulses being recorded accumulatively in the corresponding channels. A variable delay between the triggering pulse and the opening of the first channel is available so that the initial part of the decay can be omitted. The channel width can be varied and a variable width background channel is opened towards the end of the decay. A typical time sequence would be

(a) The pulsatron tube fires a 10-μs burst of neutrons and triggers the analyser;
(b) 100 ms later the first of the sixteen channels opens for 10 ms followed in succession by the remaining fifteen channels;
(c) 700 ms after the initial trigger pulse the background channel opens for 200 ms;
(d) One second after the trigger pulse the tube fires again.

Because of the limited number of counting channels available, care had to be taken that the equipment was set up on the right portion of the neutron decay curve. This was done with an initial short experiment with zero delay and a wide channel width (25 ms). From this the optimum delay and channel width were found.

For the measurements on HERO the pulsatron was run for about 15 min before taking measurements to allow the delayed neutron background to reach equilibrium. Measurements were then taken until sufficient counts were obtained, about 1000 sweeps with the analyser.

The analysis of the results was by a least squares fit to the form

$$A \exp[-\lambda t] = C - B \exp[-\delta t].$$

Here λ is prompt decay constant and δ is an effective delayed neutron decay constant. C is the corrected count and A and λ are the fitting parameters. B is obtained from the counts in the background channel. It is found that the

derived decay values are insensitive to the δ-value particularly when the system is well subcritical. For the WAGR results, therefore, the variation of the background was ignored. Each measurement was repeated several times.

7. EXPERIMENTAL RESULTS

Two sets of measurements have been analysed according to the methods outlined in the previous sections. The first set consists of measurements with the HERO reactor where the reactivity of the system was varied by changing the number of fuel channels, the overall reactor size remaining constant. In the second set the reactivity of the WAGR reactor was varied

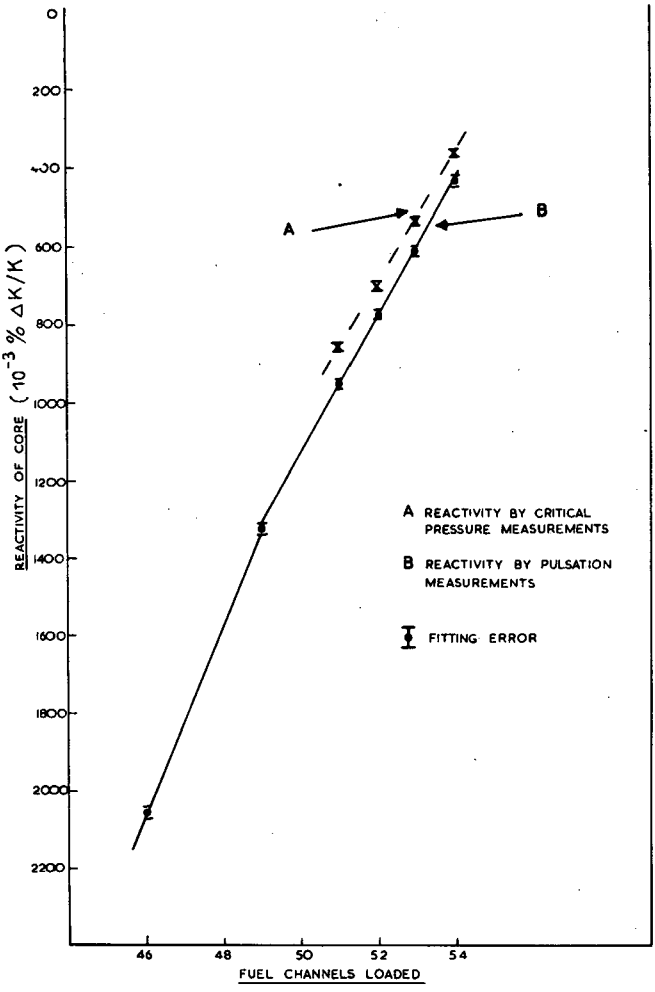


Fig. 8

Comparison of pulsed source method with air pressure coefficient method (HERO)

by pressurizing with air. All reactivity measurements are quoted here in percentage of $\Delta k/k$.

The HERO reactor with air as coolant has a critical size of 55 channels of fuel loaded with no absorbers present. Pulsatron measurements of the prompt neutron decay constant were carried out on the core built with 54, 53, 52, 51, 49 and 46 channels loaded. Independent estimates of the shutdown of the core at 54, 53, 52, and 51 channels loaded were obtained by approach-

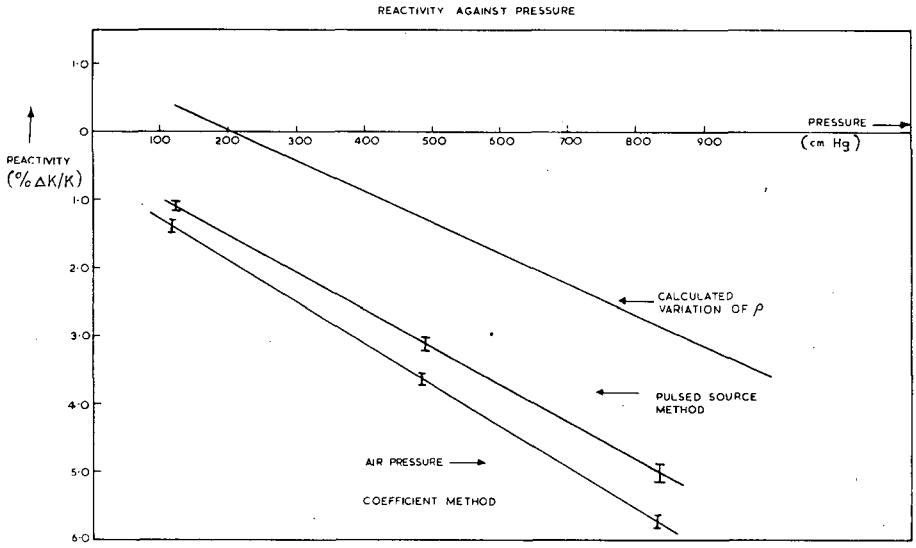


Fig. 9

Comparison of pulsed source method with air pressure coefficient method (WAGR)

to-critical counting in conjunction with the known air pressure coefficient. Using two-group lattice data it should now be possible to calculate R and α_i and, hence knowing the measured value of the prompt neutron decay constant, the shutdown reactivity of the system. However since the lattice constants available took no account of several small perturbers within the reactor, the theoretical value of reactivity was incorrect by about 0.5% $\Delta k/k$ when compared with experiment. Consequently for the comparisons here the k_∞-value for the core was reduced until the calculated reactivity of the 55-channel core agreed with the experimental value.

The pulsatron and critical pressure estimates of reactivity are given in Fig. 8. The two curves lie parallel with a difference of $\sim 0.09\%$ $\Delta k/k$. This is considered good agreement since the errors shown are least squares fitting errors. In addition to the experimental errors there is an error of $\pm$ 4% in the β-value. In the pulsatron results this would produce a systematic error in the reactivities quoted of $\sim 0.03\%$ $\Delta k/k$, decreasing β increasing the shutdown reactivity. In the critical pressure determination the error in β will produce a systematic percentage change in the quoted shutdown reactivities of 4%, decreasing β decreasing the shutdown reactivity. By

changing β from the value used of 0.0069 to 0.0074 the two curves can be made to agree within the experimental errors.

The WAGR measurements were made in a core of fixed configuration. The core was made subcritical by air poisoning and the reactivity varied by pressurizing the reactor. At various air pressures pulsatron measurements of the prompt neutron decay constant were taken and converted to shutdown reactivities using calculated values of R and α_i. These are compared in Fig. 9 with the calculated reactivities and those measured using the reactor air pressure coefficient of reactivity. This latter value was deduced from doubling time measurements with the reactor critical. The calculation of the R and α_i values was complicated by the extreme non-conformity of the core considered. The core arrangement consisted of three concentric fuel zones with a total of 15 control rods and 3 absorbers. In addition there were 4 stainless steel loop tubes and 22 vacancies. In all there were a total of 195 fuel channels out of 253 channels loaded. Considering the complexity of the core the agreement between the pulsatron and air pressure methods is good. Again the errors quoted are the experimental values and do not include the errors in β.

8. CONCLUSIONS

The theoretical examination of the prompt decay of the thermal flux in a multi-region system reveals that a relationship can be established between the decay constant λ and the effective multiplication constant k_{eff} in terms of two parameters, called for the purpose of this paper, the reactor response coefficient R and the prompt decay correction α_i, both of which depend in some degree on the way the subcritical state is achieved. The first parameter R has some physical meaning in that for a uniform bare system, it is equivalent to the mean neutron lifetime of the system and that a spot value can be measured with the system at delayed critical. However the evidence suggests that the effect on R of, say, an absorber is not only dependent on the reactivity held by the absorber, but also depends on its position, by being very strongly affected by changes in the flux patterns at the core boundaries. Consequently values of R estimated from one set of measurements do not necessarily apply to all other circumstances. With regard to the second parameter, no physical meaning can be attached to it, nor can it be measured directly. However it has been shown that under near critical conditions the value of α_i is small enough either to be ignored or that a relatively inaccurate estimate is sufficient.

Comparison with measurements taken on the WAGR and HERO reactors shows that the methods discussed here give good agreement with the air pressure technique over a wider range of reactivity even for systems with complex core arrangements.

REFERENCES

[1] SIMMONS, B.E. and KING, J.S., Nucl. Sci. Engng 3 (1958) 595-608.

[2] BARRATT, P.R., Relative validities of slowing down theories in a natural uranium water moderated lattice, Ph.D. Thesis, Birmingham University.

[3] MEISTER, H., Reactor Sci. Techn. 4 (1963) 97-114.
[4] WEINBERG, A.M. and WIGNER, E.P., The Physical Theory of Neutron Chain Reactors, University of Chicago Press, Chicago, Ill. (1958) Chap. 12, 15.
[5] MOORE, J., "Reactor physics development for advanced gas-cooled reactors", Exponential and Critical Experiments III IAEA, Vienna (1964) 3-25.
[6] HAWKINS, P.O. and SUTTON, R.S., Rev. Sci. Instrum. 31 (1960) 3.
[7] MOUNSEY, A., Private communication.

PULSED-SOURCE EXPERIMENTS WITH MULTIPLYING AND NON-MULTIPLYING HEAVY WATER SYSTEMS

E. UTZINGER, W. HEER AND H. R. LUTZ
SWISS FEDERAL INSTITUTE FOR REACTOR RESEARCH,
WÜRENLINGEN, SWITERLAND

Abstract — Résumé — Аннотация — Resumen

PULSED SOURCE EXPERIMENTS WITH MULTIPLYING AND NON-MULTIPLYING HEAVY WATER SYSTEMS. An extensive series of measurements with a pulsed source of the $T^3(d,n)He^4$ type has been performed at the subcritical facility MINOR of the Swiss Federal Institute for Reactor Research, Wurenlingen. Three types of experiments were carried out to measure:

(a) Decay constants of prompt neutron modes in natural and slightly enriched lattices;
(b) Subcritical reactivity by means of the prompt decay and delayed neutron tails in natural and slightly enriched lattices;
(c) Anisotropy of the thermal diffusion constant in D_2O containing different numbers of parallel empty tubes of various size.

The time-dependent thermal neutron flux was measured in each system at different axial positions to obtain decay constants of the prompt modes for different axial bucklings (Fourier analysis) without changing the actual height of the D_2O level. The experimental values were compared with theoretical two-group parameters. Limitations of the technique are discussed. In addition, reactivity in highly subcritical systems with $\rho \geq -40\$$ was measured directly by utilizing the delayed neutron tail of the pulses. Results are compared with static measurements and show rather good agreement.

EXPÉRIENCES A L'AIDE DE SOURCES PULSÉES SUR DES SYSTÉMES MULTIPLICATEURS ET NON MULTIPLICATEURS A EAU LOURDE. Une longue série de mesures à l'aide d'une source pulsée du type $^3T(d,n)^4He$ a été faite avec l'assemblage sous-critique MINOR de l'Institut fédéral suisse de recherches nucléaires, à Würenlingen. Il s'agissait d'expériences de trois types visant à mesurer les caractéristiques suivantes:

a) Les constantes de décroissance des modes de neutrons instantanés dans des réseaux à uranium naturel et des réseaux à uranium faiblement enrichi;
b) La réactivité sous-critique au moyen de la décroissance des neutrons instantanés et de la queue des bouffées constituée par des neutrons retardés, dans des réseaux naturels et des résaux faiblement enrichis;
c) L'anisotropie de la constante de diffusion des neutrons thermiques dans D_2O contenant des tubes vides parallèles de diverse dimension, en nombres différents.

Les auteurs ont mesuré le flux de neutrons thermiques variable dans le temps pour chaque système à différentes positions axiales en vue d'obtenir les constantes de décroissance des modes de neutrons instantanés pour différents laplaciens axiaux (analyse de Fourier) sans modifier la hauteur du niveau de D_2O. Ils ont comparé les valeurs expérimentales avec les paramètres obtenus à l'aide d'une théorie à deux groupes. Ils discutent les limitations de la technique. En outre, ils ont mesuré directement la réactivité dans des systèmes fortement sous-critiques où $\rho \geq -40\$$ en utilisant la queue des bouffées constituée par des neutrons retardés. Enfin, ils comparent les résultats avec ceux de mesures statiques et montrent qu'ils sont en assez bon accord.

ЭКСПЕРИМЕНТЫ С ПУЛЬСИРУЮЩИМ ИСТОЧНИКОМ НА НЕРАЗМНОЖАЮЩИХ И РАЗМНОЖАЮЩИХ УСТРОЙСТВАХ С ТЯЖЕЛОЙ ВОДОЙ. На подкритическом устройстве MINOR Швейцарского федерального института по реакторным исследованиям в Вюренлингене осуществлена широкая программа измерений при помощи пульсирующего источника типа $T^3(d,n)He^4$. Проведены три категории экспериментов для измерения:

а) констант распада мгновенных нейтронов в естественных и слегка обогащенных решетках;
б) уровня реактивности в подкритическом состоянии при помощи распада мгновенных

нейтронов и хвостов замедленных нейтронов в естественных и слегка обогащенных решетках; и

в) анизотропии диффузионной константы тепловых нейтронов в тяжелой воде с погруженным в нее разным количеством параллельно расположенных пустых трубок разных размеров.

Для каждого устройства поток тепловых нейтронов, зависящий от времени, измеряли в различных положениях по высоте для получения констант распада мгновенных нейтронов для различных осевых лапласианов (анализ Фурье) без изменения высоты действительного уровня тяжелой воды. Экспериментальные значения сравниваются с теоретическими двугрупповыми параметрами. Обсуждаются недостатки этого метода. В дополнение к этому путем использования хвоста замедленных пульсирующих нейтронов непосредственным образом была измерена реактивность в сильно подкритических системах с $\rho \geq -40$ \$. Результаты сравниваются со статистическими измерениями, и они дают весьма хорошее совпадение.

EXPERIMENTOS CON FUENTES PULSADAS EN SISTEMAS DE AGUA PESADA MULTIPLICADORES Y NO MULTIPLICADORES. Los autores utilizaron la instalación subcrítica «MINOR» del Eidgenossisches Institut fur Reaktorforschung de Wurenlingen para una larga serie de mediciones con una fuente de neutrones pulsados utilizando la reacción $^{3}T(d,n)^{4}He$. Llevaron a cabo tres clases de experimentos a fin de medir:

1. Las constantes de decrecimiento de los modos correspondientes a los neutrones instantáneos en reticulados de uranio natural y ligeramente enriquecido.

2. La reactividad en el estado subcrítico, partiendo del decrecimiento de los neutrones instantáneos y de los datos proporcionados por las «colas» de neutrones retardados en reticulados de uranio natural y ligeramente enriquecido.

3. La anisotropía de la constante de difusión térmica en D_2O previa introducción de un número variable de tubos paralelos de diversos tamaños.

Se midió el flujo de neutrones térmicos en función del tiempo en cada uno de los sistemas con distintas posiciones del eje, a fin de obtener las constantes de decrecimiento de los modos de los neutrones instantáneos para distintos laplacianos axiales (análisis de Fourier) sin modificar el nivel real del D_2O. Los autores comparan los valores experimentales con los parámetros de la teoría de dos grupos y examinan seguidamente las limitaciones de esta técnica. Además, midieron directamente, utilizando los datos proporcionados por la «cola» de neutrones retardados de los impulsos, los valores de la reactividad en sistemas acusadamente subcríticos con $\rho \geq -40$ dólares. Estos resultados concuerdan satisfactoriamente con los de las mediciones estáticas.

1. INTRODUCTION

The aim of the experiments discussed in this paper is to determine lattice parameters of subcritical natural uranium, heavy water assemblies by means of a pulsed neutron source. The most important information in such experiments is the decay constant of the prompt neutron flux. For that reason we have measured the decay constants (dependent on the geometric buckling) as precisely as possible and developed a theoretical interpretation of the measurements, which gives information on the lattice parameters of the assembly. In an additional experiment we measured the reactivity by means of the delayed neutron tail.

The application of the pulsed neutron method to steam- and gas-cooled heavy water assemblies (i.e. assemblies with void and streaming effects) was also considered. For this reason measurements were carried out to determine the anisotropy of thermal diffusion constants. These experiments were performed with assemblies consisting of heavy water and containing empty tubes of various sizes.

2. EXPERIMENTAL ARRANGEMENT

The experiments were carried out at the subcritical assembly MINOR of the Swiss Federal Institute for Reactor Research in Würenlingen (Fig. 1). This facility has been described in a previous paper [1]; therefore only a

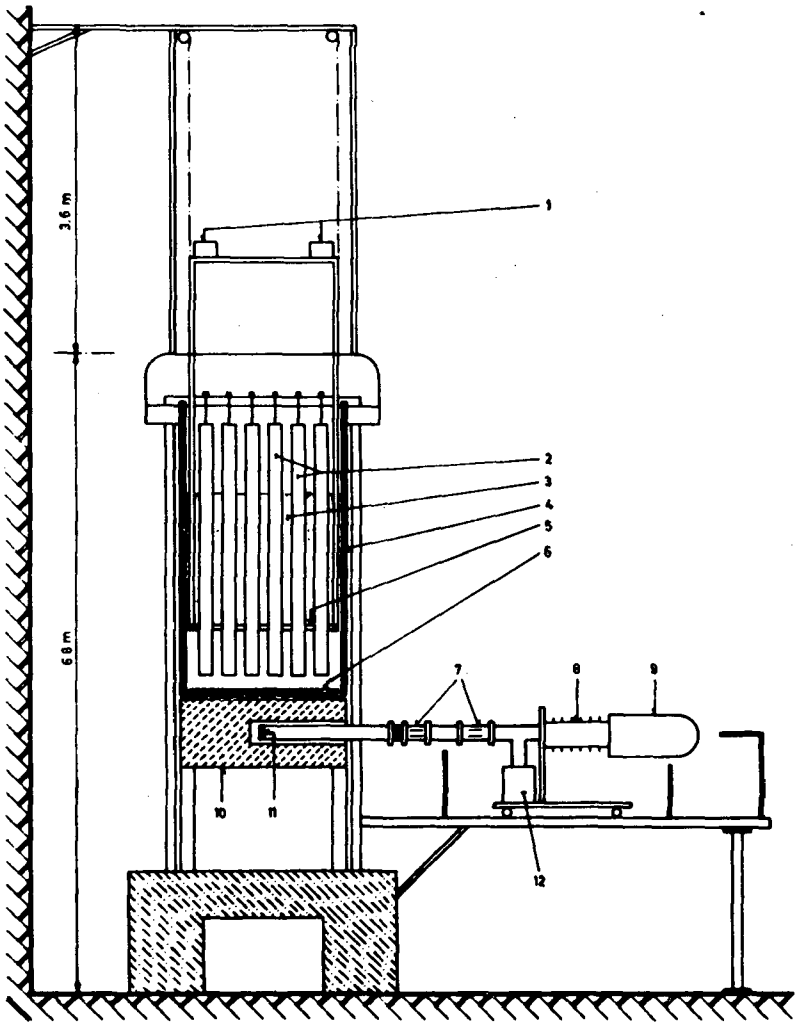


Fig. 1

Pulsed measurements at the MINOR facility

1. Pre-amplifier
2. Fuel rods
3. D_2O
4. Aluminium tank
5. Neutron counters
6. Boral plate
7. Deflection plates
8. Accelerating tube
9. High-voltage terminal with pulsed ion source
10. Graphite pedestal
11. Tritium target
12. Ion pump

few important facts are mentioned here. The tank with the heavy-water lattice cores measures 140 cm in diameter and 280 cm in height. The fuel suspension system is sufficiently flexible to accept different types of fuel elements. In our experiments three types of fuel rods were used (see Table I).

TABLE I

FUEL RODS

Name	Fuel			Cladding		
	Material	Density (g/cm^3)	Diam. (mm)	Material	Inner diam. (mm)	Outer diam. (mm)
MINOR-20	$U_{nat.}$ metal	18.94	20	Al	20.2	22.2
MINOR-17-E	U metal 0.947 wt. % U^{235}	18.8	17	Al	17.6	19.6
DIORIT	$U_{nat.}$ metal	18.90	27	Al	27	30

An accelerator of the $T^3(d, n)He^4$ type (Nuclear Texas Corporation) produces neutrons of 14 MeV. For our experiments a special type of pulsed ion source (with an extraction voltage pulsing system) was constructed. It is possible to obtain a ratio of neutron production during the pulses to neutron production between the pulses of better than 10^5 with a source intensity of about 10^{11} n/s.

The standard MINOR counting equipment was used (BF_3 counters) as neutron detectors. A TMC CN-110 analyser (with 256 channels) can be utilized; the channel width was varied between 80 and 640 μs.

3. THEORY

3.1. Decay constants of the prompt neutron flux

For the interpretation of our experiments a theory is needed, which relates the measured decay constants to the lattice parameters of the system. A first calculation shows that the one-group theory is not satisfactory for the interpretation of the precise experimental results. Therefore two-group diffusion theory is used. Although the results are better, a slight systematic trend remains. At present, however, there seems to be no better theory for an adequate solution of this problem.

The two-group diffusion equations are solved for cylindric geometry with some refinements included.

$$(D_{fa}\,\Delta_a + D_{fr}\,\Delta_r)\phi_f(r,z,t) - \Sigma_f\phi_f(r,z,t) + \frac{k_\infty \Sigma_s}{p}(1-\beta)\phi_s(r,z,t)$$

$$+ \sum_{i=1}^{N} \lambda_i C_i(r,z,t) + Q(r,z,t) = \frac{1}{v_f}\,\frac{\partial\phi_f(r,z,t)}{\partial t} \tag{1}$$

$$(D_{sa}\,\Delta_a + D_{sr}\,\Delta_r)\phi_s(r,z,t) - \Sigma_s\phi_s(r,z,t) + p\Sigma_f\phi_f(r,z,t-l_{0f})$$

$$= \frac{1}{v_s}\,\frac{\partial\phi_s(r,z,t)}{\partial t} \tag{2}$$

$$\frac{k_\infty\beta_i}{p}\,\Sigma_s\phi_s(r,z,t) - \lambda_i C_i(r,z,t) = \frac{\partial C_i(r,z,t)}{\partial t} \tag{3}$$

$$\beta = \sum_{i=1}^{N} \beta_i \tag{4}$$

where

ϕ_f, ϕ_s : fast and thermal flux respectively
v_f, v_s : average velocity of the fast and thermal neutrons respectively
D_{fa}, D_{fr}, D_{sa}, D_{sr} : axial and radial diffusion constants respectively of the fast and thermal neutrons
Σ_f, Σ_s : cross-sections for disappearance of fast and thermal neutrons respectively
k_∞ : multiplication factor of the infinite medium
p : resonance escape probability
β_i : delayed neutron fraction of the i-th group
C_i, λ_i : concentration and decay constants respectively of the delayed neutron precursors
N : number of delayed neutron groups

$l_{0f} = \frac{1}{\Sigma_f v_f}$: average neutron lifetime in the fast group (infinite medium)
$Q(r,z,t)$: source term

The aim of introducing l_{0f} in the diffusion equation of the thermal group is not to discuss the rise time of the thermal flux after a neutron burst, as is often believed. (The rise time cannot be interpreted by this theory because the source-neutrons do not have the fission spectrum.) But the l_{0f} also has an influence on the prompt neutron decay constants, which in general, is not negligible.

The diffusion equations are solved using appropriate boundary conditions and assuming an infinitely short neutron burst into the assembly at time t = 0. The corresponding solution ϕ_s (Green's function) is of interest,

because the solution for another source term Q'(t) (with the same space dependence) is given by the convolution integral

$$\phi_s'(t) = \phi_s(t) * Q'(t). \tag{5}$$

Details of the calculations and the exact solutions are given in Ref. [2]. The decay of the prompt neutron flux, which is the most interesting part of our experiments, is given by

$$\phi = \sum_{m=1}^{\infty} \sum_{n=1}^{\infty} a_{mn} J_0(\alpha_n r) \sin(\beta_m z) e^{-\gamma_{mn} t}, \tag{6}$$

where

$$\alpha_n = \left(\frac{j_{0n}}{\tilde{R}}\right) \text{ and } \beta_m = \left(\frac{m\pi}{\tilde{H}}\right),$$

j_{0n} being the n-th zero of the Bessel function of order 0, $\tilde{R}$ and $\tilde{H}$ extrapolated boundaries and a_{mn} dependent on the source-geometry. The value of the γ's has to be found by an approximation method. A very good approximation, which in our case is better than 1% is

$$\gamma_{mn} = \frac{C}{F} + \frac{AC^2}{F^3} \tag{7}$$

where

$$\left.\begin{aligned} A &= l_{0f} l_{0s} + \frac{l_{0f}^3 l_{0s}}{2 l_f l_s} + l_{0f}^2 l_{0s} \left(\frac{1}{l_f} + \frac{1}{l_s}\right) \\ F &= l_{0f} l_{0s} \left(\frac{1}{l_f} + \frac{1}{l_s}\right) + \frac{l_{0f}^2 l_{0s}}{l_f l_s} \\ C &= \frac{l_{0f} l_{0s}}{l_f l_s} - k_\infty (1 - \beta) \end{aligned}\right\} \tag{8}$$

with

$$l_{0s} = \frac{1}{\Sigma_s v_s}$$

$$l_f = \frac{l_{0f}}{1 + \tau_a \beta_m^2 + \tau_r \alpha_n^2}$$ average lifetime of the fast neutrons in the finite system

$$\left.\begin{aligned} \tau_a &= \frac{D_{fa}}{\Sigma_f} \\ \tau_r &= \frac{D_{fr}}{\Sigma_f} \end{aligned}\right\}$$ $\tau_{a,r}$, axial and radial Fermi age

$$l_s = \frac{l_{0s}}{1 + L_a^2 \beta_m^2 + L_r^2 \alpha_n^2}$$ average lifetime of the thermal neutrons in the finite system

$$\left.\begin{aligned} L_a^2 &= \frac{D_{sa}}{\Sigma_s} \\ L_r^2 &= \frac{D_{sr}}{\Sigma_s} \end{aligned}\right\} \quad L_{a,r}\text{, axial and radial diffusion length}$$

3.2. Anisotropy of thermal diffusion constants

Measurements of the diffusion constants were performed to check different theories. Decay constants of assemblies of heavy water with empty tubes of various sizes have been determined. In this experiment one-group theory can be used. (Only the time interval where the flux spectrum has a Maxwellian spectrum is of interest.)

$$(D_r \Delta_r + D_a \Delta_z - \Sigma_a)\phi = \frac{1}{v}\frac{d\phi}{dt} \tag{9}$$

The resulting thermal flux ϕ after injection of a neutron burst is

$$\phi(r, z, t) = \sum_{m=1}^{\infty}\sum_{n=1}^{\infty} a_{mn} J_0(\alpha_n r)\sin(\beta_m z)e^{-\gamma_{mn}t} \tag{10}$$

with

$$\gamma_{mn} = \Sigma_a v + \overline{D_r v}(\alpha_n^2) + \overline{D_a v}(\beta_m^2) \tag{11}$$

Diffusion cooling is neglected. If the assembly consists of pure heavy water, D_r is equal to D_a.

3.3. Reactivity measurements

Great efforts have been undertaken to extend the various methods of reactivity measurement (modified pulsed source method, $k\beta/l$ method) to our far subcritical heavy water systems. The principle of these experiments is to measure not only the prompt neutron flux, but also the delayed neutron tail. All these methods can be reduced to two basic formulas.

For simplicity we suppose first, that the repetition rate R of the neutron bursts is large compared with all decay constants of the delayed neutron precursors and small compared with the decay constant of the prompt neutron flux. The neutron burst shall be infinitely short.

The first formula, initiated by GOZANI [3], is based on the supposition that the delayed neutron distribution does not contain higher geometric harmonics. In this case one finds [3]

$$-\rho = RA/\gamma B, \tag{12}$$

where

ρ = reactivity in \$-units
R = repetition rate
A, γ = amplitude and decay constant respectively of the asymptotic prompt neutron flux
B = constant flux originating from the delayed neutrons.

γ and A can be determined if one waits until the higher harmonics in the prompt neutron part have decreased sufficiently; then one measures only the asymptotic part.

The second formula, initiated by GARELIS and RUSSELL [4], respects the higher delayed neutron harmonics in a one-group approximation

$$\int_0^\infty n_p(t)\,[e^{\alpha_c t} - 1]\,dt = \frac{B}{R} \tag{13}$$

$$-\rho = \frac{\gamma - \alpha_c}{\alpha_c} \tag{14}$$

where n_p is the prompt neutron flux.
The first expression represents an equation to determine α (n_p, B and R are measured quantities); γ is determined in the same manner as in the first case.

The formulas in both cases cannot be applied directly to our measurements. Corrections have been developed for

(a) Finite pulse width;
(b) Repetition rate - incomplete decay of the prompt neutron flux when starting the next neutron pulse;
(c) Repetition rate - decay of the delayed neutron flux between the pulses.

Correction (a) is applied to Eq.(13) by separating the two integrals. The correction to $\int_0^\infty n_p(t)dt$ is equal to 0; the correction to $\int_0^\infty n_p \exp(\alpha_c t)dt$ depends only on α_c (and the pulse width), but not on the amplitudes and decay constants of the different modes.

The assumptions of the second method (one-group theory, α_c independent of mode) have been checked for some examples.

4. ANALYSIS OF EXPERIMENTAL DATA

We have tried to determine the prompt decay constants as precisely as possible. Since the neutron flux consists of a sum of exponential terms (Eqs.(6) and (10)) this determination is not easy. In principle one could wait until the higher harmonics have decreased sufficiently: then one measures only the term with the smallest decay constant. This method fails if the fundamental mode is not excited with a predominant amplitude, i.e. if a_{11} is small compared with other a_{mn}. In this case one has to wait too long. Calculations have shown that this method cannot give better accuracy than about 5% in our far subcritical assembly.

(a) Position of the neutron source. The best position would be in the centre of the assembly. This is not possible in the MINOR-facility for technical reasons (in addition one has to consider the perturbation by the installation of the pulsed neutron source). In our case the tritium target (source of 14-MeV neutrons) is placed in the centre of the pedestal near the

bottom of the tank. This arrangement gives small amplitudes of higher radial harmonics, but large amplitudes of axial harmonics.

(b) Position of neutron counters. The detector can be placed at a zero of $\sin(\beta_m z)$ or $J_0(\alpha_n r)$: a series of harmonics with index m or n can be avoided. But this method is less effective, because other harmonics have a large amplitude at this place. The use of counters, which detect a flux integral, is more effective. We used long (20 in) and thin ($\frac{1}{2}$ in) BF_3 counters. These detectors are placed along a radius in such a manner that the first and second radial harmonics are detected with an efficiency of less than 1% of the fundamental mode (Fig. 2).

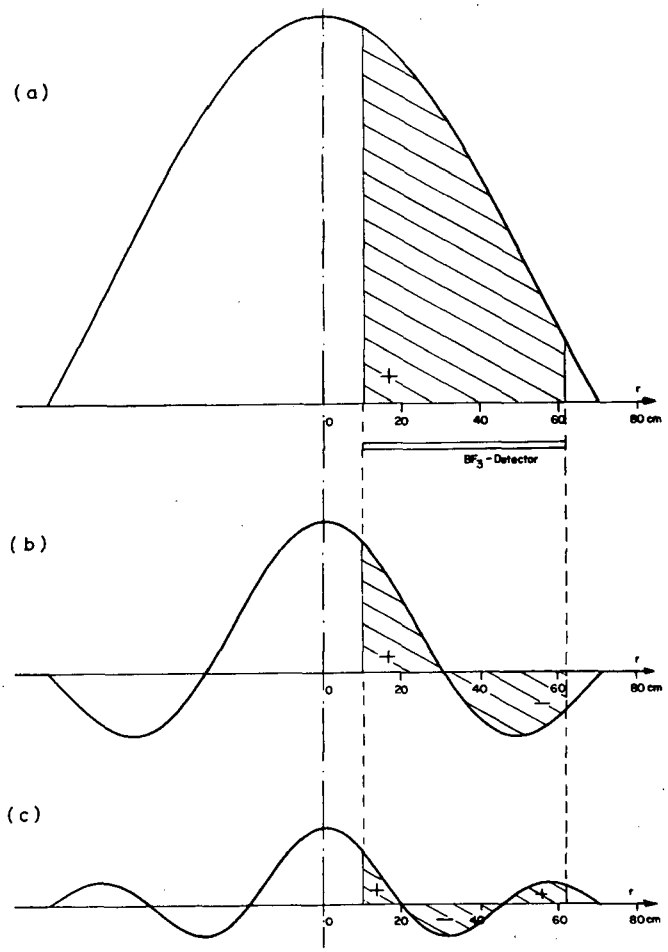


Fig. 2

Detector arrangement in the MINOR facility

(a) $J_0\left(\frac{j_{01}}{\tilde{R}} r\right)$ (b) $J_0\left(\frac{j_{02}}{\tilde{R}} r\right)$ (c) $J_0\left(\frac{j_{03}}{\tilde{R}} r\right)$

By these two improvements only the fundamental mode is measured. On the other hand a very large amount of higher axial harmonics is observed. We take advantage, however, of this fact in measuring the time distribution of the neutron flux (with the above described counters) at different axial positions (Fig. 3). For each time interval a Fourier analysis of the resulting

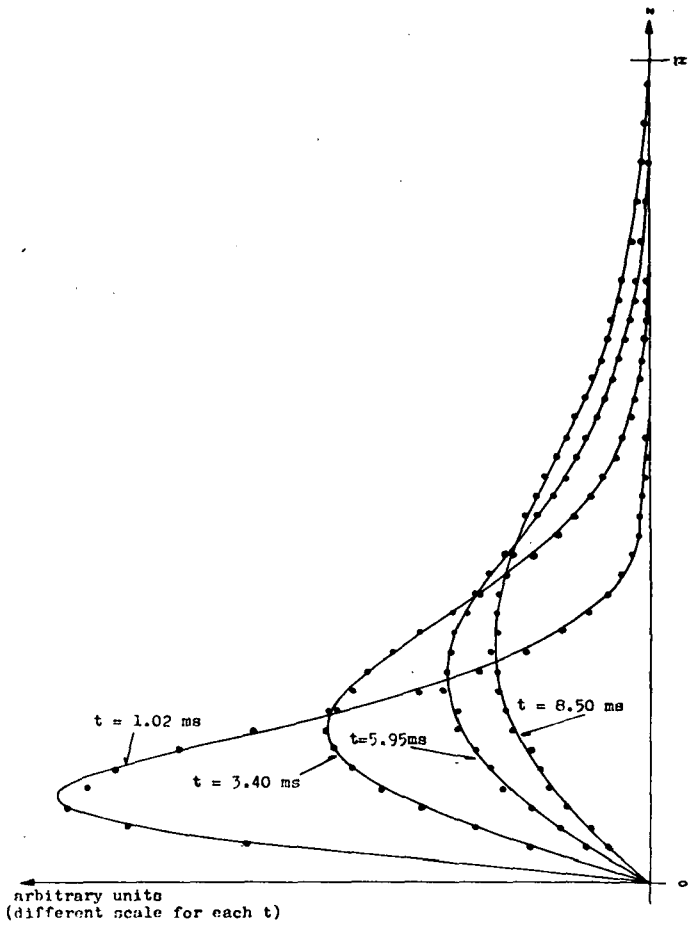


Fig. 3

Axial flux distribution at different times
(t = time after neutron burst)

axial flux distribution is carried out. These Fourier coefficients as a function of time are exponential functions with the desired decay constants (see Figs. 4 and 5) [5]. This method has the additional advantage that decay constants of assemblies with different geometric bucklings can be determined without change of the actual size (each Fourier coefficient corresponds to a different geometric buckling). The time distribution (normally, 128 time intervals were used) was measured at up to 30 axial positions.

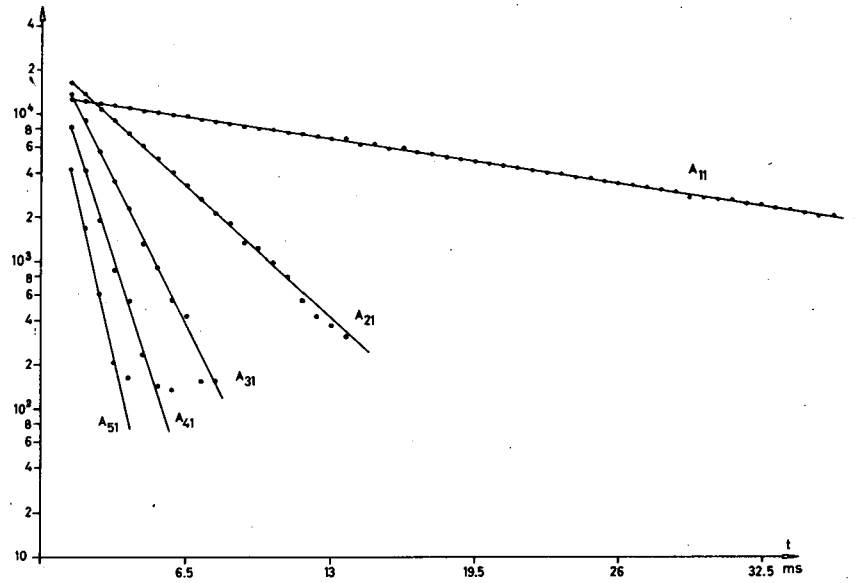


Fig. 4

Fourier coefficients $A_{mn}(t)$ for MINOR-17-E rods, 10-cm lattice pitch

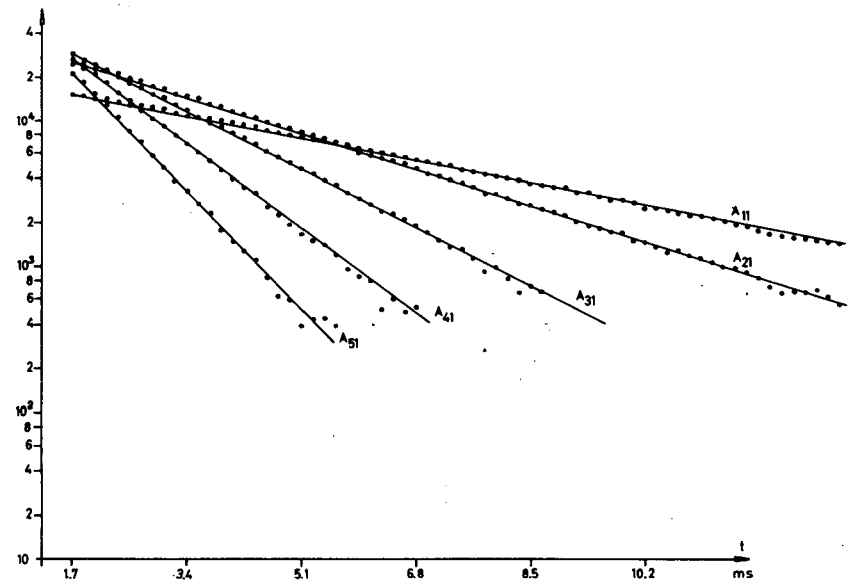


Fig. 5

Fourier coefficients $A_{mn}(t)$ for MINOR-20 rods, 16-cm lattice pitch

5. RESULTS AND CONCLUSIONS

5.1. Prompt decay constants

Measured and calculated decay constants (according to Eq. (7)) are given in Tables II, III and IV. Table II contains two theoretical values; in the first case Σ_a (and L^2) is taken from the Swedish "burn-up" programme, the second value corresponds to a diffusion length, determined by the Amouyal-Benoist method. The material buckling is taken from exponential experiments.

In the case of the MINOR-17-E elements (Table III) we have determined the diffusion length L^2 and the material buckling K^2 from the pulsed measurements. Table V shows the results from pulsed and exponential experiments.

TABLE II

DECAY CONSTANTS OF LATTICES WITH MINOR-20 RODSS

Lattice pitch (cm)	B^2 (μB)[a]	$\gamma_{exp.}$ (s^{-1})	$\gamma_{theor.}$ (L^2 from burn-up programme)	$\gamma_{theor.}$ (L^2 Amouyal-Benoist method)
8	1247	267 ± 1	257.2	254.6
	1715	492 ± 4	475.9	471.7
	2496	839 ± 8	817.2	810.9
	3589	1270 ± 10	1254.6	1246.3
	4993	1768 ± 15	1763.7	1754.2
10	1250	185 ± 1	178.9	177.4
	1718	363 ± 4	355.0	352.5
	2499	641 ± 6	633.5	629.7
	3592	992 ± 10	996.8	991.9
	4996	1393 ± 15	1428.9	1423.4
12	1250	183 ± 1	182.1	181.0
	1718	338 ± 4	333.9	332.2
	2499	580 ± 6	576.6	574.1
	3592	893 ± 10	897.6	894.5
	4996	1247 ± 10	1286.0	1282.6
14	1259	194 ± 1	194.0	193.4
	1727	333 ± 4	330.8	330.0
	2508	550 ± 6	551.1	550.2
	3601	827 ± 10	845.9	845.1
	5005	1158 ± 10	1206.8	1206.6
16	1267	211 ± 1	211.7	211.0
	1735	335 ± 4	339.1	338.1
	2516	527 ± 6	545.5	544.4
	3609	805 ± 8	824.0	822.7
	5013	1110 ± 10	1168.1	1167.0

[a] $1\ \mu B = 10^{-6}\ cm^{-2}$.

TABLE III

DECAY CONSTANTS OF LATTICES WITH MINOR-17-E RODS

Lattice pitch (cm)	B^2 (μB)[a]	$\gamma_{exp.}$ (s^{-1})	$\gamma_{theor.}$ (s^{-1})	$\gamma_{theor.}$ with corrected data (s^{-1})
10	1316	52.99 ± 0.4	44.99	52.7
	1991	320 ± 3	291	310
	3116	712 ± 11	673	709
	4691	1095 ± 30	1165	1220
12	1307	107 ± 1	100.2	106
	1991	328 ± 3	317	324
	3131	670 ± 7	658	668
	4727	1093 ± 25	1104	1117
14	1339	154 ± 1	148	154
	2062	365 ± 3	356	361
	3267	687 ± 7	685	690
	4954	1099 ± 30	1122	1126
16	1354	186 ± 1	181	185
	2083	378 ± 3	376	380
	3298	687 ± 7	690	692
	4999	1111 ± 30	1109	1111
18	1345	208 ± 2	204	206
	2065	391 ± 4	389	389
	3265	684 ± 8	687	684
	4945	1074 ± 30	1090	1084

[a] $1\ \mu B = 10^{-6}\ cm^{-2}$.

The agreement between theoretical and experimental values is good, although a small systematic error is observed. In the case of the DIORIT elements the differences are larger.

A comparison between theoretical (also static) and pulsed values is difficult because of the uncertainty in the diffusion lengths. But two conclusions are obvious:

(a) A systematic difference is observed between the bucklings obtained by static and by pulsed measurements in the undermoderated range: the static values are always larger.

(b) There are increasing discrepancies between theoretical and experimental decay constants with increasing geometric bucklings. This effect may be explained by spectrum effects, which are most pronounced in the undermoderated region.

5.2. Reactivity measurements

Reactivity measurements of assemblies with DIORIT rods have been performed (see Table VI). The reactivity was determined according to Eqs.

TABLE IV

DECAY CONSTANTS OF LATTICES WITH DIORIT RODS

Lattice pitch (cm)	B^2 $(\mu B)^a$	$\gamma_{exp.}$ (s^{-1})	$\gamma_{theor.}$ (s^{-1})
10	1274	310 ± 2	284
	1860	598 ± 4	561
	2837	1030 ± 10	987
	4203	1539 ± 30	1523
12	1293	218 ± 3	203
	1899	469 ± 4	441
	2909	823 ± 8	811
	4324	1240 ± 20	1285
14	1292	201 ± 2	192
	1913	427 ± 4	405
	2947	770 ± 12	739
	4395	1180 ± 30	1174
16	1313	204 ± 2	204
	1962	415 ± 4	405
	3044	750 ± 15	724
	4558	1189 ± 30	1142
18	1328	223 ± 3	219
	1982	414 ± 4	406
	3071	708 ± 8	704
	4597	1099 ± 20	1100

[a] $1\ \mu B = 10^{-6}\ cm^{-2}$.

(12) and (13) and the corresponding corrections for finite pulse width and repetition rate were included. Three counter positions were chosen: position 1, 45 cm, position 2, 75 cm and position 3, 105 cm above the bottom of the tank. Position 3 is the most favourable; the amount of higher harmonics is very large at position 1.

The asymptotic prompt neutron decay constant in Table VI is taken from the Fourier analysis method. The values in Table VI are calculated by means of a new programme, described in Ref.[10]. The agreement of measured and theoretical values is not bad, if one considers the difficulties of such measurements in the far subcritical range and the very large amount of higher harmonics.

In our experiments the corrections are in many cases large. The experimental conditions can be improved. Because of the complexity of the different corrections these improvements could well be applied by an online computer. Further experiments of this kind are planned.

TABLE V

MEASURED AND THEORETICAL L^2 AND K^2 OF MINOR-17-E LATTICES

	Diffusion lengths		Material bucklings	
Lattice pitch (cm)	$L^2_{theor.}$ (cm^2)	$L^2_{exp.}$ (cm^2)	$K^2_{exponential\ experiment}$ (μB)	$K^2_{pulsed\ experiment}$ (μB)
10	141	124 ± 4	1227 ± 4	1215 ± 7
12	207	200 ± 6	1026 ± 6	1012 ± 7
14	285	285 ± 8	861 ± 5	842 ± 8
16	374	374 ± 10	717 ± 5	704 ± 8
18	475	475 ± 12	587 ± 5	577 ± 6

TABLE VI

REACTIVITY MEASUREMENTS WITH DIORIT RODS

Lattice pitch (cm)	Counter position	γ (s^{-1})	α_c (s^{-1})	$-\rho$ Eq. (12) and corrections ($)	$-\rho$ Eq. (13) and corrections ($)	$-\rho_{theor.}$ with $\beta = 0.0070$ ($)
8	1	660	31.4 ± 0.8	15.0 ± 3.0	19.8 ± 1.5	24.3
	2		31.1 ± 0.8	20.0 ± 2.5	20.2 ± 1.5	
	3		35.5 ± 0.8	25.8 ± 2.0	17.6 ± 1.5	
10	1	310	19.5 ± 0.7	7.5 ± 0.5	15.2 ± 0.5	14.8
	2		20.3 ± 0.7	10.4 ± 1.5	14.2 ± 0.6	
	3		21.2 ± 0.7	16.0 ± 1.0	13.6 ± 0.6	
12	1	217	13.4 ± 0.7	11.0 ± 1.5	15.2 ± 0.7	14.6
	2		14.6 ± 0.7	13.4 ± 1.0	13.8 ± 0.7	
	3		14.6 ± 0.7	15.3 ± 1.0	13.8 ± 0.5	
14	1	198	10.4 ± 0.7	15.8 ± 1.0	18.0 ± 0.5	18.9
	2		10.9 ± 0.7	18.8 ± 1.0	17.0 ± 0.5	
	3		11.0 ± 0.7	17.3 ± 1.0	17.1 ± 0.3	
16	1	204	8.9 ± 0.4	20.1 ± 2.5	21.9 ± 0.7	26.2
	2		9.2 ± 0.4	25.7 ± 2.5	21.5 ± 0.7	
	3		8.6 ± 0.4	27.6 ± 2.5	22.7 ± 0.7	
18	1	223	6.7 ± 0.4	19.6 ± 3.0	32.5 ± 1.5	37.0
	2		7.6 ± 0.4	32.7 ± 3.0	28.5 ± 1.5	
	3		7.4 ± 0.4	34.2 ± 3.0	29.4 ± 1.5	

Note:

Only statistical error is respected; systematic errors, i.e. harmonics in the case of Eq. (12) and one-group approximation in the case of Eq. (13) are neglected.

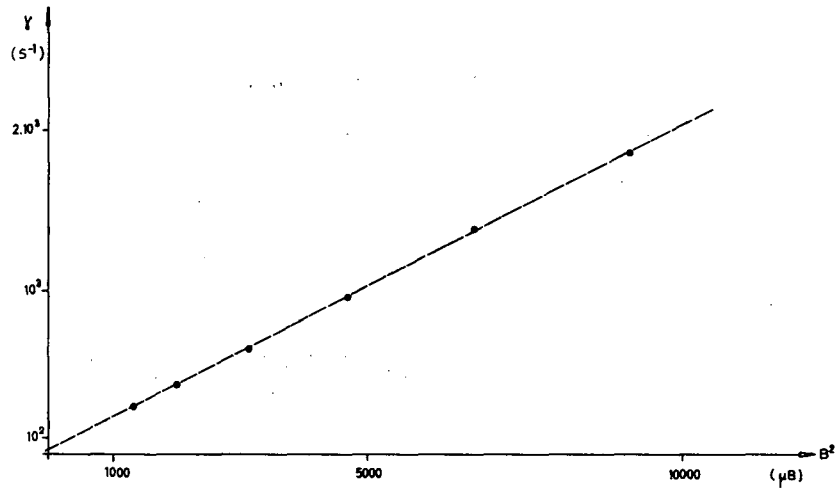


Fig. 6

Decay constants of heavy water (99.85%, 22°C)
($1\ \mu B = 10^{-6}\ cm^{-2}$)

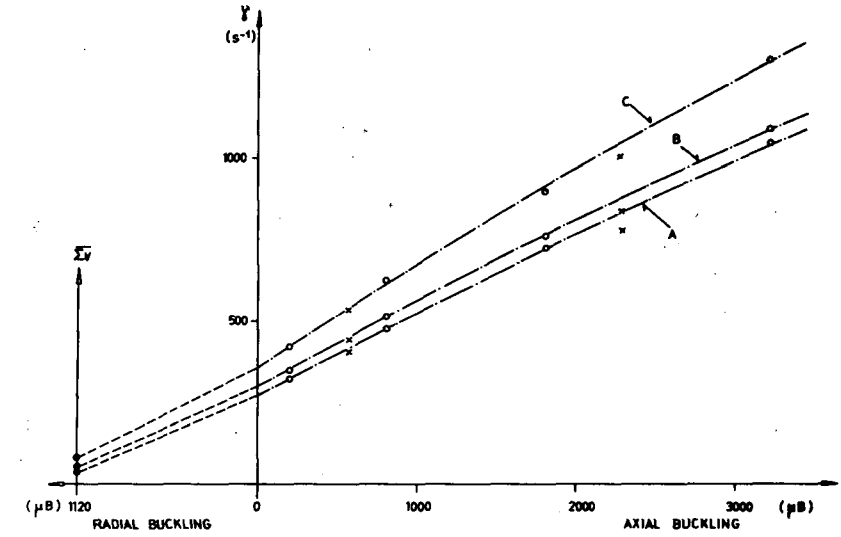


Fig. 7

Decay constants of heavy water containing empty tubes (diam. 76 mm)
($1\ \mu B = 10^{-6}\ cm^{-2}$)

Lattice pitch A: 32 cm
B: 24 cm
C: 16 cm
O Actual height 220 cm
× Actual height 130 cm

TABLE VII

THEORETICAL AND EXPERIMENTAL DIFFUSION CONSTANTS

Tube diam. (mm)	Lattice pitch (mm)	$\overline{\Sigma_a v}$ (s^{-1})	D_a, theor. (cm)	D_a, exp. (cm)	D_r, exp. (cm)	D* (cm)	D** (cm)	D*** (cm)
144	320	61.1	1.795	1.41 ± 0.05	0.97 ± 0.02	1.38	1.29	1.11
144	240	90.0	2.548	1.96 ± 0.08	1.12 ± 0.02	1.81	1.65	1.41
76	320	36.6	0.969	1.04 ± 0.04	0.85 ± 0.02	0.92	0.90	0.89
76	240	46.6	1.079	1.08 ± 0.05	0.91 ± 0.02	0.98	0.96	0.93
76	160	75.1	1.394	1.27 ± 0.07	1.02 ± 0.02	1.18	1.14	1.09

* BEHRENS [7] ** BENOIST [8] *** CARTER [9]

5.3. The thermal diffusion constant of heavy water

The thermal diffusion constant of heavy water at a concentration of 99.85% and 22°C was determined

$$\overline{vD} = (2.02 \pm 0.01) \times 10^5 \text{ cm}^2/\text{s}$$

This result is in excellent agreement with a value of Ref. [5] (see also [6]). Figure 6 shows the curve decay constant versus geometric buckling.

In the same manner axial diffusion constants of assemblies containing empty tubes are measured (Fig. 7). If the axial diffusion constant and the absorption term are known, the radial diffusion constant can also be determined (Eq. (11)).

The experimental values of the diffusion constants are always smaller than the theoretical values (see Table VII). This result is not evident. Because of the streaming effect one would expect the contrary. The following explanations could be possible:

(a) Average neutron energy too low (diffusion cooling);
(b) Systematic error because of the simple diffusion theory (average over the Maxwellian spectrum);
(c) Asymptotic axial flux distribution not a sine function (because of streaming effects).

It is certain that (c) has an influence, especially in cases of larger geometric buckling. But this effect cannot explain the too small decay constants at the smallest geometric bucklings. Further investigations are necessary to clear this point.

REFERENCES

[1] MEIER, R. W., LUTZ, H. R. and UTZINGER, E., Exponential and Critical Experiments II IAEA, Vienna (1964) 59-83.

[2] UTZINGER, E., Untersuchung von unterkritischen Natururanschwerwasserreaktoren mit Hilfe einer gepulsten Neutronenquelle, EIR-Bericht No. 73.

[3] GOZANI, T., A modified procedure for the evaluation of pulsed source experiments in subcritical reactors, Nukleonik 8. Heft (1962).

[4] GARELIS, E. and RUSSELL, J. L., Theory of pulsed neutron source measurements, Nucl. Sci. Engng 16 (1963).

[5] MEISTER, H., Pulsed neutron experiments on subcritical heavy water natural uranium lattices, Reactor Sci. Tech. 17 (1963).

[6] SPRINGER, T. et al., On the determination of the diffusion constants of H_2O, phenyls, ZrH and D_2O by neutron single-scattering experiments, Proc. 3rd UN Int. Conf. PUAE, 1964, A/Conf. 28/P/763.

[7] BEHRENS, D. J., The effect of holes in a reacting material on the passage of neutrons, with special reference to the critical dimension of a reactor, Rpt AERE T/R 103 (1958).

[8] BENOIST, P., A general formulation of the diffusion coefficient in a heterogeneous medium which may contain cavities, Rpt AERE-Trans 842 (SPN 522).

[9] CARTER, C., Streaming due to holes in a reactor, Rpt AERE-R 3367 (1960).

[10] GOZANI, T., DEMARMELS, P., HÜRLIMAN, T. and WINKLER, H., "Modified pulsed source techniques", these Proceedings II.

PULSED NEUTRON MEASUREMENTS ON A HEAVY WATER POWER REACTOR (MZFR) AT ZERO ENERGY

G. BRONNER AND W.-H. DIO
REAKTOR-VERSUCHSSTATION,
SIEMENS-SCHUCKERTWERKE AG, GARCHING
AND
G. SCHLOSSER
ABTEILUNG REAKTOR ENTWICKLUNG,
SIEMENS-SCHUCKERTWERKE AG,
ERLANGEN, FEDERAL REPUBLIC OF GERMANY

Abstract — Résumé — Аннотация — Resumen

PULSED NEUTRON MEASUREMENTS ON A HEAVY WATER POWER REACTOR (MZFR) AT ZERO ENERGY. The pulsed neutron method was used for zero-power measurements in the core of a heavy water reactor. Various methods were used for the evaluation of the pulsed measurements. The so-called "integral" evaluation methods are based on theories published by Sjöstrand and Gozani; so far they have been applied mainly to light water reactors. These methods use not only the prompt neutron decay constant but also the information contained in the delayed neutron tails to determine the reactivity. For measurements on the heavy water reactor, however, the methods had to be modified so as to adequately take into account the time dependence of the delayed neutrons. The fraction of the delayed neutrons was calculated using a reasonable assumption for its time dependence. All the information needed could be obtained from the measurements. These methods are well suited for hand calculations to yield the reactivity with proper accuracy. An analytical procedure was applied to check the results of the integral methods. This essentially involves the exact calculation of the time dependence of the delayed neutron fraction by an iteration procedure.

The results of the different evaluation methods mentioned above are compared by plotting them as functions of the D_2O level and of the boron concentration. Due to the inclined control rods the flux distribution is distorted in a rather complicated manner when the rods are inserted. Therefore the time dependence of this distribution was measured for different positions of the pulsed neutron source. It was possible to find one position for which the influence of higher modes on the measurements of the shutdown reactivity was sufficiently small.

Finally it is shown that the values of $\left(\frac{\delta\rho(H, c_i)}{\delta(1/H^2)}\right)_{H=H_i}$ and $\left(\frac{\delta\rho(H_i, c)}{\delta c}\right)_{c=c_i}$ (ρ reactivity, H_i critical D_2O level for boron concentration c_i) obtained by period measurements in the slightly supercritical state and pulsed measurements in the subcritical state are in excellent agreement.

MESURES FAITES A LA PUISSANCE ZÉRO DANS UN RÉACTEUR DE PUISSANCE A EAU LOURDE (MZFR), PAR LA MÉTHODE DES NEUTRONS PULSÉS. Les auteurs ont employé la méthode des neutrons pulsés des mesures à la puissance zéro dans le cœur d'un réacteur à eau lourde et utilisé diverses méthodes pour évaluer les mesures relatives aux bouffées. Les méthodes d'évaluation dites «intégrales» se fondent sur les théories publiées par Sjöstrand et Gozani; jusqu'ici, elles ont été appliquées principalement à des réacteurs à eau légère. Ces méthodes de détermination de la réactivité n'utilisent pas seulement la constante de décroissance des neutrons instantanés mais aussi les renseignements que donne la queue des bouffées constituée par des neutrons retardés. Cependant, pour ce qui est des mesures relatives aux réacteurs à eau lourde, il a fallu modifier les méthodes pour tenir compte des variations des neutrons retardés en fonction du temps. Les auteurs ont calculé la fraction des neutrons retardés en se fondant sur une hypothèse raisonnable touchant cette variation. Les mesures ont permis d'obtenir tous les renseignements nécessaires. Ces méthodes conviennent très bien pour calculer la réactivité avec la précision voulue sans l'aide de machines. Ils ont analysé les résultats des méthodes intégrales aux fins de vérification. Pour cela, il leur a fallu calculer exactement, par une méthode d'itération, les variations de la fraction des neutrons retardés en fonction du temps.

Ils comparent les résultats des différentes méthodes d'évaluation indiquées plus haut en les considérant comme les valeurs de fonctions du niveau de D_2O et de la concentration du bore et en les portant sur un graphique. Par suite de l'inclinaison des barres de commande, la distribution du flux subit une distorsion assez complexe au moment de l'introduction des barres. En conséquence, les variations de cette distribution en fonction du temps ont été mesurées pour différentes positions de la source de neutrons pulsés. Il a été possible de déterminer une position dans laquelle l'influence des modes supérieurs sur les mesures de la réactivité d'arrêt a été suffisamment faible.

Enfin, les auteurs montrent qu'il existe un très bon accord entre les valuers de $\left(\frac{\delta\rho(H, c_i)}{\delta(1/H^2)}\right)_{H=H_i}$ et de $\left(\frac{\delta\rho(H_i, c)}{\delta c}\right)_{c=c_i}$ (ρ est la réactivité, H_i est le niveau de D_2O à l'état critique pour la concentration du bore c_i) que l'on obtient par la méthode de la période constante pour l'état légèrement surcritique et par la méthode des neutrons pulsés pour l'état sous-critique.

ИЗМЕРЕНИЯ ИМПУЛЬСНЫХ НЕЙТРОНОВ НА ТЯЖЕЛОВОДНОМ ЭНЕРГЕТИЧЕСКОМ РЕАКТОРЕ ПРИ НУЛЕВОЙ МОЩНОСТИ. Метод импульсных нейтронов использовался для измерений нулевой мощности в активной зоне тяжеловодного реактора. Для оценки измерений импульса использовались различные методы. Методы так называемой "интегральной" оценки основаны на теориях, опубликованных Сьестрандом и Гозани; до сих пор они применялись главным образом к легководным реакторам. Эти методы используют не только постоянную распада мгновенных нейтронов, но также и информацию, содержащуюся в следах запаздывающих нейтронов для определения реактивности. Однако для измерений на тяжеловодных реакторах эти методы необходимы модифицировать с тем, чтобы должным образом учесть временную зависимость запаздывающих нейтронов. Доля запаздывающих нейтронов рассчитывалась при разумном учете ее временной зависимости. В результате этих измерений можно получить всю необходимую информацию. Эти методы хорошо подходят для расчета выхода реактивности с достаточной точностью. Для проверки результатов интегральных методов применялась аналитическая процедура. Это по существу связано с точным расчетом временной зависимости доли запаздывающих нейтронов, что достигается с помощью процедуры повторения.

Результаты различных вышеуказанных методов оценки сравниваются между собой путем помещения их как функции уровня D_2O и концентрации бора. Из-за наклона регулирующих стержней распределение потока искажается довольно сложным образом в то время, когда стержни введены. Поэтому временная зависимость этого распределения измерялась для различных положений источника импульсных нейтронов. Оказалось возможным найти одно положение, для которого влияние более высоких форм на измерение реактивности остановленного реактора было достаточно малым.

И, наконец, показывается, что величины $\left(\frac{\delta\rho(H, c_i)}{\delta(1/H^2)}\right)_{H=H_i}$ и $\left(\frac{\delta\rho(H_i, c)}{\delta c}\right)_{c=c_i}$ (ρ – реактивность, H_i – критический уровень D_2O для концентрации бора c_i), полученные периодическими измерениями в слегка надкритическом состоянии, а также измерения импульсов в подкритическом состоянии, хорошо между собой согласуются.

MEDICIONES POR EL METODO DE LOS NEUTRONES PULSADOS REALIZADAS EN UN REACTOR DE POTENCIA DE AGUA PESADA (MZFR) A ENERGIA NULA. Los autores han empleando el método de los neutrones pulsados para realizar mediciones a energía nula en el cuerpo de un reactor de agua pesada. Siguieron diversos métodos para evaluar los resultados de esas mediciones. Los métodos denominados de evaluación «integral» se besan en teorías dadas a conocer por Sjostrand y Gozani, y hasta la fecha se habían venido aplicando principalmente a los reactores de agua ligera. Estos métodos emplean para la determinación de la reactividad no sólo la constante de decrecimiento de los neutrones inmediatos, sino también los datos relativos a las «colas» de neutrones retardados. Ahora bien, para efectuar mediciones en un reactor de agua pesada, fue preciso modificar esos métodos a fin de tener debidamente en cuenta la variación de la población de neutrones retardados en función del tiempo. Se calculó la fracción de esos neutrones asignando un valor hipotético razonable a su variación en función del tiempo; las mediciones proporcionaron todos los datos necesarios. Estos métodos se prestan bien al cálculo manual para determinar el valor de la reactividad con la debida precisión. A fin de verificar los resultados de los métodos de evaluación integral,

se empleó un procedimiento analítico, el cual requiere un cálculo exacto por un procedimiento iterativo de la variación de la fracción de neutrones retardados en función del tiempo.

Los autores comparan los distintos métodos de evaluación anteriormente mencionados recurriendo a su representación gráfica en función del nivel D_2O y de la concentración de boro. Debido a la inclinación de las barras de control, la distribución del flujo experimenta una distorsión un tanto compleja cuando se introducen las barras. Por ello, se midió la variación de esta distribución en función del tiempo para distintas posiciones de la fuente de neutrones pulsados y se pudo encontrar una posición en la cual la influencia ejercida por los armónicos superiores sobre los resultados de las mediciones de la reactividad de parada era suficientemente pequeña.

Por último, los autores demuestran que existe una concordancia muy satisfactoria entre los valores $\left(\frac{\delta\rho(H, c_i)}{\delta(1/H^2)}\right)_{H=H_i}$ y $\left(\frac{\delta\rho(H_i, c)}{\delta c}\right)_{c=c_i}$ (en donde ρ es la reactividad y H_i el nivel crítico del D_2O para una concentración c_i de boro) obtenidos por medición del período en un estado ligeramente supercrítico, y las determinaciones realizadas con neutrones pulsados en el estado subcrítico.

1. INTRODUCTION

With zero-energy measurements on a power reactor it is of great advantage to use the pulsed neutron source method. The time for such experiments is generally limited and a computer is not always available in this phase. Therefore it is desirable to evaluate pulsed neutron measurements by methods which yield reactivity values with proper accuracy within the shortest possible time using only simple tools. In favourable cases it is then possible to complete the evaluation whilst the measurements for the persisting experiment are being made. This helps to reveal any irregularities as long as the measurements are repeatable.

Using the integral evaluation method of pulsed measurements [1, 2] it is possible to obtain the reactivity of a subcritical state from a single measurement. In this way it is no longer necessary to relate to a "normalizing measurement", i.e. to the determination of the generation time Λ for the critical reactor, which, independent of the method selected, is always somewhat tedious. Moreover, errors in Λ are not introduced into the results of all measurements.

In view of the above considerations the integral evaluation method was modified so that it can also be applied in a simple way to systems with a long generation time. This method was utilized for quick evaluation of the pulsed measurements on the zero-energy assembly of the MZFR (D_2O natural uranium reactor). The suppositions of the integral method [2] were assumed to be valid for this reactor since its reflector thickness (about 30 cm) was small in comparison to the core dimensions (radius about 150 cm, height 150-350 cm) and the measured reactivities never exceeded the value of -10 \$.

For a few measurements, an analytical method for the determination of the reactivity was used, too, and thus it was possible to check the results of the modified integral method.

2. SURVEY OF VARIOUS METHODS USED FOR DETERMINING THE REACTIVITY FROM PULSED MEASUREMENTS

The time behaviour of the fundamental mode $n_o(t)$ in a subcritical reactor following the injection of a short neutron burst (δ-pulse) can be represented by a sum of exponential functions: $n_{oE}(t) = \sum_0^m A_j e^{-\omega j t}$ (subscript E denoting a single pulse). The values ω_j are obtained as solutions of the inhour equation

$$\omega = \frac{\beta - \rho}{\Lambda} + \frac{1}{\Lambda} \sum_{i=1}^{m} \frac{\beta_i \lambda_i}{\omega - \lambda_i} \qquad (1)$$

where ρ is the reactivity of the system, Λ the generation time, m the number of delayed neutron groups, β_i the effective fraction and λ_i the decay constant of the i-th group.

The algebraically largest value of of ω, denoted by ω_o, is always greater than λ_i. Furthermore, if the condition $\omega_o \gg \lambda_i$ is satisfied, then $\omega_o \gg \omega_j (j \geq 1)$ and if the amount of the term $\frac{1}{\Lambda} \sum_{i=1}^{m} \frac{\beta_i \lambda_i}{\omega_o - \lambda_i}$ is negligible when compared to ω_o, then $\omega_o \approx (\beta - \rho)/\Lambda$ and we obtain the known relationship

$$\omega_o = \frac{\beta - \rho}{\Lambda} = \frac{1 - k_{eff}(1 - \beta)}{\Lambda k_{eff}} = -\frac{k_p - 1}{l} = \alpha \qquad (2)$$

where α is the decay constant of the prompt neutrons, k_{eff} the effective multiplication factor, k_p the prompt multiplication factor and l the neutron lifetime. $A_o e^{-\omega_o t} = A_o e^{-\alpha t}$ then represents the time profile of the density of prompt neutrons. Substituting the reactivity ρ^* (\$) related to β into Eq. (2), we obtain

$$\rho^* = 1 - \alpha \frac{\Lambda}{\beta} \qquad (2')$$

When Λ is known or is determined from a pulsed neutron measurement with known reactivity, e.g. $\rho = 0$, the decay constant α measured in a subcritical state yields directly the associated reactivity ρ. This is, however, subject to the condition that Λ remains constant over the entire reactivity range under investigation or that deviations from the value obtained from the "normalizing measurement" can be treated theoretically.

For H_2O-moderated systems the condition $\omega_o \gg \lambda_i$ is in general satisfied over the entire range $\rho \leq 0$, because of the short neutron generation time $\Lambda (\approx 10^{-4}$ s). With graphite-moderated or D_2O-moderated reactors the generation time is appreciably longer ($\approx 10^{-3}$ s) and the term

$$\frac{1}{\Lambda} \sum_{i=1}^{m} \frac{\beta_i \lambda_i}{\omega_o - \lambda_i}$$

can only be ignored for reactivities $\rho < -5\%$. For measurements in the range $-5\% < \rho < 0$ the complete Eq. (1) must be used instead of Eq. (2). Furthermore,

$\omega_o \gg \omega_j$ $(j \geq 1)$ no longer holds true; determining ω_o from the measured $n(t)$ requires an analysis in which the time variation from $\omega_j (j \geq 1)$ of the "background" can no longer be neglected in the range of the usual measuring intervals T of about $10/\omega_o$ [3].

With N δ-source pulses following each other in regular time intervals of length T for $N\,\omega_j T \gg 1$ (state of equilibrium), the expression for the single pulse

$$(T = \infty)\; n_{oE}(t) = \sum_{j=0}^{m} A_j e^{-\omega_j t}$$

becomes

$$n_o(t) = \sum_{j=0}^{m} \frac{A_j}{1 - e^{-\omega_j T}} e^{-\omega_j t}$$

Since for pulsed experiments $\omega_o T$ is always $\gg 1$, the amplitude A_o remains unchanged, but there is a significant increase in "background" as compared with the single pulse.

The method for the evaluation of pulsed measurements described in section 3 takes account of the time dependence of the "background" by a linear approximation. The analytical method (section 4) used in conjunction with some measurements for purposes of comparison is based on a least-squares fit of the theoretical time behaviour of the entire density $n_{oE}(t)$.

2.1. *Sjöstrand's method*

SJÖSTRAND [1] showed that by using the information contained in the fraction of the delayed neutrons resulting from periodic pulsing there is no need for a normalizing measurement of Λ for the determination of ρ. The method developed by him is based on the following considerations.

If $M_{tot} = \frac{1}{1 - k_{eff}}$ is the total multiplication to which a source neutron of the fundamental mode is subjected in the reactor with the multiplication factor k_{eff} and if

$$M_p = \frac{1}{1 - k_p} = \frac{1}{1 - k_{eff}(1 - \beta)}$$

is similarly the prompt multiplication, then

$$\frac{M_\rho}{M_{tot} - M_p} = \frac{1 - k_{eff}}{k_{eff}\beta} = \frac{-\varrho}{\beta} = -\varrho^* \qquad (3)$$

(In the following $M_p/(M_{tot} - M_p)$ will be denoted as the multiplication quotient.)

If the reactor is excited to the state of equilibrium (precursors of the delayed neutrons in the saturation) by periodic source pulses (repetition time T) we find for the fundamental mode that the density of prompt neutrons $n_{op}(t)$ integrated over a measuring interval T is proportional to the prompt multiplication, and the density $n_o(t)$ (also integrated over an interval T) is proportional to the total multiplication. Thus, we obtain

$$\frac{\int_0^T n_{op}(t)dt}{\int_0^T n_o(t)dt - \int_0^T n_{op}(t)dt} = \frac{M_p}{M_{tot} - M_p} = -\varrho^* \quad . \tag{4}$$

Determining the reactivity by this method presupposes that the fraction of the density of prompt neutrons $n_{op}(t)$ can be obtained from the measured $n_o(t)$. This is a simple matter if the conditions $\alpha \approx \omega_o$ and $\omega_o \gg \omega_j$ $(j \geq 1)$ are satisfied. If this is the case the prompt neutron density $n_{op}(t)$ is given by $A_o e^{-\alpha t} = A_o e^{-\omega_o t}$ and can be easily determined from $n_o(t)$ since the density of delayed neutrons – then identical to

$$\sum_{j=1}^{m} A_j e^{-\omega_j t}/(1-e^{-\omega_j t})$$

– can be taken as constant during the decay of $n_{op}(t)$.

If the above conditions are no longer satisfied, ω_o has to be obtained from an analysis of $n_o(t)$ and the fraction of the density of prompt neutrons can no longer be determined in a simple way (section 3). Independently of this, difficulties will arise if the measured n(t) contains higher modes, since then the direct use of Eq. (4) would lead to errors in the reactivity values.

For his reactivity determinations on the D_2O reactor SR1 Sjöstrand eliminated these two influences by theoretical corrections.

2.2. Gozani's method

With the method for the evaluation of pulsed neutron measurements published by GOZANI [2] the reactivity is also calculated from the multiplication quotient of Eq. (3); however, the contribution of the fundamental mode to the prompt neutron density is obtained by a simple extrapolation method. This method presupposes that the time variation of the source strength during the pulse is known. Gozani bases its derivation on periodic rectangular pulses of duration d with repetition time T and makes the assumption that the above conditions $\alpha \approx \omega_o$ and $\omega_o \gg \omega_j$ are satisfied. The extrapolation method is shown in Fig. 1. B is the constant "background" of the delayed neutrons and n_d the maximum value of the density of prompt neutrons in the fundamental mode at the end of the source pulse. It is determined from an extrapolation of the exponential part for $t > t_w$ of $n_{op}(t)$ into the range $t < t_w$. For the reactivity ρ^* we then obtain the following relationship

$$-\rho^* = \frac{n_d d}{1-e^{-\alpha d}} \Big/ BT \tag{5}$$

Since this method does not permit the higher modes of the delayed neutrons to be eliminated, the reactivity values thus determined are invariably subject to systematic errors. The errors are, however, appreciably smaller than those obtained by the direct application of Eq. (3) since the amplitudes of the higher modes compared to that of the fundamental mode of the delayed neutron density are very much smaller than in the prompt fraction.[1]

[1] The k β/l method proposed by GARELIS and RUSSELL [4] cannot be applied in a simple manner to systems with long generation times. Therefore we could not use this method – already employed by us with advantage to experiments on H_2O systems – to evaluate our zero-energy measurements on the MZFR.

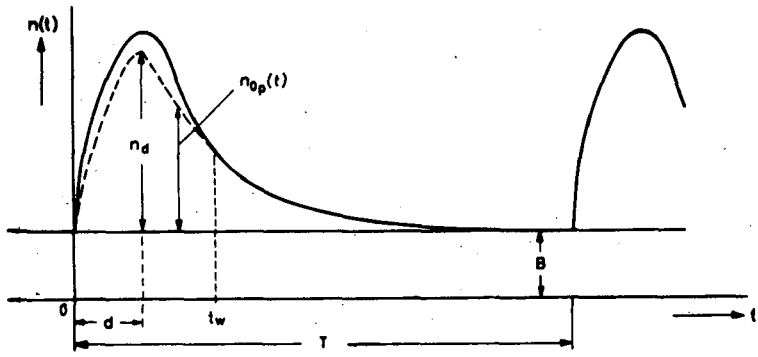


Fig. 1

Gozani's method of reconstructing the prompt main mode

Gozani applied this method to the evaluation of pulsed measurements on the H_2O swimming pool reactor SAPHIR.

In the following it is shown that the two methods can be modified so that, even with the exclusive use of experimental data, they allow quick determination of the reactivity on systems with long neutron generation time in the range $\rho^* < -1\ \$$.

3. SIMPLE EXTENSION OF THE INTEGRAL METHOD FOR REACTIVITY MEASUREMENTS ON SYSTEMS HAVING LONG GENERATION TIMES

In carrying out pulsed neutron measurements on systems having long generation times (D_2O, graphite) the "background" B can no longer be assumed to be constant for the duration of the measuring interval ($T \approx 10/\omega_0$) for reactivities $\rho > -5\%$. The obvious thing to do is to use a linear approximation for its time variation since then the necessary data can be taken in a convenient way from the experiment. To illustrate the method it will be best to start with periodic δ-source pulses. Then

$$B(t) = \sum_1^m \frac{A_j}{1-e^{-\omega_j T}} \cdot e^{-\omega_j t} \approx \sum_1^m \frac{A_j}{1-e^{-\omega_j T}}(1-\omega_j t) = B(0) - \frac{B(0)-B(T)}{T}\, t$$

The value B(T) is measured directly at the end of the measuring interval when $A_0 e^{-\omega_0 t}$ has practically decayed to zero; the slope $s = -[B(0) - B(T)]/T$ and with this B(0) must be determined from the recorded n(t). Of the various possible methods mainly one method was used, in which s and also ω_0 can be calculated from the ratio of partial integrals of n(t) which are free of harmonics (Appendix 1).

For s and ω_0 we find the following formulas:

$$s = -\frac{2(I_2^2 - I_1 I_3)}{2I_2(T-t_2)^2 - I_1(T-t_3)^2 - I_3(T-t_1)^2}$$

$$\omega_0 = \frac{1}{t_3 - t_1} \ln \frac{I_1 + s/2(T-t_1)^2}{I_3 + s/2(T-t_3)^2}$$

where $I_k = \int_{t_k}^{T} n(t)dt - B(T) \cdot (T-t_k)$, with k = 1, 2, 3 and $t_2 = (t_1+t_3)/2$.

Substituting ω_o into Eq. (1) we obtain

$$\omega_o = \alpha + \frac{1}{\Lambda} \sum_{1}^{m} \frac{\beta_i \lambda_i}{\omega_o - \lambda_i}$$

from which the value α can be calculated. Since the second term on the right-hand side only represents a correction for $\rho \leqq 0$ it will suffice to determine the necessary value of Λ from the simplified relationship $\omega_o = (\beta - \rho)/\Lambda$ by using an approximate value for ρ (e.g. from the integral method with constant background).

The integral method requires that the neutron density n(t) be divided into a prompt and a delayed fraction; however, a spurious background caused by spontaneous fission, etc. has to be eliminated. With periodic δ-pulses this separation is a simple matter: With each pulse the neutron density $n_d(t)$ of the fundamental mode is suddenly raised by $\sum_{0}^{m} A_j = A$. This can be directly measured with a true fundamental mode excitation and in the presence of higher modes it can be obtained from the relationship $A = A_o + B(0) - B(T)$ where A_o can be determined by extrapolation of the function $A_o e^{-\omega_o t}$ and B(0) from B(T) and s. The increase A corresponds to the increase in the prompt neutron density $n_{op}(t)$ since the density of the delayed neutrons cannot vary suddenly. Since the prompt neutron density of the preceding pulses has completely decayed up to this moment, A represents just the value of the prompt neutron density of the fundamental mode at the time t = 0. If α is used, the value of the integral of $n_{op}(t)$ during the measuring interval is now obtained from

$$\int_{0}^{T} n_{op}(t)dt = \frac{A}{\alpha}$$

Forming now the "prompt harmonic-free" total integral

$$I_f = \frac{A_o}{\omega_o} + \frac{B(0) + B(T)}{2} \cdot T$$

and subtracting A/α gives the fraction of the delayed neutrons which, however, contains the contribution of the delayed higher modes as does Gozani's expression, Eq. (5).

The reactivity is given by

$$\rho^*[\$] = - \frac{A}{\alpha} / (I_f - \frac{A}{\alpha}) \qquad (6)$$

To check the influence of higher modes, ρ^* can also be determined by the simple integral method Eq. (4), yielding

$$\rho^* = - (\int_{0}^{T} n(t)dt - I_f + \frac{A}{\alpha}) / (I_f - \frac{A}{\alpha}) \qquad (7)$$

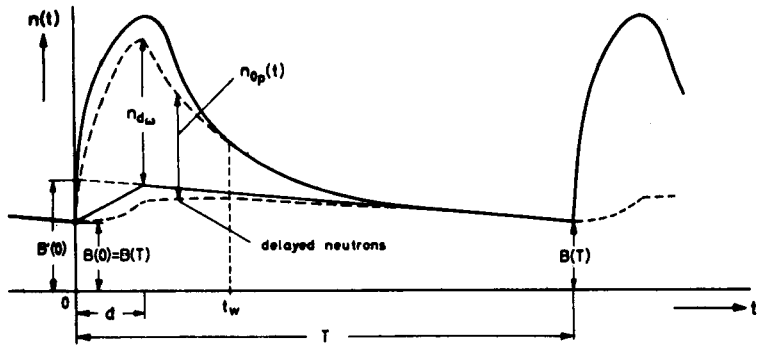


Fig. 2

The reconstruction of the prompt main mode for the modified integral method

For the rectangular source pulses (duration d) which are generally used the conditions are not quite so simple (Fig. 2). The integrals A_o/ω_o and A/α change to the form of Eq. (5) $n_{d\omega}\, d/(1 - e^{-\omega_o d})$ and $n_{d\alpha}\, d/(1 - e^{-\alpha d})$, and the "background" B(t) must be represented by two linear functions (Fig. 2).

$$B(t) = B(T) + [B'(0) - B(T)]\left(\frac{t}{d} - \frac{t}{T}\right);\ 0 \leq t \leq d$$

$$B(t) = B'(0) - \frac{B'(0) - B(T)}{T}\, t;\ d \leq t \leq T$$

where B'(0) is the extrapolated value for t = 0.

s, ω_o, and α can again be determined in the same way as for the δ-pulses; the values B'(0) and $n_{d\omega}$ are obtained by extrapolation. Obviously, however, the value of $n_{d\alpha}$ cannot any longer be obtained by simple measuring. Generalizing the conditions for δ-pulses the rectangular pulses can be treated (Appendix 2) and the following relation between $n_{d\omega}$ and $n_{d\alpha}$ is found

$$n_{d\alpha} = \frac{1 - e^{-\alpha d}}{1 - e^{-\omega_o d}}\ \frac{\omega_o}{\alpha}\ \left(1 + \frac{1 - e^{-\omega_o d}}{\omega_o d}\ \frac{B'(0) - B(T)}{n_{d\omega}}\right) n_{d\omega}$$

The prompt fraction of the fundamental mode thus is

$$\int_0^T n_{0p}(t)\, dt = \frac{n_{d\alpha} d}{1 - e^{-\alpha d}}$$

The "prompt harmonic-free" total integral I_f now takes the form

$$I_f = \frac{n_{d\omega}\, d}{1 - e^{-\omega_o d}} + \frac{B'(0) + B(T)}{2}\, T - \frac{B'(0) - B(T)}{2}\, d$$

Thus, Eq. (6) becomes

$$\rho^*[\$] = -\left(\frac{n_{d\alpha}\, d}{1 - e^{-\alpha d}}\right) \Big/ \left(I_f - \frac{n_{d\alpha}\, d}{1 - e^{-\alpha d}}\right)$$

and Eq. (7)

$$\rho^*[\$] = -\left(\int_0^T n(t)\,dt - I_f + \frac{n_{d\alpha}\, d}{1 - e^{-\alpha d}}\right) \Big/ \left(I_f - \frac{n_{d\alpha}\, d}{1 - e^{-\alpha d}}\right)$$

4. ANALYTICAL METHOD FOR CHECKING THE MODIFIED INTEGRAL METHOD

The analytical evaluation method used by us is an ALGOL-programmed fit method. For the one-group model the neutron density $n_E(t)$ following a single δ-pulse or rectangular pulse is represented by as many delayed neutron groups as desired. The values of λ_i and β_i of these groups to be substituted into $n_E(t)$ are considered to be sufficiently well known while the properties of the source pulse are experimentally determined. The problem of determining the two parameters ρ and Λ from a curve $n_E(t)$ can be reduced to the fitting of ρ if Λ is determined first for a state of known reactivity. A measurement on the critical reactor with $\rho = 0$, for example, gives a value for the generation time Λ_k (more exactly: a fit parameter for λ_i and β_i). The values of Λ for states with changed geometry can then be obtained from Λ_k by small corrections. For the subcritical states then it is only necessary to determine the reactivity ρ.

Since an analysis taking into account higher modes is not reliable enough we confine ourselves in each case to those sections of the decay curves which are nearly free of higher modes. With the aid of the computer programme the curve $n_E(t)$ for a single pulse is reconstructed from the function n(t) for periodic source pulses measured with a multichannel time analyser. Then, either with $\rho = 0$ and an initial value $\Lambda_k^{(1)}$ (critical reactor) or with Λ (calculated from Λ_k) and an initial value $\rho^{(1)}$ (subcritical reactor) the programme computes the roots of the inhour equation $\omega_j^{(1)}$ and the amplitudes $A_j^{(1)}$. Writing

$$n^{(1)}(t) = n_E(t) - \left(\sum_{j=1}^{m} A_j^{(1)} e^{-\omega_j^{(1)} t}\right)_{theor.}$$

would give

$$n^{(1)}(t) = A_o^{(1)} e^{-\omega_o^{(1)} t}$$

in the case of correct parameters. For the specified initial values a value $\omega_o^{(2)}$ can now be determined from $n^{(1)}(t)$ by the method of least squares fitting (with a weighting function which takes into account the fraction $\sum_1^m A_j^{(1)} e^{-\omega_j^{(1)} t}$ and the counting statistics); the inhour equation then gives an improved value, $\Lambda^{(2)}$ or $\rho^{(2)}$. After a few iterations no further improvement of the results is obtained.

5. DESCRIPTION OF THE REACTOR AND EXPERIMENTAL ARRANGEMENT

The pulsed neutron experiments described below were performed on the zero-energy assembly of the Mehrzweck-Forschungsreaktor (MZFR) which at present is being erected on the site of the Kernforschungszentrum, Karlsruhe. The MZFR is a D_2O-moderated and D_2O-cooled pressure-vessel reactor employing UO_2 of natural isotope composition as fuel; it has a thermal output of 200 MW. A detailed description of this reactor is given in [5]. The zero-energy measurements required special measuring devices and easy access to the reactor core. Since these conditions would have been difficult to meet on the completed reactor, the zero-energy measurements were made on an assembly set up solely for this particular purpose.

The core was built up step by step to its full size ($R_c \approx 150$ cm, $H_c \approx 350$ cm) with the original fuel rods in a steel tank of a shape similar to that of the moderator vessel of the MZFR. Also, the original control rods were used in the same array as on the MZFR; they were inserted obliquely from the top into the core. Details of the zero-energy assembly are given in [6]. Pulsed measurements were carried out on the fully charged assembly.

A Philips neutron generator with sealed-off neutron tube was used as pulsed neutron source. The maximum possible pulse duty factor d/T was 10%. The minimum pulse repetition frequency was 0.7 c/s, corresponding to $T \approx 1.4$ s. The neutron source strength during the pulse was about 10^9 n/s. The neutron tube was accomodated preferably in a "thimble" which projected from the bottom into the reflector close to the centre line.

BF_3 counters were used as neutron detectors. They could be displaced vertically in thin-walled axially parallel aluminium tubes which were inserted into the reactor at different radial positions and reached down to the lower core edge. A TMC-256-channel time analyser which was triggered by the neutron generator was used for recording the detector pulses. A delay circuit enabled the neutron burst to start simultaneously with the first recording channel. The inherent background was recorded by a separate

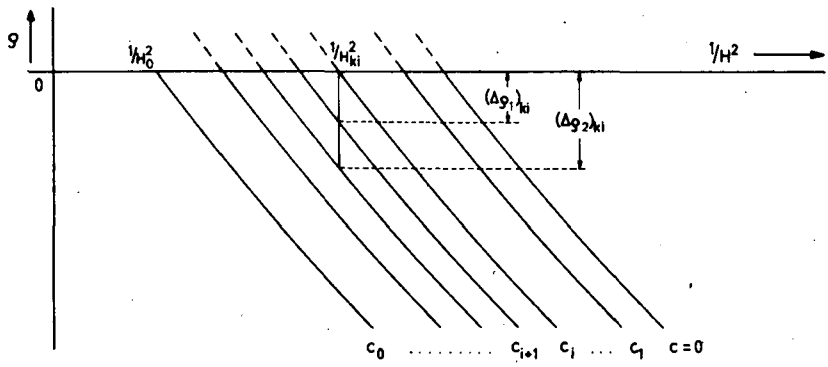


Fig. 3

Schematic presentation of the function $\rho(1/H^2, c_i)$ where ρ is the reactivity, H the water level, c the boron concentration, $H_{ki}(c_i)$ the critical water levels and H_0 the water level at full height

counter. The time analyser and counter were checked for equal counting efficiency.

The spacing between the source pulses with 10^7 to 10^8 neutrons per burst was selected as $T \approx 12/\omega_0$. Assurance thus was given that the prompt neutron density had decayed practically to zero at the end of the interval T and the fraction of the delayed neutrons of the total background measured could be determined with a sufficiently high accuracy. In the worst case the inherent background was equal in magnitude to that produced by the periodic pulsing. In most cases by properly locating the detector and source it could be ensured that the higher modes in the prompt fraction had decayed after a waiting time t_w of $2/\omega_0$ to $3/\omega_0$. The prompt fundamental mode could then be reconstructed with reasonable accuracy.

6. MEASUREMENTS AND RESULTS

6.1. Experiments for determining excess reactivity

The pulsed neutron method was used on the fully charged reactor for measuring the neutron generation time Λ and the shutdown reactivity of the control rods and for determining the excess reactivity. A brief description of the experiments for determining the excess reactivity is given first. With this procedure, a detailed description of which is given in [6], the excess reactivity of the reactor is reduced in steps by adding boron, the differential quotient

$$\left(\frac{\partial \varrho(H_i, c)}{\partial c}\right)_{c=c_i} = -\varkappa(c_i)$$

being determined in each case from measured reactivity ρ as a function of the water level H at a constant boron concentration c_i. (H_i is the critical water level at a boron concentration c_i.) In [6] it is shown how the excess reactivity of the fully charged unpoisoned reactor can be calculated from κ.

The measurement of the reactivity as a function of the water level also yields the differential quotient

$$\left(\frac{\partial \varrho(H, c_i)}{\partial (1/H^2)}\right)_{H=H_i}$$

Like κ, this was, furthermore, determined by period measurements in the slightly supercritical range, thus enabling a comparison to be made between period and pulsed neutron measurements.

The neutron generation time was determined from pulsed neutron measurements on the critical reactor. For $\rho = 0$ the background is especially high and its time dependence is greatly pronounced because of the very small value of ω_0 obtained in this case. Nevertheless, as the values of Table I show, fairly good results are obtained by representing the time-dependent background by a linear function.

Table II permits a comparison to be made of the reactivity values which result from measurements with a varying water level in the range $\rho < 0$ by

TABLE I

COMPARISON OF THE EVALUATION METHODS FOR NEUTRON GENERATION TIME Λ_k IN THE CRITICAL REACTOR FOR DIFFERENT STATES OF POISONING

Boron concentration	Critical water level	Modified integral method (section 3)		Analytical method (section 4)	
c (ppm B)	H_k (m)	ω_{0k} (s^{-1})	Λ_k (ms)	ω_{0k} (s^{-1})	Λ_k (ms)
0	1.732	8.1 ± 0.3	0.935 ± 0.04	8.22 ± 0.04	0.92 ± 0.02
1.5858	1.868	8.0 ± 0.3	0.945 ± 0.04	8.15 ± 0.04	0.93 ± 0.02
8.670	4.123	8.6 ± 0.3	0.875 ± 0.04	8.80 ± 0.05	0.855 ± 0.03

Note: The water level is measured from a plane 0.360 m below the lower fuel edge, corresponding approximately to the bottom of the equivalent bare reactor. The effective fraction of delayed neutrons was calculated to be $\beta_{eff} = 7.13 \times 10^{-3}$ for the MZFR core.

TABLE II

COMPARISON OF THE EVALUATION METHODS FOR MEASUREMENTS OF THE REACTIVITY AS A FUNCTION OF THE WATER LEVEL H IN THE RANGE $\rho < 0$

Boron concentration	Water level	Modified integral method			Analytical method	
c (ppm B)	H (m)	ω_0 (s^{-1})	$-\rho$ (%)	$-\rho\omega$[a] (%)	ω_0 (s^{-1})	$-\rho$ (%)
0	1.732	8.1	0	0	8.22	0
	1.667	15.9	0.82	0.76	15.9	0.74
		15.5	0.81	0.72	16.0	0.75
		15.8	0.78	0.75	16.0	0.75
	1.591	26.1	1.78	1.74	27.2	1.79
	1.519	38.1	3.03	2.90	39.2	2.93
		37.9	2.89	2.88	38.8	2.89
	1.426	55.1	4.92	4.57	57.3	4.66
		55.8	4.96	4.64	55.4	4.48
	1.371	69.7	5.91	6.00	69.3	5.82
3.705	2.028	16.0	0.72	0.73	16.7	0.77
	1.806	35.6	2.61	2.57	37.9	2.67
	1.667	52.9	4.36	4.22	55.6	4.30
8.493	3.459	15.1	0.57	0.57	15.3	0.58
	3.018	23.0	1.26	1.28	23.5	1.30
	2.698	31.6	2.05	2.05	32.2	2.06
	2.477	39.0	2.72	2.71	40.0	2.75
	2.270	48.1	3.58	3.54	49.0	3.55

[a] Calculated from the inhour equation.

the modified integral method[2] and by the analytical method. As can be seen the results generally are in good agreement. Greater differences are obtained only for the measurements c = 0, H = 1.667 m and c = 0, H = 1.426 m. This can be attributed most likely to disturbances of the inherent background during the recording.

For an additional comparison the column giving the results from measurements by the modified integral method also contains reactivity values ρ_ω computed from ω_0 with the aid of the inhour equation, Eq. (1). For the boron concentrations, c = 3.075 ppm B and c = 8.493 ppm B, for which measurements in the critical state were not available the required particular Λ_k was

[2] Those delayed photoneutrons ($\lambda_i < 10^{-3}\ s^{-1}$) which are not excited to the state of equilibrium during a pulsed neutron experiment do not contribute to the total β (7.13×10^{-3}) by more than 3×10^{-5}. Therefore the error introduced in the calculation of ρ(%) from the measured ρ^*(\$) by using the value of β containing those fractions, too, is insignificant.

determined by the usual extrapolation method. The calculation of ρ_ω took into account the variation of Λ with the water level.

6.2. *Comparison of the results from pulsed neutron and period measurements*

Figure 3 schematically shows the relationship between ρ, water level H, and boron concentration c in the form of a set of curves. The pulsed neutron experiments yielded the function $\rho\,(1/H^2,\ c_i)$ in the subcritical range. Since after evaluation by the modified integral method the measurements showed that the functions $\rho\,(1/H^2, c_i)$ can be fairly well approximated by straight lines the differential quotients

$$\left(\frac{\partial \varrho(H, c_i)}{\partial (1/H^2)}\right)_{H=H_i}$$

were determined from the slope of these straight lines. These differential quotients could be obtained also from period measurements by the method usually employed for measuring level coefficients. As can be seen from Fig. 4 the values obtained by these two experimental methods are in fairly good agreement.

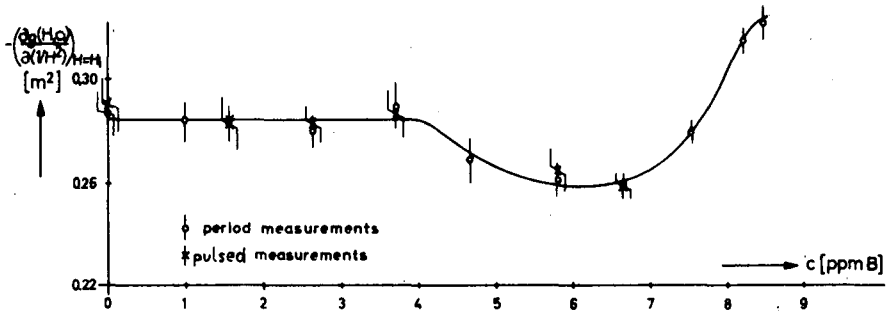


Fig. 4

Measured values of $-[\partial\rho(H, c_i)/\partial(1/H^2)]_{H=H_i}$

The value $\kappa\,(c_i)$ can be determined directly from the curve segments $\rho\,(1/H^2, c_i)$ measured in the range $\rho < 0$. The increments $\Delta\rho_1$ can be taken directly from the curve segments and used for forming the quotients of the differences $[(\Delta\varrho/\Delta c)_1]_{H_i}$ which represent first approximate values for $\kappa(c_i)$. Plotting these quotients versus the associated values for Δc and extrapolating to $\Delta c = 0$ the partial differential quotient $(\partial\varrho/\partial c)_{c=c_i} = \varkappa(c_i)$ is obtained directly. With period measurements, however, κ has to be determined [6] from the relationship

$$-\varkappa(c_i) \equiv \left(\frac{\partial \varrho(H_i, c)}{\partial c}\right)_{c=c_i} = \left(\frac{\partial \varrho(H, c_i)}{\partial (1/H^2)}\right)_{H=H_i} \cdot \frac{d(1/H_i^2)}{dc}$$

Figure 5 shows the results for $\kappa(c_i)$ obtained by both methods. The agreement between the values is satisfactory.

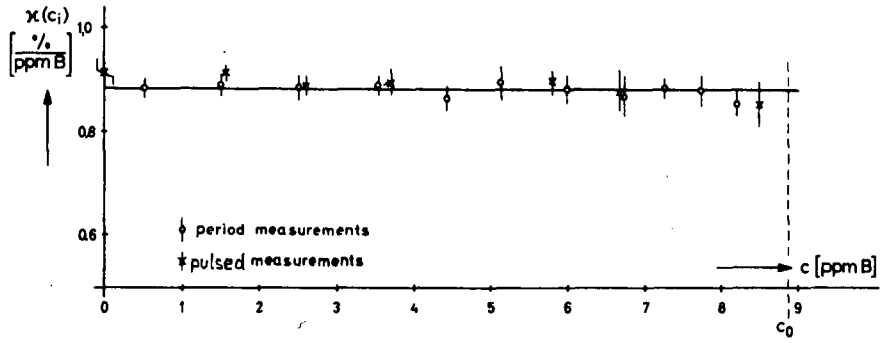


Fig. 5

Experimental values of $\kappa(c_i) = -[\partial\rho(H_i, c)/\partial c]_{c=c_i}$

6.3. *Measurement of the shutdown reactivity*

The shutdown reactivity is denoted as the amount of (negative) reactivity of the unpoisoned and fully charged reactor in which all the control rods are completely inserted. The reactor with inserted inclined control rods has a very complex density distribution for the fundamental mode, which is not symmetrical to the centre plane through the core but has a maximum in the upper half of the core. With the pulsed neutron source at the lower core edge only a very weak excitation of the fundamental mode was obtained. With n(t) measured at the technically possible detector positions, the decay of the prompt main mode up to the moments of the order of magnitude of $5/\omega_0$ was distorted by higher modes; the measurements could not be evaluated. A decisive improvement with respect to the excitation of the fundamental mode could be obtained by arranging the source on the cover of the reactor vessel. This is pronounced particularly in Fig. 6 which represents time-dependent axial distributions measured for the two source positions. When the source is positioned at the bottom the prompt main mode is not established even after 130 ms ($\approx 5/\omega_0$); however, with the source arranged on the cover the asymptotic distribution is already attained after about 30 ms ($\approx 1/\omega_0$). The axial density distribution of the delayed neutrons is shown in the diagram too.

The values obtained for the negative reactivity of the reactor with inserted control rods from two runs are given in Table III. The value of

TABLE III

VALUES FOR NEGATIVE REACTIVITY OF REACTOR WITH INSERTED CONTROL RODS

$-\rho_I$ (%)	$-\rho\omega$ (%)
3.20 ± 0.1	3.36 ± 0.3
3.18 ± 0.1	3.32 ± 0.3

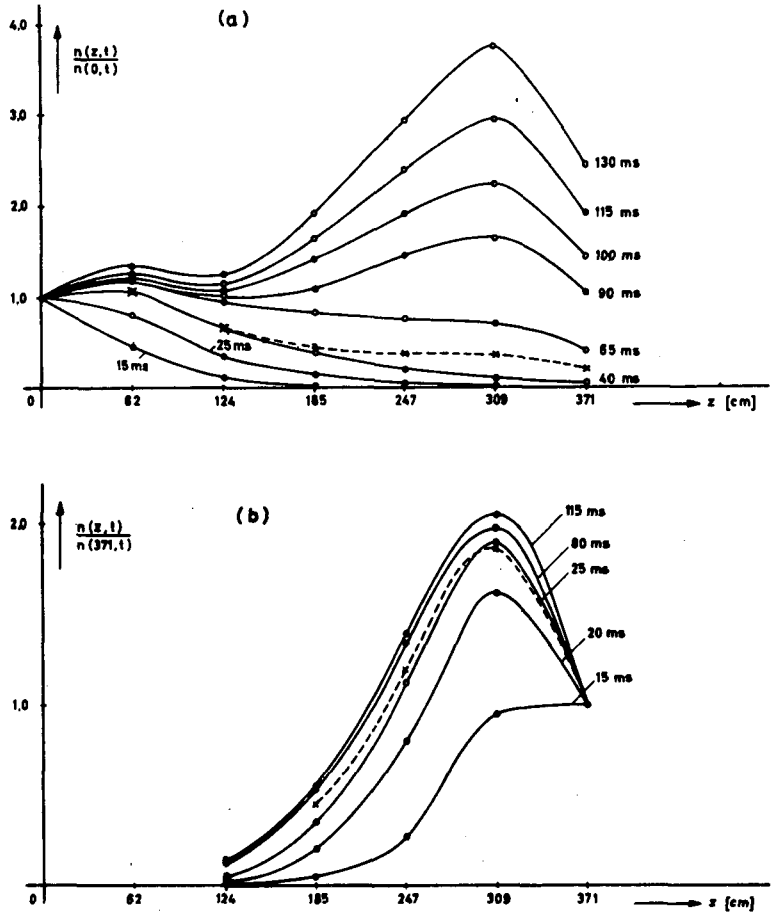


Fig. 6

Time dependence of axial flux distribution following a neutron burst; water level at full height, all control rods inserted

(a) Neutron source below
(b) Neutron source above

O Flux of prompt neutrons
× Flux of delayed neutrons

$-\rho_I$ was obtained by the modified integral method and $-\rho_\omega$ (with ω_o measured) from the inhour equation, Eq.(1). The required Λ was calculated from the value of the generation time measured for $\rho = 0$ (undisturbed reactor, water level lowered).

When the reactivity influence of the detector was taken into account, a shut-down reactivity $\rho_A = (3.1 \pm 0.2)\%$ was obtained. Rod drop measurements yielded $\rho_A = 2.9\%$.

7. CONCLUSIONS

For the evaluation of pulsed neutron measurements on a D_2O reactor in the range $0 > \rho > -6\%$ a modified form of the integral method was used on a fairly large scale. A linear approximation allowed for the time dependency of the background which could no longer be neglected because of the long generation time.

The data required for setting up the approximation could be taken in a simple way from the experiment itself, so that the desired quick and simple evaluation could be rendered possible. The results were in fairly good agreement with the values obtained by an analytical method with the aid of a computer.

APPENDIX

1. Determination of $s = -\frac{B(0)-B(T)}{T}$ and ω_o

In the absence of higher modes a semi-log plot of $n(t)-B(T)$ initially yields a nearly linear decrease, which is followed by a part having varying slope caused by the faulty background corrections. In the presence of higher modes this linear part is also limited from the beginning of the interval. Let these perturbations caused by higher modes vanish at time t_w. If three points t_k ($k = 1, 2, 3$) are selected, namely $t_1 = t_w$, $t_2 = t_1 + \Delta t$ and $t_3 = t_1 + 2\Delta t$, where $\Delta t \approx 1/\omega_o$, and if $n(t)-B(T)$ is integrated from t_k to T, the following expression is obtained:

$$I_k = \int_{t_k}^{T} n(t)dt - B(T)\cdot(T - t_k) \quad .$$

According to our approximation these integrals are equal to the sum of the terms $\frac{A_o}{\omega_o} e^{-\omega_o t_k}$ and $-\frac{s}{2}(T-t_k)^2$. For the determination of s we find the following condition:

$$\frac{I_1 + {}^{s}/_{2}(T-t_1)^2}{I_2 + {}^{s}/_{2}(T-t_2)^2} = e^{\omega_o \Delta t} = \frac{I_2 + {}^{s}/_{2}(T-t_2)^2}{I_3 + {}^{s}/_{2}(T-t_3)^2}$$

If the I_k are determined essentially by their exponential parts, quadratic terms of s may be neglected, and we obtain

$$s = -\frac{2(I_2^2 - I_3 I_1)}{2I_2(T-t_2)^2 - I_1(T-t_3)^2 - I_3(T-t_1)^2}$$

and

$$\omega_o = \frac{1}{2\Delta t} \ln \frac{I_1 + {}^{s}/_{2}(T-t_1)^2}{I_3 + {}^{s}/_{2}(T-t_3)^2}$$

2. Rectangular neutron pulses

With regard to rectangular neutron pulses there is no jump of the neutron density at t = 0, which could be used for the determination of the prompt amplitude. However, the ratio of the integral of the prompt part to the integral of the course determined by ω_o remains unchanged, when the shape of the source pulse is altered.

$$\frac{A/\alpha}{A_o/\omega_o} = \frac{n_{d\alpha}\; d/(1-e^{-\alpha d})}{n_{d\omega}\; d/(1-e^{-\omega_o d})}$$

Using $A = A_o + B_\delta(0) - B_\delta(T)$ (where δ stands for a δ-shaped pulse) one obtains

$$n_{d\alpha} = \frac{1-e^{-\alpha d}}{1-e^{-\omega_o d}}\;\frac{\omega_o}{\alpha}\;\left(1+\frac{B_\delta(0)-B_\delta(T)}{A_o}\right) n_{d\omega}\;.$$

But now the ratio $[B_\delta(0)-B_\delta(T)]/A_o$ is not known, since it is determined by quantities only occuring in the case of δ-pulses. For finding this, a δ-pulse is chosen which at t = 0 produces the same number of source neutrons as the rectangular pulse of width d. Hence it follows, that the integral values remain unchanged, and we obtain

$$A_o = \frac{n_{d\omega}\, d}{1-e^{-\omega_o d}}\;\omega_o$$

and

$$B_\delta(T)T + [B_\delta(0) - B_\delta(T)] = B(T)T + [B'(0) - B(T)]\;\frac{T-d}{2}$$

Furthermore the relation between $B_\delta(T)$ and B(T) has to be established. If the rectangular pulse is considered to be an integral over appropriately normalized δ-pulses, the result is

$$B(T) = \frac{1}{d}\int_0^d \left[B_\delta(0) - \frac{B_\delta(0)-B_\delta(T)}{T}\;(T-t')\right] dt'$$

$$= B_\delta(T) + \frac{d}{2T}\left[B_\delta(0) - B_\delta(T)\right]\;.$$

Hence it follows

$$B_\delta(0) - B_\delta(T) = B'(0) - B(T),$$

i.e. the difference is equal for both pulse shapes and, consequently, may be determined from the values measured for the rectangular pulse. Then

$$n_{d\alpha} = \frac{1-e^{-\alpha d}}{1-e^{-\omega_o d}}\;\frac{\omega_o}{\alpha}\;\left(1+\frac{1-e^{-\omega_o d}}{\omega_o d}\;\frac{B'(0)-B(T)}{n_{d\omega}}\right)\; n_{d\omega}$$

REFERENCES

[1] SJÖSTRAND, N. G., Ark. Fys. 11 (1956) 233.
[2] GOZANI, T., Nukleonik 4 (1962) 348.
[3] KÜCHLE, M., Exponential and Critical Experiments II IAEA, Vienna (1964) 575-85; SAGOT, M., TELLIER, H., JACQUEMART, R. and KREMSER, J., Exponential and Critical Experiments III IAEA, Vienna (1964) 163-89; SASTRE, S., WEINSTOCK, E. V., Nucl. Sci. Engng 20 (1964) 359.
[4] GARELIS, E. and RUSSELL, J. L., Nucl. Sci. Engng 16 (1963) 263.
[5] ZIEGLER, A., Atomwirtschaft, VII 1 (1962).
[6] BEHRENS, E., BRONNER, G., DIO, W. H., GRÜN, A. E., RITZ, H. and SCHLOSSER, G., Nukleonik, to be published.

ÉTUDE DES MILIEUX MULTIPLICATEURS HOMOGÈNES A L'AIDE DE SOURCES PULSÉES DE NEUTRONS

J. G. BRUNA, J. P. BRUNET, J. BUCHET, M. HOUELLE ET H. TELLIER
CENTRE D'ÉTUDES NUCLÉARIES DE SACLAY, FRANCE

Abstract — Résumé — Аннотация — Resumen

STUDY OF HOMOGENEOUS CORE ASSEMBLIES USING PULSED NEUTRON SOURCES. The pulsed neutron technique was here applied to the study of light-water-moderated homogeneous core assemblies. Using fissile materials in solution form it is easy to achieve large variations in geometrical buckling and moderation ratio. In the initial series of experiments, the fuel consisted of U^{235} or U^{233} in the form of uranyl nitrate. The solution concentrations used varied from 44 to 326 g of uranium per litre. Adoption of a coherent series of cross-sections made it possible to deduce, from the variations in the prompt neutron decay constant as a function of geometrical buckling, data on the non-leakage probability and the slowing-down area. We adopted effective cross-sections calculated on the basis of assimilating light water to a secondary differential thermalizer. Interesting comparisons are made possible by the use of two fissile materials with markedly different η and resonance capture values.

In a second series of experiments, devoted mainly to safety measures, we were able to deduce the maximum permissible concentrations in various containers at processing plants by measuring the prompt neutron decay constants in weak plutonium nitrate solutions.

ÉTUDE DES MILIEUX MULTIPLICATEURS HOMOGÈNES A L'AIDE DE SOURCES PULSÉES DE NEUTRONS. La technique des neutrons pulsés a été appliquée à l'étude des milieux multiplicateurs homogènes modérés à l'eau légère. L'emploi de matériaux fissiles, sous la forme de solutions, permet d'obtenir facilement de grandes variations du laplacien géométrique et du rapport de modération. Dans une première série d'expériences, le combustible était constitué par de l'uranium-235 ou de l'uranium-233 sous forme de nitrate d'uranyle. La concentration des solutions utilisées a varié entre 44 et 326 grammes d'uranium par litre. Des variations de la constante de décroissance des neutrons prompts en fonction du laplacien géométrique, les auteurs ont déduit, en adoptant un jeu cohérent de sections efficaces, des renseignements intéressant la probabilité de non-fuite et l'aire de ralentissement. Ils ont adopté les sections efficaces effectives calculées en assimilant l'eau légère à un thermaliseur différentiel secondaire. L'emploi de deux matériaux fissiles ayant un η et des captures résonnantes notablement différentes permet des comparaisons intéressantes.

D'une seconde série d'expériences principalement axées sur des mesures de sécurité, il est possible de déduire, par l'intermédiaire de la mesure des constantes de décroissance des neutrons prompts dans des solutions de nitrate de plutonium faiblement concentrées, les concentrations maximales admissibles dans divers récipients des usines de traitement chimique.

ИЗУЧЕНИЕ ГОМОГЕННЫХ РАЗМНОЖАЮЩИХ СРЕД С ПОМОЩЬЮ ИМПУЛЬСНЫХ НЕЙТРОННЫХ ИСТОЧНИКОВ. При изучении гомогенных размножающих сред, где замедлителем служит обычная вода, был применен импульсный метод. Использование делящихся материалов в виде раствора позволяет легко достигать больших изменений геометрического лапласиана и коэффициента замедления. В первой серии опытов топливом служили уран-235 или уран-233 в виде уранила нитрата. Концентрация примененных растворов колебалась между 44 и 326 г урана на 1 л. Из изменений константы распада мгновенных нейтронов в зависимости от геометрического лапласиана, с применением соответствующего подбора эффективных сечений, нами были получены данные относительно вероятности утечки и площади замедления. Мы применили эффективные сечения, рассчитанные на основе ассимиляции обычной воды с вторичным дифференциальным термализатором. Использование двух делящихся материалов, у которых существенно различаются η и резонансные интегралы, позволяет получать интересные сравнения.

Из второй серии опытов, касающихся главным образом мер безопасности, стало воз-

можным вывести концентрации, максимально допустимые в цехах заводов по химической обработке, через измерение констант распада мгновенных нейтронов в растворах нитрата плутония слабой концентрации.

ESTUDIO DE MEDIOS MULTIPLICADORES HOMOGENEOS CON AYUDA DE FUENTES DE NEUTRONES PULSADOS. Los autores han aplicado la técnica de los neutrones pulsados al estudio de medios multiplicadores homogéneos moderados con agua ligera. El empleo de materiales fisionables en forma de solución permite modificar fácil y ampliamente el laplaciano geométrico y la razón de moderación. En la primera serie de experimentos se empleó como combustible ^{235}U o ^{233}U en forma de nitrato de uranilo. La concentración de las soluciones utilizadas osciló entre 44 y 326 g de U/ℓ. De las variaciones de la constante de decrecimiento de los neutrones rápidos en función del laplaciano geométrico, los autores han deducido, eligiendo un conjunto coherente de secciones eficaces, datos sobre la probabilidad de no escape y sobre el área de moderación. Para ello eligieron secciones eficaces efectivas calculadas equiparando el agua ligera a un termalizador diferencial secundario. El empleo de dos materiales fisionables caracterizados por valores muy diferentes de η y de la sección eficaz de captura por resonancia permite establecer interesantes comparaciones.

En la segunda serie de experimentos, orientados principalmente a la medición de factores de seguridad, los autores pudieron deducir, por determinación de las constantes de decrecimiento de los neutrones inmediatos en soluciones diluidas de nitrato de plutonio, las concentraciones máximas admisibles para diversos tipos de recipientes empleados en las instalaciones de tratamiento químico.

1. INTRODUCTION

La facilité de mise en œuvre et la souplesse d'emploi de la technique dite des neutrons pulsés font que son application à l'étude des milieux multiplicateurs se développe de plus en plus dans de nombreux laboratoires. Les expériences réalisées à Saclay ces dernières années eurent essentiellement pour objet la détermination du rapport de la fraction effective des neutrons retardés au temps de vie des neutrons prompts ou l'étalonnage d'antiréactivités réalisées de diverses manières: barre de contrôle, empoisonnement du modérateur ou substitution d'éléments de combustible [1]. Bénéficiant des installations mises au point pour la mesure des masses critiques des solutions, les expériences pulsées furent dernièrement orientées vers l'étude des milieux multiplicateurs homogènes modérés à l'eau légère, le combustible étant de l'uranium-235 ou de l'uranium-233 sous forme de nitrate d'uranyle. L'emploi des solutions permet d'obtenir facilement des variations importantes du laplacien géométrique et du rapport de modération. Il était donc possible de mesurer la réponse impulsionnelle de milieux multiplicateurs aussi bien au voisinage de la criticité que pour des états très sous-critiques obtenus directement par diminution du niveau de la solution, donc avec une géométrie se prêtant, en principe, aisément à une interprétation théorique. Des variations de la constante de décroissance des neutrons prompts en fonction de la géométrie il est possible de déduire, pour chaque concentration et en se donnant un jeu cohérent de sections efficaces, des renseignements intéressant la probabilité de non-fuite. D'autre part, l'emploi de deux matériaux fissiles ayant un η notablement différent permet une comparaison intéressante. Il est également possible de déduire des mesures de constantes de décroissance à géométrie fixe et concentrations variables des renseignements intéressant la sécurité des installations de traitement des matériaux fissiles, et en particulier de déterminer les concentrations maximales admissibles dans des récipients donnés. C'est dans

ce but qu'une série d'expériences a été réalisée à Dijon à l'aide de solutions de nitrate de plutonium faiblement concentrées.

2. PRINCIPE DES MESURES

Les expériences effectuées sur les milieux multiplicateurs à l'aide de sources pulsées de neutrons consistent à injecter dans le milieu de brèves impulsions de neutrons et à étudier le comportement, en fonction du temps, du flux induit dans la pile. Un certain temps après l'impulsion de neutrons, temps nécessaire au ralentissement des neutrons rapides et à l'extinction des modes harmoniques, la réponse impulsionnelle d'un milieu reproducteur est une somme de fonctions exponentielles dont les constantes de décroissance sont les racines de l'équation de Nordheim. Lorsque la décroissance du flux est suffisamment rapide, les fonctions correspondant aux divers groupes de neutrons retardés peuvent être considérées comme constantes pendant la durée de l'analyse, et le comportement de la densité neutronique en fonction du temps peut être représenté par la somme d'une seule fonction exponentielle, correspondant à la décroissance des neutrons prompts, et d'une constante englobant la contribution des neutrons retardés, les fissions spontanées et, éventuellement, le bruit de fond dû à une source de démarrage. La constante de décroissance des neutrons prompts peut s'exprimer par la relation suivante:

$$\frac{1}{\theta} = \frac{1 - K_{eff}(1 - \beta_{eff})}{\tau} + \frac{\beta_{eff} K_{eff}}{\tau} \sum_i \frac{a_i \lambda_i}{\frac{1}{\theta} - \lambda_i} \qquad (1)$$

dans laquelle τ représente le temps de vie des neutrons prompts dans la pile sous-critique, λ_i les périodes des neutrons retardés et a_i leur abondance relative. k_{eff} désigne le coefficient de multiplication effectif.

Dans le cas d'un réacteur modéré à l'eau légère ne comportant pas de réflecteur, le second terme de la relation (1) qui représente l'influence des neutrons retardés peut être pratiquement négligé car $1/\theta$ est très grand devant les différents λ_i, sauf au voisinage immédiat de la criticité, et l'incertitude expérimentale est bien supérieure à la valeur du terme correctif. Il est par conséquent raisonnable d'utiliser la relation approchée

$$\alpha = \frac{1 - k_{eff}(1 - \beta_{eff})}{\tau}. \qquad (2)$$

Disposant comme paramètres expérimentaux de la hauteur de solution dans la cuve et de la concentration en combustible, il est intéressant d'exprimer α en fonction du laplacien géométrique et de dissocier l'influence du modérateur de celle du combustible [2]. $P(B_1^2, L_1^2)$ désignant la probabilité de non-fuite des neutrons en cours de ralentissement nous avons

$$\tau = \frac{1}{v\Sigma_a(1 + L_2^2 B_2^2)}, \qquad k_{eff} = \eta \epsilon p f \frac{P(L_1^2, B_1^2)}{1 + L_2^2 B_2^2},$$

soit

$$\alpha = v\Sigma_a(1 + L_2^2B_2^2) - \eta \epsilon p f (1 - \beta) v\Sigma_a P(L_1^2, B_1^2)$$

$$= v\Sigma_a + D_0B_2^2 - \eta \epsilon p f (1 - \beta) v\Sigma_a P(L_1^2, B_1^2).$$

Σ_m désignant la section efficace d'absorption du modérateur et Σ_c celle du combustible

$$\Sigma_a = \Sigma_m + \Sigma_c = \frac{\Sigma_c}{f}$$

d'où

$$\alpha = v\Sigma_m + vDB_2^2 + v\Sigma_c [1 - \eta \epsilon p(1 - \beta) P(L_1^2, B_1^2)]. \qquad (3)$$

Remarquons que, dans notre cas où le modérateur est de l'eau légère, les variations de laplacien obtenues ne sont pas suffisantes pour que l'influence du coefficient de refroidissement soit sensible. Le coefficient de diffusion $vD = D_0$ peut alors être considéré comme indépendant de B_2^2.

Lorsque la concentration en matériau fissile reste faible, le coefficient de diffusion ainsi que l'aire de ralentissement peuvent être considérés comme invariables et égaux aux constantes correspondantes du modérateur pur. α est dans cette hypothèse une simple fonction linéaire de la section efficace d'absorption du combustible, donc de la concentration, et il existe une géométrie pour laquelle la probabilité de non-fuite satisfait à la relation

$$P(L_1^2, B_1^2) = \frac{1}{\eta \epsilon p (1 - \beta_{eff})}.$$

Le laplacien géométrique correspondant est appelé «laplacien neutre» [3]; pour cette valeur la constante de décroissance d'une impulsion de neutrons est indépendante de la concentration et égale à celle que l'on obtiendrait dans le modérateur pur ayant les mêmes dimensions. Le réseau des courbes $\alpha = f(B_2^2)$ est alors concourant.

Ces résultats ne sont plus valables lorsque la concentration devient relativement importante. Les propriétés modératrices du milieu varient par suite de la présence du combustible en grande quantité. L'absorption moyenne du milieu augmente et la proportion d'eau par unité de volume décroît; il en résulte une diminution de l'absorption due au modérateur ainsi qu'une variation du coefficient de diffusion et de l'aire de ralentissement. L'intersection de $\alpha = f(B_2^2)$ avec la courbe du modérateur devient fonction de la concentration et, à géométrie constante, les variations de α ne sont plus linéaires. L'obtention d'une géométrie constante devient elle-même délicate par suite des modifications de la longueur d'extrapolation. D'autre part, lorsque le combustible est utilisé sous la forme d'une solution d'un sel métallique, il existe en fonction du rapport uranium sur modérateur un minimum du volume critique, donc un maximum du laplacien matière. Pour certaines dimensions du milieu multiplicateur la fonction $\alpha = f$ (concentration) n'est plus monotone et l'on doit observer une inversion de son sens de va-

riation pourvu que l'on puisse utiliser des solutions très concentrées en quantités suffisantes.

3. DISPOSITIF EXPÉRIMENTAL

Les expériences furent réalisées à l'aide des ensembles critiques homogènes ALECTO constitués par une cuve cylindrique d'acier inoxydable de 0,3 cm d'épaisseur et de 30 cm de diamètre extérieur, la hauteur étant de 100 cm pour l'uranium-235 et 135 cm pour l'uranium-233. Suspendue à une armature métallique, cette cuve est surmontée d'une boîte à gants contenant les mécanismes des barres de commande et de sécurité et du palpeur servant à la mesure du niveau. La solution est montée dans le cœur par le fond de la cuve à l'aide de pompes. Les solutions sont préparées dans une boîte à gants contenant le réservoir annulaire de stockage. Les variations de concentration sont obtenues par dilution en ajoutant de l'eau acidulée. Le contrôle neutronique de la montée de solution est facilité par l'emploi d'une source de démarrage de radium-béryllium. La protection biologique est assurée par une enceinte étanche entourée de murs de béton et d'un toit de paraffine. Afin de limiter au maximum l'influence des neutrons réfléchis par les parois de la protection, la cuve est soigneusement cadmiée sur toute la surface latérale ainsi que sur le fond, la présence de la boîte à gants supérieure interdisant la mise en place de cadmium au-dessus de la solution. Comme les hauteurs de solutions utilisées sont petites en comparaison de celles de la cuve, l'angle solide sous lequel est vue la partie non protégée est faible.

L'analyseur de temps est un sélecteur transistorisé TMC à 256 canaux équipé d'un tiroir «neutrons pulsés». La lecture des informations mises en mémoire s'effectue à l'aide d'une imprimante perforatrice Friden permettant une interprétation mécanographique directe [4]. Les détecteurs de neutrons sont des compteurs à trifluorure de bore dont la sensibilité est choisie, suivant l'antiréactivité, de façon à obtenir un taux de comptage tel que les pertes de comptage dues au temps mort n'excèdent pas 10% dans les premiers canaux. Ils sont placés suivant une génératrice à l'extérieur du cœur, entre la cuve et l'enveloppe de cadmium.

Les sources pulsées dont nous disposions émettent suivant la réaction (DT) 3 à $4 \cdot 10^6$ neutrons par impulsion dont la durée est de quelques microsecondes, la fréquence de répétition étant limitée à 2 ou 3 Hz. Avec cette émission il était possible de n'utiliser qu'une seule source, d'autant plus que les harmoniques spatiaux n'étaient pas à craindre étant donné les faibles dimensions des milieux étudiés. Cependant, dans l'intention de diminuer le temps d'expérimentation lors des mesures sur des configurations très sous-critiques, nous avons utilisé quatre sources, disposées à l'extérieur de la cuve contre le cadmium et déclenchées successivement. Un commutateur électronique interposé entre le sélecteur et les sources permettait de déclencher successivement l'une des quatre sources pour chaque balayage de l'analyseur. Nous obtenions ainsi une cadence quatre fois plus rapide, ce qui diminuait notablement la durée de chaque mesure. Les quatre sources n'ayant pas rigoureusement la même production de neutrons il en

résultait malheureusement des taux de comptage légèrement différents suivant la source utilisée, d'où une petite imprécision sur la correction du temps mort.

Pendant les mesures, la source de démarrage était escamotée bien que pour les très grandes antiréactivités le bruit de fond qu'elle introduit soit négligeable à l'échelle de temps d'un canal.

4. COMPOSITION DES SOLUTIONS

Nous avons utilisé, à plusieurs concentrations, des solutions dans l'eau légère de nitrate d'uranyle $(NO_3)_2UO_2$ dont l'acidité libre est maintenue voisine de 2 N. Le combustible en est soit de l'uranium-235, soit de l'uranium-233 dont la composition isotopique en poids pour cent grammes d'uranium total est indiquée dans le tableau I.

TABLEAU I

COMPOSITION ISOTOPIQUE DE L'URANIUM

Uranium-235	Uranium-233
^{235}U: 89,95 ± 0,1	^{233}U: 97,00 ± 0,04
^{238}U: 8,97 ± 0,9	^{234}U: 2,34 ± 0,02
^{234}U: 0,78 ± 0,01	^{238}U: 0,43 ± 0,01
^{236}U: 0,30 ± 0,01	^{235}U: 0,22 ± 0,01

Le mélange combustible à base d'uranium-233 contient 3,2% de thorium-232. Les quantités de combustible disponibles étaient de 5 kg pour l'uranium-235 et 3 kg pour l'uranium-233. Une analyse chimique permet de déterminer la concentration du combustible (en uranium total) et l'acidité de la solution, et de contrôler la teneur en fer (quelques dizaines de mg/l) qui pourrait provenir d'une éventuelle corrosion des parois par l'acide nitrique. Les caractéristiques des diverses solutions étudiées sont rassemblées dans le tableau II.

5. RÉSULTATS EXPÉRIMENTAUX

Nous nous étions proposés de déterminer pour plusieurs concentrations les constantes de décroissance des neutrons prompts correspondant à un certain nombre de niveaux de la solution dans la cuve, depuis la criticité jusqu'à des configurations les plus sous-critiques possibles. La limite inférieure du niveau fut déterminée par la possibilité, compte tenu du matériel dont nous étions dotés, d'observer une décroissance significative;

TABLEAU II

CARACTÉRISTIQUES DES SOLUTIONS ÉTUDIÉES

Uranium-235			Uranium-233		
Concentration (g/l)	Densité (g/cm³)	Normalité	Concentration (g/l)	Densité (g/cm³)	Normalité
43,7 ± 0,5	1,131 ± 0,002	2,00 ± 0,02	48,4 ± 0,5	1,127 ± 0,002	1,93 ± 0,02
90 ± 2	1,190 ± 0,002	2,11 ± 0,02			
231 ± 3	1,382 ± 0,002	2,08 ± 0,02	89,7 ± 1	1,177 ± 0,002	1,99 ± 0,02
281 ± 3	1,450 ± 0,002	1,93 ± 0,02			
326 ± 3	1,510 ± 0,002	1,87 ± 0,02	78,9 ± 1	1,181 ± 0,002	1,97 ± 0,02

la limite supérieure, soit par la criticité, soit par la quantité de combustible qui ne permit pas d'obtenir la taille critique dans le cas des plus fortes concentrations en uranium-235.

L'ensemble des résultats obtenus pour cinq concentrations en ^{235}U et trois en ^{233}U est rassemblé dans les tableaux III et IV. Remarquons que certaines marges d'erreur relatives aux décroissances très rapides peuvent paraître élevées. Elles sont surtout dues au fait que le tiroir équipant notre sélecteur n'est pas adapté à la mesure des constantes de décroissance très élevées. La plus petite largeur de canal est de 10 μs auxquelles il faut juxtaposer 10 μs de mise en mémoire (ce qui constitue une perte d'information importante). Le nombre de canaux intéressant la décroissance est donc relativement faible, d'où une incertitude plus grande sur la mesure de α. D'autre part, les ensembles critiques ALECTO ne permettent pas de maintenir la température constante et pour l'ensemble des expériences elle varie entre 20 et 25°C. Aucune correction ne fut possible, le coefficient de température de nos solutions n'étant pas connu.

Les variations de α sont représentées en fonction du laplacien géométrique thermique $B^2_{\frac{1}{2}}$ sur la figure 1 pour l'uranium-235 et sur la figure 2 pour l'uranium-233; y figurent également à titre de comparaison les courbes représentatives de l'eau acidulée déduites de l'absorption et du coefficient de diffusion de l'eau à 22°C [5] en tenant compte de l'acide nitrique présent. Quelques mesures effectuées sur de l'eau acidulée à 2 N (tableau V) sont en bon accord avec les valeurs calculées.

6. INTERPRÉTATION DES RÉSULTATS

Cette campagne d'expériences pulsées fut effectuée dans le double but de déterminer le laplacien neutre des solutions et de tester la possibilité, à partir des mesures de α, d'évaluer les conditions critiques d'un récipient

TABLEAU III

RÉSULTATS OBTENUS POUR CINQ CONCENTRATIONS EN URANIUM-235

B_z^2 (cm^{-2}) \ C_U (g/l)	43,7 ± 0,5	90 ± 2	231 ± 3	281 ± 3	326 ± 3
0,05845	7600 ± 300	8150 ± 250	-	-	-
0,05656	7150 ± 300	7810 ± 150	11 360 ± 150	12 100 ± 150	12 820 ± 200
0,05323	-	7077 ± 150	-	-	11 720 ± 200
0,05039	7050 ± 200	6726 ± 150	8 523 ± 100	9 740 ± 120	10 560 ± 200
0,04585	6000 ± 100	5514 ± 120	6 000 ± 80	7 210 ± 100	8 065 ± 150
0,04402	-	-	-	-	6 550 ± 150
0,04304	-	-	-	-	5 490 ± 100
0,04242	5596 ± 100	4405 ± 60	3 703 ± 50	4 292 ± 60	-
0,04037	-	-	2 128 ± 30	2 381 ± 30	-
0,03919	-	-	1 035 ± 20	1 110 ± 20	-
0,03865	4717 ± 60	3158 ± 40	-	-	-
0,03596	4000 ± 50	2010 ± 15	-	-	-
0,03399	3436 ± 40	1222 ± 10	-	-	-
0,03249	3185 ± 40	587 ± 5	-	-	-
0,03215	-	420 ± 3	-	-	-
0,03207	-	385 ± 3	-	-	-
0,03195	-	334 ± 2	-	-	-

de géométrie donnée lorsque les quantités de matériaux fissiles disponibles sont insuffisantes pour obtenir la criticité. Nous avons, de plus, à l'aide des valeurs de sections efficaces communément admises, ajusté une probabilité de non-fuite rendant correctement compte des résultats expérimentaux.

a) Variations de α à géométrie constante

L'ensemble des résultats permet de connaître les variations de α en fonction de la concentration à hauteur constante. La figure 3 montre clairement que la plage de concentration dans laquelle ces variations peuvent être considérées comme linéaires doit être extrêmement réduite, une courbure significative apparaissant déjà entre 44 et 90 g/l. Il est donc hasardeux de prétendre déterminer la concentration critique d'un récipient en extrapolant les mesures effectuées à faibles concentrations; ceci conduirait

toutefois à une concentration inférieure à la concentration critique vraie, ce qui pourrait à la rigueur suffire lorsqu'on se limite à des études de sécurité. Le nombre de concentrations étudiées n'est pas suffisant pour préciser le minimum des variations de α mais il serait intéressant de pouvoir effectuer des rapprochements entre le lieu de ce minimum et le minimum

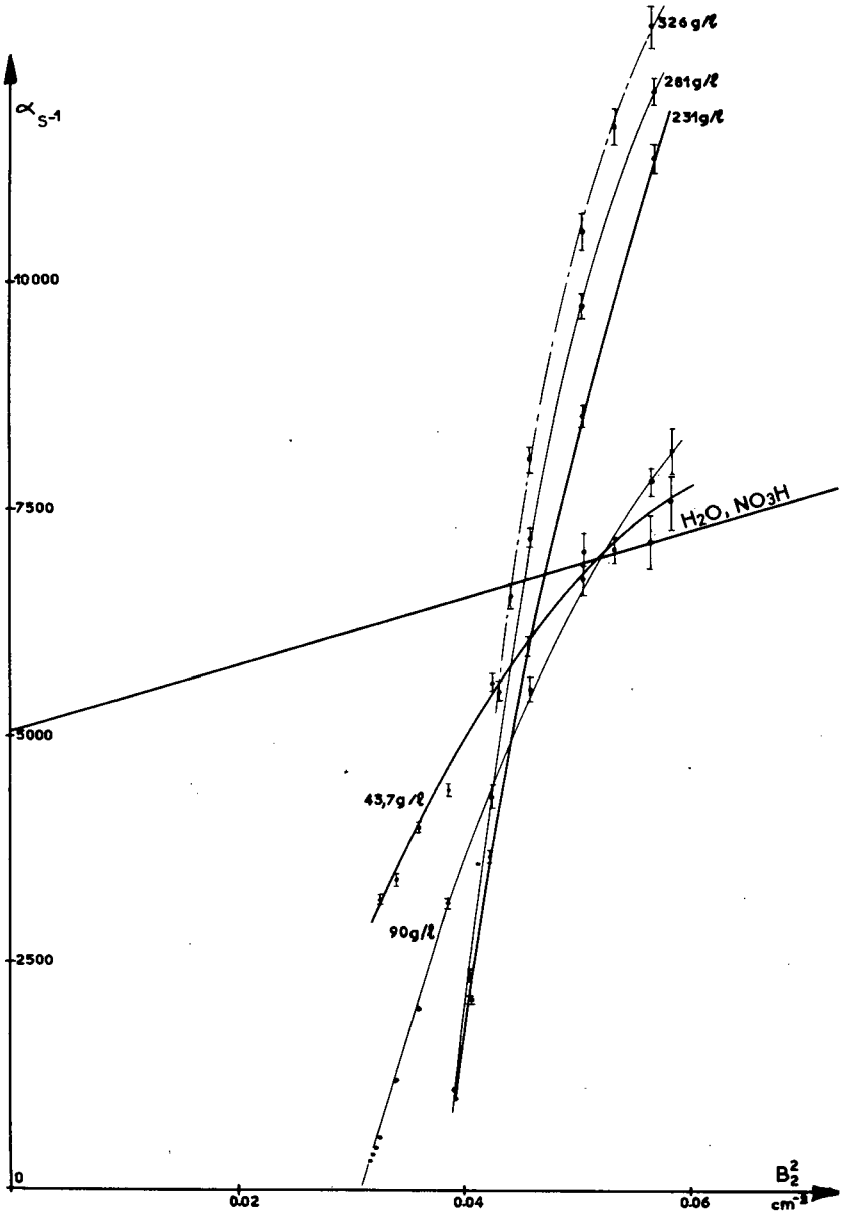


Figure 1

Variation de α en fonction du laplacien géométrique thermique pour l'uranium-235.

TABLEAU IV

RÉSULTATS OBTENUS POUR TROIS CONCENTRATIONS EN URANIUM-233

C_{UT} (g/l) / B_2^2 (cm^{-2})	48,4 ± 0,5	78,9 ± 1*	89,7 ± 1
0,06716	-	7650 ± 200	-
0,06383	-	7075 ± 200	-
0,05856	-	6820 ± 200	-
0,05656	-	-	5860 ± 200
0,05303	-	5440 ± 100	-
0,05223	-	-	4935 ± 100
0,05039	5210 ± 200	-	4200 ± 100
0,04585	-	-	2314 ± 50
0,04459	-	2670 ± 50	-
0,04402	3940 ± 100	-	1480 ± 20
0,04242	-	-	820 ± 10
0,04183	-	-	600 ± 10
0,04114	-	-	320 ± 5
0,04004	-	570 ± 10	-
0,03399	1450 ± 20	-	-
0,03168	652 ± 10	-	-
0,02989	118 ± 3	-	-

* Expériences réalisées avec une cuve de 25 cm de diamètre.

de volume critique, ainsi que d'effectuer des mesures au voisinage du second zéro de la fonction $\alpha = f(C)$ dans le cas d'un laplacien géométrique inférieur au laplacien matière maximum. La quantité de matière fissile disponible ne permit pas cette dernière série de mesures.

b) Aire de ralentissement

La connaissance de la constante de décroissance et l'adoption d'un jeu de sections efficaces permet de déterminer la probabilité de non-fuite en choisissant $P(L_1^2, B_1^2)$ comme paramètre inconnu. Le combustible intervenant sous la forme d'un sel, nous avons introduit la capture de l'anion en utilisant la relation suivante:

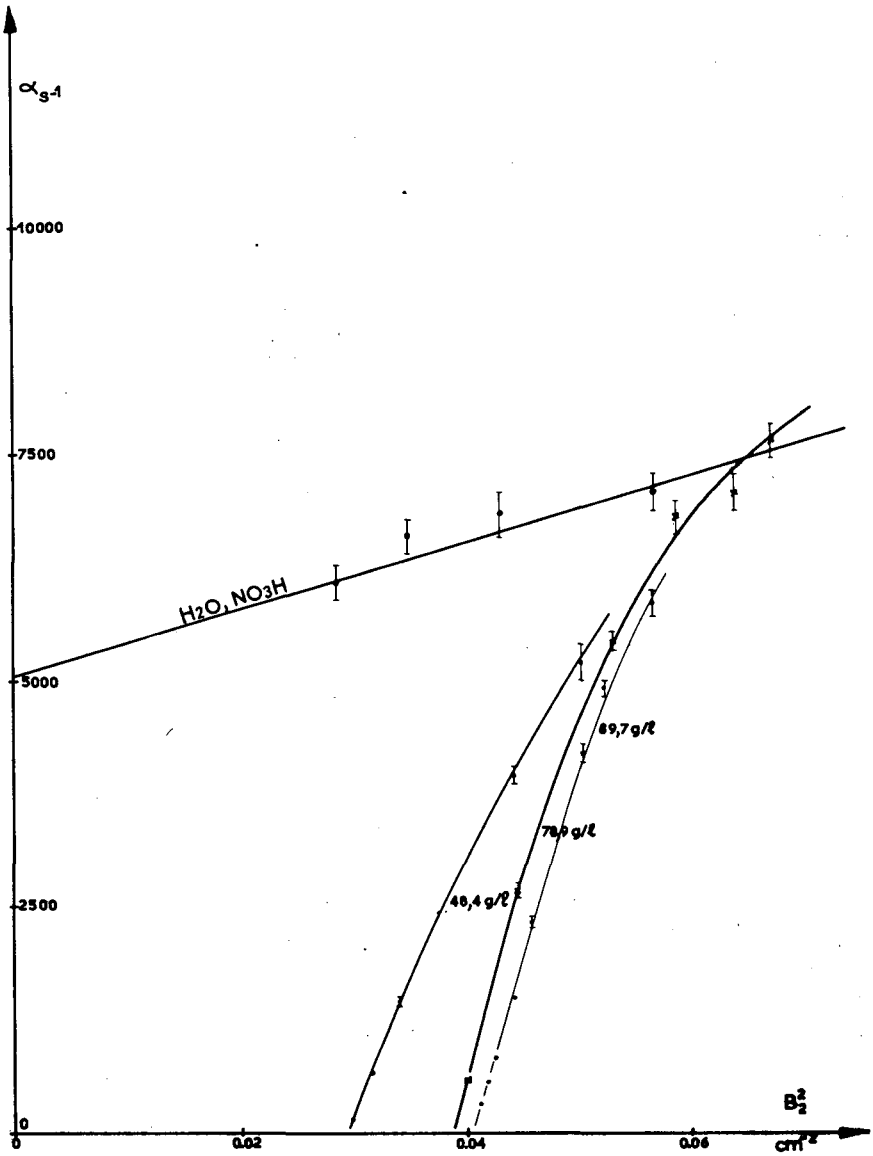


Figure 2

Variation de α en fonction du laplacien géométrique thermique pour l'uranium-233.

$$\alpha = \nu\Sigma_m + D_0B_2^2 + \nu\Sigma_{sel}\left[1 - \frac{\Sigma_{métal}}{\Sigma_{sel}}\eta\epsilon p(1-\beta_{eff})P(L_1^2, B_1^2)\right]. \qquad (4)$$

Les sections efficaces macroscopiques du modérateur, du combustible, et des divers absorbants sont calculées à partir des nombres de noyaux déduits de l'analyse chimique et des sections efficaces microscopiques suivantes:

TABLEAU V

MESURES SUR L'EAU ACIDULÉE A 2 N

B_z^2 (cm^{-2})	0,05656	0,04297	0,03451	0,02863
$\alpha_{exp}(s^{-1})$	7080 ± 250	6900 ± 250	6600 ± 250	6100 ± 200
$\alpha_{calculé}$	7211	6695	6373	6150

$^{238}U = 2,75$ b, $^{234}U = 93$ b et $^{232}Th = 7$ b;

Azote = 1,88 b et hydrogène = 0,33 b. [6]

Pour l'uranium-235 et l'uranium-233 nous avons adopté les sections efficaces effectives,

$$\hat{\sigma} = \frac{\int \sigma(E)\Phi(E)dE}{\int \frac{v_0}{v}\Phi(E)dE}.$$

Elles sont calculées en assimilant l'eau acidulée à un thermaliseur différentiel secondaire, les deux fonctions le caractérisant étant celles du modèle Nelkin-Soulé pour l'eau légère (voir tableau VI). Ces calculs étant limités à une énergie de 1,63 eV il fut tenu compte des fissions et des captures produites à des énergies supérieures en calculant p et ϵ à l'aide des intégrales effectives de résonance [5]. Ces intégrales étant mesurées pour un seuil de 0,45 eV, nous leur avons soustrait la quantité

$$I = \int_{0,45}^{1,63} \sigma(E)\,\frac{dE}{E}$$

déterminée à l'aide des sections efficaces du BNL 325.

η est alors calculé par la relation $\eta = \nu\hat{\Sigma}_g/\hat{\Sigma}_a$ en adoptant $\nu = 2,4498$ pour l'uranium-235 et 2,5091 pour l'uranium-233 [7].

Il est tenu compte de la variation du coefficient de diffusion avec l'absorption du milieu en utilisant la relation suivante [8]:

$$D = \frac{\Sigma_d}{3(\Sigma_a + \Sigma_d)^2}.$$

Les laplaciens géométriques sont calculés en adoptant des longueurs d'extrapolation égales à 2,5 cm pour le groupe rapide et 0,3 cm pour le groupe thermique. Compte tenu des imprécisions introduites par les con-

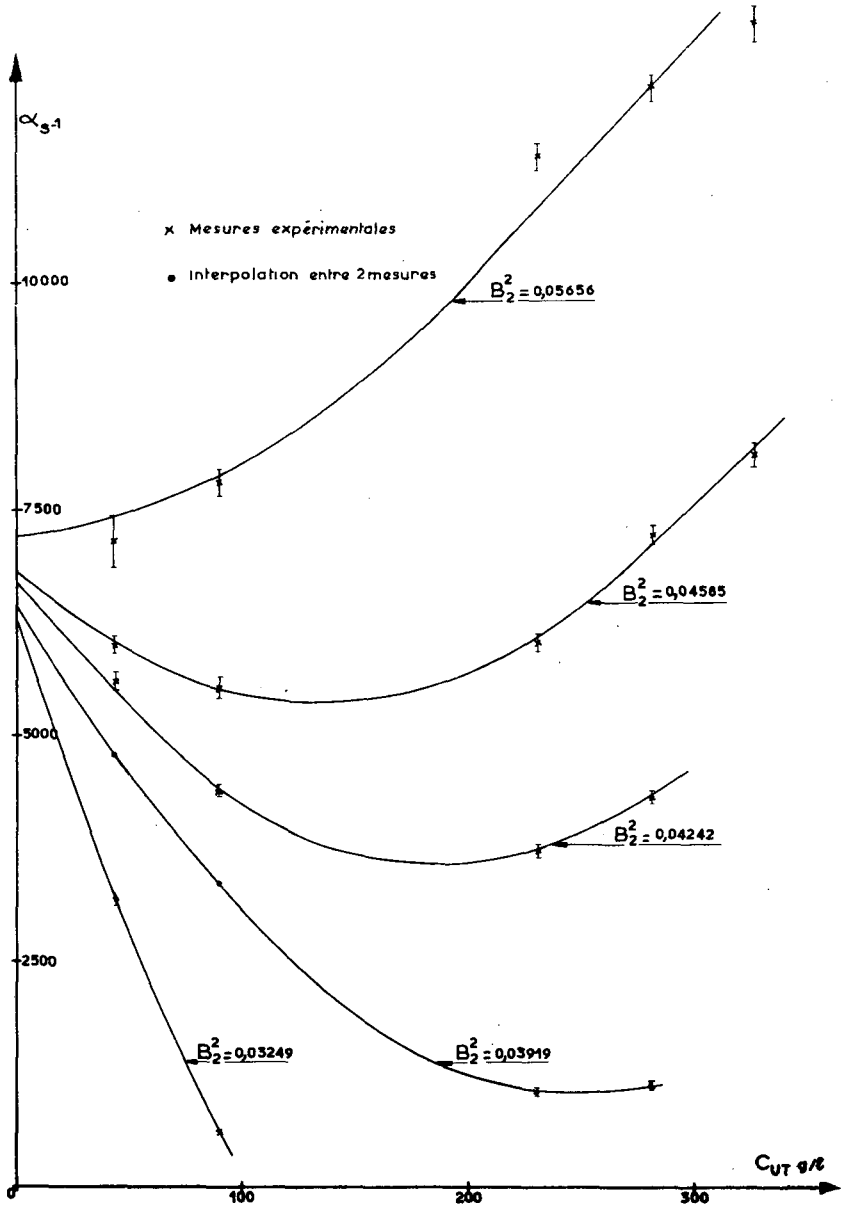


Figure 3

Uranium-235 – $\alpha = f(C_{UT})$.

ditions aux limites - effet réflecteur dû à la cuve et dissymétrie axiale (la frontière inférieure est constituée par la cuve et la supérieure par de l'air) - les longueurs d'extrapolation furent considérées comme indépendantes de la concentration.

TABLEAU VI

SECTIONS EFFICACES EFFECTIVES ET AIRE DE RALENTISSEMENT

Concentration (g/l)	Uranium-235					Uranium-233		
	43,7	90,0	231	281	326	48,4	78,9	89,7
σ_f (b)	549,02	542,42	525,73	520,83	516,70	542,45	546,89	548,72
σ_c (b)	669,40	662,42	644,80	639,63	635,29	598,35	602,04	603,58
L_1^2 (cm^2)	27,0	27,3	30,8	32,8	34,8	30,0	31,9	32,2

Les valeurs de $P(B_1^2, L_1^2)$ ainsi déterminées sont telles que pour $B_1^2 < 0,036$ cm^{-2} ($B_1^2 < 0,042$ pour la cuve 250) les variations de $(1/P - 1)$ sont proportionnelles à B_1^2. La figure 4 représente à titre d'exemple les variations de l'inverse de la probabilité de non-fuite rapide obtenues dans le cas de la solution à 90 g/l d'uranium-235 et de celle à 48,4 g/l d'uranium-233. Le modèle de YUKAWA fut alors utilisé pour représenter le ralentissement:

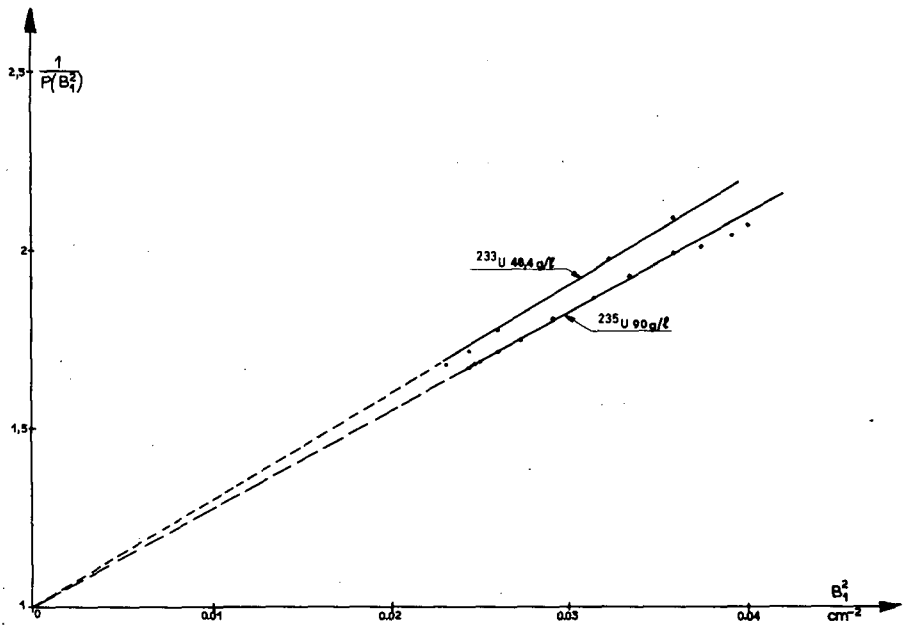


Figure 4

Inverse de la probabilité de non-fuite.

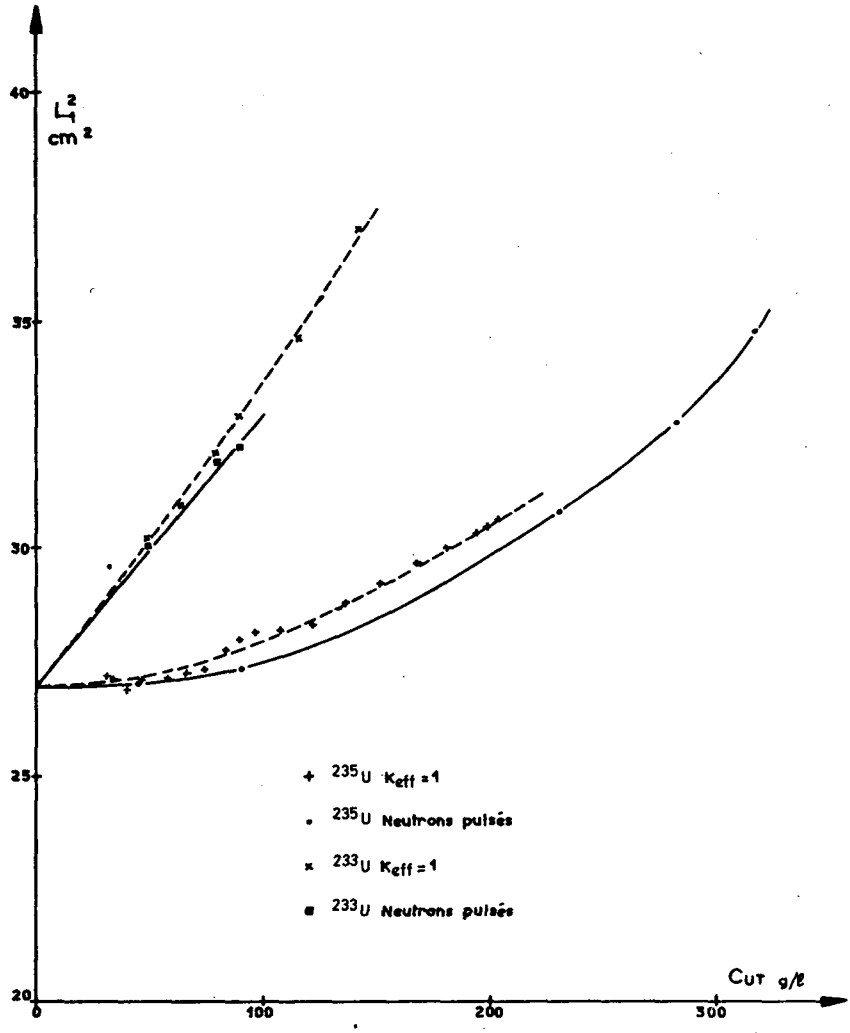


Figure 5

Aire de ralentissement des solutions de nitrate d'uranyle.

$$P(L_1^2, B_1^2) = \frac{1}{1 + L_1^2 B_1^2}.$$

Les mesures correspondant à des laplaciens supérieurs à 0, 036 (ou 0, 042) sembleraient indiquer une courbure dont le signe, non constant, ne doit pas être considéré comme significatif. Ceci peut provenir soit d'une mesure erronée de α due au spectre non encore en équilibre, soit d'un mauvais calcul du laplacien géométrique. La hauteur devenant faible devant le diamètre il peut apparaître des variations de longueurs d'extrapolation axiale qui interviennent sur le terme principal. Les points correspondants ne furent pas utilisés dans le calcul de L_1^2 par la méthode des moindres car-

rés. Les résultats sont consignés dans le tableau VI et représentés par la figure 5.

L'extrapolation des courbes de cette figure à une concentration nulle semble cohérente avec la valeur de 27 cm^2 désormais admise pour l'eau pure, mais il existe une importante différence dans le comportement des deux corps fissiles. En effet, alors que le ralentissement n'est pratiquement pas affecté par la présence de noyaux d'uranium-235 lorsque la concentration reste inférieure à une centaine de grammes par litre, il en est tout autrement pour l'uranium-233, cas où, même pour de faibles concentrations, apparaît une très forte variation de L_1^2.

Ces résultats sont, par contre, très éloignés des 21, 2 cm^2 trouvés par CAMPBELL et STELSON [9] dans le cas des solutions de fluorure d'uranyle UO_2F_2, sans être nécessairement incompatibles, les distances d'extrapolation utilisées par ces auteurs n'étant pas précisées.

En effet, les valeurs de l'aire de ralentissement ainsi déterminées sont très sensibles à la distance d'extrapolation rapide ϵ_1 utilisée. Plusieurs calculs effectués à l'aide des résultats expérimentaux obtenus dans le cas de la solution à 90 g/l d'uranium-235 et utilisant des valeurs de ϵ_1 comprises entre 2 et 3 cm ont conduit à la variation suivante:

$$\frac{d L_1^2}{d \epsilon_1} = + 3,3 \text{ cm}^2/\text{cm}.$$

Une détermination de l'aire de ralentissement par une méthode statique fut également effectuée en interprétant les dimensions critiques expérimentales à l'aide du même formalisme et des mêmes valeurs des diverses sections efficaces. B_{1c}^2 et B_{2c}^2 désignant les laplaciens géométriques critiques, nous pouvons alors écrire

$$(1 + L_1^2 B_{1c}^2)(1 + L_2^2 B_{2c}^2) = \eta \epsilon p f.$$

Les résultats obtenus sont aussi représentés sur la figure 5, figure qui permet de constater que l'accord entre les deux méthodes est assez satisfaisant. Néanmoins, il semble exister un écart systématique, un peu plus accentué pour l'uranium-235 que pour l'uranium-233, les valeurs obtenues par méthode cinétique étant un peu plus faibles. Remarquons que le sens de cet écart peut s'expliquer par la présence, lors des expériences pulsées, d'une protection de cadmium autour de la cuve, protection qui provoque un léger gain de réactivité en jouant le rôle d'un réflecteur pour les neutrons rapides fuyant hors du cœur.

c) Laplacien neutre

La notion du laplacien neutre, correspondant à la géométrie pour laquelle le temps de vie des neutrons prompts est indépendant de la concentration, ne conserve sa signification que lorsque les propriétés modératrices de la solution peuvent être considérées comme constantes. Ceci peut se produire pour une gamme de concentrations plus ou moins étendue suivant le corps fissile. En toute rigueur, nous ne devons pas obtenir une constante

mais simplement une fonction dont la dérivée à l'origine $\left(\frac{d\alpha}{dc}\right)_{c=0}$ s'annule.

Pratiquement, et compte tenu des erreurs expérimentales, nous pouvons admettre pour les solutions d'uranium-235, dont l'aire de ralentissement reste invariable jusqu'à 90 g/l, α comme constant dans cette gamme de concentrations pour un laplacien géométrique $B_2^2 = 0,052 \pm 0,001$ cm^{-2} soit $B_1^2 = 0,0369 \pm 0,0007$ cm^{-2}.

Dans le cas des solutions d'uranium-233, dont le η est supérieur, l'intersection avec la courbe du modérateur pur ne se réalise que pour des laplaciens géométriques plus élevés et nous ne l'avons que difficilement ob-

TABLEAU VII

COMPOSITION ISOTOPIQUE DU PLUTONIUM

Isotope	^{239}Pu	^{240}Pu	^{241}Pu
Teneur exprimée en g d'isotopes pour 100 g de Pu	96,77 ± 0,04	3,00 ± 0,03	0,12 ± 0,01

tenue. En effet, bien que l'environnement des deux ensembles critiques ne soit que très légèrement différent et que les cuves soient identiquement cadmiées, les réflexions parasites se révélèrent beaucoup plus importantes dans le cas de l'uranium-233. Elles ne permirent pas l'exploitation des mesures effectuées avec de faibles hauteurs de solution. Nous avons par la suite repris une série d'expériences à l'aide d'une cuve de 25 cm de diamètre en utilisant une concentration de 78,9 g/l. Il fut alors possible d'obtenir l'intersection de la courbe $\alpha = f(B_2^2)$ de la solution avec celle du modérateur pur, pour $B_2^2 = 0,064 \pm 0,002$ cm^{-2}. Les solutions d'uranium-233 méritent que l'on fasse une remarque. En effet, nous avons vu que leur aire de ralentissement variait très rapidement d'une quantité importante et cela même pour des concentrations très faibles. L'on conçoit alors qu'il ne puisse plus exister de point de concours des courbes $\alpha = f(B_2^2)$ comme dans le cas de l'uranium-235. La notion de laplacien neutre ne doit donc plus être considérée comme valable dans de telles conditions. Les impératifs du programme de mesures n'ont malheureusement pas permis de vérifier expérimentalement cette hypothèse.

7. MESURES SUR LE PLUTONIUM

Le milieu actif étudié était une solution nitrique de $(NO_3)_4$Pu d'acidité maintenue autour de 2 N, de concentration en plutonium variant de 0 à 20,2 g/l. Les résultats de l'analyse isotopique du plutonium sont rassemblés dans le tableau VII; le tableau VIII groupe les résultats de l'analyse chimique.

Le récipient qui contenait la solution active était une cuve cylindrique en acier inoxydable de diamètre extérieur égal à 300 mm dont les parois avaient 3 mm d'épaisseur, le fond 6,5 mm environ. La cuve était placée

TABLEAU VIII

COMPOSITION CHIMIQUE DES SOLUTIONS

N° de la solution	Concentration en Pu (g/l) à 2% près	Acidité libre en normalité (N) à 2% près	NO_3 en normalité (N) à 1% près	Densité à 0,1% près	Fer (mg/l) à 10% près
1	0	2,00	2,00	1,067	6,7
2	0,035	2,05	2,05	1,067	18,5
3	0,030	1,95	1,95	1,067	11
4	6,40	2,20	2,44	1,087	72,5
5	8,10	2,03	2,22	1,082	105
6	11,7	2,59	2,93	1,110	130
7	18,4	1,91	2,36	1,099	412
8	20,2	1,83	2,30	1,099	240

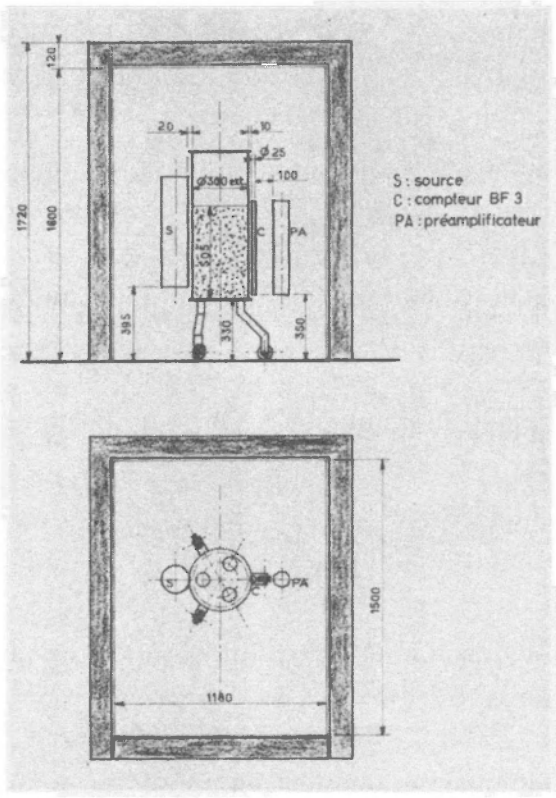


Figure 6
Positions des compteurs et de la source.

à l'intérieur d'un château de paraffine tapissé intérieurement de cadmium (fig. 6).

Le générateur de neutrons émet une bouffée d'environ 10^6 neutrons rapides pendant 1,5 μs. La fréquence de pulsation était de 4 c/s. Il nous a paru nécessaire de contrôler en permanence l'état de ces sources; un détecteur (scintillateur SPF + P. M.) placé près de la source délivre un courant dont l'amplitude est proportionnelle au flux de neutrons émis.

La chaîne de détection doit être peu sensible au rayonnement γ et avoir un temps de résolution faible. Une première chaîne à compteur BF_3 (4 NE 31) présentait un temps de résolution de 5 μs et un rendement de 4 cps par 1 $n/cm^2 \cdot s$. Une chaîne plus rapide (1 μs de temps de résolution) fut utilisée afin de réduire la durée des manipulations. Le P. M. était un 56 AVP avec scintillateur verre-^{6}Li. Sur cette chaîne, un créneau de tension appliquée sur la dynode focalisatrice du P. M. permettait un blocage de la voie détection au moment de la bouffée de neutrons. La position des compteurs est donnée sur la figure 6.

L'étude de la décroissance est faite à l'aide d'un analyseur à 400 canaux (SA 40) fonctionnant en multi-échelles. Nous avons utilisé les canaux 0 à 99 pour stocker le bruit de fond. Au canal 100 la source est déclenchée, on enregistre ensuite l'évolution neutronique jusqu'au canal 399. Une horloge extérieure détermine la vitesse de balayage des 400 canaux (15 μs par canal pour la plus rapide, soit 12 μs pour la mise en mémoire et 3 μs de temps d'enregistrement).

Résultats et interprétation

Les mesures ont été effectuées sur deux géométries:

1. Hauteur de solution active égale à 50,5 cm, $B_z^2 = 0,0284$ cm^{-2}. (Dans le calcul de B_z^2, on considère que les parois et le fond de la cuve font partie du milieu actif, la longueur d'extrapolation est égale à 0,3 cm).
2. Hauteur de solution égale à 28,3 cm, $B_z^2 = 0,0360$ cm^{-2}. Les résultats obtenus sont groupés dans le tableau IX.

Les courbes de la figure 7 représentent la variation de α avec C pour les deux géométries.

Le but des expériences réalisées à la Station de criticité de Dijon est d'essayer d'appliquer la technique des neutrons pulsés à la détermination de la concentration critique d'un assemblage de géométrie déterminée en partant d'états sous-critiques.

Considérons l'expression

$$\alpha = v\,[(\Sigma_a + DB^2) - \nu\Sigma_f(1 - B)P(B^2)].$$

Elle se décompose comme suit:

$$\alpha = \alpha_0 - AN_{Pu},$$

N_{Pu} = nombre de noyaux de plutonium par cm^3,
α_0 = constante de décroissance de l'assemblage de même géométrie mais ne contenant que le modérateur, ici de l'acide 2 N.

$$A = \nu\nu G_f [(1 - B)P(B^2) - (1 + \frac{\sigma_c}{G_f})].$$

On voit que N_{Pu} n'intervient pas dans A. Expérimentalement on a vérifié sur les deux géométries étudiées que A reste constant de 0 à 20,2 g/l.

Si l'on admet que A ne varie pas de la concentration nulle à la concentration critique, α sera une fonction linéaire de N_{Pu} ; il suffit alors d'effectuer, à géométrie constante, des mesures de α sur l'assemblage étudié contenant d'abord le modérateur, ensuite des solutions de concentrations en matériau fissile différentes mais éloignées de la concentration critique, puis d'extrapoler linéairement à $\alpha = 0$ pour obtenir la concentration correspondant à l'état prompt critique.

En réalité A sera influencé par la concentration en noyaux fissiles d'autant plus que le milieu sera peu modéré, l'extrapolation linéaire donnera tout de même une limite inférieure de la concentration critique, la concavité des courbes $\alpha = f(N_{Pu})$ étant tournée vers les α positifs; dans le cas d'une géométrie sûre, la concentration critique n'existe pas, la valeur obtenue sera donc sûre a fortiori.

La droite des moindres carrés tracée dans le cas où $B_z^2 = 0,0284$ cm^2 (fig. 7) extrapolée à $\alpha = 0$ donne Cp = 45,8 g/l, avec $\beta = 220$ pcm, on obtient une limite inférieure de la concentration «critique retardé» $C_R = 44,5$ g/l.

Les expériences réalisées à Saclay sur l'assemblage ALECTO [10] de dimensions identiques à celui que nous avons utilisé aboutissent par l'approche habituelle à une concentration correspondant à l'état critique retardé de 43,6 g/l pour une hauteur de solution égale à 50,5 cm et une teneur en ^{240}Pu de 1,48%.

On n'a pas effectué l'extrapolation linéaire dans le cas $B_z^2 = 0,0360$ cm^{-2}, la concentration critique étant trop éloignée.

TABLEAU IX

PLUTONIUM-239

N° de la solution étudiée	Concentration en Pu (g/l)	Acidité en normalité (N)	α (s^{-1})	
			$B_z^2 = 0,0284$ cm^{-2}	$B_z^2 = 0,0360$ cm^{-2}
1	0	2,05	5820 ± 250	
2	0,035	2,05	5720 ± 250	
3	0,03	1,95		7060 ± 100
4	6,40	2,20	4670 ± 150	6465 ± 150
5	8,1	2,03	4380 ± 250	
6	11,7	2,59	3960 ± 180	6380 ± 120
7	18,4	1,91	3390 ± 240	
8	20,2	1,83	3220 ± 120	5800 ± 100

Dans le domaine de concentration étudiée, la méthode aboutit à des résultats satisfaisants.

Dans une prochaine campagne les expériences seront poursuivies sur des géométries différentes et jusqu'à la concentration «critique retardé».

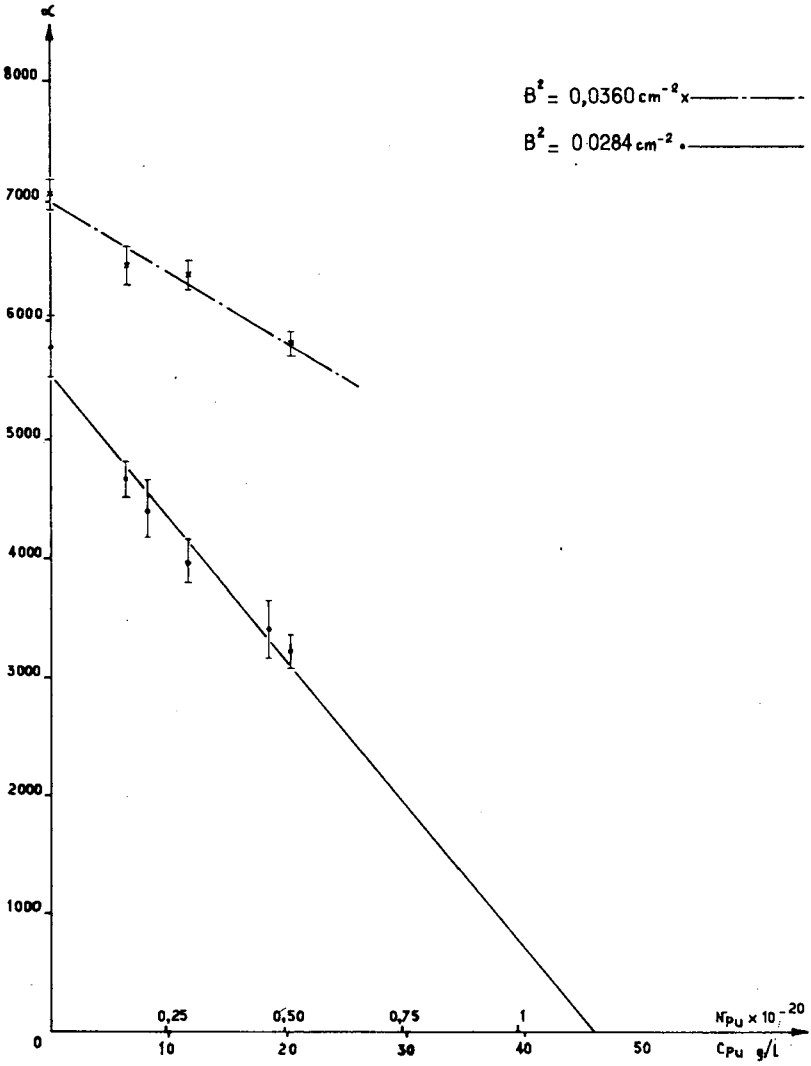


Figure 7

Variation de α pour deux géométries (plutonium).
$\alpha = f(C_{Pu})$.

8. CONCLUSION

Le temps limité pendant lequel les assemblages critiques furent disponibles et l'emploi d'un analyseur en temps n'ayant pas une largeur de canal suffisamment faible influencèrent beaucoup la précision des résultats

expérimentaux obtenus dans le cas des milieux très sous-critiques. De plus, la géométrie des réacteurs ne remplissait pas les conditions idéales d'exécution de mesures fines, la présence d'un plateau support et, au fond de chaque cuve, du dispositif d'introduction et d'évacuation de la solution provoque des perturbations locales dans la distribution du flux. Malgré cela il nous parut possible de déduire, des mesures de la constante de décroissance des neutrons, des renseignements concernant l'aire de ralentissement des solutions de sels fissiles dans l'eau. Une interprétation identique a déjà été effectuée dans le cas hétérogène d'assemblages graphite-^{235}U [11, 12]. Un point délicat lié aux milieux modérés à l'eau légère, donc de dimensions réduites, est constitué par le choix des longueurs d'extrapolation dont l'influence est très grande. Une variation avec les dimensions géométriques peut introduire une erreur systématique sur la détermination de $P(B_1^2, L_1^2)$. Les valeurs de l'aire de ralentissement ainsi obtenues ne devront donc être utilisées que dans un formulaire utilisant les mêmes distances d'extrapolation. L'ensemble de ces expériences prouve qu'il est possible d'effectuer et d'interpréter des mesures en neutrons pulsés sur des milieux reproducteurs très sous-critiques. Indépendamment de ces interprétations, les expériences en neutrons pulsés peuvent fournir des résultats intéressant la sécurité des installations nucléaires.

RÉFÉRENCES

[1] SAGOT, M., TELLIER, H., JACQUEMART, R. et KREMSER, J., «Technique des neutrons pulsés appliquée aux assemblages critiques et sous critiques», Exponential and Critical Experiments III, AIEA, Vienne (1964) 163.

[2] MEGHREBLIAN, R. and HOLMES, D., Reactor analysis, McGraw Hill Company (1960) chap. 9-2.

[3] CAMPBELL, E. and STELSON, P., Reactor parameters of a Small Subcritical Reactor by Pulsed Neutron Technique, ORNL 2076 (1956).

[4] MORIER, F. et TELLIER, H., VOLUBILIS: Code de calcul pour l'interprétation des expériences de cinétique pulsée, Note CEA 517 (1963).

[5] LOPEZ, W. and BEYSTER, J., "Measurement of Neutron Diffusion Parameters in Water by Pulsed Neutron Method", Nucl. Sci. and Engng 12 (1962) 190.

[6] PONTIS, C., Table des sections efficaces des éléments pour les neutrons thermiques, Note CEA 238 (1958).

[7] WESTCOTT, C.-H. Effective Cross Section Values for Well Moderated Thermal Reactor Spectra, CRRP 960 (1960).

[8] WEINBERG, A. and WIGNER, E., The Physical Theory of Neutron Chain Reactor, The University of Chicago Press (1958) 196.

[9] CAMPBELL, E. and STELSON, P., Measurement of Thermal Neutron Relaxation Times in Subcritical Systems, ORNL 2204 (1956).

[10] BRUNA, J.-G., BRUNET, J.-P., CLOUET D'ORVAL, C. et KREMSER, J., Expérience de criticité sur une solution de plutonium et d'uranium enrichi à 90%, Rapport CEA 2453 (1964).

[11] FULTZ, S., The Time Dependent Thermal Neutron Flux from a Pulsed Subcritical Assembly, Nucl. Sci. and Engng 6-313 (1959).

[12] PURICA, I. K., SEFERIAN, N. et RĂCĂTĂIANU, E., «Etude d'un ensemble sous-critique par la méthode de la caractéristique de fréquence», Exponential and Critical Experiments III, AIEA, Vienne (1964) 71.

DISCUSSION

(on the foregoing four papers)

C.A. PRESKITT: May I comment on the papers presented by Mr. Sherwin and Mr. Bronner? The former paper reports that the factor α_i remains in the vicinity of zero when a reactor is made subcritical by the addition of air pressure. The latter reports that good results were obtained in the analysis of pulsing experiments in systems made subcritical by the addition of boron poison. Both these results indicate that the neutron-generation time is nearly constant when the reactor is made subcritical by these means, which is exactly what one would expect for cases of this sort. This follows from the fact that the transient solution is equivalent to making the reactor critical again by removing 1/v poison and from the assumption that the fundamental prompt mode remains identical to the static distribution. This is true irrespective of the complexity of the reactor provided the poison is uniform.

J. SHERWIN: What you say is true for simple systems. The system I was describing, however, was of the WAGR type and had an extremely complex core. What I said was that the α_i term was negligible in the expression $\lambda = (1/R)[1 - k_{eff}\ (1 - \beta)\ (1 + \alpha_i)]$ but that the R value, which is related to the generation time Λ, was not linear with k_{eff}. Hence Λ will not be constant. The deviation of R versus k_{eff} was not large but had a significant effect on the comparison with the air-pressure reactivity scale.

E. GARELIS: I have a question on Mr. Bronner's paper. If the assemblies had been pulsed at a faster rate, would a constant delayed contribution have been obtained, in particular in the more subcritical cases?

G. BRONNER: In our reactor (MZFR) we usually had higher modes lasting for $\approx 1/\omega_0$ to $2/\omega_0$; thus only after this time was it possible for us to make an accurate analysis. We feel that proper determination of ω_0 requires about 5 e-foldings. But then in the total time, about t/ω_0, the background has decreased and therefore it seemed best to take background decay into account also. For this a point is needed where the ω_0 decay has died out ($T \approx \mu/\omega_0$) and therefore we used T-values of this order.

J. SHERWIN: I wonder whether anyone would care to comment on the accuracy of the delayed-neutron data, particularly for plutonium, and to discuss the impact on the inhour and $(k\beta/\ell)$ techniques of the errors involved.

G.R. KEEPIN: The accuracy of Pu^{239} delayed-neutron data is a few per cent (average 3-4%) for the least-squares-fitted periods and abundances[1]. These errors were determined in the computer least-squares-fitting process and do not include systematic errors which may arise in measured delayed-neutron gross decay curves. However, the accuracy of delayed-neutron data for the major fissionable materials has been demonstrated by several independent kinetic experiments, including period-reactivity measurements done by independent methods (e.g. in the case of Pu^{239}, measurements on the bare Pu^{239} critical assembly JEZEBEL) and the Laplace transform method[2] of generating the period-reactivity relation without introducing ana-

[1] Roughly the same accuracy applies to other fissionable species, with the exception of U^{235}, for which a somewhat better accuracy has been obtained.

[2] KEEPIN, G.R., Physics of Nuclear Kinetics, Addison Wesley, Reading, Mass. (1965).

lysed delayed-neutron groups. Comparisons for six fission species of Laplace-transformed period-reactivity relations with corresponding inhour relations calculated from basic delayed-neutron data show excellent agreement (~ 0.1% mean deviation) over the complete reactivity region from delayed through prompt critical[2]. Such precise agreement over a range of periods from ~1 ms to ~10^3s provides a stringent check on the least-squares analysis of measured delayed-neutron decay curves. The errors of a few per cent on individual delayed-neutron group periods and abundances are thus effectively reduced (by a factor of 2 or more) when these parameters are closely coupled as in the usual reactor kinetic relations (e.g. period-reactivity relations, the $(k\beta/\ell)$ technique, rod-drop analysis, etc.).

In addition it should be remembered that the relative importance or "effectiveness" of delayed neutrons can change the effective values of delay group abundances and thus affect the accuracy of all calculated kinetic relations, including inhour and $(k\beta/\ell)$ techniques. Delayed-neutron effectiveness factors (relative to prompt-neutron effectiveness) are computed by adjoint flux and spectrum weighting and are dependent on details of individual reactor geometry and composition and therefore do not lend themselves to generalization. It may be noted, however, that delayed-neutron effectiveness factors can be as large as 1.3 - 1.4 (as in some water-moderated systems) or can be several per cent less than unity (e.g. in small fast Pu systems)[3]. Thus uncertainties in delayed neutron effectiveness values can become an appreciable source of error, in some cases overshadowing errors associated with measured values of the delayed-neutron parameters.

S. SCOTT: A number of speakers have drawn attention to the difficulty of using high pulsing rates as a result of the overlapping of one pulse on another. This can be overcome quite easily by applying a correction for the prompt-neutron component "hidden" by the following pulse. We have used a correction which is based on the assumption that the prompt mode at this time is a single exponential, and we have found it to be quite accurate.

G. BRONNER: With our method of linear approximation of the decaying background we need a point (T) where only parts of the decays of ω_j with $j > 0$ are present. We can then determine s, ω_0, and A_0 by using three parts of the integral of $[n(t) - B(T)]$. If a fraction of the ω_0-decay is still present at the beginning of the next pulse, it would be necessary to use four parts of that integral and the method would then become rather cumbersome. Moreover, if one uses a duty cycle up to 10%, and is therefore forced to use all formulas in the generalized form for finite pulse-length, one cannot use any simple one-exponential decay description of the prompt part.

[3] Op. cit.

THE COMMON BELGONUCLEAIRE -CEN PROGRAMME FOR THE SURVEY STUDY OF UO_2-PuO_2-H_2O LATTICES BY THE PULSED NEUTRON TECHNIQUE*

J. DEBRUE AND F. MOTTE
CENTRE D'ÉTUDE DE L'ÉNERGIE NUCLÉAIRE, MOL,
AND
R. DELRUE, E. FOSSOUL, M. STIÉVENART AND G. TAVERNIER
SOCIÉTÉ BELGE POUR L'INDUSTRIE NUCLÉAIRE (BELGONUCLÉAIRE),
BRUSSELS, BELGIUM

Abstract — Résumé — Аннотация — Resumen

THE COMMON BELGONUCLÉAIRE-CEN PROGRAMME FOR THE SURVEY STUDY OF UO_2-PuO_2-H_2O LATTICES BY THE PULSED NEUTRON TECHNIQUE. In the frame of the work performed on plutonium recycling in light water reactors, a good deal of effort is devoted to the determination of the PuO_2-UO_2-H_2O lattice nuclear parameters. The scarcity and the cost of plutonium at high 240 content is such that one must rely on experimental methods involving small quantities of fuel, in other words subcritical assemblies. The pulsed neutrons technique has been chosen as a valuable, handy and fast tool for survey studies of plutonium-fuelled lattices.

Such a survey aims at the measurement of several integral parameters such as infinite multiplication factor, material bucklings, temperature coefficients etc. for different kinds of fuel (U-enrichment, Pu content, Pu^{240} isotopic content etc.), lattices (rod diameter, water-to-fuel ratio poisoning, etc.) and temperatures. As a first step in the programme, a 5% enriched UO_2 lattice has been studied by the proposed technique, and preliminary results pertaining to that particular experiment are given in the present paper. The experimental programme for the future will deal very soon with plutonium-fuelled lattices and a tentative schedule is given for the next years to come.

PROGRAMME COMMUN BELGONUCLÉAIRE-CEN POUR L'ÉTUDE DES RÉSEAUX UO_2-PuO_2-H_2O PAR LA MÉTHODE DES NEUTRONS PULSÉS. Dans le cadre des travaux effectués sur le réemploi du plutonium dans les réacteurs à eau légère, une grande activité est consacrée à la détermination des paramètres nucléaires des réseaux PuO_2-UO_2-H_2O. Le combustible à forte teneur en ^{240}Pu est si rare et si coûteux qu'il faut s'en tenir aux méthodes expérimentales qui ne font intervenir que de très petites quantités de combustible, en d'autres termes à des assemblages sous-critiques. La méthode des neutrons pulsés a été choisie parce qu'elle est à la fois précieuse, pratique et rapide pour les études générales sur les résaux au plutonium.

Une étude de ce genre vise à mesurer plusieurs paramètres intégraux, tels que le facteur de multiplication infini, les laplaciens matière, les coefficients de température, etc. pour différents combustibles (enrichissement en U, teneur en Pu, teneur isotopique en ^{240}Pu, etc.), différents réseux (diamètre des barres, rapport eau/combustible, empoisonnement, etc.) et différentes températures. Comme première opération dans le cadre du programme, les auteurs ont appliqué la méthode proposée à un réseau de UO_2, enrichi à 5%; le mémoire fournit les résultats préliminaires de cette expérience. Des expériences prochaines porteront sur des réseaux au plutonium; les auteurs esquissent le programme provisoire pour quelques années.

СОВМЕСТНАЯ ПРОГРАММА ИССЛЕДОВАТЕЛЬСКОГО ЯДЕРНОГО ЦЕНТРА БЕЛГОНУКЛЕЭР ПО ОБЗОРНОМУ ИЗУЧЕНИЮ РЕШЕТОК $UO_2-PuO_2-H_2O$ МЕТОДОМ ИМПУЛЬСНЫХ НЕЙТРОНОВ. В рамках работ по повторному плутониевому циклу на водяных реакторах большие усилия прилагаются для определения ядерных параметров решеток $PuO_2-UO_2-H_2O$.

Небольшие количества и стоимость плутония с большим содержанием плутония-240 заставляют полагаться на экспериментальные методы, связанные с небольшими количествами топлива, другими словами, иметь дело с подкритическими сборками.

* Work performed under sharing contract 001-64-1-TRUB with EURATOM.

Метод импульсных нейтронов был выбран как ценное, удобное и быстрое средство проведения обзорного изучения решеток плутониевого топлива.

Такой обзор имеет целью измерение нескольких интегральных параметров, таких как K ∞, лапласианы материала, температурные коэффициенты и т.д. для различных видов топлива (обогащение ураном, содержание плутония, изотопное содержание плутония-240 и т.д.) и температур.

В качестве первого шага этой программы с помощью предлагаемого метода изучалась решетка, обогащенная UO_2 до 5%, и в настоящем докладе приводятся предварительные результаты, касающиеся этого эксперимента.

Будущая экспериментальная программа будет связана с решетками плутониевого топлива, и приводится предварительный план работы на несколько лет.

PROGRAMA CONJUNTO DE LA BELGONUCLÉAIRE Y EL CEN PARA EL ESTUDIO PANORAMICO DE RETICULADOS DE UO_2-PuO_2-H_2O MEDIANTE LA TECNICA DE LOS NEUTRONES PULSADOS. Como parte de los trabajos que se realizan sobre el reciclado del plutonio en reactores de agua ligera, se ha procurado determinar los parámetros nucleares de reticulados de PuO_2-UO_2-H_2O. La escasez y el elevado costo del plutonio con alto contenido de ^{240}Pu obligan a recurrir a métodos experimentales que exijan pequeñas cantidades de combustible, es decir, a métodos a base de conjuntos subcríticos. Los autores han elegido la técnica de los neutrones pulsados por considerarla valiosa, sencilla y de rápidos resultados para realizar estudios panorámicos de reticulados de Pu.

Un estudio de esta índole tiene por objeto medir diversos parámetros integrales tales como las constantes de multiplicación correspondientes a medios infinitos, los laplacianos materiales, los coeficientes de temperatura, etc., para distintos tipos de combustible (según el enriquecimiento del U, el contenido de Pu, el contenido de isótopo ^{240}Pu, etc.), reticulados (según el diámetro de las barras, la razón agua/combustible, el envenenamiento, etc.) y temperaturas. En la primera etapa del programa se ha estudiado con dicha técnica un reticulado de UO_2 enriquecido al 5%; se dan los resultados preliminares del experimento. El programa previsto incluye la realización muy en breve de experimentos con reticulados de Pu, y los autores exponen el plan de trabajo establecido para los próximos años.

1. INTRODUCTION

In the frame of work performed on plutonium recycling in light water reactors, the Centre d'Etude de l'Energie Nucléaire (CEN) and Belgo-Nucléaire have installed as a first step an experimental set-up for the study of subcritical uranium oxide, light water lattices by the pulsed neutron technique.

The fuel used for these experiments is the 5% enriched UO_2 fuel of the research reactor THETIS which is now under construction at Ghent University. Lattices having volumetric H_2O-UO_2 ratios ranging from 1.5 to 9.35 are studied at room temperature in that facility.

Most of these experiments are essentially approaches-to-critical performed with great care and by using different measurement techniques simultaneously. The measurements performed on the lattice of the THETIS reactor (pitch: 15.42 mm; H_2O/UO_2 = 4.13) will be checked by the THETIS critical experiment scheduled at the end of summer 1965. Results obtained from this survey programme should allow a thorough evaluation of the pulsed neutron technique potential to deal with lattice parameter measurement in the subcritical range (k = 0.7 and 0.98). Besides, the experience acquired during this first part of the programme will help a great deal in the future work on PuO_2-UO_2-H_2O lattices.

2. DESCRIPTION OF THE EXPERIMENTAL APPARATUS

The pulsed neutron facility which has been erected to study 5% enriched UO_2-H_2O lattices is located in an auxiliary building of the reactor BR 1 at Mol. The experimental set-up is composed of the classical components, i.e. a pulsed neutron generator and its control apparatus, an aluminium tank containing the water which acts as moderator as well as reflector and shielding, a mechanical support for the fuel elements, detectors and accessories, which is positioned in the centre of the water tank, several detectors and their associated counting circuits (multichannel, monitoring scalers, health physics, etc.), a demineralization circuit for the water, a shielding wall mainly for fast neutrons, which surrounds the tank and neutron generator, and a loading platform which is placed just above the tank.

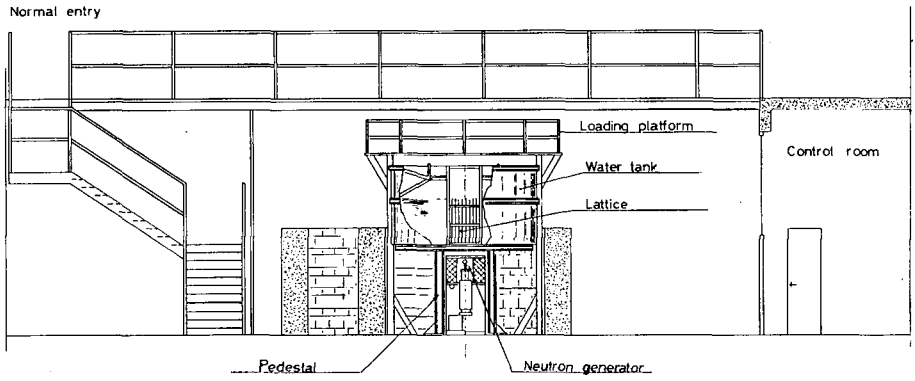


Fig. 1

Vertical cross-section of the pulsed neutron facility

The neutron generator, a S.A.M.E.S. (BS 1 type), accelerates 150-keV deuterons on to a tritiated target; the source neutrons have then a mean energy of 14 MeV. This generator, which uses a vacuum pump, could not be placed inside the tank.

The tank is placed, by use of a pedestal, above the neutron generator in such a way that the neutron source (target) is placed on the vertical axis of the assembly. The diameter of the tank is 220 cm and its height is 125 cm (see Fig. 1).

The mechanical support of the lattice is made of an aluminium frame and plexiglas grids as shown in Fig. 2. Three horizontal grids are used; one of them, having a thickness of 10 mm, is placed beneath and supports the lattice, the other two grids, having a thickness of 5 mm, serve as guides during the loading. Several sets of grids will be used to realize five different lattice spacings (five values of the H_2O-UO_2 ratio ranging from 1.51 to 9.35). The support grid is placed in the centre of the tank in the lower position in order to have the lattice as close as possible to the pulsed neutron source.

Five hundred fuel elements are available; they are 706 mm long and have an outside diameter of 8 mm. The thickness of the stainless steel clad-

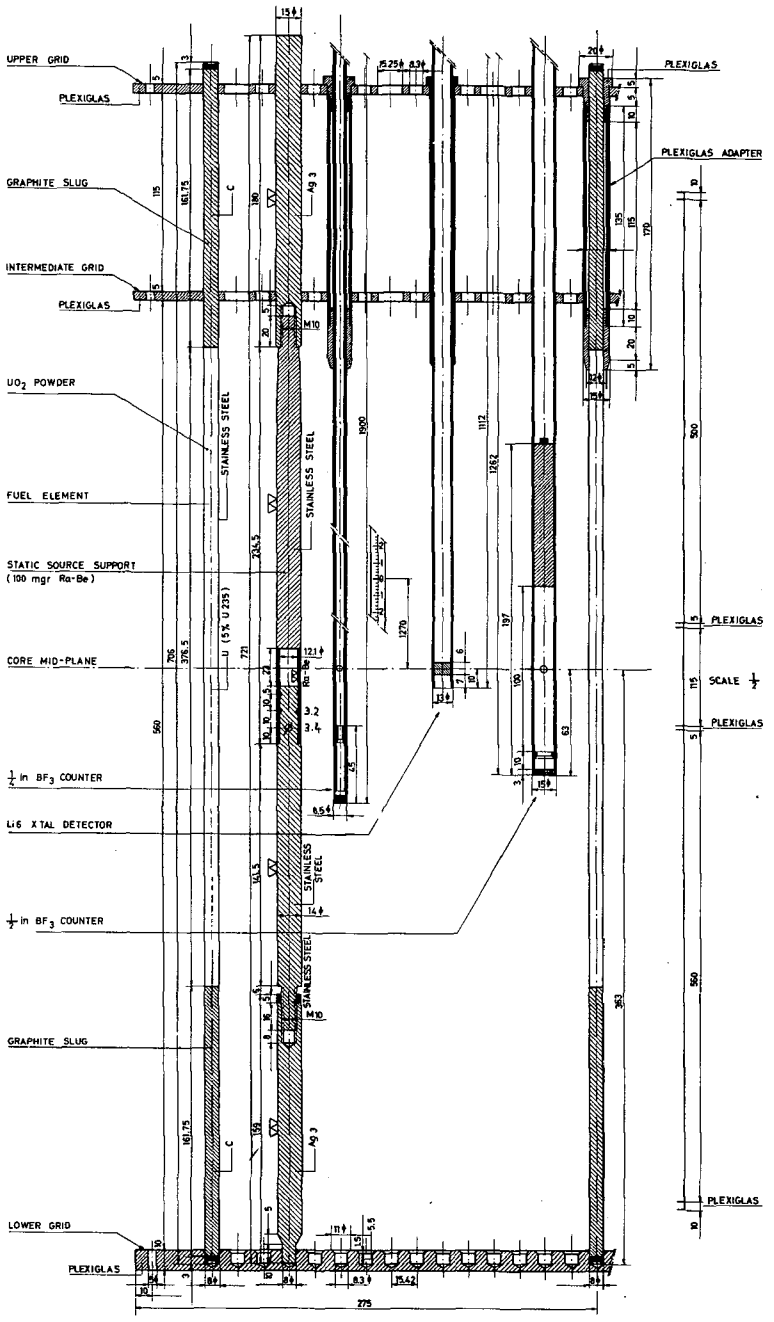


Fig. 2

Mechanical support of the lattice vertical cross-section

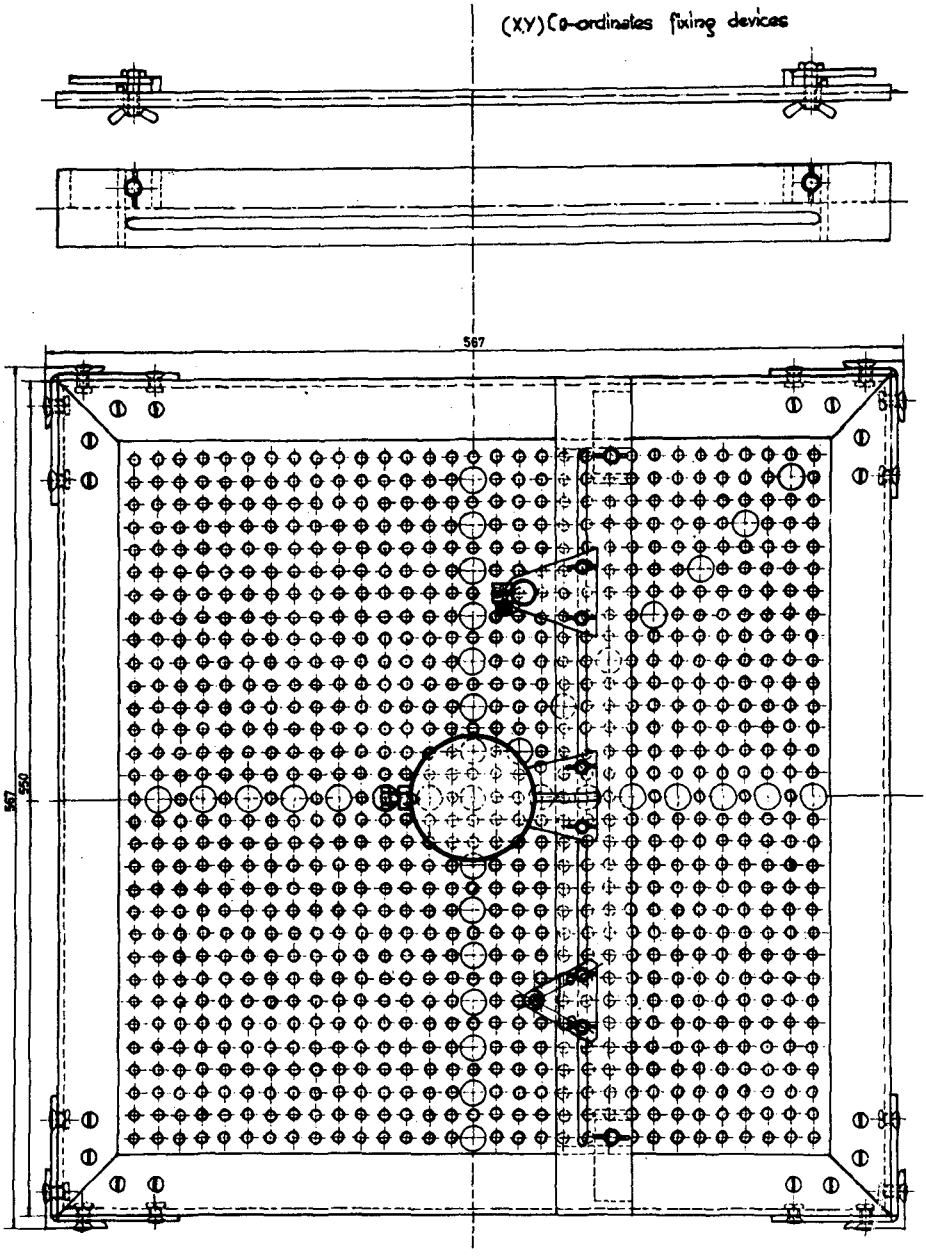


Fig. 3

Mechanical support of the lattice plane view

ding is 0.2 mm. The active length is 376.5 mm long and is filled with 5% enriched UO_2 powder; the density of the fuel is 8.5 g/cm^3 and has been obtained by vibration. On each side of the active length, a 161.75-mm-long graphite slug has been placed and sealed with the UO_2 powder (see Fig. 4).

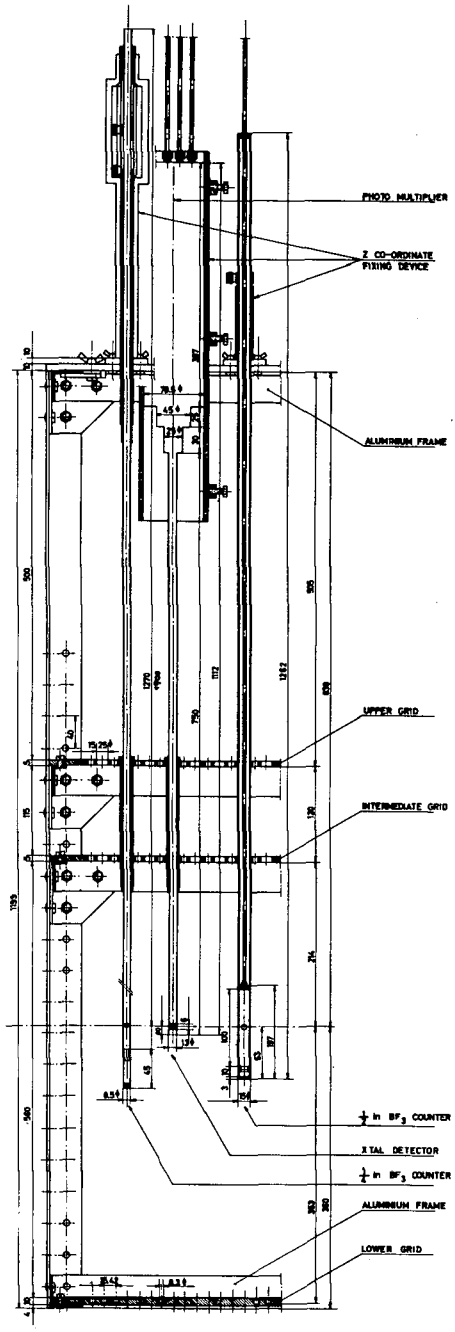


Fig. 4

Detailed view of the lattice and accessories

For large lattice spacings, the plexiglas grids have been drilled according to the desired lattice pitch; the normal diameter of the holes is 8.3 mm, but some holes on the two axes of the upper grids (see Fig. 3) have been drilled with a diameter of 15.25 mm to allow the use of detectors and a static Ra-Be source inside the core. Plexiglas adapters are then used to allow the placement of fuel element in these holes as seen in Fig. 4. For small lattice spacings, small detectors ($\leqslant$ 8.5 mm diam.) only are to be used and other grids are to be built.

A static Ra-Be source can also be used; it is generally placed in the centre of the core (X = 0, Y = 0, Z = 0).

Three detectors are used now, they are : a 1/2-in diam. BF_3 proportional counter, a Li^6 Xtal (9-mm diam.) mounted on a light guide plus a photomultiplier and a 1/4-in diam. BF_3 proportional counter. Three adequate positioning devices are used with them as shown in Figs. 2 and 3. Another 1-in diam. BF_3 proportional counter surrounded by a paraffin cylinder and an outer cadmium shield serves as monitor counter when the accelerator is used, it is located near the neutron generator below the water tank.

No fast control devices have been provided; just a slow dump of the water tank is available.

The water height has been choosen nearly equal to the length of the fuel elements (700 mm); the lattices which are assembled in the tank are then reflected radially by a nearly infinite thickness of pure water, though the axial reflector, which is 162 mm thick, has a mixed composition (water, graphite and steel).

With the subcritical facility described above, a lattice having the same pitch as the one of the THETIS reactor is being tested now. Out-of-core as well as in-core measurements are done. The flexibility of the facility and the reproducibility of the measurements are excellent.

3. EXPERIMENTAL PROGRAMME

The experimental programme which has just started consists mainly in cold clean approaches-to-criticality by varying the loading, i.e. the total number N of fuel elements forming the core. It is also foreseen to perform some measurements on poisoned lattices and some void coefficient measurements.

Since the type of fuel elements is unique, the only geometrical parameters which are varied are the lattice spacing and the external shape of the assembly (cylinder, square, slab).

3.1. Experimental techniques

During approaches-to-critical, three types of measurement are done at succeeding steps of the loading and are interpreted on the spot in five different ways. This immediate interpretation of experimental data aims at the fast determination of the subcriticality of the assembly as well as the extrapolated critical mass of the lattice. A more detailed interpretation of the experiment will be done later to determine lattice parameters such

as k_∞ and the prompt neutron lifetime. The three types of measurement techniques are the following.

(a) The static inverse multiplication

This is done by using a static Ra-Be source (100 mg). The space neutron density distribution is measured and the integral over the core volume is evaluated; the inverse of it is then plotted as a function of the loading and the extrapolated critical mass is determined.

(b) The source-jerk technique

A measurement of the reactivity of the assembly is performed by measuring the decay of the neutron density after the extraction of the static source (or the extinction of the neutron generator). The measured parameter is the ratio R.

$$R = n(o) / \int_{\Delta t} n(t)\,dt,$$

where n(o) is the neutron density just before the source jerk, n(t) is the neutron density after the source jerk, and Δt is some integration time after the source jerk. A comparison of measured values of R with a theoretical curve gives the reactivity of the assembly.

(c) The pulsed neutron method

The pulsed neutron method is considered as being the most valuable technique for far subcritical measurements and it is the basis of the programme. The following data and information are gathered by using this method.

(i) An inverse multiplication measurement is made by registering the mean neutron density $\bar{n}$ over the pulsation period T.

$$\bar{n} = \frac{1}{T} \int_0^T n(t)\,dt$$

$1/\bar{n}$ is then plotted as a function of the loading and the value of the extrapolated critical mass is determined.

(ii) A measurement of the reactivity is made by the "area method", i.e. by measuring the ratio of the total prompt neutrons P to the total delayed neutrons D.

$$\$ = P/D.$$

(iii) The main information which is finally drawn from the pulsed neutron measurements is the prompt neutron decay constant $\alpha(s^{-1})$. From this

TABLE I

GEOMETRICAL CHARACTERISTICS OF LATTICES TO BE STUDIED

Lattice n°	Lattice pitch (mm)	Grid basic pitch (mm)	H_2O/UO_2	Calculated critical number of rods for cylindrical configuration
I	10.9	10.9	1.51	1300
II	13.0	13.0	2.63	630
III (THETIS)	15.42	15.42	4.13	462
IV	18.4	13.0	6.33	442
V	21.8	15.42	9.35	627

measurement, the reactivity is derived in two ways. First, using a calculated value of β (delayed neutron fraction) and l (prompt neutron lifetime), the reactivity is derived through the following relation:

$$\delta k = \frac{\alpha l + \beta}{1 - \beta} \quad \text{with} \quad \alpha < 0$$

Secondly, using an extrapolated value of α at delayed criticality in the following relation, another value of the reactivity is derived.

$$\frac{\delta k}{k\beta} = 1 - \frac{\alpha}{\alpha_c}.$$

The value α_c is obtained by extrapolation of the experimental α-curve, α_c corresponding to the extrapolated critical mass obtained by the other techniques.

Using these techniques simultaneously, a fast and accurate determination of the extrapolated critical mass as well as the variation of the reactivity as a function of the loading has been made possible.

3.2. Schedule for experiment on UO_2-H_2O lattices

The first part of the programme which deals with the lattice parameter measurements of 5% enriched UO_2-H_2O assemblies started with measurements on the THETIS lattice. Four other lattices are to be studied experimentally; they are described in Table I.

The measurements being performed now on the THETIS lattice are the following: (i) subcritical measurement as a function of loading for different radial shapes (circular, square and slab); (ii) subcritical measurement as a function of poisoning ($\leqslant$ 1.500 ppm of boric acid) and (iii) void coefficient

TABLE II

SCHEDULE OF SUBCRITICAL MEASUREMENTS ON 5% ENRICHED UO_2-H_2O LATTICES

Scope of experiment	Lattice pitch (mm)	Grid basic pitch (mm)	H_2O/UO_2	Boric acid content (weight ppm)
Detailed study of the THETIS lattice	15.42	15.42	4.13	-
	15.42	15.42	4.13	0 - 1.500
Survey study of water to fuel ratio	21.80	15.42	9.35	-
	13.00	13.00	2.63	-
	18.40	13.00	6.33	-
	10.90	10.90	1.51	-
Void coefficient measurement of the THETIS lattice	15.42	10.90	4.13	-

measurement by use of empty microtubes which will be distributed throughout the core. Most of these measurements will be checked by the critical experiment of the THETIS reactor.

The measurements foreseen on the other four lattices comprise approaches-to-critical in a single macroscopic geometry (cylinder). These survey experiments aim at determining the influence of the water-to-fuel ratio on the lattice parameters as determined or inferred by different conventional and pulsed methods.

Table II gives a schedule of the experiments on the 5% enriched UO_2-H_2O lattices.

3.3. Future work on PuO_2-UO_2-H_2O lattices

The work described so far pertains only to the preliminary part of the programme which deals with measurements of the lattice parameters of PuO_2-UO_2-H_2O lattices. The next and more important part of the programme will begin at the end of this year when the first plutonium fuel loading will be available. This first plutonium fuel will consist of a mixed oxide with 3% enriched uranium and 2% plutonium content. The pulsed experiments will be performed in other facilities, but with the same techniques.

The CEN facility VENUS will first be used for cold clean lattices. Its use will give valuable check points for the analysis of particular lattices at large pitch. However, most experiments will be of the subcritical type.

In addition to VENUS, a pressurized subcritical facility is envisaged, to

investigate hot lattices and temperature coefficients. A typical feature of this programme is the low requirement of fuel, a fact of the utmost importance with regard to plutonium which is not only expensive but quite scarce for some high Pu^{240} content.

4. REMARKS AND PRELIMINARY RESULTS

The experiments performed during the first weeks of the programme demonstrated the flexibility of the facility. This flexibility permits most of the time to be devoted to measurements. It also gives confidence concerning the completion and success of the parametric study now under way.

The choice of facility components, as well as their arrangement, has proved quite judicious; biological shielding has allowed the experimental set-up and measuring apparatus to be concentrated in a small working area. Accelerator and detector characteristics and the associated electronics lead to good conditions for precise measurements in reduced time intervals.

Although the reactivity attained so far is rather low, extrapolated critical masses as obtained by different techniques are in satisfactory agreement; approaches-to-critical curves entirely support the safety criteria adopted. These criteria guarantee the safe loading of the subcritical assemblies with no hindrance to the experimental programme progress.

With regard to pulsed neutron measurements in particular, there is evidence for the existence of two time constants: they seem to characterize the decay of two neutron populations coming from primary neutrons slowed down in the core and in the reflector respectively. From measurements performed thus far, a determination of the variation of these decay constants with the fuel loading was possible.

DISCUSSION

See the discussion after the paper "Pulsed neutron studies of BeO natural uranium lattices" (SM-62/41) by B.V. Joshi et al., these Proceedings II.

STUDY OF SOLID-MODERATED ENRICHED URANIUM EPITHERMAL SYSTEMS BY THE PULSED NEUTRON TECHNIQUE*

J. R. MORTON III
UNIVERSITY OF CALIFORNIA,
LAWRENCE RADIATION LABORATORY,
LIVERMORE, CALIF., UNITED STATES OF AMERICA

Abstract — Résumé — Аннотация — Resumen

STUDY OF SOLID-MODERATED ENRICHED URANIUM EPITHERMAL SYSTEMS BY THE PULSED NEUTRON TECHNIQUE. The pulsed neutron technique has been applied to subcritical assemblies to accumulate data useful for the testing of multigroup calculational methods. The measurements were generally of two types: studies designed to examine the properties of fuel-moderator systems, and studies of the effects of various single perturbations upon the fuel-moderator system. The pulsed neutron method is particularly suited to the latter type application because the relative worth of such a perturbation can be measured quite directly with high precision.

The subcritical assemblies used for this purpose were semi-homogeneous systems composed of fully enriched uranium foils with moderators of thin blocks of either graphite or beryllium oxide. These systems emphasized simple idealized geometries rather than detailed mockups of specific configurations. The fuel densities of nearly all the systems were sufficiently high to produce epithermal neutron spectra. The assemblies can be characterized by their moderator-fuel ratios. The BeO-moderated systems ($\rho_{BeO} = 2.86$ g/cm^2) were BeO/U^{235} = 123, 247, 329, 493, and 3830; their prompt neutron decay constants at delayed critical, $\alpha_c (= \beta_{eff}/\ell^*)$, were 590, 270, 192, 123, and 21.5 s^{-1} (±3%). The graphite-moderated systems ($\rho_C = 1.64$) were C/U^{235} = 598, 1200, 2280, and 9103 with corresponding α_c values: 150, 70, 38, and 9.5 s^{-1} (±3%). A sensitive test of multigroup cross-sections was performed using the measured values of α_c and $\Delta\alpha/\Delta B^2$ with calculated values of $\Delta k/\Delta B^2$ to deduce β_{eff}. Deviations from the expressed β_{eff} may be attributed to deficiencies in cross-sections. Perturbations studied yielded the worths of reflector materials in slab geometry adjacent to one face of a subcritical assembly and absorber samples in slab or bar geometries centrally located within an assembly. Such measurements permit direct deduction of reflector savings or poison costs to core reactivity; more refined analysis permitted evaluation of scattering and absorption cross-sections and resonance integrals. Reflector studies were made with systems having BeO/U^{235} = 247; absorber studies were made with systems with BeO/U^{235} = 247 and 493, and C/U^{235} = 598.

ETUDE DE SYSTÈMES A NEUTRONS ÉPITHERMIQUES, A URANIUM ENRICHI ET A RALENTISSEUR SOLIDE, PAR LA MÉTHODE DES NEUTRONS PULSÉS. L'auteur a appliqué la méthode des neutrons pulsés à des assemblages sous-critiques pour accumuler des données utiles en vue du contrôle des méthodes de calcul à plusieurs groupes. Dans l'ensemble, ces mesures ont été de deux types: a) études sur les propriétés des systèmes composés d'un combustible et d'un ralentisseur; b) études des effets de diverses perturbations isolées sur un système composé d'un combustible et d'un ralentisseur. La méthode des neutrons pulsés convient parfaitement à ce dernier type d'application parce que l'on peut mesurer assez directement et avec une grande prévision la réactivité relative d'une perturbation.

Les assemblages sous-critiques utilisés à cet effet étaient des systèmes semi-homogènes à géométrie simple formés de feuilles d'uranium pleinement enrichi et de minces blocs de graphite ou de glucine. Les densités de combustible dans presque tous les systèmes étaient suffisamment élevées pour produire des spectres de neutrons épithermiques. Ces assemblages peuvent être caractérisés par leur rapport ralentisseur-combustible. Pour les systèmes ralentis au BeO ($\rho_{BeO} = 2,86$ g/cm^2), les rapports étaient les suivants: BeO/^{235}U = 123, 247, 329, 493 et 3830; leurs constantes de décroissance des neutrons instantanés à l'état critique retardé, $\alpha_c (= \beta_{eff}/\ell^*)$, étaient: 590, 270, 192, 123 et 21,5 s^{-1} (±3%). Pour les systèmes ralentis au graphite ($\rho_C = 1,64$), les rapports étaient les suivants: C/^{235}U = 598, 1200, 2280 et 9103 et les valeurs correspondantes de α_c: 150, 70, 38 et 9,5 s^{-1} (±3%). L'auteur a effectué un contrôle très sensible d'un ensemble de sections

* Work performed under Atomic Energy Commission Contract No. W-7505-eng-48.

efficaces en utilisant les valeurs mesurées de α_c et de $\Delta\alpha/\Delta B^2$ avec les valeurs calculées de $\Delta k/\Delta B^2$ pour déduire β_{eff}. On peut expliquer les écarts par rapport à la valeur prévue pour β_{eff} par des insuffisances dans les sections efficaces.

Les perturbations étudiées ont fourni les réactivités de matériaux utilisés comme réflecteur dans une géométrie de plaques adjacent à une face d'un assemblage sous-critique et d'échantillons d'absorbants dans des géométries de plaques ou de barres placées au centre d'un assemblage. De telles mesures permettent de déduire directement les gains en réactivité du cœur dus au réflecteur ou les pertes dues au poison; une analyse plus fine a permis d'évaluer les sections efficaces de diffusion et d'absorption et les intégrales de résonance. Les études sur les réflecteurs ont été faites avec des systèmes dont le rapport BeO/ ^{235}U était 247; les études sur les absorbants ont été faites avec des systèmes dont les rapports BeO/^{235}U étaient 247 et 493, et le rapport C/ ^{235}U était 598.

ИЗУЧЕНИЕ ЭПИТЕРМИЧЕСКИХ СИСТЕМ С ОБОГАЩЕННЫМ УРАНОМ И ТВЕРДЫМ ЗАМЕДЛИТЕЛЕМ ПРИ ИСПОЛЬЗОВАНИИ МЕТОДОВ С ИМПУЛЬСНЫМИ НЕЙТРОНАМИ. Метод с импульсными нейтронами применен к подкритическим сборкам для накопления данных, полезных при проверке многогрупповых вычислительных методов. В общем производились два типа измерений: исследования, предназначенные для изучения свойств систем топлива-замедлителя и исследование воздействия различных единичных возмущений на систему топливо-замедлитель. Метод с импульсными нейтронами является особенно подходящим в последнем случае, потому что может быть измерена непосредственно и с высокой точностью относительная величина такого возмущения.

Подкритические сборки, использованные для этой цели, были полугомогенными системами, состоящими из фольги из полностью обогащенного урана с замедлителями из тонких блоков графита или окиси бериллия. Эти системы представляли собой простые идеализированные геометрии, а не детальные модели особых конфигураций. Плотности топлива почти всех систем были достаточно высокими, чтобы давать спектры надтепловых нейтронов. Сборки можно характеризовать соотношением между топливом и замедлителем. Системами с замедлителем из BeO (ρ_{BeO} = 2,86 г/см^2) были BeO/U^{235} = 123, 247, 329, 493 и 3830; их постоянные распада мгновенных нейтронов при критичном α_c (= $\beta_{эфф}/\ell^*$) с учетом запаздывающих нейтронов составляли 590, 270, 192, 123 и 21,5 сек$^{-1}$ (±3%). Системы с графитовыми замедлителями (ρ_c = 1,64) представляли C/U^{235} = 598, 1200, 2280 и 9103 с соответствующими значениями α_c : 150, 70, 38 и 9,5 сек$^{-1}$ (±3%). Чувствительный контроль за многогрупповыми сечениями осуществлялся с использованием измеренных величин α_c и $\Delta\alpha/\Delta B^2$ при расчетных значениях $\Delta k/\Delta B^2$ для выведения $\beta_{эфф}$. Отклонения от ожидаемых значений $\beta_{эфф}$ могут быть отнесены к недостаточным значениям сечений.

Изучаемые возмущения дали сведения о величинах материалов отражателя в геометрии пластины, прикрепленных к одной поверхности подкритической сборки, и об образцах поглотителя в геометриях пластины или бруска, расположенных в центральной части сборки. Такие измерения позволяют непосредственно вычислить экономию на отражатель или цену отравления в реактивности активной зоны; более тщательный анализ позволяет произвести оценку сечений рассеяния и резонансных интегралов. Были проведены исследования отражателей на системах, имеющих BeO/U^{235} = 247; были проведены исследования поглотителя на системах с BeO/U^{235} = 247 и 493 и C/U^{235} = 598.

ESTUDIO DE SISTEMAS EPITERMICOS DE URANIO ENRIQUECIDO Y MODERADOR SOLIDO MEDIANTE LA TECNICA DE LOS NEUTRONS PULSADOS. El autor ha empleado la técnica de los neutrones pulsados en experimentos con conjuntos subcríticos, con el propósito de acopiar datos que permitan verificar la validez de los métodos de cálculo de varios grupos. Las determinaciones correspondieron, en general, a dos tipos distintos: estudios con miras a examinar las propiedades de sistemas de combustible y moderador, y estudios de los efectos que las diversas perturbaciones ejercen por separado, sobre el sistema de combustible y moderador. El método de los neutrones pulsados se presta especialmente a este último tipo de estudio debido a la posibilidad de medir directamente, con alta precisión, la importancia relativa de la perturbación de que se trata.

Los conjuntos subcríticos empleado con este fin consistían en sistemas semihomogéneos formados por láminas de uranio totalmente enriquecido y bloques de grafitos o de BeO como moderador. Estos sistemas representaban geometrías sencillas e idealizadas más bien que maquetas detalladas de configuraciones concretas. En casi todos los sistemas, la densidad del combustible era lo suficientemente elevada para producir

espectros de neutrones epitérmicos. Los conjuntos podían caracterizarse por sus razones moderador/combustible. Los sistemas moderados con BeO (ρ_{BeO} = 2,86 g/cm²) presentaban razones BeO/^{235}U = 123, 247, 329, 493 y 830; las correspondientes constantes de decrecimiento de los neutrones inmediatos en el estado crítico retardado, $\alpha_c (=\beta_{ef}/\ell^*)$, eran de 590, 270, 192, 123 y 21,5 s^{-1} (± 3%). Los sistemas moderados por grafito (ρ_C = 1,64) presentaban razones C^{235}U = 598, 1200, 2280 y 9103, con valores de α_c de 150, 70, 38 y 9,5 s^{-1} (± 3%) respectivamente. Se efectuó un sensible ensayo de las secciones eficaces de varios grupos empleando los valores medidos de α_c y de $\Delta\alpha/\Delta\beta^2$ y los valores calculados de $\Delta k/\Delta\beta^2$ para deducir el valor de β_{ef}. Las desviaciones observadas respecto del valor previsto de β_{ef} podían atribuirse a valores incorrectos de las secciones eficaces.

Las perturbaciones estudiadas proporcionaron los valores relativos de materiales reflectores en una geometría de placas adyacente a una de las caras de un conjunto subcrítico, así como de muestras de material absorbente en geometrías de barras o de placas colocadas en el centro de un conjunto. Esas mediciones permiten deducir directamente de la reactividad del cuerpo las economías debidas al reflector o los costos de envenenamiento; un análisis más detenido permitió evaluar las secciones eficaces de dispersión y de absorción, así como las integrales de resonancia. Los estudios sobre el material reflector se realizaron con sistemas que presentaban una razón BeO/^{235}U = 247, mientras que los estudios sobre los materiales absorbentes se efectuaron con sistemas de BeO/^{235}U = 247 y 493, y C/^{235}U = 598.

1. INTRODUCTION

For a number of years our Laboratory has had a continuing interest in homogeneous, solid-moderated systems fuelled with fully-enriched uranium. Since the systems of interest have had substantially epithermal neutron spectra, with their well-known resonance complications, intensive experimental effort has been required in support of design calculations. Because of its directness and high precision, the pulsed neutron method for study of subcritical systems has been a major tool in this programme. These studies were generally of two types: those designed to examine the properties of simple fuel-moderator systems and those designed to determine the effects of various perturbations on the fuel-moderator system.

2. EXPERIMENTS

2.1. General

The subcritical assemblies used for this programme were semi-homogeneous parallelepipeds composed of fully-enriched uranium foils (93.2% U^{235}) and moderators of thin blocks of either graphite or beryllium oxide. The emphasis for these systems was to obtain assemblies substantially free from extraneous structural perturbations and in geometries which could be treated with exactness; therefore, analysis could be concerned essentially with the nuclear properties of the systems. This programme did not include study of detailed mock-ups of specific configurations. The neutron spectra of the various systems were controlled by varying the fuel density; in this report the assemblies and their spectra are characterized by the gross molar moderator-fuel ratios. Critical measurements on systems of this type were described in Refs. [1] and [2].

2.2. Subcritical assemblies

2.2.1. Uranium foils

The enriched uranium foils were 13.35 cm (5.25 in) square with nominal thicknesses of 0.003 and 0.005 cm (0.001 and 0.002 in); they were coated with a fluorocarbon plastic layer about 0.00064 cm thick. The individual foils had average U^{235} isotopic weights of 8.49 and 16.1 g for the 0.003 and 0.005 cm thicknesses, respectively. The fluoroplastic (CF_2) was found to contain no impurity in concentration greater than 1 ppm by chemical analysis; nuclear magnetic resonance tests showed the hydrogen content to be less than 3 parts per thousand.

2.2.2. Beryllium oxide moderator material

The BeO blocks were of two sizes: 15.25 cm × 15.25 cm × 2.54 cm (6 in × 6 in × 1 in) and 15.25 cm × 15.25 cm × 1.27 cm (6 in × 6 in × 0.5 in), with a 0.038-cm (0.015-in) deep by 13.65-cm (5.375-in) wide recess on one face to hold the fuel foils. The average weight of the blocks was 1690 or 825 g, depending upon the size range. The average BeO density in the usual assembly volume, including the voids for containing the fuel foils, was 2.86 g/cm^3. Study of the moderator material by use of the pulsed neutron method indicated the impurity concentration of neutron absorbers to be less than 1 mb per BeO molecule.

TABLE I. Major impurities in ATJ graphite

Element	Concentration (ppm)
B	14.4
Ca	200
Al	200
Mg	30
Fe	600
Ag	6
Cu	500
Ti	60

2.2.3. Graphite moderator material

The ATJ graphite blocks also were of two sizes: 15.25 cm × 15.25 cm × 1.27 cm (6 in × 6 in × 0.5 in) and 15.25 cm × 45.8 cm × 2.54 cm (6 in × 18 in × 1 in) with a 0.025-cm (0.010-in) recess in the top to accommodate the fuel foils. There were two types of 15.25-cm square graphite blocks: solid blocks with an average weight of 499 g, and slotted blocks, used for pallets in stacking the assemblies, with an average weight of 306 g; the larger blocks had an average weight of 3014 g. Most assemblies were con-

structed with a plane of slotted blocks every 15.25 cm of assembly height. The major impurities in the graphite are listed in Table I.

2.2.4. Arrangement of assemblies – BeO systems

The individual BeO-moderated assemblies customarily had fixed base dimensions with variable heights. The systems were constructed in two parts; the lower part, with fixed height, was raised vertically to contact a 0.048-cm thick stainless steel diaphragm which supported the upper part. For the later assemblies the lower parts rested upon a 0.64-cm boral plate; the sides of both portions of the assemblies were enclosed in a supporting framework of boral plates and aluminium angle braces to preserve the dimensional stability and minimize wall-return from the test cell. The support framework caused a small but measurable decrease in the prompt neutron decay constant, which may account for variations in otherwise identical assemblies described below. A reader interested in critical dimensions is also advised to consult Ref. [2].

2.2.5. Arrangement of assemblies – graphite systems

The various graphite-moderated assemblies were also constructed with fixed base dimensions and variable heights. These systems were built on a low-mass table surrounding a graphite housing containing poison rods. The assemblies were quite similar to those described in Ref. [1] except for changes which reduced the control void volume. When measurements were performed, the poison rods were withdrawn from the assembly. The graphite assemblies rested upon a boral plate 0.32-cm thick to minimize reflection from the support structure. The problem of wall-return appeared to be unimportant in pulsed neutron measurements with these systems; this conclusion was based upon the lack of detectable changes in the decay constants when the sides were enclosed in 0.64-cm boral plates.

2.3. Pulsed neutron technique

In the pulsed neutron technique the measured parameter is the prompt neutron decay constant α which characterizes the decay of the neutron population in a subcritical system following introduction of a short burst of neutrons [3]. The pulsed neutron source used was an "Omnitron" [4] which generates bursts of 14-MeV D-T neutrons. The source produced bursts of about 10^5 neutrons with a pulse width of 2 μs; frequencies varied over the range 6 to 130 s^{-1}, depending upon the system of interest. The decays were observed using a 256-channel time analyser; channel widths were varied from 30 to 650 μs. The leakage flux from the assemblies was generally observed using either a 3.8-cm ($1\frac{1}{2}$ in) diameter $Li^6I(Eu)$ scintillator or a 12.7-cm (5-in) diameter Li^6-loaded plastic scintillator (NE 421)*. In every case the pulsed source and neutron detector were centrally located on adjacent faces of an assembly, which seemed to minimize modal interferences.

* Manufactured by Nuclear Enterprises Ltd., Winnipeg, Canada.

TABLE II. Summary of prompt neutron decay constants for BeO-moderated systems

Assembly height (cm)	Prompt neutron decay constants				
	$\frac{BeO}{U^{235}}=123$[a]	$\frac{BeO}{U^{235}}=247$[b]	$\frac{BeO}{U^{235}}=329$[c]	$\frac{BeO}{U^{235}}=493$[d]	$\frac{BeO}{U^{235}}=3830$[e]
46.2	2670				
47.0		1628			
47.5	1900				
48.3		1224			424
48.6	1100				
49.6	590[f]	802			
50.8		443	814	914	313
51.8		270[f]			
52.1			550	723	
53.4			291	540	212
53.6			192[f]		
54.6				365	
55.9				206	119
56.7				123[f]	
57.2					81.3
58.5					37.9
59.2					21.5[f]
63.5		1812[g]			
68.6		1153			
71.1		857			
73.7		595			
74.9		464			
76.2		351			
77.2		265[f]			

[a]Base dimensions were 61 × 61 cm; fuel planes were 0.042 cm thick uranium, spaced 2.620 cm apart. BeO assembly density: 2.77 g/cm^3. Aluminum spacer strips 0.081 cm thick were used to provide space for the fuel planes.

[b]Base dimensions were 61 × 61 cm; reproduced from Ref. [8] for comparison. Fuel planes were 0.020 cm thick uranium, spaced 2.54 cm apart. BeO assembly density: 2.86 g/cm^3.

[c]Base dimensions were 61 × 61 cm; fuel planes were 0.015 cm thick uranium, spaced 2.54 cm apart. BeO assembly density: 2.86 g/cm^3.

[d]Base dimensions were 61 × 61 cm; reproduced from Ref. [9] for comparison. Fuel planes were 0.005 cm thick uranium, spaced 2.54 cm apart. BeO assembly density: 2.86 g/cm^3.

[e]Base dimensions were 91.5 × 91.5 cm; fuel planes were 0.003 cm thick uranium, spaced 5.08 cm apart. BeO assembly density: 2.86 g/cm^3.

[f]These values were obtained by extrapolating to delayed critical a curve of prompt decay constant (α) versus M^{-1}.

[g]For data from here down the base dimensions were 61 × 45.8 cm, other properties were as described in footnote b.

2.4. *Treatment of data*

Within a short time following an injected pulse of neutrons, a sub-critical assembly attains a "stable" or "fundamental" mode which has the form of a single exponential decaying to a constant background. For these experiments, early data channels which obviously failed to follow an exponential-type decay were rejected; the remaining data were processed using FRENIC, a computer programme which effects a least-squares fit to a sum of exponentials and computes the decay constant [5]. This programme also prints out a comparison plot of both the experimental and the fitted data. A typical example of such a plot is shown in Fig. 1. Inspection of the plots permits evaluation of both the overall fit produced and the rejection of early channels, where the higher modes occur.

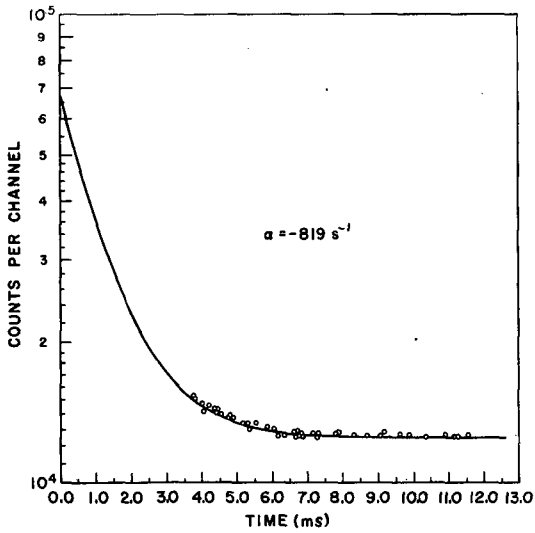


Fig. 1

Typical plot of pulsed neutron data fitted by computer processing.
The continuous curve is the fitted data; scattered points are experimental.
Over most of the data experimental and fitted values coincide.

3. RESULTS

3.1. *BeO-moderated subcritical systems*

For each type of assembly, measurements were made as follows: Beginning with an assembly of fixed base dimensions and tall enough to be within several centimetres of critical ($k_{eff} \sim 0.95$), both α and the inverse multiplication of a radioactive source were determined. These measurements were repeated for incremental increases in assembly height to the nearest complete layer below delayed critical. Partial layers beyond that point were also used so that values could be obtained within a few cents of delayed critical. The value of α_c was determined by extrapolating to delayed critical a

TABLE III. Summary of prompt neutron decay constants for graphite-moderated systems

Assembly height (cm)	Prompt neutron decay constants			
	$\frac{C}{U^{235}}=598$[a]	$\frac{C}{U^{235}}=1200$[b]	$\frac{C}{U^{235}}=2280$[c]	$\frac{C}{U^{235}}=9103$[d]
91.5	733	583	---	
92.8	592	---	---	
97.0	---	496	---	
95.4	397	---	---	
96.6	276	377	---	
98.1	150[e]	---	---	
99.1		258	393	
100.4		204	---	
101.7		149	---	
103.2		70[e]	---	
104.2			269	
106.8			208	
109.3			157	
110.6			129	
111.8			102	
113.1			74.8	
114.9			38[e]	
127.0				87.7
132.2				59.2
134.8				45.7
137.2				33.5
138.5				26.6
139.8				20.4
142.0				9.5[e]

[a]Base dimensions were 123 × 123 cm; fuel planes were 0.005 cm thick uranium, spaced 1.27 cm apart. The average moderator density in the assembly was 1.64 g/cm^3.

[b]Base dimensions were 123 × 123 cm; fuel planes were 0.005 cm thick uranium, spaced 2.54 cm apart. The average moderator density in the assembly was 1.64 g/cm^3.

[c]Base dimensions were 123 × 123 cm; fuel planes were 0.003 cm thick uranium, spaced 2.54 cm apart. The average moderator density in the assembly was 1.64 g/cm^3.

[d]Base dimensions were 154 × 154 cm; fuel planes were 0.003 cm thick uranium, spaced 10.2 cm apart. The average moderator density in the assembly was 1.67 g/cm^3.

[e]These values were obtained by extrapolating to delayed critical a curve of prompt decay constant versus relative inverse multiplication.

graph of α versus M^{-1}, the relative inverse multiplication. The systems studied and the pulsed neutron data are summarized in Table II. These data are as presented in Ref. [6] with one correction. If necessary the assembly dimensions can be converted to geometric buckling by use of the extrapolation distance of 1.3 cm, which was determined by neutron flux traverses.

3.2. Graphite-moderated subcritical systems

The technique used for the graphite-moderated systems was essentially the same as that described for the BeO-moderated assemblies. The systems studied and the pulsed neutron data are listed in Table III. These data are essentially refinements of measurements of KLOVERSTROM and KOMOTO [7]. The measurements discussed here differ from the earlier work in the following ways: (1) the assembly structure was improved in the way mentioned in section 2.2.5; (2) the pulsing and inverse multiplication measurements were performed concurrently on the same configurations, rather than

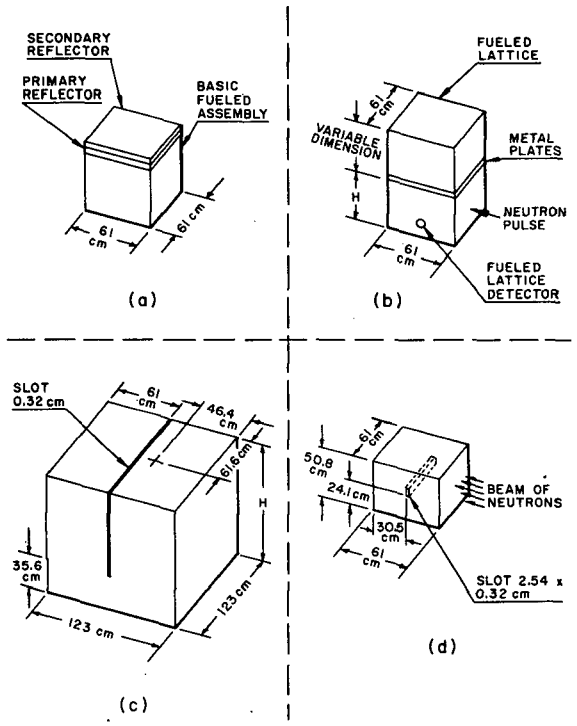


Fig. 2

Sketches of experimental arrangements:
(a) reflector studies;
(b) absorbers in slab geometry in a BeO system;
(c) absorbers in slab geometry in a graphite system;
(d) absorbers in bar geometry in a BeO system.

TABLE IV. Reflector materials

Material	Thickness (cm)	Surface density (g/cm^2)
Aluminum, type 1100F (99% purity)	0.64	1.72
Beryllium oxide	1.27	3.61
Brass, half-hard	0.32	2.68
Copper, #129 hard	0.32	2.96
Hastelloy R-235 (Ni 63.95%, Cr 15.24%, Fe 9.85%, Mo 5.49%)	0.64	4.92
Nickel, cold-rolled annealed	0.32	2.81
René 41 (Ni 53.23%, Cr 19.06%, Co 11.04%, Mo 9.93%, Ti 3.18%)	0.95	7.82
Steel, cold-rolled	0.30	2.57
Stainless steel, type 304	0.32	2.44

TABLE V. Variations of decay constants with thicknesses of various reflectors

Reflector material	Assembly height (cm)	Reflector thickness (cm)	Reflector surface density (g/cm^2)	α (sec^{-1})	Reflector material	Assembly height (cm)	Reflector thickness (cm)	Reflector surface density (g/cm^2)	α (sec^{-1})
BeO	47.0	1.27	3.61	1231	Copper	48.3	0.32	2.96	1134
		2.54	7.22	852			0.64	5.92	1052
		3.81	10.83	507			0.95	8.88	968
	44.4	2.54	7.22	1665			1.27	11.84	896
		3.81	10.83	1283			1.59	14.80	828
		5.08	14.44	883			1.90	17.76	758
		6.35	18.05	548			2.22	20.72	704
	39.4	7.62	21.66	1742			2.54	23.68	646
Ni	48.3	0.32	2.81	1061			2.86	26.64	581
		0.64	5.62	913			3.18	29.60	533
		0.95	8.43	783			3.49	32.56	487
		1.27	11.24	648			3.81	35.52	444
		1.59	14.05	545	Brass	48.3	0.64	5.36	1067
		1.90	16.86	446			1.27	10.72	923
		2.22	19.67	365			1.90	16.08	793
	47.0	1.90	16.86	840			2.54	21.44	679
		2.22	19.67	748			3.18	26.80	579
		2.54	22.48	664			3.81	32.16	489
		2.86	25.29	575	Aluminum	49.5	0.64	1.72	774
		3.18	28.10	506			1.27	3.44	730
		3.49	30.91	441			1.90	5.16	700
		3.81	33.72	385			2.54	6.88	663
Hastelloy R-235	47.0	0.64	4.92	1386			3.18	8.60	627
		1.27	9.84	1140			3.81	10.32	597
		1.90	14.76	984	Steel	48.3	0.60	5.14	1039
		2.54	19.68	833			1.20	10.28	872
		3.18	24.60	720			1.80	15.42	732
		3.81	29.52	607			2.40	20.56	607
René R-41	47.0	0.95	7.82	1249			3.00	25.70	509
		1.90	15.64	1014			3.60	30.84	416
		2.86	23.46	816					
		3.81	31.28	689					
Stainless steel T-304	48.3	0.64	4.88	1033					
		1.27	9.76	858					
		1.90	14.64	710					
		2.54	19.52	586					
		3.18	24.40	482					
		3.49	29.28	429					
		3.81	34.16	381					

TABLE VI. Variations of decay constants with thicknesses of composite reflectors

Primary reflector			Secondary reflector			Tertiary reflector			α
Material	Thickness (cm)	Surface density (g/cm^2)	Material	Thickness (cm)	Surface density (g/cm^2)	Material	Thickness (cm)	Surface density (g/cm^2)	(sec^{-1})
BeO	7.62	21.66	Hastelloy	0.64	4.92	-	-	-	1504
				1.27	9.84				1319
				1.90	14.76				1175
				2.54	19.68				1076
				3.18	24.60				990
				3.81	29.52				937
BeO	7.62	21.66	René	0.11	0.98	-	-	-	1619
				0.95	7.82				1392
				1.90	15.64				1239
				2.86	23.46				1125
				3.81	31.28				1059
BeO	5.08	14.44	Ni	2.54	22.48	-	-	-	1185
						Hastelloy	0.64	4.92	1088
							1.27	9.84	1021
							1.90	14.76	963
							2.54	19.68	908

having their assembly height dependences determined in separate series of experiments; and (3) the measurements were made with faster and more dependable electronic equipment.

3.3. Perturbed systems

The perturbations of interest to these studies were reflectors and localized absorbers. In each case the measured effects of the perturbations are related to their resonance integrals for scattering, absorption, or both. The general arrangements for the various experiments are shown in Fig. 2.

3.3.1. Studies of reflectors

The assembly used for the reflector studies had a BeO–U^{235} ratio of 247 and base dimensions of 61 cm × 61 cm. The general experimental procedure followed was to determine first the decay constant for the unreflected reference assembly selected for a series of measurements. Reflectors were

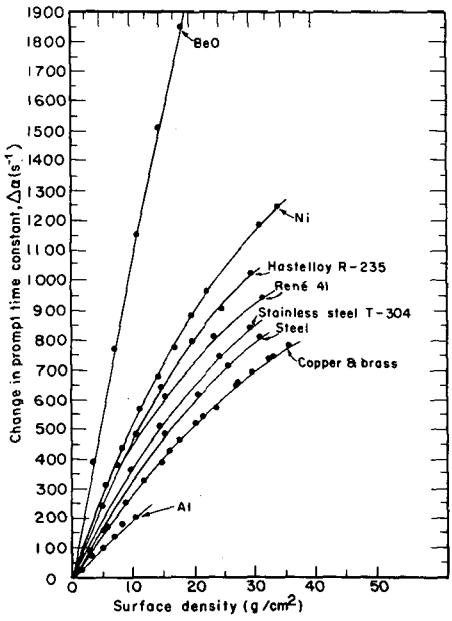


Fig. 3

Change in decay constant as a function of surface density for various reflector materials

then constructed on the top surface only, usually in the form of 61-cm square plates. The type of arrangement used is sketched in Fig. 2(a). This particular arrangement was chosen to limit analysis to a one-dimensional problem. For the measurements involving combinations of reflector materials, the material in contact with the basic assembly constituted the "primary reflector"; the next group of material was the "secondary reflector", and

so on. The decay constant was measured over a range of thicknesses for each type of reflector. Various properties of the reflector materials studied are shown in Table IV. The experimental results are shown in Table V for systems with single reflectors. Data for systems with composite reflectors are given in Table VI. Figure 3 summarizes the results of Table V in a plot of the decay constant change versus reflector surface density. Other graphical summaries of these data are given in Reference [8].

TABLE VII. Properties of absorbers

Material	Thickness	Surface density (g/cm^2)	Analytical data
Nickel	0.32	2.81	(ppm) P<50, S<50; (wt %) B<0.0005, Cd<0.005,[a] Co 0.005-0.05, Cu 0.02-0.2, Fe 0.01-0.1, Mn 0.03-0.3, Mo<0.0005, Si 0.003-0.03, Ti 0.002-0.02.
Ingot iron	0.32	2.45	(wt %) C 0.021, Mn 0.020, P 0.003, S 0.023, Si 0.004, Cu 0.132
Cobalt	0.038 0.093	0.320 (av.) 0.700 (av.)	Spec. (Max. wt %) Ni 0.4, Mn 0.03, Si 0.03, trace of elements, Co 99.5 min. Analysis B 0.0003-0.003
Gold	0.003 0.025	0.0564 (av.) 0.498 (av.)	Not analyzed; density variation within each foil $\leq 2\%$
Hastelloy R-235	0.25	2.07	(wt %) Cr 15.54, Fe 10.13, C 0.13, Si 0.23, Co 0.14, Mn 0.01, Mo 5.54, P 0.001, S 0.007, Al 2.01, Ti 2.60, B 0.003, Ni - balance
René 41	0.112	0.986	(wt %) Cr 19.08, Fe 0.94, C 0.11, Si 0.17, Co 10.94, Mn 0.03, Mo 9.98, S 0.010, Al 1.48, Ti 3.08, B 0.006, Ni - balance
Boron-loaded stainless steel	0.025	0.198	(wt %) Cr 17.86, Ni 13.73; Fe 63.79, Cd<0.01,[a] Co 0.02-0.2, Cu 0.04-0.4, Mn>2, Mo 0.004-0.04, Si 0.01-0.1, Ti 0.0004-0.004, Gd, Dy, Sm,<0.01[a] B 1.00, B^{10}/B^{11} ratio 0.246

TABLE VII. (Continued)

Material	Thickness	Surface density (g/cm^2)	Analytical data
Boral	0.32	0.846	B 17.1%
BeO	1.27	3.61	Neutron absorbers <1 mb/Be atom
U^{238}	0.021	0.398 (0.303)[b]	0.2 - 0.3% U^{235}
Cd	0.013	0.117	Not analyzed
Niobium	0.140	1.170	1% Zr; (ppm) Ni 600; O 500; Cu 30; Fe 200; N, Mo, Si, Ti 100; Al 40; C 50; H 1.
Zirconium	0.32	2.18	(ppm) Cr, Cu, Mg, Mn, Mo, Na, Ni, Pb, Ti, V, W<20; Al 25; B, Cd<0.3; C 224; Fe 285; Hf 75; Si 52; Sn<50; H 28; N 40; O 1180.
Yttria (Y_2O_3)	1.26	6.01	(ppm) C 4800; F 10; P, Mo, Sn, V, Tu, Rh, Eu, Co, In, Dy, Ti, Ho, Nd, Ta<10; Ba, Gd, B, Mn, Au, Ag, Tb<1; Cr, K, Lu, Cd<5; S 130; Al, Cu 1.0; Ca 20; Fe, Na 30; Mg 40; Ni 10; Si 120; Sm<50; Li<0.5; Hf, Er<100, Y 100

[a] Not detected.

[b] Averaged over cross-section of BeO assemblies.

3.3.2. Studies of absorbers in slab geometry in BeO systems

There were two groups of studies with absorbers in slab geometry in BeO-moderated systems. In some earlier measurements, successive increments of absorbers were introduced centrally into an assembly with a constant quantity of fuel-moderator material, the decay constant being determined as a function of increasing quantity of absorber present. For later measurements, after the first increment of absorber was introduced into the assembly and the decay constant determined, fuel and moderator material were added to increase the assembly height and bring the value of α to approximately the value of the same type of assembly without the absorber. Successive measurements were made, first adding increments of absorber and then fuel-moderator material until the desired total thickness of absorber was present. This then allowed a deduction of the equivalent in un-

TABLE VIII. Summary of absorber data in BeO assemblies

$\frac{BeO}{U^{235}}$ ratio	Assembly height (cm)	Absorber characteristics				α (sec^{-1})
		Material	Location: H (cm)	Thickness (cm)	Surface density (g/cm^2)	
123	48.6	Boron steel	26.3	0.025	0.198	1842
	50.0	Boron steel	26.3	0.025	0.198	1110
247	50.9	René	40.7	0.112	0.986	674
	51.0	Hastelloy		0.254	2.07	632
	50.9	Niobium		0.140	1.170	688
	51.1	Boral		0.32	0.846	2375
	51.1	Iron		0.32	2.45	555
	51.4			0.64	4.90	672
	51.8			0.95	7.36	783
	52.1			1.27	9.81	904
	52.4			1.59	12.26	976
	52.7			1.90	14.71	1046
	53.0			2.22	17.16	1110
	53.3			2.54	19.62	1168
	76.2[a]	Au	43.2	0.025	0.498	1650
	82.5[a]					1151
	87.6[a]					705
	50.8		25.4	0.003	0.0564	1102
	50.8			0.025	0.498	2658
	50.8	U^{238}		0.021	0.303	806
	50.8			0.042	0.606	946
	50.8	Co		0.038	0.320	1637
	54.6			0.038	0.320	489
	54.7			0.076	0.640	1353
	57.3			0.076	0.640	656
	51.1	Zr	40.7	0.32	2.18	485
	51.4			0.64	4.36	546
	51.8			0.95	6.54	597
	52.1			1.27	8.72	654
	52.4			1.59	10.90	708
	52.7			1.90	13.08	758
	53.0			2.22	15.26	816
	53.3			2.54	17.44	871
	54.6	Cd	25.4	0.013	0.117	1708
	58.4			0.013	0.117	630
	51.1	Ni	35.6	0.32	2.81	952
	51.1			0.32	2.81	632
	51.4			0.64	5.62	1035
	51.4			0.64	5.62	775
	51.8			0.95	8.43	1126
	51.8			0.95	8.43	646
	52.1			1.27	11.24	968
	52.1			1.27	11.24	752
	52.4			1.59	14.05	1030
	76.2[a]	Boron steel	43.2	0.025	0.198	708
	77.5[a]					584
	78.8[a]					478
	80.0[a]					370
	76.2[a]			0.050	0.396	986
	80.0[a]					653
	82.6[a]					461
	83.8[a]					347
493	56.0	René	35.6	0.112	0.986	649
	59.8			0.112	0.986	243
	59.9			0.224	1.972	568
	63.7			0.224	1.972	212
	56.1	Hastelloy		0.254	2.07	631
	59.9			0.254	2.07	222
	60.2			0.508	4.14	567
	62.7			0.508	4.14	326
	55.9	Au		0.003	0.0564	513
	58.4			0.003	0.0564	222
	55.9			0.025	0.498	1376
	66.0			0.025	0.498	365
	55.9	Co		0.038	0.320	847
	61.0			0.038	0.320	293
	61.0			0.076	0.640	714
	66.1			0.076	0.640	226
	66.2			0.114	0.960	540
	68.7			0.114	0.960	302
	68.8			0.208	1.660	768
	73.9			0.208	1.660	274
	56.2	Ni		0.32	2.81	782
	61.3			0.32	2.81	244
	61.6			0.64	5.62	682
	65.4			0.64	5.62	319
	65.7			0.95	8.43	647
	69.5			0.95	8.43	275
	69.8			1.27	11.24	543
	72.4			1.27	11.24	313
	72.7			1.59	14.05	542
	75.2			1.59	14.05	267
	75.6			1.91	16.86	443
	76.8			1.91	16.86	315
	77.2			2.22	19.67	466
	80.0			2.54	22.48	318
	80.3			2.86	25.29	453
	81.6			2.86	25.29	282
	56.2	Iron		0.32	2.45	563
	58.7			0.32	2.45	271
	59.1			0.64	4.90	564
	61.6			0.64	4.90	306
	61.9			0.95	7.36	558
	64.4			0.95	7.36	321
	64.8			1.27	9.81	550
	68.6			1.27	9.81	187
	68.9			1.59	12.26	392
	70.2			1.59	12.26	285
	71.4			1.59	12.26	167
	70.5			1.90	14.71	467
	73.0			1.90	14.71	228
	73.3			2.22	17.16	392
	74.6			2.22	17.16	270
	74.9			2.54	19.62	414
	76.2			2.54	19.62	292
	55.9	Boron steel	27.9	0.025	0.198	804
	55.9	BeO		1.27	3.61	308
	55.9	Y_2O_3		1.26	6.01	1101
	58.4					771
	61.0					473
	62.2					340

[a]Assembly base dimensions 61 × 45.8 cm.

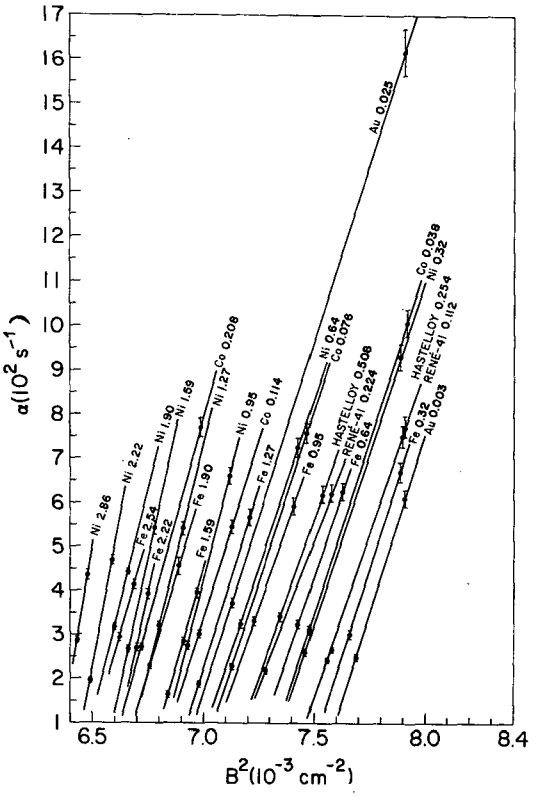


Fig. 4

Summary of α versus B^2 for absorbers of various thicknesses; indicated thicknesses are in centimetres.

poisoned assembly height for each system containing an absorber by referring to the decay data of Table II. The sample materials used in these experiments and their known properties are listed in Table VII. A typical assembly arrangement is shown in Fig. 2(b). The measured data are summarized in Table VIII. With one exception, all the assemblies had base dimensions of 61 cm × 61 cm. Most of the data for the $BeO/U^{235} = 493$ assembly were treated in terms of the inferred equivalences between absorbers and fuelled lattice material in Ref. [9]; Figure 4 summarizes part of these data.

3.3.3. Studies of absorbers in slab geometry in graphite systems

The studies of absorbers in slab geometry in graphite-moderated systems were performed in essentially the same manner as was described in section 3.3.2. They differed in that the absorber slabs were introduced vertically into the system by use of a slot, as shown in Fig. 2(c). Many of the samples described in Table VII were also used in these experiments. The measured decay constant data are shown in Table IX. The assembly used for this set of measurements had a $C-U^{235}$ ratio of 598 and base dimensions of 123 cm

TABLE IX. Summary of absorber data in graphite systems

Assembly height (cm)	Absorber characteristics				α (sec^{-1})
	Material	Dimensions (cm)	Thickness (cm)	Surface density g/cm^2	
91.4	-	-	-	-	717
94.0	-	-	-	-	539
95.3	-	-	-	-	430
96.5	-	-	-	-	328
98.3[a]	-	-	-	-	155[a]
96.5	U^{238}	120 × 40	0.020	0.398	436
97.8	↓	↓	0.020	0.398	322
96.5	↓	↓	0.041	0.796	489
97.8	↓	↓	0.041	0.796	377
96.5	Cd	121.9 × 30.5	0.013	0.117	827
97.8	↓	↓	↓	↓	721
100.3	↓	↓	↓	↓	521
102.9	↓	↓	↓	↓	308
96.5	Boron steel	124.5 × 30.5	0.025	0.198	461
97.8	↓	↓	0.025	0.198	352
96.5	↓	↓	0.051	0.396	562
99.1	↓	↓	0.051	0.396	350
96.5	Co	123.2 × 30.5	0.076	0.640	740
99.1	↓	↓	↓	↓	546
101.6	↓	↓	↓	↓	340
96.5	Au	121.9 × 30.5	0.003	0.053	640
97.8	↓	↓	↓	↓	357
99.1	↓	↓	↓	↓	244
96.5	↓	↓	0.025	0.498	820
99.1	↓	↓	↓	↓	626
100.3	↓	↓	↓	↓	522
102.9	↓	↓	↓	↓	318

[a]Values extrapolated to delayed critical.

× 123 cm. Since the slot slightly perturbed the decay constant for the assembly, values for the assembly without absorbers are also given. From flux plots the extrapolation length for this system is taken to be 1.92 cm [7].

3.3.4. Studies of absorbers in bar geometry in BeO systems

For studies of absorbers in bar geometry the assembly was arranged as shown in Fig. 2(d). Two series of such measurements were made: The first set had a slot as shown in the figure, which produced no measurable effect in the decay constant of the system. The second series used a slight-

TABLE X. Summary of bar absorber properties

Material	Thickness (cm)	Surface density (g/cm^2)	Analytical data
Hf	0.081	1.05	(ppm) Al<25; B 0.2; C 60; Co, V<5; Cr 90; Fe<50; Mg, Mn, Ni<10; N 95; O 180; Pb 5; Si 90; Ti 10; Zr 19000.
Eu_2O_3	0.076		(wt %) Gd<0.005,[a] Sm 0.02-0.2, Dy<0.005, B<0.0001,[a] Cd<0.0001, Ir<0.001.
Gd_2O_3	0.076		(wt %) Eu 0.02-0.2, Sm<0.03, Dy<0.005, B 0.001-0.01, Cd 0.00005-0.0005, Ir<0.001.
Sm_2O_3	0.076		(wt %) Eu>0.1, Gd 0.02-0.2, Dy 0.02-0.2, B 0.005-0.05, Cd<0.0001, Ir<0.00
Hastelloy	(see Table VII)		
Au	(see Table VII)		
Cd	(see Table VII)		
René	(Analysis of Table VII is typical)		
Boral	(see Table VII)		

[a] Not detected.

ly larger slot (0.48 cm × 3.81 cm × 61 cm) with its lower edge at 25.4 cm above the base of the assembly; the larger slot changed the decay constant slightly from the value given in Table II. The value of α_{DC} was not changed, however. The BeO-U^{235} ratio of the assembly was 247, and the assembly dimensions were constant for both series of measurements. Analytical data for those bar absorbers which were analysed are given in Table X. The data from the pulsed neutron data are given in Table XI. Figure 5 shows a plot of absorber surface density with the change in decay constant produced for several absorbers.

3.4. Limits of uncertainty

The moderator-fuel ratios listed in this report are gross molar ratios uncorrected for self-shielding. A qualitative series of self-shielding studies for BeO-moderated systems was described in Ref. [2]. Calculated magnitudes of this effect are given in Ref. [10]. The uncertainties in the decay constants were estimated, based upon attainable reproducibility for like systems. The decay constants within a particular series of measurements with a given assembly generally have precision of about 0.5%. Whenever the assemblies have been re-constituted, the statistics of the moderator and fuel may contribute to as much as a four-fold increase in the range of errors. Of course, the differences taken to show a change in decay constants have a somewhat greater range of uncertainty.

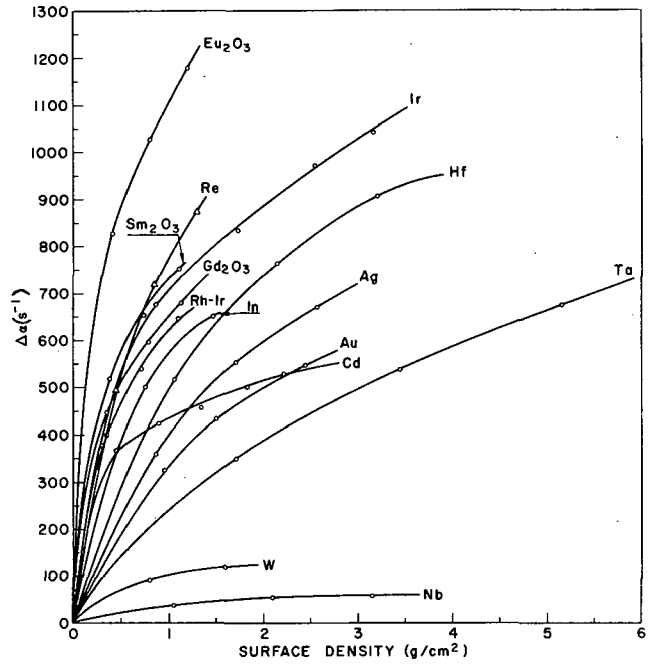


Fig. 5

Change in decay constant as a function of surface density for various absorber materials in bar geometry.

3.5. Discussion

3.5.1. Principles of pulsed neutron measurements

Operationally and conceptually the pulsed neutron technique is relatively simple. The time behaviour of the neutron population in a multiplying system is given by the kinetic equations

$$\frac{dn}{dt} = [k(1 - \beta) - 1]\,\frac{n}{\ell^*} + \Sigma_i \lambda_i C_i; \quad \frac{dC_i}{dt} = \frac{k\beta_i n}{\ell^*} - \lambda_i C_i \,. \tag{1}$$

In these equations, k, β and ℓ^* are effective values for the multiplication factor, delayed neutron fraction, and prompt neutron lifetime, and λ and C are decay constant and concentration for each delayed neutron precursor. The pulsed neutron method makes use of suitable apparatus which permits a separation in time of the prompt and delayed neutrons leaking from a subcritical system following injection of a short burst of neutrons. Much of the earlier use of this method has been reviewed in Ref. [3]. Following attainment of the "stable" mode mentioned in section 2.3. the prompt neutron population is observed to behave as a single decaying exponential, characterized by a decay constant α which can be defined by

TABLE XI. Summary of bar absorber data in BeO systems

Material	Dimensions (cm)	Thickness (cm)	Surface density (g/cm^2)	α (sec^{-1})
Series 1[a]				
Ta	61 × 2.54	0.102	1.70	803
		0.208	3.44	990
		0.312	5.17	1129
Hf		0.081	1.05	969
		0.165	2.14	1202
		0.246	3.21	1358
Hastelloy		0.254	2.07	509
René		0.358	2.94	623
Ag		0.081	0.86	804
		0.162	1.71	1006
		0.243	2.57	1123
Au		0.048	0.95	777
		0.076	1.49	882
		0.125	2.44	999
Nb		0.122	1.05	488
		0.244	2.10	507
		0.366	3.13	510
Cd		0.056	0.44	802
		0.109	0.88	894
		0.163	1.33	909
		0.216	1.78	953
		0.269	2.23	979
W		0.079	0.80	517
		0.158	1.58	544
Rh 80% - Ir 20%		0.025	0.35	825
		0.050	0.71	964
		0.075	1.07	1071
Ir		0.012	0.29	796
		0.038	0.86	1102
		0.076	1.73	1260
		0.114	2.59	1397
		0.140	3.17	1468
In		0.102	0.74	980
		0.204	1.47	1129
Boral		0.32	0.83	1305
	61 × 1.27	0.32	0.83	971

TABLE XI. (Continued)

Material	Dimensions (cm)	Thickness (cm)	Surface density (g/cm^2)	α (sec^{-1})
Series 2[b]				
None	-	-	-	537
Cd	61 × 2.54	0.013	0.129	843
		0.025	0.254	878
		0.038	0.376	907
Au	61 × 2.54	0.003	0.057	591
		0.005	0.113	622
		0.008	0.170	647
BN	61 × 2.49	0.163	0.344	1408
		0.326	0.694	1653
Sm_2O_3	61 × 2.52	0.076	0.370	1055
		0.152	0.731	1186
		0.228	1.101	1289
Eu_2O_3		0.076	0.417	1364
		0.152	0.789	1564
		0.228	1.206	1716
Gd_2O_3		0.076	0.355	985
		0.152	0.784	1132
		0.228	1.136	1218
Sm_2O_3[c]		0.076	0.370	1116
Eu_2O_3[c]		0.076	0.417	1393
Gd_2O_3[c]		0.076	0.355	1049

[a]Slot at height of 24.1 cm.

[b]Slot at height of 25.4 cm.

[c]For these measurements the samples were shielded on each side by 0.013 cm Cd.

$$\alpha = \frac{1 - k(1 - \beta)}{\ell^*} , \tag{2}$$

with the notation defined above. Then at delayed critical

$$\alpha_{DC} = -\frac{\beta}{\ell^*} . \tag{3}$$

For some change within a system which causes a change in α, the reactivity has been deduced through the relation

$$\rho(\$) = \frac{\alpha - \alpha_{DC}}{\alpha_{DC}} . \tag{4}$$

Use of the above relations is generally based upon a very simplified model which assumes a single neutron energy group and an unchanging lifetime, ℓ^*. Recently there have been some modifications of these general ideas. GARELIS and RUSSELL [11] have devised a procedure for deducing the reactivity of a subcritical system from a single pulsed measurement, using the decay constant and an integral relation for deducing $k\beta/\ell^*$. This method has the advantages of avoiding the need for measuring α_{DC} or the possibility of a changed lifetime; the method is also claimed to be modally independent, which is supported by the data of Ref. [12]. A somewhat simpler procedure has been discussed by LEWINS [13], which deduces reactivity directly in dollars simply by dividing the time-integrated prompt neutrons by time-integrated delayed neutrons, without making use of the decay constants at all. The reactivities calculated by these various methods all converge near critical to values determined by methods other than pulsing [14], and the various pulsing methods are reasonably self-consistent within 10$ of criticality. There have been efforts to calculate decay constants directly [15, 16]; however, success has not been notable for systems which were not sufficiently thermal to be suitable for two-group treatments. Further developments in pulsed neutron theory which are amenable to practical applications will be most welcome. It is hoped that the data of this article may prove helpful for this purpose.

3.5.2. Applications of pulsed neutron measurements

The most popular use of pulsed neutron studies has been for calculation of reactivities by use of the relations discussed previously. Their use in our Laboratory for development of multigroup calculations has not been concerned explicitly with reactivities, however. Epithermal assemblies and reactors are, unfortunately, sensitive to the nuclear cross-sections of their constituents over the entire range of energy, from 10 MeV to thermal energies. Consequently, agreement with a handful of experiments cannot possibly assure complete confidence in the computing machinery. The simplest and most obvious test for such a calculation is to reproduce the measured critical mass of a given multiplying system; however, agreement between experiment and calculation in such a case is not an unequivocal test [17]. A somewhat more rigorous check can be performed by correlating with the critical masses in a series of systems in which the spectrum is varied by varying the fuel density. Such treatments were discussed by STONE and LINGENFELTER [17] with the data of KLOVERSTROM et al. [2]. To further test the multigroup codes, a procedure is outlined below in which the pulsed neutron data are employed. It is believed that this series of tests is particularly sensitive to the absorption cross-sections in the region of the median fission energy of the system, and that by treating a large number of assemblies of different fuel loadings, many of the groups of absorption cross-sections can be tested.

In this treatment, which was mentioned in Ref. [6], use is made of Eq. (2) with the assumptions that the prompt lifetime is insensitive to the changes of buckling considered in this article. (Arguments to justify this latter assumption are given in the Appendix.) If Eq. (2) is differentiated with respect to k, for $k \sim 1$, $\beta \ll 1$,

$$\frac{d\alpha}{dk} = -\frac{1}{\ell^*}, \tag{5}$$

so

$$\ell^* = -\frac{dk}{d\alpha} \approx -\frac{(\Delta k/\Delta B^2)}{(\Delta\alpha/\Delta B^2)}, \tag{6}$$

in which B^2 is the geometric buckling.

In actual practice, pulsing measurements have been customarily performed with assemblies which are parallelepipeds having constant base dimensions and variable heights. In the spirit of Eq.(6) then

$$\ell^* \approx -\frac{(\Delta k/\Delta H)}{(\Delta\alpha/\Delta H)}, \tag{7}$$

in which H is the height of the assembly under consideration. At delayed critical, by Eq.(3),

$$\beta = -\ell^*\alpha_{DC}. \tag{8}$$

By use of Eqs.(7) and (8), β can be evaluated from the quantities α_{DC} and $\Delta\alpha/\Delta H$ determined experimentally, and $\Delta k/\Delta H$ calculated for the same system by use of a multigroup method. The derived β should be related to the detailed properties of the entire system. A value for β can be determined in an alternate way for the same fuel-moderator system and multigroup method: it is the calculated change in k for the system found by subtracting delayed neutrons from the fission spectrum. This second β should be sensitively related to the size of the assembly and the properties of the moderator, which are usually well known. If the details of the calculation and cross-sections are quite good the two derived values of β should agree quite closely; however, this is not always the case. Where the credibility of the computational method has been otherwise established, lack of agreement may be attributed to deficiencies in cross-sections.

For studies of perturbed systems, the assumption is made that systems which have like values of the decay constant α also should have like values of k; this implies a corollary assumption of a constant lifetime, which is somewhat difficult to justify. For systems with absorbers, the invariance in α_{DC} caused by introducing a localized absorber and the relative insensitivity to absorber thickness of the slope $\Delta\alpha/\Delta B^2$, as shown in Fig. 4, are taken to be indications that the lifetime does not change greatly in this type of assembly. This is consistent with the findings of BENGSTON et al. [18], and was also discussed in Ref. [9]. For a given perturbation then, the resonance integral for its material in a region of uncertainty might be adjusted to produce an overall k for the perturbed system which agrees with k for the unperturbed assembly having the same α. An overall summary of the results of these methods is contained in Ref. [10].

4. CONCLUSION

The results of an extended series of pulsed neutron studies on simple systems have been presented. These data may be used directly for empirical evaluations of systems; they may also be used for correlations with multigroup calculations by use of simple methods which have proven to be useful for this purpose at our Laboratory.

ACKNOWLEDGEMENTS

The following individuals were participants in various parts of the measurements described in this article: F.A. Kloverstrom, D.E. Kraft, F. Shon, J.M. Piowaty, T. Weirich, L.L. Gardner and J. Petruzzi.

REFERENCES

[1] REYNOLDS, H.L., Proc. 2nd UN Int. Conf. PUAE 12 (1958) 632.
[2] KLOVERSTROM, F.A., DECK, R.M. and REYENGA, A.J., Nucl. Sci. Engng 8 (1960) 221-25.
[3] BECKURTS, K.H., Nucl. Instrum. Meth. 11 (1961) 144-68.
[4] GOW, J.D. and RUBY, L., Rev. sci. Instrum. 30 (1959) 315-17.
[5] KEEPIN, G.R., WIMETT, T.F. and ZEIGLER, R.K., J. nucl. Energy 6 (1957) 1.
[6] MORTON, J.R., Trans. Amer. nucl. Soc. 7 (1964) 284-86.
[7] KLOVERSTROM, F.A. and KOMOTO, T.T., Pulsed neutron source studies of graphite-enriched uranium systems, Rpt UCRL-5477 (9 Feb. 1959).
[8] MORTON, J.R., SHON, F.J., WEIRICH, T.F. and GARDNER, L.L., Reactivity effects of various reflectors on near-homogeneous BeO-moderated, oralloy-fueled systems, Rpt UCRL-6729 (Jan. 2 1962).
[9] MORTON, J.R., PIOWATY, J.M., PETRUZZI, J. and GARDNER, L.L., to be published in Nucl. Sci. Engng.
[10] DOYAS, R.J. and CANFIELD, E.H., A new derivation of multigroup cross sections for BeO- and graphite-moderated systems, Rpt UCRL-7827 (1964).
[11] GARELIS, E. and RUSSELL, J.L., Nucl. Sci. Engng 16 (1963) 263-70; GARELIS, E., Nucl. Sci. Engng 18 (1964) 242-45.
[12] BROWN, J.R. et al., Measurements of subcritical reactivity using a pulsed-neutron source, Rpt GA-4838 (1964).
[13] LEWINS, J.L., Nucl. Energy (Nov. 1963) 316-18.
[14] KOLAR, O.C. and KLOVERSTROM, F.A., Nucl. Sci. Engng 10 (1961) 45-52.
[15] FULTZ, S.C., Nucl. Sci. Engng 6 (1959) 313-19.
[16] HENRY, A.F., Proc. of 2nd Symp. on Application of Pulsed Neutron Source Techniques, Rpt UCRL-5665 (Livermore) (1958) 108-24.
[17] STONE, S.P. and LINGENFELTER, R.E., Neutron diffusion theory programs and their application to simple critical systems, Rpt UCRL-5913 (1960).
[18] BENGSTON, J. et al., Proc. 2nd UN Int. Conf. PUAE 12 (1958) 63.

APPENDIX *

If, instead of assuming constant ℓ^* as in the derivations of Section 3.5.2., ℓ^* is assumed to be a function of k, differentiation of Eq. (2) with respect to k gives

* The discussion of this appendix was stimulated by ideas obtained from R.W. Albrecht, University of Washington (Seattle).

$$\frac{d\alpha}{dk} = -\frac{1}{\ell^{*2}}\frac{d\ell^*}{dk} - \frac{(1-\beta)}{\ell^*} + \frac{k(1-\beta)}{\ell^{*2}}\frac{d\ell^*}{dk} \tag{A.1}$$

$$= \frac{\beta - 1}{\ell^*} + \frac{1}{\ell^{*2}}\frac{d\ell^*}{dk}[k(1-\beta) - 1]\ ; \tag{A.2}$$

then from the definition of α of Eq. (2)

$$\frac{d\alpha}{dk} = \frac{\beta - 1}{\ell^*} + \frac{1}{\ell^{*2}}\frac{d\ell^*}{dk}(-\alpha\ell^*)\ . \tag{A.3}$$

Rearranging and taking

$$-\alpha\ell^* = \frac{\alpha\beta}{\alpha_{DC}} = \beta(1 + \$) \tag{A.4}$$

(here, \$ denotes the number of dollars below delayed critical)

$$\ell^* = -\frac{dk}{d\alpha}\left[1 - \beta - \beta(1+\$)\frac{d\ell^*}{\ell^* dk}\right]\ . \tag{A.5}$$

and Eq. (A.5) is identical in form to Eq. (6) except for the second and third terms in the bracket. The validity of the simplified Eq. (6), depends upon the magnitude of the quantities in these added terms. From elementary one-group thermal reactor theory

$$\ell^* = \frac{\ell_0}{1 + L^2B^2} \quad \text{and} \quad k = \frac{k_\infty}{1 + L^2B^2}\ . \tag{A.6}$$

Differentiating with respect to buckling,

$$\frac{d\ell^*}{dB^2} = \frac{-L^2\ell_0}{(1 + L^2B^2)^2} \quad \text{and} \quad \frac{dk}{dB^2} = \frac{-L^2k_\infty}{(1 + L^2B^2)^2}\ . \tag{A.7}$$

Therefore

$$\frac{d\ell^*}{\ell_0} = \frac{dk}{k_\infty}\ , \tag{A.8}$$

and multiplying by $1 + L^2B^2$ gives

$$\frac{d\ell^*}{\ell^*} = \frac{dk}{k}\ . \tag{A.9}$$

Rearranging then,

$$\frac{d\ell^*}{\ell^* dk} = k^{-1} \sim 1 \tag{A.10}$$

for near-critical. A two-group approach also yields a value near unity for the above quantity. The above result may be substituted into Eq. (A.5) to give

$$\ell^* = -\frac{dk}{d\alpha}\left[1 - \beta - \frac{\beta}{k}(1 + \$)\right] . \tag{A.11}$$

For near-critical conditions ($k \sim 1$) this can be further simplified, taking $\beta = 0.007$,

$$\begin{aligned} \ell^* &= -\frac{dk}{d\alpha}[1 - 2\beta - \beta\,\$] \\ &= -\frac{dk}{d\alpha}[0.986 - 0.007\,\$] \quad . \end{aligned} \tag{A.12}$$

Equation (A.12) then shows that near critical the constant lifetime approximation does not introduce excessive error. Hence for 2$ subcritical the correction is about 3%. For 10$ subcritical the correction is about 8%.

It is well to point out that this argument applies in the case of a change in k caused by a change in buckling, but it would not necessarily be true in the case of a change due to changing the quantity of fuel present. An increase in the quantity of fuel would increase both the number of fissions and captures in the system. The lifetime would be decreased on both accounts while the reactivity effects would tend to cancel.

ÉTUDE DE RÉSEAUX A PAS VARIABLE URANIUM-EAU LÉGÈRE PAR DES MESURES CINÉTIQUES ET STATIONNAIRES

P.H. GAVIN
ÉCOLE POLYTECHNIQUE DE L'UNIVERSITÉ DE LAUSANNE, SUISSE*

Abstract — Résumé — Аннотация — Resumen

KINETIC AND STEADY-STATE MEASUREMENTS OF VARIABLE-PITCH ENRICHED URANIUM, LIGHT WATER LATTICES. The decay of the neutron flux in a subcritical reactor after a sudden shutdown (following steady-state operation) can be analysed into a series of spatial and time harmonics. Spatial harmonics can be deduced from steady-state operation. The time constants of exponentials are characteristic of the core assembly and in a two-group theory the lattice and reactivity parameters can be deduced from measurements of flux in relation to time. These parameters are determined experimentally for various bare cores composed of enriched UO_2 rods in light water and are used to study a variable-pitch lattice and predict its kinetic and steady-state behaviour.

ÉTUDE DE RÉSEAUX A PAS VARIABLE URANIUM ENRICHI-EAU LÉGÈRE PAR DES MESURES CINÉTIQUES ET STATIONNAIRES. La décroissance du flux de neutrons dans un réacteur sous-critique, après l'arrêt brusque d'un régime stationnaire, peut se décomposer en harmoniques du lieu et du temps. Les harmoniques du lieu se déduisent du régime stationnaire. Les constantes de temps des exponentielles sont caractéristiques du milieu multiplicateur, et dans une théorie à deux groupes, on peut déduire de la mesure du flux en fonction du temps les paramètres du réseau et la réactivité. Ces paramètres ont été déterminés expérimentalement pour différents cœurs sans réflecteur, composés de barres de UO_2 enrichi dans l'eau légère. On utilise ensuite ces paramètres pour l'étude d'un réseau à pas variable, et pour prédire son comportement cinétique et stationnaire.

ИЗУЧЕНИЕ РЕШЕТОК ОБОГАЩЕННЫЙ УРАН–ОБЫЧНАЯ ВОДА С ПЕРЕМЕННЫМ ШАГОМ ПУТЕМ КИНЕТИЧЕСКИХ И СТАЦИОНАРНЫХ ИЗМЕРЕНИЙ. Уменьшение потока нейтронов в подкритическом реакторе после быстрой остановки может происходить в гармониках места и времени. Гармоники места выводятся из стационарного режима. Постоянные времени показательных функций являются характерными данными размножающей среды, и по двухгрупповой теории можно путем измерения потока во времени вывести параметры решетки и реактивность. Эти параметры были определены экспериментальным путем для различных активных зон без отражателей, состоящих из стержней из обогащенного UO_2, помещенных в обычную воду. В дальнейшем эти параметры использовались для изучения решетки с переменным шагом и выяснения ее кинетических и стационарных свойств.

ESTUDIO, MEDIANTE MEDICIONES CINETICAS Y ESTACIONARIAS, DE RETICULADOS DE URANIO-AGUA LIGERA DE PASO VARIABLE. El decrecimiento del flujo neutrónico en un reactor subcrítico, después de una interrupción brusca de su funcionamiento en régimen estacionario, puede descomponerse en armónicos espaciales y temporales. Los primeros se deducen del regimen estacionario. Por su parte, las constantes de tiempo de las ecuaciones exponenciales son características del medio multiplicador de que se trate, y empleando una teoría de dos grupos, pueden deducirse los parámetros del reticulado y la reactividad partiendo de los valores medidos del flujo en función del tiempo. El autor ha determinado experimentalmente estos parámetros para diversos cuerpos de reactor desprovistos de reflector, constituidos por barras de UO_2 enriquecido, sumergidas en agua ligera. Seguidamente, se ha servido de estos parámetros para estudiar un reticulado de paso variable y predecir su comportamiento cinético y estacionario.

* Subside n° 2807 du Fonds national suisse de la recherche scientifique.

1. DÉTERMINATION DES CONSTANTES D'UN RÉSEAU RÉGULIER

Un milieu multiplicateur de neutrons peut être étudié, dans une théorie de diffusion à deux groupes, si l'on connaît certains paramètres caractéristiques de ce milieu. Ce sont: K, coefficient de multiplication du milieu infini, L_1^2 et L_2^2 , aires de ralentissement et de diffusion des neutrons, enfin l_{01} et l_{02}, vies des neutrons rapides et thermiques dans le milieu infini. La détermination de ces paramètres dans un assemblage sous-critique peut se faire par l'analyse des cartes de flux radiale et axiale en régime stationnaire, et par l'analyse de la décroissance dans le temps, en différents points, du flux thermique des neutrons, après la coupure brusque d'un régime stationnaire.

Les mesures ont été faites sur différents réseaux d'oxyde d'uranium enrichi modéré à l'eau légère, dans l'assemblage sous-critique CACTUS de l'Ecole polytechnique de Lausanne [1].

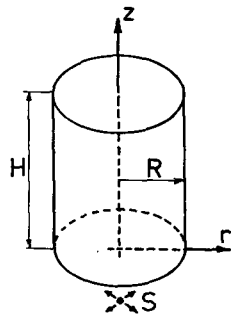


Figure 1

Choix des coordonnées et position de la source.

1.1. Cas stationnaire

Cinq sources Pu-Be placées dans un bloc de graphite sous le réseau alimentent le milieu multiplicateur.

Dans un cœur nu, le flux thermique a la forme (fig. 1)

$$\phi_2 = AJ_0(\alpha r)\exp(-\gamma z)$$

si l'on se trouve assez loin de la source.

Des cartes de flux radiales et axiales permettent de déterminer α et γ, avec

$$\text{laplacien matière } \mu^2 = \alpha^2 - \gamma^2.$$

Dans un cœur réfléchi radialement, le flux thermique suit la loi

$$\phi_2(r, z) = [AJ_0(\alpha r) + CI_0(\alpha^* r)] \exp(-\gamma z),$$

avec $\mu^2 = \alpha^2 - \gamma^2$, $\nu^2 = \alpha^{*2} + \gamma^2$.
μ^2 et ν^2 ont leur définition habituelle [2], et valent respectivement

$$\mu^2 = \frac{K-1}{L_1^2 + L_2^2}, \qquad \nu^2 = \frac{K-1}{L_1^2 + L_2^2} + \frac{1}{L_1^2} + \frac{1}{L_2^2}. \tag{1}$$

L'adjonction d'un réflecteur apporte une donnée de plus, par comparaison entre le milieu étudié et un modérateur connu. Une carte de flux radiale permet de déterminer α et α^*, d'où μ^2 et ν^2.

1.2. Cas cinétique

1.2.1. Instrumentation

Les mesures cinétiques ont été faites au moyen d'une source de neutrons pulsée Philips [3] émettant des neutrons de 14 MeV de façon continue ou en impulsions de 2 μs à 3 ms de durée, à une fréquence variant entre 10 c/s et 10 Kc/s. Pour obtenir un régime permanent au cours de l'impulsion, il faut que celle-ci soit assez longue (2 à 3 ms). Ainsi la fin de l'impulsion correspond pratiquement à la coupure brusque d'un régime permanent. Le taux de répétition doit être faible, pour que l'amplitude des neutrons retardés soit minimale. En effet, il faut attendre que le flux ait décru de plusieurs décades pour atteindre la période stable, qui serait alors noyée dans le fond des neutrons retardés si le taux de répétition était trop élevé. Les mesures ont été faites avec un analyseur à 68 canaux Rohlwes, synchronisé sur la fin de l'impulsion de neutrons. La longueur des canaux est variable de 0,5 μs à 100 s, par facteur ×1, ×2, ×5; le temps de passage entre deux canaux successifs est inférieur à 0,5 μs. Les valeurs les plus couramment utilisées étaient les suivantes:

Taux de répétition: 10 c/s à 50 c/s,
Impulsion de neutrons: 200 μs à 2 ms de durée et 10^7 neutrons/impulsion,
Largeur des canaux: 50 ou 100 μs.

1.2.2. Théorie

La variation dans le temps du flux de neutrons thermiques a été étudiée par plusieurs auteurs [4, 5]. En fait, l'énergie des neutrons de source est très différente de l'énergie de fission, et il faut tenir compte de ce fait pour l'analyse des résultats, car la forme du flux est fortement modifiée.

On écrit les équations de diffusion à trois groupes, avec

ϕ_0 = flux des neutrons rapides dû aux neutrons de source de 14 MeV> E> coupure thermique,
ϕ_1 = flux des neutrons rapides de fission, énergie de fission > E> coupure thermique,
ϕ_2 = flux thermique.

De plus, on décompose le flux thermique en deux termes. Le premier terme

ϕ_2' représente le flux thermique dû au ralentissement des neutrons de fission, et le second terme ϕ_2'' représente le flux thermique dû au ralentissement des neutrons de 14 MeV. On a donc

$$\phi_2 = \phi_2' + \phi_2'' .$$

Pour chacun de ces groupes, on a les équations de diffusion suivantes, en tenant compte d'un seul groupe de neutrons retardés:

$$D_0\nabla^2\phi_0 - \Sigma_0\phi_0 = \frac{1}{v_0}\frac{\partial\phi_0}{\partial t} ,$$

$$D_1\nabla^2\phi_1 - \Sigma_1\phi_1 + K(1-\beta)\Sigma_2\phi_2 + \lambda C = \frac{1}{v_1}\frac{\partial\phi_1}{\partial t} ,$$

$$D_2\nabla^2\phi_2' - \Sigma_2\phi_2' + \Sigma_1\phi_1 = \frac{1}{v_2}\frac{\partial\phi_2'}{\partial t} ,$$

$$D_2\nabla^2\phi_2'' - \Sigma_2\phi_2'' + \Sigma_0\phi_0 = \frac{1}{v_2}\frac{\partial\phi_2''}{\partial t} ,$$

$$\frac{\partial C}{\partial t} = -\lambda C + K\beta\Sigma_2\phi_2 . \qquad (2)$$

On ne tient pas compte des fissions rapides produites par le groupe zéro. Le flux de chaque groupe doit satisfaire une équation aux valeurs propres du type

$$\nabla^2\phi = -B^2\phi .$$

Chacun de ces flux, ainsi que la concentration des précurseurs, se décompose en composantes radiale, axiale, et temporelle.

$$\begin{aligned} &\phi_g(r,z,t) = R_g(r)\cdot Z_g(z)\cdot T_g(t), \\ &C(r,z,t) = R_g(r)\cdot Z_g(z)\cdot T_g(t), \end{aligned} \qquad g = 0, 1, 2, \text{ indice de groupe.} \qquad (3)$$

Il est possible de placer la source sous le réseau de telle manière qu'il n'y ait qu'un harmonique radial. Alors

$$R_g(r) = R(r) = J_0(\alpha r),$$

$$Z_g(z)\cdot T_g(t) = \sum_j C_{gj}\sin\gamma_j z\cdot T_g(t) = \sum_j \sin\gamma_j z\cdot T_{gj}(t). \qquad (4)$$

On remplace les équations (4) dans le système (2), et en utilisant les propriétés d'orthogonalité du sinus, on obtient autant de systèmes que de j. Le système (2) devient

$$-T_{0j}(1+L_0^2B_j^2)=l_{00}\frac{dT_{0j}}{dt},$$

$$-T_{1j}(1+L_1^2B_j^2)+\frac{K(1-\beta)\Sigma_2}{\Sigma_1}T_2+\frac{\lambda C_{1j}}{\Sigma_1}=l_{01}\frac{dT_{1j}}{dt},$$

$$-T'_{2j}(1+L_2^2B_j^2)+\frac{\Sigma_1}{\Sigma_2}T_{1j}=l_{02}\frac{dT'_{2j}}{dt}, \qquad (5)$$

$$-T''_{2j}(1+L_2^2B_j^2)+\frac{\Sigma_0}{\Sigma_1}T_{0j}=l_{02}\frac{dT''_{2j}}{dt},$$

$$\frac{dC_j}{dt}=-\lambda C_j+K\beta\Sigma_2T_{2j},$$

avec

$$B_j^2=\alpha^2+\gamma_j^2, \qquad \alpha=\frac{2405}{R}, \qquad \gamma_j=\frac{j\pi}{H}, \qquad (6)$$

$l_{0g}=1/v_g\Sigma_g$ = vie des neutrons du groupe g en milieu infini.

Par simplification d'écriture, on omet dès à présent l'indice j, que l'on replacera quand il sera nécessaire de bien faire ressortir les harmoniques axiaux-temporels. On applique au système (5) la transformation de Laplace, avec

$$\frac{dT_g}{dt} \sqsubset s\overline{T}_g-T_g(0),$$

s = variable de Laplace,

$T_g(0)$ = flux des neutrons du groupe g en t = 0, c'est-à-dire à la fin de l'impulsion de neutrons.

On résout le nouveau système par rapport à T_2, en tenant compte des équations de couplage

$$C(0)=\frac{K\beta\Sigma_2}{\lambda}T_2(0),$$

$$T'_2(0)=\frac{\Sigma_1T_1(0)}{\Sigma_2(1+L_2^2B^2)},$$

$$T''_2(0)=\frac{\Sigma_0T_0(0)}{\Sigma_2(1+L_2^2B^2)}, \qquad (7)$$

et

$$K_{ej} = \frac{K}{(1+L_1^2B_j^2)(1+L_2^2B_j^2)},$$

$$l_{gj} = \frac{l_{og}}{1+L_g^2B_j^2} = \text{vie des neutrons en milieu fini.} \qquad (8)$$

On obtient, après simplifications,

$$\overline{T_2} = \frac{T_2(0)(1+l_1 s)(s+\lambda)[l_2(1+l_0 s)+l_0] + T_2(0)(1+l_0 s)K_e\beta + T_2'(0)(l_1-l_0)(s+\lambda)}{l_0 l_1 l_2\left(s+\frac{1}{l_0}\right)(s+\lambda)\left(s-\frac{K_e-1}{l_1+l_2}\right)\left(s+\frac{1}{l_1}+\frac{1}{l_2}+\frac{K_e-1}{l_1+l_2}\right)} \qquad (9)$$

$$= \frac{A_0}{s+\frac{1}{l_0}} + \frac{A_1}{s-\frac{K_e-1}{l_1+l_2}} + \frac{A_2}{s+\frac{1}{l_1}+\frac{1}{l_2}+\frac{K_e-1}{l_1+l_2}} + \frac{A_3}{s+\lambda}.$$

On revient à la fonction initiale

$$T_2(t) = A_0 e^{r_0 t} + A_1 e^{r_1 t} + A_2 e^{r_2 t} + A_3 e^{r_3 t} \qquad (10)$$

avec

$$r_0 = -\frac{1}{l_0}, \quad r_1 = \frac{K_e-1}{l_1+l_2}, \quad r_2 = -\left(\frac{1}{l_1}+\frac{1}{l_2}+\frac{K_e-1}{l_1+l_2}\right), \quad r_3 = -\lambda. \qquad (11)$$

Les quatre termes de l'équation (10) ont la signification suivante :

- $A_0 e^{r_0 t}$ décroissance du flux thermique dû au ralentissement des neutrons de 14 MeV,
- $A_1 e^{r_1 t}$ décroissance du flux des neutrons prompts dont le premier harmonique r_{11} donnera la période stable,
- $A_2 e^{r_2 t}$ régime transitoire très court à la coupure de la source,
- $A_3 e^{r_3 t}$ décroissance du flux des neutrons retardés.

Revenant à l'indice d'harmonique j, on peut écrire le flux thermique sous la forme

$$\phi_2(r, z, t) = J_0(\alpha r) \cdot \sum_j \sin \gamma_j z \cdot T_{2j}(t).$$

L'indice j doit être affecté aux constantes r et A de l'équation (10), les constantes r augmentant en valeur absolue avec j (équations (11), (8) et (6)).

Dans l'expression (10), le dernier terme, qui représente les neutrons retardés, peut être considéré comme une constante. En effet, les périodes stables mesurées sont de l'ordre de 1000 s^{-1}, ce qui est très grand par rap-

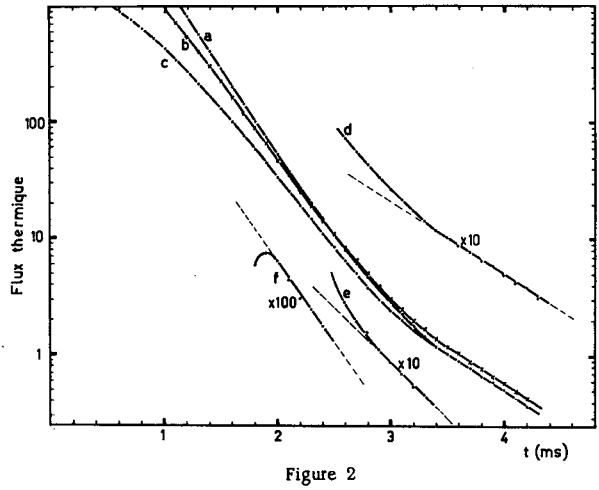


Figure 2

Décroissance type, après soustraction des neutrons retardés. Réseau UO_2 enrichi à 1,8%, W/U = 3,5.

a) mesure faite en z = H/3,
b) mesure faite en z = H/2,
c) mesure faite en z = 2H/3,
d) 1er harmonique axial $B_g^2 = 107 \cdot 10^{-4}$ cm^{-2},
e) 2e harmonique axial $B_g^2 = 126 \cdot 10^{-4}$ cm^{-2},
f) 3e harmonique axial $B_g^2 = 158 \cdot 10^{-4}$ cm^{-2}.

port à λ (environ 0,08 s^{-1}). On soustrait donc la contribution des neutrons retardés du flux mesuré. Le troisième terme disparaît très rapidement, on le néglige. Par contre le premier subsiste un temps non négligeable par rapport à la constante de temps stable. La présence des neutrons de source d'une part et du grand nombre d'harmoniques axiaux d'autre part nous oblige d'attendre que le flux ait décru d'un facteur 1000 environ avant d'atteindre la période stable (fig. 2).

Les premiers harmoniques axiaux ont l'allure représentée par la figure 3.

La somme de ces harmoniques représente la carte de flux axiale stationnaire.

Si l'on place successivement le détecteur (compteur BF_3) en z = H/3, z = H/2, z = 2H/3, on peut isoler les différents harmoniques de la façon suivante:

On additionne les décroissances mesurées en z = H/3 et z = 2H/3. On obtient deux fois le premier harmonique, alors que les harmoniques 2, 3, 4, donnent une contribution nulle. L'harmonique 5 décroît assez vite pour être négligé. Le fondamental F(t) qui reste a la forme (j = 1):

$$F(t) = A_0 \exp(-t/l_0) + A_1 \exp\left(\frac{K_e - 1}{l_1 + l_2} t\right). \qquad (12)$$

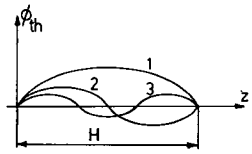


Figure 3

Forme des trois premiers harmoniques axiaux.

K_e est le coefficient de multiplication effectif du premier harmonique, il est donc directement relié à la réactivité du réseau. La connaissance de F(t) permet de déterminer $(K_e - 1)/(l_1 + l_2)$ et l_0. De façon semblable, la soustraction des mêmes décroissances en $z = H/3$ et $z = 2H/3$ isole l'harmonique 2. Cette détermination est cependant moins bonne, car il reste l'harmonique 4, et il est difficile d'en déduire le second harmonique de la contribution des neutrons de 14 MeV. Enfin l'harmonique 3 se détermine de la décroissance mesurée en $z = H/2$ de laquelle on soustrait le fondamental défini par l'équation (12).

Il est nécessaire, pour faire cette analyse, que l'erreur statistique des mesures soit très faible.

On a obtenu ainsi trois valeurs de $r_1 = (K_e - 1)/(l_1 + l_2)$ pour trois valeurs de $B_j^2 = \alpha^2 + (j\pi/H)^2$, $j = 1, 2, 3$.
D'après (11) et (8)

$$r_{1j} = r_1(B_j^2) = \frac{K_e - 1}{l_1 + l_2} = \frac{\mu^2 - B_j^2}{a + bB_j^2};$$

en négligeant les termes en B^4,

$$a = \frac{l_{01} + l_{02}}{L_1^2 + L_2^2}, \qquad b = \frac{l_{01} L_2^2 + l_{02} L_1^2}{L_1^2 + L_2^2}. \tag{13}$$

La courbe $r_1(B_j^2)$ est une hyperbole équilatère et il est possible de déterminer a et b par la méthode des moindres carrés; a et b sont des carac-

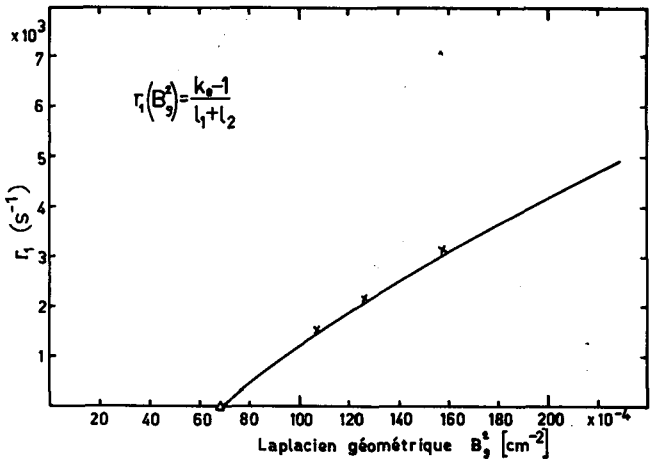


Figure 4

Variation de la période stable r_1 en fonction du laplacien géométrique B_g^2.

—— calculé d'après la référence [8],
Δ mesuré en stationnaire,
× mesuré en cinétique.

Réseau UO_2 enrichi à 1,8% ^{235}U, W/U = 3,5.

téristiques du milieu infini (fig. 4). Dans l'expression (10) on peut facilement déterminer les amplitudes A des différentes exponentielles. Ceci n'a pas grand intérêt, sauf pour la valeur A_3, amplitude des neutrons retardés. Pour ce faire, on multiplie l'équation (7) par $s+\lambda$, puis on fait tendre s vers $-\lambda$. On obtient, en négligeant λ devant $1/l$

$$A_3 = \frac{T_2(0)K_e\beta}{-l_1 l_2 \frac{K_e-1}{l_1+l_2}\left(\frac{1}{l_1}+\frac{1}{l_2}+\frac{K_e-1}{l_1+l_2}\right)} \cong -\frac{T_2(0)K_e\beta}{K_e-1} = -\frac{T_2(0)\beta}{\rho}. \qquad (14)$$

On retrouve une expression connue reliant le rapport n_p/n_d à la réactivité, qui est donc encore valable lorsque les neutrons de source ont une énergie différente de l'énergie de fission. $T_2(0)$ est la valeur du flux thermique à la fin de l'impulsion, en $t = 0$.

La valeur de β est tirée de la référence [7]. Le rapport β/ρ varie cependant avec le lieu, et il convient d'en tenir compte en appliquant cette relation [8].

Les relations (1), (13) et (14) sont suffisantes pour déterminer entièrement les constantes du réseau de la théorie à deux groupes, c'est-à-dire K, L_1^2, L_2^2, l_{01} et l_{02}, ainsi que d'autres grandeurs, par exemple la durée de vie l_{00} des neutrons de source.

2. ÉTUDE D'UN RÉSEAU NON RÉGULIER

Il est souvent intéressant d'utiliser des réseaux non réguliers, dans lesquels la concentration en combustible dépend du lieu. On peut obtenir ainsi un flux plus plat et une température plus uniforme. Si l'on dispose de barres de combustible, on les concentre davantage au centre du réseau. A chaque barre on associe une cellule, c'est-à-dire un certain volume de modérateur. Ceci permet de définir un rapport local volume de modérateur/volume de combustible = W/U et d'attribuer à cette cellule les constantes globales déterminées dans la première partie, pour un réseau régulier de même W/U.

On homogénéise ainsi le réseau non régulier, mais les constantes nucléaires seront fonction du lieu. Pratiquement, on conserve la symétrie cylindrique. L'équation de diffusion, qui a la forme

$$\operatorname{div}(D\,\overrightarrow{\operatorname{grad}}\,\phi) - \Sigma\phi + S = \frac{1}{v}\frac{\partial\phi}{\partial t}$$

devient

$$(\overrightarrow{\operatorname{grad}}\,D \cdot \overrightarrow{\operatorname{grad}}\,\phi + D\nabla^2\phi)_r + (D\nabla^2\phi)_z - \Sigma\phi + S = \frac{1}{v}\frac{\partial\phi}{\partial t},$$

puisque D est fonction du rayon mais non de la hauteur.

On étudie successivement les cas stationnaire et cinétique.

2.1. *Cas stationnaire*

Les équations de diffusion de la théorie à deux groupes donnent

$$\begin{aligned} \operatorname{div}(D_1 \overrightarrow{\operatorname{grad}}\,\phi_1) - \Sigma_1\phi_1 + K\Sigma_2\phi_2 &= 0, \\ \operatorname{div}(D_2 \overrightarrow{\operatorname{grad}}\,\phi_2) - \Sigma_2\phi_2 + \Sigma_1\phi_1 &= 0, \end{aligned} \tag{15}$$

dans lesquelles toutes les constantes nucléaires sont fonction du lieu.

Supposons que les flux aient les solutions suivantes, valables pour un cœur nu sous-critique:

$$\begin{aligned} \phi_1 &= \sum_i A_{1i} J_0(\alpha_i r)\exp(-\gamma z), \\ \phi_2 &= \sum_i A_{2i} J_0(\alpha_i r)\exp(-\gamma z). \end{aligned} \tag{16}$$

$\sum_i A_i J_0(\alpha_i r)$ représente le mode fondamental du flux radial, qu'on analyse selon les fonctions de Bessel. On remplace ces solutions dans le système (12) après avoir calculé div(D grad ϕ), et on obtient deux équations à 2i inconnues, les A_{1i} et A_{2i} .

Pour déterminer complètement les A_i , on utilise les propriétés d'orthogonalité des fonctions de Bessel, ou on suppose que le système est satisfait en i points sur le rayon. On obtient un système de 2i équations homogènes. On détermine γ en annulant son déterminant, puis on résout le système. Les solutions (16) se vérifient par une carte de flux radiale et axiale (fig. 5).

Cas cinétique

Par analogie avec les équations valables pour le cœur régulier, on suppose que la solution a la forme

$$\phi_g(r, z, t) = \sum_i A_{gi} J_0(\alpha_i r) \cdot \sum_j \sin \gamma_j z \cdot T_{gj}(t) .$$

g = 1, 2, indice de groupe.
On introduit cette solution dans le système (17):

$$\begin{aligned} \operatorname{div}(D_1 \overrightarrow{\operatorname{grad}}\,\phi_1) - \Sigma_1\phi_1 + K\Sigma_2\phi_2 &= \frac{1}{v_1}\frac{\partial\phi_1}{\partial t}, \\ \operatorname{div}(D_2 \overrightarrow{\operatorname{grad}}\,\phi_2) - \Sigma_2\phi_2 + \Sigma_1\phi_1 &= \frac{1}{v_2}\frac{\partial\phi_2}{\partial t}, \end{aligned} \tag{17}$$

que l'on résout par rapport à T_2.

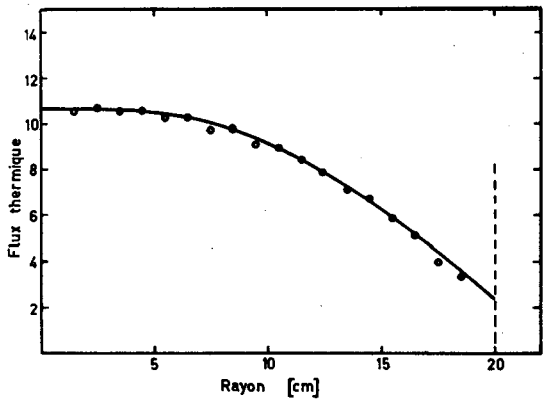


Figure 5

Carte de flux radiale.

294 barres UO_2. W/U = 2,5 en r = 0 et W/U = 4 en r = 20.
Période stable: r = 1150 ± 50 s^{-1}.

—— calculé,
O mesuré.

On a vu dans la première partie que la source n'avait pas d'influence sur la période stable du réseau. Ici, seule la période stable nous intéresse, il n'y a donc pas lieu de faire le calcul selon la théorie à trois groupes ou avec les neutrons retardés.

Les propriétés d'orthogonalité du sinus permettent d'obtenir un système pour chaque harmonique axial.

Après avoir remplacé ϕ par sa valeur dans le système (17), on multiplie chaque terme par r et on intègre sur le rayon entre 0 et R. Il reste alors un système ne contenant que T_1 et T_2, et on peut résoudre ce système par une méthode semblable à celle exposée dans la première partie. Si l'on pose

$$p_g = \sum_i A_{gi} \int_0^R \left\{ J_0(\alpha_i r)(1 + L_g^2 B_i^2) + \alpha_i J_1(\alpha_i r) \frac{dD_g}{dr} l_{og} \right\} r dr,$$

$$q_g = \sum_i A_{gi} \int_0^R l_{og} J_0(\alpha_i r) r dr,$$

$$s_1 = \sum_i A_{1i} \int_0^R \frac{l_{02}}{l_{01}} J_0(\alpha_i r) r dr,$$

$$s_2 = \sum_i A_{2i} \int_0^R \frac{K l_{01}}{l_{02}} J_0(\alpha_i r) r dr,$$

$$B_i^2 = \alpha_i^2 + \left(\frac{\pi}{H}\right)^2,$$

T_2 sera solution de l'équation du deuxième ordre

$$\frac{d^2T_2}{dt^2} + \left(\frac{p_2}{q_2} + \frac{p_1}{q_1}\right)\frac{dT_2}{dt} + \frac{p_1p_2 - s_1s_2}{q_1q_2}T_2 = 0,$$

d'où l'on peut définir K_{eff} et les vies moyennes

$$\bar{l}_1 = \frac{q_1}{p_1}, \qquad \bar{l}_2 = \frac{q_2}{p_2}, \qquad K_e = \frac{s_1s_2}{p_1p_2}. \tag{18}$$

On a fait des mesures sur un cœur nu d'un diamètre de 40 cm et d'une hauteur de 117 cm, composé de barres d'oxyde d'uranium enrichi à 1,8% disposées de façon que le rapport W/U varie de façon quasi continue de 2,5 au centre à 4 à l'extérieur.

La figure 5 montre les résultats du calcul et des mesures et donne la constante de temps de la période stable.

RÉFÉRENCES

[1] VITTOZ, B. et al., « Assemblage sous-critique à uranium enrichi et eau légère », Exponential and Critical Experiments I, AIEA, Vienne (1964) 355-370.
[2] GLASSTONE, S. and EDLUND, M., Nuclear Reactor Theory, Van Nostrand, New-York (1952).
[3] REIFENSCHWEILER, O., Nucleonics 18 12 (1960) 69-71.
[4] FULTZ, S.C., Nucl. Sci. and Engng 6 (1959) 313-319.
[5] SIMMONS, B.E. and KING, J.S., Nucl. Sci. and Engng. 3 (1958) 595-608.
[6] AUDINET, M. et al., Rapport CEA 807 (1958).
[7] KEEPIN, G.R. and WIMETT, T.F., Nucleonics 16, 10 (1958) 86.
[8] RUTGERS, E., Helv. phys. Acta, à paraître.

PULSED NEUTRON STUDIES OF BeO-NATURAL URANIUM LATTICES

B. V. JOSHI, V. R. NARGUNDKAR AND K. SUBBARAO
ATOMIC ENERGY ESTABLISHMENT TROMBAY, BOMBAY, INDIA

Abstract — Résumé — Аннотация — Resumen

PULSED NEUTRON STUDIES OF BeO-NATURAL URANIUM LATTICES. The use of the pulsed neutron method for determination of the diffusion parameters and multiplication constants of lattices is described. The diffusion parameters and multiplication constants of BeO-natural uranium lattices are obtained by this method. The uranium rods used were 2.92 cm diameter clad in aluminium 0.072 cm thick and were arranged vertically in channels of square cross-section 5 cm × 5 cm, in a square lattice of pitch 15 cm. The neutron bursts were produced from a cascade accelerator by pulsing the ion source and using the Be(d, n) reaction. The detectors were enriched boron trifluoride proportional counters. The space and time harmonics were eliminated as described by the authors in another paper at this Symposium. The decay constant of the fundamental mode was determined for several bucklings, far from criticality. In these calculations the effect of diffusion cooling and anisotropy was taken into account. All the diffusion and multiplication constants were determined by the method of least squares fit by three different approaches. The prompt critical buckling was determined by solving the decay constant equation for $\lambda = 0$. The final results are:

Diffusion length L = 15.2 cm
Absorption constant $\lambda_0 = 762.5\ s^{-1}$
Diffusion coefficient $D = 1.761 \times 10^5\ cm^2/s$
Diffusion cooling constant $C = -8.766 \times 10^5\ cm^4/s$
Age $\tau = 150.7\ cm^2$
Infinite multiplication factor $k_\infty = 1.126$
Prompt critical buckling $B^2 = 3.00 \times 10^{-4}\ cm^{-2}$

ÉTUDES DE RÉSEAUX URANIUM NATUREL-GLUCINE, PAR LA MÉTHODE DES NEUTRONS PULSÉS. Les auteurs décrivent l'utilisation de la méthode des neutrons pulsés pour la détermination des paramètres de diffusion et des constantes de multiplication des réseaux. Cette méthode permet d'obtenir les paramètres de diffusion et les constantes de multiplication du réseau uranium naturel-glucine. Les barres d'uranium utilisées avaient un diamètre de 2,92 cm et un gainage d'aluminium d'une épaisseur de 0,072 cm; elles étaient disposées verticalement dans des canaux de section carrée 5 × 5 cm dans un réseau carré dont le pas était de 15 cm. Les bouffées de neutrons étaient produites par la réaction Be(d, n), la source de deutérons pulsés étant un accélérateur à cascade. Les détecteurs étaient des compteurs proportionnels au BF_3. Les harmoniques du lieu et du temps ont été éliminées de la façon décrite par les auteurs dans un autre mémoire présenté au même colloque. Les auteurs ont déterminé la constante de décroissance du mode fondamental pour plusieurs laplaciens, loin de l'état critique. Dans ces calculs, ils ont tenu compte de l'effet de refroidissement par diffusion et de l'anisotropie. Ils ont déterminé toutes les constantes de diffusion et de multiplication en ajustant les données de trois manières différentes par la méthode des moindres carrés. Ils ont obtenu le laplacien pour l'état critique instantané en résolvant l'équation de la constante de décroissance pour $\lambda = 0$. Les résultats définitifs qu'ils ont obtenus sont les suivants:

Longueur de diffusion L = 15,2 cm
Constante d'absorption $\lambda_0 = 762,5\ s^{-1}$
Coefficient de diffusion $D = 1,761 \cdot 10^5\ cm^2/s$
Constante de refroidissement par diffusion $C = -8,766 \cdot 10^5\ cm^4/s$
Age $\tau = 150,7\ cm^2$
Facteur de multiplication infini $k_\infty = 1,126$
Laplacien pour l'état critique instantané $B^2 = 3,00 \cdot 10^{-4}\ cm^{-2}$

ИССЛЕДОВАНИЕ РЕШЕТОК BeO–ПРИРОДНЫЙ УРАН С ПОМОЩЬЮ ИМПУЛЬСНЫХ НЕЙТРОНОВ. Описывается применение метода импульсных нейтронов для определения диффузионных параметров и постоянных размножения решеток. С помощью этого метода получены диффузионные параметры и постоянные размножения для решеток BeO–природный уран. Использовавшиеся урановые стержни имели в диаметре 2,92 см и были покрыты алюминием толщиной в 0,072 см. Они были расположены вертикально в каналах, имеющих квадратное сечение 5 × 5 см в квадратной решетке с шагом 15 см. Импульсы нейтронов получали с помощью каскадного ускорителя в результате пульсирования источника ионов и использования реакций Be (d, n). Детекторами служили пропорциональные счетчики из обогащенного трехфтористого бора. Пространственные и временные гармоники были устранены с помощью метода, описанного Джоши и другими в 1965 году. Постоянная распада основного состояния определена для нескольких лапласианов при состоянии, далеком от критического. В этих вычислениях принимали в расчет эффект диффузионного охлаждения и анизотропии. Все постоянные диффузии и размножения определяли методом аппроксимации наименьших квадратов тремя различными подходами. Мгновенный критический лапласиан определен путем разложения уравнения постоянной распада для $\lambda = 0$. Окончательными результатами являются:

Диффузионная длина $L = 15{,}2$ см.
Постоянная абсорбции $\lambda_0 = 762{,}5$ сек$^{-1}$.
Диффузионный коэффициент $D = 1{,}761 \cdot 10^5$ см^2 сек$^{-1}$.
Постоянная диффузионного охлаждения $C = -8{,}766 \cdot 10^5$ см^4 сек$^{-1}$.
Возраст $\tau = 150{,}7$ см^2.
Коэффициент неограниченного размножения $k_\infty = 1{,}126$.
Мгновенный критический лапласиан $B^2 = 3{,}00 \cdot 10^{-4}$ см$^{-2}$.

ESTUDIO DE RETICULADOS DE BeO-URANIO NATURAL CON AYUDA DE NEUTRONES PULSADOS. Los autores describen el empleo del método de los neutrones pulsados para determinar los parámetros de difusión y las constantes de multiplicación de diversos reticulados. Empleando este método, han obtenido los parámetros de difusión y las constantes de multiplicación en reticulados de BeO-uranio natural. Las barras de uranio empleadas medían 2,92 cm de diámetro, estaban revestidas de una capa de aluminio de 0,072 cm de espesor, y se hallaban colocadas verticalmente en canales de sección cuadrada de 5 cm de lado, en un reticulado cuadrado de 15 cm de paso. Las ráfagas de neutrones se produjeron con un acelerador de cascada pulsando la fuente de iones y empleando la reacción Be(d, n). Como detectores se emplearon contadores proporcionales de BF_3 enriquecido. Los armónicos espaciales y temporales se eliminaron por el método descrito por Joshi y sus colaboradores en otra memoria presentada en este simposio. Se determinó la constante de decrecimiento del modo fundamental para diversos laplacianos cuando la criticidad estaba muy lejos de alcanzarse. En estos cálculos se tuvo en cuenta el efecto del enfriamiento por difusión, así como el de la anisotropía. Todas las constantes de difusión y de multiplicación se determinaron mediante ajuste por cuadrados mínimos siguiendo tres procedimientos distintos. El laplaciano crítico inmediato se obtuvo resolviendo la ecuación de la constante de decrecimiento para $\lambda = 0$. Los resultados finales fueron los siguientes:

Longitud de difusión $L = 15{,}2$ cm.
Constante de absorción $\lambda_0 = 762{,}5$ s^{-1}.
Coeficiente de difusión $D = 1{,}761 \cdot 10^5$ cm^2/s.
Constante de enfriamiento por difusión $C = -8{,}766 \cdot 10^5$ cm^4/s.
Edad $\tau = 150{,}7$ cm^2.
Factor de multiplicación infinita $k_\infty = 1{,}126$.
Laplaciano crítico inmediato $B^2 = 3{,}00 \cdot 10^{-4}$ cm^{-2}.

INTRODUCTION

Natural uranium-BeO lattices have been investigated by BENOIST et al. [1] by the steady state method. They obtained a value of $(5.44 \pm 0.02) \times 10^{-4}$ cm^{-2} for the delayed critical buckling. In the pulsed neutron experiments with

lattices we obtain a number of multiplication constants and diffusion parameters in a relatively simple way. The prompt critical buckling is obtained from these. The theory underlying the experiment has been discussed in the literature [2, 3, 4, 5].

EXPERIMENTAL APPARATUS

The pulsed neutron source and the time analyser have been described earlier [6]. The assembly was a heterogeneous lattice of natural uranium rods in beryllium oxide. The rods were 2.92 cm in diameter clad in 0.076-cm aluminium. They were arranged vertically in channels of square cross-section 5 cm × 5 cm in a square lattice of pitch 15 cm. The channels were lined with 0.076-cm thick aluminium. The assembly sizes range from 105 cm×105 cm×100 cm to 90 cm×60 cm×30 cm (buckling range from 2.62×10^{-3} to 1.29×10^{-2} cm^{-2}). Throughout the experimental investigation the room temperature was maintained between 75 and 79°F. The choice of counting rate, channel width, pulse width and delay was made as described in our earlier paper [6]. For each buckling, counting was stopped when a total of 200 000 counts were accumulated in the first channel. This was done in three sets for cross checking.

ELIMINATION OF THE SPACE HARMONICS

The target was arranged on the top of the assembly as shown in Fig. 1. The target height was between 20 to 30 cm from the top surface, as this was found to minimize the amplitude of the harmonics in the assembly. The second and third harmonics in the z-direction were eliminated by placing the counter vertically with the position and length of the counter such that the positive and negative contributions of each harmonic were cancelled out. The third harmonic in the x-direction was eliminated by placing the counter at a nodal point. For asymmetric source positions the second harmonic in the x-direction was eliminated by placing the counter at positions (A) and (B) (Fig. 1) and taking equal counts in each position. The third harmonic contribution in the y-direction was minimized by giving adequate delay (two and half fundamental decay times). Higher harmonics would be insignificant. The elimination of the harmonics was tested as described earlier [6].

CALCULATION OF DECAY CONSTANT

A fraction of the fission neutrons was emitted as delayed neutrons. The thermal neutron density is then given by

$$n(t) = A \exp(-\lambda t) + B \exp(-\lambda_d t),$$

where λ_d is the average radioactive decay constant of the precursors.

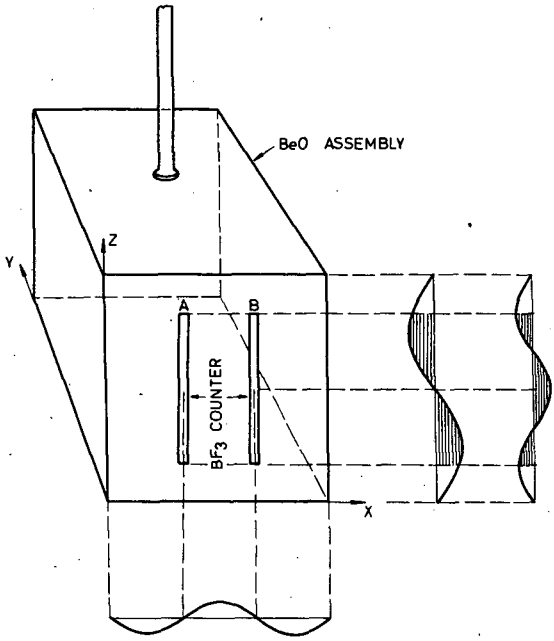


Fig. 1

Experimental arrangement of source and detectors

Since λ_d is very small compared to λ, the effect of delayed neutrons is simply to cause a uniform background B_0.

$$n(t) = A \exp(-\lambda t) + B_0$$

The decay constant was calculated by Behren's method. Constant background B_0 was eliminated as explained in an earlier paper [6]. The calculations were done on CDC-3600 computer.

CALCULATION OF BUCKLINGS

The medium is slightly anisotropic mainly because of the vertical air gaps between the rods and the channel walls. This is taken into account by correcting the purely geometric buckling for anisotropy in the following manner. We can write

$$M^2B^2 = M_\perp^2 B_x^2 + M_\perp^2 B_y^2 + M_{\parallel}^2 B_z^2,$$

where M^2 is the effective migration area for a cubical medium, $M_\perp^2$ and $M_{\parallel}^2$ are the migration areas in transverse and axial directions respectively and B^2 is the effective geometric buckling. The anisotropy is defined by

$$M_{\parallel}^2 / M_\perp^2 = 1 + \epsilon.$$

From these equations we obtain

$$B^2 = \frac{1}{(1+\epsilon/3)} \left[B_x^2 + B_y^2 + (1+\epsilon) B_z^2\right],$$

where $\epsilon = 0.051$.

CALCULATION OF DIFFUSION AND MULTIPLICATION PARAMETERS

For a multiplying medium the expression for the decay constant is given by

$$\lambda = \lambda_0 + DB^2 + CB^4 - \lambda_0(1-\beta)k_\infty e^{-B^2\tau},$$

where β is the delayed neutron fraction, k_∞ is the infinite medium multiplication constant, τ is the age of neutrons and the other constants have their usual meaning. The extrapolation length used for calculation of bucklings was 0.7194λ [7, 8]. The anisotropy is ignored for calculating λ_{tr}.

Because of the exponential on the right-hand side, a direct least squares fit is not possible. Also, in the buckling range studied here and with the order of τ known [1], it is not possible to expand the exponential into a power series of small number of terms. The problem was approached in the following way: The least squares fit was made by three different methods.

(1) Multifit method

The fitting was divided into two parts, the parabola and the exponential. After an initial estimate of λ_0, D and C was made and these values were assumed, a linear fit was made for

$$\log \left[\frac{(\lambda_0 + DB^2 + CB^4) - \lambda}{(1-\beta)\lambda_0}\right] = \log k_\infty - B^2\tau$$

to estimate k_∞ and τ. These values of k_∞ and τ were used to obtain new values of λ_0, D and C from the parabola fit. The process was repeated until a self-consistent set of values of λ_0, D, C, k_∞ and τ was obtained.

(2) Direct fit

Some initial values were assigned to the five parameters, and the weighted sum of the squares of the residuals was calculated. The values of the parameters were then altered by trial in successive steps in such a way as to decrease the weighted sum. This was continued until no further decrease in the weighted sum was possible by any changes up to a given accuracy in the parameters. Thus the values of the parameters were obtained for which the weighted sum of the squares of the residuals was the least.

(3) Partial expansion method

The equation for λ can be written as

$$\lambda + \lambda_0 k_\infty (1-\beta)\left\{\exp(-B^2\tau) - \left[1 - B^2\tau + \frac{(B^2\tau)^2}{2}\right]\right\} = \lambda_0' + D'B^2 + C'B^4,$$

where

$$\lambda_0' = [1 - k_\infty (1-\beta)]$$

$$D' = D + k_\infty \lambda_0 \tau (1-\beta)$$

$$C' = C - \frac{k_\infty \lambda_0 \tau^2}{2}(1-\beta)$$

After some reasonable initial values for λ_0, k_∞ and τ were assumed, a least squares fit was made to the above equation to estimate λ_0', D' and C' with iteration on λ_0'. The values of k_∞ and τ were those for which weighted sum of the square of the residuals was the least.

The five parameters λ_0, D, C, k_∞ and τ were calculated by each one of the above three methods and are shown in Table I. The decay constant equation was then solved for $\lambda = 0$ to obtain prompt critical buckling.

TABLE I

CALCULATION OF THE FIVE PARAMETERS BY THREE LEAST-SQUARE FITTING METHODS

Method	λ_0 (s^{-1})	D (10^5 cm^2/s)	C (10^5 cm^4/s)	τ (cm^2)	k_∞
Multifit	753.0	1.769	-8.896	151.6	1.128
Direct fit	764.2	1.758	-8.696	150.7	1.126
Partial expansion	762.5	1.761	-8.766	150.7	1.126

Note: An estimation of errors on these parameters is being attempted.

ACKNOWLEDGEMENTS

We gratefully extend our thanks to Messrs. M. S. Kamath and S. K. Eligar for their help with electronics and readings. We are also grateful to the accelerator staff for operation of the accelerator. Our sincere thanks are due to Dr. R. Ramanna for his interest in the work.

REFERENCES

[1] BENOIST, P., *et al.*, Proc. 2nd UN Int. Conf. PUAE (1958).
[2] VON DARDEL, G. F. and SJÖSTRAND, N. G., Progress in Nuclear Energy Series 1, Physics and Mathematics 2 (1958).
[3] KLOVERSTROM, F. A. and KOMOTO, T. T., Rpt UCRL-5477 (1959).
[4] MEISTER, H., Nucl. Energy 17 (1963).
[5] FULTZ, S. C., Nucl. Sci. Engng 6 (1959) 313.
[6] JOSHI, B. V., NARGUNDKAR, V. R. and SUBBARAO, K., "Diffusion parameters of BeO by pulsed neutron method", these Proceedings I.
[7] GELBARD, E. M. and DAVIES, J. M., Nucl. Sci. Engng 13 (1962) 237.
[8] WILLIAMS, M. M. R., J. nucl. Energy. A/B 17 (1963) 55.

DISCUSSION

(on papers SM-62/71, SM-62/13 and SM-62/41).

M. STIÉVENART: I should like to make a comment on the subject of the experiment described by Mr. Preskitt in connection with the source-jerk technique. We have also performed such measurements using H_2O-U_2O reflected assemblies. The variations were rather weak and they were confined to a small area around the source where they were due to first-flight source neutrons. Far away from the source the measured parameter was fairly space-independent.

C.A. PRESKITT: The space dependence is quite low in the source-jerk experiment if the system is near critical. Could you tell me what the reactivity was in the system you have just mentioned?

M. STIÉVENART: In the measurement I mentioned the reactivity was such that the k_{eff} varied between 0.72 and 0.86. The space dependence of the measured parameter was found to be weak far away from the source for four assemblies in this range of k.

C.A. PRESKITT: There is another effect that is liable to be of importance in the source-jerk experiment. If a 14-MeV source is used, the source will become distributed and the space dependence will be less. This is actually mentioned in my paper.

J. SHERWIN: Calculations and measurements made at Windscale indicate that spatial effects are present in source-jerk measurements. We have found that in reflected systems the corrections to be applied tend to be constant over a large fraction of the system. In other words after about 0.8 R, where R is the radius of the fuel region, the corrections to be applied are constant. We have concluded from this that it is better to put detectors in the outer regions and calculate the correction rather than to minimize the correction by careful positioning of the detector.

A. HENRY (Chairman): For source-jerk, rod-drop and pulsed-neutron experiments, one can frequently analyse data much more consistently by assuming that the flux at any time can be expressed as the sum of two flux shapes, each with its own time behaviour. This simple extension of the conventional procedure has recently been applied to the rod-drop experiment and has made it possible to arrive at a meaningful interpretation of data which otherwise would be uninterpretable.

J. SHERWIN: One of the assumptions made in the papers presented is that the distribution of the prompt and delayed fast neutrons in non-uniform systems is the same. We have made four-group calculations at Windscale of the prompt and delayed fast neutrons and have found that the ratio of delayed to prompt neutrons is not constant across the core of non-uniform systems. What impact does this have on the methods discussed in the papers?

C.A. PRESKITT: This assumption was not made in my studies and the effect of any such variation is included in the results reported.

A. HENRY: It seems to me that the primary purpose of performing pulsed-source experiments is to check the validity of some numerical model to be used for describing the reactor. In view of this, why do we not avoid using reactivity in this connection and instead compare directly measured and calculated prompt die-away constants?

C.A. PRESKITT: I agree with you entirely that the decay constant is a more important quantity than the reactivity. At least, this is true insofar as the physicist is concerned. On the other hand, for reactor operators and safety experts it is more convenient to deal with reactivity and we should therefore make some attempt to determine this quantity.

M.N. MOORE: I should like to ask Mr. Preskitt a question. In his eigenfunction expansion of the space dependence in terms of eigenfunctions of Laplacian, what boundary conditions were employed to define the functions vanishing on the extrapolated boundary or boundary conditions somewhere within the system?

C.A. PRESKITT: We used the eigenfunctions which vanish at the extrapolated boundary of the entire system.

M.N. MOORE: I take it then that essentially you used the method of Foderaro and Garabedian?

C.A. PRESKITT: Yes, you will find several references in our paper to earlier work by Garabedian and collaborators.

M. STIÉVENART: We have performed a number of experiments on light-water reflected lattices and have detected phenomena of the same type as described in Mr. Preskitt's paper.

At the centre of the core the flux-time variation is the sum of two contributions, a prompt contribution and a slower one. We have tried to derive two decay constants from these measurements. The fast decay constant seems to be in good agreement with the α derived from a $1/v$ poisoned reactor calculation and there seems to be a simple relationship between the second decay constant and the first. These measurements are described in my paper (SM-62/13).

S. SCOTT: With reference to paper SM-62/41, it seems to me that the magnitude of the source term in the expression for λ should be increased by the factor $e^{\lambda\tau_1}$, where τ_1 is the neutron slowing-down time, since the overall neutron density is decaying.

B.V. JOSHI: I am not sure whether this is necessary. Perhaps this appears as a constant multiplying factor for the amplitude of neutron density and does not enter into the expression for the decay constant.

SUBCRITICALITY DETERMINATION ON A REFLECTED GRAPHITE SYSTEM BY THE PULSED NEUTRON METHOD

K. SUMITA AND Y. KANEKO
JAPAN ATOMIC ENERGY RESEARCH INSTITUTE,
HIGASHINODA, MIYAKOJIMA-KU, OSAKA, JAPAN.

Abstract — Résumé — Аннотация — Resumen

SUBCRITICALITY DETERMINATION ON REFLECTED GRAPHITE SYSTEM BY THE PULSED NEUTRON METHOD. The usual concept of reactivity is based on the treatment of a persisting mode of neutron multiplication. The experimental methods for reactivity measurement in a highly subcritical system which are based on the measurement of the persisting mode have theoretical and experimental difficulties. The other reactivity measurement methods, which are based on that of the prompt mode (pulsed neutron experiment, Rossi-α method, etc.), have other difficulties, because the prompt neutron lifetime changes depending on subcriticality, and the relation with the method based on persisting mode is very complicated in a reflected system.

The purpose of the present work is to establish another concept to avoid the above-mentioned problem, and to describe exactly the situation of neutron multiplication in a reflected subcritical system. The concept is that the prompt neutron decay constant of fundamental mode α should be used directly as a measure of neutron multiplication, because this quantity satisfies the following two sufficient, fundamental requirements: to be uniquely measurable free from space dependence and detector specification, and to be calculable from the fundamental Boltzmann equations. To prove that α does satisfy these requirements, a series of pulsed experiments was made at various subcritical states in a reflected graphite-moderated enriched fuel system (SHE).

The experimental results confirmed that α_{00} has the same value at any point of core and reflector, by means of the separation of spatial harmonics, using bare and cadmium-covered BF_3 counters. The state of SHE is changed by diminishing the core with or without a centre control rod and by adding distributed poison to the core or to the reflector.

The multigroup subcritical kinetics of the reflected reactor have been extended, and a direct comparison between the experimental results from pulsed neutron experiments and the calculated values from multigroup treatment using P_1 and S_4 approximation with regard to the above-mentioned systems has been made to investigate this concept. Calculated values of α_{00} for the core-diminished subcritical status with and without a control rod showed fairly good agreement with the measured values. In addition the time-dependent spectra changes of the subcritical systems were also investigated in the experiments.

DÉTERMINATION, PAR LA MÉTHODE DES NEUTRONS PULSÉS, DE LA SOUS-CRITICITÉ D'UN SYSTÈME A RÉFLECTEUR, RALENTI AU GRAPHITE. La notion habituelle de réactivité est fondée sur l'analyse du mode fondamental de multiplication des neutrons. Les méthodes expérimentales de mesure de la réactivité dans les systèmes très sous-critiques ont recours à la mesure des modes fondamentals et présentent des difficultés d'ordre théorique et expérimental. Les autres méthodes reposant sur la mesure du mode des neutrons instantanés (expérience avec les neutrons pulsés, méthode α de Rossi, etc.) soulèvent d'autres problèmes, parce que la durée de vie des neutrons instantanés varie en fonction de la sous-criticité et, dans un système à réflecteur, la relation avec la méthode fondée sur le mode fondamental est très compliquée.

Le mémoire a pour objet de proposer une nouvelle idée permettant d'éviter les problèmes précités, et de décrire rigoureusement le processus de multiplication des neutrons dans un système sous-critique à réflecteur. Cette idée est qu'il faut utiliser directement la constante α de décroissance du mode fondamental des neutrons instantanés pour mesurer la multiplication des neutrons parce que cette valeur répond à deux conditions nécessaires et suffisante: être mesurable indépendamment de l'espace et d'une spécification de détecteur, et être calculable à partir des équations fondamentales de Boltzmann. Pour vérifier que tel est bien le cas, il a été procédé à une série d'expériences au moyen des neutrons pulsés, à différents états sous-critiques, dans un système à combustible enrichi, ralenti au graphite, avec réflecteur (SHE).

Les résultats expérimentaux ont confirmé que, par séparation des harmoniques du lieu à l'aide d'un compteur BF_3 avec et sans revêtement de cadmium, α_{00} a la même valeur à tous les points du cœur et du réflecteur. On modifie l'état de SHE par diminution des dimensions du cœur avec ou sans une barre de contrôle centrale et par adjonction de poison réparti dans le cœur et le réflecteur.

Pour approfondir cette idée, on a déterminé la cinétique du réacteur à réflecteur à l'état sous-critique dans une théorie à plusieurs groupes et procédé à une comparaison directe entre les résultats des expériences au moyen des neutrons pulsés et les valeurs calculées dans une théorie à plusieurs groupes, en utilisant l'approximation P_1 et S_4 pour les systèmes précités. Les valeurs calculées de α_{00} pour l'état sous-critique du cœur dont les dimensions sont réduites avec et sans une barre de contrôle concordent assez bien avec les valeurs mesurées. Les variations de spectra dépendant du temps des systèmes sous-critiques ont également été étudiées au cours des expériences.

ОПРЕДЕЛЕНИЕ ПОДКРИТИЧНОСТИ В ГРАФИТОВОЙ СИСТЕМЕ С ОТРАЖАТЕЛЕМ МЕТОДОМ ИМПУЛЬСНЫХ НЕЙТРОНОВ. Обычная концепция реактивности основана на решении проблемы устойчивого режима размножения нейтронов. При применении экспериментальных методов измерения реактивности в сильно подкритической системе, которые основаны на измерении устойчивого режима, возникают теоретические и экспериментальные трудности. При других методах измерения реактивности, которые основаны на измерении мгновенного режима (эксперимент с импульсными нейтронами, альфа-метод Росси и т.д.) возникают другие трудности в связи с изменениями времени жизни мгновенных нейтронов в зависимости от подкритичности, и связь с методом, основанным на устойчивом режиме, является очень сложной в системе с отражателем.

Назначение данной работы состоит в том, чтобы разработать новую концепцию с целью устранения вышеупомянутой проблемы и точного описания процесса размножения нейтронов в подкритической системе с отражателем. Концепция заключается в том, что постоянную распада мгновенных нейтронов в основном состоянии α следует применять непосредственно в качестве мерила размножения нейтронов, так как такое количество удовлетворяет следующим двум основным требованиям, достаточным для обеспечения возможности однозначного измерения независимо от пространственной и энергетической зависимости и возможности расчета на основании уравнения основного состояния.

Для достижения этой цели проведена серия экспериментов с импульсными нейтронами в различных подкритических состояниях в системе с отражателем, графитовым замедлителем и обогащенным топливом (SHE).

Было экспериментально подтверждено, что α_0 имеет такое же значение в любой точке активной зоны и отражателя при разделении пространственных гармоник при использовании неэкранированного счетчика BF_3 с кадмиевой оболочкой. Состояние SHE изменяется путем уменьшения величины активной зоны, путем увеличения отравления активной зоны и отражателя.

Многогрупповое кинетическое уравнение в подкритическом состоянии реактора с отражателем расширено, и для изучения этой концепции проведено непосредственное сравнение между экспериментальными результатами, полученными из экспериментов с импульсными нейтронами, и расчетными значениями в результате многогруппового решения вышеупомянутых систем с применением приближения $P-1$. Расчетные значения α_0 для ослабленного подкритического состояния активной зоны достаточно хорошо согласовывались с измеренными значениями. Кроме того, исследовались также ядерные характеристики подкритических систем.

DETERMINACION DE SUBCRITICIDADES EN UN SISTEMA CON REFLECTOR DE GRAFITO POR EL METODO DE LOS NEUTRONES PULSADOS. El concepto usual de reactividad está basado en el análisis del modo persistente de la multiplicación neutrónica. Los métodos experimentales de medición de la reactividad en un sistema altamente subcrítico, que parten de la medición del modo persistente, presentan ciertas dificultades teóricas y experimentales. Los demás métodos de determinación de la reactividad, basados en la medición del modo debido a los neutrones inmediatos (experimento con neutrones pulsados, método de Rossi α, etc.) y en la del modo debido a los neutrones retardados, entrañan otras dificultades que derivan del hecho de que la vida media de los neutrones inmediatos varía en función de la subcriticidad, y su relación con el método basado en el modo persistente resulta muy compleja en un sistema con reflector.

El objeto del estudio emprendido por los autores es establecer otro concepto para evitar el problema anteriormente mencionado, así como describir exactamente las condiciones de multiplicación neutrónica en un

sistema subcrítico provisto de reflector. La idea es que la constante de decrecimiento de los neutrones inmediatos correspondiente al modo fundamental, α, debería poder servir de medida directa de la multiplicación neutrónica. Esta idea se basa en el hecho de que esta magnitud satisface las dos siguientes condiciones esenciales y suficientes: poder medirse exenta de la dependencia espacial y característica del detector, y poder calcularse partiendo de las ecuaciones fundamentales de Boltzmann. A fin de comprobar que α satisface esas condiciones, se realizó una serie de experimentos con neutrones pulsados en diversos estados subcríticos de un sistema de combustible enriquecido, con moderador y reflector de grafito (SHE).

Los resultados experimentales obtenidos después de proceder a la separación de los armónicos espaciales, empleando contadores de BF_3 con y sin revestimiento de Cd, confirmaron que el valor de α_{00} permanece constante en todos los puntos del cuerpo del reactor y del reflector. El estado del sistema SHE se modificó reduciendo la masa en el cuerpo del sistema con o sin barra de control central e incorporando veneno distribuido en el cuerpo o en el reflector. Los autores ampliaron la cinética subcrítica de varios grupos del reactor con reflector y procedieron a una comparación directa entre los resultados de experimentos realizados con neutrones pulsados y los valores calculados a partir del tratamiento de varios grupos, empleando el cálculo de aproximación P_1 y S_4, de los sistemas anteriormente mencionados, a fin de investigar este concepto. Los valores calculados de α_{00} para el estado subcrítico con el cuerpo de masa reducida con o sin barra de control central concordaron satisfactoriamente con los valores medidos. Además, se investigaron experimentalmente las variaciones espectrales dependientes del tiempo en los sistemas subcríticos.

1. INTRODUCTION

Recently, the pulsed neutron method, which is based on the measurement of the decaying prompt mode of neutron multiplication, has been developed and highly evaluated as a powerful method to measure the dynamic reactivity in a wide range of subcriticality. In a bare system the relation between the persistent mode and the prompt mode is rather simple, so that it is possible to measure by the pulsed neutron method the value of dynamic reactivity in the dollar unit and the ratio of prompt neutron lifetime l to effective delayed neutron fraction β_{eff} appearing in the same inhour equation on the one-group model. [1, 2].

Some efforts to apply this method in the highly subcritical and reflected system have been made. In the highly subcritical system, the prompt neutron lifetime changes with the subcriticality, so that correction of this effect must be considered. [3, 4] In the reflected system, the relation between the persistent mode and the prompt mode is so complicated, and the value of $k_{eff,d} \cdot \beta_{eff}/l$ ($k_{eff,d}$ being the effective multiplication factor corresponding to the persistent mode) changes so much with subcriticality, that it becomes actually impossible to reduce the value of dynamic reactivity based on the persistent mode from the prompt neutron decay constant α_0 of the fundamental mode without simplifying or neglecting the treatment of delayed neutrons [4-6]. No other methods guarantee obtaining the true value of dynamic or static reactivity in a highly subcritical and reflected system. [7]

The purpose of the present work is to establish a new concept to avoid the above-mentioned experimental and theoretical difficulties; this concept provides an accurate representation of the neutron multiplication in a reflected system. The basic idea is to use the prompt neutron decay constant α_{00} of the fundamental mode, in other words, the eigenvalue itself of the time-dependent neutron balance equation in the given nuclear systems, directly as a measure of neutron multiplication. This concept has already been suggested by BACH et al. [8], but its adequacy to the following require-

ments has not been investigated. This quantity must be proved to satisfy the following two necessary and sufficient, fundamental conditions: To be uniquely measurable independently of spatial effects and detector specification, and to be directly calculable from the fundamental equation on neutron transportation. In the present work, it is confirmed that the pulsed neutron method can measure the value of α_{00} uniquely and that value can be calculated in a way similar to the usual multigroup-multiregion criticality calculation in the reflected, enriched, uranium-graphite system, in the full range from the delayed critical state to the moderator case with or without centre control rod.

2. PRINCIPLE

Neutron density in the multiplying system after a pulsed neutron burst is given by

$$N(\vec{r}, v\vec{\Omega}, t) = \sum_{h=0}^{\infty} a_{nm} N_{nm}(\vec{r}, v\vec{\Omega})\, e^{-\alpha_{nm} t}, \ldots \tag{1}$$

where

$$a_{nm} = \iiint N^{+}_{nm}(\vec{r}, v\vec{\Omega}) N(\vec{r}, v\vec{\Omega}, 0)\, dv\, d\vec{\Omega}\, dV, \tag{2}$$

$N(\vec{r}, v\vec{\Omega}, t)dV\, d\vec{\Omega}$ is the number of neutrons belonging to $dv\, d\vec{\Omega}$ at time t in a volume element dV around the point $\vec{r}$, $\vec{\Omega}$ being a unit vector in the direction of motion, and v the neutron velocity. $N_{nm}(\vec{r}, v\vec{\Omega})$ is the normalized eigenfunction, α_{nm} the eigenvalue for the following Boltzmann Eq.(3), $N^{+}_{nm}(\vec{r}, v\vec{\Omega})$ its adjoint function and $N(\vec{r}, v\vec{\Omega}, 0)$ the injected pulsed neutron density.

$$v\vec{\Omega} \cdot \operatorname{grad} N_{nm} + [-\alpha_{nm} + v(\Sigma_a + \Sigma_s)] N_{nm}$$

$$= \iiint N_{nm}(\vec{r}, v', \vec{\Omega}') \left\{ \frac{\nu \Sigma_f(v')}{4\pi} \left[(1-\beta) X_p(v) + \sum_{i=1}^{6} \frac{\lambda_i \beta_i X_i(v)}{\lambda_i - \alpha_{nm}} \right] \right. \tag{3}$$

$$\left. + \Sigma_s(v'\vec{\Omega}' \to v\vec{\Omega}) \right\} dv'\, d\vec{\Omega}'$$

where Σ_a is the macroscopic absorption cross-section, Σ_s the scattering cross-section, $\Sigma_s(v'\vec{\Omega}' \to v\vec{\Omega})$ the scattering cross-section for neutrons scattered from $dv'\, d\vec{\Omega}'$ to $dv\, d\vec{\Omega}$ and Σ_f the fission cross-section. $X_p(E)$ is the prompt fission spectrum, $X_i(E)$ the delayed neutron spectrum, ν the yield of neutrons per fission and β and β_i the delayed neutron fraction and that of the i-th group of precursors, respectively. Subscripts n and m indicate n-th

spatial and m-th energetic harmonic modes. The boundary condition is that $N_{nm}(\vec{r}, v\vec{\Omega})$ is a continuous function of $\vec{r}$ at the inner interface and equals zero on the free surface for all $\vec{\Omega}$ entering the system.

It must be noted that the right side of Eq.(1) includes the modes associated with the delayed neutrons, but those modes are functions varying so slowly with time that they are observed as constant background in almost every pulsed neutron experiment. Thus discussions about those modes can be neglected here. It must be proved that α_{00} can be measured free from spatial and energetic harmonic contamination. Some numerical investigations revealed that the ratio of the spatial harmonic decay constant α_{ij} to the fundamental decay constant α_{00} became smaller with increasing subcriticality. For cases when the multiplying systems were made subcritical by removing fuel materials, the ratio of each mode still remained larger than those in a pure moderator system. This would indicate easier separation of harmonic contamination in pulsed experiments with a subcritical system than in pulsed experiments with a pure moderator system, for instance diffusion coefficient measurements.

As for the experimental procedure, some methods have been developed to find α_{00} more precisely from the response of the detectors. One of these is the Fourier-transform method by which the component of the fundamental mode can be eliminated by Fourier-transforming to the response of the detectors located at different positions in the system. The other is the multimode fitting method, by which the component of the fundamental mode can be eliminated by fitting the response of a single counter to the sum of the fundamental mode and higher harmonic modes.

Accompanying spatial harmonics, there exists an energetically higher mode $N_{om}(\vec{r}, v\vec{\Omega})$ which has no spatial mode, but has m energetic modes. FURUHASHI [9] suggested that neutrons associated with the energetic higher modes cannot be detected by a 1/v counter in the infinite systems. How rapidly do energetically higher modes die out compared with the fundamental one? The inverse of the difference between the α_{00} and α_{01}, the thermalization time constant, is a measure of the speed of neutron thermalization. Some experiments [10] have shown that the thermalization time constant in a fuel containing a graphite system is slightly shorter than that in a pure graphite system, and that the energy which injected neutrons reach asymptotically is higher in the fuel-containing graphite assembly than in the pure graphite assembly. It is well known that the thermalization time constant in the pure moderator system is much shorter than the neutron lifetime in the fuel-containing moderator system. It can be considered that the above arguments are also valid for systems using other types of moderators, e.g. H_2O, D_2O, Be, etc, mainly because thermalization time constants are much shorter than the prompt neutron lifetime in the corresponding systems.

This shows that it is possible to obtain enough statistical data to determine α_{00} before neutrons die away. It is, established in principle, from the above discussion that when enough time elapses after neutron injection, the magnitude of the fundamental mode $N_{00}(\vec{r}, v\vec{\Omega})$ prevails over those of the harmonic modes at any point of the system and for all neutron velocities. Thus, it must be possible to measure α_{00} independently of spatial effects and detector specification. Ambiguity still remains for the case in which a

strong absorber is inserted. The preceding discussion for the determination of α_{00} can be applied to this case, but the harmonic contamination is so complicated and strong in a highly subcritical case that, for general discussion, it cannot be denied that α_{00} is sometimes not measurable, even if experimental endeavours attempt to eliminate the harmonic contamination.

Equation (3) is the same as the critical equation for the fictitious system with, however, the absorption cross-section and fission spectrum replaced by

$$\Sigma_a - \frac{\alpha_{00}}{v} \quad \text{and} \quad X_p(v)(1-\beta)+\sum_i \frac{\lambda_i \beta_i X_i(v)}{\lambda_i - \alpha}$$

When the contribution of the delayed neutron can be neglected in highly subcritical states, the calculational procedure then consists of searching for the value of α_{00} for which the static multiplication factor $k_{eff,s}$ assumes $1/(1-\beta)$, where β is the actual delayed neutron fraction. Thus the numerical method developed for critical mass calculation is almost directly applicable to a solution of Eq. (3). In addition to the conventional multigroup treatment, the value of the effective negative absorption cross-section $-\alpha_{00}/v$ must be evaluated precisely, especially for the thermal group, because this determines the rate of the thermal leakage which is relatively pronounced in the core-diminished, highly subcritical systems. The thermal neutron spectrum by which cross-sections are averaged is preferably calculated space-dependently on the neutron decaying state. Actual calculating methods are described in section 4.

The above discussion contains the fundamental assumption that the Boltzmann equation has a discrete eigenvalue for fundamental modes. The existence of continuous eigenvalues, as the solution of that equation, is now the important problem in reactor theory. The experimental results of present work cannot directly contribute to the discussion of this kind of fundamental and rigorous problem. But if the principle is extended to contain the continuous eigenvalues, it will still be a fairly good approximation for such a small buckling graphite system, in practice, to adopt the value of the measured and calculated α as the measure of subcriticality under the above-mentioned assumption.

3. EXPERIMENTS

Two series of pulsed neutron experiments were made at various subcritical states in SHE, (Semi-Homogeneous Critical Assembly at the Japan Atomic Energy Research Institute [11]). One series of experiments was to prove the spatial and energetic independence of α_{00} at various points in the various subcritical states of SHE-V and SHE-VI under various core configurations (experiment A), and the other was to measure the value of α_{00} for comparison with the calculated value for the core-diminished case in the same SHE-VI with and without control rods in the centre of the core region (experiment B).

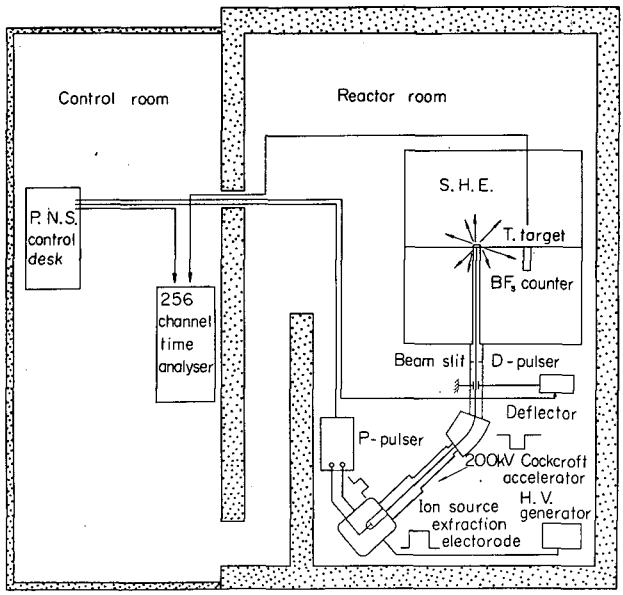


Fig. 1

Experimental arrangement

3.1. *Experimental arrangement (See Fig. 1)*

SHE has a side-reflected cylindrical core consisting of fuel pellets of a homogeneous mixture of 20% enriched UO_2 and graphite grains, a graphite moderator and a graphite side reflector of thickness 80 to 90 cm (See Fig. 2). The overall carbon-U^{235} atomic ratio of the core region is 5378(SHE-V) and 4328(SHE-VI) for experiments A and B.

For experiment A, the degree of subcriticality in SHE was changed either by reducing the core loading (Pattern F), or by charging cadmium strips uniformly to the core (Pattern C), to the inner reflector (Pattern R) or to both (Pattern C + R). Subcriticality is higher with the higher serial number of experiment in the respective patterns. The cadmium strip is 0.6 mm thick, 5 mm wide and 1234 mm in length. The number of strips distributed in SHE at each pattern is shown in Table I.

For experiment B, core configurations were changed in a way similar to pattern F of experiment A. In addition to core-diminished cases, B_4C graphite grey rods or Cd black rods were inserted into the centre of the core region of each configuration. The control rods are 42 mm in diameter; each section is 1250 mm in length. The grey rods, Nos. 1 and 7, contain 0.01 and 0.986 g/cm^3 of B_4C powder in the graphite powder, respectively. The black cadmium rods have a 1-mm thick cadmium plate on the surface of rods.

The experiments were made with the JAERI-TOHIBA compact pulsed neutron source [12], which was operated at 100-μs pulsed width, with a repetition rate of 1/20 to 5 pulses per second. It was intended to get the maximum ratio of the peak intensity of pulsed neutrons to the average intensity of

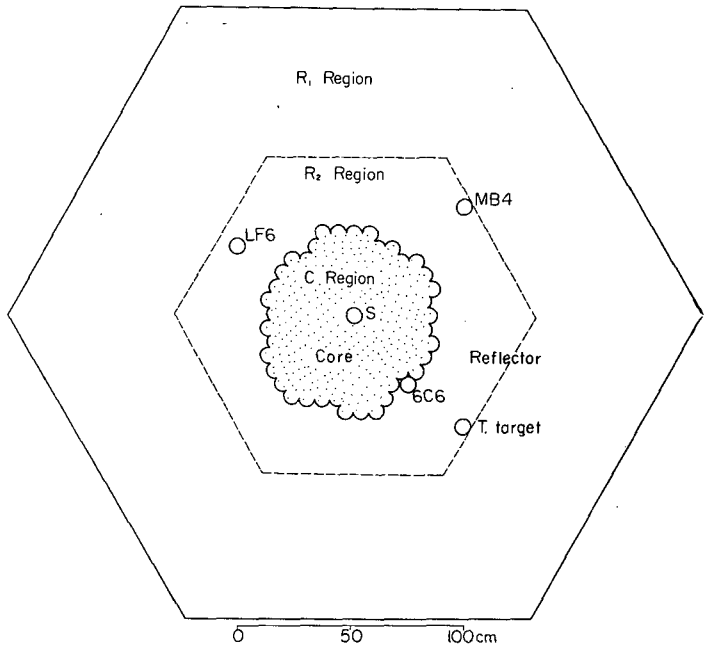


Fig. 2

Cross-sectional view of SHE

background neutrons induced from the operation of the accelerator. Two distinguished designs were adapted to obtain the above-mentioned feature. The pulsing of the probe voltage of a RF ion source was used synchronously with the pulsing of the deflector voltage for the post-accelerated deuteron beam. Another method was the use of a beam analysing magnet for the post-accelerated beam. The above-mentioned ratio obtained was 10^{-5} and this ratio was good enough to measure the α_{00} in the state very close to delayed critical in this experiment, although the assembly had the spontaneous fission neutrons from U^{238}. The tritium target of the pulsed neutron source producing 14-MeV D-T neutrons was placed at the position MC9 (See Fig. 2) in both series of experiments.

The time-analyser part of the measuring system was a 256-channel time analyser consisting of a TMC Model CN-110 and Model 212. The detectors used in the experiments were HITACHI EB 125 M-type BF_3 counters (25 mm in diameter and 300 mm in length), bare or covered with a filter of cadmium 0.6 mm thick or gadolinium 0.05 mm thick.

With each pattern of experiment A, counter positions 6C6 LF6 were selected to emphasize the radial harmonic effect on the prompt neutron decay, other positions, S and MB4, were selected to reject the same harmonic effect (See Fig. 2). Two monitoring BF_3 channels for normalization were provided within all the experiments.

The prompt cadmium ratio, i.e. the thermal-to-epithermal neutron density ratio, in a prompt mode was determined in the same pattern as ex-

TABLE I

PROMPT NEUTRON DECAY CONSTANTS FOR THE VARIOUS CORES

Core number	Core configuration		Number of fuel rods	Number of Cd strips	Measured	Calculated
F-1	SHE-V		222	0	6.5 ± 0.1	
F-2	C/U^{235} = 5378		180	0	42.1 ± 0.8	
F-3	Reflected assembly		120	0	93.4 ± 3.0	
F-4			73	0	140.0 ± 3.0	
C-1	Reflected and poisoned assembly	Cd strips in core region	221	36	98.5 ± 2.0	
C-2			221	72	167.3 ± 3.2	
C-3			221	108	208.0 ± 5.0	
C-4			221	144	219.6 ± 4.4	
C+R-1		Cd strips in core and reflector	221	48	114.0 ± 2.2	
C+R-2			221	96	191.3 ± 5.0	
C+R-4			221	204	289.1 ± 5.3	
R-1		Cd strips in reflector	221	72	125.0 ± 1.0	
R-2			221	144	248.0 ± 2.2	
R-3			221	216	345.0 ± 1.0	
R-4				288	387.0 ± 7.0	
F'-3	SHE-VI C/U^{235} = 4328 Reflected assembly		73	0	124.8 ± 1.3	
C'-2	Reflected and poisoned assembly	Cd strips in core	221	72	140.0 ± 0.8	
C'-4			221	144	211.3 ± 0.9	
C'+R'-2		Cd strips in core and reflector	221	96	90.6 ± 0.6	
C'+R'-4			221	204	225.2 ± 1.0	
R'-2		Cd strips in reflector	221	144	126.7 ± 0.7	
R'-4			221	288	179.5 ± 2.7	
	SHE-VI Reflected assembly		192	0	3.5 ± 0.1	9.5
			190	0	5.8 ± 0.1	
			184	0	12.3 ± 0.1	18.0
			182	0	14.3 ± 0.2	
			170	0	28.0 ± 0.1	31.5
			158	0	38.5 ± 0.2	42.0
			146	0	49.4 ± 0.2	53.0
			122	0	72.2 ± 0.1	74.7
			98	0	95.7 ± 0.3	95.6
			74	0	118.0 ± 0.4	117.0
			50	0	139.0 ± 0.6	138.0
			26	0	160.0 ± 0.6	160.0
			0	0	191.0 ± 4.8	191.5

periment A, taking the ratio from the counting rate of the bare BF_3 counter to that from the cadmium filter-covered one for the prompt decaying state, after background subtraction. In experiment B, the prompt gadolinium ratio was measured in the same manner as the cadmium ratio.

In experiment B the detector was located at the end of fuel channel S for the core containing more than 184 fuel rods, to avoid the counting loss by high neutron intensity. For other smaller cores, the detector position was selected to 6B3 for minimum higher harmonic effects. The prompt gadolinium ratio was measured at the detector position S by a gadolinium-filtered BF_3 counter.

3.2. Experimental results

The data for the thermal neutron density, which decays after the contribution of the higher harmonics becomes negligible (about 10 ms), was fitted to the following formula by the least-squares fitting method using IBM 7044 [13].

$$K_{10}e^{-\alpha_{10}t} + K_{00}e^{-\alpha_{00}t} + \text{constant background.} \tag{4}$$

For this fitting, a correction of 2 μs for the resolution time of the measuring system was made. The delayed mode contribution of background to the decay constant of the prompt mode was neglected in this processing because this did not cause an error of over 1%. Most of the values of α_{00} determined from these experiments have statistical and systematic errors less than 3%, after the correction for the inserted counters, filters and the extention tube of the accelerator had been made.

From experiment A, experimental results on the SHE-V and SHE-VI core using a bare BF_3 counter show that the prompt neutron decay constant of the fundamental mode is uniquely a measurable quantity (after a short transient resulting from the prompt harmonic decay) under all varieties of conditions, such as different core configuration (See Figs.3 and 4). The results using a cadmium-covered BF_3 counter show common values between epicadmium and thermal neutrons under all conditions, but the transient parts of epicadmium neutrons die out more rapidly as compared to thermal neutrons (See Figs.5 and 6). It is moreover to be noted that from the epicadmium neutron decay one can determine α_{00}, free from harmonic contamination, more easily than from thermal neutron decay in very highly subcritical state. Separation of harmonics has been performed for all conditions and it has been proved that the changes in the ratio of harmonic mode to that of the fundamental mode agree in trend with theoretical prediction for each counter position.

In the case of the C pattern, the value of α_{00} showed a distinct tendency to saturate, together with rapidly increasing signs of harmonic contamination as the number of cadmium strips increased (See Fig. 7). At the same time, the prompt cadmium ratio decreased slightly. It can be explained from these experiments that the core region behaves as a pure absorber after a certain number of cadmium strips are added to the core, and that the thermal parts of the reactor neutron remain mostly in the reflector region (See Fig. 8).

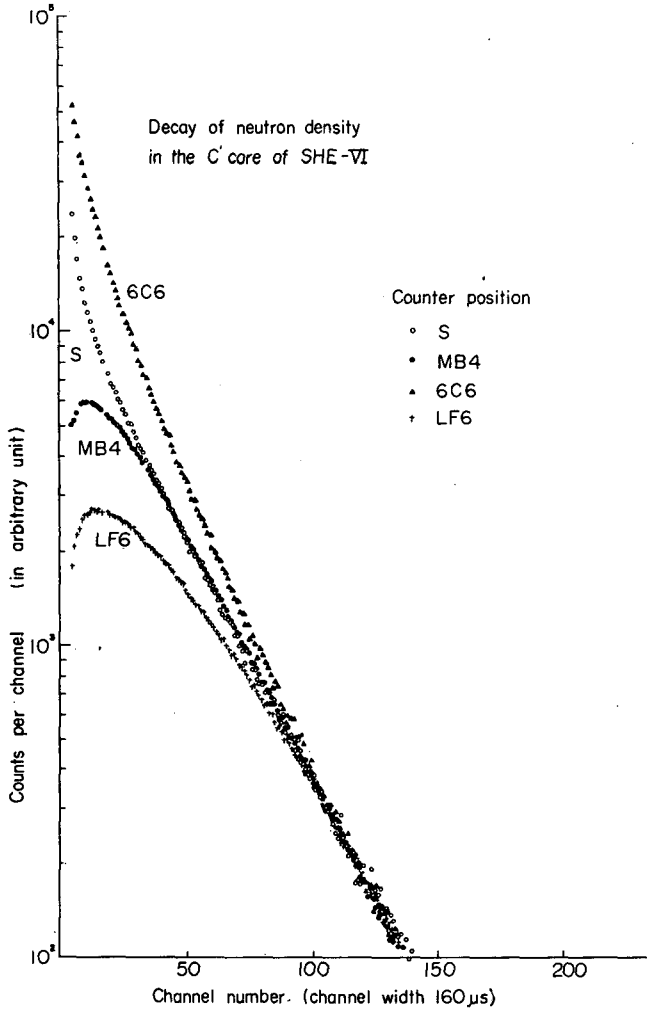


Fig. 3

Time response for the bare BF_3 counter in the core-reduced SHE-VI

In the case of the R pattern, the value of α_{00} showed a slowly saturating tendency and only weak signs of harmonic contamination with similar cadmium addition. No significant change was found in the prompt cadmium ratio. These results show that this operation has an effect of gradually making SHE bare from the viewpoint of neutron multiplication. In the case of the C+R pattern, the tendency and harmonic contamination of α_{00} showed characteristics intermediate between the two preceding cases.

In contrast to the case where cadmium was added, with the F pattern the value of α_{00} increased almost linearly with the number of loaded fuel rods, and a softening tendency of the neutron spectrum was discerned from the fact that the prompt cadmium ratio for the F-3 core was about twice as

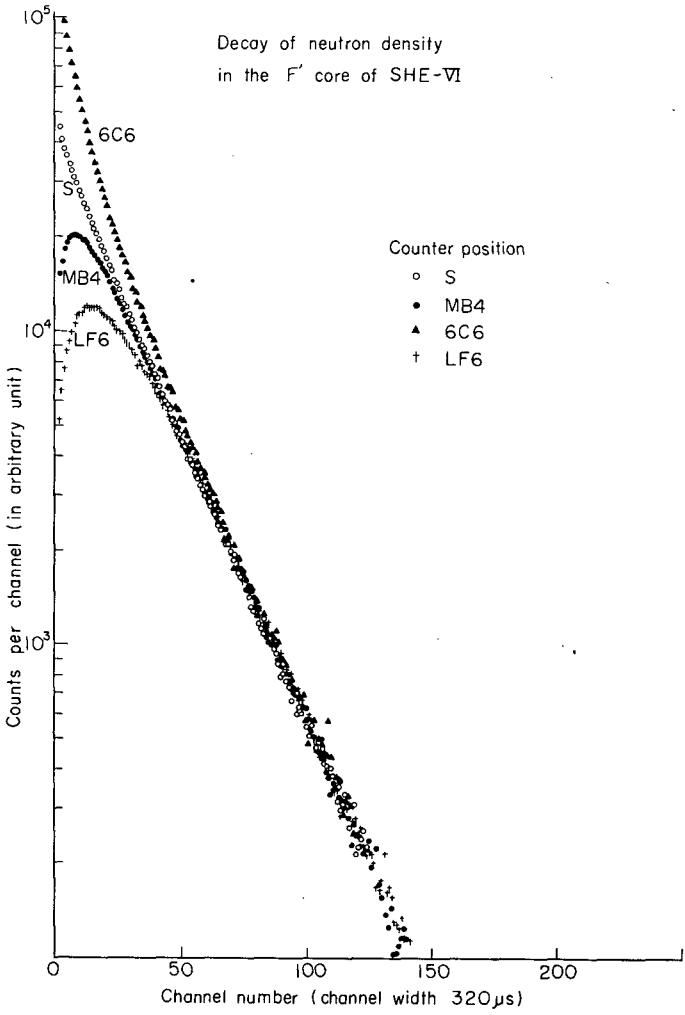


Fig. 4

Time response for the bare BF_3 counter in the core-poisoned SHE-VI

much as the value of the static cadmium ratio at the delayed critical state (See Fig. 8). This tendency is probably caused by fictitious negative thermal absorption $-\alpha_{00}/v$.

From experiment B, the nearly linear relation between the value of α_{00} and the number of loaded fuels was confirmed more precisely. (Fig. 9). A similar tendency was observed in the case with the central control rod. This is not a general relation applicable for other assemblies, but a very interesting and useful result in SHE.

The increment of the decay constant α_{00} when control rods were inserted for the various grades of subcriticality is shown in Fig. 10 along with the calculated values. It was found that those increments from the insertion of

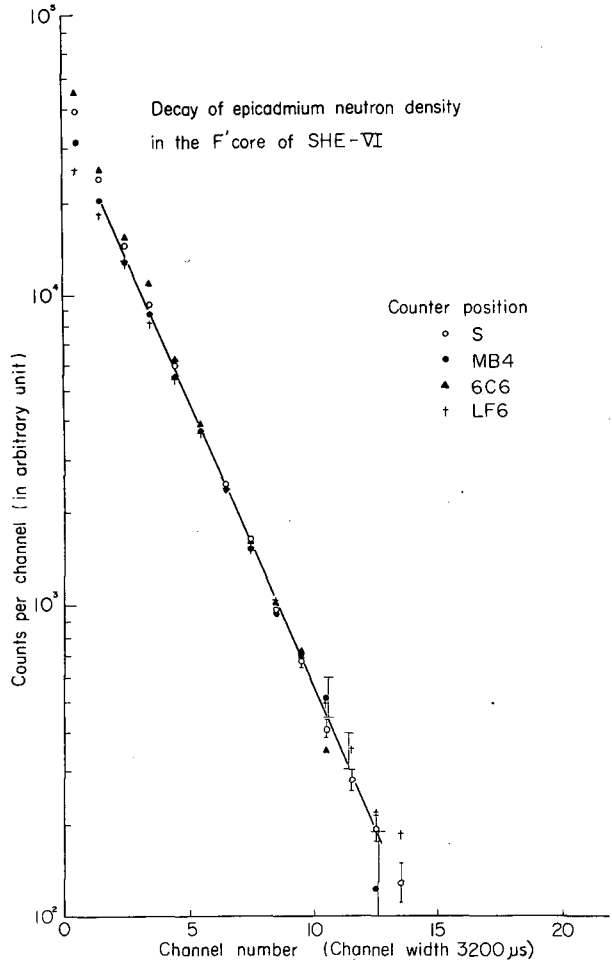


Fig. 5

Time response for the cadmium filter-covered BF_3 counter in the core-reduced SHE-VI

the control rod No. 7 increased most markedly with the increase of loaded fuel numbers.

The prompt gadolinium ratios show another interesting result, namely that the ratio does not change much in the range from the critical mass to half that value: in other words, the neutron spectrum change of the prompt mode is not so distinguished in this range. But distinguished changes appeared in very highly subcritical states (See Fig. 9). The time-dependent prompt gadolinium ratio was also measured, by taking the ratio of the counting rate from the bare BF_3 counter to that from the gadolinium filter-covered BF_3 counter. The results show that after pulsed neutron injection the ratio was established in 3 to 4 ms in a pure graphite system, 2 to 3 ms in the 13 fuel rods system, and in less time in the state containing more than 13 fuel

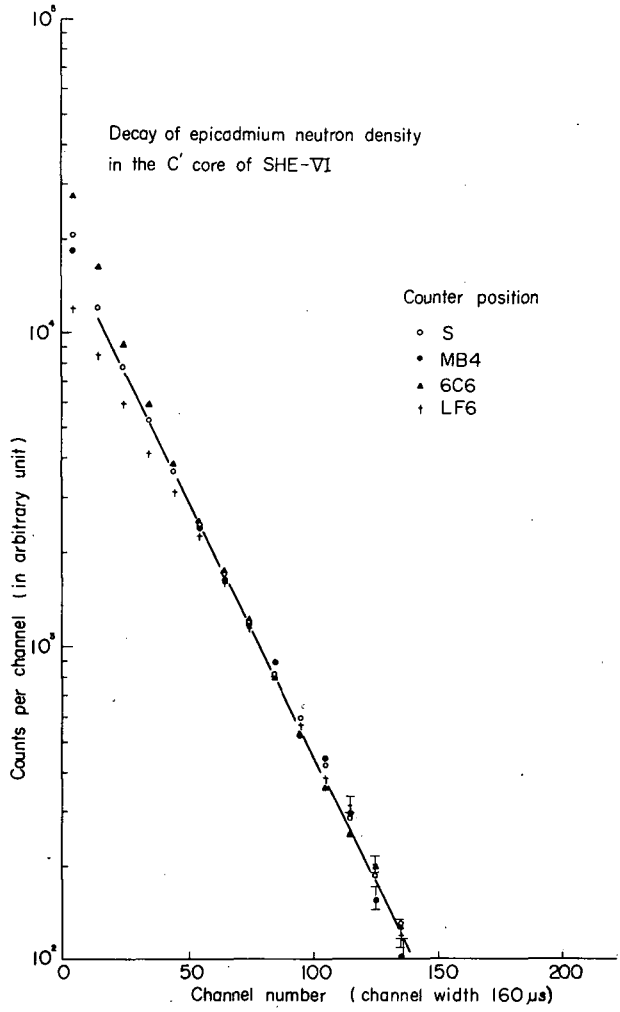


Fig. 6

Time response for the cadmium filter-covered BF_3 counter in the core-poisoned SHE-VI

rods. Then the determination of α_{00} by elimination of the error resulting from the neutron spectrum transient of the prompt mode can be made automatically at the same time as the elimination of the spatial harmonic contamination in this experiment.

4. CALCULATION

In the graphite-moderated system, the decay constant α_{00} is most precisely obtainable as an eigenvalue for the Boltzmann Eq. (3). In the present work, two methods of calculation were adopted. One of them is the multi-

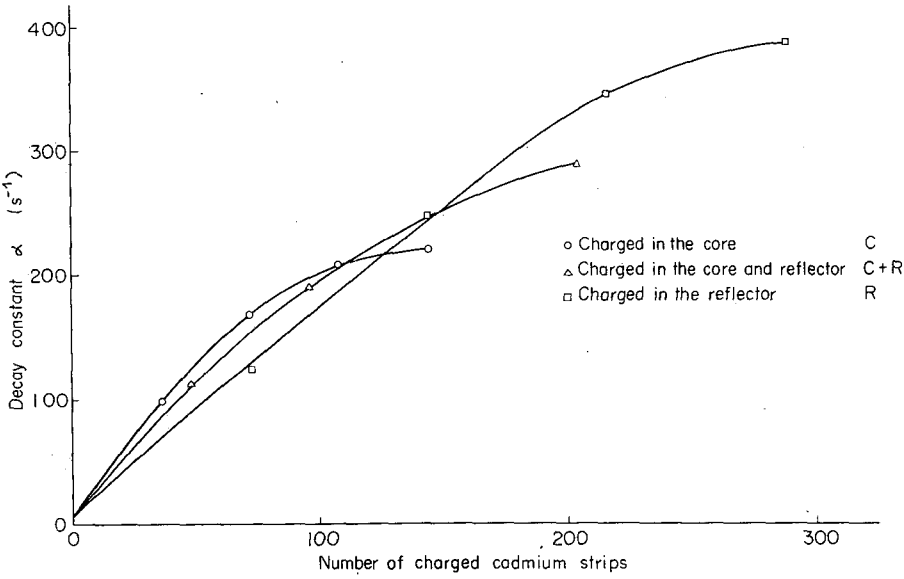


Fig. 7

Prompt neutron decay constant versus number of the loaded cadmium strips in SHE-V

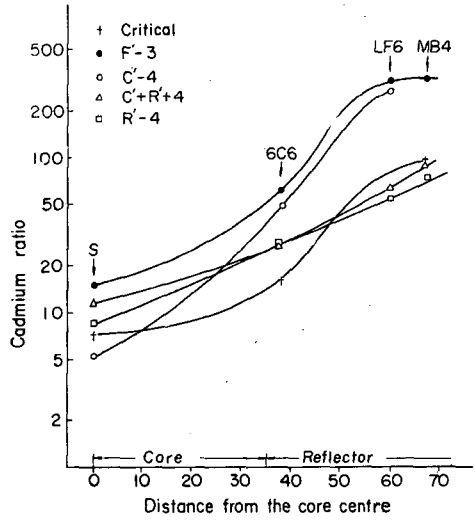


Fig. 8

Prompt cadmium ratio in the highly subcritical SHE-V

group P_1 equation which was solved numerically using the code MEID-P_1 (one-dimensional, 34-group and multiregion, P_1 approximation code) [14] for the core-diminished case of experiment B. In this calculation, the contribution of delayed neutrons was neglected.

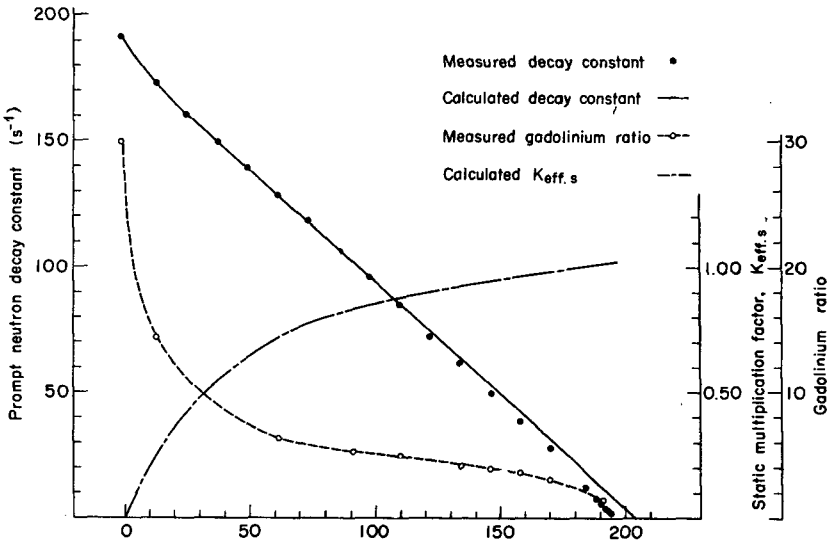


Fig. 9

Prompt neutron decay constant versus number of the loaded fuel rods in SHE-VI

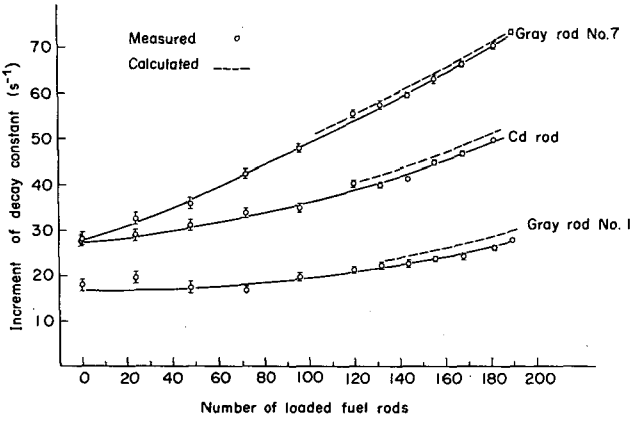


Fig. 10

Increment of prompt neutron decay constant when control rods are inserted in SHE-VI

In the calculational procedure, space dependence of thermal and fast neutron spectra was included in the following manner. The whole region was divided into a core and three reflector regions, and for each region thermal constants of the infinite systems were specified. In the case of the pure moderator system, Maxwellian-weighted thermal cross-sections were used. Critical experiments performed independently of the pulsed experiment proved that the above calculational method and input data gave a static multiplication factor $k_{eff,s}$ within an error of 1%.

Calculated decay constants α_{00} for various grades of subcriticality in

the case of the diminished core are shown in Fig. 9 and Table I, together with the measured values of α_{00}. Calculated values of α_{00} by the 34-group model agree well with the experimental values over the entire range of subcriticality. The correction to the epithermal neutron spectrum in decaying modes is automatically included in the calculational procedure. The spectrum correction for the decaying state in the thermal group is not made in these calculations. The error from thermal spectrum softening is estimated to be within 1.5% in the range of $\alpha < 100$. For the very small core, the P_1 model is not expected to be a good approximation, and the thermal constants of the infinite system are also used for the small core. In spite of those treatments, the results of calculation showed a satisfactory agreement with experimental values for the small core in the present work and a tendency toward slightly poor agreement in the system close to the delayed-critical state.

The value of $k_{eff,s}$ was also calculated by the usual method using the same code for the comparison between α_{00} and $k_{eff,s}$ (See Fig. 9).

For the case in which a strong absorber is inserted, the numerical calculation by the transport treatment is necessary, because the changes of neutron flux are so large near the strong absorber that the diffusion model is not valid in this region.

In the present work, the calculation for the case in which control rods are inserted is made by using the SNACK-I code [15] based on the S_4 approximation, (9-group, 5-region). The $k_{eff,s}$ was also calculated by GSN-2C code [16] (S_4 approximation, 9-group, 5-region).

Macroscopic cross-sections for fast 8-groups by the SNACK-I code were calculated as average values from the 63-groups by the MEID-P_1 code (age-diffusion approximation, 63-groups) [17-18]. $<1/v>_{1\text{ to }8}$ was calculated by the average spectrum MEID-62 group, and $<1/v>_9$ is adopted as the same value of the MEID-P_1 case for the core and the reflector. In the above calculations, using the SNACK-I code, the contributions of the delayed neutrons were neglected. The results of the calculation showed a fairly good agreement with the experimental increment values (See Fig. 10). A calculation for α_c, prompt neutron decay constant at delayed critical state, was performed, using the SNACK-I code, with a result of 5.8. This value showed a fairly good agreement with the experimental result of 6.1 ± 0.2.

5. DISCUSSION AND CONCLUSION

After all investigations about the concept of determining subcriticality, it is concluded that the prompt neutron decay constant α_{00} of the fundamental mode has a unique value for a given system, free from spatial dependence and detector specification. Direct comparison was made between accurately measured values of α_{00} and calculated values of α_{00} over a wide range of subcriticality for various core configurations, resulting in fairly good agreement. Such a direct comparison does not prove successful if the usual dynamic or static reactivity concept is used, except near the critical point; this is the most valuable point in the α_{00} concept.

The greatest inconvenience of this concept is that the value itself does not represent a measure of the distance from the critical point, so that in

comparing one reactor with another, the distance from the critical point cannot be discussed only by means of α_{00}. This kind of comparison is easier with the usual reactivity concept. It is, therefore convenient to adopt a reduced subcriticality unit: $\Delta\alpha = (\alpha_{00} - \alpha_c)/\alpha_c$, where α_c is the value of α_{00} at delayed critical. This value is very close to the usual dynamic reactivity near the critical point, although α_c varies with critical core configuration.

If the above-described characteristics of the method for determining α_{00} are used, the following applications can be expected, although further efforts are needed to improve the method of calculation for the complicated cases.

(1) Replacement of the expensive critical experiment by the subcritical pulsed neutron experiment. In some stages of fuel loading in a subcritical system, it is possible to check the code and the nuclear data used in the nuclear design. For example, the critical mass can be predicted accurately from a few measured values of α_{00} for the highly subcritical state.

(2) Prediction of excess reactivity. As compared to the usual critical experiments, a more reliable estimation of large reactivity can be obtained from data extrapolated from the subcritical to supercritical state.

(3) Measurement of reactor physics constants in enclosed systems. Measurements which must be performed outside a system can be used to study nuclear characteristics of high temperature and high pressure in enclosed systems.

ACKNOWLEDGEMENTS

The authors wish to thank Messrs. R. Kurokawa, F. Akino (JAERI) and A. Takahashi (Osaka University) for their co-operation in the experiments and calculations. They would also like to acknowledge their deep appreciation of the useful suggestions given by Dr. K. Inoue (JAERI) and Mr. M. Akanuma (JAERI) for the calculations.

REFERENCES

[1] SIMMONS, B.E. and KING, J.S., Nucl. Sci. Engng 3 (1958) 595-608.
[2] FULTZ, S.C., Nucl. Sci. Engng. 6 (1961) 313-19.
[3] DE SAUSSURE, D. et al., Nucl. Sci. Engng 9 (1961) 291-98.
[4] SUMITA, K. et al., J. atom. Energy Soc. Japan 4 (1962) 825-34.
[5] FRAUDE, A., Nukleonik 4 (1962) 84-94.
[6] GOZANI, T., Nukleonik 5 (1963) 55-62.
[7] SUMITA, K. and KANEKO, Y., J. nucl. Sci. Technol., to be published.
[8] BACH, D.R. et al., Nucl. Sci. Engng 11 (1961) 199-210.
[9] FURUHASHI, A., J. atom. Energy Soc. Japan 4 (1962) 677-84.
[10] KANEKO, Y. et al., Trans. 1964 Ann. Mtg. of Atomic Energy Soc. Japan (1964) 84.
[11] INOUE, K. et al., Rpts. JAERI-4014 (1960) and JAERI-1032 (1962).
[12] SUMITA, K. et al., Trans. of 1961 Nat. nucl. Congr., Tokyo (1961) 141.
[13] AKINO, F. et al., JAERI- Memo 1795 (1963).
[14] KANEKO, Y. et al., Trans. of 1965 Ann. Mtg of Atomic Energy Soc. Japan (1965) E-38.

[15] INOUE, K., to be published, JAERI Rpt.
[16] AKANUMA, M., to be published, JAERI Rpt.
[17] AKANUMA, M., to be published, JAERI Rpt.
[18] INOUE, K., to be published, JAERI Rpt.

ÉTALONNAGE DE BARRES DE CONTRÔLE DANS LES RÉSEAUX URANIUM-NATUREL GRAPHITE

S. FUSTER, M. SAGOT, A. TARABELLA ET H. TELLIER
CENTRE D'ÉTUDES NUCLÉAIRES DE SACLAY,
FRANCE

Abstract — Résumé — Аннотация — Resumen

CALIBRATION OF CONTROL RODS IN NATURAL URANIUM-GRAPHITE LATTICES. Application of the pulsed neutron technique to natural uranium, graphite-moderated lattices raises some problems as regards both experimentation and interpretation. The large amount of fuel results in background due to the numerous spontaneous fissions and necessitates the use of sources which are powerful enough but which do not disturb the lattice. As a result of their large size, graphite reactors, when used as pulsed sources, have spatial harmonics which decrease with constants close to that of the fundamental mode, so that the sources and detectors have to be carefully sited. Neutron lifetime is relatively long and the induced flux falls off sufficiently slowly for the decay of the first delayed neutron groups to be detectable during the analysis. All these problems have been studied in a series of preliminary measurements carried out on the MARIUS experimental critical stack, during which several prototype control rods were calibrated in various lattices. The experiments were subsequently extended to power reactors by measuring the negative reactivity of a number of rod clusters at the EDF2 nuclear power station.

ÉTALONNAGE DE BARRES DE CONTRÔLE DANS LES RÉSEAUX URANIUM NATUREL-GRAPHITE. L'application de la technique des neutrons pulsés aux réseaux à uranium naturel modérés au graphite pose certains problèmes à la fois d'expérimentation et d'interprétation. Le tonnage important de combustible conduit à un bruit de fond dû aux fissions spontanées en nombre élevé, il nécessite l'emploi de sources qui soient suffisamment intenses, mais ne perturbent pas pour autant le réseau: étant donné leurs grandes dimensions, les réacteurs à graphite possèdent en régime impulsionnel des harmoniques spatiaux décroissant avec des constantes proches de celle du mode fondamental, ce qui nécessite un positionnement soigné des sources et des détecteurs. Enfin, la durée de vie des neutrons est relativement longue et le flux induit décroît suffisamment lentement pour que la décroissance des premiers groupes de neutrons retardés soit sensible pendant la durée d'analyse. Tous ces problèmes ont été étudiés au cours d'une série de mesures préliminaires effectuées sur l'empilement critique expérimental MARIUS, expériences au cours desquelles plusieurs barres de contrôle prototypes furent étalonnées dans différents réseaux. Les expériences furent par la suite étendues aux réacteurs de puissance en procédant à la mesure de l'antiréactivité de certains groupes de barres de la centrale nucléaire EDF2.

КАЛИБРОВКА РЕГУЛИРУЮЩИХ СТЕРЖНЕЙ В РЕШЕТКАХ ИЗ ЕСТЕСТВЕННОГО УРАН-ГРАФИТА. В результате применения метода импульсных нейтронов к решеткам на природном уране с графитовыми замедлителями возникают некоторые проблемы, которые одновременно носят характер эксперимента и интерпретации. Значительный тоннаж топлива приводит к возникновению фонового шума, который проявляется в результате самопроизвольного деления в большом количестве, а это заставляет применять достаточно интенсивные источники, но без существенных возмещений в самой решетке; графитовые реакторы с учетом их больших размеров обладают на импульсном режиме пространственными гармониками, которые уменьшаются с постоянными, близкими к постоянной основной гармоники, что обусловливает необходимость в тщательно выбранном расположении источников и детекторов. Наконец, время жизни нейтронов является относительно продолжительным, и поэтому поток спадает достаточно медленно для того, чтобы распад первых групп запаздывающих нейтронов оказывал влияние во время проведения анализа. Все эти проблемы были изучены при проведении серии предварительных измерений, осуществленных на экспериментальной критической загрузке реактора MARIUS. Во время этих опытов несколько прототипных регулирующих стержней были калиброваны в различных решетках. Затем опыты были перенесены на энергетические реакторы, когда были проведены измерения компенсирующей способности определенных групп стержней на ядерной электростанции EDF 2.

CALIBRACION DE BARRAS DE CONTROL EN RETICULADOS DE URANIO NATURAL-GRAFITO. El empleo de la técnica de los neutrones pulsados para estudiar los reticulados de uranio natural moderados por grafito plantea ciertos problemas, tanto experimentales como de interpretación. La presencia de varias toneladas de combustible ocasiona cierto ruido de fondo, debido al elevado número de fisiones espontáneas que se producen, lo que exige el empleo de fuentes de suficiente intensidad sin que por ello se introduzcan perturbaciones en el reticulado. Dadas sus grandes dimensiones, los reactores moderados por grafito presentan, al funcionar en régimen de impulsos, armónicos espaciales que decrecen con constantes próximas a la del modo fundamental, lo que obliga a elegir cuidadosamente la posición de las fuentes y de los detectores. Por último, la vida media de los neutrones es relativamente larga y el flujo inducido disminuye con suficiente lentitud para que el decrecimiento de los primeros grupos de neutrones retardados pueda percibirse durante todo el análisis. Los autores han estudiado todos estos problemas en el curso de una serie de mediciones preliminares efectuadas en el conjunto crítico experimental MARIUS, durante las cuales se calibraron en diversos reticulados varias barras de control empleadas como prototipo. Estos experimentos se ampliaron seguidamente a los reactores de potencia, procediéndose a la medición de la antirreactividad de ciertos grupos de barras en la central nucleoeléctrica EDF2.

1. INTRODUCTION

Au nombre des problèmes qui se posent aux physiciens chargés des projets de réacteurs, on peut citer le choix des barres de contrôle dont la distribution, le nombre et la position dans le cœur ont de notables conséquences sur la construction, le fonctionnement et la sûreté de l'installation. Aussi a-t-on souvent recours à l'expérience lorsque les méthodes de calcul ne sont pas jugées suffisantes pour déterminer ce choix.

En France, les études expérimentales de la filière uranium naturel-graphite sont principalement menées sur l'empilement critique froid MARIUS et plus récemment sur l'empilement chaud CÉSAR. En outre, au cours des démarrages des centrales de puissance, des expériences systématiques ont permis de mesurer l'efficacité de l'ensemble des barres ainsi que des groupes spécialisés (pilotage, compensation, sécurité).

Parmi les techniques employées, la méthode de pulsation, qui a été progressivement appliquée à presque tous les types de réacteurs, n'a guère tenté les expérimentateurs de la filière uranium naturel - graphite, ceci pour plusieurs raisons:

- Les conditions d'application de cette méthode sont assez défavorables. Ces réacteurs sont de grandes dimensions. Il en résulte que certains harmoniques spatiaux ont une antiréactivité voisine de celle du fondamental et s'éteignent difficilement. Le temps de vie des neutrons prompts ayant d'autre part une valeur relativement élevée, il est nécessaire de tenir compte de l'évolution des neutrons différés durant la période analysée. Ces conditions se rencontrent de la même manière dans les réacteurs à eau lourde [1, 2]. Enfin, le flux dû aux fissions spontanées est élevé en raison de la masse d'uranium importante présente dans le milieu. Pour observer la réponse impulsionnelle du réacteur dans de bonnes conditions, il est donc nécessaire de disposer de sources intenses.

- Les installations disponibles sont le plus souvent des réacteurs de production sur lesquels on trouve peu de dispositifs expérimentaux (canaux de mesure, voies d'accès). D'autre part le temps d'expérimentation concédé au physicien est très réduit.

- Enfin, on peut en général introduire de l'air à pression variable dans les caissons de ces réacteurs. Cette méthode d'empoisonnement à l'air per-

met de déterminer simplement, par mesure critique, la majeure partie des efficacités recherchées des barres, ce qui semble diminuer a priori l'intérêt des mesures sous-critiques en général moins précises.

Cependant, la méthode de pulsation appliquée à ces réacteurs peut donner des résultats intéressants. Outre la détermination de β/θ, elle permet l'étalonnage des groupements de barres dont l'efficacité ne peut être atteinte par la méthode d'empoisonnement à l'air: c'est le cas de toutes les configurations sous-critiques à la pression atmosphérique. En particulier, l'antiréactivité «toutes barres basses» est un paramètre important tant du point de vue de la sûreté que pour la vérification expérimentale des calculs théoriques.

Avant de tenter une application de la méthode à la centrale nucléaire EDF2 de Chinon, nous avons voulu faire une série d'expériences sur l'empilement critique expérimental MARIUS où le temps nous était moins compté.

Nous relatons ici les résultats obtenus et les difficultés rencontrées.

2. MÉTHODE

2.1. Principe

Suivant une méthode désormais classique, nous déterminons tout d'abord la constante de décroissance des neutrons prompts α selon le mode fondamental de leur distribution spatiale pour des états du réacteur dont on connaît l'antiréactivité:

$$\alpha = -\frac{\rho_0 - \beta}{\theta_c}, \qquad \alpha > 0. \tag{1}$$

ρ_0 est l'antiréactivité du mode fondamental $\rho_0 = \frac{k_{eff} - 1}{k_{eff}}$; $\beta = \sum_{i=1}^{n} \beta_i$. β_i est la fraction effective des neutrons retardés émis avec la constante de décroissance λ_i. Nous tenons compte dans le calcul du recyclage rapide dans le ^{238}U et du coefficient d'importance dû à la faible énergie d'émission des neutrons [3]. θ_c est le temps de vie des neutrons dans le réacteur exactement critique.

En comparant ces valeurs de α avec celles que l'on obtient en pulsant le réacteur contenant des éléments absorbants d'efficacité inconnue, on peut déduire leur antiréactivité.

L'équation (1) suppose que la relation

$$\theta = \theta_c \cdot k_{eff} \tag{2}$$

est exacte. θ est le temps de vie des neutrons dans le milieu dont le facteur de multiplication est k_{eff}.

La relation (2) n'est rigoureuse (dans la théorie à un groupe) que pour un milieu multiplicateur homogène (ce qui est le cas d'un réseau empoisonné de façon uniforme ou celui d'un milieu dont on fait varier les dimensions géométriques). Nous avons cependant admis qu'elle était encore vérifiée

dans le cas où l'on ne s'écartait pas trop de ces conditions. Lorsqu'il n'en était pas ainsi nous avons été amenés à faire des corrections que nous décrirons ci-dessous.

2.2. Influence des neutrons retardés

Dans les milieux étudiés, l'hypothèse de la constance des neutrons différés n'est pas suffisante. Les temps d'analyse peuvent atteindre 0,7 s, les émetteurs de neutrons retardés peuvent donc décroître de façon significative durant cette période, au moins en ce qui concerne les plus rapides.

La réponse impulsionnelle du milieu multiplicateur à une seule émission très brève de neutrons, que nous supposons pour l'instant répartie suivant le fondamental spatial, s'écrit pour $t > 0$

$$n(t) = \sum_{j=0}^{n} a_j \exp(-\omega_j t) + n_f . \tag{3}$$

$n(t)$ est la densité neutronique au temps t après l'impulsion,
n_f la densité neutronique constante due aux fissions spontanées.
Les $-\omega_j$ sont les racines de l'équation de Nordheim

$$\rho_0 = s\theta_c + s\sum_{i=1}^{n} \frac{\beta_i}{s+\lambda_i} . \tag{4}$$

Pour les antiréactivités élevées
- ω_0 est voisin de α,
- les ω_j sont peu différents des λ_i $(i = j)$.

Pour des antiréactivités faibles (quelques centaines de pcm par exemple) elles diffèrent plus ou moins de ces valeurs. Ceci est surtout important pour le couple ω_0, α; nous décrirons ci-dessous la correction permettant de passer de l'un à l'autre. D'une façon générale on a

$$\sum_{i=1}^{n} \lambda_i + \alpha = \sum_{j=0}^{n} \omega_j .$$

Les amplitudes a_j ont pour expression

$$a_j = S_0 \frac{\theta_c}{\theta_c + \sum_{i=1}^{n} \frac{\beta_i \lambda_i}{(\lambda_i - \omega_j)^2}} . \tag{5}$$

S_0 est l'amplitude du terme source suivant le mode fondamental (la suite des fonctions propres représentant chaque mode harmonique étant supposée orthonormée).

On montre que

$$\sum_{j=0}^{n} a_j = S_0.$$

Lorsque la pulsation est effectuée de façon récurrente, nous tenons compte de l'empilement des termes exponentiels en substituant aux a_j les termes

$$A_j = a_j \left[\frac{1}{1 - \exp(-\omega_j T)} - \frac{1}{N} \frac{\exp(-\omega_j T)[1 - \exp(-N\omega_j T)]}{[1 - \exp(-\omega_j T)]^2} \right],$$

T étant la période de récurrence, et N le nombre de cycles observés. Nous supposons qu'aucune pulsation n'a précédé la période d'enregistrement.

Le principe de notre dépouillement consiste à soustraire de la densité neutronique observée n(t) la somme des termes

$$\sum_{j=1}^{n} A_j \exp(-\omega_j t) \tag{6}$$

à décroissance lente, que nous calculons en utilisant

- les constantes connues des émetteurs différés,
- des valeurs approchées de l'amplitude A_0, du temps de vie θ_c et de l'antiréactivité. Un processus d'itération nous permet, bien entendu, un ajustement de ces données.

Nous isolons ainsi dans les valeurs expérimentales les termes

$$A_0 \exp(-\omega_0 t) + n_f.$$

Un programme de moindres carrés nous permet ensuite d'optimiser les valeurs de A_0, ω_0 et n_f.

Signalons ici que, dans un but de simplification, nous n'avons fait intervenir dans le calcul de (6) que deux groupes de neutrons différés, ceux dont les constantes de décroissance sont les plus élevées. Nous avons regroupé les constantes propres à ^{235}U et à ^{238}U. Les groupes que nous négligeons ont donc au maximum un λ de 0,3 s^{-1} [4]. Nous pensons néanmoins qu'il est préférable de faire intervenir tous les groupes d'émetteurs différés dans ce calcul; un programme mécanographique destiné à en tenir compte est en cours d'élaboration.

Pour des états peu sous-critiques, comme nous le signalons ci-dessus, ω_0 et α diffèrent l'un de l'autre. Nous utilisons les relations ci-dessous pour faire les corrections utiles

$$\alpha = \frac{\omega_0}{1 - \frac{1}{\rho_0 - \beta} \sum_{i=1}^{n} \frac{\beta_i \lambda_i}{\omega_0 - \lambda_i}}, \tag{7}$$

$$\alpha = \omega_0 - \frac{1}{\theta_c} \sum_{i=1}^{n} \frac{\beta_i \lambda_i}{\omega_0 - \lambda_i} \cdot \qquad (8)$$

Lorsque l'antiréactivité est connue, la relation (7) est applicable. Lors de l'étalonnage des éléments de contrôle, la réactivité est inconnue mais le temps de vie a déjà été déterminé et on peut utiliser la relation (8). Dans les calculs faits avec ces formulations, tous les émetteurs différés ont été pris en compte.

2.3. Problèmes posés par les harmoniques spatiaux

Si la fin de la décroissance est très influencée par les neutrons différés, le début en est perturbé par la présence d'harmoniques spatiaux traduisant les phénomènes de propagation de l'onde neutronique issue de la source.

On sait que la cinétique de chaque mode harmonique est semblable à celle du fondamental. Les termes que l'on doit modifier dans les expressions écrites sont l'antiréactivité, qui devient celle de l'harmonique considéré, ainsi que l'amplitude du terme source qui lui est rattaché. La répartition des neutrons thermiques naissants issus de la source étant difficile à prévoir, le calcul a priori de ces termes à partir de considérations géométriques nous paraît hasardeux.

Nous avons recherché la solution de ce problème en implantant les sources de façon à exciter au minimum les harmoniques les moins sous-critiques (harmonique 1 azimutal, 2 axial par exemple). Nous décrivons pour chaque expérience les précautions prises.

3. DISPOSITIF EXPÉRIMENTAL

3.1. Sources de neutrons

Les sources utilisées ont été fabriquées au CEA, où elles sont à peu près exclusivement adoptées pour l'étude des milieux multiplicateurs thermiques. Elles utilisent la réaction (d, t) et émettent des neutrons de 14 MeV [5, 6].

Nous avons utilisé quatre sources de ce type sur MARIUS (diamètre 98 mm); sur EDF2 un progrès de fabrication nous a permis d'employer un modèle de diamètre plus réduit (68 mm), le nombre des sources étant de trois. Dans tous les cas elles étaient déclenchées simultanément. L'émission de chaque unité est de quelques millions de neutrons par impulsion.

3.2. Matériel de détection

Les détecteurs utilisés sont des compteurs à BF_3. L'électronique qui leur est associée a fait l'objet d'études suivies qui ont permis d'abaisser considérablement les temps de résolution (4 μs à MARIUS, 1 μs à EDF2). Elle est maintenant entièrement transistorisée et permet de réaliser le mélange des impulsions issues de plusieurs compteurs.

3.3. Sélecteur

Nous avons utilisé un sélecteur à 256 canaux de fabrication TMC équipé de son tiroir standard «neutrons pulsés». Les organes de sortie permettent la perforation d'une bande qui facilite le calcul mécanographique ultérieur.

4. EXPÉRIENCES RÉALISÉES SUR MARIUS

4.1. Description du réacteur et des réseaux étudiés

MARIUS est un ensemble critique modéré au graphite qui utilise comme combustible des barreaux d'uranium naturel sous forme de cartouches gainées du type G2 [7]. L'empilement à axe horizontal est un cylindre de 6 m de diamètre et de 5,80 m de longueur. Il comprenait à l'époque des expériences deux zones distinctes: une zone centrale carrée de 144 canaux au pas de 22,4 cm et une zone périphérique au pas de 19,2 cm. Le nombre de canaux chargés de la zone périphérique est variable suivant la composition de la zone centrale. Le cœur est entouré d'un réflecteur de graphite massif correspondant aux canaux non chargés en uranium et remplis par des rondins de graphite. La zone périphérique est chargée par des cartouches de 31 mm de diamètre dans des canaux de 70 mm de diamètre. 24 canaux correspondant aux angles de la partie centrale sont chargés par des tubes de 29,1 × 45 mm. Les 120 canaux restants ont été chargés de quatre façons différentes (tableau I) et constituèrent ainsi quatre réseaux distincts. Les zones centrale et périphérique comprennent le même nombre de cartouches par canal, l'épaisseur du réflecteur axial est par conséquent uniforme.

TABLEAU I

CHARGEMENT DE LA ZONE CENTRALE ET TAILLE CRITIQUE

Réseau	Diamètre du combustible (mm)	Diamètre du canal (mm)	Nombre de cartouches par canal	Taille critique en nombre de canaux
1	31	70	16	238
2	31	140	16	376
3	31	110	12	373
4	32 canaux Ø 50 autres canaux Ø 31	110	12	433

4.2. Dispositions expérimentales

Quatre sources synchronisées ont été mises en place dans les réflecteurs axiaux, en bout du combustible, dans les canaux les plus proches de l'axe de la pile. Chaque réflecteur recevait deux sources de manière à éliminer au mieux les harmoniques axiaux d'ordre pair au cas où le nombre de neutrons émis par chaque source différerait. Le détecteur était situé contre le cœur dans le plan médian. D'autres positions ont été étudiées pour mettre en évidence les harmoniques axiaux et radiaux afin de choisir les conditions expérimentales permettant d'atténuer au maximum leur effet.

L'antiréactivité due au matériel expérimental varie avec les réseaux étudiés (30 à 60 pcm), elle a été mesurée par divergence et nous en tenons compte dans notre dépouillement.

4.3. Détermination de β et β/θ_c

La détermination de $\alpha(\rho)$ a été faite en pulsant le réacteur déchargé d'un certain nombre de canaux périphériques.

Pour chaque état du chargement, l'antiréactivité a été calculée en utilisant le code RIFIFI [8]. Les longueurs d'extrapolation axiales dans les zones centrale et périphérique qui interviennent dans ce calcul ont été déterminées expérimentalement par des cartes de flux. Cette manière de faire varier l'antiréactivité est moins précise que l'empoisonnement à l'air que nous avons employé sur EDF2, mais c'était la seule accessible.

Il est d'autre part certain que la relation (2) permettant d'écrire α sous la forme

$$-\frac{\rho_0-\beta}{\theta_c}$$

n'est pas satisfaite. En effet, le déchargement périphérique entraîne l'augmentation de l'épaisseur du réflecteur. Le temps de vie des neutrons est de ce fait bien supérieur à ce que la relation (2) ferait prévoir.

Une correction a dû être introduite pour tenter de linéariser la fonction de $\alpha(\rho_0)$. Elle n'est qu'approchée. Nous calculons les temps de vie θ_c dans des milieux ayant la même configuration radiale que ceux que nous étudions mais une longueur les rendant critiques.

Ces temps de vie sont exprimés par

$$\theta_c = \frac{\int_{V_1} \phi_2^* \phi_2 \, d\vec{r}}{\nu\Sigma_f \int_{V_2} \phi_1^* \phi_2 \, d\vec{r}},$$

V_1 = volume du réacteur, V_2 = volume du cœur.

Les flux sont calculés à l'aide du code RIFIFI. θ_{co} étant le temps de vie calculé pour la configuration initiale qui rend le réacteur réellement critique,

$$\alpha_{\text{corrigé}} = \alpha \cdot \frac{\theta_c}{\theta_{co}}.$$

Il serait difficile de justifier rigoureusement cette correction. Il nous semble cependant qu'elle rend compte en grande partie de l'effet perturbateur que nous avons ainsi tenté d'éliminer. Il est néanmoins certain que les variations du temps de vie constituent un point délicat dans l'interprétation de ces expériences.

Pour les quatre réseaux étudiés, les valeurs de ω_0 et de α, les variations relatives des temps de vie et les valeurs de α corrigées sont indiquées dans le tableau II. Chaque valeur de α est obtenue avec une incertitude de 1 à 2%.

Nous avons admis que les α corrigés étaient connus à 3% près.

La figure 1 représente les variations de α corrigé en fonction des antiréactivités calculées. L'extrapolation à zéro de ces droites permet de déterminer β pour chaque réseau. Les résultats sont en bon accord avec les valeurs calculées sauf en ce qui concerne le réseau 2. Dans ce réseau le canal a un diamètre de 140 mm. Les fuites axiales, qui sont très importantes, ont dû être mal interprétées dans le calcul des antiréactivités. Le tableau III fournit les éléments utiles aux comparaisons. Les valeurs expérimentales de α à la criticité ne sont pas en bon accord avec celles qui sont issues du calcul. Le désaccord dépasse les marges d'erreur. Il semble que les temps de vie calculés soient systématiquement trop faibles.

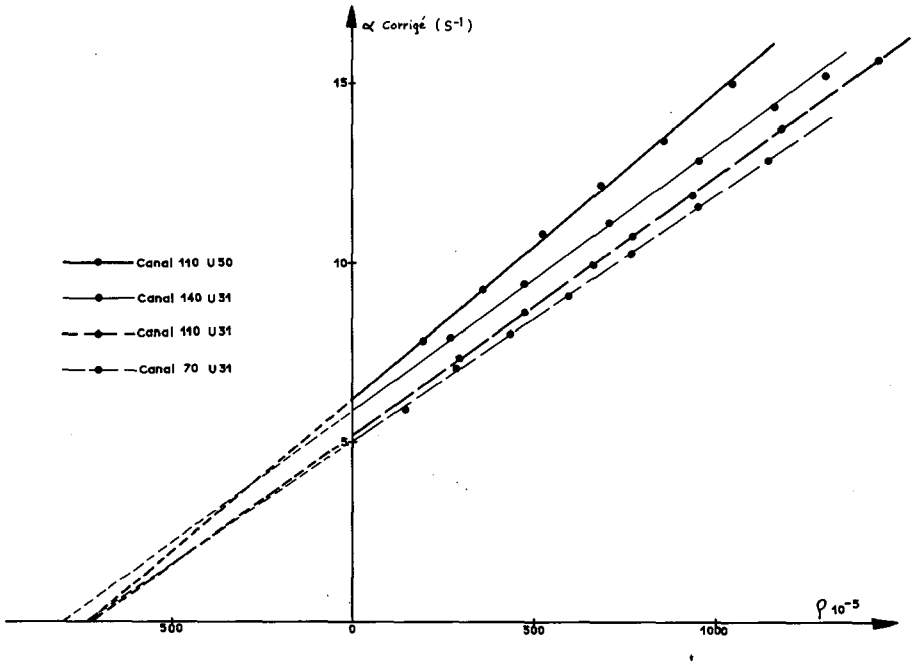


Fig. 1

MARIUS - Etalonnage.

TABLEAU II

APPROCHES SOUS-CRITIQUES

Réseau	Antiréactivité 10^{-5}	ω_o (s^{-1})	α	$\frac{\theta_c}{\theta_{co}}$	$\alpha_{corrigé}$ (s^{-1})
1	144	6,34	5,84	1,0069	5,88
	287	7,36	6,96	1,0141	7,06
	438	8,17	7,83	1,0236	8,01
	599	9,06	8,76	1,0335	9,05
	770	10,08	9,82	1,0441	10,25
	953	11,18	10,95	1,0554	11,56
	1150	12,22	12,01	1,0676	12,82
2	272	8,22	7,82	1,0132	7,92
	477	9,48	9,14	1,0256	9,36
	705	11,00	10,72	1,0368	11,11
	956	12,44	12,20	1,0500	12,81
	1162	13,70	13,49	1,0604	14,30
	1309	14,38	14,18	1,0676	15,14
3	298	7,65	7,24	1,0147	7,35
	474	8,69	8,35	1,0248	8,56
	668	9,90	9,60	1,0359	9,94
	773	10,55	10,28	1,0418	10,71
	939	11,53	11,29	1,0511	11,87
	1182	13,07	12,86	1,0642	13,69
	1450	14,65	14,47	1,0783	15,60
4	198	8,20	7,76	1,0097	7,84
	359	9,46	9,09	1,0181	9,25
	525	10,83	10,52	1,0252	10,78
	684	12,05	11,78	1,0327	12,16
	858	13,10	12,85	1,0406	13,37
	1049	14,51	14,29	1,0487	14,99

TABLEAU III

VALEURS DE β ET DE β/θ_c (MARIUS)

Réseau	Valeurs calculées			Valeurs expérimentales	
	θ_c (μs)	β 10^{-5}	α à la criticité (s^{-1})	β 10^{-5}	α corrigé à la criticité
1	1327	724	5,46	730	5,0 ± 0,2
2	1161	723	6,23	800	5,8 ± 0,2
3	1176	723,3	6,15	715	5,2 ± 0,2
4	1036	723,3	6,98	730	6,2 ± 0,2

4.4. Etalonnage de barres de contrôle

Des mesures de l'efficacité de diverses barres de contrôle prototypes ont été réalisées dans les quatre réseaux. Les barres, placées dans un canal central, soit circulaire d'un diamètre de 70, de 90 ou de 110 mm, soit carré de 80 ou de 98 mm de côté, traversaient l'empilement de part en part, y compris les réflecteurs axiaux. Plusieurs types de barres ont été utilisés: des tubes de carbure de bore d'un diamètre extérieur de 35, 50 et de 75 mm, une barre d'un diamètre de 100 mm dont le gainage extérieur pouvait être soit de l'aluminium soit du fer et dont l'intérieur pouvait être rempli de rondins de graphite. Ont également été étalonnées une barre grise et une barre noire du réacteur EDF1 (de 62 mm de diamètre) et, à titre de comparaison, un tube de cadmium de 0, 8 mm d'épaisseur et de 50 mm de diamètre, et un jeu de cartouches de fer type G2 de 31 mm de diamètre. Pour chaque mesure, la configuration du réseau correspondait, à une fraction de canal près, au chargement critique du réacteur propre. Nous tenons bien entendu compte de cet état initial dans l'élaboration des efficacités mesurées. Des valeurs de α obtenues, on déduit immédiatement l'antiréactivité des absorbants introduits en utilisant les droites de la figure 1.

Pour chaque réseau et chaque géométrie du canal central les résultats des étalonnages sont consignés dans le tableau IV.

La barre de 75 mm de diamètre a été étalonnée dans le réseau 1 pour divers enfoncements relatifs x, les résultats (fig. 2) sont en bon accord avec une loi de variation de la forme

$$\rho = \frac{2\rho M}{\pi} \int_0^x \sin^2 \pi x \, dx.$$

L'examen des résultats obtenus sur MARIUS nous a montré que, sous réserve de quelques précautions expérimentales, la méthode de pulsation fournissait des résultats intéressants. Une campagne de mesure sur EDF2 a donc été décidée, à titre d'essai.

TABLEAU IV

ÉTALONNAGE DE BARRES DE CONTRÔLE
(Antiréactivité exprimée en pcm)

Réseau	Canal 70 U31	Canal 140 U31	Canal 110 U50			Canal 110 U31				
Canal central (dimensions en mm) / Barre (diamètre en mm)	Ø 90	Ø 90	Ø 70	Ø 90	Ø 110	Ø 70	Ø 90	Ø 110	Carré 80	Carré 98
Ø 35	1024	608	-	384	-	-	697	-	708	727
Ø 50	1233	788	-	496	-	-	858	-	872	907
Ø 75	1469	976	-	594	-	-	1068	-	1060	1113
Ø 62 noire	-	924	550	569	599	946	1000	1068	1001	1053
Ø 62 grise	-	314	160	162	215	358	373	373	367	379
Ø 31 Fe	-	-	-	147	-	-	303	-	-	-
Ø 50 Cd	-	696	-	430	-	-	820	-	-	-
Ø 100 Al	-	-	-	-	-	-	-	1322	-	-
Ø 100 Fe	-	-	-	-	751	-	-	1258	-	-
Ø 100 Fe + C	-	-	-	-	749	-	-	1279	-	-

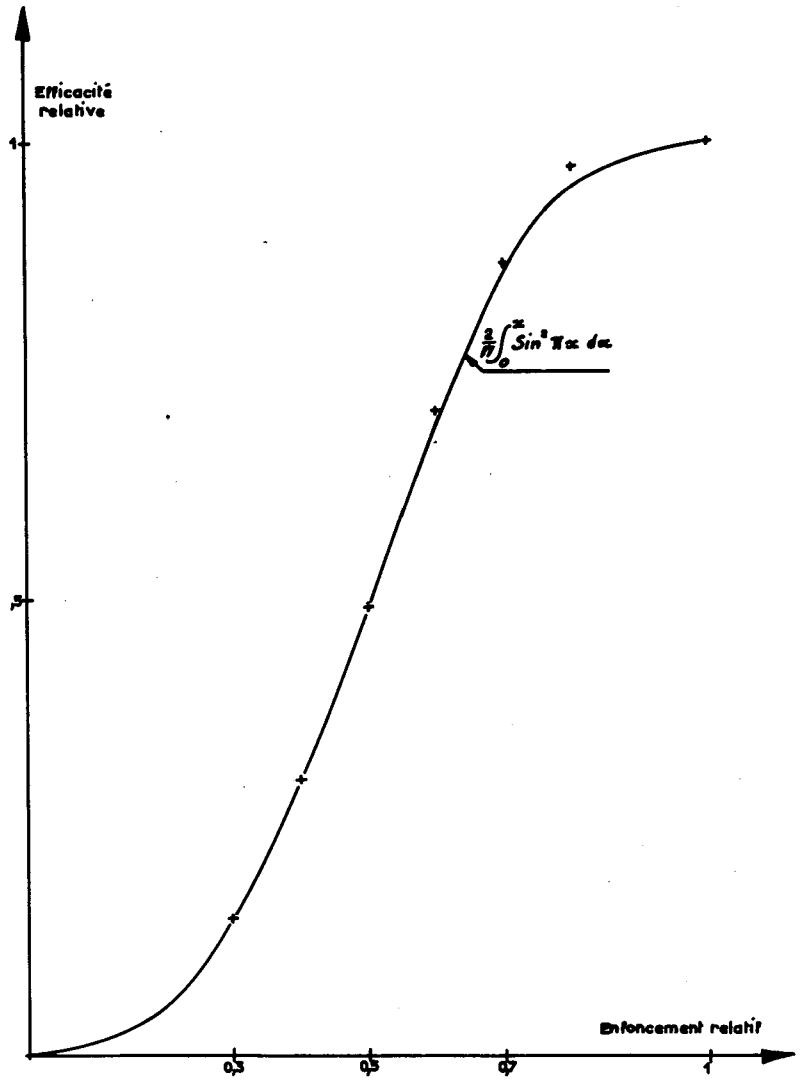


Fig. 2

Etalonnage de la barre Ø 75.

5. EXPÉRIENCES RÉALISÉES SUR EDF2

5.1. Description du milieu multiplicateur EDF2

Nous ne pouvons donner ici qu'une description très succincte.

L'empilement de graphite contenu dans un caisson en acier est cylindrique et vertical. Sa hauteur totale est de 8, 40 m, son rayon de 7, 20 m.

Le milieu actif est un réseau à pas hexagonal de 22,5 cm. Le nombre de cellules est de 2671. Le réflecteur radial a une épaisseur de l'ordre du mètre. Il est partiellement empoisonné par des poteaux métalliques ayant un rôle mécanique (corset). Les canaux chargés de combustible reçoivent 12 cartouches dont la longueur est de 60 cm. Le combustible (uranium naturel + 1% de Mo) est tubulaire (diamètre extérieur: 40 mm; diamètre intérieur: 18 mm).

Le chargement réalisé lors des essais que nous décrivons comprenait plusieurs zones (outre le réflecteur):

- Une zone centrale dite zone 11/12 de 450,62 cm de rayon. Elle comprend 1453 cellules, une cellule sur 12 n'est pas chargée.
- Une zone périphérique dite zone 2/3 de 611 cm de rayon constituée par 1218 cellules, une cellule sur 3 n'est pas chargée.

Dans chaque zone les cellules non chargées d'uranium reçoivent soit des rondins de graphite soit des barres de contrôle. La masse totale de graphite est de 2200 tonnes, celle d'uranium environ 260 tonnes.

Les éléments de contrôle se décomposent comme suit:

- Barres de compensation à court terme: 70 barres noires
- Barres de compensation à long terme: 6 barres grises
- Barres de pilotage: 6 barres grises
- Barres de pilotage spatial: 18 barres en 6 secteurs de 3 barres grises
- Barres de sécurité: 4 barres noires.

La figure 3 montre leur implantation dans le réacteur.

5.2. *Dispositions expérimentales adoptées*

Lors des essais à faible puissance, un certain nombre de puits de mesure avaient été installés de façon provisoire dans le cœur du réacteur. Ils étaient constitués par des tubes de magnésium-zirconium (diamètre intérieur: 100 mm) scellés à leur partie inférieure. Ils permettaient une manipulation relativement aisée du matériel en gardant le réacteur sous pression d'air.

Les trois sources pulsées de neutrons ont été disposées dans le canal central du réacteur en K 05 (fig. 3), la source médiane à mi-hauteur de l'empilement ($z = 0$), les deux autres sources symétriques de celle-ci en $z = \pm 60$ cm.

Les trois compteurs ont été installés dans les puits M 17, M 23 et F 05, ces points sont radialement situés à peu près au nœud de l'harmonique 2 radial du réacteur nu équivalent. Azimutalement ils sont à 120° l'un de l'autre. La cote des compteurs était celle du nœud de l'harmonique 3 axial; c'est-à-dire aux 2/3 de la hauteur de l'empilement à partir du bas.

Le temps d'expérimentation dont nous avons pu disposer (vingt heures environ) ne nous a pas permis d'essayer d'autres dispositions géométriques de notre appareillage.

Les positions adoptées permettent d'éliminer:

- les harmoniques azimutaux,
- les harmoniques 2 et 3 radiaux,
- l'harmonique 2 radial dans la mesure où la complexité du milieu ne déforme pas trop les fonctions propres.

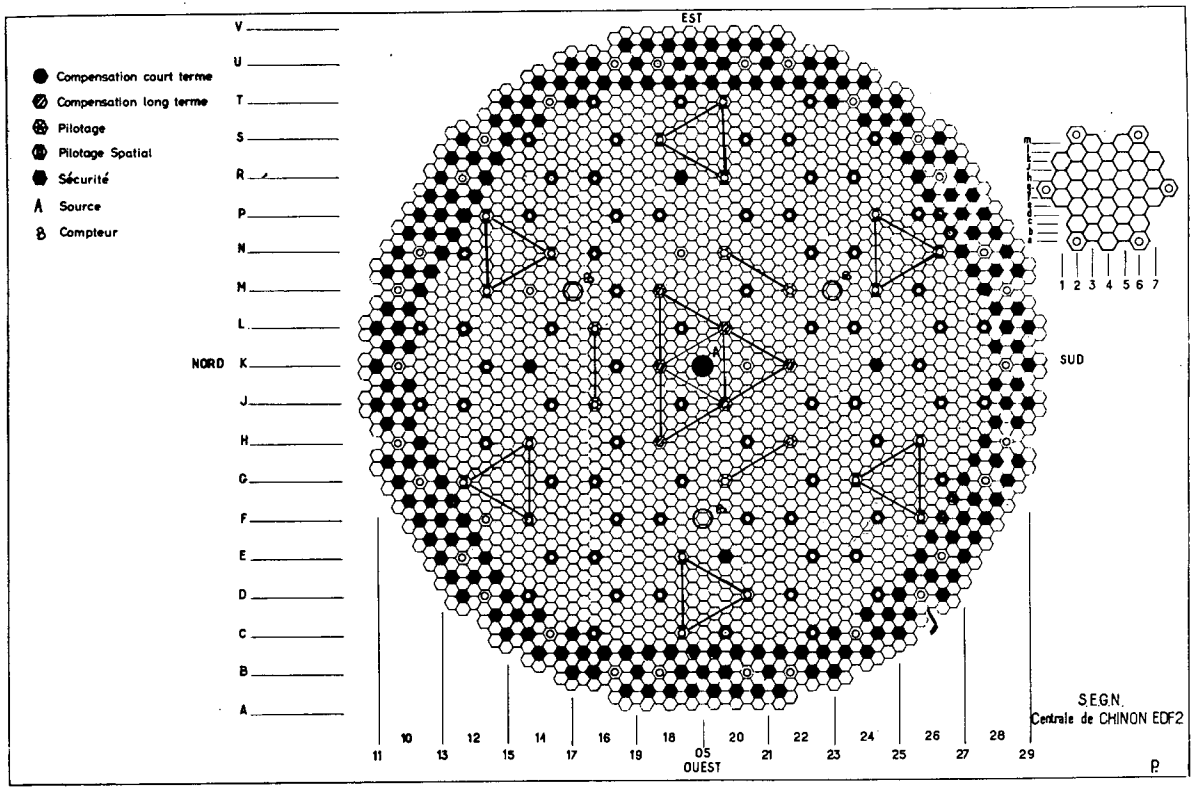


Fig. 3

Implantation des barres de contrôle.

L'antiréactivité due à la présence du matériel expérimental dans le milieu, mesurée par divergences, était de 75 pcm.

5.3. Mesures faites sur le réacteur empoisonné à l'air

La méthode d'empoisonnement à l'air permet d'obtenir très aisément des états sous-critiques bien connus. Le calcul des antiréactivités est immédiat, on a:

$$P = (\text{pression réalisée} - \text{pression critique}) \times \frac{\partial \rho}{\partial \rho}.$$

La pression critique et le terme $\partial\rho/\partial\rho$ sont déterminés expérimentalement par approche sur-critique.

L'ensemble des résultats expérimentaux obtenus sur EDF2 montre que le coefficient de pression $\partial\rho/\partial\rho$ est pratiquement indépendant de la pression et de l'état des barres.

Le tableau V rassemble les résultats obtenus aux diverses pressions étudiées.

Le coefficient de pression était de 527 pcm/b à la température de 40°C, la pression critique de 5,648 b (matériel expérimental en pile). Le milieu étant empoisonné de façon homogène, nous n'avons pas fait de corrections en ce qui concerne le temps de vie θ_c.

La figure 4 est une représentation de ces résultats. La valeur de β que l'on peut en déduire, $\beta = 720 \pm 20$ pcm, est en bon accord avec la valeur calculée $\beta = 709,8$ pcm. Il n'y a donc pas de désaccord significatif dans nos mesures de réactivité (temps de doublement du flux critique et pulsation). La valeur de $\alpha_c = 6,75 \pm 0,2$ s^{-1} est en relativement bon accord avec le calcul (6,38 s^{-1}).

Il aurait été intéressant de dépasser la pression de 9 b qui était malheureusement une limite, à cette température, liée à la tenue mécanique du caisson en acier du réacteur.

TABLEAU V

VALEURS DE α EN FONCTION DE L'ANTIRÉACTIVITÉ (EDF2)

Pression de l'air (b)	Antiréactivité	ω_0 (s^{-1})	α (s^{-1})
6,050	$212 \cdot 10^{-5}$	9,25 ± 0,15	8,85 ± 0,15
6,138	$258 \cdot 10^{-5}$	9,55 ± 0,15	9,16 ± 0,15
7,148	$790 \cdot 10^{-5}$	14,15 ± 0,2	13,9 ± 0,2
8,144	$1315 \cdot 10^{-5}$	19,3 ± 0,4	19,2 ± 0,4
8,946	$1738 \cdot 10^{-5}$	23,2 ± 0,5	23,1 ± 0,5

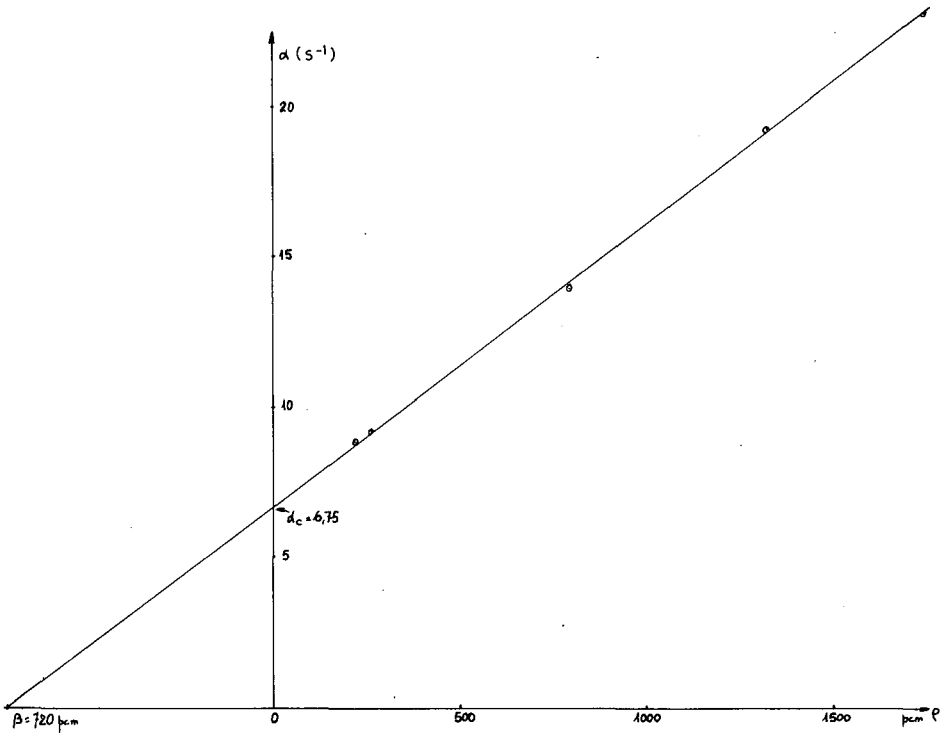


Fig. 4

EDF2-variations de α en fonction de l'antiréactivité.

5.4. Etalonnage des éléments de contrôle

Le peu de temps dont nous disposions ne nous a pas permis de faire un grand nombre de mesures. Nous avons étudié deux groupements:

Groupe des barres de divergence et de sécurité

Il est constitué par les barres de sécurité (R 18, K 14, E 20 et K 24) et les barres dites de divergence durant les essais à faible puissance (J 14, F 16, F 22, P 22 et L 24). Ce lot de barres a été étudié pour recouper une expérience faite par empoisonnement à l'air. L'efficacité déterminée par cette méthode est de 955 ± 15 pcm.

La pulsation a été faite à une pression d'air (5, 788 b) voisine de la pression critique. La valeur de α mesurée est de $16,5 \pm 0,3\ s^{-1}$. L'efficacité déduite de cette mesure est de 965 ± 40 pcm. On voit que l'accord entre les deux méthodes est excellent.

Efficacité de l'ensemble des barres du réacteur

Cette configuration dite « rideau renforcé » comprend toutes les barres à l'exclusion des quatre barres de sécurité.

La mesure se situe dans le domaine des antiréactivités importantes (8 à 10 β). Il est certain que c'est dans ce cas que se présentent le maximum de difficultés, en particulier, en ce qui concerne les harmoniques spatiaux.

La mesure a été faite à deux pressions d'air différentes. Le tableau VI résume les résultats obtenus. Ils sont à comparer avec l'efficacité calculée: 8116 pcm. Les marges d'erreur indiquées tiennent compte

- Des incertitudes dues à l'extrapolation de la droite $\alpha(\rho)$. L'empoisonnement dû à la présence des barres étant quasiment homogène nous pensons que les variations de θ_c peuvent être négligées devant les autres sources d'erreur.
- Des incertitudes propres à la mesure de α. Pour tenter de mettre en évidence des harmoniques spatiaux nous avons systématiquement fait varier le nombre des canaux voisins de l'origine des temps qui étaient susceptibles d'être perturbés. Les retards ainsi introduits à l'analyse sont de 1 à 4 fois la constante de temps $1/\alpha$. Les marges d'erreur indiquées englobent les résultats obtenus. Cette méthode nous a montré que notre calcul de l'évolution lente du bruit de fond dû aux émetteurs retardés devait être perfectionné. Nous pensons aussi que les marges d'erreurs pourraient être réduites si l'évolution de la croissance initiale du flux en fonction des antiréactivités était étudiée.

6. CONCLUSIONS

Les résultats obtenus, sur EDF2 en particulier, montrent que la méthode peut s'appliquer aux réacteurs de production.

Lorsque les antiréactivités à mesurer sont de l'ordre du millier de pcm, on obtient rapidement des résultats avec une précision de 3 à 4%. Le gain de temps réalisé peut justifier une précision un peu moins bonne que celle que l'on obtient en employant la méthode d'empoisonnement à l'air. Pour des antiréactivités plus importantes, la méthode paraît actuellement un peu moins sûre mais il est certain que les grandeurs à mesurer sont difficiles à atteindre même par d'autres méthodes.

TABLEAU VI

EFFICACITÉ DE L'ENSEMBLE DES BARRES

Pression d'air	1,010 b	6,707 b
α mesuré	$58,5 \pm 2\ s^{-1}$	$82 \pm 4\ s^{-1}$
Antiréactivité correspondante	5520 ± 300	8030 ± 500
$(P_c - P) \times \frac{\partial \rho}{\partial \varrho}$	2440 ± 25	-558 ± 6
Efficacité totale	7960 ± 300	7470 ± 500

REMERCIEMENTS

Les expériences effectuées sur le réacteur EDF2 ont été aimablement autorisées par les différents services de l'Electricité de France chargés de la réalisation et l'exploitation des centrales de Chinon, que nous tenons à remercier.

Nous adressons nos compliments à l'équipe des électroniciens du Service des expériences neutroniques pour l'excellent fonctionnement du matériel qui a été mis en œuvre dans les meilleurs délais.

RÉFÉRENCES

[1] KÜCHLE, M., "Pulsed-neutron Measurements on a Heavy Water Reactor at Zero Energy", Exponential and Critical Experiments II IAEA, Vienna (1964) 575.

[2] FRAUDE, A., Nukleonik 4 (1962) 84.

[3] RAIEVSKI, V. et TANGUY, P., Effet des fissions rapides sur la cinétique d'un réacteur thermique, Note CEA 161 (1956).

[4] MORIER, F. et TELLIER, H., Volubilis: Code de calcul pour l'interprétation des expériences de cinétique pulsée, Note CEA 517 (1963).

[5] SAGOT, M. et TELLIER, H., Etude d'un réacteur à combustible légèrement enrichi (RUBÉOLE) à l'aide de sources pulsées de neutrons, Rapport CEA 2201 (1962).

[6] JACQUEMART, R., Application de la méthode des neutrons pulsés sur les piles ALIZÉ et AQUILON, Rapport CEA R 2376 (1963).

[7] TESTE du BAILLER, A., MARIUS: Empilement expérimental critique, Rapport DEP 10 (1960).

[8] AMOUYAL, A., BACHER, P., LAGO, B., MENGIN, F. et PARKER, E., RIFIFI: Méthode de calcul analytique de la condition critique et des flux d'une pile, Rapport CEA 1398 (1960).

FAR SUBCRITICALITY MEASUREMENTS BY THE PULSED NEUTRON TECHNIQUE*

M. PETROVIĆ
BORIS KIDRIČ INSTITUTE OF NUCLEAR SCIENCE
BELGRADE, YUGOSLAVIA

Abstract — Résumé — Аннотация — Resumen

FAR SUBCRITICALITY MEASUREMENTS BY THE PULSED NEUTRON TECHNIQUE. Subcriticality measurements of the Argonaut reactor were performed with the reactivity as far as -15 $. Data are obtained by measuring the time and space distribution of the decaying neutron after the injected burst. The reactor was made subcritical with dummy fuel plates inserted into the system instead of fuel plates. Dummy fuel plates were made with the same absorption cross-section as the fuel.

The Kaman Pulsatron was used as the pulsed neutron source. To minimize generation of the higher modes in the initial flux distribution, attention was paid to the positioning of the neutron source. The BF_3 counters and the TMC multichannel analyser were used for detection, time analysis and registration. The data were processed using the ZUSE Z-23 digital computer. The results of measurements show the limit of the method.

MESURE DE LA SOUS-CRITICITÉ PAR LA MÉTHODE DES NEUTRONS PULSÉS. Les mesures de la sous-criticité du réacteur ARGONAUTE ont été effectuées à un niveau de réactivité allant jusqu'à 15 dollars. Les données ont été obtenues en mesurant la distribution, en fonction du temps et de l'espace, des neutrons en voie de décroissance après injection de la bouffée de neutrons. Le réacteur a été rendu sous-critique en plaçant dans le système de fausses plaques de combustible au lieu des plaques normales, les premières ayant la même section efficace d'absorption que les secondes.

On a utilisé le pulsatron Kaman comme source de neutrons pulsés. Pour réduire au minimum l'apparition des modes élevés dans la distribution de flux initiale, on a soigné le positionnement de la source de neutrons. On a utilisé des compteurs au BF_3 et l'analyseur multicanal TMC pour analyser et enregistrer les données qui ont été traitées à l'aide de la calculatrice numérique ZUSE Z-23. Les résultats des mesures indiquent les limites de la méthode.

ИЗМЕРЕНИЕ ГЛУБОКОЙ ПОДКРИТИЧНОСТИ С ПОМОЩЬЮ ИМПУЛЬСНЫХ НЕЙТРОНОВ. Измерения подкритичности реактора "Аргонавт" осуществляли с реактивностью до 15 долларов. Данные получали путем измерения распределения распадающихся нейтронов по времени и пространству после инжектирования импульса. Реактор был доведен до подкритичности с помощью ложных топливных пластин, вставленных в систему вместо топливных пластин. Ложные топливные пластины имели такое же сечение поглощения, как и топливо.

В качестве источника импульсных нейтронов применяли пульсатрон Камана. Чтобы уменьшить возникновение более высоких типов распределения первоначального потока, уделяли внимание расположению нейтронного источника. Для анализа времени обнаружения и регистрации использовали счетчики BF_3 и многоканальный анализатор TMC. Данные обрабатывали с помощью цифровой вычислительной машины ZUSE Z-23. Результаты измерений демонстрируют пределы этого метода.

MEDICION DE SUBCRITICIDADES MUY ACUSADAS EMPLEANDO EL METODO DE LOS NEUTRONES PULSADOS. El autor ha medido la subcriticidad del reactor «Argonaut» obteniendo reactividades de hasta -15 dólares. Consiguió los datos midiendo la distribución espacial y temporal de la población neutrónica en decrecimiento después de aplicada la ráfaga. Se consiguió la subcriticidad del reactor introduciendo en el sistema placas de combustible simuladas en lugar de placas verdaderas. La sección eficaz de absorción de las placas simuladas era igual a la del combustible. Como fuente de neutrones pulsados se empleó un Pulsatron Kaman. A fin de reducir al mínimo la generación de modos superiores en la distribución inicial del flujo, la

* The experimental part of this work was performed at the International Institute of Nuclear Science and Engineering, Argonne, Ill., USA.

posición de la fuente neutrónica se eligió con sumo cuidado. Para la detección, el análisis de tiempos y registro de datos, se utilizaron contadores de BF_3 y un analizador multicanal TMC. Los datos se trataron empleando una calculadora numérica ZUSE Z-23. El autor expone los resultados de las mediciones, en los que se reflejan las limitaciones del método empleado.

INTRODUCTION

As has been reported [1] the pulsed neutron technique affords accurate reactivity determination over a wide reactivity range.

The errors in the far subcriticality measurements may be a result of higher modes of neutron distribution which do not decay fast enough compared with the fundamental one, or to the change in the neutron lifetime affected by the added absorber. In inhomogeneous or highly reflected reactors higher modes of neutron distribution and neutrons arriving from the reflector can cause additional errors.

The subject of this paper is the pulsed neutron measurement of the reactivity on the highly reflected reactor Argonaut.

EXPERIMENTAL METHOD AND RESULTS

The measurements were performed on the Argonaut one-slab reactor core [2]. The reactor was critical with 93 fuel plates with all control rods almost completely out.

The reactor was made subcritical by replacing the fuel plate with a boral plate having the same absorption cross-section. In such an experimental arrangement the prompt neutron lifetime for the subcritical reactor will be the same as for the critical. This also allowed easier calculation of the reactor subcriticality.

The boral plates were selected according to the transmission measurement data. Measurements were made with both the critical and subcritical reactor with 4, 8 and 14 boral plates.

The Kaman pulsatron was used as the pulsed neutron generator. The pulsatron was mounted on the top of the reactor on the central line of the reactor core. This arrangement was chosen so as to have the initial neutron flux distribution closer to the distribution of the fundamental mode.

A small BF_3 counter (2 cm × 2 cm) was used as a neutron detector. The detector was located along the z-axis of the core slab to measure the time and spatial distribution. A TMC multi-channel analyser with a pulsed neutron logic unit was used. The decay constants α were found by fitting a single exponential function to the data. Numerical analysis was performed on the ZUSE Z-23 digital computer. Another BF_3 counter located in the thermal column was used as a monitor to normalize the data for spatial distribution measurements.

To check the measurement of the critical reactor we obtained the prompt lifetime by the reactor oscillator method. The data obtained by the pulsed neutron technique and the oscillator method differ by less than 2% (186 and 183 μs). The data for the critical reactor are given in Fig. 1. The reactivity

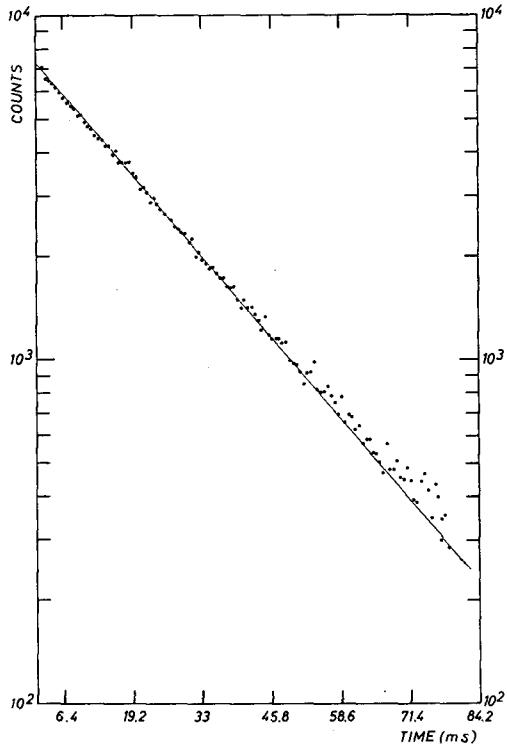


Fig. 1

Time response for critical reactor

worth of the fine control rod was measured by the pulsed neutron and rod drop techniques and the results were in good agreement.

For the configuration of the pulsed neutron source and the reactor, most of the higher modes in the distribution are generated in the direction of the z-axis. The time and space distribution is measured (Fig. 2) in this direction to observe when a single fundamental mode remained, i.e. what part of the decay curve (Fig. 3) has to be used for calculating the decay constant.

In all cases the reactivities were computed with the relation

$$R = \alpha/\alpha_c - 1$$

The results for three different boral plate loadings are plotted in Fig. 4. One measurement was made without water as the moderator in the core; the result is also given in Fig. 4.

COMPARISON OF MEASURED AND CALCULATED RESULTS

The magnitude of the reactivity change obtained by replacing one fuel plate by a boron plate, according to the perturbation theory is approximately

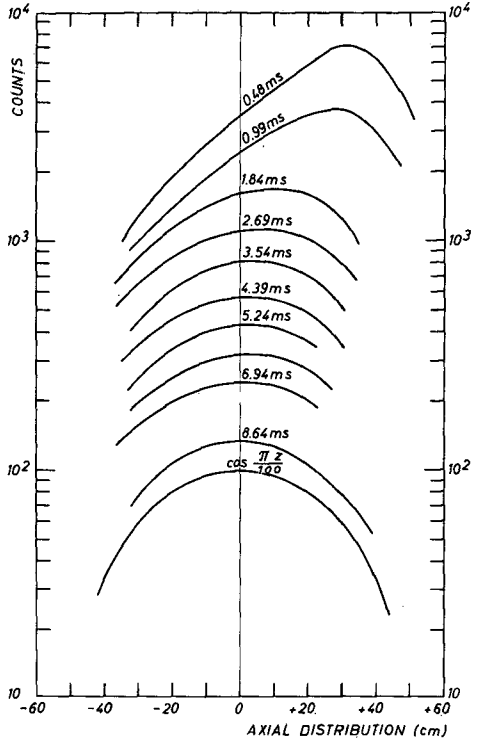


Fig. 2

One-dimensional spatial neutron flux distribution

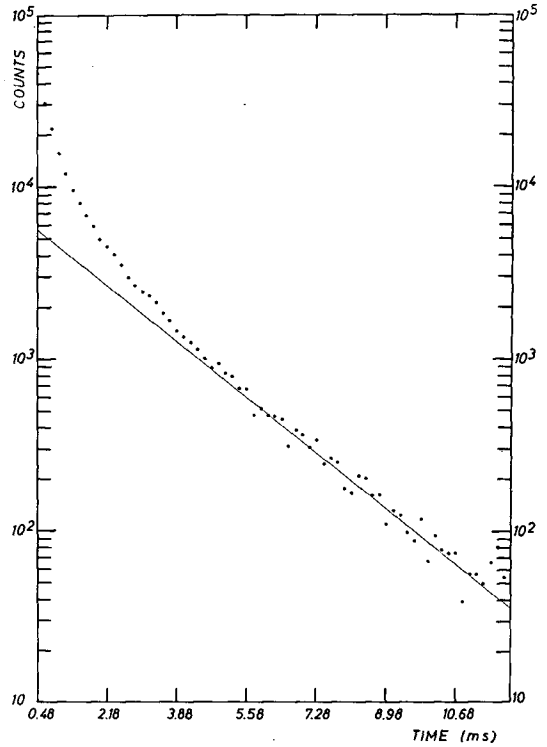


Fig. 3

Time response for subcritical reactor

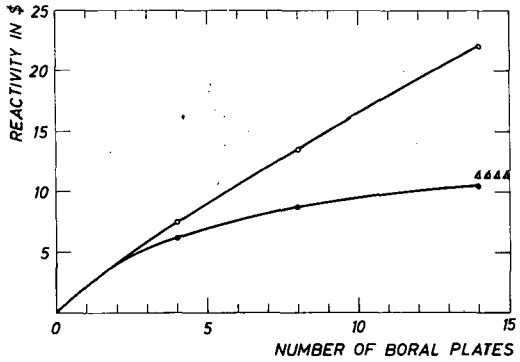


Fig. 4

Reactivity measurement for three different boral plate loadings

o Calculated
• Measured
Δ Measured reactivity without water

equal to the reciprocal of the number of fuel plates in the core weighted by the reactor important function. For a particular plate location the total reactivity for 4, 8 and 14 plates is calculated and given in Fig. 4.

The measured data are in good agreement with the calculated up to the -5$ subcritical reactor. For -10 $ to -15 $ of reactivity, discrepancies rapidly rise up to 25 and 40%, respectively.

The neutron decay constant of a reactor without water as the moderator is the same as the decay constant of the graphite block of the same size as the reactor thermal column. From these results it can be seen that the decay constant of the highly subcritical Argonaut reactor is greatly influenced by the neutrons from the reflector, i.e. the thermal column. After the burst of neutrons from the pulsatron there is a transient period until the decay constant reaches the value of a neutron decay constant of the graphite reflector. The reactor then acts as a booster to the pulsed neutron source. The data of the reactor neutron-decay in this transient period cannot be used.

In conclusion we may say that even for such an inhomogeneous highly reflected reactor as the Argonaut, the pulsed neutron technique affords accurate reactivity determination up to -5 $ of reactivity.

ACKNOWLEDGEMENT

The author wishes to thank Dr. W. Sturm for his suggestions concerning the work and Messrs. K. Ruzicht and D. Cokinos for their valuable contributions to the experimental part of this work.

REFERENCES

[1] SIMMONS, B.E. and KING, J.S., A pulsed neutron technique for reactivity determination, NSE 595 (1958) 3 p.

[2] LENNOX, D.H. and SPINRAD, B.I., Interim report on "ARGONAUT", ANL-5552 (1956).

ОПРЕДЕЛЕНИЕ ПАРАМЕТРА β/ℓ ГРАФИТО-ВОДЯНОГО РЕАКТОРА НУЛЕВОЙ МОЩНОСТИ "АННА" ПРИ ПОМОЩИ ИМПУЛЬСНОГО ИСТОЧНИКА НЕЙТРОНОВ

С. ХВАЩЕВСКИ и К. ДЫБОВСКИ
ИНСТИТУТ ЯДЕРНЫХ ИССЛЕДОВАНИЙ ПАН, ЦВИРК
ПОЛЬША

Abstract — Résumé — Аннотация — Resumen

DETERMINATION OF β/ℓ IN GRAPHITE-WATER ZERO-POWER ANNA REACTOR BY THE PULSED NEUTRON SOURCE. Using a pulsed source we measured the parameters β/ℓ_{kr} and reactivity of the control and safety components of the ANNA reactor. Since the lifetime of prompt neutrons in ANNA is of the order of that of delayed neutrons, the correction factors for β/ℓ_{kr} and reactivity were calculated by reference to the attenuation constant of the prompt neutrons. The methods of processing the results are also given.

MESURE AU MOYEN D'UNE SOURCE DE NEUTRONS PULSÉS, DU PARAMÈTRE β/ℓ DU RÉACTEUR ANNA DE PUISSANCE ZÉRO, RALENTI AU GRAPHITE ET REFROIDI A L'EAU. Au moyen d'une source de neutrons pulsés, les auteurs ont mesuré les paramètres β/ℓ_{kr} et les antiréactivités des éléments de réglage et de sécurité du réacteur ANNA. Etant donné que dans ce réacteur les neutrons instantanés ont une durée de vie analogue à celle des neutrons retardés, ils ont calculé les coefficients de correction pour β/ℓ_{kr} et pour la réactivité en se fondant sur la constante d'amortissement des neutrons instantanés. Ils indiquent en outre des méthodes pour le traitement des résultats obtenus.

ОПРЕДЕЛЕНИЕ ПАРАМЕТРА β/ℓ ГРАФИТО-ВОДЯНОГО РЕАКТОРА НУЛЕВОЙ МОЩНОСТИ "АННА" ПРИ ПОМОЩИ ИМПУЛЬСНОГО ИСТОЧНИКА НЕЙТРОНОВ. При помощи импульсного источника нейтронов измеряли параметры $(\beta/\ell)_{кр}$ и реактивности управляющих и защитных элементов в реакторе "Анна". Поскольку время жизни мгновенных нейтронов в реакторе "Анна" порядка времени жизни запаздывающих нейтронов, рассчитаны поправочные коэффициенты для $\beta/\ell_{кр}$ и реактивности от постоянной затухания мгновенных нейтронов. Приводятся также приемы обработки результатов.

DETERMINACION DEL PARAMETRO β/ℓ DEL REACTOR ANNA, POTENCIA NULA, MODERADO POR GRAFITO Y REFRIGERADO POR AGUA, CON AYUDA DE UNA FUENTE DE NEUTRONES PULSADOS. Con ayuda de una fuente de neutrones pulsados, los autores han medido los parámetros β/ℓ_{kr} y reactividad correspondientes a los elementos de regulación y seguridad del reactor ANNA. Como la vida de los neutrones inmediatos es en este reactor análoga a la de los neutrones retardados, los autores calcularon el coeficiente de corrección para β/ℓ_{kr} y para la reactividad, basándose en la constante de atenuación de los neutrones inmediatos. Los autores indican, además, los métodos para el tratamiento de los resultados obtenidos.

ВВЕДЕНИЕ

Измерение параметров реактора при помощи импульсного источника нейтронов основано на исследовании хода временной зависимости плотности нейтронов в реакторе после инжекции в него нейтронного импульса. Установив асимптотическое распределение, зависимость плотности нейтронов от времени можно записать в следующем виде:

$$N(t) = N_0 \exp(-\alpha t) + N_d(t),$$

где α – постоянная затухания мгновенных нейтронов, N_d – фон запаздывающих нейтронов.

Анализ результатов этих измерений основан на уравнениях кинетики точечного реактора:

$$\frac{dN}{dt} = \left(k\frac{\beta}{\ell}\right)_{эф}\left(\rho - 1\right)N + \sum_{i=1}^{\ell} C_i \lambda_i + S,$$

$$\frac{dC_i}{dt} = \left(k\frac{\beta}{\ell}\right)_{эф} a_i N - C_i \lambda_i ,$$

где ρ – реактивность в долларах, $a_i = \frac{\beta_i}{\beta}$.

В случаях, когда параметр $\left(\frac{\beta}{\ell}\right)_{кр} >> \lambda_{макс}$, можно пренебречь влиянием запаздывающих нейтронов на постоянную затухания мгновенных нейтронов и применять следующие приближенные формулы [1]:

$$\rho = \left(\frac{\alpha}{\left(k\frac{\beta}{\ell}\right)_{эф}} - 1\right),$$

$$\left(\frac{\beta}{\ell}\right)_{кр} = \left(k\frac{\beta}{\ell}\right)_{эф,кр} = \alpha_{кр},$$

где $\alpha_{кр}$ – постоянная затухания мгновенных нейтронов в критическом реакторе.

В дальнейших измерениях считаем с некоторым приближением, что параметр $\left(k\frac{\beta}{\ell}\right)_{эф} = \left(\frac{\beta}{\ell}\right)_{кр} = \text{const}$ и тогда:

$$\rho = \left(\frac{\alpha}{\alpha_{кр}} - 1\right).$$

При $\left(\frac{\beta}{\ell}\right)_{кр} \approx \lambda_{макс}$ эти приблизительные формулы сопряжены с довольно большими ошибками. В этом случае мы используем некоторые поправочные коэффициенты, полученные из анализа численных решений уравнения обратных часов [2]. Для определения величины $\left(\frac{\beta}{\ell}\right)_{кр}$ реактора мы используем следующие соотношения:

$$\left(\frac{\beta}{\ell}\right)_{кр} = \alpha_{кр} - A\left(\frac{\beta}{\ell}\right)_{кр}$$

Величина $A\left(\frac{\beta}{\ell}\right)_{кр}$, график которой приведен на рис. 1, при больших значениях $\left(\frac{\beta}{\ell}\right)_{кр}$ равна $\bar{\lambda} = \frac{\Sigma \beta_i \lambda_i}{\beta} = 0{,}411\ сек^{-1}$. В случае малых значений

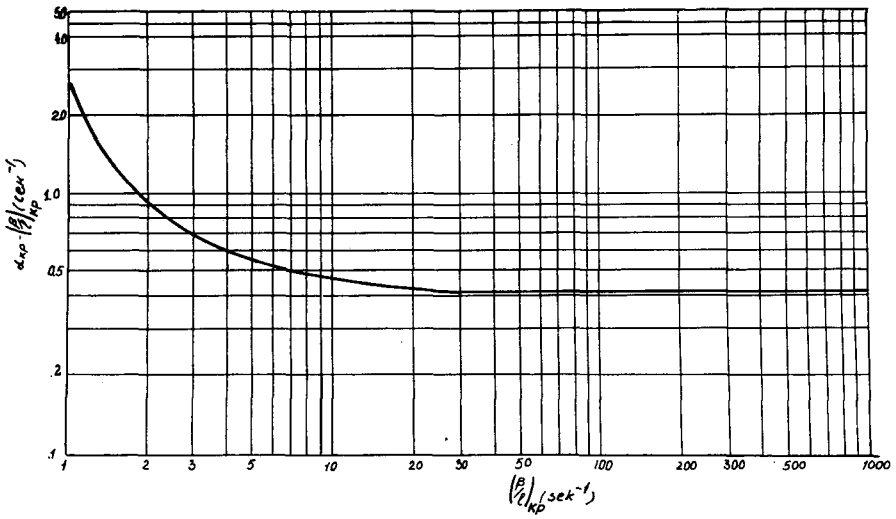


Рис.1

Зависимость поправочного коэффициента А от $\left(\frac{\beta}{\ell}\right)_{кр}$.

$\left(\frac{\beta}{\ell}\right)_{кр}$ влияние запаздывающих нейтронов на α сказывается сильней и поэтому при $\alpha_{кр} < 20$ сек$^{-1}$ нужно принимать во внимание коэффициент, величина которого больше 0,411 сек$^{-1}$.

Реактивность системы была определена при использовании следующего соотношения:

$$\rho = \frac{\alpha}{(k\frac{\beta}{\ell})_{эф}} - B(\alpha) - 1.$$

График функции В приведен на рис.2. Из рисунка видно, что увеличением α поправочный коэффициент стремится к 0.

Следующим довольно сложным вопросом является переменный во времени фон запаздывающих нейтронов, особенно при измерениях с постоянными затухания $\alpha < 30$ сек$^{-1}$. В этих случаях наибольший вклад в переменную составляющую фона вносят нейтроны из наиболее быстро распадающейся группы запаздвающих нейтронов. Если принять, что величина переменной составляющей фона мала по сравнению с основным эффектом и, что плотность нейтронов после инжекции меняется по экспоненциальному закону:

$$N(t) = N_0 \exp(-\alpha t) + N_d,$$

где N_d – постоянная составляющая фона, то получим для переменной составляющей следующее выражение:

$$N_d(t) = \frac{k\beta_6 \lambda_6 N_0}{\ell \alpha^2 (1-k)^2} \left\{ \exp(-k\tau) - \exp(-\tau)[\tau(1-k)+1] \right. ,$$

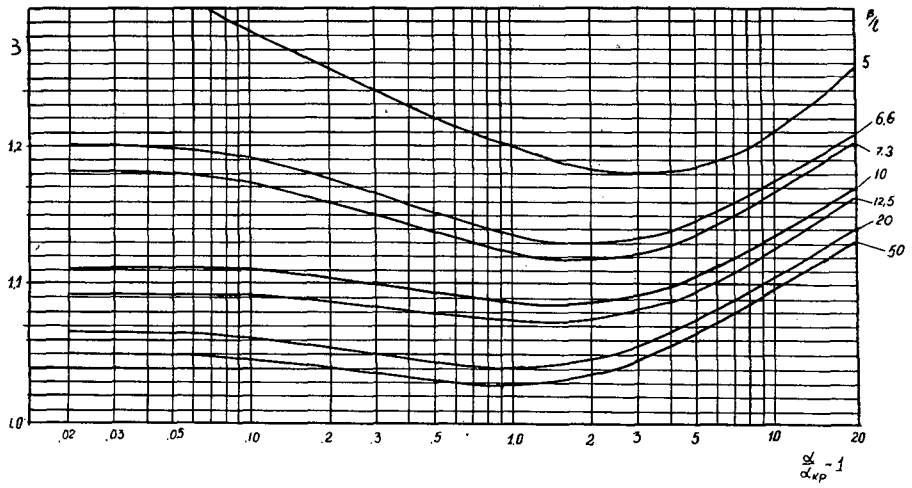


Рис.2

Зависимость поправочного коэффициента B от α.

где $\beta_6 \lambda_6$ – эффективная доля и постоянная распада 6-й группы запаздывающих нейтронов,

$$\tau = \alpha t ,$$

$$k = \frac{\lambda_6}{\alpha} .$$

Решение это было сравнено с решением, полученным при помощи аналоговой машины. Результаты согласуются в пределах точности аналоговой машины.

Идеальным способом удаления переменного фона, было бы составление соответствующих таблиц для вычитания фона. Были приняты и эти меры, но поскольку такая процедура довольно кропотлива, был разработан другой метод получения постоянных затухания с учетом фона. Этот метод приводится ниже.

ЭКСПЕРИМЕНТАЛЬНАЯ УСТАНОВКА

В измерениях применялся построенный авторами импульсный источник нейтронов ИГН-200 [3]. Источник представляет собою линейный ускоритель дейтонов до энергии 200 кэв с импульсным ионным источником [4]. Нейтроны возникали в облучаемой дейтонами тритиевой мишени. В описанных измерениях генератор испускал нейтронный импульс длительностью 300 мксек и количеством нейтронов $2 \div 4 \cdot 10^7$. Частота следования импульсов $1 \div 10$ в сек.

Импульсы нейтронов инжектировались в реактор "АННА" [5]. Это реактор нулевой мощности с графито-водяным модератором и графитовым отражателем. Топливо-обогащенный до 20% уран. Реактор управляется при помощи подвижного тепловыделяющего элемента (ПТВЭЛ) и компенсационного стержня (КС). В реакторе имеются четыре стержня аварийной защиты (СА3).

Мишень импульсного источника нейтронов располагалась внутри отражателя на середине высоты активной зоны. Пропорциональные счетчики BF_3 для регистрации плотности нейтронов располагались также внутри отражателя. Импульсы, полученные из счетчиков после соответствующего усиления, подавались на вход 400-канального временного анализатора СТ-400 ДМ. Для увеличения точности измерений применялся внешний стабилизированный кварцом генератор канальных импульсов. Анализатор запускался от стартовых импульсов, которые через световую линию запускали тоже ионный источник генератора нейтронов.

ОБРАБОТКА РЕЗУЛЬТАТОВ

Полученные при помощи временного анализатора результаты обрабатывались при помощи кода "КАНДИДЕ" [6] на вычислительной машине "УРАЛ-2". Вычисления в коде идут следующим путем:

1. Коррекция входных данных на мертвое время анализатора.
2. Вычитание заданного постоянного фона.
3. Подсчет в заданном интервале каналов по формулам взвешанных наименьших квадратов логарифмического коэффициента затухания.

В коде предусмотрена возможность проведения нескольких итераций для уточнения величины фона.

Обычная зависимость плотности нейтронов в реакторе от времени приведена на рис.3. После инжекции плотность нейтронов сначала быстро

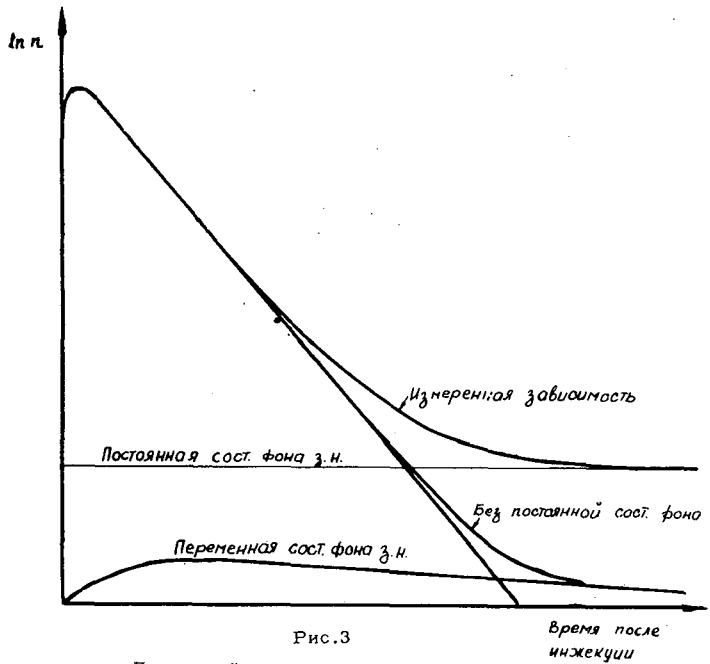


Рис.3

Примерный ход зависимости плотности нейтронов в реакторе после инжекции нейтронного импульса.

возрастает, потом начинает экспоненциально убывать до некоторого уровня. Уровень этот является величиной постоянной составляющей фона и находится из количества импульсов, подсчитанных в последних каналах анализатора при условии, что время анализа $T > (10/\alpha)$.

Для проведения дальнейших расчетов необходим правильный выбор пределов области, в которой производится расчет логарифмического коэффициента затухания. Чтобы избавиться от влияния высших гармоник особенно при измерениях больших значений α, нужно выбрать такой начальный канал анализируемой области, чтобы влияние высших гармоник было несущественным.

Кстати, нужно отметить, что амплитуда высших гармоник очень сильно зависит от взаимоположения в реакторе источника нейтронов и детектора. Идеальным с этой точки зрения оказался центр активной зоны, но по техническим причинам мы не могли проводить измерений в этой точке. Поэтому был найден измерительный канал в отражателе, в котором детектор регистрировал наименьшую амплитуду высших гармоник.

Начальный канал определяли во время обработки результатов. При закрепленном номере конечного канала области,в которой производится расчет, изменяли номер начального канала.Полученная таким образом зависимость α от номера начального канала достигает при некотором канале максимальной величины. Именно этот канал в дальнейшем считается начальным. Пример такой зависимости приведен на рис.4.

Для исключения влияния на результаты измерений переменной составляющей фона запаздывающих нейтронов можно применять вычитание аналитически рассчитанного фона. Метод этот довольно трудоемкий. По-

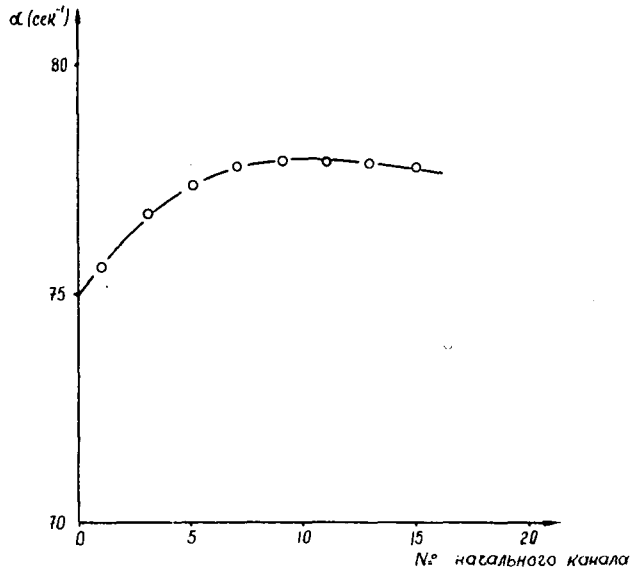


Рис.4

Пример зависимости α от номера начального канала. Номер конечного канала 75.

этому с целью получения величин,свободных от фона,применялась следующая процедура анализа результатов.

При определенном номере начального канала производился расчет коэффициентов затухания для нескольких номеров конечных каналов. Зависимость α от номера конечного канала экстраполировалась к нулю, и полученная таким образом величина α_0 принималась за истинную постоянную затухания мгновенных нейтронов. На рис.5 приведен пример зависи-

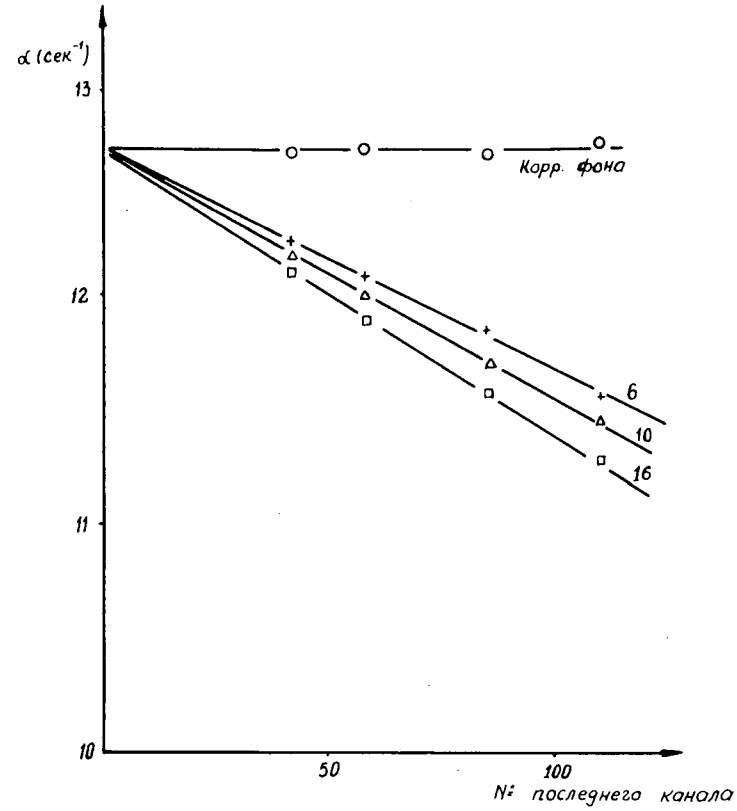


Рис.5

Пример зависимости α от номера конечного канала. Цифры при прямых означают номер начального канала. На рисунке приведены также α,полученные после коррекции данных на переменный фон

мости α от номера конечного канала для нескольких номеров начальных каналов. Как видно из рисунка, эти зависимости представляют собою прямые линии,пересекающие ось ординат в одной точке.

Для проверки были проведены расчеты для этих же результатов после учета переменного фона. В этом случае получено $\alpha_{кор}$, не зависящее от номера конечного канала и равное α_0. Подобные расчеты были успешно проведены еще для нескольких результатов измерений.

Величина $\alpha_{кр}$ должна быть измерена в критическом реакторе на за-

паздывающих нейтронах. Большой фон запаздывающих нейтронов и некоторые технические трудности делают невозможным проведение этих измерений. Поэтому величина $\alpha_{кр}$ получена из экстраполяции подкритических измерений, проделанных при помощи ПТВЭЛ или КС. Для измерений использовалось регулирующее устройство, обладающее при данной загрузке зоны линейной зависимостью реактивности от положения.

РЕЗУЛЬТАТЫ ИЗМЕРЕНИЙ

Измерения были проделаны для трех конфигураций активной зоны реактора. Конфигурации эти представлены на рис.6. На этом же рисунке обозначены также положения мишени источника и детектора. Основной загрузкой реактора является конфигурация № 1. В остальных конфигурациях возрастает отношение массы графита в активной зоне к массе воды и топлива.

В таблице приведены результаты измерений α и реактивностей ПТВЭЛ и САЗ. Для конфигурации № 1 даны для сравнения величины реактивности, измеренные при помощи метода сброса стержня [7]. Причиной появле-

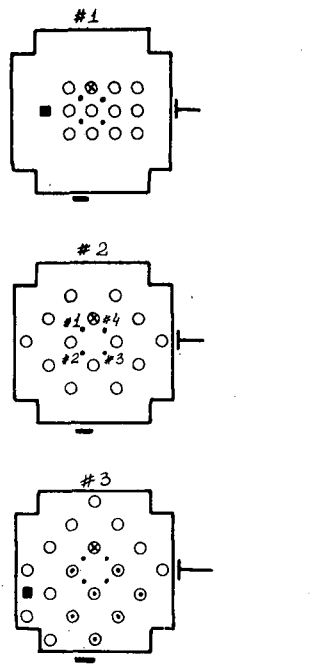


Рис.6

Схемы конфигураций активной зоны, для которых были проведены измерения.

- Тэпловыд. элемэнт в воде
- Тэпловыд элемент без воды
- Подвижный ТВЭЛ
- Стержень аварийной защиты
- Компенсационный стержень
- Детектор
- Мишень генератора нейтронов

Таблица 1

РЕЗУЛЬТАТЫ ИЗМЕРЕНИЙ $(\beta/\ell)_{кр}$ И РЕАКТИВНОСТЕЙ ПТВЭЛ И СА3

		Зона №1	Зона № 2	Зона №3
α сек$^{-1}$		12,85 ±0,08	7,85 ±0,1	7,21 ±0,08
$\left(\frac{\beta}{\ell}\right)$ сек$^{-1}$		12,5 ±0,1	7,48 ±0,15	6,84 ±0,1
ПТВЭЛ	α сек$^{-1}$	78,7 ±0,3		54,8 ±0,1
	ρ $	5,56 ±0,09		7,02 ±0,1
СА3 №1	α сек$^{-1}$	82,97 ±0,2	73,9 ±0,12	54,83 ±0,2
	ρ $	5,62 ±0,7 (6,36)	8,42 ±0,06	7,5 ±0,1
СА3 №3	α сек$^{-1}$	98,9 ±0,4		
	ρ $	6,88 ±0,1 (9,45)		
СА3 №1,3	α сек$^{-1}$	138,1 ±0,4	114,9 ±0,3	91,4 ±0,2
	ρ $	9,99 ±0,1	13,6 ±0,15	12,35 ±0,15
СА3 №1,2,3,4	α сек$^{-1}$	175,0 ±0,7	154,7 ±0,5	127,9 ±0,5
	ρ $	12,9 ±0,2	18,72 ±0,2	17,7 ±0,2

Величины реактивности, приведенные в скобках, получены методом сброса стержня.

ния некоторых различий между результатами этих двух методов может быть непостоянство параметра $\left(k\frac{\beta}{\ell}\right)_{эф}$ при возрастании отрицательной реактивности.

На рис.7 представлена зависимость реактивности и коэффициента затухания мгновенных нейтронов от положения ПТВЭЛ.

Как видно из приведенных результатов, величина α очень чувствительна к изменению реактивности реактора вплоть до больших отрицательных ρ(-20 долларов). Кроме этого, как показали измерения,

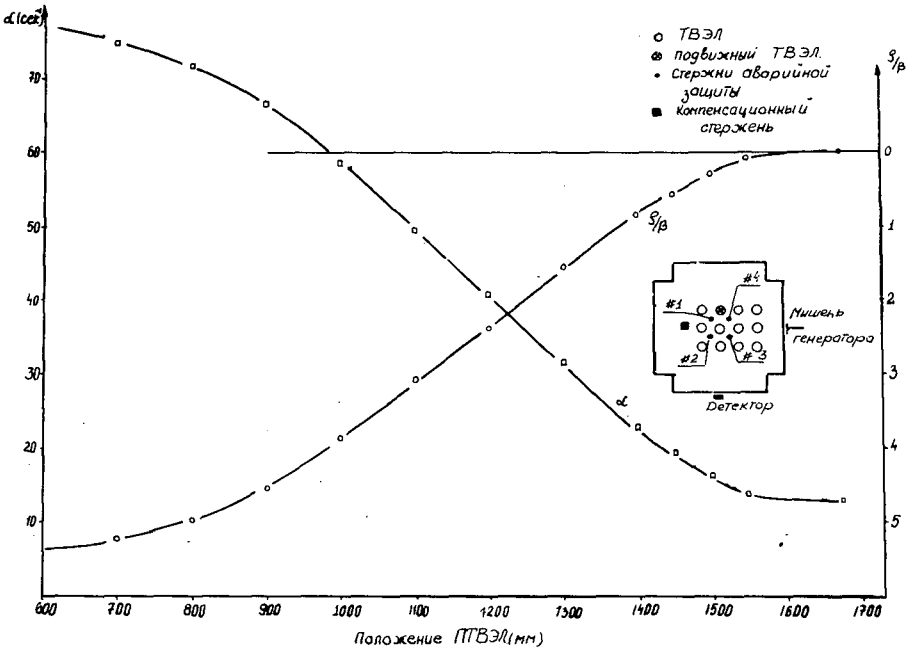


Рис.7

Зависимость реактивности и постоянной затухания α от положения ПТВЭЛ.

величину эту можно измерять с большой точностью даже при больших $-\rho$. К сожалению нет однозначной связи между α и ρ, поскольку параметр $\left(k\frac{\beta}{\ell}\right)_{эф}$, определенный при $\rho = 0$, вероятно изменяется с возрастанием ρ.

Этот пробел до некоторой степени заполняет работы Гарелиса [8] и Гозаньего [9], но точность, с которой в этих работах определяется параметр $\left(k\frac{\beta}{\ell}\right)_{эф}$, во многом уступает точности определения α.

Авторы считают своим приятным долгом выразить благодарность сотрудникам Вычислительной лаборатории Отделения физики реакторов, в особенности Т. Куликовской за помощь в проведении вычислений, а также сотрудникам Лаборатории эксплоатации критических сборок, и прежде всего Е. Кубовскому и К. Яблонскому за помощь в проведении измерений.

ЛИТЕРАТУРА

[1] BECKURTS K.H. Nucl.Instrum.Meth. 11 (1961) 144.
[2] BOUŻYK J., SUWALSKI W. (To be published).
[3] CHWASZCZEWSKI S. Nukleonika 5 (1960) 355–360.
[4] CHWASZCZEWSKI S., DYBOWSKI K. Nukleonika 9 (1964) 897.
[5] ARKUSZEWSKI J. et al. Symposium in Amsterdam in 1963. IAEA, Proc. Vol.III, pp.333–354, Vienna, 1964.

[6] ARKUSZEWSKI J., KULIKOWSKA T. KANDIDE-kod analizujacy neutronowe doświadczenia impulsowe. Spraw. Z.IX–A.
[7] BOUŻYK J. et al. (To be published).
[8] GARELIS et al. NSE 16 (1963) 263–270.
[9] GOZANI T. Nukleonik 4 (1962) 348–349.

PULSED NEUTRON REACTIVITY MEASUREMENTS IN THE NEAR-CRITICAL STATE

K. EINFELD, H. HENNIES, G. MEMMERT AND W. ULLRICH
INTERATOM,
BENSBERG, FEDERAL REPUBLIC OF GERMANY

Abstract — Résumé — Аннотация — Resumen

PULSED NEUTRON REACTIVITY MEASUREMENTS IN THE NEAR-CRITICAL STATE. Measured and calculated thermal neutron decay constants λ are reported for various 5% enriched zirconium hydride moderated lattices, using UO_2 and $ZrH_{1.7}$ rods in an aluminium matrix. By performing measurements in the critical and in near-critical states values of β/ℓ could be determined. The resulting β/ℓ values were used to calculate reactivity worths of different absorber rods and absorber arrangements from the measured decay constants. Several measurements were evaluated applying the modified pulsed source technique of Garelis and Russell.

MESURE DE RÉACTIVITÉ DE NEUTRONS PULSÉS AU VOISINAGE DE L'ÉTAT CRITIQUE. Les auteurs présentent les constantes λ de décroissance des neutrons thermiques qu'ils ont mesurées et calculées pour divers réseaux enrichis à 5%, ralentis à l'hydrure de zirconium, en utilisant des barres de $ZrH_{1.7}$ et de UO_2 dans une matrice d'aluminium. En effectuant des mesures à l'état critique et au voisinage de l'état critique, ils ont pu déterminer les valeurs de β/ℓ. Les valeurs obtenues pour β/ℓ ont servi pour déterminer l'effet sur la réactivité de différentes sortes de barres et de dispositifs d'absorption à partir des constantes de décroissance des neutrons mesurées. Les auteurs ont évalué plusieurs grandeurs en appliquant la méthode modifiée de la source pulsée de Garelis et Russell.

ИЗМЕРЕНИЯ РЕАКТИВНОСТИ ИМПУЛЬСНЫХ НЕЙТРОНОВ В СОСТОЯНИИ, БЛИЗКОМ К КРИТИЧЕСКОМУ. Сообщается о измерениях и вычислениях постоянных λ распада тепловых нейтронов для различных решеток с замедлителем в виде обогащенного до 5% гидрида циркония с использованием стержней UO_2 и $ZrH_{1.7}$ в алюминиевых матрицах. При проведении измерений в критическом и близком к критическому состояниях можно определять значения β/ℓ. Полученные результаты значений β/ℓ применяли для вычисления значений реактивности различных поглощающих стержней и поглощающих устройств за счет измеренных постоянных распада. Целый ряд измерений оценивали с помощью усовершенствованного метода пульсирующих источников Гарелиса и Расселла.

MEDICIONES DE LA REACTIVIDAD, EN EL ESTADO CRITICO Y EN EL PROXIMO A LA CRITICIDAD, CON AYUDA DE NEUTRONES PULSADOS. Los autores facilitan los valores experimentales y teóricos de las constantes λ de decrecimiento de los neutrones térmicos para diversos reticulados enriquecidos al 5% y moderados por hidruro de zirconio, empleando barras de UO_2 y $ZrH_{1.7}$ en una matriz de Al. Realizando mediciones en el estado crítico y en el próximo a la criticidad, pudieron determinar los valores de β/ℓ. Estos valores se utilizaron para calcular, partiendo de las constantes de decrecimiento medidas, los valores de la reactividad correspondientes a distintas barras y configuraciones de material absorbente. La evaluación de algunas de las mediciones se realizó aplicando la técnica modificada de la fuente de neutrones pulsados, ideada por Garelis y Russell.

1. INTRODUCTION

During the past years various reactor experiments have shown that zirconium hydride (ZrH_x) is a suitable moderator material. Homogeneous, fully enriched reactor systems such as TRIGA [1], SNAP 10A/2 [2] and SNAP 8 [3] have used this moderator. At present, a power reactor experiment is under development [4], which uses sodium as a coolant and ZrH_x

as a moderator in a slightly enriched, heterogeneous core lattice. To determine the nuclear characteristics of such a reactor system, a series of nuclear experiments was performed from January 1962 through March 1965 to furnish test cases for the theoretical models being used in the calculation of the core characteristics. During the different phases of the experimental programme the pulsed neutron source technique was applied to a rather large extent. The experiments can be divided into the following three phases.

In the first phase the nuclear properties of the moderator itself were determined by measuring the neutron spectrum in a block of ZrH_x by the time-of-flight method at three different temperatures (20, 335, 555°C) [5]. In the same ZrH_x block the thermal neutron decay constant in a pulsed neutron experiment was measured as a function of temperature up to 450°C.

During the second phase the thermal neutron decay constant λ of slightly enriched heterogeneous UO_2-ZrH_x lattices was determined in a subcritical facility up to a $k_{eff} = 0.95$ [6]. At room temperature the reactivity worth of different reflector arrangements and of control rods were measured by the pulsed neutron method. The same method was used to determine the isothermal coefficient of reactivity up to a temperature of 450°C for two lattices of different heterogeneity.

As a result of the good agreement obtained between the theoretical calculations of λ and the experimental values, it was decided to include during the third phase of measurements in a critical facility a rather large number of pulsed neutron experiments. In this way it was possible to cover the complete range of λ-values from very low fuel loadings up to the critical state of different core configurations. For several of these configurations β/l was determined by extrapolating the λ-values to the critical state. Furthermore, the reactivity worth of different absorbers and absorber configurations was measured. The results of the experiments during the third phase and a discussion on them are the subject of this paper.

2. CRITICAL FACILITY AND LATTICE CONFIGURATIONS

Several cylindrical core configurations were investigated with the critical assembly KNK mounted on the split table machine of the critical facility at the Reaktorzentrum Geesthacht [7]. Fuel, moderator and reflector rods were loaded in a honeycomb matrix made of aluminium, which could be separated in two symmetrical halves for loading and shutdown (see Fig. 1). The matrix consisted of about 6000 Al tubes having a hexagonal cross-section with an inner diameter of 16.6 mm and forming a hexagonal lattice with a pitch of 18.2 mm. The UO_2 fuel was 5.03% enriched and clad with Zircaloy of 0.4-mm thickness. The diameter of the UO_2 pellets was 14.0 mm. The moderator ($ZrH_{1.7}$) consisted of pellets with 15.1-mm diameter having a hydrogen density of 6.2×10^{22} H-atoms/cm^3. Fuel cartridges and moderator were filled into V2A steel tubes of 0.3-mm wall thickness and 16.1-mm o.d. The axial and radial reflector were composed of steel rods. Further details are given in Ref. [7].

The different lattice configurations (KNK I, KNK II, KNK IV) are shown in Fig. 2; their geometrical data are given in Table I. Different core

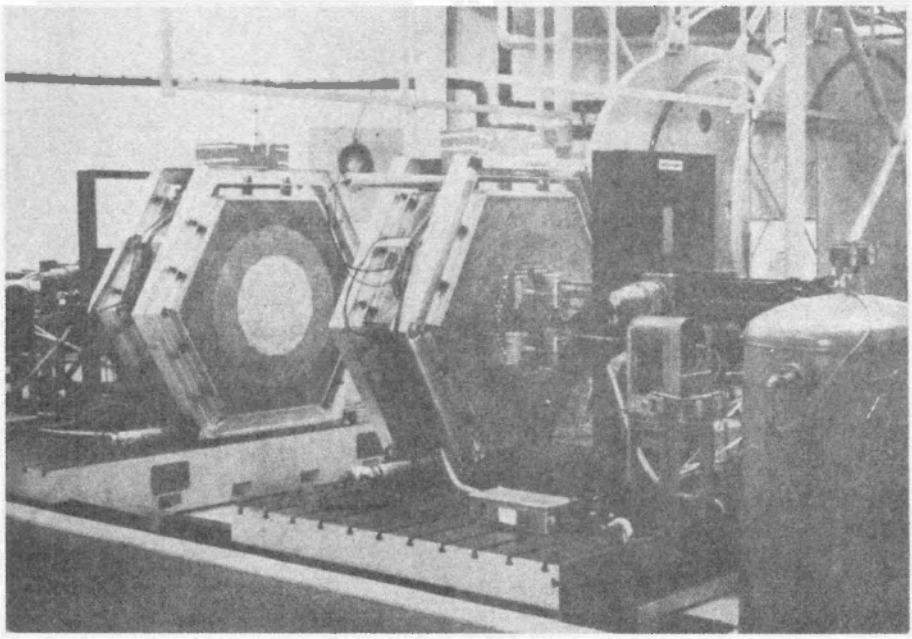


Fig. 1

Critical assembly KNK

loadings of KNK I and KNK IV were investigated, while KNK II was used to measure shutdown worths of control rods at the critical core loadings. The critical core loading amounted to 320 fuel rods at KNK I and 72 fuel clusters at KNK II. A critical assembly of KNK IV could not be established because of the limited amount of $ZrH_{1.7}$ available. The position of the steel radial reflector was not changed for the different fuel loadings of KNK I. Starting from a critical loading the positions of the unloaded fuel rods were filled with $ZrH_{1.7}$ so that a two-zone radial reflector was built up.

Four different absorber materials were investigated: B_4C, Borax ($Na_2B_4O_7 \cdot 10\ H_2O$) and mixtures of B_4C + 40 vol.% $ZrH_{1.7}$ and B_4C + 60 vol.% $ZrH_{1.7}$. The absorbers were filled in stainless steel tubes of 16.1-mm o.d., 0.3-mm wall thickness and 120-cm length. The average density was 1.43 g/cm^3 for B_4C, 0.94 g/cm^3 for Borax and 5.62 g/cm^3 for $ZrH_{1.7}$ in the mixtures. Single absorber rods were exchanged with the inner fuel rod of the fuel cluster in the core centre and in three clusters which were symmetrically positioned around the core centre on a circle with a mean radius of 17 cm. Clusters of seven absorber rods were inserted instead of the central fuel cluster and instead of eccentric clusters with 17-cm distance from the core centre. Further measurements were performed with single absorber rods in a central moderator zone, in which the positions of the central fuel clusters were loaded with $ZrH_{1.7}$ (see Fig. 2).

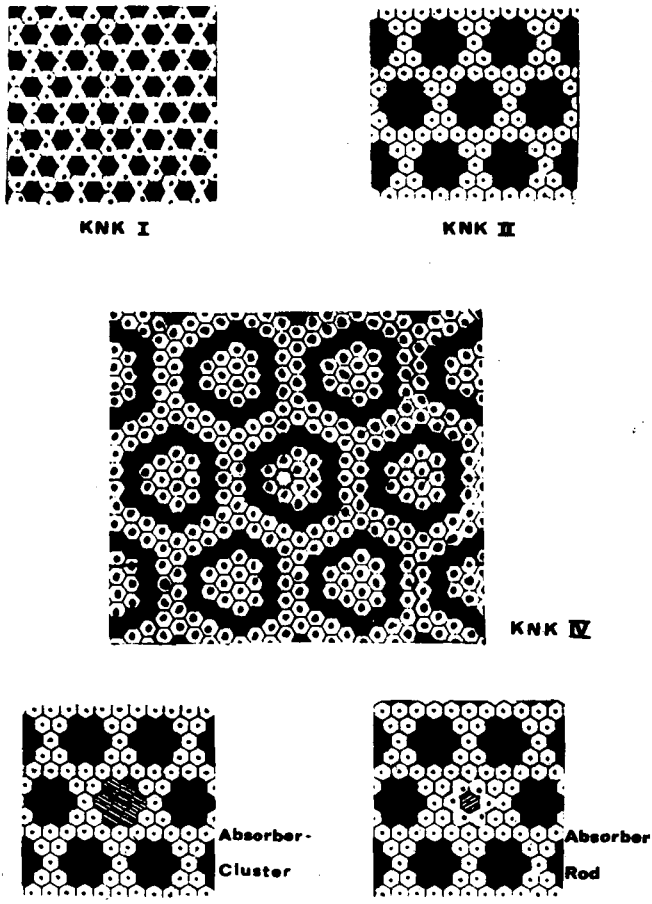


Fig. 2

Lattice and absorber configurations

3. EXPERIMENTAL METHODS

3.1. Measurements of thermal neutron decay constants

The measured parameter is the fundamental mode decay constant of the thermal neutron flux after injection of a short burst of fast neutrons in the core.

Short bursts (15-30 μs) of 14 MeV-(d, t)-neutrons were produced with the Philips sealed-off neutron tube PW 5301 [8, 9] which generated 4×10^4 neutrons per 20-μs burst. Some measurements could be performed with a new, considerably improved version of the Philips tube, giving a yield ten times higher [10]. The neutron tube was positioned in the radial reflector, in which matrix tubes could be removed (see Fig. 3).

TABLE I

GEOMETRICAL DATA

Assembly	$\frac{V_{ZrH}}{V_{UO_2}}$	Number of fuel rods (clusters)	Core length (cm)	Core radius (cm)	Radial reflector (cm)	Axial reflector (cm)
KNK I	2.33	320 (critical	80	29.7	1.1 ZrH+17 steel	19
		315	80	29.5	1.4 ZrH+17 steel	19
		305	80	29.0	1.8 ZrH+17 steel	19
		290	80	28.3	2.6 ZrH+17 steel	19
		260	80	26.8	4.1 ZrH+17 steel	19
		230	80	25.2	5.7 ZrH+17 steel	19
KNK II	1.50	72 clusters (critical)	80	32.5	20 steel	19
KNK IV	2.56	23 clusters	80	31.8	20 steel	19
		19 clusters	80	29.0	20 steel	19
		7 clusters	80	17.5	20 steel	19

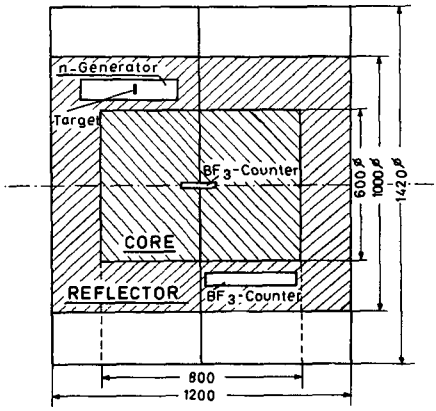


Fig. 3

Neutron generator and detector position

A small BF_3 counter (5 EB 40/13, 20th Century Electronics) could be placed at various positions of the central matrix channel, and a larger BF_3 counter (40 EB 70/50/G, 20th Century Electronics) was used in the radial reflector (see Fig. 3).

Neutron flux decays were observed using a 256-channel time analyser, which was started at the end of the fast neutron pulse. The normally installed background channel and time delay was removed to make possible an analysis of the decay curves by the method of Garelis and Russell (see section 5). The measured data were processed using a computer programme which makes a least-squares fit to a sum of exponentials and computes the decay constant [6]. The decay constants are estimated to have an uncertainty of ±2% based on the precision of repetitive measurements with different detector positions.

3.2. Determination of β/l

$\beta/l = \lambda_c$ is the prompt neutron decay constant for the reactor pulsed at delayed critical. The difficulty, namely, that all neutrons injected into the critical reactor are conserved and give an increasing strong background, was avoided by applying the following procedure: After some hundred bursts the pulsing and data collection were stopped, and the reactor was made subcritical with a calibrated control rod. After almost all neutrons had died away, the control rod was set in the critical position again and pulsing continued. The procedure was repeated about hundred times. This method is quite tedious and the result was not very satisfactory (bad statistics).

It is easier to measure the decay constants for various well-known subcritical states of the assembly and to extrapolate to a critical core loading. The reactor was made subcritical by period-calibrated control rods, rod-drop-calibrated safety rods (fuel withdrawal) and fuel unloading. The reactivity loss by unloading fuel was determined by the source-jerk technique using the Philips neutron tube, which could be switched off in about 1 ms.

4. THEORETICAL METHODS

As described in [6], direct methods were used to solve the multi-group diffusion equations to calculate either the decay constant λ or the multiplication constant k_{eff}. Again the group constants were determined by cell calculations, in which the code PEGGI (similar to MUFT IV) was used in the fast energy groups with the heterogeneity of the cell becoming apparent in the self-shielding factors which give the ratio between effective and infinitely diluted resonance integrals. The associated Dancoff corrections were determined by Monte-Carlo calculations, which seemed to be more accurate in the case of two-dimensional lattices of complicated structure. In the thermal energy group only one-group methods were used; however, instead of one-dimensional S_n-calculations, Monte-Carlo methods were performed which have practically the accuracy of two-dimensional transport theory.

An important parameter in all pulsed neutron investigations is β_{eff}, the effective fraction of delayed neutrons per fission. The value of β_{eff} varies in different systems mainly because of two effects, namely

(1) The fractions of delayed neutron for U^{235} and U^{238} are fairly different, so that β_{eff} is dependent upon the enrichment and upon the shape of the neutron energy spectrum.

(2) The energy of the delayed neutrons is small compared with the energy of the fission neutrons so that the leakage of the delayed neutrons is smaller, and their contribution to k_{eff} is more significant.

The average $\bar{\beta}$ for the mixture of isotope was calculated by

$$\bar{\beta} = \frac{\beta^5 (\overline{\nu\Sigma_f^5}) + \beta^8 (\overline{\nu\Sigma_f^8})}{(\overline{\nu\Sigma_f^5}) + (\overline{\nu\Sigma_f^8})},$$

where $(\nu\Sigma_f^5)$ and $(\nu\Sigma_f^8)$ are the energy and volume averages of the fission cross-sections in the whole core. Consequently, β_{eff} is determined by

$$(1-\beta_{eff}) = (1-\bar{\beta}) \frac{k_{eff}\ (\text{prompt neutrons})}{k_{eff}\ (\text{prompt+delayed neutrons})}$$

Here for instance k_{eff} (prompt neutrons) is the multiplication constant calculated by using the fission spectrum of the prompt neutrons only. Another important parameter connected with β_{eff} is $\lambda_c = \beta_{eff}/l$, where l is the neutron lifetime. Because λ_c is equal to the decay constant in the delayed critical state, a λ-calculation for the theoretically determined critical state was made. The deviations between theoretical and experimental values (Table III) are probably caused more by errors in l than in β_{eff}.

A considerable part of the theoretical work was devoted to the calculation of the shutdown reactivity of different control rods. For this purpose a control cell was defined (Fig. 2) which comprised the control rod and a surrounding cylindrical core zone. Within this cell a version of the code PEGGI (improved version of MUFT IV), which considered the flux depression in the control region by the flux disadvantage factors, was applied. These disadvantage factors were calculated by multigroup-S_n-code (for instance with ten energy groups).

Both codes were used iteratively and finally led to three-group cross-sections for the epithermal energy region. A similar approach was followed in the thermal region, with the exception that instead of S_n-calculations two-dimensional Monte-Carlo methods were used. These four-group constants, together with those for core and reflector, were applied in a diffusion code (similar to WANDA) and gave shutdown reactivities Δk_{eff} shown in Table V. The system with eccentric control rods was calculated by a two-group code which contained the control rods as singularities [11, 12]. The characteristic parameters of these singularities were matched to the aforementioned homogenized four-group calculation for control rods in such a way that the shutdown reactivity for central rods calculated by the homogenized method and by the singularity method led to exactly the same values.

5. RESULTS AND DISCUSSION

5.1. λ for different core configurations

The measured and calculated decay constants for different fuel loadings of KNK I and KNK IV are given in Table II. The difference between k_{eff} (experiment) and k_{eff} (theory) has been calculated using

$$\lambda = \frac{1}{l}[1-k_{eff}\ (1-\beta)] \tag{1}$$

which gives

$$\Delta k_{eff} = -\frac{\Delta\lambda}{\lambda}\left[\frac{1}{1-\beta} - k_{eff}\right],$$

with k_{eff} and λ the calculated reactivity and decay constants, respectively, and Δk_{eff} the reactivity equivalent of the deviation $\Delta\lambda = \lambda$ (experiment) - λ (theory). The results for KNK I are shown in Fig. 4.

5.2. Determination of β/l

Results of the β/l determination are given in Table III together with calculated values of β and β/l. For the nearly critical state, Eq. (1) can be transferred into

$$\lambda = k\beta/l(1+\rho)\ , \tag{2}$$

where ρ is the reactivity in dollar units. This relation was used to determine β/l in KNK I, and KNK II, for which measurements near critical could be performed. For KNK II, measured decay constants are plotted versus measured reactivities in Fig. 5. In the case of KNK IV, the assembly was about 6 to 8 $ subcritical. Equation (1) was used for the β/l determination. The error in the extrapolated β/l is much higher because of the uncertainty

TABLE II

DECAY CONSTANTS FOR DIFFERENT CORE CONFIGURATIONS

KNK I Number of fuel rods	λ (s^{-1}) experiment	theory	Δk (%) [k_{eff}(exp) - k_{eff}(theory)]
315	304 ± 3	220	0.38
305	460 ± 5	354	0.46
290	710 ± 10	590	0.50
260	1250 ± 30	1140	0.49
230	2200 ± 300	1780	2.45

KNK IV Number of fuel elements	λ (s^{-1}) element	theory	Δk (%) [k_{eff}(exp) - k_{eff}(theory)]
23	1487 ± 20	-	-
19	1926 ± 30	1626[a] 1410[b]	1.0 1.8
7	7068 ± 200	6730	1.0

a) Square core area approximation.
b) Cylindrical core area approximation.

of the k_{eff} values measured by the source-jerk technique. Because of this uncertainty, several pulsed neutron measurements on KNK IV have been evaluated applying the method of GARELIS and RUSSELL [13], which gives $k_1\beta/l_1$. The reactivity worths determined are listed in Table IV together with results of the source-jerk measurements. The results of the two different methods are in fair agreement. The measurements were performed by varying the source and detector positions and the neutron pulse repetition rate. The detector was located in different positions in the core and the reflector. The calculated $k_1\beta/l$ for the same core configuration but for different detector positions differed by about 10%. Great care was necessary in the determination of the delayed neutron tail because of a considerable background which had to be measured separately. Reproducible results were obtained from measurements with the detector in the core centre, while measurements in the steel reflector were difficult because of the low neutron flux intensities.

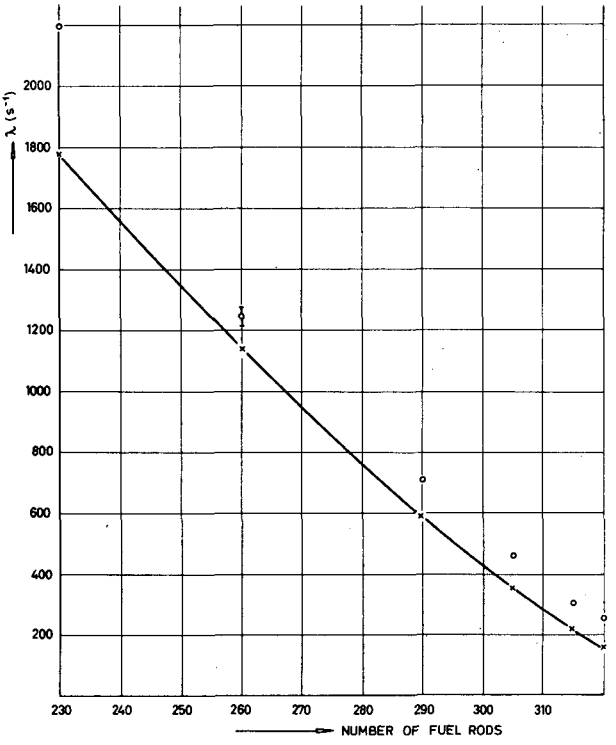


Fig. 4

Decay constants for different loadings of KNK I

TABLE III

β/l FOR DIFFERENT CORE CONFIGURATIONS

Assembly	β (theory)	β/l (theory) (s^{-1})	β/l (experiment) (s^{-1})
KNK I	0.00736	250	223 ± 4
KNK II	0.00749	275	258 ± 5
KNK IV	0.00729	-	205 ± 20

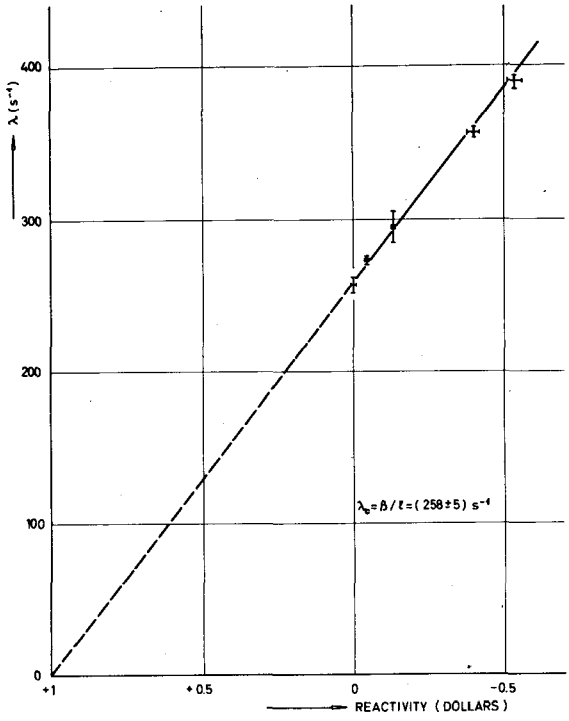


Fig. 5

Determination of β/l for KNK II

TABLE IV

SHUTDOWN REACTIVITIES FOR DIFFERENT LOADINGS OF KNK IV

Assembly	Measured reactivity [$]	
	Source-jerk technique	Garelis-Russell method
25 fuel elements	4.8 ± 0.6	5.2 ± 0.5
23 fuel elements	6.3 ± 0.8	6.2 ± 0.6
19 fuel elements	8.4 ± 1.0	8.9 ± 1.0

5.3. Reactivity worths of different absorbers in KNK II

The results of reactivity measurements on absorber rods and clusters in KNK II are summarized in Table V. The listed experimental values of

TABLE V

DECAY CONSTANTS AND REACTIVITY WORTHS OF DIFFERENT ABSORBER CONFIGURATIONS IN ASSEMBLY KNK II

Absorber	Position	λ (s^{-1}) experiment	Δk_{eff}(%) experiment	Δk_{eff}(%) theory
B_4C	Central moderator zone	1021 ± 20	2.24 ± 0.11	1.96
B_4C+40 vol. % ZrH rod	Central moderator zone	979 ± 20	2.11 ± 0.11	-
B_4C+60 vol. % ZrH rod	Central moderator zone	971 ± 20	2.08 ± 0.11	-
Borax rod	Central moderator zone	908 ± 15	1.90 ± 0.09	1.48
B_4C cluster	Central	1678 ± 30	4.16 ± 0.22	4.22
Borax cluster	Central	1459 ± 25	3.52 ± 0.19	3.69
3 B_4C cluster	17 cm from core centre	3229 ± 100	8.71 ± 0.40	8.28
3 Borax cluster	17 cm from core centre	2750 ± 100	7.30 ± 0.35	7.30
Borax cluster	17 cm from core centre	1115 ± 50	2.51 ± 0.11	2.29
B_4C rod	Centre of central fuel cluster	635 ± 20	1.10 ± 0.05	-
Borax rod	Centre of central fuel cluster	500 ± 10	0.72 ± 0.03	-
B_4C+40 vol. % ZrH rod	Centre of central fuel cluster	577 ± 10	0.94 ± 0.04	-
B_4C+60 vol. % ZrH rod	Centre of central fuel cluster	558 ± 10	0.88 ± 0.04	-
3 B_4C rods	Centre of fuel cluster 17 cm from core centre	985 ± 30	2.13 ± 0.10	-
3 Borax rods	Centre of fuel cluster 17 cm from core centre	750 ± 20	1.45 ± 0.07	-

Δk have been calculated using Eq.(1) with the experimentally determined β/l. The theoretical values for Δk are uncertain with an absolute error $\pm 0.2\%$. This uncertainty is caused by the statistical errors of the Monte-Carlo calculations and by the fact that the centre of the core and therefore the position of the control rods is not well defined in cores which are not of exact cylindrical shape.

It has been assumed that the prompt neutron lifetime does not change with reactivity. This is certainly not correct for the large reactivities which were obtained when fuel clusters were unloaded and absorber clusters inserted into the core. Corrections have, however, not been applied. The change in Δk is small and within experimental error for single rods; for a single B_4C cluster the lifetime change would be about 4%.

6. CONCLUSIONS

It has been shown that there is good agreement between the theoretical and the experimental decay constants λ for the different core loadings of KNK I. The rather large discrepancy at the lowest fuel loading probably results from poor statistics in the measurement of the neutron decay. Because of the irregular core boundaries of KNK IV, the agreement between the theoretical and the experimental values of the decay constant λ is not so good, and it is felt that two-dimensional calculations would give better results for the theoretical λ-values. The deviations of about 10% between the experimental and the theoretical values of β/l are probably the result of a simplified treatment of the thermal group in the calculation of neutron lifetime l. Therefore, it is planned to use multigroup transport theory methods. The evaluation of pulsed neutron measurements on KNK IV, applying the method of Garelis and Russell, has shown that shutdown reactivities agreed with values measured by the source-jerk technique. In this case the method gave results with satisfactory engineering accuracy. The results of the absorber measurements on KNK II show good agreement between the theoretical and experimental values of shutdown reactivity for the cluster cases. In the case of the less important single rods the differences are somewhat larger because of the smaller diameter of the absorbers.

The theoretical and experimental investigations on $ZrH_{1.7}$-moderated, low-enriched lattices have shown that the pulsed neutron technique is a powerful tool to determine shutdown reactivities of absorbers and neutron decay constants for different core loadings which can be used to calculate the reactivity values. Only short measuring times in the range of 30 - 60 min are needed to obtain results with satisfactory accuracy.

ACKNOWLEDGEMENTS

This work has been sponsored by the Bundesministerium für Wissenschaftliche Forschung, Bonn. We acknowledge with pleasure the helpful assistance of Dr. Wrobel of Reaktorzentrum Geesthacht, who was in charge of the operation of the critical facility, and his staff.

REFERENCES

[1] BJÖRNERUD, E.K. and STERN, M.O., Elektrotechnik und Maschinenbau 78 (1961) 576.
[2] ANDERSON, G.M., Astronautics and Aerospace Engng (May 1963) P. 27.
[3] JOHNSON, L.E. and GOETZ, C.A., AIAA Electric Propulsion Conf., Colorado Springs (March 1963).
[4] HARDE, R. and STÖHR, K.W., Proc. 3rd UN Int. Conf. PUAE, 1964, P/537.
[5] EINFELD, K. and RUPPERT, E., to be published in Nukleonik.
[6] EINFELD, K., MEMMERT, G., ULLRICH, W. and WIESNER, S., Proc. 3rd UN Int. Conf. PUAE, 1964, P/645.
[7] BRANDSTETTER A. and HENNIES, H., Atomkernenergie 9 (1964) 259.
[8] REIFENSCHWEILER, O. and VAN DORSTEN, A.C., Phys. Verh. (Mosbach) 8 (1957) 163.
[9] REIFENSCHWEILER, O., Philips Res. Rpts. 16 (1961) 401.
[10] ELENGA, C.W. and REIFENSCHWEILER, O., "The generation of neutron pulses and modulated neutron fluxes with sealed-off neutron tubes", these Proceedings II.
[11] SCALETTAR, R. and NORDHEIM, L.W., Rpt MED C-42.
[12] FRÖHLICH, R., Nukleonik 2 (1960) 192.
[13] GARELIS, E. and RUSSELL, J.L., Jr., Nucl. Sci. Engng 16 (1963) 263.

DISCUSSION

(on the foregoing five papers)

J. RUSSELL: A great deal of evidence has been presented at this Symposium which indicates that under certain conditions the fundamental decay mode for a non-multiplying system does not exist because the lowest discrete eigenvalue lies within the continuum. I wonder whether anything similar can occur in a multiplying assembly. In other words, are there multiplying assemblies which do not have fundamental decay modes?

M. STIÉVENART: There would seem to be no mathematical reason why the fundamental eigenvalue could not join the continuum. We have searched for a reason and have been unable to find one.

E. SILVER: There is a range of reactor conditions where the core is highly loaded and the reflector has low absorption and hence long lifetime. Under such conditions, the reflector lifetime can be of the same order of magnitude as the core-generation time or it can be greater. In such a case, particularly if the reflector generation time is greater, the asymptotic decay is characteristic of the reflector and provides little if any information about the core multiplication. Such "reflector-moderated" reactor systems have been investigated at Oak Ridge, and this effect has been observed.

Y. KANEKO: To yield good statistics after the neutron spectrum reaches the asymptotic spectrum, λ_1-λ_0 must be large in comparison with λ_0, where λ_1 and λ_0 are the first energetic decay constant and the fundamental decay constant, respectively.

I have made an analysis of time-dependent neutron-thermalization phenomena in multiplying systems in a case where the system was infinite and was characterized by 1/v absorption and a given fission cross-section. My conclusion was that λ_1, λ_2, λ_3 ... are the same in multiplying systems as the corresponding values in non-multiplying systems and that only λ_0 changes. It is therefore concluded that it is possible to obtain good statistics in a multiplying system before the neutrons die away.

A. HENRY (Chairman): Could Mr. Hennies please tell me what nuclear model was used to analyse his experiments?

H.H. HENNIES: We carried out four-group diffusion calculations to obtain decay constants and k_{eff}-values, homogenizing the materials in the core. For the absorber rods we defined a control cell where the flux depression was taken into account by appropriate disadvantage factors.

M. SAGOT: It was pointed out at the 1963 Amsterdam Symposium on Exponential and Critical Experiments[1] that safety-rod calibration measurements could be carried out in the Dresden reactor by means of the pulsed-neutron method following the inception of full-power operation. Can anyone give any details of this work?

P. MEYER: We have carried out measurements of this sort in the Humboldt Bay reactor. The results of the experiments are reported in the references given in my paper[2].

---

[1] INTERNATIONAL ATOMIC ENERGY AGENCY, Exponential and Critical Experiments (3 vols.) IAEA, Vienna (1964).

[2] MEYER, P., "An experimental study of the (kβ/ℓ) pulsed neutron source technique in light water assemblies" (SM-62/68) these Proceeding II.

G.R. KEEPIN: I would like to draw attention once again to the important role of delayed and prompt-neutron effectiveness in detailed reactor-kinetics calculations. As we all know, the measured delayed-neutron yields and fractions vary by an order of magnitude among the different fission species. However, there can be even further variation in the values of effective delayed-neutron yields among the different fissioning species in a given reactor depending on its geometry and composition. Neutron-effectiveness calculations become particularly important in mixed isotopic systems, as for example breeder reactors which combine fissionable materials of very different delayed-neutron (and hence kinetic) characteristics. Unfortunately the detailed computation of neutron effectiveness is rather complex, requiring (in addition to prompt and delayed neutron energy spectra) a knowledge of adjoint-flux distribution throughout the representative positions in the assembly; nevertheless for some types of systems detailed effectiveness calculations have been carried out numerically in multigroup-diffusion or transport theory formulation. As future kinetics experiments – including pulsed neutron measurement on multiplying systems – become more precise, there will be a correspondingly greater need for more detailed computations of both prompt and delayed-neutron effectiveness.

A. HENRY: I should like to add one brief comment, namely that in space-time calculations it may be necessary not only to use effective values for β but also to use adjoint-weighted few-group parameters.

J. SHERWIN: We have examined the β_{eff} value for systems of the AGR type. If we define a factor X (sometimes referred to as an effectiveness factor γ) such that $\beta_{eff} = X\beta$, where β is the measured physical value, we find that X is less than 1.0 for large systems of the AGR type. This appears to be a consequence of the fact that the birth energy of the delayed neutrons is below the fast-fission threshold in U^{238}.

C.A. PRESKITT: In connection with this question of the "effectiveness" of delayed neutrons, I think it is important to remember that this is entirely determined by one's definition of reactivity. This has been shown by Henry, Gozani, Gross and Marable, and others. In the case of some definitions of reactivity, usually referred to as dynamic reactivity, the "effectiveness" is unity, i.e. $\beta_{eff} = \beta$.

A. HENRY: It also has to be borne in mind, however, that adjoint weighting yields a theoretical expression for reactivity which is correct to the second order in errors in the flux, whereas weighting with unity (which leads to $\beta_{eff} = \beta$, the physical quantity) results in a theoretical expression for reactivity having a first-order error in the flux which may be of the same order as the reactivity itself. Because of this danger, I favour adjoint weighting and effectiveness calculations.

FAST NEUTRON SYSTEMS

(Session V)

PULSED NEUTRON EXPERIMENTS ON FAST AND INTERMEDIATE SYSTEMS

F. STORRER
EURATOM-CEA ASSOCIATION FOR FAST NEUTRONS
CENTRE D'ÉTUDES NUCLÉAIRES DE CADARACHE
FRANCE

Abstract — Résumé — Аннотация — Resumen

PULSED NEUTRON EXPERIMENTS ON FAST AND INTERMEDIATE SYSTEMS. Experimental and theoretical aspects of the work which has been done on the pulsing of fast and intermediate assemblies are critically reviewed. It is indicated that much less work has been done on the theoretical analysis of such experiments than has been the case for thermal neutron systems. The essential differences between the experimental and theoretical aspects of pulsed experiments on fast and thermal systems are indicated; the areas where research is in progress and where more research is called for are outlined. Special emphasis is placed on the comparison between different types of kinetic experiments. It is shown that all these experiments, including the modulated experiments, the noise experiments and also static source amplification experiments, can be considered as special cases of a more general class of experiments in which the neutron density is a function of time, space and energy. The different objectives of such experiments are discussed as well as the choice of the experiment which will best meet any particular objective.

EXPÉRIENCES, AU MOYEN D'UNE SOURCE PULSÉE, SUR DES SYSTÈMES A NEUTRONS RAPIDES ET INTERMÉDIAIRES. L'auteur procède à un examen critique des aspects expérimentaux et théoriques des travaux relatifs aux bouffées dans les assemblages à neutrons rapides et à neutrons intermédiaires. Il fait observer que l'analyse théorique de telles expériences a donné lieu à beaucoup moins de travaux qu'il n'y en a eu pour les systèmes à neutrons thermiques. L'auteur indique les différences essentielles entre les aspects expérimentaux et théoriques des expériences avec neutrons pulsés sur des systèmes à neutrons rapides et à neutrons thermiques. Les domaines où progresse la recherche et ceux où il faut l'intensifier sont définis. L'auteur met l'accent sur la comparaison entre différents types d'expériences cinétiques. Il montre que toutes ces expériences, et notamment les expériences modulées, les expériences par l'intermédiaire du bruit et aussi les expériences par amplification d'une source statique, peuvent être considérées comme des cas particuliers d'une classe plus générale d'expériences dans laquelle le nombre volumique de neutrons est une fonction du temps, du lieu et de l'énergie. Il traite des différents objectifs de ces expériences et de la manière de choisir l'expérience qui convient le mieux à un objectif donné.

ЭКСПЕРИМЕНТЫ С ИМПУЛЬСНЫМИ НЕЙТРОНАМИ НА БЫСТРЫХ И ПРОМЕЖУТОЧНЫХ СИСТЕМАХ. Дается критический обзор экспериментальных и теоретических аспектов работ по пульсирующим сборкам на быстрых и промежуточных нейтронах. Указывается, что гораздо меньшая работа была проведена по теоретическому анализу таких экспериментов, чем для устройств, работающих на тепловых нейтронах. Отмечается существенная разница между экспериментальными и теоретическими аспектами экспериментов на пульсирующих нейтронах в зависимости от того, работает ли устройство на быстрых или на тепловых нейтронах. Указываются те области, в которых в настоящее время проводятся исследования, а также те области, в которых желательно развить дальнейшие исследования. Особое внимание уделяется сравнению различных видов кинетических экспериментов. Отмечается, что все эти эксперименты, включая эксперименты модуляции, эксперименты по шумам, а также эксперименты по усилению статических источников можно рассматривать как частные случаи экспериментов более общей категории, в которых плотность нейтронов является функцией времени, пространства и энергий. Обсуждаются различные цели такого рода экспериментов, а также выбор тех экспериментов, которые наилучшим образом соответствуют конкретной задаче.

EXPERIMENTOS CON NEUTRONES PULSADOS EN SISTEMAS RAPIDOS E INTERMEDIOS. El autor examina detenidamente los aspectos experimentales y teóricos de la labor que se ha realizado en conjuntos rápidos e

intermedios empleando neutrones pulsados, y señala el hecho de que la atención dedicada al análisis teórico de estos experimentos ha sido mucho menor que la prestada a los sistemas de neutrones térmicos. Expone las diferencias esenciales que existen, tanto en el plano experimental como en el teórico, entre las determinaciones con neutrones pulsados realizados en sistemas rápidos y los llevados a cabo en sistemas térmicos. Delimita las esferas en que se están realizando investigaciones y las que requieren un esfuerzo mayor. Hace especial hincapié en la necesidad de comparar los resultados de los distintos tipos de experimentos cinéticos. Pone de manifiesto que todos estos experimentos -modulados, sobre el ruido y también sobre amplificación estática de la fuente- pueden considerarse como casos especiales dentro de una misma categoría más general de experimentos en los que la densidad neutrónica varía en función del tiempo, del espacio y de la energía. El autor examina los distintos objetivos que se persiguen con dichos estudios, así como la elección del tipo de experimento que permitirá alcanzar con mayor facilidad un objetivo determinado.

I. INTRODUCTION

Pulsed experiments, or more generally kinetic experiments on fast and intermediate systems, can be classified into four types, according to the input and to the presence or absence of thermal feedback.

(1) Input: time-dependent source; no feedback.
(2) Input: time-dependent source; with feedback.
(3) Input: time-dependent reactivity; no feedback.
(4) Input: time-dependent reactivity; with feedback.

This paper surveys only the first type, which is ideally suited for the study of basic neutronics, since it involves no other phenomena and since the relation between input and any arbitrary output (e.g. flux, reaction rate) is perfectly linear, a property which greatly simplifies the analysis.

Just a few comments about the three other types: type 2 has to the author's knowledge never been put into practice. As is the case for type 4, an experiment of this type should find a possible use in a measurement of feedback. Such an experiment was suggested by FOSSOUL [1]. Type 3 is suited for reactivity measurements (rod drop or asymptotic period), studies in neutronics (especially in its linear range: zero power transfer function), and is used also to provide neutron bursts (IBR reactor of the USSR). Type 4 is mainly used for measurements of feedback (transfer function at power) and for safety studies (SEFOR) and also to provide neutron bursts (Godiva).

The burst production aspects of types 3 and 4 are covered in the session on pulsed reactors and neutron sources of these Proceedings. In experiments of types 3 and 4 the transients are normally slow enough for their neutronic aspect to be treated by a conventional point kinetics model in space and energy. On the contrary, the main problems which arise in type 1 are caused by the departure from this point model.

From now on I shall concentrate on experiments of type 1. Their linear nature has a direct consequence: the responses to different time-dependences of the source are directly linked together by very simple mathematics.

One can forget the physics when comparing responses of pulsed (single pulse or repetitive pulses [2]), modulated and static experiments, and also the cross correlation between output and input in random-noise experiments [3].

Pulsed experiments are stressed in this paper. Modulated techniques are discussed at this meeting [4], as well as their application to fast systems [5, 6]. Occasional references to them are made in this paper, particularly

the area method of SJÖSTRAND [7] and a modified version suggested by CADILHAC et al. [6].

While discussing pulsed experiments, the classical problem of discrete eigenvalues and eigenfunctions will of course repeatedly come up notwithstanding Corngold's personal remark that "we theoreticians should impose on ourselves a moratorium on this subject, so as not to scare off the experimentalists". I will try however to put this problem into its proper perspective.

Strictly speaking a discrete eigenvalue can exist only for critical or supercritical systems, since in subcritical systems one can always find mechanisms for transient modes which, however faint, decay slower than any calculated discrete mode. Such slowly decaying transient modes can arise from delayed neutrons, from reflected neutrons, from very high energy neutrons (where the cross-section decreases as $1/E$ or $1/v^2$) or, in the case of fast systems, from very slow neutrons. For practical purposes – for our experimentalists – it will suffice that there be a sharp peak in the continuous eigenvalue distribution, or in other words that there be a time range in which an exponential decay with a well-defined decay constant predominates.

I will not insist here on the possible applications of pulsed neutron work since such considerations are not proper to fast systems. The main purpose of such experiments may be to provide either a direct measure of a quantity of interest or an integral check of basic data or of methods of calculation. Kinetic experiments obviously have greater potentialities than static experiments, the latter being a poor particular case of the former. In addition kinetic experiments have the advantage over static experiments of bringing in the velocity of the neutrons as an essential variable, and not only indirectly through the energy dependence of the cross-sections. This property, which is abundantly exploited in time-of-flight experiments, makes it possible to measure or to influence neutron spectra, as is discussed in some detail in [6].

Pulsed experiments, which have now become very common on thermal systems – multiplying or not – have not as yet been widely applied to fast and intermediate systems. This is one of the reasons why this paper will not be limited to a survey of past experimental and theoretical work. Most of the work is still to be done, and part of this paper will be devoted to the programme of various organizations and to speculations as to what will or should be done and how it could be done. Theoretical aspects will be stressed, for no other reason than my personal tendencies.

II. ESSENTIAL CHARACTERISTICS OF FAST AND INTERMEDIATE SYSTEMS

The essential characteristic of these systems is that practically no neutrons reach thermal energies, so that no upscattering can take place. Of course, even in Godiva, and a fortiori in more dilute systems, a lone neutron may at times escape all the traps and reach thermal energies and even be upscattered, but the point is that these events are so few that they may be neglected. Thus, only through multiplication can there be a feedback from low to high neutron energies. I need not add that zero-velocity neutrons, which seem to bother the thermal-system theoretician, never enter into the

picture. Another consequence of the high energy of the neutrons is that the medium with which they collide can be considered as a collection of free atoms (except in Doppler effect calculations), thus avoiding many complications. On the other hand considerable complications arise from the fact that neutron reactions take place over a wide range of energies, in which the collision rates differ by orders of magnitude. As an example Fig. 1

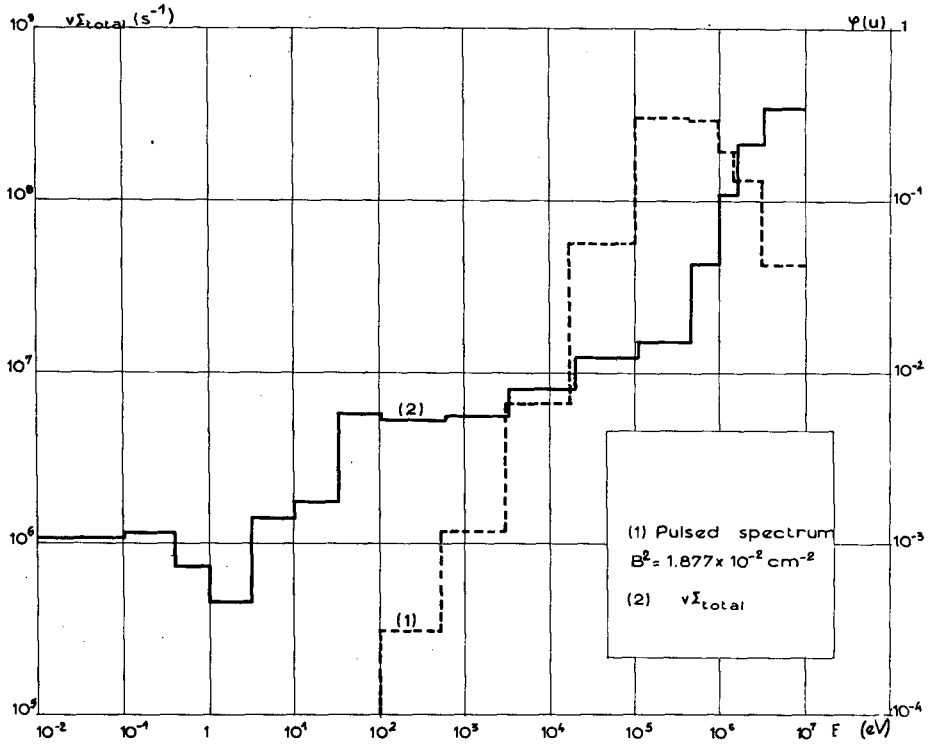


Fig. 1

Calculated spectrum and collision rate for a typical pulsed fast system

shows the asymptotic spectrum, and also the collision rate $v\Sigma$ as a function of energy, for a typical pulsed fast system. In thermal systems most of the reactions take place in a narrow energy band, with low collision rates, while the slowing-down process, which fortunately involves much higher collision rates, may be rather simply described, often by a steady-state kernel. No such privileged energy exists in fast systems. Except in very special cases, a monoenergetic treatment is of no value. As will be seen later, the wide range of collision rates gives rise to a wide range of continuum eigenvalues. Only in multiplying systems, and even then not too far below criticality, can a discrete eigenvalue pull itself out of this continuum. For higher spatial modes the lower multiplication further reduces the possi-

bility of having a discrete eigenvalue. The fact that "upscattering" can only be the result of a fission, and also the important role of inelastic scattering in fast systems, makes the mathematical treatment of these systems quite different from that of thermal systems.

Finally, pulsed experiments on fast systems differ from those on thermal systems by the instrumentation required. Typical decay periods vary from about 10^{-8} s for low-reactivity, hard spectrum assemblies to about 10^{-5} s for near-critical, soft spectrum assemblies. The source pulse cut-off has to be short compared to the decay period of the assembly. The beam-deflection method is therefore used to provide short pulses. On the output side, detectors with short time resolution (a few 10^{-9} s) and fast electronics are required. The instrumentation requirements are similar to those of fast neutron time-of-flight experiments. Because of the high dead-time of the time delay analysers which are presently available, the detection rate has to be limited to one count per pulse, and high pulse repetition frequencies are required to achieve good statistics in a reasonable time. This subject is treated in the session on pulsed reactors and neutron sources these Proceedings [8].

III. NON-MULTIPLYING SYSTEMS

In such systems, no discrete eigenvalue can exist, since in the absence of upscattering, the spectrum shifts continuously towards low energies. In a multigroup representation, the matrix is triangular, and the eigenvalues are the diagonal elements, which are the group removal rates. These tend to a continuous spectrum when the number of groups increases.

A single discrete eigenvalue would exist in the trivial, and fictitious, case where there is no slowing down and where the removal rate by absorption and leakage is independent of energy, i.e. where the removal cross-sections have a $1/v$ dependence. The eigenvalue is this constant removal rate, while the eigenfunction is then arbitrary, since there is no coupling between different energies.

Another trivial case is that in which the removal rate is independent of energy, but with slowing down. The spectrum is then continuously softened (i.e. no eigenfunction) but the total neutron population as well as the total absorption and leakage rates decay with a single decay constant, the removal rate.

The absence of discrete eigenvalues does not make pulsed experiments on non-multiplying systems a priori useless, even though the interpretation is made more difficult. It is always possible to compare a calculated and an experimental time-dependent behaviour of some measurable quantity and to try to derive from this comparison some information on the validity of basic data or of a theoretical method. As is discussed in section V of this paper, pulsing of non-multiplying systems can also be performed to measure spectra by time-of-flight.

In this section the past and present work on pulsed non-multiplying systems is reviewed. It will be apparent that the shrewdness of experimenters often makes up for the basic complexity of these experiments, and that more information can be obtained than can be a priori conjectured.

The first experiments were carried out at Los Alamos twenty years ago [9]. The experimenters were then interested, apparently for a very practical reason, in the time and energy dependence of the neutrons reflected back into fast cores by reflectors in U, WC and BeO. A periodically pulsed (or modulated) source of D-D neutrons was located at the centre of the spherical cavity within the approximately spherical reflectors. The energy of the source ranged from 2.1 to 3.1 MeV. U^{235}, U^{238} and Np^{237} fission detectors were also located in the cavity and the resolving time of the apparatus was of the order of 10^{-7} s, the pulse width being about 10^{-6}s. Use of delay lines for each detector makes only one pulse-time analyser circuit necessary. The measurements were also performed without a reflector, so that the reflected neutrons could be obtained by subtraction. The measurements agreed well with the results obtained by a crude calculation. The theory however was here of secondary importance, since the goal was the measurement of directly useful properties of reflectors.

Pulsed experiments on assemblies of bismuth, lead and natural uranium have been carried out at the Massachusetts Institute of Technology by BEGHIAN and co-workers [10]. Bursts (3×10^{-9} s long) of monoenergetic neutrons of variable energy were obtained by a Van de Graaf generator through the $Li^7(p, n)$ Be^7 reaction. A scintillation counter with a 1-in diameter by 1-in thick plastic phosphor was used to measure the neutron flux. Standard nanosecond neutron time-of-flight equipment was used, with an overall resolution of about 4×10^{-9} s.

The detectors were biased so as not to count neutrons which had lost more than 300 keV (for the 0.84-MeV source) or 600 keV (for the 1.26-MeV source). The decay curves observed for assemblies of various sizes could over some time interval be approximated by exponentials, with decay periods ranging from (6 to 30)$\times10^{-9}$s. This exponential behaviour can be explained by the quasi-monoenergetic nature of these experiments: because of the detector bias, most of the inelastically scattered neutrons are not counted, and for the heavy nuclei in these assemblies elastic moderation is negligible (energy loss during a mean neutron lifetime of 20 and 50 keV for uranium and lead respectively). These experiments are indeed analysed by the authors on the basis of a one-velocity model. It is shown that it is possible to measure fast diffusion coefficients and the sum of absorption and inelastic cross-sections. Transport corrections to the diffusion approximations are made. This may however be superfluous in view of the errors introduced by the one-velocity approximation. There is for example a discrepancy of a factor of 4 between the experimental value of the coefficient of the B^4 term and that obtained from NELKIN's [11] transport solution. For the same reason; I do not quite agree with the authors when they indicate that these experiments can serve as a check on the validity of the assumptions of transport theory.

A P_N solution with Marshak boundary conditions as carried out for this experiment by Cockrell and co-workers [12] also seems too refined.

I would add also that these experiments should be considered as integral checks of cross-sections rather than as their direct measurements.

Beghian and co-workers extended this technique to iron, a medium weight nucleus, where energy degradation by elastic scattering becomes important [13, 14]. The average energy loss over a neutron lifetime ranges

in this case from 30 to 100 keV. Such an energy loss does not so much affect the one-velocity theory as it has an effect on the counting rate, since the detector efficiency varies with energy. The authors took this into account by adding a fictitious cross-section to the non-elastic cross-section. The experimental curve still had an exponential behaviour over more than a decade.

Similar measurements have been made on medium weight nuclei (Fe, Cu, C) by d'OULTREMONT and co-workers [15]. The source neutron energies were 1.4, 1.1, 0.89 and 0.67 MeV. The experimental results are well confirmed by Monte-Carlo and P_1 calculations.

In Japan, HIRAOKA and co-workers [16] pulsed lead and natural uranium assemblies. In this case however the neutrons were obtained by D-T (14 MeV) and D-D reactions (4.8 MeV maximum). The pulse width was 4 ns, time resolution, 5.6 ns and the detector was a 1-in diameter × 1-in thick LiI scintillator. Decay curves have been measured for neutron energies in the ranges 0.8 - 1.2 MeV, 2.5 - 3.5 MeV and 4.5 - 5.8 MeV. For lead, in all combinations of source energy, detectors energy, and assembly size, a smooth quasi-exponential behaviour was observed with a decay period which is a systematic function of the energy, thus confirming that no asymptotic spectrum exists. For natural uranium a similar behaviour was observed, except that for a detection energy above 2.5 MeV and after about 30 ns a second exponential behaviour is observed with a longer decay period, which is independent of the source energy and of the detection energy, and seems actually close to the only decay period observed at lower energy. Thus it appears that an asymptotic spectrum is reached. The authors conjecture that this is indeed the case, because of the multiplying nature of natural uranium. Calculations by STORRER and STIÉVENART [17] indicate that no asymptotic spectrum could be obtained, because of the low multiplication factor of natural uranium. We arrived however at the conclusion that in pure U^{238} an asymptotic spectrum could eventually be obtained through multiplication, but only for those neutrons which are above the fission threshold.

In natural uranium, this "asymptotic" mode for fast neutrons can exist only as long as neutrons are not fed back from lower energies through U^{235} fission. It is possible that the initial steep exponential behaviour which was observed for high energy neutrons corresponds to this initial "asymptotic" mode for fast neutrons.

The second and slower apparent exponential decay is hard to explain; the experimenters show a large discrepancy between experimental and calculated value, but it is not clear how this calculated value was obtained.

Further experimental work has been performed in Japan and theoretical analysis is in progress [18].

The measurement of the capture cross-sections of various materials below 50 keV with a lead slowing-down-time spectrometer is a very interesting and special application of pulsed experiments [19, 20]. This technique is based on the fact that a burst of monoenergetic neutrons injected in a lead assembly retains a narrow energy spread while slowing down. Thus, as in time-of-flight spectroscopy, there is a very close relation between time and energy. By adding a small quantity of capturing material to the lead, it is possible to deduce the capture cross-section of this material as a function

of energy from the variation of the reaction rate as a function of time. It is reported in [20] that the measurements are not accurate above 20 keV.

IV. MULTIPLYING SYSTEMS

Except for the original work at Livermore reported in 1957, very little experimental and theoretical work was done in this field until very recently. The pace is now picking up, but most of the work remains to be done and many questions have not been answered yet. Past and present work will be reviewed in this section in more or less chronological order, jumping back and forth from experiment to theory.

At Livermore PASSELL, BENGSTON and co-workers [21, 22, 23, 24] pulsed bare enriched uranium spheres of various diameters. The source neutrons (14 MeV) were produced by sweeping an accelerator beam over a tritiated target. Pulse width was 10^{-8} s. The leakage flux was detected by a Hornyak fast neutron detector which fed, through a time-to-height converter, a multichannel pulse height analyser, the ultimate channel width being of the order of 3×10^{-9} s. After the initial space and energy transients, a purely exponential behaviour was observed, with decay periods varying with the diameter of the assembly from about 15 to more than 100 ns. The experimental decay constants agree within 4 to 9% with the values calculated by a three-group S_n code. The method consists in the determination of the capture cross-section λ/v which has to be subtracted to make the system critical. This method of calculation is of course the best, since it can be used in principle with the most refined (steady state) multigroup diffusion or transport codes, which can best take the detailed geometry and cross-section data into account.

Under those conditions a comparison of calculation and experiment provides an excellent check on the validity of the codes, including the cross-sections, which are used for steady state calculations. Unfortunately, as will be seen later, this method, when blindly applied, breaks down in most cases. Even for these highly enriched uranium assemblies, the method does not work, except very near critical, if groups are added at the low energy end. The reason for this break-down is that in most cases λ is, strictly speaking, not the smallest discrete eigenvalue at all, but a peak in a continuous eigenvalue spectrum or at best a discrete eigenvalue surrounded by an infinity of discrete or continuous eigenvalues. We see later however that this method, which we will call "the steady state code method", can often be rescued in practice, by choosing an adequate group structure and not allowing groups below a certain energy. This can only be done however after a thorough theoretical analysis which will lead to an understanding of the problem. Such an analysis is greatly facilitated if the asymptotic reactor theory is used, i.e. if one expands the spatial distribution in terms of $e^{i\vec{B}\cdot\vec{r}}$ functions. Either diffusion or asymptotic transport theory can be used. We will not delve here into the problem of finding the adequate B^2 (plus eventually higher B^2 eigenvalues) for a given bare assembly. I will just refer to the work of INÖNÜ (25) and GELBARD and DAVIS [26] for the determination of adequate extrapolation distances. In 1963, BORGWALDT [27] performed a

series of 8-group diffusion fundamental mode calculations on bare uranium spheres of various sizes and enrichments. In such calculations the leakage is represented by a DB^2 cross-section and the decay constants α_i are the eigenvalues of the multigroup matrix. In addition to the α_i's, Borgwaldt determined for the various modes the flux and adjoint flux spectra (eigenvectors) as well as their relative "intensities" for a given source spectrum. He arrived at the conclusion that pulsed experiments were not promising for $k < 0.7$, mainly because the relative intensity of the fundamental mode was too small.

At about the same time, STORRER and STIÉVENART [17] proposed a simplified approach to the fundamental mode calculation for multiplying systems, which is based on only one assumption, i.e. that the spectrum of the neutrons emerging from a fission is independent of the energy of the incident neutron and of the nuclide which underwent fission. This approach can be used as well with a multigroup or a continuous energy model, and with both diffusion or asymptotic transport theory. This method was later extended to time-independent problems [28] and then generalized to provide a description for a wide class of experiments, including modulated experiments [29]. It is briefly described here as it applies to pulsed experiments. It consists in expressing the solution for a multiplying medium in terms of solutions for a non-multiplying medium (the same medium with $\nu = 0$), which thus involves only slowing down, since there is no upscattering in fast systems.

When a burst of arbitrary spectrum is injected into a multiplying medium, we look first at the neutrons coming directly from the source, not via a fission. For these neutrons the medium can be considered as a non-multiplying one (same cross-section but $\nu = 0$), and the flux $\phi_1(E, t)$ before fission is obtained by a slowing-down calculation. When $\phi_1(E, t)$ has been calculated, the source $S_1(t)$ of first fissions can be found by

$$S_1(t) = \int \nu\Sigma_f(E)\phi_1(E, t)\,dE$$

$\phi_1(E, t)$ depends evidently on the spectrum of the burst. For a burst with the fission spectrum, $\phi_1(E, t)$ will be particularized as $\phi_f(E, t)$ and the source of first fissions as $K(t)$

$$K(t) = \int \nu\Sigma_f(E)\phi_f(E, t)\,dE$$

$k(p)$, Laplace transform of $K(t)$, is the transfer function between successive (prompt) fission sources; let us note that

$$k(0) = \int_0^\infty K(t)\,dt = k_{eff,p}$$

where the subscript p refers to prompt neutrons. Similarly $s_1(p)$ and $s(p)$ are the Laplace transforms of $S_1(t)$ and of the total fission source $S(t)$.

It is shown in the reference that

$$\boxed{s(p) = \frac{s_1(p)}{1 - k(p)}}$$

This is a generalization of the subcritical multiplication formula.

As for the total fission source S(t), it will be obtained from s(p) by an inverse Laplace transformation.

It should be noted that the solution S(t) for a multiplying system, can be obtained from the transfer functions $s_1(p)$ and $k(p)$, which are very similar and can be calculated by slowing-down calculations in a non-multiplying medium.

When evaluating S(t) contributions will come from the singularities of s(p).

In a multigroup approach, $s_1(p)$ and $k(p)$, which are easy to calculate since the slowing down matrix is triangular, have in general the same poles. The poles of s(p) are then the roots of

$$\boxed{k(p) = 1}$$

There are n such roots in a n-group calculation and the largest root in algebraic value corresponds to the fundamental decay mode of the system. In the continuous model, there may be contributions from poles of s(p), and from other singularities, which can give rise to a continuum of modes.

It can easily be seen [29] that for any discrete mode, with eigenvalue α_i, the corresponding spectrum is given by $\varphi_f(E, \alpha_i)$, the Laplace transform of the slowing-down flux following a fission burst, evaluated at $p = \alpha_i$. Furthermore, the "intensity" of a given mode α_i is given by the residue of s(p) at $p = \alpha_i$, which can be expressed as

$$r(\alpha_i) = - \frac{s_1(\alpha_i)}{[d\,k(p)/dp]_{p=\alpha_i}}$$

Multigroup "k(p) method" calculations have been carried out in [17], for highly enriched uranium spheres. It is seen that, with a given group structure characterized by the $v_i\Sigma_i$, which are the group removal rates (by absorption, slowing down and leakage) the smallest decay constant $\lambda_i = -\alpha_i$ can never be larger than $(v\Sigma)_{min}$, which usually corresponds to the lowest energy group. When λ_1 is well separated from $(v\Sigma)_{min}$, the residue $\tau(\alpha_1)$ is large, indicating a high intensity in the fundamental mode. However if k_{eff} decreases (increase of B^2 or decrease of ν), λ_1 tends to $(v\Sigma)_{min}$, but at the same time $\left(\frac{dk(p)}{dp}\right)_{p=\alpha_1}$ increases and the intensity of the α_1 mode tends to zero. This means that there are very few neutrons in the α_1 mode, and that the role of the fundamental mode is taken over by α_2, which we called a pseudo-fundamental mode. It would indeed have been the fundamental mode if the (lowest energy) group corresponding to $(v\Sigma)_{min}$, in which there are very few neutrons anyway, had been left out. This behaviour can rather intuitively be described as follows: when k_{eff} decreases, the "fundamental" α crosses the $-(v\Sigma)_{min}$ value (from α_1 it becomes α_2), dragging along with it an important residue, while leaving behind a parasitic low residue mode with $\alpha_1 \simeq -(v\Sigma)_{min}$. It is no wonder that difficulties arise when one tries to find the "pseudo-fundamental" eigenvalue α_2 by a steady state code: since α_2 is smaller than $-(v\Sigma)_{min}$, the removal rate $(v\Sigma)_{min} + \alpha_2$ becomes negative in the lowest energy

group. As was said above however, the "steady state code method" could be rescued by dropping this group, or eventually several groups at the low energy end.

Before going into some more theoretical considerations, both with a multigroup and with a continuous energy model, I should say a few words about the pulsed experiments which are performed in the Karlsruhe SUAK facility, since our theoretical work is illustrated by attempts at their interpretation.

The SUAK facility is described in [5]. Very interesting experimental results are presented and I am sure that our German colleagues will have done outstanding theoretical work in trying also to interpret them.

The attempts made in France are presented in [6] for the multigroup method, and in [30] for the continuous energy method. In [6] the multigroup k(p) technique is carried out one step further. After s(p) has been obtained, without discarding any group, S(t) is obtained by a Laplace inversion and $-S'(t)/S(t)$ is then calculated numerically and plotted as a function of time. Such a plot obtained from the 16-group Hansen Roach set is shown in Fig. 2 for SUAK assembly No. 2 (k ranging from 0.81 to 0.87, depending on the

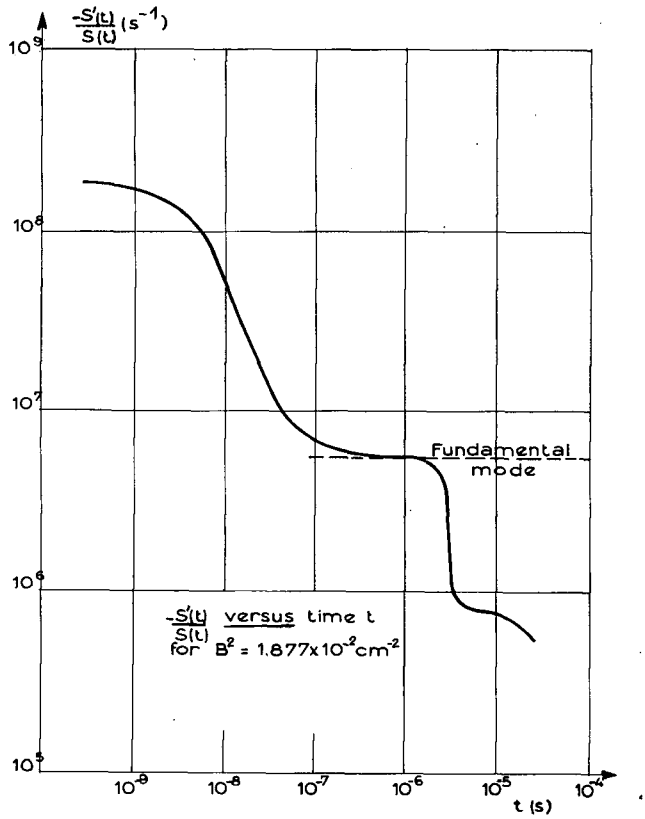


Fig. 2

Dependence of $\frac{-S'(t)}{S(t)}$ on time for $B^2 = 1877 \times 10^{-2}$ cm^{-2}

cross-section set). If a true asymptotic mode existed, this function should tend for large t to the decay constant $\lambda_1 = -\alpha_1$. It is seen however that for a time interval ranging from about 0.5 to 1.5 μs after the burst, the curve stays on a plateau at $\lambda = 5.4 \times 10^6\ s^{-1}$, or $\lambda^{-1} = 187$ ns. After about 4μs a new, less well-defined plateau is reached with λ about $0.8 \times 10^6\ s^{-1}$. In Table I, the first seven eigenvalues λ_i are indicated together with their relative intensity. This quantity is defined by $\frac{r(\lambda_i)/\lambda_i}{\sum_j (\lambda_j)/\lambda_j}$. For each mode, it is

TABLE I

RELATIVE INTENSITY OF EIGENVALUES

λ_I	λ ($10^6\ s^{-1}$)	Relative intensity
λ_1	0.47	$<10^{-6}$
λ_2	0.75	0.6×10^{-5}
λ_3	1.11	1.2×10^{-5}
λ_4	1.14	-1×10^{-5}
λ_5	1.4	0%
λ_6	1.8	0%
λ_7	5.4	41.3%

proportional to the residue divided by the decay constant, and thus proportional to the integral over all time of the contribution of this mode to S(t).

It is seen that the relative intensities of the first six modes are negligible, while almost half of all the fissions are in the seventh mode, which corresponds to the plateau of Fig. 2. Thus for all practical purposes λ_7 corresponds to a pseudo-fundamental mode, and the first six modes are low intensity parasitic modes. It is interesting to note that this information can be obtained either from Fig. 2 or from Table I, but better yet from both. A computer code has been written in Cadarache which calculates automatically both sets of data.

This pseudo-fundamental decay constant λ_7 could have been obtained directly as λ_1, if the six lowest energy groups, down from 30 eV, had been discarded. Figure 1 shows the spectrum of the pseudo-asymptotic mode. It can be seen that there are practically no neutrons below 100 eV.

Now that we know how many groups should be discarded, we can try to obtain a better value for the decay constant by the use of a steady state code, such as a two-dimensional S_n code. This however is not possible if the parasitic groups are not discarded, since negative cross-sections would appear in these groups.

The time constant $\lambda_7^{-1} = 187$ ns is in fair agreement with the experimental value 220 ns. A better theoretical value could be obtained by choos-

ing a finer group structure in the important region above 30 eV, and by using an S_n code.

A plot of $-S'(t)/S(t)$ for the first SUAK assembly (k_{eff} ranging from 0.71 to 0.75 depending on the cross-section set) is shown in Fig. 3. Here the plateau is very poorly defined, with a decay constant of about 8×10^6 s^{-1}. This

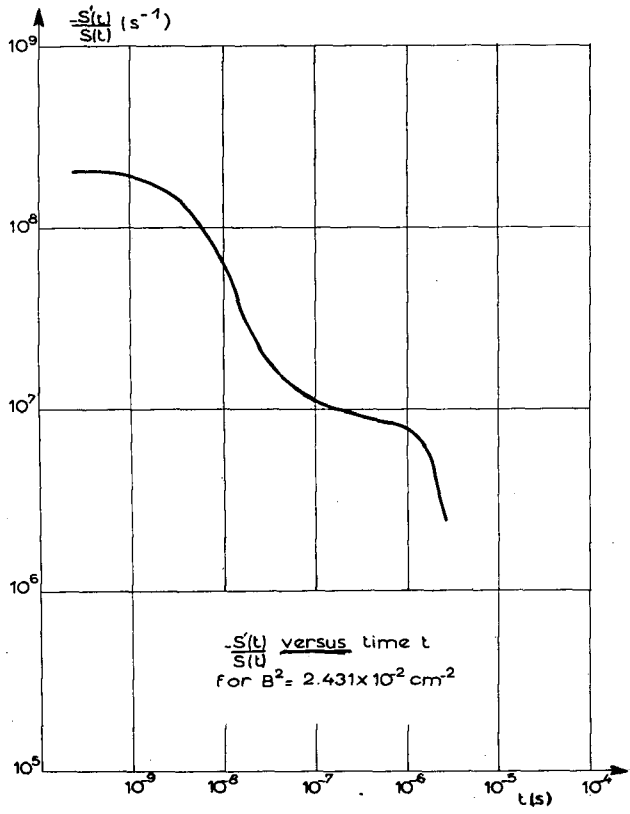


Fig. 3

Dependence of $\frac{-S'(t)}{S(t)}$ on time for $B^2 = 2431 \times 10^{-2}$ cm^{-2}

time it is λ_{10}, with a relative intensity of 37.5% but there are some more slowly decaying modes with relative intensities of about 1%.

Thus it seems that for SUAK-type assemblies it is difficult to find a well-defined pseudo-asymptotic decay constant when k_{eff} is smaller than about 0.8.

CADILHAC et al. [30] have used the k(p) method with a continuous energy model in diffusion theory. This method gives a clearer insight into the qualitative structure of time-dependent phenomena since a multigroup method always exhibits artificial features related to the choice of the energy groups. However for quantitative evaluations a multigroup method must always be used, at least for part of the calculation.

By using rather general slowing-down kernels it is found that k(p) can be written as $k(p) = \int_{\lambda_0}^{\lambda_1} K(\lambda) d\lambda / (\lambda + p)$. Note that in a multigroup representation

k(p) is also given by such an expression, with $K(\lambda) = \sum_{j=1}^{n} K_j \delta(\lambda-\lambda_j)$, which is certainly only an approximation to the true $K(\lambda)$. k(p) is a regular analytic function of p outside the negative real axis, and also on the part of the negative real axis outside the interval from $-\lambda_0 = -(v\Sigma)_{min}$ to $-\lambda_1 = -(v\Sigma)_{max}$. It is shown that S(t) is then given by $S(t) = \int_{\lambda_0}^{\lambda_1} \gamma(\lambda) e^{-\lambda t} \alpha\lambda$ plus eventually a discrete exponential mode $\gamma_\alpha e^{-\alpha t}$ if k(p) = 1 has a root $-\alpha$, with $\alpha < \lambda_0 = (v\Sigma)_{min}$. If this is not the case, no discrete fundamental mode exists: S(t) is a continuous combination of decaying exponentials. However if the distribution $\gamma(\lambda)$ shows a sharp peak around some value of λ, this value, which is larger than $(v\Sigma)$ will be a "pseudo-mode" and S(t) will possibly behave like the corresponding exponential during a finite time interval. This is in qualitative agreement with what was found by a multigroup method.

Cadilhac and co-workers then introduce a very interesting technique which combines the quantitative advantages of the multigroup method and the qualitative advantages of the continuous energy method. They try to deduce the cumulative function $c(\lambda) = \int_{\lambda_0}^{\lambda_1} K(\lambda) d\lambda/\lambda$ from its multigroup step approximation $\sum_{\lambda_j < \lambda} K_j/\lambda_j$. If simple analytical expressions of $c(\lambda)$ can be fitted, the further numerical evaluations can be carried out with the continuous energy model. This procedure was successful for hard spectrum assemblies, but not for very dilute assemblies, because of the complex structure of $K(\lambda)$ when the spectrum is very degraded.

Both the multigroup and continuous energy models seem to indicate that
(1) When k_{eff} is small (B^2 large) there is only a continuous distribution of modes.
(2) When k_{eff} increases, a peak develops in this continuous distribution $\gamma(\lambda)$, and moves to the right as it becomes larger and sharper.
(3) If $(v\Sigma)_{min} > 0$, there is a value of k_{eff} above which this peak pops out of the continuum and becomes a true discrete eigenvalue $\lambda_1 < (v\Sigma)_{min}$.

The range of k_{eff} for which a discrete eigenvalue exists is strongly dependent on the relative values of $(v\Sigma)_{min}$ and of the inverse of the lifetime. Indeed, for a not too highly subcritical system, the asymptotic decay constant is given approximately by $\alpha = (1-k)/\ell$ (= absorption rate − production rate). Thus a discrete eigenvalue should exist for $(1-k)/\ell < (v\Sigma)_{min}$ or $k > 1-\ell(v\Sigma)_{min}$.

This range of values of k is unfortunately narrow, but we have seen that the pulsed technique can be extended to lower values of k, as long as pseudo-asymptotic modes can be defined and measured.

There is an excellent qualitative agreement between our results, and those obtained by CORNGOLD [31, 32, 33] for thermal non-multiplying systems.

As a next theoretical step the continuous energy model should be treated with asymptotic transport theory. Similarly to [32] one should find that the branch cut for k(p) and s(p) along the real axis is replaced by a curve of singularities, described by $\lambda = -v\Sigma(v) \pm iBv$, where the maximum value of the real part is again $-(v\Sigma)_{min}$. I close this theoretical section by mentioning

the paper of STIÉVENART [34], in which he treats both the multigroup and continuous energy model.

I conclude this section of the paper by continuing the review of the experimental work. In the paper by COMTE et al. [35] pulsed plutonium cores are surrounded by uranium or copper reflectors. WEALE and PATERSON [36] report measurements of α on uranium and plutonium-fuelled fast reactor assemblies in VERA at Aldermaston, both by the pulsed and by the Rossi-α method. In Sweden the pulsed source technique has been used by BRUNFELTER and KOCKUM [37] to measure negative reactivities ranging from 0.05 to 5% in the first core of the Swedish fast critical assembly FR-0. The data have been processed according to the theories of GARELIS and RUSSELL [38] and GOZANI [39].

Finally pulsed neutron work will be performed on critical or subcritical fast assemblies at Argonne National Laboratory [40], General Atomics [41], Los Alamos [42] and Cadarache [6].

V. APPLICATION TO TIME-OF-FLIGHT FAST NEUTRON SPECTROMETRY

Fast non-multiplying and multiplying assemblies can also be pulsed to measure fast spectra by time-of-flight techniques. The extension of this technique to fast neutron spectra was made possible by the development of high intensity, short duration pulsed neutron sources. A high intensity is required because of the long flight paths necessary for good resolution and because of the severe limitation imposed on the repetition frequency by the increase of the pulse duration along the flight path.

Several experiments have been performed on non-multiplying systems. An electron Linac is generally used to produce high intensity pulses of photofission neutrons in a uranium target.

The duration of the neutron pulse leaving the assembly is often short compared to the required time resolution, so that the pulse can be treated as instantaneous. The measured leakage spectrum is then in effect identical to the leakage spectrum which would exist in presence of a static source.

KATO and co-workers [40] measured in this way the spectrum leaking from a large depleted uranium block using a 50-m flight path. Spectral indices were also measured. The experimental results are compared with those obtained by a multigroup transport theory analysis.

Similar measurements were performed at General Atomic by RUSSELL et al. [43]. Several experiments have been completed on geometries designed to be calculable by specific computer codes. In particular, leakage spectra from a few keV to a few MeV were measured for a 6-in diameter sphere with a central source. Results are compared with multigroup transport theory.

At Harwell GAYTHER and GOODE [44], using a 60-m flight path, measured spectra from 1 keV to 5 MeV emerging from the surface or from a central re-entrant hole of uranium and sodium spheres. A comparison is given between measured and theoretical spectra.

The time-of-flight technique has also been applied to multiplying assemblies by PATERSON and WEALE [45, 46]. The spectrum of a beam extracted

from plutonium- and uranium-fuelled VERA assemblies was measured in the range of 100 eV to 50 keV. In these multiplying assemblies much lower yields, as can be obtained from a positive ion electrostatic accelerator through 14 D-T reaction, are adequate.

Since these assemblies are only a few per cent subcritical, the decay periods of the neutron pulses (about 4 μs) exceed the required time resolution (about 1 μs). Fortunately however, because the pulse shape is well defined and accurately measurable, it is possible to predict its effect on the detector time-distribution and thereby to make an improvement in the effective resolution of the system. The authors comment that "the neutron pulse could in principle be obtained by a fast chopper method but because of the high reactor power requirement and the difficulties of designing a chopper which is adequately opaque to fast neutrons but does not degrade the observed spectrum, the pulsed source technique seems at present to be the more practical method". A crucial problem in this experiment is to establish a means of beam extraction and collimation which ensures that the energy distribution in the extracted beam is the same as that in the reactor core. This problem seems to have been adequately solved. Similar experiments are also performed with the SUAK assembly [5].

If spectrometry of reactor neutrons up to 50 keV by time-of-flight proves to be successful, it will be a very valuable tool to fast reactor physicists, since no other satisfactory method exists in this energy range, which is very important for large dilute fast reactors, particularly as regards the Doppler effect.

VI. VARIOUS REMARKS AND CONCLUSIONS

1. The Garelis-Russell $k\beta/\ell$ method

This method [38], which is derived from one-velocity diffusion theory for bare assemblies, is probably not applicable to fast systems since it assumes that $v\nu\Sigma_f$ is independent of energy. It will be interesting to hear what results the Swedes have obtained with this method on their FR-0 critical assembly [37].

2. The area method for measuring reactivity in dollars

This method, as suggested by SJÖSTRAND [7], is probably difficult to apply to fast assemblies, since the measurement of the transient part of the pulse requires a very high time resolution, between 1 and 10 ns. In [6] we present a modulated version (frequency as low as 10 c/s) of the area method in which a resolution of about 10^{-3} s would be adequate, This version should be particularly suited to fast assemblies, because of the very large difference between the time constants of prompt and delayed neutrons.

3. Reflected neutrons

Pulsed neutron experiments could be perturbed by neutrons scattered by walls and floors. For this reason the SUAK assembly is placed in a thin walled room [5]. Since a large fraction of the room-scattered neutrons is

thermal [47], something could be gained by surrounding the assembly with a thermal neutron absorber. The fraction of thermal neutrons could also be increased by adding moderator material to walls and floors. BEGHIAN and co-workers [10] have observed in their experiments that the residual spectrum from the scattered neutrons was time-independent and constant over the sweep period. The time-dependent characteristics of reflected neutrons are briefly treated in [6]. Their influence on the experiments is a function of their time constants and of their relative contribution to the overall neutron balance. They could be treated as delayed neutrons or as another group of low energy neutrons with their time constant substituted for $(v\Sigma)^{-1}$. They could eventually give rise to parasitic modes or contribute to the delayed neutron background (probably the case for thermal neutrons, because of their large time constant).

Similar problems arise when the assembly is surrounded by a reflector. But in this case the time constants are usually much shorter, and the relative contribution of the reflected neutrons to the total neutron population is much larger. When this relative contribution is very large, the mathematical treatment becomes much more complex.

Along similar lines an interesting experiment was performed at Oak-Ridge by MICHALCZO [48] (see KEEPIN [49]). Two 93%-enriched U^{235} metal slabs (8 in × 10 in surface area) were separated by various distances from 0 to 5 in, and α measured as a function of separation distance in the just critical system (maintained by varying slab thickness). These data show that α is significantly dependent upon the neutron flight time across the gap between the two metal slabs, in quantitative agreement with transport theory.

4. *Subcritical assemblies as amplifiers*

In normal operation the burst duration of the IBR reactor is too long (36 μs) for spectrometry in the resonance region [50]. Burst duration may be reduced drastically by using IBR under subcritical conditions as a multiplier of fast neutrons injected into the reactor by an external source.

A similar use of a uranium metal multiplying assembly was reported [51].

5. *Conclusions*

The pulsing of fast assemblies is still a very new field. More experimental data and more theoretical work are needed to assess the potentialities of the various types of experiments which were mentioned in this survey. It is hard to forecast if they will be performed as extensively as has been the case for thermal systems.

REFERENCES

[1] FOSSOUL, E. A., "Doppler effect in fast reactors for non-uniform heating and temperature distribution". Proc. Conf. on Breeding, Economy and Safety in Large Fast Reactors, Rpt ANL-6792 (1963).

[2] GARELIS, E., Nucl. Sci. Engng 18 (1964) 242-45.

[3] UHRIG, R. E., Symposium on Noise Analysis in Nuclear Systems, Rpt TID 7679.

[4] UHRIG, R. E., "Techniques closely related to pulsed neutron research" (SM-62/76), these Proceedings II.

[5] BORGWALDT., H., KÜCHLE. M., MITZEL, F. and WATTECOMPS, E., "SUAK, a fast subcritical facility for pulsed neutron measurements", (SM 62/2), these Proceedings II.
[6] CADILHAC, M., GOVAERTS, P., HAMMER, P., MOORE, M., NICOLAENKO, B. and STORRER, F., "Comparative study of several types of pulsed and modulated experiments on fast neutron multiplying media", (SM-62/87), these Proceedings II.
[7] SJÖSTRAND, N.G., Ark. Fys. 11 (1956) 233-46.
[8] DUQUESNE, H., GERBIER, R., LYON, F. and SCHMITT, A., « Système à fréquence et largeur d'impulsion réglables, permettant la pulsation et la modulation de milieux multiplicateurs à neutrons rapides », (SM-62/85), these Proceedings II.
[9] KUPFERBERG, K.M. et al., Lifetime of neutrons in reflectors, Rpt LA-2743 (1962).
[10] BEGHIAN, L.E., RASMUSSEN, N.C., THEWS, R. and WEBER, J., Nucl. Sci. Engng 15 (1963) 375-81.
[11] NELKIN, M., Nucl. Sci. Engng 7 (1960) 210-16.
[12] COCKRELL, R.G., PEREZ, R.B. and DALTON, G.R., Nucl. Sci. Engng 19 (1964) 423-30.
[13] BEGHIAN, L.E., PROFIO, A.E., WEBER, J. and WILENSKY, S., Nucl. Sci. Engng 17 (1963) 82-89.
[14] BEGHIAN, L.E. and WILENSKY, S., "The pulsed neutron technique applied to fast non-multiplying assemblies" (SM-62/74), these Proceedings II.
[15] DECONNINCK, G., d'OULTREMONT, P. and STIÉVENART, M., "Contribution to the study of fast neutron non-multiplying assemblies by the pulsed neutron technique", (SM-62/14) these Proceedings II.
[16] HIRAOKA, T., IIJIMA, T., HIRAKAWA, N., NAKAMURA, T. and NOZAWA, M., J. Nucl. Sci. Technol. 1 (1964) 108-09.
[17] STORRER, F. and STIÉVENART.M., Contribution to the theory of the pulsed neutron technique applied to fast multiplying systems, Rpt EUR 593.e (1964).
[18] SUMITA, NAKAMURA, T. and HIRAOKA, T., Personal communication through the courtesy of S. Nomoto.
[19] KAPCHIGASHEV, S.V. and POPOV, Y.P., Sov. atom. Energy 15 (1964) 808-14. Translated from Atomnaja Energija 15 (1963) 120-26).
[20] MITZEL, F. and PLENDL, H.S., Nukleonik 6 (1964) 371-79.
[21] PASSELL, L., ABRAMSON, R.H., ANDRE, C. and PEREZ-MENDEZ, V., Rpt UCRL 4673 (1956).
[22] PASSELL, L., BENGSTON, J. and BLAIR, D.C., Rpt. UCRL 4808 (1957).
[23] BENGSTON, J. and PASSELL, L., Rpt UCRL 4998 (1957).
[24] BENGSTON, J., Proc. 2nd UN Int. Conf. PUAE 12 (1958) 63.
[25] INÖNÜ, E., Proc. 2nd UN Int Conf. PUAE 16 (1958) 701.
[26] GELBARD, E.M. and DAVIS, J.A., Nucl. Sci. Engng 13 (1962) 237-44.
[27] BORGWALDT, H., personal communication, 1963.
[28] STORRER, F., GOVAERTS, P., EBERSOLDT, F. and STIÉVENART, M., Rpt. EUR 1910 e.
[29] STORRER, F., GOVAERTS, P., EBERSOLDT, F. and HAMMER, P., A method for calculating the flux evolution in a fast neutron multiplying medium as a function of time, space and energy, Trans. Amer. nucl. Soc. 7 2 (Nov. 1964).
[30] CADILHAC, M., GOVAERTS, P., HAMMER, P., MOORE, M., NICOLAENKO, B. and STORRER, F., "Contribution to the theory of pulsed and modulated experiments on fast neutron multiplying media" (SM-62/86) these Proceedings II.
[31] CORNGOLD, N., MICHAEL, P. and WOLLMAN, W., Nucl. Sci. Engng 15 (1963) 13-19.
[32] CORNGOLD, N., Nucl. Sci. Engng 19 (1964) 80-90.
[33] CORNGOLD, N. and MICHAEL, P., Nucl. Sci. Engng 19 (1964) 91-94.
[34] STIÉVENART, M. and EMILE, E.," Theoretical considerations concerning the pulsation of fast subcritical assemblies" (SM 62/12), these Proceedings II.
[35] COMTE, R., MASSIEUX, J. and ROCHE, M., « Mesures par neutrons pulsés sur des assemblages à neutrons rapides » (SM 62/84), these Proceedings II.
[36] WEALE, J.W. and PATERSON, W.J., "Measurements of the prompt neutron decay constant of the VERA reactor using the pulsed source method" (SM 62/26), these Proceedings II.
[37] BERGSTRÖM, A., BRUNFELTER, B. and KOCKUM, J., "Determination of neutron lifetimes and reactivities in the fast critical FR-0 assembly" (SM-62/29), these Proceedings II.
[38] GARELIS, E. and RUSSELL, J.L., Nucl. Sci. Engng 16 (1963) 263-70.
[39] GOZANI, T., Nukleonik 4 (1962) 84.
[40] KATO, W.Y., MEISTER, H.H., MAIN, G.W., RUSSELL, J.L. and CROSBIE, K., "fast reactor physics parameters from a pulsed source" (SM 62/56), these Proceedings II.
[41] Nucl. Industry (April 1965).

[42] ORNDOFF, J., personal communication.
[43] RUSSELL, J. L. et al.,"Neutron spectra in bulk media by time-of-flight", (SM 62/61), these Proceedings II.
[44] GAYTHER, D. and GOODE, P. D.," Measurements of fast neutron spectra in reactor materials" (SM 62/23) these Proceedings II.
[45] PATERSON, W.J. and WEALE, J.W., J. British nucl. Energy Soc. (Oct. 1964) 311-19.
[46] PATERSON, W.J. and WEALE, J.W., "Some measurements of fast reactor spectra by the time-of-flight technique using a pulsed neutron source", (SM 62/27), these Proceedings II.
[47] OTSTAVNOV, P.S., Sov. atom. Energy 16 2 (Feb. 1964).
[48] MICHALCZO, J.T., Rpt ORNL-TM-470 (1963).
[49] KEEPIN, G.R., Pulsed neutron research in neutron and reactor physics, Atom. Energy Rev. 2 2(1964) 75/95.
[50] BUNIN, B.N. et al.,Proc. 3rd UN Int. Conf. PUAE, 1964, P/324.
[51] Proc. EANDAC Conf., Neutron Time-of-flight methods, Session III, EURATOM, Brussels (Sept. 1961).

DISCUSSION*

N. CORNGOLD: I should like to point out that there are fundamental differences between discrete eigenvalues in their proper sense and the pseudo-discrete" eigenvalues which Dr. Storrer has discussed. The former is an intrinsic property of the system, while the latter depend on the scheme of approximation, the initial conditions, and also on the nature of the system. The evaluation of the relative importance of these factors is an interesting theoretical problem.

F. STORRER: I agree. However, I think that with proper initial conditions a well-defined pseudo-asymptotic mode can be measured and calculated and that a comparison of calculated and experimental values can provide an excellent check on the basic data and on the methods of calculation. If we limited ourselves to eigenvalues in their proper sense, we would deprive ourselves of this very interesting possibility.

L. BEGHIAN: Does the neutron inelastic process lead to a bunching of the energy spectrum, thus giving rise to predominant modes?

F. STORRER: It may, but one cannot discuss a fundamental-mode spectrum without taking into account the multiplication of the assembly. In the absence of multiplication, neutrons can only slow down and no asymptotic spectrum can be obtained.

M. NELKIN: You mentioned that the quasi-fundamental mode could be identified from its intensity. Could it not also be readily identified from the associated eigenfunction?

F. STORRER: Yes, this probably can be done. The "parasitic" eigenfunctions show marked discontinuities. The pseudo-fundamental eigenfunction is well-behaved and is positive everywhere if one discards the low-energy tail, in which there are practically no neutrons anyway. If one does not discard the low-energy tail, this eigenfunction is not well-behaved either.

N. CORNGOLD: Would Dr. Storrer care to discuss the types of multiplying systems which give a unique pseudo-mode having a quite physical eigenfunction associated with it.

F. STORRER: Strictly speaking, a true discrete fundamental mode can only exist for critical or supercritical systems and does not exist for the

* See also discussion of paper "Fast reactor physics parameters from a pulsed source" (SM-62/56), these Proceedings II.

subcritical state since one can always find a mechanism which brings in a very slowly decaying neutron population (very slow neutrons and neutrons reflected by the walls). However, one can define a pseudo-fundamental mode down to a k_{eff}-value of about 0.8 in the case of the SUAK assembly. To do this, low-intensity parasitic modes have to be neglected. The pseudo-fundamental eigenfunction can only be defined above a certain energy, i.e. it cannot be extended to low energies where the removal rate $v\Sigma$ is smaller than the decay constant of the pseudo-fundamental mode.

P. DAITCH: Would you not agree that there is a difference between the pulsed problem in moderators and in fissionable systems? In the case of moderators an operator is involved that may be symmetrized and the eigenfunctions have reasonable orthogonal properties, which necessitates the presence of the lowest eigenfunctions to keep the flux positive. On the other hand, the non-self-adjoint fission operator has a different orthogonality weighting function, which allows one practically to retain the positive definite nature of the flux while neglecting the lowest and other eigenfunctions.

F. STORRER: A difference of this sort certainly does exist but I would guess that one could obtain very different results in the case of thermal non-multiplying systems too – if I may venture into that field for a moment – if one excited different eigenfunctions by changing the energy of the source.

In the fast systems described in the paper the flux and the pseudo-fundamental eigenfunction are positive definite only in the energy range which was adopted and not below that range.

K.H. BECKURTS: I have two questions relating to the $S'(t)/S(t)$ curves shown in Fig. 2 of your paper. These curves were derived for the total fission rate. Have you also calculated such curves for actual reaction rates as observed experimentally, for instance with a recoil proton detector? I should also be interested to hear whether you have considered the possibility of deriving correction factors F(t), as referred to in my paper*, in order to increase the region of "fundamental-mode decay" in the evaluation of such experiments. I think this method might increase the accuracy of α-determinations.

F. STORRER: The correction factors F(t) which you introduced for non-multiplying systems are certainly very useful but I am not sure whether they can be extended to multiplying systems.

As for your other question, S(t) of course gives the reaction rate directly for a fission detector with the same isotopic composition as the fuel in the assembly. The flux at any energy can be easily obtained by a convolution of S(t) and of a time dependent slowing-down kernel. As is indicated in my paper, this is particularly easy in a time interval in which S(t) varies exponentially. Thus, when the logarithmic derivative of S(t) reaches a plateau, the logarithmic derivative of any reaction rate would also reach a plateau.

---

* BECKURTS, K. H., "A review of pulsed neutron experiments on non-multiplying media" (SM-62/1) these Proceedings I.

MESURES PAR NEUTRONS PULSÉS SUR DES ASSEMBLAGES CRITIQUES

R. COMTE, J. MASSIEUX ET M. ROCHE
CENTRE D'ÉTUDES NUCLÉAIRES DE SACLAY, FRANCE

Abstract — Résumé — Аннотация — Resumen

PULSED NEUTRON MEASUREMENTS IN FAST ASSEMBLIES. Kinetic measurements with pulsed neutrons were performed in fast subcritical assemblies with a plutonium core (5-8.7 kg) and a uranium (9 cm) or copper (2-7 cm) reflector. The apparatus is described and the data are then presented and discussed. The results obtained by the pulsed neutron and by conventional methods are compared. The paper ends with a discussion of some aspects of the signal-to-noise ratio and the performance of the accelerator and electronics system, with a view to improving the accuracy of the method.

MESURES PAR NEUTRONS PULSÉS SUR DES ASSEMBLAGES A NEUTRONS RAPIDES. Des mesures cinétiques par neutrons pulsés ont été effectuées sur des assemblages sous-critiques à neutrons rapides, dont le cœur est en plutonium (5 à 8,7 kg) et le réflecteur en uranium (9 cm) ou en cuivre (2 à 7 cm). L'appareillage est décrit, puis les résultats des mesures sont présentés et discutés. Une comparaison est faite entre les résultats obtenus par la méthode des neutrons pulsés et par les méthodes classiques. La dernière partie développe certaines considérations sur le rapport signal sur bruit, sur les performances de l'accélérateur et de l'électronique, en vue d'améliorer la précision de la méthode.

ИЗМЕРЕНИЯ С ПОМОЩЬЮ ИМПУЛЬСНЫХ НЕЙТРОНОВ НА БЫСТРЫХ СБОРКАХ. Кинетические измерения с помощью импульсных нейтронов проводились на подкритических сборках на быстрых нейтронах, активная зона которых состояла из плутония (5–8,7 кг), а отражатель – из урана (9 см) или из меди (2–7 см). Дается описание оборудования, приводятся и обсуждаются результаты измерения. Сравниваются результаты, полученные методом импульсных нейтронов и обычными методами. В последней части приводятся некоторые замечания по поводу отношения сигнала к шуму, а также данных об импульсном источнике (ускорителе) и электронной аппаратуре с тем, чтобы улучшить точность метода.

MEDICIONES CON NEUTRONES PULSADOS EN CONJUNTOS RAPIDOS. Los autores han efectuado mediciones cinéticas por el método de los neutrones pulsados, en conjuntos subcríticos de neutrones rápidos cuyo cuerpo estaba constituido por Pu (5, 0 a 8, 7 kg) rodeado de U (9 cm) o de Cu (2 a 7 cm) en calidad de reflector. Describen los instrumentos empleados, y analizan los resultados de las mediciones. Comparan los resultados obtenidos por el método de los neutrones pulsados con los logrados por los métodos clásicos. En la última parte de la memoria formulan diversas consideraciones sobre la relación señal-ruido y sobre los rendimientos del acelerador y del equipo electrónico, con miras a aumentar la precisión del método empleado.

1. GÉNÉRALITÉS

1.1. Mesures cinétiques par neutrons pulsés - Principe - But

Les méthodes expérimentales utilisées pour l'étude des réacteurs ont pour objet de déterminer en premier lieu les dimensions critiques, puis les paramètres cinétiques et enfin les répartitions de flux et les perturbations.

La méthode des neutrons pulsés, qui consiste à injecter de manière cyclique une brève bouffée de neutrons, introduit le paramètre α, dont l'extrapolation vers $\alpha = 0$ donne la dimension critique prompte. On conçoit donc qu'une approche sous-critique soit réalisée par cette méthode.

D'autre part, la théorie simple à un groupe donne la valeur de α en fonction du coefficient de reproduction prompt, K_p, et du temps de vie τ

$$\alpha = \frac{I - K_p}{\tau}.$$

Lorsque l'on obtient la valeur de τ pour l'état critique retardé, on en déduit, par la relation

$$\alpha_c = \frac{\beta}{\tau},$$

le rapport entre β et le temps de vie, d'où la valeur du temps de vie si l'on a pu évaluer β en pcm.

Cette méthode donne également la valeur de β, chiffrée en paramètre de chargement ou en équivalent de barre. La méthode des neutrons pulsés donne des résultats du même ordre que la méthode dite «α Rossi», mais son domaine d'application pratique est situé plus bas dans l'échelle des réactivités.

1.2. Description des assemblages étudiés

1.2.1. RACHEL

L'assemblage RACHEL [1, 2] est constitué par un cœur en plutonium δ et par un réflecteur en uranium naturel, d'une épaisseur de 93 mm. La géométrie est sphérique. L'approche sous-critique a été réalisée en ajoutant des plaquettes de plutonium et des rondelles d'uranium dans le plan équatorial qui sépare les deux hémisphères de l'assemblage.

On a pu ainsi atteindre l'état critique, avec une masse brute de plutonium de 7099 g (soit une masse corrigée de 6820 g en déduisant l'influence des vides et des gaines). Un jeu de barres de contrôle permet d'effectuer les divergences et les stabilisations désirées.

1.2.2. JACINTHE

L'assemblage sous-critique JACINTHE est constitué par un cœur en plutonium δ, d'une masse de 9 kg environ, entouré d'un réflecteur en cuivre, d'une épaisseur variant entre 2 et 14 cm. La géométrie est cylindrique avec un rapport $H/D \simeq 1$. L'approche sous-critique a été réalisée par la méthode des comptages, et l'extrapolation a donné une épaisseur critique de 7,0 cm.

Les mesures par neutrons pulsés ont été entreprises afin de déterminer l'état critique prompt et ainsi d'évaluer β en épaisseur de réflecteur.

2. DESCRIPTION DE L'APPAREILLAGE

2.1. Générateur de neutrons pulsés

2.1.1.

Le générateur de neutrons pulsés est un accélérateur de 150 kV, utilisant la réaction $T(D, n)^4He$.

Le débit continu maximum est de 10^9 neutrons de 14 MeV par seconde.

2.1.2.

La pulsation est réalisée par déflexion sinusoïdale du faisceau après accélération. Les plaques de déflexion électrostatiques sont situées à la sortie de l'accélérateur. On trouve ensuite des lèvres, faiblement écartées, situées à 60 cm environ, puis la cible, située à 200 cm de la déflexion.

Ainsi le faisceau n'atteint la cible que pendant les brefs instants où il n'est pas intercepté par les lèvres. Le champ de déflexion est d'environ 3000 V/cm. Les fréquences de pulsation sont comprises entre 200 kc/s et 1 Mc/s. La durée des bouffées est d'environ 2 à 6% de la période de pulsation. Cette dernière est choisie pour être 10 fois plus grande que la période de décroissance de l'assemblage étudié.

2.1.3.

Le faisceau issu de la source est composé de plusieurs types d'ions, dont les vitesses après accélération sont différentes (en particulier les ions D^+ et D_2^+, en proportion de 2 à 1 suivant les réglages de l'accélérateur). Par conséquent, après la déflexion électrostatique, les ions D_2^+ vont prendre du retard sur les ions D^+ et ainsi, donner une deuxième bouffée de neutrons, moins intense puisque la section efficace de la réaction $T(D, n)^4He$ diminue avec l'énergie des deutons. Dans les conditions définies au paragraphe précédent, la différence des temps de vol, c'est-à-dire l'intervalle de temps entre ces deux bouffées, est de 240 ns.

Pour éliminer les ions moléculaires, une deuxième déflexion électrostatique est installée à mi-chemin entre la première déflexion et la cible. Elle est normalement alimentée par une tension élevée (600 V); lors du passage des D^+, elle tombe à une valeur nulle pour remonter ensuite à 600 V en moins de 60 ns; ainsi lorsque les retards sont correctement ajustés, les ions moléculaires ne peuvent atteindre la cible. Dans les expériences ultérieures, prévues avec un autre accélérateur, ce dispositif d'élimination sera remplacé par une déflexion magnétique permanente qui apportera en outre une amélioration du rapport signal sur bruit.

Lorsque la période de pulsation est de 240 ns ou un sous-multiple, il est possible de caler la bouffée d'ions moléculaires en même temps que la bouffée d'ions atomiques.

2.1.4.

La cible, en cuivre recouvert de titane tritié, est refroidie par circulation d'eau. Elle est placée contre la partie externe du réflecteur

de l'assemblage. Cette condition est nécessaire pour avoir le maximum de neutrons injectés dans l'assemblage qui possède une source interne importante (due au plutonium-240).

Un quartz escamotable placé au voisinage des lèvres permet d'ajuster la focalisation à cet endroit pour que les limites des bouffées soient très brèves.

Une installation de télévision a été utilisée pour les réglages, mais ce procédé n'est pas facilement exploitable en raison de sa dynamique insuffisante et des «traînées».

Le réglage de la focalisation est d'abord dégrossi par observation visuelle sur le quartz sans pulsation, et achevé d'après la forme des bouffées.

2.2. Electronique

Le diagramme d'ensemble est représenté à la figure 1.

2.2.1. Détection

Le détecteur placé contre l'assemblage, à l'opposé de la cible, est un scintillateur plastique (1'' × 1''/2) associé à un photomultiplicateur 56 AVP.

Le temps de montée des impulsions est de 5 ns environ. Ensuite, un amplificateur à large bande permet d'augmenter l'amplitude des impulsions pour actionner correctement le sélecteur à une bande.

Ce dispositif détecte donc les neutrons et les gamma sortant de l'assemblage. Parmi les neutrons, il faut essayer de sélectionner ceux qui ont une énergie correspondant à l'énergie moyenne du spectre neutronique de l'assemblage et éviter de compter ceux qui ont une énergie élevée.

Compte tenu de la réponse d'un scintillateur plastique aux neutrons, l'usage d'un sélecteur à une bande permet de détecter les protons de recul correspondant à la bande (ΔE), c'est-à-dire que les neutrons d'énergie supérieure à $E + \Delta E$ sont détectés avec une efficacité approximativement constante, compte non tenu de la section efficace de la réaction (n, p). On voit immédiatement l'intérêt du sélecteur par rapport à un discriminateur habituel qui donnerait une efficacité croissante avec l'énergie des neutrons (même restriction que ci-dessus).

Le sélecteur fonctionne suivant le principe rapide-lent en coïncidence et son retard interne est relativement indépendant du temps de montée des impulsions (fig. 2). L'information temps est recueillie par un amplificateur saturé, dont la sortie, après un retard, chemine à travers une porte. Cette porte est actionnée par la voie de sélection d'amplitude. Pour l'ensemble de la chaîne de détection, on observe ainsi un jitter inférieur à 3 ns.

2.2.2. Convertisseur temps-amplitude

Comme il n'existe pas actuellement d'analyseur rapide de temps, il est nécessaire d'utiliser un convertisseur temps - amplitude et un analyseur multicanaux.

Le convertisseur temps - amplitude est présenté en tiroirs fonctionnels: un tiroir sélecteur à une bande, décrit ci-dessus; un tiroir dit «temps de

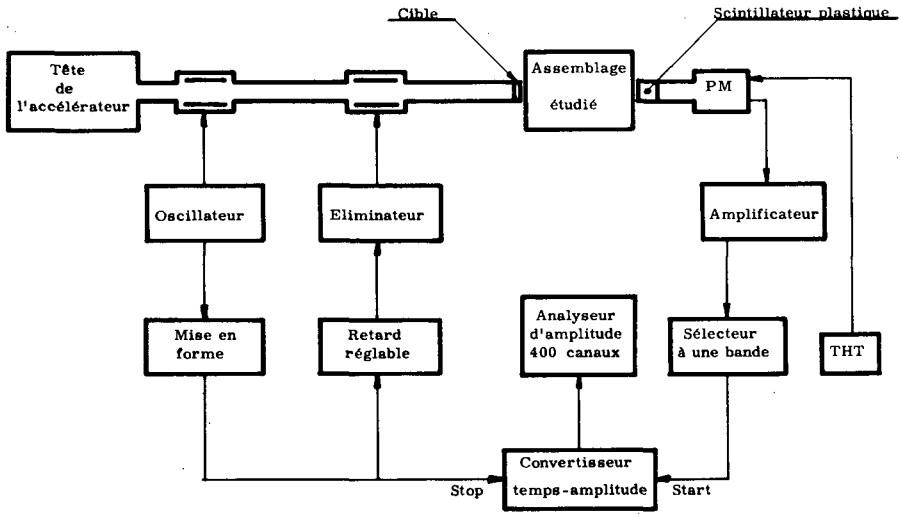


Fig. 1

Diagramme d'ensemble.

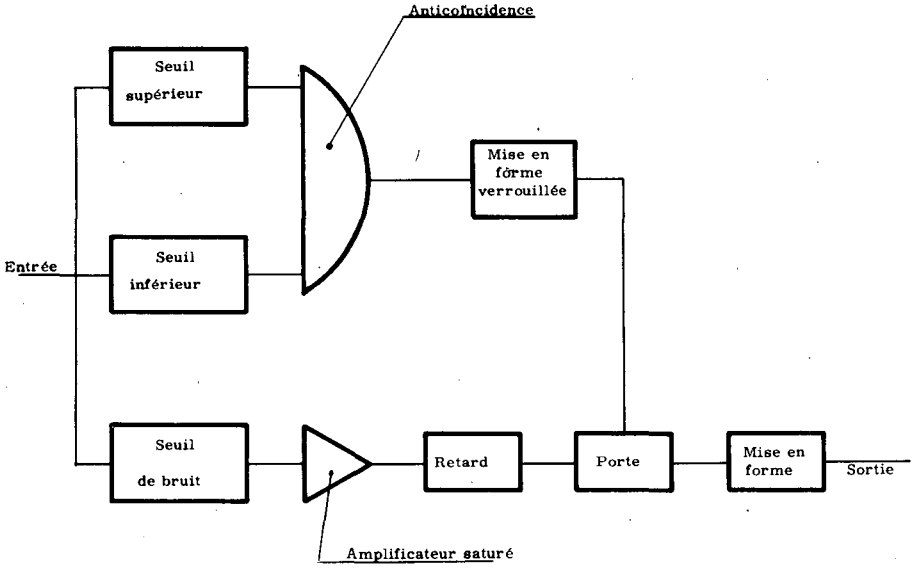


Fig. 2

Sélecteur à une bande.

vol» reçoit la sinusoïde provenant de la déflexion du faisceau, pour donner une impulsion qui représente le repère en temps de chaque bouffée; enfin, un tiroir de conversion contient les circuits formant la dent de scie, qui commence après une impulsion «start» en provenance du sélecteur à une

bande et est interrompue après l'impulsion «stop» suivante. Après mise en forme, le sommet de la dent de scie est envoyé dans un analyseur multicanaux.

Plusieurs circuits de paralysie ont été introduits pour éviter que le tiroir de conversion ne puisse fonctionner lorsqu'il n'est pas dans son état de repos; de nombreux essais ont été effectués avec des trains d'impulsions, pour vérifier que le convertisseur est effectivement verrouillé pendant son temps de récupération.

Le principal inconvénient de l'ensemble (convertisseur temps - amplitude, analyseur) est de ne pouvoir enregistrer qu'une seule impulsion par cycle. Pour éviter de faire des corrections trop nombreuses dans les dépouillements, il est nécessaire que la probabilité de détecter plus d'un neutron par cycle soit faible, autrement dit, les taux de comptage sont limités à 10^{-2} ou 10^{-3} de la fréquence de pulsation.

2.3. Etalonnages

Les étalonnages constituent une partie très importante des manipulations, car ils permettent le dépouillement et le passage au temps réel. Il existe plusieurs méthodes d'étalonnage qui se recoupent plus ou moins, mais chacune fournit une seule des grandeurs nécessaires.

2.3.1. Mesure de la fréquence de pulsation

Cette méthode est très simple; elle fournit la période de pulsation, c'est-à-dire le temps écoulé entre le premier canal utile et le dernier canal utile de l'analyseur, si toutefois la gamme du convertisseur temps - amplitude est supérieure à la période de pulsation.

2.3.2. Mesure de la largeur relative des canaux

On utilise autant que possible l'appareillage expérimental de manière à conserver tous les phénomènes parasites tels que: ondulation, induction, réflexions. L'oscillateur de pulsation actionne la voie «stop», mais la voie «start» est actionnée par une source aléatoire. Les comptages dans chaque canal sont proportionnels à la largeur du canal considéré.

Du fait que l'ensemble convertisseur temps - amplitude, analyseur multicanaux n'est pas en général linéaire, on sera amené à corriger les comptages expérimentaux en tenant compte de l'étalonnage ci-dessus.

Cette méthode peut même donner la largeur effective de chaque canal si l'on mesure les nombres totaux d'impulsions «start» et «stop» ainsi que la durée de l'étalonnage par la formule

$$\Delta t_i = \frac{n_i \times T}{N_{start} \times N_{stop}}$$

où Δt_i désigne la durée du canal i, n_i le nombre de coups stockés dans le canal i, N_{start} et N_{stop} les nombres d'impulsions «start» et «stop» accumulés pendant la durée T de l'étalonnage.

2.3.3. Mesure de la position des canaux

Nous venons de mesurer la durée relative (ou même absolue) de chaque canal. Il est nécessaire de connaître la position de certains canaux par rapport à un canal origine. Il est possible de l'obtenir en additionnant les largeurs des canaux intermédiaires, mais une mesure indépendante est préférable. Cet étalonnage est effectué à partir d'un pilote à quartz déclenchant simultanément un oscilloscope et un générateur de deux impulsions déphasables; ce générateur actionne les voies «start» et «stop». L'oscilloscope, en expansion, présente la deuxième impulsion et un marqueur à haute fréquence (50 Mc/s) en balayage alterné. Il suffit de déplacer l'impulsion déphasable d'un certain nombre de marqueurs et de lire le numéro d'ordre des canaux de l'analyseur. La précision absolue de la méthode est supérieure à 10 ns.

2.4. Dépouillements

Les dépouillements présentés dans cette communication ont été effectués sans l'aide de machines électroniques; un programme est en cours de mise au point et sera utilisé pour les mesures à venir.

Le résultat brut d'une mesure de décroissance se présente sous la forme d'une série de nombres représentant les comptages dans chacun des canaux et plusieurs corrections sont effectuées avant l'interprétation effective.

2.4.1. Correction de pertes de comptage

Le temps mort de l'analyseur (environ 115 μs en moyenne) introduit une perte qui peut être négligée, car elle correspond à un certain nombre de bouffées perdues et n'influe donc pas sur la forme de la décroissance. Par contre, le convertisseur temps - amplitude, qui n'analyse au plus qu'une impulsion par bouffée, introduit une déformation de la décroissance. La correction à effectuer est simple dans son principe, mais nous avons préféré adopter des taux de comptage peu élevés pour l'éviter.

Appelons N, le nombre total d'impulsions «stop» arrivées pendant la durée de la mesure, et n_i le comptage obtenu dans le canal i.

Après une bouffée, il est possible de compter un coup dans le canal i, sauf si un coup a été compté dans un des canaux 1 à i - 1. Par conséquent, le nombre de coups du canal i doit être corrigé par le facteur

$$\frac{1}{N - \sum_{j=1}^{j=i-1} n_j}.$$

2.4.2. Correction de largeur de canaux

Les comptages n_i correspondent à une largeur de canal Δt_i. Il est donc nécessaire de rapporter les n_i à une largeur de canal constante. Pour cela, on utilise l'étalonnage 2.3.2.

2.4.3. Correction de position de canaux

Le numéro d'un canal n'est pas lié linéairement à l'écart de temps entre le milieu du premier canal et le milieu du canal considéré. Il est nécessaire d'utiliser l'étalonnage 2.3.2. pour déterminer cet intervalle de temps souvent à un facteur constant près; le facteur constant est déterminé ou recoupé par l'étalonnage 2.3.3.

2.4.4. Détermination du paramètre α

Après ces corrections, les nombres obtenus représentent l'évolution du taux de comptage en fonction du temps. On retranche le bruit de fond, qui est obtenu par le comptage avant la bouffée *, puis on ajuste l'exponentielle par la méthode des moindres carrés, en retouchant au besoin le bruit de fond.

3. RÉSULTATS EXPÉRIMENTAUX

3.1. Mesures effectuées sur RACHEL

3.1.1. Conditions expérimentales

Les mesures par neutrons pulsés ont été effectuées sur des chargements peu réactifs, entre -600 pcm et -8000 pcm de l'état critique. On envisage actuellement d'effectuer une série d'expériences sur des chargements plus réactifs.

Dans le tableau I, l'écart de masse par rapport à l'état critique est corrigé pour tenir compte de la présence de gaines et de jeux, suivant les valeurs données dans la référence [1]. L'écart de réactivité en pcm est déduit de l'équivalent pcm - gramme calculé.

En principe, pour chaque chargement une mesure est effectuée barres entrées et une mesure barres sorties.

3.1.2. Discussion des résultats

Les résultats sont rassemblés dans le tableau I.

La figure 3 représente la variation de α en fonction de l'écart de masse de l'état critique. Cette variation est linéaire jusque vers 1000 g (environ 4500 pcm). Les chargements comprennent alors trois plaquettes. A partir de 1000 g, la courbe s'incurve légèrement, mais il faut noter que ces chargements ne comprennent plus que deux, une ou zéro plaquettes, d'où un manque de précision par suite des corrections de vides et de gaines.

Un ajustage par moindres carrés sur les mesures effectuées pour un écart de masse jusqu'à 1000 g donne les valeurs suivantes:

$$-\alpha \cdot 10^6 = 0{,}585\ \Delta M(g) + 1{,}265 \cdot 10^6 \quad \text{barres sorties,}$$

$$-\alpha \cdot 10^6 = 0{,}618\ \Delta M(g) + 0{,}118 \cdot 10^6 \quad \text{barres entrées.}$$

* A condition que les périodes de neutrons retardés soient au moins 10 fois supérieures à la période de pulsation et que cette dernière soit également supérieure à la période de décroissance prompte.

TABLEAU I

RACHEL – VARIATION DE α EN FONCTION DE ΔM

Fréquence de pulsation (kc/s)	Ecart de masse M (g)	1 - K (pcm)	$-\alpha(10^6 s^{-1})$	
			Barres entrées	Barres sorties
215	171	665	1,25	2,27
215	265	1090	1,67	2,82
215	376	1590	2,34	3,38
451	376	1590	-	3,54
451	489	2100	3,28	4,15
451	583	2520	3,74	4,65
451	693	3020	4,36	5,24
940	693	3020	-	5,42
940	864	3780	-	6,75
940	1069	4700	6,57α	7,45
940	1444	6400	8,25	9,43
940	1876	8350	11,61	-

On voit que l'équivalent masse des barres semble diminuer légèrement avec la réactivité, alors que pendant l'approche par comptages on avait observé une efficacité constante en inverses de comptage.

La pente moyenne de la variation de α avec ΔM est

$$\Delta\alpha/\Delta M = -0{,}601 \cdot 10^6 \ s^{-1} \cdot g^{-1} .$$

Compte tenu de la détermination de l'état critique par d'autres méthodes, on obtient la valeur de α_c, soit:

$$\alpha_c = -3{,}2 \cdot 10^5 \ s^{-1} .$$

La méthode «α Rossi» donne

$$\alpha_c = -2{,}9 \cdot 10^5 \ s^{-1} .$$

La discordance peut s'expliquer par une erreur dans les corrections de vides et de gaines, car les mesures «α Rossi» ont été effectuées sur un assemblage à quatre plaquettes, alors que les mesures par neutrons pulsés utilisaient des chargements de zéro à trois plaquettes.

La valeur obtenue pour β est

$$\beta = 53{,}5 \text{ g Pu}.$$

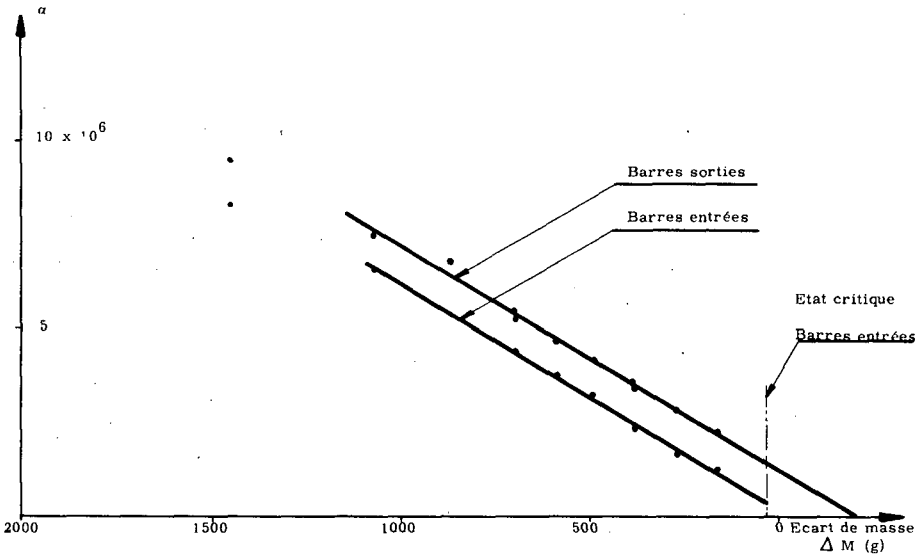


Fig. 3

RACHEL - Variation de α en fonction de la masse du cœur.

A l'aide de la valeur de β en pcm, on peut déterminer le temps de vie à l'état critique

$$\tau = 7{,}5 \cdot 10^{-9} \text{ s.}$$

On pourra noter que certaines mesures (tableau I) ont été effectuées avec des fréquences de pulsations différentes, c'est-à-dire dans des conditions indépendantes. Les valeurs trouvées de α diffèrent alors de moins de 5%.

3.1.3. Temps de vie

Au cours de l'approche sous-critique par comptages [1] nous avons constaté que les comptages C étaient liés à l'écart de masse ΔM de l'état critique par la formule

$$1/C = A_1 \cdot \Delta M,$$

A_1 étant une constante. Or les comptages C des neutrons de fuite sont liés à K par la formule

$$C = A_2 \frac{1 - K/\eta}{1 - K} = A_2 \frac{1 - K/\eta}{\Delta K}$$

avec A_2 = constante;

$$\eta = \frac{\nu \sigma f}{\sigma_c + \sigma_f},$$

d'où, par élimination de C,

$$\frac{\Delta K}{\Delta M} = \left(1 - \frac{1}{\eta} + \frac{\Delta k}{\eta}\right) \cdot \frac{A_2}{A_1}.$$

Le terme en $\Delta K/\eta$ est négligeable,
donc

$$\frac{\Delta K}{\Delta M} = p_c.$$

Par conséquent, à la précision des mesures près, l'équivalent masse du pcm, p_c, est constant dans une très large gamme au-dessous de l'état critique (plusieurs milliers de pcm).

Par ailleurs, au cours de l'approche par neutrons pulsés nous avons constaté que α était lié à l'écart de masse ΔM par la formule

$$\alpha - \alpha_c = A_3 \cdot M$$

où A_3 = constante.
Or

$$(\alpha - \alpha_c) = \frac{K-1}{\tau} = \frac{\Delta K}{\tau}.$$

Par suite

$$\frac{\Delta K}{\tau} = A_3 \Delta M,$$

soit

$$\tau = \frac{p_c}{A_1} = \tau_c.$$

Le temps de vie est donc lié à l'équivalent pcm - gramme et, à la précision des mesures près, il est constant dans une très large gamme de réactivité.

3.2. Mesures effectuées sur JACINTHE

3.2.1. Conditions expérimentales

L'approche par neutrons pulsés a été effectuée plusieurs semaines après l'approche par comptages, d'où quelques variations dues à un défaut de reproductibilité des chargements.

Les mesures concernent des assemblages réfléchis avec une épaisseur de cuivre comprise entre 2 et 6,5 cm. Une perturbation a permis d'obtenir les coefficients de multiplication K à partir de l'équivalent calculé pcm - gramme surface.

TABLEAU II

JACINTHE - APPROCHE SOUS-CRITIQUE
Valeur des inverses de comptage et
de α en fonction de l'épaisseur du réflecteur

Epaisseur du réflecteur (cm)	Inverse du comptage chaîne I	Inverse du comptage chaîne III	$-\alpha(10^6\ s^{-1})$
2			29,5
3	36,99	33,94	20,2
4	27,38	23,35	12,2
5	15,80	14,021	10,5
5,5	10,78	9,057	6,10
6	6,913	5,882	3,41
6,5	3,679	3,021	2,09

3.2.2. Discussion des résultats

Les résultats sont rassemblés dans le tableau II.

Les figures 4 et 5 représentent respectivement l'approche par comptage et l'approche par neutrons pulsés. Les abscisses, où sont portées les épaisseurs de réflecteur, ont une échelle logarithmique.

Dans l'extrapolation par moindres carrés, le réflecteur de 2 cm a été négligé.

On a trouvé ainsi les valeurs suivantes:

Epaisseur critique (chaîne de comptage axiale) = 7,05 cm,
Epaisseur critique (chaîne de comptage latérale) = 6,94 cm,
Epaisseur critique prompte (neutrons pulsés) = 7,18 cm.

On pourrait obtenir la valeur de β en épaisseur de réflecteur en faisant la différence de ces valeurs extrapolées, mais en raison de la dispersion des points expérimentaux, on ne pourrait guère se fier au résultat. (On trouve $\beta = 0,18 \pm 0,05$ cm de réflecteur).

L'état critique retardé étant connu avec une précision insuffisante, il est possible de connaître α_c et τ_c à l'aide des valeurs de K déterminées par d'autres mesures (section 3.2.1.), pour une configuration sous-critique.

En effet, le coefficient de multiplication du réflecteur de 6,5 cm est $K = 0,993$, et comme $\beta = 200$ pcm, on a

$$\alpha_{6,5} = \frac{0,993 + 0,002 - 1}{\tau_{6,5}},$$

soit

$$\tau_{6,5} = 4,5 \cdot 10^{-9}\ s.$$

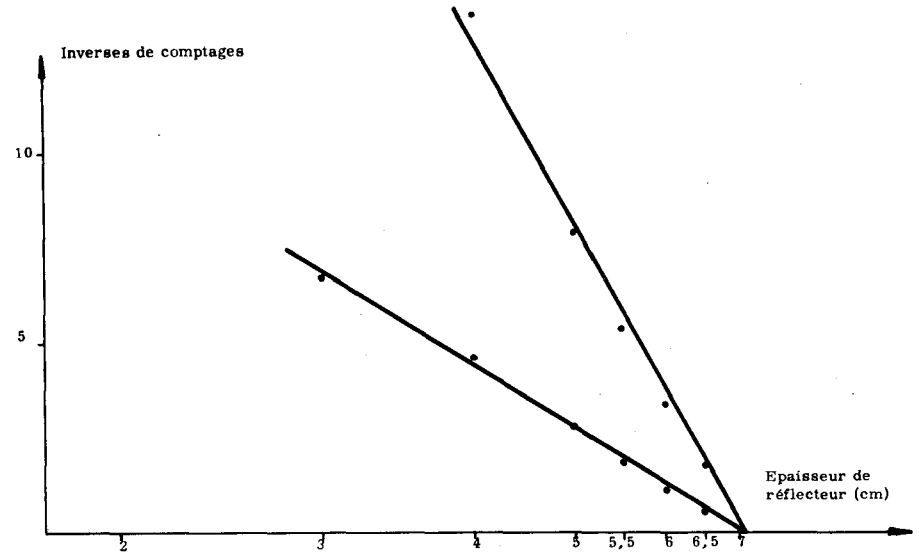


Fig. 4

JACINTHE - Approche sous-critique par comptages.

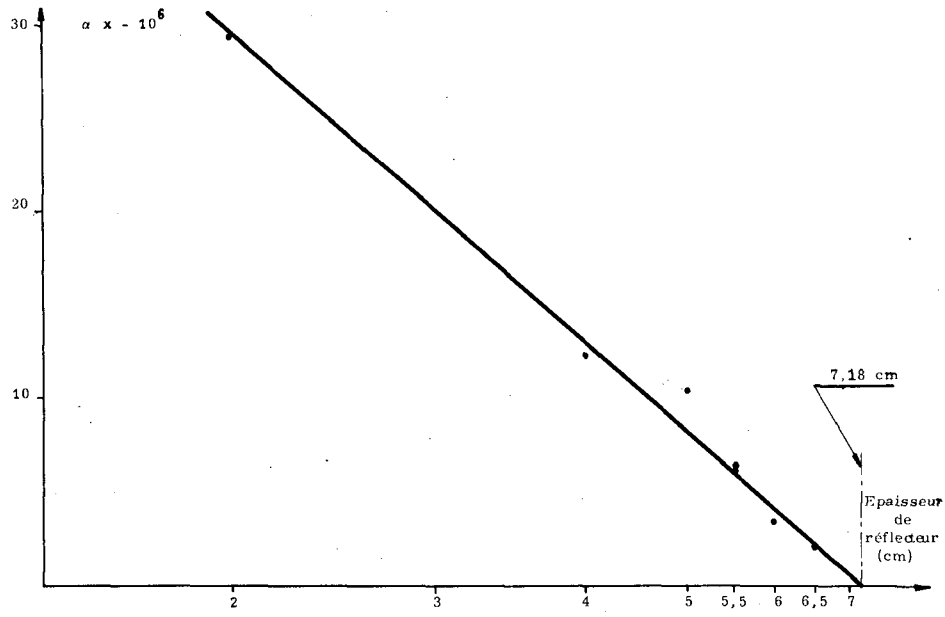


Fig. 5

JACINTHE - Approche sous-critique par neutrons pulsés.

Une discussion analogue à celle de la section 3.1.3. montre que le temps de vie reste pratiquement constant depuis l'état critique jusqu'à une antiréactivité de quelques milliers de pcm.

On obtient donc

$$\alpha_c = -4{,}7 \cdot 10^5 \ s^{-1}.$$

4. ÉTUDE DU RAPPORT SIGNAL SUR BRUIT

Par de simples considérations statistiques, il est facile de mettre en évidence que le dépouillement des résultats expérimentaux est d'autant plus précis que la partie exponentielle de la décroissance se détache mieux du niveau résiduel.

Or les mesures effectuées ont montré que le rapport signal sur bruit était inférieur à celui qui avait été évalué a priori.

Le calcul suivant met en évidence les facteurs à améliorer pour augmenter le rapport signal sur bruit, ainsi que l'influence des paramètres cinétiques sur ce dernier.

4.1. Rapport signal sur bruit dans la méthode des neutrons pulsés

4.1.1. Notations

Si = Signal = Nombre de neutrons présents dans l'assemblage au sommet de la bouffée et liés aux bouffées;

Br = Bruit = Nombre de neutrons présents dans l'assemblage non correlés en chaîne prompte avec les bouffées;

$R = Si/Br$ = Rapport signal sur bruit;

A = Nombre de fissions primaires induites chaque seconde par les neutrons pulsés de l'accélérateur;

B = Nombre de fissions primaires induites chaque seconde par les neutrons non pulsés * de l'accélérateur;

N = Fréquence de pulsation;

ν_0 = Nombre de neutrons produits par fission provoquée par des neutrons de 14 MeV;

ν = Nombre de neutrons produits par fission provoquée par des neutrons de fission (où éventuellement, par fission spontanée);

S = Nombre de fissions spontanées par seconde;

$\alpha = (K_p - 1)/\tau$; β; K = paramètres cinétiques classiques.

4.1.2. Valeur du terme «Signal»

Chaque bouffée produit A/N fissions primaires, soit $(A/N)[\nu_0/(1-K_p)]$ neutrons prompts. Le nombre λ de neutrons présents au sommet de la bouffée est donc

$$\lambda = \frac{-\alpha}{1-K_p} \cdot \frac{A}{N} \cdot \nu_0.$$

---

* Ces neutrons sont dus à des deutons déchargés et non défléchis, et au «halo» du faisceau [3].

Il faut ajouter à ce terme un facteur d'accumulation de niveau dû au fait qu'une nouvelle bouffée est injectée avant que les décroissances précédentes soient achevées.

Le niveau résiduel avant la deuxième bouffée est égal à $\lambda \exp(\alpha/N)$, soit, si l'on tient compte de toutes les bouffées précédentes,

$$\lambda \left[\exp\left(\frac{\alpha}{N}\right) + \exp\left(\frac{2\alpha}{N}\right) + \dots \right] = \frac{\lambda \exp\left(\frac{\alpha}{N}\right)}{1 - \exp\left(\frac{\alpha}{N}\right)}.$$

On écrit donc

$$Si = \frac{-\alpha}{1 - K_p} \cdot \frac{A}{N} \cdot \nu_0 \left[1 + \frac{\exp\left(\frac{\alpha}{N}\right)}{1 - \exp\left(\frac{\alpha}{N}\right)} \right].$$

4.1.3. Valeur du terme «Bruit»

4.1.3.1. Bruit dû aux neutrons retardés

En supposant la période de pulsation inférieure à la plus courte des périodes des neutrons retardés, le bruit de fond dû à ces derniers est sensiblement constant.

Chaque seconde, A fissions primaires engendrent $A\nu_0/(1-K)$ neutrons, soit $\beta A\nu_0/(1-K)$ neutrons retardés, qui n'ont pas de corrélation prompte avec la pulsation.

4.1.3.2. Bruit dû à la source interne

Il s'écrit $S\nu/(1-K)$. Bien entendu, ce bruit n'a aucune corrélation avec la pulsation.

4.1.3.3. Bruit dû à la source pulsée de neutrons

Des expériences ont montré que, sans «assemblage», l'accélérateur pulsé donne une émission continue de neutrons de 14 MeV, dont l'amplitude est comprise entre 0,1% et 1% de celle du sommet de la bouffée. Contrairement à ce que l'on pourrait croire a priori, cette émission constitue le terme fondamental du bruit de fond. Nous ne considérons pas les neutrons issus des réactions DD, car on peut diminuer considérablement leur importance relative en choisissant la très haute tension de l'accélérateur et en adoptant un jeu de lèvres ayant un angle solide très faible par rapport à l'assemblage étudié.

Soit B le nombre de fission initiales induites chaque seconde par les neutrons non pulsés, c'est-à-dire entre chaque bouffée. Le nombre total de neutrons produits par ces fissions primaires est donc

$$\frac{B\nu_0}{1-K}.$$

4.1.4. Expression du rapport signal sur bruit

Jusqu'ici, nous avons considéré les niveaux neutroniques et non les taux de comptages. Si le détecteur utilisé enregistre avec une égale probabilité tous les neutrons issus de l'assemblage, le rapport des comptages est égal au rapport des niveaux. On a par suite

$$R = \frac{Si}{Br} = \frac{\dfrac{-\alpha}{1-K_p} \cdot \dfrac{A}{N} \cdot \nu_0 \left[1 + \dfrac{\exp\left(\dfrac{\alpha}{N}\right)}{1 - \exp\left(\dfrac{\alpha}{N}\right)} \right]}{\dfrac{\beta A \nu_0}{1-K} + \dfrac{S\nu}{1-K} + \dfrac{B\nu_0}{1-K}},$$

soit, si l'on note que $\exp(\alpha/N) \ll 1$ (voir section 4.1.5.1.)

$$R = \frac{1}{\beta + \dfrac{S}{A} \cdot \dfrac{\nu}{\nu_0} + \dfrac{B}{A}} \cdot \frac{1-K}{1-K_p} \cdot \frac{-\alpha}{N}.$$

4.1.5. Discussion

La formule précédente renferme trois facteurs.

4.1.5.1.

Le facteur $-\alpha/N$ représente le rapport de la période de pulsation à la période de décroissance. D'après les notations, le nombre de neutrons par bouffée est A/N; on améliore donc le rapport R en diminuant N, mais alors les bouffées deviennent plus longues. Lorsqu'elles atteignent l'ordre de grandeur de α, il faut introduire un facteur supplémentaire. Par ailleurs, la diminution de N conduit à augmenter la durée des mesures dans la même proportion, afin de conserver la précision statistique (voir section 2.2.2.). Une valeur intéressante de α/N est $|\alpha/N| = 10$ *.

4.1.5.2.

Le terme $(1-K)/(1-K_p)$ dépend uniquement de l'assemblage étudié. Il varie de 1 pour $(1-K) \gg \beta$ à 0 pour $K = 1$, et est égal à 1/2 pour $1-K = \beta$. Ce terme montre bien la limitation de la méthode des neutrons pulsés vers les fortes réactivités.

4.1.5.3.

Le terme $1/(\beta + S/A \cdot \nu/\nu_0 + B/A)$ montre l'importance relative des différentes sources de neutrons. Pour $A \gg S$ et $A \gg B$, la limite de ce rapport serait $1/\beta$.

---

* Soit $\exp(\alpha/N) = 5 \cdot 10^{-5}$.

Or un accélérateur électrostatique, si l'on ne prend pas de précautions spéciales, donne un rapport B/A compris entre 0,1 et 1 * .

C'est donc le terme B/A qui est prépondérant dans le rapport R, car on a en général A > S.

Pour diminuer B/A, il faut

a) Avoir une bonne focalisation de l'accélérateur;
b) Diminuer les recombinaisons d'ions, c'est-à-dire améliorer le vide et éviter les dégazages par impact du faisceau;
c) Utiliser une extension coudée sur l'accélérateur, avec déflexion magnétique permanente.

Nous avons effectué quelques essais en plaçant la pulsation électrostatique avant l'aimant d'analyse. Ainsi, toutes les particules neutres ou polyatomiques sont éliminées par l'aimant, alors qu'avec la disposition habituelle, où la pulsation est placée après l'aimant, les ions rechargés entre ce dernier et les plaques de déflexion viennent augmenter le terme B.

4.2. Rapport signal sur bruit, dans la méthode «α Rossi»

La formule fondamentale de la méthode «α Rossi» est la suivante:

$$P(t)dt = Cdt + \frac{E K_p^2}{2(\bar{\nu})^2 (1 - K_p)\tau} \cdot \overline{\nu(\nu - 1)} \exp(\alpha t) dt,$$

où E = Efficacité du détecteur.

P(t) dt représente la probabilité de compter un coup après un premier coup enregistré. Le terme Cdt représente la probabilité d'avoir un coup non lié à la chaîne. On peut donc écrire

$$P(t)dt = \frac{ES\bar{\nu}}{1 - K} dt + \frac{K_p^2 E}{2(\bar{\nu})^2 (1 - K_p)\tau} \cdot \overline{\nu(\nu - 1)} \exp(\alpha t) dt.$$

Le rapport signal sur bruit R(αR) s'écrit alors

$$R = \frac{K_p^2}{(1 - K_p)\tau} \cdot \frac{\overline{\nu(\nu - 1)}}{2(\bar{\nu})^3} \cdot \frac{(1 - K)}{S},$$

$$R = \frac{\overline{\nu(\nu - 1)}}{2(\bar{\nu})^3} \cdot \frac{K_p^2 (1 - K)}{1 - K_p} \cdot \frac{1}{S\tau}.$$

4.3. Comparaison des rapports signal sur bruit

Soit R(NP) le rapport Si/Br de la méthode des neutrons pulsés et R(αR) le rapport Si/Br de la méthode «α Rossi».

* A représente 0,1 à 1% du débit neutronique qui serait obtenu en arrêtant la pulsation de l'accélérateur (voir section 4. 1. 3. 3.).

4.3.1. Influence de la réactivité

On voit que, à côté des termes constants $\alpha/N \simeq 10$ et $\overline{\nu(\nu-1)}/2\bar{\nu}^3 \simeq 0{,}1$, figure un terme de réactivité qui varie approximativement de la même manière dans les deux formules, bien que le terme K_p^2 soit légèrement défavorable vers les basses réactivités dans la méthode «α Rossi». Au voisinage de $K = 1$, les valeurs de R augmentent lorsque K diminue, mais on ne constate pas d'avantages très nets pour l'une ou l'autre des méthodes.

4.3.2. Influence des sources

Dans la méthode des neutrons pulsés, il y a intérêt à augmenter le débit de la source de neutrons pulsés, c'est-à-dire A, jusqu'à obtenir $S/A < (B/A+\beta)$*. Le terme $1/(\beta+S/A\cdot\nu/\nu_0+B/A)$ garde alors une valeur constante.

Par contre, dans la méthode «α Rossi», l'efficacité des détecteurs conduit à augmenter S lorsque la réactivité diminue, afin de ne pas allonger indéfiniment la durée des mesures.

Il est nécessaire de conserver $S/(1-K) = \text{constante}$, de manière à conserver des taux de comptage sensiblement constants au-dessous d'une certaine réactivité; le terme $1/S$ devient alors supérieur au terme $1/(\beta+S/A\cdot\nu/\nu_0+B/A)$ et la méthode des neutrons pulsés devient plus avantageuse, indépendamment d'autres considérations théoriques.

4.3.3. Conclusion

D'après l'étude des rapports signal sur bruit, on voit que les facteurs permettant de comparer les domaines de réactivité où ces méthodes peuvent être appliquées sont les suivants:

a) La limite supérieure de réactivité est fixée d'une part, dans les deux méthodes, par le terme $(1-K)/(1-K_p)$ qui tend vers 0 lorsque K tend vers 1, et d'autre part

- dans la méthode «α Rossi», par le temps de vie des neutrons dans l'assemblage considéré et par l'importance de la source spontanée.
- dans la méthode des neutrons pulsés, par la puissance supplémentaire dégagée dans l'assemblage par les chaînes de fissions que l'accélérateur y induit, ce qui oblige à limiter la réactivité pour empêcher un échauffement exagéré ou une irradiation du personnel lorsque les protections n'ont pas été calculées en conséquence.

b) La limite inférieure de réactivité est fixée dans la méthode «α Rossi» par l'efficacité des détecteurs, qui ne peut être augmentée indéfiniment, ce qui conduit à ajouter une source supplémentaire. Dans les mesures par neutrons pulsés, aucune limitation n'apparaît.

Bien entendu, les performances de l'accélérateur ou de l'électronique peuvent conduire à une résolution insuffisante pour effectuer les mesures selon l'une ou l'autre méthode dans les assemblages rapides très sous-critique.

---

* Le terme B/A dépend de la géométrie de l'accélérateur et non de son débit.

5. CONCLUSION GÉNÉRALE

L'ensemble des mesures effectuées a démontré la nécessité d'utiliser, dans le domaine des assemblages critiques en neutrons rapides, des appareillages présentant des caractéristiques très poussées, pour obtenir une précision convenable. L'amélioration systématique du rapport signal sur bruit doit être recherchée en premier lieu par une adaptation judicieuse du générateur de neutrons: obtention d'une focalisation très fine, mise en place d'un système d'analyse du faisceau, éventuellement montage d'une pulsation avec regroupement.

Les résultats obtenus sur des assemblages dont la réactivité était comprise entre −10 000 pcm et −500 pcm montrent que les décroissances peuvent être décrites par une seule exponentielle. L'application de la théorie à un groupe nous a permis d'en déduire le coefficient de décroissance α_c à l'état critique et le temps de vie des différents systèmes, et de montrer que ce dernier restait sensiblement constant dans le domaine de réactivité considéré.

RÉFÉRENCES

[1] CLAIR, C., «Propriétés neutroniques de l'assemblage critique RACHEL», Physics of Fast and Intermediate Reactors I AIEA, Vienne (1962) 321.

[2] BOURGEOIS, P. et al., «Description de l'assemblage critique RACHEL», Physics of Fast and Intermediate Reactors I, AIEA, Vienne (1962) 313.

[3] FRIEDMAN, E. and GORNI, S., Modifications in the Post-Acceleration Pulsing Systems of Texas Nuclear Neutron Generator, Nucl. Instrum. Meth. 23 1 (1963) 155-6.

BIBLIOGRAPHIE

BENGSTON, J., "Determination of Prompt Neutron Decay Constants of Multiplying Systems", Proc. 2nd UN Int. Conf. PUAE 12 (1958) 63-71.

UNIVERSITY OF CALIFORNIA, Proceedings of the Second Symposium on the Application of Pulsed Neutron Source Techniques, Lawrence Radiation Laboratory, Berkeley, California (December 4 and 5, 1958), UCRL-5665.

KEEPIN, G. R., Pulsed Neutron Techniques, LAMS - 2215 (1958), 28 pp.

DISCUSSION

W. KATO: At what point does one find a difference between the pulsed-neutron technique and the Rossi-α technique?

R. COMTE: In both cases the prompt neutron decay constant, α, varies linearly with the plutonium mass of the assembly within the reactivity limits I have indicated. The α-values obtained with the Rossi-α technique are lower than those obtained with the pulsed-neutron method. However, by extrapolating to the critical state one can obtain α_c values that differ by less than 5% provided that certain cladding corrections are made.

D. STEGEMANN: Can you give any explanation for the discrepancies you found between the pulsed-source and the Rossi-α technique at the lower reactivity states in your system?

R. COMTE: I cannot tell you whether this discrepancy results from a difference between the two phenomena or to the apparatus. I think that the electronic apparatus for time measurement is much more sensitive with the Rossi-α technique.

DETERMINATION OF NEUTRON LIFETIMES AND REACTIVITIES IN THE FAST CRITICAL FR-0 ASSEMBLY*

A. BERGSTRÖM, B. BRUNFELTER AND J. KOCKUM
RESEARCH INSTITUTE OF NATIONAL DEFENCE,
STOCKHOLM, SWEDEN

Abstract — Résumé — Аннотация — Resumen

DETERMINATION OF NEUTRON LIFETIMES AND REACTIVITIES IN THE FAST CRITICAL FR-0 ASSEMBLY. The pulsed source technique has been used to measure negative reactivities ranging from 0.05 to 10% in the first core of the fast critical assembly FR-0. The loading contains a 20% enriched uranium metal core with a thick copper reflector.

The decay constant of the main mode has been deduced by a least squares fitting to the measured data, approximating the higher modes with one second exponential decay. The reactivities have been calculated according to formulae given by Garelis et al. and by Gozani. The decay constant is determined with a relative statistical uncertainty of about ± 3%, the reactivity with an uncertainty of ± 4%. Comparisons have been made with Rossi-α measurements.

When trying to evaluate the lifetime with the aid of one-region kinetic equations, it is found that the lifetime increases 40% between criticality and 1% subcriticality. The value of the lifetime obtained is about 60% too high compared to 14-group calculations. Two-region kinetic equations using separate lifetimes in core and reflector give closer agreement between theory and experiment.

DÉTERMINATION DE LA DURÉE DE VIE ET DE LA RÉACTIVITÉ DE NEUTRONS DANS L'ASSEMBLAGE CRITIQUE A NEUTRONS RAPIDES FR-0. La méthode de la source pulsée a été utilisée pour mesurer des anti-réactivités allant de 0,05 à 10% dans le premier cœur de l'assemblage critique à neutrons rapides FR-0. Il s'agissait d'un cœur à uranium métallique, enrichi à 20%, avec un épais réflecteur en cuivre.

Les auteurs ont déduit la constante de décroissance du mode principal par un ajustement aux données mesurées selon la méthode des moindres carrés en exprimant d'une manière approchée les modes supérieurs avec une décroissance exponentielle d'une seconde. Les réactivités ont été calculées selon les formules données par Garelis et al. et par Gozani. La constante de décroissance est déterminée avec une incertitude statistique relative d'environ ±3%, et la réactivité avec une incertitude de ± 4%. Les mesures ont été comparées aux mesures de α de Rossi.

Si l'on essaie d'évaluer la durée de vie à partir d'équations cinétiques à une région, il s'avère que la durée de vie augmente de 40% entre la criticité et l'état inférieur de 1% à la criticité. La valeur de la durée de vie obtenue est environ 60% trop élevée par rapport aux calculs à 14 groupes. On obtient un meilleur accord entre la théorie et l'expérience avec des équations cinétiques à deux régions dans lesquelles on utilise des durées de vie différentes dans le cœur et le réflecteur.

ОПРЕДЕЛЕНИЕ ВРЕМЕНИ ЖИЗНИ НЕЙТРОНОВ И РЕАКТИВНОСТЕЙ В БЫСТРОЙ КРИТИЧЕСКОЙ СБОРКЕ FR-0. Метод импульсных нейтронов применялся для измерения отрицательных реактивностей в диапазоне 0,05—10% в первой активной зоне быстрой критической сборки FRO. Загрузка состояла из стержня металлического урана 20%-ного обогащения с толстым медным отражателем.

Константа распада основного состояния была выведена подгонкой измеренных данных *методом наименьших квадратов с приближением к более высоким видам с одной второй* экспоненциального распада. Реактивности рассчитаны в соответствии с формулами, предложенными Е.Гарелисом и другими и Т.Гозани. Константа распада определена с относительной статистической неопределенностью до ± 3%, а реактивность с неопределенностью ± 4%. Даются сравнения с результатами измерений по методу α-Росси.

---

* Experimental work performed at AB Atomenergi, Studsvik, Nyköping, Sweden.

При попытке сделать оценку продолжительности жизни с помощью кинетических уравнений одной зоны установлено, что продолжительность жизни возрастает на 40% между критичностью и 1% подкритичности. Полученные значения продолжительности жизни на 60% выше по сравнению с 14-групповыми расчетами. Двухзональные кинетические уравнения, использующие отдельные продолжительности жизни в активной зоне и в отражателе, позволяют получить лучшее согласие теории с экспериментом.

DETERMINACION DEL PERIODO DE LOS NEUTRONES Y DE REACTIVIDADES EN EL CONJUNTO CRITICO DE NEUTRONES RAPIDOS FR-0. Los autores han empleado la técnica de los neutrones pulsados para medir reactividades de valor negativo, comprendidas entre el 0,05 y el 10%, en el primer cuerpo del conjunto crítico de neutrones rápidos FR-0. La carga de este conjunto estaba constituida por U metálico enriquecido al 20%, con un reflector de Cu de gran espesor.

La constante de decrecimiento del modo fundamental se dedujo mediante el ajuste por el método de los cuadrados mínimos a los datos medidos, asimilando los armónicos de grado superior a un segundo decrecimiento exponencial. Los valores de la reactividad se calcularon con arreglo a las fórmulas propuestas por Garelis y sus colaboradores y por Gozani. La constante de decrecimiento se determinó con una incertidumbre estadística relativa de aproximadamente ± 3%, y el valor de la reactividad con una incertidumbre de ± 4%. Los resultados se compararon con los obtenidos por la técnica de Rossi-α.

Al tratar de determinar el período con ayuda de ecuaciones cinéticas para una sola región, se comprobó que dicho parámetro aumenta un 40% al pasar de la criticidad a una subcriticidad del 1%. El valor obtenido para el período es un 60% demasiado elevado en comparación con el resultante del cálculo para 14 grupos. Las ecuaciones cinéticas para dos regiones, que emplean períodos distintos para el cuerpo y el reflector, permiten conseguir una mayor concordancia entre los resultados teóricos y los experimentales.

INTRODUCTION

The pulsed source technique has been used rather extensively to measure reactivity and neutron life time [1-5]. In this type of measurement, short bursts of neutrons are periodically introduced into the subcritical reactor and the neutron population is measured as a function of time. Three different time behaviours can be observed (see Fig. 3): the build-up of a prompt neutron population and decay of high energy and spatial modes, the exponential decay of the fundamental prompt mode, and finally a practically constant delayed neutron population governed by the mean fission rate.

One-group, one-region reactor kinetic equations give the following expression for the fundamental mode decay constant

$$\alpha = \frac{\rho - \beta}{\ell (1 - \rho)}, \qquad (1)$$

where the reactivity $\rho = (k - 1)/k$, k is the effective multiplication constant, β the effective fraction of delayed neutrons and ℓ the mean prompt neutron lifetime.

By introducing the two-region (core-reflector) model proposed by COHN [6], KISTNER [7] shows that the fundamental decay constant is split in two. The kinetic equations in this notation with one group of delayed neutrons are

$$\left.\begin{aligned} \frac{dN_c}{dt} &= \frac{k_c(1-\beta)-1}{\ell_c} N_c + \frac{k_{rc}}{\ell_r} N_r + \lambda C \\ \frac{dN_r}{dt} &= -\frac{N_r}{\ell_r} + \frac{k_{cr} N_c}{\ell_c} \\ \frac{dC}{dt} &= -\lambda C + \frac{\beta k_c}{\ell_c} N_c \end{aligned}\right\} \quad (2)$$

where

N_c = total number of neutrons in core

N_r = total number of neutrons in reflector

C = total number of delayed neutron precursors

k_c = probability that a disappearing core neutron will give rise to a new fission neutron in the core

k_{rc} = probability that a disappearing reflector neutron will reappear in the core

k_{cr} = probability that a disappearing core neutron will reappear in the reflector

ℓ_c = prompt neutron lifetime in core

ℓ_r = neutron lifetime in reflector

λ = mean decay constant of delayed neutron precursors

$$\lambda_c = \frac{1-k_c(1-\beta)}{\ell_c}$$

$$\lambda_r = \frac{1}{\ell_r}$$

For a short neutron pulse the following solution is obtained when the delayed neutrons are neglected

$$\left.\begin{aligned} N_c(t) &= N_0 \frac{\lambda_c+\alpha_2}{\alpha_2-\alpha_1}\left[e^{\alpha_1 t} - \frac{\lambda_c+\alpha_1}{\lambda_c+\alpha_2} e^{\alpha_2 t}\right] \\ N_r(t) &= N_0 \frac{\lambda_c+\alpha_2}{\alpha_2-\alpha_1} \frac{\lambda_c+\alpha_1}{\lambda_{rc}}\left[e^{\alpha_1 t} - e^{\alpha_2 t}\right] \\ \alpha_{1,2} &= -\frac{\lambda_c+\lambda_r}{2} \pm \sqrt{\left(\frac{\lambda_c+\lambda_r}{2}\right)^2 - \left(\lambda_c\lambda_r - \frac{k_{cr}\,k_{rc}}{\ell_c\ell_r}\right)} \end{aligned}\right\} \quad (3)$$

When the reflector becomes less effective, that is $k_{cr}\,k_{rc}$ approaches zero, $N_c(t)$ approaches $N_0 e^{\alpha_1 t}$ with $\alpha_1 = -\lambda_c = \alpha$.

By using one-velocity diffusion theory for a bare reactor, GARELIS and RUSSELL [3] have shown that the parameter $\gamma = k\beta/\ell$ can be determined from the following expression

$$\int_0^\infty N_p(t) \exp(\gamma t)dt - \int_0^\infty N_p(t)dt = \frac{N_d}{F} \quad (4)$$

Here $N_p(t)$ is the prompt neutron counting rate at time t, N_d the delayed neutron counting rate, and F the burst frequency. The reactivity and lifetime are calculated from the expressions

$$-\rho = \beta \frac{\alpha - \gamma}{\gamma} \tag{5}$$

and

$$\ell = \frac{\beta}{\gamma(1-\rho)} \tag{6}$$

WALLACE [8] has pointed out approximations necessary to derive Eq.(3) in a multi-energy case and the necessity to justify these approximations experimentally.

GOZANI [4] gives the following expression for the reactivity

$$-\rho = \beta \frac{F}{N_d} \frac{C}{\alpha} \tag{7}$$

Here C is the amplitude of the main mode (with decay constant α) extrapolated back to zero time.

With the assumption of only one exponential decay, Eqs.(5) and (7) can be shown to be identical. With the same assumption, both equations give

$$-\rho = \beta \frac{F}{N_d} \int_0^\infty N_p \, dt \tag{8}$$

and

$$\ell = \frac{N_d + F \int_0^\infty N_p \, dt}{N_d + \beta F \int_0^\infty N_p \, dt} \cdot \frac{\beta}{\alpha} \tag{9}$$

In other words, the reactivity is given by the ratio of the total number of prompt neutrons to delayed neutron counting rate, while the deduced lifetime is inversely proportional to α.

The decay constant for fission chains (α) may in fast reactors also be determined by the so-called Rossi-α technique [9-10]. In this type of measurements, one or two detectors are placed in the reactor, which is kept at a constant power, and the time distribution between two consecutive pulses is recorded. α can be deduced from the deviation from a statistical distribution. KISTNER [7] has deduced expressions similar to Eq.(3) for the reflected case.

EXPERIMENTAL EQUIPMENT

The FR-0 core I is an approximately circular cylinder of 20% enriched uranium-metal surrounded by a thick copper reflector (Table I). The fuel consists of square plates loaded in vertical tubes on a split table (Fig. 1). One of the table halves is remotely moved close to the other during approach-to-criticality. The control rods are loaded as ordinary fuel tubes and fuel is taken out of, and copper is brought into, the core when they are driven out to decrease the reactivity.

The neutron source used is a Texas Nuclear Model 9505 neutron generator. Deuteron ions are accelerated to 150 keV before striking a tritium target placed as shown in Fig. 1, where they produce 14-MeV neutrons. The deuteron beam is cut into 1-μs or longer square pulses before acceleration and these can be further chopped by applying a 500 kc/s sinusoidal voltage to a pair of deflector plates in the post-acceleration drift tube. To reduce the background between pulses, a square voltage pulse synchronous to the pre-acceleration pulsing is applied to a second couple of deflector plates in the drift tube. The frequency of the pre-acceleration pulsing can be varied up to 50 kc/s.

TABLE I

DATA FOR FR-0 CORE 1

Critical mass (kg)	365
Height (cm)	30.1
Equivalent radius (cm)	15.3
Reflector thickness (cm)	
Top and bottom	40.9
Axial	34.3
Core composition (vol.%)	
U^{235}	17.6
U^{238}	70.1
Fe	4.8
Ni	0.5
Cr	1.2
Teflon (CF_2)	0.2
Void	5.6
Reflector composition (vol.%)	
Copper	88.5
Steel	6.5
Void	5.0

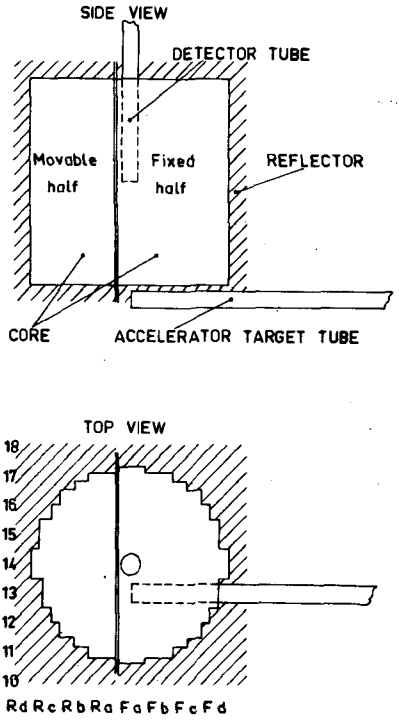


Fig. 1

Geometrical set-up of the experiment

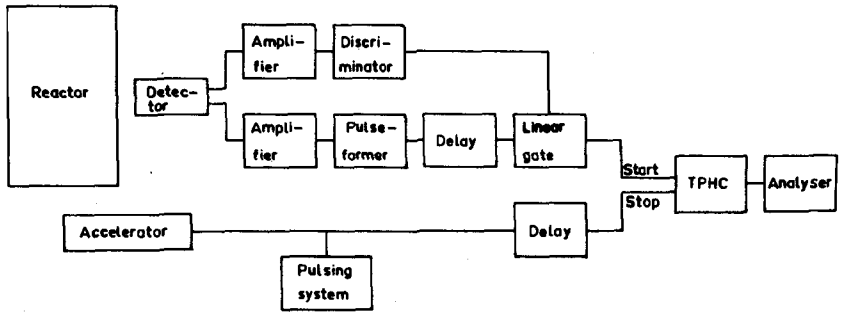


Fig. 2

Block diagram of the electronics

A block diagram of the time-measuring electronics is shown in Fig. 2. The detector is a stilbene scintillator recording proton recoils. The difference in pulse form between electron and proton pulses is used to discriminate against γ-rays reducing the γ-ray sensitivity by a factor grater than 10^3 [11]. At the same time a lower cut-off at about 0.5-MeV proton energy is introduced.

The proton pulses pass a gate and start a time-to-pulse-height converter (TPHC). The stop pulse is obtained from the pulsing system. The range of the TPHC and the delay of the stop-pulse is chosen in such a way that the time immediately before and after each burst is scanned while the rest of the time is discarded. In this way the time resolution is kept high enough even at low burst frequencies. Zero time is deduced by extrapolating the rising part of the recorded pulse-height spectrum (Fig. 3) back to background level giving an uncertainty of ± 0.5 channels (0.12 or 0.25 μs).

In the Rossi-α measurements the same type of electronics has been used. The detector has been a He^3 filled proportional counter which both starts and stops the TPHC. To ensure that the same pulse does not both start and stop the TPHC, a time delay of 2 μs is inserted in the start line.

EXPERIMENT

The method was tested on control rods where the reactivity was known from inverse multiplication and rod drop measurements. The technique was

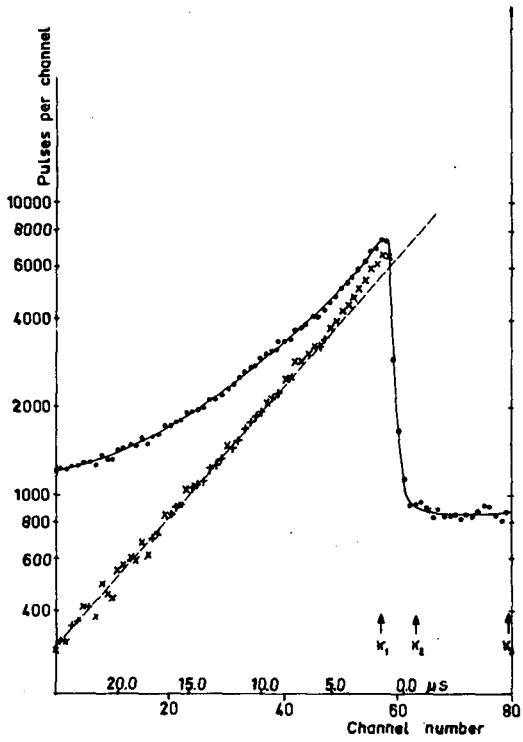


Fig. 3

Recorded pulse-height (time) spectrum (ρ= 0.72%)

● Dead-time-corrected spectrum

× Spectrum with the delayed neutron contribution subtracted

– – – Main mode decay obtained with the GAP programme

then used when determining the reactivity worth of a central air gap of varying width.

The reactivity range covered was 5×10^{-4} to 10^{-1}. The burst frequency was chosen to give a ratio between maximum prompt neutron counting rate and delayed neutron background of about 8 or higher. The intensity of the deuteron beam or the burst width was adjusted to give a probability not higher than 5% for two counts per burst. The second of these counts is lost and this effect has to be corrected for. The burst widths were either 300 ns or 1 μs. A typical measuring time to get about 3% accuracy in the α-determination was about half-an-hour. A constant background due to multiplication of spontaneous fission neutrons from U^{238} had to be determined after each run. The time calibration was made either with a pulse generator giving two output pulses with variable known delay or by using a radioactive source instead of reactor in the start chain (Fig. 2). This source gives statistically distributed start pulses. From the mean number of start pulses per second, the stop frequency and the registered counting rate per channel of the multichannel analyser, the time per channel can be deduced. The two methods agree within 1/2%. The second method also gives a good test of the linearity of the system. An increase of the channel-width of about 3% over the whole range had to be corrected for.

Preliminary measurements did not show any pronounced geometrical variation in the ratio of excitation between the main mode and higher modes. During most of the reported measurements the detector was kept in the central fuel element 17 cm above the bottom surface of the core.

DATA EVALUATIONS

The recorded time distribution is first corrected for start losses in the TPHC. Ignoring second-order terms, and using the recorded pulse-height spectrum in the corrections, one may express the corrected number of pulses in channel i as

$$N_{exp}(t_i) = \frac{N(t_i)}{T_m F \tau \left[1 - \sum_{i+1}^{\kappa_2} \frac{N(t_i)}{T_m F} - \frac{T_d - (\kappa_2 - i)\tau}{(\kappa_3 - \kappa_2)\tau} \sum_{\kappa_2}^{\kappa_3} \frac{N(t_i)}{T_m F} \right]} \qquad (10)$$

where $N(t_i)$ is the number of counts in channel i, T_m the total measuring time, F the burst frequency, τ the channel-width and T_d the time range of the TPHC. The channel numbers κ_2 and κ_3 are defined in Fig. 3.

The corrected time distribution $N_{exp}(t_i)$ contains contributions from initial transients, which may be expressed as several superimposed exponential distributions, but which after some few channels (κ_1 in Fig. 3) are supposed to be adequately represented by one additional exponential term in the assumed theoretical distribution

$$N_{theor}(t_i) = C\, e^{\alpha t_i} + C'\, e^{\alpha' t_i} \qquad (11)$$

The four parameters C, C', α and α' were determined from the experimental values using the GAP language [12] and a least-squares criterion. The parameters C and C' in the expressions (11) above define a linear sub-space in the function space and are therefore for each α and α' uniquely solved by GAP from the equations of the normal to the point $N_{exp}(t)$ in function space. Determination of the parameters α and α' in expressions of the type given in Eq. 11 often lead to convergence difficulties if a linearization by Taylor expansion is used. For this reason a straightforward scanning with logarithmically equal intervals in the interesting domain of the $\alpha\alpha'$-space was employed before starting an iterative procedure. This also ensures that the lowest existing minimum is found. The error in α is dominated by the uncertainty of whether or not Eq.(11) is an adequate representation also of the transient behaviour close to channel κ_1. Little can be deduced from the experiment about the validity of Eq.(11), although the increase in κ^2-values obtained for runs with increasing statistical accuracy indicates that Eq.(11) may not give a completely correct description of the experimental data. Also, the two exponents are rather close to each other ($0.1 < \alpha/\alpha' < 0.4$). The criterion quantity forms a narrow valley on the $\alpha\alpha'$ plane, and the error in α should be measured as the necessary change in α to obtain a significant change in the criterion inside the valley. From these considerations the error in α is estimated to about ± 3%.

Before solving γ in the integral Eq.(4) by GAP [12] the equation was reformulated as

$$\sum (N_{exp}(t_i) - N_d\tau)\exp(\gamma t_i) - \sum (N_{exp}(t_i) - N_d\tau) = \frac{N_d}{F} \qquad (4b)$$

where $N_d = \sum_{\kappa_2}^{\kappa_3} \frac{N_{exp}(t_i)}{(\kappa_3 - \kappa_2)\tau}$

From Eqs.(8) and (9) the statistical uncertainty in ℓ and ρ may be calculated as $\left(\frac{\Delta\ell}{\ell}\right)^2 \cong \left(\frac{\Delta\rho}{\rho}\right)^2 = \left(\frac{\Delta F}{F}\right)^2 + \left(\frac{\Delta N_d}{N_d}\right)^2 + \left(\frac{\Delta[N_i - N_d]}{[N_i - N_d]}\right)^2$. The uncertainty in zero time (Δt_0) gives a systematical error $\Delta\rho/\rho = \alpha\Delta t_0$ to the ρ-values calculated according to Eq.(4) which is included in Table II. The corresponding error in γ is an order of magnitude smaller and thus neglectable.

RESULTS

(a) Start rod measurements

The recorded data from a typical measurement are shown in Fig. 3 together with a curve where the constant delayed neutron background is subtracted. The calculated main mode decay is also shown.

Figure 4 shows the reactivity worth of the rod, calculated from Eqs.(5) and (7), as a function of rod position as well as the results of inverse multiplication measurements. The same data are given in Table II together with

TABLE II

REACTIVITY OF START ROD (STS1) AND SCRAM ROD (SCS2)

Rod position (cm)	Reactivity (%)			
	Eq. (5)	Eq. (7)	Inverse mult.	Rod drop
STS1 12.1	0.26 ± 0.01	0.26 ± 0.01	0.25	
STS1 24.5	0.75 ± 0.02	0.72 ± 0.03	0.66	
STS1 32.0	0.91 ± 0.03	0.88 ± 0.03	0.81	
STS1 39.4	0.92 ± 0.03	0.86 ± 0.03	0.87	
STS1 49.5	1.03 ± 0.03	0.96 ± 0.04	0.98	
STS1 62.0	1.23 ± 0.04	1.16 ± 0.05	1.17	
STS 74.5	1.43 ± 0.04	1.31 ± 0.07	1.34	
SCS2 71.0	1.88 ± 0.06	1.75 ± 0.09		1.72

the results of a measurement on one of the scram rods which has been calibrated with the rod drop technique. The relatively good agreement between the results of Eqs (5) and (7) indicates that one exponential decay dominates the prompt neutron population. The results obtained from Eq. (5) seem to lie, systematically, about 5% above the inverse multiplication and rod drop values. In Fig. 4, ℓ-values from Eq. (6) are also given showing a large increase in neutron lifetime with increasing negative reactivity.

Figure 5 gives the α-values obtained with the pulsed source technique and the Rossi-α technique. The results of applications of one- and two-region kinetic models to the problem are also shown. The Rossi-α measurements were made on a spherical core of the same composition as the cylindrical core in the pulsed source measurements. α_1 and α_2 have been calculated according to Eq. (3). The following expressions have been used in the critical state. Leakage through the outer reflector surface has been neglected.

$$\left.\begin{aligned} k_c &= \frac{P_c}{A_c + J_+} = 0.431 \\ k_{cr} &= \frac{J_+}{A_c + J_+} = 0\ 665 \\ k_{rc} &= \frac{J_-}{J_+} = \frac{J_+ + A_c - P_c}{J_+} = 0.858 \end{aligned}\right\} \qquad (12)$$

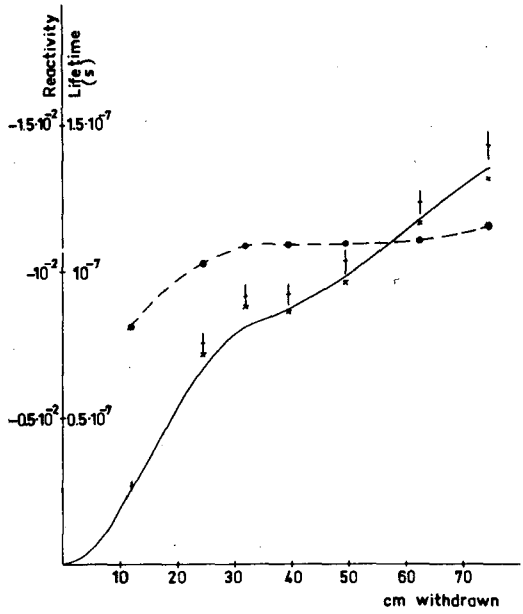


Fig. 4

Reactivity and lifetime as a function of the position of start rod 1

—— Reactivity measured by the inverse multiplication technique

† Reactivity measured by the pulsed source method, evaluated as $-\rho = \beta \frac{\alpha - \gamma}{\gamma}$ (Eq.(5))

× Reactivity measured by the pulsed source method, evaluated as $-\rho = \beta \frac{F}{N_d} \frac{C}{\alpha}$ (Eq.(7))

-●- Lifetime evaluated as $\ell = \frac{\beta}{\gamma(1-\rho)}$ (Eq.(6))

where

P_c = the neutron production in the core

A_c = the neutron absorption in the core

J_+ = the outward integrated current through the core-reflector interface

J_- = the inward integrated current through the core-reflector interface.

These quantities have been evaluated in one-group diffusion theory for spherical geometry. This rather crude approximation is justified by results of flux shape measurements using fission chambers with different energy response. These measurements all give cosine axial distributions with almost the same extrapolated length [13]. The one-group cross-sections have been condensed from a 14 group set [14]. ℓ_r and ℓ_c are calculated in 14-group formalism as

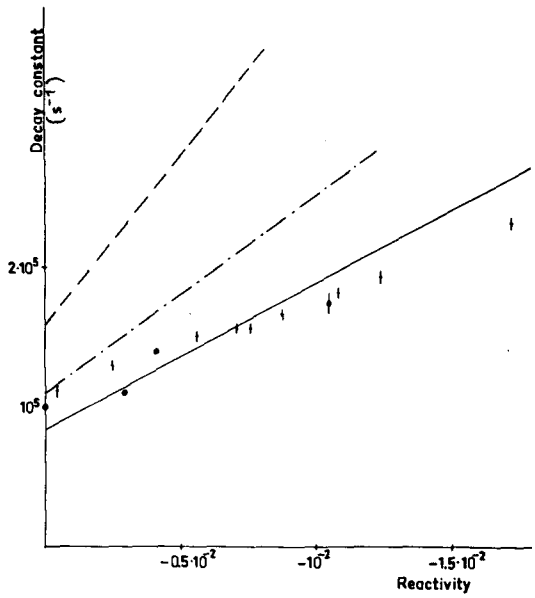


Fig. 5

Decay constant as a function of reactivity

† Pulsed source measurements
● Rossi-α measurements
——— $-\alpha_2(\rho)$ derived from Eqs.(3) (10) and (11) as described in text
-·-·- $-\alpha(\rho)$ derived from Eq.(1) with $\ell = \frac{\ell_c + (1-k_c)\ell_r}{k_c}$
– – – $-\alpha(\rho)$ derived from Eq.(1) with $\ell = \ell_c + \ell_r$

$$\left.\begin{aligned} \ell_c &= \frac{\sum_1^{14} \int_{\text{core}} \frac{1}{v_i}\,\phi_i \phi_i^*\,dV}{\int_{\text{core}} \sum_{i=1}^{14} \nu\Sigma_{fi}\phi_i \sum_{j=1}^{14} \chi_j \phi_j^*\,dV} = 2.87\times 10^{-8}\ \text{s} \\ \ell_r &= \frac{\sum_1^{14} \int_{\text{reflector}} \frac{1}{v_i}\,\phi_i \phi_i^*\,dV}{\int_{\text{core}} \sum_{i=1}^{14} \nu\Sigma_{fi}\phi_i \sum_{j=1}^{14} \chi_j \phi_j^*\,dV} = 2.08\times 10^{-8}\ \text{s} \end{aligned}\right\} \quad (13)$$

where χ_j is the fraction of fission neutrons borne in group j. ϕ_i and ϕ_i^* have been obtained by S_n calculations [14]. COHN [6] gives the following ex-

pression for the total prompt neutron lifetime $\ell=[\ell_c+(1-k_c)\ell_r]/k_c$ which in this case gives $\ell = 7.13\times10^{-8}$. In one region formalism $\ell=\ell_r+\ell_c = 4.95\times10^{-8}$ s.

With these approximations $-\alpha_1 = 6.80\times10^{7}$ s and $-\alpha_2 = 8.3\times10^{4}$ s. The high value of $-\alpha_1$ causes the corresponding decay to be hidden among the higher modes while it is possible to identify α_2 as the measured α.

To estimate the variation of α_2 with reactivity it has been assumed that the decrease in reactivity is entirely caused by a decrease in the production term P_c when the rod is pulled out of the reactor. This gives the solid line in Fig. 5. The dashed line represents Eq. (1) with $\ell = 4.95\times10^{-8}$ s; the dashed-dotted line represents Eq. (1) with $\ell = 7.13\times10^{-8}$ s.

(b) Reactivity of a central air gap

The result of measurements of the reactivity change when the two reactor tables are separated is shown in Fig. 6. Separations between 0.3 and 30 mm were investigated giving reactivity changes between 0.05 and 12%.

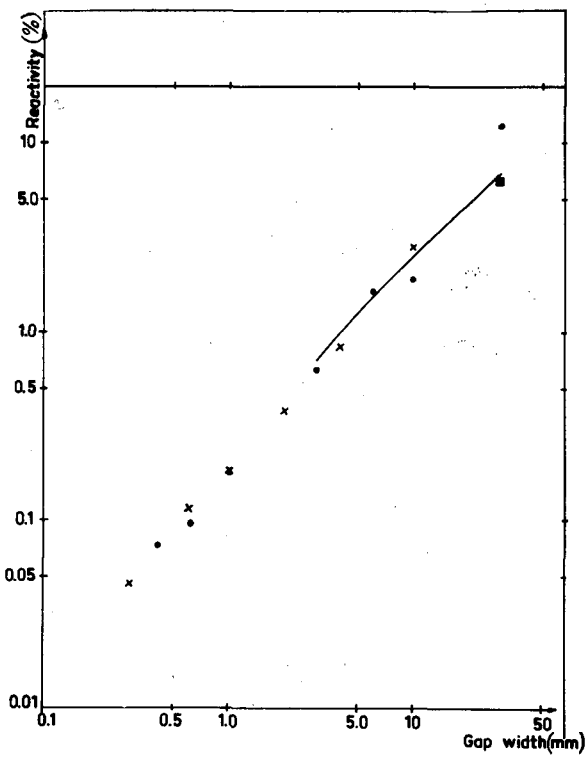


Fig. 6

Reactivity of a central air gap

× Detector in the fixed half (Fa14)
● Detector in the movable half (Ra14)
■ Result of a six-group, two-dimensional S_n calculation
— Results of diffusion theory calculations

Two detector positions (tube Fa14 and Rb14, Fig. 1) were used. The variation of α with reactivity is very similar to the data given in Fig. 5 in the reactivity range also covered in the start rod measurements. (The $\rho = 5 \times 10^{-4}$ point in Fig. 5 is taken from this set of measurements.)

The curve in Fig. 6 represents a diffusion theory calculation on a bare reactor and the theoretical point (filled square) at 30 mm a six-group two-region S_n calculation [14].

DISCUSSION

Figure 5 shows the invalidity of Eq. (1) when the probability is large that a core neutron has experienced a previous collision in the reflector. A six-group two-dimensional calculation [14] was performed to investigate if the overall neutron lifetime changes when a central control rod is partly withdrawn due to the simultaneous introduction of copper into the core. However, the calculated increase of 6% is far too small to explain the apparent rise in neutron lifetime shown in Fig. 4. As a result of approximations made when evaluating α_2 (Eq. 12) and the fact that α_2 is the difference between two large quantities, the relatively good agreement between the α_2-line and the α-measurements shown in Fig. 5 might be accidental. On the other hand, an effect of this kind could explain the discrepancy between measured and calculated lifetimes reported by BRUNSON et al. [10] and the fact that the ρ-intercept in the α versus ρ line measured by PATERSON and WEALE [5] does not equal β (compare Eq. (1)). A more sophisticated theoretical treatment of the problem should be of great interest, especially in this case where the effect is large owing to the efficient reflector, and comparison between theory and experiment therefore is easy to perform.

Figure 4 shows that the pulsed source method can be used for reactivity measurements even if Eq. (1) is invalid. As pointed out by GOZANI [4], the ratio between total prompt and delayed neutron population is a unique function of reactivity and burst frequency, and Eq. (8) shows that both Eqs. (5) and (7) essentially use this ratio.

ACKNOWLEDGEMENTS

The authors want to express their gratitude for the technical assistance given by the operating crew and for the many fruitful discussions with all members of the physics group at the FR-0 reactor.

REFERENCES

[1] SJÖSTRAND, N.G., Ark. Fys. 11 (1956) 233.
[2] BECKURTS, K.H., Nucl. Instrum. Meth. 11 (1961) 144.
[3] GARELIS, E. and RUSSELL, J.L., Nucl. Sci. Engng 16 (1963) 263.
[4] GOZANI, T., Nukleonik 5 (1963) 55.
[5] PATERSON, W.J. and WEALE, J.W., J. Brit. nucl. Energy Soc. 3 (1964) 311.
[6] COHN, C.E., Nucl. Sci. Engng 13 (1962) 12.

[7] KISTNER, G., Nukleonik 7 (1965) 106.
[8] WALLACE, S.K., Nucl. Sci. Engng 21 (1965) 116.
[9] ORNDOFF, J., Nucl. Sci. Engng 2 (1957) 450.
[10] BRUNSON, G.S., CARRAN, R.N., GASIDLO, J.M. and HUBER, R.J., Rpt. ANL-6681 (1963).
[11] BRUNFELTER, B., KOCKUM, J. and STARFELT, N., Neutron Dosimetry II IAEA, Vienna (1963) 351.
[12] BERGSTRÖM, A., Proc. of EANDC Conf. on Automatic Acquisition and Reduction of Nuclear Data, Karlsruhe (1964) 512.
[13] HELLSTRAND, E. et al., AE Rpt, to be published, 1965.
[14] HÄGGBLOM, H., AE Rpt, to be published, 1965.

FAST-REACTOR PHYSICS PARAMETERS FROM A PULSED SOURCE*

W. Y. KATO, H. H. MEISTER**, G.W. MAIN
ARGONNE NATIONAL LABORATORY, ARGONNE, Ill.,
AND
J. L. RUSSELL, Jr. AND K. L. CROSBIE
J. J. HOPKINS LABORATORY,
GENERAL ATOMIC, SAN DIEGO, CALIF.,
UNITED STATES OF AMERICA

Abstract — Résumé — Аннотация — Resumen

FAST REACTOR PHYSICS PARAMETERS FROM A PULSED SOURCE. One of the more important integral parameters in fast reactor physics analysis is the neutron spectrum of a particular composition reactor core. Various methods, such as proton recoil counters and nuclear emulsion analysis, have been used to study fast reactor spectra. With the development of high intensity short-duration pulsed neutron sources, the time-of-flight technique has become suitable for fast reactor spectrum determination.

To evaluate the feasibility of measuring fast neutron spectra from a core using time-of-flight techniques, an experiment has been performed to measure the equilibrium spectrum in a large block of depleted uranium using the General Atomics Linac facilities. A ten-metric-ton block of depleted uranium was assembled to form a 81-cm cube. This block of uranium was pulsed by electron bombardment of a uranium target imbedded in the block. The spectra from various sections of the block were measured using time-of-flight techniques for a 50-m flight path. Spectral indices, such as the ratio of the fission rates of U^{238}/U^{235}, U^{233}/U^{235}, U^{234}/U^{235}, Np^{237}/U^{235}, Pu^{239}/U^{235}, were also measured. In addition, measurements of the U^{238} capture rates were obtained in various parts of the block. This paper describes the techniques used to obtain these reactor physics parameters. The experimental results such as the spectra and spectral indices are also compared with those obtained from theoretical considerations using multigroup transport theory analysis.

The pulsed neutron technique is also applicable for the measurement of such parameters as : β/ℓ, where β is the effective delayed neutron fraction and ℓ is the lifetime; neutron importance; and k_{eff}. This paper concludes with a discussion on the proposed application of a pulsed neutron source for the measurement of some of these parameters on fast reactor cores constructed on ZPR-VI, the Argonne Fast Critical Facility.

DÉTERMINATION, A L'AIDE D'UNE SOURCE PULSÉE, DES PARAMÈTRES DE LA PHYSIQUE DES RÉACTEURS A NEUTRONS RAPIDES. Un des plus importants paramètres intégraux de la physique des réacteurs à neutrons rapides est le spectre des neutrons d'un cœur de réacteur de composition particulière. On a utilisé diverses méthodes pour étudier les spectres des réacteurs à neutrons rapides, par exemple celle des tubes compteurs à protons de recul et l'analyse d'émulsions nucléaires. Maintenant que des sources à bouffées de neutrons de courte durée et à forte intensité ont été mises au point, la méthode du temps de vol peut servir pour la détermination des spectres des réacteurs à neutrons rapides.

Afin d'étudier la possibilité de mesurer sur un cœur les spectres de neutrons rapides en utilisant la méthode du temps de vol, les auteurs ont fait une expérience dont l'objet était la mesure du spectre d'équilibre dans un grand bloc d'uranium appauvri, l'accélérateur linéaire de la General Atomic étant utilisé à cette fin. Dix tonnes d'uranium appauvri ont été assemblées en un cube de 81 cm de côté. Ce bloc d'uranium a été pulsé par bombardement électronique d'une cible en uranium placée à l'intérieur. Les spectres provenant de diverses sections du bloc ont été mesurés suivant les techniques du temps de vol avec un canal de parcours de vol de 50 mètres. Des caractéristiques des spectres, telles que le rapport des taux de fission $^{238}U/^{235}U$, $^{233}U/^{235}U$, $^{234}U/^{235}U$, $^{237}Np/^{235}U$, $^{239}Pu/^{235}U$, ont été mesurés en diverses parties du bloc. Les auteurs décrivent les méthodes utilisées pour obtenir ces paramètres de la physique des réacteurs. Les résultats expérimentaux, par exemple les

* Work performed under the auspices of the United States Atomic Energy Commission.

** Visiting scientist from Kernforschungszentrum, Karlsruhe, Federal Republic of Germany.

spectres et les caractéristiques des spectres, sont également comparés à ceux qu'on obtient en partant de considérations théoriques par le recours à l'analyse suivant la théorie du transport à plusieurs groupes.

La méthode des neutrons pulsés peut aussi servir pour la mesure des paramètres suivants: β/ℓ, l'importance des neutrons et k_{eff}. Le mémoire se termine sur la discussion d'une proposition tendant à appliquer la méthode de la source de neutrons pulsés à la mesure de certains de ces paramètres dans des cœurs de réacteurs à neutrons rapides construits à ZPR-VI, l'installation critique à neutrons rapides d'Argonne.

ОПРЕДЕЛЕНИЕ ФИЗИЧЕСКИХ ПАРАМЕТРОВ БЫСТРЫХ РЕАКТОРОВ С ПОМОЩЬЮ ПУЛЬСИРУЮЩЕГО ИСТОЧНИКА. Одним из наиболее важных интегральных параметров при анализе физики быстрых реакторов является нейтронный спектр активной зоны реактора определенного состава. Для изучения спектров быстрых реакторов использовали различные методы, напрмер применяли счетчики протонов отдачи и анализ ядерной эмульсии. С разработкой источников импульсных нейтронов высокой интенсивности при малой продолжительности импульса метод определения по времени пролета стал наиболее подходящим для определения спектра быстрых реакторов.

Для оценки возможности измерения спектров быстрых нейтронов из активной зоны с использованием времени пролета был проведен эксперимент по измерению спектра равновесия в большой массе обедненного урана с использованием установок LINAC компании "Дженерал атомик". Десять метрических тонн обедненного урана собрали в куб с ребром 81 см. В урановый блок вставили урановую мишень и подвергли импульсной электронной бомбардировке. Спектры из различных секций блока измеряли с использованием метода определения по времени пролета для траектории полета в 50 м. Измеряли также спектральные показатели, такие как соотношение скорости деления урана-238/урана-235, урана-233/урана-235, урана-234/урана-235, нептуния-237/урана-235, плутония-239/урана-235. Кроме того, были получены измерения интенсивностей захвата урана-238 в различных частях блока. Описываются методы, использованные для получения этих физических параметров реакторов. Экспериментальные результаты, такие, как спектры и спектральные показатели также, сравниваются с результатами, полученными на основе теоретических соображений, с использованием анализа теории многогруппового переноса.

Метод с импульсными нейтронами применяется также для измерения таких параметров как β/ℓ, где β является фракцией эффективных запаздывающих нейтронов, а ℓ – периодом жизни, нейтронных значений и коэффициента эффективности. В заключение обсуждается применение источника импульсных нейтронов для измерения некоторых из этих параметров на активных зонах реакторов, сконструированных на базе установок ZPR-VIU, например Аргонская критическая установка на быстрых нейтронах.

OBTENCION DE PARAMETROS, EN LA FISICA DE LOS REACTORES RAPIDOS CON AYUDA DE UNA FUENTE PULSADA. Uno de los parámetros más importantes en los estudios de física de los reactores rápidos lo constituye el espectro neutrónico de un cuerpo de reactor de composición determinada. Para estudiar los espectros de los reactores rápidos, se han empleado diversos medios, como por ejemplo contadores de protones de retroceso y emulsiones nucleares. Con el perfeccionamiento de fuentes de impulsos neutrónicos de elevada intensidad y corta duración, la determinación de esos espectros puede realizarse por la técnica del tiempo de vuelo.

A fin de evaluar, empleando las técnicas del tiempo de vuelo, la posibilidad de determinar los espectros de los neutrones rápidos emitidos por un cuerpo de reactor, se ha realizado un experimento consistente en medir el espectro de equilibrio en un bloque de uranio empobrecido de grandes dimensiones, empleando el acelerador lineal (Linac) de la General Atomic. Para ello se empleó un bloque de 10 t de uranio empobrecido al que se le dio la forma de un cubo de 81 cm de arista. Este bloque fue sometido a la acción de impulsos producidos por bombardeo electrónico de un blanco de uranio situado en su interior. Se midieron los espectros correspondientes a diversas secciones del bloque, empleando técnicas del tiempo de vuelo, para una trayectoria de 50 m. También se midieron los índices espectrales, tales como las razones de los índices de fisión $^{238}U/^{235}U$, $^{233}U/^{235}U$, $^{234}U/^{235}U$, $^{237}Np/^{235}U$ y $^{239}Pu/^{235}U$. Además, se obtuvieron en diversas partes del bloque los valores del índice de captura en el ^{238}U. Los autores describen las técnicas empleadas para evaluar estos parámetros. También comparan los resultados conseguidos experimentalmente, tales como los espectros y los índices espectrales, con los obtenidos empleando el método de análisis basado en la teoría de transporte de varios grupos.

La técnica de los neutrones pulsados puede emplearse también en la medición de diversos parámetros, a saber: β/ℓ (siendo β la fracción efectiva y ℓ la vida media de los neutrones retardados), el factor de importancia neutrónica y el coeficiente k_{ef}. Por último, los autores examinan la proyectada aplicación de una

fuente de neutrones pulsados a la medición de algunos de estos parámetros en cuerpos de reactores rápidos montados en la instalación crítica de neutrones rápidos de Argonne (ZPR-VI).

INTRODUCTION

All important parameters that characterize a fast-reactor system are calculated by means of the neutron spectrum. Experimental determination of the neutron spectrum is important because it provides a means of verifying calculational techniques and averaged cross-section sets. With the gradual shift in emphasis in fast-reactor research towards large (approximately 3000-5000-litre core) dilute fast reactors with softer spectra than those currently in operation, there is greater interest in the intermediate energy neutron distribution from a few hundred electron volts to a few hundred kiloelectron volts. Many different methods have been used in an attempt to determine the core spectra using such techniques as cloud chambers [1], nuclear emulsions [2], proton recoil counters [3], helium-3 detectors, and lithium detectors with solid-state devices [4]. In thermal reactors, the Maxwellian distribution has been measured with time-of-flight techniques by means of a pulsing source or chopper [5-7]. With fast reactors whose spectra range from a few hundred electron volts upward, it becomes difficult to measure the spectra by time-of-flight techniques using a chopper to interrupt the neutron beam, because of the lack of materials that can act as a good shutter, and the difficulty of designing and constructing a fast acting shutter in order to obtain good resolution.

With the availability of high-ingensity short-duration pulsed neutron sources, it becomes possible to pulse a fast system and measure the emerging burst of neutrons by time-of-flight techniques. To determine the feasibility of measuring fast spectra with time-of-flight techniques and other reactor physics parameters with a pulsed source, a large depleted uranium assembly and auxiliary equipment was assembled at the General Atomic LINAC facilities by Argonne National Laboratory and General Atomic personnel for pulsed experiments on U^{238}. This paper presents the results of time-of-flight spectra, spectral indices, fission rates and U^{238} capture measurements from various parts of the depleted uranium assembly.

EXPERIMENTAL ARRANGEMENT

A large assembly of approximately 10 tonnes of depleted uranium (0.21% U^{235}) was assembled, as shown in Fig. 1, using 2 in × 2 in × 2 in , 2 in × 2 in × 1 in and 2 in × 2 in × 5 in depleted uranium bricks. Approximately 1700 bricks of depleted uranium were stacked in 16 layers on a movable pedestal as shown in Fig. 1. The uranium was stacked on a movable table so that one face of the 10-tonne assembly could be brought up to the electron beam tube of the LINAC.

The bricks in the ninth layer were arranged, as shown in Fig. 2, so that transverse channels 5-cm high by 5-cm wide could be made in five different positions across the layer. The bricks of uranium were so arranged that it was possible to remove 5 cm × 5 cm columns of depleted uranium for the

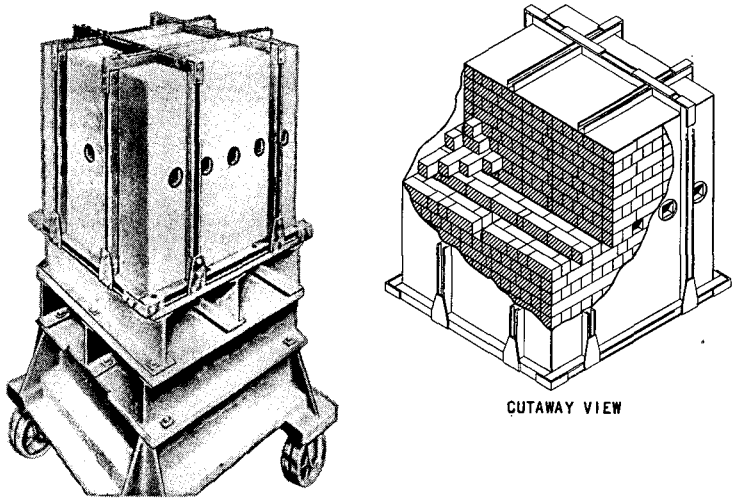


Fig. 1

Uranium block on pedestal

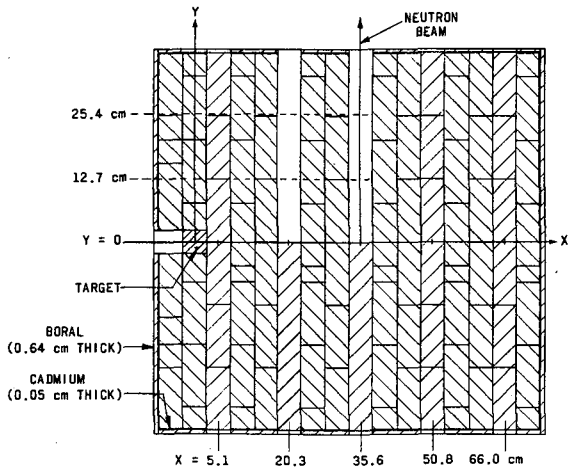


Fig. 2

Cross-section of 9th layer

insertion of counters or foils, or for the emergence of a neutron beam. The five transverse traverse channels were located at distances of 5.1, 20.3, 35.6, 50.8, and 66.0 cm (2, 8, 14, 20, 26 in) from the target.

The overall dimensions of the block were 81-cm long, 76-cm wide, and 81-cm high (32 in × 30 in × 32 in). The entire uranium assembly was covered

with a 1-mm-thick cadmium sheet and a 7-mm-thick boron-aluminium (Boral) sheet to minimize the effect of room-scattered neutrons.

A beam tube from the LINAC was arranged so that the 30-MeV electron beam would impinge upon a nickel-coated 2 in × 2 in × 2 in brick of depleted uranium whose centre is located about 8 cm (3 in) from the outside face along the centre line in the ninth layer of the large block of uranium. The centre of the target was located approximately 43.2 cm from the table top. The surface of the target block was coated with nickel to minimize oxidation of the uranium upon heating. The target was air-cooled with a small stream of air and its temperature was monitored with a thermocouple. During the experiment the beam current of the LINAC was usually adjusted so that the surface of the target was no greater than about 500° C.

The 30-MeV electron beam from the LINAC incident on the target is converted into bremsstrahlung which, in turn, produced photo-fission neutrons in the U^{238} target and surrounding material. The arrangement of the experiment with respect to the beam from the LINAC and the flight path is shown in Fig. 3.

Experimental measurements of spectra or spectral indices were made from one of the five transverse channels, shown in Fig. 1. To pin-point the

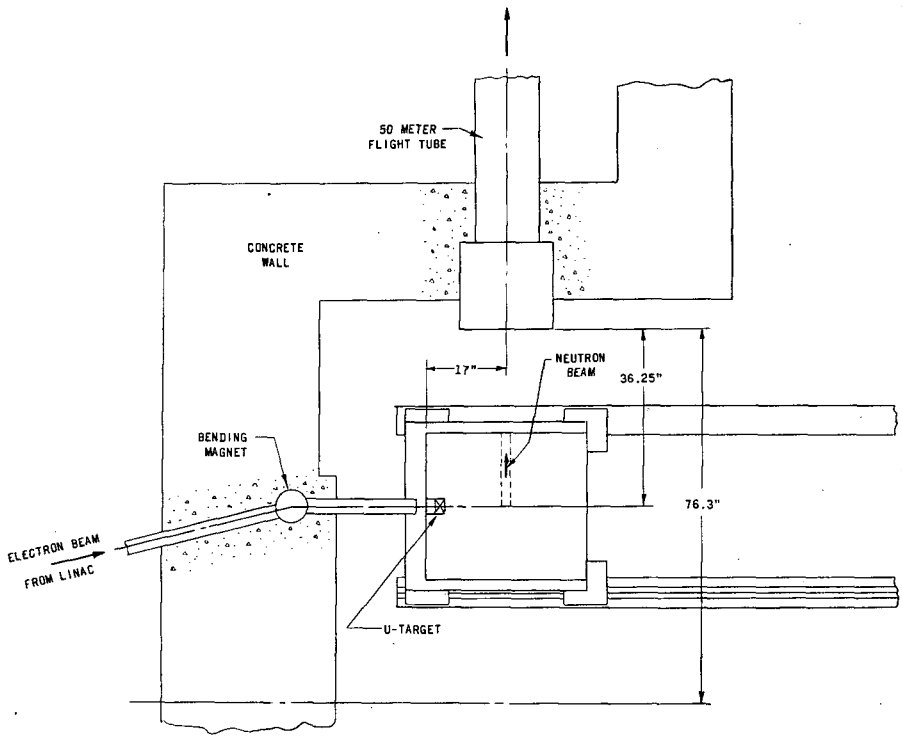


Fig. 3

Experimental arrangement of neutron flight path

positions where an experiment was conducted, a rectangular co-ordinate system is used to describe the horizontal plane locations in the ninth layer. The centre of the target block is considered to be (0, 0), the centre of the (x, y) co-ordinate system. All the measurements reported in this paper were made in the ninth layer, whose centre is 43.2 cm from the bottom of the block. All the channels, except the one where measurements were being conducted, were normally filled with depleted uranium bricks to avoid perturbations of the flux distribution. Depleted uranium bricks were used to fill the channel to the location where measurements were being conducted.

With time-of-flight measurements, the channel from which the beam was being extracted was always filled at least to the y = 0 plane. This channel was then aligned with the 50-m flight path, as shown in Fig. 3. A detailed description of the LINAC characteristics, its facilities, and 50-m flight path may be found in Reference [5].

NEUTRON DETECTORS

Three different types of neutron detectors were used for the fast spectra time-of-flight measurements: a cluster of BF_3 counters, liquid scintillator, and a B_4C block in combination with the liquid scintillator. The BF_3 counter cluster consisted of thirty-two 5-cm-(2-in)-diam. thin-walled 0.08 cm (0.30 in) $B^{10}F_3$ filled (1 atm pressure) gas counters with an active length of about 40 cm [9]. The cluster was approximately 23 cm thick, 36-cm wide, and 61-cm high (9 in × 14 in × 24 in). For measuring neutrons with energies greater than about 200 keV, a 13-cm (5-in)-diam. liquid organic scintillator [10] was used. This detector was based on observing scintillations caused by the proton recoils of scattered neutrons. The third type of detector used for time-of-flight measurements was a boron carbide and water mixture [11] and the 5-in. liquid scintillator. An aluminium box of approximately 51 cm × 25 cm × 10 cm (20 in × 10 in × 4 in) was filled with about 14 kg (30 lb) of commercial-grade boron carbide and 6 kg (14 lb) of water. The B_4C detector was placed in the neutron beam so that the 10-cm thickness dimension was in line with the flight path. The liquid scintillator was then placed directly behind the box containing the boron-carbide-water mixture in line with the flight path to observe the 0.48-MeV gamma rays emitted from the (n, α) reaction. In addition to these detectors for time-of-flight neutrons, a conventional BF_3 gas-filled counter was placed in the same room where the uranium assembly was located to monitor the overall neutron flux.

SPECTRA MEASUREMENTS

Neutron spectra measurements were attempted at the following locations in the assembly: (20.3, 0), (20.3, 12.7), (20.3, 25.4), (35.6, 0) and (50.8, 0). Measurements of the neutron spectrum at (20.3, 0) were made with the three types of detectors at the 50-m flight path station. At the other locations the principal detector was the B_4C detector. A large fraction of the 50-m neutron flight path was evacuated to a pressure of about 50 μm to minimize attenuation

of the beam by air scattering. The details of the collimator and shielding around the cell where the uranium assembly was located may be found in a paper by BEYSTER et al. [8]. The detector pulses were analysed using a TMC-CN1024 Analyser with a TMC-211 or TMC-201 logic plug-in unit for the time-of-flight measurements. The channel width used in the analyser depended on the type of detector used. With the B_4C detector, a channel width of 125 ns was used while a 500-ns width was used for the BF_3 counters and 31.25 ns for the 5-in scintillator. The data stored in the time analyser was punched out onto paper tape and was processed by using ECTOPLASM, a computer code developed by NALIBOFF [12] for reducing time-of-flight spectral information on the IBM-7044 and subsequently adapted for the CDC-3600 computer. This code corrects the data for background, either directly measured or calculated, time analyser deadtime losses, mean neutron emission time in the assembly, and source strength variations from run to run based on a monitor counting rate. The programme converts the time-dependent neutron distribution into an energy-dependent neutron spectrum. In converting from the time to energy dependence, a correction is introduced for the relative energy sensitivity of the detector. A correction for the neutron losses due to materials in the neutron beam flight path may also be introduced. The code also groups data in neighbouring energy channels to produce a neutron spectrum which has an approximately constant energy resolution at all energies. In these measurements, since there was some uncertainty on how the background should be measured, the background correction was calculated by taking the average of the last 100 analyser channels.

Spectra obtained from the time-of-flight measurements of neutrons originating from the (20.3, 0) location in the uranium assembly are shown in Fig. 4. Curves A and B are curves obtained from the same run. Curve A shows the effect of approximately 0.54 cm (0.214 in) of aluminium in the flight path. The aluminium resonances at 35.04 ± 0.09, 89 ± 1 keV and about 150 keV are clearly observed in Curve A which has not been corrected for the aluminium in the flight path. When the neutron distribution is corrected for the aluminium resonances by using the total cross-sections tabulated by HOWERTON [13], the resulting neutron distribution is given by Curve B of Fig. 4. Curve C shows the data obtained with the BF_3 counters uncorrected for material in the flight path. Since the BF_3 detector efficiency drops off rapidly at high energies, the region above 100 keV shows the effects of poor statistics. In addition, the region between 10 and 100 keV shows the effects of the aluminium resonances and possibly copper resonances. The copper resonances would be due to the copper in the brass of the BF_3 counter walls. Curves D and E were obtained using transport theory analysis described later.

A measurement of the spectrum at (20.3, 0) with the 5-in organic scintillator resulted in spectral information from about 300 keV to 10 MeV. The shape of the curve in the 300 keV to 1 MeV region is almost identical with the shape of the curve obtained with the B_4C detector in that location.

Measurement of the spectrum at (35.6, 0) is shown in Fig. 5. Only the data from the B_4C detector are shown compared with a calculated curve. The experimental data are shown uncorrected for the aluminium in the flight path.

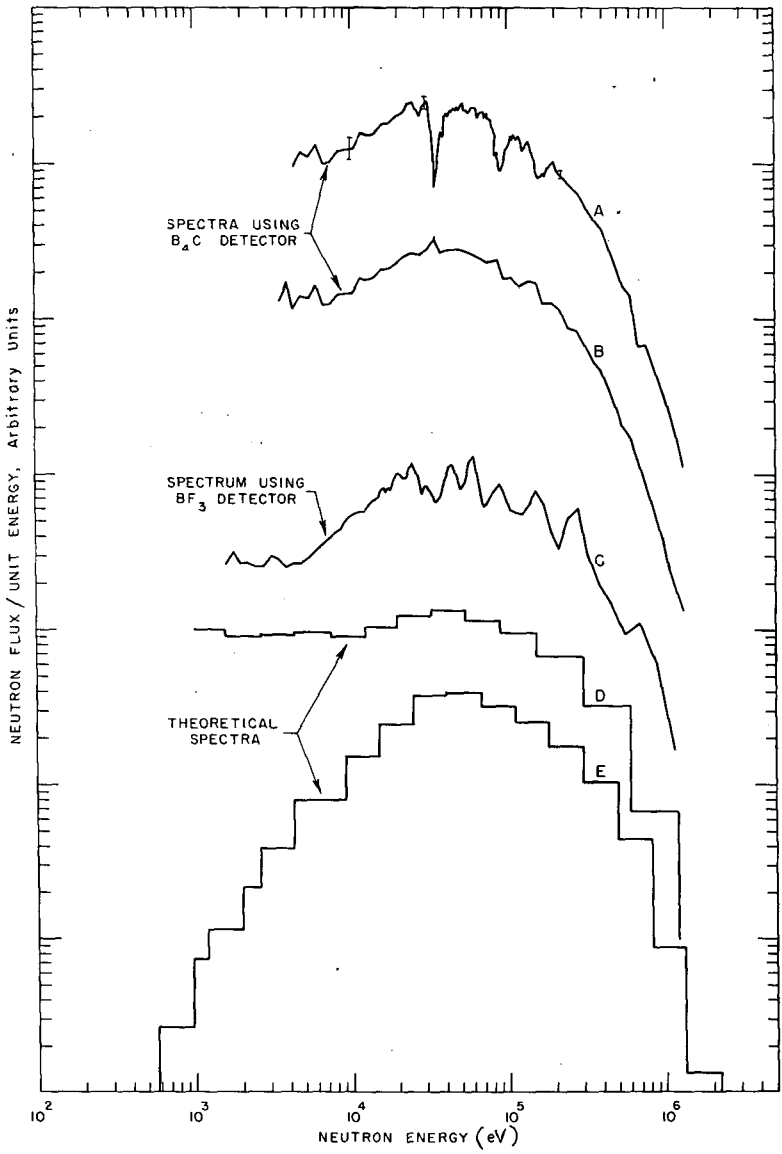


Fig. 4

Spectra at (20.3, 0)

Spectra measurements attempted at the (50.8, 0) position were not successful because of the limitations on neutron intensity due to the lack of a properly cooled target.

It should be noted that the neutrons which were observed in the time-of-flight measurements emerged either from the y = 0 plane or a plane pa-

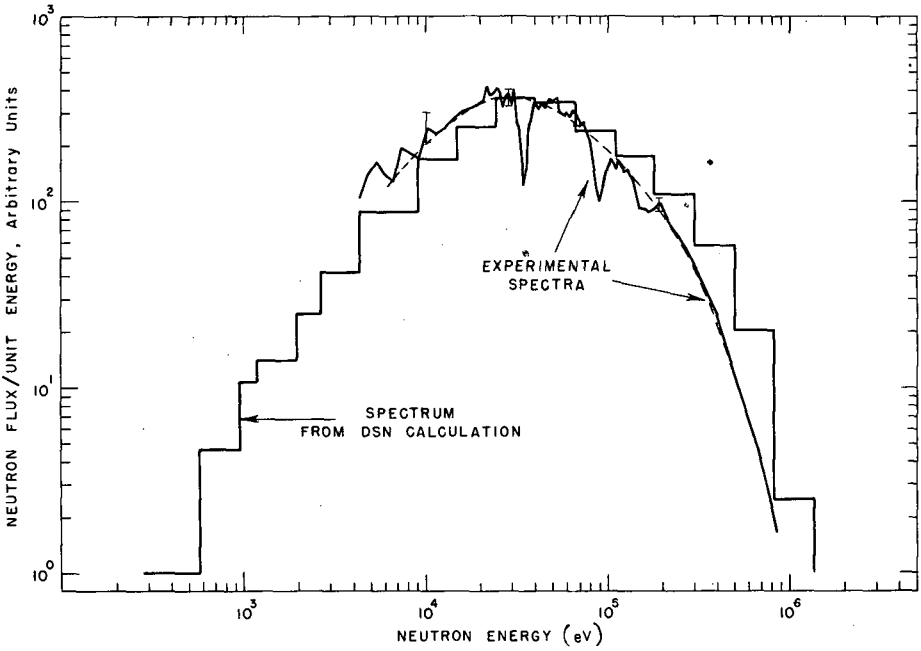


Fig. 5

Spectrum at (35.6, 0)

rallel to the y = 0 plane. For the measurements from the y = 0 plane, the neutrons emerged essentially at a 90° angle from the incident electron beam. To see whether an angular dependence of the spectra exists, measurements were obtained from (20.3, 0), (20.3, 12.7) and (20.3, 25.4) locations since the neutrons would be from positions at different angles with respect to the incident electron beam.

Experimental spectra obtained at (20.3, 0), (20.3, 12.7) and (20.3, 25.4) are compared in Fig. 6. The data shown in this figure, however, do not show strong angular dependence effects. A summary of the LINAC conditions, analyser channel widths, and time to obtain the aforementioned data are given in Table I.

COMPARISON WITH THEORY

One purpose of the uranium spectrum measurements was to provide a means of evaluating methods used to calculate fast and intermediate neutron spectra. Although the geometry is not one-dimensional, and a two- or three-dimensional neutron transport calculation would be more rigorously applicable, a one-dimensional calculation is a reasonable approximation for comparison with the measured spectra near the source. The measured

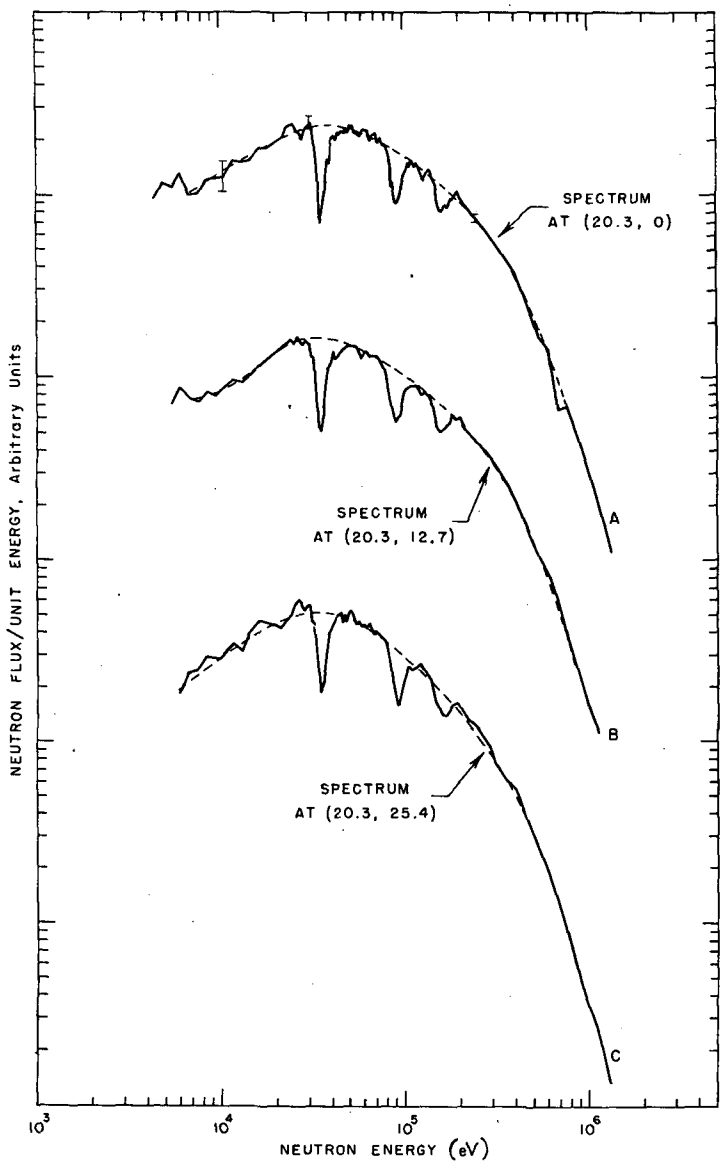


Fig. 6

Experimental spectra at different locations

neutron spectra near the source and far from the boundaries should be qualitatively the same as those of a point source in large spheres - a one-dimensional problem. The first efforts to calculate the spectra obtained in various parts of the assembly were with one-dimensional, multigroup trans-

TABLE I

TIME-OF-FLIGHT PARAMETERS

Run No.	Curve	Position (x,y)	Run Time, min	Detector	LINAC		Analyzer	
					Flt. Path (m)	Burst Width (nsec)	Channel Width (nsec)	Total Counts
6	Fig. 5	(35.6,0)	142	B_4C + 5" Scintillator	50	100	125	--
10	Curve A & B, Fig. 4	(20.3,0)	59	B_4C + 5" Scintillator	50	20	125	300,400
11		(20.3,0)	63	5" Scintillator	50	20	31-1/4	302,400
13	Curve C,Fig. 4	(20.3,0)	157	BF_3 Counters	50	100	500	293,000
15	Curve B,Fig. 6	(20.3,12.7)	44	B_4C + 5" Scintillator	50	50	125	305,000
16	Curve C,Fig. 6	(20.3,25.4)	33	B_4C + 5" Scintillator	50	100	125	145,000

port-theory computer codes. Two codes, the GAPLSN [14] and DSN (ANL - RE 209) [15], were used with GAM II [16] to obtain the cross-section set for the former code and cross-section set 199 [17], a modified YOM [18] set, in the latter case to calculate the spectra in the depleted uranium assembly.

The function of GAPLSN was to calculate the neutron distribution in an assembly of specified geometry and cross-sections. This is a distribution in angle, energy, and space.

Besides cross-sections and geometry, it was necessary to specify the neutron source spectrum and spatial distribution. The source was confined to a small volume near the surface struck by the electron beam, so it is sufficient for our calculation to represent the source as a small, central, volumetric neutron source. The angular distribution of the neutrons from the experimental source appears to be isotropic [19]. The neutron energy distribution from small uranium spheres has been measured above 0.5 MeV and from this it was inferred that the photo-neutron spectrum is not a simple fission neutron spectrum.

The geometry of the experiment was approximated in the calculation as a point source in an uranium metal sphere, 61 cm (2 ft) in diameter. The meshes chosen were S-8, P-1, 17 energy groups, and 150 space points. The photo-neutron spectrum of U^{238} has not been measured, so that of a lead source was used. For computational purposes, this consisted of a fission neutron spectrum shape from 0.5 to 5.5 MeV, the fission spectra multiplied by a factor of two above 5.5 MeV (to account approximately for direct interaction neutrons), and a $1/\sqrt{E}$ variation below 0.5 MeV.

The results of the GAPLSN calculation are shown by Curve D in Fig. 4. Since the experimental spectra (Curves A, B, and C) were obtained at an angle of 90 degrees to the source, the calculated curve is obtained by averaging angular groups 5 and 6.

The DSN calculation using a modified 18-group YOM cross-section set was done assuming a fission spectrum source, isotropic scattering, and an S-8 approximation. In this calculation a 3-region problem was chosen to represent the geometry of the experiment. The first region of 0.83-cm radius was the origin of the fission source. The region from 0.83 cm to 89 cm represented the uranium assembly in spherical geometry and the third region the void external to the assembly. The calculated results which represent the total flux at (20.3, 0) are shown in Curve E in Fig. 4. There is reasonable agreement between shapes of the theoretical curves (D and E) above about 30 keV and a wide discrepancy below this value. The difference in the two theoretical curves is due to differences in such factors as resonance self-shielding, assumed shape of the fission neutron spectrum, shape of the source neutron distribution, and the number of down-scattering groups.

Comparing the experimental (Curve B) and the theoretical spectra (Curves D and E), there appears to be qualitative agreement in the shapes of spectra above about 30 keV. The experimental curve lies between the two theoretical curves below 30 keV. In addition, if one compares the shapes of the experimental and theoretical curves closely the peak of the experimental spectrum appears to be shifted slightly towards the lower energy region.

Another comparison between experimental data and theoretical calculations is shown in Fig. 5 for the spectrum at (35.6, 0). The theoretical

curve was that obtained using the DSN code. If one compares the experimental and theoretical curves in Figs. 4 and 5, it is found that there is qualitative agreement in the shapes of the curves above about 30 keV. The theoretical spectrum of Fig. 5 seems to indicate a slightly harder spectrum than that obtained from experimental measurements. There are large discrepancies between experiment and theory in the lower energy regions; this indicates that further effort, both experimentally and theoretically, is needed.

FISSION DETECTORS

To obtain spectral indices to compare with those obtained from the time-of-flight spectra data or theoretical spectrum calculations, two types of special fission detectors were used: small gas-flow-type fission chambers and solid-state devices.

The small absolute gas-flow-type fission chambers used to measure effective fission cross-section ratios were of parallel-plate design similar to those described by KIRN [20]. The body of the chambers (5-cm diam., 1.9-cm long) was made with thin aluminium (0.05-cm-thick) walls to minimize spectral distortion caused by inelastic scattering. Each counter contained about 400 μg of fissionable material electroplated to a density of about 100 μg per cm^2 on a 0.025-cm-thick stainless-steel plate, which also formed the bottom of the fission chamber. The collecting electrode was held by a Kovar seal at a distance of 0.7 cm from the fissionable layer. An RG-71 pulse cable leading to the preamplifier outside the uranium assembly was connected to the chamber by a 10-cm-long aluminium extension tube in order to keep moderating material away from its sensitive area. The fission chambers were operated as gas-flow counters, with a 90% argon and 10% methane mixture, and a collecting voltage of about 300 V.

A conventional preamplifier and fast pulse amplifier (Argonne Type A-156) were used with the counters. A typical pulse-height distribution obtained with one of these counters in a fast spectrum is shown in Fig. 7. Fission and alpha pulses appear to be well separated so that less than 1% of the total fission pulses is lost in the alpha background when the discriminator is set slightly above the alpha edge. The rise time of the amplifier (~80 ns) was short enough to minimize pile-up of alpha pulses even when Pu^{239} and Pu^{240} samples were used.

The solid-state counters which were used to measure the effective fission ratios were constructed using surface barrier detectors. The counters were 1.1-cm in diameter, 1.2-cm long, with a wall thickness of 0.05 cm. Each counter contained a 0.012-cm-thick stainless-steel disk, located 0.06 cm from the sensitive face of the detector, on which was electroplated a coating of fissionable material. The thickness of the coatings ranged from 50 to 100 μg/cm^2. The counters were operated at a bias voltage of 50 V and were used with a low-noise, charge-sensitive preamplifier.

Plates coated with U^{233}, U^{234}, U^{235}, U^{238}, Np^{237}, Pu^{239}, and Pu^{240} were available for fission rate measurements. Since the detectors could take only one plate at a time, it was necessary to interchange plates in order to obtain fission rates for the different fissile isotopes.

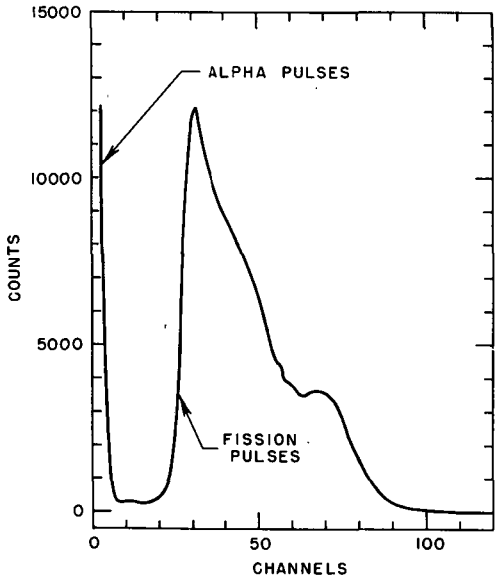


Fig. 7

Pulse-height distribution for fission chamber

Either the fission chambers or the solid-state detectors were placed inside one of the transverse channels, shown in Fig. 1, extending into the interior of the uranium assembly. They were supported by the thin 5-cm^2 aluminium framework which was inserted into the channel so that the sensitive area of the counter was facing the surface of the depleted uranium column from the opposite half of the channel, either at the (20.3, 0) or (36.6, 0) position.

FISSION RATE MEASUREMENTS

Two types of fission rate measurements using the solid-state and gas-flow detectors were of interest in the assembly: the observation of the die-away of the neutron spectrum, and the time-averaged fission rate.

During the initial testing of the fission chambers in the accelerator beam, an additional background was observed in the gas-flow chambers which appeared about 10 μs after each accelerator burst. These background pulses were caused partially by the intense gamma radiation produced in the target and partially by pick-up of the radio frequency voltage of the accelerator through the preamplifier input and power supply. It was found that the amplitude of these background pulses was proportional to the average beam current; thus, by running the accelerator at a reduced beam intensity, it was found possible to keep these pulses below the threshold of the discriminator so that fission-rate measurements could be made. Generally, when fission-rate measurements were made with the gas-flow counter, a beam current of the

order of 10% of that used for the time-of-flight measurements was used. It was found that this background was rather high at the (20.3, 0) position, so that it was possible to make die-away measurements only at the (35.6, 0) position with the gas-flow counters.

The solid-state detectors, which had a better shielded preamplifier, showed a much lower amplitude for the background signal. Because of the long rise time (> 1 μs) on the low-noise preamplifier (Tennelec Model 100-A) used with the solid-state detectors, only the time-averaged fission rates were measured at the (20.3, 0) position. Three types of corrections were introduced to the counting rate in order to obtain correct fission ratios: (1) corrections for counting losses, (2) normalization for variations of beam intensity, and (3) corrections for the fission contributions of impurity isotopes. Corrections for counting losses were necessary even at relatively low average counting rates because of the pulsed operation of the neutron source and the short decay time of the neutron spectrum. The experimentally determined time-averaged fission ratios at (20.3, 0) are given in Table II. For comparison, fission ratios obtained from the DSN calculation are also given in the same table.

Two types of fission-rate measurements were made at the (35.6, 0) position with gas-flow fission chambers: a time-averaged fission-rate determination using a conventional 1-Mc scaler and fast amplifier, and a time-dependent fission rate with the TMC 1024 channel time analyser and the TMC 201 logic plug-in unit.

The time-dependent fission rates after the injection of the neutron burst were measured for the following isotopes: U^{233}, U^{235}, Np^{237}, Pu^{239}, and Pu^{240}. Typical die-away or burst decay curves are shown in Figs. 8 and 9 for U^{235} and Pu^{239}, respectively. A channel width of 62.5 μs was used with the analyser to obtain these decay curves.

TABLE II

TIME-AVERAGED FISSION RATIOS AT (20.3, 0)

	Experimental	Calculated (DSN-Spectra)
U^{233}/U^{235}	1.678 ± 0.020	1.569
U^{234}/U^{235}	0.133 ± 0.003	0.171
U^{238}/U^{235}	0.0091 ± 0.0003	0.00643
Np^{237}/U^{235}	0.182 ± 0.003	0.148
Pu^{239}/U^{235}	———	1.114
Pu^{240}/U^{235}	———	0.157

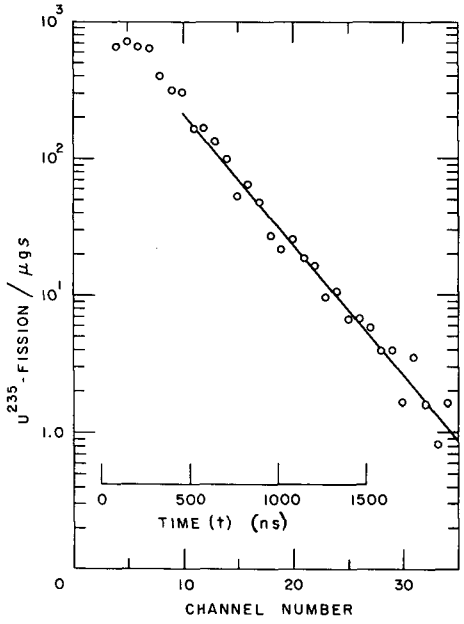


Fig. 8

Time dependence of U^{235} fission rate at (35.6, 0)

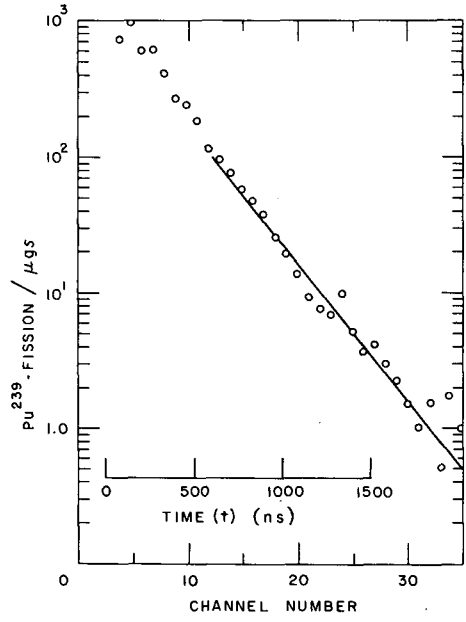


Fig. 9

Time dependence of Pu^{239} fission rate at (35.6, 0)

It is expected that higher spatial and energy modes of the flux distribution will prevail in the first part of the decay curves; however, the data for the U^{233} and U^{235} isotopes indicate that the data can be approximated by a single exponential function $e^{-\alpha t}$ over most of the curve. An exponential fit for times greater than 500 ns yields values of $1/\alpha$ for five different isotopes at (35.6, 0) as follows: U^{233}, 261 ± 15 ns; U^{235}, 284 ± 15 ns; Np^{237}, 274 ± 30 ns; Pu^{239}, 263 ± 15 ns; and Pu^{240}, 274 ± 25 ns. It was not possible to obtain a decay curve with the U^{238} detector because of limited intensities. These results indicate that after a transition time of about 500 ns, a time-asymptotic spectrum is established which decays exponentially.

The variation of the neutron spectrum as a function of time after the injection of the neutron burst was studied by plotting the fission ratios, σ_f^z/σ_f^{25}, as a function of time. The curves shown in Fig. 10 show the dependence of the fission ratios with time at the (35.6, 0) location. With the exception of those of U^{233}/U^{235} and Pu^{239}/U^{235} which are not too sensitive to spectrum changes, the other fission ratios indicate a decreasing value or a softening of the neutron spectrum with time. After about 500 ns, the fission ratios within experimental error arrive at a constant value which is characteristic of the establishment of a time-asymptotic spectrum. The asymptotic values of σ_f^z/σ_f^{25} which have been obtained by adding all the channels with $t > 500$ ns are given in Table III. The time-averaged fission ratios obtained using a conventional scaler are also listed in Table III. The limits of error in Table III are based on statistical counting uncertainties only. They do not

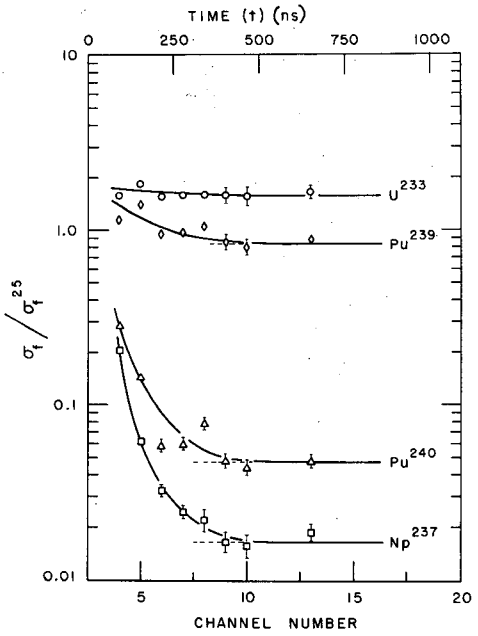


Fig. 10

Fission ratios at (35.6, 0)

TABLE III

FISSION RATIOS AT (35.6, 0)

	Experimental (Time Averaged)	Calculated (DSN-Spectra)	Experimental-Asymptotic
U^{233}/U^{235}	1.599 ± 0.024	1.548	1.59
U^{234}/U^{235}	0.0909 ± 0.0015	0.107	----
U^{238}/U^{235}	0.0031 ± 0.0004	0.00252	----
Np^{237}/U^{235}	0.0836 ± 0.0018	0.0877	0.0246
Pu^{239}/U^{235}	1.012 ± 0.016	1.060	0.819
Pu^{240}/U^{235}	0.1011 ± 0.002	0.0925	0.0463

include uncertainties such as that in the quantity of material coated on the plates. It is expected that uncertainties due to the coating material are less than 1% for the U^{235} and U^{238} detectors, and of the order of 3% for U^{233}, U^{234}, Pu^{239}, and Pu^{240}. For comparison purposes fission ratios obtained from the DSN calculation are also given in Tables II and III for the (20.3, 0) and (35.6, 0) locations.

FOIL ACTIVATION MEASUREMENTS

The U^{235} and U^{238} fission and U^{238} capture distributions were measured in the assembly by irradiating 0.013-cm-thick foils of 93% enriched uranium, weighing about 0.3 g each and (0.2 wt.% U^{235}) depleted uranium foils of about 1 g each. These foils were wrapped in aluminium foil and placed at various positions in the assembly for irradiation. The irradiation was carried out at the same time that time-of-flight spectra measurements were in progress from the (20.3, 0) position. The foils were analysed for Mo^{99} to determine fission rates and Np^{239} was separated radiochemically and analysed by techniques of References [21] and [22]. The variation of the beam intensity during the run was monitored with the BF_3 counter and corrections to determine the fission and capture rates were based on the monitor counting rates.

The U^{235} fission distribution in the assembly as measured by this activation technique is shown in Fig. 11. The axial (along the x axis) fission distributions appear to approach an exponential $e^{-\alpha t}$ decay. The U^{235} and U^{238} fission rates and U^{238} capture rates are tabulated in Table IV. The time-averaged U^{238}/U^{235} fission ratio using the activation techniques was only obtainable at x = 20.3 and 35.6 because of limited neutron intensity. The U^{238} capture to the U^{235} fission ratios and the U^{238}/U^{235} fission ratios are given in Table V. There are considerable uncertainties in these U^{238}/U^{235} fission

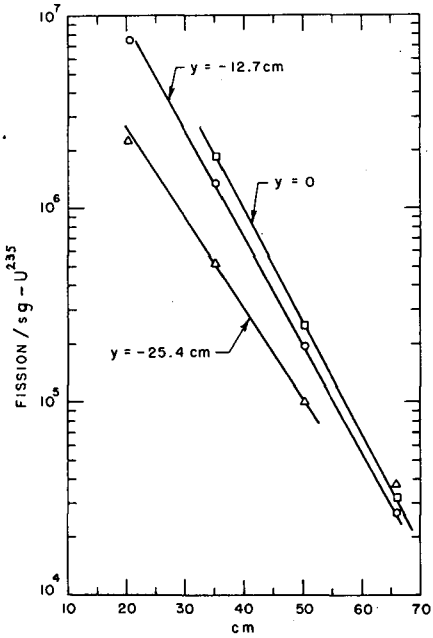


Fig. 11

U^{235} fission distributions

ratios because of the low Mo^{99} activity in the U^{238} foils. Theoretically determined U^{238} capture/U^{235} fission calculated from the DSN calculations are also given in the table.

Since an asymptotic spectrum is not established for points less than about 50 cm from the source [23], it is possible to obtain only a rough estimate of the diffusion length in depleted uranium from the decay curves given in Fig. 11. These curves give a value of 7.5 ± 0.4 cm for the axial decay length. Assuming a value of 2.5 cm for the radial extrapolation length and the values of 81 cm and 76 cm for the height and width, a value of L = 8.2 cm for the diffusion length is obtained. This is considerably smaller than the value of 9.17 ± 0.18 obtained by CHEZEM [23] so that it would appear definite that an asymptotic spectrum has not been established in this region.

CONCLUSIONS

These experiments have shown that a LINAC provides a high-intensity short-duration neutron burst for neutron spectra measurements from a fast assembly using time-of-flight techniques. Spectra from a fast-reactor assembly may be measured with good resolution from a few kiloelectron volts to about 10 MeV. The B_4C detector has been shown useful up to about 2 MeV. Its basic limitation is due to the uncertainty in its response function above

TABLE IV

U^{238} CAPTURE AND U^{235} FISSION DISTRIBUTION*

Position	Captures/sec/g-U^{238}	Fissions/sec/ g-U^{235}	Fissions/sec/ g-U^{238}
(20.3,0)	----	----	----
(35.6,0)	2.62×10^5	2.02×10^6	1.14×10^4
(50.8,0)	3.75×10^4	2.69×10^5	----
(66,0)	4.58×10^3	3.39×10^4	----
(20.3,-12.7)	1.06×10^6	7.97×10^6	9.17×10^4
(35.6,-12.7)	1.92×10^5	1.43×10^6	8.43×10^3
(50.8,-12.7)	3.02×10^4	2.08×10^5	----
(66,-12.7)	4.08×10^3	2.85×10^4	----
(20.3,-25.4)	3.03×10^5	2.44×10^6	1.38×10^4
(35.6,-25.4)	8.28×10^4	5.59×10^5	6.16×10^3
(50.8,-25.4)	1.51×10^4	1.06×10^5	----
(66,-25.4)	2.58×10^3	3.97×10^4	----

LINAC (Run No. 13)

Rep. rate 360/sec

Burst width 100 nsec

BF_3 monitor 2.3×10^5 c/m

* Capture and Fission rates normalized to source intensity during Run No. 13 in the time-of-flight spectra measurements.

2 MeV. For higher energies the liquid scintillator would be the more appropriate detector to be used. The measured gross neutron spectrum is in qualitative agreement above 30 keV with the theoretically calculated spectrum. Below 30 keV there are large discrepancies between experiment and theory which require further effort for clarification. The time-of-flight technique with a LINAC could produce high-energy resolution spectra to obtain the fine structure in the spectrum. This might be a means to check the methods for obtaining averaged cross-section sets useful in reactor analysis. The experiments also gave a survey of the time-space dependence of fission rates and spectral indices, although statistical accuracy was, in some cases, limited by low neutron intensities.

TABLE V

U^{238} CAPTURE AND U^{235} FISSION RATIO DISTRIBUTIONS

Position (x,y)	$\sigma_c^{U^{238}}/\sigma_f^{U^{235}}$ Experimental	Calculated	$\sigma_f^{U^{238}}/\sigma_f^{U^{235}}$
(20.3,0)	———	0.160	———
(35.6,0)	0.131	0.141	0.0038
(50.8,0)	0.141	0.143	———
(66,0)	0.137	0.146	———
(20.3,-12.7)	0.135		0.0097
(35.6,-12.7)	0.136		0.0040
(50.8,-12.7)	0.146		———
(66,-12.7)	0.145		———
(20.3,-25.4)	0.127		0.0038
(35.6,-25.4)	0.150		0.0093
(50.8,-25.4)	0.143		———
(66,-25.4)	0.066		———

The neutron intensity with the air-cooled U^{238} target provided a sufficient intensity to measure the U^{235} fission and U^{238} capture rates throughout the assembly by radiochemical separation techniques. Measurements of fission ratios with solid-state detectors and gas-flow-type absolute counters was possible at the x = 20.3 and 35.6 positions. The gamma sensitivity of the gas-flow counters and radio-frequency noise pick-up made it necessary to operate the LINAC at reduced intensities, so it was not possible to obtain spectral indices measurements at distances greater than about 35 cm from the target where an asymptotic spectrum might be expected.

Fission rates were measured at (35.6, 0) as a function of the time after the injection of the neutron burst. The die-away curves for U^{233} and U^{235} can be approximated by a single exponential with a decay time of about 270 ns. The variation of the fission ratios with time indicates a softening of the neutron spectrum during a transition time of about 500 ns, after which an exponentially decaying asymptotic spectrum is established.

For future experiments it is desirable to improve the statistical accuracy by increasing neutron intensity. The development of a liquid metal or water-cooled target which could be embedded in an assembly would give a considerable improvement in the neutron intensity without significantly increasing room background. Improved shielded electronics would also help by reducing the radio-frequency noise pick-up. Since solid-state detectors are relatively insensitive to gamma rays, larger detectors would also aid in increasing the counting rate so that spectral indices could be made throughout an assembly. A thorough investigation of the time-space dependence of the fission rates in the assembly plus the time-of-flight spectra from different locations would give additional information to check calculation techniques and cross-sections for improvement of our understanding of fast-reactor physics.

FUTURE PULSED SOURCE EXPERIMENTS WITH CRITICALS

In addition to the measurement of spectra and spectral indices, the pulsed source technique is useful for the measurement of the decay constant α close to critical in a reactor. The measurement of α close to critical provides a value of the ratio of the effective delayed-neutron fraction and the neutron lifetime. This ratio has been measured in fast criticals conventionally using the ROSSI [24, 25] technique. The Rossi technique is applicable provided that there are few inherent source neutrons in the assembly. If an assembly has a large inherent source due to such isotopes as Pu^{240} in the assembly, it becomes difficult to measure α with the conventional Rossi technique. In such situations the pulsed neutron source technique would be useful in providing a value for α. The pulsed source technique also provides a method for measuring the subcriticality of a system [5, 6] when other methods are inadequate. Another parameter which may be measured using a pulsed source technique is the neutron importance as a function of position in the core for a particular neutron distribution of the source.

The measurement of these parameters will be attempted on the Argonne National Laboratory's fast critical facilities in the near future. The Laboratory has three highly flexible critical facilities in operation at the present time, ZPR-3 [26], ZPR-6 [27], and ZPR-9. ZPR-3 is at present being used to investigate small plutonium-fuelled fast reactors. The ZPR-6 is being used for the investigation of large dilute reactors ($\sim$ 1000-3000-litre core), while ZPR-9 is being used for the study of tungsten-based light-metal-reflected fast reactors. The ZPR-3 facility has a small pulsed neutron source which is being used for β/ℓ or alpha measurements. The ZPR-6 and ZPR-9 complex also has a pulsed neutron source on order for alpha and reactivity measurements. A comparison of the important characteristics of the pulsed neutron sources which are or will be available to Argonne's fast critical facilities are given in Table VI.

ACKNOWLEDGEMENTS

The authors would like to express their appreciation to L.R. Dates (ANL) who designed the components for the uranium pedestal, to J.R. Brown (GA)

TABLE VI

ARGONNE FAST CRITICAL'S PULSED SOURCES CHARACTERISTICS

	ZPR-3	ZPR-6
Generator type	High voltage transformer drift tube	High voltage transformer drift tube
Accelerating voltage (keV)	150	200
Nuclear reaction	$H^2(H^3n)He^4$	$H^2(H^3,n)He^4$
Neutron production rate (n/sec)	10^{11}	5×10^{11}
Pulse repetition rate (pulses/sec)	$10\text{-}10^5$	$10\text{-}10^5$
Pulse width (μsec)	1 min	1 min
Duty cycle	Up to 100%	Up to 100%
Maximum target current in pulsed mode (mA)	———	3.4
Maximum beam current continuous (mA)	1	2
Ion source	R.F.	Penning

and W. Mowry (GA) who assisted in assembling and dismantling the experimental equipment, and J. Trimble (GA) and R. Hackney (GA) who assisted in the data reduction and theoretical calculations. Appreciation is expressed to R. Armani and his group (ANL) who analysed the activity of uranium foils by radiochemical techniques. Acknowledgement is also extended to D. Meneghetti (ANL) for helpful discussions on the theoretical analysis of spectra from a uranium assembly.

REFERENCES

[1] LICHTENBERGER, H. V., THALGOTT, F. W., KATO, W. Y. and NOVICK, M., "Operating Experience and Experimental Results Obtained from a NaK Cooled Fast Reactor," Proc. Intern. Conf. Peaceful Uses At. Energy, Geneva, 1955, Vol. 3, United Nations, New York (1956), P/813, 345.

[2] REDMAN, W. C. and ROBERTS, J. H., "Some Current Techniques of Fast Neutron Spectrum Measurements," Proc. Intern. Conf. Peaceful Uses At. Energy, Geneva, (1958), P/597, 72.

[3] BENNETT, E. F., Trans. Am. Nucl. Soc. 7, No. 2 (1964) 369.

[4] HUBER, R. J., Trans. Am. Nucl. Soc. 7, No. 2 (1964) 368.

[5] KEEPIN, G. R., At. Energy Rev. 2, No. 2, IAEA, Vienna (1964).

[6] BECKURTS, K. H., Nucl. Instr. Methods 2 (1961) 144-168.

[7] STONE, R. S. and SLOVACEK, R., Nucl. Sci. Eng. 6 (1959) 461-465.

[8] General Atomic Linear Accelerator Facility, USAEC Report, GA-1855 (Rev.).

[9] BEYSTER, J. R., et al., Nucl. Sci. Eng. 9 (1961) 168-184.

[10] BEYSTER, J. R., et al., "Integral Neutron Thermalization," USAEC Report, GA-4659 (January 24, 1964).

[11] RUSSELL, J. R., et al., "Neutron Spectra in Bulk Media by Time-of-Flight," Proc. IAEA Symp. Pulsed Neutron Research (1965) SM 62/61.

[12] NALIBOFF, Y. D., "FORTRAN ECTOPLASM Program," USAEC Report, GAMD-2887 (January 25, 1962).

[13] HOWERTON, R. J., "Tabulated Neutron Cross Sections, Part I: 0.001-14.5 MeV," USAEC Report, UCRL-5226 (May 1958).

[14] ALEXANDER, J. H., HINMAN, G. W., and TRIPLETT, J. R., "GAPLSN, A Modified DSN Program for the Solution of the One-Dimensional Anisotropic Transport Equation," USAEC Report, GA-4972 (March 1964).

[15] CARLSON, B., LEE, C., and WORLTON, J., "The DSN and TDC Neutron Transport Codes," USAEC Report, LAMS-2346 (February 1960).

[16] JOANOU, G. D. and DUDEK, J. S., "GAM-II, A B_3 Code for the Calculation of Fast-Neutron Spectra and Associated Multigroup Constants," USAEC Report, GA-4265 (September 1963).

[17] BHIDE, M. G. and HUMMEL, H. H., "Calculations of the Doppler Coefficients for Large Ceramic Fueled Fast Reactor," USAEC Report, ANL-6601 (August 1962).

[18] YIFTAH, S., OKRENT, D., and MOLDAUER, P. A., "Fast Reactor Cross Sections," Pergamon Press, New York (1960).

[19] TRIMBLE, G. D., HOUGHTON, G. K., and AUDAS, J. H., "Measurement of Neutron Spectra in Liquid Hydrogen," USAEC Report, GA-5750 or NASA-CR-54230 (1964).

[20] KIRN, F. S., "Neutron Detection with an Absolute Fission Counter," Proc. IAEA Symp. Neutron Dosimetry, IAEA, Vienna (1963) Vol. II.

[21] KATO, W. Y., KIRN, F. S., and REDMAN, W. C., "Measurement of the Conversion Ratio for a Fast Breeder Reactor," Reactor Operational Problems, (HUGHES, D. J., et al., eds.) Pergamon Press, New York (1957), Vol. II.

[22] SMITH, R. R., et al., "The Breeding Ratio of a Plutonium Loading in EBR-I," USAEC Report, ANL-6789 (February 1964).

[23] CHEZEM, C. G., Nucl. Sci. Eng. 8 (1960) 652-669.

[24] ORNDOFF, J., Nucl. Sci. Eng. 2 (1957) 450.

[25] BRUNSON, G. S., et al., "A Survey of Prompt-Neutron Lifetimes in Fast Systems," USAEC Report, ANL-6681 (August 1963).

[26] BRITTAN, R. O., et al., "Hazards Evaluation Report on the Fast Reactor Zero Power Experiment (ZPR-III)," USAEC Report, ANL-6408 (1961).

[27] KATO, W. Y. and DATES, L. R., "Design and Construction of the Argonne Fast Critical Facility (ZPR-VI)," Physics of Fast and Intermediate Reactors, IAEA, Vienna (1962) Vol. I.

DISCUSSION

D. STEGEMANN: My question is concerned with the low-energy tail of your measured spectra. If one looks at the figures in your paper one finds that the measured points stop at around 5 to 10 keV. Given a flight path of 50 m and the intensity of a Linac, it should be easy to go to 100 eV. Why was this not possible?

W. KATO: Our intensity was limited by the target. We did not use the full intensity of the Linac and thus we could not measure spectra at energies lower than those indicated.

J. RUSSELL: The results of these spectrum measurements reveal the presence of many low-energy neutrons which are indicated by one transport-theory code and cross-section set but not by the others. This means that it may be very difficult to apply the calculational method described by Mr. Storrer[1] to determine whether a pulsed-neutron-measured decay can be a "fundamental mode".

I should also like to ask Mr. Storrer whether the presence of the low-energy neutrons in bulk U^{238} means that fast reactors with U^{238} reflectors do not have a fundamental mode of decay.

F. STORRER: In the experiments mentioned by Dr. Kato one is really measuring the spectrum produced by a static source so that no eigenvalue problem arises in the calculation. In fast-reactor blankets, the low-energy neutrons are not produced by U^{238} since U^{238} provides very little elastic moderation below the inelastic threshold.

As for the discrepancy between the calculated and experimental low-energy spectra, let me say that apparently nobody has as yet been able to calculate adequately the low-energy tail in fast reactors, as is evidenced by the disagreements between calculated and experimental lifetimes of critical assemblies.

M. POOLE: Have you investigated the effect of room-return reactions on the spectrum, i. e. are sufficient room-return reactions present to distort the spectrum in the uranium appreciably? Such an error cannot be easily allowed for on the basis of a background measurement.

W. KATO: No investigations of this sort were carried out.

M. POOLE: What percentage of background was present at various energies?

W. KATO: At high-energy regions the background was 5-10%; at about 10 keV it was 40 - 50%.

M. POOLE: How was the sensitivity of your counter determined as a function of energy?

W. KATO: We calculated the efficiency of the B_4C detector. Information on this is given in another paper[2] of these Proceedings.

---

[1] See STORRER, F., "Pulsed neutron experiments on fast and intermediate systems" (SM-62/88), these Proceedings II.

[2] See RUSSELL, J. L. et al., "Determination of neutron spectra in bulk media by time of-flight" (SM-62/61), these Proceedings II.

SUAK, A FAST SUBCRITICAL FACILITY FOR PULSED NEUTRON MEASUREMENTS*

H. BORGWALDT, M. KÜCHLE, F. MITZEL AND E. WATTECAMPS
KERNFORSCHUNGSZENTRUM KARLSRUHE,
FEDERAL REPUBLIC OF GERMANY

Abstract — Résumé — Аннотация — Resumen

SUAK, A FAST SUBCRITICAL FACILITY FOR PULSED NEUTRON MEASUREMENTS. SUAK is a small unreflected unmoderated assembly fuelled with 20% enriched uranium. The fuel is in the form of thin plates of 2 in × 2 in × 1/8 in which are held in square tubes. The tubes are closely packed together, so that assemblies of different size and composition can be realized. The maximum size is a cube of about 35-cm side length. The maximum value of k_{eff} is 0.90.

To reduce the backscattering of neutrons the assembly is located in the centre of a thin-walled building surrounded at a distance of 25 m by a wall for radiation protection. The control room is embedded in this wall. With a 200-keV pulsed neutron generator, measurements of the prompt neutron decay with different detectors and measurements of spectra by the time-of-flight technique are performed. A description of the assembly is given. First preliminary results are presented and compared with calculations.

SUAK – ASSEMBLAGE SOUS-CRITIQUE A NEUTRONS RAPIDES POUR LES MESURES AU MOYEN DES NEUTRONS PULSÉS. SUAK est un petit assemblage sans réflecteur ni ralentisseur où le combustible utilisé est de l'uranium enrichi à 20%. Le combustible se présente sous forme de plaques minces de 5×5×0,32 cm placées dans des tubes de section carrée. Les tubes sont groupés et serrés les uns contre les autres de manière à réaliser des assemblages de dimension et de composition variées. La dimension maximum est un cube de 35 cm environ de côté. La valeur maximum de k_{eff} est 0,90.

Pour que la rétrodiffusion des neutrons soit moins importante, l'assemblage est placé au centre d'une construction à parois minces entourée à une distance de 25 m par un mur de protection contre les rayonnements. La salle de contrôle est aménagée dans ce mur. Avec un générateur de neutrons pulsés de 200 keV, on procède à des mesures de la constante de décroissance pour les neutrons instantanés avec différents détecteurs ainsi qu'à des mesures de spectres par la méthode du temps de vol. Les auteurs décrivent l'assemblage et donnent les premiers résultats provisoires qu'ils comparent à ceux des calculs.

SUAK – ПОДКРИТИЧЕСКАЯ СБОРКА НА БЫСТРЫХ НЕЙТРОНАХ ДЛЯ ИЗМЕРЕНИЯ ИМПУЛЬСНЫХ НЕЙТРОНОВ. SUAK является небольшой сборкой без отражателя и без замедлителя, заполненной ураном, обогащенным до 20%. Топливо находится в форме тонких пластин размером 2×2×1/8 дюйма, которые помещены в четырехугольные трубы. Трубы тесно упакованы так, что можно получать сборки различных размеров и состава. Сборка максимального размера представляет собой куб с ребром около 35 см. Максимальное значение коэффициента эффективности равняется 0,90.

Чтобы уменьшить обратное рассеяние нейтронов сборка размещается в центре помещения с тонкими стенами, которое окружено на расстоянии 25 м стеной для радиационной защиты. Контрольное помещение вделано в-эту стену. При наличии генератора импульсных нейтронов с энергией в 200 кэв производятся измерения распада мгновенных нейтронов с помощью различных детекторов, а также измерения спектров с помощью метода времени пролета. Дается описание сборки. Приводятся и сравниваются с расчетами первые предварительные результаты.

EL «SUAK»: INSTALACION SUBCRITICA RAPIDA PARA MEDICIONES POR EL METODO DE LOS NEUTRONES PULSADOS. El «SUAK» constituye un conjunto de pequeñas dimensiones, desprovisto de reflector y de moderador, alimentado con U enriquecido al 20%. El combustible empleado presenta la forma de

* The work was performed within the scope of the Fast Breeder Project-Association Karlsruhe-Euratom.

placas de 50, 8×50, 8×3, 1 mm dispuestas en el interior de tubos de sección cuadrada. Estos tubos se agrupan apretadamente, de modo que pueden formar conjuntos de dimensiones y composición distintas. El tamaño máximo que pueden presentar es el de un cubo de unos 35 cm de arista. El valor máximo de k_{ef} alcanza a 0,90.

Para reducir la retrodispersión de los neutrones, el citado conjunto se coloca en el centro de una estructura de paredes delgadas rodeada, a una distancia de 25 m, por un muro de protección contra las radiaciones. La sala de control se encuentra embutida en ese muro. En dicha instalación se efectúan mediciones del decrecimiento de la población de neutrones rápidos, empleando un generador de neutrones pulsados de 200 keV, así como mediciones de los espectros por el método del tiempo de vuelo. Los autores describen el conjunto, y presentan los resultados preliminares obtenidos comparándolos con los del cálculo.

1. INTRODUCTION

In the physics of thermal reactors a large amount of information has been obtained from the measurement of space and time eigenvalues of clean lattices. For fast systems with their very broad and system-dependent energy spectrum the situation is much less favourable. Nevertheless, some exponential experiments have been performed [1]. Whereas in an exponential experiment a large amount of expensive material is wasted in the region where the spectrum reaches its asymptotic shape, this is not the case in a pulsed neutron measurement. Therefore, the application of the pulsed source technique to fast systems seems to be attractive. However, since the asymptotic spectrum is only established via the multiplication process, a fairly high multiplication is required to get good time eigenvalues. If the amount of fuel available is limited, this can best be achieved with as little structural material as possible. For easier interpretation of the measurements an unreflected homogeneous system should be used. This leads to a small compact design with a relatively hard neutron spectrum.

Such an assembly has moreover the advantage of being very well suited for spectrum measurements by the time-of-flight technique since the short decay time allows very short flight paths to be used. This more than compensates the disadvantage of having only a small fraction of neutrons in the energy range where time-of-flight methods are applicable. Of course, the spectrum of such an assembly is quite different from that which is expected for a large dilute fast breeder. Nevertheless, calculational methods and cross-section sets can be checked in that energy range where the Doppler effect is important and where no other techniques of spectrum measurement exist.

Therefore, in Karlsruhe in the framework of the fast breeder project, in addition to the large critical facility SNEAK and the coupled fast-thermal reactor STARK, the small flexible fast subcritical assembly SUAK has been constructed, the fuel of which will later be used in the SNEAK assembly.

2. DESCRIPTION OF THE FACILITY

The subcritical assembly consists of thin plates (2 in×2 in×1/8 in) of 20% enriched uranium, which are held in aluminium square tubes of 1-mm wall thickness. The tubes are closely packed together to form parallelepipeds of 27.0, 32.3, or 37.7-cm side length, respectively. The height

of the assembly is variable up to 35.1 cm by changing the filling height of the platelets. The tubes are closed at the top and at the bottom with 3 cm aluminium plugs and set with pins on an aluminium base plate of 3.0 cm thickness. To reduce backscattering of neutrons this assembly is located 5 m above the ground in the centre of a thin-walled building of dimensions 10 m×15 m×10 m. 3.5 m above the ground there is a grid on which the accelerator and auxiliary equipment is mounted. Figure 1 shows an artist's view of the assembly.

For radiation protection the building is surrounded at a 25-m distance by a wall of 5.5 m height in which the control room is embedded. An evacuated flight tube of 50-cm diameter and variable length up to 22 m leads radially from the assembly to the wall. It is mounted on a bridge on which the heavily shielded detector can be moved on wheels to seal the end of the flight tube. An extension of the flight tube to 50 m is under construction.

The accelerator is a 200 keV Cockcroft-Walton type generator constructed by EYRICH [2] and produces neutrons by the $T(d, n)He^4$ reaction. With a combined beam extraction and beam deflection pulsing device, neutron bursts of 0.1-μs width and triangular shape are produced at a repetition rate of up to 4×10^4 c/s.

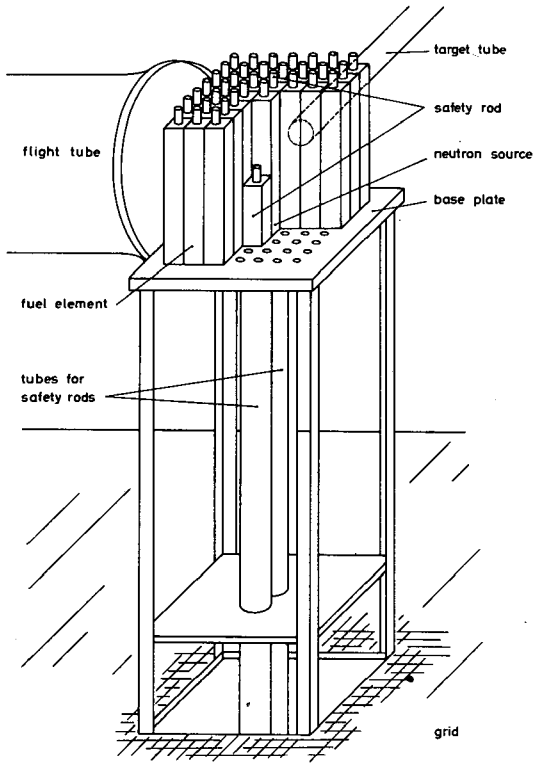


Fig. 1

SUAK assembly

When building up the assembly the approach-to-criticality was controlled by a multiplication measurement. For that purpose a Po-Be source was inserted at the bottom of the central fuel element, and the neutron flux as a function of the number of fuel elements was measured with three long counters placed on different sides of the assembly at a distance of about 1 m. Two of the central elements acted as safety rods. They were not plugged at the base plate but movable by control rod drives from below. At a preset flux level they would drop out of the assembly, thus reducing the multiplication.

Since it was not allowed to go to a higher multiplication than corresponds to $k_{eff} = 0.90$, a fairly accurate determination of k_{eff} during the build-up of the assembly was necessary. Therefore, the expected counting rate as a function of the number of fuel elements N was calculated using several hundred spatial harmonic modes. In view of the small number of elements and the odd shape of the configurations during build-up of the assembly, a value, that was obtained from the same configuration but with the elements filled with lead, was subtracted from each counting rate. This greatly reduced shadowing and scattering effects from single elements. When plotting this corrected inverse multiplication $1/M$ versus $1/\sqrt{N}$ an approximately straight line was found for $M > 5$ which could be extrapolated to give the critical mass. Adjusting the calculation to this value the k_{eff} of the assembly was found. In practice the agreement between the experimental and theoretical critical number of fuel elements was so good that only an adjustment of 0.5% in k_{eff} was required.

3. THE THEORY UNDERLYING THE PULSED NEUTRON MEASUREMENTS

In view of the small size and the simple shape of the SUAK assemblies the decay of the neutron field after injection of a neutron burst was treated in a space-independent multigroup diffusion approximation. Leakage was taken into account by introduction of a buckling B^2 that was calculated from the geometrical dimensions with an extrapolation length of $d = 0.71\ \bar{\lambda}_{tr}$, where [3]

$$\bar{\lambda}_{tr} = \sum_{i=1}^{G} \phi_i \phi_i^* \lambda_{tr,i}^2 \Big/ \sum_{i=1}^{G} \phi_i \phi_i^* \lambda_{tr,i} \quad . \tag{1}$$

ϕ_i and ϕ_i^* are the static flux and importance spectra and G is the number of groups.

The top and bottom plug and the base plate were taken into account by calculating the savings with a one-dimensional multigroup diffusion code [4]. This approximation was checked by measuring the reactivity effect of an additional aluminium plate of 3-cm thickness placed at one side of the assembly. The measured and calculated values agreed well within the limits of error. The error introduced from the diffusion approximation was checked by comparing a static S_4 calculation with a diffusion calculation. The S_4 calculation gave a k_{eff} which was about 2% higher.

The multigroup constants used were based on the Karlsruhe version of the 16-group cross-section set of YIFTAH, OKRENT, and MOLDAUER [5] (YOM) and on the 26-group data of ABAGJAN, BAZAZJANC, BONDARENKO and NIKOLAEV [6] (ABN) which include corrections for resonance self-shielding.

Three types of solutions of the multigroup diffusion equation have been used. In view of the short prompt neutron decay times and high repetition rates of pulsing, the delayed neutrons were always treated as a constant background.

(a) Determination of decay constants

The multigroup equations were Laplace transformed and written in a form that helps to find the time eigenvalues

$$\frac{1}{k(p, B^2)}\left[\sum_{j=1}^{G} (\nu\sigma_f)_j \phi_j(p)\right]\chi_i + \sum_{j=i+1}^{G} \sigma_s(i, j)\phi_j(p) - \left(\sigma_{rem,i} + D_i B^2 + \frac{p}{v_i}\right)\phi_i(p) = 0 \qquad (2)$$

with the normalization of ϕ_j :

$$k(p, B^2) = \sum_{j=1}^{G} (\nu\sigma_f)_j \phi_j(p).$$

Here p is the Laplace parameter, the ϕ_j are the transformed group fluxes, ν is the average number of prompt fission neutrons and $\sigma_s(i, j)$, $\sigma_{rem,i}$, and σ_{fi} are the macroscopic group transfer, removal, and fission cross-sections, respectively. χ_i is the fraction of the fission spectrum in the i-th-group, D_i is the diffusion coefficient, and k(p) is the Laplace transform of the first generation multiplication kernel which is an obvious generalization of k_{eff} of the stationary reactor theory.[1] Eigenvalues of Eq. (2) are the p-values for which $k(p_n) = 1$; $n = 1, 2, \ldots G$ [7]. The most positive eigenvalue should be the fundamental mode decay constant.

But for fast systems with a low multiplication ($k_{eff} < 0.90$) it happens that whereas the bulk of neutrons are decaying exponentially with a time constant

$$\alpha \approx \frac{1 - k_{eff}(1 - \beta)}{\ell}$$

there is a small fraction of low energy neutrons not participating in this time behaviour, but decaying more slowly and in a non-exponential way. These had to be described by continuous eigenvalues.

---

[1] $1/k(p)$ can be described as the factor by which ν had to be multiplied to make p and B^2 exist in the reactor at the same time.

In the multigroup calculations the existence of these neutrons is reflected in the fact that the decay constant of the bulk of neutrons we are looking for is not necessarily the most positive eigenvalue but is followed by others. However, if the multiplication is not too low, the interesting mode can easily be found since it is the first eigenvalue p_n coming from positive p-values, which is clearly distinguished from any pole of k(p) [7]. This phenomenon is illustrated in Fig. 2.

(b) Calculation of the complete time behaviour of the neutron decay

When the multiplication is too low ($k_{eff} < 0.80$) the first part of the decay of the neutron field after a pulse is strongly influenced by energy harmonics, whereas the last part is governed by the low energy neutrons mentioned above. Therefore, no decay constant can be extracted from the measured time behaviour. To be able to interpret measurements even in that case the complete time behaviour of the neutron field after a pulse has been calculated.

For that reason a Fourier series expansion of the time dependence of the neutron flux with a rectangular source distribution has been performed

$$\phi(t) = \mathrm{Re} \sum_{n=0}^{\infty} \phi_n \, e^{i\omega_n t} . \qquad (3)$$

The Fourier coefficients were calculated from the multigroup diffusion equations with that source. Up to a hundred frequencies have been included. Moreover, the energy distribution of the source and the energy sensitivity of the detector could be taken into account.

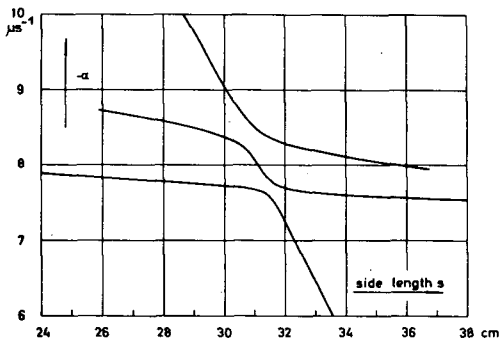


Fig. 2

Prompt neutron decay constant as calculated from the 16-group YOM set

The prompt neutron decay constant as calculated from the 16-group YOM set versus the sidelength s of a cube consisting of 20% enriched uranium. The usual continuous shape is interrupted, and it is the fundamental mode only for s > 32 cm. For 31 cm < s < 32 cm it is the first harmonic, for s < 31 cm it is the second harmonic and so on.

Calculations with the 16-group YOM set and with the 26-group ABN set, which extends down to the thermal region, showed a fairly good exponential decay for $k_{eff} > 0.70$.

(c) Correlation between decay constant, reactivity and neutron lifetime

In the interpretation of pulsed neutron measurements the relation

$$\alpha = \frac{1 - k_{eff}(1-\beta)}{\ell} \tag{4}$$

is often used, where α is the prompt neutron decay constant and ℓ is the neutron lifetime. To check the validity of this equation a power series expansion of $1/k(p)$ in the vicinity of $p = 0$ was made

$$\frac{1}{k(p)} = \frac{1}{k(0)}[1 + \ell_1 p + \ell_2 p^2 + \ell_3 p^3 + \dots],$$

where $k(0) = k_{eff}(B^2)(1-\beta_{eff})$ and ℓ_1 is the neutron lifetime. The correction terms to Eq. (4), ℓ_2 and ℓ_3 were computed from a third-order perturbation theory. For $k_{eff} = 0.87$ the correction amounts to about 10% in α.

4. MEASUREMENTS OF THE NEUTRON DECAY

From the calculations of the time decay of the neutron field it turned out that a good exponential could only be expected for $k_{eff} > 0.7$. On the other hand, for safety reasons the systems were restricted to $k_{eff} < 0.90$. Since moreover the amount of fuel available was limited to 120 kg U^{235} in the form of 20% enriched uranium no large variation in size and composition was possible but the system with the highest multiplication was built up. This was a block consisting of 6×6 elements filled up to the top with 20% enriched uranium only. Any additional material would have reduced the multiplication or would have softened the neutron spectrum too much. The parameters of the assembly are given in Table I.

The assemblage was interrupted at 5×5 elements to perform check measurements. These data are also given in Table I. Since the decay times of these systems were in the range of 100 to 200 ns, a timing accuracy of about 10 ns was required. This was achieved with a Stilbene scintillator used for proton recoil measurements and fission counters operating with cross-over-pick-off gates. The Stilbene crystal was fixed between two multipliers. A slow coincidence from the two was used for noise suppression; pulse shape discrimination as proposed by OWEN [8] gave a signal free of γ-background from one multiplier and a triple coincidence of these signals opened a gate for the fast signal taken from the anode of the other multiplier.

A TMC 256-channel time analyser with the model 219 plug-in unit was used, capable of channel width down to 10 ns. The target current pulse triggered the analyser.

TABLE I

MEASUREMENTS OF NEUTRON DECAY

Atomic densities of the assemblies		$N\text{-}U^{235} = 0.821 \times 10^{22}/cm^3$ $N\text{-}U^{238} = 3.284 \times 10^{22}/cm^3$ $N\text{-}Al^{27} = 0.437 \times 10^{22}/cm^3$
Experimental critical mass corrected for savings		248 ± 10 kg U^{235}
Assembly number	1	2
Number of elements	25	36
Loading (kg U^{235})	82.24	118.5
Size including savings (cm)	26.9×26.9×38.3	32.3×32.3×38.3
Geometric buckling B^2 (cm^{-2})	2.431×10^{-2}	1.877×10^{-2}
k_{eff} from 1/M measurements	≈ 0.75	0.86 ± 0.01
k_{eff} from pulsed measurements (area method)	-	0.88 ± 0.02
k_{eff} calculated from ABN set	0.765	0.864
k_{eff} calculated from YOM set	0.754	0.843
$\left(\frac{1}{\alpha}\right)_{measured}$ (ns)	no exponential decay	230 ± 3
$\left(\frac{1}{\alpha}\right)_{calc.\ ABN}$ (ns)	122	205
$\left(\frac{1}{\alpha}\right)_{calc.\ YOM}$ (ns)	108	176

For the measurements with the 25-element assembly the target was outside and one element was withdrawn to insert a U^{235} fission counter in a position where the most important spatial harmonics were suppressed.

The measured time dependence of the neutron intensity after subtraction of the constant delayed neutron background is given in Fig. 3. When the tran-

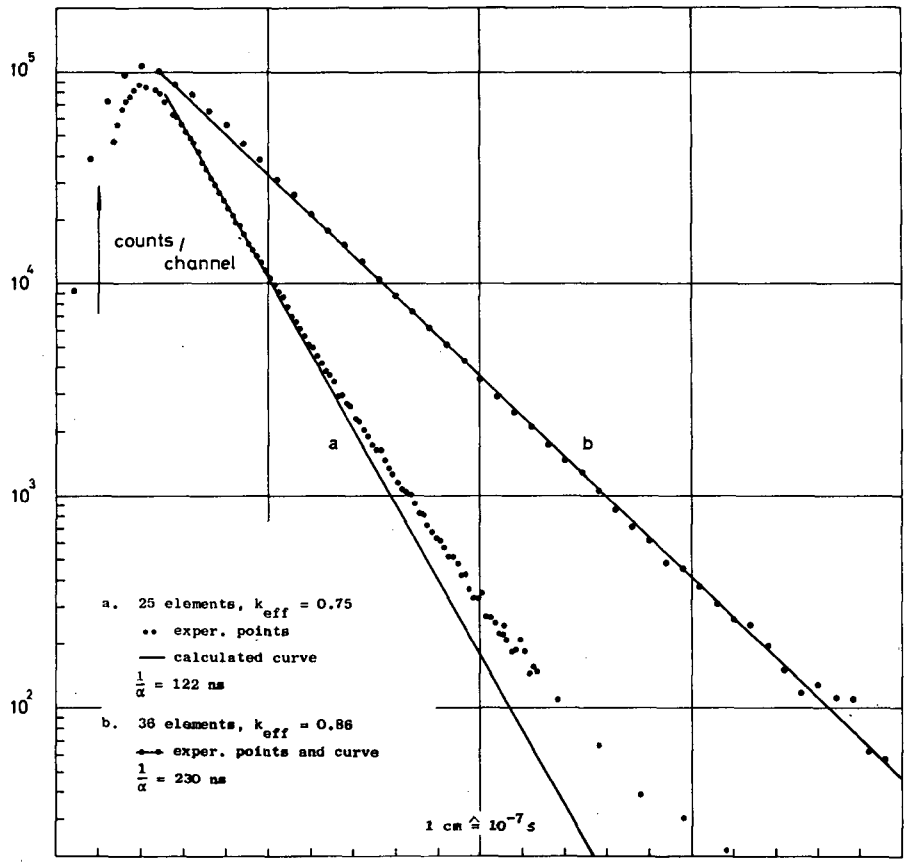


Fig. 3

Time decay of the neutron flux

sients have died away there is a small interval where the time behaviour looks exponential but then it is followed by a slower decaying tail of much higher intensity than predicted by the calculation which is also included in the figure. The calculation was performed for the unperturbed case with the ABN cross-section set [6]. Measurements with the unperturbed assembly and the proton recoil detector outside showed a time behaviour that differed mainly in the transients.

The 36-element assembly measurements have been made with fission counters[2], coated with Np^{237}, U^{238} and U^{235}, located inside and outside the assembly. When inserted in the assembly the counters were completely embedded in the fuel so that the perturbation now was relatively small. A good exponential decay was always observed. Because of energy harmonics

[2] *Twentieth Century Electronics type FC 165.*

there was a small difference in the transients between the Np^{237} and the U^{235} fission counter measurements and a larger difference betwen the U^{235} and the U^{238} results for the time interval from the beginning up to 400 ns. The time decay as measured with a Np^{237} fission counter outside the assembly is included in Fig. 3. No calculated curve is given but the decay times are compared in Table I.

The experimental decay time is about 15% longer than predicted by the calculation based on the ABN cross-sections and 30% longer than calculated from the YOM data. Since the agreement in $1 - k_{eff}$ is much better this seems mainly to be a result of errors in the calculation of the neutron lifetime. A calculation with the ABN set without correction for resonance self-shielding showed that there is practically no self-shielding in the SUAK assemblies. Therefore, the difference in the lifetimes as calculated from the YOM and from the ABN data must be caused by differences in the cross-sections.

The values in the table are taken from eigenvalue calculations, but practically the same values were found from a plot of the time-dependent neutron flux.

To check the influence of backscattered neutrons a measurement with the assembly covered with cadmium was made. No difference in the neutron decay apart from the reflector effect of cadmium was observed.

An additional check was the determination of reactivity from the ratio of the time-averaged prompt and delayed neutron fluxes as proposed by GOZANI [9]

$$\frac{\bar{\Phi}_{\text{prompt}}}{\bar{\Phi}_{\text{delayed}}} = -\frac{\rho}{\beta_{\text{eff}}} .$$

Since the prompt neutron decay time is short and the repetition rate is high, room return neutrons would give an almost constant background. This adds to the delayed neutron flux and leads to a wrong experimental flux ratio. This is particularly serious for systems which are subcritical to this extent.

For the determination of the fundamental mode, prompt neutron flux the finite width of the source burst had to be taken into account. Though the almost triangular shape of the source burst has been measured, some uncertainty is caused by this correction. β_{eff} was determined from the measured fractions of U^{238} and U^{235} fissions of the assembly. The minor importance of the delayed neutrons was taken into account. As an average from different measurements with the fission counter inside and outside of the assembly,

$$k_{eff} = 0.88 \pm 0.02$$

was obtained.

An evaluation with the method as proposed by GARELIS and RUSSELL [10] gave the same result well within the limits of error. The fact that the value is higher than the result of the stationary measurement could be explained in the way that $(17 \pm 5)\%$ of the constant background results from room-scattered neutrons. However, in view of the uncertainties from the

finite pulse-width correction, from the determination of β_{eff}, and from a possible presence of delayed neutron harmonics, the conclusion is not very stringent.

In addition to the measurements with the unperturbed assembly, the reactivity effects of an aluminium plate and of the withdrawal of single elements have been determined by the pulsed source method.

5. MEASUREMENTS OF NEUTRON SPECTRA BY THE TIME-OF-FLIGHT TECHNIQUE

If the build-up and decay of the neutron field in an assembly after a neutron burst injection is short compared with the flight-time of the neutrons from the assembly to the detector, what is measured is essentially the stationary spectrum of the subcritical assembly with a continuously running source. This, of course, differs from the spectrum of the critical assembly and from the asymptotic spectra in time or in space. But if it is just this spectrum which we calculate, no fundamental problems of interpretation of the measured spectra arise. The spectrum is highly space dependent, however, and so far measurements from two positions have been made:

(1) The spectrum from the centre of the assembly. Here, no flux gradient difficulties appear if the target position is also at the centre of the assembly.

(2) The leakage spectrum from the surface. Here, no beam extraction problems arise.

In both cases, however, the problems of neutron collimation and determination of the background have to be solved first. Since the measurements started very recently, the investigations so far have concentrated mainly on these points.

A large-area neutron detector of high sensitivity in the keV-region but with moderate time resolution properties is required. Therefore, a Li^6-loaded glass scintillator of 4 3/16-in diameter and 1-in thickness was chosen. This detector is very sensitive to keV-neutrons, but it is also black to slow neutrons and sensitive to γ-rays. This is particularly serious since the assembly is completely unshielded. Therefore, the scintillator is surrounded by a heavy shield consisting of concentric annular cylinders of 4 mm of B^{10} powder, 5 cm of lead and 40 cm of a mixture of paraffin and Li_2CO_3 which has an overall length of 170 cm. The whole shield is placed on a trolly. The flight tube is of variable length ranging from 5 to 22 m. It is evacuated and sealed on both sides by 2 and 1.5 mm aluminium windows, respectively. In the flight tube steel collimators of 20-cm thickness were placed at 1/4, 2/4 and 3/4 of the flight path. Their inner part consisted of replaceable annular cylinders of CUNIFER 30 to adjust the opening of the collimator to the requirements of the experiments. The outer diameter of 41 cm was chosen to prevent primary source neutrons from hitting the shield.

To measure the spectrum from the centre of the assembly a difference technique was applied which allows the most reliable background determination. For these measurements, the central row of fuel elements was replaced by a horizontally stacked row which left the dimensions of the assembly un-

changed. The fuel of the central element of this row could be removed to generate a horizontal through-channel of 5 cm × 5 cm. This channel could be loaded half from the side opposite to the detector.

For spectrum measurements from the centre, all collimators but the first one had an inner diameter of 12.5 cm. The latter selects a circular area of 35 cm^2 centred at the beam hole axis, that means 25 cm^2 from the central region and 10 cm^2 from the surface.

The spectrum from the central region of the assembly is obtained by subtracting the time-of-flight distribution with the through-channel from the time-of-flight distribution obtained with the channel loaded with fuel up to the centre. It has not been investigated whether the spectrum in the beam differs from the spectrum in the centre of the assembly. Wall-scattering effects at the extraction channel were certainly reduced by the difference method. Since the withdrawal of the fuel plug from the central channel reduces the multiplication of the assembly by $\Delta k_{eff} = 0.014$ it also reduces the background. Therefore, the measurements were normalized to the same counting rate of a long counter.

For the measurements of the leakage spectrum from the surface of the assembly, all collimators had an inner diameter of 12.5 cm which selected a circular area of 123 cm^2 at the centre of one side of the assembly. Much attention has been given to the determination of the background. To gain a better understanding of the methods used, different sources of background have to be distinguished, the most important ones being,

(1) Permanent background caused by
   (a) Radioactive impurities contained in the Li^6-glass scintillator,
   (b) Cosmic radiation,
   (c) Photomultiplier noise.

(2) Time-independent background from the accelerator caused by
   (a) Delayed neutrons,
   (b) Prompt neutrons slowed down in the shield.

(3) Time-dependent background caused by
   (a) Air, wall and ground-scattered neutrons,
   (b) Beam neutrons scattered in the detector shield which, therefore, are detected at a time later than corresponds to their flight-time,
   (c) Neutrons scattered at the inner collimator walls,
   (d) Neutrons penetrating the collimator,
   (e) Prompt γ-rays from fission and inelastic scattering,
   (f) Neutrons and γ-rays from the accelerator produced outside the assembly and not shadowed by the collimator.

The permanent background has been measured when the accelerator was switched off. Its contribution was respectively 0.2, 1.8 and 12% at neutron energies of 300, 100 and 10 keV.

The time-independent background was measured in the time channels preceding the accelerator burst. It amounts to 0.8, 5 and 32% of the signal at neutron energies of 300, 100 and 35 keV, respectively. To measure the time-dependent background different methods have been investigated:

(1) To determine the γ-background time-dependent pulse height spectra of the Li^6-detector have been measured with a time resolution of 500 ns. From each spectrum the γ-ray contribution has been obtained by proper extrapolation of the pulse-height spectrum from the region where no neutrons can occur into the region used for neutron detection.

(2) Furthermore, the γ-ray background has been determined with a Li^7-detector which is insensitive to neutrons, but equally sensitive to γ-rays as the Li^6-detector.

(3) Shadowing the detector by 20 cm CUNIFER 30 practically suppresses the neutron beam and allows determination of background type 3(a) and (f). An additional plate of 10 cm plastic placed at the back of the first collimator should transform background type 3(d) to an almost time-independent background. A measurement with such a plate showed that the effect was very small.

(4) The background, type 3(b) and (c), is the most difficult to measure. Here, a plug is required which is transparent to all neutrons, except for the neutrons in the energy range to be measured. For these it should be completely black. This can be approximated for selected energies by a material with black resonances. Since the cross-section peaks at the different resonances are of different height, the thickness of the transmission probe has to be optimized for each energy.

(5) Furthermore, in the energy region between resonances it is possible to determine the background from extrapolation of the transmission of probes of different thickness to zero transmission using the known total cross-section.

So far, measurements have been made with a flight path of 11.5 m at assembly No. 2. The target was located at the centre of the assembly. The build-up and decay of the neutron field after the neutron burst had a half-width of 300 ns. The repetition frequency of the accelerator was 25×10^3 c/s and the intensity was 10^4 neutrons per burst. A TMC 256 channel analyser with a model 201 plug-in unit was set at a channel width of 125 ns. Other data of the measurements are listed in Table II. The background measurements for the leakage spectrum are illustrated in Fig. 4. The close agreement between the results from the shadow-cone and from the black resonance measurements indicates that the background type 3(b) and (c) is rather small.

The time-of-flight distributions have been corrected for background, for the transmission of the aluminium windows and for the energy dependence of the Li^6 detector. The detector has previously been calibrated in the energy range from 50 to 320 keV with monoenergetic neutrons from a Van de Graaff generator. The measured sensitivity curve corresponds to the expected efficiency as deduced from the Li^6 (n, α) cross-section.

No resolution correction has been applied so far. Since the main purpose of the measurements is to check calculations, this correction could be avoided entirely, when measured and calculated time-of-flight distributions are compared.

In Fig. 5 the measured parts of the spectra are given together with the calculated flux shapes. The measurements are normalized so as to agree with the calculation at about 100 keV. The one-dimensional 16-group diffusion calculation based on the YOM data serves only as a rough indication

TABLE II

SPECTRUM MEASUREMENTS

Type of measurement	Neutron energy (keV)	Energy resolution (%)	Signal / Background	Statistical error (%)	Running time (h)
Leakage spectrum	88	10	5.0	1	8
from the surface	35	6.5	1.32	2.5	
Beam spectrum	88	10	0.74	2.2	40
from the centre	35	6.5	0.36	6.1	

of the SUAK spectra. For comparisons with the measurements, more sophisticated calculations will be used later. The measured spectra are much softer than the calculated ones. No conclusion should be drawn, however, unless the measurements are extended to lower as well as to higher energies. Here, it seems possible to go up to more than 1 MeV. If the length of the flight path and the channel width are optimized, the counting rate per channel Z is given by

$$Z(t) = \text{const.}\eta(E)\phi(E)\alpha^2 \left(\frac{\Delta E}{E}\right)^4,$$

where η is the sensitivity of the detector, $\phi(E)$ is the neutron spectrum, and α is the prompt neutron decay constant. Since ϕ is increasing, where η is decreasing, similar counting rates at the same resolution can be expected for higher energies than have been obtained so far. The approximate resolutions obtainable at various energies for the flight paths foreseen are given in Table III.

ACKNOWLEDGEMENTS

The authors would like to acknowledge the great help they have had from D. Schreier throughout the work; they are indebted to W. Eyrich for setting up and servicing the accelerator. Thanks are also due to K.H. Beckurts for many suggestions and stimulating discussions.

REFERENCES

[1] SNELL, A.H., Rpt CF-589 (1943); MARTENS, F.H., Rpt ANL-5379 (1955); CHEZEM, C.G., Nucl. Sci. Engng 8 (1960) 652; BEETS, C., CAMPAN, J.L., DECKERS, H. and ZALESKI, C.P., React. Sci. Techn. 16 (1962) 221; BONDARENKO, I.I., GOLUBEV, V.I., ZVONAREV, A.V., NIKOLAEV, M.N., ORLOV, M.J. and UZNADZE, O.P., Atom. Energ. 17 (1964) 113.

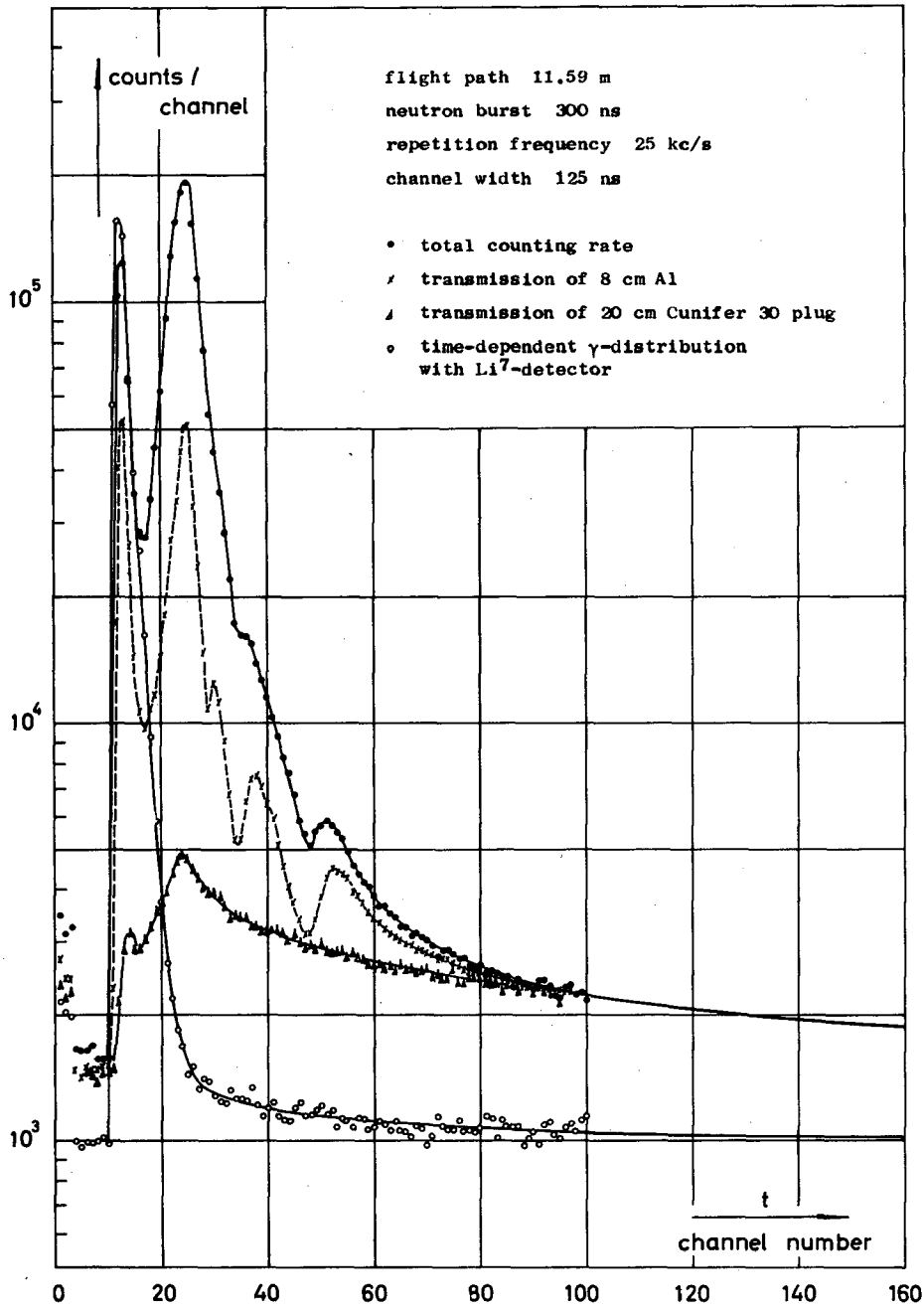


Fig. 4

Time-of-flight distributions for leakage spectrum

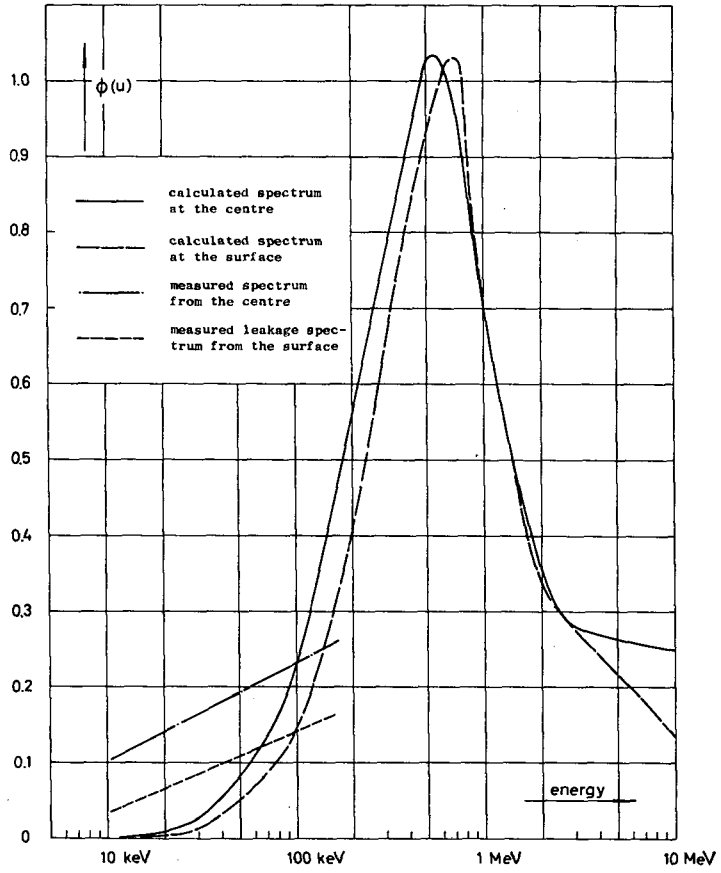


Fig. 5

Spectra of the SUAK assembly

TABLE III

ENERGY RESOLUTION FOR DIFFERENT FLIGHT PATHS

ΔE/E (%)	s = 5.5 m (keV)	11.5 m (keV)	21.5 m (keV)	55 m (keV)
5	4.5	18	76	390
10	18	86	300	1.5

[2] EYRICH, W., Nukleonik 4 (1962) 167.
[3] BORGWALDT, H., Nukleonik 5 (1963) 27.
[4] MÜNZNER, W., Internal Karlsruhe Rpt INR-103 (1964).
[5] YIFTAH, S., OKRENT, D., MOLDAUER, P.A., Fast Reactor Cross Sections, Pergamon Press, N.Y. (1960).
[6] ABAGJAN, L.P., BAZAZJANC, N.D., BONDARENKO, I.I. and NIKOLAEV, M.N., INDSWG-17 (1963).
[7] STORRER, F. and STIÉVENART, M., Rpt EUR 593e (1964).
[8] OWEN, R.B., Nucleonics 17 (1959) 92.
[9] GOZANI, T., Nukleonik 4 (1962) 348.
[10] GARELIS, E. and RUSSELL, J.L., Nucl. Sci. Engng 16 (1963) 263.

DISCUSSION

J. RUSSELL: I notice that the data reported are higher than the theoretical values by a factor of 10. Is this correct?

M. KÜCHLE: Yes, it is. However, the measurements extend only to E ≈ 100 keV and are normalized to agree with the calculated curve at that point. Only if the measurements were extended to higher energies could one attempt to draw any conclusions.

SOME MEASUREMENTS OF FAST REACTOR SPECTRA BY THE TIME-OF-FLIGHT TECHNIQUE USING A PULSED NEUTRON SOURCE

W.J. PATERSON, W.B. McCORMICK AND J.W. WEALE
ATOMIC WEAPONS RESEARCH ESTABLISHMENT,
ALDERMASTON, UNITED KINGDOM

Abstract — Résumé — Аннотация — Resumen

SOME MEASUREMENTS OF FAST REACTOR SPECTRA BY THE TIME-OF-FLIGHT TECHNIQUE USING A PULSED NEUTRON SOURCE. The zero-energy fast reactor VERA is equipped with a pulsed neutron source and a 50-m neutron flight path and these facilities have been used for time-of-flight neutron spectrometry in the energy range 100 eV to 50 keV. The results are discussed and are compared with calculated values.

MESURES DE SPECTRES DANS UN RÉACTEUR A NEUTRONS RAPIDES PAR LA MÉTHODE DU TEMPS DE VOL, AU MOYEN D'UNE SOURCE PULSÉE. Le réacteur à neutrons rapides VERA, de puissance zéro, est doté d'une source de neutrons pulsés et d'un canal de 50 m pour le parcours de vol des neutrons; ces moyens ont été utilisés aux fins de la spectrométrie des neutrons à l'aide d'appareils à temps de vol pour des énergies comprises entre 100 eV et 50 keV. Les auteurs discutent les résultats et les comparent aux valeurs calculées.

НЕКОТОРЫЕ ИЗМЕРЕНИЯ СПЕКТРОВ БЫСТРЫХ РЕАКТОРОВ МЕТОДОМ ПО ВРЕМЕНИ ПРОЛЕТА С ПОМОЩЬЮ ИСТОЧНИКА ИМПУЛЬСНЫХ НЕЙТРОНОВ. Реактор на быстрых нейтронах нулевой мощности VERA оборудован источником импульсных нейтронов с траекторией полета нейтронов 50 м, и эти установки использовались для спектрометрических измерений нейтронов по времени в диапазоне энергии 100 эв–50 кэв. Обсуждаются результаты, которые сравниваются с расчетными данными.

MEDICION DE ESPECTROS EN UN REACTOR RAPIDO POR EL METODO DE TIEMPO DE VUELO EMPLEANDO UNA FUENTE PULSADA. El reactor rápido de potencia nula «VERA» está dotado de una fuente de neutrones pulsados y de una trayectoria de vuelo de los neutrones de 50 m de longitud, que se han empleado en mediciones de espectrometría neutrónica por el método del tiempo de vuelo en el intervalo de energías comprendido entre 100 eV y 50 keV. Los autores examinan los resultados obtenidos y los comparan con los valores calculados.

1. INTRODUCTION

In currently proposed designs for fast power reactors a significant fraction of the neutron flux is in the energy range below 50 keV and measurement of the neutron energy spectrum in this range is particularly important for checking calculations of the Doppler temperature coefficient. The time-of-flight method is the only one available which gives a detailed spectrum over the range from 50 keV down to, say, 50 eV and this method is being used on the zero-energy fast reactor VERA [1]. The reactor is operated in the subcritical state and is provided with a pulsed neutron source to define the starting time of the extracted neutron beam. The degree of subcriticality has to be carefully chosen so as to ensure that the multiplication of source neutrons is sufficient to produce a representative reactor energy spectrum but not so large that the reactor pulse is too wide for adequate resolution. We have found that adequate resolution can be obtained with a reactor multi-

plication of 20 and a flight path of 50 m provided that allowance is made for the reactor pulse shape when analysing the time distributions to deduce the spectra. In this way results have been obtained from 500 eV to 150 keV for a plutonium-graphite system and from 50 eV to 50 keV for a uranium-graphite-polythene system.

The principles of the method are illustrated in Figs.1, 2, 3 and 4. Figure 1 shows the neutron time distribution produced in a typical fast reactor spectrum by a short pulse of neutrons and the way in which this shape is modified by neutron flight time over 30 m. Figure 2 shows the general layout of the VERA reactor system with its pulsed accelerator and its neutron flight tube. Figures 3 and 4 show the way in which the pulsed source and the beam extract tube are accommodated.

In the present paper the accuracy and limitations of the technique are discussed and some recent measurements on the VERA fast reactor are described.

2. BEAM EXTRACTION AND COLLIMATION

It is essential to establish a method of beam extraction and collimation which ensures that the energy distribution in the extracted beam is the same as that in the reactor core. A hole is made through the reflector and core to the point where the spectrum is to be measured, usually the core centre, and the collimator is designed so that a direct path to the detector exists

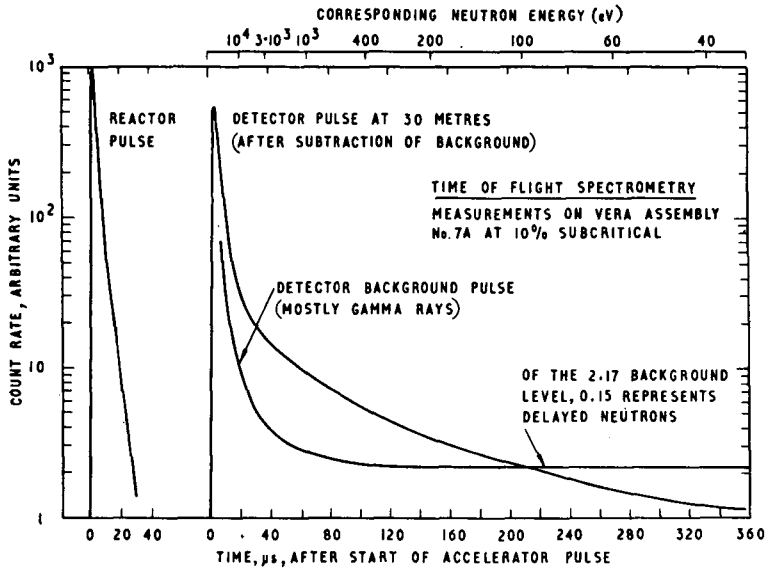


Fig. 1

Typical neutron flux versus time distributions obtained in the reactor core and in the flight tube at 30 m

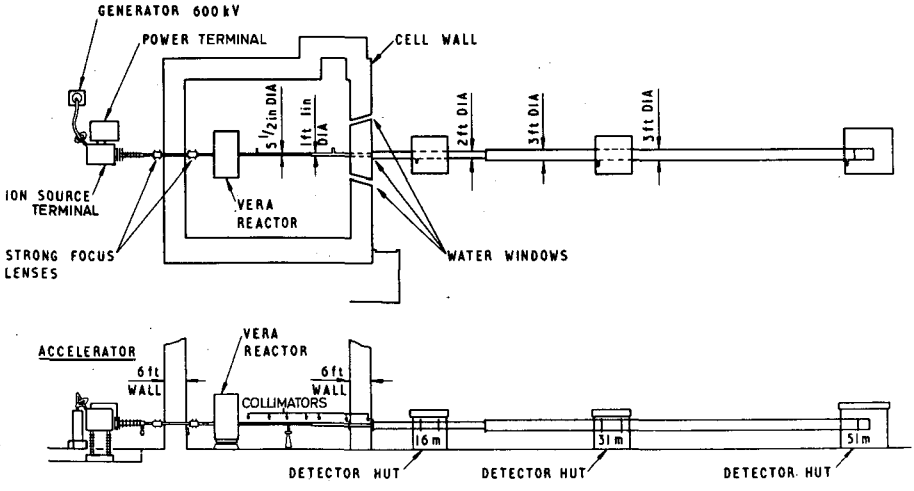


Fig. 2

VERA time-of-flight tube and accelerator

only for those reactor neutrons which are emitted from the core surface at the end of the hole. We have to establish two points: first, that the neutrons emitted from the surface at the end of the hole accurately represent the neutron spectrum that would exist at that point in the core if the hole were not present; secondly, that the measurements are not affected by neutrons scattered to the detector from the collimator or from the reactor environment generally. Figure 2 shows the flight-tube layout and Fig. 3 shows the arrangement of the accelerator source and the beam extract hole in VERA Assembly 7A. The extract beam hole is shown at its maximum size, that is $2\frac{1}{2}$ in high and 3.4 in wide. When a smaller beam hole is required it is obtained by packing extra core material to line the full size hole. The beam hole within the reactor is not sealed but the main flight tube is evacuated to prevent neutron scattering in the air and the neutron beam from the reactor enters the flight tube through a 0.015-in-thick aluminium membrane. The flight tube increases in diameter as the distance from the reactor increases so that there is no possibility of reactor neutrons striking the flight tube walls beyond the collimator. To avoid interposing a second and much thicker diaphragm in the neutron path at the detector end of the flight tube the complete detector is mounted within the flight tube. The 6-ft-thick concrete walls of the reactor cell provide an effective shield for the detector against scattered neutrons and for this reason all collimating apertures are placed within the reactor cell.

The efficacy of the beam extraction and collimating system has been checked by comparing certain spectrum-sensitive reaction rates in the reactor core and in the extracted and collimated beam with the reactor running at steady power. The spectrum indicators were: U^{238} fission (threshold 1.2 MeV); U^{235} fission (sensitive to all energy neutrons and particularly to thermal neutrons); and proton scattering in hydrogen gas (with an electronic

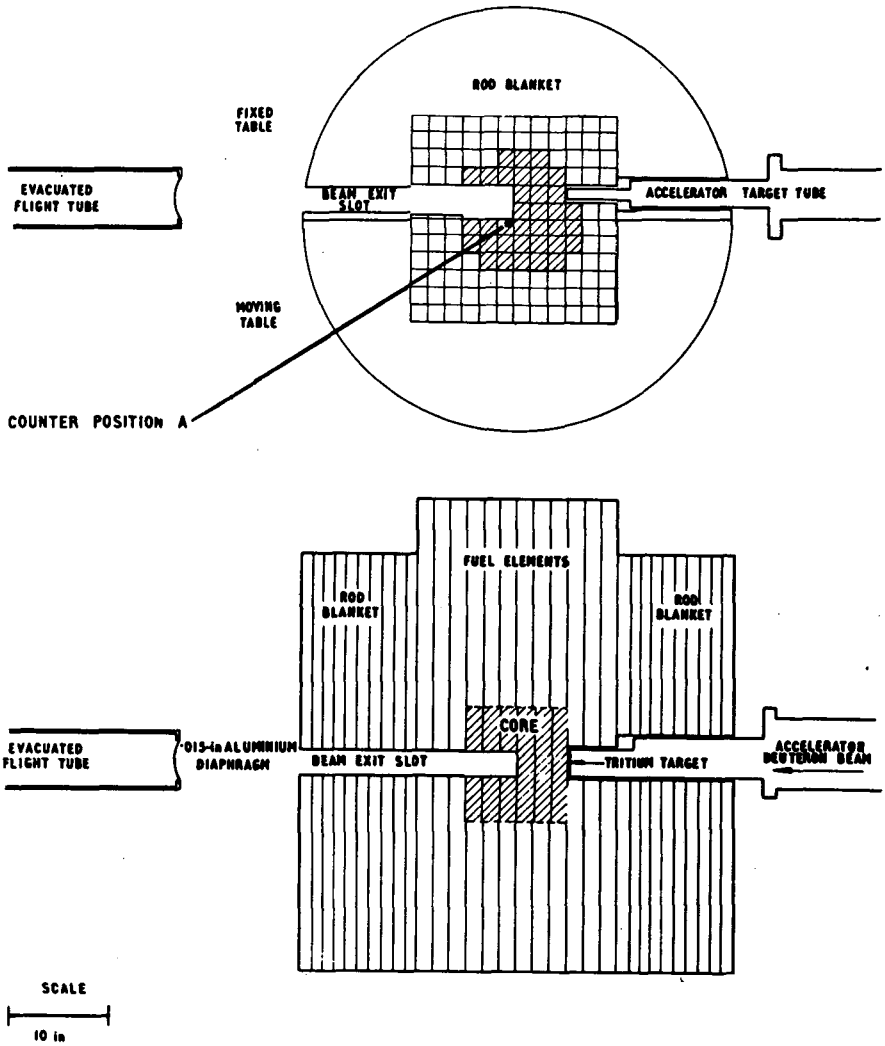


Fig. 3

Detailed arrangement of accelerator source and flight tube in VERA 7A
Above: horizontal section
Below: vertical section

bias adjusted so that the counter responded only to neutrons of energy above 240 keV). The fission rates were measured by cylindrical fission chambers and the hydrogen scattering was measured by a hydrogen-filled proportional counter. Tests were done with the extract beam hole as shown in Fig. 3. The reaction rates were first measured at position A, with and without the beam extract hole, to look for any distortion of the reactor core spectrum caused by insertion of the beam hole. The reaction rates were then measured

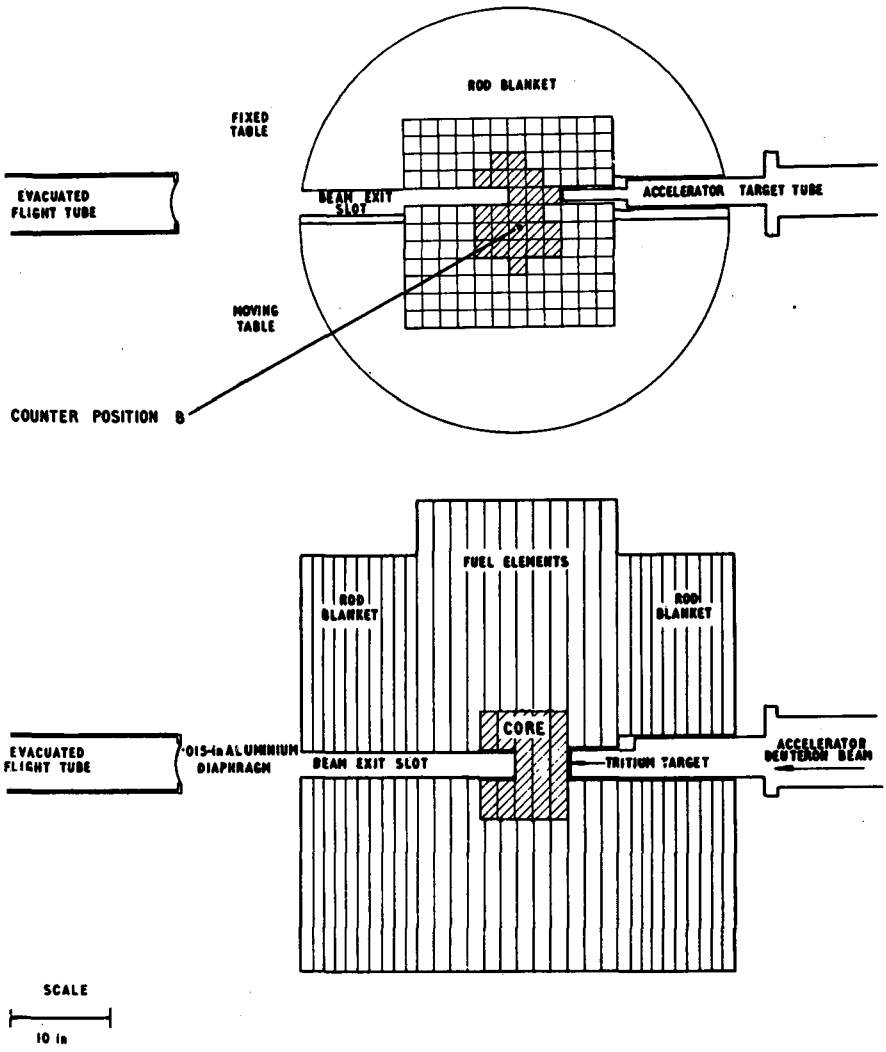


Fig. 4

Detailed arrangement of accelerator source and flight tube in VERA 11A
Above: horizontal section
Below: vertical section

in the extracted beam at a distance of 15 m from the core, using a number of borated-wax collimators spaced along the tube, so that there was no direct path to the detector from any part of the steel tube wall within the reactor cell. The results of these tests are summarized in Table I.

The effect of beam hole size on the emerging spectrum has also been investigated by comparing time-of-flight measurements with two different hole sizes (3.4 in wide by 2.5 in high and 1.7 in wide by 2.5 in high)

TABLE I

REACTION-RATE RATIOS IN THE CORE AND IN THE EXTRACTED BEAM

	Measurements in the core (position A)			Measurements in the beam at 15 m, using a core beam-hole 3.4 in wide and 2.5 in high
	Without beam-hole	With core beam-hole 1.8 in wide and 3 in high	With core beam-hole 3.4 in wide and 2.5 in high	
$\frac{U^{238}\ \text{fissions/g}}{U^{235}\ \text{fissions/g}}$	0.0376 ± 0.0015	0.0372 ± 0.0015	0.039 ± 0.002	0.038 ± 0.003
$\frac{\text{H recoils (> 240 keV)}}{U^{235}\ \text{fissions/g}}$	-	-	1.48 ± 0.08	1.53 ± 0.08

Note: The beam-hole in the reflector was 2.5 in square for all the tests.

in Assembly 7A at the same reactivity. Over the energy range investigated (100 eV to 30 keV) the spectra are in good agreement.

We conclude from these results that the insertion of the beam hole does not cause any large distortion of the core spectrum in the vicinity of the extract point and that there are no gross differences between the spectrum in the core and that in the extracted beam.

3. RESOLUTION

Our aim has been to measure the low energy spectra in fast reactor assemblies with an accuracy sufficient to check Doppler coefficient calculations. If these calculations are to be accurate to, say, ±20% the spectrum calculations must have a rather better accuracy, and we have taken the experimental requirement to be the measurement to ±5% of the relative neutron flux in a succession of energy groups of 0.25 lethargy width. Although the main contribution to the Doppler coefficient is below 10 keV we require the time-of-flight results to extend up to 50 keV so that they can be checked against proton-recoil measurements. At 50 keV an uncertainty of ±20% in energy corresponds to ±1.6 μs in flight time over 50 m whereas the decay of the reactor pulse may itself be several μs if the system has a mulitplication of 20. At first sight therefore, the resolution of the system appears inadequate. However, because the reactor pulse shape is well defined and accurately measurable, it is possible to calculate its effect on the detector time distribution and thereby to make an improvement in the effective resolution of the system. By this means we have been able to make measure-

ments up to 50 keV or to 200 keV, depending on the characteristics of the reactor.

Allowance for the reactor pulse shape is made by an iterative procedure, as follows:

(1) An approximate spectrum $\phi_1(E)$ is derived from the detector time distribution $D_1(t)$ by assuming a reactor pulse width of zero.

(2) From $\phi_1(E)$ and the measured reactor pulse shape the corresponding detector time distribution $D_2(t)$ is calculated. This will, of course, be different from the actual observed time distribution.

(3) From the time distribution $D_2(t)$ a new spectrum $\phi_2(E)$ is derived, again assuming a reactor pulse width of zero.

The difference between the spectra $\phi_1(E)$ and $\phi_2(E)$ represents the effect of assuming zero reactor pulse shape in the analysis of the time distribution $D_2(t)$. The approximate spectrum $\phi_1(E)$ can therefore be made more accurate by multiplying its component energy groups by the ratio of corresponding energy group intensities in $\phi_1(E)$ and $\phi_2(E)$. Thus a new spectrum $\phi_3(E)$ is derived. Then items (2) and (3) are repeated starting with $\phi_3(E)$ as the approximate spectrum and in this way another set of correction ratios to apply to $\phi_1(E)$ is produced and another improvement in accuracy is obtained in deriving a spectrum $\phi_4(E)$. The iteration is repeated until the correction factors deduced cease to change significantly. It is necessary to introduce a degree of smoothing by combining the correction ratios into larger groups. Each energy group component of the approximate spectra is multiplied by the correction ratio of the larger group to which it belongs, rather than by an individual correction ratio, and this leads to more rapid convergence and to a minimization of the effects of statistical errors. The validity of the procedure has been established satisfactorily by practical tests. An ideal smooth spectrum was generated and combined with a reactor pulse shape to produce a time distribution; typical experimental errors were then added and the result was analysed by the above method. In this way the possible improvements in effective resolution were determined for a variety of typical experimental results.

In the analysis it has been assumed that the neutron spectrum remains constant during the reactor pulse. This can only be approximately true because the time required to slow down fission neutrons into the lowest energy groups is comparable with the reactor pulse length. The validity of the approximation has been tested by calculations taking into account the time-dependence of the spectrum and by experiments using spectrum-dependent detectors. The spectrum was calculated by the Monte-Carlo method and by time-dependent diffusion theory as a function of time after the insertion of a short pulse of 14-MeV neutrons. The system used for this test was the spherical equivalent of VERA 5A, 5% subcritical, and the source pulse was introduced at the centre. After initial fluctuations during the first microsecond, the Monte Carlo calculation showed a spectrum which was constant for all energy groups above 42 eV and the diffusion theory calculation showed a spectrum which had appreciable time dependence below 10 eV. The pulse was followed for 10 μs in the Monte-Carlo calculation and for 35 μs in the diffusion theory calculation. Experimentally the time dependence was studied by measuring the reactor pulse shape with neutron detectors of different energy sensitivities. The measurements were made in a system

having the same core composition as VERA 7A and 10% subcritical. The source pulse was 2 μs wide. Ratios of count rates as a function of time in the different detectors are listed in Table II.

There is no significant difference between the U^{238} fission counter, the hydrogen-recoil counter and the boron-covered U^{235} fission counter, but the bare and cadmium-covered results show appreciable count-rate increases in the later stages of the pulse. It appears that this effect is caused by neutrons of energy less than 1 eV.

On the basis of these experiments, supported by the calculations described above, we conclude that there is no significant error introduced into the analysis of the time-of-flight results by assuming a time-independent spectrum provided that the reactor pulse shape is taken as that measured with a counter insensitive to neutrons below a few eV. We have used the U^{238} fission chamber result in analysing the VERA results.

4. DERIVATION OF THE IN-CORE SPECTRUM OF THE CRITICAL SYSTEM

The pulsed time-of-flight technique measures the spectrum in a beam extracted from a subcritical system. This may differ from the spectrum in the critical system because:

(a) The subcritical system contains a 14-MeV neutron source whereas all the neutrons in a critical system arise from fission.

TABLE II

COUNT RATES COMPARED WITH U^{238} FISSION RATE AS A FUNCTION OF TIME AFTER THE SOURCE PULSE
(Normalized to unity at zero time)

Detector / Time after source pulse (μs)	U^{238} fission counter	H recoil counter, detecting protons above 50 keV	U^{235} fission counter	U^{235} fission counter covered with boron having 15% transmission at 1 eV	U^{235} fission counter covered with 0.07 cm of Cd
0	1	1.0	1.0	1.0	1.0
10	1	1.03	1.21	1.11	1.22
20	1	1.06	1.27	1.04	1.25
30	1	1.04	1.36	1.04	1.26
40	1	1.05	1.49	1.04	1.30
50	1	1.05	1.58	1.04	1.35
60	1	0.97	1.62	0.95	1.30

Note: Standard deviations of these ratios range from 0.02 at 10 μs to 0.10 at 60 μs.

(b) The pulsed source will produce higher harmonic modes of neutron flux distribution and these will be associated with different energy spectra because leakage rates vary with harmonic content and with energy.

(c) The spectrum of the fundamental mode distribution in a subcritical system will differ from that in the critical system because of the higher leakage rate in the former.

We have accumulated some experimental evidence from which the importance of these effects can be judged. The change in the U^{238}-U^{235} fission cross-section ratio produced by changing from a self-sustaining critical to subcritical systems containing a 14-MeV source has been measured in VERA 7A in the counter hole position A shown in Fig. 3. In two subcritical systems at $5\frac{1}{2}$% and 11% subcritical the U^{238}-U^{235} fission ratio was found, in each case, to be 0.91 of its value in the critical system. However in VERA 11A the U^{238}-U^{235} fission cross-section ratio measured in a 5% subcritical system agreed to within 0.5% with the value measured at the same position in a critical system. The time-of-flight spectra have been measured at different degrees of subcriticality in the two VERA experiments described and discussed later in this paper. The effect of higher harmonic modes generated by the pulsed source has been tested to some extent by measuring the reactor pulse shape in different positions within the core and reflector in both experiments. There is no evidence of any spatial variation of the decay constant and from this we conclude that harmonic effects are not important.

Given that the beam spectrum is representative of the spectrum in the critical system, it remains to normalize the scale of measurements to correspond with measurements made in the critical system using other techniques. The complete reactor spectrum in VERA assemblies is covered in three energy ranges by the three techniques: Photo-emulsion, hydrogen-filled proportional counter, time-of-flight spectrometry. It is possible to normalize these to coincide in the overlapping regions of the energy range, but it is desirable to check this procedure by obtaining each measurement in absolute terms if possible. This is straightforward for the proton-recoil methods but requires a two-stage normalization for the time-of-flight results. First, the ratio of core centre flux in the subcritical system, ϕ_{CS}, to beam flux at the detector at the same reactor power, ϕ_{BS}, is determined by installing U^{235} fission counters at these two positions. We thus obtain a constant

$$R = \frac{\phi_{CS}(E)}{\phi_{BS}(E)}$$

which is dependent on geometry but independent of energy. Next the time-of-flight spectrum is measured in the extracted beam for the subcritical system,

$$\phi_{BS}(T_0 F) = \frac{C(E)}{\eta(E)}$$

where C(E) is the detector count rate and $\eta(E)$ its efficiency. At the same time as this experiment is done the subcritical spectrum at the reactor

centre in the energy range adjacent to that covered by the time-of-flight technique is measured by a hydrogen proportional counter. We denote this as ϕ_{CS} (proportional counter). The core centre spectrum corresponding to the region of the time-of-flight measurement is then determined as

$$\phi_{CS}(T_0F) = R\phi_{BS}(T_0F)$$

and $\phi_{CS}(T_0F)$ is then directly comparable with ϕ_{CS} (proportional counter). Since calculation shows that the ratio of flux in the proportional counter region (up to 100 keV) to the flux in the time-of-flight region is the same for the critical and subcritical systems, a proportional counter measurement in the critical system provides the ratio required to normalize the time-of-flight result to the critical reactor equivalent.

5. DETERMINATION OF DETECTOR EFFICIENCY

The detector consists of an array of seven Li^6-loaded glass scintillators mounted inside the flight tube. Each scintillator is 6.3 cm diameter by 2.5 cm thick and contains about 12 g of Li^6. The overall array diameter is 23 cm. The efficiency of this detector as a function of energy has been calculated using a Monte-Carlo programme in which the array was simplified to a single cylinder 30 cm diameter and 2.5 cm thick. The calculated efficiencies for this arrangement were 7% smaller than those calculated for an infinite plane detector of the same thickness and no variation of this difference with energy was evident. The accuracy of these calculations is within ±2% but the $Li^6(N,\alpha)$ cross-section data used [2] have a 10% uncertainty over most of the relevant energy range and further checks on the detector efficiency are desirable. A possible method which is being tested is to produce an accurately known neutron spectrum over the relevant energy range by mounting a simple polythene sphere around a 14-MeV neutron source. The emergent spectrum can be accurately calculated and the nuclear data for hydrogen and carbon are well-known. A comparison of calculated and measured count rates in the Li detector could therefore be used to determine the detector efficiency more accurately.

6. TIME-OF-FLIGHT MEASUREMENTS ON VERA REACTOR ASSEMBLIES

Measurements of spectra have been made on the fast reactor assemblies VERA 7A and VERA 11A. The detailed compositions and dimensions of these assemblies are listed in Table III. Assembly 7A is fuelled with uranium at an effective enrichment of 30%, together with some graphite and polythene to enhance the neutron flux in the low energy regions. The flux distribution is similar to that expected in a large fast reactor of the type now being designed for electricity generation. Assembly 11A is fuelled with plutonium and has a considerably harder spectrum than Assembly 7A. The experimental core arrangements are shown in Figs. 3 and 4. The pulsed source conditions were: pulse width, 2 μs; source strength, 10^{12} n/s during the pulse; pulse repetition rate, 500 s^{-1}. Measurements were made for VERA 7A at $K_e = 0.945$

TABLE III

SIZE AND COMPOSITION OF VERA REACTOR ASSEMBLIES

Assembly number	Composition of core (atoms/cm^3 × 10^{-22})										Core dimensions		Critical mass (kg U^{235} or Pu^{239})
	U^{235}	U^{238} (including U^{234} and U^{236})	Pu^{239} (including 0.4% of Pu^{241})	Pu^{240}	Cu (including solder, etc.)	Fe	Cr	Ni	C	H	Height H (in)	Diam. of equal cross-section cylinder D (in)	
5A	0.6605	0.0504	-	-	-	0.628	0.164	0.0688	5.461	0.655	11.2	12.6	58.5
7A	0.568	1.223	-	-	-	0.628	0.164	0.0688	3.580	0.575	13.2	14.3	75.5
11A	-	-	0.724	0.037	0.796	0.607	0.158	0.0665	4.606	-	8.56	10.61	33.1

Note: The reflector in all cases is a cylinder of overall height of 41 in and overall diameter of 46 in with effective composition as follows:

Element	Atoms/cm^3 × 10^{-22}
U^{235}	0.025
U^{238}	3.44
Fe	0.646
Cr	0.168
Ni	0.071

and $K_e = 0.89$ (8 dollars and 16 dollars subcritical, respectively) and for VERA 11A at $K_e = 0.97$ and $K_e = 0.95$ (10 dollars and 17 dollars subcritical respectively).

For VERA 7A the observed time-distributions are shown in Figs. 6 and 7 and the deduced spectra in Fig. 8. For VERA 11A the observed time-distributions are shown in Figs. 9 and 10 and the deduced spectra in Fig. 11. Comparisons with calculation are shown in Fig. 5.

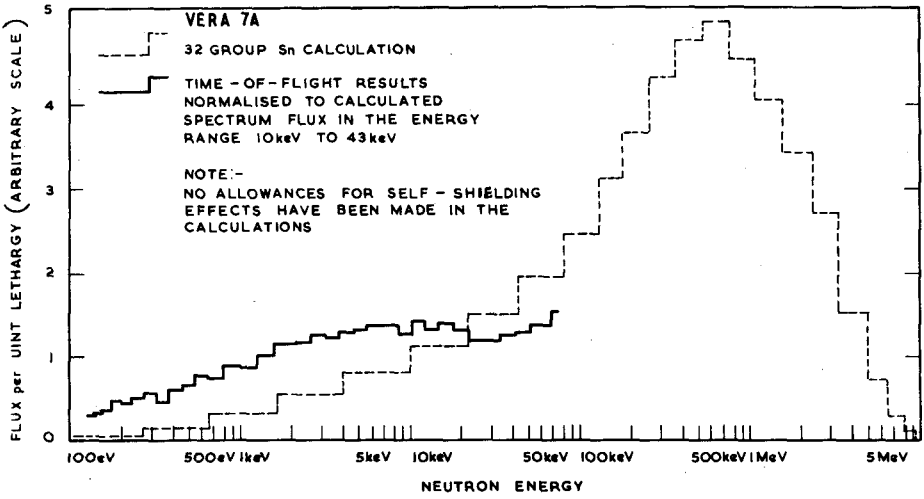
7. DISCUSSION

The results obtained on the VERA reactor indicate that time-of-flight spectrometry can be developed into a reliable and accurate technique in fast reactor physics. The spectral index measurements and the fact that the spectrum is not affected by changing the beam hole size provide some evidence that the extracted beam spectrum is characteristic of that in the reactor core. There is also theoretical and experimental evidence that spectrum time-dependence is not a serious problem. There is some experimental evidence that the spectrum is not very dependent on the degree of subcriticality and for the energy range below 100 keV, this is supported by theoretical studies but further work is necessary to establish a relation between the spectra in the critical and subcritical systems. Further work is also necessary to study heterogeneity effects and to establish the results on an absolute scale in relation to equivalent reactor power.

Comparison of the present results with calculation indicate that the calculated spectra contain relatively too few neutrons in the low energy groups.

ACKNOWLEDGEMENTS

We are indebted to Mr. J. B. Parker for time-dependent spectrum Monte-Carlo calculations and for calculations of the detector efficiency, to Dr. A. Brickstock for time-dependent diffusion calculations, and to Mr. E.D. Pendlebury for Carlson calculations of spectra in critical and subcritical systems. Acknowledgment is also due to members of the VERA reactor experimental and operating teams for the experimental work.



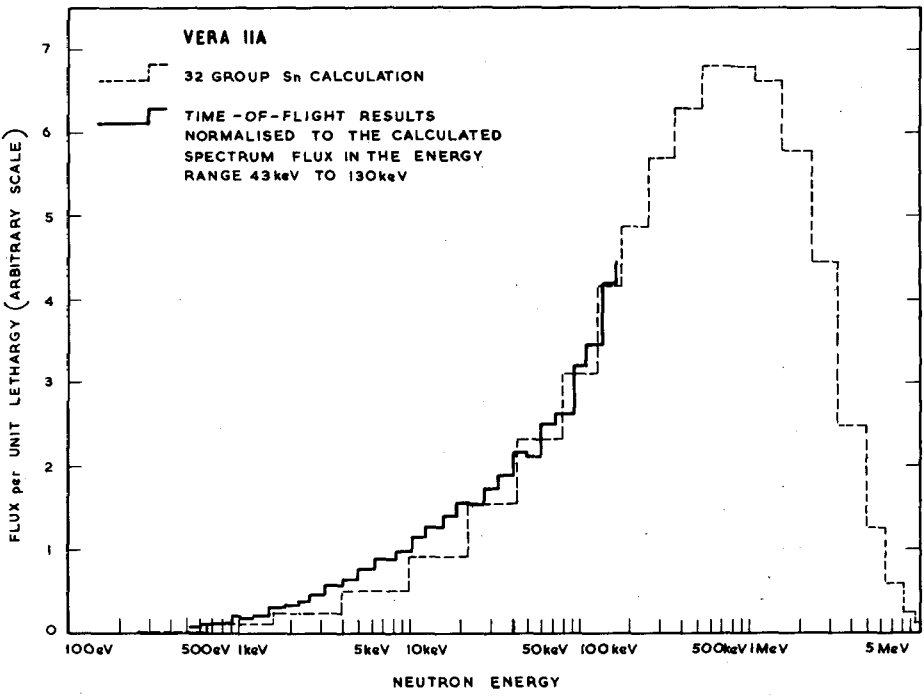


Fig. 5

Comparison of calculated core centre spectra for VERA 7A and 11A critical assemblies with spectra measured by time-of-flight

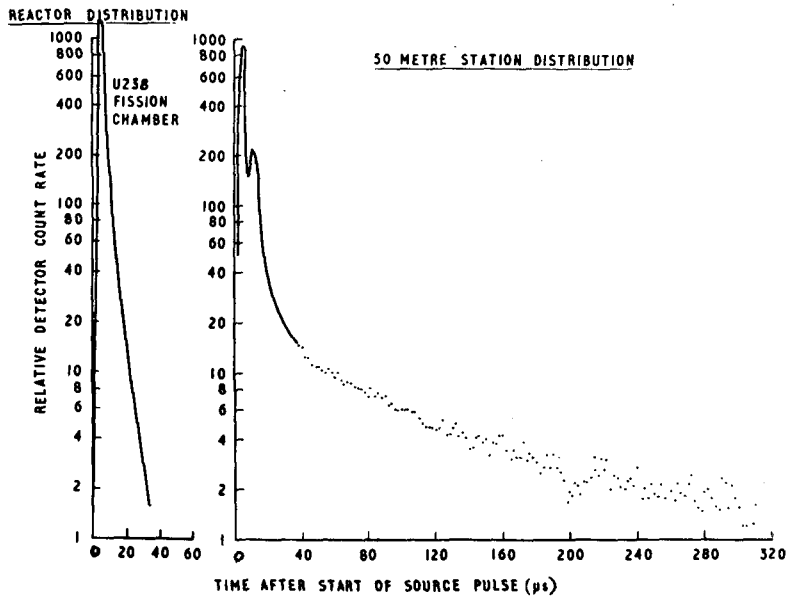


Fig. 6

Neutron time distributions for VERA 7A
(11% subcritical)

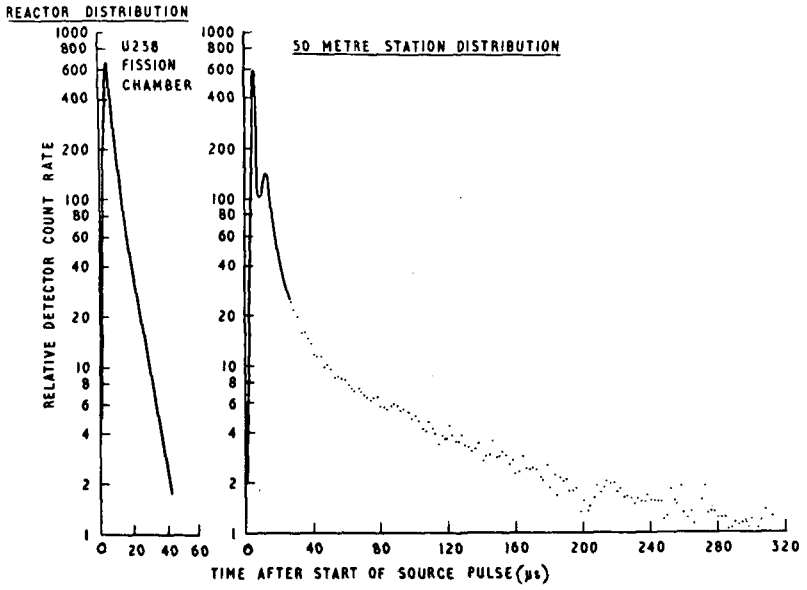


Fig. 7

Neutron time distributions for VERA 7A
(5.5% subcritical)

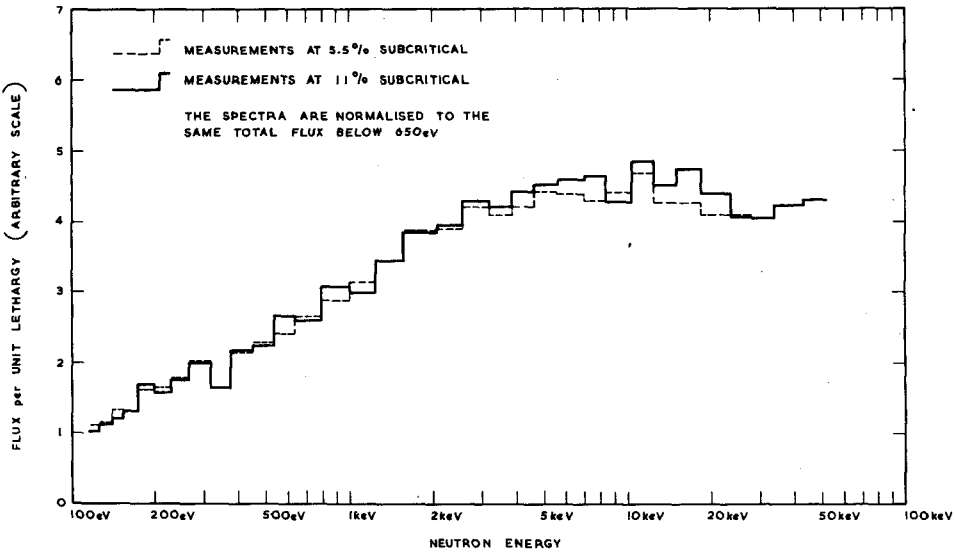


Fig. 8

Neutron energy spectra deduced from measurements on VERA 7A

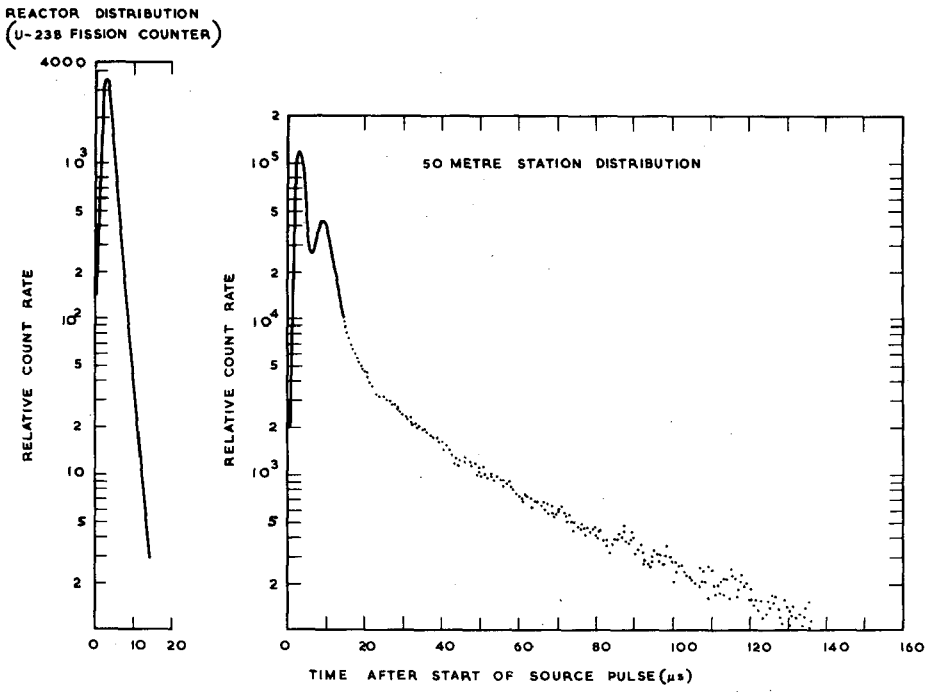


Fig. 9

Neutron time distributions for VERA 11A
(5% subcritical)

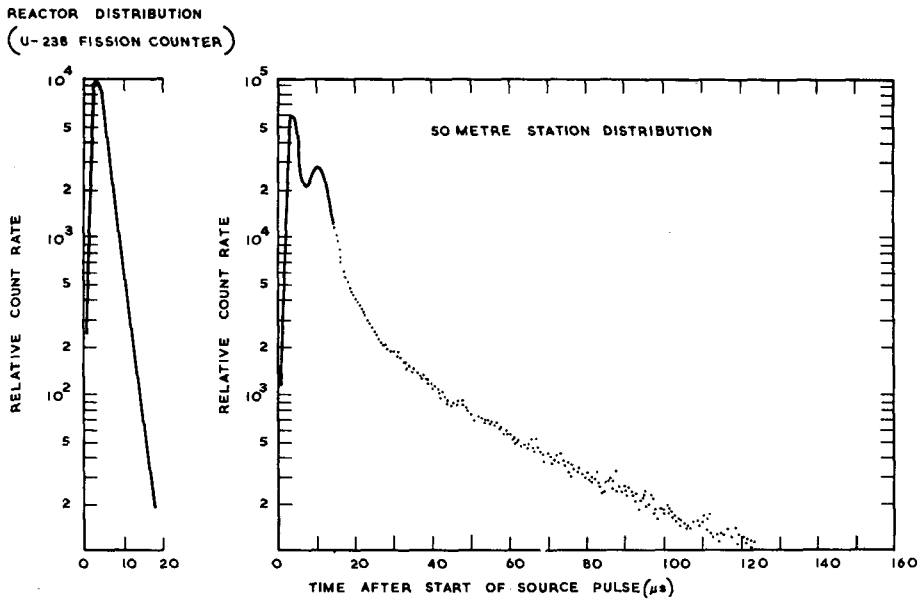


Fig. 10

Neutron time distributions for VERA 11A
(3% subcritical)

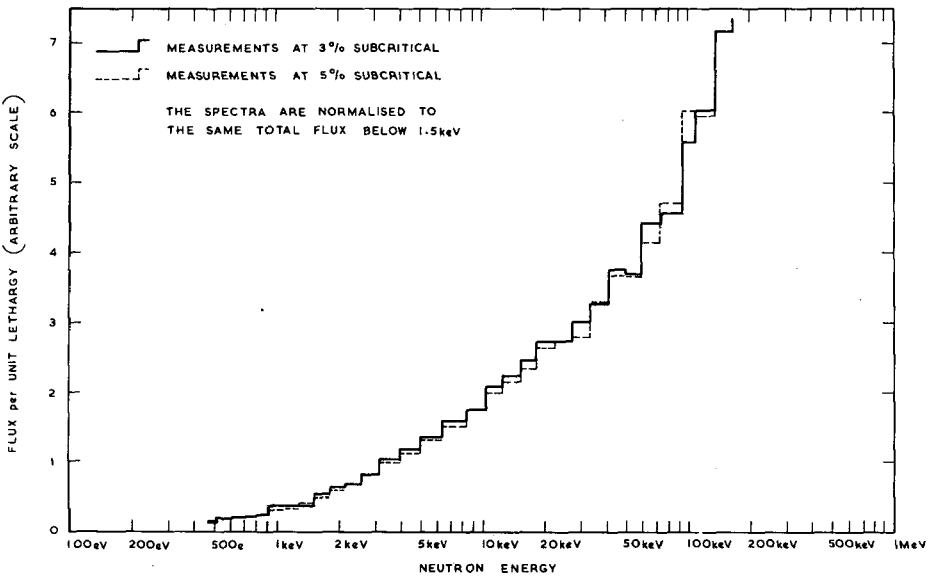


Fig. 11

Neutron energy spectra deduced from measurements on VERA 11A

REFERENCES

[1] WEALE, J.W. et al. "Operating experience with the zero-energy fast reactor VERA", Exponential and Critical Experiments I IAEA, Vienna (1964) 159-93.

[2] PENDLEBURY, E.D., Neutron cross-sections of Li^6 in the energy range 0.001 eV to 15 MeV, Rpt AWRE 0-60/64 (1964).

DISCUSSION

W. KATO: Could you please clarify your statement that the spectrum is independent of subcriticality?

W.J. PATERSON: We have compared U^{238}/U^{235} fission cross-section ratios measured in critical VERA 7A and 11A systems with ratios measured in the same systems at subcritical containing a 14-MeV source. For system 11A the ratios at critical and at 5% subcritical were identical. In a 7% subcritical VERA 7A system the U^{238}/U^{235} fission cross-section ratio was found to be 1.02 times its value in the critical system.

Time-of-flight spectrum results in VERA 7A at $5\frac{1}{2}$ and 11% subcritical have the same shape as do the measurements at 5 and 3% subcritical in VERA 11A.

Thirty-two-group S_n calculations disagree with these fission-ratio measurements and predict a much larger proportion of high-energy flux in the subcritical systems but these calculations predict little change, with reactivity, of the spectrum shape below about 100 keV.

MEASUREMENTS OF FAST NEUTRON SPECTRA IN REACTOR MATERIALS

D. B. GAYTHER AND P. D. GOODE
ATOMIC ENERGY RESEARCH ESTABLISHMENT,
HARWELL, DIDCOT, BERKS.
UNITED KINGDOM

Abstract — Résumé — Аннотация — Resumen

MEASUREMENTS OF FAST NEUTRON SPECTRA IN REACTOR MATERIALS. To test theoretical methods of calculating neutron spectra in fast reactors, a series of measurements of spectra in simple assemblies of pure materials has been made. The Harwell 45-MeV electron Linac produced a pulse of fast neutrons in a natural uranium target which was placed at the centre or on the side of the assembly and the spectrum of neutrons emerging from its surface or from a central re-entrant hole was measured by the time-of-flight technique. A flight path length of 60 m was used and the maximum time resolution was 1 ns/m. The spectrum measurements covered the energy range 1 keV to 5 MeV using three types of neutron detector. For energies from 5 keV to 1 MeV a boron plug detector was used which consisted of a thin walled aluminium container packed with B^{10} metal, the γ-rays from the $B^{10}(n,\alpha\gamma)$ reaction being detected in 4 NaI crystals mounted on photomultipliers. Measurements in the range 0.5 to 5 MeV were made with a plastic scintillator and the low energy region was covered with a Li^6 glass scintillator. To obtain an energy spectrum from the observed time-of-flight, data allowance had to be made for the energy dependence of the efficiencies of the detectors. These were determined by direct comparison with a calibrated long counter using the Harwell 3-MeV pulsed Van de Graaff as a monoenergetic source of neutrons. The experimental method is described and a comparison is given between measured and theoretical spectra.

MESURES DE SPECTRES DE NEUTRONS RAPIDES DANS DES MATÉRIAUX POUR RÉACTEURS. En vue d'éprouver les méthodes de calcul des spectres de neutrons dans des réacteurs à neutrons rapides, les auteurs ont fait une série de mesures de spectres dans des assemblages simples de matériaux purs. A Harwell, l'accélérateur linéaire d'électrons de 45 MeV a envoyé une bouffée de neutrons rapides dans une cible à uranium naturel placée au centre ou sur le côté de l'assemblage et les auteurs ont mesuré le spectre des neutrons émergeant de la surface de l'assemblage ou d'une cavité centrale par la méthode du temps de vol. Ils ont utilisé un canal de 60 m pour le parcours de vol des neutrons, la résolution maximum en temps étant de 1 ns/m. Ils ont mesuré les spectres pour des énergies comprises entre 1 keV et 5 MeV en employant trois types de détecteurs de neutrons. Pour des énergies comprises entre 5 keV et 1 MeV, il s'agissait d'un détecteur au bore qui consistait en une enceinte d'aluminium à parois minces remplie de ^{10}B métallique, les rayons γ de la réaction $^{10}B(n, \alpha\gamma)$ étant décelés dans 4 cristaux de NaI montés sur des photomultiplicateurs. Pour les énergies comprises entre 0,5 et 5 MeV, c'était un scintillateur en matière plastique et pour la bande à faible énergie, un scintillateur en verre au ^6Li. Afin d'obtenir un spectre énergétique en partant des données observées par la méthode du temps de vol, il a fallu tenir compte du fait que l'efficacité des détecteurs varie avec l'énergie. Cette efficacité a été déterminée par comparaison directe avec un compteur long étalonné, le Van de Graaff pulsé de 3 MeV de Harwell servant de source de neutrons monoénergétiques. Les auteurs décrivent la méthode expérimentale et comparent les spectres mesurés et les spectres théoriques.

ИЗМЕРЕНИЯ СПЕКТРОВ БЫСТРЫХ НЕЙТРОНОВ В РЕАКТОРНЫХ МАТЕРИАЛАХ. С целью проверки теоретических методов расчета спектра нейтронов в быстрых реакторах проведена серия измерений спектров в простых сборках чистых материалов. На ускорителе электронов с энергией 45 Мэв в Харуэлле получали импульс быстрых нейтронов в мишени из природного урана, которая была помещена в центре или в боковой части сборки, и спектр нейтронов, вылетающих с ее поверхности или из центрального канала вторичного попадания, измеряли методом по времени пролета. Использовали траекторию полета длиной 60 м, и максимальная разрешающая способность во времени составляла 1 наносекунду/м. Измерения спектра охватывали диапазон энергии 1 кэв–5 Мэв с использованием нейтронного детектора трех типов. В диапазоне энергии 5 кэв–1 Мэв использовался детектор с

пробкой из бора, который состоял из алюминиевого контейнера с тонкими стенками, наполненного металлическим бором-10, при этом γ-лучи, испускаемые в результате осуществления реакции бор-10 (n,αγ), обнаруживались в четырех кристаллах NaJ, смонтированных на фотоумножителях. Были проведены измерения в диапазоне 0,5–5 Мэв с помощью пластического сцинтиллятора, а область низкой энергии была охвачена с помощью стеклянного сцинтиллятора с литием-6. Чтобы получить спектр энергии на основании данных, составленных методом по времени пролета, нужно было допустить наличие зависимости энергии от эффективности детекторов. Такая зависимость определялась путем непосредственного сравнения с калиброванным "длинным счетчиком" с использованием в качестве источника моноэнергетических нейтронов ускорителя импульсных частиц Ван де Граафа с энергией 3 Мэв в Харуэлле.

Описывается экспериментальный метод, сравниваются измеренный и теоретический спектры.

MEDICION DE ESPECTROS DE NEUTRONES RAPIDOS EN MATERIALES PARA REACTORES. Con el propósito de comprobar la validez de los métodos teóricos de cálculo de los espectros neutrónicos en reactores rápidos, los autores han realizado una serie de mediciones de espectros en conjuntos sencillos de materiales puros. Para ello utilizaron el acelerador lineal (LINAC) de 45 MeV de Harwell, produciendo impulsos de neutrones rápidos dirigidos contra un blanco de uranio situado en el centro o en uno de los costados del conjunto, y midiendo por el método del tiempo de vuelo el espectro de los neutrones que emergían de su superficie o de un orificio reentrante situado en el centro. Se utilizó una trayectoria de vuelo de 60 m de longitud, siendo la resolución máxima de 1 ns/m. Las mediciones de los espectros abarcaron el intervalo de energías de 1 keV a 5 MeV, empleándose tres tipos de detectores neutrónicos. Para las energías comprendidas entre 5 keV y 1 MeV se recurrió a un detector con tapón de boro, consistente en un recipiente de aluminio de paredes delgadas lleno de ^{10}B; se detectaron los rayos γ de la reacción $^{10}B(n,\alpha\gamma)$ mediante 4 cristales de NaI acoplados a fotomultiplicadores. Las mediciones en el intervalo de 0, 5 MeV a 5 MeV se realizaron con un centelleador de plástico, y para la región de las energías bajas, se utilizó un centelleador de vidrio de ^{6}Li. A fin de obtener un espectro energético correcto partiendo de los datos del tiempo de vuelo observados, fue preciso tener en cuenta la variación del rendimiento de los detectores en función de la energía. Estos rendimientos se determinaron por comparación directa con las indicaciones de un contador «largo» calibrado, empleándose el acelerador Van de Graaff de 3 MeV, de Harwell, como fuente de neutrones monoenergéticos pulsados. Los autores describen el método experimental empleado, y comparan los espectros medidos con los teóricos.

1. INTRODUCTION

The fundamental requirements for the calculation of the properties of a fast reactor are a knowledge of the space-dependent neutron spectrum in the reactor together with the basic nuclear data of its constituent materials. A difficulty in the calculation or measurement of fast neutron spectra is the wide energy range involved. Thus in a small core the mean energy at which neutrons produce fission may be in the region of 600 keV, whereas in the large dilute systems now being considered the mean fission energy is reduced by inelastic scattering to around 200 keV. Properties such as critical size and reaction rates are largely determined by neutrons in this energy region, and can be measured readily with zero power subcritical assemblies. The Doppler temperature coefficient of reactivity, however, is mainly determined by the small population of neutrons with energies below 10 keV. Calculation of the neutron spectrum usually involves solution of the Boltzmann equation by the multigroup method. An alternative is the Monte Carlo method in which the physical situation is correctly represented, but the statistical accuracy of the solution may be severely limited by the available computer time. In the multigroup method, even with modern large computers, the physical situation must be simplified considerably. However, there is in principle no limit to the accuracy of solution. The most usual simplification is to

work with a limited number of energy groups and to use the nuclear data in the form of "group-averaged" cross-sections. This procedure presents little difficulty at the higher energies where most cross-sections and spectra vary smoothly with energy, but at lower energies, resonances in the cross-sections produce fine structure in the neutron flux. This situation is usually represented by a slowly varying spectrum combined with "self-shielded" cross-sections to account for flux dips caused by resonances.

The above considerations show that to test the methods of calculation it is important to determine experimentally (i) the exact normalization of the low energy region of the spectrum to that at high energies, and (ii) the fine structure at low energies. Existing techniques for measuring fast spectra based on proton recoil or particle reactions are capable of only poor energy resolution at energies less than (50-100) keV. The present measurements utilized the time-of-flight method which is in principle capable of high resolution over the complete spectrum. In this method a pulsed source is used to excite an assembly and the spectrum of neutrons emerging from a re-entrant hole or from the surface is determined. The measurements described in this paper are confined to blocks of pure material in simple geometry so that direct comparisons can be made to test the numerical methods and nuclear data used in calculating spectra. The results of preliminary measurements in natural uranium and sodium are presented.

2. EXPERIMENTAL METHOD

2.1. General arrangement

Figure 1 shows the general experimental arrangement used for the time-of-flight measurements and Fig. 2 shows the geometrical configuration used in the measurements on natural uranium and sodium. The source of neutrons

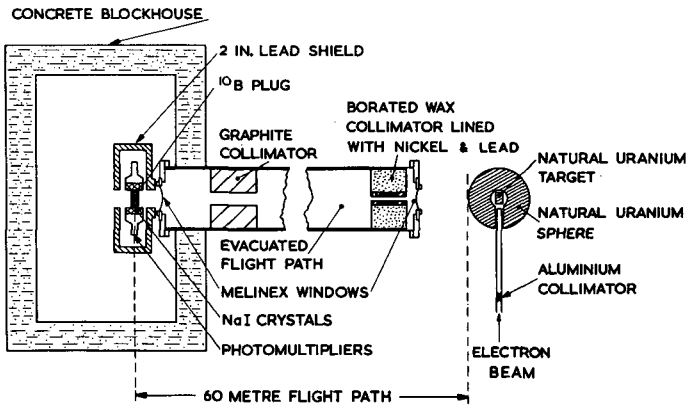


Fig. 1

General experimental arrangement

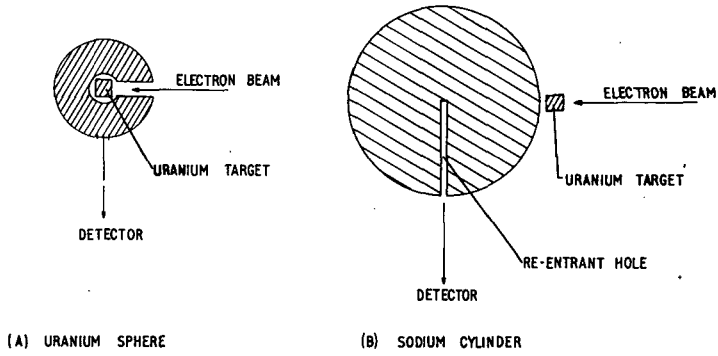


Fig. 2

Schematic arrangement for fast spectrum measurements

consisted of a small natural uranium target which was bombarded with the pulsed electron beam from the Harwell 45-MeV linear accelerator, bremsstrahlung in the target producing a fast neutron pulse from photo-fission and photonuclear reactions. Electron pulse widths of 60 ns to 1 μs were used at a maximum repetition rate of 192 pulses/s. In the natural uranium measurements the target was placed in a 9-cm diameter cavity at the centre of a 32-cm diameter sphere of the material and the leakage spectrum was measured emerging from a 5-cm diameter region on the surface of the sphere. A water-cooled aluminium collimator located in the electron drift tube confined neutron production to the target. The sodium measurements utilized a thin-walled steel tank 1 m in diameter and 1 m high filled with pure sodium; the target was placed centrally on the side of the tank and the spectrum was measured emerging from the centre of the tank through a re-entrant hole of cross-section 7.3 cm × 2.2 cm. In both measurements the neutron beam was perpendicular to the incident electron beam. The neutron beam was defined by two collimators, one of borated wax lined with lead and nickel placed near to the assembly and one of graphite located in the flight tube 3 m from the detector. The evacuated flight tube was 60 m in length and had two Melinex windows each 0.005 in thick. To minimize external background, the target cell was surrounded by 6 ft of concrete and the detector was situated in a concrete blockhouse of 2 ft wall thickness. The detector was further contained in a 2 in lead shield surrounded by a 4 in thick borated wax shield, entrance and exit holes in the detector shield allowing the neutron beam to pass through without scattering. The flight tube contained several irises with slightly larger apertures than the neutron beam to reduce the effect of scattering from the tube walls.

2.2. Neutron detectors

The requirements of a detector for fast neutron time-of-flight spectrometry are that it should have a useful and known efficiency over a wide energy range, that the efficiency should not fluctuate rapidly with energy, that it

should have a high time resolution and that it should not be affected adversely by the intense γ-flash from the target. No single detector has been found which will satisfy these criteria over the required energy range of 100 eV to 10 MeV, and three separate detectors were used whose useful energy ranges overlapped.

2.2.1. The B^{10} plug detector [1]

This is illustrated in Fig. 1, and consists of a thin-walled aluminium can 12.5 cm diameter and 4.5 cm thick packed with B^{10} metal to a density of 1.4 g/cm^3. The 480-keV γ-rays from the $B^{10}(n,\alpha\gamma)Li^7$ reaction are detected in four NaI crystals mounted on photomultipliers and located out of the neutron beam. This detector covers the energy range from about 5 keV to 1 MeV and was used for the majority of the measurements. The high energy limitation is caused by the difficulty in determining accurately the detector efficiency in the region of the resonance in the $(n,\alpha\gamma)$ cross-section at 1.9 MeV. The low energy limit depends on the particular spectrum being studied and is given by the region in which the cosmic ray background rate in the detector becomes comparable with the rate of detection of spectrum neutrons. To reduce the background rate the photomultiplier outputs were passed through a window discriminator of 20% width set to detect the 480-keV γ-ray. The window discriminator was calibrated with the 660-keV γ-rays from a Cs^{137} source.

2.2.2. The plastic detector

In this detector, the back face of a 12.5-cm diameter and 2.5-cm thick plastic disc (NATON 136) is connected by a short light pipe to two EMI 6097A photomultipliers. The outputs of the photomultipliers after amplification were taken through fast discriminators and then recorded in coincidence with a resolving time of 8 ns. The use of a coincidence technique and the selection of photomultipliers with high cathode sensitivities and low dark currents made it possible to use discriminator settings corresponding to the detection of neutrons with a minimum energy of about 35 keV. At this setting the background rate in the detector is due almost entirely to cosmic radiation. For neutron energies greater than the minimum, the detector efficiency shows an initial rapid rise, and to avoid any dependence of efficiency on slight electronic drifts recorded events below 200 keV were rejected. To minimize the paralysis time resulting from the detection of the target γ-flash, it was found necessary to use amplifiers with good overload characteristics and use double delay line pulse shaping. At 60 m the intensity of the γ-flash limits the use of this detector to a maximum energy of (5-10) MeV. The discriminator settings were calibrated with the 60-keV γ-rays from an Am^{241} source.

2.2.3. The Li^6 glass detector

This consists of an 11-cm diameter and 1.27-cm thick glass disc loaded with Li^6 (NE 905) and coupled with a short light pipe to a 5-in photomultiplier.

The output of the photomultiplier was passed through a window discriminator of 30% width, the setting of which was determined with a thermal neutron source. This detector in comparison with the B^{10} plug detector gave an improved ratio of counts-to-backgound at neutron energies less than 10 keV.

2.3. Data recording

The flight times of detected neutrons were recorded on a 4096 channel magnetic tape recorder with a channel width of either 1/16, 1/4 or 1/2 μs. The steady background present at long flight times when all the direct spectrum neutrons had died away was continuously monitored in a 100 μs gate. The target intensity was also continuously monitored with a small U^{235} fission chamber surrounded by Polythene, the events being recorded in a 100-μs gate delayed 200 μs from the neutron burst.

3. REDUCTION OF THE DATA

3.1. Corrections to be applied

The true energy spectrum is obtained from the observed time spectrum after the background has been subtracted and the appropriate factor applied for the energy dependence of the detector efficiency. A small correction is necessary to allow for the energy-dependent transmission of the two Melinex flight tube windows and a short path length in air. In addition, the observed flight times must be reduced by an amount given by the mean time after the initial burst at which neutrons of a particular energy emerge from the assembly. The actual distribution of slowing-down times to a particular energy may also affect the available resolution of the measurement. The correction for the mean slowing-down time can be measured by placing thin samples in the beam and observing the flight times at neutron resonances of accurately known energies. In the present spectrum measurements this effect was found to be small and was neglected. A choice of samples with narrow resonances and known parameters would also allow an estimate of the slowing-down time resolution to be obtained from the observed line shapes.

3.2. The measurement of background

The time-of-flight background was found to consist of a constant component mainly from cosmic rays, together with a component which decayed with time after the neutron burst. The steady component was monitored in the background gate which was delayed sufficiently to allow the time-dependent component to die away completely. The magnitude of the time-dependent component was estimated by placing samples in the beam and examining the counting rates in the troughs of "black" resonances. This technique could not be used at high energies because insufficient resolution was available and it was necessary to extrapolate the background from low energies. In both spectrum measurements the background at high energies was small, and negligible errors should be introduced in the extrapolation. In the uranium sphere measurements the total background at 1 MeV was 0.2% of the true

counts, 0.3% at 100 keV and 6% at 10 keV. In the sodium measurements the corresponding figures were 10% background at 1 MeV, 8% at 100 keV and 33% at 10 keV. The accuracy of the background determination was checked by measuring with the beam spectrum the transmissions of samples of U^{238} and carbon. The transmissions of the samples were measured accurately using the 300-m flight path total cross-section facility and bolster target of the 45-MeV linear accelerator.

3.3. The calibration of the detectors

The energy dependence of detector efficiency was measured for the B^{10} plug and the plastic detector using the pulsed Van de Graaff accelerator IBIS as a monoenergetic source of neutrons in the energy range 10 keV to 2 MeV. Events from the direct detection of neutrons were separated from background by time-of-flight analysis. The efficiency was determined by direct comparison with a calibrated Hanson-McKibben long counter. The efficiency of the long counter was known to an accuracy of about ± 3% from 20 keV to 2 MeV, and was itself calibrated against the proton recoils observed in a hydrogen-filled proportional counter. The relative efficiency curve for each counter is shown in Fig. 3; the efficiencies of the two detectors are not normalized. The boron plug measurements were unreliable below 25 keV because of high background, and the broken part of the curve is the result of a calculation which has been normalized to the measured curve in the region (25-50) keV. The plastic detector had discriminator settings corresponding

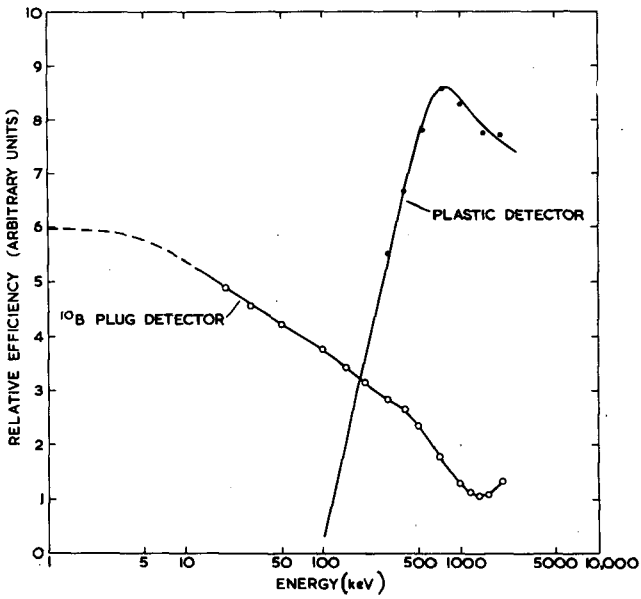


Fig. 3

Detector efficiencies

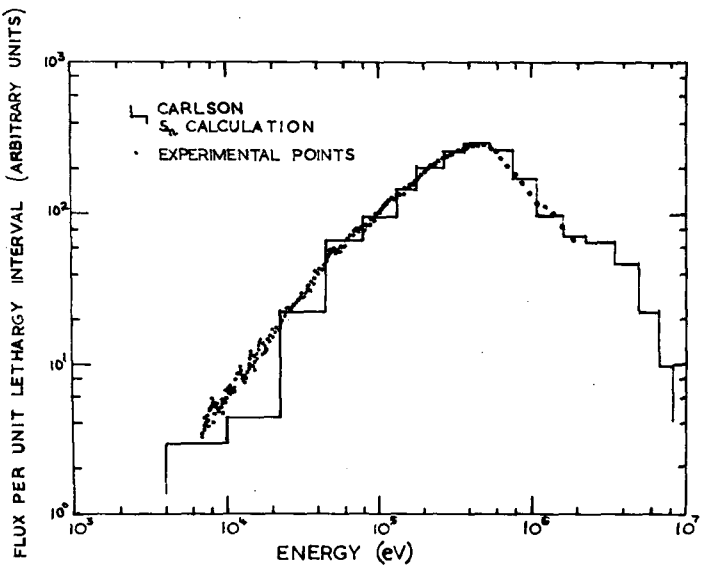
to the detection of neutrons with energies greater than about 100 keV. The time resolution of each detector was estimated from the width at half height of a γ-ray line in the time spectrum; this was 25 ns for the B^{10} plug and less than 10 ns for the plastic detector.

4. THE MEASURED SPECTRA

Figure 4 shows the measured leakage spectrum from the natural uranium sphere in comparison with a calculation [2] of the spectrum using the Carlson S_n method of solving the transport equation. The calculation was made with an IBM 7030 programme called STRAINT [3] and used the AWRE 32 group nuclear data set [4, 5]. A point isotropic fission source was assumed to be at the centre of the sphere. It can be seen that while at energies greater than 50 keV there is good agreement between the calculated and the observed spectrum, at lower energies fewer neutrons are predicted than observed.

A rigorous comparison of calculated and measured spectra will involve a knowledge of the true target neutron spectrum including its angular dependence. Preliminary measurements indicate that the target spectrum is in fact softer than the assumed fission spectrum and that, at least at the higher energies, the angular distribution is anisotropic. Further calculations have shown that the sphere leakage spectrum is not very sensitive to the source spectrum.

Figure 5 shows the measured spectrum emerging from the centre of the sodium tank. Fine structure caused by the sodium resonances can be clearly seen, the remaining structure being attributed to the presence of some iron in the beam.



6.5 1650

Fig. 4

Leakage spectrum from a natural uranium sphere

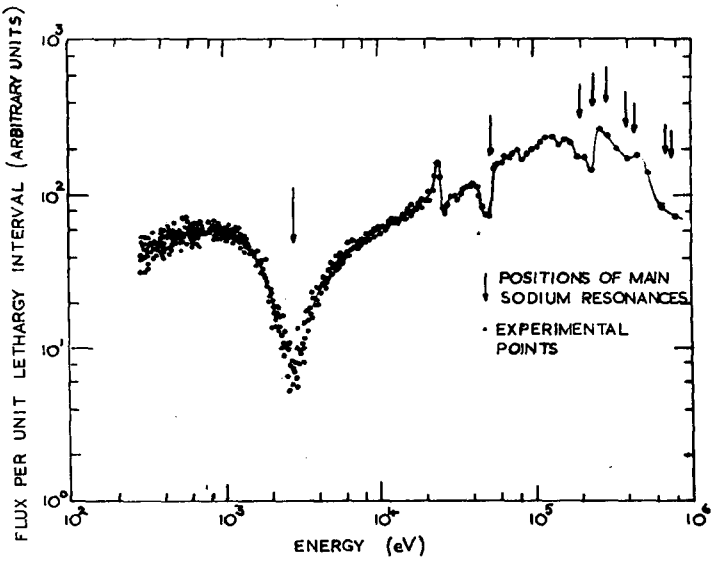


Fig. 5

Spectrum at the centre of a sodium cylinder

ACKNOWLEDGEMENTS

The authors wish to thank Dr. M. J. Poole for his advice and encouragement throughout the course of these measurements, Mr. R. H. Jones for considerable assistance with numerical analysis and Mr. G. B. Dean for help with the electronics. The detector sensitivities were measured in collaboration with Dr. M. S. Coates and Mr. D. J. Tripp. The Carlson S_n calculation was provided by Mr. E. D. Pendlebury of AWRE. The co-operation of the operating staffs of the linear accelerator and IBIS is gratefully acknowledged.

REFERENCES

[1] RAE, E. R. and BOWEY, E. M., Proc. phys. Soc. 66A (1953) 1073.
[2] PENDLEBURY, E. D., private communication.
[3] WADE, R. D., AWRE Rpt. 0-12/63 (1963).
[4] PARKER, K., AWRE Rpt. 0-82/63 (1963).
[5] PARKER, K., AWRE Rpt. 0-79/63 (1964).

DISCUSSION

J. SHERWIN: In the derivation of the group-averaged data for the STRAINT calculations, did the spectrum used in finding the averages differ considerably from that measured?

D. GAYTHER: The weighting spectrum used was constant on a lethargy scale.

DETERMINATION OF NEUTRON SPECTRA IN BULK MEDIA BY TIME-OF-FLIGHT*

J. L. RUSSELL, Jr., J.R. BEYSTER, J.R. BROWN, K.L. CROSBIE, G.K. HOUGHTON, A.E. PROFIO AND G.D. TRIMBLE
GENERAL ATOMIC DIVISION OF GENERAL DYNAMICS CORPORATION, JOHN JAY HOPKINS LABORATORY FOR PURE AND APPLIED SCIENCE, SAN DIEGO, CALIF., UNITED STATES OF AMERICA

Abstract — Résumé — Аннотация — Resumen

DETERMINATION OF NEUTRON SPECTRA IN BULK MEDIA BY TIME-OF-FLIGHT. The time-of-flight method has recently been applied to the measurement of fast neutron spectra in bulk media to study problems of computing neutron distributions in reactor and shielding geometries. The advent of the high intensity, short pulse electron linear accelerator makes possible the collection of data in reasonable time for high resolution deep penetration experiments.

Several experiments have been completed on geometries designed to be calculable by specific computer codes. Of particular interest is the class of one-dimensional geometries consisting of a central neutron source surrounded by spherical shells of homogeneous media with the outer boundary either spherical or essentially at infinity.

To evaluate the ability to calculate fast neutron spectra in high-A materials, leakage spectra from a few keV to a few MeV were measured for a 6-in diameter lead sphere with a central (γ-n) neutron source. Results are compared with multigroup transport theory using cross-sections obtained by normalizing statistical theory with cross-section data. Spectra were also obtained at the lead-graphite interface for the above sphere encased in a 5-in thick, spherical, graphite shell. As expected, comparison of theory with experiment indicates that slowing down by low-A media is much better understood than slowing down by high-A media.

The deep penetration problem, e.g. neutron shielding calculations, imposes extreme demands on computational methods both on accuracy required for input cross-sections, and on computational detail required to describe large attenuations. To study this problem, spectra were measured from 0.5 to 14 MeV for a point source, essentially infinite medium of paraffin. Measurements were made at several angles and radii out to 45-cm penetration. Results are compared with multigroup transport theory. Measurements have also been performed on a two-dimensional experiment (cylindrical medium, point source on axis) on the spectrum of deep-penetration neutrons in liquid hydrogen. This paper concludes with a discussion of some of the strengths and weaknesses of methods used to compute neutron spectra in bulk media as indicated by these experiments.

DÉTERMINATION DES SPECTRES DE NEUTRONS PAR LA MÉTHODE DU TEMPS DE VOL DANS DES MILIEUX DE GRANDES DIMENSIONS. La méthode du temps de vol a été appliquée récemment à la mesure des spectres de neutrons rapides dans des milieux de grandes dimensions, en vue d'étudier les problèmes de calcul de la distribution des neutrons dans les géométries de réacteurs et de protections. L'apparition de l'accélérateur linéaire d'électrons, à brèves impulsions et de haute énergie, a permis de recueillir des données en un temps raisonnable pour des expériences de pénétration en profondeur avec un bon pouvoir de résolution.

Les auteurs ont fait plusieurs expériences sur des géométries conçues pour pouvoir être calculées électroniquement au moyen de codes déterminés. Une classe particulièrement intéressante est celle des géométries à une dimension qui se compose d'une source centrale de neutrons entourés d'enveloppes sphériques de milieux homogènes, la frontière étant soit sphérique soit virtuellement à l'infini.

Afin de juger s'il serait possible de calculer des spectres de neutrons rapides dans des matières de numéro atomique élevé, les auteurs ont mesuré les spectres de fuite compris entre quelques keV et quelques MeV pour une sphère de plomb de 15,3 centimètres de diamètre et avec une source de neutrons centrale (γ-n). Ils confrontent les résultats avec ceux de la théorie du transport à plusierus groupes, les sections efficaces utilisées étant obtenues par un ajustement de la théorie statistique aux données relatives aux sections efficaces. Ils

* Work performed under the auspices of the United States Atomic Energy Commission, Contract No. AT(04-3)-167, Project Agreement No. 2

ont également obtenu des spectres à l'interface plomb-graphite pour la sphère ci-dessus, enfermée dans une enveloppe sphérique en graphite de 12,7 cm d'épaisseur. Comme prévu, une comparaison entre la théorie et l'expérience montre que le ralentissement dans des milieux de numéro atomique faible est beaucoup mieux compris que le ralentissement dans un milieu de numéro atomique élevé.

Pour la solution du problème de la pénétration en profondeur, par exemple dans les calculs de protection contre les neutrons, on est amené à se montrer extrêmement exigeant vis-à-vis des méthodes de calcul tant en ce qui concerne la précision nécessaire pour les sections efficaces considérées comme entrées, que le caractère détaillé des calculs qui est requis pour décrire les fortes atténuations. Pour étudier ce problème, les auteurs ont mesuré des spectres compris entre 0,5 MeV et 14 MeV, dans le cas d'une source ponctuelle et d'un milieu de paraffine virtuellement infini. Ils ont fait ces mesures pour des angles divers et des rayons allant jusqu'à 45 cm de profondeur. Les résultats sont confrontés avec ceux de la théorie du transport à plusieurs groupes. Des mesures ont été faites aussi dans une géométrie à deux dimensions (milieu cylindrique, source ponctuelle sur un axe), l'expérience portant sur le spectre de neutrons à pénétration profonde dans de l'hydrogène liquide. Les auteurs discutent des avantages et des faiblesses des méthodes utilisées pour calculer les spectres de neutrons dans des milieux à grandes dimensions tels qu'ils apparaissent à la lumière de ces expériences.

ОПРЕДЕЛЕНИЕ СПЕКТРОВ НЕЙТРОНОВ В МАССИВНОЙ СРЕДЕ ИЗМЕРЕНИЕМ ВРЕМЕНИ ПРОЛЕТА. Для изучения проблем расчета распределения нейтронов в геометриях реактора и его защиты недавно был применен метод времени пролета к измерению спектров быстрых нейтронов в массивной среде. Появление высоковольтного линейного ускорителя электронов с короткими импульсами дает возможность собирать в ограниченное время и с хорошим разрешением данные для экспериментов по глубокому проникновению.

Проведен целый ряд экспериментов в геометриях, поддающихся расчетам, по определенным кодам на счетно-решающих устройствах. Особый интерес представляет категория одномерных геометрий, состоящих из находящегося в центре источника нейтронов, окруженного сферическими оболочками из гомогенной среды, имеющей внешнюю границу в виде сферы либо бесконечности.

Для оценки возможности подсчета спектров быстрых нейтронов в материалах с большим атомным весом были измерены спектры утечки от нескольких кэв до нескольких Мэв для свинцового шара диаметром 6 дюймов с находящимся в центре источником нейтронов (γ–n). Результаты сравниваются с многогруппной теорией переноса при использовании сечений, полученных путем нормализации статистической теории с данными о сечениях. Были также получены спектры для поверхности раздела между свинцом и графитом для указанной выше сферы, заключенной в шарообразную графитную оболочку толщиной 5 дюймов. Как и следовало ожидать, сравнение теории с экспериментальными данными указывает на то, что замедление средой с малым атомным весом понимается гораздо лучше, чем средой с большим атомным весом.

Проблемы глубокого проникновения, например расчеты защиты от нейтронов, предъявляют чрезвычайно высокие требования к методам расчетов как в отношении требуемой правильности задаваемых сечений, так и в отношении детальности расчета для описания сильных ослаблений нейтронного потока. Для изучения этой проблемы были измерены спектры от 0,5 до 14 мэв для точечного источника в предположительно-бесконечной среде из парафина. Измерения производились под разными углами и по разным расходящимся радиусам вплоть до проникновения на 45 см. Результаты сравниваются с многогрупповой теорией переноса. Проведены также измерения на двухмерном эксперименте (цилиндрическая среда, точечный источник на оси) по определению спектра глубокого проникновения нейтронов в жидком водороде.

В заключение приводится обсуждение некоторых преимуществ и недостатков методов подсчета спектров нейтронов в массивной среде на основании результатов этих экспериментов.

MEDICION DE ESPECTROS NEUTRONICOS EN DIVERSOS MATERIALES POR EL METODO DEL TIEMPO DE VUELO. El método del tiempo de vuelo se ha aplicado recientemente a la medición de los espectros de neutrones rápidos en distintos materiales a fin de estudiar problemas de cálculo de las distribuciones neutrónicas en diversas configuraciones geométricas de reactor y blindaje. El perfeccionamiento del acelerador lineal de elevada intensidad, capaz de producir impulsos neutrónicos breves, permite acopiar un un plazo razonable datos relativos a experimentos de penetración profunda realizados con métodos de elevado poder de resolución.

Les autores han efectuado varios experimentos con geometrías ideadas para que pudiesen ser calculadas con claves de cómputo específicas. Ofrece particular interés el grupo de geometrías monodimensionales, constituidas por una fuente neutrónica central rodeada por capas esféricas de medios homogéneos, con un límite exterior igualmente esférico o bien situado prácticamente en el infinito.

Con el propósito de evaluar la posibilidad de calcular los espectros de neutrones rápidos en materiales de elevado número de masa, se han medido los espectros de escape neutrónico correspondientes a energías comprendidas entre algunos kiloelectronvoltios y algunos megaelectronvoltios, empleando una esfera de plomo de 15, 2 cm de diámetro en cuyo centro se hallaba una fuente neutrónica (γ-n). Los autores comparan los resultados obtenidos con los de la teoría del transporte de varios grupos, empleando secciones eficaces obtenidas por normalización de la teoría estadística sobre la base de los datos de las secciones eficaces. También se obtuvieron espectros en la superficie de separación plomo-grafito en la mencionada esfera rodeada por una capa concéntrica de grafito de 12, 7 cm de espesor. Como era de esperar, la comparación de los valores teóricos con los resultados experimentales pone de manifiesto que el conocimiento de la moderación con medios de bajo número de masa es mucho más completo que el de la moderación con medios de elevado número de masa.

El problema de la penetración profunda, es decir, los cálculos del blindaje contra los neutrones, exige la aplicación de métodos de cálculo muy perfeccionados, tanto por lo que se refiere a la precisión con que se han de indicar las secciones eficaces como respecto del detalle del cálculo que se requiere para describir grandes atenuaciones. Para estudiar este problema, se midieron los espectros correspondientes al intervalo de energías de 0, 5 MeV a 14 MeV, para una fuente puntiforme y un medio prácticamente infinito constituido por parafina. Las mediciones se realizaron con diversos ángulos y radios, para penetraciones de hasta 45 cm. Los autores comparan los resultados obtenidos con los de la teoría de transporte de varios grupos. Los autores también efectuaron mediciones del espectro de los neutrones de gran poder de penetración en hidrógeno líquido, utilizando una geometría bidimensional (medio cilíndirco y fuente puntiforme situada en el eje). Por último, los autores examinan algunas de las ventajas e inconvenientes de los métodos empleados para el cálculo de los espectros neutrónicos en diversos materiales, puestos de manifiesto en esos experimentos.

1. INTRODUCTION

Time-of-flight neutron spectroscopy dates back almost to the discovery of the neutron. But only recently have we begun to use this method to measure fast and intermediate neutron spectra in bulk media with the objective of evaluating and improving methods for calculating neutron spectra in reactors and shields. The advent of very intense, nanosecond-scale pulsed neutron sources has made practical the measurement of deep penetration neutron spectra with good resolution [1].

In the past year at General Atomic, several experiments have been completed in geometries designed to be calculable by specific computer codes. In this paper, some of the results of these experiments are discussed and compared with calculation, the experimental equipment is described, the specific experimental results are presented and compared with calculation, and some tentative conclusions are discussed.

2. EXPERIMENTAL EQUIPMENT

The neutron sources used for these measurements were (γ, n) targets of uranium or lead bombarded with a 30-MeV beam from an electron linear accelerator [2]. The Linac beam conditions used for these experiments ranged from about 0.001 to 2 A beam current, 20 to 50 ns pulse width and typically 360-pulses per second. The neutron source strength ranged from

about 10^6 to 10^{10} neutrons per pulse depending upon the requirements of the experiment [3-5].

To simplify the experimental and calculational geometry, it is highly desirable to have a neutron source which is isotropic in angle of emitted neutrons. It is not clear that target anisotropy can be made arbitrarily small since the basic photoneutron production distribution is anisotropic; the very high energy neutron production appears to be peaked in the forward direction, while the very low energy neutrons may be peaked at 90° to the incident beam. However, we have found, by considerable trial and error, that spheres of depleted uranium metal emit neutrons approximately isotropically when the electron beam impinges on the bottom of a re-entrant hole of proper depth [6]. The bottom of the hole should be two or three radiation lengths short of the centre of the sphere. Further, a 5-cm diameter sphere is probably the minimum size for which a reasonable isotropy may be obtained. The mechanism for smoothing the angular distribution is, of course, multiple scattering.

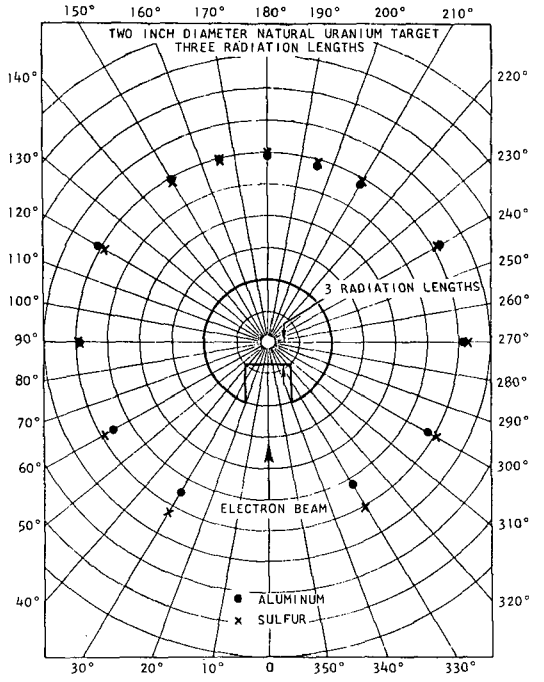


Fig. 1

Sulphur and aluminium activation data, 5 cm diameter natural uranium target

O Aluminium
× Sulphur

Figure 1 is a plot of the angular distribution of neutrons from a 2-in diameter target as measured by aluminium (7-MeV threshold) and sulphur (3-MeV threshold) foils located on a circle of 15-cm radius around the target. In Fig. 2, time-of-flight spectra at two angles are compared and support the results of the foil measurements.

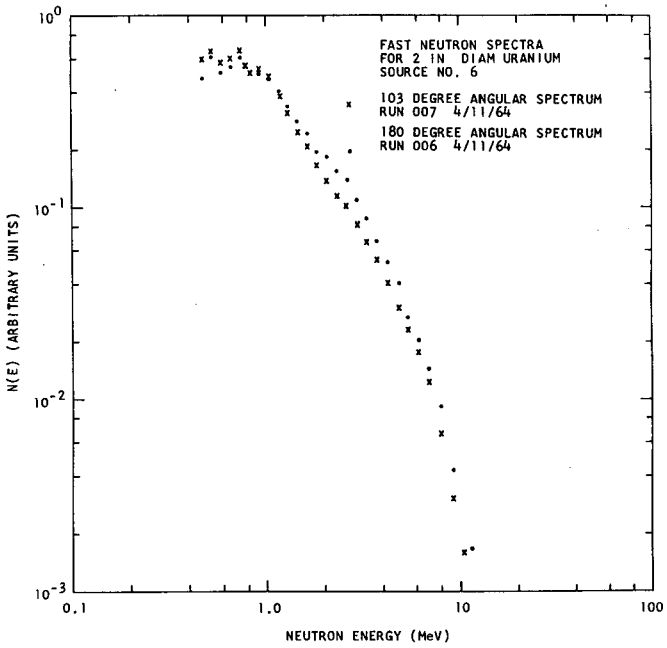


Fig. 2

Neutron time-of-flight spectra from 5 cm diameter natural uranium target

The duration of the neutron source pulse is not now a limitation on the resolution of fast spectrum measurement since such measurements have to date used pulse widths which are longer than the minimum width capability of the Linac [2, 7, 8]. The spatial thickness and slowing-down time of the experimental media place a lower limit on the resolution of the measurement of flight time in large, deep penetration geometries.

Neutrons of a particular energy emerging, after the source pulse, from a large volume of scattering material can have a large uncertainty in residence time [9-11]. This effect is small but non-negligible ($\sim$ 10 ns above 0.5 MeV) in hydrogenous media. However, the effect can become almost intolerably large in some of the high-A elements. As an example in which the moderation time can become very large, consider the spectrum emitted from a large shield of lead. The time in seconds required to slow down by elastic scattering to velocity v below the inelastic scattering threshold (0.8 MeV) is $\sim 1000/v$. (This is a simple measure of the time uncertainty, but under some conditions it would be more appropriate to use variance of the slowing-down time.) The flight time in a 50-m flight path is 5000/v. Hence, the time resolution is $\sim$ 20%, and the energy uncertainty is $\sim$40%. For this example then, a 50-m flight path is too short. Above the inelastic threshold, the inelastic slowing-down results in somewhat improved time resolution. Neutron leakage from small assemblies can also significantly reduce mean emission time. These effects must be evaluated for individual experiments. Monte-Carlo [9, 12] and transport methods [9, 13] are available for accurately describing the effect.

Resolution considerations determine the minimum acceptable flight path length. Neutron source intensity and detector size and efficiency then place a limitation on the maximum depth, or shield attenuation, which may be studied.

The flight path which was used in these experiments is designed to minimize background from neutrons and gamma rays arriving at the detector by paths other than through the appropriate collimators. The 50-m drift tube is made of three evacuated sections of roughly equal length. The pre-collimators at the source end of the flight path are easily changed to meet the requirements of a particular experiment. Figure 3 is a schematic of

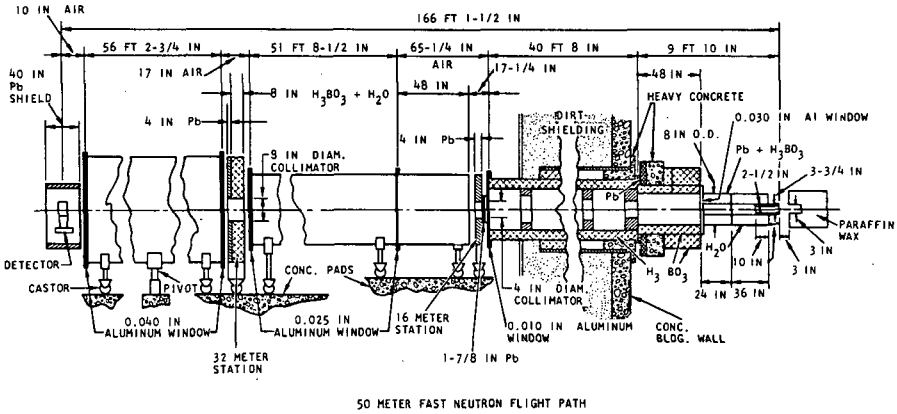


Fig. 3

Collimation system

the geometry of the pre-collimators and flight path used for a paraffin shield experiment discussed later [14].

The vacuum windows on the end of flight path sections were ~0.6 mm aluminium foils. For high energy spectra, or thermal spectra, the total cross-section of aluminium is relatively small and slowly varying with energy. This means that the correction of neutron spectrum for flight path transmission can be made accurately. However, in the intermediate energy region, the numerous aluminium resonances introduce a great deal of extraneous structure to the measured spectrum which is difficult to account for accurately. Recently, to obviate this problem, the aluminium windows were replaced by 0.12 mm Mylar of smaller diameter.

Several detectors have been used in these experiments. At energies above ~0.5 MeV, timing of the arrival of the neutron places a stringent limitation on the type of electronics which may be used for the detector. To perform adequately, the pulse height walk and time jitter should be less than ~10 ns, and it is desirable to have a detector system which can handle very high count rates, i.e. a paired pulse resolution of ~0.10 μs or less.

The only detector which has been used extensively in this high energy range is the organic scintillator viewed with a fast photomultplier. The efficiency of a standard size scintillator was carefully measured and calculated by BATCHELOR [15] at Harwell. More recent calibrations have been

made at ORNL by VERBINSKI et al. [16]. This detector is gamma sensitive, so that in some experiments some form of gamma rejection must be used. Uranium or lead filters in the flight path are effective, and the resulting flight path transmission correction for the neutron spectrum is easily applied. However, for some experiments it may be necessary to sacrifice good paired pulse resolution capability for gamma rejection by pulse shape discrimination.

The fast neutron detector used in these experiments was a 2-in diameter by 2-1/2-in high liquid scintillator without gamma rejection circuitry. The efficiency was taken from Batchelor's work; a 5-in by 5-in liquid scintillator was also used for some fast measurements, and was calibrated with respect to the 2-in detector.

Intermediate detectors cannot easily be based on proton recoil in a liquid scintillator because of the small light output from the low energy proton recoil. Some detectors which have been used more or less successfully are: banks of BF_3 counters, [17] gamma sensors viewing a slab of capturing material, lithium glass, and a gamma sensor viewing a moderated capturing slab. The intermediate data shown in this paper were taken using the 5-in liquid scintillator as a gamma detector immediately behind a 10-cm thick slab of a slurry of B_4C powder and water, each 50% by volume. Efficiency of the detector was obtained by calculating the spatial distribution of neutron captures in the slab with GAPLSN [18].

The efficiency of gamma detection as a function of position in the slab was obtained empirically with a small Cs^{137} gamma source. Overall efficiency for neutron detection was obtained at each energy by integrating the spatial capture distribution over the gamma detection efficiency. At the higher neutron energies, neutrons transmitted through the slab will result in recoil protons in the scintillator. Below that energy, however, the overall detection efficiency was quite flat. Clearly, this detector is also gamma sensitive.

The time resolution of the intermediate detector is limited primarily by the time required for the neutrons to slow down and capture in the slab. This mean time-to-capture is roughly independent of incident energy because boron is of nearly 1/v capture cross-section. This time-to-capture is approximately 0.16 μs.

Beam intensity was monitored in some experiments by activating aluminium and/or sulphur foils. Also a moderated fission chamber and a beam current integrator were used. However, any changes in source-monitor geometry may destroy the usefulness of a particular monitor for a given series of experiments. In those experiments (shielding experiments) where the flux relative to the source strength is required, care was taken to preserve source-monitor geometry.

The multichannel analyser used was a 1024 channel Model CN-1024, made by Technical Measurements Corporation, using the Model 201 plug-in unit which has time channels down to 31.25 ns width. The raw data were reduced to energy spectra using the ECTOPLASM code [19].

Although no data are available at this writing, it is in principle possible to measure the high spectrum of fast reactors by time-of-flight. The mean emission time of the prompt neutrons is approximately the prompt decay constant $\ell/(1-k_p)$. This time is 0.1 μs for a metal reactor of the Godiva

class which is 10 $-subcritical. This time spread permits an energy resolution of about 5% at 1 MeV for a 50 M metre flight path.

A facility has been fabricated (fuel, assembly machine, and instrumentation) for operation in conjunction with the Linac for time-of-flight spectrum measurements of the neutron leakage from a 17.8 cm-diameter sphere of uranium metal which is 93% U^{235}. The sphere has a 2.5-cm diameter hole, 7.6 cm deep to bring the electron beam near the centre so that the geometry can be well described by one-dimensional calculational methods.

3. EXPERIMENTAL RESULTS

Some of the data from three different experimental programmes in various stages of progress are presented in this section. In each programme the broad objectives were to evaluate computational methods and cross-sections by comparing measured with calculated spectra.

3.1. Paraffin wax

Spectra were measured in a 1.5-M cube of paraffin (CH_2 of specific gravity 0.96) (see Fig.4) [14]. A 5-cm diameter, depleted uranium metal target was used in a 15-cm diameter spherical cavity in the wax. The pre-collimator for these measurements was 6.3 cm in diameter, to view the whole

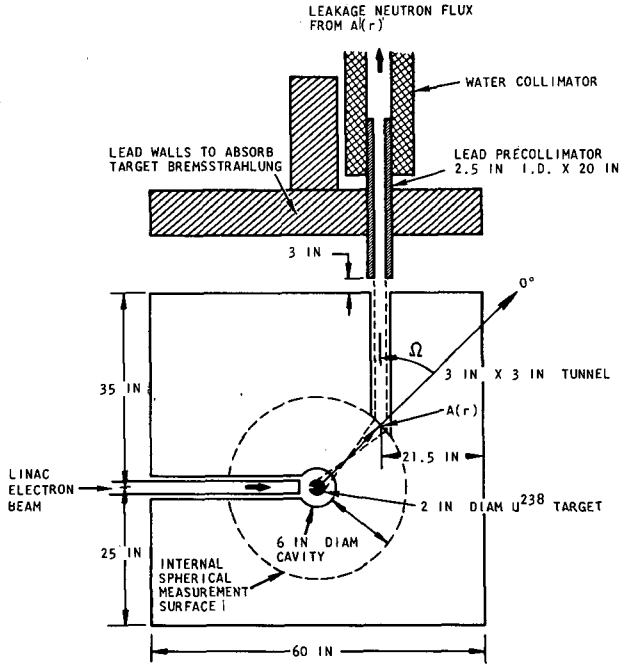


Fig.4

Plan view of experimental geometry for deep penetration measurements in paraffin

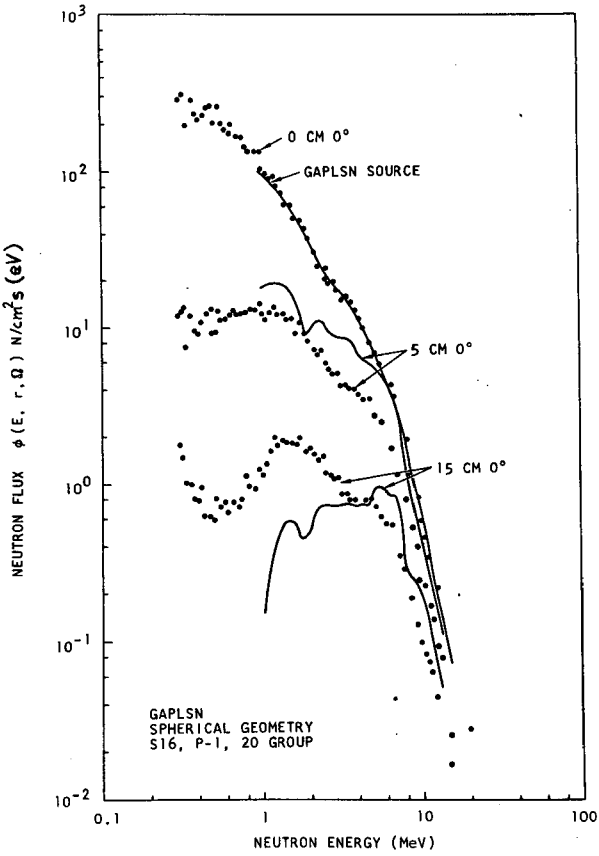


Fig. 5

Neutron spectra in paraffin (theory and experiment normalized to source)

source for the 0° measurements. The flight path is shown in Fig. 3. Figure 5 gives the data for 0° at different distances from the source viewed through a re-entrant hole in the wax block, and corresponding to penetrations of 0, 5, and 15 cm of wax. Figure 6 shows the data at 30-cm wax penetration, for angles of 16°, 32°, and 60°.

3.2. Liquid hydrogen

Spectra were measured in a large dewar of liquid hydrogen with the configuration shown in Fig. 7 [6]. The results for the 0° measurements are shown in Fig. 8 for several thicknesses of hydrogen between the source and the detector. In this experiment the uranium source was 7.6 cm diameter, and the pre-collimator was 2.2 cm diameter.

The geometry of this experiment is two dimensional (RZ).

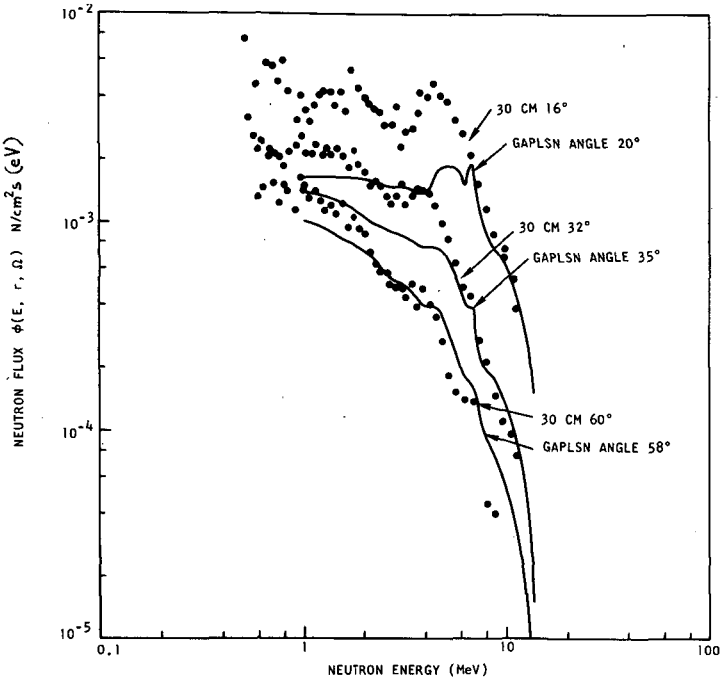


Fig. 6

Neutron spectra in paraffin (theory and experiment normalized to source in Fig. 5)

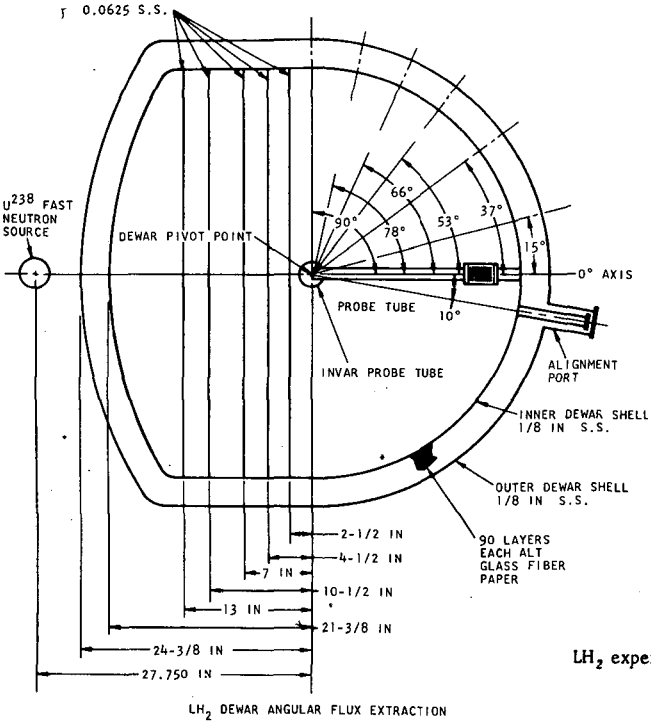


Fig. 7

LH_2 experimental dewar baffle spacings

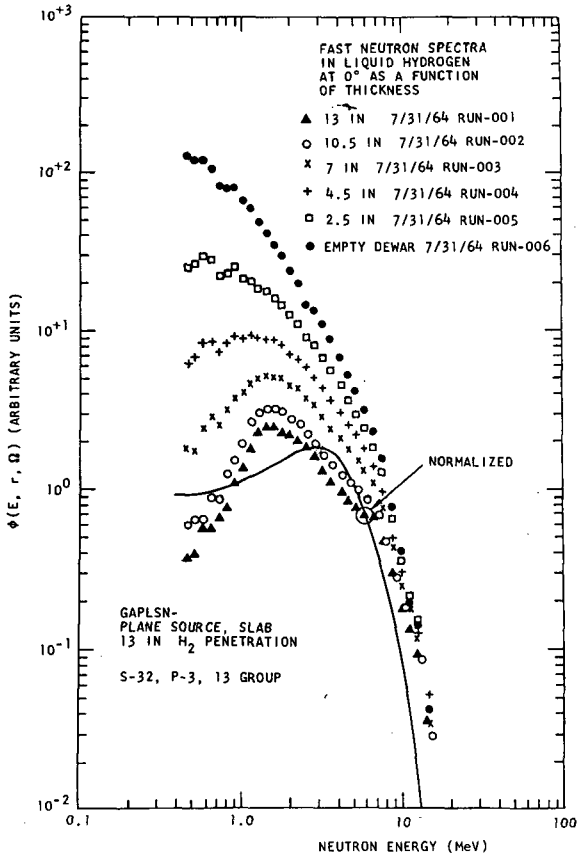


Fig. 8

Fast neutron spectra in LH_2 at 0° as a function of thickness

3.3. Lead and graphite

Figure 9 shows the neutron spectra leaking from the surface of a 12.7-cm thick shell of graphite, specific gravity 1.7, around a 15.2-cm diameter lead sphere [20]. Also shown is a spectrum without the graphite reflector. The electron beam strikes the centre of the lead through a 2.2 cm hole from the surface. This geometry was chosen so that it could be calculated with one-dimensional, spherical codes. In Fig. 10 the data are plotted without grouping and on a linear scale to show the effects of the graphite resonances on the leakage spectra.

3.4. Theory

The calculated fluxes plotted along with the data were obtained with the GAM II [21] and GAPLSN [18] codes. GAM II performs those manipulations required to convert the simple microscopic cross-sections (tabulated at 99 energy points) into a form suitable for calculating a few group, gross neutron

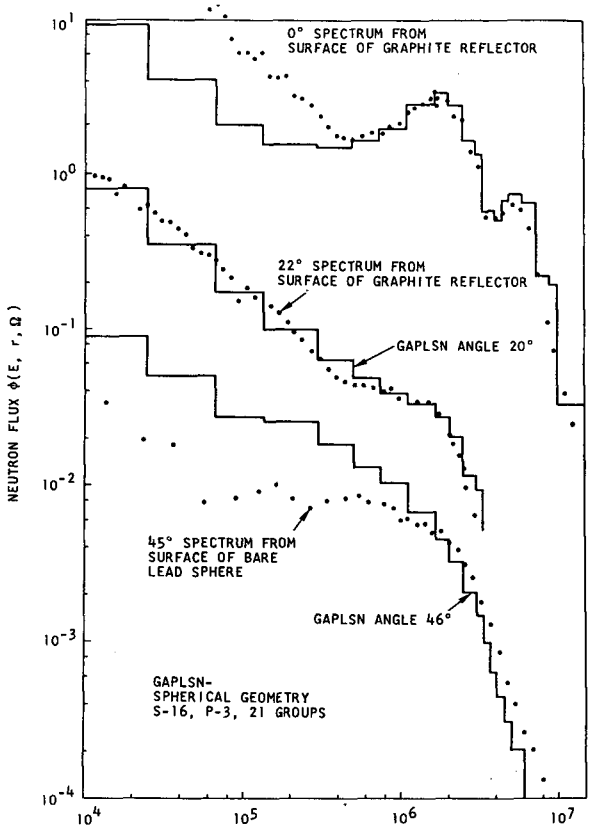


Fig. 9

Leakage spectrum from lead sphere and graphite reflected lead sphere (normalization arbitrary)

distribution. This includes calculation of the capture cross-sections in the unresolved resonance region from a statistical model with self shielding by the Nordheim integral method. The function of GAPLSN is to calculate the neutron distribution in an assembly of specified geometry and cross-section. This distribution is in angle, energy and space.

The paraffin calculation uses the 0 cm 0° data of Fig. 5 as an input source for S_{16}, P_1, 20 energy group calculation in spherical geometry. The magnitude as well as shape of the other spectra in Figs. 5 and 6 are determined.

The results of the lead-graphite calculations modified to include an excess of high energy and low energy neutrons were used as an input fission spectrum. The calculation is with S_{16}, P_3, and 21 energy groups in spherical geometry. In Fig. 10 data and calculations are shown along with the total cross-section of carbon and the assumed source for the calculation to illustrate the origin of the "fine structure" in the data.

The liquid hydrogen calculation is done in plane geometry using a fission spectrum source to examine the qualitative behaviour of the spectra. GAPLSN, being a one-dimensional code, cannot be used to describe accurately the two-dimensional geometry of the experiment.

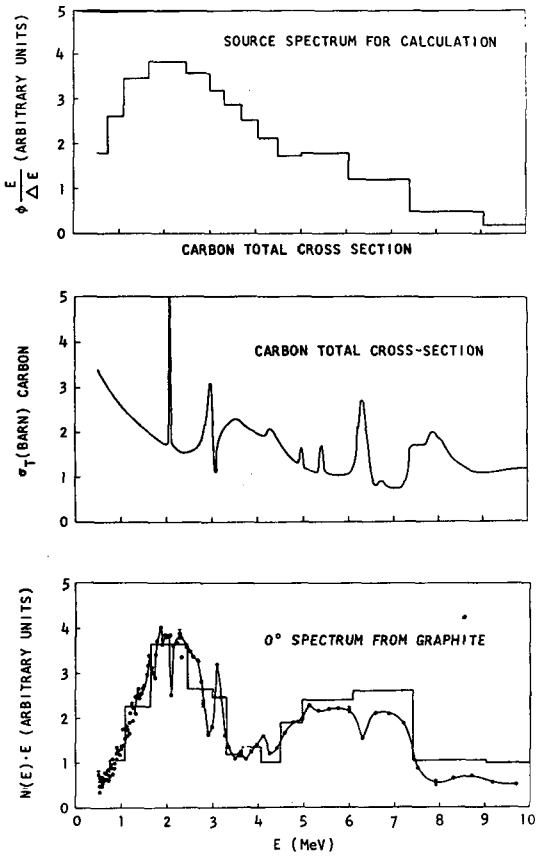


Fig. 10

Neutron leakage spectrum from graphite reflector lead sphere

4. CONCLUSIONS

The measured spectra are those at specific positions and directions. For a meaningful comparison it is necessary that the calculation be done in such a way that these particular directions be accessible. Some questions concerning the relationship of the angular resolution of the experiment relative to that of the calculation have not been completely resolved. In particular, the angular resolution of the calculation for the 0° lead-graphite leakage spectra in Fig. 9 is smaller than the experimental resolution and is believed to account for much of the discrepancy between theory and experiment. At 22°, the angular resolution is less important since the angular distribution is more slowly varying than near 0°, and the agreement is very good, as it should be since the shape of the spectrum is dominated by the well-understood elastic scattering by carbon. Also shown in Fig. 9 is the comparison for the neutron leakage for a bare lead sphere for 45°. The poor agreement suggests that while elastic scattering can be very well calculated,

cross-section data for inelastic slowing down by the high-A elements is seriously inadequate for calculating intermediate spectra. It is not generally realized that the inelastic scattering spectrum has not been measured for scattering to energies below ~100 keV. Nor has the fission spectrum been measured below ~100 keV. Yet these are the only two mechanisms by which neutrons can arrive at intermediate energies in some types of fast reactors.

The data of Fig. 10, which includes the total cross-section for carbon for comparison, show that although the average flux is handled fairly well, the "fine structure" will require more cross-section detail than can be practically handled for the present.

The deep penetration spectra are much more sensitive to angular detail in the calculation. Also, low cross-sections between resonances tend to act as "energy windows" for the deep penetration flux. A measure of the difficulty in handling these problems is indicated by the comparisons for paraffin in Figs. 5 and 6.

The liquid hydrogen comparison is qualitatively informative, but since the calculation is one dimensional only qualitative agreement is expected.

REFERENCES

[1] BLIZARD, E.P. and MITTELMAN, P.S., Recent advances in reactor shielding in the United States, Proc. 3rd UN Int. Conf. PUAE, 1964, P/260.

[2] General Atomic linear accelerator and supporting facilities, Rpt. GA-1855 Rev.(1962).

[3] BARBER, W.C. and GEORGE, W.D., Neutron yields from targets bombarded by electrons, Phys. Rev. 116 (1959) 1551.

[4] HERRING, D.F. et al., Bull. Amer. phys. Soc. 9 (1964) 32.

[5] RUSSELL, J.L. et al., Feasibility study of the accelerator pulsed fast assembly, Defense Atomic Support Agency Rpt. DASA-1470 (Dec. 1963).

[6] TRIMBLE, G.D., HOUGHTON, G.K. and AUDAS, J.H., Measurement of neutron spectra in liquid hydrogen, NASA Rpt NASA-CR-54230.

[7] BERTOZZI, W. et al., Photoneutron spectrometry by time of flight, Mass. Inst. Techn. to be published.

[8] FIRK, F.W. et al., A nanosecond neutron time-of-flight system for the Harwell 30 MeV electron Linac, Nucl. Instrum. Meth. 23 (1963) 141-46.

[9] PROFIO, A.E. et al., "Measurements and calculations of the slowing-down and migration time", these Proceedings I.

[10] PROFIO, A.E. and ECKARD, J.D., Investigations of neutron moderation with a pulsed source, Nucl. Sci. Engng. 19 (1964) 321-28.

[11] BERGMAN, A.A. et al., "A neutron spectrometer based on measuring the slowing-down time of neutrons in lead," Proc. UN Int. Conf. PUAE 4 (1956) 135-46.

[12] MICHAUDON, A., The production of moderated neutron beams from pulsed accelerators, J. nucl. Energy 17 (1963) 165-86.

[13] KOPPEL, J.U., Time dependent, space independent neutron thermalization, Nucl. Sci. Engng 12 4 (April 1962) 532-41.

[14] PROFIO, A.E. and KIRKBRIDE, T., Measurement of fast neutron spectra in an infinite medium of CH_2, Air Force Rpt. WL-TR-64-180. (GA-5973) 1964.

[15] BATCHELOR, R. et al., "The response of organic scintillators to fast neutrons, Nucl. Instrum. Meth. 13 (1961) 70.

[16] VERBINSKI, V.V. et al., Response functions of an organic scintillator to fast neutrons, Amer. nucl. Soc. Trans. 7 (Nov. 1964) 374.

[17] KATO, W.Y. et al., "Fast reactor physics parameters from a pulsed source", these Proceedings II.

[18] ALEXANDER, J.H. et al., GAPLSN - A modified DSN program for the solution of the one-dimensional anisotropic transport equation, GA Rpt -4972 (1964).

[19] NALIBOFF, Y.D., Ectoplasm Code, unpublished.
[20] RUSSELL, J.L. et al., Fast neutron spectra in a lead-graphite assembly, to be published in Amer. nucl. Soc. Trans. 1965.
[21] JOANOU, G.D. and DUDEK, T.S., GAM-II-A B_3 code for the calculation of fast-neutron spectra and associated multigroup constants, Rpt GA-4265 (1963).

DISCUSSION

M. KÜCHLE: Do you intend to check the calculated detector efficiency experimentally?

J. RUSSELL: No, not directly. It is difficult to span the range from ~ 100 eV to ~ 100 keV by a direct experimental measurement of efficiency. We are, however, attempting to check our efficiency calculations by intercalibrating a variety of calculable detectors such as lithium glass, B^{10} slab, etc.

D. GAYTHER: Detector efficiencies can be measured experimentally by comparison with a calibrated long counter if one uses a Van de Graaff accelerator as a source of mono-energetic neutrons. This technique is described in my paper* and is useful at energies greater than ~ 25 keV.

K.H. BECKURTS: It is clear from various papers presented at this Symposium that good methods have now been developed for determining fast-neutron spectra in reactor materials and in hard-spectrum subcritical assemblies. We are still faced, however, with another very important problem, namely the measurement of the low-energy part of the spectrum in realistic mock-ups of large fast-power breeders. Close-to-criticality, the relaxation times of these systems will be many many microseconds and it will be very difficult to use the standard pulsed-source time-of-flight method, especially since the equipment required is normally not available at critical assemblies. What methods ought then to be used?

W. KATO: Bennett at Argonne National Laboratory has recently made some proton-recoil-counter spectrum measurements in a core characteristic of a 2600-l fast reactor. Preliminary results indicate that the spectrum can be measured down to about 1.5 keV inside the core.

F. STORRER: Would it not perhaps be possible to improve these time-of-flight spectrum measurements by using a chopper? One would then not be handicapped by the large pulse width, which, as Dr. Beckurts just pointed out, would normally occur in pulsed assemblies close to criticality.

M. POOLE: A typical relaxation time for a large subcritical system is 2 μs. As choppers can be made to give 2-μs pulses it would certainly be possible to make equally good chopper measurements on a beam extracted from a steadily operating reactor. However, the mean power of the reactor would then be, say, 1 MW, which would mean that it could certainly not be classified as a zero-power facility and the experiment would be rather expensive. The alternative is to use a chopper to sharpen the pulse from a pulsed assembly. In this case however there is a possibility of the spectrum varying with time, and one would probably end up by carrying out a full time-dependent investigation. Such effects might be particularly serious at the

* GAYTHER, D.B. and GOODE, P.D., "Measurements of fast neutron spectra in reactor materials" (SM-62/23), these Proceedings II.

boundary between core and reflector. It is therefore my opinion that even for the large systems we shall finish up by making pulsed time-of-flight measurements using flight paths about 500 metres long.

V. RAIEVSKI (Chairman): It is not at all certain that a chopper is advantageous for analysing the low-energy spectrum in a subcritical assembly at a pulse length of 2 μs. It is difficult for a chopper to have a burst time of less than 0.5 μs so that the gain is rather small, amounting to a factor of 4. As against this, there is a considerable loss in solid angle because one is limited by the very small opening of the chopper.

THEORETICAL CONSIDERATIONS CONCERNING THE PULSATION OF FAST SUBCRITICAL ASSEMBLIES

M. STIÉVENART
SOCIÉTÉ BELGE POUR L'INDUSTRIE NUCLÉAIRE, "BELGO NUCLÉAIRE",
BRUSSELS, BELGIUM

Abstract — Résumé — Аннотация — Resumen

THEORETICAL CONSIDERATIONS CONCERNING THE PULSATION OF FAST SUBCRITICAL ASSEMBLIES. The use of a punctual multigroup energy model for interpreting time eigenvalues measured on fast neutrons subcritical bare assemblies is discussed. The inadequacies of this model are pointed out. The definition of a punctual continuous energy model is given, and the possibility of treating adequately inelastic and elastic scattering is discussed. It is also shown that the continuous energy model presented can be reduced, in some particular cases, to simpler and more classical models used in reactor physics. The energy-space-time problem is also emphasized. The possibility of using a multigroup multinodal model is discussed for interpreting the time eigenvalue measured in pulsed neutron experiments.

CONSIDÉRATIONS THÉORIQUES CONCERNANT LA PRODUCTION DE BOUFFÉES DANS DES ASSEMBLAGES SOUS-CRITIQUES A NEUTRONS RAPIDES. L'auteur discute l'emploi d'un modèle d'énergie ponctuel à plusieurs groupes en vue de l'interprétation des valeurs propres en temps mesurées pour des assemblages sous-critiques à neutrons rapides et sans réflecteur. Il signale les insuffisances de ce modèle. L'auteur définit un modèle continu et étudie la possibilité de traiter convenablement la diffusion inélastique et élastique. Il montre également que le modèle continu qu'il a défini peut être ramené, dans des cas particuliers, à des modèles plus simples et plus classiques utilisés en physique des réacteurs. L'auteur met aussi l'accent sur le problème espace-temps-énergie. Il étudie la possibilité d'utiliser un modèle à plusieurs nœuds et à plusieurs groupes pour interpréter des valeurs propres en temps mesurées dans les expériences sur les neutrons pulsés.

ТЕОРЕТИЧЕСКИЕ СООБРАЖЕНИЯ ОТНОСИТЕЛЬНО ПУЛЬСАЦИИ ПОДКРИТИЧЕСКИХ СБОРОК НА БЫСТРЫХ НЕЙТРОНАХ. Обсуждается вопрос об использовании точной многогрупповой энергетической модели для истолкования собственного значения времени, измеренного на подкритических сборках быстрых нейтронов без отражателя. Указываются недостатки этой модели. Приводится определение точной модели непрерывной энергии и обсуждается возможность обработки адекватно неупругого и упругого рассеяния. Показывается также, что модель непрерывной энергии может быть сведена в некоторых конкретных случаях к более простым и более классическим моделям, используемым в физике реакторов. Подчеркивается также проблема пространственно-временной зависимости энергии. Обсуждается возможность использования многогрупповой, многоузловой модели для интерпретации собственного значения времени, измеренного в экспериментах с импульсными нейтронами.

CONSIDERACIONES TEORICAS SOBRE EL EMPLEO DE NEUTRONES PULSADOS EN CONJUNTOS SUBCRITICOS RAPIDOS. El autor examina el empleo de un modelo puntiforme de energía de varios grupos para interpretar los valores temporales medidos en conjuntos subcríticos de neutrones rápidos desprovistos de reflector, y señala las deficiencias de dicho modelo. Define un modelo puntiforme de energía continua, y examina la posibilidad de tratar adecuadamente la dispersión inelástica y elástica de los neutrones. Demuestra asimismo que dicho modelo puede simplificarse en algunos casos particulares, quedando reducido a modelos más clásicos y sencillos empleados en física de los reactores. Por otra parte, pone de relieve la importancia del problema energía-espacio-tiempo, y examina la posibilidad de emplear un modelo de nodos y grupos múltiples para interpretar el valor temporal propio medido en experimentos con neutrones pulsados.

1. INTRODUCTION

Little information has been available up to now in the field of pulsed neutrons applied to fast neutron multiplying assemblies. This is true for the experimental field as well as for the theoretical one. The scope of the present paper is mainly to gather theoretical information which was recently obtained. This information has been derived only for multiplying assemblies.

The slowing-down and multiplication of neutrons in fast assemblies are studied using first a continuous energy model. The space effects are taken into account through the space-modes picture. General relations are drawn from this formalism and the difficulty of treating adequately the inelastic scattering is pointed out.

The multigroup energy model is also reviewed and is shown to be a particular case of the continuous energy model. Some theoretical and experimental results are compared and are shown to be in good agreement only for the near-critical state. Practical suggestions are formulated for future development.

An example of thermal and intermediate assemblies is briefly cited.

2. NOMENCLATURE

$\varphi(E,t)$: energy and time-dependent neutron flux
$F(t)$: time-dependent fission rate
$I(t)$: intensity of the external neutron source
$\Sigma_{n,\gamma}(E)$: macroscopic absorption cross-section
$\Sigma_{n,n'}(E)$: macroscopic scattering cross-section $\Sigma_{n,n'}(E)=\int_{E'} \Sigma_s(E' \to E)dE'$
$\Sigma_f(E)$: macroscopic fission cross-section
$D(E)$: diffusion coefficient
B^2 : buckling of the assembly
$v(E)$: velocity of neutrons
$\chi(E)$: fission distribution normalized to unity, $\int_E \chi(E)dE = 1$
$\chi_s(E)$: source distribution normalized to unity, $\int_E \chi_s(E)dE = 1$

3. FORMALISM IN THE CASE OF A CONTINUOUS ENERGY MODEL

We are interested in the solution of energy-time problems which are encountered in the pulsation of fast neutron subcritical assemblies. The theory of diffusion is considered a valuable tool and has been used for this study. Space effects are not considered here but, as finite dimensions of practical fast neutron assemblies must be taken into account, a leakage term has been included in the equations; it is based on the space-modes picture. The following treatment is restricted to homogeneous assemblies or equivalent homogenized ones.

Let us write the diffusion equation for the energy and time-dependent flux $\varphi(E, t)$ (delayed neutrons are ignored).

$$\Sigma_t \varphi(E, t) - \int_{E'} \Sigma_s(E' \to E)\, \varphi(E', t) dE' = -\frac{1}{v} \frac{d\varphi(E, t)}{dt} + \chi F(t) + \chi_s I(t) \qquad (1)$$

where Σ_t is the energy dependent total macroscopic disappearance cross-section, i.e.

$$\Sigma_t = \Sigma_{n,\gamma} + \Sigma_{n,n'} + \Sigma_f + DB^2,$$

$\Sigma_s(E' \to E)$ is the macroscopic differential scattering cross-section and F(t) is the fission rate related to the flux by

$$F(t) = (\nu \Sigma_f, \varphi(E, t)) = \int_E \nu \Sigma_f(E)\, \varphi(E, t) dE \qquad (2)$$

F(t) can be considered as a scalar product. The source intensity I(t) can have any time variation, but the one most often used is the pulsed one which is commonly reduced to a Dirac impulse. The following treatment is independent of the time variation of I(t) and will not be specified.

To solve the energy-time problem defined by the Eqs. (1) and (2), the Laplace transformation is used. Let p denote the Laplace variable; we have, with adequate initial conditions $[\varphi(E, 0) = 0]$, the following:

$$\left(\Sigma_t + \frac{p}{v}\right) \varphi(E, p) - \int_{E'} \Sigma_s(E' \to E)\, \varphi(E', p) dE' = \chi F(p) + \chi_s I(p) \qquad (3)$$

$$F(p) = (\nu \Sigma_f, \varphi(E, p)) = \int_E \nu \Sigma_f(E)\, \varphi(E, p) dE \qquad (4)$$

Using the linear operator concept, Eq. (3) can be put in the following form:

$$a(E)[\varphi(E, p)] = \chi F(p) + \chi_s I(p) \qquad (5)$$

where a(E) is the basic operator of the problem, i.e.

$$a(E) = \left(\Sigma_t + \frac{p}{v}\right)\left[\ldots\right] - \int_{E'} \Sigma_s(E' \to E)\left[\ldots\right] dE'$$

Equation (5) can be solved easily, provided the basic operator a(E) has an inverse operator A(E); the latter is defined by Eq. (6).

$$A(E)\{a(E)[\varphi(E,p)]\} = \varphi(E,p) \tag{6}$$

Once A(E) is known, the transforms of the fission rate F(p) and the flux $\varphi(E,p)$ are derived as follows. First, the inverse operator A(E) is applied to both sides of Eq.(5); we have then

$$\varphi(E,p) = A(E)\{\chi F(p) + \chi_s I(p)\}$$

Secondly, the fission rate transform F(p) is calculated by Eq.(4) and terms are then re-arranged, so that one obtains finally

$$F(p) = \frac{k_s(p)}{1-k(p)} I(p) = G(p)\, I(p). \tag{7}$$

k(p) and $k_s(p)$ are two scalar functions appearing quite naturally in this mathematical manipulation; they are defined by the following relations:

$$k(p) = (\nu \Sigma_f(E),\ A(E)[\chi]) = \int_E \nu \Sigma_f(E) A(E)[\chi]\, dE \tag{8a}$$

$$k_s(p) = (\nu \Sigma_f(E),\ A(E)[\chi_s])= \int_E \nu \Sigma_f(E) A(E)[\chi_s]\, dE \tag{8b}$$

The physical meaning of these two functions is shown later to be that of a multiplication factor which takes into account the distributed p/v fictitious absorber.

The main problem to be solved now is thus the calculation of the inverse operator A(E) by Eq.(6).

The multigroup energy treatment which is described in another section suggests for A(E) the following form:

$$A(E) = \frac{1}{\left(\Sigma_t + \frac{p}{v}\right)} \left\{ \left[\dots \right] + \int_{E''} \left[\dots \right] K(E'' \to E)\, dE'' \right\} \tag{9}$$

$K(E'' \to E)$ is shown hereafter to be the "slowing-down kernel"; its expression is found by replacing the operators a(E) and A(E) by their expression in Eq.(6). One obtains the following equation:

$$K(E' \to E) = \frac{\Sigma_s(E' \to E) + \int_{E''} \Sigma_s(E' \to E'') K(E'' \to E)\, dE''}{\left(\Sigma'_t + \frac{p}{v'}\right)}, \quad p \neq -v'\Sigma'_t \tag{10}$$

Let us define the "one-collision kernel" $K_1(E' \to E)$ by

$$K_1(E' \to E) = \frac{\Sigma_s(E' \to E)}{\Sigma'_t + \frac{p}{v'}} \tag{11}$$

Since we are mainly concerned with fast neutron assemblies, we have the following:

$$\Sigma_s(E' \to E) = 0 \text{ for } E' \leqslant E \text{ and } \Sigma_s(E' \to E) \neq 0 \text{ for } E' > E$$

Equation (10) can then be put into the form

$$K(E' \to E) = K_1(E' \to E) + \int_{E''} K_1(E' \to E'')K(E'' \to E)dE'' \tag{12}$$

In the most general cases, the solution of Eq. (12) is practically impossible to be obtained, provided inelastic and elastic scattering occur simultaneously. However, this equation has been solved several times for the static case and for different assumptions; an example of such solutions is given later for the time-dependent case.

The analytical and rigorous solution of the equation can be obtained as a sum of successive integrals of $K_1(E' \to E)$. One can indeed check that the following form of $K(E' \to E)$ is the solution of Eq. (12).

$$K(E' \to E) = \sum_{n=1}^{\infty} K\ (E' \to E) \tag{13}$$

with

$$K_n(E' \to E) = \int_{E''} K_1(E' \to E'')K_{n-1}(E'' \to E)dE'', \quad n = 2, 3, \ldots, \infty. \tag{14}$$

Equation (14) shows that $K_n(E' \to E)$ is the probability that a neutron is slowed down from E' to E through n collisions; consequently, one can see from Eq. (13) that $K(E' \to E)$ is the total probability that a neutron born at energy level E' reaches the energy level E. $K(E' \to E)$ is generally a complex number according to the complex nature of the Laplace variable p.

Let us write now k(p) and $k_s(p)$ with the aid of Eq. (9)

$$k(p) = \int_E \frac{\nu \Sigma_f(E)}{\left(\Sigma_t + \frac{p}{v}\right)} \left[\chi(E) + \int_{E'} \chi(E')K(E' \to E)dE'\right] dE \tag{15a}$$

$$k_s(p) = \int_E \frac{\nu \Sigma_f(E)}{\left(\Sigma_t + \frac{p}{v}\right)} \left[\chi(E) + \int_{E'} \chi_s(E')K(E' \to E)dE'\right] dE \tag{15b}$$

If $K(E' \to E)$ is the slowing-down probability, it is then evident that $k(p)$ and $k_s(p)$ are the multiplication factor, respectively, for fission neutrons and external source neutrons. $k(p)$ can also be considered as the transfer function linking successive generations of fission neutrons, and $k_s(p)$ can be regarded as the conversion factor, or transfer function, linking external source neutrons and fission neutrons.

The order of integration in Eq. (15a) may be inverted; we have

$$k(p) = \int_E \chi(E) \int_{E'} \frac{\nu \Sigma_f(E')}{\left(\Sigma'_t + \frac{p}{v}\right)} \left[\delta(E - E') + K(E \to E') \right] dE'$$

In such a manner, one makes evident the energetic adjoint ψ; one can show indeed, by solving the adjoint problem, that ψ is as follows

$$\psi(E, p) = \int_{E'} \frac{\nu \Sigma_f(E')}{\left(\Sigma'_t + \frac{p}{v}\right)} \left[\delta(E - E') + K(E \to E') \right] dE'$$

ψ measures the number of fission neutrons created per incident neutron of energy E; one has also

$$k(p) = \int_E \chi(E) \psi(E, p) dE = (\chi, \psi)$$

$$k_s(p) = \int_E \chi_s(E) \psi(E, p) dE = (\chi_s, \psi).$$

As predicted by Eqs. (10), (15a) and (15b), the functions $K(E' \to E)$, $k(p)$ and $k_s(p)$ may have singularities on the negative part of the real axis in the complex plane. Provided the energy range of interest is limited (example: 0.025 eV $\leq E \leq$ 10 MeV), it may be assumed that the negative singular part of the real axis is also limited,

$$-(\Sigma v)_{max} \leqq p_{singular} \leqq -(\Sigma v)_{min}$$

generally, $(\Sigma v)_{min}$ corresponds to the thermal energy range.

The functions $k(p)$ and $k_s(p)$ may be regarded as analytic functions throughout the complex plane except within a small countor γ around the real axis part defined by the inequality written above. These functions tend to zero when p tends to ∞.

The resultant transfer function $G(p)$, which is the Laplace transform of the impulse response $h(t)$ is also an analytic function throughout the complex plane except within the contour γ and small circles C_j around the roots of the following equation

$$h(t) = L^{-1}\left\{G(p)\right\} = L^{-1}\left\{\frac{k_s(p)}{1 - k(p)}\right\}$$

$$k(p) = 1 \tag{16}$$

The roots of this equation may be real or complex conjugate. According to the mathematical nature of k(p), Eq.(16) can have only one real root α_1 on the right of $-(\Sigma v)_{min}$; it is the fundamental eigenvalue $-(\Sigma v)_{min} < \alpha_1$. Eventual complex conjugate roots of Eq.(16) are thought to exist in the case of a fuel having resonance(s).

The impulse response h(t) may be calculated by the following classic relation,

$$h(t) = \frac{1}{2i\pi} \oint_G \frac{k_s(p)}{1 - k(p)} \exp(pt)\, dp \tag{17}$$

G is a contour including all singularities of the resultant transfer function G(p) (Fig. 1). Provided the time eigenvalues α_j of the assembly, which are

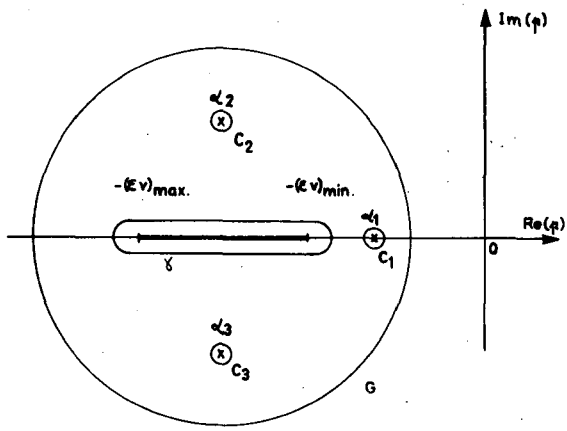


Fig. 1

Location of singularities and poles of functions k(p), $k_s(p)$, G(p) and integration contours

the solution of Eq.(16), are isolated and of first order, their contribution to the right side of Eq.(17) is of the exponential form; one has

$$h(t) = \sum_j R_j \exp \alpha_j t + \frac{1}{2i\pi} \oint_\gamma \frac{k_s(p)}{1 - k(p)} \exp(pt)\, dp \tag{18}$$

The residue R_j corresponds to the eigenvalue α_j, i.e.

$$R_j = \frac{1}{2i\pi} \oint_{C_j} \frac{k_s(p)}{1 - k(p)}\, dp = \frac{k_s(\alpha_j)}{-\left[\frac{dk}{dp}\right]_{p=\alpha_j}} = \frac{k_s(\alpha_j)}{l_j} \tag{19}$$

$l_j = -\left[\frac{dk}{dp}\right]_{p=\alpha_j}$ plays the role of a neutron production time.

The second term on the right side of Eq. (18) is of the continuum type and gives then a contribution which is not an exponential function.

The correct calculation of quantities and functions intervening in Eqs. (18) and (19) for practical fast neutron assemblies is very difficult or perhaps impossible. The main facts contributing to this situation are the following:

(1) The fission spectrum cannot be considered as being narrow compared with the energy range of interest in a practical fast assembly.

(2) The slowing down of neutrons in a fast assembly is performed with comparable importance by many elements (fuel, structure, coolant, cladding, etc.)

(3) The slowing down of neutrons by inelastic scattering is very important and should be treated as correctly as possible.

(4) The practical lower energy limit is not defined.

For these reasons, another calculation model has been used and a detailed study is given in the following section.

4. FORMALISM FOR THE MULTIGROUP ENERGY MODEL [1, 2]

The multigroup energy model is a less elaborate model than the continuous one described in the previous section, but it is more easily handled and many cross-section sets are now available for it. It is customary to derive the multigroup equations by adequately averaging cross-sections and flux in the integral Eq. (1); while doing that, one finds for the Laplace transform of the variables the following system of equations (N energy groups are considered):

$$\left[\Sigma_{ti} + \frac{p}{v}\right]\phi_i(p) - \sum_{j=1}^{i-1} \Sigma_{i \leftarrow j}\, \phi_j(p) = \chi_i F(p) + \chi_{s,i} I(p) \qquad (20a)$$

$$F(p) = \sum_{i=1}^{N} \nu \Sigma_{fi}\, \phi_i(p) \qquad (21a)$$

The previous equations are written in matrix form for convenience and for comparison with the continuous energy model.

$$|a(p)|\, \bar{\phi}(p) = \bar{\chi} F(p) + \bar{\chi}_s I(p) \qquad (20b)$$

$$F(p) = (\overline{\nu \Sigma}_f, \bar{\phi}(p)) \qquad (21b)$$

Provided thermal neutrons may be taken into account by only one energy group, the basic matrix $|a(p)|$ is triangular; we have

$$\left.\begin{aligned} a_{ij} &= 0 \qquad i < j \\ a_{ij} &= -\sum_{i \leftarrow j} \qquad i > j \\ a_{ii} &= \frac{p}{v_i} + \Sigma_{t,i} \\ \Sigma_{t,i} &= \Sigma_{n\gamma,i} + \Sigma_{nn',i} + \Sigma_{f,i} + D_i B_i^2, \quad \Sigma_{nn',i} = \sum_{k=i+1}^{N} \sum_{k \leftarrow i} \end{aligned}\right] \tag{22}$$

For the same reason, the inverse matrix $|A(p)|$ is also triangular

$$\left.\begin{aligned} &|A(p)|\ |a(p)| = |1| \\ &A_{ij} = 0 \\ &A_{ii} = \frac{1}{a_{ii}} \\ &A_{ij} = A_{ii} \sum_{k=j}^{i-1} (-a_{i,k}\ A_{k,j}) \qquad i > j \end{aligned}\right] \tag{23}$$

The matrices $|a(p)|$ and $|A(p)|$ play here exactly the role of the operators a(e) and A(e) defined for the continuous energy model. Consequently, the solution of Eqs. (20b) and (21b) is obtained by the same mathematical manipulation as the one used previously; we have then

$$\phi(p) = |A(p)|\,(\bar{\chi}\,F(p) + \bar{\chi}_s\,I(p)) \tag{24}$$

$$F(p) = \frac{k_s(p)}{1 - k(p)}\,I(p) = G(p)\,I(p) \tag{25}$$

$$k(p) = (\overline{\nu\Sigma_f},\ |A(p)|\bar{\chi}) \tag{26}$$

$$k_s(p) = (\overline{\nu\Sigma_f},\ |A(p)|\bar{\chi}_s) \tag{27}$$

In the case of the multigroup treatment, the expression of the slowing-down kernel can also be derived simply. It may be checked indeed that the quantity K_{ij} defined hereafter measures the slowing-down probability that

a neutron borne in energy group j reaches the energy group i by slowing down.

$$K_{ij} = -\sum_{k=j}^{i-1} a_{i,k} A_{kj} \qquad \text{for } i > j \tag{28}$$

We also have

$$A_{ij} = A_{ii}\, K_{ij} \qquad \text{for } i > j$$

It can be seen easily that the slowing-down kernel K_{ij}, which is defined by Eq.(28), is an analytic function in the complex plane; it has i-j poles, that is at points of the negative part of the real axis which correspond to the neutron disappearance probability p_k

$$p_k = -(\Sigma_t v)_k, \qquad j \leqslant k \leqslant i \leqslant N$$

Consequently, the functions k(p) and $k_s(p)$ also have poles at $p=p_k$ (k = 1, 2, . . . , N). These poles are bounded by two limits:

$$-(\Sigma_t v)_{max} \leqq p_k \leqq -(\Sigma_t v)_{min}$$

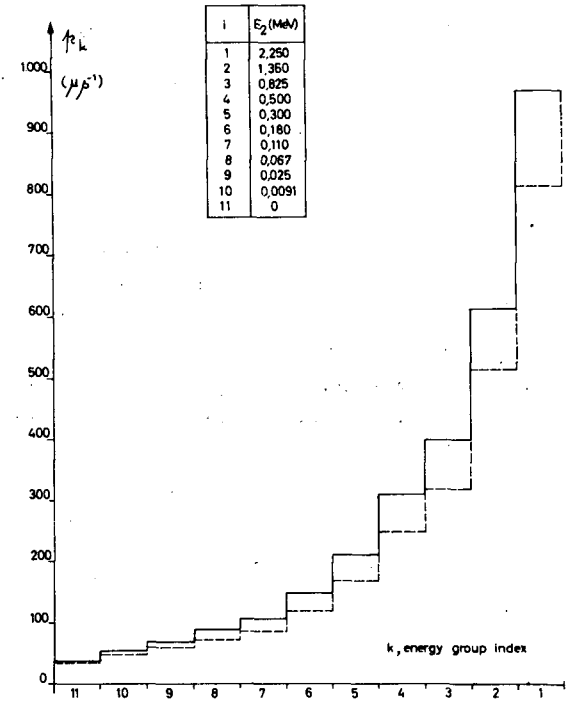
For fast neutron assemblies, it may generally be considered that the modulus of p_k increases regularly when energy increases (see for example Fig. 2). For intermediate and thermal neutron assemblies, this may be very different because of eventual resonance(s). Figure 3 shows the variation of k(p) on the real axis for two spheres of highly enriched (93%) uranium metal. Figure 4 shows the variation of k(p) in the complex plane for the corresponding critical sphere. As the number of poles of k(p) is equal to the number of energy groups, it is evident that k(p) depends strongly on the groups boundaries in the perturbed zone of the complex plane which lies around the poles, Far from this zone, multigroup models using different cross-section sets and the continuous model give probably the same k(p) function. Figure 5 shows, for example, the variation of k(p) on the real axis for three different multigroup structures.

As k(p) and $k_s(p)$ have the same poles, the resultant transfer function G(p) has poles only at the zeros of the denominator of G(p), if the source spectrum $\overline{\chi}_s$ has components in the same energy groups as the fission spectrum $\overline{\chi}$

$$G(p) = \frac{k_s(p)}{1 - k(p)} ,$$

that is at the time eigenvalues α_j which are the roots of Eq.(16)

As k(p) is an analytic function having N isolated poles, Eq.(16) has N roots. One of them is always real and located on the right of $-(\Sigma v)_{min.}$; it is the fundamental time eigenvalue α_1. The other eigenvalues can be real



i	E_2(MeV)
1	2,250
2	1,350
3	0,825
4	0,500
5	0,300
6	0,180
7	0,110
8	0,067
9	0,025
10	0,0091
11	0

Fig.2

Variation of the neutron disappearance probability for two spheres of enriched (93%) uranium metal (11 groups ANL).

—— Diam. = 13.0 cm (k_{eff} = 0.74)

– – – Diam. = 17.6 cm (k_{eff} = 1.00)

or complex conjugate (their real part is always negative), but for most of fast neutron assemblies, they are all real negative numbers regularly separated by the poles $p_k (k = 1, 2, \ldots, N)$. Figure 6 shows the variation of the fundamental eigenvalue α_1 for Godiva and for different multigroup cross-section sets; experimental results are also represented [3]. Figure 7 shows, in the case of the Y.O.M. (Yiftah, Okrent and Moldauer) cross-section set [4], the variation of the low-order eigenvalues versus the diameter of the spherical assembly (Godiva). It is evident from these theoretical results that, when the assembly goes far away from criticality, "eigenvalues which can be measured" correspond merely to transient energetic modes according to the fact that the fundamental energetic mode has then a very weak importance.

The impulse response of the assembly can be expressed as a simple function using the residue corresponding to each eigenvalue α_j.

$$h(t) = \sum_{j=1}^{N} R_j \exp(\alpha_j t) = \sum_{j=1}^{N} \frac{k_s(\alpha_j)}{l_j} \exp(\alpha_j t) \qquad (29)$$

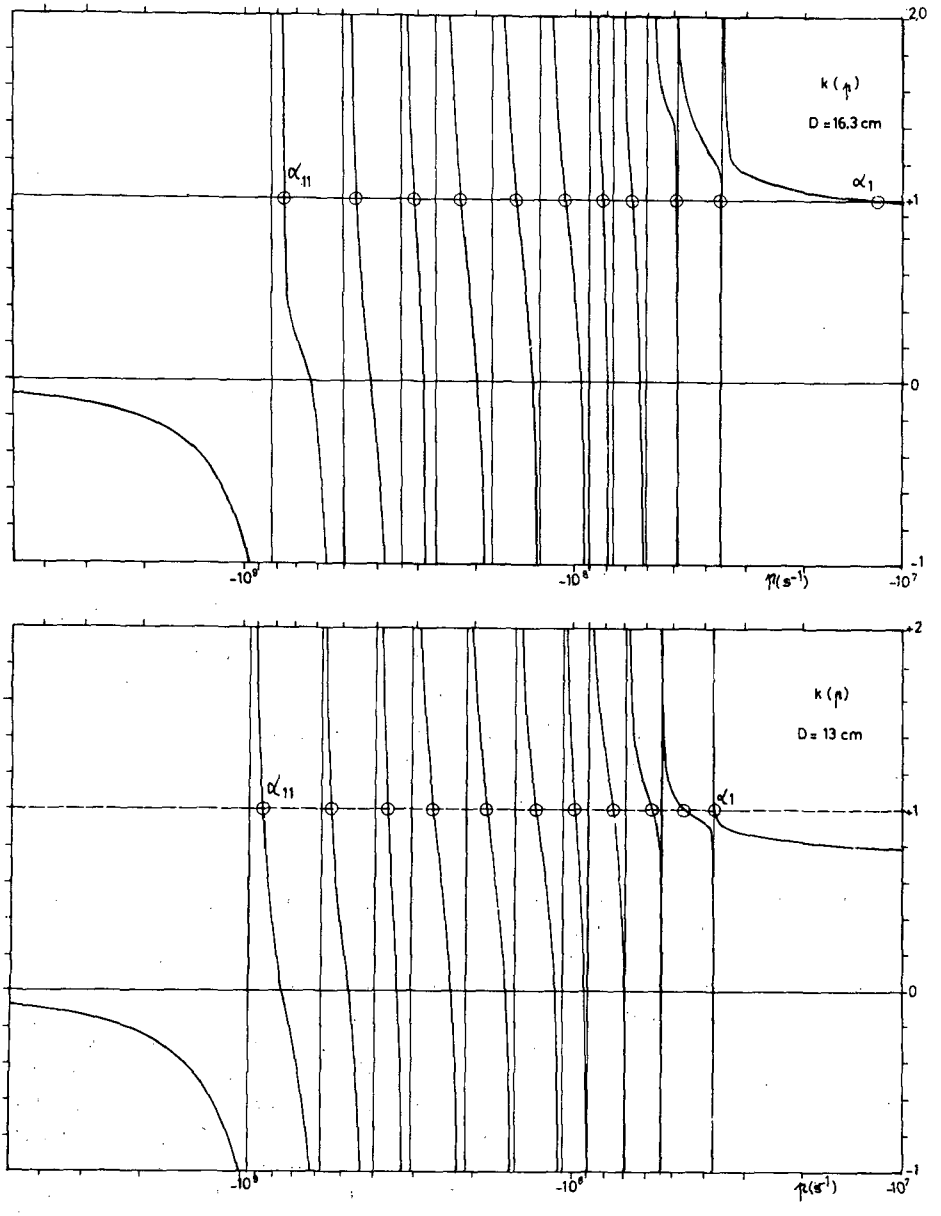


Fig. 3

Variation of k(p) for two spheres of enriched (93%) uranium metal (11 groups ANL cross-section set).

○ Time eigenvalues

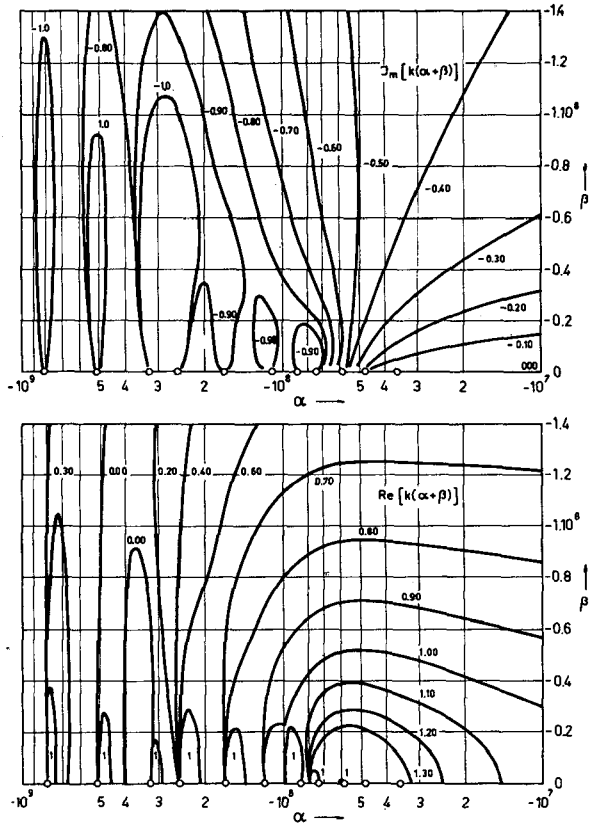


Fig. 4

Variation of $k(\alpha + j\beta)$ in the complex plane for a sphere of enriched (93%) uranium metal (diameter 17.6 cm).

O Pole of $k(\alpha + j\beta)$

The classical form given in Eq. (19) for the residue R_j is still valid. When comparing Eqs. (29) and (18), we see that the continuum-type contribution pertaining to the continuous energy model has been replaced in the present case by a sum of exponential terms corresponding to high order eigenvalues α_j $(j = 2, \ldots, N)$.

For assemblies in the near-critical state, the previous calculations have shown that the multigroup energy model is adequate to calculate the impulse response. A continuous energy model does not seem to be necessary for such assemblies.

For assemblies far from criticality ($k_{eff} \ll 1$), the importance of the fundamental (energetic) mode becomes very small compared with the importance of the high order (energetic) modes according to the preferential increase of l_1 (see also Fig. 3). It should be interesting for assemblies far from criticality to get a continuous energy model to replace the fictitious first-order eigenvalue contributions of the multigroup model by an adequate

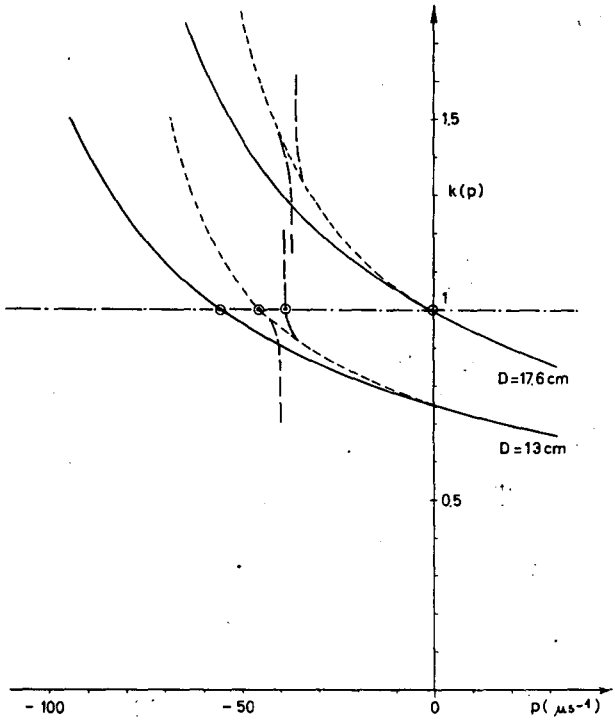


Fig. 5

Variation of k(p) for two spheres of enriched (93%) uranium metal.

⊙ Time eigenvalues
—— 3-groups ANL 5.800
----- 6-groups Belgonucléaire
– – – 11-groups ANL 5.800

continuum-type contribution. But, it is felt now that the continuous energy model should be used to compute the slowing down in the low energy part of the spectrum, while the high energy part of it could be related by a multi-group energy model. Such a mixed model, let us say a semi-continuous model, should be interesting to develop. Indeed, in this way, the inelastic scattering could be handled easily provided fast reactor cross-section sets are available for it, while the elastic slowing down would be handled by a continuous model which is now under development.

5. SOLUTION OF THE SLOWING-DOWN PROBLEM IN A PARTICULAR CASE

It has been seen in section 3 that the main problem to be solved is the calculation of the slowing-down kernel $K(E' \to E)$, that is, to find the solution of Eq. (12). This equation was solved more than twenty years ago [5] for different static cases corresponding to different assumptions on the one-

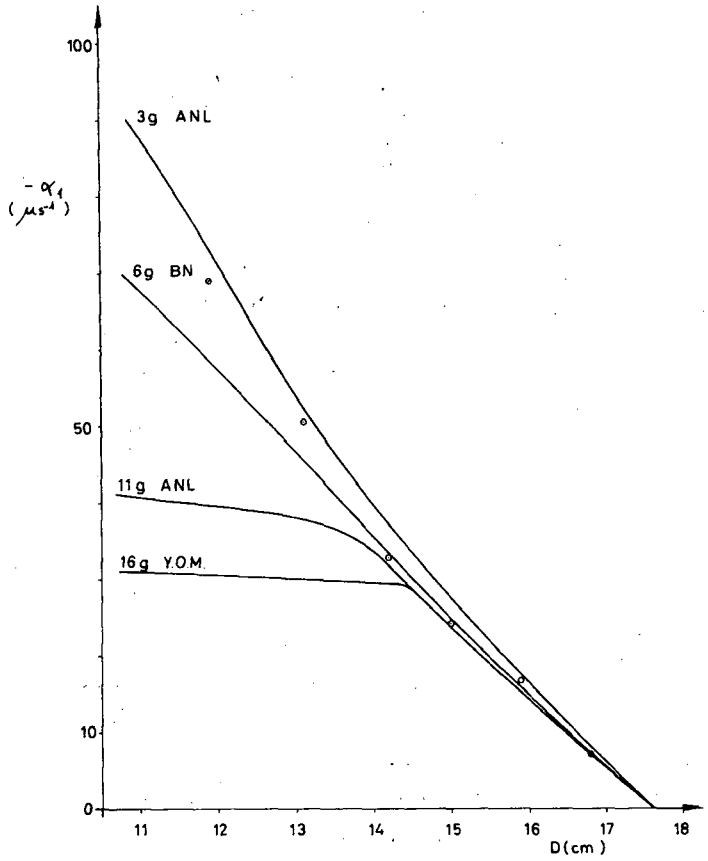


Fig. 6

Variation of the fundamental eigenvalue α_1 for Godiva and for different cross-section sets.

⊙ Experimental results [3]

collision kernel $K_1(E' \to E)$. These calculations are now being reviewed in different dynamic cases, that is for $p \neq 0$. We give here only a short example of such a case.

Let us assume that the slowing down of neutrons between energies E' and E is performed elastically and isotropically by free protons: Eq. (12) can now be written in the following form:

$$K(E' \to E) = K_1(E') \left\{ 1 + \int_E^{E'} K(E'' \to E) dE'' \right\} \qquad (30)$$

with

$$K_1(E') = \Sigma_s(E') / E' \left(\frac{p}{v} + \Sigma_t' \right) \qquad (31)$$

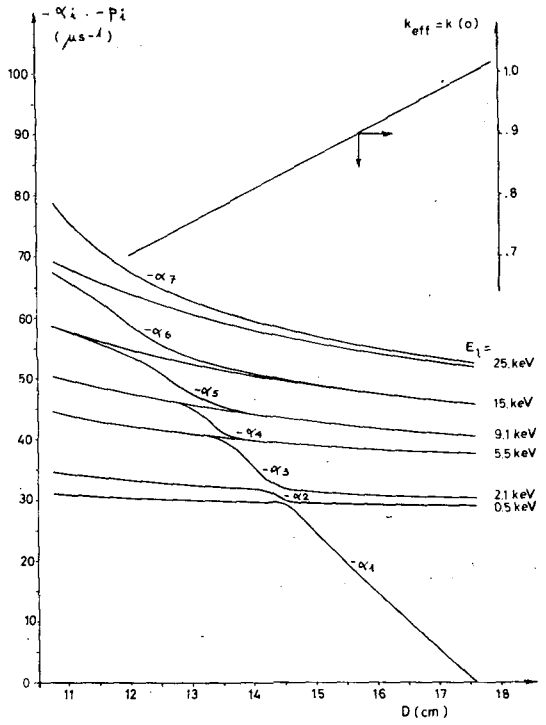


Fig. 7

Eigenvalues α_i as functions of diameter of the sphere (Godiva) (Y.O.M. 16-groups cross-sections [4]).

$\Sigma_s(E')$ is the macroscopic scattering cross-section at initial energy E'.

The solution of Eq. (30) is the following [5]:

$$K(E' \to E) = K_1(E') \exp \int_E^{E'} K_1(E'')dE'' \qquad (32)$$

or

$$K(E' \to E) = \frac{\Sigma_s(E')}{\left(\frac{p}{v'} + \Sigma_t'\right)} \left(\frac{1}{E}\right) \exp \left[- \int_E^{E'} \frac{\frac{p}{v''} + (\Sigma_t'' - \Sigma_s'')}{\frac{p}{v''} + \Sigma_t''} \frac{dE''}{E''} \right] \qquad (33)$$

One recognizes in Eq. (33) the fast non-leakage and absorption escape probabilities intervening under the form of an exponential function, including p/v absorption.

The k(p) function can then be calculated.

$$k(p) = \int_0^\infty \frac{\nu \Sigma_f(E)}{\left(\frac{p}{v} + \Sigma_t\right)} \left\{ \chi(E) + \int_0^E \chi(E') K_1(E') \exp \int_E^{E'} K_1(E'')\, dE''\, dE' \right\} dE$$

Moreover, if the fission spectrum is considered as an energetic Dirac impulse (that is a typical assumption in the case of thermal and intermediate reactor), we have, if $\bar{E}_f$ represents the mean fission neutron energy,

$$k(p) = \left[\frac{\nu \Sigma_f}{\frac{p}{v} + \Sigma_t} \right]_{E = \bar{E}_f} \left\{ 1 + \frac{\Sigma_s(\bar{E}_f)}{\nu \Sigma_f(\bar{E}_f)} \int_0^{\bar{E}_f} \frac{\nu \Sigma_f(E)}{\left(\frac{p}{v} + \Sigma_t(E)\right)} \times \left[\exp - \int_E^{\bar{E}_f} \frac{\frac{p}{v'} + (\Sigma_t' - \Sigma_s')}{\frac{p}{v'} + \Sigma_t'} \left(\frac{dE'}{E'}\right) \right] \left(\frac{dE}{E}\right) \right\}$$

The calculation of the impulse response h(t) can be done provided other assumptions are formulated concerning the source neutron spectrum $\chi_s(E)$ and the energy variation of cross-sections.

Other cases are now being studied which deal with the moderation of neutrons by heavy elements.

6. CONCLUSIONS

A general formalism has been elaborated for the calculation of the impulse response of multiplying assemblies. Mainly fast neutron assemblies have been considered, but it can be also used for intermediate and thermal neutron assemblies. The formalism can be applied either to a continuous energy model or to a multigroup model.

It has been shown that the multigroup model is adequate to predict time eigenvalues near the critical state, but is inadequate to study assemblies far from criticality. A practical semi-continuous energy model is suggested for future development.

REFERENCES

[1] STIÉVENART, M., Pulsation d'assemblages sous-critiques à neutrons rapides, Rpt. BN 6212-31 (1962)

[2] STORRER, F. and STIÉVENART, M., Contribution to the theory of the pulsed neutron technique applied to fast multiplying systems, Rpt. EUR 593.e. (1964).

[3] BENGSTON, J., Proc. 2nd UN Int. Conf. PUAE 12 (1958) 63.

[4] YIFTAH, S., OKRENT, D. and MOLDAUER, P.A., Fast Reactor Cross-sections, Pergamon Press, Oxford (1960).

[5] PLACZEK, G., On the theory of the slowing down of neutrons in heavy substances, Phys. Rev. 69 (May 1946) 9-10.

CONTRIBUTION TO THE THEORY OF PULSED AND MODULATED EXPERIMENTS ON FAST NEUTRON MULTIPLYING MEDIA

M. CADILHAC, P. GOVAERTS, P. HAMMER, M. MOORE
B. NICOLAENKO AND F. STORRER
ASSOCIATION EURATOM-CEA POUR LES NEUTRONS RAPIDES,
CENTRE D'ÉTUDES NUCLÉAIRES DE CADARACHE, FRANCE

Abstract — Résumé — Аннотация — Resumen

CONTRIBUTION TO THE THEORY OF PULSED AND MODULATED EXPERIMENTS ON FAST NEUTRON MULTIPLYING MEDIA. The authors study the structure of the analytical function k(p) introduced by Storrer and Stiévenart (EUR 593 e), to disclose the core conditions which it may be possible to obtain in the course of pulsed and modulated experiments.

In the case of pulsed experiments, the existence of a well-defined persistent exponential mode cannot necessarily be assumed at the outset. The initial formula used is one in which energy is viewed continuously, so as to obviate the artificial features introduced by the usual multigroup method. Using quite general hypotheses, it can be shown that k(p) takes the form:

$$k(p) = \int_{\lambda_0}^{\lambda_1} \frac{\kappa(\lambda)d\lambda}{\lambda + p}$$

From this, it can be deduced that the time distribution of pulse-triggered fissions is only dominated asymptotically by a pure exponential mode for core assemblies. The multigroup method provides a stepped approximation of the cumulant of $\kappa(\lambda)$. It is useful to consider the synthetic forms of $\kappa(\lambda)$, involving a few parameters whose values have to be adjusted. For example, $\kappa(\lambda)$ can be considered proportional to $(\lambda - \lambda_0)^s(\lambda_1 - \lambda)^s$, especially as this expression is suggested by rigorous calculation of $\kappa(\lambda)$ in a model in which the slowing-down is expressed by a nucleus of the Wigner or Greuling-Goertzel type and the cross-sections obey certain simple analytical laws. Various illustrations and applications of the methods described are given.

CONTRIBUTION A LA THÉORIE DES EXPÉRIENCES PULSÉES ET MODULÉES SUR DES MILIEUX MULTIPLICATEURS A NEUTRONS RAPIDES. On étudie la structure de la fonction analytique k(p), introduite par Storrer et Stiévenart (EUR 593 e), en vue de mettre en évidence des caractéristiques de milieux multiplicateurs que l'on puisse espérer atteindre par des expériences pulsées et modulées.

En ce qui concerne les expériences pulsées, l'existence même d'un mode exponentiel persistant bien défini ne peut être admise à priori. On part d'une formulation où l'énergie est traitée de façon continue, afin d'écarter des particularités artificielles dues à la méthode multigroupe habituellement utilisée. On peut montrer sous des hypothèses très générales que k(p) prend la forme

$$k(p) = \int_{\lambda_0}^{\lambda_1} \frac{\kappa(\lambda)d\lambda}{\lambda + p}$$

On en déduit que la distribution dans le temps des fissions engendrées par une impulsion n'est dominée asymptotiquement par un mode exponentiel pur que pour des milieux suffisamment multiplicatuers. La méthode multigroupe fournit une approximation en escalier de la cumulée de $\kappa(\lambda)$. Il est utile de considérer

des formes synthétiques de $\kappa(\lambda)$, dépendant d'un petit nombre de paramètres dont les valeurs doivent être ajustées. On peut prendre par exemple $\kappa(\lambda)$ proportionnel à $(\lambda-\lambda_0)^r(\lambda_1-\lambda)^s$; cette expression est d'ailleurs suggérée par un calcul rigoureux de $\kappa(\lambda)$ dans un modèle dans lequel le ralentissement est exprimé par un noyau du type de Wigner ou de Greuling-Goertzel, les sections efficaces suivant par ailleurs certaines lois analytiques simples. On donne enfin diverses illustrations et applications des méthodes exposées.

ВКЛАД В ТЕОРИЮ ИМПУЛЬСНЫХ И МОДУЛИРУЕМЫХ ОПЫТОВ В РАЗМНОЖАЮЩИХ СРЕДАХ НА БЫСТРЫХ НЕЙТРОНАХ. Исследуется структура аналитической функции k(p), предложенной Сторрером и Стивенаром (EUR 593 e), для определения характеристик размножающих сред, которые, возможно, могут быть получены с помощью импульсных и модулируемых опытов.

Что касается импульсных опытов, то нельзя предположить заранее наличие хорошо определенной устойчивой экспоненциальной гармоники. Исходят при этом из формулы, где энергия рассматривается как постоянная величина, чтобы устранить особенности, связанные с обычно используемым многогрупповым методом. Можно показать, что в свете существующих очень общих гипотез k(p) принимает вид:

$$k(p)=\int_{\lambda_0}^{\lambda_1}\frac{\kappa(\lambda)\,d\lambda}{\lambda+p}$$

Из этого выводят, что распределение по времени делений, вызванных импульсом, в общем не определяется асимптотически чистой экспоненциальной гармоникой, а вытекает из постоянного спектра констант распада. Многогрупповой метод дает постепенное приближение совмещения $\kappa(\lambda)$. Целесообразно рассмотреть синтетические формы $\kappa(\lambda)$, содержащие небольшое количество параметров, значения которых должны быть уточнены. Можно,например,взять $\kappa(\lambda)$, пропорциональное $(\lambda-\lambda_0)^r\ (\lambda_1-\lambda)^s$, это выражение к тому же обусловливается точным расчетом $\kappa(\lambda)$ в модели, а замедление выражено ядром типа Вигнера или Грелинга-Горцеля, в то время как эффективные сечения следуют, в частности, некоторым простым аналитическим законам.

Наконец, приводятся различные иллюстрации и говорится о применении изложенных методов.

APORTACION A LA TEORIA DE LOS EXPERIMENTOS DE PULSACION Y DE MODULACION EN MEDIOS MULTIPLICADORES DE NEUTRONES RAPIDOS. Los autores estudian la estructura de la función analítica k(p), propuesta por Storrer y Stiévenart, a fin de poner de manifiesto diversas características de medios multiplicadores que cabe determinar mediante experimentos de pulsación y modulación.

Por lo que respecta a los experimentos de pulsación, ni siquiera puede admitirse a priori la existencia de un modo exponencial persistente bien definido. Los autores parten de una formulación en la que se trata a la energía de una forma continua, a fin de descartar toda particularidad artificial debida al método de varios grupos habitualmente utilizado. Puede demostrarse, recurriendo a hipótesis muy generales, que k(p) adopta la forma

$$k(p)=\int_{\lambda_0}^{\lambda_1}\frac{\kappa(\lambda)d\lambda}{\lambda+p}.$$

De aquí se deduce que, en general, la distribución temporal de las fisiones producidas por un impulso está sólo dominada asintóticamente por un modo exponencial puro para medios suficientemente multiplicadores. El método de varios grupos proporciona una aproximación escalonada de la expresión de $\kappa(\lambda)$. Resulta útil considerar formas sintéticas de $\kappa(\lambda)$,que dependen de un pequeño número de parámetros cuyos valores es preciso ajustar. Puede tomarse, por ejemplo, $\kappa(\lambda)$ proporcional $(\lambda-\lambda_0)^r(\lambda_1-\lambda)^s$; esta expresión, por lo demás, es resultado indirecto de un cálculo riguroso de $\kappa(\lambda)$ aplicado a un modelo en el que se expresa su moderación mediante un núcleo de Wigner o de Greuling-Goetzel, en tanto que las secciones eficaces siguen determinadas leyes analíticas sencillas. Terminan citando diversos ejemplos de los métodos descritos y describiendo algunas de sus aplicaciones.

1. INTRODUCTION

This report deals with the mathematical treatment of the prompt neutron kinetics in fast neutron systems. We are mainly interested in subcritical multiplying systems, considering, for the sake of simplicity, homogeneous media and using buckling terms to take spatial dependence into account. Delayed neutrons are ignored.

The formulation of energy-dependent problems in these systems usually rests on the multigroup description. But this method cannot give clear insight into the qualitative structure of time-dependent phenomena since it exhibits artificial features related to the choice of the energy groups. Moreover, the ability of multigroup data available to give good quantitative descriptions of transient spectra is not established a priori.

Therefore, we have used a continuous energy variable, to obtain general properties for the time evolution of quantities of interest. This evolution has been characterized by some functions of a continuous decay variable λ. For certain simple examples these functions are elementary; for real cases, they can be deduced from multigroup information by using appropriate models.

The formulation described seems to be suitable for a proper interpretation and discussion of pulsed and modulated experiments in fast systems.

2. FUNDAMENTAL DEFINITIONS AND FORMULAE

Let us consider the following problem: at time $t = 0$, a unit fission burst is introduced into the system; what can be said about the resulting distribution in time of fissions G(t)? The fission spectrum being fixed, G(t) can be deduced from the distribution in time of first generation fissions, K(t) (fissions directly induced by the initial neutrons). In fact, the Laplace transforms of G(t) and K(t) are related by

$$g(p) = \frac{k(p)}{1 - k(p)} \tag{1}$$

k(0) is the effective prompt multiplication factor.

The functions g(p) and k(p) have been introduced and their properties have been investigated by using the multigroup method in a previous paper of STORRER and STIEVENART [1]. In this case g(p) and k(p) are rational functions and the poles of k(p) are on the negative part of the real axis. G(t) and K(t) then appear as sums of a finite number of exponential terms, but this number, as well as the decay constant and the amplitude associated to each mode, depends on the particular group structure. However, the expression

$$K(t) = \sum_{j=1}^{N} \kappa_{(j)} e^{-\lambda_{(j)} t} \tag{2}$$

may be written as

$$K(t) = \int_{\lambda_0}^{\lambda_1} \kappa(\lambda) e^{-\lambda t} d\lambda \tag{3}$$

where $\lambda_0 < \lambda_{(j)} < \lambda_1$ and

$$\kappa(\lambda) = \sum_{j=1}^{N} \kappa_{(j)} \delta[\lambda - \lambda_{(j)}] . \tag{4}$$

It is natural to assume the existence of a regular function $\kappa(\lambda)$, Eq. (4) being only an approximate expression of it, owing to the multigroup model. Then

$$k(p) = \int_{\lambda_0}^{\lambda_1} \frac{\kappa(\lambda)}{\lambda + p} d\lambda \tag{5}$$

must be a regular analytic function of p outside the negative real axis; this is indeed the case if the scattering cross-section is bounded (sufficient, but not a necessary condition, proved in the Appendix). It is readily seen that when

$$p \to -\lambda \quad \text{(real negative)}$$

k(p) tends in general to a complex limit

$$k(p) \to \theta(\lambda) \pm i\pi\kappa(\lambda) \tag{6}$$

(upper sign for Im $p > 0$)

$\theta(\lambda)$ being the Cauchy principal value integral,

$$\theta(\lambda) = \int_{\lambda_0}^{\lambda_1} \frac{\kappa(\lambda')}{\lambda' - \lambda} d\lambda' \tag{7}$$

(Hilbert transform of $\kappa(\lambda)$).

3. FURTHER PROPERTIES OF k(p): SIMPLE EXAMPLES

k(p) is the average, over the fission spectrum, of the function m(E, p) defined by the equation

$$\left(\Sigma(E) + \frac{p}{v}\right) m(E, p) = \int_0^E \Sigma_s(E \to E')\, m(E', p) dE' + \nu\, \Sigma_f(E) \tag{8}$$

with usual notations and $\Sigma(E) = \Sigma_{tot}(E) + D(E)B^2)$. As shown in the Appendix, $m(E, p)$ is regular for a complex p different from all values of $-v\Sigma(E)$ corresponding to energies smaller than E. As a consequence, the lower limit λ_0 of the $\kappa(\lambda)$ distribution is the minimum of $v\Sigma$.

To obtain examples of explicit $\kappa(\lambda)$ functions, we have considered simple scattering kernels. Assuming that fission neutrons are produced at a definite energy E_1, using the hydrogen slowing-down kernel and constant cross-sections, one obtains by solving Eq. (8)

$$k(p) = k(0)\left[1 - \frac{p^r(\lambda_1 + p)^{1-r} - p}{(1-r)\lambda_1}\right] \tag{9}$$

with $r = 2\Sigma_a/\Sigma$ and $\lambda_1 = v_1\Sigma$. Then one obtains from Eq. (6):

$$\kappa(\lambda) = k(0)\frac{\sin \pi r}{\pi(1-r)\lambda_1}\lambda^r(\lambda_1 - \lambda)^{1-r}; \quad 0 < \lambda < \lambda_1 \tag{10}$$

More generally, if $\Sigma_s(E' \to E)$ is taken as a product of a function of E and a function of E' (E' > E), Eq. (8) can be reduced to a first-order differential equation and $\kappa(\lambda)$ can be, in principle, determined by analytical methods. Thus the Wigner or Greuling-Goertzel models [2] with $1/v^\ell$ cross-sections ($0 \leqslant \ell < 1$) lead to

$$\kappa(\lambda) = a\lambda^r(\lambda_1 - \lambda)^s; \quad 0 < \lambda < \lambda_1 \tag{11}$$

where a, r, s and λ_1 are constants.

The Fermi model (heavy moderator) corresponds to infinite λ_1 and s ($c = s/\lambda_1$ being fixed)

$$\kappa(\lambda) = a\lambda^r e^{-c\lambda} \tag{12}$$

The expression

$$\kappa(\lambda) = a(\lambda - \lambda_0)^r(\lambda_1 - \lambda)^s; \quad \lambda_0 < \lambda < \lambda_1, \tag{13}$$

provides a convenient synthetic model for general discussions. Its ability to represent actual systems will be examined in section 5.

4. ANALYSIS OF THE FUNCTION G(t)

The problem of deducing G(t) from $\kappa(\lambda)$ is solved by using the set of Eqs. (5), (1) and

$$G(t) = \frac{1}{2i\pi}\int_\Delta g(p)e^{pt}\,dp, \tag{14}$$

where Δ is the imaginary axis (Laplace inversion formula). The structure of G(t) can be investigated by the usual change of the path of integration; for this, one must be careful of the singularities of g(p), namely, the branch cut of k(p) ($-\lambda_1 < p < \lambda_0$) and possible poles from roots of

$$k(p) = 1 . \tag{15}$$

It is easily shown that this equation can have only one root (which is real) $p = -\alpha > -\lambda_0$ when $\kappa(\lambda)$ is never negative; we shall assume that such is the case. Thus two situations can arise.

(a) If g(p) has no pole, it is possible to express G(t) as an integral along the branch cut:

$$G(t) = \int_{\lambda_0}^{\lambda_1} \gamma(\lambda) e^{-\lambda t} d\lambda \tag{16}$$

with

$$\gamma(\lambda) = \frac{1}{2i\pi} \lim_{0 < \epsilon \to 0} [g(-\lambda - i\epsilon) - g(-\lambda + i\epsilon)] \tag{17}$$

By using Eq. (6), one obtains

$$\gamma(\lambda) = \frac{\kappa(\lambda)}{[1 - \theta(\lambda)]^2 + \pi^2 \kappa^2(\lambda)} \tag{18}$$

(b) g(p) has a real pole, $-\alpha$, which involves an additional exponential term in the expression of G(t)

$$G(t) = \gamma_\alpha e^{-\alpha t} + \int_{\lambda_0}^{\lambda_1} \gamma(\lambda) e^{-\lambda t} d\lambda \tag{19}$$

with

$$\gamma_\alpha = - \frac{1}{dk(p)/dp} \Bigg|_{p = -\alpha} .$$

In the latter case since $\alpha < \lambda_0$, the isolated exponential dominates for large values of t: there is a fundamental mode with a well-defined decay constant α; on the other hand, instead of discrete harmonics, there is a bundle of continuous higher modes.

In the former case, Eq. (16), no separated fundamental mode exists; the time signal G(t) is a continuous combination of decaying exponentials. However, if the distribution $\gamma(\lambda)$ shows a peak around some value of λ, this value will be a "pseudo-mode" and G(t) will possibly behave like the corresponding exponential during a finite time interval. From Eq. (18), it is clear that such peaks are to be found in the neighbourhood of roots of the equation:

$$\theta(\lambda) = 1 \tag{20}$$

When a discrete fundamental mode does exist from a mathematical point of view, case (b), it may happen that this mode has too small an amplitude γ_α, or is not sufficiently separated from the continuous spectrum (α near λ_0), so that it has no physical importance. This situation has been considered in the case of multigroup formulations in [1].

5. APPLICATION TO GIVEN SYSTEMS

We have investigated a number of specific media, divided into three main classes.

(a) High density media, for example, 93.5% enriched uranium, with a mean neutron generation time τ_1 of about 5 ns.

(b) Dilute media (20% enriched uranium and structure material: iron or aluminium) with $\tau_1 \sim 20$ ns; we particularly considered the SUAK assemblies [3], for which results of pulsed experiments are available [4].

(c) Very dilute systems, corresponding, for instance, to the following volume fractions:

Uranium oxide (20% enriched)	35%
Iron	15%
Sodium	50%

with τ_1 as large as 200 ns.

Calculations were made by using the 16-group ANL constants [5] to determine the poles $-\lambda_{(j)}$ of the related approximate k(p) and the corresponding residues $\kappa_{(j)}$; then we tried to deduce the cumulative function $c(\lambda) = \int_{\lambda_0}^{\lambda} \kappa(\lambda) d\lambda/\lambda$ from its step approximation $\sum_{\substack{\lambda < \lambda \\ (j)}} \kappa_{(j)}/\lambda_{(j)}$. This process is successful when one deals with concentrated or moderately dilute media, cases (a) and (b), for which regular $c(\lambda)$ clearly appear. In most cases, simple analytical expressions of $\kappa(\lambda)$ can be fitted; thus, Eq. (13) was found to be quite appropriate to represent Godiva and other high density systems (see Fig. 1).

For very dilute systems, however, it was not possible to obtain a well-defined $\kappa(\lambda)$ by this method, because of the lawless values of many residues $\kappa_{(j)}$; this fact is probably related to a complex structure of the real $\kappa(\lambda)$, owing to the complicated shape of the total cross-section in the low energy region; more theoretical work should be done to investigate the influence of this shape, including the effects of the resonances.

A crude model may be used in every case to account for essential features: taking $\kappa(\lambda)$ as a constant a for $\lambda_0 < \lambda < \lambda_1$ and zero outside this interval (this is a particular case of Eq. (13) with r = s = 0), one obtains three parameters which can be chosen so as to keep the multiplication factor

$$k(0) = \int_0^\infty K(t)dt = \int_{\lambda_0}^{\lambda_1} \kappa(\lambda) \frac{d\lambda}{\lambda} = a \ln \frac{\lambda_1}{\lambda_0} \tag{21}$$

and the first two moments τ_1 and τ_2 of the generation time

$$\tau_1 k(0) = \int_0^\infty tK(t)dt = \int_{\lambda_0}^{\lambda_1} \kappa(\lambda)\frac{d\lambda}{\lambda^2} = a\left(\frac{1}{\lambda_0} - \frac{1}{\lambda_1}\right) \tag{22}$$

$$\tau_2 k(0) = \int_0^\infty t^2K(t)dt = 2\int_{\lambda_0}^{\lambda_1} \kappa(\lambda)\frac{d\lambda}{\lambda^3} = a\left(\frac{1}{\lambda_0^2} - \frac{1}{\lambda_1^2}\right) \tag{23}$$

If $k(0)$, τ_1 and τ_2 are known from the usual multigroup calculations, Eqs.(21),

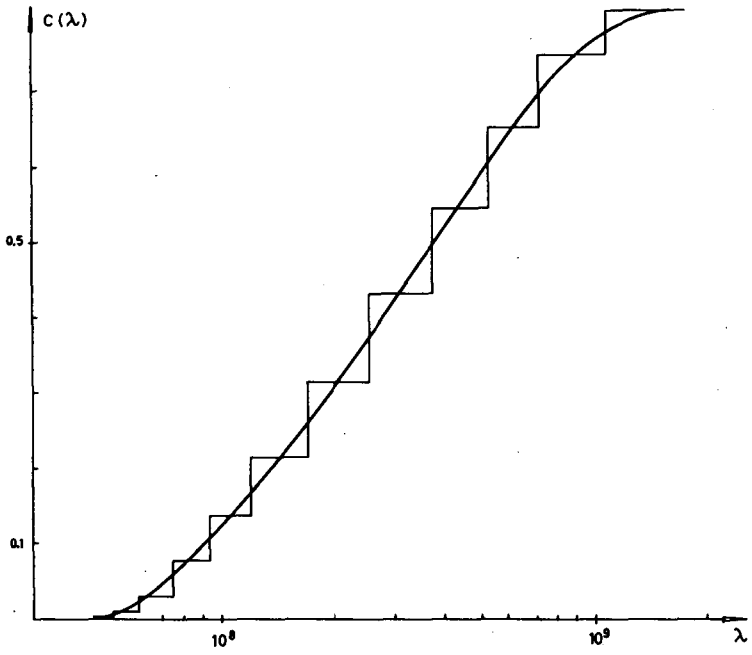


Fig. 1

93.5% enriched uranium

$k(0) = 0.81$, $\tau_1 = 5.2$ ns, $\tau_2 = 93$ ns²

Cumulative functions

(a) 16-group calculations
(b) Least squares fit

$\lambda_0 = 4.8 \times 10^7$, $\lambda_1 = 1.8 \times 10^9$, $r = 0.33$, $s = 1.7$

(22) and (23) can be solved easily by iteration. This model has the advantage of analytical simplicity

$$k(p) = a \ln \frac{p + \lambda_1}{p + \lambda_0} \tag{24}$$

$$\theta(\lambda) = a \ln \frac{\lambda_1 - \lambda}{\lambda - \lambda_0} \tag{25}$$

and

$$\gamma(\lambda) = \frac{a}{\left[a \ln \frac{\lambda_1 - \lambda}{\lambda - \lambda_0} - 1\right]^2 + \pi^2 a^2}; \quad \lambda_0 < \lambda < \lambda_1 \tag{26}$$

There is always a discrete fundamental mode α given by

$$\frac{\lambda_1 - \alpha}{\lambda_0 - \alpha} = \exp\left(\frac{1}{a}\right) \tag{27}$$

See Figs. 2 and 3. To illustrate this point, the values corresponding to the SUAK experiments [3] are shown in Table I. An experimental value of

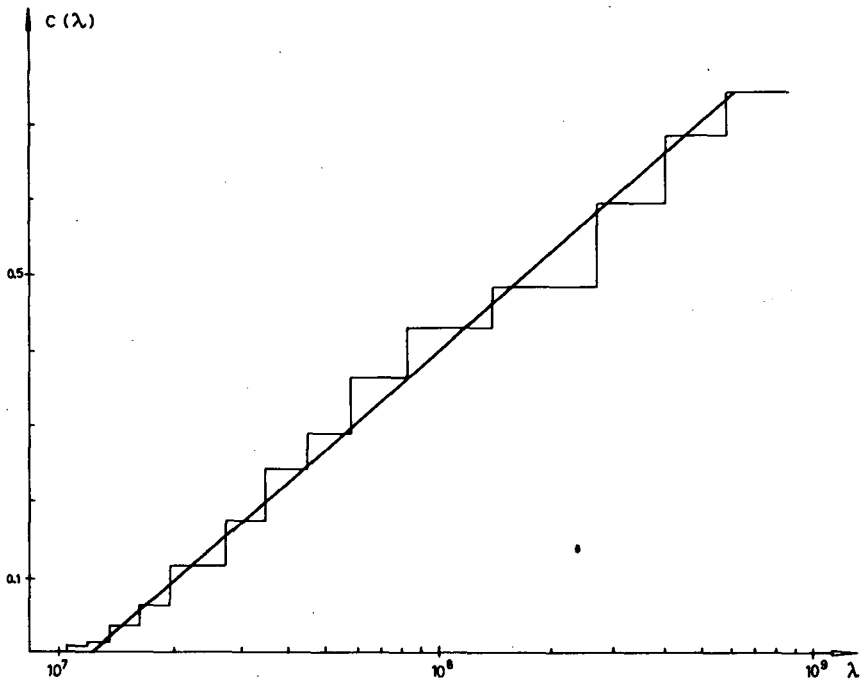


Fig. 2

SUAK (first experiment)

Cumulative functions

(a) 16-group calculations
(b) crude model (r = s = 0)

$\alpha = 4.5\ \mu s^{-1}$ has been observed in the second case, corresponding to a well-separated theoretical value.

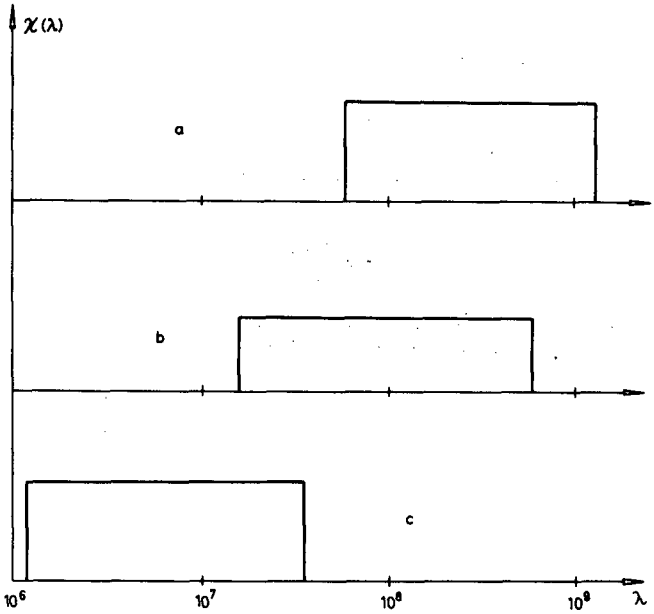


Fig. 3

Comparison of $\kappa(\lambda)$ ($r = s = 0$) for the three kinds of systems considered in section 5

6. CONCLUSION

We have shown the interest of analysing a time signal as a combination of decaying exponentials

$$G(t) = \int \gamma(\lambda)\, e^{-\lambda t}\, d\lambda \qquad (28)$$

generally including discrete and continuous contributions. Such a representation enables one to realize, for example, the reason why one cannot point out a well-defined fundamental mode by pulsing a system which is too subcritical. In principle G(t) itself may be experimentally determined (pulsed experiment), as well as its Fourier transform

$$g(i\omega) = \int \frac{\gamma(\lambda)}{\lambda + i\omega}\, d\lambda \qquad (29)$$

(modulated experiment); but these experiments give only partial information concerning $\gamma(\lambda)$ (discrete decay constants, moments such as $k(0)$, τ_1, τ_2). Moreover, the latter are physically related only to values of λ bounded by $1/\Delta t$, where Δt is the resolution time. Therefore simple models introducing a limited number of parameters should account for the main experimental aspects of the kinetics of prompt neutrons in fast systems. (See Figs. 4 and 5.)

TABLE I

EXPERIMENTAL VALUES FROM SUAK

Case	k(0)	τ_1 (ns)	τ_2 (ns²)	a	λ_0 (μs^{-1})	λ_1 (μs^{-1})	α (μs^{-1})
1	0.74	21	1800	0.19	12	590	9.0
2	0.85	25	2300	0.23	11	410	5.2

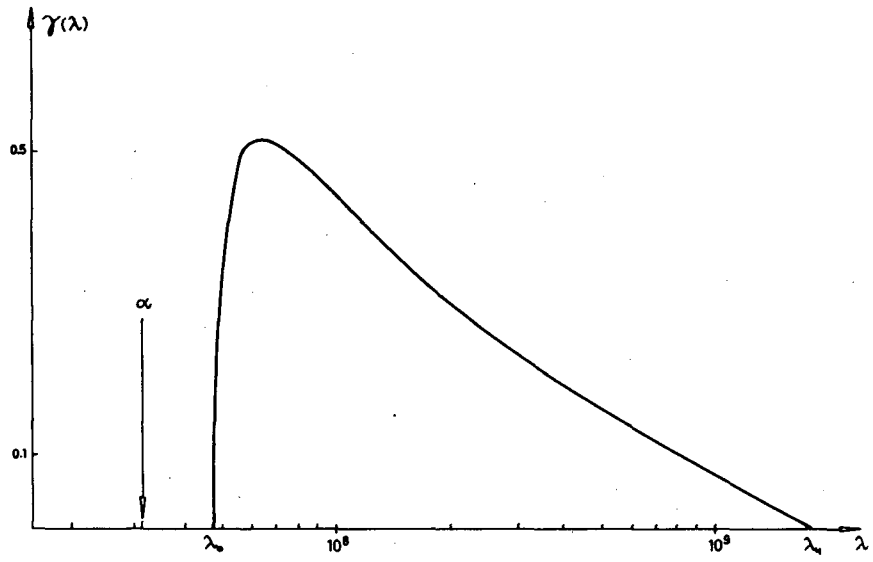


Fig. 4

The function $\gamma(\lambda)$ and the isolated decay constant α deduced from the fit shown on Fig. 1

ACKNOWLEDGEMENTS

We wish to thank Drs. Borgwaldt and Küchle, who discussed the experiments of section 5(b) with us and kindly communicated their data before publication.

APPENDIX

To prove that Eq. (8) has a solution for every complex p different from all values of $-v\,\Sigma(E)$ (in particular for p outside the real axis), we can start from the following mathematical assumptions, which are physically reasonable,

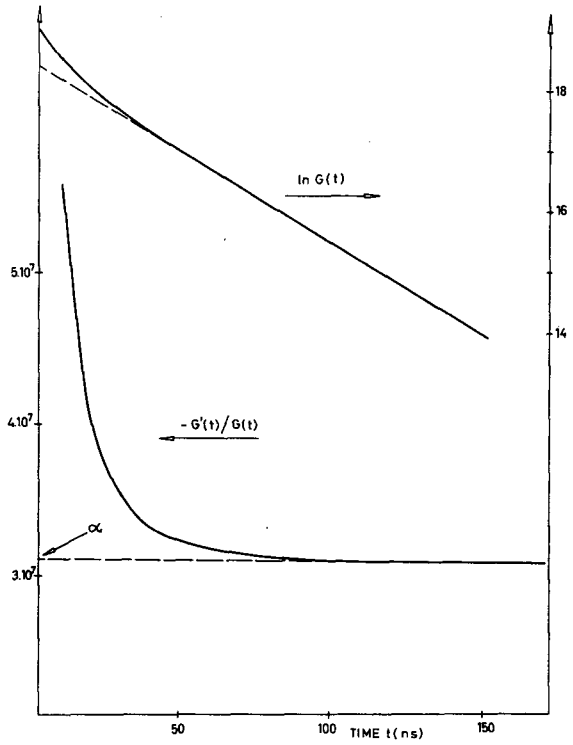


Fig. 5

An example of time response: ln G(t) and its derivative from the data of Fig. 4

$$\nu v \Sigma_f(E) \quad \text{and} \quad \frac{\int_0^E \Sigma_s(E \to E') E'^{\alpha} dE'}{(\alpha+1)\ E^{\alpha}}$$

are bounded for every $\alpha > 0$. The latter condition holds for elastic and inelastic scattering if $\Sigma_s(E)$ is bounded. If the functions $m_\ell(E, p)$ defined by

$$m_0(E) = \frac{\nu \Sigma_f(E)}{\Sigma(E) + \frac{p}{v}}$$

$$m_\ell(E, p) = \frac{1}{\Sigma(E) + \frac{p}{v}} \int_0^E \Sigma_s(E \to E')\, m_{\ell-1}(E', p) dE'; \quad \text{for } \ell > 0 \qquad (30)$$

are introduced, it is readily shown that the series

$$\sum_{\ell=0}^{\infty} m_\ell(E, p)$$

converges and gives the solution of Eq. (8). (Compare with the Neumann expansion for the solution of a Volterra integral equation.)

REFERENCES

[1] STORRER, F. and STIÉVENART, M., Rpt. EUR 593 e (1964).
[2] BECKURTS, K.H. and WIRTZ, K., Neutron Physics, Springer Verlag, Berlin (1964).
[3] BORGWALDT, D., KÜCHLE, M., MITZEL, F. and WATTECAMPS, E., SM 62/2, these Proceedings.
[4] BORGWALDT, D. and KÜCHLE, M., private communication.
[5] YIFTAH, S., OKRENT, D. and MOLDAUER, P.A., Fast Reactor Cross-Sections, Pergamon Press, N.Y. (1960).

DISCUSSION

N. CORNGOLD: Do you believe that changing the simple analytical form of $K(\lambda)$ so as to include effects of fluctuating cross-sections would improve the agreement between your theoretical and experimental data.

M. CADILHAC: The fluctuations of the effective cross-sections should only require the use of more complex $K(\lambda)$ functions to the extent that $v\Sigma_t$ is not an increasing function of energy (resonance range for diluted media, for example). The analytical form I have indicated is certainly not the only one which is of interest.

CONTRIBUTION TO THE STUDY OF FAST NEUTRON NON-MULTIPLYING ASSEMBLIES BY THE PULSED NEUTRON TECHNIQUE

G. DECONNINCK
CENTRE DE PHYSIQUE NUCLÉAIRE, LOUVAIN
AND
P. d'OULTREMONT* AND M. STIÉVENART
SOCIÉTÉ BELGE POUR L'INDUSTRIE NUCLÉAIRE, BRUSSELS, BELGIUM

Abstract — Résumé — Аннотация — Resumen

CONTRIBUTION TO THE STUDY OF FAST NEUTRON NON-MULTIPLYING ASSEMBLIES BY THE PULSED NEUTRON TECHNIQUE. Pulsed neutrons experiments have been performed on non-multiplying and poorly moderating materials (Fe, Cu, C). The energy of the source neutrons was chosen to be 1400, 1100, 890 and 670 keV. The time variations of the leakage flux have been measured for different locations of the detector. The former was shown to be strongly dependent on the latter. A systematic study of these experiments has been done by the Monte Carlo method using a semi-continuous energy model. The results given by this method are in good agreement with the experimental results and, moreover, the Monte Carlo method is a very useful tool to study the energetic degradation of the primary neutrons. The propagation of the incident neutrons in such assemblies has also been studied by the time-dependent P_1 approximation. This method gives analytical results which are also in good agreement with the experimental results.

CONTRIBUTION A L'ÉTUDE DES ASSEMBLAGES NON MULTIPLICATEURS A NEUTRONS RAPIDES PAR LA MÉTHODE DES NEUTRONS PULSÉS. Des expériences au moyen de neutrons pulsés ont été réalisées sur des matières non multiplicatrices et médiocrement ralentisseuses (Fe, Cu, C). Les énergies suivantes ont été retenues pour les neutrons émis par la source: 1400 keV, 1100 keV, 890 keV et 670 keV. Les variations dans le temps du flux de fuite ont été mesurées pour différentes positions du détecteur. Les auteurs ont procédé à une étude systématique de ces expériences au moyen de la méthode de Monte-Carlo en utilisant une formulation où l'énergie est traitée de façon semi-continue. Les résultats obtenus par cette méthode concordent bien avec les résultats expérimentaux et, en outre, la méthode de Monte-Carlo est un instrument très utile pour l'étude de la diminution d'énergie des neutrons primaires. Les auteurs ont aussi étudié la propagation des neutrons incidents dans de tels assemblages par l'approximation P_1 variable dans le temps. Cette méthode donne des résultats qui concordent eux aussi de façon satisfaisante avec les résultats expérimentaux.

ВКЛАД В ИЗУЧЕНИЕ ПОДКРИТИЧЕСКИХ СБОРОК НА БЫСТРЫХ НЕЙТРОНАХ МЕТОДОМ ИМПУЛЬСНЫХ НЕЙТРОНОВ. Эксперименты с импульсными нейтронами проводили на неразмножающих и плохо замедляющих материалах (Fe, Cu, C). Энергия нейтронного источника колебалась в пределах 1400, 1100, 890 и 670 кэв. Временные вариации потока утечки измеряли в различных местах расположения детектора. Было показано, что первые сильно зависят от вторых. Систематическое изучение этих экспериментов проводили методом Монто-Карло с использованием полунепрерывной энергетической модели. Результаты, полученные с помощью этого метода, хорошо согласуются с экспериментальными результатами, и более того, метод Монто-Карло является очень полезным для изучения энергетической деградации первичных нейтронов. Распространение бомбардирующих нейтронов в таких сборках изучали также с помощью приближения с зависимой от времени величиной P_1. Этот метод дает аналитические результаты, которые также хорошо согласуются с экспериментальными результатами.

CONTRIBUCION AL ESTUDIO DE LOS CONJUNTOS NO MULTIPLICADORES RAPIDOS POR LA TECNICA DE LOS NEUTRONES PULSADOS. Los autores han realizado experimentos con neutrones pulsados en materiales

* Present address: Centro Comune di Ricerche, Ispra, Varese, Italy.

no multiplicadores y de escasas propiedades moderadoras (Fe, Cu, C). Las energías de los neutrones emitidos por la fuente eran las siguientes: 1400, 1100, 890 y 670 keV. Han medido la variación temporal del flujo neutrónico para distintas posiciones del detector, y comprobaron que aquélla depende considerablement de éstas. Han efectuado un estudio sistemático de estos experimentos, por el método de Monte Carlo, empleando un modelo de energía semicontinua. Los resultados obtenidos por este método concuerdan satisfactoriamente con los resultados experimentales y, además, el método de Monte Carlo constituye un instrumento muy útil para estudiar la degradación energética de los neutrones primarios. También han estudiado la propagación de los neutrones incidentes en esos conjuntos, empleando para ello la aproximación de P_1 en función del tiempo. Este método ha proporcionado resultados analíticos compatibles con los datos experimentales.

1. INTRODUCTION

Pulsed experiments in the fast neutron field have been rather scarce until now [1, 2, 3]. Moreover, their interpretation has been done in analogy with pulsed experiments in the thermal field, with the hope of measuring bucklings, elastic and inelastic cross-sections, and even angular distributions [4]. To check these possibilities, simple experiments have been carried out: carbon, iron and copper blocks have been excited by 1.4, 1.1, 0.87, 0.67 MeV; monoenergetic neutron pulses and leakage fluxes have been measured as functions of time. Since the obtained spectra are strongly dependent on the detector position, the interpretation of such experiments should take the neutron wave propagation into account and the mathematical expression of the neutron density should be non-separable in time and space variables. Monte-Carlo calculations have been very useful in enlightening the problems. Moreover, a simple analytical method, the P_1 time-dependent approximation, has given results in agreement with experiments and Monte-Carlo calculations.

2. EXPERIMENTAL APPARATUS

Experiments have been carried out at the Nuclear Physics Centre of the University of Louvain with a 4.4-MeV Van de Graaff accelerator delivering 3 ns pulses at 5 MHz frequency. A usual time-of-flight measurement device has been used; it includes an ELDORADO time-to-pulse-height converter, a single channel pulse-height analyser as discriminator and a RIDL 400-channel analyser. Neutrons are detected by an organic scintillator (stilbène) coupled with a RCA 5810-A photomultiplier. The time resolution of the apparatus is of the order of the neutron pulse duration. As the objective was the study of the behaviour of the neutron cloud taken as a whole, no special precaution was taken to refine energy resolution.

Neutrons were produced by $Li^7(p,n)Be^7$ reaction on a 50-keV thick lithium target evaporated on a gold backing. Since assemblies were 40 cm from the target, the angular distribution of the source neutrons added some spreading in the neutron energy spectrum. The total uncertainty of the neutron source energy was about 100 keV. All assemblies were rectangular blocks. The leakage fluxes were measured on the source-side (reflected fluxes) and on the opposite side (transmitted fluxes). The detector was always put on the axis of the accelerator beam.

3. EXPERIMENTAL RESULTS

Figures 1A and 1B give an example of transmitted and reflected fluxes following injection of 1.4-MeV neutron bursts into a 30 cm × 40 cm × 40 cm copper block. These spectra are not corrected for background and for non-

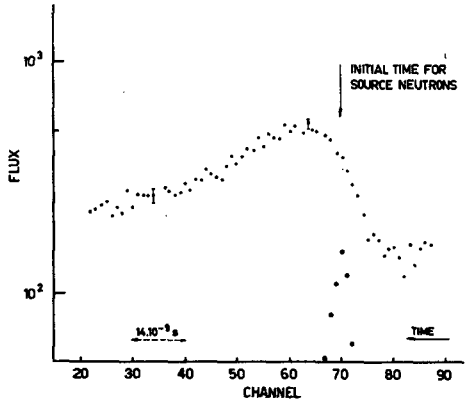


Fig. 1A

Transmitted flux spectrum; copper block 30×40×40 cm
1.408-MeV source neutrons

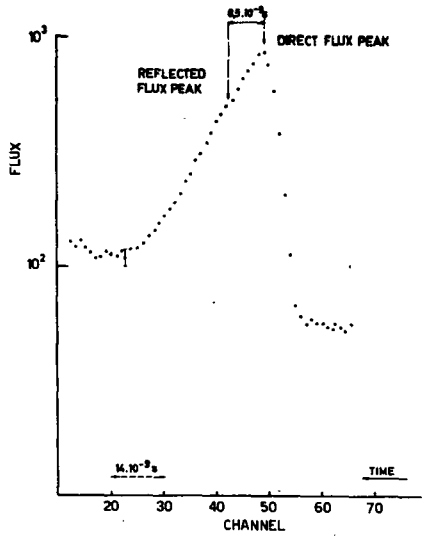


Fig. 1B

Reflected flux spectrum; copper block 30×40×40 cm
1.408-MeV source neutrons

linearity of the time-to-pulse-height converter. After such corrections, the spectra obtained were handled by least square analysis using a Fortran programme written for the IBM 1620 [5]; in this way, an exponential func-

tion is obtained which fits better the observed decay. This procedure has no other object than to give the possibility of comparing different spectra and was not used to determine "decay constants" of some hypothetical spatial modes. Table I collects experimental results: indicated errors are only the result of counting statistics and do not take experimental errors into account; these may be estimated to ≈15%. Moreover, the determination of the background is partially an arbitrary matter because the pulsing frequency is a little bit too high for such experiments and, when counting rate is poor, a supplementary error of some per cent may be introduced.

4. ANALYSIS OF EXPERIMENTAL RESULTS

Three interesting facts appear from Table I and Figs. 1A, 1B, 2A and 2B:

(1) The decay in time of transmitted and reflected fluxes is different.

(2) When the neutron wave is moving away from the source, its initial slope changes in sign.

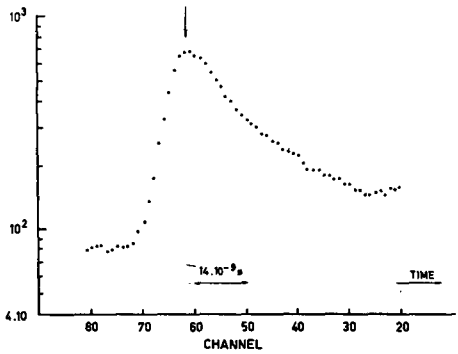


Fig. 2A

Transmitted flux; Cu 20×40×40 cm
E_n = 1.408-MeV source neutrons

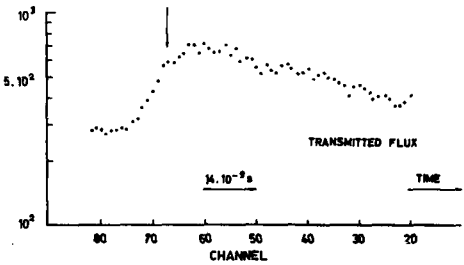


Fig. 2B

Transmitted flux; Cu 20×40×40 cm
E_n = 0.672-MeV source neutrons

(3) The thicker the assembly, the slower the asymptotic decay of the transmitted fluxes. This is also true for the reflected fluxes, but in a different way and to a lesser extent.

To clarify point (2), we have plotted on Figs. 2A and 2B the time variation of the transmitted flux for one copper block excited by 1.408- and 0.672-MeV neutrons (the time scale is the same as in Figs. 1A and 1B). The arrow indicates the time-of-arrival of source neutrons at the observation point. After this time, the slope can be measured and Figs. 2A and 2B show that it has changed in sign. This effect results in an increase of the scattering cross-section of copper when energy decreases: (σ_s(1.408 MeV),

TABLE I

EXPERIMENTAL RESULTS

Assembly (cm × cm × cm)		Source neutron energy (MeV)	Decay constant (Transmitted flux) ($10^7 s^{-1}$)	Decay constant (Reflected flux) ($10^7 s^{-1}$)
Carbon	36×36×36	1.408	4.184 ± 0.23	8.464 ± 0.35
	36×36×36	1.099		8.718 ± 1.32
	18×36×36	1.090	7.153 ± 0.14	11.013 ± 1.45
Iron	40×30×30	1.408	6.523 ± 0.62	
	40×30×30	1.099	5.387 ± 0.38	
	40×30×30	0.891	4.629 ± 0.24	
	40×30×30	0.786	2.750	
	40×30×30	0.672	3.560	
	20×30×30	1.408	10.638 ± 0.03	
Copper	30×40×40	1.408	3.992 ± 0.27	8.045 ± 0.08
	30×40×40	1.099	2.349 ± 0.36	6.184 ± 0.13
	30×40×40	0.891		5.268 ± 0.10
	30×40×40	0.679		3.328 ± 0.11
	20×40×40	1.408	6.002 ± 0.38	
	20×40×40	1.099	4.849 ± 0.07	
	20×40×40	0.891	3.680 ± 0.10	
	20×40×40	0.679	2.613 ± 0.25	

σ_s (0.672 MeV) = 4 b). Such an energetic effect is equivalent to the increase of the total number of mean free paths between the source and the observation point; but a quantitative interpretation of this phase variation is difficult. However, Monte-Carlo calculations and P_1 approximation, both used in a one-velocity model, give valuable information about this phenomenon.

As far as the evolution of the flux decay in terms of the block size is concerned (point (3)), this is generally accepted to be in reasonable agreement with the elementary diffusion theory [2, 3]. However, it would be surprising that this may be quite right for several reasons. As a matter of fact, one must bear in mind that the establishment of a neutron population at the equilibrium is only possible by collisions with the moderating nuclei. Two extreme possibilities can be envisaged:

(1) The medium is poorly moderating (lead or uranium) and its mean free path is large. In this case, there are not many collisions per unit of time and, when the neutron population reaches the equilibrium, its density becomes so weak, because of the leakage, that it is no longer detectable (see Fig. 5).

(2) The medium is more moderating and its mean free path is so small that the neutrons are performing many collisions before leaving the medium. Now, and for small assemblies (4 to 8 mean-free-paths thick), equilibrium is quickly reached, but energy degradation is so important that it is impossible to consider the neutron cloud as monoenergetic and the decay is not at all exponential.

At least, let us point out that a "trapping effect", similar to the one existing for beryllium in the thermal field [6], has been observed in the case of the 780-keV resonance of the Fe^{56}: it can be seen from Table I that 670-keV neutrons (σ_s = 2.3 b) are decaying faster than 780-keV neutrons having however a greater velocity (σ_s = 3.5 b).

5. ANALYSIS OF PULSED EXPERIMENTS BY THE MONTE-CARLO METHOD

To get an empirical knowledge of the behaviour of the neutrons in such experiments, a great number of them have been simulated by the Monte-Carlo method. A simple Fortran programme has been written for the IBM 7090 and operated at the Euratom Research Centre, Ispra. The programme allows the geometry of the assemblies to be taken into account exactly. The following approximations have been used:

(1) Neutrons are undergoing only elastic collisions.

(2) Neutron angular distribution is approximated by: $\sigma_{el\,s}(\theta) \sim \sigma_0(1+\omega_1 \cos\theta)$ with the LANGSDORF's values of ω_1 [7].

Results* are:

(1) The time variation of reflected and transmitted total fluxes.

(2) The time variation of partial fluxes in a multigroup energy model for these two flux waves.

The following information has been obtained:

(1) Figures 3A and 3B show the time variation of fluxes transmitted and reflected by 6, 12, 20 and 30-cm-thick copper blocks having 40 cm × 40 cm

* Some results have been checked by the TIMDC programme and agreement is good.

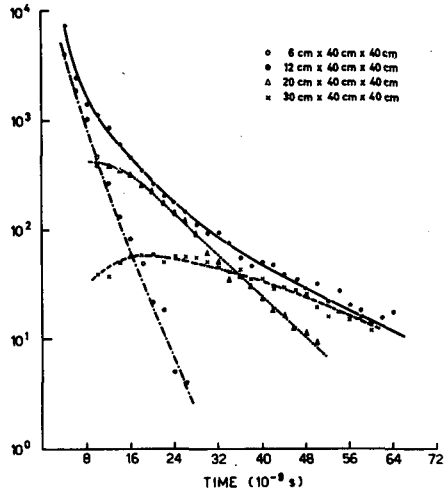


Fig. 3A

Monte-Carlo calculations, transmitted fluxes in Cu blocks
$E_n = 1.09$ MeV

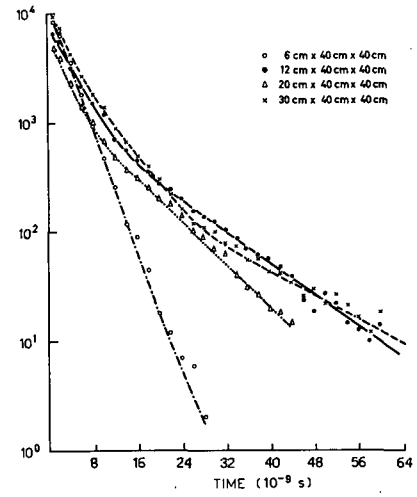


Fig. 3B

Monte-Carlo calculations, reflected fluxes in Cu blocks
$E_n = 1.09$ MeV

cross-section. These blocks have been excited by 1.099-MeV neutron pulses of $\delta(t)$ duration and, in this case, diffusion is taken as isotropic. Two facts must be pointed out:

(a) When the thickness of the block increases, the decay rate of the reflected flux decreases until it reaches a minimum value (20 cm and 30 cm blocks have the same decay rate). For thickness greater than 6 or 7 mean free paths, the blocks may be considered as infinite for the time during which there are enough neutrons for detection.

(b) The decay rate of the transmitted flux, immediately after the arrival of neutrons at the observation point, decreases monotonously when the size of the assembly increases. For small assemblies, it is greater than the one of the reflected flux, due to a transport effect of source neutrons. For large assemblies the contrary is true, but there exists a particular thickness for which the two decays are identical. Nevertheless, for all assemblies, both fluxes tend to decay with the same rate a long time after the arrival of the first neutrons at the observation point. One also sees that the wave phase is changing in the same way as indicated by Figs. 2A and 2B.

(2) Six- and 12-cm-thick copper blocks have also been studied, copper nuclei being assumed infinitely heavy. This leads to a one-velocity model. A phenomenon, which is partly hidden by the energy degradation in the actual experiments, appears here: after the transient period, while reflected and transmitted fluxes are decaying differently, they have an identical decay which agrees reasonably with elementary diffusion calculations (the decay constant $\alpha = vDB_g^2$, where v is the neutron velocity, D the diffusion coefficient and B_g^2 the geometrical buckling. Calculations are shown in Table II and Fig. 4.

TABLE II

ONE-VELOCITY CALCULATIONS

Copper block (cm)	α(Monte-Carlo) (s^{-1})	α(Diffusion theory) (s^{-1})
9×60×60	10.31×10^7	9.03×10^7
12×60×60	6.83×10^7	6.45×10^7

Here B_g^2 has been calculated with an extrapolation length of $0.71\ \lambda_{tr}$. Agreement is better with a $0.57\text{-}\lambda_{tr}$ extrapolation length which corresponds to Mark's boundary conditions. This fact has also been pointed out in the MÜLLER abd KSCHWENDT's work [13].

(3) The results for numerous cases of experiments are shown in Table I. Table III allows the comparison of experimental and Monte-Carlo results. Let us point out two facts:

(a) Agreement between both investigation methods is generally well excepted when the experiment has been done during such a time period that, because of the energy degradation of the neutrons, the mean energy of the neutron population becomes lower than the first inelastic level (~ 800 keV in iron and copper). In these cases, Monte-Carlo calculation, which does not take inelastic scattering into account, indicates a slower decay than experiment. A good example are the results on the 30 × 30 × 40 cm copper block excited by 1.408-MeV neutrons (Fig. 6 and Table III).

(b) A detailed study of the energy spectrum evolution as a function of time (Fig. 5) shows that, even for copper and iron, the energy is suf-

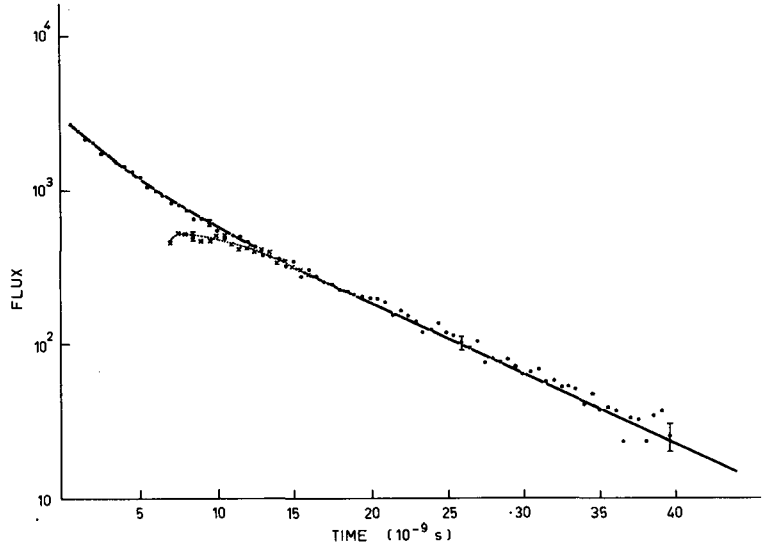


Fig. 4

Monte-Carlo calculations for Cu^{63}, 9 cm × 60 cm × 60 cm, without moderation
$E_n = 1$ MeV

—●— Reflected flux
...x... Transmitted flux

ficiently degraded so that the mean energy of the transmitted flux may be at least 300 keV lower than the one of source neutrons. Under these conditions, it seems difficult to measure cross-sections by pulsed technique with an exception perhaps for the heaviest media, if one can define an analytical model able to describe the transient states of the neutron cloud.

Anyway, the measurement of reflected flux seems to be more interesting than that of transmitted flux because it is possible, by this technique, to eliminate geometrical effect if large and thick assemblies are used.

(4) One of BEGHIAN's experiments [2] has been simulated, i.e. excitation of a 8 in × 8 in × 8 in lead block by 1.24-MeV neutrons (Fig. 6). During a time period which is long, making allowance for the detection possibilities, the neutron population is not at equilibrium. A decay rate of 16×10^7 s^{-1} has been obtained, as Beghian obtained, but it does not seem correct to interpret this decay rate, which corresponds to a transient state, by the elementary diffusion theory.

6. THE P_1 TIME-DEPENDENT APPROXIMATION

6.1. The formalism

The whole of the preceding observations aims at finding an analytical model able to take the neutron wave propagation into account. Thus, a wave

TABLE III

COMPARISON BETWEEN EXPERIMENTAL RESULTS AND MONTE-CARLO CALCULATIONS

Assembly (cm × cm × cm)		Neutron energy (MeV)	Decay constant - Transmitted flux (10^7 s^{-1})				Decay constant - Reflected flux (10^7 s^{-1})			
			I[a]	II[b]	III[c]	Experimental	I	II	III	Experimental
Carbon	36×36×36	1.408			5.55	4.18 ± 0.23			8.81	8.46 ± 0.35
	12×36×36	1.408		5.34	5.34		10.21			
	12×36×36	1.099	13.1	5.31	5.31	7.153 ± 0.14	9.45	5.31		
Iron	40×30×30	0.786			2.66	2.75	8.23	4.52		
	40×30×30	0.672			3.21	3.56	7.71	3.21		
Copper	30×40×40	1.408			2.93	3.99 ± 0.27	10.21	3.02	7.86	8.04 ± 0.08
	30×40×40	1.039			2.51	2.35 ± 0.36	10.11	2.84	6.04	6.184 ± 0.13
	20×40×40	1.408		4.06	5.45	6.00 ± 0.38	9.62	4.12		
	20×40×40	1.099			4.45	4.89 ± 0.07	10.0			
	20×40×40	0.679		2.81	2.41	2.613 ± 0.25	10.2	2.81		
Lead (in)	8 × 8 × 8	1.240			16.1	16 ± 0.31[d]	11.8	11.8		

a Decay rate of the transitory fluxes.

b Decay constants of the fluxes when equilibrium is attained.

c Decay constants of the fluxes calculated on the same time period as in the experimental measurement. Agreement between Monte-Carlo and experiment may be estimated comparing column III and "Experimental".

d BEGHIAN et al. [2].

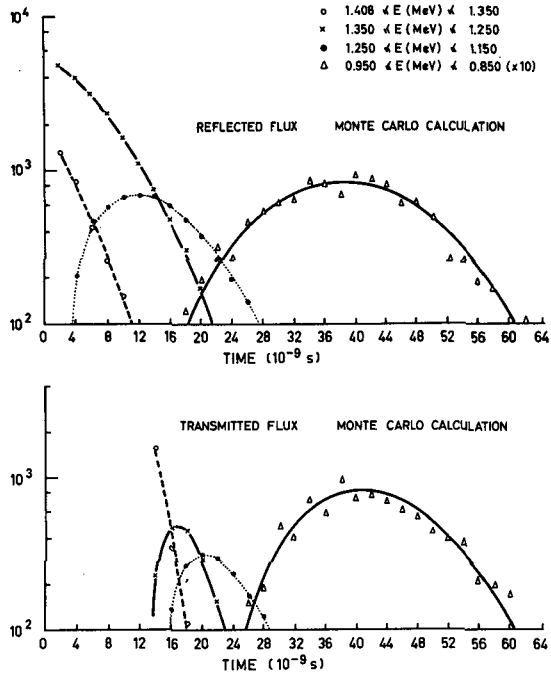


Fig. 5

Energetic spectrum of the leakage fluxes of a 20 cm × 40 cm × 40 cm Cu block pulsed by 1.408-MeV neutrons

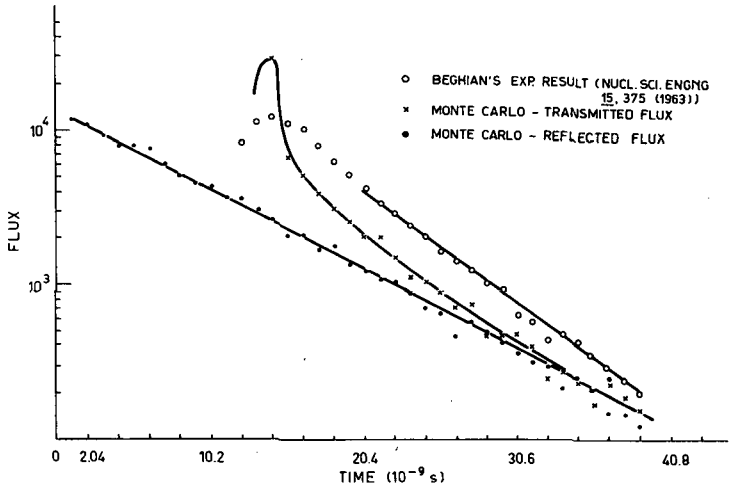


Fig. 6

Leakage fluxes in a 8 in × 8 in × 8 in lead block pulsed by 1.24-MeV neutrons

equation is required and it is well known [6, 8] that such an equation is displayed by the P_1 approximation of the time-dependent Boltzmann's equation. If the one-velocity model is assumed to be valid, one has the following equations:

$$\left(\Sigma_a + \frac{1}{v}\frac{\delta}{\delta t}\right)\phi_0(r,t) + \frac{\delta}{\delta r}\phi_1(r,t) = 0$$

$$\frac{\delta}{\delta r}\phi_0(r,t) + 3\left(\Sigma_{tr} + \frac{1}{v}\frac{\delta}{\delta t}\right)\phi_1(r,t) = 0\,, \tag{1}$$

where $\phi_0(r,t)$ and $\phi_1(r,t)$ are the two first moments of the neutron flux expansion in Legendre polynomials:

$$\phi(\vec{r},t) = \frac{1}{4\pi}\sum_{l=0}^{\infty}(2l+1)P_l(\cos\theta)\phi_l(r,t)$$

and where other symbols have their usual meaning,

In a semi-infinite medium ($0 \leq r \leq \infty$), the system (1) can be solved by two successive Laplace transforms on time and space variables. This method has the advantage of allowing an easy use of the initial and boundary conditions. One obtains, for the neutron density:

$$\phi_0(r,t) = \frac{\sqrt{3}}{4} S\left[(\Sigma_{tr} + \Sigma_{tot}(1-c))\, I_0 + (\Sigma_{tr} - \Sigma_{tot}(1-c))\right.$$

$$\left.\frac{t}{\sqrt{t^2-\mu^2}} I_1\right] \exp -\frac{v}{2}(\Sigma_{tr} + \Sigma_{tot}(1-c))t\,, \tag{2}$$

where

c = number of secondary neutrons born in a collision

$$\mu = \frac{r}{v}\sqrt{3}$$

$I_i = I_i\left[\frac{v}{2}(\Sigma_{tr} - \Sigma_{tot}(\sec))\sqrt{t^2-\mu^2}\right]$ (modified Bessel function of first kind)

S = source intensity.

On the other hand, in an infinite slab of thickness a, one obtains, by using the Laplace transform on time alone

$$\phi_0(r,t) = \frac{1}{\sqrt{3}} S\, e^{-at} \sum_{n=1}^{\infty}(-1)^n [I_0(b(t^2-\mu_0^2)^{\frac{1}{2}}) - I_0(b(t^2-\mu_1^2)^{\frac{1}{2}})] \tag{3}$$

where

$\mu_0 = (r+2n\,a)\sqrt{3}/v$

$\mu_1 = (2\,a\,(n+1)-r)\sqrt{3}/v$

$a = \frac{v}{2}(\Sigma_{tr} + \Sigma_{tot}(1-c))$

$b = \frac{v}{2}(\Sigma_{tr} - \Sigma_{tot}(1-c))$

The right-hand sides of Eqs.(2) and (3) are non-separable in time and space and describe a wave front propagation followed by an asymptotic stationary neutron distribution. Furthermore, the solution of Eq.(3) contains real arguments even if a is small. This fact agrees with LEHNER and WING's results [11] but is at variance with other authors' conclusions [4, 12], who obtain oscillating fluxes when the assembly dimensions are decreasing below some limits. It is probable that these oscillating solutions appear because separable Ansatz are used a priori. Moreover, this separability introduces spatial eigenvalues whose significance is physically questionable because, during the interesting time interval, fluxes are very far from equilibrium. At last, we may note that Monte-Carlo calculations have been carried out on media for which oscillatory fluxes have been foreseen [4] and that no special behaviour has been pointed out.

6.2. Results of calculation

By using Eqs.(2) and (3) neutron fluxes in several media, finite or infinite, have been calculated for a monoenergetic $\delta(t)$ neutron source. Figure 7

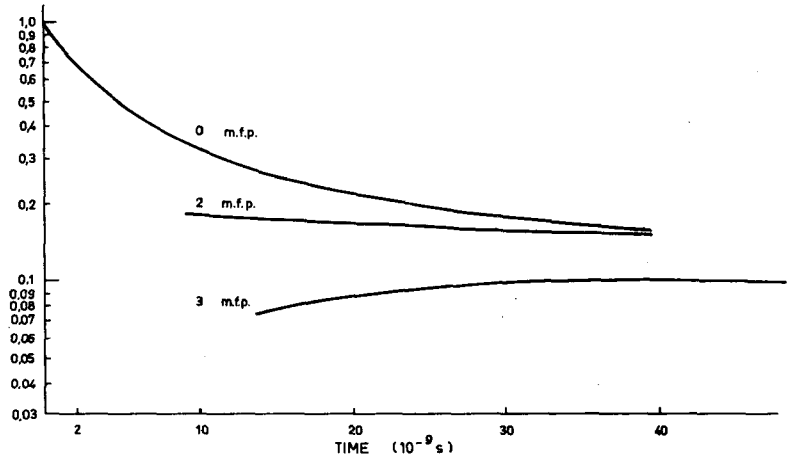


Fig. 7

Time-dependent spectra in an infinite Cu block, assuming no moderation
$E_n = 1$ MeV
P_1 approximation

shows neutron density versus time curves for 1-MeV neutrons in a copper infinite medium, assuming no moderation. Density is calculated at 0, 2 and 3 mean free paths apart from the source. In Fig.8, results are collected for a similar calculation performed on an artificial infinite medium ($\Sigma_a = 0.2$ cm^{-1}, $\Sigma_s = 1.8$ cm^{-1}, $\lambda_{tot} = 0.5$ cm; isotopic diffusion) which has also been studied by the Monte-Carlo method [13]. Neutron density in a 5 mean-free-path radius sphere of the same material has also been calculated (Fig.9).

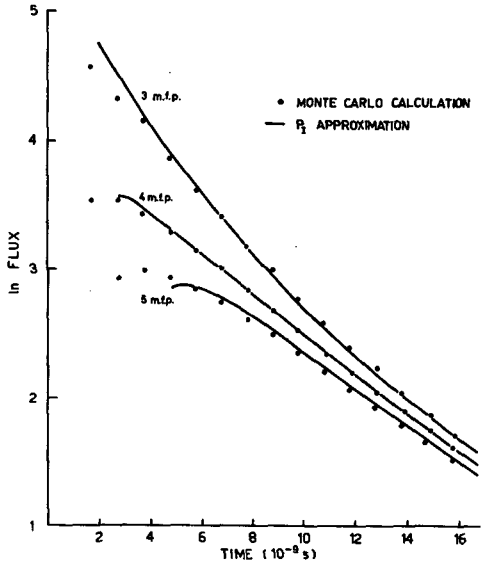


Fig. 8

Time-dependent spectra in an infinite non-moderating medium
$E_n = (10^9 \text{ cm/s})^2 \times M_n/2$

• Monte Carlo calculation
— P_1 approximation

From these results, it can be concluded that:

(1) Agreement between the P_1 and Monte-Carlo approximation is fairly good when the distance between the source and observation point is more than 3 mean free paths. This fact might be expected because P_1 approximation describes a wave travelling with the velocity $v' = v/\sqrt{3}$, where v is the neutron velocity, and it is easy to show that, after a run of 4 mean free paths in an isotopic diffusion medium, the mean velocity of the neutron population in the propagation direction of the wave achieves a value very close to v'.

(2) During its travel, the wave becomes deformed and its phase changes sign in a manner similar to the one indicated by Monte-Carlo results and, as far as one can check, by experiments. It is easy to calculate, in terms of the cross-sections, the point at which the change of sign of the wave phase appears. Perhaps this fact could be useful for cross-section measurements.

7. CONCLUSIONS

These experimental, numerical and analytical studies on pulsed assemblies lead to the following conclusions:

(1) Concerning the evolution of the neutron density, it seems sure that a short burst of fast neutrons is propagated in moderating media like a front wave. This wave has a phase which changes during the propagation, making

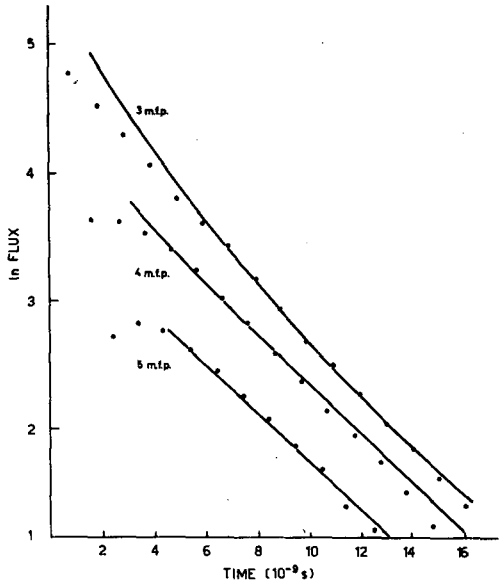


Fig. 9

Time-dependent spectra in a sphere of non-moderating medium
$E_n = (10^9\ cm/s)^2 \times M_n/2$

• Monte Carlo calculation
—— P_1 approximation

the transient part of the time behaviour of the fluxes strongly dependent on the distance from the source where they are observed. At least, the wave passage is followed by the establishment of a neutron density at equilibrium which, in the case where moderating effect is weak, seems to decay exponentially. If moderation is important, the decay law has not been dedermined; this problem joins the thermalization one.

(2) Concerning the measurement possibilities offered by pulsed experiments with fast neutrons in the field of cross-sections, geometry effects, angular distributions, etc., these depend on the possibility of correctly interpreting transient fluxes because, experimentally, stationary neutron densities are very difficult to reach. In some case, P_1 approximation has appeared to be a useful tool.

ACKNOWLEDGEMENTS

This paper releases some results of work done as fulfilment of a Ph.D. thesis [14]. One of the authors (P. d'Oultremont) takes pleasure in thanking Dr. G. Deconninck for his valuable and friendly leadership and Messrs. V. Raievski and G. Tavernier for numerous discussions and advice. The BelgoNucléaire gave an important financial support and Euratom granted a fellowship.

REFERENCES

[1] BENGSTON, J., Proc. 2nd UN Int. Conf. PUAE 12 (1958) 63.
[2] BEGHIAN, L.E., RASMUSSEN, N.C., THEWS, R. and WEBER, J., Nucl. Sci. Engng 15 (1963) 375.
[3] BEGHIAN, L.E., PROFIO, A.E., WEBER, J. and WILENSKY, S., Nucl. Sci. Engng 17 (1963) 82.
[4] COCKRELL, R.G., PEREZ, R.B. and DALTON, G.R., Nucl. Sci. Engng 19 (1964) 423.
[5] SERVAIS, F. and JANSSEN, J., Détection de neutrons pulsés - Programme d'exploitation des mesures par moindres carrés, Rpt. BN 6407-15 (1964).
[6] DE SAUSSURE, G., Proc. Brookhaven Conf. on Neutron Thermalization, Rpt. BNL-719 IV (1962) 1158.
[7] LANGSDORF, A., LANE, R.O. and MONAHAN, J.E., Neutron scattering angular distribution, Rpt. ANL-5567 (1961).
[8] DI PASQUANTONIO, F., Energia Nucl. 11 (1964) 465.
[9] WEINBERG, A.M. and WIGNER, E.P., The Physical Theory of Neutron Chain Reactors, Univ. of Chicago Press, Chic., Ill. (1958).
[10] IBSIN, H.S., Introductory Nuclear Reactor Theory, Reinhold, N.Y. (1963).
[11] LEHNER, J. and WING, G.M., Comm. pure appl. Math. 8 (1955) 217.
[12] DAITCH, P.B. and EBEOGLU, D.B., Proc. Brookhaven Conf. on Neutron Thermalization, BNL-719, IV (1962) 1132.
[13] MÜLLER, K.H. and KSCHWENDT, H., Internal Rpt, Euratom, Ispra (1964).
[14] d'OULTREMONT, P., «Pulsation d'ensembles sous-critiques par des neutrons rapides», Ph.D. Thesis, Univ. of Louvain (1965).

DISCUSSION

L. BEGHIAN: It is not clear to me what the energy response was of the detector you used. By using a biased detector and confining ourselves essentially to the one-velocity case, we have measured the decay spatially over the surface of lead cubes and we have found that within experimental error there is a single mode of decay. This would seem to contradict your results.

P. D'OULTREMONT: Did you measure your spectrum on the same face of the block or on the opposite face?

L. BEGHIAN: We measured all over the surface of the cube.

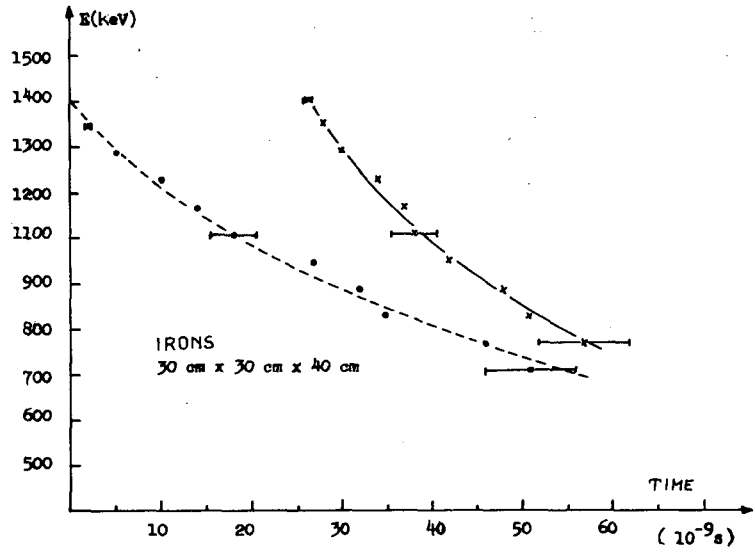
P. D'OULTREMONT: And you never saw anything of this sort?

L. BEGHIAN: No. But we did find - and this is quite important - that difficulties were liable to arise if we weren't careful with our shielding. With careful shielding of the detector, however, we found that within experimental error there seemed to be a single decay constant, provided we used a biased detector and were therefore limited to the one-velocity case.

P. D'OULTREMONT: All I can say is that when I performed these experiments I relied entirely on your experimental data.

L. BEGHIAN: The work I have just mentioned was never actually published, but we did it to check that we had a single mode of decay.

P. D'OULTREMONT: I can see why you emphasize the purely monoenergetic aspect of your experiments. We did our measurements in the same spirit. The main problem here would seem to be whether it is possible to interpret such measurements by assuming a steady-state spatial neutron distribution since, in the case of iron for example, the velocity at which the energy is degraded is such as to make it impossible for the establishment of spatial modes to occur. The following figure shows the results of a Monte-Carlo calculation from which the value of this velocity can be obtained.



Monte-Carlo evolution of mean neutron velocity in leakage fluxes
E_n = 1.408 MeV

--- Reflected flux
—— Transmitted flux

L. BEGHIAN: I think we may be talking about two completely different things. I'm talking of a one-velocity case, where, allowing for a slight amount of elastic moderation, one selects for detection only those neutrons which have undergone no degradation.

P. D'OULTREMONT: Does this also apply to the case of lead?

L. BEGHIAN: In all cases we made a selection. If we put in 1-MeV neutrons we detected only 1-MeV emerging neutrons within a spread of 100 kV. I agree that if the energy softening is taken into account then it is impossible to say what happens. One does not observe discrete eigenvalues if one observes, shall we say, the total neutron flux; a continuum of eigenvalues is observed, and one would expect this.

P. D'OULTREMONT: Is it possible to attribute a buckling to your flux or not? On the basis of these measurements and the Monte-Carlo calculation it seems to me that it is not because there is no equilibrium of the flux inside.

L. BEGHIAN: That is precisely the point. One cannot attribute a buckling to the flux. It depends on what you mean by the flux, the flux at what energy?

P. D'OULTREMONT: If one inserts 1-MeV neutrons inside the block, for example, is it possible to attribute a buckling to the flux at 1-MeV neutrons or not?

L. BEGHIAN: We believe it is, and, as I hope to show* we believe that we have shown the existence of modes even for the smallest assemblies.

---

* See BEGHIAN, L.E. and WILENSKY, S., "The pulsed neutron technique applied to fast non-multiplying assemblies" (SM-62/74), these Proceedings II.

P. D'OULTREMONT: It will be interesting to see your data, because this is not my view.

A. HENRY: Could you perhaps give some additional information on the nature of your Monte-Carlo calculations? If you have available a Monte-Carlo code which exactly describes your experiment, then this can be used directly to verify the cross-sections being tested. If not, I should think you could design a code and an experiment which would be capable of testing cross-sections exactly. This procedure would avoid the difficulties raised by using some approximate theoretical model.

P. D'OULTREMONT: With the Monte-Carlo code the geometry of the experiments is taken into account exactly. The approximations used relate to

(a) The angular neutron distribution at the time of the collisions – this is allowed for by a P_1 (cos θ) development limited to the first order of σ_s;

(b) The energy spectrum, which is approximated by a multigroup distribution. (Most of the calculations were done with 15 groups with a width of 100 keV, obtained on the basis of the effective cross-sections of Langsdorf et al. (Rpt. ANL 5567).)

I fully agree with what you say on the utilization of Monte-Carlo calculations in conjunction with experimental data to determine effective cross-sections. The only thing is that this method would probably be extremely expensive.

THE PULSED NEUTRON TECHNIQUE APPLIED TO FAST NON-MULTIPLYING ASSEMBLIES*

L. E. BEGHIAN AND S. WILENSKY
MASSACHUSETTS INSTITUTE OF TECHNOLOGY,
CAMBRIDGE, MASS., UNITED STATES OF AMERICA

Abstract — Résumé — Аннотация — Resumen

THE PULSED NEUTRON TECHNIQUE APPLIED TO FAST NON-MULTIPLYING ASSEMBLIES. A nanosecond pulsed Van de Graaff accelerator has been used to study the behaviour of fast neutrons in non-multiplying metal assemblies.

A pulsed neutron source technique has been utilized to measure fast non-elastic cross-sections for iron. The method employed is similar to that used to measure absorption cross-sections in thermal assemblies, with the exception that the fast decay times are of the order of nanoseconds rather than microseconds. Nanosecond bursts of monoenergetic neutrons are injected into various size iron assemblies. The neutron flux in these assemblies is observed to decay exponentially with a characteristic decay constant. The decay constant is composed of a sum of terms which represent neutron loss due to leakage and energy degradation. Energy degradation represents a neutron loss since a biased neutron detector is used. The removal term due to elastic and non-elastic scattering can be determined by measuring the decay constant as a function of assembly size. A theoretical development is presented for calculating the fraction that the elastic scattering contributes to the removal term, hence the non-elastic cross-section can be determined. The theoretical treatment for calculating the elastic contribution has been verified experimentally. The non-elastic cross-section for iron has been measured by this technique for primary neutron energies between 0.8 and 1.5 MeV.

The pulsed source technique described above has been used to measure decay constants for lead slabs. The experiment approximates the assumptions which are generally made when solving the time-dependent Boltzmann transport equation (i.e. one-dimension, one-velocity). Decay constants have been measured for 28 in × 32 in lead slabs of 2, 4, 6 and 8-in thickness. The results, after being corrected for energy degradation and finite assembly, are compared with the approximate solutions of the Boltzmann transport equation.

APPLICATION DE LA MÉTHODE DES NEUTRONS PULSÉS AUX ASSEMBLAGES NON MULTIPLICATEURS A NEUTRONS RAPIDES. Les auteurs ont utilisé un accélérateur Van de Graaff à impulsions de l'ordre de la nanoseconde pour étudier le comportement de neutrons rapides dans des assemblages métalliques non multiplicateurs.

Ils ont mesuré les sections efficaces non élastiques du fer pour les neutrons rapides. La méthode employée est semblable à celle qu'on utilise pour mesurer les sections efficaces d'absorption dans des assemblages à neutrons thermiques, avec cette différence que les temps de décroissance pour les neutrons rapides sont de l'ordre de la nanoseconde et non de la microseconde. Des bouffées de neutrons monoénergétiques d'une nanoseconde sont introduites dans des assemblages en fer de dimensions diverses. On remarque que dans ces assemblages le flux de neutrons décroît exponentiellement avec une constante de décroissance caractéristique. La constante de décroissance est composée d'une somme de termes qui représentent la perte de neutrons due aux fuites et à la dégradation en énergie. La dégradation en énergie représente une perte de neutrons, car un détecteur de neutrons dont les données sont entachées d'une erreur systématique est utilisé. On peut déterminer le terme correspondant à la diffusion élastique et inélastique en mesurant la constante de décroissance considérée comme une fonction des dimensions de l'assemblage. Suit un développement théorique pour le calcul de la fraction de ce terme qui est due à la diffusion élastique et, par conséquent, pour la détermination de la section efficace non élastique. Le procédé théorique de calcul de cette fraction a fait l'objet de vérifications expérimentales. Les auteurs ont mesuré la section efficace non élastique du fer par cette méthode pour des énergies de neutrons primaires comprises entre 0,8 et 1,5 MeV.

La méthode de la source pulsée décrite ci-dessus a été utilisée pour mesurer des constantes de décroissance pour des plaques de plomb. Les conditions de l'expérience sont approximativement conformes aux

* This work was supported by the National Science Foundation.

hypothèses généralement admises lorsqu'on résout l'équation de transport de Boltzmann qui est fonction du temps (c'est-à-dire une dimension, une vitesse). Les constantes de décroissance ont été mesurées pour des plaques de plomb de 70 cm × 80 cm et de 5, 10, 15 et 20 cm d'épaisseur. Après correction pour tenir compte de la dégradation en énergie et des dimensions finies de l'assemblage, les résultats sont comparés aux solutions approchées de l'équation de transport de Boltzmann.

ПРИМЕНЕНИЕ МЕТОДА ИМПУЛЬСНЫХ НЕЙТРОНОВ ПРИ ИЗУЧЕНИИ ПОВЕДЕНИЯ БЫСТРЫХ НЕЙТРОНОВ В НЕРАЗМНОЖАЮЩИХ СБОРКАХ. Ускоритель Ван-де-Граафа с наносекундными импульсами использовали для изучения поведения быстрых нейтронов в неразмножающих металлических сборках.

Для измерения сечений неупругого рассеяния железа на быстрых нейтронах применили метод импульсного источника нейтронов, аналогичный методу, применяемому для измерения сечений поглощения в тепловых сборках, за исключением того, что время быстрого спада измеряется нано-, а не микросекундами. Наносекундные импульсы моноэнергетических нейтронов инжектируются в железные сборки различных размеров. Отмечено, что поток нейтронов в этих сборках спадает экспоненциально с характеристической постоянной спада. Постоянная спада состоит из суммы членов, которые представляют собой потерю нейтронов вследствие утечки и потери энергии. Потеря энергии представляет собой потерю нейтронов, поскольку используется пороговый нейтронный детектор. Член утечки за счет упругого и неупругого рассеяния можно определить путем измерения постоянной спада в зависимости от размера сборки. Представлен теоретический вывод для расчета доли упругого рассеяния в члене утечки и, следовательно, можно определить сечение неупругого рассеяния. Теоретическая трактовка для расчета вклада упругого рассеяния проверена экспериментальным путем. Сечение неупругого рассеяния железа измерено с помощью этого метода для первичной энергии нейтронов в диапазоне 0,8–1,5 Мэв.

Вышеописанный метод импульсного источника нейтронов был использован для измерения постоянной спада в отношении свинцовых пластин. Экспериментальные данные примерно согласуются с предположениями, которые обычно делают при решении больцмановского уравнения переноса с временной зависимостью (т.е. одномерное, односкоростное). Постоянные спада измерены для свинцовых пластин размером 28 × 32 дюйма и толщиной 2; 4; 6 и 8 дюймов. После внесения поправки на потерю энергии и конечные размеры сборки результаты сравниваются с приблизительными решениями больцмановского уравнения переноса.

APLICACION DE LA TECNICA DE LOS NEUTRONES PULSADOS A CONJUNTOS RAPIDOS DE MATERIALES NO MULTIPLICADORES. Los autores han empleado un acelerador Van de Graaff, que emitía ráfagas de neutrones pulsados del orden del nanosegundo, para estudiar el comportamiento de los neutrones rápidos en conjuntos de metales no multiplicadores.

Emplearon esta técnica de la fuente de neutrones pulsados a fin de medir las secciones eficaces de dispersión inelástica de los neutrones rápidos en el Fe. El método empleado es análogo al utilizado para medir las secciones eficaces de absorción en conjuntos térmicos, salvo el hecho de que los tiempos de decrecimiento de los neutrones rápidos son del orden del nanosegundo más bien que del microsegundo. En estos experimentos, se inyectaron ráfagas de neutrones monoenergéticos, del orden del nanosegundo, en conjuntos de Fe de diversas dimensiones. Se observó que, en esos conjuntos, el flujo neutrónico decrece exponencialmente con una constante característica. Esta constante de decrecimiento está constituida por una suma de términos que representan la pérdida de neutrones debidos al escape y a la degradación energética. Esta última representa una pérdida de neutrones toda vez que se emplea un detector neutrónico polarizado. El término de eliminación correspondiente a la dispersión elástica e inelástica puede determinarse midiendo la constante de decrecimiento en función de las dimensiones del conjunto de que se trate. Los autores exponen un procedimiento teórico que permite calcular la medida en que la dispersión elástica contribuye al término de eliminación, con lo que puede calcularse subsiguientemente la sección eficaz de dispersión inelástica. El procedimiento teórico se ha comprobado experimentalmente para calcular la contribución de la dispersión elástica. Empleando esta técnica, se ha medido la sección eficaz de dispersión inelástica correspondiente al Fe, para energías de los neutrones primarios comprendidas entre 0,8 y 1,5 MeV.

Esta técnica de empleo de una fuente de neutrones pulsados se ha utilizado también para medir las constantes de decrecimiento en placas de Pb. Las condiciones de experimentación se aproximan a los supuestos que suelen formularse cuando se resuelve la ecuación de transporte de Boltzmann en función del tiempo (es decir, una sola dimensión y una sola velocidad). Los autores han medido las constantes de decrecimiento

en placas de plomo de 71×81 cm, con espesores de 5, 10, 15 y 20 cm, y comparan los resultados alcanzados, una vez corregidos para tener en cuenta la degradación energética y el conjunto finito,con las soluciones aproximadas de la ecuación de transporte de Boltzmann.

1. INTRODUCTION

In a prior series of experiments the decay of the fast neutron flux in non-moderating metal assemblies of lead, bismuth and uranium has been studied following the injection of a pulse of monoenergetic neutrons of width of a few nanoseconds [1].

The flux has been found to decay exponentially with a decay constant in the nanosecond range given by

$$\lambda = v\,\Sigma_{nel} + vDB_g^2 + CB_g^4, \tag{1}$$

where λ is the decay constant, v the neutron velocity, B_g^2 the geometric buckling, C a constant, Σ_{nel} the macroscopic non-elastic cross-section and D the fast diffusion coefficient for an infinite medium given by

$$D = \frac{1}{3\Sigma_t(1-\mu_0)} \cdot \frac{1}{1 - \frac{4}{5}\frac{\Sigma_{nel}}{\Sigma_t} + \frac{\mu_0}{1-\mu_0}\frac{\Sigma_{nel}}{\Sigma_t}}. \tag{2}$$

Σ_t is the total macroscopic cross-section and μ_0 the average cosine of the angle of scattering. It was further shown that if the differential cross-section for elastic scattering is expanded in terms of Legendre polynomials

$$\sigma_d = \frac{s}{4\pi}\sum_{r=1}^{\infty}[1 + \omega_r p_r(\cos\theta)] \tag{3}$$

then $\mu_0 = \omega_1/3$. The geometrical buckling for a rectangular block is given by

$$B_g^2 = \pi^2\left[\frac{1}{(a+2\lambda_{ext})^2} + \frac{1}{(b+2\lambda_{ext})^2} + \frac{1}{(c+2\lambda_{ext})^2}\right], \tag{3a}$$

where a, b, and c are the three assembly dimensions and the extrapolated length (λ_{ext}) is given by

$$\lambda_{ext} = \frac{0.71}{(\Sigma_t - \Sigma_{nel})(1-\mu_0)}. \tag{3b}$$

These experiments showed that Eq.(1) is consistent with cross-section measurements obtained by other methods.

A method of measuring Σ_{nel} was also developed. This cross-section is the sum of the non-elastic scattering and absorption cross-sections. The decay constant λ is measured as a function of B_g^2 by using different assembly sizes. A least squares fit is made to the values of λ obtained, with the constraint that the slope at $B_g^2 = 0$ is equal to vD, leaving the terms $v\Sigma_{nel}$ and C to be determined by best fit. The term D is a function of Σ_t (assumed known from other measurements) and Σ_{nel} which is still to be determined. B_g^2 is a function of the elastic scattering cross-section which makes B_g^2 an implicit function of Σ_{nel} since the elastic scattering cross-section is found by subtracting Σ_{nel} from Σ_t. To find Σ_{nel} an IBM 7090 code has been written, as follows.

A value of Σ_{nel} is chosen to calculate D and the values of B_g^2. A least squares fit is made and the resultant Σ'_{nel} is calculated from best fit. Σ'_{nel} is compared with Σ_{nel} and if $\Sigma'_{nel} \neq \Sigma_{nel}$ the process is repeated with a new Σ_{nel} until $\Sigma'_{nel} = \Sigma_{nel}$.

The purpose of the present work is to extend this technique to medium and medium-light nuclei (and iron in particular) where energy degradation from elastic scattering becomes important. In the present work neutron lifetimes ranged from 6×10^{-9} to 20×10^{-9} s. The average number of collisions in the assembly in this time is vT/λ_{tr}, where T is neutron lifetime. Since $\lambda_{tr} \approx 5.5$ cm and $v \approx 1.3\times 10^9$ cm/s, this average number ranges from 1 to 4. This produces energy loss from elastic scattering of from 30 to 100 keV. This range of energy loss will not materially affect the one-velocity transport theory but on the other hand could have an appreciable effect on the efficiency of the neutron detector. Since both the mean energy and shape of the injected neutron pulse will change with time, the neutron detection efficiency will also change with time, and this will effect the measured decay constant. It has been shown [2] that under the above conditions the expression for λ becomes

$$\lambda = v[\Sigma_{nel} + \Sigma_p] + vDB_g^2 + CB_g^4, \tag{4}$$

where

$$\Sigma_p = \frac{b\overline{\Delta E}}{\lambda_{tr}} \tag{5}$$

$\overline{\Delta E}$ is the average loss per collision, λ_{tr} is the transport mean free path and b is a parameter of the detector efficiency $\eta(E)$. It will also be shown that the efficiency $\eta(E)$ is a function of E (the neutron energy) given by

$$\eta(E) = \eta(E_0)[1 - b(E_0 - E)], \tag{6}$$

where b is a constant over the range of energies considered. Σ_p is a "pseudo" cross-section since it depends on instrumental as well as nuclear parameters.

The measurements made on iron to be described below have been used to check the validity of the expression of Σ_p. Since the first level in Fe^{56}

is at 850 keV, $\Sigma_{nel} = 0$ for primary neutron energies < 850 keV (the absorption cross-section is negligible). Hence measurements of λ versus B_g^2 will yield a direct determination of Σ_p. Σ_p can also be calculated from the independently known quantities b, $\overline{\Delta E}$ and λ_{tr}. The measured and calculated values agree closely as will be seen. For neutron energies greater than 850 keV the quantity $(\Sigma_{nel} + \Sigma_p)$ can be measured and hence Σ_{nel} determined by subtracting the calculated value of Σ_p.

2. EXPERIMENTAL APPARATUS

The neutron source used was the pulsed Massachusetts Institute of Technology Rockefeller Generator [3] which can generate pulse widths of 3×10^{-9} s at a repetition rate of 8 Mc/s. A more detailed description of the electronic detecting equipment is being published elsewhere [4].

The pulsed proton beam from the generator passes through an electrostatic pick-up system which provides the zero timing pulse after amplification [3]. The neutrons are generated by the $Li^7(p, n)Be^7$ reaction. A metallic lithium target (50 ± 10) keV thick was used. To restrict the angular spread of the emitted neutrons, a lithium loaded paraffin collimator was inserted between the neutron source and assembly (Fig. 1). The calculated

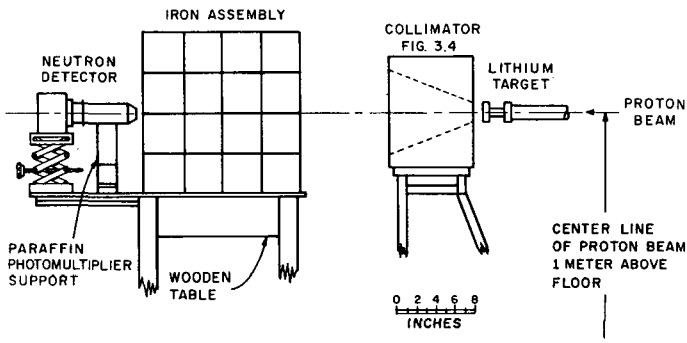


Fig. 1

Geometry for decay measurements of iron assemblies

energy spread with collimator in place was between 20 to 30 keV depending on the neutron energy.

An RCA 7264 photomultiplier with a Pilot B plastic phosphor was used as the detector. A fast output from the photomultiplier collector was used to actuate the time to pulse height converter for timing purpose. A linear signal taken from the seventh dynode is amplified by a conventional linear amplifier and is used to trigger a single channel pulse height analyser which is preset for a given pulse height acceptance range. This in turn is used to gate the signal from the converter, thus allowing pulse height, as well as time, selection. The acceptance range of the single channel analyser (called the "window") determines the relative detector efficiency for a neutron of a given energy and consequently the value of b in the expression for Σ_p

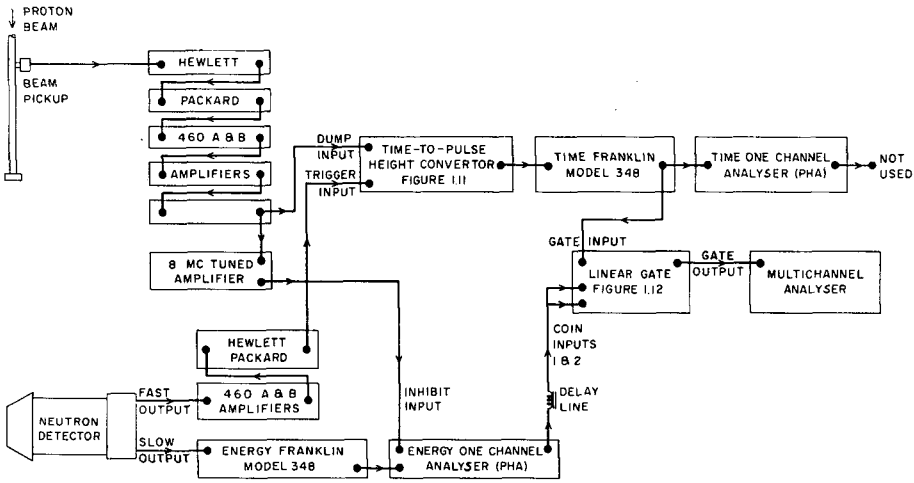


Fig. 2

Block diagram for electronic time-of-flight system

(Eqs. (5) and (6)). The output from the gate is fed into a 256 channel analyser. A block diagram of the time-of-flight system is shown in Fig. 2.

The next section describes the procedure for measuring the value of b which is necessary for calculation of Σ_p.

3. MEASUREMENT OF DETECTOR EFFICIENCY

As mentioned earlier a selected portion of the detector pulse height spectrum can be accepted by the energy window. For a given window setting we wish to determine the detector efficiency as a function of neutron energy. This is accomplished by measuring the detector pulse height spectrum for a series of different neutron energies and normalizing these to the same total neutron flux. The relative efficiency for detecting neutrons of energy E_1 relative to neutrons of energy E_2 will be given by

$$\eta_{1\text{-}2} = \frac{\int_{w_1}^{w_2} F_1(p)dp}{\int_{w_1}^{w_2} F_2(p)dp} \qquad (7)$$

where F_1 and F_2 are the normalized number of pulses per unit interval for energies E_1 and E_2, respectively, and w_1 and w_2 are the lower and upper acceptance levels of the window.

A block diagram of the apparatus used for measuring and normalizing the pulse height spectrum is shown in Fig. 3. Normalization to the same number of detected neutrons is accomplished by use of a scaler which records all pulses. The scaler (dead-time 0.7 μs) counting rate was the order

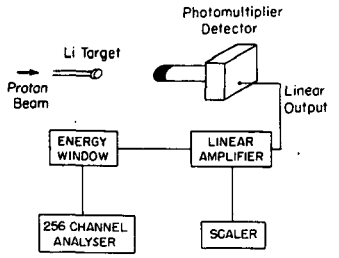


Fig. 3

Block diagram for measuring the detector efficiency

of 20 000 counts/s of which 3000 counts/s were caused by photomultiplier noise.

The above results were multiplied by $(1 - e^{-\Sigma_H x})$ to normalize to the same number of incident neutrons, where Σ_H is the macroscopic hydrogen scattering cross-section for the Pilot B plastic phosphor and x is the phosphor thickness (1 in). A correction was also made for the multichannel analyser dead-time.

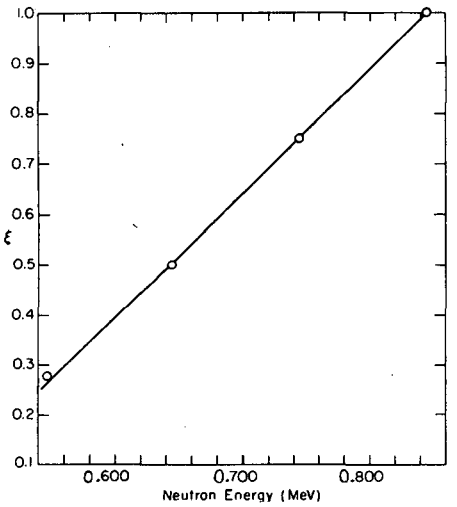


Fig. 4

Detector efficiency as a function of neutron energy

A typical efficiency curve is shown in Fig. 4 for $bE_0 = 1.8$. It should be pointed out that the linear assumption (Eq. (6)) is not valid over large energy changes (~ 1 MeV), but over the energy loss encountered (~ 200 keV) it was possible to adjust the energy window to yield a linear efficiency curve. It should also be noted that for certain window settings b can become negative because the detection efficiency increases with decreasing neutron energy.

4. CROSS-SECTION MEASUREMENT

Measurements of the non-elastic cross-section for iron were made for neutron energies between 740 keV and 1.52 MeV. The quoted value of energy is a mean energy averaged over a 100 keV spread. The uncertainty in the mean energy is ± 21 keV. The energy spread results from three factors: (1) the target thickness (50 ± 10 keV), (2) spread from angle of emission from lithium target (20 to 30 keV, depending on neutron energy) and (3) energy loss by elastic collisions (40 to 70 keV, depending on decay constant). The value of energy-dependent parameters such as Σ_t and w_1 were obtained by averaging over the appropriate energy spread.

A table of λ's and block size are shown in Table I. A typical decay curve is shown in Fig. 5 with background subtracted. Two plots of B_g^2 versus λ are shown in Fig. 6. The values of buckling were limited to values between 0.008 cm^{-2} and 0.017 cm^{-2}. The lower limit is imposed because larger assembly size would involve a poor or unusable signal-to-noise ratio. The upper limit is imposed to the primary pulse width, and the block dimensions become comparable to the extrapolated length.

The lowest neutron energy used (740 keV) is below the non-elastic threshold for iron (850 keV) so the $\Sigma_{nel} = 0$. The extrapolation of λ versus B_g^2 gives a direct measurement of Σ_p which can be compared to the calculated value. (See Table II.) The results agree within the quoted errors.

Values of σ_{nel} as functions of energy are given in Table III. It should be noted that the value σ_{nel} correponds to the inelastic scattering cross-section (n, γ processes may be neglected) from the 850 keV level in iron. This is because for each primary energy and corresponding window setting the inelastically scattered neutron is below the threshold for detection. Measurements for two different values of b were made at each energy so each entry is an average of two different measurements. In each case the two values were within the experimental uncertainty of each other. In the calculation of non-elastic cross-sections, the total cross-section values were obtained from BNL 325, and the values of w_1 from Cox*. The individual errors quoted are compounded of errors from three sources; (1) the most probable error caused by the least squares fit, (2) the quoted uncertainty in w_1 (10%) and (3) the uncertainty in the total cross-section. The last uncertainty was not quoted but was assumed to be 5% which is a typical value for this type of measurement. The uncertainty in Σ_{nel} from errors (2) and (3) were found by increasing Σ_t and w_1 by 5 and 10%, respectively, and noting the effect on Σ_{nel}. It was also found that changes in Σ_t and w_1 had a negligible effect on the least squares fit error; so the total error in Σ_{nel} could be considered to be made up of independent errors (1), (2) and (3).

Figure 7 shows the results plotted with measurements made by other methods. The Σ_p's, except near the threshold, were less than 10% of the non-elastic cross-section so an error in Σ_p would only produce an error in Σ_{nel} of second order.

---

* COX, S.G. (Argonne National Laboratory), private communication.

TABLE I

EXPERIMENTAL DECAY CONSTANTS

Assembly size (in)	Decay constant (10^7 s^{-1})	Decay constant (10^7 s^{-1})
Average neutron energy = 0.74 MeV	$bE_0 = 1.75$	$bE_0 = 2.85$
12 × 12 × 12	8.66 ± 0.30	9.93 ± 0.35
12 × 12 × 18	8.01 ± 0.44	8.47 ± 0.35
12 × 18 × 18	4.66 ± 0.24	6.77 ± 0.28
18 × 18 × 18	4.54 ± 0.23	6.01 ± 0.30
Average neutron energy = 0.93 MeV	$bE_0 = 0.082$	$bE_0 = 1.53$
12 × 12 × 12	10.20 ± 0.20	11.79 ± 0.24
12 × 12 × 18	8.47 ± 0.25	10.35 ± 0.31
12 × 18 × 18	6.90 ± 0.28	8.87 ± 0.35
18 × 18 × 18	5.10 ± 0.26	5.56 ± 0.28
Average neutron energy = 1.04 MeV	$bE_0 = 0.21$	$bE_0 = 0.51$
12 × 12 × 12	11.18 ± 0.22	13.72 ± 0.27
12 × 12 × 18	11.00 ± 0.33	12 10 ± 0.36
12 × 18 × 18	9.35 ± 0.37	11.89 ± 0.48
18 × 18 × 18	7.35 ± 0.38	8.04 ± 0.40
Average neutron energy = 1.15 MeV	$bE_0 = -0.24$	$bE_0 = 0.80$
12 × 12 × 12	11.04 ± 0.22	15.71 ± 0.31
12 × 12 × 18	10.50 ± 0.32	12.88 ± 0.39
12 × 18 × 18	9.43 ± 0.38	12.08 ± 0.48
18 × 18 × 18	6.66 ± 0.33	8.78 ± 0.44
Average neutron energy = 1.27 MeV	$bE_0 = 0.20$	$bE_0 = 0.63$
12 × 12 × 12	9.20 ± 0.18	11.30 ± 0.23
12 × 12 × 18	9.16 ± 0.27	10.73 ± 0.32
12 × 18 × 18	8.78 ± 0.35	10.73 ± 0.41
18 × 18 × 18	8.40 ± 0.42	9.27 ± 0.46

TABLE I (cont.)

Average neutron energy = 1.39 MeV $bE_0 = -0.33$		
12 × 12 × 12 12 × 12 × 18 12 × 18 × 18 18 × 18 × 18	13.23 ± 0.26 12.47 ± 0.37 11.37 ± 0.45 9.81 ± 0.49	
Average neutron energy = 1.52 MeV		
	$bE_0 = -2.01$	$bE_0 = -1.84$
12 × 12 × 12 12 × 12 × 18 12 × 18 × 18 18 × 18 × 18	13.15 ± 0.26 12.08 ± 0.36 11.78 ± 0.47 11.85 ± 0.59	14.75 ± 0.30 13.51 ± 0.39 12.47 ± 0.50 12.00 ± 0.60

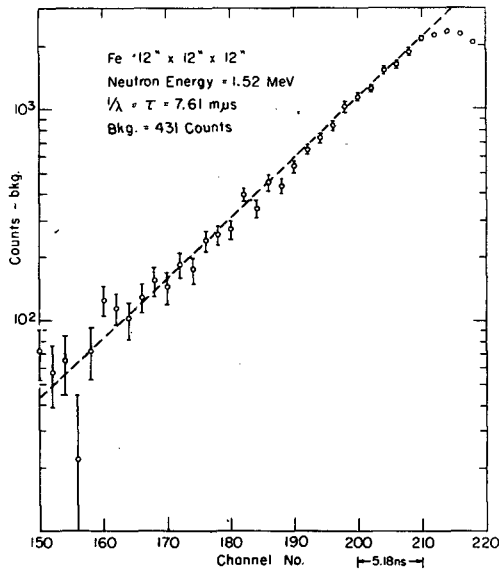


Fig. 5

A typical neutron decay curve

5. DECAY MEASUREMENTS IN LEAD SLABS

Theoretical investigations have appeared in the literature [5-8] which showed good agreement between diffusion theory and the various approximate

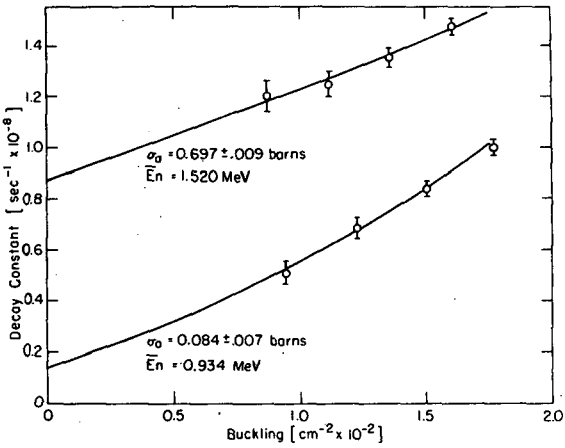


Fig. 6

Decay constant versus geometrical buckling for two neutron energies

TABLE II

PSEUDO CROSS-SECTIONS

bE_0	Calculated from least squares fit (b)	Calculated from detector efficiency (b)
1.75	0.174 ± 0.046	0.201 ± 0.020
2.85	0.354 ± 0.011	0.310 ± 0.039

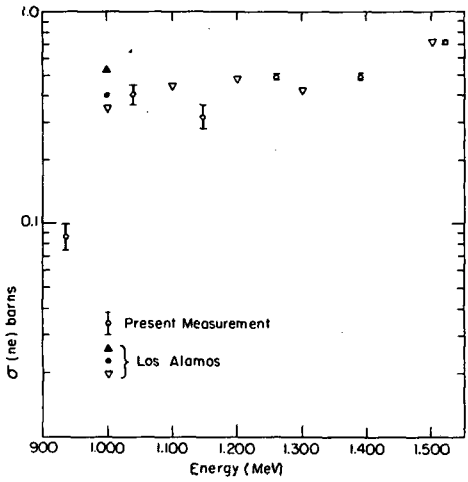


Fig. 7

Non-elastic cross-section for iron

solutions (p_1, p_2, etc.) of the one-dimensional, one-velocity Boltzmann transport equation to assembly dimensions as small as three or four mean free neutron path lengths. Although the agreement is good above three or four mean free path lengths there are discrepancies for assembly dimensions of less than this value. Some of the solutions predict a finite value of the decay constant as the assembly thickness goes to zero. The maximum value of the decay constant for thin slabs, in the absence of non-elastic scattering, is given by two of the theoreticians [7, 8] as $v\Sigma_{total}$, where v is the neutron velocity and Σ_{total} is the total macroscopic cross-section. The pulsed neutron technique offered a method for experimentally measuring decay constants in thin assemblies which can be compared to theoretical results.

A lead assembly lends itself to the experiment described above since elastic moderation is small (velocity change of the order of 2%) and slab geometry could be erected from 2 in × 4 in × 8 in lead bricks. The experimental geometry is shown in Fig. 8. The lead walls studied were 28 in high and 32 in wide. Decay constants for four different thicknesses (2 in, 4 in, 6 in and 8 in) were measured. The paraffin cone was used to shield the detector from prompt target neutrons for the 2 in and 4 in thick measurements. The two larger assemblies did not require the cone as the wall thickness (> 3 mean free path lengths) was enough to attenuate the prompt beam.

The primary neutron energy for the experiment was 0.84 MeV. The energy gave a small non-elastic scattering cross-section of approximately 100 mb. The energy PHA (see Fig. 2) was set to eliminate all neutrons which lost more than 450 keV. The setting of the energy PHA gave a pseudo removal cross-section of 64 mb. The decay constants of the lead assemblies were determined by using FRANTIC [9] to fit the experimental decay data to an exponential plus background.

Results of the lead slab decay experiment are given in Table IV. Since the experiments were conducted on finite assemblies with small pseudo and

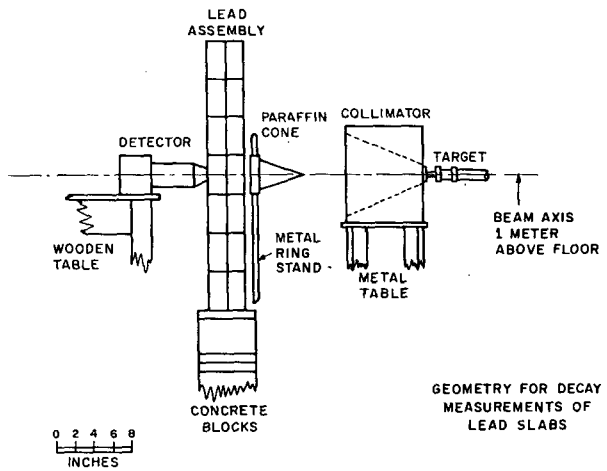


Fig. 8

Geometry for decay measurements of lead slabs

TABLE III

NON-ELASTIC IRON CROSS-SECTION

Neutron energy (MeV)	Cross-section (b)	Error (b) from		
		Least squares fit	Uncertainty in ω_1	Uncertainty in total cross-section
0.93	0.087 ± 0.012	0.008	0.005	0.007
1.04	0.406 ± 0.044	0.043	0.001	0.006
1.15	0.321 ± 0.037	0.034	0.004	0.008
1.28	0.490 ± 0.013	0.012	0.005	0.003
1.39	0.491 ± 0.013	0.012	0.003	0.007
1.52	0.713 ± 0.018	0.013	0.005	0.011

TABLE IV

DECAY CONSTANTS FOR LEAD SLABS

Slab thickness (in)	Decay constant (measured) (10^{-9} s^{-1})	Dimensionless corrected decay constant	B_{g0}^2/B_{g1}^2
2	0.1175 ± 0.0015	0.435 ± 0.0063	0.950
4	0.0775 ± 0.0013	0.274 ± 0.0054	0.913
6	0.0656 ± 0.0019	0.217 ± 0.0079	0.867
8	0.0535 ± 0.0018	0.158 ± 0.0075	0.809

Note: $\Sigma_t = 0.190\ cm^{-1}$; $v = 1.265 \times 10^9$ cm/s and $v(\Sigma_{nel} + \Sigma_{pseudo}) = 0.00684 \times 10^9\ s^{-1}$.

non-elastic cross-sections, corrections had to be made before the results could be compared with the theory of an infinite slab with no absorption. The decay constant for an infinite assembly with no absorption is given by

$$\lambda_0 = [\lambda_{measured} - v(\Sigma_{nel} + \Sigma_{pseudo})]\,(B_{g0}^2/B_{g1}^2),$$

where B_{g0}^2 is the buckling (Eq. (3a)) of a one-dimensional slab and B_{g1}^2 is

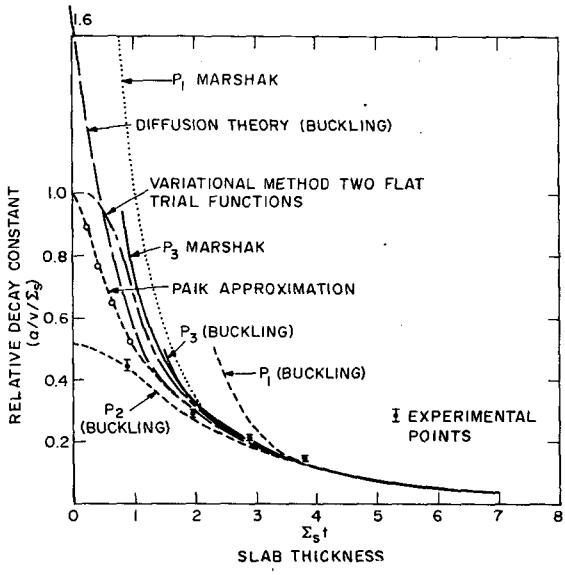


Fig. 9

Asymptotic decay constants for slabs

the buckling of the actual assembly. The results are plotted in Fig. 9 with some of the theoretical solutions of the transport equation.

The experimental results obtained with the 2-in slab is less than the theoretical prediction. This discrepancy may be a result of the experimental geometry or the effect of the decay time becoming of the order of the neutron burst width. A computational method is being developed to measure decay times of the order of the pulse width and future work will investigate the effect of the detector-slab geometry.

6. CONCLUSIONS

It has been found that the pulsed neutron source technique can be of great value in conducting investigations in the field of fast neutron physics.

By introducing the concept of a pseudo cross-section, to account for elastic moderation, the pulsed source technique is very useful for measuring neutron removal cross-sections. The method possesses the advantage that no corrections are necessary for multiple scattering and angular distribution effects which are inherent in other methods (e.g. the sphere technique). Determination of non-elastic cross-section to an uncertainty of 10% appears to be possible.

The pulsed source method is also a valuable tool for experimental investigation of neutron transport in the low MeV energy range and yield valuable data to corroborate various theoretical work.

REFERENCES

[1] BEGHIAN, L.E., RASMUSSEN, N.C., THEWS, R.T. and WEBER, J. Nucl. Sci. Engng 15 (1963) 357-81.
[2] BEGHIAN, L.E., PROFIO, A.E., WEBER, J. and WILENSKY, S., Nucl. Sci. Engng 17 (1963) 82-89.
[3] BEGHIAN, L.E. and SALOMAA, M.R. Nucl. Instrum. Meth. 17 (1962) 181-87.
[4] BEGHIAN, L.E. and KEGEL, G.H.R., in Spectroscopy of Gamma Radiation, to be published by Fordan and Breach, N.Y.
[5] CASE, K.M., Ann. Phys. (N.Y.) 9 (1960) 1-9.
[6] COCKRELL, R.G., PEREZ, R.B. and WALTON, G.R., Nucl. Sci. Engng 19 (1964) 423-26.
[7] JUDGE, F. and WAITCH, P.B., Trans. Amer. nucl. Soc. 6 (1963) 291-92.
[8] PAIK, N.C., private communication.
[9] ROGERS, P.C., Massachusetts Institute of Technology, Laboratory for Nuclear Science, Techn. Rpt. No.76 (June 1962).

DISCUSSION

R. BEDNARZ: I would like to comment on this paper and my comment also has a bearing on the paper presented by Dr. Beckurts[1]. The theorems obtained by Albertoni and Montagnini are valid for inelastically scattering moderators in the high-energy region. The difference between the high-energy region and the thermal region is that in the former the contribution from the border of the continuous part of the spectral plane is much more important. In your investigations was there any dependence on the energy distribution of the initial conditions?

L. BEGHIAN: I must emphasize again that I have restricted myself to one velocity. I don't have a distribution of energy in the pulse.

R. BEDNARZ: If another laboratory did similar investigations with a completely different accelerator, would the results be the same?

L. BEGHIAN: As far as I can see, they would not. Two laboratories have in fact done similar experiments and we violently disagree[2].

R. BEDNARZ: That is what I would have expected.

M. NELKIN: I would like to emphasize once more what the speaker has already pointed out, namely that, provided this experiment is done in the properly idealized way so that the detector is biased not to detect neutrons which have lost energy, a one-velocity transport theory is applicable for which we already have the theorems and for which we know that the eigenvalue does exist, at least in the idealization of the slab. Furthermore, in a one-velocity transport theory we know that the decay constant as a function of buckling does curve upward, as was shown in the experiment, that is to say that the equivalent of a diffusion-cooling coefficient has the opposite sign than for thermal-neutron diffusion. This is very easy to show for one velocity. In other words, the results really do look very plausible and look like the kind of things you would expect for one-velocity transport.

E. ARAI: Did you calculate C from your measured points or did you give it as a correction?

---

[1] BECKURTS, K.H., "A review of pulsed neutron experiments on non-multiplying media" (SM-62/1), these Proceedings I.

[2] See discussion following the paper "Contribution to the study of fast neutron non-multiplying assemblies by the pulsed neutron technique" by G. Deconninck at al. (SM-62/14), these Proceedings II.

L. BEGHIAN: I want to make one thing clear. C does not represent a diffusion cooling; it is merely, if you like, an arbitrary expansion in terms of buckling. It is purely and simply a Taylor expansion, and this is a concept we no longer use because we believe we are able to solve the Boltzmann equation as exactly as we want. But, I repeat, C is not a diffusion-cooling term. This is only applicable in cases of inhomogeneous spectra, such as occur in thermal assemblies, where the fast neutrons leak more quickly than the slower ones. C is purely a curve fitting, purely a Taylor expansion.

E. ARAI: If you have calculated from the measured points, you should have more measured values. Four points are not sufficient.

L. BEGHIAN: That is true but we haven't just made a least-squares fit. The process we employed is a reiterative one. What we have done is to ensure that the slope at the beginning of the curve is in fact vD_0; the slope of the λ-versus-Bg^2 curve should be vD_0. And D_0 we calculate. What we do is to assume a given removal cross-section and this gives us the intercept on the curve. We then plot our curve and if the slope doesn't come out right we reiterate the process until it does. Even with four points this is a very powerful method for curve fitting. I quite agree with you, however, that four points are not good enough; but the trouble is that, if you want more points for smaller Bg^2 the assembly becomes so large that the signal-to-noise ratio becomes very poor indeed. This is a limitation, I agree.

E. SILVER: Did you make any systematic investigation into the effect of the detector-bias setting on the value of C you obtained?

L. BEGHIAN: In a roundabout way this is related to the pseudo-cross-section and the only way we checked on this was to calculate our pseudo-cross-section and then actually to measure it. The fictitious cross-section can actually be measured. And the agreement was extremely good. I see your point, though. You are in fact saying that increasing the size of the assembly will affect the expansion and this is connected with the number of elastic collisions that are obtained.

E. SILVER: That is correct.

L. BEGHIAN: We did not carry out any special investigations because of the fact that we actually measured and calculated the pseudo-cross-section, and the calculations turned out to be so accurate that we now think we understand how to remove the energy loss due to elastic scattering.

R. BOOTH: It might be useful to carry out another type of experiment to supplement the one presented in this paper. In this experiment one would measure the propagation of the fast-neutron pulse in the medium and one could apply the same analysis as is performed in the thermal-pulse-propagation experiments to determine the scattering and diffusion parameters. The question of what buckling to use would probably not be so important in the pulse-propagation experiment as it is in the die-away experiment and I think one could determine this more easily if a constant energy spectrum were present.

L. BEGHIAN: Yes, I am sure that this is one of the next steps we must take – to investigate the pulsed propagation of fast assemblies with a Fourier analysis, in the same way as done with thermal assemblies. I've already had informative discussions with Dr. Booth and Dr. Moore on this question, and they've convinced me. I shall now try to convince my own people that this should be done.

PULSED REACTORS AND NEUTRON SOURCES

(Session VI)

FAST BURST REACTORS IN THE UNITED STATES OF AMERICA

T.F. WIMETT
UNIVERSITY OF CALIFORNIA,
LOS ALAMOS SCIENTIFIC LABORATORY,
LOS ALAMOS, N.MEX., UNITED STATES OF AMERICA

Abstract — Résumé — Аннотация — Resumen

FAST BURST REACTORS IN THE UNITED STATES OF AMERICA. Early in 1953, the bare uranium metal reactor, Lady Godiva, produced self-quenching fission bursts for the first time. Since then, seven progeny of Godiva have been produced in the USA, and at least two more are nascent. Fast burst reactors which have operated in the USA are listed in Table I, which shows time of start-up, nominal fission yield per burst and full width of pulse at half maximum power. The first five employ enriched uranium metal (~93.5% U^{235}); the three latest models contain an alloy of uranium and molybdenum which permits operation at higher temperatures, hence higher fission densities. Essential design features of these reactors with regard to a variety of pulse irradiation applications are discussed together with mechanical limitations and some advanced design proposals.

RÉACTEURS A NEUTRONS RAPIDES PULSÉS, AUX ÉTATS-UNIS D'AMÉRIQUE. Au début de 1953, le réacteur sans réflecteur à uranium métallique, appelé Lady Godiva, a produit pour la première fois des bouffées de neutrons de fission autoextinguibles. Depuis lors, sept réacteurs du type Godiva ont été construits aux Etats-Unis et deux autres au moins sont en voie de réalisation. Le tableau I donne la liste des réacteurs de ce genre qui fonctionnent aux Etats-Unis; il indique la date de démarrage, le rendement de fission nominal par bouffée et la largeur totale des impulsions à la moitié de la puissance maximum. Les cinq premiers réacteurs utilisent l'uranium métallique enrichi (environ 93, 5% de ^{235}U); les trois derniers modèles fonctionnent avec un alliage d'uranium et de molybdène qui permet d'opérer à des températures plus élevées et d'obtenir par conséquent des densités de fission plus élevées. L'auteur discute les caractéristiques essentielles de ces réacteurs en ce qui concerne diverses utilisations du rayonnement pulsé, ainsi que leurs limitations mécaniques et certains projets de modèles perfectionnés.

БЫСТРЫЕ ИМПУЛЬСНЫЕ РЕАКТОРЫ В США. В начале 1953 года впервые реактор с металлическим ураном без отражателя, "Леди Годайва", произвел самогасящиеся импульсы деления. С тех пор в США были произведены семь реакторов типа "Годайва" и, по крайней мере, еще два находятся в стадии разработки. Быстрые импульсные реакторы, которые работают в США, перечислены в табл.1, в которой даны дата пуска, номинальное количество делений на импульс и полная длительность импульса при половине максимальной мощности. В первых пяти реакторах используется обогащенный металлический уран (~93,5% урана-235); три последних модели работают на сплаве урана и молибдена, что позволяет осуществлять эксплуатацию при более высоких температурах; отсюда более высокие плотности деления. Обсуждаются существенные особенности конструкции этих реакторов в отношении различных видов применения импульсного облучения вместе с механическими пределами и некоторыми предложениями в отношении усовершенствования конструкции.

REACTORES DE NEUTRONES RAPIDOS PULSADOS EN LOS ESTADOS UNIDOS DE AMERICA. A principios de 1953 el reactor Lady Godiva (sin reflector, alimentado con uranio metálico) produjo por primera vez impulsos de neutrones de fisión autoextinguibles. Desde entonces, en los Estados Unidos se han construido siete reactores de este tipo y se están construyendo otros dos. Los cinco primeros reactores emplean uranio metálico enriquecido (~ 93, 5%, de ^{235}U); los tres últimos funcionan con una aleación de uranio y molibdeno que les permite alcanzar temperaturas más altas y, por consiguiente, obtener densidades de fisión más elevadas. En la memoria se examinan las características esenciales de todos estos reactores desde el punto de vista de sus aplicaciones en las irradiaciones pulsadas, así como sus restricciones mecánicas y algunos proyectos de modelos perfeccionados.

1. INTRODUCTION

Historically, the development of fast prompt-burst reactors was an outgrowth of a programme to determine the behaviour of supercritical systems, particularly to confirm the effectiveness of thermal expansion in quenching reactivity. The experimental behaviour of the early simple versions has been used accordingly as a basis for normalizing fast-reactor-dynamics calculations [1]. While such operation comes closer than usual to damaging conditions, careful attention to operational control has resulted in the generation of many thousands of prompt bursts on the first series of fast-burst reactors without serious incident[1].

Reactors of the first series are fabricated from highly enriched (~93.5% U^{235}) cast uranium metal, and include Lady Godiva and Godiva II at Los Alamos Scientific Laboratory (LASL), Kukla and Fran at Lawrence Radiation Laboratory (Livermore, Calif.), and SPR I at Sandia Corporation. Near-fission-spectrum neutron bursts from these reactors have been employed in (1) basic fission studies, e.g. the extensive measurements of delayed neutron and delayed gamma parameters [2], (2) radiation dosimetry, (3) calibration of radiation alarms for criticality accidents, (4) radiobiology and (5) interaction of radiation with matter such as germanium crystals [3, 4].

Maximum burst yields in the first series generally are limited by fuel integrity as a result of severe shocks associated with the rapid temperature increases. Pure uranium metal, particularly as cast, is subject to surface roughening, anisotropic crystal growth, and internal void formation. Such effects were observed and were presumably caused by burst thermal cycling or irradiation and occurred for temperature rises (from ambient) ~200°C — far below the melting temperature. Mechanical shock to structural members is also a limiting factor in most of the early burst machines. (Fran is an exception that is discussed later.)

To increase the fission yield per burst, efforts have been directed toward the development of cores which maintain dimensional stability when subjected to more extreme temperature cycles than may be tolerated in normal uranium metal. There also have been attempts to eliminate inertial difficulties related to the quenching delay associated with the finite time for translating fission energy into surface or volume expansion. This delay leads to an effective broadening of the bursts at a given yield. The second series of burst reactors as referred to here are those which employ an alloy or uranium, specifically 10 wt.% molybdenum (U-10 wt.% Mo), in which extensive metallurgical tests have indicated relatively small crystal growth and excellent phase stability during or following repeated large temperature cycles (~500°C). Included in this reactor series are HPRR (Health Physics Research Reactor) at Oak Ridge National Laboratory, Molly-G or FBR (Fast Burst Reactor) at White Sands Missile Range, and Super Kukla at Lawrence Radiation Laboratory; three additional models similar to HPRR and Molly-G are in the final planning stages, one at Sandia Corporation, one at Aberdeen

[1] Two oversized bursts were experienced on Lady Godiva (which was not specifically designed as a burst reactor) as a result of errors in operational control. Damage suffered included bending of core supports, breaking of assembly bolts, and deformation of central fuel plates in the second and more extreme excursion.

Proving Grounds, and one at LASL. None of these reactors has produced more than a total of ~300 bursts to be compared with many thousands for a typical reactor of the first series. Accordingly, such devices may be considered in a relatively early stage of development.

2. PROCEDURE FOR BURST GENERATION

All reactor systems discussed here, except where noted, employ the same basic procedure for prompt burst production, namely: (1) establishment of the delayed critical control rod positions by low power operation with the burst rod withdrawn; (2) retraction of the safety block to permit decay of delayed neutron precursors born during the steady-state operation; (3) re-insertion of the safety block followed shortly by the rapid insertion of the burst rod (worth ~1 $ excess reactivity) to boost the reactivity to the pre-determined super-prompt-critical value; (4) automatic withdrawal (scram) of safety block and rods triggered by detection of power level in the burst. If an external neutron source is used during the steady-state operation, it is generally withdrawn to a less effective position during the burst mode in order to minimize "pre-initiation", or the generation of a burst before maximum excess reactivity is achieved, i.e. before the burst rod is fully inserted.

3. REACTOR DESIGNS AND DESCRIPTIONS

Table I lists startup dates for the burst reactors considered here together with some pertinent characteristics. The first three are not in operation currently, but are included for historical interest.

Lady Godiva and Kukla

Lady Godiva [3, 5], designed and constructed by Los Alamos Scientific Laboratory, was basically spherical in shape ~6.8-in diameter with two horizontal parting planes to permit disassembly into three roughly equal-mass sections for large shutdown effectiveness. Kukla [6], shown in Fig. 1, was designed and constructed by Lawrence Radiation Laboratory and is similar to Lady Godiva, except that it is mechanically supported from underneath rather than by hangers as in the original, and, in addition, employs a cylindrical safety block (~7-kg uranium) which is withdrawn for shutdown. Both use motor-driven screw actuators for uranium control rods and pneumatic cylinders for high-speed actuation of the safety blocks and burst rods. The exposed uranium surfaces of Kukla are nickel-flashed and overplated with 0.010 - 0.015 in of cadmium to eliminate corrosion and to reduce neutron room-return effects, while the surface of Godiva is bare. Total fuel mass is ~53 kg in each reactor. The detailed burst behaviour of Kukla is assumed to be identical to that of Godiva, which is discussed in the literature [3].

Godiva II

Essentially a near-cylindrical version of Lady Godiva, Godiva II [7] was designed specifically as a burst irradiation reactor with emphasis on struc-

TABLE I

FAST BURST REACTORS

Reactor	Initial burst operation (yr)	U^{235} mass (kg)	Burst yield (fissions)	Burst width (μs)	Repetition interval (h)	α_R (per μs)
Lady Godiva	1953	50	2×10^{16}	35	~1	1.09
Godiva II	1957	54	2.5×10^{16}	35	~1	1.05
Kukla	1961	50	2×10^{16}	35	~1	(1.09)
SPR I (Routine operation)	1961	54	2×10^{16}	42	~1	(1.05)
Fran	1962	59	4×10^{16}	40	1-2	~0.7
HPRR	1962	97	1.8×10^{17}	48	1-2	0.55
Molly-G or FBR	1964	81	1.2×10^{17}	35	1-2	0.77
Super Kukla (Preliminary data)	late 1964	1000	$\sim 2 \times 10^{18}$	~950	~8	~0.05

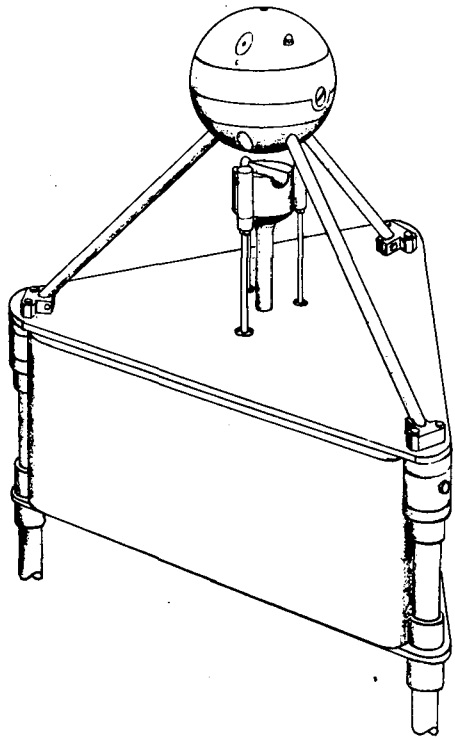


Fig. 1

Sketch of Kukla showing safety block and control rods withdrawn

tural stability. With temperature excursions limited to ~200°C in the region of maximum power density, about 2000 prompt bursts were produced in 3 yr without observable deterioration.

As shown in the drawing of Fig. 2, the large cylindrical safety block that enters the core from underneath serves two purposes: (1) it provides a large (~50 $) shutdown reactivity, and (2) it serves to partition the reactor along the radius in such a fashion that shock waves originating at the centre are prevented from travelling to the surface of the stationary part or, stated differently, the natural period of mechanical vibration is thereby reduced. This reduction is reflected in a smaller "inertial effect"[2]. To facilitate irradiation operations, the core was mounted on a small portable stand which houses all actuating machinery, control element position sensors and electrical interlocks.

SPR I

A second model of the Godiva II core, now identified as SPR I, was fabricated at LASL for operation in the Sandia Pulse Reactor Facility (SPRF)

[2] As defined in [3], the inertial effect arises from the delay required for a pressure wave to travel from the interior of a fuel piece to a surface where the major reactivity quenching takes place. To first order, a delay, τ, increases burst yield by the factor $(1+\alpha^2\tau^2)$.

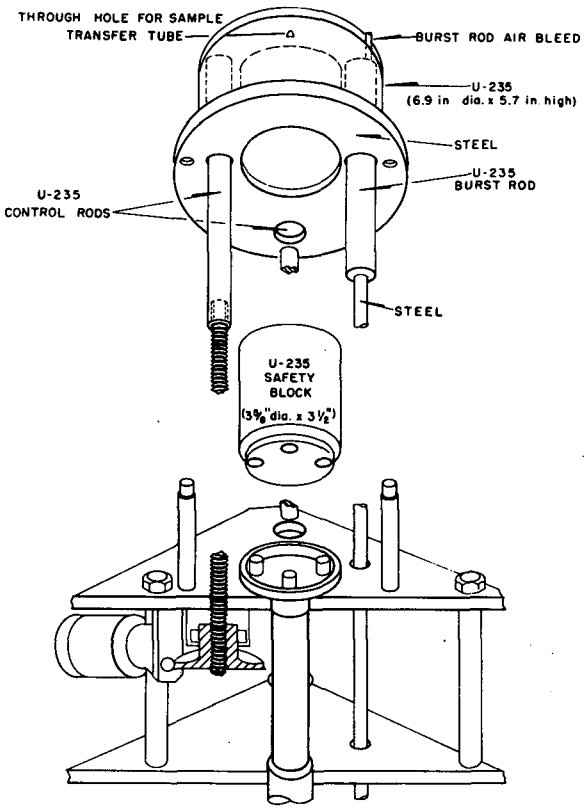


Fig. 2

Drawing of Godiva II showing core detail

at Sandia Corporation. The core fits with a clearance ~1 cm inside a perforated protective screen visible in the photograph, Fig. 3. This core was nickel-flashed as was the original, and additionally was overplated with cadmium to reduce neutron coupling with the variety of objects to be irradiated externally. Experience with such reactors has demonstrated some burst lengthening as a result of neutron back scattering from massive samples placed nearby even if there is cadmium shielding. The reactor stand is supported on a hydraulically operated elevator which lowers it into a pit after operation. A 12-in-thick lead radiation shield slides over the pit to permit personnel entry into the building soon after a burst has been produced[3].

In normal operation, burst reactors of the first series characteristically produce a prompt pulse in which the peak power is of order 10^4 MW followed by a "plateau" [7] level of order one-half megawatt. The duration of the plateau depends upon the response time of the scram system and is ~30 ms. Another characteristic of such reactors is the random variation in delay

[3] The γ-radiation level at 1 m from the Godiva II core 15 min after a burst of 2×10^{16} fissions is ~25 r/h at a normal operating frequency of one burst per hour.

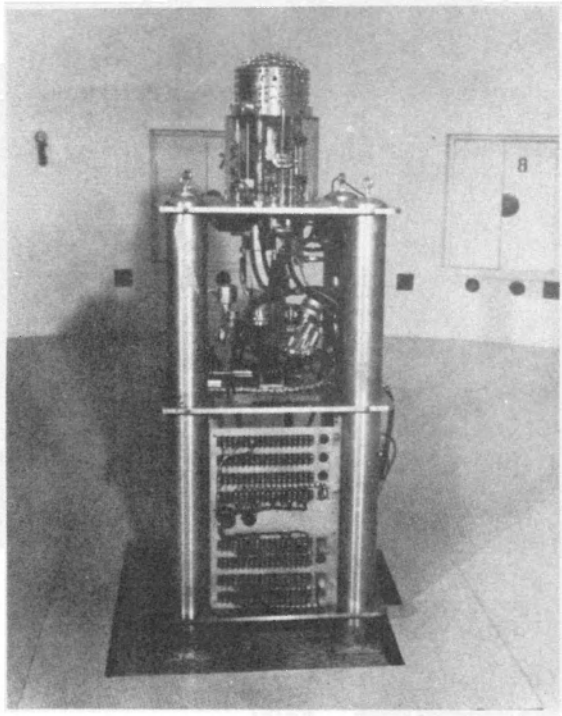


Fig. 3

SPR I reactor stand with core inside protective perforated screen

time, the interval between the attainment of maximum reactivity and the time of peak burst power. With no external neutron source, the mean delay time for Godiva II is ~3 s [7], and is ~80 ms for SPR I with a Pu-Be source of 5×10^4 n/s at a distance of 20 in from the core. To reduce the undesirable plateau duration and also to provide more precise timing of the power pulse, P.D. O'Brien of Sandia Corporation has developed a technique of programmed burst initiation in SPR I by which a short pulse of neutrons is introduced at the instant maximum reactivity is attained. Burst initiation time is predictable within 1 - 2 μs and the plateau duration is reduced to a few milliseconds by pre-programming the scram so that reactor disassembly coincides in time with the trailing edge of the prompt pulse. The neutron generator used for burst programming produces ~10^8 14-MeV neutrons in a 10-μs pulse and is located 8 ft from the reactor core.

Fran

The Fran design of Lawrence Radiation Laboratory represents an attempt to maximize the attainable burst yield in a pure uranium assembly. The major innovation lies in the mechanical arrangement for supporting the stationary fuel plates. In earlier designs, threshold damage produced by shock waves is usually associated with the larger components where stress

buildup is greatest and tends to concentrate in the fuel support bolts. Because of criticality considerations in the casting of fuel components, a typical stationary section in a fast-burst reactor consists of several discs or annular pieces which must be clamped together in a reproducible fashion. Uranium bolts generally used for this purpose are first to yield under shock forces produced during the power transient in the fuel plates. In the Fran design as illustrated in Fig. 4, clamping is accomplished externally by means

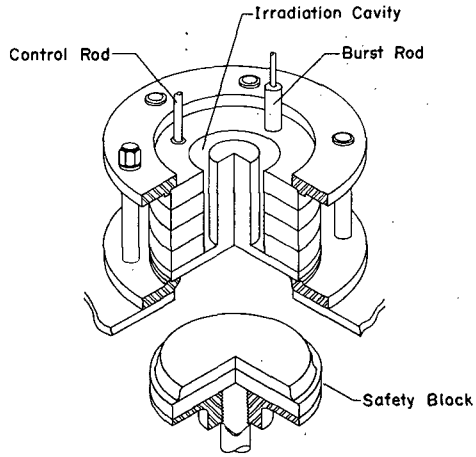


Fig. 4

Isometric drawing of Fran showing core details and supports
The diameter of fuel sections is ~7 in.
The steel supports are indicated by shading in the cut-away.

of two 3/4-in-thick steel rings which overlap the ends of the cylindrical stack of five annular fuel pieces, and by six 3/4-in steel bolts that penetrate only the steel rings and are located ~1/2 in away from the fuel surface. As the fuel expands during a burst, the steel support plates deflect with a very large effective spring constant. Burst temperature excursions approaching 350°C have been obtained and burst widths ~30 μs with negligible permanent deformation in either the steel supports or fuel plates. That crystal growth effects are less than observed in earlier models may be explained on the basis of improved casting techniques which result in finer uranium grain structure.

To reserve the central core volume for a large annular sample irradiation void (4-in deep, 1/2-in thick, and 3 1/8-in outside diameter), bottom fuel discs (~1/5 total mass) are mounted on a movable support to serve as the safety block. Control and burst rods necessarily enter the stationary section from above to avoid interference with safety block motion. The Fran safety block (rather than the burst rod) provides the rapid reactivity insertion for burst generation.

Health Physics Research Reactor, HPRR

Designed and constructed by the NDA Division of United Nuclear Corporation with the support of critical experiments performed by Oak Ridge National Laboratory [8], the HPRR is the first fast-burst reactor to depart from an unalloyed uranium-metal assembly. An alloy of uranium with 10 wt.% molybdenum was selected not only for its excellent crystal-phase and chemical stability, but also because appropriate heat treatment develops higher tensile strength than uranium by a factor ~4 at room temperature. The reactor core, shown in the photograph of Fig. 5, is basically an 8-in-diameter

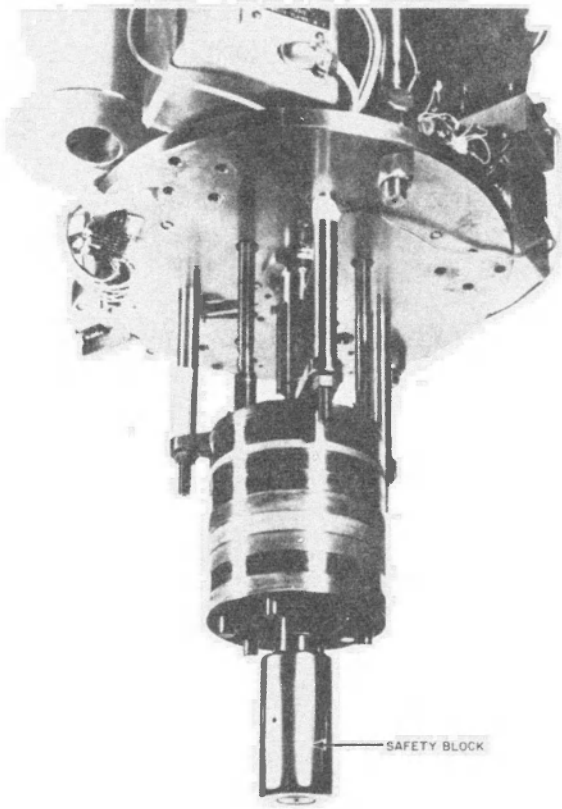


Fig. 5

View of HPRR with protective tube removed to expose safety block

cylinder of U-10 wt.% Mo alloy with a 2-in-diameter stainless steel inner core whose purpose is to reduce peaking in the fission-power distribution. The alloy contains 90 wt.% uranium of which 93.2% is U^{235}, and its total mass is ~115 kg. The stationary section, which is suspended from above as shown in the illustration, is ~9-in high and consists of ten annular pieces of several thicknesses bolted together by nine hollow fuel bolts 3/4 in in diameter. The safety block is a 3.5-in-diameter fuel annulus threaded onto

a steel centre plug which in turn is threaded to a smaller-diameter shaft extending upward out of the core where it is magnetically coupled to actuators. For reactivity shutdown, the safety block is thus driven out of a central cavity at the bottom of the stationary section. The usual complement of two control rods and a burst rod are actuated from above, and also enter the core from above. All exposed U-Mo surfaces are nickel plated.

Reactor portability is achieved in the HPRR system by suspending the reactor and its actuating mechanisms from a movable crane which raises the reactor from an irradiating site and transports it to a distant shielded location, thus increasing residual radiation attenuation by separation distance.

In preliminary operations of HPRR, burst yields in excess of 10^{17} fissions were readily obtained with some minor shock damage observed and corrected, and it is safe to say that the maximum yield is shock-limited. However, the maximum observed temperature increases of $\sim 500°C$ may be considered an upper limit for routine operation because of the onset of U-Mo phase transformation beyond $\sim 500°C$.

The HPRR reactor generates "tail-less" bursts or prompt power pulses which are not followed by the plateau mentioned previously. This useful phenomenon, first observed in Lady Godiva, is caused by rapid displacement of the safety block as a result of mechanical shock. In HPRR, a shock wave causes separation of the armature from the safety block latching magnet, and a compressed spring ejects the safety block to yield an effective scram in $\sim 225\ \mu s$.

Molly-G

Except for the core, the White Sands Missile Range (WSMR) Fast Burst Reactor (FBR) was designed and developed by Kaman Nuclear, a subsidiary of Kaman Aircraft Corporation. The core was designed by WSMR engineering staff with consultation services provided by Los Alamos Scientific Laboratory and Sandia Corporation. The core, illustrated in Fig. 6, is similar to HPRR in its cylindrical shape and use of the U-10 wt.% Mo alloy. To satisfy requirements for irradiation applications, the core is mounted on a small stand similar to that of Godiva II or SPR I (hence its nickname "Molly-G" for molybdenum-alloy Godiva). The portable stand is normally fastened to an elevator which is used to lower the assembly into a shielded pit (as in SPR I) inside a large reactor building; otherwise the assembly may be transported readily on a fork lift to an outdoor site for free space experiments.

The core is 8 in in diameter and 7 5/8-in high. The safety block is ~ 4 in in diameter and 5 3/4-in high with a stainless steel core 1.25 in in diameter; its withdrawal reduces reactivity by ~ 30 \$. The total mass of U-Mo is ~ 97 kg in this configuration.

Reactivity control is accomplished by the usual two control rods and a burst rod (~ 1.5 \$ each); in addition, there is provision for stepwise adjustments of ~ 1 \$ by means of a mass-adjustment or shim ring shown at the top of the core in the figure. A shim ring of iron adds ~ 1 \$ while one of U-Mo adds ~ 3 \$ in reactivity. The fuel rings are bolted together and to the support plate by three 3/4-in bolts. Those shown in the drawing and current-

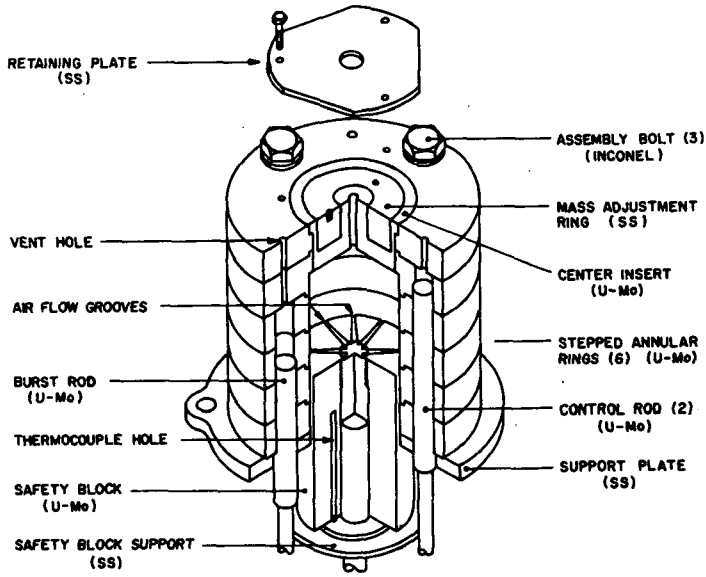


Fig. 6

Molly-G core detail

ly in use are made of a special high-strength nickel alloy, Inconel X, which exhibits a yield strength of $\sim 180\,000$ lb/in^2. U-Mo bolts have also been fabricated with a predicted yield strength $\sim 110\,000$ lb/in^2 at room temperature but the value decreases to $\sim 80\,000$ lb/in^2 at $\sim 200°$C, which is the predicted bolt temperature at the instant of maximum burst stress. Experiments are in progress at WSMR to determine the bolt material best suited for the purpose.

During a preliminary series of bursts at LASL to establish limits for routine operation, the maximum burst temperature increase observed on Molly-G was 480°C in the zone of peak power density. The resultant shock experienced by the assembly (Inconel) bolts exceeded the yield point to produce a net elongation of ~ 0.02 in in each bolt. Following this large burst and several at somewhat lower yields, the core was disassembled for examination. Additional damage revealed was a permanent downward bowing of ~ 0.05 in in the 1/2-in stainless steel support plate, a warping of the upper retaining plate, and elongation of the smaller bolts used to attach it.

In operation at WSMR, the core has produced ~ 300 bursts of $\sim 6 \times 10^{16}$ fissions with peak temperature increases in the neighbourhood of 250°C without observable damage. The shock-induced separation of the safety block magnet produces an early effective scram very similar to that described in HPRR operation.

Super Kukla

The largest and highest-yield burst reactor of the second series or U-Mo devices is Super Kukla. The basic design [9] was developed by Lawrence

Radiation Laboratory (LRL), and the assembly machine was constructed by the Baldwin-Lima-Hamilton Company with technical direction by LRL. The reactor went into operation in December 1964, and only preliminary experimental results are available at this time. The reactor is designed to serve as a prompt burst irradiation source for a wide variety of samples which may be exposed externally or in a large internal cavity.

The core structure is illustrated in Fig. 7. Basically a cylindrical shell open at the top, it includes a cavity 18 in in diameter and ~24-in high. The wall thickness is 6 in. The height is variable and nominally 37 in at critical

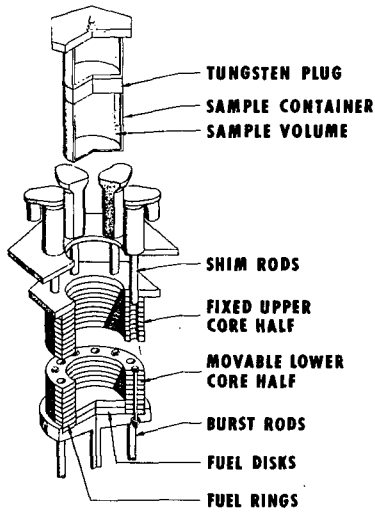


Fig. 7

Exploded view of Super Kukla

with no reactivity perturbation in the cavity. The shell is composed of a stack of U-10 wt. % Mo alloy rings in which the uranium is enriched to 20% U^{235}. The top of the cavity is reflected by means of a 6-in-thick tungsten disc attached to the sample container. Total fuel mass is ~5000 kg. Large critical mass adjustments can be made by changing discs at the bottom of the lower core half. For continuous control, a gang of six shim rods operated individually or in combination enter the core from above and employ double-ballscrew actuators. A similar gang of rods enters from below into the lower core half and is used as a burst rod driven by a double-action hydraulic cylinder. Reactor shutdown is accomplished by dropping the lower core half, which is also hydraulically actuated. Figure 8 shows the assembled reactor in the shutdown state but with the burst rod gang at its inserted position, hence protruding from the lower core half. The sample can is also visible as it hangs below the upper core half.

The maximum temperature increase observed in preliminary operations is 140°C, which corresponds to a total yield of $\sim 2 \times 10^{18}$ fissions, by far the largest fast burst yield obtained under controlled conditions. The design yield figure for this device is $\sim 5 \times 10^{18}$ fissions. No inertial shock effects

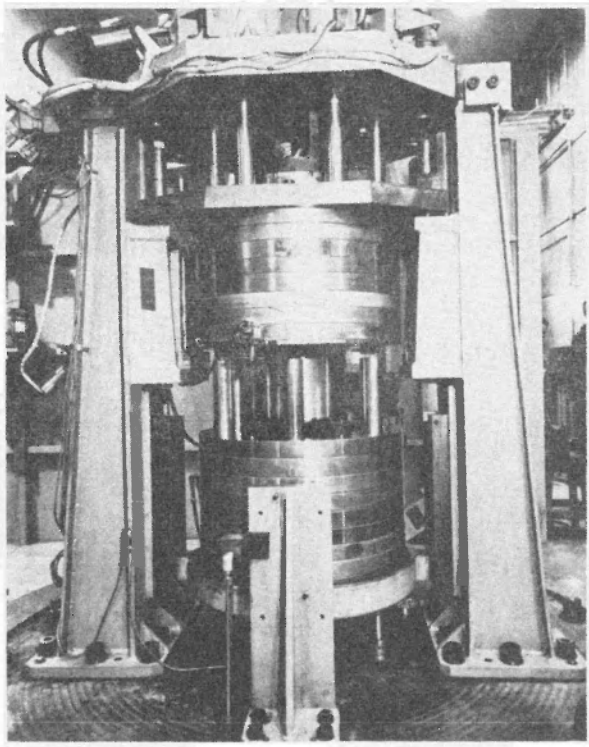


Fig. 8

Super Kukla in shutdown state but with burst rods at inserted position
Sample container is visible at the centre.

have been experienced to date. Large telescoped cylindrical springs with extremely high spring constants are incorporated for vertical shock suppression in the fuel stacks.

The burst generation procedure followed in Super Kukla operations differs in two aspects from that outlined in section 2. First, in step (1), section 2, the delayed critical operation is performed with the burst gang inserted, hence the burst gang is withdrawn in step (2) and the shim rods adjusted so that re-insertion of the ~7-$ burst rod gang leads to the desired prompt reactivity. Secondly, the neutron source remains in place during the burst mode as will be explained in section 5.

4. REACTOR PERFORMANCE

Neutron spectra

Neutron energy spectra for representative burst reactors may be described by the group parameters given in Table II using the six energy groups of G.E. HANSEN [10]. The first line shows the fission-neutron energy spec-

TABLE II

BURST REACTOR AND FISSION SPECTRA

Spectrum	0 - 0.1 (MeV)	0.1 - 0.4	0.4 - 0.9	0.9 - 1.4	1.4 - 3	3 - ∞	Mean energy $\bar{E}$ (MeV)	Comments
Fission spectrum	0.014	0.090	0.180	0.168	0.344	0.204	1.95	LAMS-2543
Godiva leakage	(0.02)	0.160	0.274	0.157	0.246	0.143	1.55	Experimental LA-1670
Godiva leakage	0.020	0.162	0.259	0.160	0.258	0.141	1.56	DSN[a], Hansen 6 group
Godiva central	0.029	0.199	0.256	0.150	0.239	0.127	1.45	DSN, Hansen 6 group
Molly-G leakage	0.023	0.171	0.264	0.167	0.246	0.129	1.49	DDK[b], Hansen 6 group
Super Kukla leakage	0.045	0.342	0.303	0.113	0.127	0.069	0.99	DSN, Hansen 16 group
Super Kukla central	0.072	0.411	0.267	0.093	0.104	0.054	0.85	DSN, Hansen 16 group
Super Kukla central (with 6-in U^{238} below cavity)	0.100	0.440	0.254	0.081	0.083	0.042	0.74	DDK, Hansen 6 group

[a] DSN refers to one-dimensional neutron transport calculation [11].

[b] DDK refers to LASL two-dimensional transport calculation (S_4 approximation in this case).

trum for comparison purposes. The next two permit comparison between experiment and transport calculation of Godiva leakage spectra. The spectrum calculated for Molly-G is in good agreement with that for HPRR, hence typical of highly enriched U-10 wt.% Mo reactors. The Godiva data apply for all reactors of the first series discussed here. The neutron spectrum calculated for Super Kukla displays a higher contribution at lower energies owing to the low uranium enrichment and presence of massive steel components. Mean spectral energy $\bar{E}$ shown in the table was calculated by employing group energy factors that include fission-spectrum weighting [10].

Kinetics

The kinetic behaviour of the burst reactors considered here is described adequately by means of a one-energy-group, space-independent analytical model with the assumption that reactivity is a linear function of fission yield. With a first order perturbation correction for the inertial lag discussed in section 2, analytical solutions so obtained are:

$$P = \frac{\rho_0 \alpha}{2b}(1 + \alpha^2\tau^2) \tag{1}$$

$$Y = \frac{2\rho_0}{b}(1 + \alpha^2\tau^2), \tag{2}$$

where P is peak burst power, Y is total prompt fission energy yield, b is a quenching constant giving the reactivity change per unit fission energy released in a particular reactor, ρ_0 is the initial excess prompt reactivity, α is the reciprocal stable reactor period, and τ is the inertial time constant. The full burst width measured at half maximum power is given by $\Delta t = 3.52\,\alpha^{-1}$ for $\alpha\tau \ll 1$, and experimentally, $\alpha\Delta t$ decreases slowly with $\alpha\tau$ to ~ 3 as $\alpha\tau$ approaches unity. Assuming reactivity is sufficiently above prompt critical that delayed neutrons play no role, $\alpha = \rho_0 \alpha_R$, where $\alpha_R \equiv \beta'/\ell$, $\ell \equiv$ prompt neutron lifetime, $\beta' \equiv$ effective delayed neutron fraction, ρ_0 is expressed in dollars ($), Eqs. (1) and (2) become

$$P = \frac{\alpha^2}{2b\alpha_R}(1 + \alpha^2\tau^2), \tag{3}$$

$$Y = \frac{2\alpha}{b\alpha_R}(1 + \alpha^2\tau^2), \tag{4}$$

and, effectively, the quenching coefficient is the product $b\alpha_R$.

Observed peak burst power for the different reactors is shown plotted against burst width Δt in Fig. 9. The inverse square dependence on Δt for large Δt as predicted by Eq. (3), with $\alpha \sim \Delta t^{-1}$, is clearly evident, and the influence of the inertial or bracketed term may be correlated with the logarithmic slope changes evident in the plots for the Godivas, Molly-G and HPRR. The limited data for Super Kukla does not display the inertial effect owing to relatively long burst widths obtained. Noting that the quenching factor b varies inversely with core mass and that α_R observed for Super

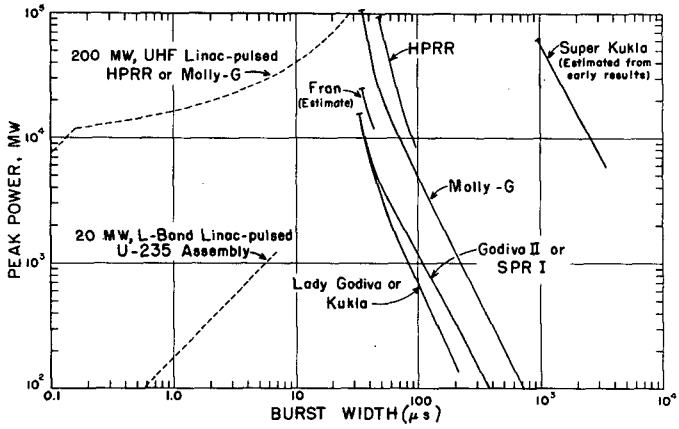


Fig. 9

Burst peak power as a function of width

Kukla (see Table I) is considerably smaller than for the other reactors discussed, Eq. (3) correctly predicts much higher peak powers for a given burst width in Super Kukla than for the smaller reactors. Similarly, the observed increase in burst power of HPRR over that of Molly-G as Δt approaches 50 μs may be correlated with three factors of the expression in Eq. (3). First, the mass ratio as it affects quenching constant b yields an enhancement of 1.19 for HPRR; secondly, the inverse ratio of the respective values for α_R yields the ratio 1.4; finally, the inertial factor contributes the ratio 1.4; finally, the inertial factor contributes the ratio 1.56 for $\Delta t = 50$ s (using values for τ as deduced from the data, namely 20 μs for HPRR and 12 μs for Molly-G). The product of these three ratios is the predicted power ratio of 2.7, which is in fair agreement with observation.

Table III lists available neutron burst fluxes as calculated or estimated by the author from experimental or design data obtained in four different representative burst reactors. Note the gradual increase in flux integral (nvt) from Godiva II at 2.5×10^{14} to $\sim 10^{15}$ in Super Kukla while the maximum flux ($nv = 2 \times 10^{19}$) is that of Molly-G. This is, of course, a result of considerably shorter burst widths in Molly-G than in the high-yield Super Kukla which in turn result from the difference in neutron lifetimes ($\ell \sim 10^{-8}$ s in Molly-G and $\sim 1.5 \times 10^{-7}$ s in Super Kukla). The flux integral available in the cavity of Super Kukla exhibits a nearly flat spatial distribution as shown by the calculated curves of Fig. 10. The upper curve shows the radial flux distribution near the central region and includes the maximum cavity flux. The lower curve shows the minimum cavity flux which occurs near the tungsten plug at the top of the cavity. These results were obtained by two-dimensional transport calculation (DDK) at LASL and apply to a particular core geometry, e.g. with 6 in of U^{238} at the bottom of the cavity.

To estimate the yield of thermal neutrons per burst with different amounts of neutron moderation, calculations were performed on a spherical reactor (Godiva) surrounded by plastic (Lucite) moderators of different thicknesses. Between the moderator and reactor was placed a 1/2-in layer of

TABLE III

BURST NEUTRON FLUX IN TYPICAL BURST REACTORS

Reactor	Peak nv(n/cm².s)		Flux integral nvt (n/cm²)	
	Available external	Available central	Available external	Available central
Godiva II or SPR I	3×10^{17}	4×10^{18}	2×10^{13}	2.5×10^{14}
Fran	6×10^{17}	1×10^{19}	3×10^{13}	5×10^{14}
Molly-G	1.5×10^{18}	2×10^{19}	7×10^{13}	9×10^{14}
Super Kukla (from design figures)	3×10^{17}	4×10^{18}	1.5×10^{14}	2×10^{15}
Super Kukla (from early experimental data)	6×10^{16}	9×10^{17}	6×10^{13}	8×10^{14}

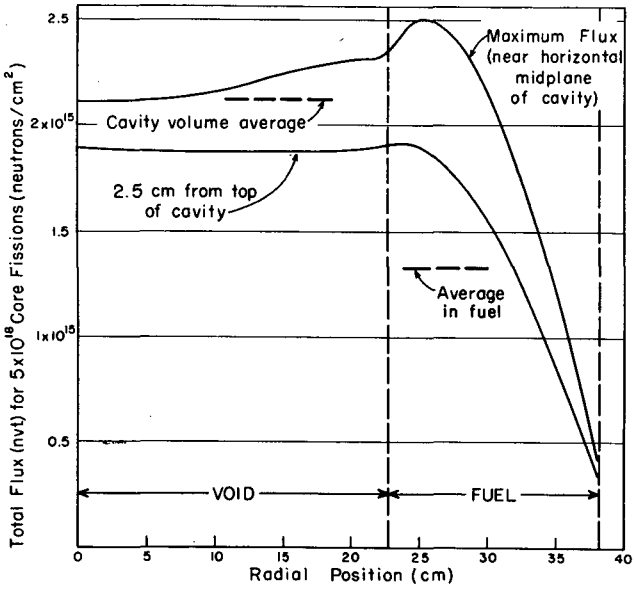


Fig. 10

Total flux as a function of radius in Super Kukla

heavily loaded boral to minimize burst broadening from coupling between reactor and moderator. The calculations were performed using the LASL one-dimensional transport code, DTK, with sixteen energy groups [10]. Results in the form of differential leakage parameters for energy groups up to 10^5 eV are shown in Fig. 11. By extrapolation on the basis of total burst fissions, a total predicted thermal flux for Molly-G is indicated on the curves. Thus for a burst of 10^{17} fissions, a total thermal flux of 2.2×10^{12} n/cm^2 is available from a 2-in moderator. Assuming the pulse is lengthened by die-away time to $\Delta t = 100\ \mu s$, this corresponds to a peak thermal flux, nv = 2.2×10^{16} n/cm^2 · s.

5. REACTOR SAFETY

Because of low repetition rates, time-averaged operating power levels for fast burst reactors are generally less than a kilowatt. This means that the radioactive fission fragment inventory is small and its dispersal as a result of an explosive accident generally would not be a matter of public-safety concern. Questions of more legitimate concern are those associated with possible low-level disruptive damage which may accompany the step-wise assembly necessary for prompt burst production. Protection of operating personnel from direct radiation is provided by remote operation from a distant or well-shielded control room.

In burst reactor operation, two occasions arise in which an unexpected power excursion may occur as a result of inadvertent reactivity additions

introduced, for example, by neutron reflectors near the bare core. The first occasion is during the initial approach-to-critical (step (1), section 2), and the second is when the safety block and burst rod are inserted (step (3)). A specified slow rate of reactivity addition, coupled with the presence of a suitable neutron source, provide the customary safeguard in step (1). During step (3), when at most a weak neutron source is present, safety resides chiefly in careful operational control so as to avoid accidental reactivity changes after the delayed-critical check. Furthermore, the accidental addition of more than a half-dollar excess reactivity between steps (2) and (3) will normally be discovered either by means of visual reactor surveillance or by a detectable increase in power level before burst rod insertion. The possibility remains, however, of an oversized burst caused by the accidental addition of up to one-half dollar at this point. That possibility is normally considered to define the maximum credible accident that serves as a basis for judging the need for containment or confinement.

For most fast burst reactors, there is a basic incompatibility between absolute safeguards against unplanned prompt excursions and the capability for reproducible burst generation. A sufficiently large neutron source will lead to a buildup in neutron population and initiate reactivity quenching by fission energy release, hence prevent an accidental prompt excursion at the available reactivity insertion rate. But the same source, by pre-initiation, may prevent attainment of the superprompt state necessary for an intentional burst. The problem of predicting energy release under ramp conditions has been considered by HANSEN [12] who shows that the probability of the neutron population remaining below a specified level at a particular reactivity depends primarily upon the time fluctuation in establishment of a persistent neutron chain, and secondarily on the time fluctuation in growth of a chain. BELL et al. [13] have developed a machine code which approximates this probability in terms of a probability-distribution generating function. Solutions obtained by the (Bell) code for cases of interest are shown in Fig. 12 where the probability that the reactor neutron population remains less than an arbitrary value of 10^5 neutrons is plotted versus reactivity, ρ_p, for different ramp rates and neutron source strengths, s. The upper curve is representative of burst rod reactivity insertion without an external source for many of the small burst reactors. The spontaneous fission source strength S_0 in Godiva II is $\sim$100 n/s but is often increased to 300 n/s by reactor multiplication after safety block insertion and before burst rod insertion, while the natural source for Molly-G and HPRR is about twice that of Godiva II. The burst reactivity insertion rate currently used on Super Kukla is $\sim$40 \$/s and the natural source is $\sim 6 \times 10^4$ n/s. The appropriate probability function is as shown in the figure. Clearly, there is finite probability of reaching $\rho_p = 0.5\$$ with no excursion taking place in operation of Godiva II and Super Kukla without external source if the ramp (inadvertently) reaches such reactivity. By increasing the (normal mode) source strength to higher values as shown on the lower curves, the probability of exceeding $\rho_p = 0.5\$$ without burst initiation may be reduced to a negligible level for either device.

To examine the problem of burst pre-initiation, we determine the probability that the neutron population at ρ_p will be equal to or greater than that corresponding to a full amplitude burst. Functions so obtained are presented

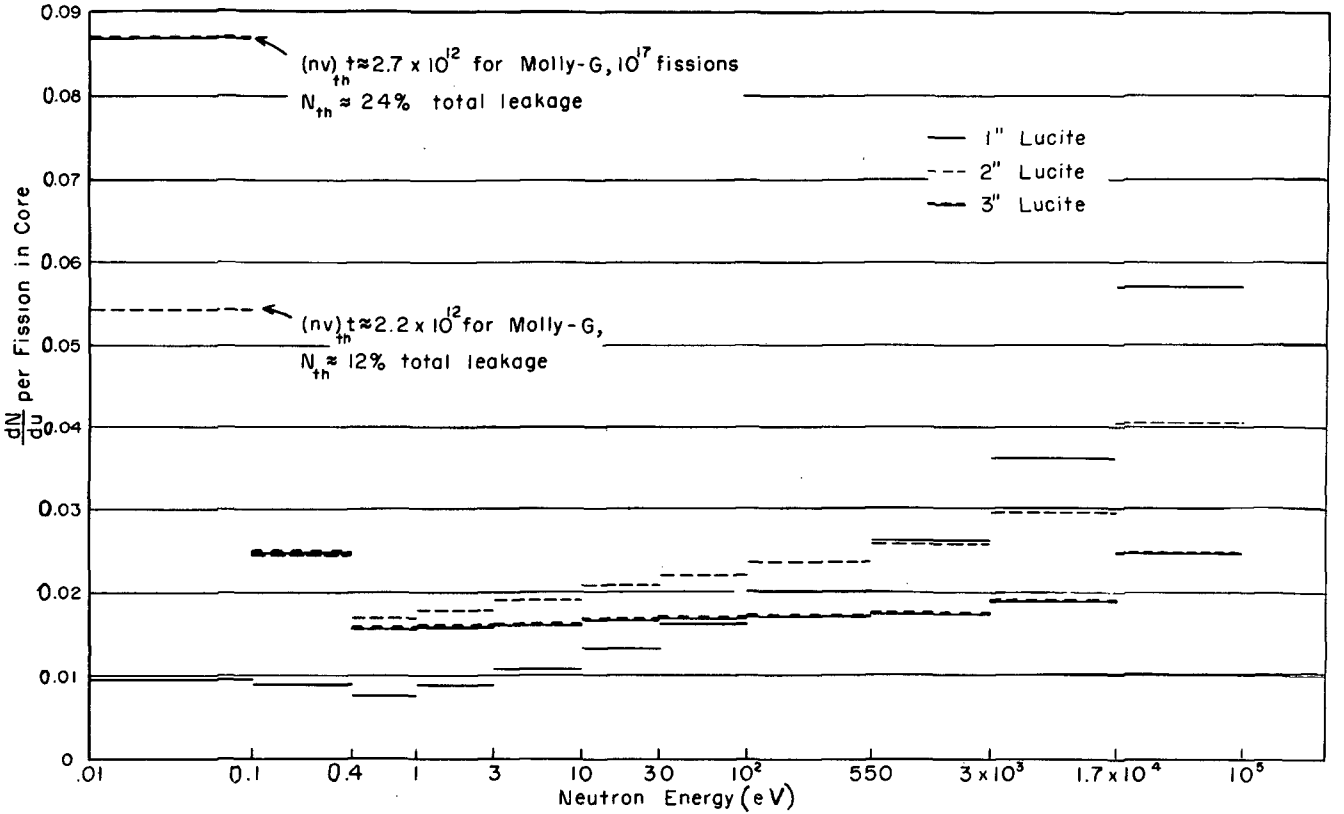


Fig. 11

Leakage neutron energy distribution computed for different thicknesses of Lucite surrounding Godiva-like burst reactor
Ordinate is neutrons per core fission per lethargy interval with an interval of 2.3 chosen for the thermal group.

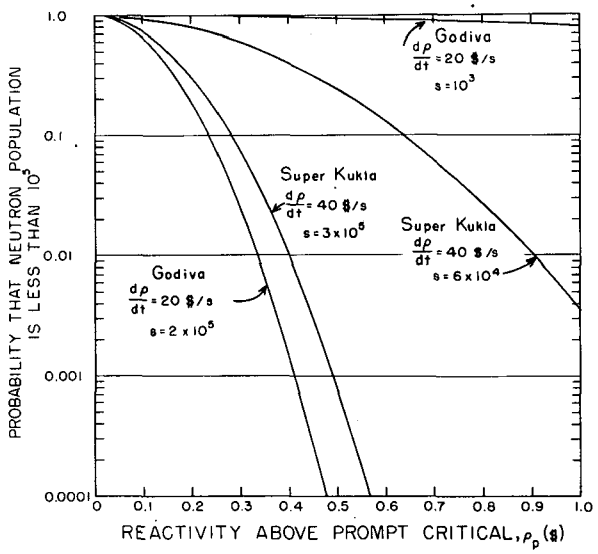


Fig. 12

Probability that core neutron population is below 10^5 neutrons for different reactivity insertion rates

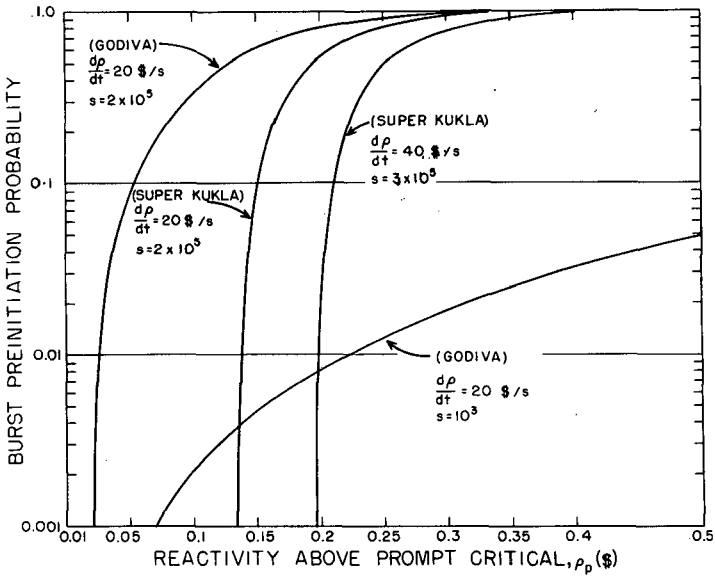


Fig. 13

Burst pre-initiation probability for different reactivity insertion rates

in Fig. 13. From the upper curve, it is apparent that a neutron source of $2.\times 10^5$ n/s for Godiva, which provides protection against excessive bursts as shown in Fig. 12, results in a 35% pre-initiation probability at the maximum operating reactivity, $\rho_p = 0.1\$$. For Super Kukla, on the other hand,

the "safe" source of 3×10^5 n/s permits operation with negligible pre-initiation probability up to $\rho_p = 0.2\$$ which is very near the design-maximum operating point.

6. PRESENT STATUS AND FUTURE PLANS

The limit of peak power in self-quenching bursts is presently $\sim 10^4$ MW as obtained in Molly-G. The maximum yield is ~ 60 MJ in the 5000-kg Super Kukla. The shortest burst width obtained is ~ 30 μs as observed in the smaller reactors having short neutron lifetimes.

For high intensity bursts less than 35 μs in width, BEYSTER and RUSSELL [14] and others at General Atomic have been investigating the bombardment of a super-critical fast reactor with the electron beam of a high current linear accelerator (Linac). They have obtained bursts up to 300 MW peak power and ~ 3 μs wide by pulsing a bare U^{235} supercritical reactor with a 20 MW L-band Linac. Because core requirements are very similar to those for short-burst generation in a self-quenching burst reactor, namely, short neutron lifetime and a shock-resistant core structure, the small U-Mo reactors discussed here are optimum choices for bombardment. The upper dashed curve in Fig. 9 shows performance predicted for the pulsing of a Molly-G type reactor using a proposed 200 MW Linac[4]. The lower curve shows predicted operation with currently available equipment. These results are taken from Ref. [14].

To further extend the range of operation of bursts from fast reactors as illustrated in Fig. 9, high-strength fuel alloys are being examined at LASL. A new scheme of burst generation is being developed at Sandia Corporation for use on a U-Mo reactor in which a burst is pulse-initiated the instant a fly-through burst rod attains maximum reactivity. This is expected to result in more reproducible "tail-less" bursts. A new shock-resistant core concept shown in Fig. 14 is being developed at LASL which includes centre-of-mass support and spring clamping.

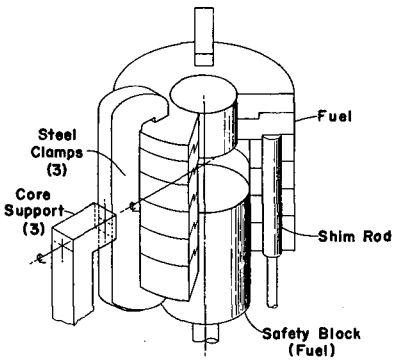


Fig. 14

New LASL reactor design concept for shock suppression

[4] Estimated values for pulsed currents generated by the 200-MW accelerator are more than 10 times that of the 20-MW accelerator at short pulse lengths, because the larger machine is specifically designed to store and utilize RF energy in the microwave cavities.

ACKNOWLEDGEMENTS

The author wishes to acknowledge contributions from P.D. O'Brien of Sandia Corporation, J.T. Milhalczo of ORNL, R.L. Long of WSMR, F.A. Kloverstrom and D. Stillman of LRL. He is indebted to LASL personnel, R.E. Anderson and M.A. Riedel for programming DDK computations, G.I. Bell for computations with his code, and to G.E. Hansen, J.D. Orndoff and H.C. Paxton for helpful suggestions.

LIST OF SYMBOLS

α = reciprocal stable reactor period

$\alpha_R = \frac{\beta'}{\ell}$ = Rossi-alpha at delayed critical

b = quenching constant usually in dollars per joule fission energy released during burst

β' = effective delayed neutron fraction relative to prompt neutrons

ℓ = prompt neutron lifetime in reactor

n = neutron density (n/cm^3)

N(E) = number of neutrons at energy E which leak out of moderator surrounding the reactor

P = burst fission power in watts

ρ = excess reactivity

ρ_p = excess reactivity relative to prompt critical

ρ_0 = initial excess reactivity relative to prompt critical describing reactor state just before burst initiation

s = neutron source strength in neutrons per second

Δt = burst width measured at half-maximum power

τ = reactor inertial time constant (s)

u = neutron lethargy

v = neutron velocity (cm/s)

Y = burst fission energy yield in joules

REFERENCES

[1] BRITTAN, R.O., Some problems in the safety of fast reactors, Rpt ANL-5577 (1956); STRATTON, W.R. et al., "Analysis of prompt excursions in simple systems and idealized fast reactors", Proc. 2nd Int. Conf. PUAE 12 (1958) 196-206.

[2] KEEPIN, G.R. et al., Delayed neutrons from fissionable isotopes of uranium, plutonium and thorium, J. nucl. Energy 6 (1957) 1/2; Phys. Rev. 107 (1957) 1044; FISHER, P.C. and ENGLE, L.B., Delayed gammas from fission of Th-232, U-233, U-235, U-238 and Pu-239, Phys. Rev. 134 4b (1964) B796-B816.

[3] WIMETT, T.F. and ORNDOFF, J.D., "Applications of Godiva II neutron pulses", Proc. 2nd Int. Conf. PUAE 10 (1958) 449-60.

[4] STEIN, H.J., Transitory electrical properties of n-type germanium after a neutron pulse, J. appl. Phys. 31 (1960) 1309.

[5] PETERSON, R.E. and NEWBY, G.A., Nucl. Sci. Engng 1 (1956) 112-25.

[6] CHRISTIE, E.R. and MAR, B.W., The Kukla prompt critical assembly, Rpt UCRL-6105 (1960).
[7] WIMETT, T.F. et al., Nucl. Sci. Engng 8 (1960) 691-708.
[8] MIHALCZO, J.T., Superprompt-critical behavior of an unmoderated, unreflected uranium-molybdenum-alloy reactor, Nucl. Sci. Engng 16 (1963) 291-98.
[9] GILBERT, W.S. et al., Rpt UCRL-7695 (1964).
[10] HANSEN, G.E. and ROACH, W.H., Six and sixteen group cross sections for fast and intermediate critical assemblies, Rpt LAMS-2543 (1961).
[11] CARLSON, B.G. and BELL, G.I., Proc. 2nd Int. Conf. PUAE 16 (1958) 535-49; CARLSON, B.G., Solution of the transport equation by S_n approximations, Rpt La-1891 (1955).
[12] HANSEN, G.E., Assembly of fissionable material in the presence of a weak neutron source, Nucl. Sci. Engng 8 (1960) 709-19.
[13] BELL, G.I. et al., Probability distribution of neutrons and precursors in a multiplying assembly I and II, (a) Ann. Phys. (N.Y.) 21 (1963) 243; (b) Nucl. Sci. Engng 16 (1963) 118-23.
[14] BEYSTER, J.R and RUSSELL, J.L., Rpt GA-6168 (1965).

DISCUSSION

W. KLEY: Is the rather long burst width of Super Kukla due to moderation effects of neutrons in the sample inside the reactor or is it essentially the geometrical dimensions of the cavity that result in long neutron lifetime due to flight-time effects?

T. WIMETT: The lifetime is certainly affected by both sample perturbation and by the geometric effect. However, the preliminary data which I presented are based on behaviour with no samples present. I believe that work is being done at Lawrence Radiation Laboratory on developing neutron shielding in the cavity in order to decouple samples from the reactor.

M.J. POOLE: Can you explain why at pulse lengths of, say, 0.2 μs a factor of ~ 1000 is given as peak power for a stated factor of only 10 in Linac power?

J. RUSSELL: The curve of peak power versus pulse width for the 20-MW Linac is for a conventional L-band (1200-megacycle) machine. The curve for the 200-MW Linac refers to a lower-frequency machine which stores a large amount of microwave energy in its waveguides so that at short pulses the current can be increased. At very short pulse lengths it might operate at ~ 10 000 MW.

Y. POPOV: As regards the operation of a Linac in conjunction with the core, do you rely on mechanical displacement of the parts of the core?

T. WIMETT: Let me point out that we have not used a Linac for neutron production at Los Alamos. However, it is true that mechanical displacement as it applies to reactor scramming is essential to reduce multiplication of neutrons emitted by the precursors which are born during the burst. Because it is supercritical the reactor must in any case be scrammed in a short time.

J. RUSSELL: Is the IBR pulsed with a Linac at the present time?

Y. POPOV: No, it is not. For some time it has been triggered by a pulsed beam of electrons from a microtron.

THE PULSED FAST REACTOR AS A SOURCE FOR PULSED NEUTRON EXPERIMENTS

V. RAIEVSKI, W. KLEY, R. HAAS, J. LARRIMORE, T. ASAOKA,
K. GIEGERICH, R. MISENTA, J. RANDLES, G. RICCOBONO,
H. RIEF, F. SCIUTO, H. WUNDT
EURATOM, ISPRA, ITALY
G. TAVERNIER, J. VAN DIEVOET, J. VAN MIEGROET
BELGONUCLÉAIRE, BRUSSELS, BELGIUM
AND
H. HILDENBRAND, H. R. SCHWARZ
SIEMENS-SCHUCKERTWERKE, ERLANGEN, FEDERAL REPUBLIC OF GERMANY

Abstract — Résumé — Аннотация — Resumen

THE PULSED FAST REACTOR AS A SOURCE FOR PULSED NEUTRON EXPERIMENTS. A large part of neutron physics experiments at reactors make use of pulsed beam methods, or could use this technique. It is therefore evident that a pulsed fast reactor is a very important economic and powerful neutron source. The physics layout of this reactor is discussed in detail and the choices of the free reactor parameters in relationship to reactor physics, the experimental needs and metallurgical limitations are explained.

It is shown that even with the very conservative values of fuel burn-up chosen, mean specific power production and pulsation device safety, the performance figures for pulsed neutron experiments in the thermal and sub-thermal energy region compare favourably with those obtained at high flux reactors, which are close to the upper limits of possible development. The optimization of the moderators, which serve as sources for thermal and cold neutrons, and the interaction of the moderators on the reactor performance characteristics are discussed. The epithermal neutron source is also described. Finally, some safety considerations, which are specific for the pulsed nature of the reactor, are presented.

LE RÉACTEUR A NEUTRONS RAPIDES PULSÉS COMME SOURCE DE NEUTRONS PULSÉS EN PHYSIQUE EXPÉRIMENTALE. Pour un grand nombre d'expériences sur la physique des neutrons faites avec des réacteurs, on utilise ou on peut utiliser les méthodes des faisceaux pulsés. Il est donc évident qu'un réacteur à neutrons rapides pulsés constitue une source de neutrons très importante, économique et puissante. Dans le mémoire, les auteurs étudient de façon détaillée l'aménagement du réacteur du point de vue de la physique, et expliquent le choix des paramètres de réacteur libres dans ses rapports avec la physique des réacteurs, ainsi que les besoins en matière d'expérience et les limitations qu'imposent les métaux utilisés.

Il est démontré que, même en choisissant très prudemment les valeurs du taux de combustion de la puissance spécifique moyenne et de la marge de sécurité pour le dispositif de pulsation, on obtient pour les expériences faites au moyen de neutrons pulsés dans les gammes d'énergie thermique et sub-thermique des résultats qui peuvent avantageusement être comparés à ceux obtenus dans les réacteurs à haut flux, qui sont proches de la limite maximum de développement possible. Les auteurs discutent l'optimisation des ralentisseurs servant de source de neutrons thermiques et froids, notamment l'action des ralentisseurs sur les caractéristiques de performance du réacteur. Ils décrivent également la source de neutrons épithermiques. Enfin, ils exposent certaines considérations de sécurité spéciales à la nature du réacteur à neutrons pulsés.

БЫСТРЫЙ ИМПУЛЬСНЫЙ РЕАКТОР КАК ИСТОЧНИК ИМПУЛЬСНЫХ НЕЙТРОНОВ ДЛЯ ПРОВЕДЕНИЯ ЭКСПЕРИМЕНТОВ. Большая часть экспериментов по нейтронной физике на реакторах проводится или может проводиться с помощью методов *пульсирующих пучков*. Отсюда явствует, что быстрый импульсный реактор является очень важным, экономичным и мощным источником нейтронов.

Подробно рассмотрены физические характеристики такого реактора и даны объяснения по поводу выбора свободных параметров реактора с точки зрения физики реактора, экспериментальных потребностей и металлургических ограничений.

Показано, что даже при выборе очень умеренных значений для выгорания топлива, среднего удельного энерговыделения и безопасности пульсирующего устройства, характеристики экспериментов с импульсными нейтронами в области тепловых и подтепловых энергий выгодно отличаются от тех, которые получены на реакторах с высокой плотностью нейтронных потоков, являющихся почти пределом возможного усовершенствования.

Рассмотрены вопросы оптимизации замедлителей, играющих роль источников тепловых и холодных нейтронов, включая их влияние на рабочие характеристики реакторов. Описан также источник надтепловых нейтронов.

В заключение изложены некоторые соображения о безопасности, связанные с импульсным характером реактора.

EMPLEO EN FISICA EXPERIMENTAL DE LOS REACTORES DE NEUTRONES RAPIDOS PULSADOS. En muchos de los experimentos de física neutrónica que se efectúan con reactores se utilizan o se pueden utilizar métodos a base de haces pulsados. Es evidente, por lo tanto, que un reactor de neutrones rápidos pulsados constituye una fuente neutrónica muy importante, económica y potente. En la memoria se examinan detalladamente las características físicas del reactor, así como la elección de sus parámetros libres, en relación con la física de los reactores, con las necesidades experimentales y con las limitaciones que imponen los metales empleados.

Se ha demostrado que aun cuando se elijan con gran prudencia los valores del grado de combustión, de la potencia media específica y del margen de seguridad para el dispositivo de pulsación, los resultados experimentales obtenidos con neutrones pulsados en las regiones de energía térmica y subtérmica se pueden comparar favorablemente con los alcanzados en los reactores de flujo elevado, que son muy difíciles de perfeccionar. En la memoria se estudian las condiciones óptimas de los moderadores que sirven de fuente de neutrones térmicos y fríos, y en especial su influencia sobre el rendimiento del reactor. Se describe también la fuente de neutrones epitérmicos. Por último se exponen ciertas cuestiones de seguridad que son inherentes a los reactores de neutrones pulsados.

1. INTRODUCTION

For about two years, the Reactor Physics Department of EURATOM has been investigating the possibility of using a fast pulsed reactor for beam research [1, 2]. A 150 000 u. c.* contract was signed in 1964 with the firms Belgonucléaire and Siemens-Schuckertwerke with the aim of arriving at a complete design of the reactor and an assessment of its construction and operation costs.

The contract was divided into two parts: (a) part one, a five months exploratory phase, during which time different technical solutions were investigated to determine the technical specifications, and (b) part two, five months, during which a detailed design will be made, based on the established technical specifications. Part one ended in December 1964, and part two started in March 1965. Thus the design and cost estimate of the fast pulsed reactor (called SORA) is expected to be ready by August 1965.

In addition to the contract a number of theoretical studies have been performed which are described in this paper, and the following experimental studies have been undertaken: (a) a joint United States-EURATOM critical experiment is being made at the Oak-Ridge National Laboratory, (b) a physical mock-up of the hydrogen scatterer, used as a source of cold and thermal neutrons, is being tested with the 1-MeV Van de Graaff of Ispra, and (c) some experimental studies are being made on the fast safety system at the EURATOM Centre in Ispra.

---

* u. c. unité de compte, unit of monetary measure.

2. GENERAL DESCRIPTION

SORA is designed as a research reactor for pulsed neutron beam research, over a range of neutron energies from cold neutrons to keV neutrons. The prototype for the SORA reactor is the periodically pulsed fast reactor which has been operating in the USSR since 1960 [3].

The SORA reactor is a 1-MW fast, liquid metal cooled reactor (design mean power for the first core is 0.6 MW). Reactivity variations are obtained with a pulsation device operating adjacent to the reactor core. A horizontal cross-section of the reference reactor is shown in Fig. 1, a horizontal cross-section of the core and reflector in Fig. 2, and a vertical cross-section through the reactor and the pulsation device in Fig. 3.

The core volume is about 6 l. The critical volume can be adjusted by changing the fuel height and by using dummy fuel elements. The first core consists of about 120 closely packed cylindrical fuel elements (outer diameter 15 mm). Each element is made of a highly enriched uranium-molybdenum (10 wt.%) alloy section (h: 240 mm) and a 120-mm molybdenum top reflector, in an Incoloy cladding. The core is contained in a double-walled irregular hexagonal shaped vessel. The NaK coolant enters through a central pipe below the core, flows upward through the core, and leaves the vessel from an upper coolant plenum.

A fast neutron reflector (h: 440 mm; thickness, about 180 mm) surrounds the vessel on each side of the hexagon, except the one toward the pulsation device. The inner, most efficient part of the reflector is made of molybdenum; the outer layer is of stainless steel. The reflector houses two hydrogenous scatterers in cryostats, which are used as moderators, and the safety and control rods. These are all located close to the vessel. A boron layer through the reflector completely shields the core from thermal and epithermal neutrons produced in the scatterers (This is necessary to have a sufficiently short effective generation time for the reactor core.)

Shielding comprises a graphite thermal shield (about 45 cm thickness) around the fast reflector and a lateral biological shield made of high density iron concrete (density 4.2) to minimize the thickness (140 cm) on the experimental side. The reflector safety and control rods, cryostats, thermal shield, pulsation device, and its housing are cooled by an auxiliary gas cooling system, using gas with low oxygen content to avoid a fire in case of NaK leakage.

The control and safety rods are all reflector control rods. These are (see Fig. 2):

(a) Two safety rods (Nos. 14 and 15 in Fig. 2) made of molybdenum. A pneumatic device actuated by an electro valve can withdraw each rod and bring the reactor below prompt criticality in less than 50 ms after a scram signal arises; delayed criticality is reached in about 200 ms.

(b) An adjustment rod (No. 18) made of tungsten with $B_4^{10}C$ follower. This rod is used as a calibrated rod for approach-to-pulsed-criticality. It has two insertion speeds corresponding respectively to 2.5 and 0.6 pcm*/s.

(c) A regulation rod (No. 19) identical to the adjustment rod which is used as a fine control rod during the start up procedure.

---

* pcm = pour cent mille or 10^{-5}.

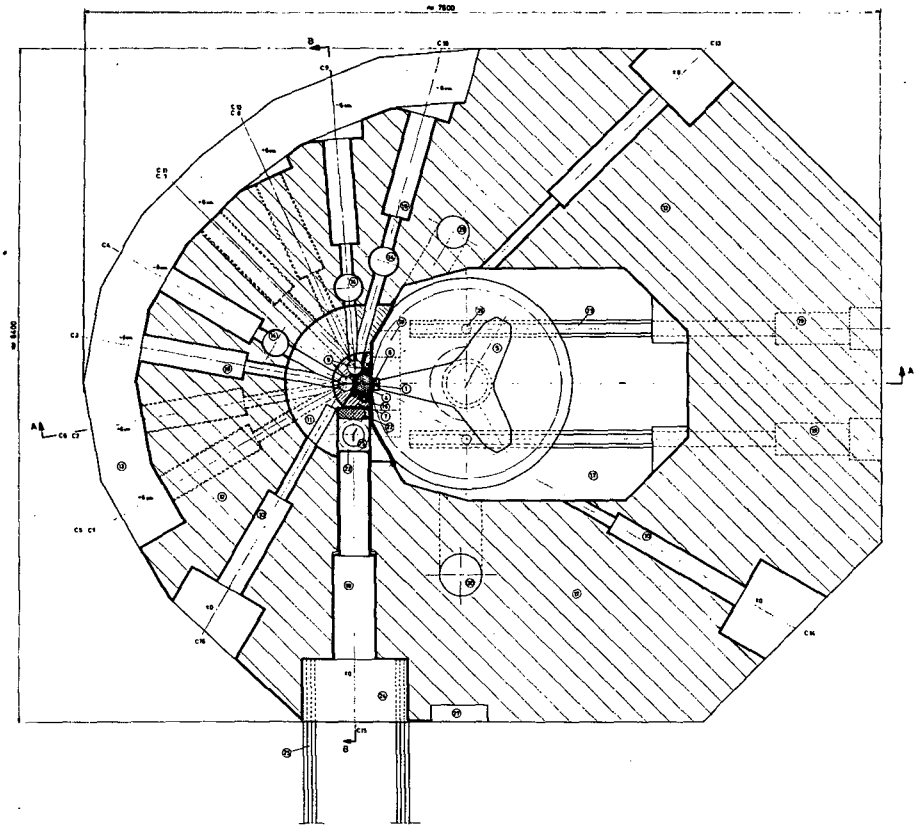


Fig. 1

Reactor block, general layout of horizontal section

(1) Core
(2) Upper reflector
(3) Fuel assembly support plates
(4) Reactor vessel
(5) Pulsation device
(6) Moving reflector (Source S3)
(7) Stationary reflector
(8) Lower stationary reflector
(9) Scatterer loading tube (source S1 and S2)
(10) Beam channel (C1-C16)
(11) Thermal shield
(12) Biological shield
(13) Beam-port slot
(14) Shutter tube
(15) Irradiation tube
(16) Control rod
(17) Pulsation cell
(18) Shutter SH1
(19) Handling channels
(20) Pulsation-cell plug
(21) Compensation block
(22) Moderator block (source S4)
(23) Tight beam-channel insert
(24) Beam-port block
(25) Rails
(26) Pulsation device fixation and adjustment
(27) Installation duct
(28) Installation gallery
(29) Duct for primary NaK loop
(30) Duct for auxiliary cooling

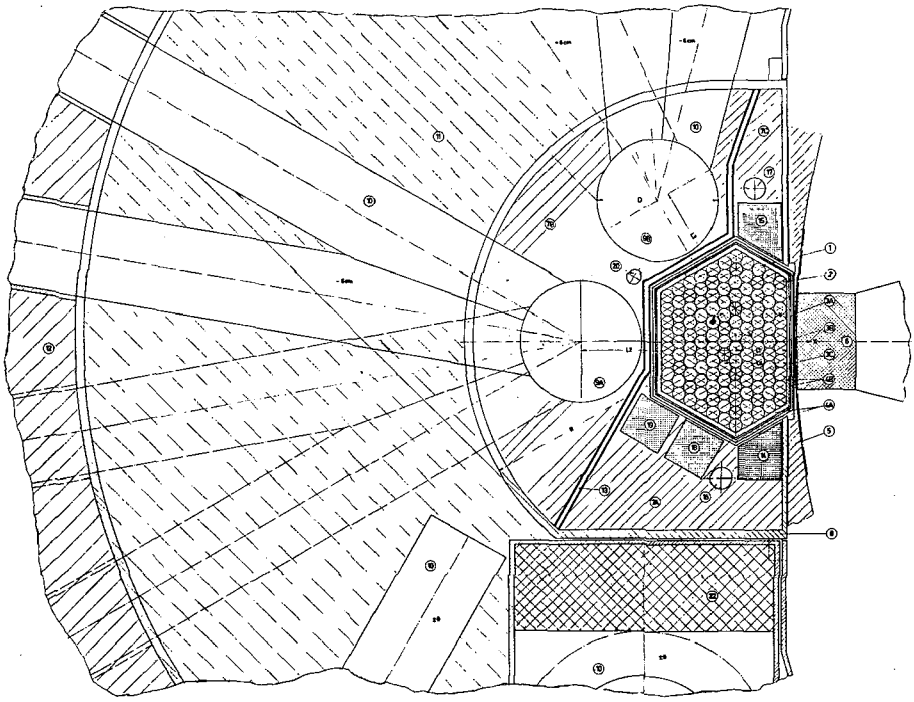


Fig. 2

Reactor, horizontal section

(1) Fuel rod
(2) Trim rod
(3A) Central assembly
(3B) Middle assembly
(3C) Outer assembly
(4A) Reactor vessel (double walled)
(4B) Reactor vessel (window region)
(5) Housing of the pulsation device
(6) Moving reflector (source S3)
(7A) Stationary reflector A
(7B) Stationary reflector B
(7C) Stationary reflector C
(8) Reflector structure
(9A) Scatterer (source S1)
(9B) Scatterer (source S2)
(10) Beam hole
(11) Thermal shield
(12) Biological shield
(13) Boron layer
(14) Safety rod
(15) Safety rod
(16) Fast control rod
(17) Slow control rod
(18) Adjustment rod
(19) Regulation rod
(20) Start-up source
(21) Compensation block (below the core)
(22) Moderator block (source S4)

(d) A compensation block (see Fig. 3), which is a tungsten annular plug below the reactor. Its function is strictly limited to the compensation of reactivity variations from burn-up and changes in the experimental facilities.

(e) A slow automatic control rod (No. 17), which is a tungsten cylindrical rod with a reactivity worth of 40 pcm. It is moved step by step to keep the fast automatic control rod in the centre of its range.

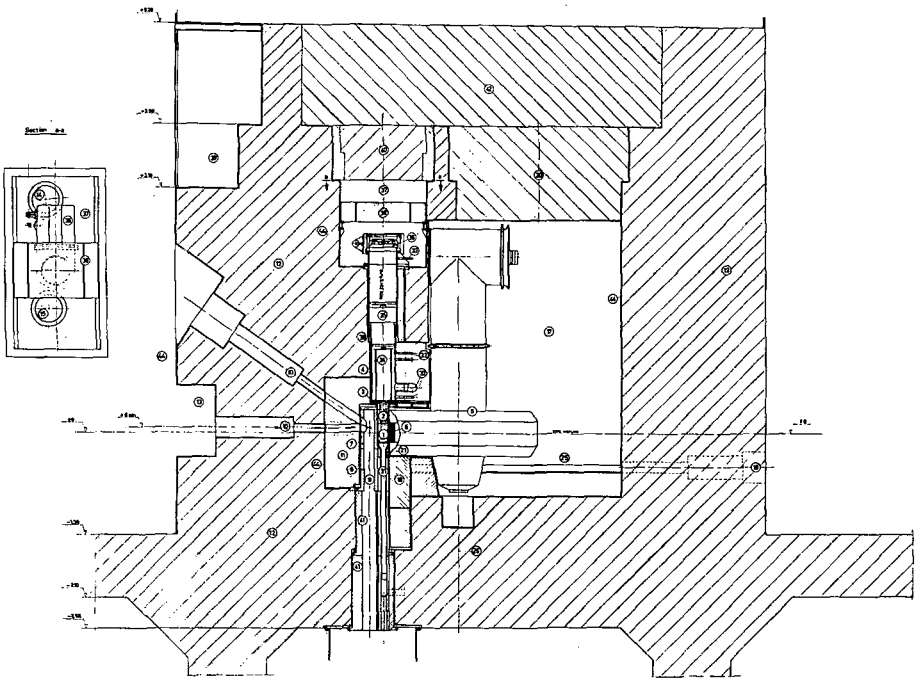


Fig. 3

Reactor block, general layout of vertical section

(1) Core
(2) Upper reflector
(3) Fuel assembly support plates
(4) Reactor vessel
(5) Pulsation device
(6) Moving reflector (source S3)
(7) Stationary reflector
(8) Lower stationary reflector
(9) Scatterer loading tube (source S1 and S2)
(10) Beam channel (C1-C16)
(11) Thermal shield
(12) Biological shield
(13) Beam-port slot
(14) Shutter tube
(15) Irradiation tube
(16) Control rod
(17) Pulsation cell
(18) Shutter SH1
(19) Handling channels
(20) Pulsation-cell plug
(21) Compensation block
(22) Moderator block (source S4)
(23) Tight beam-channel insert
(24) Beam-port block
(25) Rails
(26) Pulsation device fixation and adjustment
(27) Installation duct
(28) Installation gallery
(29) Duct for primary NaK loop
(30) Duct for auxiliary cooling
(31) Coolant inlet
(32) Coolant outlet
(33) Cover gas connection
(34) Hold down device
(35) Vessel shield plug
(36) Reactor vessel closure
(37) Operation pit
(38) Shutter SH2
(39) Vessel lining tube
(40) Top shield plug
(41) Bottom shield plug
(42) Movable shielding
(43) Tube shield plug
(44) Lining

(f) A fast automatic control rod (No. 16), which is a molybdenum half cylindrical, rotary rod having a reactivity worth of 10 pcm. The maximum reactivity insertion rate is 20 pcm/s.

Reactivity pulses are obtained by moving a beryllium block reflector close to the unreflected side of the hexagonal core. The reflector block dimensions (height 24 cm, width 11 cm, thickness 7 cm) and the tip velocity (283 m/s) come from reactor physics considerations on reflector worth, background and pulse shape. To achieve these specifications, the beryllium block is fastened to a large propeller driven by a 3000 rpm electrical motor, so that the beryllium block describes a 180-cm diameter trajectory, passing 50 times per second the unreflected side of the core.

The propeller is preferred to a wheel to get a lighter device, simplifying the design of shaft and bearings. Titanium alloy is preferred to steel as material, both from weight and from activation considerations. The propeller has a vertical axis of revolution. It consists of an arm of uniform stress carrying the reflector block and two shorter compensation arms. It is located in an aluminium housing filled with helium gas to reduce frictional power losses.

The shaft consists of two conic hollow shaft butts screwed to the propeller. Bearings are oil lubricated, and located far enough away to be sufficiently shielded from radiation.

Safety features incorporated in the pulsation device system are:

(a) A safety factor greater than 6. The safety factor is defined as the quotient of the calculated nominal stress in the most strained cross-section of a piece (a factor 2 has been allowed for stress concentration) and the yield-stress of the material used (0.2% plastic deformation). A test rotor must sustain a spin test at twice the nominal rotation speed without measurable deformation in regions of stress concentration.

(b) The beryllium block and the propeller are divided into two identical parts by a median plane, so that in case the beryllium block or a part of the arm close to the beryllium block breaks loose, this would affect only half of the pulsation device. The remaining part and, in particular, the shaft are designed to resist the resulting unbalanced forces.

(c) In case of a failure of the bearings or of the shaft, emergency bearings close to the propeller would maintain the propeller at its normal position of rotation.

The region between core and beryllium block, called the window, is a delicate part of the design. Reactor physics considerations on the worth of the beryllium block limit the gap between core and beryllium to about 10 mm total, of which less than 7 mm is material. This requires both a thin vessel window (7 mm total) and a thin housing window (2 mm at the centre).

3. EXPERIMENTAL FACILITIES

The reactor is used mainly as an intense pulsed source of cold, thermal and epithermal neutrons (a few eV). Some experiments are also forseen in the keV region using a very long flight path (up to about 1 km). The reactor is equipped with a total of 16 beam tubes.

Four sources of slowed-down neutrons are provided:

(a) A hydrogenous moderator in a cryostat (diam., 140 mm; height, 240 mm) located in a vertical channel close to the core boundary (see Fig. 2) is the source for thermal neutrons. Light water ice will be used as hydrogenous material, to avoid reactivity variations. The source can be loaded and unloaded from below through a vertical channel. Six beam tubes look at this source, two pairs of horizontal beam tubes at two different levels, and one pair of slanted tubes. The inner diameter of the narrow beam hole section is 10 cm; the distance from the source axis to the outer end of the beam tube is 200 cm. Two of the horizontal beam tubes are equipped with a vertical shutter, or a rotating chopper (diam., 25 cm; distance from the source axis, 75 cm) to cut out the pulse background.

(b) A second hydrogenous moderator in a cryostat as a cold source, located close to another side of the core. The layout of the source and the beam tubes are similar to those of the thermal neutron source.

(c) The beryllium block moving reflector is a source for neutrons in the keV region. Two horizontal beam tubes look at this source; one of them may be used with a flight path of up to 1 km.

(d) A large horizontal beam tube (diam., 28 cm) with its inner end at the boundary of the fast neutron reflector and the graphite thermal shield is a second source of epithermal neutrons.

4. EXPECTED REACTOR PERFORMANCE

The fast pulsed reactor is a remarkable instrument for pulsed neutron beam experiments [4]. The pulsed neutron technique is widely used for diffraction, inelastic scattering and nuclear physics, where choppers are operated with a stationary reactor. A chopper has a duty cycle of the order of 5×10^{-3} so only a small fraction of the neutrons injected in the beam are used for the experiments. Advantages of a fast pulsed reactor are:

(a) The duty cycle can be nearly 0.7; this means that 70% of the power is produced during the pulses and used for the experiment. Taking into account the factor of 5×10^{-3}, a 1-MW pulsed reactor gives the same counting rate as an identical stationary reactor with the same experimental layout and operated at a power of 140 MW.

(b) The fast core is more concentrated. The maximum thermal flux in the central hydrogen scatterer is $4 \times 10^{13} n/cm^2$ s-MW at stationary operation, a figure about twice higher than for an optimized thermal reactor. This advantage is still more important for epithermal neutrons for which intensity is proportional to the specific power (6-1 core for SORA, about 90-1 for a thermal reactor), as the scatterer has dimensions not negligible compared to the core and cannot be placed in contact with it, the practical gain as compared to an optimized externally moderated reactor is about three, which is smaller than the core volume ratio. The maximum epithermal flux in the scatterer is 0.7×10^{13} n/cm^{2}s-MW in the energy interval 22.6-0.414 eV. In addition, for these neutrons, the reactor pulse (50 μs) is not broadened by the moderator.

(c) The spectrum of slowed-down neutrons can be properly selected by adjusting the temperature and the thickness of the hydrogen source. A cold source can be used with reasonable cooling requirements.

(d) A low pulse repetition rate can be selected without loss in counting rate.

(e) There is low background between the pulses.

(f) Thinner shielding can be used.

A major disadvantage is the large width ($\sim 90\ \mu s$) of the thermal neutron pulse in the scatterer. Combining the advantages (a), (b) and (c), a 1-MW fast pulsed reactor is equivalent for the counting rate to a 280-MW stationary reactor for cold and thermal neutrons and to about a 420-MW stationary reactor for epithermal neutrons, using the same experimental layout, but with the disadvantage of a larger pulse (90 μs for thermal, and 50 μs for epithermal neutrons). This pulse can be shortened using a synchronized chopper but at the expense of a reduction of the duty cycle. For example, a 20-μs chopper suitable for cold and thermal neutron experiments would reduce the counting rate by 3.7 and a 5-μs chopper suitable for epithermal neutrons would give a reduction factor of 8 (assuming a Gaussian for the pulse shape). In these two extreme cases, the 1-MW pulsed fast reactor would still be comparable for cold and thermal neutrons to a 70-MW stationary reactor, and for epithermal neutrons to a 50-MW stationary reactor, with the advantage of lower background, lower pulse repetition rate and thinner shielding which still makes the instrument attractive.

These very simplified considerations, which could be elaborated more in detail, illustrate clearly the advantages of a fast pulsed reactor for pulsed neutron beam experiments.

It is convenient for easy comparison with a steady state reactor to consider the use of choppers with small burst width (in this case the optimum experimental layout for the steady state reactor is transposed to the pulsed reactor without any change). But, optimum use of the pulsed reactor would be generally with a long flight path and a background chopper (cutting the wings of the pulse). Thus almost all neutrons fed into the beam are used for the experiment. The following situations may be considered.

(a) Cold neutrons

Because of the low repetition rate (50 c/s), flight paths as long as 10 or 20 m can be used without overlap. For these neutrons, neutron conducting tubes as proposed by MAIER-LEIBNITZ [5] will allow a long flight path without loss of intensity. These tubes would be very suitable for diffraction-type experiments. For inelastic scattering a chopper may sometimes be necessary to shorten the pulse width.

(b) Thermal neutrons

Use of a long flight path does not mean necessarily a loss of intensity. If a good angular definition of the beam is required, as is often the case, large counters covering the full solid angle would give no loss at all, for instance a 1° collimated beam would cover a 35-cm diameter counter at

20 m. If good angular definition is not required, the long flight path would give a loss of intensity; thus a special chopper would be needed to shorten the pulse. However, loss of intensity would be partially compensated by the small shielding thickness which allows the use of a 6° collimated beam impinging on the sample.

(c) Epithermal neutrons

For these neutrons, a special chopper would be necessary to get good resolution. For these neutrons the operation of the pulsed reactor with an accelerator would considerably increase the performance.

5. OPERATION OF A PULSED REACTOR WITH AN ACCELERATOR

A present-day electron Linac may produce intense pulses of neutrons of the order of 10^{14} n/s with a duration of 2 μs. This intensity is still far below the intensity of a pulsed reactor giving 0.8×10^{17} n/s at a power of 1 MW, of which about half is available as leakage neutrons. For cold and thermal neutrons, the short pulse of the accelerator will not compensate for the disadvantage of the comparatively low intensity. The moderator would always broaden the pulse up to about 90 μs. Even for epithermal neutrons in the 1-eV range, the intensity is too low. For this range, amplification by a reactor of the number of neutrons produced by the accelerator is advantageous. This was done already using subcritical fast assemblies called boosters [6].

The amplification by a booster merely results from the lengthening of the accelerator pulse by chain generations; there is no amplification of the peak intensity. Amplification is simply related to the prompt negative reactivity ϵ_p by the relation $A = 1/\epsilon_p$. This gives the ratio of the number of neutrons produced by the reactor pulse to the number injected by the accelerator pulse. The width of the reactor pulse is $A\tau$, where τ is the mean lifetime of the neutron in the booster.

The desired pulse width limits the amplification. For instance, if $\tau = 2 \times 10^{-8}$ s and a 5-μs pulse is required, the amplification cannot exceed 250. However, for such pulses a limitation arises from background and not from the pulse width requirement. In a repetitively pulsed booster, the fraction of the total power in the pulse is $1 - \beta/\epsilon_p$. The fraction β/ϵ_p of the power between the pulses gives rise to a background. In the above-mentioned example, using a U^{235} booster ($\beta = 0.0064$), the prompt reactivity must be higher (in absolute value) than β, so amplification cannot exceed $1/\beta = 150$. The situation can be substantially improved using a plutonium booster ($\beta = 0.002$) but even in this case amplification would be limited below 100 to get an acceptably low background.

A pulsed reactor excited by an accelerator would operate like a booster during the pulse. If the reactor pulse is short compared to the time for the reflector block to move past the window, reactivity may be considered as constant during the pulse. So the pulse amplification and the pulse width are still given by the simple relation ($A = 1/\epsilon_p$, $\theta = A\tau$), but the reactivity

between the pulse is changed by the wheel rotation to a more negative value ϵ_0. Thus ϵ_p and ϵ_0 are different; this means that amplification and background are independent quantities. For instance higher amplification than the limit value $1/\beta$ for a booster can be obtained with low background.

To take again the previous example, an amplification of 250 would be acceptable with a U^{235} core. In this case, the reactor is delayed-supercritical and prompt-subcritical during the pulse. In the SORA case fuelled with U^{235}, $\epsilon_0 = 5\beta$, which means that 80% of the power is in the pulse. The Linac intensity required to match the reactor power would be $\frac{0.8}{250} \times 10^{17} = 3 \times 10^{14}$ n/s. This is a very high value for the present day Linac, but it can be expected in the future. There is no advantage to having pulses shorter than 5 μs; the spread of time distribution of 1-eV neutrons in a hydrogenous target is already of this order [7].

6. REACTOR STATICS

This section summarizes the time-independent stationary and semi-stationary neutron transport problems which have been studied for the SORA reactor. In these studies the time scale of reactivity changes is assumed to be long compared to the mean generation time of neutrons. This assumption implies that an equilibrium distribution of neutrons is achieved, even when the reactivity changes very rapidly.

As the reactor consists of a highly enriched small core surrounded by a very heterogeneous system of reflectors and scatterers, precise methods of solving the neutron transport equation are required. Two methods have been used: the Carlson S_n and the Monte Carlo method.

(a) The S_n method

The S_n method has mainly been used for calculating problems which require a precise geometrical treatment in the x-y plane but which are insensitive to the heterogeneity of the system in the z-direction. For the solution of these problems, the 2 DXY code has been adapted and a set of axial bucklings has been introduced to account for the finite extension of the reactor in the z-direction.

A number of test calculations were carried out and compared with experimental results available in the literature, to confirm the accuracy of the method and to check the basic nuclear data. The cross-sections used for the S_n calculations are based on the 18-group (10-MeV thermal) set of LASL. All the calculations have been performed with the S_4 approximation.

(b) The Monte Carlo method

The Monte Carlo programme (TIMOC) was developed to solve three-dimensional criticality problems, particularly related to the moving reflector. This programme deals with all nuclear phenomena including anisotropic scattering and inelastic scattering either by using the level excitation or the statistical model. The code computes the effective multiplication factor,

the reactivity worth of the moving reflector at different positions, the mean generation time of neutrons and the neutron spectra at different points of interest. A special perturbation method is applied to study the reactivity changes caused by small displacements of the moving reflector or other small effects.

As a result of the comparison of TIMOC calculations with the experimental results, 33 energy groups (10 MeV-0.1 eV) have been used with cross-sections which are taken mainly from the YOM (Yiftah-Okrent-Moldauer) 16-group set and, in the lower energy range, from the LASL (Los Alamos Scientific Laboratory) set. Also, a 26-group Russian cross-section set (1964) was tested and gave similar results.

Under the above-mentioned assumptions of semi-stationary conditions, the following problems were studied:

(a) Calculations for the various core sizes and core compositions, which led to the reference design. The required k_{eff} of 1.03 is obtained with about 57 kg of U^{235} for the most reactive condition (cold state at the beginning of life with all control rods in and the moving reflector in its most reactive position). The approximate relation between k_{eff} and critical mass is $3(\Delta k_{eff}/k_{eff}) = (\Delta \text{cm}/\text{cm})$.

(b) Reactivity worth of the moving reflector and choice of a suitable material. Among the different materials which were considered in the calculations, beryllium showed the largest reactivity worth followed by nickel which is about 16% less effective. To achieve more than the necessary 5 $ reactivity change, a comparatively large section of the reflector has to be moved. This led to the irregularly shaped hexagonal cross-section of the core with its 11-cm window width and its height of 24 cm.

(c) Optimization of the scatterers to maximize the intermediate, thermal and subthermal neutron production.

(d) Choice of the stationary reflector to decrease the core size and mean generation time. To prevent long-lived neutrons from returning to the core and to keep the core generation time below 20 ns, calculations showed that it is necessary to introduce boron shields.

(e) The time behaviour of the reactivity change caused by the moving reflector, which was calculated by the TIMOC code as a real three-dimensional problem by placing the moving reflector at different positions in front of the window.

(f) Reactivity changes caused by control rods and mechanical instabilities. The molybdenum safety rods will have a reactivity worth of nearly 0.8% k_{eff} when all other control rods are inserted. The worth of the tungsten adjustment and regulation rod with a B_4C follower will be about 0.8% k_{eff} each. The compensation block will have a worth of about 1%. One possible mechanical instability could be small displacements of the moving reflector perpendicular to the window. The evaluated effect is about 70 pcm/mm.

(g) Input parameters for the kinetic equations to analyse the pulse characteristic, as described in the following section.

Because of the difficulty of calculating accurately reactivity effects of reflecting materials outside of the compact SORA core, even with the sophisticated methods used, a critical-experiment programme has been undertaken in co-operation with the United States Atomic Energy Commission to check the above calculational results.

7. PULSE KINETICS

Owing to the presence of neutrons with lifetimes which are long compared to the power pulse width (these neutrons originate mainly from the hydrogenous scatterers), the familiar one-group space-independent kinetic equation cannot be applied to analyse the pulse characteristics of the SORA reactor. Since these slow neutrons will behave in a similar manner to the delayed neutrons during the power pulse, they must be treated separately from the other neutrons with very short lifetimes. On the other hand, the pulse characteristics of thermal neutrons in the scatterers will be different from those in the core because of the very dissimilar neutron characteristics. Hence, the separation of the scatterers from the core is necessary, in addition to the separation of slow and fast neutrons. For this reason, a few space-point kinetics in a few energy-group model has been developed.

By multiplying both sides of the reactor equations which describe the time behaviour of neutrons in a certain energy range by the importance function and performing integrations over all solid angles of neutron velocity, over all energies and over certain space regions, one obtains a set of kinetic equations in which the coupling between different space regions does not appear explicitly. To simplify the problem, the following assumptions were introduced: (a) the spatial distribution and energy spectrum of the fast neutrons are the same as for the steady state condition described by the static reactor equation, and (b) the time behaviour of slow neutrons in the core-region is independent of that in the scatterer-region, while the slow neutron spatial distribution and energy spectrum in both regions are the same as for the steady state.

These assumptions are quite reasonable for evaluating the pulse characteristics of the SORA reactor. For the fast neutrons, the generation time, diffusion time from the core to the scatterers and the slowing-down time in the scatterers are all very short compared to the power pulse width, while for the slow neutrons, the absorber layer installed between the two regions produces a very effective decoupling. The assumptions have also been applied to consider the graphite shielding located outside the stationary reflector.

Hence, for the reference design of the reactor, it was possible to construct a 3-energy-group (fast, intermediate and thermal), 3-space point (core, hydrogen scatterers, and graphite shield) model, with all input parameters (the mean generation times and so on), except the effective multiplication factor k_1 for the fast neutrons independent of the time. These time-independent parameters were obtained by the use of the static regular and adjoint fluxes obtained from the multigroup S_4 calculations. The influence of the moving reflector on these parameters has been examined and found to have a small effect on the pulse characteristics.

The stationary pulse characteristics have been calculated using the "pulsed criticality" condition, i.e. the condition giving time-independent pulse amplitudes [8, 9, 10].

The boundary energy between fast and intermediate groups was 454 eV; the boundary between intermediate and thermal groups was 0.414 eV. Some pulse calculations for an epithermal group (22.6-0.414 eV) have also been

made. For the periodic variation of k_1, a parabolic form, $k_1(t) = k_{1m} - \alpha(vt)^2$, has been assumed.

Values used for the principal parameters were
$\beta = 0.0064$,
k_0 (multiplication factor between pulses) = 0.9744,
$\alpha = 7\ m^{-2}$,
v (moving reflector velocity) = 283 ms, and
f (pulse repetition rate) = 50 pulses per second.

The results obtained are as follows:

Maximum effective multiplication factor (k_{1m})	1.0075
Power amplification factor (ratio of maximum power to power between pulses)	1400
Ratio of mean power to power between pulses	5
Power pulse half width (μs)	50
Thermal flux amplification factor (scatterer region)	700
Thermal flux pulse half width (scatterer region) (μs)	90

Thus the maximum of the thermal neutron burst in the central hydrogenous scatterer would be 5.5×10^{15} n/cm^2 s at 1-MW mean power and 50 c/s pulse repetition rate. The maximum of the epithermal neutrons burst (energy range 22.6-0.414 eV) would be 2×10^{15} n/cm^2 s with a 50-μs half width. The leakage flux at the surface of the scatterer is strongly peaked forward. A multiple collision calculation has been performed by Asaoka to calculate the ratio of the leaking neutrons per unit solid angle in the forward direction at the surface of the scatterer to the isotropically distributed neutron flux at the maximum position; this factor was found to be 0.7. Thus the number of neutrons feeding the beam tubes can be computed on the basis of 4×10^{15} n/cm^2 s isotropic flux at the surface of the scatterer, with a 90-μs pulse width and 50 c/s, for thermal neutrons, and 1.4×10^{15} n/cm^2 s with a 50-μs pulse width for epithermal neutrons.

8. DYNAMICS AND CONTROL

The fast dynamics of SORA including kinetics, heat transfer, and control, have been simulated on the Ispra analog computers. The main purpose of this study was to design a reasonable and safe automatic fast control device.

The principal difficulty in the simulation was that the expected output variables (fluxes or power) vary over several decades, which is inconvenient for analogue simulation. A special electronic steering unit, called SIOUX [11], was developed which switched the respective variables from one scale factor to another as soon as some limit voltages were reached. Since the commutations for different variables do not all occur simultaneously, a very precise electronic device was necessary. In fact, for the first time a floating point technique was applied to analog computers in this manner.

To account for the relatively long-lived prompt neutrons from the H_2O-scatterers, a multigroup one-point kinetics model was developed and ap-

plied. The coefficients were taken from S_n transport calculations; the reactivity input pulse shape came from static Monte Carlo computations.

The heat transfer from the fuel to the NaK coolant and outside the core was of minor importance during the 50 periods (1 s of real time) which could be simulated within nearly 2 h. The periodic fuel temperature was about 0.5 pcm. The dynamic behaviour is thus relatively independent of the power level at which the reactor is operated.

As is done also for the IBR reactor, Dubna, USSR, we choose the energy per period as control input signal. The difference between this m-th period energy and the reference energy is used as control input during the (m + 1)-th period. After a suitable amplification, this quantity feeds the armature windings of a DC motor so that, with a certain time constant, the energy difference is proportional to the angular velocity of the control rod driving motor.

The result, as illustrated in Fig. 4, was that with control time constants less than the period length (20-30 ms), a very satisfactory transient behaviour could be achieved. With an optimized amplification, the decay period of the transients could be reduced to 0.8 s after + 16 pcm reactivity steps, which in reality would never occur. The rotary fast control rod is coupled without any gearing to the motor shaft. The inertia of the rotor will be large enough so that modifications of the load do not modify the time constant.

The reactor, being prompt critical during some microseconds, is very sensitive to small modifications of its average reactivity level, so that it can be shut down by a small reactivity insertion. This aids the safety in case of emergency.

9. EXCURSION ANALYSES

Because of the novelty of the pulsed reactor concept, considerable effort has been given to assessing the reactor behaviour under postulated accident conditions. In studying excursions in SORA it has been found convenient to divide the work into two sections: (a) the study of power pulses which are accidentally large but not large enough to vaporize the fuel and destroy the core and (b) the study of destructive power pulses. In this paper, we discuss only the second class of problems since it bears most directly on the safety of the system.

In these problems, attention is focused on very serious accident conditions. Although it is known from the start that such conditions are almost impossible, it is now a well-established philosophy to consider the so-called "maximum credible accident" and to evaluate from this the most extreme hazard that can occur. In the case of the SORA reactor, the worst credible accident takes the form of a fracture of the titanium rotor during the normal pulsed operation of the system, the collision of the broken fragment with the core, the consequent insertion of an abnormally large reactivity pulse and the generation of such a large nuclear excursion that the vapour pressure of the overheated fuel destroys the core explosively.

To estimate the mechanical energy release in such an accident, it has been necessary to couple two quite separate physico-mathematical models.

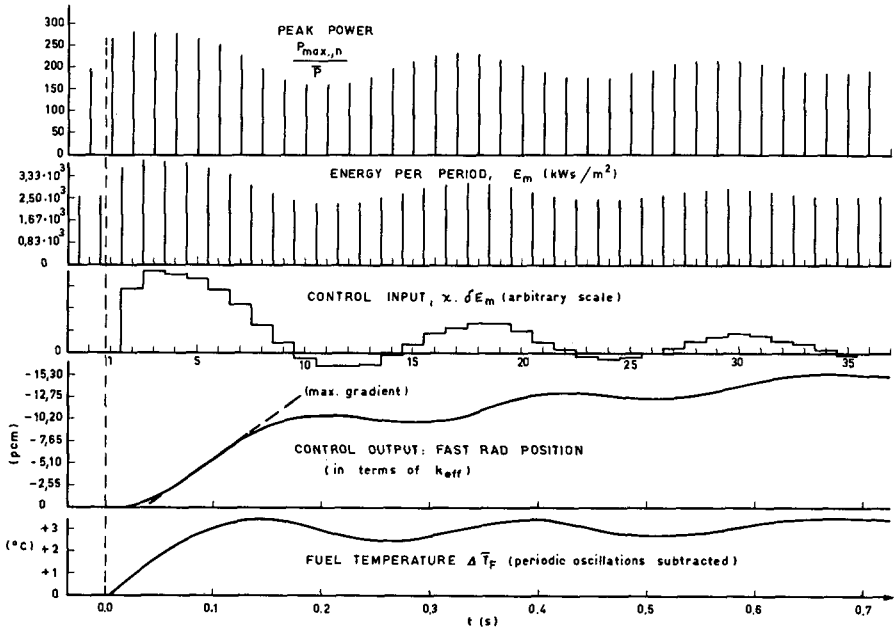


Fig. 4

Transient behaviour (schematized) after + 16-pcm reactivity step.

These are: (a) a model which describes the mechanical aspect of the accident – the motion of the broken fragment of the rotor, its collision with and compression of the core and the resultant reactivity input as a function of the time, and (b) a model which, given the reactivity input as a function of time, describes the nuclear excursion, the connected fuel vapour pressure, the movement of the core material (core destruction) under the influence of this pressure and the termination of the excursion from the explosive expansion of the system.

(a) Mechanical model

In the pulsation device in SORA, the titanium rotor and beryllium reflector block are fabricated in two identical pieces. Thus if a fracture should develop, it will occur in only one half of the rotor at any one time. Thus, the amount of energy which is available for compression of the core, in the event of an actual breakage, is reduced by a factor of two without in any way reducing the strength of the device. This is a very great advantage from the safety point of view.

In the event of a maximum credible accident, one of the halves of the rotor will break away at an instant when it is approaching the core. The broken fragment will then travel outwards from its normal circular path and strike the core in the window region with the beryllium block foremost. The reactivity input will thus be made up of three separate, pulse-like compo-

nents; one as the unbroken half-rotor swings past the window, a second when the fragment of the broken half-rotor strikes and compresses the core, and a third when the fragment slides past the window under its own inertia. These three pulses are separated in time from each other when the angular position of the rotor at the instant of fracture is small (< 5°) or large (>20°), but mutually augment each other at some intermediate angle. When a fracture occurs at this angle, the ingoing accidental reactivity pulse has its largest value and likewise the destructive energy release.

(b) Nuclear model

The main nuclear model used to describe the excursion and destruction of the system is an adaption of the well-known Bethe-Tait model [12]. Its essential features are:

(i) Spherically symmetric, spatially parabolic approximations to the power and reactivity worth distributions,
(ii) Linear relations between the energy per unit mass of fuel and vapour pressure, and
(iii) Core explosion treated like an expanding liquid.

(c) Numerical results

Attempts are still under way to improve on the above models and particularly on certain assumptions about details which have been made in the mechanical model. In the meantime, many numerical results have been obtained and from these the following conclusions have been drawn. For accidents in which the fracture occurs in the beryllium block or to its fixation onto the titanium rotor, the mechanical energy released by the induced nuclear excursion is always zero (i.e. fuel vaporization does not occur). For accidents in which very large fragments of the rotor break away, studies are being undertaken to determine an absolute upper limit of the energy release. Preliminary results based on a conservative model indicate an upper limit of a few hundred kilograms of equivalent TNT, which would be contained within the building. It should be recognized that the very high mechanical safety factors in the rotor design make accidents of this sort extremely improbable.

10. CONCLUSION

Studies made up to now show that the construction and safe operation of a 1-MW fast pulsed reactor is possible. In this case the mean specific power 0.17 MW/l is still low compared to those of present-day fast power reactors. Thus in principle an increase up to a power of 5 MW is imaginable. However, with the present design power, the reactor is a very valuable source for accurate measurement with cold, thermal and epithermal neutrons. Improvements foreseen in the present design include use of plutonium fuel in later core loadings, which would give better pulse characteristics and a higher mean power than the uranium core (higher intensity, sharper pulse, much lower background). Another possible improvement

for epithermal neutrons would be the coupling of the pulsed reactor with a high intensity Linac. Provisions are made in the present design not to exclude this possibility if it appears feasible in the future.

ACKNOWLEDGEMENTS

The authors are very indebted to Mr. Guéron who has always actively supported this programme and to Messrs. Jacrot and Maier-Leibnitz for many helpful discussions.

The work reported in this paper was performed by a large number of individuals at the Ispra Research Center of EURATOM, at Belgonucléaire and at Siemens-Schuckertwerke.

REFERENCES

[1] RAIEVSKI, V., The SORA reactor, Rpt. EUR-1643e (1964).
[2] LARRIMORE, J. A. and RAIEVSKI, V., Design considerations for the pulsed source reactor SORA, Trans. Amer. nucl. Soc. 7 (Nov. 1964) 2, 513.
[3] BLOKHIN, G. E. et al., "A pulsed fast reactor", (in Russian) Physics of Fast and Intermediate Reactors III IAEA, Vienna (1961) 399.
[4] HAAS, R. and MØLLER, H. B., A study of the performance of neutron beam experiments at the pulsed fast reactor SORA, Rpt. EUR-490 (1963).
[5] MAIER-LEIBNITZ, H., Uses for the pulsed Triga reactor, Rpt. GA-3075 (1962).
[6] POOLE, M. J. and WIBLIN, E. R., Proc. 2nd UN Int. Conf. PUAE 14 (1958) 266.
[7] MICHAUDON, A., The production of moderated neutron beams from pulsed accelerators, React. Sci. Engng 17 (July 1963) 4-5.
[8] BONDARENKO, I. I. and STAVISKI, Yu. Ya., Pulsed operation of a fast reactor, Atomnaja Energija 7 (1959) 417; Reactor Sci. Techn. 14 (1961) 55.
[9] BLAESSER, G., MISENTA, R. and RAIEVSKI, V., The kinetic theory of a fast reactor periodically pulsed by reactivity variations, Rpt. EUR-493 (1964).
[10] STIEVENART, M., Etude des caractéristiques d'un réacteur à impulsion, Rpt. BN 6203-25 (1962).
[11] VAN WAUWE, A., The SIOUX, system, Rpt. EUR-1914 (1964).
[12] BETHE, H. A. and TAIT, J. H., U. K. A. E. A. Rpt. RHM (50)/113 (1956).

DISCUSSION

W. GLÄSER: Do you believe that an advantage of a factor of 10 over a very high flux reactor, e.g. the HFBR, holds true for all types of scattering experiments in condensed matter now being performed. I am thinking especially of work with high angular resolution, in which only small samples can be used.

V. RAIEVSKI: No general figure of merit can be established for this type of reactor. Each experiment has to be considered separately. Generally speaking, it may be said that in experiments involving mono-energetic neutrons, in which a high duty cycle is possible with the sample under study, the intensity of a pulsed reactor will be lower by a factor of 2 or 3 than that of a steady-state 100-MW reactor for any experiment performed on small samples and with high angular resolution; for experiments on large samples, where

large solid angles are possible, a pulsed reactor will be better by a factor of as much as 50 or 100.

In experiments in which blank spectra are used, the duty cycle is always limited by the frame overlap of the pulses. In this case the duty cycle is determined by the energy resolution. In experiments where high resolution is required, a pulsed reactor will be superior to a steady-state reactor; where use can also be made of total reflection tubes for the beam, it may be as much as 4-8 times as advantageous as the steady-state type. A further advantage of the pulsed reactor is the low background: in some experiments this advantage may be considerable, although it is difficult to calculate.

H. POLLAK: What is the shape of the neutron pulses you obtain? At first glance it would appear to be sinusoidal, but this shape could be modified by delayed neutrons.

V. RAIEVSKI: The exact pulse shape was calculated by means of a 3-dimensional Monte-Carlo code (TIMOC), which was developed especially for this purpose. A critical experiment which will be getting under way at Oak Ridge very shortly will enable us to check the results of this code. As a first approximation, one can always represent the upper part of the pulse by a Gaussian, and this is what we do in our calculations.

H. POLLAK: In your oral presentation you mentioned a figure of 1400 for the ratio of signal (neutron pulse) to background between the pulses. Does this ratio correspond to peak power or is it the ratio of the integrated flux to the background over a period of 50 ms?

V. RAIEVSKI: The figure of 1400 is the ratio of peak power to power between pulses or, if you prefer, the ratio of signal to background. The ratio of peak power to average power is 270 at 50 Hz.

Y. POPOV: When do you expect to complete your project?

V. RAIEVSKI: Obviously, this is an important question and one which is of concern to us. For the time being, the appropriate departments of the Commission have been authorized to draw up detailed plans for the reactor with a view to determining costs. A contract relating to this study, which is to be completed in August 1965, has been signed with Belgonucléaire and Siemens Schuckertwerke AG. At the same time, we are working with the USAEC on a critical experiment at Oak Ridge for the purpose of measuring the important physical parameters of the reactor there. At the Ispra Centre we have begun a neutron thermalization study on a mock-up of the SORA cold source, which receives a supply of neutron pulses from a Van de Graaff generator. Once these studies have been completed, the Commission will be in a position to decide how this project should be followed up.

T. F. WIMETT: The ratio of peak power to background which you report implies a constant repetition frequency. I would like to ask why you exclude the possibility of lowering the frequency to improve this ratio?

V. RAIEVSKI: In the case of the IBR reactor, the pulse repetition frequency is obtained by the coincidence ("beat frequency") between two rotating modulator wheels. For reasons of structural and operational simplicity, we use only one wheel, thereby fixing the repetition frequency at 50 Hz, which is a suitable frequency for most of the experiments being considered.

It is true that the signal-to-background ratio can be improved by reducing the frequency, but we are then faced with the problems you mention in con-

nection with your own paper (SM-62/53), i.e. the thermal cycling of the fuel elements. This is an important reason, with a reactor of considerable average power, for not using a high frequency.

M.J. POOLE: I would like to ask a general question. In view of the background problem, has there been any consideration by Euratom or in the United States of the possibility of using a plutonium fuel in pulsed reactors to decrease the background between pulses?

V. RAIEVSKI: Owing especially to the small delayed-neutron fraction involved, the use of a plutonium core would give us a background five times as small as that with a uranium-235 core. In our project, we have considered the use of such a core in later loadings. The present volume of the tank would permit the use of a plutonium loading in ceramic or cermet form.

G.R. KEEPIN: With reference to Dr. Poole's general question, I might mention that a Pu booster was proposed by Rex Fluharty (National Reactor Testing Station, Idaho Falls, USA) at the EANDC Symposium on Neutron Time-of-Flight Methods held at Saclay in 1961*. He proposed the use of molten Pu alloys – for example Pu-Fe – as a neutron booster (subcritical multiplying system) to be used in conjunction with a pulsed-neutron source, such as a linear accelerator. This proposed scheme involved the continuous removal of delayed fission products from a molten plutonium loop, and a cooling scheme using liquid sodium coolant. Obviously there would be very difficult chemical and metallurgical problems associated with handling a Pu-Fe alloy in the molten state, and as far as I am aware, the proposal has not been actively pursued.

On another topic, I believe the IBR fast-burst machine at the JINR, Dubna (USSR), uses Pu in the stationary part of the IBR critical configuration, and U^{235} in the rotary part. In contrast to the usual concept of a "self-quenching" burst reactor, the IBR depends upon physical separation rather than inherent shut-down mechanisms for burst termination**.

Y. POPOV: I would like to point out that the reduction in the velocity of rotation of the reflector also leads to a delay of the pulse in time, and this can be a disadvantage in a number of experiments. It might be mentioned that in individual experiments with thermal and cold neutrons, the IBR, operating at an average power of 2 kW, can achieve the required statistical accuracy that we get with steady-state reactors operating at several tens of MW.

M. STIÉVENART: I would like to make a comment on improving the ratio of maximum power to background in a reactor of the SORA type. If such a reactor is operated with a liquid fuel circulating at a given velocity, the amount of precursors is reduced before the beginning of the pulse and this is equivalent to a reduction of the effective delayed neutron fraction, which is a function of the velocity of the fuel and therefore causes an increase in the ratio of maximum power to background. This notion is independent of the nature of the fuel. Such a procedure would ultimately be limited by the delayed neutrons of long half-life.

---

* Neutron Time-of-Flight Methods, Proceedings of EANDC Symposium, Saclay, July 1961. Euratom, Brussels (1961).

** BUNIN., B.N., et al., Proc. 3rd UN Int. Conf. PUAE (1964) Paper 28/P/324.

J. RUSSELL: Have you looked into the possibility of using an accelerator to pulse the SORA? At a prompt multiplication of 1000, all you would need is a 3×10^{13} neutron source to operate SORA at 1 MW.

V. RAIEVSKI: Coupling a Linac with the reactor would enable us to reduce the pulse-width to a few microseconds while keeping the same number of neutrons per pulse. This procedure would be highly advantageous in experiments with epithermal neutrons but would be of no advantage in work with thermal or cold neutrons, owing to the inevitable prolongation of the pulse in the hydrogenous moderator. A study of this subject has been made and is included in the paper, where the conclusion is reached that a Linac producing 3×10^{14}n/s would be required for this reactor. We have made provision in the present reactor for installing such an accelerator later on.

D. BRETON (Chairman): Could Mr. Popov tell us whether experiments of this kind are planned at the Dubna reactor?

Y. POPOV: No, they are not. At present, we are conducting successful experiments on "triggering" a fast pulsed reactor by means of a microtron.

THE TRANSIENT CHARACTERISTICS OF A NEW PULSE RESEARCH REACTOR

J. MacPHEE
ATOMICS DIVISION, AMERICAN MACHINE AND FOUNDRY COMPANY,
YORK, PA.,
AND
R. F. LUMB
WESTERN NEW YORK NUCLEAR RESEARCH CENTER, INC.,
BUFFALO, N. Y.,
UNITED STATES OF AMERICA

Abstract — Résumé — Аннотация — Resumen

THE TRANSIENT CHARACTERISTICS OF A NEW PULSE RESEARCH REACTOR. A new concept in research reactors has recently been proof-tested by the Western New York Nuclear Research Center, Inc. on the Campus of the State University of New York at Buffalo. The new core was designed by AMF Atomics to be compatible with existing physical facilities and replaces a highly-enriched uranium-aluminium plate-type core. Called PULSTAR for ease of reference, the new core consists of uranium dioxide, enriched 6% in the isotope U^{235}. Sintered oxide pellets clad with Zircaloy comprise the fuel rods, 25 of which, in a 5×5 array, are incorporated in the 3 in × 3 in box of the fuel assembly. An eccentric nosepiece on the fuel assembly provides two orientations on the grid plate. Adjacent assemblies rotated 180° generate half-inch water gaps in which the six silver-indium-cadmium control blades operate. The pulsing capability is accomplished by fixing one control blade to the piston of a pneumatic cylinder. Standard AMF cantilever rod drives, as originally installed, are utilized to position all rods.

PULSTAR was designed for 5-MW steady state operation capable of pulsing to 10 000-MW peak power in a burst with a width, at half height, of less than 10 ms. The Doppler broadening of the U^{238} resonance absorption peak provides the prompt shutdown. The heavily loaded, undermoderated core which results from these specifications provides some unique operating characteristics. The paper presents detailed physics parameters, such as prompt neutron lifetime, void, temperature and power coefficients of reactivity, and highlights the assets accruing from low xenon poisoning. The transient characteristics are described including data on period versus reactivity, power versus period, energy versus period, burst shape parameters, and fuel and clad temperatures. Also included are neutron spectrum data and flux distribution in the experimental facilities.

CARACTÉRISTIQUES DU RÉGIME TRANSITOIRE D'UN NOUVEAU RÉACTEUR DE RECHERCHE A NEUTRONS PULSÉS. Le Western New York Nuclear Research Center Inc. a récemment soumis à des essais un réacteur de recherche d'une conception nouvelle, à l'université de l'Etat de New York, à Buffalo. Le cœur de ce nouvel appareil a été conçu par la Division atomique de l'AMF de façon à pouvoir être utilisé dans les installations existantes et remplacer le cœur constitué par des plaques d'aluminium et d'uranium très enrichi. Appelé PULSTAR, ce nouveau cœur est constitué par du bioxyde d'uranium enrichi à 6% d'uranium-235. Des pastilles d'oxyde fritté gainées de Zircaloy constituent les barreaux de combustible qui, au nombre de 25, sont disposés en cinq assemblages de cinq, de manière à constituer un élément combustible de 7, 6 cm de côté. Une manette excentrée placée sur l'élément permet de lui donner deux orientations différentes sur la plaque. Après rotation de 180°, les assemblages adjacents présentent entre eux des espaces intercalaires de 1, 25 cm dans lesquels s'insèrent les six lames de commande en argent, indium et cadmium. La possibilité de produire une bouffée est obtenue en fixant une lame de commande au piston d'un cylindre pneumatique. Les mécanismes courants AMF, à cantilever, de commande des barreaux, installés à l'origine, sont utilisés pour placer tous les barreaux dans la position voulue.

PULSTAR a été conçu pour fonctionner à 5 MW en régime normal et pouvoir atteindre 10 000 MW au moment d'une bouffée de neutrons ayant une largeur, à la moitié de la puissance maximum, inférieure à 10 ms. L'élargissement Doppler du pic d'absorption par résonance ^{238}U entraîne un arrêt rapide. Le cœur fortement chargé et sous-ralenti qui résulte de ces spécifications permet d'obtenir des caractéristiques de

fonctionnement tout à fait particulières. L'auteur présente de façon détaillée certains paramètres de physique tels que la durée de vie des neutrons instantanés et les coefficients de puissance, de température et de vide; il expose les avantages résultant du faible empoisonnement au xénon. Il décrit les caractéristiques du régime transitoire et fournit notamment des données sur la constante de temps selon la réactivité, la puissance et l'énergie selon la constante de temps ainsi que les paramètres de forme des bouffées et les températures du combustible et de la gaine. Figurent aussi dans le mémoire des données sur le spectre des neutrons et la distribution du flux dans l'installation expérimentale.

ПЕРЕХОДНЫЕ ХАРАКТЕРИСТИКИ НОВОГО ИМПУЛЬСНОГО ИССЛЕДОВАТЕЛЬСКОГО РЕАКТОРА. Западный нью-йоркский ядерный исследовательский центр провел недавно при государственном нью-йоркском университете в Буффало опытные испытания новой концепции исследовательских реакторов. Атомный отдел AMF сконструировал новую активную зону, которая должна быть совместима с существующими физическими установками и должна заменять активную зону типа пластины из высокообогащенного урана и алюминия. Реактор получил название "Пальстар", а новая активная зона состоит из двуокиси урана, обогащенной до 6% изотопом урана-235. Таблетки шлакованной окиси, покрытые циркаллоем, образуют топливные стержни, 25 из которых, в системе 5 × 5, вмонтированы в кассету топливной сборки размером 3 × 3 дюйма.

Эксцентричный наконечник топливной сборки обеспечивает две ориентации на трубной решетке. Соседние сборки, повернутые на 180°, образуют водный зазор в полдюйма, в котором вращаются шесть управляющих лопастей из серебра-индия-кадмия. Пульсация достигается за счет прикрепления одной управляющей лопасти к поршню пневматического цилиндра. Приводы управляющих стержней с противовесами по стандартам AMF, как это устанавливается первоначально, используются для того, чтобы ставить в свое положение все стержни.

"Пальстар" сконструирован таким образом, чтобы работать постоянно при 5 Мгвт, давая пульсацию пиковой энергии до 10 000 Мгвт при импульсе по ширине, при половинной амплитуде менее чем в 10 мсек. Допплеровское расширение резонансного поглощения пика урана-238 позволяет осуществлять быстрое выключение. Сильно загруженная, недостаточно замедляемая активная зона, которая дает такие результаты в связи со своими спецификациями, обеспечивает некоторые уникальные эксплуатационные характеристики. Дается детальное описание физических параметров, таких как время жизни мгновенных нейтронов, вакуум, температура, коэффициент мощности реактивности и придается большое значение высокой загораемости активов, возникающей в результате низкого отравления ксеноном. Переходные характеристики описываются вместе с данными по периоду в отношении к реактивности, мощности в отношении к периоду, энергии в отношении к периоду, параметров конфигурации импульса и температур топлива и покрытия. Включены также данные о нейтронном спектре и распределении потока на экспериментальных установках.

CARACTERISTICAS DEL REGIMEN TRANSITORIO DE UN NUEVO REACTOR DE INVESTIGACION DE NEUTRONES PULSADOS. El Western New York Nuclear Research Center, Inc. ha ensayado recientemente un nuevo tipo de reactor de investigación en la Universidad del Estado de Nueva York (Buffalo). La American Machine and Foundry construyó el cuerpo del reactor de manera que se pudiera emplear en las instalaciones existentes en lugar del actual cuerpo de placas de uranio altamente enriquecido y aluminio. El nuevo cuerpo se denomina PULSTAR y está constituido por dióxido de uranio enriquecido al 6% en ^{235}U. Las 25 barras combustibles, formadas por pastillas sinterizadas de óxido revestidas de zircaloy, están ordenadas en cinco grupos de cinco para formar elementos combustibles de 7, 6×7, 6 cm. Una excéntrica colocada en la parte superior del elemento combustible permite darle dos orientaciones en la rejilla. Con un giro de 180°, los conjuntos adyacentes dejan entre sí espacios de 1, 25 cm en los que se insertan las 6 láminas de control de plata, indio y cadmio. Los impulsos se obtienen fijando una lámina de control en el pistón de un cilindro neumático. Para poner en posición todas las barras, se utilizan mecanismos corrientes AMF en cantilever.

El PUSTAR se construyó para que funcionase a 5 MW en régimen estacionario y para que pudiese alcanzar 10 000 MW con impulsos neutrónicos de anchura inferior a 10 ms a la mitad de la altura. El ensanchamiento Doppler del pico de absorción por resonancia del ^{238}U permite una parada rápida. Gracias a este cuerpo muy cargado y poco moderado se obtienen características de funcionamiento únicas en su género. La memoria expone detalladamente algunos parámetros físicos: por ejemplo, la vida media de los neutrones instantáneos y los coeficientes de potencia, temperatura y vacío, así como las ventajas resultantes del bajo envenenamiento por xenón. Se describen las características del régimen transitorio y en especial se dan datos relativos al período en función de la reactividad, la potencia y la energía en función del período, y los parámetros de la forma del impulso y las temperaturas del combustible y del revestimiento. Igualmente se presentan datos acerca del espectro neutrónico y de la distribución del flujo en la instalación experimental.

1. INTRODUCTION

The purpose of this paper is to present recent data on a new pulse research reactor. Conceived by the Atomics Division of the American Machine and Foundry Company, and designed to meet the specifications of the Western New York Nuclear Research Center, the reactor is currently undergoing testing at Buffalo, New York. The significant nuclear parameters are presented and pulse performance to date is described. A discussion of the significance of the data and extrapolation to other core configurations is also presented. To provide a proper perspective, a history of the project and some design features are included.

2. PROJECT HISTORY

The Western New York Nuclear Research Center, Inc. (NRC) is an entirely-owned subsidiary of the State University of New York, located on the Campus at Buffalo, New York. Its principal objective is to provide to the scientific community highly specialized tools, services and materials in support of nuclear research and development activities. The conceptual design of NRC was completed in April 1959 and construction was essentially finished by January 1961. One of the principal tools available at NRC was a 1 MW nuclear research reactor which first achieved criticality on 24 March 1961, and was operated at 1 MW in June of that year.

The facilities and services of NRC are generally available to the faculty and students of the State University of New York and considerable activity has developed over the years. Industrial utilization of the facilities also accounts for a significant fraction of the Center's efforts. A general view of the reactor facility is given in Fig. 1.

In the latter part of 1962, considerable interest was expressed in, and a need indicated for, a pulse reactor facility in New York State. NRC could see nothing inherently incompatible in a reactor having both high steady state power and pulsing capability; consequently, reactor designers were approached by NRC for their concepts of converting the MTR-type core (Materials Testing Reactor) to one having such capabilities. The design specifications called for compatibility with the installed physical facility, requiring a minimum cost and inconvenience associated with the conversion. A power level of 2 MW with the 1200-gal/min installed cooling capacity, convertible to 5-MW operation, was the steady state specification. In the pulse mode, a peak power of 10 000 MW with a pulse width at half height of 10 ms was specified. AMF Atomics' conceptual drawings and calculations of a slightly enriched UO_2 core and associated control system, dubbed "PULSTAR" for ease of reference, were judged to best meet these specifications.

In March 1963, an agreement between AMF and NRC was reached to design, install and proof-test a new reactor core based upon this concept. NRC agreed to procure the fuel, compile a Safety Analysis report, install the new equipment and carry out the test programme required to attain the design output. AMF agreed to complete the development work, prepare fabrication drawings and specifications for new equipment including fuel,

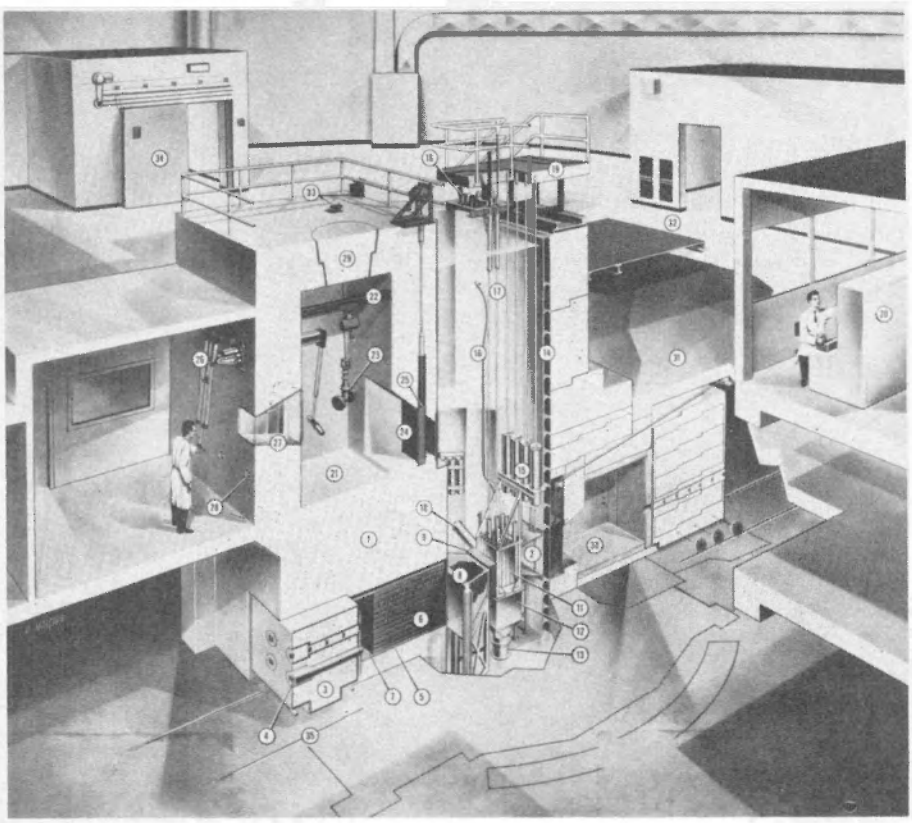


Fig. 1

Nuclear Research Center reactor facility

develop test procedures in co-operation with NRC and provide supervisory personnel during installation and testing. In addition, AMF supplied new control rod assemblies, the pulse rod mechanism, the pulse control system and miscellaneous equipment needed for the conversion.

3. DESIGN SUMMARY [1]

The reactor fuel consists of sintered UO_2 pellets, enriched by 6% in the isotope U^{235}. Forty pellets are stacked 24 in high and clad in a Zircaloy-2 tube. Twenty-five of these tubes, called rods, assembled in a regular 5 X 5 array and incorporated in a box constitute a fuel assembly, or fuel element. Grids in the top and bottom fixture of the box maintain orientation of the rods; a slot and key arrangement prevents rotation. Small bearing pads, oriented 90° apart radially and 6 in apart axially, further fix the rods so that only vertical movement is possible.

The nosepiece of the fuel element is eccentric so that there are two possible orientations on the grid plate. Rotation of two elements 180° out of phase results in a $\frac{1}{2}$-in gap between elements. It is in this gap that the control rod shrouds are installed.

The control rods are silver-indium-cadmium blades approximately $4\frac{1}{2}$ in wide and 3/16 in thick, clad with 0.003 in of nickel plate. An extension rod runs up through the shroud to contact the magnets which are attached to the rack of the rack and pinion drive cantilevered from the operating bridge. There are nominally six rods in the core region; four are utilized as shim-safety rods, one as a regulating safety rod and one as the pulse rod.

The pulse rod is identical with the other five control rods, except for the fashion in which it is attached to the drive mechanism. The pulse rod extension is attached to a piston inside an air cylinder. A collar on the rack of the cantilevered drive mechanism engages a fork on the rod extension so that the rod can be positioned in the core. The pulse is achieved by exhausting to atmosphere the top portion of the pneumatic cylinder. The stored energy of the high pressure gas below the piston ejects the pulse rod in less than 200 ms. A limit switch at the extreme travel of the pulse rod reverses the gas flow and slowly (1-2 s) returns the pulse rod to the core region as far as the collar on the rack of the drive mechanism permits.

The development of reactors such as PULSTAR has resulted in a general revision of the conventional thinking of rod drive speeds in inches per minute, reactor periods in seconds, and safety in terms of rapid rod insertion, to rod motion and reactor period in milliseconds, and internal shutdown mechanisms such as the Doppler coefficient for safety. This results in fairly simple control and instrumentation requirements. However, because it was already installed, there was substantially no change made in the steady state control and instrumentation system in conversion to the new reactor facility.

Pulse instrumentation in a separate instrument rack was added and tied into the steady state control system. The compensated ion chamber feeding the linear recorder of the steady state instrumentation was also incorporated into the pulse instrumentation. The current from this chamber is fed to a precision resistor and the voltage drop is displayed on the dual trace oscilloscope, providing a means for ascertaining reactor period. Two miniature fission chambers are installed in the core region. Their signals are fed to linear amplifiers. The amplified signal from one chamber is converted to a logarithmic signal which is displayed on the oscilloscope to provide information with regard to pulse shape and peak power. A camera attachment converts this display to a permanent record.

The second fission chamber signal is amplified and the output applied simultaneously to a power peak following unit and a power integrating unit. The peak following unit consists basically of a diode connected so that a condenser may be charged, but not readily discharged. This provides an output voltage from the unit which represents the peak power. The power integrating unit consists of an operational amplifier with capacitance feedback and resistive input, providing the time integral of the input voltage pulse. The output voltages of each unit can be selectively displayed on a digital voltmeter, directly reading peak power in MW up to 10 000 MW and energy in hundreds of MW-s.

The steady state and transient control systems are interlocked through a mode switch. The transient control system is de-energized when the switch is in the steady state mode, precluding an inadvertant pulse. Further, the reactor can be operated in steady state mode only when the pulse rod is in the fully withdrawn position. Other interlocks provide for bypassing certain scram functions (high power, short period, etc.) when the pulse button is activated in the pulse mode. Electrical timers control return of the pulse rod to the core, re-instatement of the bypassed scrams, and re-setting of the pulse control circuits.

4. RESULTS TO DATE

Before initiating the pulse testing programme, an extensive measurement programme was undertaken at low power to determine the significant nuclear parameters. The test core chosen, Fig. 2, consisted of 20 fuel as-

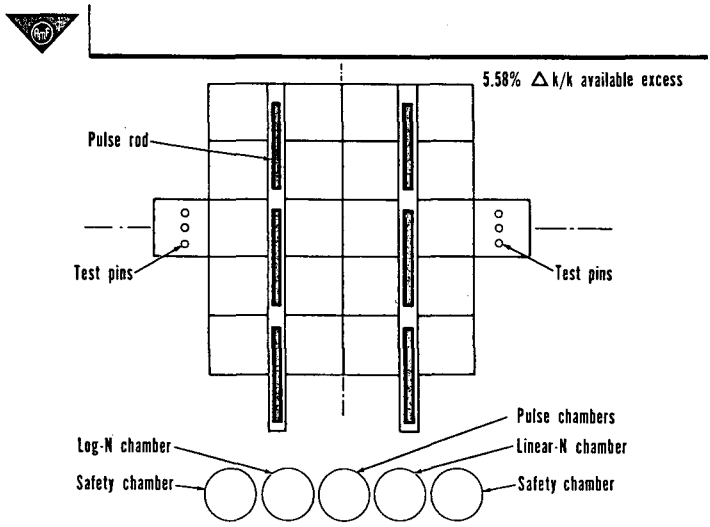


Fig. 2

Pulse test core

semblies in a regular 5 × 4 array, with six test fuel rods located in the reflector. Because of the strong flux peaking in the reflector, these test rods were exposed to power densities greater than the hottest rod in the core by a factor of 1.8 as determined by wire activation and confirmed by gamma scanning of fuel rods. The excess reactivity of the test core was 5.5% ΔK/K including the test rods. Control rod worth totalled > 12% ΔK/K and the pulse rod was worth 2.5% ΔK/K.

Table I lists the significant nuclear parameters. It is interesting to note, from the point of view of reactor safety, that the moderator temperature coefficient is large, and negative over the entire range of operating

TABLE I

PULSTAR PARAMETERS

Fuel	
Material	UO_2
Enrichment	6%
Form	Pellets
Cladding	Zircaloy-2
Moderator and coolant	Light water
Reflector	Light water
20 Element core	
Size (in)	12 × 15 × 24
UO_2 loading (kg)	286
Uranium loading (kg)	252
U^{235} loading (kg)	15.1
Moderator temperature coefficient at 100°F (ΔK/°F)	-8×10^{-5}
Void coefficient (ΔK/% void)	-0.4%
Doppler coefficient at 100°F (ΔK/°F)	-2.4×10^{-5}
Prompt neutron lifetime (μs)	29
Effective delayed neutron fraction (%)	0.76

temperatures (15–45°C). Similarly, the void coefficient is quite large and negative. These coefficients reflect the high fuel-to-water ratio.

The Doppler coefficient was first measured in steady state operation by subtracting the reactivity deficit caused by moderator temperature coefficient from the total power coefficient [2]. The Doppler coefficient proved to be large and negative, substantially the value predicted. It was later confirmed from the characteristics of the transients.

The thermal neutron flux in the experimental facilities are substantially the same as those previously experienced with a MTR-type core. The peak thermal flux in the reflector at 2 MW is approximately 2.4×10^{13} n/cm^2 s and in a flux trap in the centre of the core, 5.6×10^{13} n/cm^2 s. The fast flux above 10 keV at the face of the core at 2 MW is approximately 8×10^{12} n/cm^2 s at the end of a voided beam tube.

The pulse test programme was designed presuming we knew nothing about the transient characteristics of the core. All transients have been run with natural convection cooling. Also, during the steady state tests, the reliability of the pulse instrumentation was demonstrated.

In a series of steady state power runs the ability of the Doppler coefficient to compensate for a significant reactivity insertion was ascertained. This reactivity was then inserted in a series of ramps approaching a step input.

Once the ability to accommodate these transients was demonstrated, similar reactivities were inserted as step functions using the pulse mechanism. The amount of reactivity inserted was then gradually increased with accompanying increases in peak power. The performance followed prediction quite well: as the pulse sharpened up, the total energy in the pulse decreased to a minimum and then began to increase. During the programme the temperature and strain of test rod cladding was measured. Pressure was monitored at the top and side of the core. Reactor period, peak power and integrated energy were monitored and recorded. At pre-determined energy releases, the test pins were inspected visually and dimensionally. Repetitive pulses at various energy releases demonstrated the reproducibility of the system.

The value of β, the effective delayed neutron fraction, for the test core is 0.76% $\Delta K/K$. When the transients initiated resulted in a prompt critical excursion (reactivity inserted > 0.76% $\Delta K/K$), it became possible to measure the prompt neutron lifetime from the relationship:

$$1/T = \frac{\delta K - \beta}{l}$$

or

$$l = T(\delta K - \beta).$$

Figure 3 is a plot of the prompt reactivity inserted ($\delta K - \beta$) versus the reciprocal period generated ($1/T$) for a series of periods ranging from 300 to 5 ms. The slope gives a value of 29 μs for the apparent prompt neutron lifetime of the test core.

To date, the reactor has been pulsed repetitively to 3700-MW peak power. This involved a reactivity insertion of 1.9% $\Delta K/K$ and a total energy release of 47 MW-s with a reactor period of 2.8 ms. The pulse shape is quite symmetrical except for the tail (see Fig. 4), and can be approximated by the equation:

$$E_m = 1.94\ P_m\ T$$

where

E_m = energy to peak power in MW-s,
P_m = peak power in MW and
T = period in seconds.

In the lower energy pulses, the ratio of the total energy to the energy at the peak is approximately 2.1 and increases slightly in the more energetic pulses to approximately 2.25. Maximum UO_2 temperatures at the hot-spot were estimated to be 2900°F, equivalent to a specific energy release of 540 W-s/g.

Plots of peak power versus reciprocal power and energy-to-peak power versus reciprocal power, Figs. 5 and 6, fit the predicted curves quite well, approximating straight lines at periods shorter than 8 ms. These relationships can be approximated by:

$$P_m = (2.87 \times 10^{-3})\alpha^{2.41}$$

$$E_m = (1.37 \times 10^{-2})\alpha^{1.26}.$$

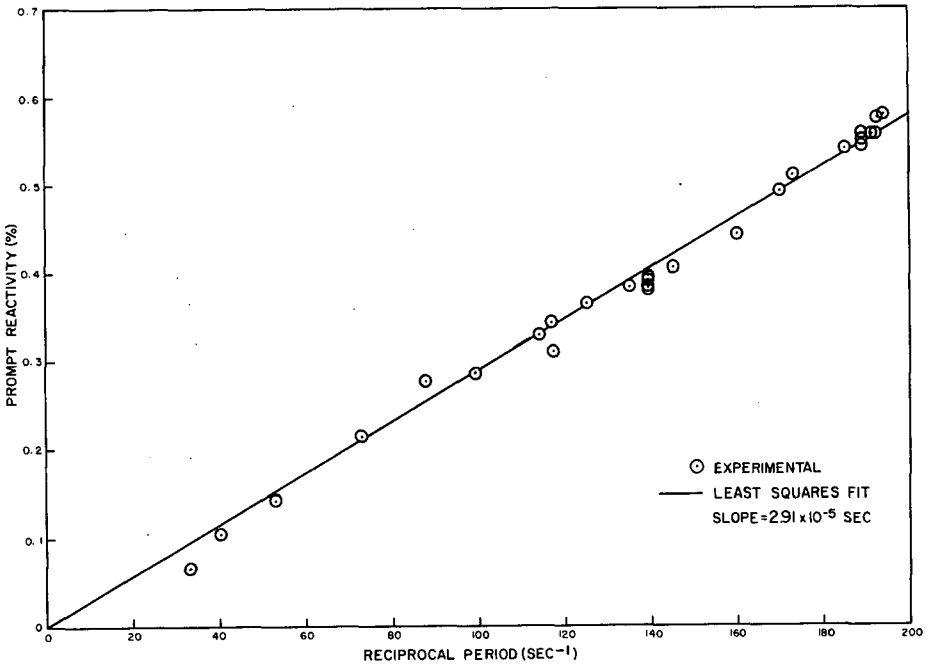


Fig. 3

Prompt reactivity versus reciprocal period (from shim-rod calibration)

The approximations hold quite well for periods shorter than 8 ms as is demonstrated by the plotted data. This gives us considerable confidence in our ability to predict the performance of the core at higher energy releases.

5. IMPLICATIONS

A maximum specific energy release of 540 W-s/g of UO_2 has been achieved safely in a 20 element core to date. This corresponds to a maximum energy density of 2.2 MW-s per litre of core. Although these values coincide with the design targets, there are indications that the use of forced convection cooling during pulsing will enable us to go to significantly higher energy releases. However, even if this potential for higher specific energy is ignored, the implications of present levels with respect to larger cores is extremely interesting. Before proceeding to an extrapolation to larger cores, some discussion of the test core is in order, because the unique characteristics of very small UO_2 cores do not permit direct extrapolation.

The very small size of the test core increases the importance of the reflector which manifests itself in a lengthening of the prompt neutron lifetime. Thus, if core size were the only parameter changed, a larger core would have a shorter prompt neutron lifetime. Consequently, the peak power in a large core would be higher, for a given energy release.

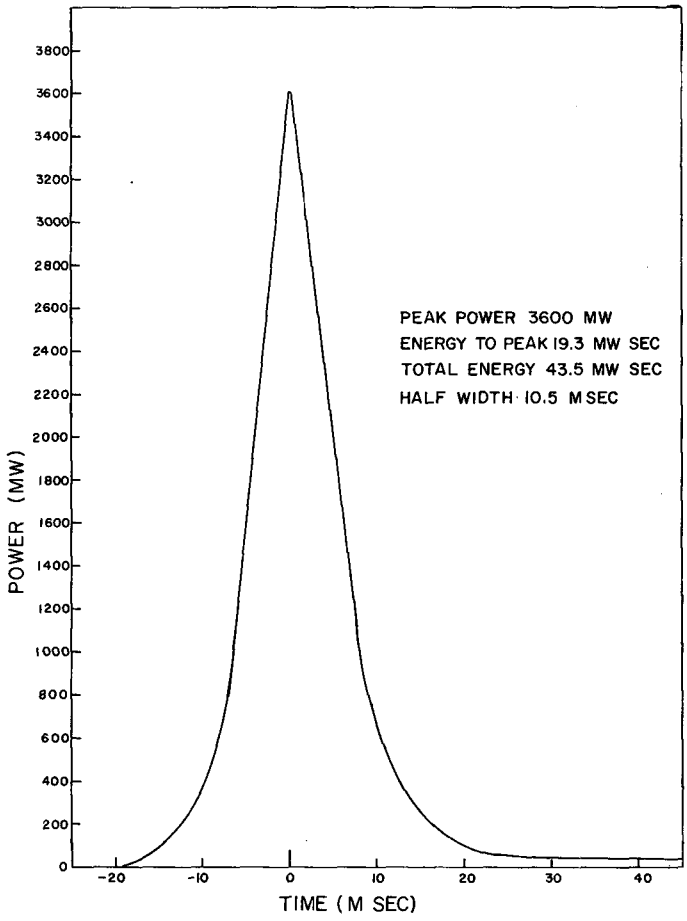


Fig. 4

Linear plot of typical 2.8-ms pulse

Another effect of a small core geometry is a larger hot-spot factor. Unlike highly enriched cores, the hot-spot in the test core occurred at the edge of the core. This was a result of the very large thermal neutron flux peak in the reflector (relative to the average in the fuel) brought about by the heavy U^{235} loading in the fuel. In larger cores, fuel enrichment and hence fuel loading would be reduced. This would reduce the magnitude of the reflector flux peak relative to the average in the core, which would in turn, reduce the value of the hot-spot at the core edge and thus the overall hot-spot factor.

Two core sizes have been selected to illustrate the implications of PULSTAR performance to date: a thirty element PULSTAR core, which represents the ultimate or design PULSTAR core configuration;and a core the same size as TREAT [3], to permit a more meaningful comparison with a graphite-moderated pulsed reactor.

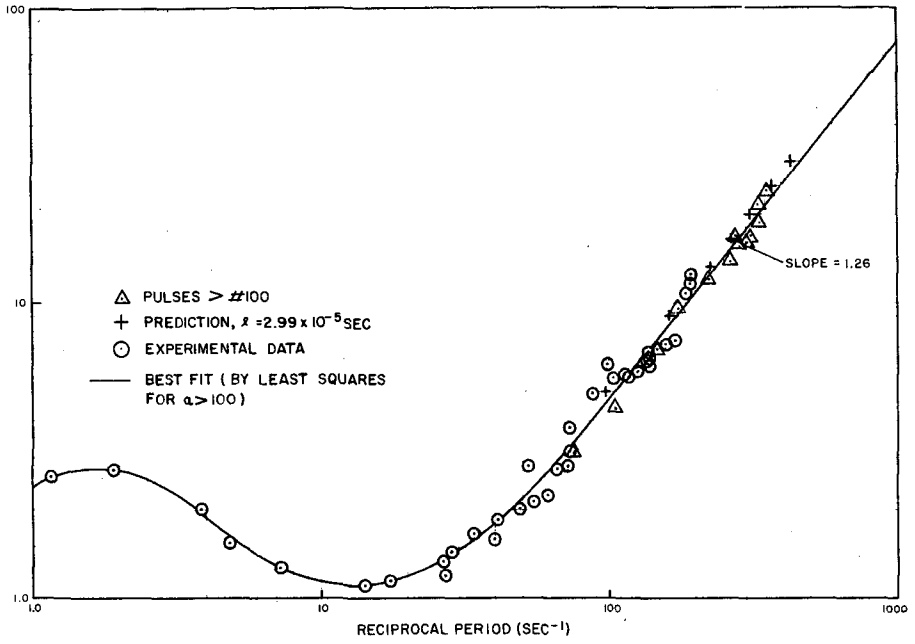


Fig. 5

Energy-to-peak power versus reciprocal period

TABLE II

EXTRAPOLATION OF PULSTAR PERFORMANCE TO LARGER CORES

Type of core	30-element PULSTAR	TREAT-size core
Overall size (in)	15 × 18 × 24	60 diam. × 48 high
Core volume (*l*)	106	2220
UO_2 loading (kg)	429	9000
Ratio of maximum-to-average power density	2.8	2.5
Maximum energy density (MW-s/l)	2.2	2.2
Average energy density (MW-s/l)	0.785	0.88
Pulse performance		
Energy release (MW-s)	83	2000
Prompt lifetime (μs)	25	25
Period (ms)	2.36	2.36
Peak power (MW)	8400	200 000

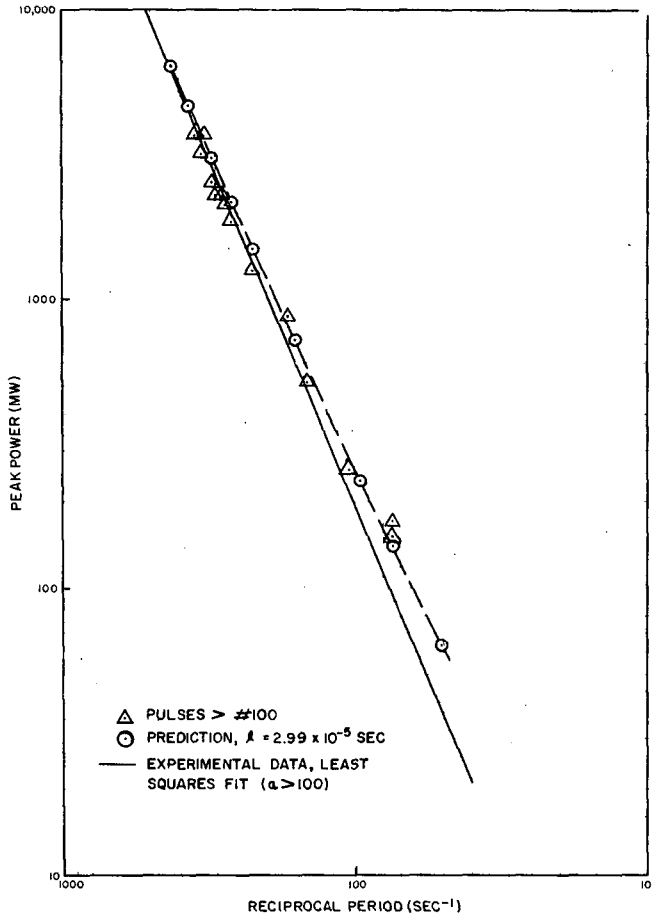


Fig. 6

Peak power versus reciprocal period

The performance of these two cores, based on a maximum UO_2 temperature of 2900°F and a specific energy release of 540 W-s/g of UO_2 (both of which have been achieved in the PULSTAR core at NRC), is given in Table II. These extrapolations show that a very modest increase in performance of the NRC PULSTAR core is needed to achieve the design power of 10 000 MW. In addition, these data show that the performance of large oxide-fuelled pulsed reactors compares extremely well with that of graphite-moderated pulsed reactors, exemplified by the TREAT design. Although not indicated in Table II, it should also be pointed out that at these specific energies, pulsed fuel meltdown experiments can be conducted in internal flux trap facilities in these cores. This latter fact is supported by data on the core shown in Fig. 2 which showed that the flux in an internal flux trap is over four times the maximum in the core and over twice the value in the special fuel pins in the reflector (which reached a UO_2 temperature in ex-

cess of 4000°F). Therefore, it may be concluded that in spite of the fact that the full potential of PULSTAR at NRC has not been reached as yet, the performance to date represents a significant contribution to the technology of pulse reactors.

REFERENCES

[1] MacPHEE, J. and LUMB, R.F., The design of PULSTAR, a pulse-steady state research reactor, to be published.

[2] LUMB, R.F. and MacPHEE, J., Considerations in formulating a test program for a new transient reactor, to be published.

[3] OKRENT, D. et al., The reactor kinetics of the transient reactor test facility, Rpt ANL 6174 (Sept. 1960).

DISCUSSION

J.W. WEALE: Could Dr. Lumb say a little more about the damage to the fuel elements which he observed at high temperatures and indicate whether there is any evidence that the UO_2 fuel will have a long lifetime under these conditions of operation.

R.F. LUMB: It is rather difficult to make any precise statements about the expected lifetime of the UO_2 pellets. We have only some 133 transients with this particular core. The test pins in the reflector did undergo some mechanical damage, in the form of accelerated corrosion, as a result of the transients. The temperatures in the clad exceeded 1200° C. This is a fairly severe situation in that the phase transition point is of course exceeded. It should be pointed out that this high temperature, which came about as a result of local film blanketing of the clad, was highly localized, occurring only at certain points on the fuel surface. For example, in certain cases it amounted to only 15% of the circumference of a section through the hottest spot in the fuel pin. However, because we did go through the phase transition and because certain stresses existed in one segment of the fuel, and also because we naturally had relaxation in another segment of the fuel, we encountered what might be called a warping of the fuel, i.e. it showed some degree of bowing and twisting, with the result that the pins were obviously of no further use to us.

As I indicated in my presentation, we plan to continue work with the test core (in which there was no damage to the fuel), using forced cooling. We expect to make good progress in eliminating the film blanketing. As regards the lifetime of the UO_2, we cannot say with certainty how many times we shall be able to pulse the reactor in this fashion. Our calculations indicate that it is really fatigue of the clad that is the serious concern. On the basis of very conservative estimates, we think that we should be able to get a significant number of pulses, say, 800-1000, before serious fatigue begins to limit the life of the core. I'm sorry that I cannot give you a more definitive answer.

D. BRETON (Chairman): Before we proceed to the next paper, I shall call upon Mr. Russell, who wishes to comment briefly on recent work with the TRIGA reactor.

J. RUSSELL: At General Atomic we have a continuing programme for systematically improving the fuel element and design of the pulsed TRIGA reactor. As a part of this development programme, reactivity insertions of up to 5.0 $ have been performed safely in our prototype reactor. The properties of a 5.0 $ pulse are the following: a peak power of 8400 MW, a pulse width at half maximum of 5.5 ms and a peak fuel temperature of 846°C.

These large reactivity insertions were made in a core using TRIGA fuel elements constructed from a U-ZrH alloy with an H/Zr atomic ratio of 1.7 and clad with 20-mil 304 stainless steel. This fuel has the advantage of being single phase well above 1000°C. A potential limitation on the maximum temperature to which the fuel may be subjected results from the diffusion of hydrogen from the fuel to the interstices in the fuel can at the higher temperatures. This causes increasing pressure within the fuel can with increasing fuel temperature. However, it should be noted that for a temperature of 800°C the predicted equilibrium hydrogen pressure from this fuel is only 2.5 atm.

The peak reactor power during the transient can be described by Scalettar's* variable heat capacity modification of the Fuchs-Nordheim model of reactor response to step reactivity insertions.

Comparison of experimental and calculated values of prompt energy release versus prompt reactivity insertion are in agreement and again indicate the applicability of this model.

During the test programme to reach reactivity insertions of 4.8$, there was some experimental evidence of film boiling in the region of the hotter fuel elements. Computer calculations which consider the temporal changes in clad temperature and heat flow indicate that film boiling is possible during the large reactivity insertions. While film boiling in itself is not deleterious to the reactor operation it can allow clad temperatures to reach values at which stress relieving may occur in the clad. To reduce the possibility of film boiling, it may be desirable to introduce a thermal barrier between the fuel and cladding.

A special fuel element having such a thermal barrier was constructed. This element was provided with both temperature- and pressure-sensing instrumentation. The fuel content was increased 50% over that of a standard fuel element to reach higher fuel temperatures than the rest of the core during a transient.

This special element has been placed in the region of highest core flux and subjected to 125 pulses at 4.6$ reactivity insertions and 28 pulses at 4.8$ reactivity insertions. Examination of the cladding has indicated that film boiling did not occur on this element.

The reactor core has been pulsed over 6000 times, including 1000 times at reactivity insertions of 4 $ or more. The same core is also used for steady-state operation at powers up to 1.5 MW (th).

---

* SCALETTAR, R., The Fuchs-Nordheim Model with variable heat capacity. Nucl. Sci. Engng., 16 (1963) 459-460.

TWO COMPACT, HIGH-INTENSITY PULSED NEUTRON SOURCES

W. EYRICH AND A. SCHMIDT
KERNFORSCHUNGSZENTRUM KARLSRUHE,
FEDERAL REPUBLIC OF GERMANY

Abstract — Résumé — Аннотация — Resumen

TWO COMPACT, HIGH-INTENSITY PULSED NEUTRON SOURCES. Advanced experiments on the kinetic behaviour of neutrons in matter, especially neutron spectrum measurements, require compact pulsed neutron sources with high intensity and great flexibility. To fulfil the needs of an extended research programme at Karlsruhe, two special sources of 14-MeV neutrons have been developed during the last years. These are:

1. A high-power neutron pulse generator with duoplasmatron source (W. Eyrich). The maximum instantaneous source power of this device is more than 3×10^{13} n/s. A duoplasmatron ion source supplies deuteron currents up to 500 mA. Due to a novel design of the accelerator, it is possible to accelerate these currents up to 140 keV and shoot them directly onto a titanium-tritium target. The target may be brought near the experimental setup to a distance of 27 mm. The pulse duration of the deuteron pulse is now 8 to 50 μs, the recurrence frequency up to 400 c/s. The high voltage may be applied either as a DC or as a pulsed voltage to the accelerating electrode which also contains the target. The plasma current in the duoplasmatron is up to 40 A during pulses. In the intervals between pulses the discharge is quenched. This device has been operating successfully for more than two years.

2. The neutron flash tube (A. Schmidt). In this device, deuterons are generated by means of an intense pulsed RF-discharge in deuterium gas at a pressure of about 10^{-3} Torr. Peak deuteron currents up to 15 A are extracted through a circular emission orifice in the discharge vessel. By a pulsed 150-kV voltage which is applied to a very short acceleration gap, the deuterons are accelerated directly onto a tritium target. Up to 500 pulses per second of about 2-μs duration can be delivered. The neutron yield is about 5×10^8 neutrons per pulse. The target is on ground potential and readily accessible so that the neutron output into nearly 2π solid angle can be utilized. A special feature of the neutron flash tube is the gas pressure regulating system which includes a titanium sputtering pump, simultaneously acting as a controllable replenisher system.

Design and construction of both devices, as well as operation experience, are discussed in detail.

DEUX SOURCES DE NEUTRONS PULSÉS A HAUTE INTENSITÉ ET DE FAIBLE ENCOMBREMENT. Les expériences avancées sur le comportement cinétique des neutrons dans la matière, notamment les mesures du spectre des neutrons, nécessitent des sources de neutrons pulsés ayant un faible encombrement, une haute intensité et une grande souplesse. Pour répondre aux besoins d'un vaste programme de recherches entrepris à Karlsruhe, deux sources spéciales de neutrons de 14 MeV ont été mises au point au cours des dernières années. Ce sont:

1. Un générateur de bouffées de neutrons de grande puissance ayant un duoplasmatron comme source (W. Eyrich). La puissance maximum instantanée de cet appareil comme source est supérieure à $3 \cdot 10^{13}$ n/s. Le duoplasmatron comme source d'ions fournit des courants de deutérons atteignant jusqu'à 500 mA. L'accélérateur étant d'une conception nouvelle, il est possible d'accélérer ces courants jusqu'à 140 keV et de les diriger directement sur la cible de titane-tritium. On peut approcher la cible à 27 mm du dispositif expérimental. La durée d'impulsion de la bouffée de deutérons est actuellement de 8 à 50 μs, sa fréquence de 400 Hz. On peut appliquer la haute tension, soit sous forme d'un courant continu, soit sous forme d'une tension pulsée, à l'électrode d'accélération qui contient également la cible. Le courant de plasma dans le duoplasmatron monte à 40 A pendant les bouffées. Dans les intervalles, la décharge est coupée. Cet appareil a fonctionné avec succès pendant plus de deux ans.

2. Un tube à bouffées de neutrons (A. Schmidt). Dans cet appareil, on produit des deutérons au moyen d'une décharge H. F. pulsée intense dans du deutérium sous une pression d'environ 10^{-3} mm de Hg. Des courants de deutérons atteignant des pointes de 15 A sont extraits par un orifice circulaire d'émission pratiqué dans l'enceinte de décharge. En appliquant une tension pulsée de 150 kV pendant une très courte interruption de l'accélération, on accélère directement les deutérons sur une cible de tritium. On peut ainsi produire jusqu'à

500 bouffées par second, leur durée étant d'environ 2 μs. Le rendement en neutrons est d'environ $5 \cdot 10^8$ neutron par bouffée. La cible est au potentiel de la terre et elle est facilement accessible de manière que l'on puisse utiliser les neutrons produits dans un angle solide voisin de 2π. Ce tube produisant des bouffées de neutrons présente comme caractéristique particulière d'être équipé d'un système spécial de régulation de la pression du gaz.

Les plans, la construction ainsi que le fonctionnement de ces deux appareils sont examinés de façon détaillée dans le mémoire.

ДВА КОМПАКТНЫХ ИСТОЧНИКА ИМПУЛЬСНЫХ НЕЙТРОНОВ ВЫСОКОЙ ИНТЕНСИВНОСТИ. Для усовершенствованных экспериментов по кинетическому поведению нейтронов в веществе, особенно по измерениям нейтронных спектров, требуются компактные источники импульсных нейтронов с высокой интенсивностью и большой гибкостью. Для того, чтобы выполнить требования расширенной программы исследований в Карлсруэ, в последние два года были разработаны два специальных источника нейтронов с энергией в 14 Мэв, а именно:

1. Генератор импульсных источников высокой интенсивности со сдвоенным плазматронным источником (В. Эрих). Максимальная мгновенная мощность источника в этом устройстве составляет более $3 \cdot 10^{13}$ н/сек. Сдвоенный плазматронный источник ионов поставляет дейтериевые токи до 500 ма. Благодаря новизне конструкции ускорителя можно увеличивать энергию этих частиц до 140 кэв и направлять их непосредственно на титано-тритиевую мишень. Мишень можно подносить к экспериментальной установке на расстояние до 27 мм. Протяженность дейтериевого импульса составляет в настоящее время от 8 до 50 мксек, а частота повторяемости до 400 ц/сек. Высокое напряжение можно подавать или в виде постоянного тока, или как импульсное напряжение на ускоряющий электрод, в котором также содержится мишень. Плазменный ток в сдвоенном плазматроне составляет во время импульсов величину до 40 а. В интервалах между импульсами происходит разряд. Это устройство успешно работает в течение уже более двух лет.

2. Нейтронная пламенная трубка (А. Шмидт). В этом устройстве частица дейтерия генерируется посредством интенсивного импульсного радиочастотного разряда в дейтериевом газе при давлении около 10^{-3} мм ртутного столба. Пик дейтериевых токов до 15 а отводится через круглое эмиссионное отверстие в разрядную колбу. Посредством импульсного напряжения 150 кэв, которое подается на очень короткий зазор ускорения частицы дейтерия ускоряются и направляются непосредственно на тритиевую мишень. Таким образом можно направить до 500 имп/сек за период времени приблизительно в 2 мксек. Выход нейтронов составляет около $5 \cdot 10^8$ н/имп. Мишень заземлена и легко доступна так, что можно использовать выход нейтронов с твердым углом, равным почти 2π. Особой чертой трубки нейтронной вспышки является система, регулирующая давление газа, которая включает титано-разбрызгивающий насос, одновременно действующий в качестве контролируемой системы наполнения.

Подробно обсуждается конструкция и изготовление обоих устройств, а также опыт, накопленный при работе с ними.

DOS FUENTES DE NEUTRONES PULSADOS DE ALTA INTENSIDAD Y PEQUEÑAS DIMENSIONES. Para efectuar experimentos avanzados sobre el comportamiento cinético de los neutrones en la materia, y en particular para medir espectros neutrónicos, se necesitan fuentes de neutrones pulsadas que sean de pequeñas dimensiones, alta intensidad y gran flexibilidad de funcionamiento. Para atender a las necesidades de un vasto programa de investigación que se está desarrollando en Karlsruhe, estos últimos años se han construido dos fuentes especiales de neutrones de 14 MeV:

1. Un generador de impulsos neutrónicos de gran potencia, que utiliza como fuente un duoplasmatrón (W. Eyrich). La potencia instantánea máxima de esta fuente es superior a $3 \cdot 10^{13}$ n/s. El duoplasmatrón proporciona haces de deuterones de hasta 500 mA. Gracias a algunas características nuevas del dispositivo, es posible acelerar estos haces hasta 140 keV y dirigirlos directamente hacia un blanco de titanio-tritio. Este blanco puede acercarse hasta 27 mm del dispositivo experimental. En la actualidad se emplean impulsos de deuterones que duran de 8 a 50 μs, y cuya frecuencia es de 400 Hz. La alta tensión puede aplicarse en forma de corriente continua o en forma de tensión pulsada al electrodo de aceleración, que también contiene el blanco. La intensidad de la corriente plasmática en el duoplasmatrón es de 40 A como máximo durante los impulsos. En los intervalos, los impulsos se extinguen. Este dispositivo ha funcionado con éxito durante más de dos años.

2. Tubo de impulsos neutrónicos (A. Schmidt). En este dispositivo los deuterones se generan por medio de una intensa descarga de radiofrecuencia pulsada en deuterio a una presión de 10^{-3} torr aproximadamente. Por

un orificio circular de emisión hecho en el recinto de descarga se extraen haces de deuterones de 15 A como máximo. Aplicando una tensión pulsada de 150 kV a una zona de aceleración de dimensiones reducidas, los deuterones son acelerados directamente hacia el blanco de tritio. Así pueden obtenerse hasta 500 impulsos por segundo de una duración de 2 μs aproximadamente. El rendimiento es de unos $5 \cdot 10^8$ neutrones por impulso. El blanco se encuentra al potencial de tierra y es de fácil acceso, de manera que el rendimiento neutrónico puede aprovecharse en un ángulo sólido de casi 2π. Una de las características particulares de este tubo de neutrones pulsados es un sistema regulador de la presión del gas que comprende un absorbedor de titanio que desempeña al mismo tiempo función de sistema de reposición graduable.

En la memoria se examinan detalladamente los planos, la construcción y el funcionamiento de ambos dispositivos.

1. INTRODUCTION

For advanced neutron decay measurements and for time-of-flight application higher neutron intensities are required than can be achieved with the conventional present-day Cockcroft-Walton type neutron generators. Electron linear accelerators are extremely strong pulsed neutron sources; however, they are very expensive and their flexibility is limited. To have a flexible device easily transportable to any experimental set-up, two types of small powerful neutron generators have been developed in our laboratory. To meet the urgent needs, an accelerator with stationary high-voltage power supply operating with a pulsed duoplasmatron ion source [1-3] was built. For long range applications a more ambitious "neutron flash tube" has been developed which is based on a pulsed RF-discharge combined with a pulsed acceleration voltage. Both accelerators produce 14-MeV neutrons from the $H^3(d, n)He^4$ reaction and use tritium targets.

2. A HIGH-POWER NEUTRON PULSE GENERATOR WITH DUOPLASMATRON SOURCE*

The basic disadvantage of the conventional accelerators is the large distance between the ion source and the target. Space charge and lens aberration limit the beam current, and the highest value we could achieve with accelerators built in our laboratory was 26 mA [4]. To avoid these difficulties, in the design described below, the focusing device was deleted and the target was set close enough to the extraction channel to get the total ion current from a duoplasmatron ion source on to the target in spite of space charge effects. The position was chosen to achieve a complete and uniform target loading. A second unusual design principle was to connect the target with the high voltage and to have the ion source at ground potential. This greatly facilitates the power supply since all the auxiliary equipment is now on ground potential and does not have to be powered via insulating transformers.

On this basis the construction was made to meet the following requirements as well:

(1) The background between the neutron bursts should be zero.

* By W. Eyrich

(2) The target should be positioned as closely to the surface of the accelerators as possible to keep the efficient solid angle of source neutrons high.
(3) The overall dimensions should not be larger than about 1 m^3.
(4) The accelerator should be reliable enough to run continuously for days.

The following specifications were obtained:

Burst length:	5 - 50 μs
Repetition rate:	up to 400 s^{-1}
Acceleration voltage:	120 kV
Maximum ion current:	500 mA on target.

The instantaneous neutron production rate amounts to about 2×10^{13} s^{-1}. The average current is limited by the target cooling to 2 mA.

2.1. Description of the accelerator

Figure 1 shows a sectional drawing of the neutron generator and Fig. 2 gives a photographic view from the side with the ion source removed. In the sectional drawing, Fig. 1, the accelerator is cut perpendicular to the view of the photograph so that here the ion source is located on the top (parts 1-6, Fig. 1). Below the source is the hollow accelerating electrode connected to negative high voltage (parts 9 and 10) with the ion inlet opening on its top (8); the exchangeable neutron generating target is at the bottom (10).

In addition, the electrode contains channels (11) to extract the neutral gas; these channels are so designed that no electric lines of force are able to deflect the ion beam within the electrode. In the lower part the electrode contains a ring channel (22) for the oil cooling of the target. The electrode is supported by two porcelain insulators (13 and 14)[1]. Both insulators are cone-shaped and have a boring in the axial direction. The negative high voltage is fed to the accelerating electrode through the insulator (13) by a high-voltage cable (18). Insulator (14) contains the target-cooling supply. For that purpose, boring (17) is separated in the axial direction by a partition wall of teflon, and the two halves thus generated serve as the inlet and outlet of the annular cooling oil channel. The extraction electrode is contained in a steel housing (12) kept under an internal pressure of about 8×10^{-5} Torr during operation, or 5×10^{-7} Torr, if no gas is introduced. This vacuum is generated by an oil diffusion pump flanged onto the housing. Two tube adapters (15, 16) securing the support insulators, are flanged onto the housing. One adapter (16) is equipped with a metal bellows to take up the differences in length of the supporting insulators. The porcelain parts are each supported by screw collar flanges (23, 24) screwed onto the flanges of the adapters and pressing a bead of the insulator against a rubber seal. On one side of the high-voltage input the screw collar flange (23) has a groove, housing a current transformer coil for measuring the pulse currents flowing to the extraction electrode. At the top the steel housing is closed by the ion source, and at the bottom by a thin-walled top lid (21).

[1] Another accelerator was built having one insulator only.

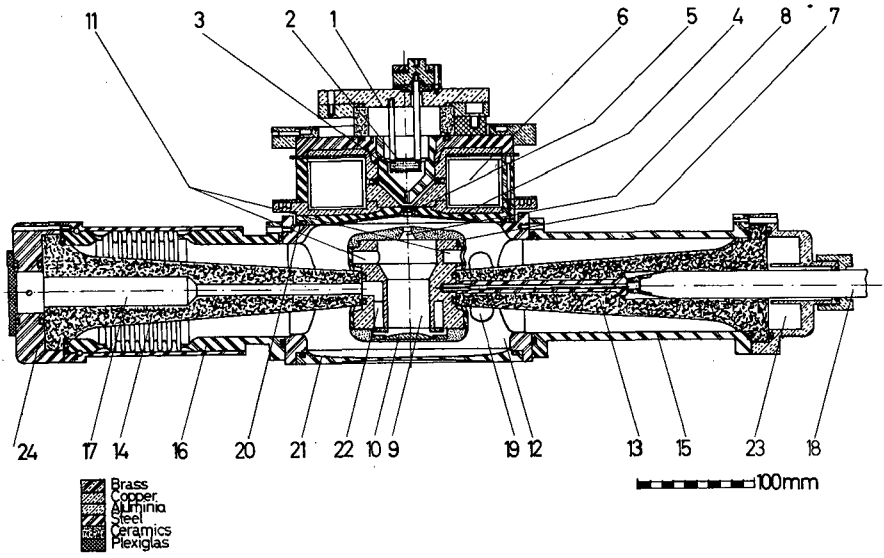


Fig. 1

Sectional view of the neutron generator with duoplasmatron source

1-6 Duoplasmatron ion source

1	Cathode
2	Hot cathode (emission up to 40 A)
3	Intermediate electrode
4	Anode
5	Ion emitter
6	Magnet coil

7-11 and 22 collector electrode with target

7	Collector electrode
8 and 9	Ion flight channel
10	Target
22	Cooling oil channels
12	Steel housing
11	Gas extraction channels
13	Supporting insulators with current input
14	Supporting insulators with cooling oil pipe 17
15	Steel tube adapter with flange for connecting supporting insulator
16	Adapter with metal bellows
17	Cooling oil pipe
18	150-kV high-voltage cable
19	Connection bore to vacuum pump
20	High-vacuum seal
21	Top lid
23	Collar flange with current transformer for measuring ion pulses
24	Collar flange

2.2. The ion source

The duoplasmatron ion source [1-3] is composed of a cathode (1, 2), an intermediate electrode (3) and an anode (4). The cathode consists of a helically wound tape, 12-mm wide and 130-mm long of thrice-folded nickel screen (mesh size 0.04 mm, thickness of wire 0.03 mm). For activation it is thinly coated with a mixture of 50% strontium carbonate and 50% barium carbonate dissolved in amyl acetate. This type of cathode supplies currents up to 40 A at 900°C and has a very long life at this operating temperature, and when the cathode is cold, air can be admitted without any disadvantage. The cathode tape is mounted on a flange by two rods. One rod acts at the same time as the current input. The cathode flange (1) is placed upon a

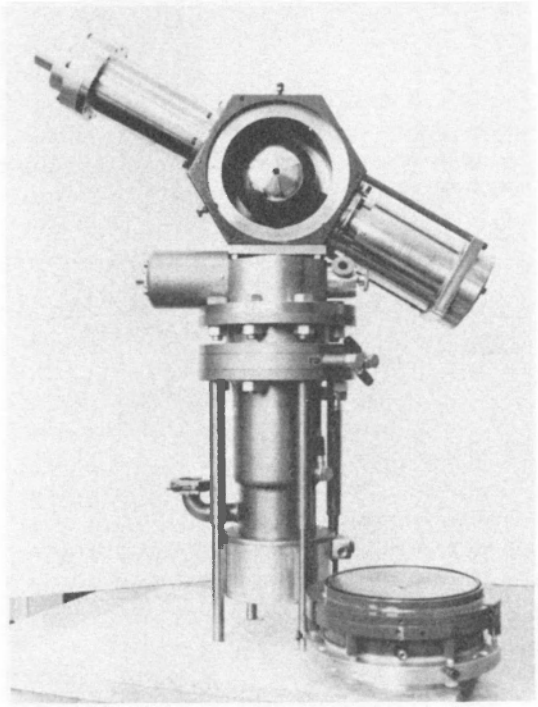


Fig. 2

Neutron generator with duoplasmatron source

porcelain spacer ring which is attached to the intermediate electrode (3) and screwed onto the intermediate electrode flange through an insulation. The intermediate electrode (3) surrounds the cathode and, in its cone-shaped section, has a channel 4 mm in diameter for the plasma to flow to the anode. The intermediate electrode is made of steel and is mounted in a steel flange with copper discs brazed to it for better heat removal.

The anode serves as the end flange of the ion source. It consists of a steel plate containing a molybdenum insert (5) in its centre with a hole of 1.2-mm diameter and 0.5-mm length drilled in its top, which then widens up to 8 mm in the downward direction. Again, copper inserts are brazed onto the steel plate for good heat removal; these inserts contain the channels through which the coolant is pumped. However, these channels are not required for our pulsed operation because the average power of the ion source is very low. It is sufficient to use a strong blower to remove the heat from the electrode flanges, shaped like cooling fins. The anode has a wide groove (6) to contain the excitation coil generating the magnetic field between anode and intermediate electrode. The groove is closed by the intermediate electrode flange. A pertinax disc and a vacuum seal of silicone rubber insulate the two electrodes from each other. The anode is secured to the intermediate electrode by plastic screws. The palladium gas inlet valve is screwed onto the cathode flange.

2.3. Operation of the generator

The ignition of the discharge is initiated by a square wave pulse of about 300-V amplitude applied to the cathode, the anode remaining on ground potential. The arc current then increases to 40 A, the arc voltage being 90 V. The current is limited by a total resistance of 10 Ω (R_3, R_4 of Fig. 3).

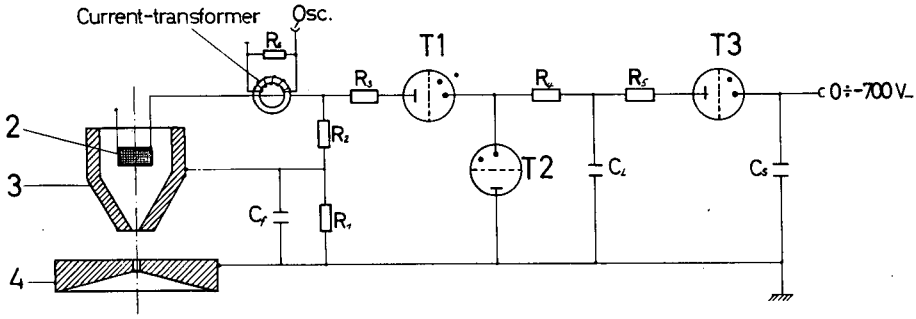


Fig. 3

Principle diagram of the pulsing device of the duoplasmatron ion source

The intermediate electrode is fed by a voltage divider. To facilitate ignition the intermediate electrode is connected to the anode by a capacitor of 0.1 μF (C_f, Fig. 3). Immediately after ignition the current of the intermediate electrode drops to nearly zero, and the electrode reaches a steady state potential of +40 V with respect to the cathode. At the end of the pulse a short circuit caused by the triggering of thyratron T_2 removes the arc voltage. To excite the gas discharge in the ion source a pressure of about 0.12 Torr is required. The cathode saturation current has to exceed 20 A. If the emission of the cathode is less, ignition of the plasma will occur either not at all, or only after some delay. If the pressure is too low, the discharge, if occurring at all, will break down before the end of the pulse, or plasma oscillations will appear. The latter happens when the high ion current decreases the pressure in the source below the value necessary for discharge. Between the intermediate electrode and anode an axial inhomogeneous magnetic field is used to focus the plasma onto the 1.2-mm diameter hole in the anode. In this way, it is possible to compress to 1/10 the cross-section of the plasma filament emitted from the 4-mm diameter channel of the intermediate electrode, thus causing an increase in plasma current through the opening in the anode of more than ten times the original value.

The plasma passing the anode opening of 1.2-mm diameter diverges in the widening bore, there forming a plasma boundary from which the ions are emitted. By means of the extraction electrode the acceleration voltage is applied. The ions leaving the plasma boundary thus are forced to form a space-charge limited beam and are accelerated to pass the extraction electrode channel. Behind the channel the beam diverges owing to space charge, reaching a diameter of 30 mm at the target distance of 80 mm.

The extracted ion current is roughly determined by the parallel beam space-charge formula

$$I_{\text{deuteron}} = 3.84 \times 10^{-8} \frac{F}{d^2} \times U^{3/2},$$

where

U = extraction voltage in volts

d = distance in cm between extraction electrode and anode of the duoplasmatron ion source = 0.8 cm

F = emission area in cm^2. This is the area of the boring of 0.5 cm^2 in the anode.

At an extraction voltage of 60 kV this gives I = 0.28 A and at 120 kV, I = 1.38 A.

At an accelerator voltage of 120 kV the ion current was measured and the neutron source strength was determined by means of foil activation. The pulse current from direct measurement was 0.5 A, while the current deduced from activation via neutron yield was 0.31 A. Under these conditions an instantaneous source strength of 1.9×10^{13} n/s was obtained; that means 1.5×10^8 or 9.5×10^8 neutrons per burst for 8 or 50 μs pulse width, respectively.

The value of the ion current calculated from the space charge law is not reached, since not only atomic ions but also a major portion of molecular ions are accelerated, and since at high current intensities the beam broadens to such an extent that it hits the extraction electrode. This distance of the target has been chosen so as to make the space-charge broadened ion beam cover the whole target of 35-mm diameter in as uniform a way as possible. In this case the target has its maximum lifetime, which was about 15 mAh in our normal applications. To keep the accessible solid angle of source neutrons high, the target, kept at high voltage in the high vacuum, is 2.3 cm away from the top lid.

2.4. Electric equipment

The electric equipment consists essentially of a high-voltage device and a pulsing device. The high-voltage device supplies the negative DC accelerating voltage which is variable up to 150 kV. An automatic current control switches the device off as soon as the current exceeds the nominal value of 10 mA. To prevent every flashover from switching the high-voltage device off, a delay element has been built in. A protective resistor of 10 kΩ is included in the input line. The high-voltage supply is made with a flexible high-tension lead, the shielding of which is grounded via a protective resistor of 10 kΩ.

The pulsing device supplies pulsing currents up to 50 A and a pulse voltage variable from 90 to 300 V. The pulse duration can be selected by a rotary switch between 8 and 50 μs. The maximum repetition frequency is 400 c/s. The limit is set by the thyratrons. The pulsing device contains three thyratrons. These can be triggered one after the other by a control device which is externally triggered. The first thyratron triggered is T_1 thereby connecting C_L through R_3 and R_4 with the cathode of the ion source (see Fig. 3). At the end of the pulse, triggering of thyratron T_2 removes the arc voltage again and discharges C_L through R_4 until both thyratrons are switched off. Then T_3 is triggered and reloads C_L from C_S which is ten times larger and is connected with the power supply. In thyratrons filled

with inert gas this cycle is finished after 2 μs and can then be triggered again. In case of a false triggering sequence of the thyratrons an excess-current switch disconnects the DC supply for a short time.

2.5. *Operating experience*

Since the completion of the first duoplasmatron accelerator in July 1962 three more neutron generators using this principle have been built. These neutron generators have been used in measurements where a high neutron intensity is important or where the neutron generator had to be small. The following measurements have been carried out with these neutron generators: Measurements of thermalization time in graphite [5], measurement of the decay constant in extremely small graphite assemblies [6], measurement of the diffusion length in neutron fields decaying with time [7], pulsed reactivity measurements on the fast-thermal Argonaut reactor STARK [8] and an activation analysis. Neutron spectrum measurements using this accelerator are in preparation.

The following experience has been obtained in the course of these measurements: The first cathode we used was a tape of 12-mm width and 100-mm length cut out of a nickel screen (mesh size 0.6-mm thickness of 0.15-mm wire). This tape was coated with a mixture of nickel powder, barium and strontium carbonate dissolved in amyl acetate [2]. The tape supplied a good electron yield, but after a short time it burnt out starting at the edge. To eliminate this we then used a tape of molybdenum. It also proved to be unsuitable because the active layer flaked off. Therefore we now make the tape as described in section 2.2. This type of cathode has been in operation in our laboratory for several hundred hours. To protect the cathode we originally filled the neutron generator with nitrogen when changing the target. However, this precaution proved to be unnecessary. A target change can be carried out with an experiment interruption of about 2 h.

The type of diffusion pump oil used strongly influenced the dielectric strength of the accelerator. Use of a high-vacuum carbon oil, e.g. Diffilen, gave good dielectric strength at the beginning, but after some time an electrode current up to some milliampères started to flow due to the Malter effect. An inspection of the extraction electrode revealed a brown coating on it around the extraction opening. After removal of this film the old dielectric strength was restored for a short time. Fouling of this type was considerably reduced when using silicone oil DC 705. This oil permits operation of the accelerator at an extraction voltage of 120 kV for a long time without causing any electron background to arise. Silicone oil DC 705 also allows the neutron generators to be run with diffusion pumps cooled by air instead of water. By using these pumps it is possible to perform experiments in which the use of water would be impossible for safety reasons.

Viton O-ring seals, which we used for high vacuum sealing in general, were found to be inappropriate for the ion source because of fluorine gas emission. This emission, which can be detected from the change in the plasma colour, causes a sharp drop in the ion current. Silicone rings do not show this disadvantage.

The cooling oil circuit is hermetically sealed. Care has to be taken to prevent air bubbles being pumped around in it, because otherwise there may be flashover in the cooling oil channels of the inlet and outlet lines.

The types of cooling oil we tested were transformer oils, Dowtherm A, and very light viscous silicone oil. Of these, silicone oil proved to be best because at lower pumping power it has a higher circulation rate than the other coolants. Its dielectric strength is as good as that of transformer oil.

The measurements revealed that the neutron source intensity between the bursts was in fact essentially zero.

3. THE NEUTRON FLASH TUBE*

In this accelerator neutron source, the D-T reaction is used to produce 14-MeV neutrons with a peak instantaneous rate of about 2.5×10^{14} n/s. Thus, during each 2-μs burst 5×10^8 neutrons are generated.

A maximum pulse repetition rate of 250 s^{-1} can be used, giving an average source strength of more than 10^{11} n/s. Therefore the device may also serve as a strong source of fast neutrons as required for activation purposes and activation analysis systems.

The accelerator tube is operated as a valved-off, closed, low-pressure discharge system whose pressure is uniform and held constant by a special replenisher system. It is filled with a mixture of equal parts of deuterium and tritium gas, deuterium being supplied by means of an electrically heated nickel diffusion leak and absorbed in the replenisher. The tritium is supplied by insertion of a fully saturated tritium-deuterium target. The initial neutron yield is about three times as high as the above figure which refers to the equilibrium conditions reached after approximately two hours of operation, when half the tritium content of the target has been replaced by deuterons from the beam. The neutron yield then remains constant for at least 25 h of operation at an average neutron output of 10^{11} n/s. After longer operating times, the neutron source strength decreases owing to target sputtering. The sputtering target can be easily replaced by a fresh one, requiring only half-an-hour to mount and a subsequent period of four hours to pump the system down again.

As the target is operated at ground potential and readily accessible, small samples up to 40-mm diam. can be irradiated at a distance of less than 5 mm from the 50-mm diam. target surface. Big assemblies can be irradiated at a closest distance to the target of about 25 mm, so that the neutron output into nearly 2π solid angle can be utilized.

There is no spurious neutron production during the pulse intervals, since no acceleration voltage exists then.

3.1. Operating principles of the accelerator (see Fig. 4)

The ions, deuterons and tritons, are generated by means of an intense pulsed high-frequency discharge in the gas mixture at a pressure of about 2×10^{-3} Torr. The discharge is excited inductively inside a cylindrical Pyrex

* By A. Schmidt

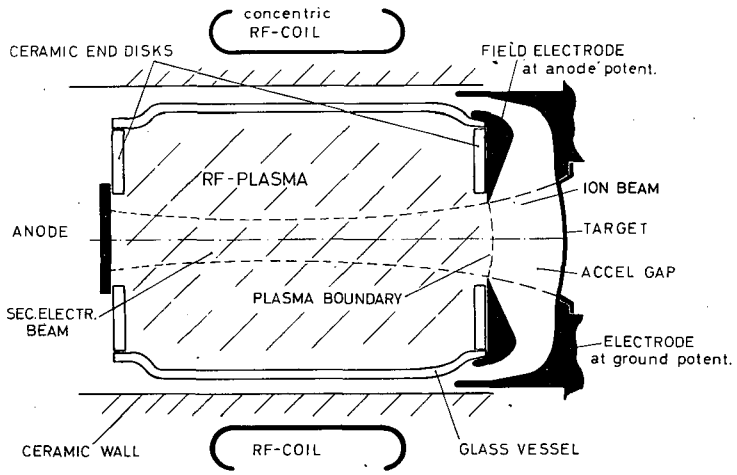


Fig. 4

Principle of the neutron flash tube accelerator

vessel of about 1.3-l volume. The peak power of the RF-pulse is about 200 kW at a frequency of 40 Mc/s. The pulse lasts for 12.5 μs, which is the time needed to fully dissociate the gas content of the discharge vessel and to achieve enough ionization to obtain peak ion current densities of 1-2 A/cm^2 at the boundary of the excited plasma. The ions impinging on the target surface cause the release of secondary electrons at a rate of about four electrons per ion. These electrons pass the accelerating gap in the opposite direction, thereby gaining the same amount of energy as the ions. These electrons form a convergent beam that passes through the emission orifice and the plasma vessel to strike a water-cooled anode at the other end. The total pulse current is in the range 50-75 A.

At the time of maximum plasma density and, correspondingly, of the highest emission current (10-15 A) through the circular emission orifice, a high-voltage pulse of 2 μs duration is applied to the high-voltage end flange of the tube, raising the potential of the discharge plasma to +150 kV within about 0.5 μs. Thus the ions leaving the plasma boundary within the emission orifice are accelerated towards the target electrode, which is held at ground potential. This acceleration takes place across a very short gap of only about 2.5 cm, extending between the ion-emitting plasma boundary and the active target surface. By means of a properly chosen geometry for the electrodes which determine the potential distribution around the beam, and by a properly adjusted curvature of the plasma boundary (for a fixed acceleration voltage this is steadily controllable by the applied RF-power), a divergent, nearly rectilinear space-charge-limited ion flow is obtained. This results in an almost uniform loading of the 50-mm diam. active target surface, whose backing is water-cooled.

3.2. The construction of the accelerator tube (see Fig. 5)

The tube is constructed as a ceramic-metal sealed system. The outer vacuum envelope consists of a hollow cylindrical ceramic tube which has

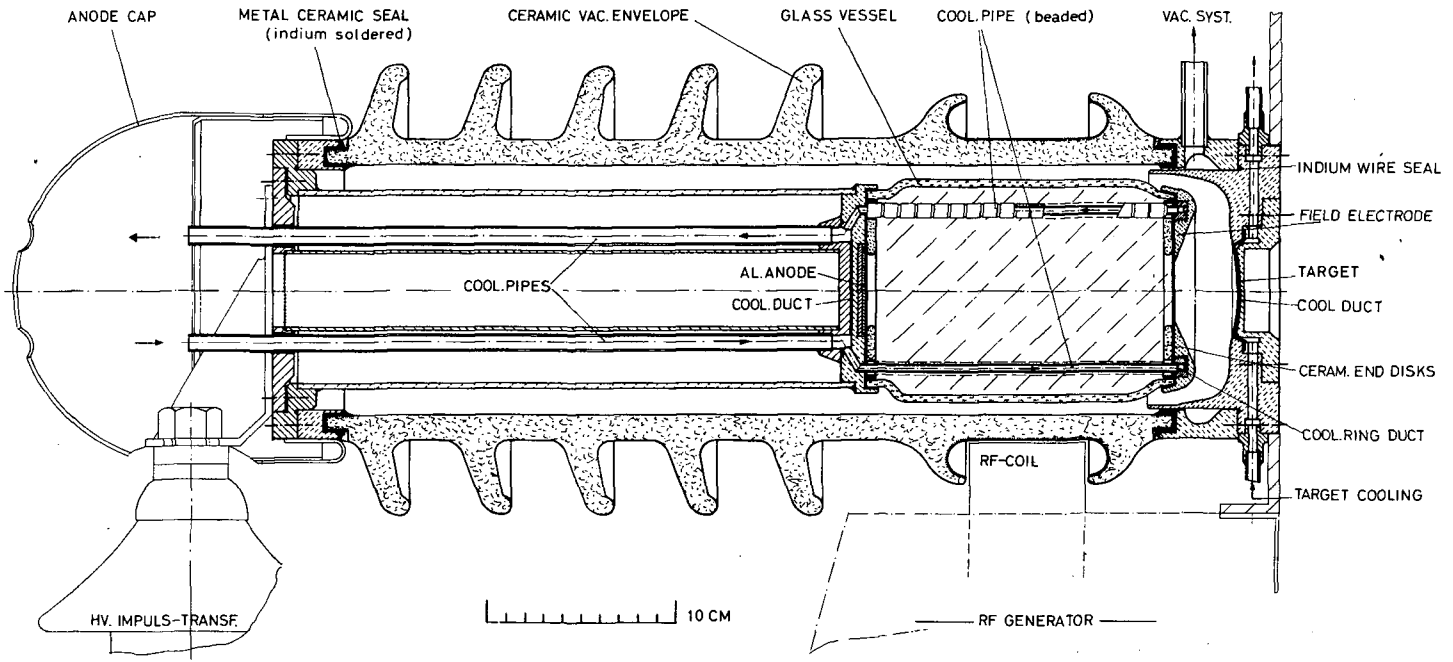


Fig. 5

The accelerator tube

a convoluted outer surface to increase the creep distance with respect to high voltage flashover. The single RF-coil winding is located near the target end of this ceramic body, and its conductor is made by burnt-in silver paint to which silver-plated contacts are soldered. The edge of the coil as well as the ends are rounded off by an overlap of the ceramic to avoid sharp edges and to increase the spark-over voltage at the coil ends. The ends of the ceramic envelope are also silver coated and soft soldered with an indium silver alloy to two annular stainless-steel flanges; to these latter are bolted the end flanges with the joints sealed by indium wire. At the centre of the target end flange, a thick copper-backing tritium-titanium target is inserted and sealed directly by a step-flange seat against the water-cooling duct which carries the water at the rear of its backing. The other end flange is the high voltage terminal; it carries the anode support to which the inner discharge chamber is fixed.

This inner discharge chamber consists of a Pyrex glass cylinder and two separate annular ceramic end disks of high alumina ceramic. One of these is clamped directly to the water-cooled anode body, which also carries one end of the Pyrex glass cylinder. Two small cooling tubes near the inner walls of the discharge cylinder extend from the anode body to the field electrode structure at the other end of this cylinder. There is a metal ring provided with a cooling duct inside which is fed from the two diametrically located cooling tubes. The latter are shielded against the discharge by ceramic beads which are strung on these tubes. The field electrode is screwed onto the cooling metal ring by means of an inside thread on the latter and surrounds the emission orifice in front of the target. The second ceramic end disk is fixed by clamps to the cooling ring, thus shielding the discharge from the field electrode structure. The centre hole of the ceramic disk allows the discharge to reach the emission orifice. The whole inner discharge chamber system, as supported by the anode body at one side and clamped to it by means of the field electrode structure at the other side (the clamping stresses are supported by the two cooling ducts) is located in the centre of the coil section of the outer ceramics insulator vacuum envelope.

There is a small cylindrical gap between the freely supported Pyrex discharge vessel and the inner wall of the outer ceramic envelope, which acts as an insulating vacuum space. Since the operating pressure of the system is low, no RF-discharge is excited in this region.

To ensure a low background of X-rays from the impinging fast electrons, the anode is made of an aluminium disc which is soldered to the stainless steel anode structure via a heat-distributing copper body. Inside the anode support but not included inside the vacuum system, the anode cooling ducts are located. Cooling of the target as well as of the anode is done with ordinary water in a series flow. There are no insulation difficulties from the conductivity of the water.

At the maximum pulse repetition rate of 250 c/s the average power loading of the target is about 1.2 kW, corresponding to a specific load of 60 W/cm^2. The average ion current is 8 mA ($\hat{=}$ 0.4 mA/cm^2). The anode under these conditions is loaded by about 4 kW over an area of about 5 cm^2 ($\hat{=}$ 800 W/cm^2). This heat flow, by means of the copper insert, is distributed to an area of 25 cm^2 which is cooled away by a fast waterflow at a

rate of 160 W/cm². A load of about 800 W is transferred by a part of the secondary electrons to the edge of the emission-orifice which is cooled by another waterflow.

Under full load conditions, about 600 W of RF-power are transferred to the discharge plasma. By means of wall losses, this power is transferred to the Pyrex discharge vessel at a maximum rate of 1 W/cm², heating the Pyrex to about 400°C. This heat is radiated to the wall of the ceramic vacuum envelope where it is conducted away to the outside which is air-cooled. The temperature of the ceramic envelope rises to about 80°C.

3.3. The vacuum system (see Fig. 6)

The appendage system for pumping and pressure regulation is attached to the target flange of the accelerator tube by means of a copper gasket. It consists of a 1 l/s Vacion ion-sputtering pump which is used for the final pumpdown of the system after a fresh target has been inserted, and can

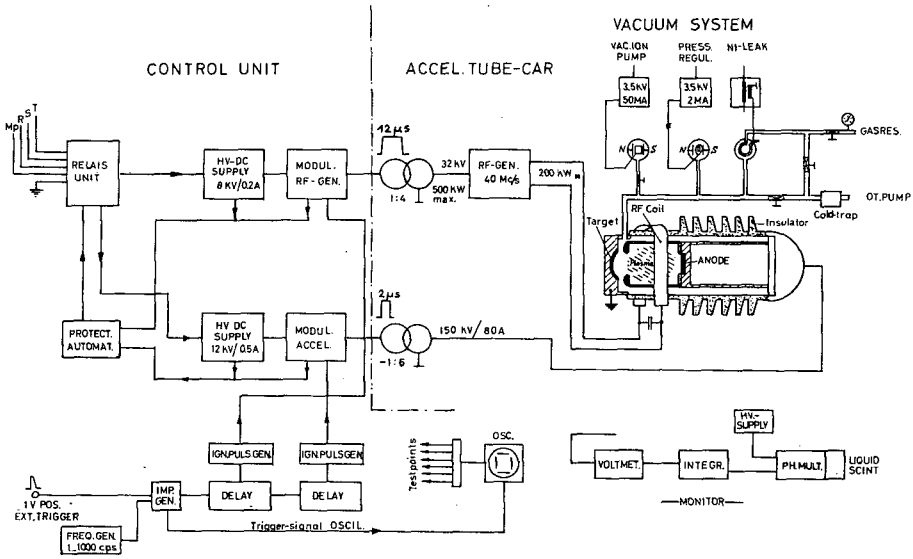


Fig. 6

Lay-out block diagram

be valved-off during the operation of the tube with a Granville-Philips valve. A small electrically heated nickel diffusion leak serves for letting in small amount of deuterium gas. A second Granville-Philips valve serves to close the system from the mechanical forepump which acts as a roughing pump for the initial pumpdown of the system after target exchange. This small two-stage mechanical pump has an end vacuum of 10^{-5} Torr if the liquid nitrogen cold trap is used. Also attached to the vacuum appendage system is the pressure regulator.

The pressure regulator (Fig. 7) is a special small ion sputtering pump which simultaneously acts as a hydrogen replenisher, as its titanium

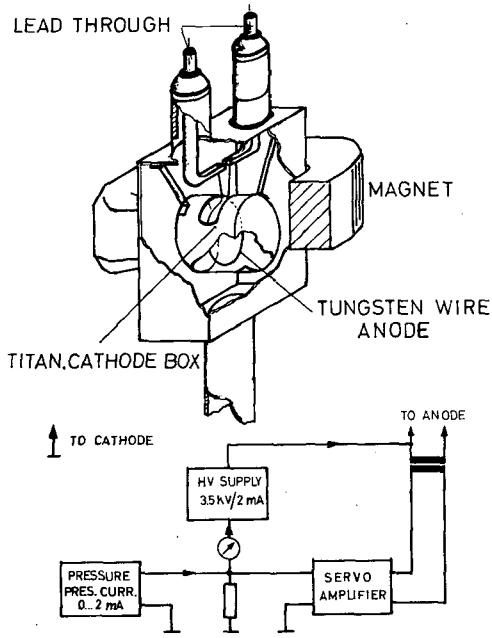


Fig. 7

Pressure control system

cathodes can be heated to release their stored hydrogen content. By means of the pump current the pressure can be measured and controlled automatically to a pre-set value with the aid of an amplifier acting on the heater. At the same time the system acts as a selective pump, removing all other gases from the system except the hydrogen isotopes, thus keeping the tube clean during operation [9].

By careful construction of this system it is possible to hold all the built-in titanium at the same temperature. Also, it is designed so that no sputtered material can get outside to colder surfaces where it would pump off hydrogen in an uncontrolled manner. A nearly fully closed cylindrical titanium cathode box surrounds a tungsten wire anode ring, which is held by two feed-through insulators and can be heated from a small insulation transformer. The system, which is thermally well insulated, is mounted in a stainless steel envelope which fits into a small 1 kG permanent magnet. It works like a small ion sputtering pump at a speed of about 0.1 l/s, using a voltage of 3 kV. The cathode box can be fairly uniformly heated by irradiation of the inside tungsten anode to temperatures up to 700°C and stores easily 10–20 cm^3 of NTP hydrogen. When the accelerator is not used, this pump is cooled down and removes all the discharge gas down to at least 10^{-6} Torr before the discharge extinguishes.

3.4. The lay-out of the equipment (Fig. 6)

The whole device consists of two parts: the accelerator tube carriage (Fig. 8) and the control unit (Fig. 9). The latter contains the main supplies

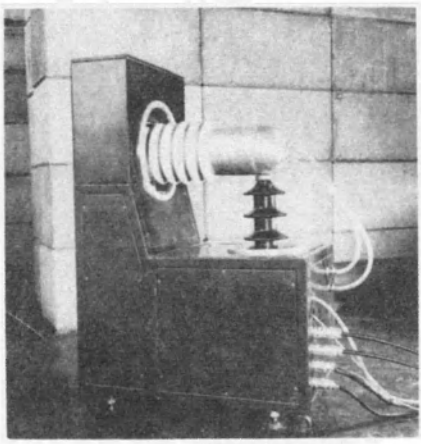


Fig. 8

Accelerator tube carriage

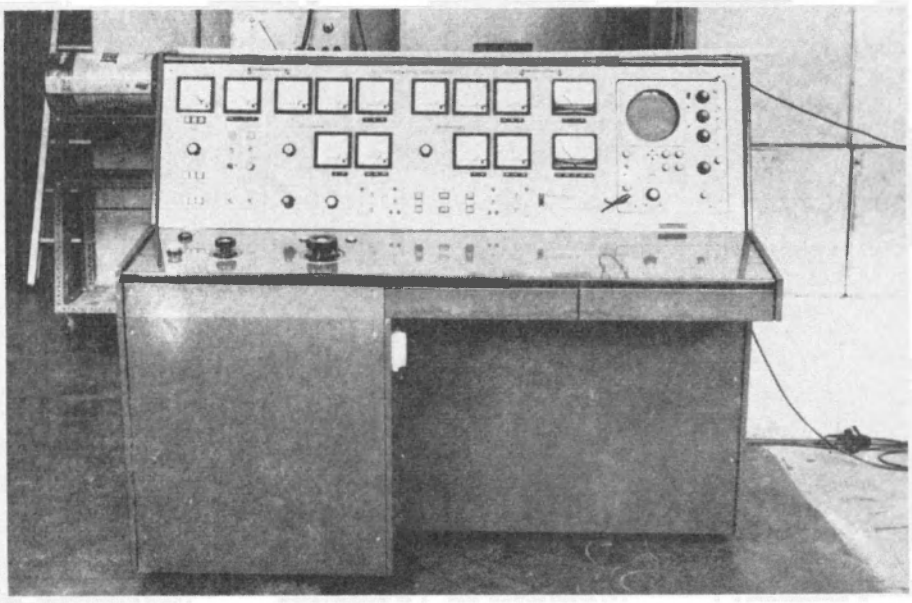


Fig. 9

Control unit

and the timing and control equipment to drive the two high-power line-type pulsers. The power pulses are fed through cables to the accelerator carriage.

The accelerator tube carriage contains the accelerator tube, the arrangement for evacuation, gas filling and pressure regulation, the cathode

pulsed RF-generator with its pulse transformer and the high-voltage 150-kV accelerator pulse transformer. The accelerator tube is mounted horizontally on the carriage with the target side of the tube resting at the front part of the carriage frame. Above the target end flange is mounted the appendage vacuum system. The target is easily accessible from the front. The anode terminal of the tube is directly supported by the high voltage output terminal of the acceleration voltage pulse transformer.

Near the target end of the tube, below the single RF-coil winding, the pulsed RF-oscillator power generator is assembled. It consists of four radiation-cooled transmitting tubes (Telefunken RS 639) in push-pull operation. Two tubes are operated in parallel on each side of the tank circuit which consists of the coupling coil around the flash tube and a single 50-pF vacuum capacitor.

The output amplitude of the pulse moderator which drives the RF pulse-generator is steadily variable by means of a manually controlled variac. This modulator delivers at maximum -8 kV peak voltage pulses with a duration of 12.5 μs into a load of 125 Ω. At the maximum pulse repetition rate 1.6 kW are delivered to the load. These pulses are transformed by the RF-generator pulse-transformer at a ratio of 1:4 to -32 kV peak voltage pulses which are fed to the cathodes of the RF-generator. At peak pulse voltage the RF-voltage at the terminals of the coupling coil is about 50-kV peak RF. The centre tap of the coupling coil is connected to a small 100-W power supply. This excites the RF-generator during the intervals between pulses to get a small constant pre-ionization inside the discharge vessel. In this way, statistical starting effects are avoided.

The accelerator pulser output amplitude is steadily variable by a motor-driven variac; it is capable of delivering pulses with -25 kV peak voltage and 2-μs duration into a 50-Ω load at a pulse repetition rate of 250 s^{-1}. The peak power is 12.5 MW. These pulses are fed to the tube carriage by a matched cable, and are transformed in the accelerator pulse transformer at a ratio of -1:6 to +150 kV at an impedance level of 1800 Ω which matches the resistance of the accelerator tube. The maximum average power of the pulser is 6 kW.

The device can be triggered externally as required by the experiments. The minimum interval between pulses has to be 4 ms. The input signal fires a blocking oscillator which delivers a trigger pulse to a waveform monitoring oscilloscope. With the aid of a lumped parameter delay-line switch, two pulses can be selected which drive the power-switching hydrogen thyratrons. The first one fires the RF-generator pulser, the second one, after a time delay of 12 μs, drives the accelerator pulser. The time delay between these pulses corresponds to the build-up time of the discharge plasma in the flash tube.

3.5. Operating experience

The neutron flash tube system in its present form as displayed in Figs. 8 and 9 was completed in September 1964. Before this, experiments had been performed with preliminary glass accelerator tubes. To avoid contamination problems in these early investigations, the tube was mostly operated with light hydrogen fillings. Because an unconvoluted tube and improper

RF-coil construction was used, this system was not stable against outside flashover at voltages above 100 kV. The present assembly does not show this effect; it has operated at voltages up to 160 kV without outside flashover. Operation at higher voltages was not possible so far owing to limitations in the pulse transformer. A disappointing feature of the new system was the breakdown of the inner discharge vessel which was originally made from a high alumina ceramic. This was therefore replaced by a Pyrex vessel which gave successful operation.

During the last two months, test runs with tritium-titanium targets and a tritium-deuterium gas mixture were made. A very satisfactory performance of the device over extended periods of time was observed at the following parameters:

Accelerator voltage:	140 kV
Target ion current:	15 A (this measurement goes back to a calorimetric calibration)
Repetition rate:	150-200 s^{-1}
Pulse length:	2 μs.

The neutron yield showed a strong decrease initially but then remained constant for more than 20 h. It was possible to operate the device completely unattended for periods of several hours. This is facilitated by an automatic overload and mismatch protection system incorporated in the pulsers' control circuits.

An absolute source strength measurement was made, using the $Al^{27}(n,\alpha)N^{24}$ and the $F^{19}(n,2n)F^{18}$ reactions. The induced activities were absolutely determined by the 4π-β-γ coincidence method. These determinations were performed at an accelerator voltage of 105 kV with the pulse parameters as above. Both measurements were in good agreement and a source strength of $(2 \pm 0.2) \times 10^8$ neutrons per pulse was found. Extrapolating this value to 140 kV, the source strength of the flash tube is 5×10^8 neutrons per pulse.

ACKNOWLEDGEMENTS

The author gratefully acknowledges the assistance of Mr. H. Dohrmann during all phases of this work. Special thanks are due to Prof. Dr. K.H. Beckurts who sponsored the development of this work with great interest.

REFERENCES

[1] V. ARDENNE, M., Tabellen der Elektronenphysik, Ionenphysik und Übermikroskopie I II, VEB-Verlag, Berlin (1956).
[2] FRÖHLICH, H., Nukleonik 1 (1958) 184.
[3] KISTEMACHER, J., ROL, P.K., SCHUTTEN, J. and DE VRIES, C., Z. Naturf. 10a (1955) 850.
[4] EYRICH, W., Nukleonik 4 (1962) 167.
[5] SCHWEICKERT, H., Diploma Thesis, Karlsruhe, 1964.
[6] KÜCHLE, M., unpublished.
[7] ARAI, E. and KÜCHLE, M., Nukleonik, in press.
[8] EDELMANN, M., KUSSMAUL, G., MEISTER, G., STEGEMANN, D. and VÄTH, W., "Pulsed source and noise measurements on the STARK reactor at Karlsruhe", these Proceedings II.
[9] DOHRMANN, H. and SCHMIDT, A., to be published.

DISCUSSION

K. SUMITA: What is the maximum ratio of the peak intensity of pulsed neutrons to the time-average background neutrons due to operation of the accelerator?

A. SCHMIDT: The interpulse production of background neutrons from both sides is zero, since with the duoplasmatron source the ion source discharge is fully quenched in that it is short-circuited. With the neutron flash tube generator, there is no acceleration voltage during the intervals between pulses.

K. SUMITA: Have you attempted to analyse the ion beam coming from the ion source? What is the fraction of monatomic D in the beam?

A. SCHMIDT: We did not measure the atomic beam content with either of our devices. With the duoplasmatron neutron generator, our operating conditions were essentially the same as those described by V. Ardenne and H. Fröhlich. Therefore the beam composition measured by these authors should also apply in our case and would amount to at least some 70% under these heavily pulsed conditions. The discharge colour appears to be quite red, which is a qualitative indication of a high atomic percentage of the beam.

A high atomic content (nearly 90%) can also be assumed with the neutron flash tube by reason of the discharge colour, which again is a bright red. The discharge power level is so high that nearly complete dissociation of the gas content takes place during the build-up time of the plasma and this is enhanced by step-processes within the discharge at these high electron temperatures and plasma densities.

S. CHWASZCZEWSKI: In the flash-type pulse tube, use is made of a pulse transformer and a high-frequency generator (~100 kW). Could you indicate what level of radiointerference is liable to overload the measurement apparatus?

A. SCHMIDT: The rf-interference generated during the rf-pulse and high-voltage pulse decay very rapidly at the end of the neutron pulse, since no further rf-power is then being applied. At that time the small preheating power also vanishes for 1 ms. So no interference is generated during the measurement time.

To avoid long-term overload disturbances in the measuring device during the time of the rf-pulse, consistent shielding of the measuring device is desirable, and double shielding in the case of the detectors and preamplifiers. If the overload capacity and the recovery time of the amplifier are sufficient, single constant interference pulses coincident with the rf-pulse can easily be gated off. Field strength measurements have not been made, but in an open-wire loop of about 1 m^2 in area located near the control desk (a cable distance of 6 inches from the source), about 1V rf-pulse voltage is induced (as measured with an oscilloscope).

W. NAGEL: In the Eyrich accelerator one irradiates a tritium target with a deuterium beam. What can you say on the subject of neutron output versus time? Do you observe any decrease?

A. SCHMIDT: The neutron output of this accelerator is related to the normal dilution of the target tritum content due to the impinging deuteron beam, the tritium evolved being pumped off. The half-life of the target is

about 7h at full output. This half-life is rather large, owing to the nearly uniform beam loading of our fairly large target (diam. 35 mm).

W. NAGEL: Has your group any experience with rare-earth targets (especially erbium)? These could be expected to have a higher hydrogen loading and better temperature resistance.

A. SCHMIDT: Thus far we have used only tritium-titanium targets. Later, however, we shall try to use erbium targets too, the more so since our own facility for making tritium targets is now in operation.

R. GERBIER: On the use of rare earths in tritiated targets, I can report that for the past two years we have been experimenting with erbium at CEN, Grenoble, in the hope of being able to work at higher temperatures, corresponding to higher beam powers. We have encountered some disappointments in that the erbium targets, just like those of titanium, undergo destruction at temperatures at which the hydride would ordinarily be stable under the pressures which are used. We believe that the phenomenon of cathode pulverization is responsible for these difficulties, but we are not making any systematic measurement of this sputtering.

J.E. BOUNDEN: I do not think that sputtering should have been causing the trouble since SERL measurements of the sputtering rate for erbium by 100-keV hydrogen isotope ions suggest that this is in agreement with the theoretical value and this theoretical value does not differ widely from that for titanium.

THE GENERATION OF NEUTRON PULSES AND MODULATED NEUTRON FLUXES WITH SEALED-OFF NEUTRON TUBES

C. W. ELENGA AND O. REIFENSCHWEILER
PHILIPS RESEARCH LABORATORIES,
N. V. PHILIPS' GLOEILAMPENFABRIEKEN, EINDHOVEN, NETHERLANDS

Abstract — Résumé — Аннотация — Resumen

THE GENERATION OF NEUTRON PULSES AND MODULATED NEUTRON FLUXES WITH SEALED-OFF NEUTRON TUBES. Results of experiments with sealed-off neutron tubes are reported with particular reference to the generation of neutron pulses and modulated neutron fluxes. The mean neutron output of the normal (Philips) tube during continuous and pulsed operation was from 1 to 5×10^8 n/s. The output during pulses was 10^9 n/s, the pulse duration within the range from 5 μs to 10 s. The life of the tested tubes was several 1000 h. Experiments have been carried out on the modulation of the neutron output in accordance with an arbitrary time function. It was found possible to generate, for example, sinusoidal modulated fluxes in the frequency range between 1 and 1000 c/s.

A special tube for pulsed operation, based on the normal tube, has been developed. With a mean output of 1 to 2.5×10^8 n/s this tube yields about 5×10^{10} n/s during pulses in the range from 3 to 500 μs. These neutron tubes have a wide range of application by reason of their reliability, their long life, their simplicity, ruggedness and small size (diameter 7 cm, length about 50 cm).

PRODUCTION DE BOUFFÉES DE NEUTRONS ET DE FLUX DE NEUTRONS MODULÉS DANS DES TUBES A NEUTRONS SCELLÉS. Le mémoire expose les résultats d'expériences effectuées dans des tubes à neutrons scellés, plus particulièrement en ce qui concerne la production de bouffées de neutrons et de flux de neutrons modulés. En fonctionnement continu et pulsé, le rendement moyen en neutrons du tube courant (Philips) a été de 1 à 5.10^8 n/s. Le rendement pendant les bouffées a été de 10^9n/s, la durée des boufées étant comprise entre 5 μs et 10 s. La durée de service des tubes essayés a été de plusieurs milliers d'heures. Des expériences ont été effectuées sur la modulation de la production de neutrons conformément à une fonction de temps arbitraire. On a constaté qu'il était possible de produire des flux modulés sinusoïdaux, par exemple, dans la gamme des fréquences comprises entre 1 et 1000 Hz.

Pour le fonctionnement pulsé, on a mis au point un tube spécial dérivé du tube courant. Ayant un rendement moyen de 1 à $2,5 \cdot 10^8$ n/s, ce tube produit environ $5 \cdot 10^{10}$ n/s pendant des bouffées d'une durée comprise entre 3 μs et 500 μs. Ces tubes à neutrons peuvent recevoir de très nombreuses applications du fait de leur fiabilité, de la longueur de leur durée de service, de leur simplicité, de leur robustesse et de leurs petites dimensions (7 cm de diamètre et environ 50 cm de longueur).

ГЕНЕРАЦИЯ НЕЙТРОННЫХ ИМПУЛЬСОВ И МОДУЛИРОВАННЫХ ПОТОКОВ НЕЙТРОНОВ В ЗАПАЯННЫХ НЕЙТРОННЫХ ТРУБКАХ. Сообщаются результаты экспериментов с запаянными нейтронными трубками с особым упором на генерацию нейтронных импульсов и модулированных потоков нейтронов. Средний выход нейтронов для обычной трубки (фирмы Филипс) во время непрерывной и импульсной работы составлял от 1 до $5 \cdot 10^8$ н/сек. Выход нейтронов во время импульсов составлял 10^9 н/сек, а продолжительность импульса находилась в диапазоне от 5 мксек до 10 сек. Срок службы испытанных трубок — 1000 часов. Были проведены эксперименты по модулированию нейтронного выхода в соответствии с произвольной временной функцией. Оказалось возможным генерировать, например, синусоидально модулированные потоки в диапазоне частоты от 1 до 1000 ц/сек.

Для работы с импульсами была разработана специальная трубка, в основу которой положена обычная трубка. При среднем выходе от 1 до $2,5 \cdot 10^8$ н/сек эта трубка дает $5 \cdot 10^{11}$ н/сек во время импульсов в диапазоне от 3 до 500 мксек. Эти нейтронные трубки находят широкое применение в силу своей надежности, длительного срока службы, простоты, прочности и небольшого размера (диаметр 7 см, длина около 50 см).

EMPLEO DE TUBOS SELLADOS PARA PRODUCIR NEUTRONES PULSADOS Y FLUJOS NEUTRONICOS MODULADOS. En la memoria se exponen los resultados de las experiencias hechas con tubos neutrónicos sellados, en especial por lo que se refiere a la producción de neutrones pulsados y de flujos neutrónicos modulados. El rendimiento medio del tubo de modelo corriente (Philips), en régimen continuo y pulsado, era de 1 a $5 \cdot 10^8$ n/s. El rendimiento durante los impulsos era de 10^9 n/s y la duración de los impulsos estaba comprendida entre 5 μs y 10 s. La vida útil de los tubos ensayados era de varios miles de horas. Los autores efectuaron experimentos sobre la modulación neutrónica con arreglo a una función de tiempo escogida arbitrariamente. Se comprobó que, por ejemplo, era posible generar flujos sinusoidales modulados de frecuencia comprendida entre 1 y 1000 Hz.

Para el funcionamiento pulsado los autores construyeron un tubo especial derivado del corriente. Con un rendimiento medio de 1 a $2,5 \cdot 10^8$ n/s, este tubo produce aproximadamente $5 \cdot 10^{10}$ n/s durante los impulsos en el intervalo comprendido entre 3 μs y 500 μs. Estos tubos generadores se prestan a muchas y muy diversas aplicaciones debido a su funcionamiento seguro, a su larga vida útil, a su construcción simple y robusta y a su reducido tamaño (7 cm de diámetro y unos 50 cm de longitud).

1. INTRODUCTION

Ion accelerators have proved most advantageous for generating neutron pulses. Techniques for producing the high energy ion pulses necessary for the generation of neutron pulses have reached an advanced stage of development during recent years. However, accelerator neutron sources are generally complicated, non-mobile and expensive installations.

Mainly in consequence of the availability of tritium in adequate quantities it has become possible in recent years to build more compact and transportable versions of the accelerator-type neutron generating equipment. On the basis of the T(d, n)-reaction a fairly high neutron yield can be obtained with a relatively low accelerating voltage of, for example, 100 to 200 kV. In virtue of this, several types of equipment of this kind have been built, in which the ion accelerator and all auxiliary apparatus are mounted on trolleys. So far an essential drawback of these ion accelerators working with tritium targets has been that the life of the targets is limited.

The neutron generator can be made more compact by making the ion accelerator in the form of a sealed-off tube, thus eliminating the need for a pumping arrangement and a continuous gas supply for the ion source. In recent years in the Philips Research Laboratories investigations have been undertaken, which are related to the design problems presented by such sealed-off neutron tubes. After further development work, in co-operation with the Electron Tubes Division of our company, the tubes have reached the production stage. In this work we have concentrated on reliability and long life. It has proved possible to fabricate sealed-off neutron tubes suitable for pulsed neutron research with a life of several 1000 h. A complete neutron generator comprising this sealed-off neutron tube with control cabinet, voltage supply units and cable connections has been developed by the Industrial Equipment Division.

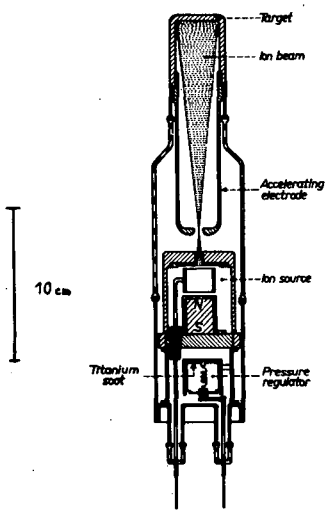
Two experimental neutron tubes, both for continuous and pulsed operation, and with an average neutron output of 5×10^7 n/s, were described for the first time in 1957 at the Deutsche Physikertagung at Heidelberg [1]. Later a more complete account of our neutron tubes and the underlying research work was given [2, 3]. In the meantime sealed-off neutron tubes have been described by other authors [4-7].

For the sake of completeness a short description of the design and performance of our tube is given. This is followed by a rather more detailed account of the operation of the neutron tube and results of experiments with it, with particular reference to the generation of neutron pulses and modulated neutron fluxes.

2. DESIGN AND PERFORMANCE OF THE NEUTRON TUBE

2.1. Generation and acceleration of the ions

Figure 1(a) is a sectional drawing of our neutron tube. A Penning ion source is used for generating the ions. The gas filling is deuterium or a mixture of tritium and deuterium. The Penning ion source is particularly suitable for sealed-off neutron tubes because it works at a relatively low gas pressure and is simple, robust and stable in operation. As the magnetic



(a)

Fig. 1(a)

Sectional drawing of the neutron tube

field of our ion source is supplied by a small permanent magnet placed inside the ion source chamber, only one voltage is needed for the gas discharge. Also, it is a very simple matter to generate ion current pulses by pulsing this discharge voltage. Under DC operation the source mainly supplies molecular ions; this drawback is eliminated by operating the source with high current pulses. Under these operating conditions, the high charge-carrier density causes such a high partial pressure of atomic hydrogen that a large percentage of atomic ions is formed.

The ions leaving the ion source are accelerated in a single stage accelerating system. They enter the field-free space inside the accelerating

electrode as a slim divergent beam and strike a target containing tritium. Ion source and accelerating system work stably over a wide range of gas pressures, from about 10^{-4} to a few times 10^{-2} mm Hg. The ion source operates at voltages from several 100 V to several kilovolts, and the accelerating system can operate at voltages from 100 to 200 kV.

2.2. The target

An essential drawback of the conventional tritium targets, generally used in accelerator neutron sources so far, has been their limited life. Because there is naturally no question of replacing targets in sealed-off neutron tubes, these targets are not suitable in a tube which is desired to have a long life. A solution to this problem has been found in the drive-in targets (self-loading targets) which were investigated earlier in connection with the D(d, n)-reaction [8]. In these targets a deuterium content is built up gradually by ion bombardment. We arrived at a simple and effective self-loading target for the T(d, n)-reaction by filling the tube with an equal mixture of tritium and deuterium [2, 3]. Once established, the state of saturation of the tritium-deuterium mixture in the target will maintain itself throughout the life of the tube, and there will be no drop in the neutron yield. As a system for the drive-in target a titanium-plated silver disc has proved to be very suitable.

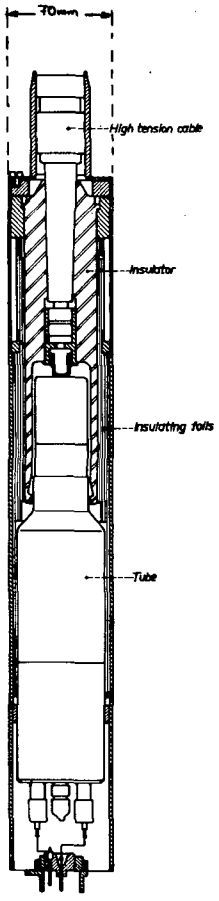
2.3. The pressure regulator

When the tube is in operation a regulating device has to keep the pressure level constant by compensating gas clean-up in the discharge and sometimes also by absorbing the filler gas released by certain constructional parts when heated. For this purpose a special pressure regulator [9] is employed, which has the advantage, as against other devices of this kind, that equilibrium pressure establishes itself very quickly. In this pressure regulator titanium is deposited as a true powder (particle size about 100 Å) on the inner wall of a metal cylinder by evaporating the titanium in an argon atmosphere. After this powdered titanium has been made to absorb the deuterium-tritium mixture, the gas pressure inside the tube can be adjusted by heating the metal cylinder to a certain temperature.

2.4. Neutron tube with metal casing

To strengthen the tube and make it convenient to handle it has been enclosed in a metal cylinder of 7 cm diameter and about 50 cm long, as shown in Fig. 1(b). Ion source and pressure regulator, at earth potential, are fed by a cable connected at one end of the metal casing. The negative high tension for the target is supplied by a high tension cable through an insulator at the other end of the casing.

This compact and robust version of the neutron tube in the cylindrical metal casing makes it very suitable for a wide range of applications, e.g. in reactor physics, and in oil-well logging.



(b)

Fig. 1(b)

The tube enclosed in its metal casing

3. OPERATION OF THE TUBE

For loading the neutron tube one needs a negative high tension supply for the accelerating voltage, a power unit supplying 2 to 3 kV for the ion source and a heater current supply for the pressure regulator. The neutron yield can be adjusted to the desired value by varying the accelerating voltage, or alternatively by varying the gas pressure or the voltage on the ion source, both of which affect the target current.

We normally operate the tube at an accelerating voltage of 125 kV and, under DC conditions, at a target current of 100 μA. The ion source voltage is then between 2 to 3 kV, the discharge current of the ion source about 0.3 mA, the gas pressure about 10^{-3} mm Hg. About 80% of this current is due to ions hitting the target; the remaining 20% are electrons accelerated

in the opposite direction. The neutron output under these conditions is between 1 and 2.5×10^8 n/s, depending on the quality of the target. The neutron tube can however be operated without difficulty at twice the nominal target current, i.e. at 200 μA. The neutron output in this region is still a reasonably linear function of the target current, lying between 2 to 5×10^8 n/s.

The gas pressure inside the tube can be stabilized automatically without difficulty. As pressure gauge, up till now, the Penning ion source has been used, the discharge current of which at a given ion source voltage provides a measure for the gas pressure. Stabilization of the gas pressure is achieved by regulating the pressure regulator voltage via an electronic regulating system in such a way that the discharge current of the ion source, and with it the gas pressure, remains constant.

For generating neutron pulses only the ion source voltage is pulsed. The same accelerating voltage is used as under continuous operation. Pulsing of the accelerating voltage, as would be quite feasible, has not been used by us so far. The maximum neutron output during the pulse intervals is about ten times greater than it is under continuous operation with a target current of 100 μA; it is thus about 10^9 n/s. The same mean neutron output can be reached as under DC operation.

With target currents higher than about 300 μA the relative increase in the backward accelerated electrons is greater than that in the ions, owing to the increasing gas pressure, this in its turn being caused by the higher probability of ionizing impacts between fast charge-carriers and gas molecules. To get an intermittent neutron output of 10^9 n/s a target current of 2 mA and an ion source current of 3 mA are needed. The ion source voltage is not critical; a suitable value is 3 kV.

The pulse duration can be varied at will over a wide range. The shortest pulses used so far had a duration of about 3 μs, the longest pulses a duration of 10 s. The maximum permissible duty cycle is given by the condition that the mean neutron output should be about the same as that achieved under continuous operation with a target current of 100 μA. With an intermittent neutron yield of 10^9 n/s, thus the maximum duty cycle is 10%.

Random-distributed neutron pulses, sometimes employed in reactor physics, can also be generated. Another important mode of the neutron yield, important for similar applications are step functions of the neutron output. These too, we have generated with our neutron tube. In both cases the target current, and with it the neutron output, are controlled by the ion source voltage.

Several tubes from the production line have been life-tested under DC and pulsed operation at full output for periods exceeding 1000 h. Two tubes were working steadily for nearly 8000 h, one of them under pulsed operation with a pulse duration of 100 ms and a repetition rate of 1 pulse per second. No fall-off in neutron yield or in reliability could be detected during or after these tests.

4. DEVELOPMENT OF AN IMPROVED TUBE FOR PULSED OPERATION

Because the intermittent neutron output of our normal neutron tube is too low for some applications, investigations were carried out with a view

to increasing this output. The Penning ion source of the neutron tube described above can deliver higher ion currents than are needed for the generation of 10^9 n/s. But then the gas pressure is so high that most of the current through the tube consists of backward accelerated electrons. Moreover, the tube shows tendency to high-voltage breakdown which affects its reliability. To increase the maximum obtainable pulse intensity the ion source has to be improved in such a way that a sufficiently high current is obtained at a sufficiently low gas pressure.

All-important for the efficient functioning of the Penning discharge are the strength and shape of the magnetic field. In the Penning ion source of our normal neutron tube the magnetic field falls off sharply along the tube axis in the direction of the exit canal of the ion source as shown in Fig. 2(a).

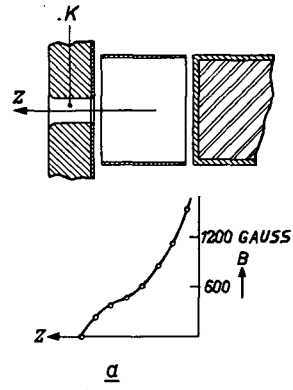


Fig. 2(a)

Sectional drawing of discharge chamber and plot of magnetic field strength along the tube axis of the Penning ion source of the conventional neutron tube

As a result many electrons are lost prematurely by hitting the anode. An essential improvement in ion source functioning was obtained by placing an annular permanent magnet M at the side of the exit canal K inside the ion source (Fig. 2(b)). Moreover, in the cathode opposite the exit canal K a cylindrical cavity was drilled as described first by KELLER [10]. Figure 2(b) also shows that the magnetic field strength is more constant along the tube axis inside the ion source.

Firstly, experiments were done with this ion source in a special arrangement enabling the electrodes to be changed easily. The ion source chamber and the anode each had a window to allow visual observation of the discharge. In these experiments the discharge was fed by a pulse-forming network. The ions leaving the ion source were accelerated to 20 keV. The value of the ion current was determined by calorimetry.

It has been found that at gas pressures ranging from $(1\text{-}2)\,10^{-2}$ mm Hg, which values are tolerable in sealed-off neutron tubes, a useful ion current of more than 100 mA could be generated with the improved ion source. The maximum ion current obtained so far in this mode of operation was 330 mA. To strike the discharge a special voltage spike of 1500 V was applied to the ion source. Thereafter the discharge is sustained by a voltage of 500 V

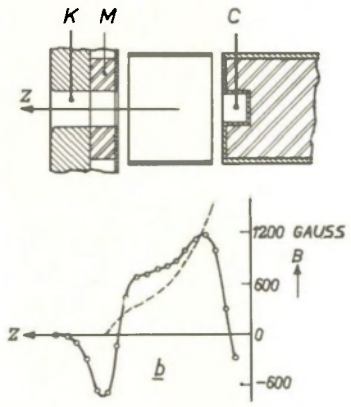


Fig. 2(b)

The same for the improved neutron tube yielding higher pulse outputs

supplied by the pulse-forming network. In these experiments the pulse duration was 20 μs, the repetition rate 50 pulses per second.

Figure 3 is a photograph of the discharge. It can be seen that the discharge is concentrated into a cylindrical region of about 5 mm diameter. Figure 4 shows the neutron tube embodying the improved ion source. The

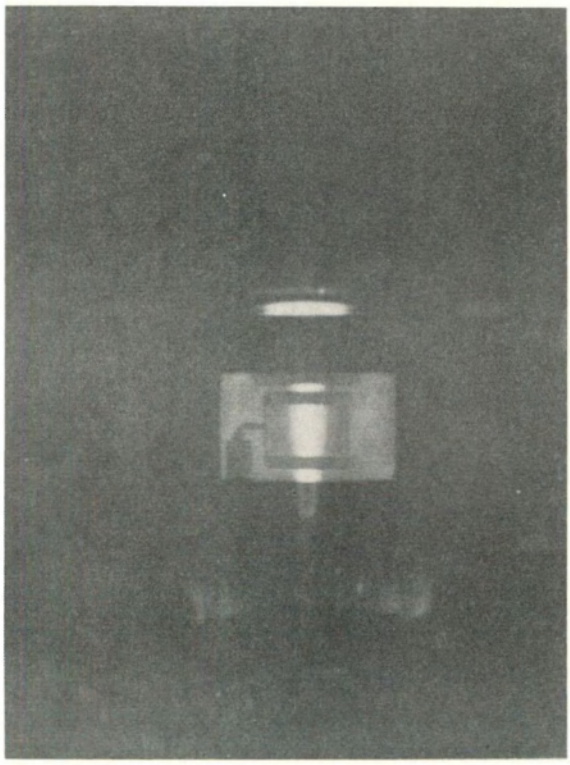


Fig. 3

Photograph of the discharge

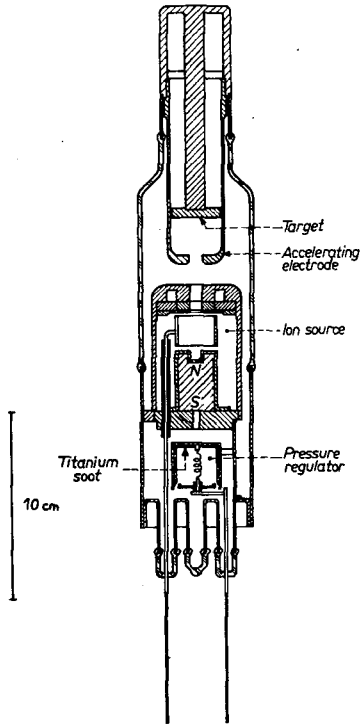


Fig. 4

Sectional drawing of the improved version of the neutron tube yielding higher pulse outputs

target is placed at a shorter distance from the ion source than in the normal neutron tube because the ion beam has a larger aperture angle, mainly as a consequence of space charge repulsion in the region where the ion beam is narrow.

So far the ion source of these tubes has been operated by the pulse generator used in our normal neutron generator. This has the advantage that pulse length and repetition rate can be chosen at will but the disadvantage that the discharge current of the ion source, and with it the target current, and the pulse output are limited. With this power supply a pulse yield of about 5×10^{10} n/s with a pulse length between 3 μs and 500 μs could be obtained. It was also possible to generate the short pulses of 3-μs duration with an intermittent output of a few times 10^{11} n/s. Probably this output can also be obtained during longer pulses, if the ion source supply is adapted.

Figure 5 shows oscillograms of the ion source voltage pulse, the ion source current pulse and the neutron pulse for a typical mode of operation. The intermittent ion source current was 1.25 A with an ion source voltage of about 600 V, and the intermittent neutron output was 5×10^{10} n/s. The intermittent target current was 28 mA. The pulse duration was 50 μs and the duty factor 0.5%. Experiments with this improved tube will be continued.

The new tube passed its first practical test when it was used by EINFELD, HENNIES, MEMMERT and ULRICH [11] in reactivity measure-

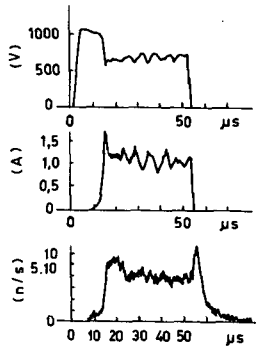


Fig. 5

Oscillograms of ion source voltage pulse, ion source current pulse and neutron pulse

ments, as described at this Symposium. It has been shown that the time taken for the measurements was reduced by a factor of about 10.

An experimental neutron tube for a mean output of 10^{10} n/s embodying the same ion source has been developed in our laboratories. This tube will be suitable not only for applications in pulsed neutron research, but also for activation analysis. In this connection it may be of interest to mention that in activation analysis pulsed neutron sources will be useful for detecting isotopes with half-lives of the order of milliseconds [12, 13]. The tube will be described in more detail later.

5. THE GENERATION OF MODULATED NEUTRON YIELDS

Some time ago we were asked[1] to look into the possibility of generating sinusoidally modulated neutron yields. The frequency had to be between 1 and 1000 c/s, the distortion less than 1% and the drift in the mean yield level was required to be less than 1% per hour. Experience gained so far regarding control and stabilization of our neutron tube suggested that prospects of solving this problem were good.

As the neutron output at constant gas pressure and constant accelerating voltage is proportional to the target current, it is possible to generate a neutron yield modulated in accordance with an arbitrary time function by transferring the appropriate waveform or other pattern to the target current and at the same time stabilizing the accelerating voltage and the gas pressure. The best way to vary the target current quickly is to alternate the ion source voltage.

Figure 6 is the block circuit. The target current is transformed by the resistor R into a voltage signal, which is compared with the voltage signal representing the given time function. The difference between the two voltages regulates via an amplifier the ion source voltage in such a way that

[1] By W. Rotter, Common Group, Centre d'études de l'énergie nucléaire – EURATOM, Mol, Belgium.

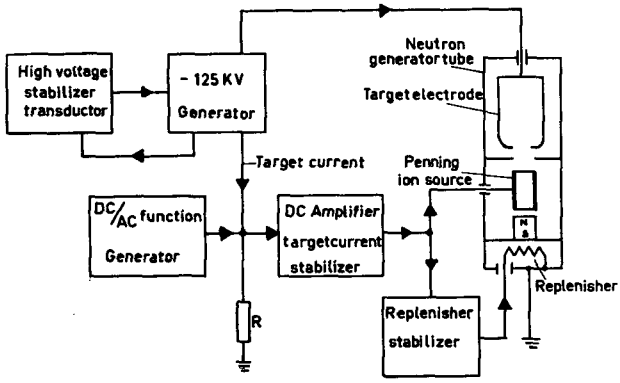


Fig. 6

Schematic electronic circuit for the generation of modulated neutron outputs

this difference is reduced to zero. For the generation of the sinusoidal modulated voltage a function generator is used. The accelerating voltage is stabilized by a specializer at 1‰, for a main voltage fluctuation of 10%.

The gas pressure is stabilized by a method similar to that described when the normal operation of the tube was dealt with. Instead of the ion source current the mean discharge voltage of the ion is used to stabilize the gas pressure. This offers no difficulties as long as the variation of the target current and with it the variation of the ion source voltage are fast compared with the time constant of the pressure regulating system. As this time constant is several seconds the lower limit to the frequencies obtainable is about 1 c/s. For the generation of lower frequencies it would be possible to average out, electronically, the ion source voltage over a longer period or to incorporate a special pressure gauge in the neutron tube.

It is possible to generate a sinusoidally modulated neutron output with a frequency up to at least 1000 c/s. The maximum modulation depth is about

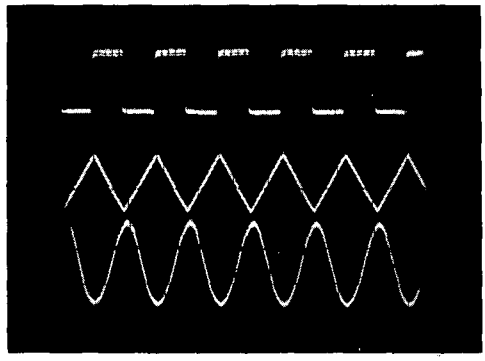


Fig. 7

Oscillograms of several time functions of the neutron output at a frequency of 10 c/s: sine, triangle and square wave

50%, the distortion of the given sine-wave not more than 1%. The drift in the mean neutron output was found to be smaller than 1% during 1 h. Figure 7 shows oscillograms of several time functions of the neutron output at a frequency of 10 c/s: a sine, a triangle and a square wave.

It is, of course, possible with this method to generate neutron yields modulated in accordance with an arbitrary time function within the possible frequency range. This was demonstrated very impressively by the transmission of a musical signal by modulation of the neutron output. The target current, and with it the neutron intensity, was modulated by the signal voltage from a gramophone pick-up. The neutron yield was measured with a plastic scintillator and the voltage signal coming from the photomultiplier was fed to a loudspeaker via an amplifier.

A stabilized neutron output can be regarded as a special kind of time function, namely a constant in time. To obtain this a stable value must be conferred on the target current by means of a stable voltage applied across resistor R (Fig. 4).

In another method for stabilizing the neutron output, this output is measured by a stable detector and one of the operating parameters of the tube is regulated by an electronic system in such a way that the measured detector signal remains constant. The detector used in our experiments was a BF_3 counter whose count rate was held constant by automatic control of the accelerating voltage. Also, the ion source voltage could be used, of course, for the regulation of the neutron output. The neutron yield was monitored by a second independent BF_3 counter. The neutron tube and the two BF_3 counters were placed inside a large water-filled tank. The counting rate of both BF_3 counters was about 10^4 counts/s. Comparison of intervals 1 s long showed that the difference in the neutron yield during such intervals was not greater than 1% over a total period of one hour. It is thus shown that this method affords about the same degree of stability of the neutron output as is theoretically possible with the given statistical information.

The method of regulating the neutron output by controlling the count rate of a neutron detector in accordance with a time function, as employed in principle in the above stabilization method for a constant neutron output, could also be used for generating a modulated neutron output. Then the count rate must be made to follow the prescribed time function. The best procedure for making the neutron detector independent of the influence of the surrounding matter would be to measure the neutron output inside the tube, by counting the alpha-particles associated with the generated neutrons from the T(d, n)He^4 reaction.

6. CONCLUSION

The neutron tubes described in this paper have a wide range of applications by reason of their reliability, their long life, the ease with which the neutron output can be regulated and – where necessary – stabilized, the possibility of generating neutron pulses, and the simplicity, ruggedness and small size of the tubes. In the field of reactor physics this has been proved by many investigators. An essential advantage is that the parameters of

interest in a multiplying system, i.e. the reactivity and the lifetime of neutrons, can be determined by several different and independent methods without changing the experimental arrangement. In this connection we will only refer to the paper by ROTTER [14].

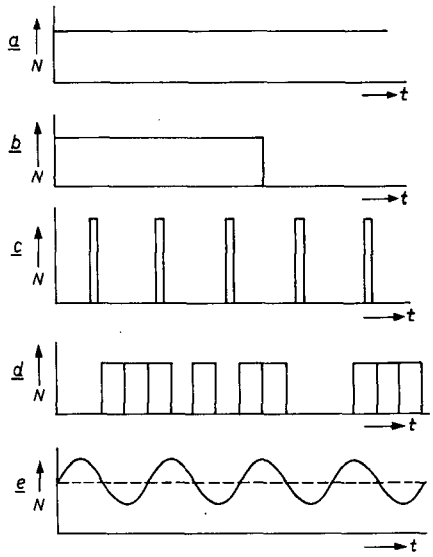


Fig. 8

Modes of neutron output useful in reactor physics investigations

Figure 8 shows the different modes of neutron output of our tube which can be applied in the field of reactor physics: stabilized constant neutron outputs, step functions of the neutron output, neutron pulses, random-distributed neutron pulses and sinusoidally modulated neutron yields or neutron outputs modulated in accordance with other time functions. Our neutron tube is also especially suitable for the application in oil-well logging. Another important field of application is in neutron and reactor physics training, a good example for which can be found in the Schule für Kerntechnik at the Kernforschungszentrum Karlsruhe.

ACKNOWLEDGEMENTS

We wish to thank Mr. Eijmberts for his assistance in carrying out the experiments.

REFERENCES

[1] REIFENSCHWEILER, O. and VAN DORSTEN, A.C., Phys. Verh. (Mosbach) 8 (1957) 163.
[2] REIFENSCHWEILER, O., Nucleonics 18 12 (1960) 69-71.

[3] REIFENSCHWEILER, O., Philips Res. 16 (1961) 401-18.
[4] GOW, J.D. and POLLOCK, H.C., Rev. sci. Instrum. 31 (1960) 235-40.
[5] HAWKINS, P.O. and SUTTON, R.W., Rev. sci. Instrum. 31 (1960) 241-48.
[6] FRENTROP, A.H. and SHERMAN, H., Nucleonics 18 12 (1960) 72-74.
[7] CARR, B.J., Nucleonics 18 12 (1960) 75-76.
[8] FIEBIGER, K., Z. angew. Phys. 9 (1957) 213-23.
[9] REIFENSCHWEILER, O., Rev. sci. Instrum. 35 (1964) 456-60.
[10] KELLER, L.R., Helv. phys. Acta 22 (1949) 78-88.
[11] EINFELD, K., HENNIES, H., MEMMERT, G. and ULRICH, W., "Pulsed neutron reactivity measurements in the near-critical state", these Proceedings II.
[12] GLAGOLEV, V.L., KOVRIZHNYKH, O.M., MAKAROV, Yu.V. and YAMPOL'SKII, P.A., J., exptl. theoret. Phys. (USSR) 36 (1959) 1046-57; Soviet Phys. JETP 36 9 (1959) 742-51.
[13] GLAGOLEV, V.L. and YAMPOL'SKII, P.A., J. exptl. theoret. Phys. (USSR) 40 (1961) 743-48; Sov. Phys. JETP 13 (1961) 521-24.
[14] ROTTER, W., «Mesures au moyen d'une source pulsée et modulée dans un réacteur», these Proceedings II.

DISCUSSION

J. SHERWIN: What is the maximum possible distance between the tube and the EHT supply and up to what surrounding temperatures can one work with the tube?

O. REIFENSCHWEILER: Thus far we have used cable lengths of up to 30 m. We have operated the tube at surrounding temperatures of up to 100°C but so far we have not done much experimental work on the question of temperature.

M. PETROVIC: One of your neutron sources is built to provide sinusoidal output with a "clearance factor" of the order of 1% (i.e. 99% modulation). How is this achieved?

O. REIFENSCHWEILER: As pointed out in the paper, the target current which is proportional to the neutron output is compared with the prescribed signal and the difference between them is reduced to zero by an electronic feed-back system.

M. PETROVIC: What is the transfer function of the neutron source for the frequency range given in the paper?

O. REIFENSCHWEILER: The 3dB-points of the transfer function lie below 1 Hz and above 1000 Hz.

J.E. BOUNDEN: What is the output of the Philips tube when modulated sinusoidally?

O. REIFENSCHWEILER: The mean output is about 2×10^8 n/s with a modulation of 50%. In other words, the minimum value of the modulated output is 10^8 n/s and the corresponding maximum value is 3×10^8 n/s.

HIGH-OUTPUT NEUTRON GENERATING TUBES FOR REACTIVITY MEASUREMENTS

P. D. LOMER, J. E. BOUNDEN, J. D. L. H. WOOD
SERVICES ELECTRONICS RESEARCH LABORATORY,
BALDOCK, HERTS.
AND
W. J. BARNES
ATOMIC WEAPONS RESEARCH ESTABLISHMENT,
ALDERMASTON, BERKS.,
UNITED KINGDOM

Abstract — Résumé — Аннотация — Resumen

HIGH OUTPUT NEUTRON GENERATING TUBES FOR REACTIVITY MEASUREMENTS. A pulsed neutron tube capable of producing at least 10^8 neutrons per pulse in a 10-μs pulse has been developed and incorporated in a simple 9-cm diam. probe for reactivity measurements. This probe has been used in a number of zero-energy reactors. The range of these measurements can be extended by the use of the well-established technique of transfer function analysis. This extension is linked with the development of another neutron generating tube of high continuous output which is capable of modulation at frequencies up to 1000 c/s. Such a tube has been achieved by using an RF ion source from which a mixed beam of deuterium and tritium ions is accelerated onto a target loaded with a mixture of deuterium and tritium. Free tritium can be handled safely in a sealed-off tube of this type. The tube which has been developed has a continuous output of 10^{10} n/s for an accelerating voltage of 120 kV and total tube current of 1.8 mA. Since a D-T mixture is used in both ion source and target, a continuous circulation of gas between target and ion source is achieved, resulting in a stable neutron output and target lives extending to well over 100 h. The neutron output can be modulated by varying the power supplied to the RF ion source. Square wave modulation has been demonstrated over a range of frequencies from 0.017 c/s to 5 kc/s corresponding to pulse lengths from 30 s to 100 μs. The factors controlling the rise time of the neutron pulse are discussed. The tube has been completely contained within a metal cylinder 18 cm in diameter and 91 cm long. The power supplies, including a 120-kV accelerating voltage, are fed via plug and socket connections to one end of the cylinder, as are also the connections for the coolant hoses. The complete assembly is thus suitable for insertion into a zero-energy reactor for experimental purposes, it being possible to operate remotely the associated power and coolant supplies. The coolant liquid (with variable flow rates up to 10 l/min) is pumped under pressure (50, lb/in^2 max.) to the target, electron back stop and RF ion source which dissipate a total of approximately 800 W. The design of a complete system with all the associated equipment is described.

TUBE GÉNÉRATEUR DE NEUTRONS A HAUT RENDEMENT POUR LES MESURES DE RÉACTIVITÉ. Pour des mesures de réactivité, on a mis au point et incorporé dans une simple sonde de 9 cm de diamètre un tube générateur de neutrons pulsés pouvant produire au moins 10^8 neutrons par bouffée de 10 μs. Cette sonde a été utilisée dans un certain nombre de réacteurs de puissance zéro. On peut étendre la gamme de ces mesures en utilisant la méthode bien connue de l'analyse de la fonction de transfert. Cette extension est liée à la mise au point d'un autre tube générateur de neutrons ayant un rendement continu élevé et susceptible de modulation à des fréquences allant jusqu'à 1000 Hz. Ce tube a été réalisé à l'aide d'une source d'ions H. F. d'où un faisceau accéléré de deutérons et de tritons mélangés est dirigé sur une cible chargée d'un mélange de deutérium et de tritium. On peut manipuler en toute sécurité le tritium libre dans un tube scellé de ce genre. Le tube ainsi mis au point a un rendement continu de 10^{10} n/s pour une tension d'accélération de 120 kV et un courant total de 1, 8 mA dans le tube. Puisqu'on utilise un mélange de deutérium et de tritium à la fois pour la source d'ions et pour la cible, on obtient une circulation continue de gaz entre la cible et la source d'ions, ce qui assure un rendement stable en neutrons et, pour la cible, une durée de vie dépassant largement 100 heures. Le rendement en neutrons peut être modulé en modifiant la puissance fournie à la source d'ions H. F. On a obtenu des modulations à ondes carrées sur une gamme de fréquences comprises entre 0,017 Hz et 5 kHz correspondant à des longueurs de bouffée de 30 s à 100 μs. Les auteurs discutent les facteurs dont dépend le temps de montée de

la boufée de neutrons. Le tube tout entier a été placé dans un cylindre métallique de 18 cm de diamètre et 91 cm de long. L'alimentation, y compris une tension d'accélération de 120 kV, était assurée par un raccordement à l'une des extrémités du cylindre; cela vaut également pour les raccordements au circuit du fluide de refroidissement. L'ensemble peut donc être placé, à des fins expérimentales, dans un réacteur de puissance zéro puisqu'il est possible d'assurer à distance l'alimentation en courant et en fluide de refroidissement. Le fluide de refroidissement (dont le débit variable peut atteindre 10 l/min) est pompé sous pression (3, 50 kg/cm² au maximum) sur la cible, la butée d'arrêt des électrons et la source d'ions H. F. qui dissipent approximativement 800 W au total. Les auteurs décrivent l'ensemble du système et des appareils annexes.

ПРИМЕНЕНИЕ ТРУБОК ДЛЯ ПРОИЗВОДСТВА НЕЙТРОНОВ БОЛЬШОИ МОЩНОСТИ ДЛЯ ИЗМЕРЕНИЙ РЕАКТИВНОСТИ. Трубка для генерации импульсных нейтронов, на которой можно получать по крайней мере 10^8 н/имп в 10-микросекундном импульсе, разработана и включена в простой зонд диаметром 9 см с целью измерения реактивности. Этот зонд использовался в ряде реакторов нулевой мощности.

Диапазон этих измерений можно расширить в результате применения хорошо разработанного метода анализа передаточной функции. Такое расширение связано с разработкой другой трубки для генерации нейтронов с большим постоянным выходом, на которой можно модулировать при частотах вплоть до 1000 гц. Такая трубка сконструирована в результате использования радиочастотного источника ионов, из которого смешанный пучок ионов дейтерия и трития ускоряется на мишень, загруженную смесью дейтерия и трития. Свободный тритий можно безопасно обрабатывать в отпаянной трубке такого типа. На разработанной трубке обеспечивается постоянный выход 10^{10} н/сек при ускоряющем напряжении 120 кв и общем токе в трубке 1,8 ма. Поскольку смесь дейтерия и трития используется как в источнике ионов, так и в мишени, достигается постоянная циркуляция газа между мишенью и источником ионов, в результате достигнут устойчивый выход нейтронов и период жизни мишеней продлен свыше 100 часов.

Выход нейтронов можно модулировать путем изменения мощности, подаваемой на радиочастотный источник ионов. Модуляция квадратной волны обеспечивается в диапазоне частот от 0,017 гц до 5 кгц, что соответствует длине импульсов от 30 до 100 сек. Обсуждаются факторы, определяющие время увеличения импульсов нейтронов.

Трубка вся помещается внутри металлического цилиндра диаметром 18 и длиной 91 см. Энергия, в том числе ускоряющее напряжение величиной 120 кв, подается через пробку и розетку к одному концу цилиндра, а также на соединения для шлангов охладителя. Таким образом, полная сборка может быть помещена в реактор нулевой мощности для экспериментальных целей, при этом ею можно управлять дистанционно подачей соответственно энергии и охладителя.

Жидкость охладителя (с переменной скоростью потока вплоть до 10 л/мин.) накачивается под давлением (макс. 50 фунт/дюйм²) к мишени, стопору электронов и радиочастотному источнику ионов, которые рассеивают мощностью максимально 800 вт.

Описывается конструкция полной системы и ее оборудование.

TUBO GENERADOR DE NEUTRONES DE ALTO RENDIMIENTO PARA MEDICIONES DE REACTIVIDAD. Para medir la reactividad se ha construido y montado en una sonda corriente de 9 cm de diámetro, un tubo generador de neutrones pulsados que puede producir como mínimo 10^8 neutrones por impulso de 10 μs. La sonda se utilizó en varios reactores de potencia nula. La gama de mediciones se puede ampliar gracias al método bien conocido del análisis de la función de transferencia. Para ello se necesita construir otro tubo generador de neutrones de gran rendimiento continuo que pueda modular a frecuencias de hasta 1000 Hz. Este tubo se construyó empleando una fuente iónica de radiofrecuencias que emite un haz acelerado de deuterones y tritones mezclados; el haz se dirige hacia un blanco cargado con una mezcla de deuterio y de tritio. El tritio libre se puede manipular con toda seguridad en un tubo sellado de estas características. Este tubo generador tiene un rendimiento continuo de 10^{10} n/s a una tensión de aceleración de 120 kV, siendo la corriente total en el tubo de 1, 8 mA. Como se utiliza una mezcla de deuterio y de tritio tanto en la fuente iónica como en el blanco, se logra una circulación continua del gas entre una y otro, con lo que el rendimiento neutrónico es estable y la duración de los blancos es muy superior a 100 h. El rendimiento neutrónico puede modularse variando la potencia suministrada a la fuente iónica de radiofrecuencias. Se han obtenido ondas cuadradas en una gama de frecuencias comprendida entre 0, 017 Hz y 5 kHz, lo que corresponde a anchuras del impulso de 30 s y 100 μs, respectivamente. En la memoria se examinan los factores que regulan el tiempo de subida del impulso neutrónico. El tubo completo se coloca dentro de un cilindro metálico de 18 cm de diámetro y 91 cm de altura. La corriente, en especial la tensión de aceleración de 120 kV, se suministra mediante una conexión

en uno de los extremos del cilindro; lo mismo se hace con las conexiones de las tuberías de refrigeración. De esta manera el dispositivo completo puede utilizarse para los experimentos en un reactor de potencia nula, pues se puede regular a distancia la corriente y el flúido de refrigeración. El refrigerante líquido (cuyo caudal varía y puede llegar a 10 l/min) se bombea a presión (3, 50 kg/cm² como máximo) sobre el blanco, la trampa de electrones y la fuente iónica de radiofrecuencia que juntos disipan aproximadamente 800 W. La memoria describe el sistema completo y el equipo auxiliar.

1. INTRODUCTION

The use of a pulsed neutron source for reactivity measurements has been described by SIMMONS and KING [1], BECKURTS [2] and others [3, 4]. In these measurements, which can be made on subcritical or zero-energy reactors, the source is situated within the assembly and provides a pulse of 14-MeV neutrons. The subsequent time dependence of the neutron flux is used to measure the reactivity.

Pulsed neutron systems for reactivity measurements have been described by KELLY et al. [5] and by CARR [6]. A similar system using a tube described by HAWKINS and SUTTON [7] has been designed and used for reactivity measurement in the Zenith Reactor. All these systems used neutron tubes based on the D(t, n)He^4 reaction but were limited in output to about 10^7 neutrons per pulse.

An extension of this type of reactivity measurement to large reactor assemblies with more rapid and precise accumulation of data has been achieved with a pulsed tube capable of producing 5×10^8 neutrons per pulse in a 10-μs pulse. This tube, which has been described in Ref. [8] and is shown in Fig. 1, consists of a P.I.G. (Philips Ion Gauge) ion source from

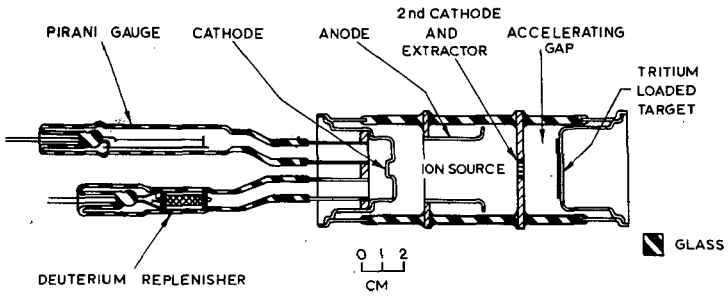


Fig. 1

Type-K neutron generator showing construction and electrode arrangement

which a beam of deuterium ions is accelerated across a 1.6-cm gap onto a tritium-loaded target. The performance characteristics of the tube are given in Fig. 2. The tube has been incorporated in a 9-cm diameter, 45-cm long probe as shown in Fig. 3. The probe is connected with a high-voltage cable to a 150-kV pulse transformer up to 7 m from the probe. The complete system will operate for well over 50 000 pulses with an output of 10^8 neutrons per pulse and has been used in several zero-energy reactors.

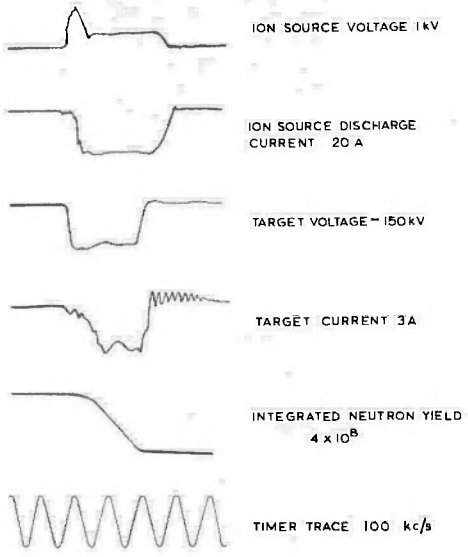


Fig. 2

Typical pulse waveforms for type-K generator

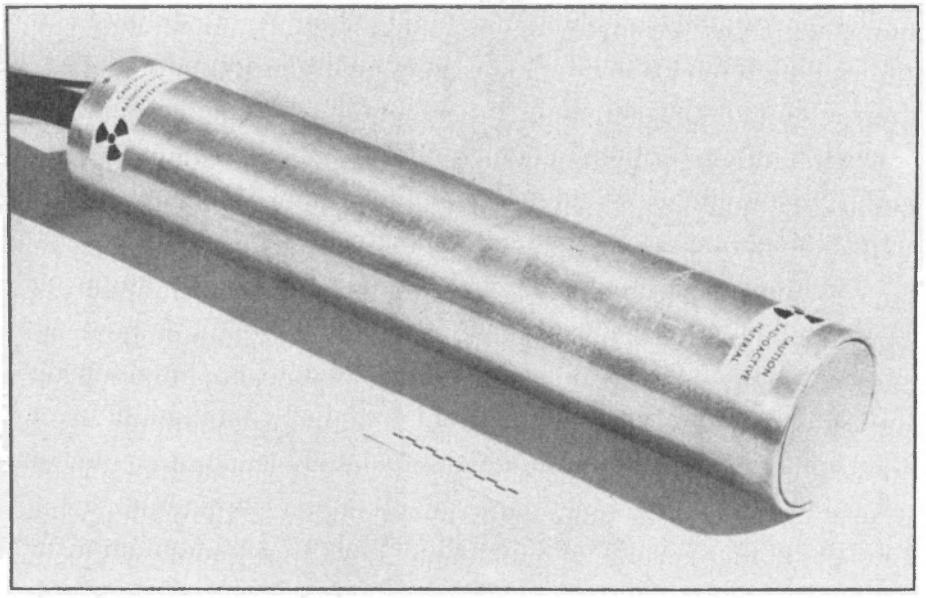


Fig. 3

Complete reactor probe containing type-K neutron generator

A further advance in this type of measurement is envisaged, in which pulses of neutrons of random pulse length are injected and the transfer function analysis technique is used. Such measurements on zero-energy reactors require a neutron output of about 10^{10} n/s with square-wave modulation at frequencies from 0.0167 c/s to 5 kc/s, corresponding to pulse lengths of from 30 s to 100 μs. A high-output neutron source suitable for this application has been developed at the Services Electronics Research Laboratory.

2. DESIGN CONSIDERATIONS

Sealed-off neutron tubes have significant advantages over either radiochemical sources or continuously pumped accelerators for this application. Radiochemical sources have inadequate outputs and cannot be modulated over the required range of frequencies. Although continuously pumped accelerators using the D-T reaction have sufficient output initially, the output decays rapidly due to dilution of the tritium-loaded target with deuterium from the ion beam. The same problem can be overcome in a sealed-off neutron tube by using a mixture of deuterium and tritium in both the target and the ion source. This solution is difficult to apply to accelerators because of the health physics problems involved in recirculating tritium gas.

3. THE TYPE-L NEUTRON SOURCE (10^{10} n/s)

3.1. Source design and construction

This source [9], which is shown in Figs. 4 and 5, will give a stable continuous output of 14-MeV neutrons at the rate of at least 10^{10} n/s for over 100 h, and is designed to meet the modulation requirements already mentioned. The source has applications in the field of neutron activation analysis as well as for reactor measurements*.

This tube uses an RF ion source to provide a beam of deuterium and tritium ions which are accelerated onto the target to produce neutrons. It operates as follows.

The replenisher is heated to give a pressure of 15 μm of a 50/50 mixture of deuterium and tritium in the tube. An RF discharge is struck in the ion source region by feeding power at a frequency of 15 Mc/s to a coil of about six turns wound around the glass ion source envelope. The glass extractor shield and the vitreous enamel prevent the metal extractor from being sputtered by the RF plasma.

Ions are extracted from the plasma through the central hole in the extractor by applying a potential of -120 kV to the target shield relative to the extractor (Fig. 6). The beam of ions formed passes through the central hole of the target shield and impinges on the target which is electrically insulated from the target shield and held at a potential of +400 V relative to it in order to suppress secondary electrons formed by the ion bombardment of the target.

---

* The source is now commercially available from Elliott Electronic Tubes, Ltd., Elstree Way, Borehamwood, Hertfordshire, England.

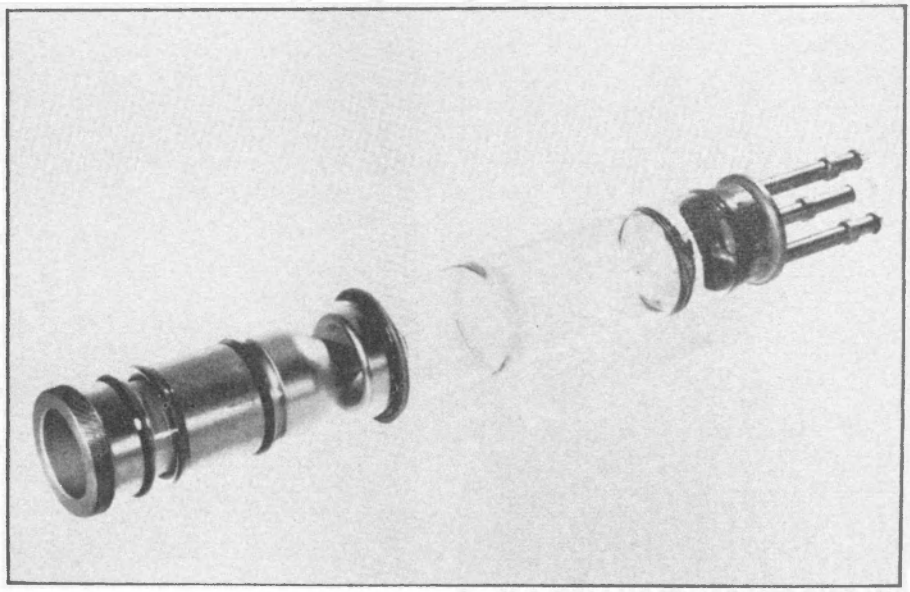


Fig. 4

Neutron generator type-L

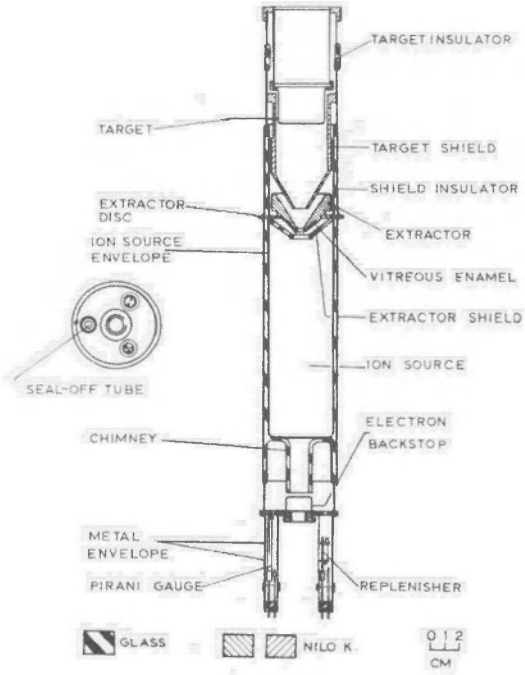


Fig. 5

Neutron generator type-L

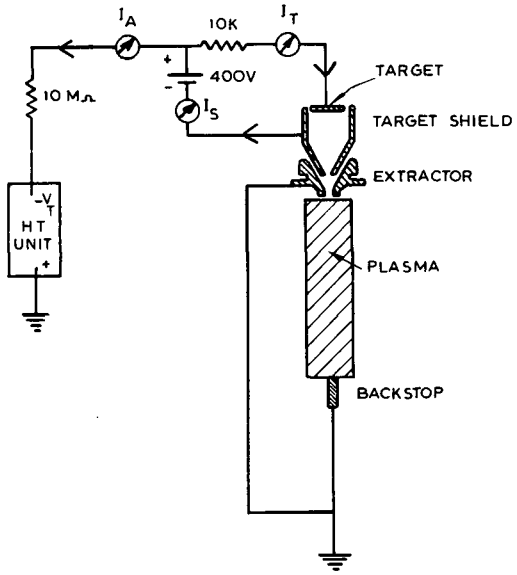


Fig. 6

High-tension circuit

This voltage also serves to collect some of the electrons formed by ionization of the gas inside the target shield by the ion beam and in fact more electrons are collected by the target than fast ions and hence the directions of the net positive currents to the electrodes are as shown in Fig. 6.

Some of the electrons formed inside the target shield and in the ion accelerating region are accelerated by the main electric field back into the ion source. This beam of backstreaming electrons impinges on the electron backstop which is a molybdenum cup, inside which coolant is circulated to dissipate the heat generated by stopping the electrons.

The target consists of a molybdenum cup which has a layer of erbium evaporated on it, in which deuterium and tritium are absorbed. Erbium is one of the rare earth materials which can be used for hydrogen isotope targets at much higher temperatures than titanium [10]. This can be important in high-power neutron tubes because of the heat dissipated by the ion beam at the target.

Breakdown between the target shield and extractor electrodes is prevented by arranging that their spacing is such that the region of operation is on the low-pressure x distance side of the minimum in the Paschen breakdown curve.

3. 2. Source operating characteristics

Figures for normal source operating conditions are given in Table I. Details of the container which has been designed for the source are given in section 4.

TABLE I

NORMAL SOURCE OPERATING CONDITIONS

Pressure	15 μm Hg
Ion source power	500 W into RF oscillator
Target voltage, V_T	100 - 120 kV
Tube current, I_A	1.6 mA
Target current, I_T	0.2 mA
Shield current, I_S	1.8 mA
Target bias voltage	400 V
Neutron output	10^{10} n/s

3.3. Modulation of the type-L neutron source

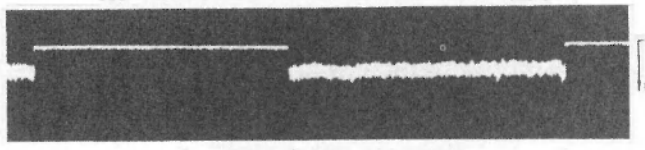
The neutron output can be modulated by modulating the RF power used to excite the ion source discharge. Square wave modulation has been carried out for frequencies ranging from 5 kc/s to 0.0167 c/s and some sample neutron yield waveforms are shown in Figs.7 and 8. To obtain these waveforms a scintillator was used which gave pulses for individual neutrons detected. The pulses were amplified and passed through a discriminator into a sample ratemeter circuit with a variable time constant, and the output from this was displayed on an oscilloscope. The ratemeter time constant was always chosen to be short compared with the neutron output pulse length being used. Thus the hash seen on the waveforms is caused by statistical fluctuations in the neutron detection efficiency.

The detection efficiency could not be raised sufficiently to make precise conclusions about the quality of the modulation at 5 kc/s. Waveforms for 1 kc/s and lower frequencies are shown and in this range it appears that a specification of pulse rise times of less than one tenth of the pulse length can be met. In general the yield cut-off at the end of the pulses is faster than the rise time especially at the lower frequencies.

An RF discharge causes an equilibrium quantity of gas to be absorbed on the walls of the ion source which is liberated fairly rapidly when the discharge ceases. With the particular RF oscillator being used it was found that for modulation frequencies less than 1 c/s this effect caused a rise in pressure in the source between pulses sufficient to cause the re-striking of the discharge to be erratic. This was overcome by maintaining a weak discharge in the source between main pulses, i.e. by having a 90% depth of modulation.

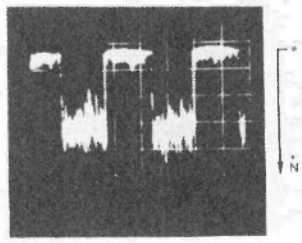
At the very lowest frequencies, e.g. see the 0.028-c/s waveform in Fig.8, in spite of the weak discharge the pressure rises sufficiently to cause a mismatch between the oscillator and the discharge resulting in a ramp at the beginning of the main neutron pulse. However, the neutron yield levels off as soon as the discharge has restored the pressure to its normal value.

At all frequencies above 1 c/s a depth of modulation of 100% was used. No examples of modulation with varying mark to space ratio have been shown

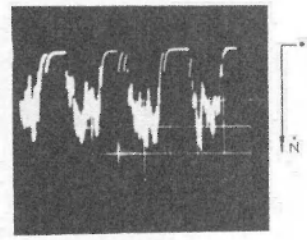


1 c/s

Depth of Modulation 90%



50 c/s



1 kc/s

Depth of Modulation 100%

$\dot{N}$ = Neutron yield per second
t = Time

Fig. 7

Neutron pulse shapes for square wave modulation



0·083 c/s Square wave modulation



0·028 c/s Square wave modulation

N = Neutron Yield t = Time
Depth of Modulation 90%. Maximum Neutron Yield during Pulses = 10^{10} neutrons/s

Fig. 8

Neutron yield waveforms

but this has been carried out. Modulation of the source by modulating the target voltage has not yet been fully investigated. This would seem to be feasible for frequencies below 1 c/s.

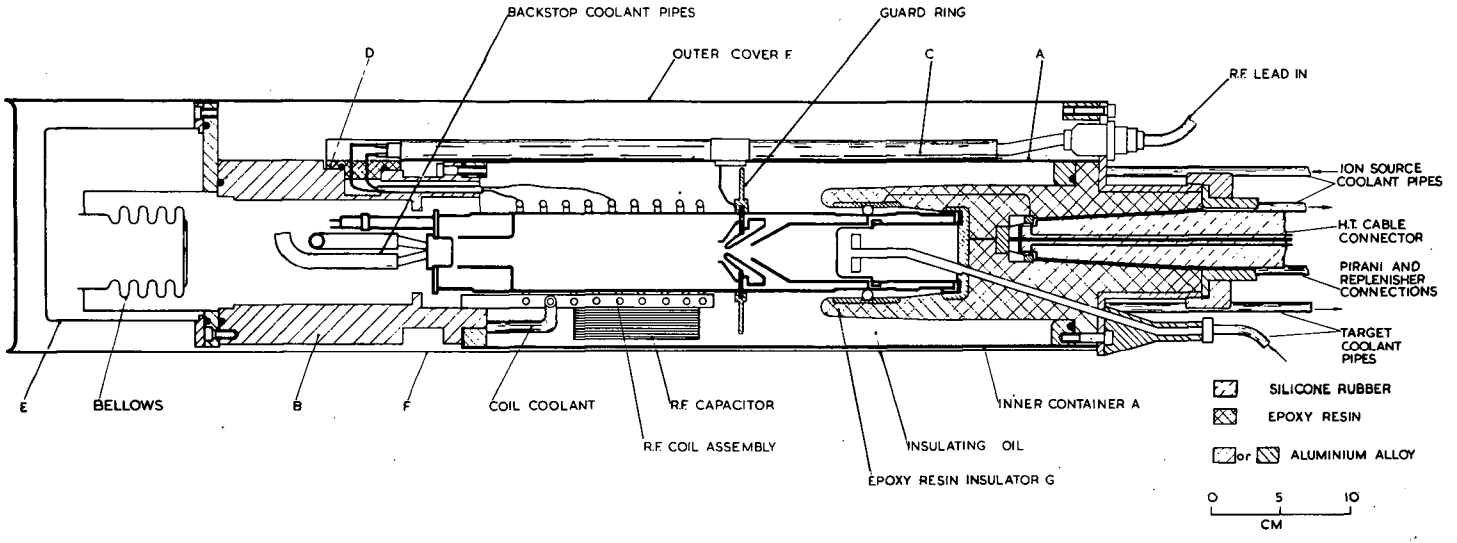


Fig. 9

Type-L source container for reactor applications

4. TYPE-L SOURCE CONTAINER FOR REACTOR APPLICATIONS

The source container, which has been developed at the Atomic Weapons Research Establishment for use in a zero-energy reactor, is shown in Figs. 9 and 10. It has been designed to be lowered into a fuel element cavity approxi-

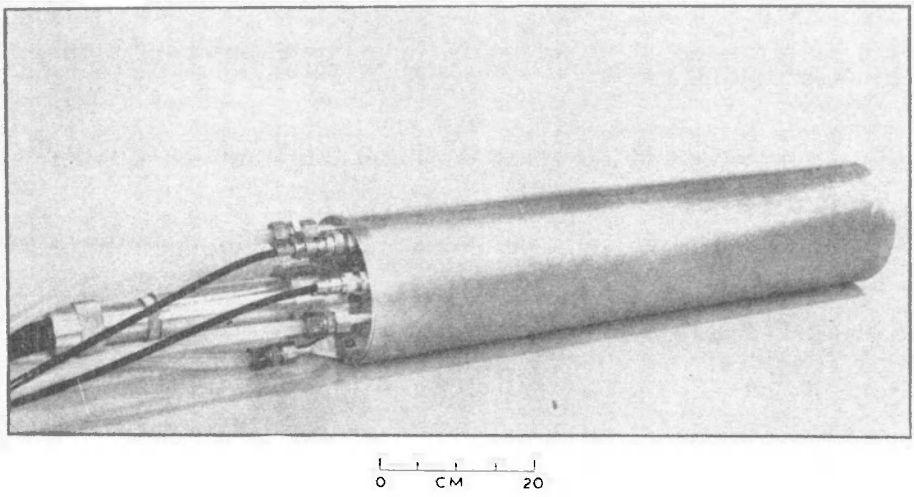


Fig. 10

Type-L neutron source container for reactor applications

mately 18 cm in diam. It has all its coolant and electrical connections emerging from one end and has been operated at a distance of 12 m from its control gear.

The constructional layout is as follows. The type-L source is screwed into the epoxy resin insulator G which has moulded-in electrodes that make electrical contact with the source target and target shield electrode. The -120 kV supply to the target is fed in via the standard high-voltage coaxial plug and socket connection on the insulator, as is also the supply for the target shield which is 400 V negative with respect to the target. Tubes are moulded into the insulator to enable the coolant fluid to be pumped to and from the rear face of the target, and there is a neoprene seal to isolate the coolant from the remainder of the container.

Clamped to the insulator is the inner container A and the main body B which are filled under vacuum with dried and filtered insulating oil to provide good electrical insulation around the source. Any expansion of the oil from temperature changes is taken up by the bellows. A guard ring is clamped to the extractor disc of the source to eliminate regions of high non-uniform electric stress around this electrode.

The whole assembly is contained within the outer cover F which is 17.5 cm in diam. and 78-cm long. Aluminium alloys are used whenever possible for metal parts as this material has a fairly short "half-life" after activation.

To excite the plasma in the ion source, RF power is led in via a cable from a variable frequency (10 - 18 Mc/s) oscillator onto the primary coil of an RF transformer which surrounds the ion source. This assembly is mounted on formers supported by the body B. The secondary coil of the transformer is shunted by a fixed 80 pF capacitor.

The pirani and replenisher circuits are protected from RF pick-up by screening of the RF lead-in and also by incorporating suitable LC filter elements.

Several coolants were considered for cooling the source. Arcton-113, i.e. CCl_2FCClF_2, fluid was finally chosen, since this, besides being a good coolant, is also a good electrical insulator, the latter being especially necessary as approximately 150 W of heat must be removed from the target which is at high voltage. The coolant enters the container through hoses made of nylon, which have the advantage of being very robust and also chemically resistant to Arcton-113. There are four coolant hoses, two for cooling the target and two for cooling the ion source end of the neutron generator. For the latter purpose the coolant passes through one of the RF coils to cool the coil and is then circulated behind the electron backstop of the source. The container has been designed for use on the DIMPLE reactor at the Atomic Energy Establishment, Winfrith.

5. CONCLUSION

Two types of compact neutron source have been developed which are in a convenient form for insertion into reactors. One gives 10-μs pulses of neutrons at up to 5×10^8 neutrons per pulse and the other gives a continuous yield of 10^{10} n/s which can be modulated over a wide range of pulse widths. These sources should prove to be valuable tools in reactor physics research and the L-tubes should be especially useful for transfer function analysis and binary cross-correlation measurements.

ACKNOWLEDGEMENTS

This paper is published by permission of the Ministry of Defence and the United Kingdom Atomic Energy Authority.

REFERENCES

[1] SIMMONS, B.E. and KING, J.S., Nucl. Sci. Engng 3 (1958) 595.
[2] BECKURTS, K.H., Nucl. Instrum. Meth. 11 (1961) 144.
[3] FULTZ, S.C., Nucl. Sci. Engng 6 (1959) 313.
[4] COPEZ, W.M. and BEYSTER, J.R., Nucl. Sci. Engng 12 (1962) 190.
[5] KELLY, R.D., HAMILTON, J.C. and BEAVIS, L.C., Rev. Sci. Instrum. 32 (1961) 178.
[6] CARR, B.J., Nucleonics 18 (1960) 75.
[7] HAWKINS, P.O. and SUTTON, R.W., Rev. Sci. Instrum. 31 (1960) 241.
[8] LOMER, P.D., WOOD, J.D.L.H. and BOTTOMLEY, R.C., Nucl. Instrum. Meth. 26 (1964) 7 - 12.
[9] BOUNDEN, J.E., LOMER, P.D. and WOOD, J.D.L.H., Nucl. Instrum. Meth. (March 1965).
[10] REDSTONE, R. and ROWLAND, M.C., Nature, Lond. 201 (1964) 1115.

SYSTÈME A FRÉQUENCE ET LARGEUR D'IMPULSIONS AJUSTABLES PERMETTANT LA PULSATION ET LA MODULATION DE MILIEUX MULTIPLIANTS SOUS-CRITIQUES A NEUTRONS RAPIDES

M. DUQUESNE*, R. GERBIER**, F. LYON* ET A. SCHMITT*
CENTRE D'ÉTUDES NUCLÉAIRES DE CADARACHE, FRANCE

Abstract — Résumé — Аннотация — Resumen

CONTROLLABLE PULSE FREQUENCY AND WIDTH SYSTEM FOR PULSING AND MODULATING FAST-NEUTRON CORE ASSEMBLIES. The authors describe a system for producing neutron bursts of independently controllable width and frequency. The rise and quenching times of these bursts are of the order of a few nanoseconds. The system is applied to high-frequency pulsed and modulated experiments. Rapidly quenched neutron bursts are produced by deflection of a pure deuteron beam which has previously been accelerated and sorted.

Ions other than atomic deuterons are removed after acceleration in a 10° magnetic sorting field. Consideration is also being given to a pre-acceleration sorting system offering the advantage of reduced bulk. The deuteron beam passes through the space between two plates where there is normally an electrostatic field which deflects the beam onto the surfaces of a diaphragm. Application of a very high potential pulse to the first plate cancels the field and thus brings the beam rapidly onto the neutron-producing target (beginning of the burst). The second plate then receives a pulse of the same type which restores the field and removes the beam from the target (end of the burst). The pulse rise time is of the order of 10 ns; disappearance from the target is faster. The duration of the burst can be controlled as required within reasonable limits by suitably increasing the interval between the two pulses.

In some cases ion transit time in the plates is not negligible in relation to the duration of the step applied to them. In such cases, one of the plates is replaced by a travelling wave line to which the two pulses are applied successively. The potential pulse thus accompanies the deuteron cluster producing the burst. The burst times can thus be reduced below 4 ns. The first stages of the voltage step generators are transistorized. The output tubes are sealed-disc valves providing a 1500-V step in a few nanoseconds. A 50-MHz double tetrode is employed for pulses for the delay line. A detection system comprises a scintillator-photomultiplier device incorporating a coincidence-anticoincidence unit, a time analyser and a digital data recorder.

SYSTÈME A FRÉQUENCE ET LARGEUR D'IMPULSIONS AJUSTABLES PERMETTANT LA PULSATION ET LA MODULATION DE MILIEUX MULTIPLIANTS SOUS-CRITIQUES A NEUTRONS RAPIDES. Les auteurs on mis au point un système permettant la production de bouffées de neutrons de largeur et de fréquence de récurrence réglables indépendamment. Les temps de montée et de descente de ces bouffées sont de l'ordre de quelques nanosecondes. Ce système est appliqué aux expériences pulsées et modulées à haute fréquence. Pour la production de bouffées de neutrons à extinction rapide, on procède par déflection d'un faisceau de deutérons purs préalablement accélérés et triés.

Les ions autres que les deutérons atomiques sont éliminés après accélération dans un aimant de tri à 10°. Les auteurs étudient également un système de triage avant accélération qui aurait l'avantage d'un encombrement réduit. Le faisceau de deutérons passe dans l'espace compris entre deux plaques où règne normalement un champ électrostatique qui défléchit le faisceau sur les parois d'un diaphragme. On applique à la première plaque une très large impulsion de tension qui annule le champ, ce qui a pour effet d'amener rapidement le faisceau sur la cible neutronigène (début de la bouffée). La deuxième plaque reçoit ensuite une impulsion du même type qui rétablit le champ et fait disparaître le faisceau de la cible (fin de la bouffée). Le front de montée des impulsions est de l'ordre de 10 ns; le temps de disparition sur la cible est inférieur à cette dernière

---

* Association EURATOM-CEA-SECNR

** Laboratoire des accélérateurs - CEN de Grenoble

valeur. La durée de la bouffée peut être réglée à volonté dans les limites raisonnables par un retard convenable de la seconde impulsion par rapport à la première.

Dans certains cas, le temps de transit des ions dans les plaques n'est pas négligeable par rapport à la durée de l'échelon qui leur est appliqué. On remplace alors l'une des plaques par une ligne à onde progressive à laquelle sont appliquées successivement les deux impulsions. L'impulsion de tension accompagne ainsi le paquet de deutérons qui produit la bouffée. Les fronts de bouffée peuvent ainsi être ramenés au-dessous de 4 ns. Les générateurs à échelon de tension sont transistorisés dans leurs premiers étages. Les tubes de sortie sont des lampes à disque scellé permettant d'obtenir un échelon de 1500 V en quelques nanosecondes. Les auteurs utilisent une double tétrode de 50 MHz pour les impulsions destinées à la ligne de retard. Le système de détection utilise un dispositif scintillateur-photomultiplicateur dont la chaîne comprend un ensemble coïncidence-anticoïncidence, un analyseur de temps et un enregistreur numérique des informations.

СИСТЕМА РЕГУЛИРУЕМЫХ ЧАСТОТЫ И ШИРИНЫ ИМПУЛЬСА, ДАЮШАЯ ИМПУЛЬС И МОДУЛЯЦИЮ РАЗМНОЖАЮЩИХ СРЕД НА БЫСТРЫХ НЕЙТРОНАХ. Нами разработана система, которая дает возможность получать нейтронные импульсы независимо от регулируемой ширины и частоты следования. Время нарастания и затухания этих импульсов составляет порядка нескольких наносекунд. Данная система используется при проведении импульсных и модулируемых опытов высокой частоты. Для получения нейтронных импульсов с быстрым затуханием применяется отклонение пучка чистых дейтонов, которые предварительно были ускорены и отобраны.

Ионы, которые не являются дейтонами, были устранены после ускорения в сортировочном магните при 10°. Нами изучалась также система отбора перед ускорением, которая имела бы преимущество в виде уменьшенных габаритных размеров. Пучок дейтонов проходит через пространство, находящееся между двумя пластинками, где обычно имеется электростатическое поле, отклоняющее пучок на стенки диафрагмы. На первую пластинку направляется очень широкий импульс напряжения, который снимает поле, и это делается для того, чтобы быстро направить пучок на мишень, генерирующую нейтроны (начало импульса). Затем вторая пластинка получает импульс того же типа, который восстанавливает поле и снимает пучок с мишени (конец импульса). Фронт нарастания импульсов порядка 10 наносекунд; время исчезновения с мишени ниже этого последнего значения. Продолжительность импульса может свободно регулироваться в разумных пределах соответствующей задержкой второго импульса по отношению к первому.

В определенных случаях время пролета ионов в пластинках имеет определенное значение по отношению к постепенной продолжительности, которая к этому времени применяется. Далее одну из пластинок заменяют увеличивающейся линией, к которой последовательно применяются два импульса. Импульс напряжения сопровождает, таким образом, сгусток дейтонов, который дает импульс.

Ступенчатые генераторы напряжения в первых ступенях имеют транзисторы. Выходными лампами являются электронные лампы с дисковыми выводами, которые дают возможность получать серию 1500 вольт в течение нескольких наносекунд. Мы используем двойные тетроды по 50 мгц для импульсов, предназначенных для линии задержки.

В системе обнаружения применяется сцинтилляционно-фотоумножающее устройство, цепь которого состоит из схемы совпадений-антисовпадений, временного анализатора и цифрового самописца информации.

SISTEMA DE FRECUENCIA Y AMPLITUD DE IMPULSO AJUSTABLES, PARA PULSAR Y MODULAR MEDIOS MULTIPLICADORES DE NEUTRONES RAPIDOS. Los autores han ideado un sistema que permite regular independientemente la amplitud y la frecuencia de los impulsos neutrónicos. El tiempo de subida y bajada de los impulsos es del orden de algunos nanosegundos. Este sistema se emplea en los experimentos con neutrones pulsados y modulados de alta frecuencia. Para producir impulsos neutrónicos de extinción rápida, se desvía un haz de deuterones puros previamente acelerados y seleccionados.

Los iones distintos de los deuterones se eliminan después de la aceleración en un imán selector de 10°. Los autores estudian igualmente un sistema para efectuar la selección antes de la aceleración que presenta la ventaja de ser de pequeñas dimensiones. El haz de deuterones atraviesa el espacio comprendido entre dos placas en las que hay normalmente un campo electroestático que desvía el haz hacia las paredes de un diafragma. Se aplica a la primera placa un fortísimo impulso de tensión que anula el campo, con lo que se dirige rápidamente el haz hacia el blanco neutronígeno (comienzo del impulso). La segunda placa recibe seguidamente un impulso del mismo tipo que restablece el campo y hace desaparecer el haz del blanco (final del impulso). El frente de subida de los impulsos es del orden de 10 ns y el tiempo de desaparición en el blanco es inferior a este valor.

La duración del impulso puede ajustarse a voluntad dentro de límites razonables retardando adecuadamente el segundo impulso con relación al primero.

En ciertos casos el tiempo de tránsito de los iones en las placas no es despreciable con respecto al tiempo durante el cual se aplica el incremento de tensión. En estas circunstancias, se sustituye una de las placas por una línea de onda progresiva a la que se aplican sucesivamente los dos impulsos. El impulso de tensión acompaña así al paquete de deuterones que produce el impulso. Los frentes de impulsos pueden reducirse, de este modo, a menos de 4 ns. Los generadores de tensión escalonada están transistorizados en sus primeras etapas. Los tubos de salida están constituidos por válvulas de disco sellado que permiten obtener un incremento de tensión de 1500 V en algunos nanosegundos. Los autores han utilizado un doble tetrodo de 50 MHz para los impulsos destinados a la línea de retardo. El sistema de detección emplea un dispositivo de centelleo y un fotomultiplicador cuyo circuito comprende un conjunto coincidencias-anticoincidencias, un analizador de tiempos y un registrador numérico.

1. INTRODUCTION

Le mémoire traite de certains problèmes liés à l'application de la technique des neutrons pulsés à l'étude physique de milieux sous-critiques à neutrons rapides. Ainsi, la bouffée de neutrons injectée dans de tels milieux doit avoir un temps d'extinction aussi court que possible, compte tenu de la plus courte période de décroissance à mesurer. Après chaque détection, le temps mort de l'appareillage d'enregistrement en mémoire de l'information est toujours grand par rapport à la période de pulsation utilisée dans ce type d'expériences. Ce temps mort introduit ou non une déformation de la décroissance enregistrée par rapport à la décroissance à mesurer, suivant la technique de détection utilisée.

Nous décrirons d'abord un système original de pulsation du faisceau d'ions issu d'un accélérateur électrostatique, ce système pouvant s'adapter à la modulation à haute fréquence en créneaux carrés de ce même faisceau.

Nous comparerons ensuite deux techniques d'enregistrement du double point de vue de la fidélité de la décroissance enregistrée et de la durée totale de l'expérience pour un même nombre d'informations enregistrées.

2. SYSTÈME DE PULSATION RAPIDE D'UN ACCÉLÉRATEUR ÉLECTROSTATIQUE

2.1. Principe du système de pulsation

2.1.1. Objet de l'étude

Nous avons pour but de créer, sur la cible d'un accélérateur électrostatique, des impulsions de courant ionique à fronts de montée et de descente plus courts que 10 ns, la durée de ces impulsions étant comprise entre 10 et 500 ns, et la fréquence de répétition étant variable à volonté. Ces exigences nous ont amenés à renoncer à une pulsation par procédé à haute fréquence [1], qui ne présentait pas la souplesse souhaitable, et à faire l'essai
a) d'un dispositif utilisant un système à deux plaques de déflexion alimentées par deux échelons de tension décalés dans le temps, suivant le principe exposé par AALAN [2], et
b) d'un dispositif original utilisant une seule plaque et une ligne à progression d'ondes alimentée par un créneau de tension [3].

2.1.2. Le système à deux plaques à échelons de tension

2.1.2.1. Disposition

Le système de déflexion présente les dispositions géométriques représentées à la figure 1.

La plaque A reçoit une impulsion de tension de durée t* dont seul le front d'attaque est raide; le front de fin d'impulsion peut être quelconque. La plaque B reçoit la même impulsion décalée de Δt ($\Delta t < t^*$).

La différence de tension $V_A - V_B$ est alors représentée par un créneau de durée Δt dont les deux fronts sont raides (fig. 2). La durée du front de

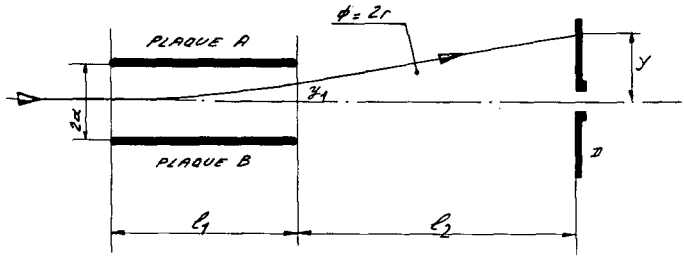


Figure 1

Disposition géométrique.

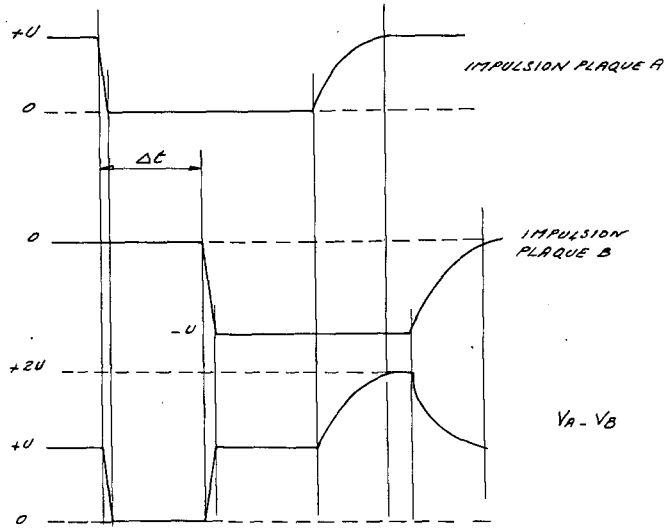


Figure 2

Forme des impulsions.

ce créneau représente le temps de balayage du faisceau entre la position défléchie (faisceau effacé) et la position directe (faisceau frappant la cible), ou inversement.

Le transitoire intéressant l'impulsion de courant ionique sur la cible dépend de ce temps de balayage et aussi du diamètre D du diaphragme (fig. 1) et du diamètre 2 r du faisceau.

2.1.2.2. Dynamique de la déflexion

L'étude théorique de la dynamique de ce système est détaillée dans le rapport cité en référence [4]. Un exemple des résultats obtenus est donné par la figure 3, qui représente le temps de balayage sur la cible t_D en fonc-

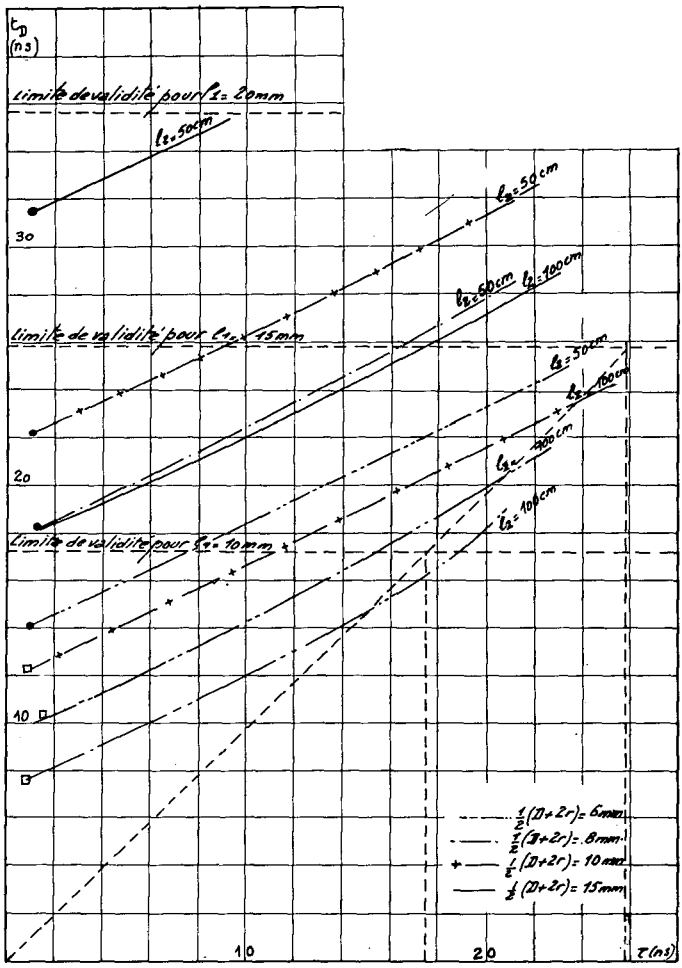


Figure 3

Système à 2 × 1 plaques.
Temps de balayage pour diverses valeurs de (D + d),
en fonction du temps de montée de l'impulsion
(E_0 = 1000 V/cm), V = 350 kV.

tion du temps de montée de l'impulsion (D représente, sur cette figure, le diamètre du diaphragme et r le rayon du faisceau d'ions).

Il est remarquable de constater qu'il est impossible d'obtenir un temps de balayage inférieur au temps de montée τ. Le mieux que l'on puisse espérer, dans le cas où τ est supérieur à 15 ns, est un temps de balayage du même ordre de grandeur; pour des τ très faibles, c'est le temps de transit dans les plaques (soit l_1/v_0 si v_0 est la vitesse longitudinale des ions) qui limite la vitesse de balayage.

2.1.3. Le système à ondes progressives

2.1.3.1. Disposition

Dans ce système, l'une des plaques est remplacée par une ligne à progression d'onde telle que la vitesse de déplacement de l'onde y soit v_0. Un créneau de tension est appliqué à cette ligne.

L'autre plaque est à un potentiel constant tel que le champ électrique, entre cette plaque et la ligne, soit nul entre la plaque et la section de ligne où se trouve appliqué le créneau. Nous considérons, ce qui revient au même, que les ions sont défléchis pendant le passage du créneau dans la ligne.

2.1.3.2. Dynamique du système

On montre [4] que, dans l'hypothèse idéale d'une montée linéaire de l'onde de tension, le temps de balayage est donné par

$$\theta = \frac{(D/2 + r)}{y_{max}} \cdot \tau$$

où y_{max} est la déviation maximale possible, compte tenu de la tension appliquée sur la ligne à progression d'ondes. θ est donc inférieur à τ (fig. 4).

2.1.4. Conclusion

Le système à deux plaques ne permet pas d'obtenir des temps de montée ou de descente de l'impulsion cible inférieurs à ceux de l'impulsion appliquée aux plaques.

Par contre, le système à onde progressive idéale amène à des temps de montée ou de descente nettement inférieurs (parfois, d'un facteur 2 ou 3) à ceux de l'impulsion appliquée à la ligne. Ce système apparaît donc nettement préférable.

Une solution approchée consisterait à avoir plusieurs paires de plaques successives alimentées avec le déphasage convenable: la réalisation pratique d'un tel appareillage pose autant de problèmes que celle d'un système à ligne à ondes progressives, et ce dernier lui a été préféré.

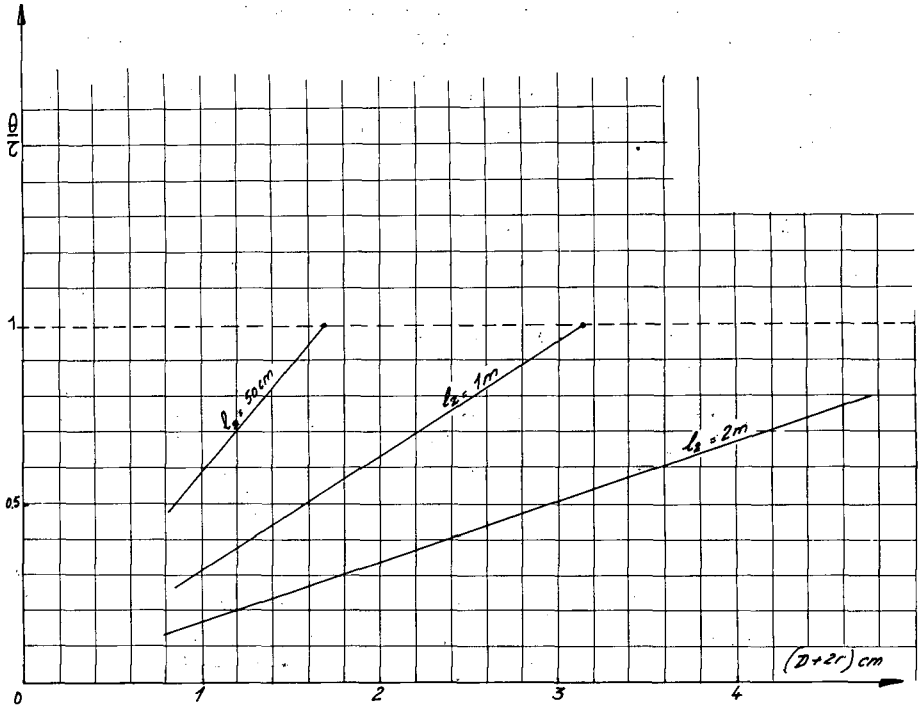


Figure 4

Temps de balayage pour une ligne à onde progressive idéale.

θ = temps de balayage,
τ = temps de montée,
E_0 = 500 V/cm,
V = 350 kV,
l_1 = 20 cm.

2.2. Description du système à ondes progressives

2.2.1. Généralités: adaptation de l'accélérateur

L'accélérateur utilisé est un SAMES électrostatique, d'une tension variable de 150 à 400 kV, et 1 mA de courant de deutons. Pour que le système de déflexion proposé soit utilisable, il faut

- obtenir de l'accélérateur un faisceau de deutons purs et suffisamment monocinétiques. Pour cela, un tri du faisceau brut est nécessaire;
- éliminer les bruits de fond neutroniques qui peuvent provenir, soit des faisceaux indésirables éliminés par le tri, soit des ions qui frappent le diaphragme de balayage ou les diaphragmes intermédiaires;
- résoudre le problème du montage sous vide d'une ligne à progression d'ondes susceptible d'être atteinte par le faisceau d'ions qui transporte une puissance notable;

- mesurer la forme de l'impulsion sur la cible sans déformer les fronts d'attaque et de descente, au moins au cours de la période de préparation des expériences.

Enfin, un générateur d'impulsions doit être conçu spécialement pour cette expérience en raison des caractéristiques très particulières qui lui sont demandées.

2.2.2. Electronique de pulsation

2.2.2.1. Générateur d'impulsion

La figure 5 présente le bloc-diagramme de l'électronique de pulsation. Le signal rectangulaire attaquant l'amplificateur de tension est fourni par

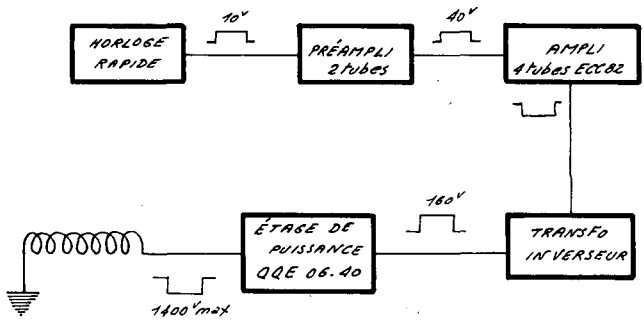


Figure 5

Schéma bloc de l'électronique de pulsation.

une horloge transistorisée. L'amplificateur (fig.6 et 7) est constitué par un préamplificateur à tubes à émission secondaire par un amplificateur distribué et par un étage de puissance. L'amplitude du signal de sortie peut être réglée de 800 à 1400 V, tout en conservant un front de montée et un front de descente de 10 ns.

2.2.2.2. Ligne à progression d'ondes

Cette ligne est constituée par un bobinage hélicoïdal en fil de cuivre argenté enroulé sur un mandrin d'araldite pure qui présente deux faces planes d'une largeur de 2 cm environ, afin d'obtenir un champ aussi uniforme que possible.

La longueur utile de ligne, dans une des réalisations ayant servi aux expériences, est de 23 cm. Telle qu'elle est dessinée, son retard électrique est de 50 ns correspondant au temps de transit dans le champ de deutons de 220 keV. Le temps de montée propre de cette ligne est de 7 ns, et son impédance caractéristique de 750 Ω.

Le conducteur de retour est constitué par un boîtier en cuivre de section rectangulaire relié à un noyau formé par une lame de cuivre disposée dans l'axe du mandrin, le tout étant à la masse. Les problèmes d'adaptation d'extrémité de ligne, qu'il faut surmonter pour éviter les réflexions, ont été ainsi correctement maîtrisés.

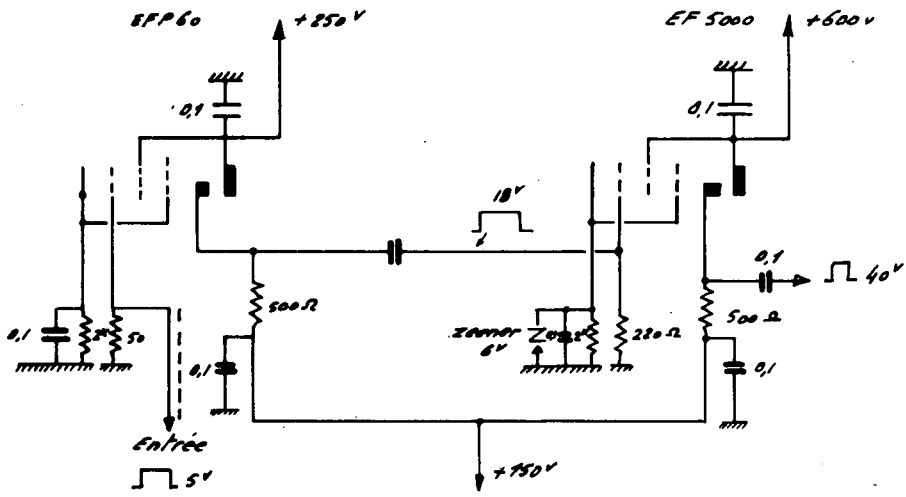


Figure 6

Détail du préamplificateur.
Préamplificateur, gain 8, temps de montée < 4 ns;
EFP 60 et EF 5000; penthode à émission secondaire.

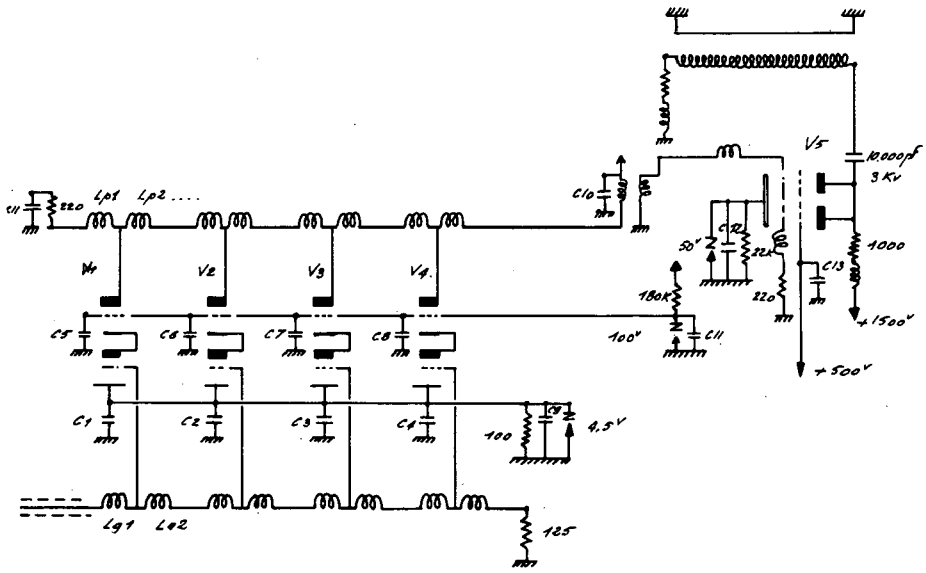


Figure 7

Ensemble de pulsation rapide.
Déflection à ondes progressives. Accélérateur GNP2. F 005-001.
C1 à C8: 1000 pf; C9 à C13: 10 000 pf; V1 à V4: E 182 CC; V5: QQE 0640;
T1: Transformateur inverseur. Tore ferrite LTT 2002.

2.2.2.3. Performances et discussion

L'impulsion de durée $\leq 1\ \mu s$ et de 1200 V d'amplitude relevée sur la ligne a des fronts de montée et de descente d'une durée inférieure à 12 ns. Elle ne présente pas d'ondulation de crête sensible. De toute façon, du fait que nous travaillons avec un diamètre de faisceau inférieur de 4 mm environ au diamètre du diaphragme balayé devant la cible, il faudrait une ondulation de près de 7% pour qu'il y ait ondulation du courant de cible.

2.2.3. Tri de faisceau et élimination du bruit de fond neutronique

2.2.3.1. Tri de faisceau

Le faisceau ne doit comporter que des ions d'un seul type (deutons) ayant tous la même vitesse. Or la source de l'accélérateur fournit normalement un faisceau complexe d'ions, parmi lesquels seulement 50 à 80% de deutons. Le tri de ce faisceau complexe est donc nécessaire pour que seuls les deutons purs entrent dans le système de déflexion, les ions moléculaires n'ayant pas la vitesse convenable.

Deux procédés différents sont employés pour ce tri:

- Tri en tête: après une pré-accélération de 20 kV [1], le faisceau est défléchi de 30° dans un analyseur placé en tête de l'accélérateur. Une lentille quadripolaire, qui suit l'analyseur, lui donne les caractéristiques requises pour l'attaque du tube accélérateur. Ce dispositif présente l'inconvénient d'exiger une forte puissance dans la tête haute tension de l'accélérateur.
- Tri après accélération: nous avons placé un aimant permanent après la fin de l'accélération. Un shunt magnétique permet de faire varier le champ magnétique autour de sa valeur moyenne (2500 G environ). L'angle de déflexion de 10° pour les deutons de 220 keV permet d'obtenir une séparation de 1 cm à 30 cm de la sortie de l'aimant.

2.2.3.2. Pulsation lente de la source

La source de l'accélérateur est allumée peu de temps (environ 2 μs) avant l'impulsion de déflexion, et éteinte aussitôt après. La synchronisation convenable est obtenue par une horloge rapide qui commande également les électroniques de comptage. Cette horloge déclenche le créneau de commande de source en avance de 2 μs sur l'impulsion électronique de déflexion.

Pour commander cette pulsation lente de source, on a préféré à tout autre système un transformateur d'isolement conçu pour fonctionner en impulsions [5] dont le détail de réalisation est représenté à la figure 8. Une différence de potentiel continue de 400 kV peut être appliquée entre primaire et secondaire: le primaire est à la référence de la masse, le secondaire à celle de la tête de l'accélérateur.

Le créneau de commande est différencié par ce transformateur; l'impulsion correspondant au début de créneau débloque l'oscillateur de 80 Mc/s de la source d'ions haute fréquence, celle-ci s'allume et le faisceau est

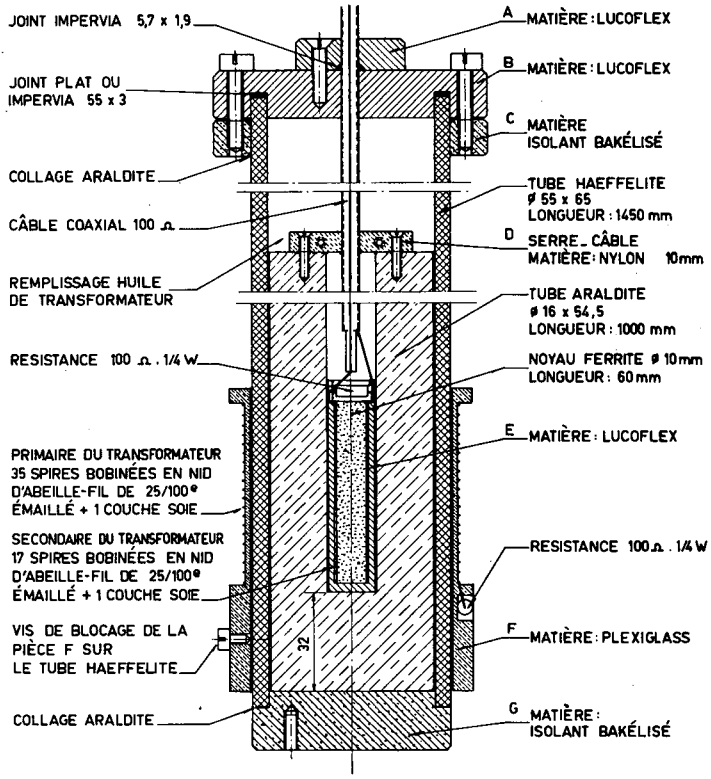


Figure 8

Transformateur d'impulsions isolé.

envoyé dans l'accélérateur. L'impulsion correspondant à la fin de créneau bloque l'oscillateur et la source s'éteint avec un retard de 1 à 2 μs [6].

2.2.3.3. Elimination du bruit de fond neutronique

Les neutrons parasites proviennent de la réaction (d, d) lorsque des ions deutérium frappent les parties de l'accélérateur qui ont pu retenir par absorption ou combinaison chimique du deutérium moléculaire ou atomique.

Le fait de ne laisser la source allumée que pendant le temps exactement nécessaire limite dans le temps la formation de neutrons parasites et diminue le risque de compter un coup fortuit entre deux bouffées. Toutefois, il est pratiquement impossible, en raison du temps de désionisation, d'obtenir une extinction de la source simultanée, ou même en avance sur l'impulsion de courant cible. Il y aura forcément un courant résiduel parasite qui viendra frapper la partie opaque du diaphragme de balayage pendant une à deux μs après la fin de l'impulsion de cible. De même le courant des molécules éliminées par l'aimant de tri frappera pendant le même temps le «beam catcher» . Enfin d'autres diaphragmes disposés sur le parcours du faisceau peuvent être des sources de neutrons de 3 MeV gênants.

Pour diminuer la quantité de neutrons parasites ainsi produits, on a choisi pour l'ensemble des diaphragmes du tantale non refroidi: à la température de fonctionnement, le tantale absorbe très peu de deutérium et le flux parasite est considérablement diminué. Par ailleurs, le canal d'entrée du réacteur n'étant pas dans l'axe des éléments de prolongateur qui précèdent le déflecteur, le blindage extérieur - polythène et cadmium - est assez efficace.

2.2.4. Détection du courant de cible

2.2.4.1. Généralités

La cible de l'accélérateur est normalement constituée par un disque supportant le tritium et refroidi à l'eau. Les capacités parasites rendent problématique la mesure correcte à l'oscilloscope de la forme de l'impulsion de courant ionique dont les fronts de montée sont inférieurs à 10 ns.

Dans ces conditions, on devra se contenter de faire une mesure soignée, sur une cible spécialement conçue, pendant la mise au point de l'appareillage qui précède l'expérience réelle. Pendant celle-ci, la cible devant être moins encombrante, il faudra accepter une mesure approximative de l'impulsion de courant. Des mesures neutroniques peuvent, d'autre part, être faites pour reconstituer la bouffée de neutrons.

2.2.4.2. Cible coaxiale

Une cible dite « coaxiale» a été étudiée et réalisée (fig. 9). Elle présente au faisceau une face plane de mêmes dimensions que les cibles neutronigènes classiques. Derrière cette face, le diamètre diminue progressivement jusqu'à permettre le raccordement sur câble coaxial de 50 Ω. Le conducteur extérieur, à la masse, présente une forme analogue de façon que tout l'ensemble soit adapté pour 50 Ω. Un diaphragme placé devant la cible protège les isolements contre un impact indésirable du faisceau. La cible est en cuivre et un circuit interne de refroidissement à eau est prévu. Les fuites résistives par l'eau de refroidissement n'entraînent pas de perturbation sensible sur la lecture de courant.

Une cible du même type a probablement déjà été utilisée par ANDERSON et SWANN [7]. La transformation d'impédance qu'elle introduit permet de réduire la déformation du temps de montée à moins de 2 ns [8]. Une telle cible peut attaquer directement un oscilloscope rapide.

2.2.5. Montage pratique

2.2.5.1. Géométrie d'ensemble

Le centrage correct d'un faisceau d'accélérateur de 6 à 8 mm de diamètre, à l'entrée de la section de déflexion qui n'offre qu'un passage utile de 20 mm, est absolument nécessaire. Le contrôle de ce centrage est obtenu au moyen de sondes tournantes en tungstène entraînées par un moteur synchrone sous vide. Ces sondes permettent d'effectuer un centrage pré-

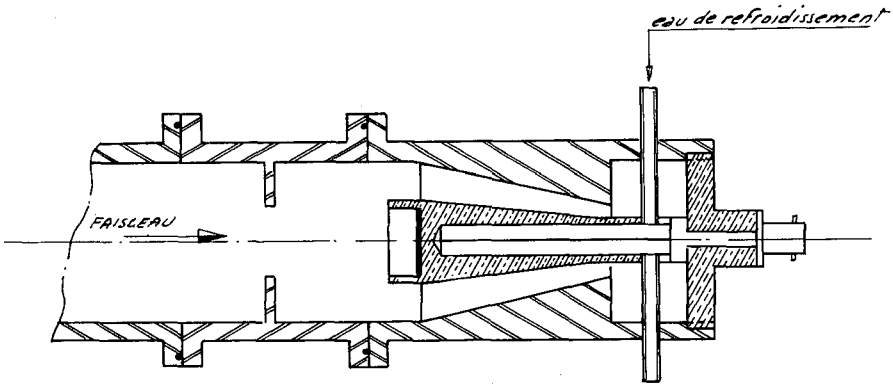


Figure 9

Cible coaxiale.

cis et de mesurer, avec un bonne approximation, le diamètre du faisceau. Une cible escamotable est utilisée pour ces mesures (fig. 10).

L'ensemble de l'appareillage occupe une place relativement importante; environ 50 cm sont nécessaires entre la trappe de sortie de l'accélérateur et le plan moyen de l'aimant de tri. L'entrée de la ligne de déflexion est à 80 cm de ce plan moyen, compte tenu du pompage différentiel nécessaire. Ce pompage pourrait être reporté entre la ligne et l'entrée du canal du réacteur, qui mesure deux mètres de long.

2.2.6. Conclusions et performances

2.2.6.1. Expérimentation

Le système qui vient d'être décrit a été expérimenté avec les valeurs suivantes des paramètres:

V = 220 kV,
E_0 = 600 V/cm (maximum 700 V/cm),
l_1 = 23 cm,
l_2 = 200 cm,
τ = 12 ns,
2 r= 1,2 cm,
D = 1,6 cm.

Le calcul fournit $y_{max} = (E_0/4\,V) l_1 (l_1 + 2\,l_2)$ = 66 mm, alors que la déviation de l'axe de faisceau en sortie de ligne est de 3,6 mm. Le temps de balayage correspondant est théoriquement

$$\theta = \left[\frac{(D/2 + r)}{y_{max}}\right] \tau = 2{,}5 \text{ ns}.$$

Cette valeur a été correctement approchée lors des essais de l'appareillage. Pour ce diamètre de faisceau, le courant de deutons est supérieur à 500 μA, et il y correspond un débit de neutrons de 14 MeV de 2 à $4 \cdot 10^{10}$ n/s. 4π avec les cibles tritiées habituelles.

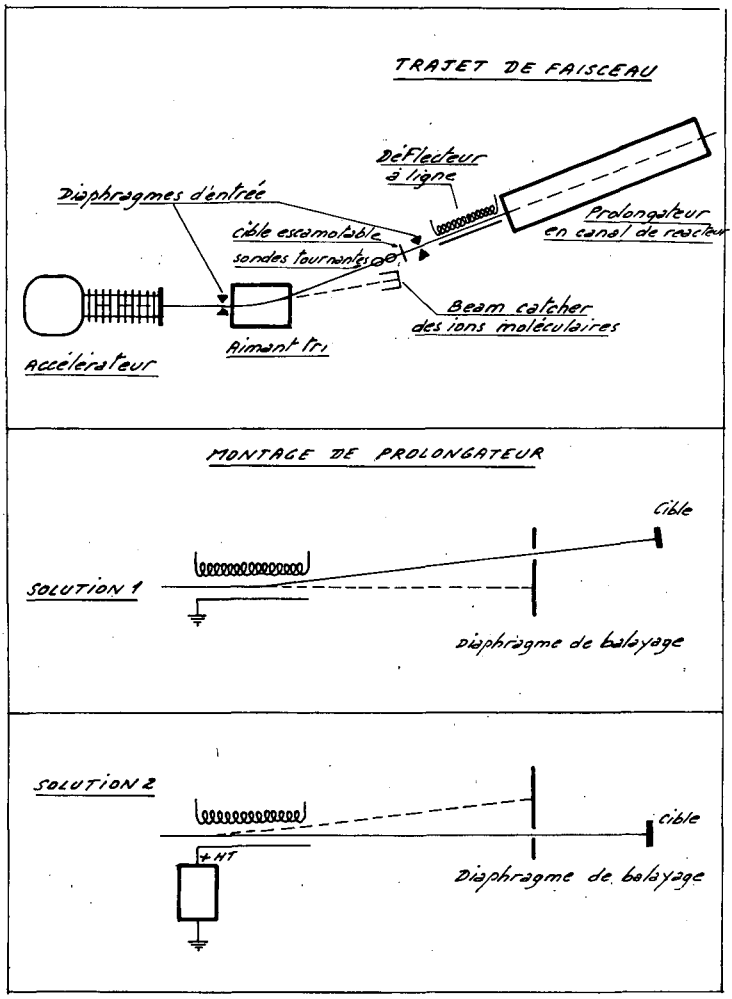


Figure 10

Trajet de faisceau.

2.2.6.2. Possibilités du système de pulsation

A l'origine, un créneau d'une durée de quelques centaines de ns est requis; il se répète à une fréquence de quelques centaines de c/s. La puissance de crête passant dans la ligne est de 4 kW, tandis que la puissance de crête supportée par le tube de sortie est seulement de 1,2 kW. Celui-ci étant donné pour une puissance moyenne de 60 W, une fréquence de répétition de plusieurs dizaines de milliers de c/s peut être atteinte (cela dépend de la durée de pulse). Quant à la durée de pulse, elle ne doit pas être supérieure à 1 μs.

2.2.6.3. Conclusion

L'appareillage décrit est simple; son efficacité est bonne, à condition que l'on adapte l'accélérateur à ce type de fonctionnement. Ses performances permettent la réalisation des expériences de pulsation d'ensembles sous-critiques à neutrons rapides, jusqu'à des fréquences de répétition voisines de 100 kc/s. L'utilisation de cet appareillage pour la modulation en créneaux peut être envisagée en modifiant l'étage de sortie de l'amplificateur de tension.

3. TECHNIQUES D'ENREGISTREMENT DE LA DÉCROISSANCE

3.1. Exposé du problème

Après injection d'une bouffée de neutrons dans un milieu sous-critique, le fondamental, en espace et en énergie de la population neutronique due à cette bouffée, décroît dans le temps suivant une loi $\phi(t)$.

Au cours d'une décroissance donnée, plusieurs neutrons peuvent exciter le détecteur. Par suite du temps mort de l'appareillage d'enregistrement en mémoire de l'information reçue par le détecteur, seule l'information provenant du premier neutron est prise en compte. Il en résulte une déformation de la décroissance mesurée $g(t)$ par rapport à la loi $\phi(t)$ à mesurer.

On démontre que*

$$g(t) = \frac{\lambda\phi(t)\exp\left[-\lambda\int_0^t \phi(u)du\right]}{1-\exp-\lambda\int_0^T \phi(u)du}, \qquad (1)$$

λ étant l'efficacité du détecteur par neutron de flux,

T la période de pulsation, $0 < t \leq T$.

Le rapport $g(t)/\phi(t)$ est donc une fonction monotone décroissante du temps.

De l'équation (1), on peut déduire

$$\phi(t) = \frac{g(u)}{\lambda\left[R-\int_0^t g(u)du\right]}, \qquad (2)$$

$$R = \frac{1}{1-\exp\left[-\lambda\int_0^T \phi(u)du\right]}.$$

La recherche de $\phi(t)$ ou d'une quantité proportionnelle à $\phi(t)$, connaissant $g(t)$, nécessite donc la connaissance de la quantité $\lambda\int_0^T \phi(u)du$ qu'il est en général difficile de déterminer avec précision.

---

* Un rapport, en cours de publication, présente le détail de l'ensemble des calculs relatifs à cette étude dont on ne présente, ici, que les conclusions essentielles.

Si $N = \lambda \int \phi(u)du$, qui représente le nombre moyen d'excitations du détecteur après l'injection d'une bouffée, est petit devant 1, a fortiori $\lambda \int_{\Omega}^{t} \phi(u)du$ est petit devant 1. Si on néglige cette dernière quantité, il y a alors proportionnalité entre g(t) et $\phi(t)$; cette approximation étant d'autant meilleure que N est petit:

$$g(t) = k\,\phi(t)(1 - N).$$

Plus précisément, si on veut que pour $t = T$ l'écart entre g(t) et $k\phi(t)$, en valeur relative, soit inférieur à 1%, il conviendra d'avoir $\bar{N} = 0{,}01$, ce qui correspond en moyenne à un enregistrement toutes les cent pulsations, sans tenir compte du temps mort τ associé à chaque enregistrement.

Si on appelle $\bar{t}$ le temps moyen qui sépare deux enregistrements successifs, dans l'hypothèse ou $\bar{N}$ est petit et en tenant compte du temps mort τ on démontre que

$$t \simeq \frac{T}{\bar{N}} + \tau \text{ à } \epsilon T \text{ près}, \quad 0 < \epsilon < 1. \tag{3}$$

Ce temps moyen est directement proportionnel à la durée totale de l'expérience.

Par exemple, pour une fréquence de pulsation de 50 kc/s ($T = 20\ \mu s$) pour $\bar{N} = 0{,}01$ et en prenant $\tau = 100\ \mu s$,

$$\bar{t} = 2100\ \mu s.$$

3. 2. Enregistrement sélectif des informations

Supposons un appareillage de détection et d'enregistrement ne prenant en compte une information que si elle provient d'une excitation unique du détecteur pendant une période. On montre que la décroissance enregistrée g'(t) est de la forme

$$g'(t) = \frac{\lambda \exp\left[-\lambda \int_0^1 \phi(u)du\right]}{1 - \exp\left[-\lambda \int_0^T \phi(u)du\right]}\,\phi(t). \tag{4}$$

La loi mesurée g'(t) est alors proportionnelle à $\phi(t)$ quel que soit $\bar{N}$, ce qui évite toutes corrections du type précédent sur g'(t).

Si on appelle $\bar{t}'$ le temps moyen s'écoulant entre deux enregistrements successifs de ce type, on montre que

$$\bar{t}' \simeq \frac{T}{\bar{N} \exp(-\bar{N})} + \tau \text{ à } \epsilon T \text{ près}, \quad 0 < \epsilon < 1, \tag{5}$$

quel que soit $\bar{N}$; τ étant fixe, $\bar{t}'$ sera minimal quand $\bar{N} = 1$ et sa valeur sera $\bar{t}' \simeq eT + \tau$.

En utilisant les mêmes valeurs numériques que précédemment, on obtient

$$\overline{t'} = 150\ \mu s,$$

à comparer avec $\overline{t} = 2100\ \mu s$.

Pour un même nombre total d'informations enregistrées au cours d'une expérience donnée, l'enregistrement sélectif des informations permet une durée totale d'expérience 13 fois plus faible que si l'on utilise le dispositif classique d'enregistrement. La réalisation du montage électronique permettant cet enregistrement sélectif ne pose aucun problème technique très difficile à résoudre.

La fonction $\overline{N} \exp(-\overline{N})$ est une fonction qui présente un minimum pour $\overline{N} = 1$. La recherche de $\overline{N} = 1$ se fait en rendant maximal le taux de comptage enregistré avec ce système de détection

- soit en faisant varier la position d'un détecteur donné par rapport au massif étudié,
- soit pour une position donnée en ajustant l'efficacité du détecteur. Cet ajustement n'est pas très critique, comme le montre la figure 11 sur laquelle on a représenté $\overline{t'}$ en fonction de $\overline{N}$ pour différentes valeurs de τ.

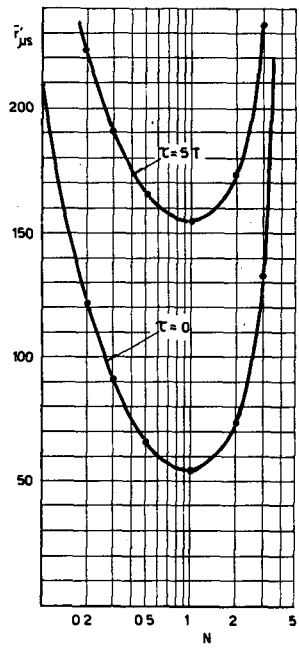


Figure 11

Temps moyen $\overline{t'}$ entre 2 enregistrements successifs.
$\overline{t'} = \overline{t'}(\overline{N})$; $T = 20\,\mu s$.

RÉFÉRENCES

[1] BERTHERY, M., Pulsation rapide par modulation de vitesse d'un faisceau de deutons de 150 keV, Rapport interne CEN-FAR DEP/SEPP 244/63 (juin 1963).
[2] AALAN, K., UCRL 5430 T.
[3] PIERSON, A., Brevet français (n° en cours d'attribution).
[4] DUQUESNE, M., Etude d'un système de déflexion rapide d'un faisceau d'ions issus d'un accélérateur électrostatique de 400 keV, Rapport interne SECNR-GES (7 mars 1965).
[5] PIERSON, A., Brevet français 982-695 du 22 juillet 1964.
[6] GRUNBERG, G., Phys. Radium, 22, suppl. au n° 11, (novembre 1961) 194A.
[7] ANDERSON, J. H. et SWANN, D., Nucl. Intrum. Meth., 30 (1964) 1-22.
[8] LEWIS, I. A. D. and WELLS, F. H., Millimicrosecond Pulse Techniques, Pergamon Press, London (1956) 96.

DISCUSSION

S. CHWASZCZEWSKI: In the system you describe, the deuteron beam falls on the target and will fall on it again from the opposite direction. How is this avoided?

R. GERBIER: In the two-voltage-step device with two plates, the beam is deflected at a given moment to twice the normal maximum amplitude. This is not so in the device using the travelling wave line. In neither system, however, does the beam at any time pass over the target parasitically (i.e. from the undesired "opposite direction").

S. CHWASZCZEWSKI: In facilities with deflected beams, there is a large background because of the DD reaction as a result of the load on the spot on which the deuteron beam falls. What is the pulse/background ratio in your facility?

R. GERBIER: We are acquainted with this phenomenon. To reduce background, we have provided for the inclusion of soft iron or tantalum diaphragms, which will be kept at a high temperature to reduce deuterium absorption. The diaphragm can also be removed quite far from the target itself in the final installation. Since this installation is not yet in operation, I cannot reply to your question in detail.

GENERAL DISCUSSION

D. BRETON (Chairman): At this time I shall call upon Mr. Bourion who wishes to comment briefly on new development work on pulsed-neutron generators.

M. BOURION: I should like to describe a neutron generator which we have developed at the Compagnie Générale de Télégraphie sans Fil. This apparatus generates neutrons in a small sealed-off tube, 4 cm in diameter and 18 cm in overall length. The tube, which has two electrodes and does not have an ion source, is operated simply by the application of high tension between the target and the anode. It is characterized by a hollow anode surrounded by a tubular magnet, and the electrode-type structure gives rise to an electron-trapping effect inside the anode which is conducive to the production of ions in this region. The ions are then accelerated towards the target by the applied potential difference. The target is a conventional tritium target in titanium, the latter being deposited on a metal support that is part of the tube envelope. The tube also has a Pirani gauge for measuring pressure and a titanium reservoir for regulating the latter.

As there are only two electrodes, the current passing through the tube is relatively high and cannot be maintained at steady state. This is therefore intrinsically a pulsed tube. The high-tension pulses applied to the electrodes are obtained by means of a transformer coupled to the tube.

The voltage of the pulse applied to the transformer primaries is only 3 kV. The pulse length is 2 μs and the repetition frequency can be set at between 0 and 25 Hz. Under these conditions, and with about 3 kV for the primary pulses, one obtains between 5×10^6 and 10^7 neutrons per pulse. A basic feature of the generator is the very small size of the probe, which enables it to be inserted with ease into a reactor channel, for example.

Investigations of neutron generation as a function of the number of pulses produced by the tube show that neutron production becomes stabilized above two million pulses. This stabilization is certainly due to the establishment of an equilibrium isotopic composition between target and beam. This is a classic phenomenon that is obtained in tubes with deliberately mixed beams. Here the effect is obtained automatically.

RELATED TECHNIQUES

(Session VII)

TECHNIQUES CLOSELY RELATED TO PULSED NEUTRON RESEARCH

R. E. UHRIG
UNIVERSITY OF FLORIDA,
GAINESVILLE, FLA., UNITED STATES OF AMERICA

Abstract — Résumé — Аннотация — Resumen

TECHNIQUES CLOSELY RELATED TO PULSED NEUTRON RESEARCH. Techniques related to pulsed neutron research involve the injection of neutrons at one of the boundaries of a nuclear system, and the localized perturbation of the neutron population then propagates throughout the system. The disturbance introduced at the boundary may be continuous, such as a sinusoidal modulation (neutron wave technique) or a pseudo-random (on-off) variation of source strength (pseudo-random pulsing), or it may be a single burst of neutrons.

Propagation of the perturbation can be dealt with as a spatially dependent pulse propagation problem. Hence, the impulse response (and source transfer function) of the system at any point can be determined from neutron wave or pseudo-random pulsing experiments which, in turn, allow the evaluation of the nuclear parameters of the system.

The neutron wave technique is used to measure diffusion parameters of moderators, the nuclear properties of subcritical assemblies, and to measure thermalization power and diffusion cooling in crystalline moderators. The pseudo-random pulsing technique was developed as a means of measuring subcriticality of nuclear systems. Cross-correlation of the input with the neutron density at several points throughout the system yields the spatially dependent impulse response of the system which can be Fourier-transformed to yield a dispersion (or transfer) function.

Other phenomena, including reflection of neutron waves from the interface between heavy water and graphite, interference between propagating disturbances and the lattice of a heavy water, natural uranium system, and neutron pulse propagation in graphite using a pulsed TRIGA reactor as an intense neutron source have been demonstrated.

Recent trends in data reduction are toward the incorporation of "on-line" digital computers for data reduction. Such techniques, now used for pulse height analysis, are being developed for multichannel time analysis for all types of pulsed neutron research. Data analysis often involves correlation and spectral density determinations to evaluate system parameters.

MÉTHODES ÉTROITEMENT LIÉES A LA RECHERCHE AU MOYEN DES NEUTRONS PULSÉS. Les techniques associées à la recherche au moyen des neutrons pulsés nécessitent l'injection de neutrons à l'une des frontières d'un système nucléaire; la perturbation locale à laquelle est soumise la population des neutrons se propage alors à travers tout le système. La perturbation provoquée à la frontière peut être continue, comme c'est le cas d'une oscillation sinusoïdale dans une expérience modulée (méthode de l'onde neutronique) ou d'une variation de la source selon une fonction pseudo-aléatoire (expérience pulsée pseudo-aléatoire), ou bien il peut s'agir d'une seule bouffée de neutrons.

Pour étudier la propagation de la perturbation, on peut la considérer comme un problème de propagation d'une impulsion variable dans l'espace. Il s'ensuit donc que la réponse du système à l'impulsion (et la fonction de transfert de la source) en un point quelconque peuvent être déterminées par une expérience modulée ou une expérience pulsée pseudo-aléatoire, ce qui permet d'évaluer finalement les paramètres nucléaires du système.

La méthode de l'onde neutronique est utilisée pour mesurer les paramètres de diffusion des ralentisseurs, les propriétés nucléaires des assemblages sous-critiques, et pour mesurer le pouvoir de thermalisation et le refroidissement par diffusion dans les ralentisseurs cristallins. La méthode pseudo-aléatoire a été mise au point pour mesurer des systèmes nucléaires à l'état sous-critique. Une corrélation entre l'entrée et le nombre volumique de neutrons en plusieurs points répartis dans tout le système fournit la réponse du système à une impulsion variable dans l'espace qui, par une transformée de Fourier, peut donner une fonction de dispersion (ou de transfert).

L'auteur a fait la démonstration d'autres phénomènes: réflexion des ondes neutroniques par l'interface eau lourde-graphite, interférence entre les perturbations qui se propagent et le réseau d'un système uranium

naturel-eau lourde, et propagation dans le graphite de bouffées de neutrons obtenues au moyen d'un réacteur TRIGA pulsé comme source intense de neutrons.

Depuis peu, on a tendance à favoriser l'incorporation de calculatrices numériques pour le dépouillement simultané des données. Ce procédé qui est maintenant utilisé pour analyser les amplitudes d'impulsions est mis au point pour être utilisé avec des analyseurs en temps multicanaux dans tous les types de recherches au moyen de neutrons pulsés. L'analyse des données implique souvent l'établissement de corrélations et la détermination de densités de spectre pour évaluer les paramètres du système.

МЕТОДЫ, ТЕСНО СВЯЗАННЫЕ С ИССЛЕДОВАНИЯМИ МЕТОДОМ ИМПУЛЬСНЫХ НЕЙТРОНОВ. Методы, связанные с исследованиями методом импульсных нейтронов, включают введение нейтронов на одну из границ ядерной системы, после чего локализованное возмущение нейтронов распространяется по всей системе. Осуществляемое на границе возмущение может быть постоянным, например, оно может представлять собой синусоидальную модуляцию (метод нейтронной волны) или псевдослучайную (по типу "включено – выключено") вариацию мощности источника (псевдослучайную пульсацию) или оно может представлять собой отдельный импульс нейтронов.

Распространение возмущения можно рассматривать как проблему распространения пространственно зависимых импульсов. Следовательно, реакцию (и передаточную функцию источника) системы на импульс в любом месте можно определить на основе экспериментов, связанных с нейтронной волной или псевдослучайной пульсацией, что в свою очередь позволяет произвести оценку ядерных параметров системы.

Метод нейтронной волны используется для измерения диффузионных параметров замедлителей, ядерных свойств подкритических сборок, а также для измерения термализационной способности и диффузионного охлаждения в кристаллических замедлителях. В качестве средства измерения подкритичности ядерных систем был разработан метод псевдослучайной пульсации. Взаимная корреляция входного сигнала с плотностью нейтронов в нескольких местах по всей системе приводит к ответному пространственно зависимому импульсу системы, который может быть разложен в ряд Фурье для получения дисперсионной (или передаточной) функции.

С помощью импульсного реактора "Трига" в качестве мощного источника нейтронов были показаны другие явления, включая отражение нейтронных волн от поверхности раздела между тяжелой водой и графитом, интерференцию между распространяющимися возмущениями и решеткой тяжеловодной системы на природном уране и распространение импульса нейтронов в графите.

В последенее время наметилась тенденция использовать цифровые вычислительные машины для обработки данных параллельно с их поступлением. Такие методы, которые в настоящее время используются для амплитудного анализа импульсов, разрабатываются для проведения анализа с помощью многоканального временного анализа в связи с всевозможными исследованиями методом импульсных нейтронов. Анализ данных часто связан с корреляцией и определениями спектральной плотности для оценки параметров системы.

TECNICAS AFINES A LAS EMPLEADAS EN INVESTIGACIONES MEDIANTE NEUTRONES PULSADOS. Las técnicas afines a las empleadas en investigaciones mediante neutrones pulsados implican la inyección de neutrones en una de las superficies de separación de un sistema nuclear, seguida de la propagación a través de todo el sistema de la perturbación localizada a que está sometida la población neutrónica. La perturbación creada en la superficie de separación puede ser de carácter continuo, como ocurre con las modulaciones sinusoidales (técnica de las ondas neutrónicas) o consistir en una variación pseudoaleatoria de la intensidad de la fuente, o en un solo impulso neutrónico.

Puede considerarse que la propagación de la perturbación representa un problema de propagación del impulso en función del espacio. Por consiguiente, la respuesta del sistema al impulso (y la función de transferencia de la fuente) en un punto cualquiera pueden determinarse mediante experimentos con ondas neutrónicas o con impulsos pseudoaleatorios, que a su vez permiten evaluar los parámetros nucleares del sistema. La técnica de las ondas neutrónicas se utiliza para determinar los parámetros de difusión en los moderadores, las propiedades nucleares de los conjuntos subcríticos y para medir el poder de termalización y el enfriamiento por difusión en moderadores cristalinos. La técnica de los impulsos pseudoaleatorios fue elaborada para medir la subcriticidad de los sistemas nucleares. Estableciendo una correlación entre los datos de entrada y la densidad neutrónica en diversos puntos del sistema, se obtiene la respuesta del sistema en función del espacio, que se puede transformar según el método de Fourier para obtener la función de dispersión (o de transferencia).

El autor ha puesto de manifiesto otros fenómenos: la reflexión de las ondas neutrónicas en la superficie de separación entre el agua pesada y el grafito, la interferencia entre las perturbaciones en propagación y la red de un sistema de uranio natural y de agua pesada, así como la propagación de impulsos neutrónicos en el grafito utilizando un reactor TRIGA pulsado como fuente de neutrones de elevada intensidad. Las recientes tendencias en materia de reducción de datos, favorecen la incorporación de calculadoras numéricas al circuito. Estas técnicas, que en la actualidad se utilizan para analizar la amplitud de los impulsos, han sido elaboradas para efectuar análisis de tiempo con aparatos multicanales en todos los tipos de investigaciones con ayuda de neutrones pulsados. El análisis de los datos obliga a menudo a establecer correlaciones y a determinar densidades espectrales para poder evaluar los parámetros del sistema.

INTRODUCTION

Most of the work discussed at this conference deals with the conventional pulsed neutron technique in which a burst of fast neutrons is injected into a nuclear system. These neutrons spread out over the entire system and are slowed down, giving a wide spatial distribution of the thermal neutron population which then dies away owing to absorption and leakage from the system. After the fundamental mode has been attained, the die-away (or decay) constant of the exponential attenuation can be used to evaluate the nuclear properties of the system.

The techniques that are discussed here aim to obtain the same nuclear properties sought by means of the conventional pulsed neutron technique, but they differ in several respects. The primary difference is that the disturbance that is introduced into the system is a disturbance of the thermal neutron density, usually at one of the boundaries of the system. As the thermal neutrons diffuse away from the source, the neutron density decreases with distance.

These experiments can be separated into transient and steady-state categories. The transient experiment, in many respects, resembles the conventional pulsed neutron experiment. In this case a transient source of thermal neutrons is introduced at one of the boundaries and the resultant disturbance is studied as it propagates throughout the system. Specifically, we are interested in the characteristics (shape, height, width, phase, etc.) of the disturbance at various positions in the assembly. For example, let us consider the case where the disturbance is a pulse of thermal neutrons. The resultant disturbance of the thermal neutron density in the assembly has a Gaussian-like shape with a dispersion that increases with time, and hence with distance from the source. One can also show that this pulse peak propagates away from the source and that the rate of propagation of the peak is related to the characteristics of the nuclear system.

The steady-state method involves the use of a thermal neutron source the output of which, in a general sense, is continuous with significant deviations from the average value. These deviations may be sinusoidal, random, pseudo-random, Gaussian, square-wave, complex wave form, etc. The objective in the experiments using any of these inputs is the same; namely, to obtain the response of the system to those variations. The method of analysis of data is dependent upon the type of disturbance used. The relative advantages of each of these methods and their interrelation are discussed in this paper.

In general, these experiments are carried out with an accelerator-type neutron source capable of producing large quantities of thermal neutrons. A Van de Graaff accelerator with energy greater than the 1.88 MeV threshold can be employed using a proton beam impinging upon a lithium target. This will yield neutrons with an energy of about 29 eV, which are readily slowed down to thermal energies. Work has also been carried out using targets that yield fast neutrons, making it necessary to employ a neutron "filter" to slow down the neutrons to thermal energies. Unfortunately, such a filter greatly attenuates the thermal neutron-source intensity. An alternate neutron source used in some work has been a "pulsing" reactor such as the TRIGA or PULSTAR. The relative advantages of each type of source will be discussed.

HISTORICAL DEVELOPMENTS OF TECHNIQUES RELATED TO PULSED NEUTRON RESEARCH

Historically, the pulsed neutron technique was used as early as 1942 by MANLY, HAYWORTH and LUEBKE [1] to observe the time decay of neutron bursts as a means of measuring the mean lifetime of thermal neutrons in water and thereby deduce the corresponding microscopic absorption cross-section of hydrogen. However, the technique apparently remained dormant until Von DARDEL published the results of a series of experiments carried out using a pulsed neutron source in 1954 [2-5]. This was followed by the presentation of the results of several investigators, using pulsed neutron techniques, at the Geneva Conference on Peaceful Uses of Atomic Energy in 1955 [4, 5]. At the same conference, a paper was presented by RAIEVSKI and HOROWITZ [6]. This paper, which was an outgrowth of a Ph.D. thesis by RAIEVSKI [7] described the technique of using a sinusoidal input of source neutrons to measure diffusion parameters of heavy water and graphite. The authors describe two experiments, both of them utilizing mechanical modulators to produce the sinusoidal variation in the neutron source strength. In one of the experiments, a beam of neutrons from a reactor was interrupted with a rotating cadmium disk to produce the modulation. In the other, a uranium absorber was mechanically rotated between a radioactive antimony source and a beryllium target, thereby sinusoidally modulating the output due to the gamma-N reaction. These experiments were supported by a theoretical development based primarily upon diffusion theory.

The significance of the Raievski-Horowitz work is that it was the first of the techniques "closely related to pulsed neutron research". The sinusoidal modulation technique is a frequency-domain technique while the pulsed neutron technique is a time-domain technique. With sinusoidal modulation, a quasi-steady state is achieved; while with the pulsed source, the neutron population is a transient quantity. With the sinusoidal modulation, the disturbance propagates away from the source, and hence the dynamic variation of the neutron population is spatially dependent. In the pulsed technique, the fundamental mode prevails during the decay of the population. Two quantities (amplitude and phase) are measured for the sinusoidally modulated experiment, while only one quantity (decay constant) was measured

for the pulsed technique. Hence, more information can be obtained from the sinusoidal modulation experiment.

It is interesting to compare the subsequent development of these two techniques, both initiated at about the same time. It appears that the pulsed neutron technique caught the imagination of reactor experimentalists throughout the world, and in the intervening ten years there has been widespread use of this technique in reactor physics measurements. The sinusoidal source modulation technique, which I shall call the "neutron wave" technique, apparently created little interest. The "neutron wave" technique was resurrected, however, in 1958 by UHRIG and his associates at Iowa State University [8-12] quite independently of the work at Saclay. A small mechanical oscillator, consisting of a drum, lined with a sinusoidal pattern of cadmium, rotated around a paraffin cylinder containing five plutonium-beryllium sources, was constructed in an attempt to measure the transfer function of a subcritical assembly. The presence of "neutron waves" was immediately noticed and the investigation was directed towards that phenomenon.

In 1961, UHRIG [13] and his associates, now at the University of Florida, began a new series of experiments using a Texas nuclear neutron generator that had been specially modified to produce sinusoidal modulation by varying the extraction voltage on the ion bottle. This accelerator was used with a 256-channel Technical Measurements Corporation time analyser and was used to gather data on neutron wave propagation. It was soon found that the 14.3-MeV neutrons from a tritium target, which were emitted due to the D-T reaction, completely masked any wave effects. Hence it was necessary to develop a means of slowing down these neutrons to thermal energy while at the same time retaining the sinusoidal nature of the output. Such a device was developed primarily by trial and error by PEREZ and HARTLEY [14], and this immediately led to successful neutron wave experiments which could and did compete, for the first time, with conventional pulsed neutron techniques.

It is apparent that the easy and convenient method of providing a burst of neutrons using a small accelerator is the primary factor which propelled the pulsed neutron techniques into prominence. Only recently have the advantages of the neutron wave technique over the pulsed neutron technique been pointed out and exploited by experimenters at the University of Florida [15-20]. Other related techniques, such as pulse propagation, pseudo-random pulsing and noise techniques, have followed in rapid succession from the neutron wave work. This work has also been helped greatly by the theoretical developments of PUROHIT [21], OHANIAN and DAITCH [22], WEINBERG and SCHWEINLER [23] and especially MOORE [24-28].

GENERALIZED IMPEDANCE CONCEPT OF A NUCLEAR SYSTEM

A nuclear system can often be considered as a generalized impedance with inputs and outputs. The classical approach in systems analysis, which usually considers only a single input, has been applied quite successfully to nuclear systems where the outputs at all points of the system are proportional [29]. Where the output varies as a function of position, spatially

dependent effects must be taken into account. Multiple input systems can generally be treated by the method of superposition providing that the system is linear, or can be linearized without introducing significant error.

Let us consider the system in Fig. 1, the dynamic characteristics of which are represented by its transfer function G(s) and its impulse response

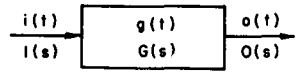


Fig. 1

Block diagram of a generalized impedance

g(t). Here the relationship between the input and the output is given by the convolution theorem to be

$$o(t) = \int_{-\infty}^{\infty} g(\lambda) i(t-\lambda) d\lambda. \tag{1}$$

In the frequency domain, this relationship becomes

$$O(s) = G(s) I(s). \tag{2}$$

If the system of Fig. 1 is a subcritical nuclear system in which the delayed neutrons can be neglected, its dynamic behaviour can be represented by

$$\frac{dn(t)}{dt} = \frac{k_p - 1}{\ell} n(t) + s(t). \tag{3}$$

Introduction of a perturbation in the source term results in a perturbation of the output and this relationship between the perturbations is given by the transfer function

$$G(s) = \frac{\Delta N(s)}{\Delta S(s)} = \frac{1}{s + \frac{1 - k_p}{\ell}} = \frac{1}{s+\alpha} \tag{4}$$

and its impulse response is

$$g(t) = e^{-\alpha t}. \tag{5}$$

This last expression indicates that the neutron population in a subcritical assembly which has been pulsed dies away exponentially with a decay constant α. The response of the system to a sinusoidal input of source strength A is readily shown to be

$$o(t) = \frac{A}{\sqrt{(\alpha^2+\omega^2)}} \cos\left[\omega t + \tan^{-1}\left(-\frac{\omega}{\alpha}\right)\right]. \tag{6}$$

The relationships expressed by Eqs. (4) and (5) are valid for any kind of

source input to the system, and several different inputs will be considered in this paper.

In many cases, the input to the system is non-deterministic in nature, and the input-output relationships must be dealt with in terms of their statistical properties. The specific physical quantities to be used here will be correlation functions and spectral densities. Let us consider the system of Fig. 2, with an input the auto-correlation function and power spectral

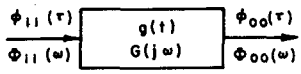


Fig. 2

Block diagram of a system with statistical input and output

density of which are $\phi_{ii}(\tau)$ and $\Phi_{ii}(\omega)$ respectively. The output has an auto-correlation function and power spectral density of $\phi_{oo}(\tau)$ and $\Phi_{oo}(\omega)$ respectively. BENDAT [30], LEE [31] and others give the relationship between the correlation functions and power spectral densities to be

$$\phi_{oo}(\tau) = \int_{-\infty} g(\lambda)d\lambda \int_{-\infty} g(\sigma)d\sigma\, \phi_{ii}(\tau+\lambda-\sigma), \tag{7}$$

$$\Phi_{oo}(\omega) = |G(j\omega)|^2 \Phi_{ii} = G(j\omega)G^*(j\omega)\Phi_{ii}(\omega). \tag{8}$$

When cross-correlations and cross-spectral densities between the inputs and the outputs are used, the input-output relationships are

$$\phi_{io}(\tau) = \int_{-\infty}^{\infty} g(\lambda)\phi_{ii}(\tau-\lambda)d\lambda, \tag{9}$$

$$\Phi_{io}(\omega) = G(j\omega)\Phi_{ii}(\omega). \tag{10}$$

The similarity between Eqs. (1) and (2) and Eqs. (9) and (10) are quite apparent.

SINUSOIDAL MODULATION (NEUTRON WAVE) TECHNIQUE

In the study of the dynamic nuclear characteristics of moderating and multiplying nuclear systems, the behaviour of the system is determined by a balance of neutrons supplied by an external source, the neutrons produced in fission, the neutrons absorbed in the various materials of the assembly, and the neutrons which leak from the system. If any of these quantities is disturbed, the others are also affected. When a sinusoidal variation of the neutron source of the form

$$\mathcal{S}(r_o, t) = \mathcal{S}_o(r_o) + \delta\mathcal{S}(r_o, t) \tag{11}$$

is introduced into the assembly, the resultant variation in the neutron flux at any point is

$$\psi(r, t) = \psi_o(r) + \delta\psi(r, t), \tag{12}$$

where r represents the general space co-ordinate and r_o represents the location of a point source. For very low frequencies, the neutron flux throughout the assembly appears to vary directly as the source strength. The contribution due to the delayed neutrons is not significant unless the multiplication is relatively large.

For a higher frequency of source oscillation, the time variation of neutron density at a point distant from the source is still sinusoidal with the frequency of the source, but it lags the source variation because of the finite time for the neutron disturbance to travel from the source to the distant point. As the frequency increases, the lag becomes greater, and at very high frequencies the variation of the neutron flux at a distant point may lag the source by several cycles. The magnitude of the lag as well as the amplitude of the disturbance at any point are influenced by the nuclear properties of the materials in the assembly. Hence the propagation of these disturbances (here called neutron waves) can be used as a means of measuring the nuclear properties of the materials in the assembly.

If the assembly is a multiplying assembly, having a moderator with a relatively low absorption cross-section and a configuration which, in a general sense, can be represented by homogeneous reactor theory, then elementary diffusion theory offers a reasonable representation of the dynamic behaviour of the system. In the case of a moderating assembly, the dominating effect is thermalization, i.e. the interaction of the slowed-down neutrons with the lattice of the moderator, and this effect must be included in the model. For high frequencies, better approximations to the Boltzmann transport equation, such as the P_1 approximation, must be used.

The time and space dependent neutron diffusion equation for a multiplying system, where the neutrons spend most of their lives as thermal neutrons, can be expressed in the form

$$\nabla^2\psi(r, t) + B_M^2\psi(r, t) = \frac{1}{vD}\frac{\partial\psi(r, t)}{\partial t}, \tag{13}$$

where

$$B_M^2 = \frac{1}{L^2}(k_p - 1) = \frac{1}{L^2}[k_\infty(1 - \beta) - 1] \tag{14}$$

$$\frac{1}{L^2} = \frac{\Sigma_a}{D} = \frac{1}{\ell_\infty vD} \tag{15}$$

and the symbols are those commonly used in reactor theory. By taking the Laplace transform, Eq. (13), we reduce the time-dependent problem to a static problem in which the neutron absorption is increased by the "time absorption" s/v, where s is the Laplace transform parameter. The result is

$$\nabla^2\psi(r, s) + \left[B_M^2 - \frac{s}{vD}\right]\psi(r, s) = \nabla^2\psi(r, s) + \beta_M^2(s)\psi(r, s) = 0, \tag{16}$$

where the complex material buckling β_M^2 is given by

$$\beta_M^2 = B_M^2 - \frac{s}{vD} . \tag{17}$$

The application of the boundary and source conditions appropriate to the particular configuration will give an expression for the neutron density. In the case of a rectangular assembly, with an isotropic point source located at the centre of the base and zero neutron flux at the extrapolated boundaries of all other sides, the result is

$$\psi(x, y, z, s) = \sum_{m=1}^{\infty} \sum_{n=1}^{\infty} A_{mn} \cos \frac{m\pi x}{a} \cos \frac{n\pi y}{b} e^{-\rho_{mn}(s)z} \left[1 - e^{-2\rho_{mn}(s)(c-z)}\right], \tag{18}$$

where A_{mn} is the coefficient for the mn-th mode of the Fourier cosine series and $\rho_{mn}(s)$ is the complex inverse relaxation length of the mn-th mode of the sinusoidal component of the neutron flux, which is

$$\begin{aligned} \rho_{mn}^2(s) &= \left(\frac{m\pi}{a}\right)^2 + \left(\frac{n\pi}{b}\right) - \beta_M^2 = B_{\perp mn}^2 - \beta_M^2 \\ &= B_{\perp mn}^2 - B_M^2 + \frac{s}{vD} = \gamma_{mn}^2 + \frac{s}{vD} . \end{aligned} \tag{19}$$

The portion of Eq. (18) in rectangular brackets, known as the end correction factor, is approximately equal to unity except near the upper end of the assembly. This correction factor is usually dropped even though it implies the assembly is infinitely long in the z-direction and that the geometric buckling is equal to its perpendicular component, i.e.

$$B_{mn}^2 = B_{\perp mn}^2 = \left(\frac{m\pi}{a}\right)^2 + \left(\frac{n\pi}{b}\right)^2 . \tag{20}$$

Hence the static inverse relaxation length is

$$\gamma_{mn}^2 = B_{\perp mn}^2 - B_M^2 = B_{mn}^2 - B_M^2 . \tag{21}$$

When the isotropic point source condition of Eq. (11) is expanded in an orthogonal set and applied to the assembly at the origin for each mode, the resultant fluctuation of neutron flux is

$$\Delta\psi(x, y, z, s) = \sum_{m=1}^{\infty} \sum_{n=1}^{\infty} \frac{\Delta S_{mn}(0, 0, 0, s)}{2D\rho_{mn}(s)} \cos \frac{m\pi x}{a} \cos \frac{n\pi y}{b} e^{-\rho_{mn}(s)z} . \tag{22}$$

The disturbance is sinusoidal with an amplitude of each mode ΔS_{mn} and a frequency ω. The solution of Eq. (22) is

$$\Delta\psi(x,y,z,t) = \sum_{m=1}^{\infty}\sum_{n=1}^{\infty} \frac{\Delta S_{mn}(0,0,0,t)\cos\frac{m\pi x}{a}\cos\frac{n\pi y}{b}}{2D[\alpha_{mn}^2 + \xi_{mn}^2]^{1/2}} e^{-\alpha_{mn}z} e^{j(\omega t - \xi_{mn}z)}, \quad (23)$$

where

$$\alpha_{mn} = \left(\frac{\Psi_{mn}^2 + \gamma_{mn}^2}{2}\right)^{1/2} \quad (24)$$

$$\xi_{mn} = \left(\frac{\Psi_{mn}^2 - \gamma_{mn}^2}{2}\right)^{1/2} \quad (25)$$

$$\Psi_{mn}^2 = \left[\gamma_{mn}^4 + \left(\frac{\omega}{vD}\right)^2\right]^{1/2}. \quad (26)$$

By expanding the source term of Eq. (22), the transfer function has been obtained by UHRIG [17] as

$$G(x,y,z,s) = \frac{\Delta\psi(x,y,z,s)}{\Delta S(x,y,z,s)} = \frac{2}{abD}\sum_{m=1}^{\infty}\sum_{n=1}^{\infty}\frac{1}{\rho_{mn}(s)}$$

$$\times\cos\frac{m\pi x}{a}\cos\frac{n\pi y}{b} e^{-\rho_{mn}(s)z}. \quad (27)$$

Similar expressions can be obtained for other geometries.

It is clear from Eq. (19) that the use of sinusoidal source and observation of the resultant sinusoidal component of the neutron flux is substantially equivalent to performing a "poisoning" experiment. Increasing the frequency of oscillation is equivalent to increasing the amount of poisoning. However, the neutron wave technique is not limited to liquid moderated systems. Furthermore, the problems of "clean-up" after a poisoning are obviated.

Use of a more sophisticated theory will aid in understanding the "wave" nature of the disturbance. Let us consider the consistent P_1 approximation to the transport equation, as given by WEINBERG and WIGNER [32], and consider the propagation of mono-energetic neutrons throughout the system. Averaging the energy dependent parameters over an assumed spectrum, e.g. over the Maxwell-Boltzmann distribution, yields the well-known telegrapher's equation

$$\frac{3D}{v^2}\frac{\partial^2\psi(r,t)}{\partial t^2} + \frac{1}{v}(1 + 3D\Sigma_a)\frac{\partial\psi(r,t)}{\partial t} = D\nabla^2\psi(r,t) - \Sigma_a(r,t) + k_{p\infty}\Sigma_a\psi(r,t). \quad (28)$$

WEINBERG and WIGNER [32] have indicated that the general solution of the telegrapher's equation shows the phenomena of retardation, that is, the solution has a well-defined wave front in addition to a residual disturbance which persists at all points traversed by the wave front. Thus, a solution to the time-dependent Boltzmann equation, in the telegrapher's equation

approximation, must have a wave front, i.e. a region beyond which there is no disturbance of the neutron density. The wave front effectively separates the medium into two regions, and an observer placed in the assembly will notice a change in the second spatial and time derivatives of the flux as the front passes through the observation point. However, the wave front is a transient which quickly dies out, and the system responds to the driving input in a steady-state manner. When a dissipative term, such as a sinusoidal source fluctuation, is introduced, the result is a spatial oscillation of the neutron flux.

The telegrapher's equation, Eq. (28), can also be changed into the form of Eq. (16) where the complex material buckling $\beta_M^2(s)$ is now defined as

$$\beta_M^2(s) = B_M^2 - (1+3D\Sigma_a)\frac{s}{vD} - \frac{3s^2}{v^2} \tag{29}$$

and the corresponding complex inverse relaxation length is

$$\rho_{mn}^2(s) = B_{mn}^2 - \beta_M^2 = B_{mn}^2 - B_M^2 + (1+3D\Sigma_a)\frac{s}{vD} + \frac{3s^2}{v^2}$$

$$= \gamma_{mn}^2 + (1+3D\Sigma_a)\frac{s}{vD} + \frac{3s^2}{v^2}. \tag{30}$$

This result expresses the square of the inverse relaxation length as a function of frequency, and is analogous to the dispersion law relating the wave numbers to the frequency in the optics of dispersive media as shown by MOORE [24, 28]. This dispersion law can be rewritten by substituting $j\omega$ for s and grouping the real and imaginary terms. The resultant equations are

$$\rho_{mn} = [X_{mn}^2 + jY_{mn}^2]^{1/2} = \alpha_{mn} + j\xi_{mn} = [(\alpha_{mn}^2 - \xi_{mn}^2) + j(2\alpha_{mn}\xi_{mn})]^{1/2}, \tag{31}$$

where

$$X_{mn}^2 = (\alpha_{mn}^2 - \xi_{mn}^2) = \gamma_{mn}^2 - \frac{3\omega^2}{v^2} \tag{32}$$

$$Y_{mn}^2 = (2\alpha_{mn}\xi_{mn}) = (1+3D\Sigma_a)\frac{\omega}{vD} \tag{33}$$

$$\alpha_{mn} = \left(\frac{\Psi_{mn}^2 + X_{mn}^2}{2}\right)^{1/2} \tag{34}$$

$$\xi_{mn} = \left(\frac{\Psi_{mn}^2 - X_{mn}^2}{2}\right)^{1/2} \tag{35}$$

$$\Psi_{mn}^2 = [X_{mn}^4 + Y_{mn}^4]^{1/2}. \tag{36}$$

Substitution of the above relationships into Eq. (28) yields the solution

$$\psi(x,y,z,t) = \sum_{m=1}^{\infty}\sum_{n=1}^{\infty} \frac{\Delta S_{mn}(0,0,0,t)\cos\frac{m\pi x}{a}\cos\frac{n\pi y}{b}}{2D(\alpha_{mn}^2 + \xi_{mn}^2)^{1/2}} e^{-\alpha_{mn}z} e^{j(\omega t - \xi_{mn}z)}. \quad (37)$$

This equation indicates that each spatial mode, which is weighted by the corresponding Fourier coefficient of the source term, propagates as a damp wave with a phase shift with respect to the original disturbance. The wave velocity for the mn-th mode is

$$V_{mn} = \omega/\xi_{mn} \quad (38)$$

indicating that neutron wave propagation is a dispersive phenomenon since the wave velocity is frequency dependent. For low frequencies, Eq. (38) reduces to

$$V_{mn} = 2vD\gamma_{mn}/(1+3D\Sigma_a) \quad (39)$$

indicating that the velocity of each mode is different, but independent of frequency. For high frequencies, Eq. (38) becomes

$$V_{mn} = v/\sqrt{3} = 0.577\ v \quad (40)$$

indicating that the wave velocity for all modes approaches 0.577 times the average neutron velocity. Hence the wave velocity for high frequencies approaches the velocity of the wave front. Actually the wave and wave front velocity are both equal to the average neutron velocity v, and the factor 0.577 is due to the inaccuracies in the P_1 approximation.

Under suitable experimental conditions, one can minimize the higher spatial modes, therefore plotting the amplitude and phase shift of a wave as a function of the source-detector distance from which can be determined both the real and imaginary part of the inverse complex relaxation length, α_{mn} and ξ_{mn} respectively. Hence, Eqs. (31) through (36) yield

$$\alpha_{mn}^2 - \xi_{mn}^2 = B_{mn}^2 - B_M^2 - \frac{\omega^2}{3v^2} = \gamma_{mn}^2 - \frac{3\omega^2}{v^2} \quad (41)$$

$$2\alpha_{mn}\xi_{mn} = (1+3D\Sigma_a)\frac{\omega}{vD}. \quad (42)$$

Hence the slope of the $(\alpha_{mn}^2 - \xi_{mn}^2)$ versus ω^2 plot yields velocity of the wave front $(v/\sqrt{3})$ and the intercept at zero frequency will determine the square of the inverse relaxation length. As the frequency increases, higher order transport corrections must be used, which will result in new terms of higher powers of frequency. The plot of $(2\alpha_{mn}\xi_{mn})$ as a function of frequency results in a straight line through the origin the slope of which is proportional to $(1+3D\Sigma_a)/vD$. The telegrapher's equation approximation of the Boltzmann transport equation should be used for high frequencies where the time be-

tween successive collisions of neutrons is comparable to the reciprocal of the angular frequency as pointed out by ALBRECHT [33] and MORTENSEN [34]. However, recent work by KUNAISH [35] has shown that the correction due to the non-Maxwellian energy distribution is much more important than the improvements achieved by the use of the P_1 approximation instead of the diffusion equation. Furthermore, the frequencies of interest in most nuclear systems, except those containing light water, do not warrant use of the P_1 approximation over diffusion theory.

In the limit of zero mean free-path and zero absorption cross-section, but infinite velocity, the telegrapher's equation reduces to the diffusion equation. It is the property of the diffusion equation that the wave front propagation velocity is infinite. However, a wave-like disturbance is propagated, and its velocity is finite and frequency dependent. Diffusion theory yields approximately the same wave velocity for low frequencies as the P_1 approximation, but gives the erroneous result that wave velocity is proportional to the square root of the frequency as ω approaches infinity. These limitations of diffusion theory have been pointed out by ALBRECHT [33], MORTENSEN [34] and KUNAISH [35].

In view of the importance of the non-Maxwellian energy distribution, reported by KUNAISH [35], let us consider the thermalization theory model in the diffusion approximation as developed for moderators by PEREZ and UHRIG [16]. The energy dependent neutron flux is developed in terms of the associated Laguerre polynomials of order one and normalized to unity. This expansion is convenient because the first term represents the Maxwellian distribution and the higher terms are perturbations. Furthermore, these polynomials are an exact solution to the heavy gas thermalization model for constant absorption cross-section.

Equations (13) through (27) are generally valid for this analysis except that Eq. (19) becomes

$$\rho_{mn}^2(s) = B_{\perp mn}^2 + \frac{\sqrt{\pi}}{2}\left\{\frac{1}{L^2}\left[1-\frac{\pi C_0}{4vD}\left(\frac{1}{L^2}+\frac{s}{vD}\right)\right]+\frac{s}{vD}\left[1-\frac{\pi C_0 s}{4v^2D^2}\right]\right\}. \quad (43)$$

For a sinusoidal input

$$s = j\omega \quad (44)$$

and separation of the real and imaginary components of Eq. (43) gives

$$\alpha_{mn}^2 - \xi_{mn}^2 = \left[B_{\perp mn}^2 + \frac{\sqrt{\pi}}{2L^2}\left(1+\frac{\pi C_0}{4vDL^2}\right)\right] + \left(\frac{\sqrt{\pi}}{2vD}\right)^3 C_0\omega^2 \quad (45)$$

and

$$2\alpha_{mn}\xi_{mn} = \left(\frac{\sqrt{\pi}}{2vD}\right)\omega - \left(\frac{\pi}{2vDL}\right)^2 C_0\omega^2, \quad (46)$$

where

$$\rho_{mn}^2(j\omega) = (\alpha_{mn} + j\xi)^2 = \alpha_{mn}^2 - \xi_{mn}^2 + j\,2\alpha_{mn}\xi_{mn} \quad (47)$$

and C_0 is the "cooling" coefficient.

Plots of $(\alpha_{mn}^2 - \xi_{mn}^2)$ and $(2\alpha_{mn}\xi_{mn})$ versus frequency for moderators are shown in Figs. 3 and 4 for diffusion theory, thermalization theory and the P_1 approximation of the Boltzmann equation. It is seen that the "corrections"

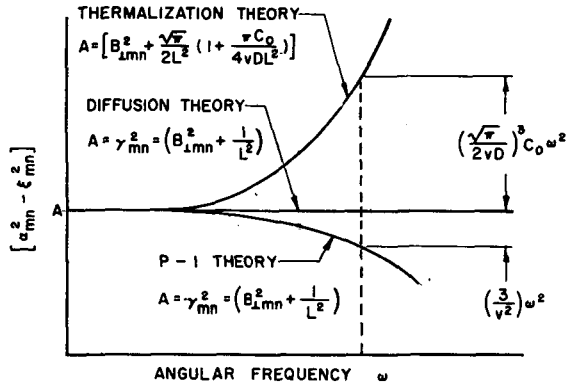


Fig. 3

Plot of $[\alpha_{mn}^2 - \xi_{mn}^2]$ versus frequency for neutron waves

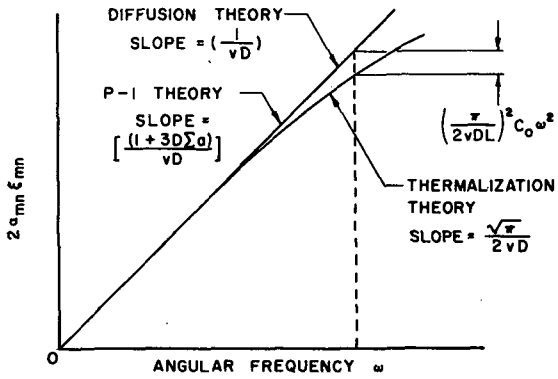


Fig. 4

Plot of $2\alpha_{mn}\xi_{mn}$ versus frequency for neutron waves

to diffusion theory for the $(\alpha_{mn}^2 - \xi_{mn}^2)$ plot for the thermalization theory and P_1 treatments are opposite in sense, with the non-Maxwellian neutron energy distribution correction being much more important in moderators. In multiplying systems, the two effects are often nearly equal in magnitude. For some systems, especially those where neutrons spend much of their lives as thermal neutrons, e. g. graphite or heavy water-moderated multiplying systems, the two effects tend to cancel out, thereby making diffusion theory appear quite valid. The "correction" for the $2\alpha_{mn}\xi_{mn}$ is quite small, even for high frequencies.

Experimental results of neutron wave experiments carried out on

graphite are reported later in this paper and compared with results of other techniques.

HETRICK and SEALE [36] have proposed that neutron waves be used to measure crystalline binding parameters of materials. Specifically they propose to carry out experiments at very low temperatures in order to increase the number of solid and liquid materials in which models for the binding of hydrogen atoms can be studied.

SQUARE WAVE PULSING

Another interesting technique related to pulsed neutron research is the square wave pulsing or modulation technique, attributed by KEEPIN [37] to Oak Ridge National Laboratory, which may also be used to determine the decay of the thermal neutron flux in a nuclear system. It has the distinct advantage of providing a means of measuring decay constants without using a multichannel time analyser. The average neutron counting rate from a nuclear system subjected to a neutron source "on-off" pulsing with a 50% duty cycle and counted only during the "off" period is

$$\dot{C} = \frac{\dot{C}_\infty}{4} \frac{f}{(\alpha/4)} \tanh\left[\frac{(\alpha/4)}{f}\right], \tag{48}$$

where $\dot{C}_\infty$ is the saturated counting rate for continuous source operation, and $\alpha/4$ is one-quarter of the decay constant of the fundamental mode which is being measured. For $f \ll \alpha/4$, the observed counting rate varies linearly with frequency, that is

$$\dot{C} = \dot{C}_\infty(f/\alpha), \tag{49}$$

while for $f \gg \alpha/4$, the counting rate is $(\dot{C}_\infty/4)$. Extrapolation of the asymptotes for high and low frequencies intersect at $f = \alpha/4$ or $\omega = \pi\alpha/2$. This is illustrated in Fig. 5, where count rate is plotted against frequency.

To measure α accurately, the range of oscillator frequencies should "straddle" the value $f = \alpha/4$ by at least one decade in each direction. A lower

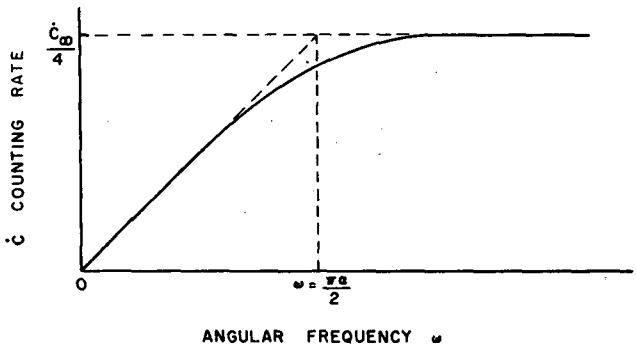


Fig. 5

Plot of counting rate versus frequency for square wave pulsing

limit on pulse length is imposed by the condition that pulse rate and decay times be small compared to pulse length. In practice, these considerations limit pulse length to a minimum of about 1 ms (f_{max}= 500 cps). Hence, measurements are limited to values of $\alpha \leq 200\ s^{-1}$.

The square wave technique can also be used in the same way as a sinusoidal input. Since the square wave can be Fourier analysed into an infinite number of harmonics of the fundamental frequency, it can be considered as the superposition of sinusoidal inputs. For a linear system, the output will be a superposition of the outputs due to the individual components of the input. It has the advantage that the data for many frequencies can be taken simultaneously. In actual practice, the number of frequencies for which measurements can be taken is limited because the amplitude of the higher harmonics decreases linearily with the order of the harmonic. This difficulty can be overcome by use of the pseudo-random binary (on-off) type of square wave pulsing discussed later.

RANDOM NOISE TECHNIQUES

The use of random noise as an input for purposes of measuring parameters of a nuclear system is under widespread investigation [38]. There are several principal advantages which may accrue from this technique. The first of these is that the random noise input may actually already exist in the reactor in that the fission process is a statistical phenomenon. Furthermore, the output of any artificial neutron source is essentially random in nature and often can serve as the input to a system. An additional advantage for "linearized" systems is that the disturbance generally is as small as it can be and still is significant, thereby obviating the problems of nonlinearities if they exist.

The relationships given in Eqs. (7) through (10) generally can be used for the determination of the impulse response or the transfer function of the system under investigation. Since it is much easier to calculate the transfer function from Eqs. (8) or (10), this is usually the technique employed. However, the original measurements taken on a system may be correlation techniques since a correlation function and the corresponding spectral density constitute a Fourier transform pair. The choice as to which measurement is actually taken is dependent upon the equipment available and the experimenter's choice.

In any practical nuclear system employing a detector for measurement, noise is introduced into the system by the detection process. Furthermore, the instrumentation involved in measuring the correlation function or the spectral density may also have dynamic characteristics $G_m(j\omega)$ which must be taken into account. Hence, a realistic block diagram of a nuclear system and instrumentation is shown in Fig. 6. The application of Eq. (8) to this system yields

$$\Phi_{oo}(\omega) = |G_R(j\omega)|^2 |G_M(j\omega)|^2 \Phi_{ss}(\omega) + |G_M(j\omega)|^2 \Phi_{nn}(\omega). \qquad (50)$$

Since the inherent fluctuations of the neutron population in a subcritical

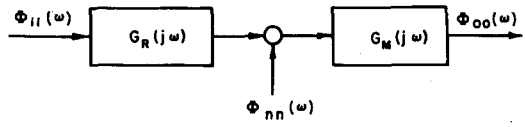


Fig. 6

Block diagram of nuclear and measuring systems

system are caused by the random release of neutrons from the neutron source, the input power spectral density $\Phi_{ii}(\omega)$ can be shown to be constant over the frequency range of interest. Furthermore, the inherent detector noise is also random and hence the $\Phi_{nn}(\omega)$ is a constant. Substitution of Eq. (4) of the transfer function into Eq. (50) and rearranging gives

$$\frac{\Phi_{oo}(\tau)}{|G_M(j\omega)|^2} = \frac{A}{\omega^2 + \alpha^2} + B . \tag{51}$$

Figure 7 shows the relationships of Eq. (51) in graphical form. Hence, the determination of the power spectral density corrected for characteristics of

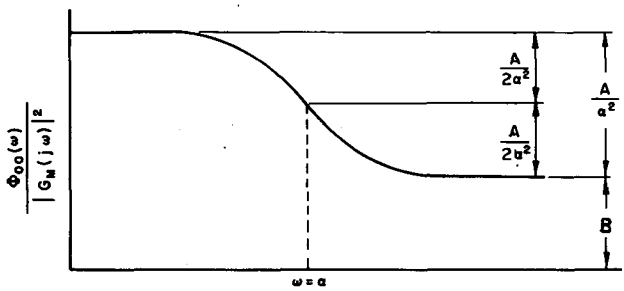


Fig. 7

Plot of $\frac{\Phi_{oo}(\omega)}{|G_M(j\omega)|^2} = \frac{A}{\alpha^2 + \omega^2} + B$

the instrumentation at several frequencies and use of a least-squares fit will allow the constants A, B and α to be evaluated. Typical results of this kind of a measurement for the University of Florida Training Reactor [39] taken by BADGLEY [40] are shown in Fig. 8. The driving function was the natural fluctuations of four Pu-Be neutron sources located in the reactor core.

It is apparent from Eq. (7) that its usefulness is limited by the complexity of trying to solve for the impulse response function. However, it can be used in certain situations. LEE [31] shows that Eq. (7) can be manipulated into the form

$$\phi_{oo}(\tau) = \int_{-\infty}^{\infty} \phi_{gg}(\lambda)\phi_{ii}(\tau - \lambda)d\lambda . \tag{52}$$

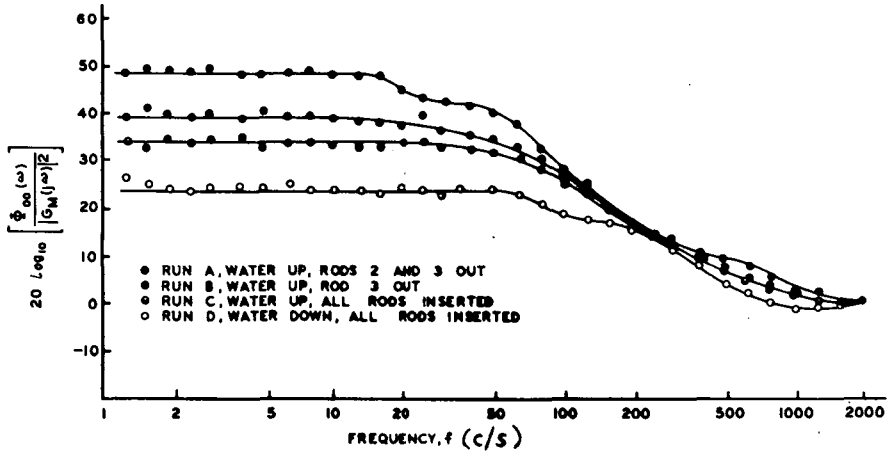


Fig. 8

Experimental measurements of power spectral density for four reactor configurations. Data are normalized to a common value at 2000 Hz.

When the input is a white noise. Eq. (52) becomes

$$\phi_{oo}(\tau) = B\phi_{gg}(\tau), \tag{53}$$

where B is a constant. For a system the impulse response of which is of the form

$$g(t) = C e^{-\alpha t} \tag{54}$$

Eq. (14) becomes

$$\phi_{oo}(\tau) = \frac{BC^2}{2\alpha} e^{-\alpha\tau}. \tag{55}$$

Unfortunately, this expression is valid only if the input disturbance of the system completely overrides all other fluctuations in the system, since it does not take into account quantities like detection noise, background, etc. Typical results from the University of Florida Training Reactor using an accelerator type neutron source producing large fluctuations are shown in Fig. 9.

The expression in Eq. (9) is also quite useful in certain instances. If the input disturbance is random, then it can be shown that

$$\phi_{io}(\tau) = A g(\tau), \tag{56}$$

where A is the constant of proportionality, i. e. the cross-correlation between the input and the output is proportional to the impulse response function. The use of the cross-correlation technique has an additional advantage in that any disturbance which is not correlated with the input disturbance does not influence the measurement significantly, provided that the

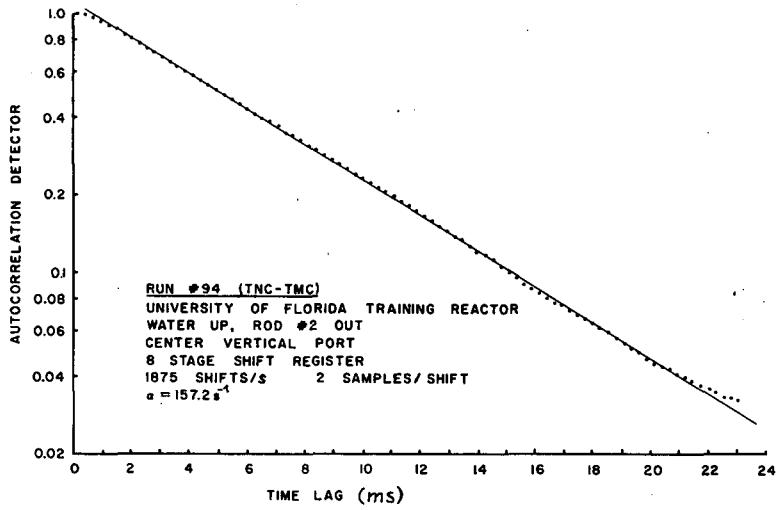


Fig. 9

Plot of auto-correlation of the detector output in the University of Florida Training Reactor

length of run is sufficiently long. The use of this technique will be illustrated in the following section on pseudo-random binary pulsing.

The relationship of Eq. (10) is quite useful since it will allow evaluation of both the amplitude and phase for the transfer function from a cross-correlation measurement between the input and the output, provided that the auto-correlation function of the input is either known or can be measured. If the input is a random noise, then $\Phi_{ii}(\omega)$ is a constant, and Eq.(10) becomes

$$\Phi_{io}(\omega) = A\,G(j\omega) \tag{57}$$

i. e., the cross-spectral density is proportional to the transfer function. Here again, both the amplitude and phase can be determined.

PSEUDO-RANDOM BINARY PULSING

In the section on random noise techniques it was shown that if the input disturbance was truly random in nature then the input-output cross-correlation function and cross-spectral density are proportional respectively to the impulse response function and the transfer function. These simple relationships are extremely attractive to the experimentalist, but unfortunately a true random signal is very difficult to obtain. In a practical situation, use of an imperfect random input may result in a significant amount of error. The reason for this is that Eqs. (56) and (57) are based on the assumption that the random signal gives an auto-correlation function which is a delta-function and a power spectral density function which is flat over all frequency ranges. This is physically unrealizable since it means that the random signal is correlated over an infinite length of time, and furthermore, it implies infinite power in the signal. For a finite length random signal, the

auto-correlation function has a finite width, and the auto-correlation has side-bands the amplitude of which may reach 5 to 10% of the peak value and are non-deterministic in nature. This leads to variations in the power spectral density and a general decrease in the higher frequency range.

To overcome these deficiencies, a pseudo-random binary variable has been used. The fact that it is binary makes it particularly applicable for an accelerator-type neutron source input because it allows the source to be simply turned on and off. The pseudo-random has statistical characteristics which, to a high degree, approximate those of a random signal. In a strict mathematical sense, the probability distribution is non-Gaussian in nature, but it very closely approximates a Gaussian distribution. The most important factor is that the auto-correlation function of this pseudo-random binary variable is deterministic in nature and approximates a delta function. Hence the exact values for the auto-correlation function can be substituted into Eq. (9) thereby providing a means of calculating the impulse response function. Furthermore, as will be seen later, the power spectral density is constant over a wide frequency range, and as a result Eq. (57) can be used over a wide frequency range. Even for high frequencies Eq. (10) can be used directly since the power spectral density is deterministic in nature.

There are two types of commonly used pseudo-random binary inputs. The first to be used with nuclear systems with the residue of the squares sequence suggested by COOPER [41] and described by ANDERSON et al. [43] for varying the reactivity input to the KIWI A' and GODIVA reactors. This sequence has been used extensively by GIBSON et al. [44] at Purdue University in their cross-correlation work, but, in general, has not gained widespread usage primarily because of the ease of generating the sequence described below.

The commonly used pseudo-random binary input variable is the "maximum length linear shift register sequence" which has been described extensively by PETERSON [45]. The use of this type of input for determining parameters related to shutdown reactivity of nuclear systems has been developed independently by STERN and VALAT [46, 47] and UHRIG [48]. This sequence is generated by use of a multi-stage shift register in which the output from the appropriate stages has been fed back through a modulo-of-two adder (an "exclusive - or" gate) to the input. The advancing of this system through its sequence is controlled by an external clock, which can operate at any desired frequency compatible with the bandwidth of the shift register components. The result is a periodic signal with a period of $N\Delta$, where N, the number of shifts (each Δ seconds long) per cycle, is given by $N = 2^n - 1$, where n is the number of stages used in the shift register.

As an example of the pseudo-random binary input variable, let us consider the output from a five-stage shift register in which the outputs of stages three and five have been fed back into the input through a modulo-of-two adder as shown in Fig. 10. The output of the fifth stage of such an arrangement is shown in Fig. 11. It is interesting to note the distribution of the length of the binary states (expressed in number of Δ time increments) in the pseudo-random variable for one period as shown in Table I. A similar pattern exists for longer sequences with the number of shorter increments increasing in a binary fashion.

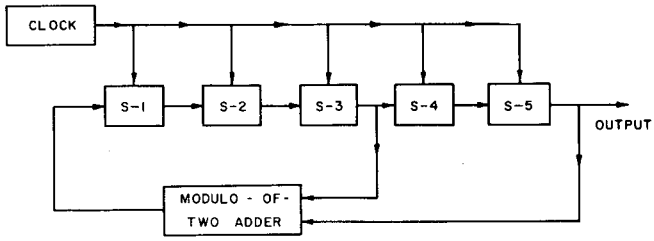


Fig. 10

Five-stage shift register with feedback to give maximum length linear shift register sequence

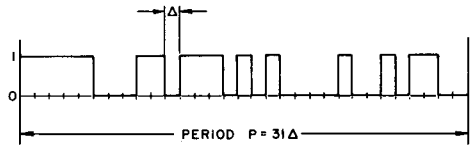


Fig. 11

Output of stage 5 of the shift register of Fig. 10

TABLE I

CONTENTS OF FIVE STAGE SHIFT REGISTER SEQUENCE

Length in Δ's	"Zero" state	"One" state
1	4	4
2	2	2
3	1	1
4	1	0
5	0	1

The auto-correlation functions of this pseudo-random binary variable is shown in Fig. 12 to be a series of triangles with base width 2Δ and unity height at intervals of NΔ separated by sidebands between triangles having a constant value of 1/N, where N is the number of shifts per cycle. The period of the auto-correlation function is the same as the period of the pseudo-random variables. It is interesting to note that as N becomes larger, the magnitude of the sidebands decreases, the triangles become narrower and the periods become longer, and the auto-correlation function, except for its periodicity, approximates a delta function more accurately. However, it should be noted that the area under the triangle above the zero axis is substantially equivalent to the area under the negative sidebands, indicating

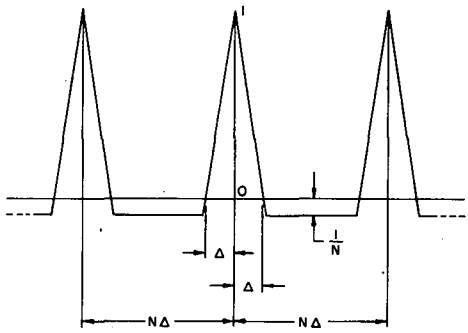


Fig. 12

Auto-correlation function of signal in Fig. 11

that the effect of the sidebands of the auto-correlation function upon the measurement should be taken into account.

The power spectral density of the pseudo-random input has several interesting features. If the auto-correlation function is treated as an aperiodic function, which is a reasonable assumption if the period is very long compared with the time of interest (i. e. the settling time of the system), then the power spectral density is continuous and is

$$\Phi_{ss}(\omega) = \frac{\Delta}{2\pi}\left\{\frac{\sin\frac{\omega\Delta}{2}}{\frac{\omega\Delta}{2}}\right\}^2. \tag{58}$$

However, if one considers the auto-correlation function as being periodic, then the power spectral density is discrete and its envelope is given by

$$\Phi_{ss}(\omega) = \frac{1}{N}\left\{\frac{\sin\frac{n\omega_1\Delta}{2}}{\frac{n\omega_1\Delta}{2}}\right\}^2, \tag{59}$$

where ω_1 is the fundamental frequency corresponding to the period of the sequence. The locus of the discrete spectrum component has the same shape as the curve for Eq. (58), the continuous case. The plot of the envelope of the discrete power spectral density of the pseudo-random binary input is shown in Fig. 13. The power spectral density is constant over the low frequency range. This is readily apparent from Eqs. (58) and (59) as the case where the $\sin(\omega\Delta/2)$ is approximately equal to $(\omega\Delta/2)$.

In practical use, the system being studied must bave a bandwidth narrower than the power spectral density of the pseudo-random input; i. e., the time constant of the system should be less than the period of the input sequence, usually by a factor of five. Furthermore, the impulse response of the system should not change significantly over one delta increment. Here again, a ratio of five between the time constant and the increment Δ is reasonable.

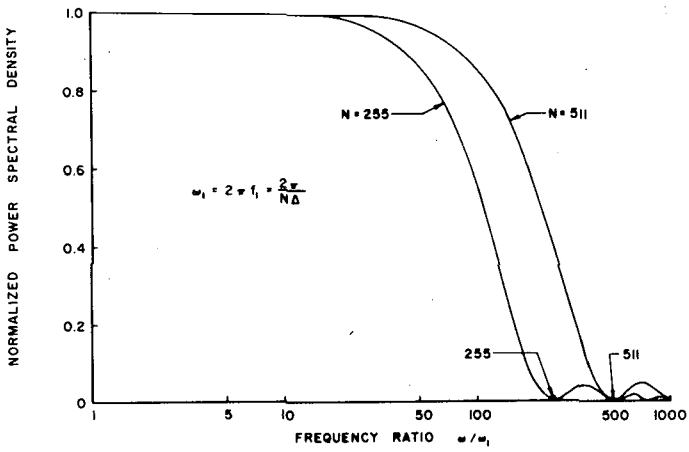


Fig. 13

Power spectral density of a pseudo-random binary variable

This means that the time interval Δ should be smaller than the bandwidth of the noise being used by a factor of at least 25.

Experimental results of cross-correlation measurements taken on the University of Florida Training Reactor are shown in Figs. 14 and 15. These

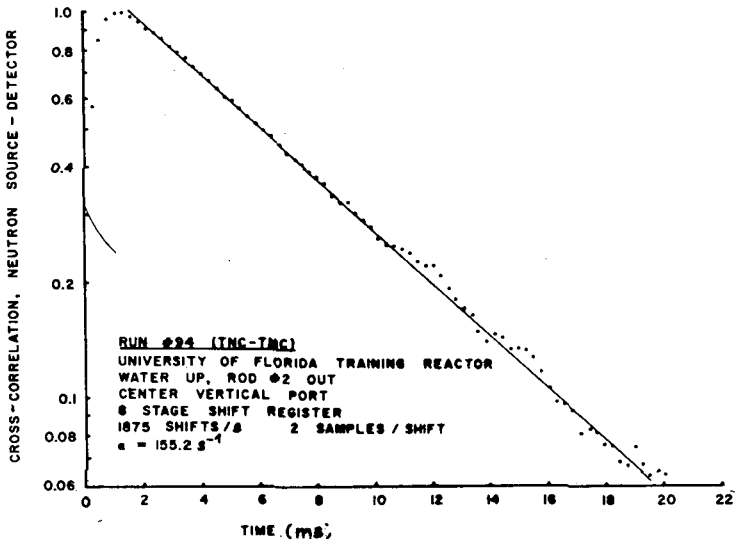


Fig. 14

Cross-correlation function of run #94 on the University of Florida Training Reactor

results are for the same run for which the auto-correlation function is shown in Fig. 9. The decay constant as determined from Fig. 14 for about 25 ms is 155.2 s^{-1}. When the data of Fig. 15 are restricted to 14 ms, the decay constant is 153 s^{-1}. Figure 15 also shows the cross-correlation between the

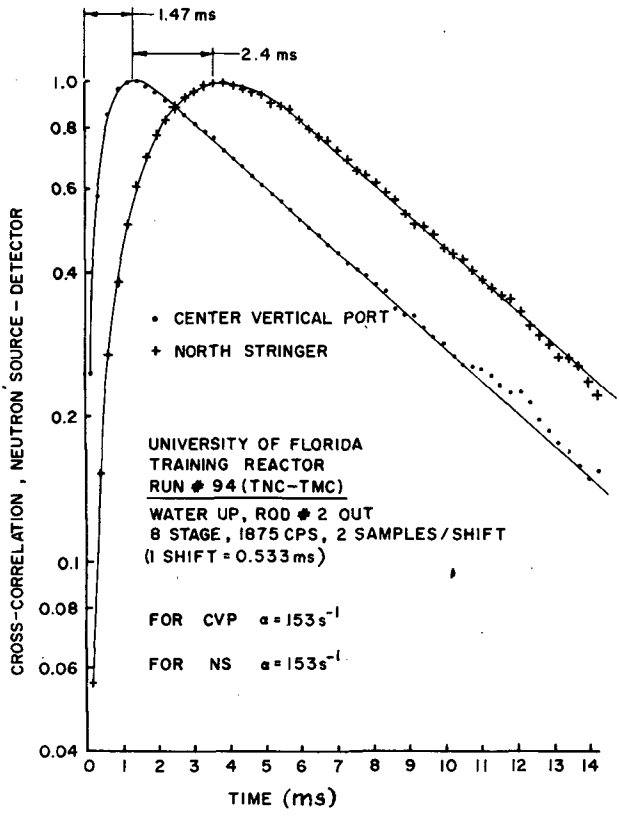


Fig. 15

Cross-correlation function of run #94 on the University of Florida Training Reactor

source and the output of a neutron detector located in the North beam port outside the core (about five feet from the neutron source). Use of a least-squares fit to the straight line (exponential) portion of the two curves gives identical decay constants of 153 s^{-1}. These values of α are in good agreement with the value of 157.2 s^{-1} obtained from the auto-correlation plot of Fig. 9.

Figure 16 shows a series of cross-correlation runs on the University of Florida UFAPA, an unreflected water-moderated, 93% enriched assembly capable of achieving an effective multiplication factor of about 0.95. Since reactivity is controlled by varying the water level in the assembly, Fig. 16 shows the cross-correlation between the neutron source and output of a detector for five different water levels. In general, these preliminary results agree within about 10% with pulsed measurements on the same assembly. This work is continuing.

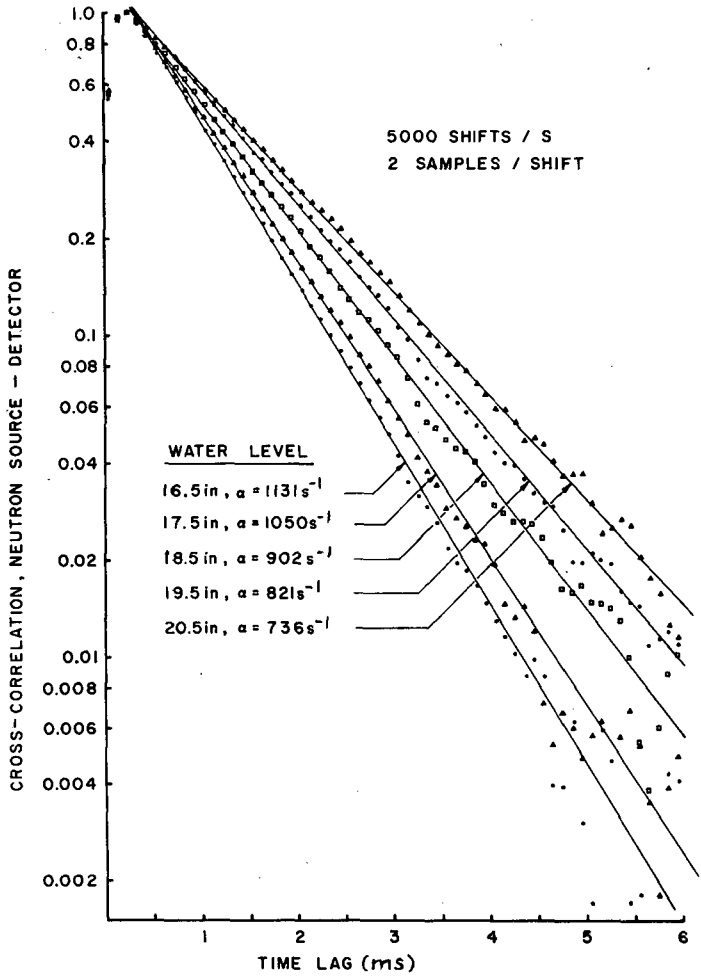


Fig. 16

Source-detector cross-correlation for UFAPA

THERMAL NEUTRON PULSE PROPAGATION

The phenomena of thermal neutron pulse propagation can be demonstrated by use of diffusion theory. Let us consider the spatially dependent transfer function derived in Eq. (27). Since the impulse response of a system can be obtained by taking the inverse Laplace transfer form of the transfer function, taking the Laplace transform of Eq. (27) will give the spatially dependent impulse response function or Green's function. This Laplace transformation has been carried out by UHRIG [17] and the result is

$$g(x, y, z, t) = \frac{2}{ab}\sqrt{\frac{v}{\pi D}}\,\frac{1}{\sqrt{t}}\,e^{-z^2/4vDt}\sum_{m=1}^{\infty}\sum_{n=1}^{\infty}\cos\frac{m\pi x}{a}\cos\frac{n\pi y}{b}\,e^{-vD\gamma_{mn}^2 t}. \quad (60)$$

This expression is quite interesting from the standpoint that it is the product of three time-dependent terms, all of them contributing to the shape of the impulse response function. Let us consider the contribution of each of these terms to the triple product. The $\exp(-vD\gamma_{mn}^2 t)$ term can be shown [17] to be substantially equivalent to the exponential decay associated with the conventional pulse neutron experiments. Hence the presence of the other two terms in the impulse response function is surprising at first. The contribution of these three terms to the impulse response function of a graphite-moderated, natural uranium-subcritical assembly is shown in

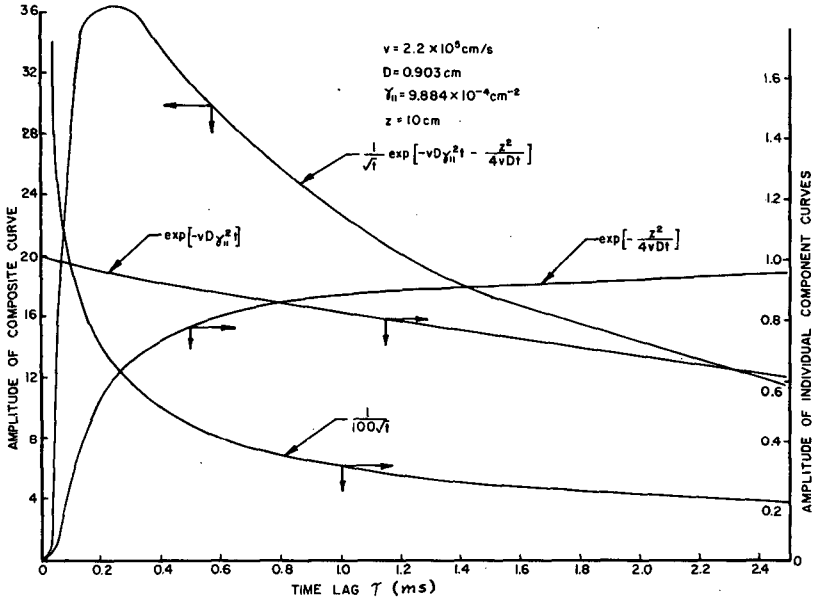


Fig. 17

Contributions of three terms of Eq. (49) to the impulse response of a graphite moderated-natural uranium subcritical assembly

Fig. 17, in which only the term for the fundamental mode is taken into consideration. It is apparent that the impulse $\exp(-z^2/4vDt)$ term is responsible for the "time delay" or retardation in the impulse response function, and that the curve goes through an inflection point where the exponent is equal to unit. Furthermore, it is seen that this term approaches unity asymptotically as time increases. The $1/\sqrt{t}$ term is an equilateral hyperbola which decreases very rapidly at first and then asymptotically approaches zero. This means that the spatially dependent impulse response function is not exponential, and cross-correlation measurements at specific positions in an assembly need to be corrected for the influence of these two terms. When the detector is large and averages the output from a large region of the assembly, the impulse response is exponential.

Another interesting comparison can be obtained by considering that portion of Eq. (60) outside the double summation signs, i. e. the multiplicative

and leakage effects are ignored, to be a Gaussian distribution term of the form

$$P(z) = \frac{1}{\sigma\sqrt{2\pi}}\, e^{-z^2/2\sigma^2}. \tag{61}$$

where the standard deviation is

$$\sigma = \sqrt{2vDt}. \tag{62}$$

Hence

$$\frac{2}{ab}\sqrt{\frac{v}{\pi D}}\,\frac{1}{\sqrt{t}}\, e^{-z^2/4vDt} = \frac{4v}{ab}\,P(z). \tag{63}$$

Equation (62) indicates that the standard deviation increases with time and that a pulse of thermal neutrons injected at the origin at time t = 0 spreads out as time increases. Hence it is apparent that a burst of thermal neutrons introduced at the origin simply dissipates in symmetrical fashion about the z = 0 plane. This is illustrated very graphically in Fig.18, which shows the

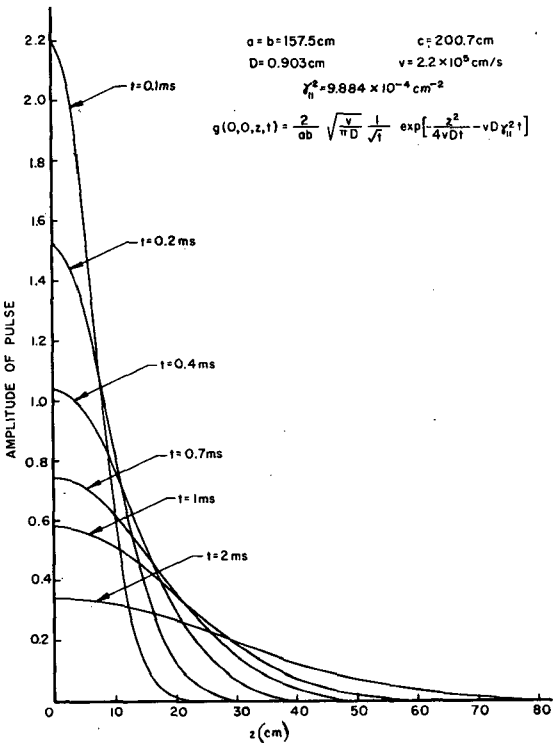


Fig. 18

Spatial distribution of neutrons in a graphite moderated-natural uranium assembly after a pulse of thermal neutrons has been ejected at the origin

spatial distribution of neutrons in a graphite-moderated natural uranium assembly after a pulse of thermal neutrons has been injected at the origin. It is apparent that the neutron density does spread out in a Gaussian-like manner about the z = 0 plane with the spatial dispersion increasing as the function of time. The variation of the neutron density as a function of time, at a specific position on the z-axis of a graphite-moderated natural uranium subcritical assembly, is shown in Fig. 19 for several positions along the

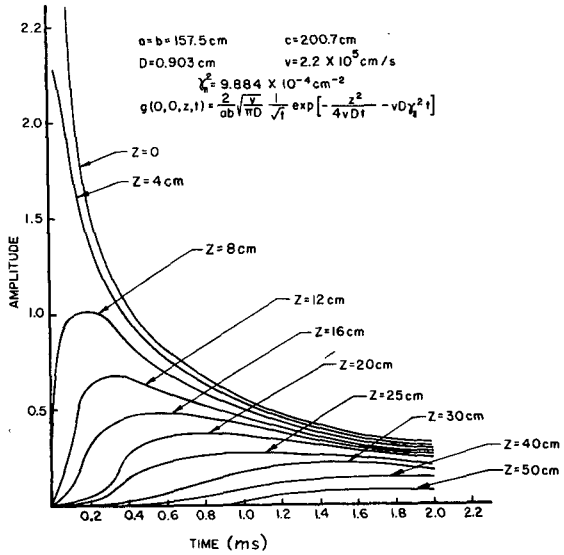


Fig. 19

The impulse response function at several positions along the z-axis of a graphite moderated-natural uranium assembly

z-axis. It is apparent that the peak value of the pulse does propagate along the z-axis as a function of time; however, the pulse spreads out severely with time and distances. Similar results were obtained from a different approach by HARTLEY [49] using diffusion theory.

Hartley also carried out experiments using a burst of thermal neutrons at the boundary. Because the accelerator used produced 14.3-MeV neutrons, it was necessary to use a "neutron filter" between the neutron source and the graphite to slow down the fast neutrons to thermal energy. Experimental measurements at four different positions obtained by HARTLEY [49] from the pulsing of a block of graphite are shown in Fig. 20. More recent data taken, using the Van de Graaff accelerator and the lithium P-N reaction to produce thermal neutrons, are shown later.

Neutron pulse propagation can also be studied using the pseudo-random binary pulsing technique. The data shown in Fig. 21 have been obtained from the University of Florida Accelerator Pulsed Assembly (UFAPA) [50] with a detector located between fuel elements at six distances from the end of the assembly where the neutron source is located. Data have been normalized to give a peak value of unity. The peculiar shape of the peak from the

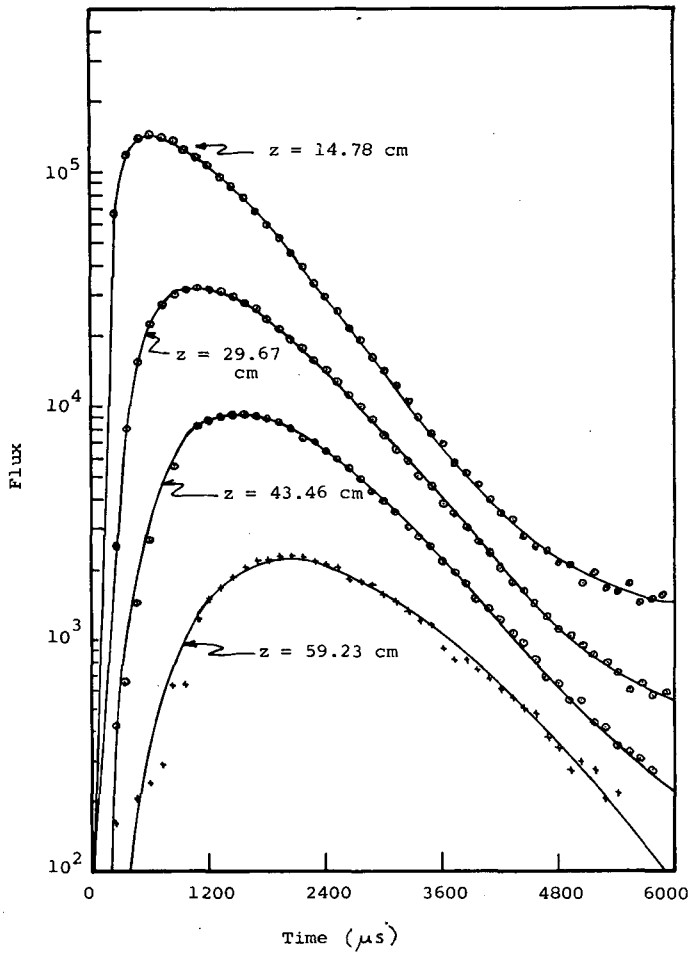


Fig. 20

Experimentally detected pulses

4-in and 8-in positions is due to the use of 14.3-MeV neutrons without a filter to thermalize them before entering the assembly. The different times at which the peak value is reached is readily apparent.

A TRIGA pulsing reactor has been used by MILEY [51] as a very high intensity source of thermal neutrons to study neutron pulse propagation in a graphite thermal column. The principal advantage over the use of accelerator-type neutron sources is intensity. This allows simplification of instrumentation and a high signal-to-background ratio since the experiment is usually not complicated by delayed neutron effects. This allows pulses to be propagated long distances before the neutron density signal becomes too small to be readily measured. The principal disadvantage of using a pulsed reactor is the wide pulse width (about 30 ms at half-peak value) which is in-

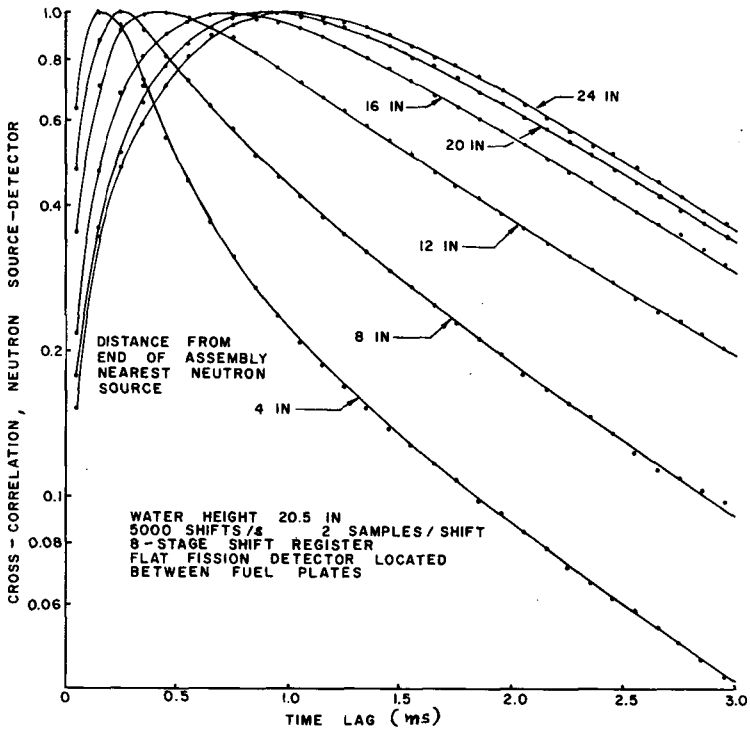


Fig. 21

UFAPA pulse propagation

herent in a thermal reactor pulse. This means that the frequency content of the pulse is limited to relatively low frequencies.

MILEY [51] has also developed several theoretical models to study pulse propagation. These models include the delta source model, the constant pulse shape model and the distributed delta source model. He has also related this work to other transient experiments with nuclear systems. His experiments to date have been limited to studying pulse shape, propagation times and inverse relaxation lengths associated with various sizes of reactor pulses in the graphite thermal column. With the number of pulsing TRIGA reactors available and the recent introduction of the PULSTAR reactor, a uranium oxide-fuelled pulsing reactor, it is likely that there will be additional work of this type undertaken.

COMPARISON OF EXPERIMENTAL RESULTS FROM DIFFERENT TECHNIQUES

Recent work by PEREZ and BOOTH [52] and OHANIAN [53] at the University of Florida has extended the thermalization treatment by using the energy-space eigenfunctions of the Boltzmann equation based upon the more

realistic scattering kernel derived by PARKS [54]. The resulting complex eigenvalue ρ^2 is again given as a series expansion in frequency.

The experimentally measured amplitude and phase shift of the thermal neutron waves, excited by both modulated and pulsed thermal neutron sources, are shown in Figs. 22 and 23. As predicted by the theory, the amplitude of

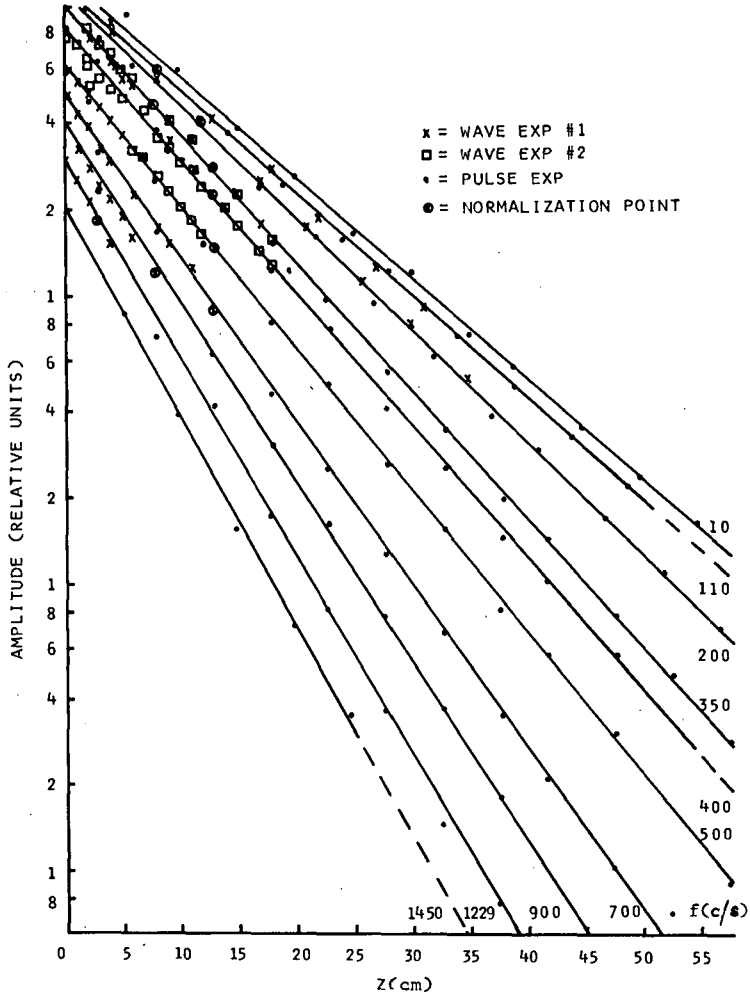


Fig. 22

Combined amplitude curves for several frequencies

the neutron wave decays exponentially and the phase lag increases linearly with distance between source and detector. The reproducibility of the data is evident from the agreement between the three independent experiments which were performed. From a least-squares fit of the above results, the values of both the real and imaginary part of the complex inverse relaxation length, α and ξ respectively, were found as a function of frequency. Com-

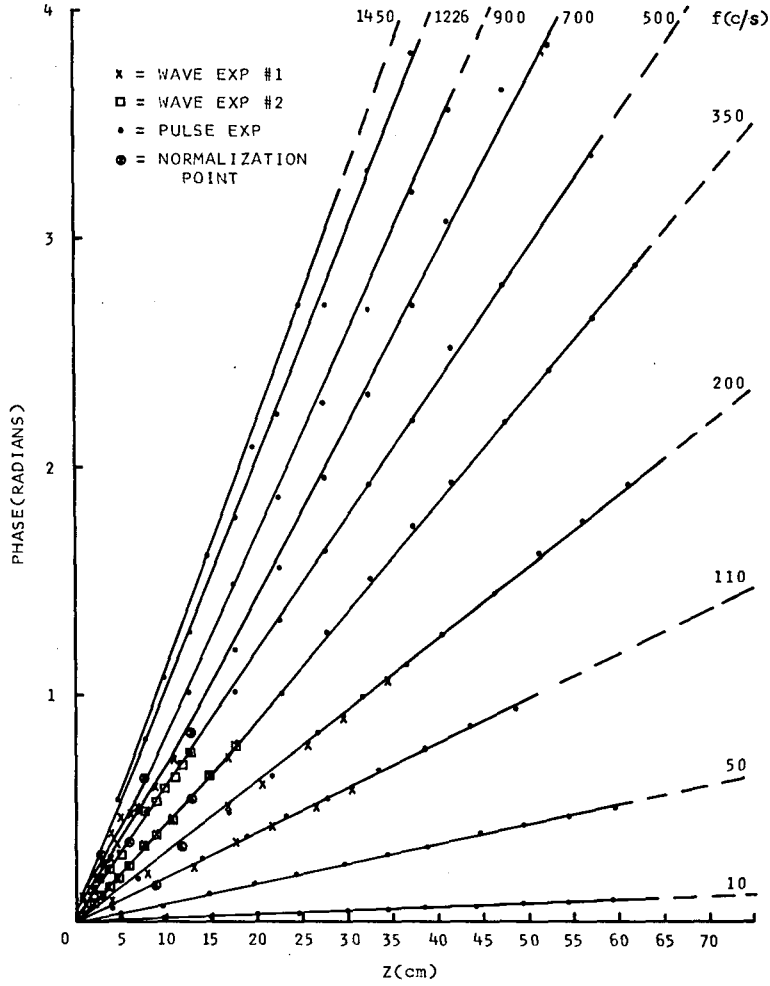


Fig. 23

Combined phase curves for several of the frequencies (some points not shown)

bination of these two independent parameters allows one to separate the diffusion effects, which are the main contributions to the function $2\alpha\xi$, from the thermalization parameters which determine the $(\alpha^2 - \xi^2)$ term.

Figure 24 shows the experimentally obtained $2\alpha\xi$ versus frequency. Agreement with the theory is very good in the full frequency range investigated. The $(\alpha^2 - \xi^2)$ function is shown in Fig. 25 where the theory shows the right general trend although it disagrees quantitatively with the experiment, even at low frequencies where modal contamination of data is not to be expected. This is a result of the extreme sensitivity of the $(\alpha^2 - \xi^2)$ curve to thermalization effects. To further illustrate the relative insensitivity of the $2\alpha\xi$ curve to thermalization effects and the strong dependence of $(\alpha^2 - \xi^2)$

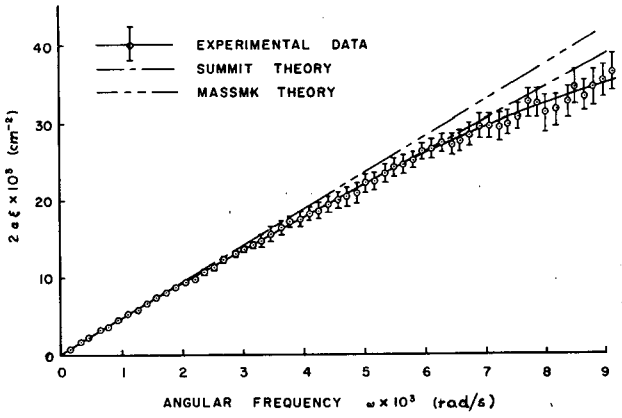


Fig. 24

Plot of $2\alpha\xi$ versus ω for graphite

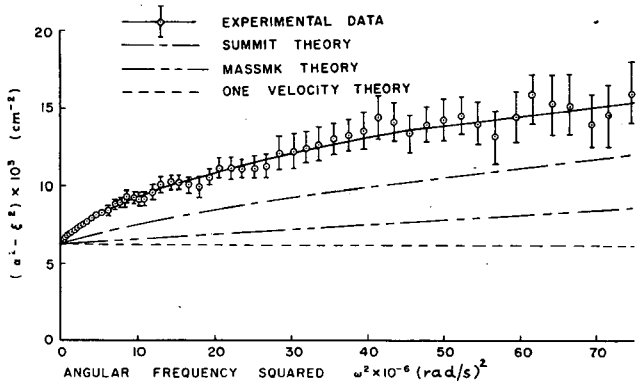


Fig. 25

Plot of $(\alpha^2 - \xi^2)$ versus ω^2 for graphite

upon these same parameters, theoretical curves obtained by the use of mass-12 scattering kernel have been included in both Figs. 24 and 25. The one-velocity prediction of a constant value for $(\alpha^2 - \xi^2)$ has also been indicated. It is to be noticed that the mass-12 theory, which presented a good agreement with Parks' kernel results, in the $2\alpha\xi$ curve, does not agree when the same comparison is made for the $(\alpha^2 - \xi^2)$ case.

The "Step-wise Multiple Regression" Code was used to least-squares fit the $2\alpha\xi$ function to an expansion in odd powers of frequency, and to least-squares fit the $(\alpha^2 - \xi^2)$ function to a similar expansion which is only dependent upon even powers of frequency. The influence of the number of terms taken in the expansions on the goodness of fit was studied by use of the "F" "Student's t" statistical tests applied to several regions of the curves. This method yielded consistent values for the first two coefficients of each expansion, which were then used to determine D_0, C_0 and F_0. The results are

TABLE II

COMPARISON OF EXPERIMENTAL AND THEORETICAL NEUTRON WAVES DATA ON GRAPHITE

	D_0 (10^{-5} cm^2/s)	C_0 (10^{-5} cm^4/s)	F_0 (10^{-7} cm^6/s)
Experimental:			
Booth-Perez (ρ = 1.60 g/cm^3)	2.19 ± 0.01	40.0 ± 2	12 ± 2
Sagot et al. (ρ = 1.619 g/cm^3)	2.19 ± 0.03	37.9 ± 4	-
Theoretical:			
Park's kernel (ρ = 1.60 g/cm^3)	2.14	21.2	-5.5

presented in Table II. Experimental results from SAGOT et al. [55] are included for comparison.

The value obtained for the diffusion coefficient D_0 agrees quite well with the results of STARR and PRICE [56], and it is consistent with the theory. The experimental value of C_0 differs by about a factor of two from the Parks' kernel prediction. It does, however, agree with the experimental values reported by Starr and Price, but does not agree with those of KLOSE [57].

The value F_0 has to be taken as tentative as it depends on the values of the coefficients of higher powers in frequency. These coefficients will affect the magnitude somewhat but not the sign. The theoretical value of F_0 agrees in both sign and magnitude with HONECK's calculations [58]. It is to be pointed out that the theoretical value would become positive for values of C_0 around 30×10^5 cm^4 s^{-1}. It is due to the relatively small theoretical prediction of C_0 that the parameter F_0 is negative. NELKIN [59], however, predicts a positive value for F_0 of the order of C_0^2/D_0, which is an approximation to a more correct form derived by PEREZ and BOOTH [52]. Obviously, work remains to be done.

There is a clear agreement between the values of D_0 and C_0 obtained from both the pulsed propagation technique and the neutron wave technique. From this viewpoint, the situation is very satisfactory. It remains, however, to study the disagreement between the experimental results and the C_0 predictions of Parks' kernel for graphite.

INSTRUMENTATION AND FACILITIES

It is apparent from the foregoing discussion that there are substantial differences between the techniques discussed and the conventional pulsed

neutron technique. Perhaps the greatest difference is the use of a thermal neutron source instead of a fast neutron source. The majority of the work carried out at the University of Florida has employed a Texas nuclear neutron generator and a neutron filter for slowing-down neutrons. The filter consists of a re-entrant tube into which the accelerator target is placed, surrounded by iron, lead, and water, as shown in Fig. 26. The resultant

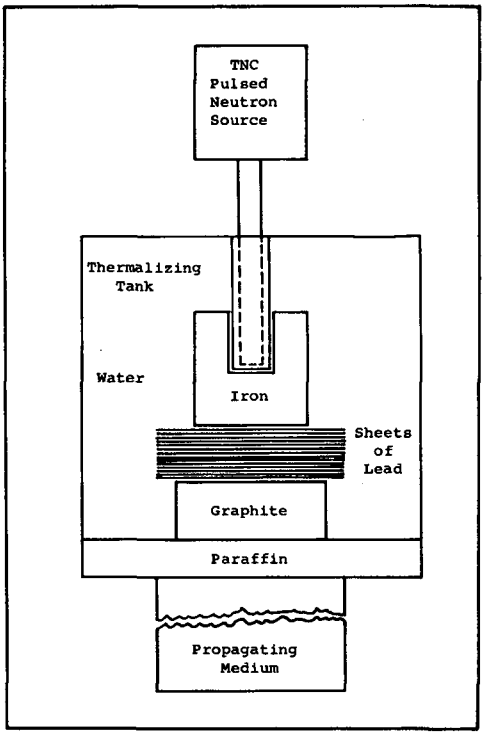


Fig. 26

Neutron filter for slowing down fast neutrons to thermal energy

flux neutron distribution is a good approximation of a cosine wave. Hence, the output of this system, feeding into a nuclear system, has the shape of the fundamental mode, a very desirable characteristic. Unfortunately, the neutron filter system reduces the intensity by about two orders of magnitude.

To overcome these difficulties, a 4-MeV Van de Graaff accelerator, recently installed, will be used as a very high intensity thermal neutron source. The principal advantage of this system is that the proton energy is above the threshold for the p-n reaction with a lithium target which produces 29-keV neutrons. This is a significant reduction in energy from the 14.3-MeV neutrons released from a tritium target. The layout of this 4-MeV Van de Graaff accelerator and shielded room is shown in Fig. 27. It is seen that the beam is sent vertically downward from the accelerator through an analysing magnet mounted on a swivel where the beam is then directed into a shielded room and against the target. Post-acceleration deflection is used

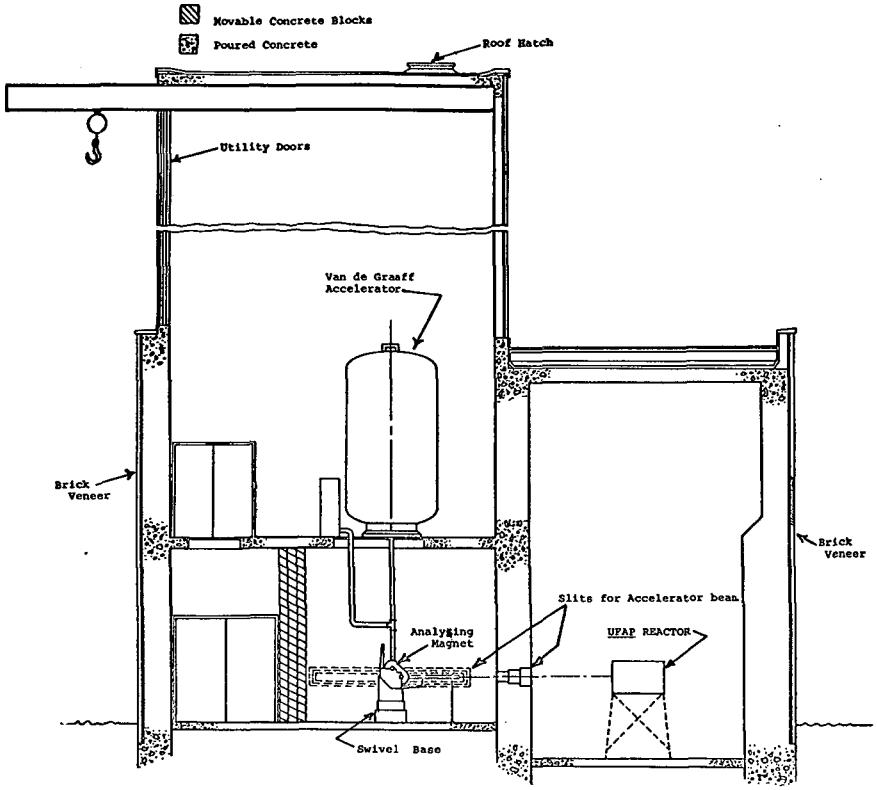


Fig. 27

View of accelerator and reactor installation

to deflect the beam on and off the target for the pulse. Sinusoidal modulation can also be carried out by using a special-shaped target or with a special sinusoidal modulation unit mounted in the terminal of the Van de Graaff accelerator.

In the experiments carried out for sinusoidal modulation, pseudo-random binary pulsing, thermal neutron pulse propagation studies, square wave pulsing, etc., the Technical Measurements Corporation multichannel time analyser system has been used. This is a commercially available instrument made in 256- and 1024-channel models, both of which will accept specialized plug-in logic modules for various kinds of nuclear measurements. The modules used in these tests were the Model 212 (pulsed neutron logic), the Model 214 (multi-scaler logic) and the Model 213 (time-of-flight logic). The Technical Measurements Corporation equipment listed above is ideally suited for conventional pulsed neutron work and has been widely used for this purpose. However, when one attempts to use any available commercial equipment for the experiments described in this paper, certain additional features are desirable.

Let us consider the pseudo-random binary pulsing using the instrumentation system shown in block diagram form in Fig. 28. In this case the

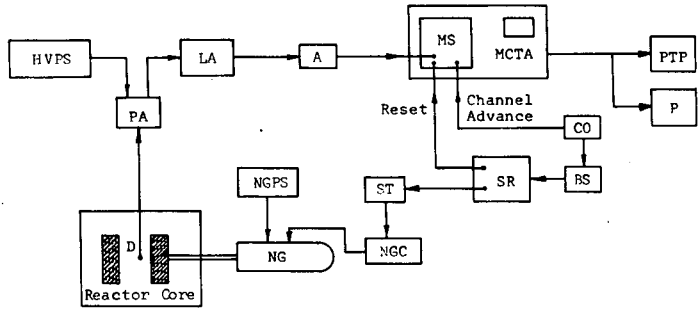


Fig. 28

Block diagram of instrumentation for pseudo-random pulsing the University of Florida Training Reactor Core

Model-214 multi-scaler logic unit is used because an external channel advance is needed. This logic unit has a minimum channel width of 100 μs including a 20-μs dead-time, thereby limiting the shift register frequency. For example, if it is desired to use four channels per shift of the shift register, the shift frequency cannot exceed 2500 shifts per second. If an eight-stage shift register is used there are 255 shifts per period, so that the use of four channels per shift requires a grand total of 1020 channels to gather the data. Because the pseudo-random binary variable is repetitious, there can be no waiting period at the end of one cycle before beginning the next one. Since the 1024-channel analyser has not swept through all its channels (i.e. there are four more channels), the reset signal is ignored, and the system must wait until the next reset signal. Hence data are counted only for every other cycle. Furthermore, the 20-μs dead-time causes an additional 20% loss of data. There is some indication that for experiments where one wants to measure the "$(k\beta/\ell)$" the loss of the background data from every other cycle is intolerable [60]. In the pseudo-random pulsing, the maximum number of channels can also be a serious limitation, i.e. under certain circumstances a 4095- or more channel system would be more desirable.

For the neutron wave experiment, it is desirable to obtain about 100 points per cycle of a sinusoidal variation of neutron density in order to fit this curve by the least-squares technique. If one uses the minimum channel interval of 20 μs (a channel of 10 μs plus 10 μs dead-time between channels), this corresponds to 2000 μs per cycle, or a maximum frequency of 500 Hz. Such a frequency is inadequate for experiments in graphite, beryllium, light water and many other materials.

In order to go to higher frequencies in neutron wave work, the Model-213 time-of-flight logic module has been used. This module has channel widths as narrow as one-quarter of a microsecond. However, when a pulse is detected, it is followed by a dead-time of 16 μs during which no pulses can be detected. Hence, while the time-of-flight logic unit can be used as a multichannel time analyser with very short channel widths, the counting rate is limited to a few thousand counts per second.

There are also other difficulties associated with these experiments which hamper data acquisition. Specifically, the pseudo-random binary pulsing requires cross-correlation which usually is carried out on a digital com-

puter. This required that the data be printed out and that cards be punched and verified before being put into the computer. Hence some of the processing of data, e.g., the correction for the effect of the sidebands, required judgment on the part of the experimenter. The processing could not be automated without an elaborate and more expensive computer programme. As a result it is often days, and sometimes weeks, between the time that an experiment is run and the time that results become known. All too often there are omissions of data or numerical errors which invalidated data, and by that time the equipment to repeat this experiment had probably been put into use in other experiments.

In view of the above considerations, it was decided to incorporate a small digital computer into the instrumentation system and to build a very high-speed digital data acquisition system to gather data into this computer. The computer chosen was the International Business Machine Model 1800 which is a 16-bit (plus memory protect and parity bits) binary computer with a

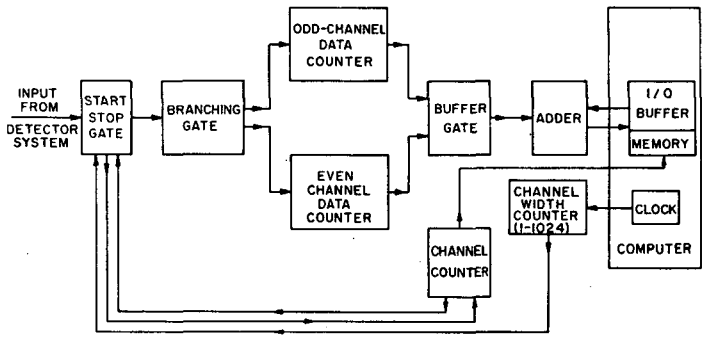


Fig. 29

Multi-channel time analyser input to the digital computer

2.00-μs memory cycle time. The input system shown in Fig. 29 has been designed with a dual-channel input system which allows channel widths as short as 2.00 μs with about 40 ns dead-time due to switching. Data are collected in one channel, while data are transferred to the memory from the other. In order to store data rapidly, a special buffer-adder is employed which allows the contents of memory to be read out, increased by the number of pulses accumulated in the previous time interval, and placed back into the same memory position, all within one memory cycle (2.00 μs). The number of channels per cycle can be varied between one and 4096 in increments of one, and the system will operate either continuously (one cycle after another), or it can be triggered by an external signal. The channel width can be varied between one and 1024 memory cycle times. The printout, punchout and data display are performed on the computer.

This system has the additional advantage that, upon completion of a run, the data can be immediately processed to determine its validity. The data will be displayed on the oscilloscope and plotted on an X-Y plotter. It can also be placed on a magnetic tape which is compatible with the University's large central digital computer.

In general, this sytem has all the features of most commercially available multichannel time analysers, with the additional advantages of 2.00 μs channel width, essentially no dead-time, variable length cycle, and the option of continuous or triggered operation. It also has the decided advantage of "on-line" computing capability so that data can be processed immediately, and the possibility of being expanded up to 32 768 channels with 2.00 μs channel widths.

The detailed design of the input system just described has been completed by DIAZ [61], and the unit is actually under construction. In addition, a 4096-channel Technical Measurements Corporation multi-parameter analyser has been purchased and will be interfaced to the IBM-1800 digital computer to process data from multi-parameter pulse height and time-of-flight measurements. The computer is scheduled for delivery in early 1966, and it is expected that this system will be operational soon after delivery.

SUMMARY

In summary, a wide variety of techniques closely related to pulsed neutron research have been described in this paper. In general, these techniques require a source of thermal neutrons which is fluctuating in a prescribed manner. Each of these techniques has its own particular advantages and disadvantages. But, taken on the whole, it is the considered opinion of the author and his associates that these techniques are extremely valuable for reactor analysis. The instrumentation used in these experiments can be fairly conventional in nature, but modern systems generally include on-line digital computing facilities which greatly increase their capability and convenience.

ACKNOWLEDGEMENT

Part of the work reported in this paper was supported by the United States Atomic Energy Commission under Contract AT(40-1)-3067, "Measurement of Reactor Shutdown Margin by Correlation Techniques". This assistance is gratefully acknowledged.

REFERENCES

[1] MANLEY, J.H., HAYWORTH, L.J. and LUEBKE, E.A., The mean life of neutrons in water and the hydrogen capture cross section, Phys. Rev. 61 (1942) 152.

[2] Von DARDEL, G.F., The interaction of neutrons with matter studied with a pulsed neutron source, Trans. R. Inst. Technol., Stockholm 75 (1954).

[3] Von DARDEL, G.F. and SJÖSTRAND, N.G., The diffusion parameters of thermal neutrons in water, Phys. Rev. 96 (1954) 1245.

[4] ANTONOV, A.V. et al., A study of neutron diffusion in beryllium, graphite, and water by the impulse method, Proc. UN Int. Conf. PUAE 5 (1956) 3.

[5] RAMANNA, R. et al., On the determination of diffusion and slowing down constants of ordinary water and beryllium oxide using a pulsed neutron source, Proc. UN Int. Conf. PUAE 5 (1956) 24.

[6] RAIEVSKI, V. and HOROWITZ, J., Determination of the mean transfer free path of thermal neutrons by measurement of the complex diffusion length, Proc. UN Int. Conf. PUAE 5 (1956) 42.
[7] RAIEVSKI, V., Etude du transport des neutrons par la méthode de modulation, Rapport CEA, No. 1095 (1953).
[8] UHRIG, R.E., Neutron waves in a subcritical assembly, Trans. Amer. nucl. Soc. 2 (1959) 2.
[9] RICCI, W.J., Transfer function of a uranium-graphite subcritical assembly, M.S. Thesis, Iowa State University, Ames, Iowa (1958), unpublished.
[10] CARIUS, R.W., Neutron diffusion in a subcritical assembly with sinusoidal source oscillation, M.S. Thesis, Iowa State University, Ames, Iowa (1959), unpublished.
[11] MERTES, F.P., Characteristics of a subcritical assembly evaluated by neutron waves, M.S. Thesis, Iowa State University, Ames, Iowa (1959),unpublished.
[12] HUSSMANN, H.L., Characteristics of neutron waves in a subcritical assembly, M.S. Thesis, Iowa State University, Ames, Iowa (1960), unpublished.
[13] UHRIG, R.E., Oscillatory techniques in a subcritical assembly, Proc. of 1961 Univ. Conf. on Subcritical Assemblies, USAEC Rpt TID-7619 (1962).
[14] PEREZ, R.B. and HARTLEY, R.H., Gainesville, Florida (1961), private communication.
[15] BOOTH, R.S., Neutron wave propagation in a subcritical assembly, M.S. Thesis, University of Florida, Gainesville, Florida (1962), unpublished.
[16] PEREZ, R.B. and UHRIG, R.E., Propagation of neutron waves in moderating media, Nucl. Sci. Engng 17 (1963) 1.
[17] UHRIG, R.E., The impulse response of an exponential assembly, Exponential and Critical Experiments III IAEA, Vienna (1964) 205-40.
[18] PEREZ, R.B., BOOTH, R.S. and HARTLEY, R.H., Experimentation with thermal-neutron wave propagation, Trans. Amer. nucl. Soc. 6 (1963) 2.
[19] PEREZ, R.B., BOOTH, R.S., DENNING, R.S. and HARTLEY, R.H., Propagation of neutron waves in subcritical assemblies, Trans. Amer. nucl. Soc. 7 (1964) 1.
[20] BOOTH, R.S., HARTLEY, R.H. and PEREZ, R.B., Application of Moore's method to the analysis of thermal neutron pulse propagation experiments, Trans. Amer. nucl. Soc. 8 (1965) 1.
[21] PUROHIT, S.N., Neutron thermalization and diffusion in pulsed media, Nucl. Sci. Engng 9 (1961) 2.
[22] OHANIAN, M.J. and DAITCH, P.B., Eigenfunction analysis of thermal-neutron spectra, Nucl. Sci. Engng 19 (1964) 3.
[23] WEINBERG, A.M. and SCHWEINLER, H.C., The theory of oscillating absorber in a neutron chain reactor, Phys. Rev. 74 (1948) 851.
[24] MOORE, M.N., The role of the dispersion law in space dependent kinetics, Proc. Conf. on Reactor Kinetics and Control, Tucson, Arizona, 1963, AEC Symposium Series No. 2, USAEC Rpt TID-7682 (1964).
[25] MOORE, M.N., The propagation of neutron bursts and the determination of the system dispersion law, Trans. Amer. nucl. Soc. 7 (1964) 2.
[26] MOORE, M.N., The noise field of a reactor, Noise Analysis in Nuclear Systems, AEC Symposium Series No. 4, USAEC Rpt TID-7679 (1964).
[27] MOORE, M.N., The determination of reactor dispersion laws from modulated neutron experiments, unpublished report, private communication (1964).
[28] MOORE, M.N., The dispersion of thermal neutron pulses in neutronic systems, unpublished report, private communication (1964).
[29] SCHULTZ, M.A., Control of Nuclear Reactors and Power Plants, 2nd ed., McGraw-Hill Book Co., New York (1961).
[30] BENDAT, J.S., Principles and Applications of Random Noise Theory, John Wiley & Sons, New York (1958).
[31] LEE, Y.W., Statistical Theory of Communications, John Wiley & Sons, New York (1960).
[32] WEINBERG, A.M. and WIGNER, E.P., The Physical Theory of Neutron Chain Reactors, Univ. of Chicago Press (1958).
[33] ALBRECHT, R.W., A transport correction to the theory of the propagation of neutron waves in moderating media, unpublished report, private communication (1964).
[34] MORTENSTEIN, G.A., Neutron wave propagation using P-1 approximations, Ph.D. dissertation, Univ. of California, Berkeley (1964), unpublished.
[35] KUNAISH, H.H., Time-, energy- and space-dependent neutron thermalization theory, Ph.D. dissertation, Univ. of Florida, Gainesville (1964), unpublished.

[36] HETRICK, D.L. and SEALE, R.L., Neutron waves and vibrational modes in moderating materials, Univ. of Arizona Engng Res. Lab. Tech. Report No. 1, Tucson, Arizona (1964).
[37] KEEPIN, G.R., Pulsed neutron techniques, LAMS 2215 (1958).
[38] UHRIG, R.E., (Ed.), Noise analysis in nuclear systems, AEC Symposium Series No.4, USAEC Rpt TID-7679 (1964).
[39] DUNCAN, J.M., University of Florida training reactor hazards summary report, Bulletin series No. 99, Florida Engineering and Industrial Experiment Station, Gainesville, Florida (1958).
[40] BADGLEY, R.W. and UHRIG, R.E., Power spectral density measurements in a subcritical nuclear reactor, Nucl. Sci. Engng 19 (1964) 2.
[41] COOPER, G., private communication (1962).
[42] ANDERSON, G.W. et al., A self-adjusting system for optimal dynamic performance, IRE Nat. Conv. Rec., Part IV (1958).
[43] BALCOMB, J.D., DEMUTH, H.B. and GYFTOPOULOS, E.P., A cross correlation method for measuring the impulse response of reactor systems, Nucl. Sci. Engng 11 (1961) 2.
[44] GIBSON, J., private communication (1962).
[45] PETERSON, W.W., Error Correcting Codes, John Wiley & Sons, New York (1961).
[46] STERN, T.E., Reactor impulse response using random source excitation and cross correlation, Noise Analysis in Nuclear Systems, AEC Symposium Series No. 4, USAEC Rpt TID-7679 (1964).
[47] STERN, T.E. et VALAT, J., Mesure des très basses réactivités à partir de la réponse impulsionnelle d'un réacteur déterminée par intercorrelation, interpretation de certains résultats, Parrott CEA-R2377, Centre d'études nucléaires de Saclay, France (1964).
[48] UHRIG, R.E., Measurement of reactor shutdown margin by noise analysis, Reactor Kinetics and Control, AEC Symposium Series No. 2, USAEC Rpt TID-7662 (1964).
[49] HARTLEY, R.H., Propagation and detection of pulses of thermal neutrons, M.S. Thesis, Univ. of Florida, Gainesville, Florida (1964), unpublished.
[50] UHRIG, R.E. et al., Summary hazards report for the University of Florida accelerator pulsed assembly, unpublished report (1964).
[51] MILEY, G.H., Reactor neutron-pulse propagation, Nucl. Sci. Engng 21 (1965) 3.
[52] PEREZ, R.B. and BOOTH, R.B., Excitation of neutron waves by modulated and pulsed sources, private communication (1964).
[53] OHANIAN, M.J., private communication (1965).
[54] PARKS, D.E. et al., Neutron thermalization in a crystalline medium in the incoherent approximation, BNL-719, Vol. 1 (1962).
[55] SAGOT, M. et al., *Technique des neutrons pulsés appliquée aux assemblées critiques et sous-critiques*, Exponential and Critical Experiments III IAEA, Vienna (1964) 163-89.
[56] STARR, E. and PRICE, G.A., Measurement of the diffusion parameters of graphite and graphite-bismuth by pulsed neutron methods, Brookhaven Int. Conf. on Neutron Thermalization, USAEC Rpt TID-4500 (1962).
[57] KLOSE, H., KUCHLE, M. and REICHARDT, W., Pulsed neutron measurements on graphite, Brookhaven Int. Conf. on Neutron Thermalization, USAEC Rpt TID-4500 (1963).
[58] HONECK, H.C., On the calculation of thermal neutron diffusion parameters, BNL 719, Vol. 1 (1962).
[59] NELKIN, M., The diffusion cooling of neutrons in a finite moderator, J. nucl. Energy 8, Pergamon Press Ltd., London (1958).
[60] GARELIS, E., private communication (1964).
[61] DIAZ, H., M.S. Thesis, University of Florida, Gainesville, Florida (1965).

DISCUSSION

N. CORNGOLD: Could Dr. Uhrig give us a little more information on the connection between the parameters appearing in his statistical analysis and the parameters of reactor physics?

R. UHRIG: What one measures in these experiments is the same Rossi-alpha as one measures by other techniques. We are also looking at the

physics of the systems as well as the mechanics involved in making the measurements. For instance, in some measurements of pseudo-random pulsing of heavy-water natural-uranium systems, we found a dip in the cross-spectral density at a frequency whose wave-length is comparable to the lattice spacing. Hence, it would appear that interference phenomena take place. Dr. Perez has also carried out wave experiments with cadmium strips equally spaced in the assembly and he obtained comparable results. He and his students have also carried out reflection experiments where neutron waves are partially reflected. We are only in the early stages of this investigation of the "optical"-type behaviour of neutron disturbances.

L. G. KEMENY*: I would like to comment on a number of points raised by this very interesting survey paper. Some of these comments are of a general nature and are pertinent to the other papers presented at this session.

In the first place, it is apparent that great progress has been made in the development of techniques closely related to pulsed-neutron research and that much useful information on reactor parameters is being obtained. It would seem however that there are some significant gaps in our understanding of stochastic processes in nuclear reactors and therefore in the conduct and interpretation of stochastic or pseudo-stochastic experiments. Detailed investigations have yet to be carried out into:

(1) the nature and degree of stationarity of fission distributions in a reactor at zero energy and at power;
(2) the formulation of stochastic models for reactors at zero energy and at power;
(3) the errors and confidence limits associated with the measurement and processing of random or pseudo-random signals, with a view to arriving at a more realistic assessment of the value of the measured parameters.

Secondly, it is of great interest to note in Dr. Uhrig's paper the exciting possibilities opened up by the use of a suitable digital computer to record and process events occurring in a reactor on an "on-line" basis. This powerful method of time analysis may eventually resolve the time scales associated with such rapid processes as neutron slowing-down or the rise time of a neutron pulse after injection.

Finally, I would like to point out that many of the experiments referred to in this paper can be simulated and planned on a suitable hybrid computing system in which the analogue side is programmed to simulate the nuclear environment or perturbation and the digital equipment is used to carry out the statistical analysis. It is thus possible and convenient to compute a variety of auto- and cross-correlograms and spectra and to study the coherence of reactor measurements made with detectors situated at various spatial positions. Models of considerable complexity can be studied in this way such as two-group diffusion simulations at zero energy or stability and control studies of boiling power reactors.

R. UHRIG: I would agree with Dr. Kemeny that there are many exciting possibilities and that much work needs to be done. We are carrying out experiments to determine the precision of the pseudo-random-pulsing technique and the influence of the characteristics of the input disturbance. For

* This comment was communicated by G.R. Keepin.

instance, when higher shift frequencies are used, the peak of the impulse-response curve shifts to the left. This is, of course, not possible physically. However, if one considers that the phenomenon is dispersive in nature, i.e. the velocity of propagation increases with frequency, then it is clear that the higher-frequency components do reach the detector sooner. We are also looking at the influence on the results of the number of data samples per shift and other variables.

There are tentative plans for a meeting on neutron noise and modulation techniques at the University of Florida in early 1966. Participants to this Symposium will receive information on the 1966 meeting as soon as it is available.

EXCITATION OF NEUTRON WAVES BY MODULATED AND PULSED SOURCES

R. B. PEREZ AND R. S. BOOTH
UNIVERSITY OF FLORIDA,
GAINESVILLE, FLA., UNITED STATES OF AMERICA

Abstract — Résumé — Аннотация — Resumen

EXCITATION OF NEUTRON WAVES BY MODULATED AND PULSED SOURCES. Placement of either a sinusoidally modulated or pulsed source of thermal neutrons at one of the boundaries of a nuclear assembly creates a disturbance which can be analysed in terms of wave components, propagating away from the localized source with frequency-dependent attenuation factors and wave velocities.

The dispersive properties of the assembly are expressed through the dispersion relation, connecting the inverse complex relaxation length (or complex wave number), $\rho(\omega)$, to the frequency of the excitation and the nuclear parameters of the system. It will be shown that the dispersion relation is of the form

$$\rho^2(\omega) = \sum_{\substack{n \\ (\text{even})}} B^{(n)}\omega^n + i \sum_{\substack{n \\ (\text{odd})}} B^{(n)}\omega^n \qquad (1)$$

where the coefficients $B^{(n)}$ are related to matrix elements of the various operators in moderating and multiplicative media.

In a neutron wave experiment one measures the attenuation factor $\alpha(\omega)$ and the phase shift per unit length $\xi(\omega)$, which satisfy the relationships

$$\alpha^2(\omega) - \xi^2(\omega) = \sum_{\substack{n \\ (\text{even})}} B^{(n)}\omega^n \qquad (2)$$

$$2\alpha(\omega)\xi(\omega) = \sum_{\substack{n \\ (\text{odd})}} B^{(n)}\omega^n . \qquad (3)$$

One has then the advantage over the conventional pulsing with fast neutrons of measuring two independent magnitudes (real and imaginary part of the wave number) from which more information can be extracted about the nuclear properties of interest.

Experiments were performed using graphite as the moderating material. Two different sources of thermal neutrons were used. In one case 14-MeV neutrons generated by a Cockcroft-Walton machine were thermalized in a tank containing several layers of iron, lead and graphite immersed in water. Lately the University of Florida 4-MeV Van de Graaff accelerator produced 29-keV neutrons from the (Li-p) reaction which were thermalized in a few inches of paraffin. In both instances the ion beams could be modulated sinusoidally or pulsed.

Fourier analysis of the slow pulses showed very good agreement with the results obtained from the sinusoidal excitation of the waves. The range of frequencies studied was between zero and 1200 c/s Least-squares fits of the experimental data with equations (4) and (5) yielded the results

$$B^{(0)} = B_\perp^2 + \frac{a_1}{L_0} = (6.6 \pm 0.1)\ 10^{-3}\ (\text{cm}^{-2}) \qquad (4)$$

$$B^{(1)} = \frac{a_2}{D_0} = (4.38 \pm 0.2)\ 10^{-6}\ (\text{cm}^{-2}) \qquad (5)$$

$$B^{(2)} = \sum_{\gamma} H_{0\gamma}/\phi_{\gamma\gamma} = (2.5 \pm 0.2)\ 10^{-10} \quad (\gamma = 0, 1, 2, \ldots 10) \qquad (6)$$

$B_\perp^2$ = Transverse buckling (cm^{-2}) = $5.96 \times 10^{-3}\ \text{cm}^{-2}$

where a_1, a_2, $H_{0\gamma}$ and $\phi_{\gamma\gamma}$ are related to matrix elements of the diffusion and thermalization operators. From Eq. (5) a value of $D_0 = (2.2 \pm 0.1) \times 10^5$ cm^2/s was found in agreement with conventional pulsed neutron measurements. Theoretical calculations using various kernels also agree with the experimental results.

EXCITATION D'ONDES NEUTRONIQUES AU MOYEN DE SOURCES MODULÉES ET PULSÉES. En plaçant une source de neutrons thermiques pulsée ou modulée sinusoïdalement à l'une des frontières d'un assemblage nucléaire, on provoque une perturbation que l'on peut analyser sous forme de composantes d'onde, se propageant à partir de la source avec des facteurs d'atténuation et des vitesses variables selon la fréquence.

Les caractéristiques de dispersion de l'ensemble sont exprimées par la relation de dispersion qui relie l'inverse de la longueur de relaxation complexe (ou nombre d'onde complexe), $\rho(\omega)$, à la fréquence de l'excitation et aux paramètres nucléaires du système. Les auteurs montrent que la relation de dispersion se présente sous la forme

$$\rho^2(\omega) = \sum_{n\ (\text{pair})} B^{(n)}\omega^n + i \sum_{n\ (\text{impair})} B^{(n)}\omega^n \tag{1}$$

dans laquelle les coefficients $B^{(n)}$ dépendent des éléments de matrice des différents opérateurs dans les milieux ralentisseurs et multiplicateurs.

Dans les expériences sur les ondes neutroniques, on mesure le facteur d'atténuation $\alpha(\omega)$ et le déphasage par unité de longueur $\xi(\omega)$, qui satisfont aux relations

$$\alpha^2(\omega) - \xi^2(\omega) = \sum_{n\ (\text{pair})} B^{(n)}\omega^n \tag{2}$$

$$2\alpha(\omega)\xi(\omega) = \sum_{n\ (\text{impair})} B^{(n)}\omega^n \tag{3}$$

Par rapport à la méthode classique des bouffées de neutrons rapides, cette façon de procéder donne alors l'avantage de mesurer deux grandeurs indépendantes (la partie réelle et la partie imaginaire du nombre d'onde) dont on peut extraire davantage de renseignements sur les propriétés nucléaires qui présentent un intérêt.

Les expériences ont été effectuées en utilisant le graphite comme ralentisseur et deux sources différentes de neutrons thermiques. Dans l'un des cas, des neutrons de 14 MeV produits par une machine Cockcroft-Walton ont été thermalisés dans un réservoir contenant plusieurs couches de fer, de plomb et de graphite immergés dans l'eau. Récemment, l'accélérateur Van de Graaff (4 MeV) de l'Université de Floride a produit à partir de la réaction (Li-p) des neutrons de 29 keV, qui ont été thermalisés dans quelques centimètres de paraffine. Dans les deux cas, on pouvait moduler sinusoïdalement ou pulser les faisceaux d'ions.

Les auteurs ont trouvé que les résultats de l'analyse de Fourier des bouffées de neutrons lents étaient en très bon accord avec les résultats obtenus par excitation sinusoïdale des ondes. La gamme de fréquence étudiée allait de zéro à 1200 Hz. L'application de la méthode des moindres carrés aux données expérimentales dans les équations (4) et (5) donne les résultats suivants:

$$B^{(0)} = B_\perp^2 + \frac{a_1}{L_0} = (6,6 \pm 0,1)\cdot 10^{-3}(\text{cm}^{-2}) \tag{4}$$

$$B^{(1)} = \frac{a_2}{D_0} = (4,38 \pm 0,2)\cdot 10^{-6}(\text{cm}^{-2}) \tag{5}$$

$$B^{(2)} = \sum_{\gamma\ (\gamma = 0, 1, 2, \ldots 10)} H_{0\gamma}/\phi_{\gamma\gamma} = (2,5 \pm 0,2)\cdot 10^{-10} \tag{6}$$

$B_\perp^2$ = Laplacien transversal (cm^{-2}) = $5,96 \cdot 10^{-3}$ cm^{-2}

dans lesquels a_1, a_2, $H_{0\gamma}$ et $\varphi_{\gamma\gamma}$ dépendent des éléments de matrice des opérateurs de diffusion et de thermalisation. A partir de l'équation (5), on a trouvé une valeur $D_0 = (2,2 \pm 0,1) \cdot 10^5$ cm²/s qui concorde avec les mesures classiques au moyen des neutrons pulsés. Les calculs théoriques au moyen de divers noyaux concordent également avec les résultats expérimentaux.

ВОЗБУЖДЕНИЕ НЕЙТРОННЫХ ВОЛН С ПОМОЩЬЮ МОДУЛИРОВАННЫХ И ИМПУЛЬСНЫХ ИСТОЧНИКОВ. Если поставить синусоидально модулированный или импульсный источник тепловых нейтронов на одну из границ ядерной сборки, то это создает нарушение, которое можно проанализировать с точки зрения волновых компонентов, распространяющихся из локализованного источника с коэффициентами ослабления, зависящего от частоты, и с волновыми скоростями.

Дисперсионные свойства сборки выражаются с помощью дисперсионного соотношения, связывающего обратную волну комплексного затухания (или комплексное волновое число), $\rho(\omega)$, с частотой возбуждения и ядерными параметрами сборки. Дисперсионное соотношение имеет следующий вид:

$$\rho^2(\omega) = \underbrace{\sum_n B^{(n)} \omega^n}_{\text{(четные)}} + i \underbrace{\sum_n B^{(n)} \omega^n}_{\text{(нечетные)}}, \tag{1}$$

где коэффициенты $B^{(n)}$ связаны с матричными элементами различных операторов в замедляющих и размножающих средах.

При эксперименте с нейтронной волной измеряется коэффициент ослабления $\alpha(\omega)$ и сдвиг фазы на единицу длины $\xi(\omega)$, которые удовлетворяют соотношениям:

$$\alpha^2(\omega) - \xi^2(\omega) = \underbrace{\sum_n B^{(n)}(\omega)^n}_{\text{(четные)}} \tag{2}$$

$$2\alpha(\omega)\xi(\omega) = \underbrace{\sum_n B^{(n)}\omega^n}_{\text{(нечетные)}} \tag{3}$$

Таким образом получают преимущество по сравнению с обычным методом с использованием пульсации с быстрыми нейтронами, которое заключается в измерении двух независимых величин (действительной и мнимой частью волнового числа), благодаря которым можно получить больше информации о ядерных свойствах, представляющих интерес.

При проведении экспериментов в качестве замедлителя использовали графит. Использовали два различных источника тепловых нейтронов. В одном случае нейтроны с энергией 14 Мэв, полученные с помощью ускорителя Кокрофта-Уолтона, были термализованы в баке, содержащем несколько слоев железа, свинца и графита, погруженных в воду. Позднее с помощью имеющегося во Флоридском университете ускорителя Ван де Граафа мощностью 4 Мэв были получены нейтроны с энергией 29 кэв из реакции (Li-p), которые были термализованы в нескольких дюймах парафина. В обоих случаях ионные пучки могли быть синусоидально модулированными или пульсирующими.

Результаты анализа Фурье, проведенного с медленными импульсами, прекрасно согласуются с результатами, полученными при синусоидальном возбуждении волн. Исследуемые частоты были в диапазоне от нуля до 1200 гц. В результате апроксимации экспериментальных данных способом наименьших квадратов с применением уравнений (4) и (5) были получены следующие результаты:

$$B^{(0)} = B_\perp^2 + \frac{a_1}{L_0} = (6,6 \pm 0,1) \cdot 10^{-3} \ (\text{см}^{-2}); \tag{4}$$

$$B^{(1)} = \frac{a_2}{D_0} = (4,38 \pm 0,2) \cdot 10^{-6} \ (\text{см}^{-2}); \tag{5}$$

$$B^{(2)} = \sum_{\gamma} H_{0\gamma} / \phi_{\gamma\gamma} = (2{,}5 \pm 0{,}2) \cdot 10^{-10} \quad (\gamma = 0,1,2, \ldots 10). \tag{6}$$

$B_{\perp}^2$ = поперечный лапласиан ($см^{-2}$) = $5{,}96 \cdot 10^{-3}$ $см^{-2}$, где a_1, a_2, $H_{0,\gamma}$ и $\phi_{\gamma\gamma}$ относятся к матричным элементам диффузионных и термализационных операторов. С помощью уравнения (5) определено, что значение $D_0 = (2{,}2 \pm 0{,}1)\ 10^5$ $см^2$ $сек^{-1}$ согласуется с обычными измерениями импульсных нейтронов (5). Теоретические расчеты с использованием различных моделей ядра также согласуются с экспериментальными результатами.

EXCITACION DE ONDAS NEUTRONICAS MEDIANTE FUENTES MODULADAS Y PULSADAS. La colocación de una fuente de neutrones térmicos modulada o pulsada sinusoidalmente en uno de los límites de un conjunto nuclear crea una perturbación que puede analizarse como si se operase con componentes de una onda que, al propagarse, se aleja de la fuente localizada, con factores de atenuación y velocidades de onda dependientes de la frecuencia. Las propiedades de dispersión del conjunto se expresan mediante la relación de dispersión, que vincula la inversa de la longitud de relajamiento compleja (o número de onda complejo), $q(\omega)$, con la frecuencia de la excitación y con los parámetros nucleares del sistema. Los autores señalan que la relación de dispersión presenta la forma

$$\rho^2(\omega) = \sum_{n\ (par)} B^{(n)} \omega^n + i \sum_{n\ (impar)} B^{(n)} \omega^n \tag{1}$$

expresión en la que los coeficientes $B^{(n)}$ están relacionados con elementos matriciales de diversos operadores en medios moderadores y multiplicadores.

En un experimento sobre ondas neutrónicas se miden el factor de atenuación, $\alpha(\omega)$, y el desplazamiento de fase por unidad de longitud, $\xi(\omega)$, que satisfacen las relaciones

$$\alpha^2(\omega) - \xi^2(\omega) = \sum_{n\ (par)} B^{(n)} \omega^n \tag{2}$$

$$2\alpha(\omega)\xi(\omega) = \sum_{n\ (impar)} B^{(n)} \omega^n. \tag{3}$$

De esta forma se tiene la ventaja, sobre el empleo del método tradicional de los neutrones rápidos pulsados, de poder medir dos magnitudes independientes (partes real e imaginaria del número de onda) de las cuales puede obtenerse más información sobre las propiedades nucleares de interés.

Los autores realizaron experimentos empleando grafito como moderador, y neutrones térmicos procedentes de dos fuentes distintas. En uno de los casos termalizaron en un tanque que contenía varias capas de hierro, plomo y grafito emergiendo parcialmente del agua, neutrones de 14 MeV generados por un aparato Cockcroft-Walton. Con el acelerador Van de Graaff de 4 MeV de la Universidad de Florida se obtuvieron, en virtud de la reacción Li-p, neutrones de 29 keV que se termalizaron en una capa de parafina de algunas pulgadas de espesor. En ambos casos, fue posible pulsar o modular sinusoidalmente los haces iónicos. El análisis por el método de Fourier de los impulsos de neutrones lentos dio resultados que concordaron con los obtenidos partiendo de la excitación sinusoidal de las ondas. El intervalo de frecuencias estudiado estuvo comprendido entre 0 y 1200 Hz. El ajuste de los datos experimentales a las ecuaciones (4) y (5) por el método de los cuadrados mínimos dio los siguientes resultados:

$$B^{(0)} = B_{\perp}^2 + \frac{a_1}{L_0} = (6{,}6 \pm 0{,}1) \cdot 10^{-3} (cm^{-2}) \tag{4}$$

$$B^{(1)} = \frac{a_2}{D_0} = (4{,}38 \pm 0{,}2) \cdot 10^{-6}\ (cm^{-2}) \tag{5}$$

$$B^{(2)} = \sum_{\gamma} H_{0\gamma}/\phi_{\gamma\gamma} = (2,5 \pm 0,2)\cdot 10^{-10} \quad (\gamma = 0, 1, 2, \ldots 10) \tag{6}$$

$B_{\perp}^{2}$ = Laplaciano transversal (cm^{-2}) = $5,96 \cdot 10^{-3}$ cm^{-2}

en donde a_1, a_2, $H_{0\gamma}$ y $\phi_{\gamma\gamma}$ están relacionados con elementos matriciales de los operadores de difusión y termalización. Partiendo de la ecuación (5), se halló un valor de $D_0 = (2,2 \pm 0,1)\cdot 10^5$ cm^2/s que concuerda con los resultados de las mediciones realizadas por el método tradicional de los neutrones pulsados. Los resultados de cálculos teóricos realizados empleando diversos núcleos concuerdan también con los datos experimentales.

1. INTRODUCTION

Historically, the problem of measuring parameters of a nuclear system has been undertaken by either static or dynamic methods. The early experimentation involved static measurements of the flux distribution in subcritical systems. By fitting the measured flux mappings to a derived theoretical prediction, diffusion parameters were obtained. The first dynamic method to be used was the classical pile oscillator technique. A representative paper in this field by WEINBERG and SCHWEINLER [1] showed that increasing the frequency of oscillation generates travelling neutron waves.

Almost simultaneously two new methods made their appearance in 1955. One, the die-away technique, was introduced by VON DARDEL [2]. In this method, a burst of fast neutrons produces a decaying, distributed source of thermal neutrons throughout the assembly, which eventually reaches an asymptotic behaviour represented by a single exponential. The decay constant is then related to nuclear and geometric parameters of the system as shown by BECKURTS [3]. The second method is based upon the sinusoidal modulation of a beam of thermal neutrons which impinge upon a boundary of the system under investigation. The sinusoidal disturbance created in this way propagates through the medium as a damped wave whose damping coefficient and phase shift per unit length are related to the diffusion and thermalization parameters of the assembly. The first experiment of this type was performed by RAIEVSKI and HOROWITZ [4]. The neutron wave technique was then neglected even though it presents the advantage over the die-away method of yielding two independent parameters, amplitude and phase shift, as opposed to just the decay constant. One reason for this was that the neutron wave experiment as performed in Ref. [4] was based upon the modulation of the neutron beam by mechanical methods which suffer from difficulties involved in obtaining reproducible wave forms and are restricted to low frequencies (UHRIG [5]). Conversely, the die-away technique utilizes electronic switching techniques to generate the neutron bursts, a method which is highly reliable and relatively easy to introduce in particle accelerators. Furthermore, important theoretical developments introducing neutron thermalization effects in the interpretation of die-away experiments (NELKIN [6], BECKURTS [7], PUROHIT [8], HÄFELE and DRESNER [9] and many others) were lacking in the neutron wave work.

In 1962, a programme to develop the field of neutron wave propagation was started at the University of Florida. Theoretical studies of PEREZ

and UHRIG [10] were able to show the relationship between the amplitude and phase shift of the neutron wave and neutron thermalization parameters. Simultaneously, BOOTH [11] and HARTLEY [12] developed an electronically modulated source of 14.4-MeV neutrons which, after being passed through a properly designed thermalizing tank, proved to be a very convenient source for thermal neutron wave experimentation. Both developments made possible the performance of neutron wave propagation studies in moderators and in subcritical assemblies [13].

This paper is concerned with the propagation of thermal neutron waves in moderating media; experimental results are presented for graphite. The relationship between the wave method and the die-away technique, as well as the advantages of the former, are also discussed.

2. THEORY*

Consider a prism-shaped moderating assembly of extrapolated dimensions a, b and c and having a plane source of thermal neutrons in the $z = 0$ face. Under the diffusion approximation the neutron field $\psi(E, x, y, z, t)$ is described by the following Boltzmann equation

$$\frac{1}{v}\frac{\partial}{\partial t}\psi(E, \vec{r}, t) = [D(E)\nabla^2 - (\Sigma_a(E) + \Sigma_s(E))]\psi(E, \vec{r}, t) + \int_{E'} dE' \Sigma_s(E', E)\psi(E', \vec{r}, t). \tag{1}$$

The pertinent boundary conditions are

$$\psi(E, x = \pm a/2, y, z, t) = \psi(E, x, y = \pm b/2, z, t) = 0 \tag{2}$$

$$-D(E)\frac{\partial}{\partial z}\psi(E, \vec{r}, t)\Big|_{z=0} = 1/2\, S(E, x, y, t). \tag{3}$$

If c is larger than a few neutron relaxation lengths, end effects may be neglected and then

$$\psi(E, x, y, z = c \to \infty, t) = 0. \tag{4}$$

The source $S(E, x, y, t)$ ($n/cm^2 s\, eV$) can change with time in any prescribed manner (i.e. pulsed variation, square wave, sine wave, etc.). Hence, to generalize the treatment it is convenient to carry out the theoretical developments in the frequency domain by defining the Fourier transforms of the neutron field and source $\psi(E, \vec{r}, \omega)$ and $S(E, x, y, \omega)$, respectively, as

$$\psi(E, \vec{r}, \omega) = \int_{-\infty}^{\infty} e^{-i\omega t}\psi(E, \vec{r}, t)dt \tag{5}$$

* For a definition of the terms, see the list of symbols at the end of this paper.

$$S(E, x, y, \omega) = \int_{-\infty}^{\infty} e^{-i\omega t} S(E, x, y, t)dt \tag{6}$$

which are related by the Fourier transform of Eqs. (1) and (3)

$$\left[D(E)\nabla^2 - \left(\Sigma_a(E) + \Sigma_s(E) + \frac{i\omega}{v}\right)\right]\psi(E, \vec{r}, \omega)$$

$$+ \int_{E'} dE' \Sigma_s(E', E)\psi(E', \vec{r}, \omega) = 0 \tag{7}$$

$$-D(E)\frac{\partial}{\partial z}\psi(E, \vec{r}, \omega)\Big|_{z=0} = \tfrac{1}{2} S(E, x, y, \omega). \tag{8}$$

We next symmetrize the kernel $\Sigma_s(E', E)$, which is accomplished by the substitution

$$\psi(E, \vec{r}, \omega) = \left[\frac{vM(E)}{D(E)}\right]^{\frac{1}{2}} \chi(E, \vec{r}, \omega), \tag{9}$$

where M(E) is the Maxwellian flux distribution. The result of this change of dependent variable is

$$(\nabla^2 - \frac{i\omega}{vD(E)})\chi(E, \vec{r}, \omega) = \int_{E'} P(E', E)\chi(E', \vec{r}, \omega)dE', \tag{10}$$

where the kernel (P(E', E) is given by

$$P(E', E) = \left\{\left[\frac{v'M(E')}{D(E)D(E')vM(E)}\right]^{\frac{1}{2}} \Sigma_s(E', E)\right.$$

$$\left. - \frac{1}{D(E')}(\Sigma_a(E') + \Sigma_s(E'))\delta(E - E')\right\} \tag{11}$$

and is symmetric, as can be easily shown by using the principle of detailed balance. The solution of Eq. (10) will be obtained by expanding the function $\chi(E, \vec{r}, \omega)$ in terms of the $\phi_{l,m}(x, y)$ eigenfuctions of the Helmholtz operator $\left\{\frac{\partial^2}{\partial x^2} + \frac{\partial^2}{\partial y^2} + B^2_{\perp l,m}\right\}$ which satisfy the orthogonal relation

$$\int_{-a/2}^{a/2}\int_{-b/2}^{b/2} dxdy\phi_{p,k}(x, y)\phi_{l,m}(x, y) = \frac{ab}{4}\delta_{p,l}\delta_{k,m} \tag{12}$$

and in terms of the energy eigenfunctions of the eigenvalue equation

$$-\rho_{0\alpha}^2 \psi_\alpha(E) = \int_{E'} P(E', E)\,\psi_\alpha(E')dE' \tag{13}$$

which, by virtue of the symmetry of the P(E', E) kernel, are real and satisfy the orthonormal relations

$$\int_E dE\,\psi_\alpha(E)\psi_\beta(E) = \delta_{\alpha\beta}. \tag{14}$$

Equation (13) is the theoretical model for a static exponential experiment in a semi-infinite moderating medium with the eigenvalues $\rho_{0\alpha}^2$ playing the role of the squared inverse relaxation lengths. The advantage of using the $\psi_\alpha(E)$ eigenfunctions for the energy expansion of Eq. (10) is that the solution for this frequency-dependent, finite medium expression can be obtained in terms of the solution of Eq. (13) for the static, semi-infinite problem. Thus, the complicated scattering kernel is incorporated into Eq. (10) through the $\psi_\alpha(E)$ in a very simple and convenient form.

Eigenvalue problems of the general form exhibited by Eq. (13) can be solved for any type of scattering kernel by following a powerful technique developed by OHANIAN and DAITCH [14]. In the present work, the solution of Eq. (13) was obtained by the Ohanian-Daitch method using both the mass-12 kernel and the more sophisticated PARKS [15] kernel for graphite. Introduction of the eigenfunction expansion

$$\psi(E, \vec{r}, \omega) = \sum_{l, m, \beta} A_{l, m, \beta}(\omega)\phi_{l, m}(x, y)\psi_\beta(E)\, e^{-\rho_{l, m} z} \tag{15}$$

into Eq. (10), and multiplication of the result by the operator

$$\int_0^\infty \int_{-a/2}^{a/2} \int_{-b/2}^{b/2} dE\,dx\,dy\,\phi_{p, k}(x, y)\,\psi_\alpha(E)$$

yields, after using the orthogonal relations (12) and (14),

$$\sum_\beta [(\rho^2 - \rho_{0\alpha}^2 - B_{p,k}^2)\,\delta_{\alpha\beta} - i\omega L_{\alpha\beta}]\,A_{p, k, \beta} = 0, * \tag{16}$$

where $\alpha, \beta = 1, 2, 3 \ldots N$ and

$$L_{\alpha\beta} = \int_E dE\,\psi_\alpha(E)\left[\frac{1}{vD(E)}\right]\psi_\beta(E). \tag{17}$$

---

* The $\rho_{0\alpha}^2$ eigenvalues for $\alpha<1$ are, in fact, particular points in the continuum eigenvalue spectrum obtained using the discrete energy representation of the eigenvalue problem, Eq. (13).

The compatibility condition of the set of homogeneous Eqs. (16) yields the following secular determinant for the eigenvalue ρ^2

$$\left|(\rho^2 - \rho_{0\alpha}^2 - B_{\perp_{p,k}})\delta_{\alpha\beta} - i\omega L_{\alpha\beta}\right| = 0; \quad \alpha, \beta = 1, 2 \ldots N \tag{18}$$

which is the dispersion law for neutron waves, relating the squares inverse relaxation length ρ^2 to the angular frequency ω. The secular determinant, Eq. (18), was solved with N = 33 terms in the eigenfunction expansion, Eq. (15). The first four of the N values of the real and imaginary part of $\rho^2_{p,k,\gamma}$ ($\gamma = 1, 2, \ldots N$) were computed for several values of ω by a direct solution of the complex secular determinant using both the mass-12 kernel and Parks kernel. The fundamental mode is compared with the experimental values in section 4. To extract the diffusion and thermalization parameters, it is convenient to express the eigenvalues $\rho^2_{p,k,\gamma}$ in an analytical form. To this end the perturbation technique developed in Ref. [10] and systematized by KUNAISH [16] is used, which gives the squared inverse relaxation length in the form of a power series in the angular frequency ω,

$$\rho^2_{p,k,\gamma} = \sum_n B^{(n)}_{p,k,\gamma} (i\omega)^n = \chi^2_{p,k,\gamma} + i\sigma^2_{p,k,\gamma}, \tag{19}$$

where the coefficients $B^{(n)}_{p,k,\gamma}$ depend on the matrix elements $L_{\alpha\beta}$ and the structure of the scattering kernel. In turn, the real and imaginary parts of the complex inverse relaxation length $\rho_{p,k,\gamma}$, $\alpha_{p,k,\gamma}$ and $\xi_{p,k,\gamma}$, respectively, are given by

$$\alpha_{p,k,\gamma} = [\tfrac{1}{2}(r_{p,k,\gamma} + \chi^2_{p,k,\gamma})]^{\frac{1}{2}} \tag{20}$$

$$\xi_{p,k,\gamma} = [\tfrac{1}{2}(r_{p,k,\gamma} - \chi^2_{p,k,\gamma})]^{\frac{1}{2}}, \tag{21}$$

where

$$r^2_{p,k,\gamma} = \chi^4_{p,k,\gamma} + \sigma^4_{p,k,\gamma} \tag{22}$$

From Eqs. (20) and (21) two very useful relations are obtained which are the basis for the experimental determination in section 5 of the diffusion and thermalization parameters

$$\alpha^2_{p,k,\gamma} - \xi^2_{p,k,\gamma} = \chi^2_{p,k,\gamma} \tag{23}$$

$$2\alpha_{p,k,\gamma}\xi_{p,k,\gamma} = \sigma^2_{p,k,\gamma}. \tag{24}$$

The perturbation treatment also gives the coefficients $A_{p,k,\alpha,\gamma}(\omega)$ in terms of a power series in ω

$$A_{p,k,\alpha,\gamma} = A^{(0)}_{p,k,\alpha,\gamma} \sum_n S^{(n)}_{p,k,\alpha,\gamma} (i\omega)^n, \tag{25}$$

where the extra subscript γ arises from the multiplicity of roots of the dispersion law, and the constants $A^{(0)}_{a,\,k,\,\alpha,\,\gamma}$ depend on the strength and spectral distribution of the source. From Eqs. (9) and (15), the Fourier transform of the flux is, after summation over the multiplicity of roots,

$$\psi(E, \vec{r}, \omega) = \left[\frac{vM(E)}{D(E)}\right]^{\frac{1}{2}} \sum_{p,\,k,\,\gamma} \phi_{p,\,k}(x, y)\phi_{p,\,k,\,\gamma}(E, \omega) e^{-\rho_{p,\,k,\,\gamma} z} , \qquad (26)$$

where

$$\phi_{p,\,k,\,\gamma}(E, \omega) = \sum_{\alpha} A_{p,\,k,\,\gamma,\alpha}(\omega)\psi_{\alpha}(E) \qquad (27)$$

is the γ energy mode associated with the eigenvalue $\rho^2_{p,\,k,\,\gamma}$. Inversion of Eq. (26) into the time domain yields the neutron field

$$\psi(E, \vec{r}, t) = \frac{1}{2\pi}\int_{-\infty}^{\infty} \psi(E, \vec{r}, \omega)\, e^{i\omega t}\, d\omega = \frac{1}{2\pi}\int_{-\infty}^{\infty} \psi(E, \vec{r}, \omega, t) d\omega. \qquad (28)$$

Equation (28) gives the neutron field as the superposition of neutron waves

$$\psi(E, \vec{r}, \omega, t) = \mathrm{Re}\left\{\left[\frac{vM(E)}{D(E)}\right]^{\frac{1}{2}} \sum_{p,\,k,\,\gamma} \phi_{p,\,k}(x, y)\, \phi_{p,\,k,\,\gamma}(E, \omega) \right.$$

$$\left. \times \exp\left[\alpha_{p,\,k,\,\gamma}\, z + i(\omega t - \xi_{p,\,k,\,\gamma}\, z)\right]\right\} \qquad (29)$$

with damping coefficients $\alpha_{p,\,k,\,\gamma}$ and phase shift per unit length $\xi_{p,\,k,\,\gamma}$. An inspection of Eq. (28) suggests several ways of performing the experiment:

(a) Excitation of the neutron field by a thermal pulse localized at one of the boundaries. To relate the measured $\psi(E, \vec{r}, t)$ to the theoretically obtained function $\psi(E, \vec{r}, \omega, t)$, one has to perform an integration over the full frequency spectrum.

(b) To avoid the complicated integration in Eq. (28), one can numerically Fourier transform the output $\psi(E, \vec{r}, t)$ for comparison with the Fourier transform found theoretically.

(c) Excitation of neutron waves by a modulated source which yields the system's frequency response directly.

Method (a) is not practical. Methods (b) and (c) are theoretically equivalent. We call them the pulsed propagation method and modulated source excitation of thermal neutron waves, respectively.

We close this section with the reminder that diffusion theory is only valid for frequencies smaller than the inverse of the time between two neutron collisions. As frequency increases, transport corrections have to be applied, KUNAISH [16]. A study of the neutron wave formalism using the Cauchy method-of-characteristics and P_1 theory reveals that transport ef-

fects introduce correction terms depending on the ratio $D\omega/c$, where c is the wave front velocity (not to be confused with the wave velocity) and D is the diffusion coefficient. Diffusion theory results are obtained in the limit $\omega/c \to 0$ or in the diffusion approximation the wave front moves with infinite speed.

3. EXPERIMENTAL TECHNIQUE, DATA ACQUISITION AND EVALUATION

3.1. Experimental technique

The experiment was performed using a stack of AGOT graphite (stack density of 1.60 g/cm^3) of dimensions 44.7 cm × 71.0 cm × 125.0 cm ($B^2_{I\,0,0}$ = 59.6×10^{-4} cm^{-2}).

The neutron source consisted of a 150-keV Texas Nuclear Corporation (TNC), Cockcroft-Walton neutron generator with both pulsing and sinusoidal modulation capabilities. To thermalize the 14.4-MeV neutrons produced by the (D, T) reaction, a thermalizer tank was designed which minimized epicadmium contamination. This last requirement was important to avoid a distributed source of thermal neutrons throughout the assembly which would mask the thermal neutron disturbance propagating from the z = 0 boundary. A drawing of the thermalizer is shown in Fig. 1.

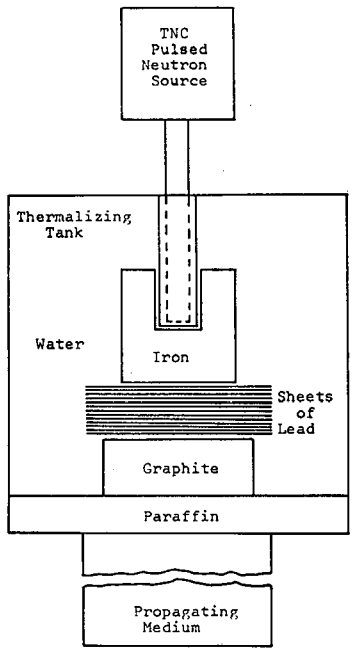


Fig. 1

Arrangement of the experiment and details of the thermalizing tank

Block diagrams for both sinusoidal and pulsed sources are shown in Figs. 2 and 3. Both of the neutron detector systems consisted of a He^3 detector connected to a Nuclear-Chicago Corporation preamplifier-scaler unit.

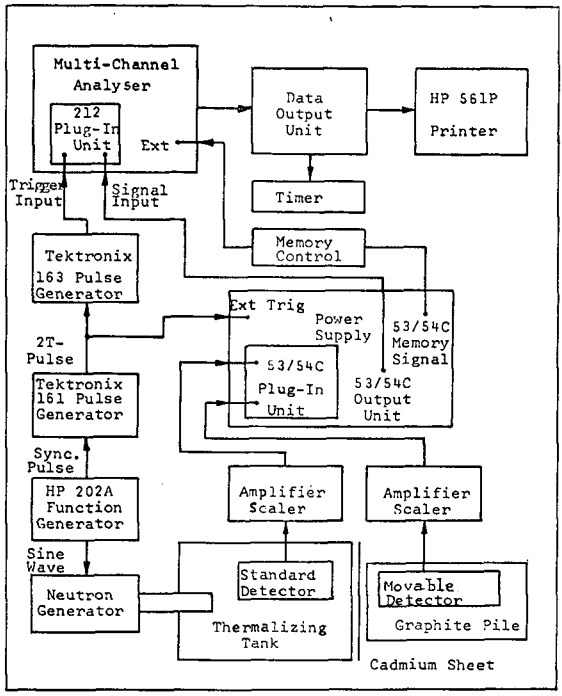


Fig. 2

A block diagram of the electronic equipment used in the wave experiment

For the wave experiment each detector output is recorded in one of the two half-memories of a 256 channel, Technical Measurements Corporation (TMC) time analyser through a system of electronic gates. A Hewlett-Packard function generator provides the sine wave for modulation of the neutron generator's extraction voltage, synchronizes the operation of the gates and triggers the TMC time analyser. For the pulse excitation technique only one detector is connected to the TMC time analyser.

3. 2. Data acquisiton and evaluation

For each frequency and detector position two runs were performed. In the second one a cadmium sheet was placed between the source and the graphite pile so that only the epithermal background was recorded. This background was then subtracted from the first run to obtain the signal resulting from only the thermal neutrons at the source. Normalization between runs was performed by recording the output of a standard detector placed in the thermalizing tank. The background corrected waves and the standard detector output were Fourier analysed to isolate the various frequency harmonics. Typical thermal neutron shapes are given in Fig. 4 for 200 c/s at several detector locations. Notice the large attenuation and phase shift as a function of distance from the source. For the pulse propagation experiment the epicadmium correction is less critical because the thermal

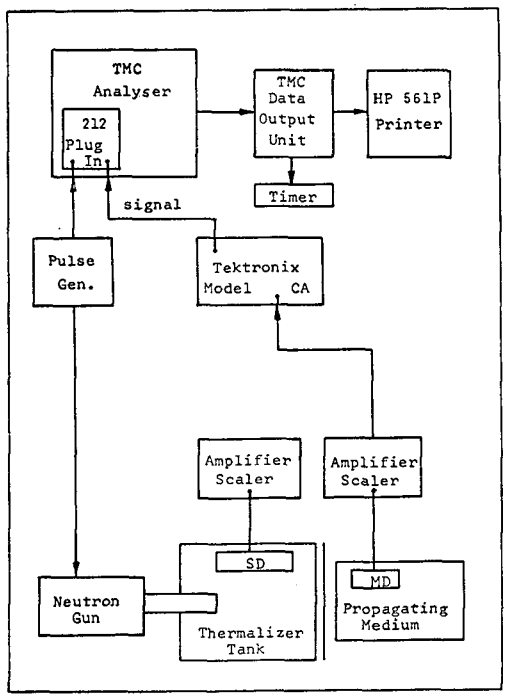


Fig. 3

A block diagram of the electronic equipment used in the pulse propagation experiment

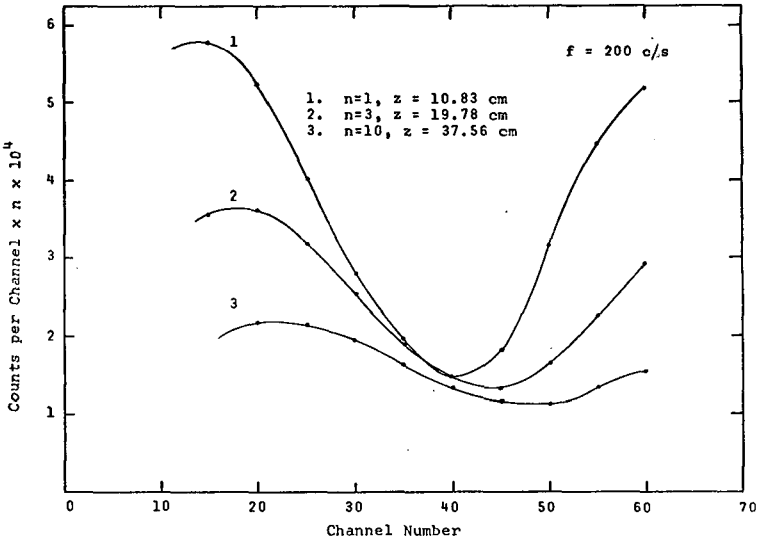


Fig. 4

Thermal wave of the 200 c/s wave experiment for several z-positions

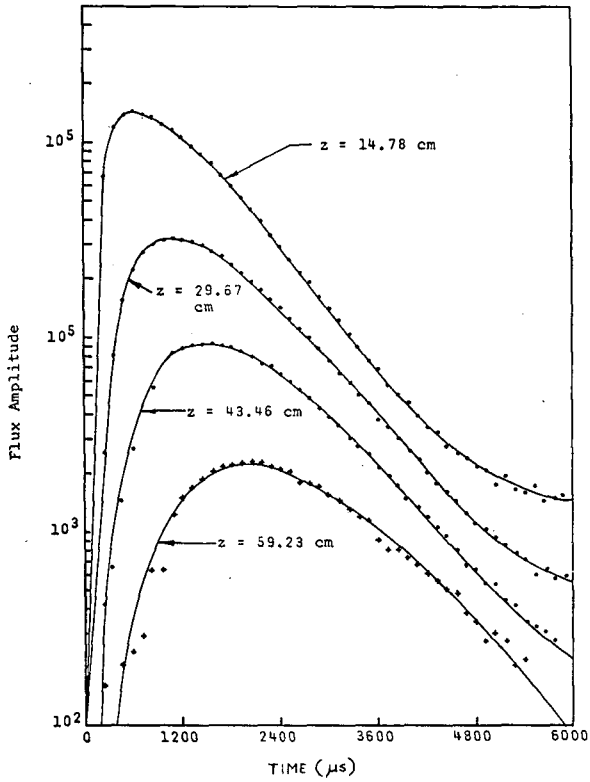


Fig. 5

Thermal pulse for the pulse propagation experiment for several z-positions

Note: See first two paragraphs of the discussion.

neutrons resulting from the epicadmium background tend to bunch up at short times after the end of the burst. A set of thermal pulses is shown in Fig. 5.

To perform the data analysis, the influence of the spatial and energy modal contamination has to be considered. The higher spatial modes are significant only at higher frequencies where leakage is not so important. Straight-forward calculations show that with a point source one would expect about 2% spatial modal contamination at a few centimetres from the source. The other complication arises from the non-Maxwellian spectral distribution which excites energy modes associated with the multiplicity of roots of the dispersion law. Computations using the Parks kernel and Eq. (18) showed the existence of only one discrete mode followed by a continuum of eigenvalues. They exhibited larger damping coefficients than $\alpha_{0,0,1}$ of the discrete mode between 0 and around 300 c/s. Beyond 300 c/s some of the continuum eigenvalues have damping coefficients which are smaller than $\alpha_{0,0,1}$.

Least squares fitting of the logarithm of the wave amplitude as a function of distance for various frequencies yielded $\alpha(\omega)$ for the fundamental mode.

Similarly, from the phase-shift linear plots, the function $\xi(\omega)$ was extracted. To minimize both the higher spatial and energy mode effects, least squares fitting codes were used, which chopped off in a step-wise fashion portions of the amplitude and phase plots until values of α and ξ were obtained which would not depend on the section on the curve analysed. The statistical errors associated with the determination of these parameters were obtained as a part of the output of the codes used in the analysis. The effect of systematic errors was studied by performing several reproducibility tests and by comparing the results obtained by the modulated source method with the ones yielded by the pulse propagation technique. The evaluation of the combined tests indicated a conservative estimate of about 2% total error (statistical and systematic).

4. COMPARISON OF THE THEORY WITH THE EXPERIMENT

It has been proposed by BECKURTS [17] that it is more useful to contrast the experimentally obtained eigenvalues with the ones computed theoretically than to compare parameters extracted from the data to their value as predicted by the theory. Consistent with this idea, Figs. 6 and 7 show the

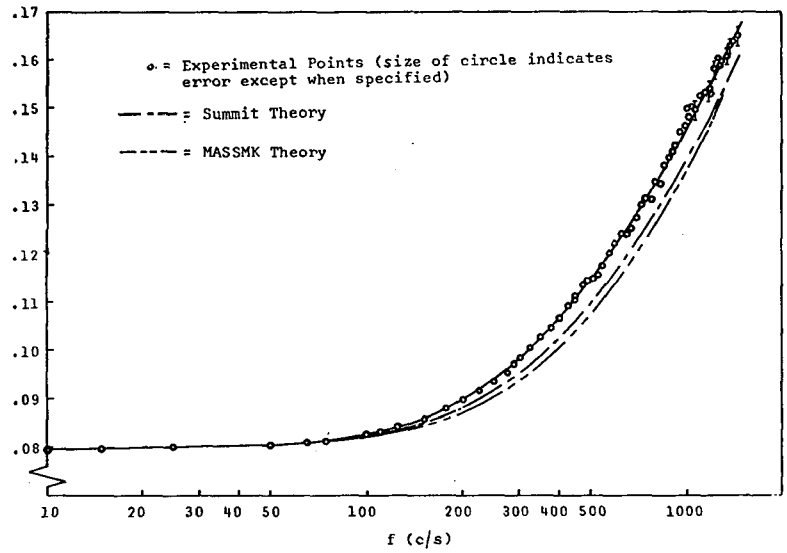


Fig. 6

Comparison of the theoretically derived α to the experimental results

real and imaginary components of the experimentally determined complex inverse relaxation length versus frequency, along with those curves from the theory using both the SUMMIT kernel and the MASSMK kernel. From an inspection of these figures, it appears that both theoretical models predict the experiment quite well up to about 500 c/s. For higher frequencies, the theory and experiment diverge slightly, with the discrepancy of the

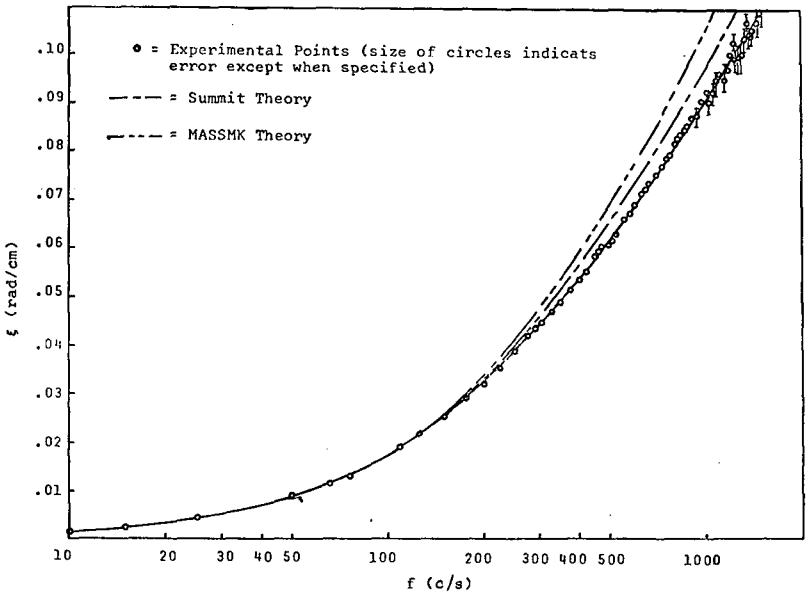


Fig. 7

Comparison of the theoretically derived ξ to the experimental results

MASSMK kernel exceeding that of the SUMMIT kernel by a noticeable amount. In the frequency range between 400 c/s and 1000 c/s the deviation between the SUMMIT kernel and the experiment rises from 4% to about 10% while, in this same frequency range, the MSSMK deviation ranges between 8 and 15%. Both theories tend to underestimate the damping coefficient α and to overestimate the phase-shift factor ξ especially at higher frequencies.

One could conclude from this direct comparison that the disagreement between theory and experiment exists only for frequencies higher than 500 c/s. However, an ambiguity exists in that this disagreement can be attributed to one or more of the following facts: (1) higher energy mode contamination, (2) higher spatial mode contamination, (3) transport effects, (4) inadequacy of the particular kernels which were used to describe the thermalization effects. From the considerations developed in section 4 about the higher energy modes, one could conclude that the modal contamination from neutron energy distribution effects will be noticeable around 500 c/s which agrees with the observation by STARR and PRICE [18], namely, that for large bucklings, waiting times of the order of two milliseconds were needed to obtain the asymptotic behaviour in die-away experiments in graphite. In terms of the neutron wave experiment, this is equivalent to the prediction that higher energy modes will become prevalent for frequencies larger than 500 c/s.

As frequency increases, all of the spatial modes associated with the fundamental energy mode approach the same values for their damping and phase shift coefficients. This is because they differ only by the transverse leakage term, $B^2_{1p,k}$, which becomes progressively less significant com-

pared to the frequency-dependent terms of ρ^2 as the frequency increases. At low frequencies these higher spatial modes can be easily discriminated against by obtaining data only at points far from the source boundary and by applying the channel-chop technique previously discussed. At higher frequencies, however, one cannot be sure that higher spatial modes are not contributing to the data since their attenuation and phase-shift factors will be nearly equal to those of the fundamental spatial model. PEREZ and UHRIG [10] estimated that for a point source in the assembly investigated here higher spatial mode contamination could become as large as 5% in the upper frequency range.

Another source of difficulty arises from the fact that transport theory should be introduced when the time between two collisions becomes of the same order of magnitude as the inverse of the frequency. This effect is less important than the thermalization effects, and it has been estimated by KUNAISH [16] to be on the order of 2%.

Hence, the direct comparison test without additional information can both preclude any firm conclusion about the disagreement between theory and experiment at the higher frequencies and lead one to assume that, since there was agreement over a reasonable range of frequencies, the diffusion and thermalization parameters derived from the theory are adequate. From this fact the question arises as to how sensitive the direct comparison test is to thermalization phenomena. Still another example of the difficulty in deriving firm conclusions concerning thermalization effects by the direct comparison of eigenvalue curves can be obtained by applying the reasoning presented thus far to typical die-away experiments. By doing this, one could conclude that diffusion theory gives adequate theoretical predictions except in the range of bucklings where the experimental data can be affected by higher energy and spatial modes as well as by transport corrections. The inadequacy of the direct comparison test is confirmed by the fact that when used to generate eigenvalue curves the MSSMK kernel, which is much less sophisticated from a thermalization viewpoint than the SUMMIT kernel, gives results which appear very similar to the SUMMIT kernel.

The difficulties encountered in the direct comparison test for both the die-away and the neutron wave experiments arise because the thermalization parameters enter as second-order effects in the frequency range in which the asymptotic mode is easily measured. To perform a meaningful comparison between the theory and the experimental results, one should be able to isolate thermalization effects from diffusion effects.

In the conventional die-away experiment this is not possible because only one quantity, the decay constant, is measured. In the neutron wave experiment, however, two independent parameters, α and ξ, are measured; and they can be combined to yield two frequency-dependent functions, $2\alpha\xi$ and $\alpha^2-\xi^2$. The former is primarily dependent upon diffusion parameters, and the latter, except for the zero-frequency intercept, is exclusively a function of thermalization parameters.

Figure 8 shows a plot of $2\alpha\beta$ as a function of frequency. Since the fundamental dependence of this function is upon diffusion parameters, the agreement between the SUMMIT theory and the experimental results appears within the experimental error over the full frequency range considered. The

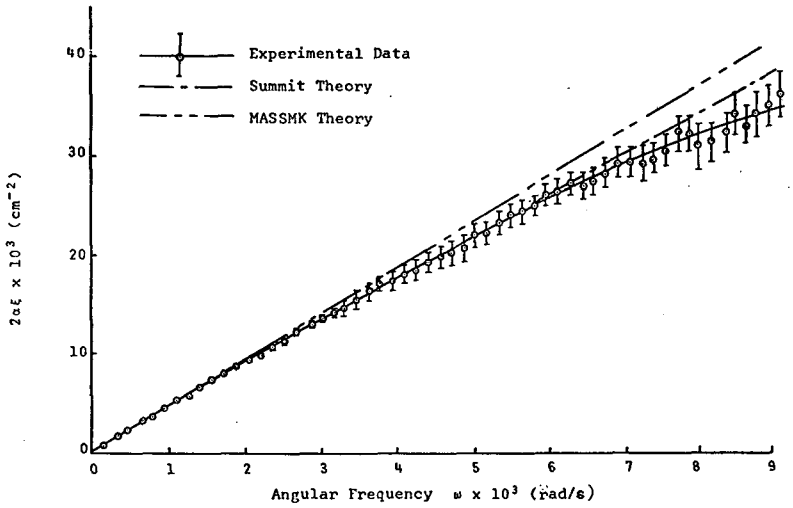


Fig. 8

Comparison of the theoretically derived $2\alpha\xi$ to the experimental results

MASSMK kernel also represents the data well in a reasonably large range of frequencies. Note that the above is especially true for frequencies less than 500 c/s where no problems associated with modal contamination and transport corrections are expected to occur.

The $\alpha^2 - \xi^2$ versus ω^2 curves, shown in Fig. 9 for the frequency range from 10 to 1400 c/s and in Fig. 10 for the frequency range below 400 c/s, indicate that sizeable differences exist among the MASSMK kernel, SUMMIT

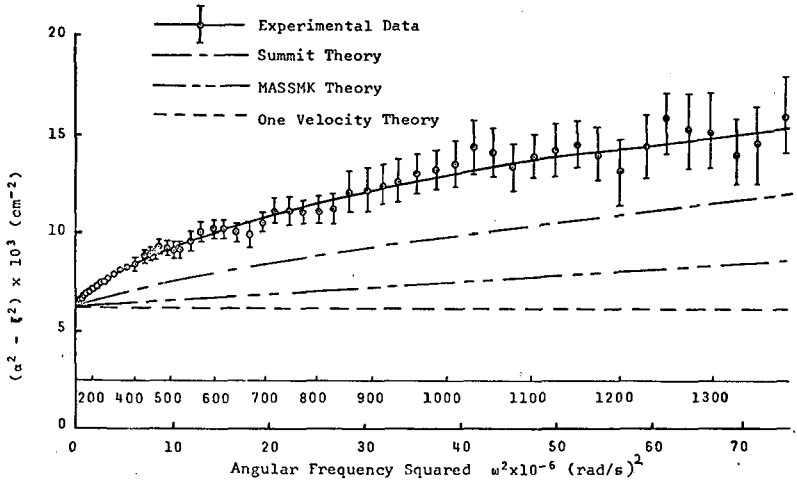


Fig. 9

Comparison of the theoretically derived $\alpha^2 - \xi^2$ to the experimental results for frequencies up to 1400 c/s

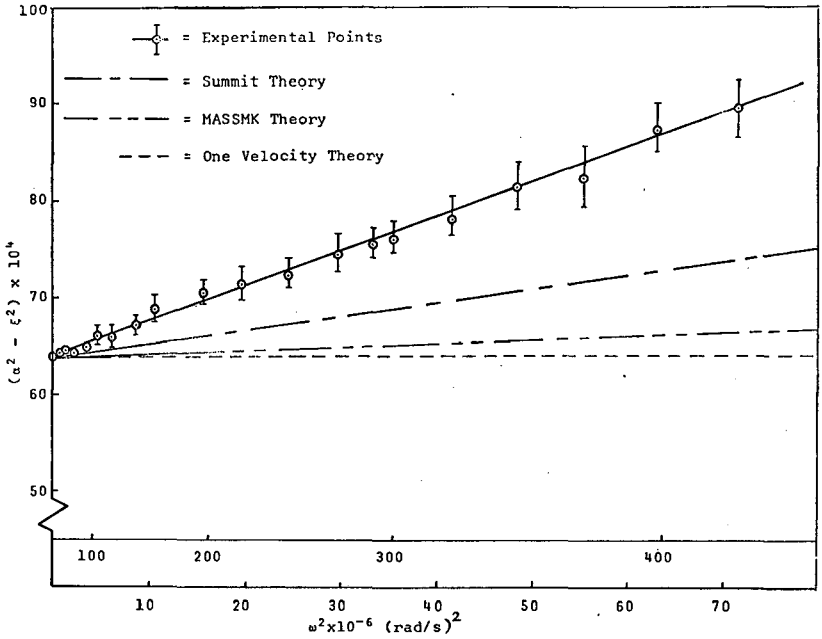


Fig. 10

Comparison of the theoretically derived $\alpha^2 - \xi^2$ to the experimental results for frequencies up to 400 c/s

kernel and the experimental results over the full frequency range. Note that the one-velocity diffusion theory model predicts a constant behaviour of $\alpha^2 - \xi^2$. Also, this is the only curve thus far presented in which noticeable differences exist between the two theories and the experimental results in the zero to 300-c/s frequency range. Therefore, this is the first instance in which the various thermalization models can be compared with the experimental results in the frequency interval where the experimental data are most accurate and reliable and with no interference arising from diffusion phenomena. In other words, the small differences in the theoretically and experimentally determined α and ξ, which are mainly caused by thermalization effects, tend to compensate in the $2\alpha\xi$ curve and to be amplified in the $\alpha^2 - \xi^2$ curve.

An inspection of Figs. 9 and 10 clearly indicates that, although the trend of the SUMMIT theory correctly describes that of the experimental results, the coefficient associated with the linear rise at low frequency will be about twice as large in the experimental curve as the one for the theory.

The real and imaginary components of ρ^2, $\alpha^2 - \xi^2$ and $2\alpha\xi$, Eqs. (23) and (24), were least-squares fit to polynomials of the form

$$\alpha^2 - \xi^2 = \sum_{\substack{n=0 \\ (\text{EVEN})}}^{N} P^{(n)} \omega^n \qquad (30)$$

$$2\alpha\xi = \sum_{\substack{n=1 \\ (\mathrm{ODD})}}^{N-1} P^{(n)}\omega^n \qquad (31)$$

so that the $P^{(n)}$ thereby determined could be compared with the coefficients $B^{(n)}$ obtained from the perturbation expansion, Eq.(19). A STEP-WISE MULTIPLE REGRESSION code was used, which applied several statistical tests to evaluate the significance of the various parameters in Eqs.(30) and (31). It was found that for the $2\alpha\xi$ curve only $P^{(1)}$ and $P^{(3)}$ were statistically significant. In the $\alpha^2 - \xi^2$ curve the $P^{(0)}$, $P^{(2)}$ and $P^{(4)}$ coefficients were found to be significant in improving the goodness of fit. The whole analysis was repeated in several portions of the experimental curve. The various coefficients determined by the method indicated above are shown in Table I.

TABLE I

EXPERIMENTAL AND THEORETICAL VALUES FOR THE $P^{(n)}$ COEFFICIENTS FOR A DENSITY OF 1.60 g/cm^3

	Polynomial fits of $2\alpha\xi$ and $\alpha^2 - \xi^2$	SUMMIT theory
$P^{(0)} \times 10^4$ (cm^{-2})	63.86 ± 0.09	63.884
$P^{(1)} \times 10^6$ (s cm^{-2})	4.64 ± 0.01	4.7386
$P^{(2)} \times 10^{10}$ (s^{2}cm^{-2})	3.92 ± 0.09	2.1143
$P^{(3)} \times 10^{14}$ (s^{3}cm^{-2})	- 1.02 ± 0.07	- 4.4903
$P^{(4)} \times 10^{18}$ (s^{4}cm^{-2})	-11.00 ± 1.00	-28.969

5. RELATIONSHIPS BETWEEN THE NEUTRON WAVE EXPERIMENT, DIE-AWAY EXPERIMENT AND THE DETERMINATION OF DIFFUSION AND THERMALIZATION PARAMETERS

The main objective of this paper is to demonstrate the effectiveness of the neutron wave technique for the determination of diffusion and thermalization parameters. To evaluate the fulfilment of this objective, the results obtained here for the experiment in graphite are compared with published results of die-away experiments where the same parameters were measured. The various complementary relationships between the two experiments are also investigated.

In the die-away experiment one measures the decay constant of the fundamental time and energy eigenfunction of the Boltzmann operator associated with the fundamental spatial mode. The real eigenvalue λ is determined as a function of the system's lowest geometric buckling, and this λ versus B^2 curve yields the parameters of interest. Consistent with current terminology, this method is referred to as a dynamic experiment. The neutron wave experiment, in contrast, is a static experiment, i.e. in the same class

as the poisoning experiment; and one measures the complex, fundamental eigenvalue ρ of the space- and energy-dependent Boltzmann operator as a function of frequency.

It has been shown in Ref. [10] that the eigenvalues λ^w and ρ^2 are mathematically related when ρ^2 is expressed in the form

$$\rho^2 = B_\perp^2 + \sum_{n=1}^{N} Q^{(n)} \left(\frac{\alpha_0 + i\omega}{D_0} \right)^n \tag{32}$$

and use is made of the relationships

$$i\omega = -\lambda^w , \tag{33}$$

where the w superscript indicates that λ^w is the eigenvalue that is to be obtained from the $Q^{(n)}$ in a neutron wave experiment and

$$-\rho = iB_z . \tag{34}$$

Substitution of the above transformation into Eq. (32) yields

$$-B_\perp^2 = -(B_z^2 + B^2) = \sum_{N=1}^{N} Q^{(n)} \left(\frac{\alpha_0 - \lambda^w}{v_0} \right)^n . \tag{35}$$

By inverting the series in $\left(\frac{\alpha_0 - \lambda^w}{v_0} \right)$ to one in B^2 one obtains

$$\lambda^w = \alpha_0 + D_0^w B^2 - C_0^w B^4 + F_0^w B^6 , \tag{36}$$

where

$$\alpha_0 = v_0 \Sigma_{a0} \tag{37}$$

$$D_0^w = v_0 / Q^{(1)} \tag{38}$$

$$C_0^w = -v_0 Q^{(2)} / (Q^{(1)})^3 \tag{39}$$

$$F_0^w = v_0 / (Q^{(1)})^5 [2(Q^{(2)})^2 - Q^{(1)} Q^{(3)}] . \tag{40}$$

The coefficients, as defined above, differ slightly from the ones measured in the dynamic die-away experiment because they were derived from the static wave experiment expressions.*

* In this context the difference between static and dynamic experiments is related to the effect upon the energy dependence of a 1/v absorber in the medium. In the die-away experiment a 1/v absorber does not affect the energy dependence of the fundamental eigenfunction (14) which, for zero buckling, is a Maxwellian. The fundamental eigenvalue of the exponential experiment is a Maxwellian distribution only in the zero absorption case. Thus, the static and dynamic experiments are equivalent only when $\alpha_0 = 0$ in the expressions for the static experiment.

In the analysis of data presented in the previous section, ρ^2 was expressed in the form

$$\rho^2 = \sum_{\substack{n=0 \\ (\text{EVEN})}}^{N-1} P^{(n)}\,\omega^n + i \sum_{\substack{n=1 \\ (\text{ODD})}}^{N} P^{(n)}\,\omega^n . \tag{41}$$

From Eqs. (32) and (41) the following connection between the $Q^{(n)}$ and $P^{(n)}$ coefficients is obtained with N = 3

$$P^{(0)} = B_1^2 + \sum_{n=1}^{3} Q^{(n)} \left(\frac{\alpha_0}{v_0}\right)^n \tag{42}$$

$$P^{(1)} = \frac{1}{v_0}\left[Q^{(1)} + 2\left(\frac{\alpha_0}{v_0}\right)Q^{(2)} + 3\left(\frac{\alpha_0}{v_0}\right)^2 Q^{(3)}\right] \tag{43}$$

$$P^{(2)} = -\frac{1}{v_0^2}\left[Q^{(2)} + 3\left(\frac{\alpha_0}{v_0}\right)Q^{(3)}\right] \tag{44}$$

$$P^{(3)} = -\frac{1}{v_0^3}\,Q^{(3)} \tag{45}$$

The $Q^{(n)}$ and α_0 / v_0 obtained from the $P^{(n)}$ by the iterative use of these expressions can be used to determine D_0^W, C_0^W, and F_0^W. For the determination of these same parameters for comparison with die-away experiments by using expressions (38), (39) and (40), the above expressions with $\alpha = 0$ should be used to determine the $Q^{(n)}$. In Table II the $Q^{(n)}$ parameters derived from Eqs. (43), (44) and (45) with $\alpha_0 = 0$ are presented. From this table and Eqs. (38), (39) and (40), the values of the dynamic α_0, D_0, C_0 and F_0 parameters were calculated and are shown in Table III. In Table IV the values for the various

TABLE II

EXPERIMENTAL AND THEORETICAL VALUES FOR THE $Q^{(n)}$ COEFFICIENTS AT A DENSITY OF 1.60 g/cm^3

	$Q^{(1)}$ (cm^0)	$Q^{(2)}$ (cm^2)	$Q^{(3)}$ (10^{-2} cm^4)
Experiment	1.020	-19.0	1.09
	±0.005	± 0.9	±0.05
Theory	1.0415	-10.3595	4.7682

TABLE III

DIFFUSION AND THERMALIZATION PARAMETERS
(Density: 1.60 g/cm^3)

	D_0 (10^{-5} cm^2/s)	C_0 (10^{-5} cm^4/s)	F_0 (10^{-7} cm^6/s)
Experiment	2.16 ± 0.01	39.0 ± 2	12.0 ± 2
Theory	2.1104	20.1553	-5.0574

TABLE IV

PARAMETERS AS DETERMINED FROM VARIOUS DIE-AWAY EXPERIMENTS COMPARED WITH THE RESULTS OF THIS WORK [a]

Year	Reference	α_0 (s^{-1})	D_0 (10^{-5} cm^2/s)	C_0 (10^{-5}cm^4/s)	F_0 (10^{-7} cm^6/s)
1961	LALANDE [19]	79.5 ± 3	2.07 ± 0.04	25.8 ± 2	-
	STARR and PRICE [18]				
1962	Type GBF	74.6 ± 0.06	2.14 ± 0.01	34 ± 3	-
	Type AA	68.1 ± 0.08	2.19 ± 0.03	41 ± 4	-
1962	STARR and de VILLIERS [20]			38 ± 5	-
1962	KLOSE et al. [b]	88.3 ± 1.2	2.13 ± 0.02	26 ± 5	-
	[21]	88.6 ± 1.6	2.11 ± 0.02	16 ± 5	-20.0 ± 10
1963	SAGOT et al. [22]	74.1 ± 3	2.19 ± 0.03	37.9 ± 4	-
1965	This work	91.0 ± 4	2.16 ± 0.01	39.0 ± 2	12.0 ± 2

[a] All values listed in the table have been corrected to a density of 1.60 g/cm^3.
[b] Both the three- and four-parameter fits are included.

diffusion and thermalization parameters that are to be compared with the die-away results are listed along with the results for several die-away experiments.* From an inspection of these tables one can conclude the following:

(1) The experimentally obtained diffusion coefficient agrees quite well with those of pulsed experiments and with the theory.

(2) The value obtained in this work for the cooling coefficient C_0 is about a factor of two higher than the one predicted by using the SUMMIT kernel

* Many of the results listed in Table IV were obtained from Ref. [22].

but is in very good agreement with the more recent die-away results. However, this result is still somewhat lower than the lower bound of 45×10^5 cm^4/s predicted for C_0 by de SAUSSURE [23].

(3) The value of F_0 obtained experimentally differs both in sign and magnitude from the one of the SUMMIT kernel and with the value obtained by KLOSE et al. [21]. HONECK [24] also used the SUMMIT kernel and obtained a value of -7.44×10^7 cm^6/s for F_0. However, NELKIN [6] predicts a positive coefficient of the order of about C_0^2/D_0 which is consistent with Eq. (40) if one neglects the contribution of $Q^{(3)}$. Inspection of this equation indicates that the sign of F_0 is determined by the magnitude of $2(Q^{(2)})^2$ compared to $Q^{(1)} Q^{(3)}$. The solution to this contradiction regarding the F_0 coefficient awaits more theoretical and experimental work.

It is the author's belief that with the introduction of electronic modulation procedures, the neutron wave method has become a highly accurate and reliable technique. This method possesses the significant advantage, among others, of isolating thermalization phenomena from pure diffusion effects, thus making possible very sensitive tests of the scattering law for moderators.

ACKNOWLEDGEMENTS

The authors gratefully acknowledge the important contribution of Dr. M.J. Ohanian to the solution of the space-energy eigenvalue problem. His help in many aspects of the paper through illuminating discussions is also appreciated.

Mr. R.H. Hartley and Mr. G.W. Fogle are responsible for several developments regarding the experimental equipment. They contributed significantly to the acquisition of data.

REFERENCES

[1] WEINBERG, A.M. and SCHWEINLER, H.C., Phys. Rev. 74 (1948) 851.
[2] VON DARDEL, G., Trans. R. Inst. Techn. Stockholm 75 (1954).
[3] BECKURTS, K.H., Nucl. Sci. Engng 2 (1957) 516.
[4] RAIEVSKI, V. and HOROWITZ, J., Proc. UN Int. Conf. PUAE 5 (1956) 42.
[5] UHRIG, R.E., Trans. Amer. nucl. Soc. 2 2 (1959).
[6] NELKIN, M.S., J. nucl. Energy 8 (1958) 59.
[7] BECKURTS, K.H., Nucl. Instrum. Meth. 11 (1961) 144.
[8] PUROHIT, S.N., Nucl. Sci. Engng 9 (1961) 157.
[9] HAFELE, W. and DRESNER, L., Rpt. ORNL-2842 (1959) 124.
[10] PEREZ, R.B. and UHRIG, R.E., Nucl. Sci. Engng 17 (1963) 90.
[11] BOOTH, R.S., Ph.D. Dissertation, Univ. of Florida (1965).
[12] HARTLEY, R.H., Master's Thesis, Univ. of Florida (1964).
[13] PEREZ, R.B., BOOTH, R.S., DENNING, R.S., and HARTLEY, R.H., Trans. Amer. nucl. Soc. 7 (1964) 49.
[14] OHANIAN, M.J. and DAITCH, P.B., Nucl. Sci. Engng 19 (1964) 343.
[15] PARKS, D.E., Rpt. GA-2438 (1962).
[16] KUNAISH, H., Ph.D. Dissertation, Univ. of Florida (1964).
[17] BECKURTS, K.H., Proc. Brookhaven Conf. on Neutron Thermalization, BNL 719 III R-1 (1962).
[18] STARR, E. and PRICE, G.A., Proc. Brookhaven Conf. on Neutron Thermalization, BNL 719 III (1962) 1034.
[19] LALANDE, G., Industries Atomiques 516 (1961) 71.

[20] STARR, E. and de VILLIERS, J.R.L., Proc. Brookhaven Conf. on Neutron Thermalization, BNL 719 III (1962) 997.
[21] KLOSE, H., KÜCHLE, M. and REICHARDT, W., Proc. Brookhaven Conf. on Neutron Thermalization, BNL 719 III (1962) 935.
[22] SAGOT, M. et al., Exponential and Critical Experiments III IAEA, Vienna (1964) 163.
[23] de SAUSSURE, G., Proc. Brookhaven Conf. on Neutron Thermalization, BNL 719. III (1962) 1158.
[24] HONECK, H.C., Proc. Brookhaven Conf. on Neutron Thermalization, BNL 719 (1962) 1186.

LIST OF SYMBOLS

$\vec{r}, E$ = vector position and neutron energy, respectively
$D(E)$ = diffusion coefficient (cm)
$\Sigma_a(E)$ = macroscopic absorption cross-section (cm^{-1})
$\Sigma_s(E', E)$ = scattering kernel ($cm^{-1}\ eV^{-1}$)
$\Sigma_s(E) = \int_{E'} \Sigma_s(E, E')dE'$, macroscopic scattering cross-section (cm^{-1})
$M(E)$ = Maxwellian distribution
$B^2_{\perp p,k}$ = transverse buckling for (p, k) spatial mode
$= \left[(2p+1)\frac{\pi}{a}\right]^2 + \left[(2k+1)\frac{\pi}{b}\right]^2$
$\phi_{p,k}(x, y)$ = eigenfunction of Helmholtz operator
$= \cos\left[(2p+1)\frac{\pi}{a}x\right]\cos\left[(2k+1)\frac{\pi}{a}y\right]$

DISCUSSION

P. d'OULTREMONT: In Fig. 5 of your paper you show different stages in the propagation of a pulse of neutrons. The experimental points are joined up by curves. Are these curves theoretical ones? At Louvain we have measured very similar phenomena for fast neutrons (≃1 MeV) and in certain cases the time-dependent P_1 approximation seems to give a fairly faithful picture of the deformations of the pulse during its movement, particularly of the displacement of the wave maximum.

R. PEREZ: I am sorry to have misled you – the figure shows only experimental points. The joining up of the points was due to the zeal of our draftsman. However, we did try to compute these pulses by solving the Boltzmann equation by Laplace transform methods, by expansion in eigenfunctions of the scattering kernel, and then inversion of the result into the time domain. This inversion proved to be very difficult. Hence we decided to develop the theory in the frequency domain and make the comparison with the Fourier transform of the pulse. This is most advantageous as higher transport approximations are much easier to handle because one replaces the operators $(\partial/\alpha\epsilon)^n$ by terms $(i\omega/v)^n$. I should also like to point out that

we are dealing with thermal systems in which the energy dependence represents a much larger effect than transport corrections.

M. N. MOORE: I should like to comment on this problem of the ability of the P_1 approximation to follow the pulse maximum. The motion of the pulse maximum may very well be described by a P_1 calculation. However, the pulse maximum is only one of the parameters that describe the shape of the pulse. The width is another. If one wants to describe the pulse shape as it is propagated, the higher-frequency components of the pulse become necessary and these high-frequency components are governed by higher-order P_n approximations.

R. PEREZ: I would tend to agree with you. Higher-order transport corrections will certainly be necessary in fast systems.

M. KAZARNOVSKY: When one examines the problem of eigenvalues for the Boltzmann equation, one is in fact studying the dependence of the eigenvalue on a geometrical parameter (buckling) – I am thinking of the case of a pure moderator. In experiments with pulsed sources this dependence decreases in the range of the positive values of the geometrical parameter B^2. In experiments involving poisoning of the moderator and a stationary source, this dependence is measured at negative values of B^2. In experiments with modulated sources the dependence decreases in the complex range. Thus, all these experiments allow us to analyse the same phenomenon; they are thus complementary and enable the results to be corrected. Each of these methods has advantages and drawbacks. It seems to me that the main difficulty with the modulated-source method is that of estimating the contribution of the higher-energy modes. Nevertheless this approach is extremely interesting and deserves the closest attention.

R. PEREZ: The neutron wave experiment allows one to explore the full complex domain because one measures both the amplitude and phase shift of the propagating wave. The analogy with the "die-away" experiment can be analytically expressed by the equalities $\omega = \alpha$, $p^2 = -B^2_z$. In fact the $2\alpha\xi$ curve in our paper is very similar to the typical $\alpha/-\beta$ curve. A full explanation of the analogy is given in a paper by Perez and Uhrig (Nuclear Science and Engineering 17 (1963) p. 90).

As for the difficulties in connection with the continuum, I should like to point out that the complex inverse relaxation lengths associated with it are only small enough to allow measurements at very high frequencies. In this case one would end up with a superposition of complex exponentials that would give rise to the onset of interference processes. The situation will be worst in a "die-away" experiment where the continuum will appear as a superposition of real exponentials, which are very difficult to analyse. Both cases however will have to be interpreted by very involved analytical techniques, although I believe it would be somewhat easier with modulated experiments.

I agree that attention should be paid to different methods with a view to improving our understanding of the phenomena arising from the interaction of neutrons with matter.

M. N. MOORE: I was very interested in the comment that was made about the interrelation between wave, pulse and poison experiments. I have found it very illuminating to unify these by the introduction of a dispersion function $Z(B^2, \lambda)$ which satisfies a dispersion law $Z(B^2, \lambda) = 0$. The pulsed

experiment demands that B^2 be real, whence λ turns out to be generally complex giving rise to time decay. The wave experiment demands that λ be real, viz. $\lambda = \omega$, whence β has to be complex giving rise to an attenuated wave. From this point of view the two experiments are related by a rotation through 90° in the complex plane.

M. COPIC: Because of the limitation on λ there is a maximum value B^{*2} in pulsed experiments beyond which we have no discrete modes. Is there a similar limitation on the frequency in (modulated) wave propagation experiments, where for frequencies larger than a certain f* value there are no discrete modes any more but only continuum?

R. BOOTH: Our theoretical calculations indicate that a discrete mode exists at all frequencies when one considers a graphite medium as described by the Boltzmann equation in the diffusion approximation. As frequency increases, the continuum energy modes begin to be propagated with complex inverse relaxation lengths, which are comparable with that of the fundamental discrete mode. Thus, as frequency increases, modal contamination increases also. I do not think that this is a serious problem since thermalization parameters can be easily obtained from the low-frequency data for which the discrete mode predominates. In fact, this energy mode contamination could be useful since it could result in a resonance effect from which more parameters could be determined.

R. PEREZ: In a normal experiment there are very few neutrons in the continuum. However, this continuum is very interesting because of its connection with the scattering kernel, and it would be very informative to feed the continuum portion of the spectra with cold neutrons, thus optimizing the neutron density in this region of continuum eigenvalues produced by the energy distribution of the neutron flux.

M. N. MOORE: I should like to comment on this question of whether there is a frequency limitation analogous to the buckling limitation in pulsed experiments. The answer is that there is. At frequencies at which the only wave that can be propagated belongs to the continuum, one finds that the wave-length is of the order of the mean free path and the phase velocity is equal to the neutron velocity. This provides some physical insight into the nature of the continuous modes. Such wave-lengths and velocities contradict hydrodynamic approximations to the Boltzmann equation. It explains why Pn multi-group approximations do not manifestly display continuous modes.

R. PEREZ: Apart from the continuum arising from the transport effects, there is also the continuum which is caused by the interaction of the neutrons with the phonon field.

P. DAITCH: I would like to draw attention to some aspects of the P-L approximations which are used to treat these problems. In the case of a uniform infinite medium all P-L approximations are exact and yield the continuum associated with energy eigenvalues. As one proceeds from this infinite case to spatially dependent cases, the eigenfunctions involve a continuum to match the angular dependence of the flux as well as its energy. The P-L approximations in this finite case yield the continuum of energy eigenvalues but their multiplicity, which includes the angular dependence at every energy, is accounted for by only a finite number of angular functions and their associated finite number of eigenvalues. This finite multiplicity

of eigenvalues represents selections from a continuum. It may be that to represent certain physical phenomena adequately one must use many of these eigenfunctions selected from the continuum, that is, go to high orders of $\overline{L}$.

COMPARATIVE STUDY OF SEVERAL TYPES OF PULSED AND MODULATED EXPERIMENTS ON FAST MULTIPLYING MEDIA

M. CADILHAC, P. GOVAERTS, P. HAMMER, M. MOORE
B. NICOLAENKO AND F. STORRER
ASSOCIATION EURATOM-CEA POUR LES NEUTRONS RAPIDES,
CENTRE D'ÉTUDES NUCLÉAIRES DE CADARACHE, FRANCE

Abstract — Résumé — Аннотация — Resumen

COMPARATIVE STUDY OF SEVERAL TYPES OF PULSED AND MODULATED EXPERIMENTS ON FAST MULTIPLYING MEDIA. A distinction is made between two types of kinetic experiment (pulsed or modulated) according to the configuration of the assembly and the source position :

(1) Critical or slightly subcritical assembly with the source in or near the core;

(2) Greatly subcritical mass fed by a source on one face, exactly as in an exponential experiment.

In both cases, the law governing the variation of the source as a function of time can be: (a) A Dirac function or one closely similar. In this case, it is a pulsed experiment; (b) A sinusoidal wave or at least a periodical function in which the fundamental component is dominant. It is then a modulated experiment; or (c) An aleatory or pseudo-aleatory function.

The paper provides a comparative study of the two aspects of these various types of experiment: (a) Fundamental integral experiments to check the basic data or methods of calculation by comparing the theoretical and experimental results; and (b) Experiments designed to determine important parameters of projected or existing reactors (e.g. determination of $\alpha - \beta/\ell$ and reactivity by the classical pulsed method, or material buckling by an exponential experiment).

As the phenomenon is perfectly linear, it is obvious that the same information can be obtained, in principle, by the method based on modulation over the entire frequency range and the pulsed method, whose spectral analysis contains all the frequencies. In practice, one or the other of these methods may be preferable, according to the purpose of the experiment. Both theoretical and experimental factors enter into the choice (e.g. accuracy of measurement and time necessary).

This abstract covers only some of the outstanding points, e.g. for type (1) experiments, the pulsed method is generally used. It takes advantage of the fact that often only the basic decay mode is measured. In this case, the neutron burst need not be an exact Dirac function. Even for a core assembly, the existence of a discrete fundamental mode is exceptional. Generally, there is a continuous spectrum of decay constants which, in certain cases, may present a very marked peak, so that a "pseudo-fundamental" mode can be defined. Even for type (1) experiments, modulation may be preferable to pulsation. This is true, for example, for the area method. Whereas this method is very difficult to apply by means of a pulsed technique, it should be possible to obtain the same result much more easily by single frequency modulation (some tens of cycles per second).

For type (2) experiments, modulation appears preferable because it is the natural extension of the classic exponential experiment, which is merely a zero frequency modulation, and because, like it, it produces an asymptotic mode, characteristic of the assembly, remote from the boundaries and sources. In this case also, a discrete asymptotic mode is not the most general one. In some cases, pulsation may be preferable for this type of experiment, if only because it gives the response to all frequencies in one operation.

ÉTUDE COMPARATIVE DE PLUSIEURS TYPES D'EXPÉRIENCES PULSÉES ET MODULÉES SUR DES MILIEUX MULTIPLICATEURS A NEUTRONS RAPIDES. Les auteurs distinguent deux types d'expériences cinétiques (pulsées ou modulées) selon la configuration de l'assemblage et la position de la source:

1. Assemblage critique ou légèrement sous-critique avec la source dans ou à proximité du cœur.

2. Massif très fortement sous-critique alimenté par une source sur une face, exactement comme une expérience exponentielle.

La loi de variation de la source en fonction du temps peut être dans les deux cas: a) Une fonction de Dirac ou une fonction qui s'en approche. Il s'agit alors d'une expérience pulsée. b) Une oscillation sinu-

soïdale ou tout au moins une fonction périodique dans laquelle la composante fondamentale est dominante. Il s'agit alors d'une expérience modulée. c) Une fonction aléatoire ou pseudo-aléatoire.

L'objet du mémoire est une étude comparative de ces divers types d'expériences sous leurs deux aspects: a) expériences intégrales fondamentales dont le but est une vérification, par comparaison des résultats théoriques et expérimentaux, des données de base ou des méthodes de calcul; b) expériences dont le but est la détermination de paramètres importants de réacteurs en projet ou existants (exemple: détermination de α-β/ℓ et de la réactivité par méthode pulsée classique, ou du laplacien-matière par une expérience exponentielle).

Le phénomène étant parfaitement linéaire, il est clair que la méthode modulée sur toute la gamme des fréquences, et la méthode pulsée, dont l'analyse spectrale contient toutes les fréquences, donnent en principe les mêmes informations. En pratique, l'une ou l'autre de ces méthodes est préférable selon le but de l'expérience. Les éléments entrant dans ce choix sont de nature théorique et expérimentale (par exemple: précision des mesures et temps nécessaires).

Seuls quelques points saillants sont mentionnés dans ce résumé. Pour les expériences de type 1, c'est la pulsation qui est généralement employée. Elle exploite le fait qu'on se limite souvent à la mesure du mode de décroissance fondamental. Dans ce cas, il n'est par nécessaire que la bouffée de neutrons soit exactement une fonction de Dirac. Il est à noter que même pour un milieu multiplicateur, l'existence d'un mode fondamental discret n'est qu'exceptionnel. En général, il y a un spectre continu de constantes de décroissance. Dans certains cas, ce spectre présente un pic très prononcé, ce qui permet de définir un mode «pseudo-fondamental».

Même pour les expériences du type 1, la modulation peut être preferable à la pulsation. C'est entre autres le cas pour la méthode des aires. Alors que cette dernière méthode est très difficile à mettre en œuvre par une technique de pulsation, la modulation à une seule fréquence (quelques dizaines de Hz) devrait donner le même résultat beaucoup plus facilement.

Pour les expériences du type 2, la modulation semble indiquée parce qu'elle est l'extension normale de l'expérience exponentielle classique, qui n'est autre qu'une modulation à fréquence nulle et que, comme elle, elle donne lieu à un mode asymptotique caractéristique du milieu, loin des frontières et des sources. Ici non plus, l'existence d'un mode asymptotique discret n'est pas la règle générale. Dans certains cas la pulsation peut être préférable pour ce type d'expériences, ne fût-ce que parce qu'elle donne en une fois la réponse à toutes les fréquences.

СРАВНИТЕЛЬНОЕ ИЗУЧЕНИЕ НЕСКОЛЬКИХ ТИПОВ ИМПУЛЬСНЫХ И МОДУЛИРУЕМЫХ ОПЫТОВ В РАЗМНОЖАЮЩИХ СРЕДАХ НА БЫСТРЫХ НЕЙТРОНАХ. Мы различаем два типа кинетических опытов (импульсные и модулируемые) в соответствии с конфигурацией сборки и расположением источника:

1) критическая или немного подкритическая сборка с источником в активной зоне или около нее;

2) очень сильный подкритический блок, питаемый источником с поверхности, точно так, как и в экспоненциальном опыте.

В том и другом случаях закон изменения мощности источника в функции времени может проявляться как: а) функция Дирака или приближающаяся к ней иная функция; В данном случае речь идет об импульсном опыте; б) синусоидальная осцилляция или по крайней мере периодическая функция, в которой основная компонента является доминирующей; в таком случае речь идет о модулируемом опыте; в) случайная или псевдослучайная функция.

Цель настоящего сообщения заключается в сравнительном изучении этих различных опытов в их двух аспектах:

а) Основные интегральные опыты, цель которых состоит в проверке, путем сравнения теоретических и экспериментальных результатов, основных данных и методов расчета.

б) Опыты, цель которых состоит в определении основных параметров проектируемых или существующих реакторов (например, определение α-β/ℓ и реактивности обычным импульсным методом или материального параметра с помощью экспоненциального опыта.

Поскольку это явление — полностью линейное, то ясно, что метод, модулируемый на всем диапазоне частот, и импульсный метод, спектральный анализ которого содержит все частоты, дают в принципе ту же информацию. На практике каждому из этих методов отдается предпочтение в зависимости от цели опыта. Входящие в этот отбор элементы носят теоретический и экспериментальный характер (например, уточнение необходимых измерений и времени).

В настоящей аннотации приводится лишь несколько характерных моментов. Для опытов типа 1) — это импульс, который обычно используется. Он основан на том обстоятельстве, что часто ограничиваются измерением основной гармоники. В данном случае нет необходи-

мости в том, чтобы нейтронный импульс точно являлся функцией Дирака. Отметим, что даже для размножающей среды наличие основной гармоники дискретного типа является исключением. В общем имеется постоянный спектр констант распада. В определенных случаях этот спектр дает ярко выраженный пик, что позволяет определить "псевдоосновной" тип. Даже в опытах типа 1) модуляции может быть отдано предпочтение перед импульсом. В числе прочих этот метод может использовать также и метод площадей. В то время, как его очень трудно использовать в случае метода пульсации, модуляция с единственной частотой (несколько десятков циклов в секунду) должна была бы дать тот же результат, но значительно более легким путем.

Для опытов типа 2) модуляция кажется предпочтительной, поскольку она является нормальным расширением обычного экспоненциального опыта, который, в свою очередь, является ничем иным, как нулевой частотной модуляцией, и поскольку данная модуляция, как и этот опыт, связана с асимптотическим методом, характеризующим среду в дали от границ и источников. К тому же наличие дискретного асимптотического метода не является общим правилом. В определенных случаях импульс может оказаться предпочтительным для данного типа опытов и не потому, что он дает одновременно ответ на все частоты.

ESTUDIO COMPARATIVO DE EXPERIMENTOS PULSADOS Y MODULADOS EN MEDIOS MULTIPLICADORES DE NEUTRONES RAPIDOS. Según la configuración del conjunto y la posición de la fuente, los autores distinguen dos tipos de experimentos cinéticos (pulsados o modulados):

1. Conjunto crítico o ligeramente subcrítico, con la fuente situada en el cuerpo o en su proximidad.

2. Conjunto muy subcrítico, con la fuente situada en una cara, exactamente como en un experimento exponencial.

En ambos casos, la ley de variación de la intensidad de la fuente en función del tiempo puede ser: a) una función de Dirac o una función análoga (experimento pulsado); b) una oscilación sinusoidal o, por lo menos, una función periódica en la que domina la componente fundamental (experimento modulado); c) una función aleatoria o pseudoaleatoria.

La finalidad de la presente memoria es proceder a una comparación de esos tipos de experimentos en sus dos aspectos: a) experimentos integrales de carácter fundamental destinados a comprobar, comparando los resultados teóricos con los experimentales, los datos básicos o los métodos de cálculo; b) experimentos para determinar los parámetros importantes de reactores en proyecto o en funcionamiento (por ejemplo, la determinación de $\alpha - \beta/\ell$ y de la reactividad por el método clásico de impulsos o del laplaciano-material por medio de un experimento exponencial).

Como el fenómeno es perfectamente lineal, es evidente que en principio se obtienen las mismas informaciones con el método de modulación en toda la gama de frecuencias y con el método de impulsos, cuyo análisis espectral contiene todas las frecuencias. En la práctica, la elección dependerá de la finalidad del experimento. Los elementos que intervienen en esta elección son de índole teórica y experimental (por ejemplo, *precisión de las mediciones* y *tiempo necesario para efectuarlas*).

A continuación se indican algunos aspectos más notables:

Para los experimentos del tipo 1, suele recurrirse al método de impulsos, que aprovecha el hecho de que a menudo sólo se mide el modo de decrecimiento fundamental. En este caso, no es imprescindible que el *impulso neutrónico se ajuste exactamente a una función* de Dirac. Cabe señalar que incluso para un medio multiplicador, la existencia de un modo fundamental discreto sólo constituye una excepción. En general, hay un espectro continuo de constantes de decrecimiento. En algunos casos, este espectro presenta un máximo muy pronunciado, lo que permite definir un modo « pseudofundamental ». Incluso para los experimentos del *tipo 1, la modulación puede ser más útil que el método de impulsos.* Por ejemplo, cuando se trata de la técnica de las áreas. Es muy difícil aplicar esta técnica por el método de impulsos, pero la modulación a una sola frecuencia (algunas decenas de Hz) debería dar el mismo resultado con mucha mayor facilidad.

Para los experimentos del tipo 2, la modulación parece indicada porque constituye la ampliación normal del experimento exponencial clásico, que *en esencia, sólo constituye una modulación de frecuencia nula* y que da igualmente lugar a un modo asintótico, característico del medio, lejos de los límites de separación y de la fuente. En este caso, la existencia de un modo asintótico discreto tampoco constituye la regla general. En ciertas ocasiones, la pulsación puede ser preferible para este tipo de experimentos, aunque sólo sea porque permite obtener en una sola operación la respuesta a todas las frecuencias.

1. INTRODUCTION

To compare the different kinds of experiments which could be performed on fast systems to assess their relative merits, a somewhat arbitrary classification of these experiments is adopted in this report. Two main types of experiments are distinguished according to the assembly configuration, the source position and the resulting mathematical treatment.

(a) Pulsed and modulated subcritical assemblies. In subcritical assemblies the source is located inside or near the core. Only bare systems are considered and the assumption is made that the flux goes to zero on the extrapolated boundary; each spatial mode is then treated separately.

(b) Pulsed and modulated exponential assemblies. The assemblies are driven by the source on one of their faces, as in a static exponential experiment, where time-dependent measurements are made as a function of position. In both cases the time variation of the source can be a delta function (pulsed experiments), a sine wave or a periodic function of time (modulated experiments), a constant (static experiments) or a random process (noise experiments).

Pulsed and modulated experiments for type (a) assemblies and modulated (wave) experiments for the type (b) assemblies are considered here. Experiments on both types of assemblies are used either as fundamental integral experiments or for the measurement of quantities of special interest (material buckling, decay constant for reactivity measurement, prompt neutron lifetime, etc.)

2. GENERAL PROPERTIES OF PULSED AND MODULATED EXPERIMENTS

The objectives and the main features of kinetic experiments are outlined first and are substantiated in further sections by numerical calculations.

These experiments are natural extensions of static ones, as the response of a pulsed experiment, when integrated over all times, yields the results of a static experiment, and the extrapolation to zero frequency of a modulated experiment yields these results as well. As pulsed and modulated experiments possess more parameters (e.g. frequency) and measured quantities (e.g. phase lag) than static ones, they potentially can yield more information even though the instrumentation has to be more elaborate. But even if one is interested only in the results of static experiments, it may be advisable to perform the corresponding kinetic experiment and to extrapolate the results to the static case. The reasons are that an extrapolation from a curve is more accurate than the measurement of only one point, and that in the kinetic experiment it is sometimes possible to eliminate or to analyse perturbing effects always present in the static experiment. An example is the problem of reflected neutrons in exponential experiments (see section 7).

Now let us examine additional information which can be obtained by kinetic experiments. In theory pulsed experiments (where the measurement is carried from $t = 0$ to $t = \infty$) and modulated experiments (over the whole

range of frequencies) contain the same information, since the latter can be obtained from the former by a Fourier analysis. In practice one or the other experiment is preferred according to what one wants to measure. The reasons for this choice are of a theoretical as well as of an experimental nature, e.g. accuracy of the measurements, time required, etc.; some of these reasons are as follows.

For the experiments on subcritical assemblies, pulsed experiments are usually performed, because one is mainly interested in the measurement of the fundamental decay mode. It is then not necessary that the burst of a neutron be a delta function. Let us note that even for a multiplying medium the existence of a discrete fundamental mode is exceptional. In general there is a continuous spectrum of decay modes; in some cases this spectrum exhibits a very sharp peak, so that it is possible to define a "quasi-fundamental" mode (see Refs. [2 and 5]).

Even in the case of experiments on subcritical assemblies, modulated experiments may be preferred to pulsed ones. This is among others the case for the area method (see Ref. [1] and section 6). While this method is rather difficult to perform in the pulsed version, a new version is presented here, which consists in a simultaneous modulation at zero frequency and at a few tens of cycles per second. This version should be much easier to apply.

For experiments on exponential assemblies, modulation seems to be well suited because it is the natural extension of the classical exponential experiment (for which the modulation frequency is zero) and because it has, just as the latter, an asymptotic mode characteristic of the medium, far from the source and the boundaries. Here too, the existence of a discrete asymptotic mode is not the general rule. In some cases, it might be more advisable to perform a pulsed experiment, if only because it gives the response to all frequencies in one measurement (see Ref. [11]). This last technique is however not discussed in this paper.

Another advantage of kinetic experiments over static ones is that the velocity v as such (i.e. besides the energy dependence of the cross-sections) has in the former a direct bearing on the neutron transport phenomena. Thus these experiments benefit from the same property which is exploited in time-of-flight spectroscopy. The sensitivity of such experiments to the velocity (a) affords a sensitive check of the spectrum and of the slowing-down processes and (b) allows a direct action on the spectrum. These two properties are illustrated by the following examples.

(1) Consider an exponential experiment on a hypothetical medium in which all cross-sections are independent of energy. In such a medium the material buckling is of course independent of slowing-down processes and its measurement cannot give any implicit information on these processes and on the spectrum. In a modulated exponential experiment one can measure, as is shown later, an analogous quantity $B^2(j\omega)$, which is of course sensitive to the slowing-down processes and to the spectrum, since the kinetic response of neutrons is dependent on their velocity v. Thus the measurement of $B^2(j\omega)$, preferably over a range of frequencies ω, does afford a check on the spectrum and on the slowing-down processes. In realistic media where the cross-sections do depend on energy, a similar reasoning is valid, since v varies more strongly with energy than do the cross-sections.

It is for a similar reason that in the fast critical experiments performed so far, a disagreement between the experimental and theoretical low energy tail of the spectrum has been deduced, not from (static) critical mass measurements, but from (kinetic) measurements of the lifetime, or from danger coefficient measurements of boron, which exhibits a 1/v cross-section.

(2) In a modulated experiment it is qualitatively obvious (and it is shown quantitatively in section 4) that both the phase lag and the attenuation of the neutron flux increase with decreasing energy and that the attenuation increases with increasing frequency. Thus an increase in ω hardens the spectrum by preferential attenuation of the low energy tail.

If one takes again a modulated exponential experiment as an example, one can expect that $dB^2(j\omega)/d\omega$ at low frequency is more sensitive to the low energy end of the spectrum, while at high frequency $B^2(j\omega)$ is more sensitive to the high energy end of the spectrum. This property of giving more weight to some part of the spectrum is a very useful characteristic of kinetic experiments.

Another example is given by the softening of the spectrum in pulsed experiments.

Thus we can say that a modulation exerts a filtering action on various kinds of neutrons. The cut-off frequency is of course inversely proportional to characteristic time constants, which are listed here in decreasing order: (a) time constants of delayed neutrons of the order of seconds, (b) time constants of reflected neutrons and (c) time constants of neutrons which stay in the assembly.

The last two types of time constants increase of course with decreasing energy. Generally, however, time constants of reflected neutrons are larger than, and well separated from, those of neutrons which stay in the assembly since (a) the flight paths are longer and (b) the energy can be made much lower by a proper choice of the reflecting surfaces.

Taking again the modulated exponential experiment as an example, let us look at $B^2(j\omega)$ as a function of frequency. At $\omega = 0$ (static experiment) $B^2(0) = B^2_m$, the material buckling. With increasing ω, $B^2(j\omega)$ takes on complex values but becomes a new real value B^2_m, p*, the prompt material buckling, when the frequency is about 10 c/s, where the delayed neutrons are filtered out. For higher frequencies, $B^2(j\omega)$ should hardly change over a few decades (see Fig. 13) if reflected neutrons are not taken into account. In practice however the reflected neutrons would gradually be filtered out and the measured value of $B^2(j\omega)$ would take on some complex values and tend to the $B^2(j\omega)$ of Fig. 13, which, if the reflected neutrons are filtered out at reasonably low frequency, should be very close to the real quantity B^2m, p. At still higher frequencies $B^2(j\omega)$ would become complex again, as indicated in Fig. 13.

3. METHODS OF CALCULATION

Based on the fact that in fast multiplying systems the neutrons gain energy only through fission and that the fission spectrum is with reasonable

* This measured value of B^2_m, p may be slighly different from the correct one because of the influence of the reflected neutrons.

approximation independent of the nuclide undergoing fission and of the energy of the incident neutron, a general theory has been developed which can be applied to pulsed, modulated and exponential fast experiments (see Refs. [2, 3 and 4]).

In this method properties of the medium are deduced from the behaviour of the function $k(p, B^2)$, the transfer function linking two successive generations of fissions in terms of p, the Laplace variable, and B, the three dimensional Fourier variable. This function is obtained from considering the "non-multiplying" medium, which is the multiplying one in which ν has been made equal to zero.

This method can be applied as well to continuous energy models and to multigroup models. The interpretation of pulsed experiments with a continuous model is given by CADILHAC et al. [5]. It sheds light on the meaning of decay constants found by multigroup calculations.

Within the framework of multigroup theory to which we limit ourselves in this paper, the method based on $k(p, B^2)$ is equivalent to the direct solution of the multigroup equations by matrix calculus. This is the classical way of treating pulsed, modulated or exponential fast experiments. But the use of $k(p, B^2)$ which takes advantage of the particular nature of the matrices involved, seems more advisable, because of its physical meaning and of the fact that, being derived for a non-multiplying medium, the contributions from the different energy groups can be calculated step by step. This makes possible an error evaluation which is much more difficult to make for the direct method. Both methods of solution are now summarized in the diffusion theory approximation and their common properties exhibited, with reference to pulsed and modulated subcritical experiments as an example. Delayed neutrons are always neglected.

3.1. Direct method

Let $\overline{\phi}$ be the flux vector with component ϕ_i in the *i-th energy group* ($i = 1..n$) and A be the matrix obtained after multiplication of the different multigroup equations by the corresponding velocity; multigroup equations for a given geometric buckling B^2 can be written as

$$(A - pI)\overline{\phi} = 0 \tag{1}$$

The decay constants are the eigenvalues $p = -\alpha_i$ of the matrix A; let $\overline{\varphi}_i$ be the corresponding eigenvectors.

If a pulse with spectrum $\overline{S}$ is injected into the medium, the neutron flux $\overline{\phi}(t)$ is given by

$$\overline{\phi}(t) = \sum_i s_i \, \overline{\varphi}_i \, e^{-\alpha_i t} \tag{2}$$

where the s_i's are the projections of $\overline{\nu S}$ on the eigenvectors $\overline{\varphi}_i$ $\overline{\nu S}$ being the vector with components $\nu_i \cdot S_i$.

For a modulated source $\overline{S}\, e^{j\omega t}$, the neutron flux becomes

$$\overline{\phi}(t) = e^{j\omega t} \sum_i \frac{s_i}{j\omega + \alpha_i} \overline{\varphi}_i = e^{j\omega t}\, \overline{\Phi}(\omega) \tag{3}$$

For a given value of ω, the numerical value of the vector coefficient of $e^{j\omega t}$ in Eq. (3) could also be found by direct inversion of the equation $(A - j\omega I)\overline{\phi} = \overline{\nu S}$ as $(A - pI)$ is not singular for p purely imaginary. This avoids the intermediate step of the determination of the eigenvalues and eigenvectors. This spectrum $\overline{\Phi}(\omega)$ can be considered as a new type of mode (not an eigenfunction), an ω-mode into which any kind of response can be expanded by Fourier analysis. Such an expansion in ω-modes is of course particularly well suited to periodic inputs, since the output can then be expressed as a discrete sum over ω-modes.

3.2. $k(p, B^2)$ method (see Refs. [2, 3, 4])

When a burst of spectrum $\overline{S}$ is injected in a given B^2 mode into the medium, the Laplace transform of the flux before first fission is denoted by $\overline{\varphi}_1(p, B^2)$ and the first fission source $s_1(p, B^2)$ is given by

$$s_1(p, B^2) = \langle \overline{\nu\sigma_f}, \overline{\varphi}_1(p, B^2) \rangle \tag{4}$$

For a burst with the fission spectrum, the notations are $\overline{\varphi}_f(p, B^2)$ and $k(p, B^2) = \langle \overline{\nu\sigma_f}, \overline{\varphi}_f(p, B^2) \rangle$; $k(0, B^2)$ is the effective prompt multiplication factor.

The total fission source $s(p, B^2)$ is expressed by

$$s(p, B^2) = s_1(p, B^2)/[1 - k(p, B^2)] \tag{5}$$

and the neutron flux $\overline{\varphi}(p, B^2)$ caused by a burst of spectrum $\overline{S}$ is

$$\overline{\varphi}(p, B^2) = \overline{\varphi}_1(p, B^2) + s(p, B^2)\overline{\varphi}_f(p, B^2) \tag{6}$$

As is indicated in Ref. [4], all expressions containing B^2 can be considered as three dimensional Fourier transforms of the corresponding point kernels in an infinite medium. In the following, the constant B^2 is dropped from the notations.

It was shown in the references that the following properties hold:

(a) The roots of $k(p) = 1$ are the eigenvalues $p = -\alpha_i$ of the matrix A.
(b) The corresponding eigenvectors are $\overline{\varphi}_f(p = -\alpha_i)$.
(c) The projections s_i of $\overline{\nu S}$ on the eigenvalues are the residues of $s_1(p)/[1 - k(p)]$.
(d) The location of the eigenvalues $-\alpha_i$ can be related to those of the non-multiplying medium (poles of $k(p)$), which are equal to $-(v\Sigma_{\text{removal}})_i$, where Σ_{removal} includes the leakage contribution $D_i B^2$.

When ν is increased from zero (non-multiplying medium) to its actual value, the roots of $k(p) = 1$ go from the poles of $k(p)$ to the eigenvalues $-\alpha_i$; if ν is further increased towards infinity, the roots will tend to the zeros of $k(p)$. Thus each eigenvalue $-\alpha_i$ can be related to a pole of $k(p)$, i.e. to an energy group.

It can be shown that for all, but the fundamental, eigenvectors, the components of the eigenvector present a maximum in the energy group to which this eigenvector is related.

(e) For a modulated source $\bar{S}\, e^{j\omega t}$, $\bar{\varphi}_f(j\omega)$, $k(j\omega)$, $s_1(j\omega)$ and $s(j\omega)$ can again be calculated directly for a given value of ω.

The total fission source is given by

$$s(j\omega) = s_1(j\omega)/[1 - k(j\omega)] \tag{7}$$

and the flux by

$$\bar{\varphi}(j\omega) = \bar{\varphi}_1(j\omega) + s(j\omega)\bar{\varphi}_f(j\omega) \tag{8}$$

It thus avoids the resolution of a linear system of n equations with n unknowns, which has to be solved when the first method is used (matrix inversion). It also avoids the preliminary determination of the eigenvalues and eigenvectors.

(f) $\bar{\varphi}_f(p, B^2)$ is the general formula giving the energy spectrum in an assembly characterized by the space transform variable B and the time transform variable p.

For example in a pulsed assembly with geometric buckling B^2, $\bar{\varphi}_f(-\alpha_1, B^2)$ is the asymptotic spectrum associated with the decay rate $e^{-\alpha_1 t}$; $\bar{\varphi}_f(j\omega, B^2)$ is the spectrum when the source is varying sinusoidally with pulsation ω.

In a modulated exponential experiment $\bar{\varphi}_f(j\omega, B^2_m(j\omega))$ is the asymptotic spectrum corresponding to the material buckling $B^2_m(j\omega)$, which is in this problem the fundamental eigenvalue.

These properties show that all the needed information can be deduced by the $k(p, B^2)$ method. All numerical evaluations have been done that way in multigroup diffusion theory.

4. PULSED AND MODULATED EXPERIMENTS ON SUBCRITICAL ASSEMBLIES

For a given geometric configuration the source spatial distribution is decomposed into the spatial eigenfunctions of the assembly, so that each spatial mode can be considered separately.

Numerical calculations always made with the Hansen Roach cross-sections set are reported for two different media. Calculations for pulsed and modulated experiments are given below. In the calculations the external source is in the highest energy group or has the fission spectrum. Similar problems are tackled with a continuous energy model in Ref. [5].

4.1. U^{235}-U^{238} medium (SUAK)

The compositions adopted are those of the first two experiments performed on SUAK at Karlsruhe. This information as well as the values of the geometric bucklings are by courtesy of BORGWALDT [6].

The SUAK atomic densities have been used as representative of a medium with rather hard spectrum but no attempt has been made to predict with high accuracy experimental results or to take care of the exact geometric configuration.

4.1.1. Pulsed experiments

The decay constants α_i have been calculated from the equation $k(p) = 1$ for the two geometric bucklings realized in the experiments. As the spectrum is hard (see Fig. 5) there are very few neutrons in the lower energy groups and the decay constants corresponding to these groups have been discarded as corresponding to pseudo-persistent modes [2]. To find out the relative importance of each mode, the residues A_i of $k(p)/[1 - k(p)]$ at the poles $-\alpha_i$ have been calculated; $k(p)/[1-k(p)]$ gives the response of a fission chamber with the composition of the medium when the burst has the fission spectrum; $k(0)/[1-k(0)]$ is the total response integrated over all times. (It is also what would be detected in a static source multiplication experiment.) A_i/α_i is

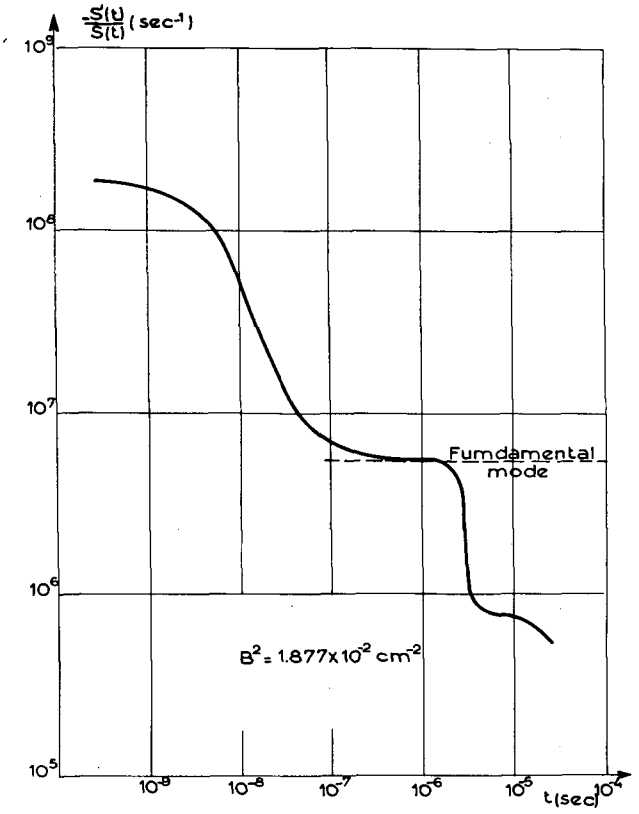


Fig. 1

SUAK
-S'(t)/S(t) versus time t

the response of the i-th mode integrated over all times; an index of the importance of each mode is the ratio A_i/α_i to $k(0)/[1-k(0)]$ expressed in per cent.

When the roots α_i (decay constants) are ordered by decreasing value, one usually observes that the importance of decay modes is negligible for decay constants smaller than a certain one (which will correspond to the fundamental mode). These smaller decay constants can then be discarded.

For $B^2 = 0.1877 \times 10^{-1}$ cm^{-2} the fundamental mode is the tenth root (importance: 42%) and corresponds to a decay $\alpha^{-1} = 187$ ns (experimental value: 220 ns); for $B^2 = 0.2431 \times 10^{-1}$ cm^{-2}, it is the seventh root (importance: 37.5%) and corresponds to $\alpha^{-1} = 119$ ns (experimental value: 120 to 130 ns). From the knowledge of the poles and the associated residues, the time behaviour can also be calculated. In Figs. 1 and 2 the logarithmic derivatives $-S'(t)/S(t)$ of the total fission source S(t) are given versus time. For $B^2 = 0.1877 \times 10^{-1}$ cm^{-2} the fundamental mode is predominant, hence $-S'/S$ tends to a constant after the fast transients have died out; the plateau around 0.75×10^6 s^{-1} corresponds to the fifteenth root, but the importance of this mode (less than 10^{-5}) is so small that it will never appear in the measurements. For $B^2 = 0.2431 \times 10^{-1}$ cm^{-2} the fundamental mode, $\alpha = 0.84 \times 10^7$ s^{-1}, is still

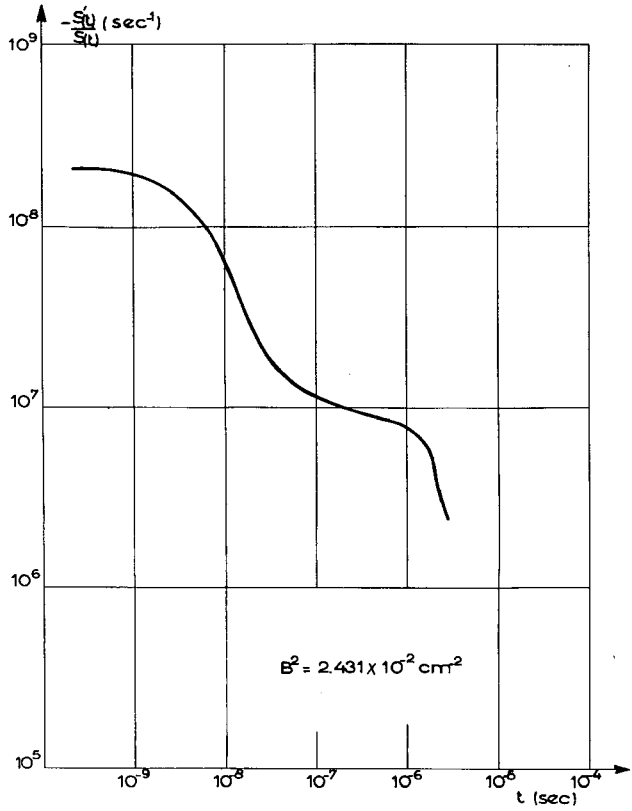


Fig. 2

SUAK

$-S'(t)/S(t)$ versus time t

dominant but the equilibrium is not reached. This illustrates very well the questions raised in [2] and analysed in [5] with the continuous energy model. It is clear that the fundamental eigenvalue is nothing but a peak in the continuous eigenvalue spectrum. The continuum on the left and right of this "eigenvalue" gives rise respectively to the transients which appear before and after the "fundamental" plateau of $-S'(t)/S(t)$. Note that if all neutrons below a certain energy were a priori neglected in the calculation, the calculated fundamental eigenvalue would effectively become discrete, with a continuum only on its left. This shows that the distinction between a discrete eigenvalue and a sharp peak in the continuous distribution is somewhat academic. For larger bucklings, there is no "fundamental" mode any more, as can be seen in Fig. 3. The decay α versus B^2 is plotted in Fig. 4,

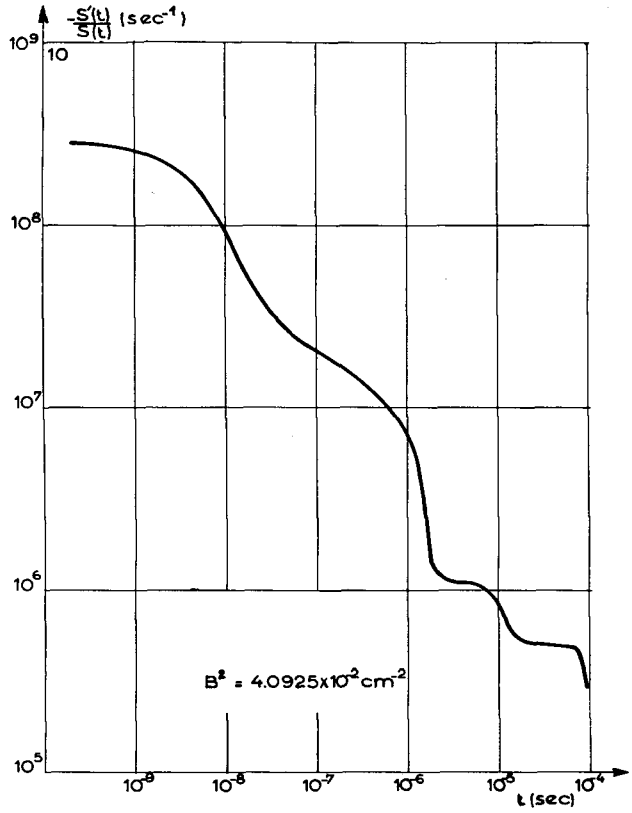


Fig. 3

SUAK

$-S'(t)/S(t)$ versus time t

and the "fundamental" spectrum for $B^2 = 0.1877 \times 10^{-1}$ cm^{-2} in Fig. 5 (pulsed curve). As was mentioned in section 2, the spectrum is markedly softened in a pulsed experiment.

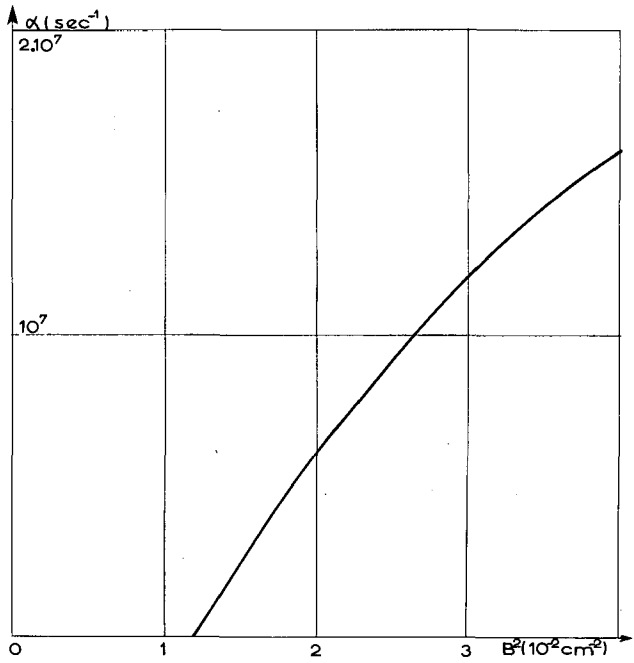


Fig. 4

SUAK

$U^{235} - U^{238}$

α versus B^2

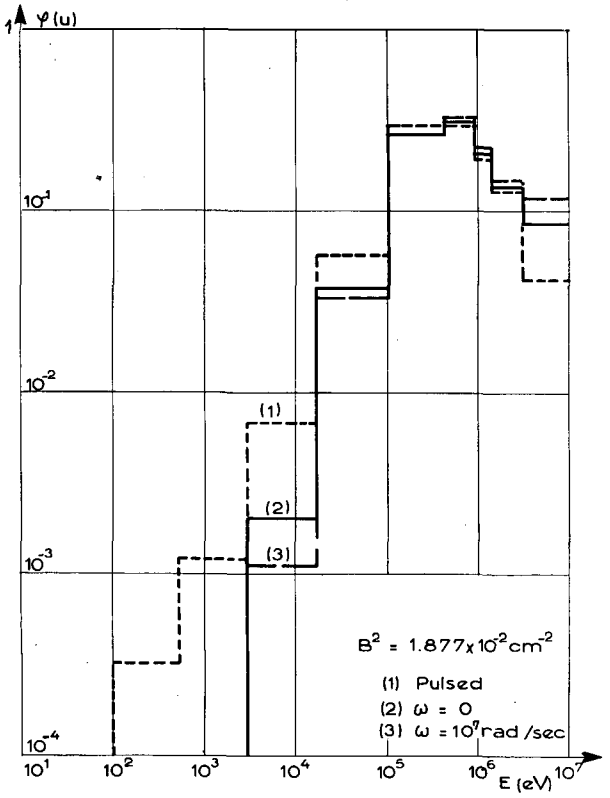


Fig. 5

SUAK spectra per unit of lethargy u

4.1.2. Modulated experiments

k(jω), s(jω) and the flux have been evaluated as a function of frequency in the range $\omega = 10^5$ to 3×10^7 rad/s. Frequencies of interest will be in the range of the α_i's, the decay constants of the pulsed experiments, i.e. between about 10^6 and 10^8 rad/s for the two geometries considered.

For $B^2 = 0.1877 \times 10^{-1}$ cm^{-2} the spectrum is drawn in Fig. 5 for $\omega = 0$ and $\omega = 10^7$ rad/s. The effect of increasing frequency is not negligible, even in this case where the static (at $\omega = 0$) spectrum is already hard. It is an illustration of properties forecast in section 2. In Fig. 6, the modulus and

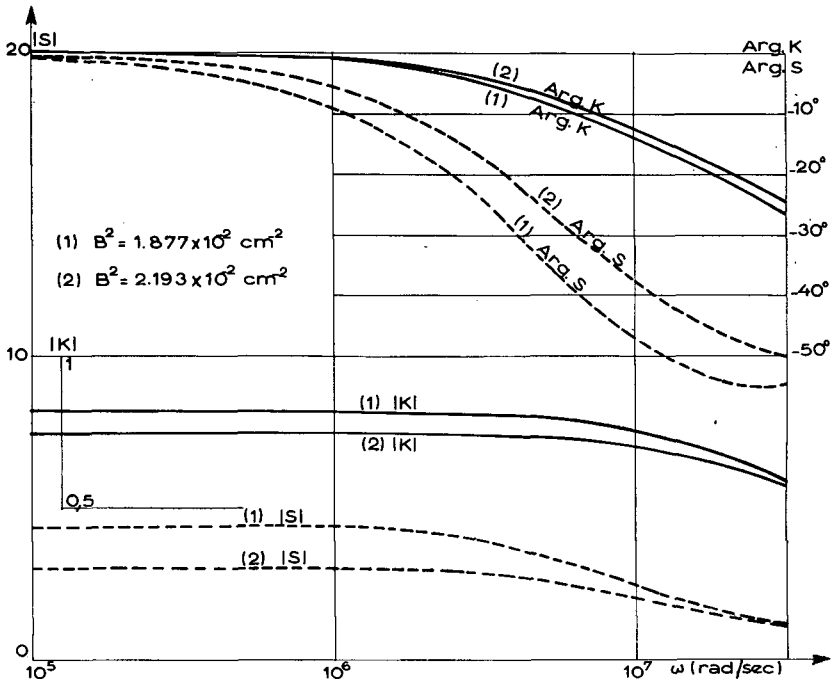


Fig. 6

SUAK modulus and phase of k(jω) and s(jω) versus frequency

the phase of k(jω) and s(jω) = k(jω)/[1 - k(jω)] are given; the phase of s(jω) is around 20° at $\omega = 3 \times 10^6$ rad/s and is sensitive to the subcriticality of the assembly. Note that s(jω) is nothing but the conventional transfer function, without the delayed neutron low frequency tail, but with energy dependence taken into account.

The slope of s(jω) at the origin is $-k'(0)/k(0) \cdot k(0)/[1 - k(0)]^2$ in which the first factor is the prompt neutron lifetime τ_1. The prompt lifetime can thus be determined from the slope of s(jω) if $k_{eff} = k(0)$ is known with sufficient accuracy. From the curve corresponding to $B^2 = 0.1877 \times 10^{-1}$ cm^{-2} and with the calculated value of k(0) one finds $\tau_1 = 2.65 \times 10^{-8}$ s^{-1}, the slope being evaluated between $\omega = 0$ and $\omega = 10^6$ rad/s.

The interpretation of pulsed and modulated multigroup results can be done with a continuous model so that k_{eff}, the first and the second time moments of k(t) are the same in both models [5]. Results from the continuous model will then be similar to those obtained by multigroup calculations, as long as the frequency remains small with respect to the prompt neutron lifetime, which is the case considered here.

4.2. Medium size, fast oxide reactor (MSFOR)

This medium is typical of a fast oxide reactor of about 800-l core. The calculations were made using Hansen Roach 16-group cross-sections.

4.2.1. Pulsed experiments

The analysis of the decay constants α_i, roots of k(p) = 1, has been made for different geometric bucklings as already explained for SUAK. In Fig. 7 the logarithmic derivative -S'(t)/S(t) is drawn for an assembly of k_{eff} = 0.975

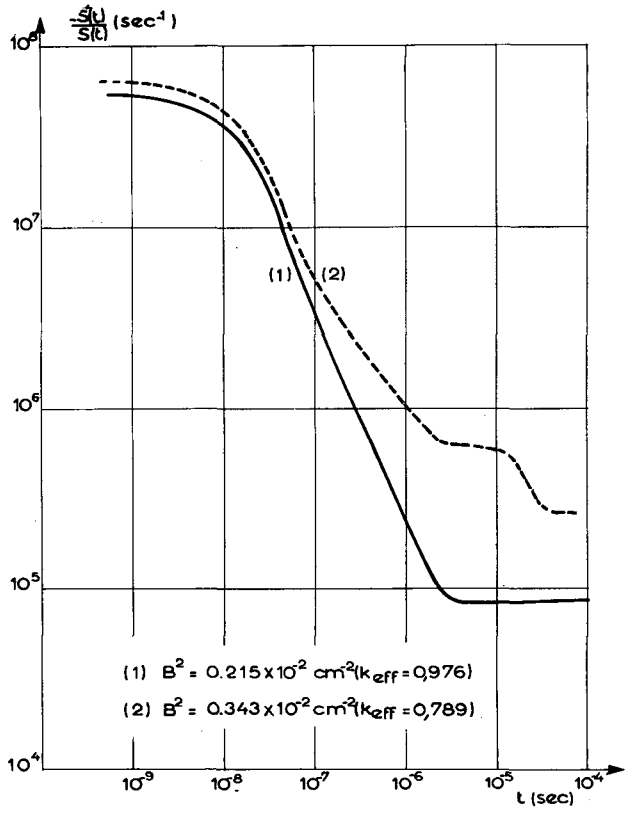


Fig. 7

MSFOR

-S'(t)/S(t) versus time t

($B^2 = 0.215 \times 10^{-2}$ cm^{-2}). There exists a fundamental mode at $\alpha = 0.85 \times 10^5$ s^{-1} (two pseudo-modes have been discarded), and its contribution $A_i k(0)/\alpha_i [1-k(0)]$ is equal to 95.5%.

For a larger buckling ($k_{eff} = 0.789$) there is still a fundamental mode at $\alpha = 6.2 \times 10^5$ (Fig. 7) with a relative importance of 42%. At larger bucklings, for example $B^2 = 0.86 \times 10^{-2}$ cm^{-2} which is a higher spatial harmonics of the first buckling considered, k_{eff} is only 0.344 and it is seen from Fig. 8 that a

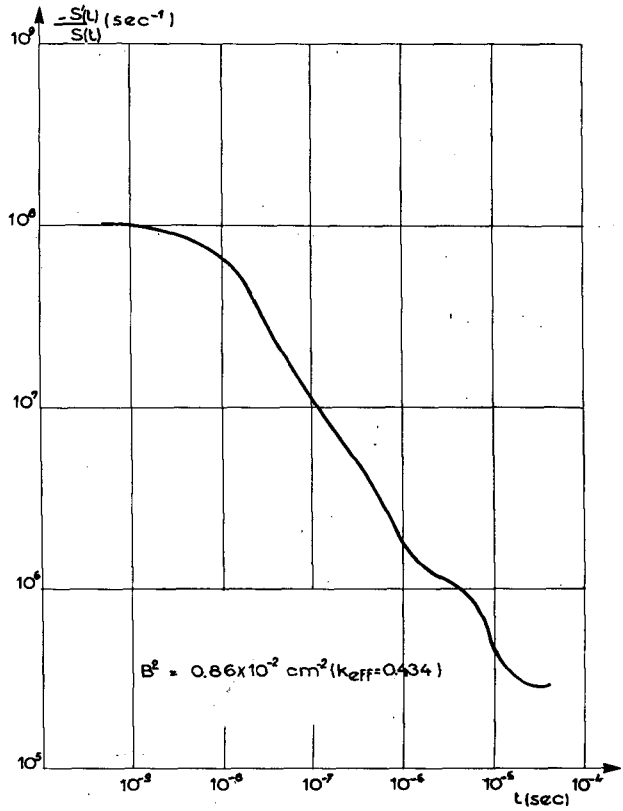


Fig. 8

MSFOR
-S'(t)/S(t) versus time t

fundamental mode does not exist any more. The slight plateau-like behaviour of -S'(t)/S(t) around 10^6 s^{-1} corresponds to only 1% of the neutrons. The fundamental spectrum for $B^2 = 0.2313 \times 10^{-2}$ cm^{-2} ($k_{eff} = 0.948$) is shown in Fig. 9.

4.2.2. Modulated experiments

The spectrum for $\omega = 0$ and $\omega = 10^7$ rad/s is given in Fig. 9 and shows a large hardening with ω. The modulus and phase of $k(j\omega)$ and of $s(j\omega)$ have been drawn in Figs. 10 and 11 as functions of frequency for three different subcriticalities. As could be deduced from the pulsed decay constants, fre-

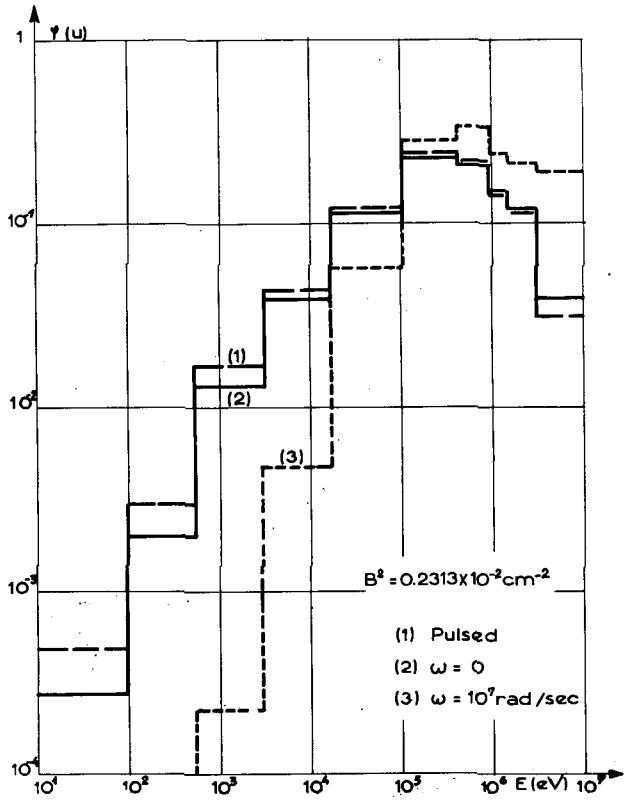


Fig. 9

MSFOR spectra per unit of lethargy u

quencies of interest are much lower than for SUAK. Noticeable phase shifts occur already at $\omega = 10^5$ rad/s and the response $s(j\omega)$ is very sensitive to the subcriticality.

The prompt lifetimes obtained from the slopes of $s(j\omega)$ are the following:

$k_{eff} = 0.976 \quad \tau_1 = 270$ ns
$k_{eff} = 0.948 \quad \tau_1 = 261$ ns
$k_{eff} = 0.789 \quad \tau_1 = 209$ ns

The phases of the fluxes in different energy groups are given in Fig. 12. It shows, as mentioned in section 2, that the lower the energy group, the larger the phase lag of the flux.

5. PULSED AND MODULATED EXPERIMENTS ON EXPONENTIAL ASSEMBLIES

The classical exponential experiment and the modulated exponential are examples of experiments of this type. The modulation technique was first

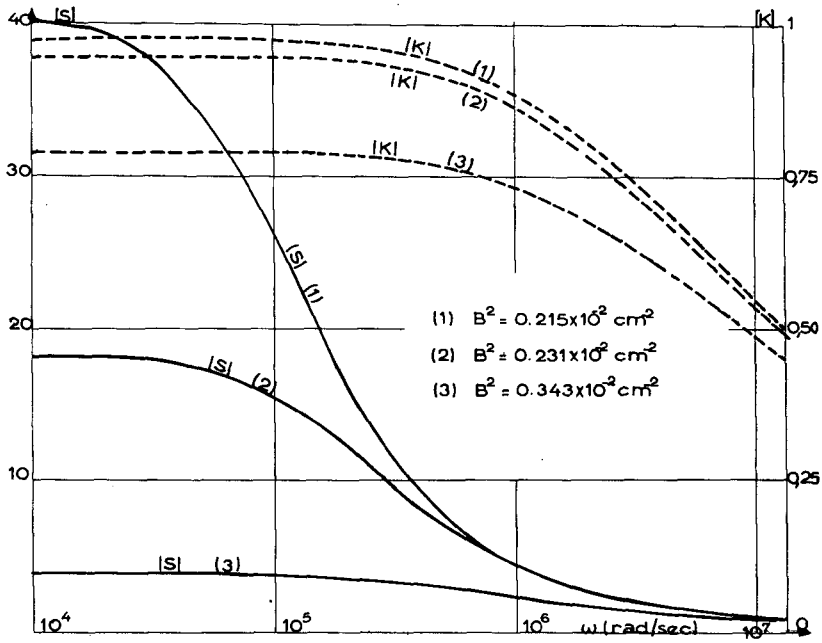


Fig. 10

MSFOR modulus of k(jω) and s(jω) versus frequency

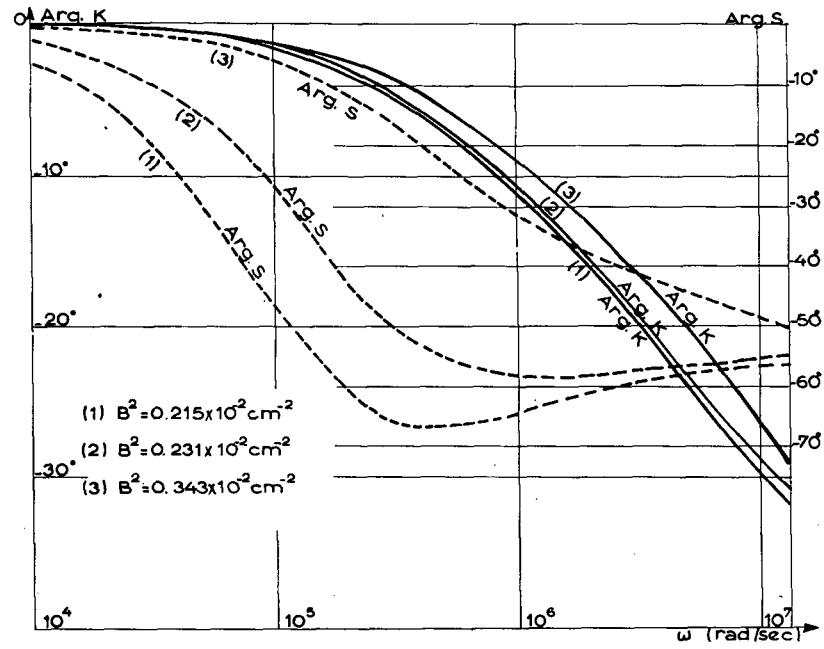


Fig. 11

MSFOR phase of k(jω) and s(jω) versus frequency

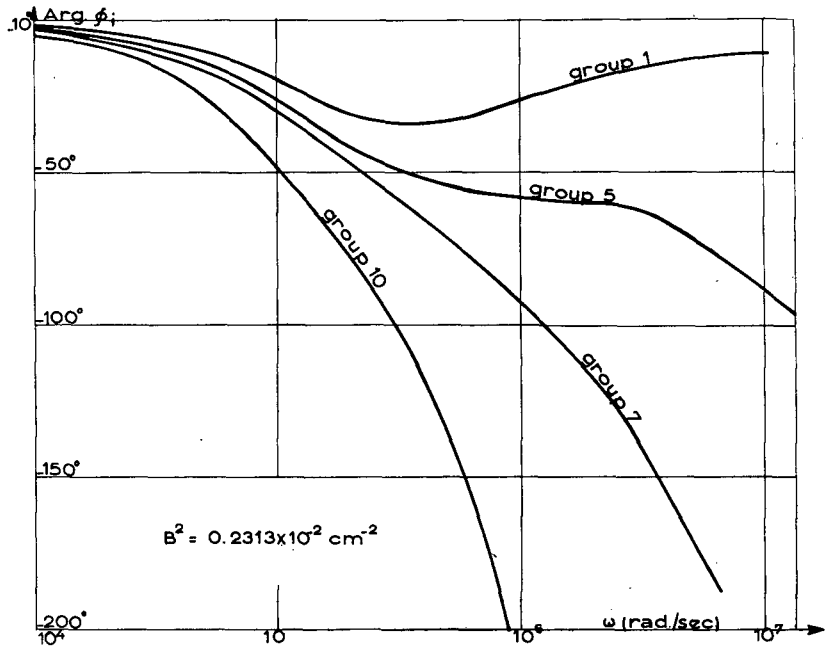


Fig. 12

MSFOR phases of flux versus ω

applied in [12] and the principle of the modulated exponential appears in [7], where the one-velocity approximation is treated.

It gives the material bucklings $B_m^2(\omega)$ as a function of ω.

$$B_m^2(j\omega) = \frac{\nu\Sigma_f - \Sigma_\alpha}{D} - \frac{j\omega}{vD} = B_m^2(0) - \frac{j\omega}{D_0} \tag{9}$$

which shows that in this model the real part of the buckling is independent of frequency and that the imaginary part is linear with frequency. The same holds in multigroup theory when vD is independent of energy, as can be seen by direct consideration of the diffusion equations. In this case $B_m^2(j\omega)$ is the largest eigenvalue of the diffusion matrix, or equivalently the largest root of $k(j\omega, B^2) = 1$.

When vD is not constant, the real and imaginary parts of $B_m^2(j\omega)$ depart from straight lines; as $\mathrm{Re}\, B_m^2(j\omega)$ is an even function of ω and $\mathrm{Im}\, B_m^2(j\omega)$ an odd function of ω, the slope of $B_m^2(j\omega)$ at the origin will be due to the imaginary part, and results from some sort of averaging of vD over the energy (analytic expressions can be obtained for few-groups models).

For a given transverse buckling B_t^2, the buckling B_z^2 in the direction of propagation is

$$B_z^2 = B_m^2(j\omega) - B_t^2 = (\alpha + j\xi)^2 \tag{10}$$

and the flux is then given by

$$\phi(E, z, t) = \varphi(E, \omega)\, e^{-\xi z}\, e^{j(\omega t + \alpha z)} \qquad (11)$$

where $\varphi(E, \omega)$ is the eigenfunction associated to $B_m^2(j\omega)$.

The relaxation length $L = 1/\xi$, the wavelength $\lambda = 2\pi/\alpha$ and the wave velocity $w = \omega/\alpha$ can be calculated as functions of the frequency, for the fundamental energy mode $B_m^2(j\omega)$ and for different transverse bucklings.

From the measurement of the flux at different z-positions and for different frequencies, the values $\alpha(\omega)$ and $\xi(\omega)$ can be evaluated, hence the material buckling $B_m^2(j\omega)$ for the B_t^2 considered.

Numerical evaluations made with the 16-groups Hansen Roach set are indicated. It was checked that in all the cases considered, the second energy mode is far beyond the fundamental one (material buckling) and can be discarded in the entire frequency range.

5.1. Composition similar to first SUAK assemblies

The variation of $B_m^2(j\omega)$ with frequency is given in Fig. 13; it is seen that in the range of frequencies considered, $B_m^2(j\omega)$ behaves as in one-group theory; the slope of Im $B_m^2(j\omega)$ corresponds to an average value $\langle vD \rangle = 0.965 \times 10^9$ cm²/s,

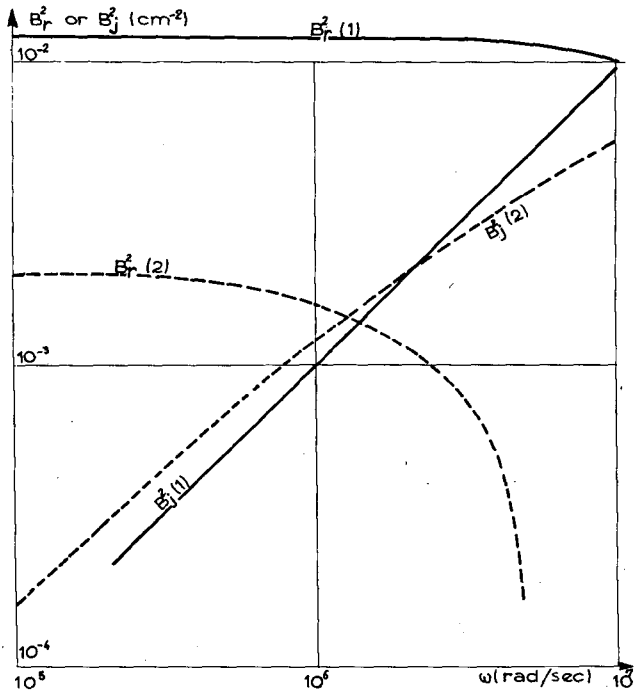


Fig. 13

Material buckling for SUAK (1) and MSFOR (2)

$B_m^2(\omega) = B_r^2 - jB_j^2$

which is a value near those obtained in groups 4 and 5 of the Hansen Roach set, where the asymptotic spectrum has its maximum (Fig. 14). In Fig. 14, the asymptotic spectrum is drawn for $\omega = 0$ and $\omega = 10^7$ rad/s; the hardening

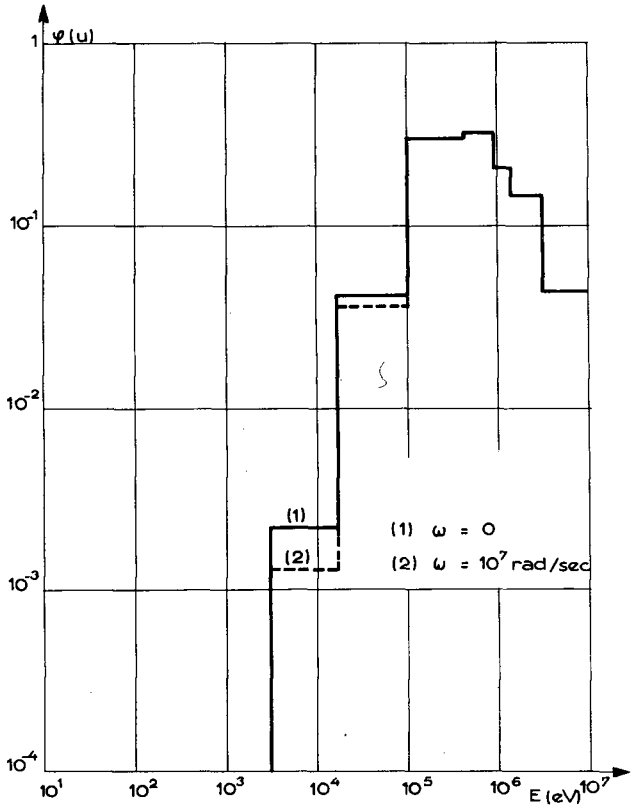


Fig. 14

SUAK asymptotic spectrum

of the spectrum is not very important, as SUAK already has a rather hard spectrum at $\omega = 0$.

The wave length and the relaxation length (Fig. 15) and the wave velocity (Fig. 16) are shown for two transverse bucklings. The indicated value of k_{eff} is that of an assembly infinite in the propagation direction and with transverse dimensions corresponding to the B_t^2 considered. These figures show that measurements of wave lengths can be performed (at $\omega = 10^6$ rad/s, λ varies between 4 and 10 m for the two curves drawn) at frequencies where the relaxation length is still reasonably large.

5.2. *Medium size, fast oxide reactor*

The comparison of $B_m^2(j\omega)$ in Fig. 13 for the former medium and for this one indicates a much more important variation of $B_m^2(j\omega)$ with frequency for

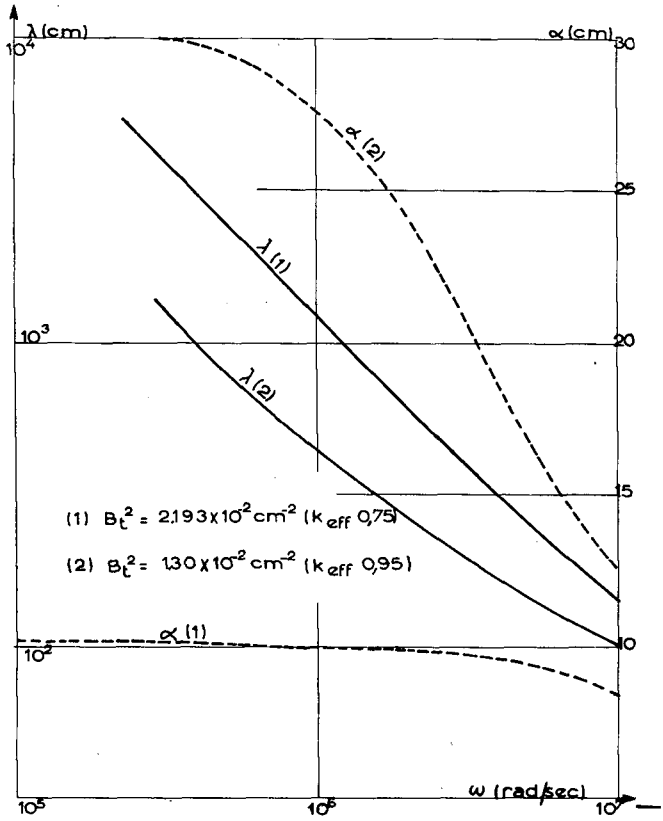


Fig. 15

SUAK wave length λ and relaxation length α

this medium. This is to be related to the softer spectrum. The evolution of the asymptotic spectrum with frequency is given in Fig. 17.

Figure 18 shows the wave length and the relaxation length and Fig. 16 the wave velocity versus frequency. To get already important phase shifts, lower frequencies than in the previous example can be chosen.

5.3. Influence of cross-section variations

It has been suggested in section 2 that $B_m^2(j\omega)$ should be rather sensitive to transfer cross-section variations, while $B_m^2(0)$ should not. Calculations have been made in which the elastic transfer cross-sections have been multiplied by a given factor, all the other cross-sections (including inelastic transfers) remaining constant. For the SUAK composition, when σ_{er} is multiplied by three, $B_m^2(0)$ increases by less than 1%, and for ω in the range 10^5 to 10^7 rad/s, the variation of $B_m^2(j\omega)$ caused by the change of σ_{er} is about 10%. Such a small effect can be explained by the hard spectrum of this medium and by the fact that σ_{er} is zero for this medium in the first four energy groups for the Hansen Roach set.

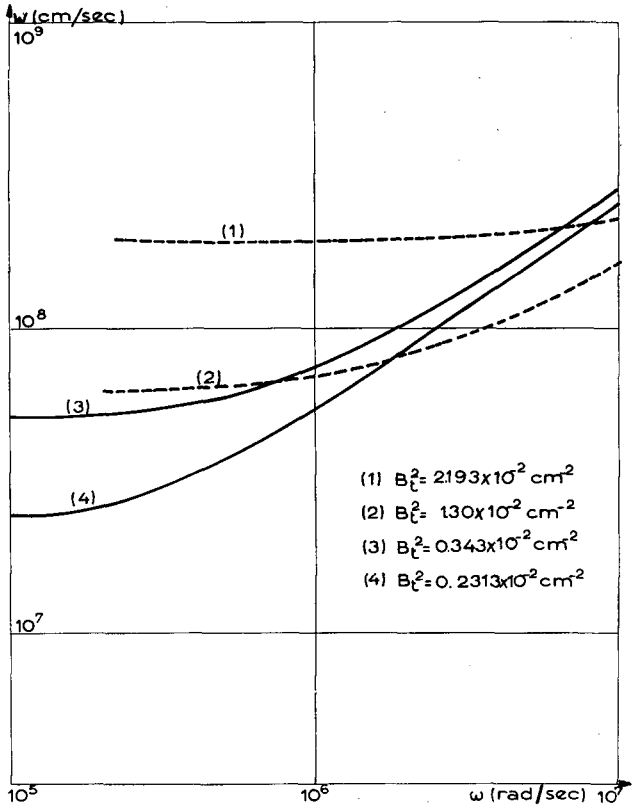


Fig. 16

Wave velocity w for
SUAK (1) and (2) and MSFOR (3) and (4)

For the medium size, fast oxide reactor, $B_m^2(0)$ is increased by 2% when σ_{er} is multiplied by two. As suggested, the effect at $\omega = 0$ is small. When the frequency is increased, both the real part and the imaginary part of $B_m^2(j\omega)$ show large variations when σ_{er} is varied by a factor of two. Then the wave length and the relaxation length in a modulated exponential experiment will change accordingly. This behaviour is shown in Fig. 19; the wave length changes by more than 50% at $\omega = 3 \times 10^5$ rad/s and the attenuation length by 20% at $\omega = 10^6$ rad/s.

5.4. *Existence of a discrete material buckling $B^2(j\omega)$*

Just as in the case of pulsed experiments where the existence of a discrete eigenvalue (decay constant) is not certain, the existence of a discrete material buckling $B^2(j\omega)$ is not a priori obvious, even in the static case. If it does exist in the static case, it may cease to exist above a certain critical frequency.

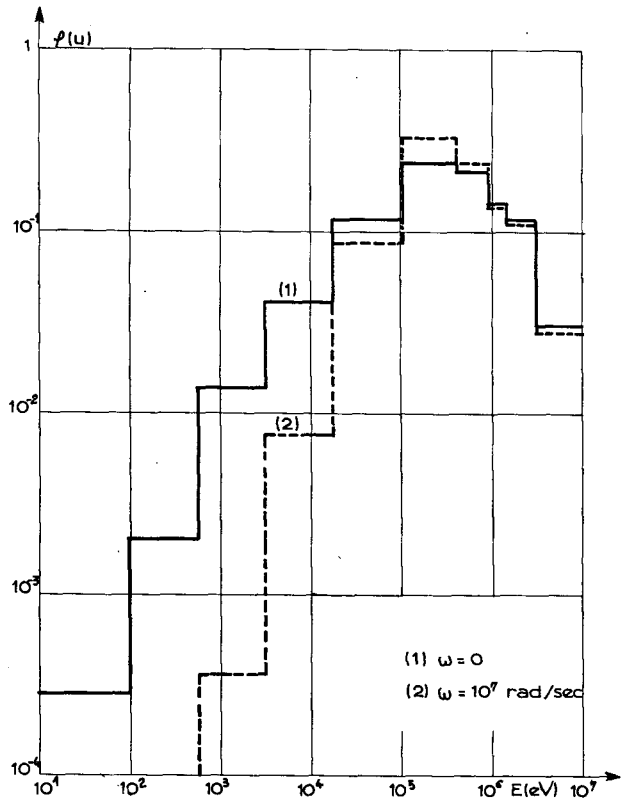


Fig. 17

MSFOR asymptotic spectrum

In the examples shown, the material buckling certainly has a well-defined discrete value, since its real part is positive while that of the transient bucklings should be negative.

The existence of a discrete material buckling is no longer obvious for media with $k_\infty < 1$, i.e. with a negative material buckling. For media with a very low value of k_∞, it is likely that no material buckling can be defined.

6. AREA METHOD

This method, proposed by SJÖSTRAND [1], in which the reactivity of a pulsed assembly is determined by comparing areas under the prompt neutron response and the delayed neutron response, is, in the proposed classification, an experiment of the subcritical assembly and is really a modulated experiment rather than a pulsed one, since it must be repetitive to attain the equilibrium state for the delayed neutrons.

It consists essentially of a modulated experiment in which the responses of the assembly to two frequencies are simultaneously measured. The first

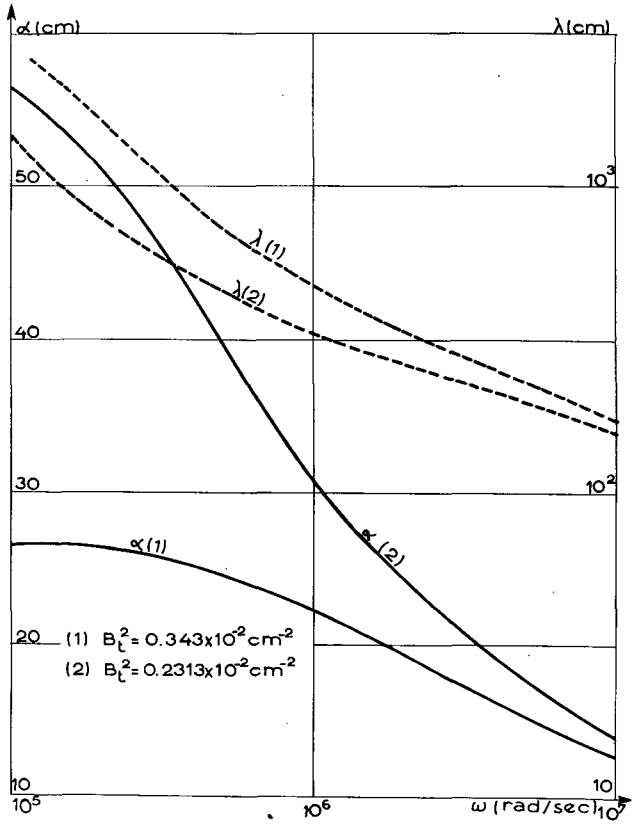


Fig. 18

MSFOR wave length λ and relaxation length α

frequency is zero, while the second is at the same time high enough for a complete attenuation of the delayed neutrons and low enough for the prompt neutrons to respond in a quasi-static manner. The area method is well adapted to fast systems, since the frequency criteria set above are satisfied over the wide plateau of the transfer function.

As suggested by Sjöstrand, the area method is as follows: short pulses are injected periodically (period chosen as indicated above). The source between pulses is zero, during a time large compared to the prompt neutron decay constant.

In this way the anti-reactivity in dollars is given by the ratio of the prompt and delayed areas A_1 and A_2 [1].

$$\rho/\beta = A_1/A_2.$$

No other information is required on the source, except that it be zero between the pulses. It is however often difficult to measure the prompt area, since the precise measurement of the prompt curve requires a very high resolution (of the nanosecond order for fast systems).

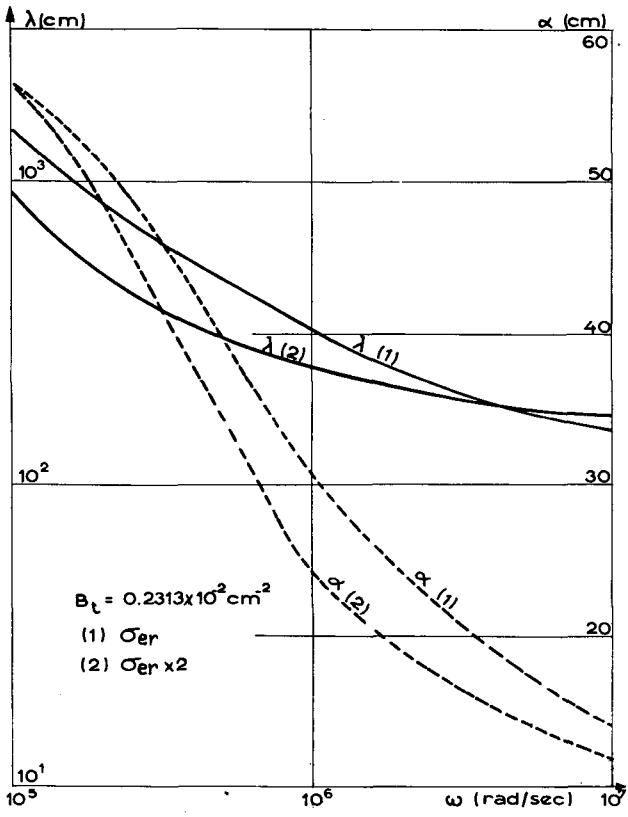


Fig. 19

MSFOR wave length λ and relaxation length α

A second version of the area method is given here. One has simultaneously a static and a modulated source

$$S(t) = A + B e^{j\omega t} \qquad \text{with } B < A.$$

If the detector is a fission detector, (same isotopic composition as the medium), the response is given by

$$R(t) \sim A \frac{S_1}{1-k} + B \frac{S_1(1-\beta)}{1-k(1-\beta)} e^{j\omega t} = C + D e^{j\omega t}$$

where S_1, as in section 3, stands for the first generation fissions. It is easy to see that

$$\frac{\beta}{\rho} = \frac{CB(1-\beta)}{AD} - 1 \simeq \frac{CB}{AD} - 1.$$

In this version of the method one has to measure the static component A and

the modulated amplitude B of the source, but the source intensity never has to be zero. It should be much easier to determine C and D in this version (eventually by a Fourier analysis) than to measure the areas in the first version. Indeed, since the frequency can be as low as 10c/s, only a very poor resolution (of millisecond order, even for fast systems) is adequate.

7. REFLECTED NEUTRONS

Modulated experiments should reduce the perturbing effect of reflected neutrons, which are obnoxious in static experiments. In classical exponential experiments, reflected neutrons are probably responsible for the large discrepancies between the fission ratios of U^{235} to U^{238} measured by different laboratories [9, 10]. Even for an outdoor assembly, the effect of ground-reflected neutrons was found important and special corrections had to be made [10]. Some simple qualitative considerations will show how modulation can help. Even in the hypothetical case that monoenergetic neutrons are emitted from a point source and are reflected directly with negligible energy loss, there would be a time spread caused by the differences of flight paths of the neutrons. Consider, for example, the ideal case of a point source situated at distance l over a reflecting plane and emitting isotropically neutrons of velocity v_0. Suppose that the neutrons after collision return to the source (180° collision) with the same velocity. The time distribution p(t) of the returning neutrons is given by

$$p(t) = \begin{cases} 0 & \text{for} \quad t < \dfrac{2l}{v_0} \\ \dfrac{1}{\pi} \dfrac{1}{t\sqrt{v_0^2 t^2/4 - l^2}} & \text{for} \quad t > \dfrac{2l}{v_0} \end{cases}$$

If the neutrons are not monoenergetic, there will be a further time spread caused by the differences of velocities. It would only be for a point source at the centre of a sphere that no time spread would take place for monoenergetic neutrons. If the source is modulated, the time spread will introduce an amplitude reduction of the reflected neutrons, as these come back with different phase shifts.

This reasoning has assumed that no moderation of the neutrons occurred. Experimental results [8] show that in a room almost all reflected neutrons are slowed down. It is then such slowed-down neutrons which must be eliminated by modulation, and this can be done at rather low frequencies. For example, time delays for neutrons of different energies to travel 2 m round trip are given in Table I.

If this phenomenon is approximated by a time variation with one time-constant, the latter should be of the same order of magnitude as the time delay; for example the time constant for neutrons of 10 keV will be around 1.5 μs, and the cut-off frequency is then $\omega = 6 \times 10^5$ rad/s.

A reason why the epithermal flux is, as observed experimentally, approximately uniform in space, could be that these neutrons suffered many collisions and travel back and forth many times, so that the time delay will

TABLE I

TIME DELAYS FOR NEUTRONS OF DIFFERENT ENERGIES

E	1 MeV	10 keV	100 eV
$\Delta t(\mu s)$	0.147	1.47	14.7

be much larger than the one indicated. Elimination of reflected neutrons by modulation would then occur at even lower frequencies than the cut-off frequencies indicated above. These qualitative estimates should be ascertained experimentally.

8. CONCLUSIONS

The different types of experiments considered in this paper will be performed with the experimental facilities available at Cadarache. A preliminary experiment will consist in the investigation of reflected neutron reduction by modulation, which can be performed with a modulated electrostatic accelerator.

The proposed version of the area method will be tried experimentally to check that its realization does not run into difficulties. Pulsed and modulated experiments of the subcritical assembly and modulated exponential experiments will also be performed, the latter with the eventual use of the fast source reactor Harmonie as an amplifier. In the case of exponential assemblies the effects of a modulated source will be investigated experimentally, particularly with reference to the possibility of reducing reflected neutron background.

Further theoretical work should be devoted to the existence of discrete modes in the static and modulated exponential experiments, and in the latter case it would be necessary to find out if there exists for a given fast medium a critical frequency above which no discrete mode exists any more. Theoretical methods used should be completed, to take into account the finite geometry of the system and the effect of going from diffusion theory to transport theory should be investigated.

REFERENCES

[1] SJÖSTRAND, N. G., Measurements on a subcritical reactor using a pulsed neutron source, Ark. Fys. 11 3 (1956).

[2] STORRER, F. and STIÉVENART, M., Contribution to the theory of the pulsed neutrons technique applied to fast multiplying systems (Paper presented at the Reactor Physics Symposium of the European Nuclear Society, Karlsruhe, April 1963) Rpt EUR/C/593 e.

[3] STORRER, F., GOVAERTS, P., EBERSOLDT, F. and STIÉVENART, M., "Contribution to the theory of exponential experiments with fast neutrons," Exponential and Critical Experiments I IAEA, Vienna (1964) 197-225.

[4] STORRER, F., GOVAERTS, P., EBERSOLDT, F. and HAMMER, P., A method for calculating the flux evolution in a fast neutron multiplying medium as a function of time, space and energy, ANS Mtg San Francisco, Nov. 1964.

[5] CADILHAC, M., GOVAERTS, P., HAMMER, P., MOORE, M., NICOLAENKO, B. and STORRER, F., "Contribution to the theory of pulsed and modulated experiments on fast neutron multiplying media," these Proceedings II.

[6] BORGWALDT, H., private communication.

[7] WEINGBERG, A. M. and WIGNER, E. P., The Physical Theory of Neutron Chain Reactors. University of Chicago Press, Chic. Ill. (1958) 436-38.

[8] OTSTAVNOV, P. S., Fluxes of fast and slowed-down neutrons in rooms, (translation), Soviet atom. Energy 16 2 (Feb. 1964).

[9] The fast exponential experiment, Rpt ANL 5379.

[10] CHEZEM, C. G., A uranium metal exponential experiment, Nucl. Sci. Engng 8 (1960) 652-59.

[11] UHRIG, R. E., "The impulse response of an exponential assembly", Exponential and Critical Experiments III IAEA, Vienna (1964) 205-39.

[12] RAIEVSKI, V. and HOROWITZ, J., Compt. Rend. 238 (1954) 1993.

MEASUREMENTS OF THE PROMPT NEUTRON DECAY CONSTANT OF THE VERA REACTOR USING THE PULSED SOURCE METHOD

J. W. WEALE, W. J. PATERSON, H. GOODFELLOW
AND M. H. McTAGGART
ATOMIC WEAPONS RESEARCH ESTABLISHMENT,
ALDERMASTON, UNITED KINGDOM

Abstract — Résumé — Аннотация — Resumen

MEASUREMENTS OF THE PROMPT NEUTRON DECAY CONSTANT OF THE VERA REACTOR USING THE PULSED SOURCE METHOD. The prompt neutron decay constant has been measured by the pulsed source method for a number of uranium-and plutonium-fuelled fast reactor assemblies. The results are discussed and are compared with values obtained on the same systems using the Rossi-α method.

MESURES DE LA CONSTANTE DE DÉCROISSANCE POUR LES NEUTRONS INSTANTANÉS DANS LE RÉACTEUR VERA, PAR LA MÉTHODE DES SOURCES PULSÉES. Les auteurs ont mesuré la constante de décroissance pour les neutrons instantanés par la méthode des sources pulsées dans plusieurs assemblages à neutrons rapides à l'uranium et au plutonium. Ils discutent les résultats de cette méthode et les comparent aux valeurs qu'on obtient pour les mêmes systèmes en utilisant la méthode α de Rossi.

ИЗМЕРЕНИЯ ПОСТОЯННОЙ РАСПАДА МГНОВЕННЫХ НЕЙТРОНОВ НА РЕАКТОРЕ "ВЕРА" МЕТОДОМ ИСТОЧНИКА ИМПУЛЬСНЫХ НЕЙТРОНОВ. Постоянная распада мгновенных нейтронов измерялась методом источника импульсных нейтронов для ряда реакторных сборок на быстрых нейтронах с топливом в виде урана и плутония. Обсуждаются результаты, которые сравниваются со значениями, полученными на тех же системах альфа-методом Росси.

MEDICION EN EL REACTOR VERA DE LA CONSTANTE DE DECRECIMIENTO DE LOS NEUTRONES INMEDIATOS, POR EL METODO DE LA FUENTE PULSADA. Con ayuda del método de la fuente pulsada, los autores han medido la constante de decrecimiento de los neutrones inmediatos en diversos conjuntos de reactor de neutrones rápidos alimentados con Y y Pu. Examinan los resultados y los comparan con los obtenidos para los mismos sistemas empleando el método de Rossi-α.

1. INTRODUCTION

In a fissile assembly whose reactivity is below prompt critical the prompt fission chains are finite and their length is characterized by a time-constant, usually denoted as α. If a large number of fission chains is initiated by the sudden injection of neutrons from a pulsed source then the rate of decay of the neutron population as a whole is determined by the same time constant. This is the basis of the pulsed source method of measuring α. The value of α for any particular system is determined by two parameters, the reactivity and the neutron lifetime. Consequently if one of these is known the other can be derived from a measurement of α. In zero-energy fast reactors the reactivity is usually measured independently and the α-measurement is used to determine the neutron lifetime. The neutron lifetime is an important quantity in kinetic studies, particularly of fast transients, and is

also a useful experimental quantity of checking neutronic calculation methods. In power reactors it is, of course, essential to have an accurate method of measuring reactivity, particularly when fuel changes are being made. The measurement of α by the pulsed source method and the derivation of reactivity from this in terms of a known neutron lifetime is a technique which may develop into an important alternative to the standard method of using calibrated control rods.

In the present paper we describe the method used to measure α in the VERA reactor and discuss the limitations of current theoretical interpretations by referring to some recent results.

2. CORE ARRANGEMENT AND PULSED-SOURCE DETAILS

VERA [1] is a zero-power fast reactor using uranium or plutonium fuel in the form of thin metal plates which can be packed into fuel elements with various diluent materials to form any required reactor composition. The compositions of the assemblies referred to in this paper are listed in Table I. The elements are packed vertically on a lattice plate in a square array. A typical configuration, showing the pulsed source located at the core-reflector boundary is illustrated in Fig. 1. The pulsed source is provided by an accelerator situated in a laboratory adjoining the reactor cell. A beam of deuterons is brought along a drift tube through the cell wall to impinge on a 2.5-cm diameter TiT target at the position where the source is required. The 14-MeV DT neutrons are emitted approximately isotropically from the target and the source is pulsed by deflecting the deuteron beam across a slit in the accelerator high voltage terminal. The pulse width is adjustable from 0.25 to 4 μs and its repetition frequency is variable from 100 to 5000 s^{-1} with a maximum duty cycle of 1%.

3. MEASUREMENT OF THE TIME DISTRIBUTION OF THE NEUTRON FLUX

The reactor flux is measured by a neutron counter - BF_3 proportional counter, U^{235} or U^{238}-coated fission chamber - which can be placed anywhere in the reactor core or reflector. Two time-sorting systems have been used to record the time distributions. The earlier measurements, on assemblies 3A and 5A, were made using a time-to-pulse height converter, in which the accelerator pulse initiated a linear voltage ramp which was then arrested by the first subsequent pulse from the detector. An output pulse, equal in height to the final ramp voltage was generated and recorded on a kicksorter. This system was replaced by a more accurate timesorter for the measurements on assemblies 11A and 11B. In this the output from an 8-Mc/s crystal oscillator is scaled down to 2, 1 or 0.5 Mc/s as appropriate and one of these pulse trains is fed to a gate unit which is opened by the accelerator modulator pulse and closed by the first subsequent detector pulse. The pulse train which passes through the gate has a length which is proportional to the delay of the detector pulse and is used to advance the channel address of a 400

TABLE I

COMPOSITION AND DIMENSIONS OF VERA ASSEMBLIES

Assembly Number	3A	5A	11A	11B
Core composition (atm/cm^3 x 10^{-22})				
U^{235}	0.619	0.6605	-	-
U^{238}	1.334	0.0504	-	-
Pu^{239}	-	-	0.724	0.724
Pu^{240}	-	-	0.037	0.037
Fe	0.628	0.628	0.607	0.607
Cr	0.164	0.164	0.158	0.158
Ni	0.0688	0.0688	0.0665	0.0665
C	3.577	5.461	4.606	4.606
H	0.0148	0.655	-	-
Cu	-	-	0.796	0.796
Core unit cell arrangement (see Note 2)	UGNGGN	GPGUGPG	GPuG	GPuG
Core dimensions				
Height (cm)	38.7	28.4	21.7	21.7
Diameter of equal-area cylinder (cm)	38.1	32.0	27.0	-
Reflector composition (atm/cm^3 x 10^{-22})				
U^{235}	0.025	0.025	0.025	-
U^{238}	3.44	3.44	3.44	
Fe	0.646	0.646	0.646	0.601
Cr	0.168	0.168	0.168	0.156
Ni	0.071	0.071	0.071	0.066
Cu	-	-	-	6.95
Reflector dimensions (overall)				
Height (cm)	104	104	104	58
Diameter (cm)	117	117	117	56
Critical mass (after correction for control rod excess) (kg U^{235} or Pu^{239})	104.3	58.5	33.1	36.5

Note: U^{238} includes a small amount of U^{234} and U^{236}.
Pu^{239} includes 0.41% of Pu^{241}.
G = Graphite, U = 93% enriched uranium.
N = Natural uranium (all 0.318-cm thick).
P = 0.0793-cm Polythene.
Pu = 0.254-cm plutonium clad in 0.0457-cm copper.

channel kicksorter (RIDL 34-12) to the channel whose number equals the population of the pulse train. A count is added to this channel and the address is then reset to await the next trigger pulse. This system provides

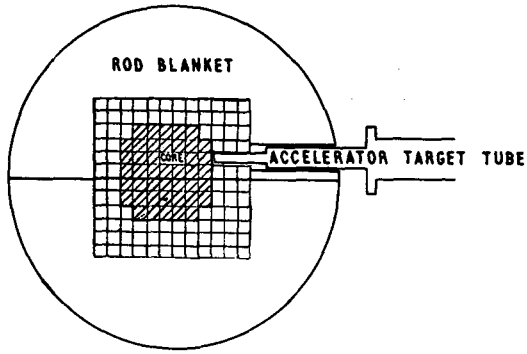


Fig. 1

Arrangement of experiment for measuring prompt chain decay constant

400 recording channels with time widths of $\frac{1}{2}$, 1 or 2 μs. With either of the time-sorter systems not more than one detector pulse can be recorded per accelerator source pulse and there is, therefore, a slight distortion of the resultant distribution because the probability of rejection of a pulse increases with its time-delay. However, since the detector count rate is typically only 0.1 per source pulse, the distortion effect is small and can be corrected with adequate accuracy.

4. REACTIVITY AND BACKGROUND LIMITATIONS

The neutron production rate in a subcritical system can be divided into two components as follows: N_p the neutron production rate in prompt chains arising directly from the source pulse and N_b the average rate of background neutron production, i.e. the rate of neutron production by processes other than prompt multiplication of pulsed source neutrons.

When a space- and energy-independent formalism are used, it can be shown (for example PATERSON and WEALE [2]) that

$$\frac{N_p}{N_b} = \frac{\alpha(1-\beta)(1-k_e)e^{-\alpha(t-W)}}{f\beta + \frac{A}{SW}(1-k_p)}, \qquad (1)$$

where

k_e = neutron reproduction constant
β = effective delayed neutron fraction
$k_p = k_e(1-\beta)$ = neutron reproduction constant excluding delayed neutrons
n = neutron population
n/τ = rate of neutron loss by absorption and leakage
τ = neutron lifetime
W = width of source pulse
t = time from beginning of source pulse

f = frequency of source pulses

$\alpha = \frac{k_p - 1}{\tau}$ = decay constant of prompt neutron chains

S = rate of production of pulsed source neutrons during pulse

A = rate of production of neutrons from sources other than the pulsed source.

For accurate measurements of α, conditions must be arranged so that the ratio N_p/N_b does not fall appreciably below unity for a period of time $(t - W)$ equal to $2/\alpha$.

In the VERA uranium experiments we found that suitable accelerator conditions were

$S = 10^9$ n/s

$W = 2$ or 3 μs

$f = 1000\ s^{-1}$.

and with these it was possible to obtain accurate measurements of α over the reactivity range from 0.08 to 7% below delayed critical. In VERA 3A, for example, there is a fairly large quantity of natural uranium giving a steady neutron source, A, of 2×10^5 n/s. The neutron lifetime, τ, is 2×10^{-7} s and the effective delayed neutron fraction, β, is 7×10^{-3}. Substituting these values into Eq. (1) we find that, at the time $t - W = 2/\alpha$, at 0.08% subcritical, $N_p/N_b = 0.54$ and at 7% subcritical, $N_p/N_b = 250$.

For this reactor, at 2% subcritical, with $f = 2.5 \times 10^3$, the rate of data accumulation was sufficient to establish the value of α to ±1% (statistical standard deviation, S.D.) in 15 min. A typical set of results is shown in Fig. 2. Curve A is the observed time distribution of neutron counts, curve B is the background observed immediately before the source pulse occurs,

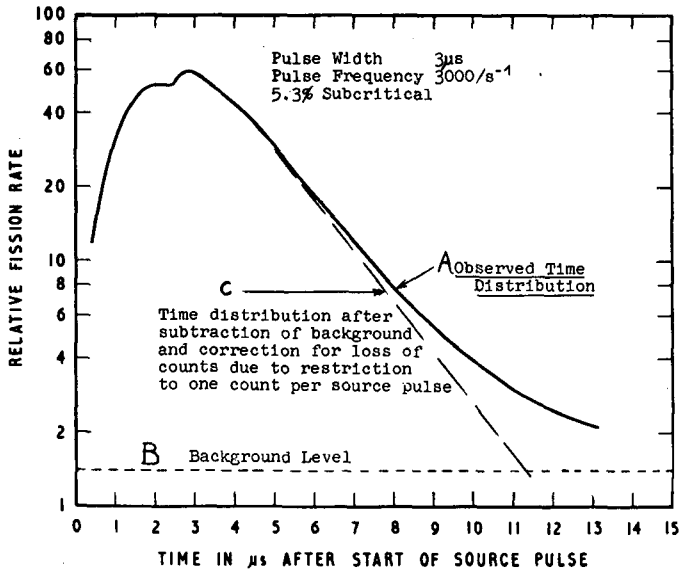


Fig. 2

Typical results (VERA 3A)

and curve C is the observed distribution after subtraction of the background and correction for the loss of counts in later channels resulting from the limitation of one count per pulse. The latter correction is small, amounting to 0.1 and 0.25% of the corrected value at times of 4 and 10 μs, respectively. The value of α is determined from curve C by fitting an exponential, weighting the results according to the inverse square of the relative standard deviation in each channel.

In the VERA plutonium assemblies the background neutron source was typically 2.5×10^6 n/s, i.e. ten times larger than in the uranium systems because of the Pu^{240} contribution. However, accurate measurements of α were possible within 0.1% of delayed critical.

5. MEASUREMENT OF REACTIVITY

The subcritical reactivity scales are deduced from the movements of calibrated control rods from their positions at delayed critical. The control rods are calibrated in absolute reactivity units by measuring the reactor periods produced by small movements of the rods and relating these periods to reactivity changes using the inhour equation. The delayed neutron data published by KEEPIN [3] have been used, taking into account the effectiveness of the delayed neutron groups of each fissile isotope relative to the prompt fission neutrons. The total effective delayed neutron fractions calculated for the VERA assemblies (using a Carlson S_n code) are given in Table II.

TABLE II

CALCULATED β_{eff} FOR THE VERA ASSEMBLIES

Assembly	Total effective delayed neutron fraction, β_{eff}
3A	$(7.30 \pm 0.31) \times 10^{-3}$
5A	$(7.54 \pm 0.30) \times 10^{-3}$
11A	$(2.96 \pm 0.30) \times 10^{-3}$
11B	$(2.12 \pm 0.20) \times 10^{-3}$

6. ROSSI-α MEASUREMENTS

To check the pulsed source technique we have repeated some of the measurements using the Rossi-α method. In this method, described for example by ORNDOFF [4], α is derived from measurements of the non-random relation between successive fission events. We followed Orndoff's procedure using two separate BF_3 proportional counters to record the time

distributions. A count in one counter was used to start a time-sorter scale which was then terminated by the first following count in the second detector. The results were analysed using the space- and energy-independent expression:

$$P(t) = Cdt + Ek_p^2 \frac{\left[\overline{\nu(\nu-1)} + \frac{2\bar{\nu}(1-k_p)\delta}{k_p}\right] e^{\alpha t}}{2\bar{\nu}^2(1-k_p)\tau} dt \qquad (2)$$

Here

- P(t) = probability of observing a count at time t after a count at time zero
- δ = the effective number of neutrons resulting from the detection process at time zero.
- C = a constant
- E = counter efficiency
- $\bar{\nu}$ = number of neutrons produced per fission; other quantities are defined as in section 4.

7. EXPERIMENTAL RESULTS

Measurements of α as a function of reactivity were made on four VERA assemblies. The dimensions and compositions of these are listed in Table I. The arrangement of each of these reactor assemblies and the positions of the pulsed source and the counters are shown in Fig. 3.

Figure 4 shows the experimental results for VERA 3A, a uranium-graphite system with a uranium enrichment of 31% and with a natural uranium reflector. The Rossi-α measurements were all made at known reactivities within the range of calibrated control rods using BF_3 proportional counters, and the pulsed source measurement made at 3.1% subcritical using a U^{235} fission counter agrees well with the Rossi-α value measured at the same reactivity. The other two pulsed source measurements were made with the two halves of the reactor assembly machine separated by 0.5 and 1.0 in and the α-values obtained are plotted in Fig. 4(b) on an extrapolated straight line drawn through the α-values between critical and 3.1% subcritical. The reactivity changes corresponding to the first and second half-inches of table movement were thus determined as $\Delta k_e = 0.0222$ and $\Delta k_e = 0.0225$, respectively. In this experiment the accuracy of measurement of α was approximately ±4% (S.D.), the main source of error arising in inadequate time-scale calibration.

Figure 5 shows results obtained with Assembly 5A, a 93% enriched uranium-graphite system containing a small amount of hydrogenous material. The flux decays plotted in Fig. 5(a), measured using a U^{235} fission counter, indicate deviations from exponential form and these deviations increase as the degree of subcriticality increases. However at reactivities between critical and 4% subcritical the flux time-decays eventually become exponential at some time after the end of the source pulse and the exponents derived from these ultimate rates of decay vary approximately linearly with reactivity as shown in Fig. 5(b). This linear relationship does not extend to more subcritical measurements For example the ultimate rate of decay predicted

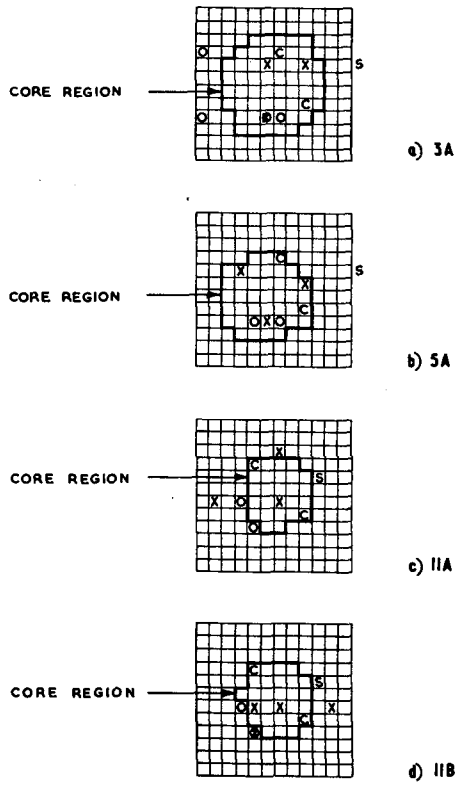


Fig. 3

Arrangement of the VERA assemblies
Note: The outer blanket of natural uranium rods is not shown in the diagrams

C: Control rods used to vary reactivity
X: Detector positions for pulsed source measurements
S: Pulsed source position
O: Rossi-α detector position

by a linear extrapolation of the α versus reactivity curve to 11% subcritical is shown as a straight dashed line in Fig. 5(a) and is much steeper than the ultimate rate of decay of the measured flux time-distribution which is plotted alongside.

Figure 6 shows the results of α-measurements on Assembly 11A, which is a plutonium-fuelled core with a natural uranium reflector. The α-values obtained with U^{235} fission detectors in the two core positions shown in Fig. 3(c) are in close agreement and the measurements in the reflector made with BF_3 proportional counters agree well with the fission counter results. At all the reactivities investigated the decay becomes exponential very soon after the end of the source pulse. If the graph of α versus reactivity is extrapolated, the intercept on the reactivity scale is 0.85 β for the pulsed curve and 1.4 β for the Rossi-α curve.

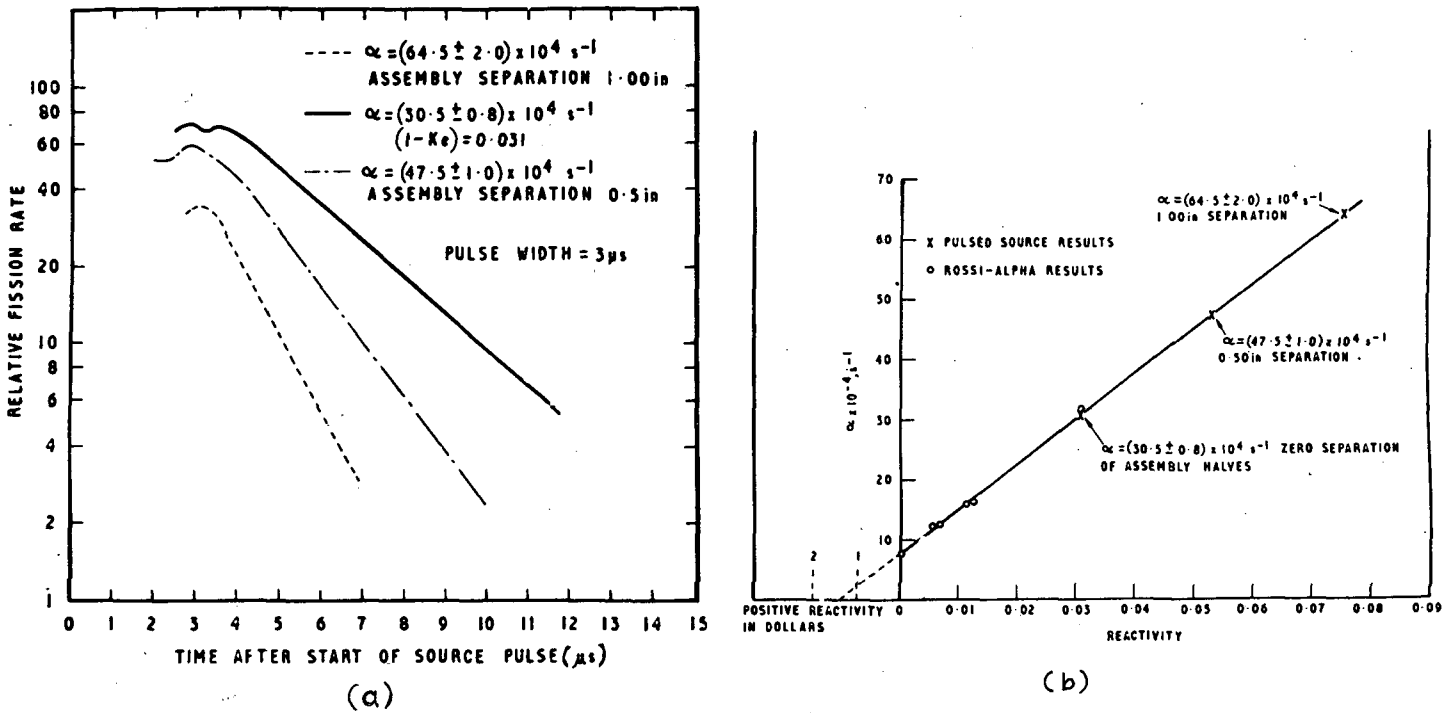
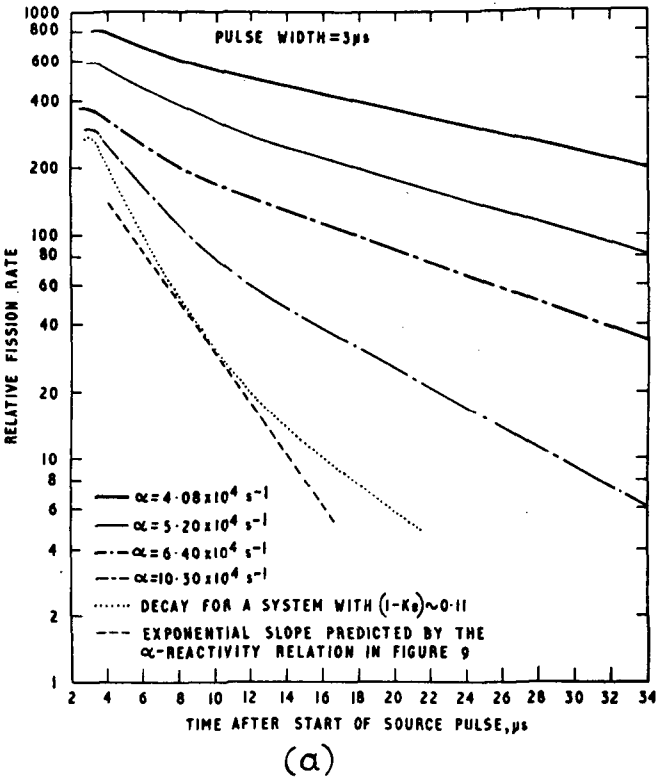


Fig. 4

Alpha measurement results (VERA 3A)



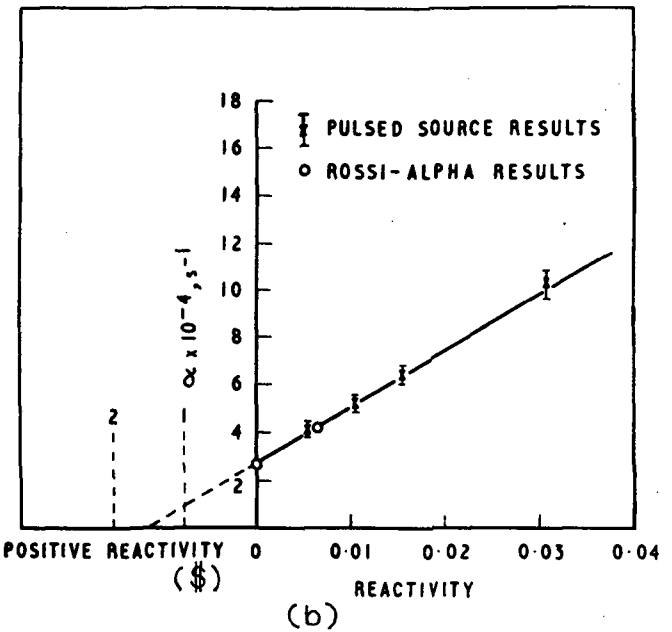
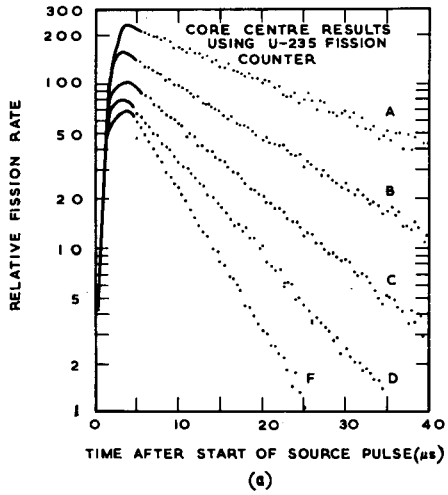
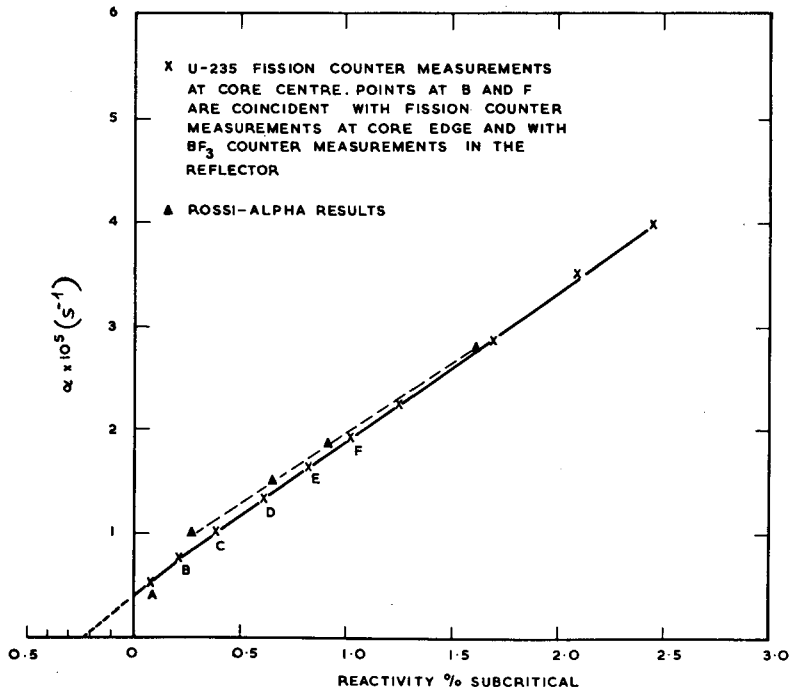


Fig. 5

Alpha measurement results (VERA 5A)



(a)



(b)

Fig. 6

Alpha measurement results (VERA 11A)

Figure 7 shows results of α-measurements on Assembly 11B, which has the same core composition as 11A but a copper reflector in place of natural uranium. The change to a copper reflector approximately doubles the effective prompt neutron lifetime of the assembly and also introduces two unexpected features. First, the neutron time distributions in systems more than 0.5% subcritical show distinct deviations from a simple exponential form. Secondly, the α-values from measurements made in the reflector with BF_3 proportional counters differ from the values obtained at the same positions using U^{235} fission counters. There is, however, no evidence of spatial dependence of α since the same value was obtained with the fission counter in all the positions shown in Fig. 3(d). Thermal neutrons in the reflector were clearly unimportant since the BF_3 counter α-value was not affected by surrounding the counter with a cadmium sheath. In the α-versus-reactivity graph, the intercept on the reactivity axis is 0.98 β.

8. DISCUSSION

If space- and energy-independence are assumed, the neutron time distribution obtained in pulsed source experiments are simple exponentials of the form

$$N(t) = N(o)e^{-\alpha t},$$

where $\alpha = \dfrac{1 - k_p}{\tau}$.

Since $k_p = k_e(1 - \beta)$, and τ is proportional to k_e, we have

$$\alpha = \frac{\beta - \varphi}{\tau_{dc}},$$

where

$\varphi = \dfrac{k_e - 1}{k_e}$ is the reactivity and

τ_{dc} is the neutron lifetime at delayed critical.

A graph of α versus ρ is therefore a straight line of slope $-1/\tau_{dc}$; the delayed critical value of α is $\alpha_{dc} = \beta/\tau_{dc}$; and α is zero at $\varphi = \beta$.

Comparing this simple theory with the experimental results in Figs. 4 to 7, it is clearly a good approximation for some systems but there are two important discrepancies.

(i) Non-exponential behaviour. The time-distributions for assembly 5A (U^{235}-graphite-polythene core with U_{nat} reflector) do not settle down to simple exponentials in the systems more than 3% (4 dollars) subcritical. The time-distributions for assembly 11B (Pu-graphite core with Cu reflector) are not simple exponentials in the systems more than 0.5% (2 dollars) subcritical.

(ii) Discrepancies on the reactivity scale. Although the relationship between α and ρ for assemblies 3A and 5A can be accurately represented by straight lines these lines do not extrapolate to the expected value (β) on

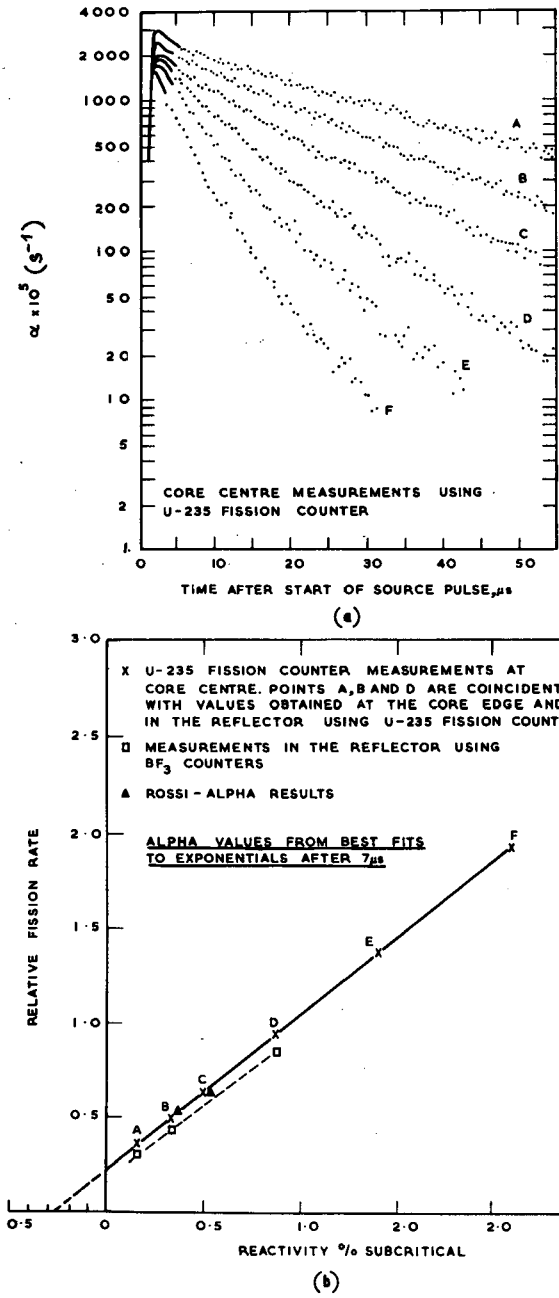


Fig. 7

Alpha measurement results (VERA 11B)

the reactivity scale at prompt critical. The intercepts are $(1.4 \pm 0.2)\beta$ for VERA 3A and $(1.5 \pm 0.3)\beta$ for VERA 5A. The errors stated are estimated limits. Such discrepancies have been observed by a number of other workers (see, for example the review by BRUNSON [5]).

It is logical to seek an explanation of these anomalies in terms of the over-simplification of the theoretical interpretation, i.e. the assumptions of spatial and energy independence.

Spatial independence implies the neglect of higher harmonic modes which might be generated by the use of a point source. However, harmonic effects would lead to a time variation of α and this would be expected in all the systems whereas there is no evidence of this in systems 3A and 11A. Moreover the Rossi-α method would be much less dependent on harmonic effects and the fact that pulsed-α and Rossi-α results agree well in systems 5A and 11B indicates that higher harmonics do not contribute significantly.

Spatial independence also implies that core and reflector neutron populations have the same α-value. Measurements in different parts of the core and reflector in the four VERA assemblies indicate no spatial variation of α but there is certainly a difference in kind in the behaviour of the copper-reflected and natural-uranium reflected systems 11A and 11B. This effect may however be explained by spectrum changes.

Energy-independence implies that the reactor energy spectrum is such that the energy-averaged values of k_e and τ do not vary significantly with time during the decay of the neutron population during the pulse. The spectrum must certainly vary with time to some extent since the initial population is of 14-MeV neutrons and the time taken to slow these down to the lowest energy groups is comparable with the reactor pulse. The questions that arise are whether this spectrum time dependence makes a significant difference to the effective value of k_e or τ during the time of the measurement and whether the values of k_e and τ during that time are the same as those that would be obtained in a steady-state system. This problem has recently been investigated theoretically by BRICKSTOCK [6]. By using a one-dimensional two-region multigroup time-dependent diffusion theory code, SWANTIME, he has shown that for VERA 5A a continual variation of α with time is predicted for a pulsed source system. The figures in Table III illustrate this effect for VERA 5A at $7\frac{1}{2}\%$ below prompt critical. (The α-values have been calculated as determined by count rate in a U^{235} fission chamber.)

The corresponding value of α derived from the expression

$$\alpha = \alpha_{dc} + \frac{1 - k_e}{k_e \tau_{dc}},$$

where τ_{dc} is the calculated lifetime at delayed critical, is $\alpha = 41.8 \times 10^4\ s^{-1}$.

Thus, for this core over the indicated time scale, a time-dependent calculation predicts an α-value which is smaller than that calculated using the equilibrium critical spectrum and which shows a marked variation with time. Brickstock attributes the difference to the relatively long time required for neutrons to be slowed down to very low energies, of the order of 1 eV. The very low energy groups are underpopulated in the early stages after the pulse and, because the slowing-down neutrons are lost to the fast groups but have

TABLE III

CALCULATED TIME DEPENDENCE OF α IN VERA 5A FOLLOWING A SOURCE PULSE AT $7\frac{1}{2}$% BELOW PROMPT CRITICAL

Time after beginning of input pulse (μs)	Apparent α-value predicted at the stated time after the beginning of the input pulse (10^4 s^{-1})	
	Homogeneous system	Heterogeneous system (Fuel plates 0.32-cm thick)
5	37.1	37.7
10	28.4	27.4
20	23.7	15.5
30	21.2	10.8
35	18.8	9.3

not yet contributed slow-group fissions, the reactor appears less reactive in the early stages. One would expect the trend to be reversed in the later stages when the very low energy groups would be overpopulated in relation to the high energy groups. The introduction of heterogeneity increases the time-dependent effect because the low energy neutrons tend to be trapped in the moderator plates producing a much greater build-up in the low groups. These predictions are in qualitative agreement with the experimental results for VERA 5A where pronounced time dependence of α was observed for well-subcritical systems. However the calculation has not yet been tested against the other VERA cores where no time-dependence was observed.

We have done some preliminary experimental studies of spectrum time-dependence in one of the VERA assemblies by measuring the pulse time-distribution with detectors of different energy sensitivities. This work is reported in the paper presented by PATERSON et al. [7]. The experiments were done on VERA 7B (an assembly of composition similar to VERA 5A but using 31% enriched uranium in the core and having a copper reflector). The reactor was 10% subcritical. The measurements showed that there was an appreciable time dependence of the spectrum but that the effect was due almost entirely to neutrons of energy below 1 eV. These measurements have not yet been repeated on the other VERA systems, but confirmatory figures have been obtained in some time-dependent spectrum calculations [7].

The discrepancy in the extrapolated intercept on the reactivity axis in Figs. 4(b) (VERA 3A) and 5(b) (VERA 5A) may be due to the presence of previously undetected delayed neutron groups which do not have any effect in the relatively long periods used for reactivity calibration. However the explanation could equally well lie in the neglect of time-dependent effects in interpreting pulsed-α measurements. Thus Brickstock's calculations of VERA 5A predict a non-linear variation of α with reactivity, the α values falling below the values expected on the simple interpretation. The results for VERA 11A, which is the only system for which we have measurements over a wide range of reactivity, extending to within 0.4% of prompt-critical, show some indication of curvature in the α-versus-ρ curve. If this effect were also present in the uranium systems it would not be detected because the measurements do not approach as closely to prompt critical, but it would be in the right direction to explain the observed discrepancy.

In VERA 11A, unlike the other three systems, the Rossi-α values measured at the blanket positions shown in Fig. 3(c) are significantly different from the pulsed source results. The Rossi-α values are larger by an amount which increases as the degree of subcriticality decreases (Fig. 6), so that a linear extrapolation predicts much larger values for α_{dc} and for the positive reactivity at $\alpha = 0$. In this connection it is also interesting to note that in general the calculated values of α_{dc} are significantly higher than the experimental values (compare, for example, DAVEY [8]).

ACKNOWLEDGEMENTS

We are indebted to Dr. Brickstock for permission to quote the results of his time-dependent diffusion theory calculations and to various members of the VERA reactor operating staff for their assistance in the experimental work.

REFERENCES

[1] WEALE, J. W. et al., "Operating experience with the zero-energy fast reactor, VERA", Experimental and Critical Experiments I IAEA, Vienna (1964).

[2] PATERSON, W. J. and WEALE, J. W., Pulsed source methods in fast reactor physics, J. Brit. nucl. Energy Soc. (Oct. 1964) 311.

[3] KEEPIN, G. R., Nucleonics 20 8 (1962) 150.

[4] ORNDOFF, J., Nucl. Sci. Engng 2 (1957) 450.

[5] BRUNSON, G. S. et al., A survey of prompt-neutron lifetimes in fast critical systems, Rpt ANL-6681 (1963).

[6] BRICKSTOCK, A., Paper to be presented at the Conf. on Application of Computing Methods to Reactor Problems, Argonne, USA (May, 1965).

[7] PATERSON, W. J., McCORMICK, W. B. and WEALE, J. W., "Some measurements of fast reactor spectra by the time-of-flight technique using a pulsed neutron source", these Proceedings II.

[8] DAVEY, W. G., A comparison of experimental and calculated prompt lifetimes and central reactivity coefficients in ZPR III assemblies and their relationship to other reactor parameters, Rpt ANL-6682.

MESURES AU MOYEN D'UNE SOURCE PULSÉE ET MODULÉE DANS UN RÉACTEUR*

W. ROTTER
CENTRE D'ÉTUDE DE L'ÉNERGIE NUCLÉAIRE,
MOL, BELGIQUE

Abstract — Résumé — Аннотация — Resumen

MEASUREMENTS WITH A PULSED AND MODULATED SOURCE IN A REACTOR. A generator with a neutron level variable in terms of any time factor has been developed by Philips Research Laboratories. Its practical use in reactor physics has been demonstrated through a series of measurements carried out in the BRO2 reactor when subcritical. The stability of this generator, and the possibility of introducing sharp variations in the neutron intensity and of pulsing the flux or modulating it sinusoidally, makes it a very versatile instrument. It enables reactivity ($\rho = \Delta k/\beta$) and neutron lifetime (ℓ/β) to be determined by different independent methods. An exact comparison can be made of these methods since they can be employed without changing the conditions under which measurements are carried out.

The following were determined: (1) ρ based on delayed neutrons, by a sudden reduction of neutron level, (2) ρ based on prompt neutrons by neutron pulses, (3) ℓ/β by a combination of (1) and (2) for $0.5\$ < \rho < 2\$$; and (4) ℓ/β based on the transfer function of the reactor for a modulated source.

The transfer functions for a reactivity oscillator and for a sinusoidally modulated source are discussed. It is shown that the measurement of ℓ/β is possible for $0.1\$ < \rho < 10\$$ by using a modulated source. The same method also gives the reactivity on the basis of the ratio of prompt neutrons to delayed neutrons for an optimal frequency, practically independently of the data for delayed neutrons and of the value of ℓ/β.

By accumulating a large number of cycles in the multi-channel analyser, better statistics for each method can be obtained. Since the neutron level from the generator is in fact sinusoidal, the response of the reactor may be integrated over each quarter of a period, as the measurement sequence is controlled by the generator; measurement time is then minimal. Observations recorded on a perforated tape are analysed by a digital computer.

MESURES AU MOYEN D'UNE SOURCE PULSÉE ET MODULÉE DANS UN RÉACTEUR. Un générateur dont le débit neutronique est variable selon une fonction du temps quelconque a été mis au point par les Laboratoires de recherches Philips. Son utilité pratique dans le domaine de la physique des réacteurs a été démontrée par une série de mesures effectuées dans le réacteur BRO2 à l'état sous-critique. Sa bonne stabilité, la possibilité de faire varier brusquement l'intensité neutronique, de pulser le débit ou de le moduler sinusoïdalement, rend ce générateur très souple. Il permet de déterminer la réactivité ($\rho = \Delta k/\beta$) et le temps de vie des neutrons (ℓ/β) d'après différentes méthodes indépendantes. Une comparaison exacte de ces méthodes est possible puisqu'elles peuvent être employées sans modifier les conditions de mesure.

On a déterminé: a) ρ sur la base des neutrons retardés, par une réduction instantanée du débit de neutrons; b) ρ sur la base des neutrons instantanés par des bouffées de neutrons; c) ℓ/β par combinaison de a) et b) pour $0,5\$ < \rho < 2\$$; d) ℓ/β sur la base de la fonction de transfert du réacteur pour une source modulée.

Les fonctions de transfert pour un oscillateur de réactivité et pour une source modulée sinusoïdalement sont discutées. Il est montré que la mesure de ℓ/β est possible pour $0,1\$ < \rho < 10\$$ en utilisant une source modulée. La même méthode fournit aussi la réactivité à l'aide du rapport des neutrons instantanés aux neutrons retardés pour une fréquence optimale, pratiquement indépendamment des données relatives aux neutrons retardés et de la valeur de ℓ/β.

Par accumulation d'un grand nombre de cycles dans l'analyseur multicanal, la statistique peut être améliorée pour chaque méthode. Le débit du générateur étant bien sinusoïdal, la réponse du réacteur peut être intégrée sur chaque quart d'une période, étant donné que la chaîne de mesure est pilotée par le générateur;

* Travail effectué dans le cadre de l'association CEN-EURATOM, chargée d'exploiter le réacteur BR2 et les installations connexes - (contrat 006/60/5 BRAB).

le temps de mesure est donc minimum. Les observations enregistrées sur bande perforée sont dépouillées par une calculatrice numérique.

ИЗМЕРЕНИЯ В РЕАКТОРЕ С ПОМОЩЬЮ ИМПУЛЬСНОГО И МОДУЛИРУЕМОГО ИСТОЧНИКА. Генератор, выход нейтронов которого изменяется в зависимости от функции какого-то времени, был разработан в исследовательских лабораториях Филипса. Его практическая польза в области физики реакторов была продемонстрирована на серии измерений, проведенных в реакторе BR-O 2 в подкритическом состоянии. Хорошая устойчивость, возможность производить резкие изменения интенсивности нейтронного потока, импульсировать выход или модулировать его синусоидально, – все это делает такой генератор очень гибким. Он позволяет устанавливать реактивность ($\rho = \Delta k/\beta$) и время жизни нейтронов (ℓ/β) по различным независимым методам. Точное сравнение этих методов возможно, поскольку последние могут быть использованы без изменения условий измерения.

Установлено: 1) ρ на основе запаздывающих нейтронов путем мгновенного уменьшения выхода нейтронов; 2) ρ на основе мгновенных нейтронов путем использования импульсов нейтронов; 3) ℓ/β путем соединения 1) и 2) для $0{,}5\ \$ < \rho < 2\ \$$; 4) ℓ/β на основе передаточной функции реактора для модулируемого источника.

Обсуждаются передаточные функции для осциллятора реактивности и для синусоидально модулируемого источника. Показано, что измерение ℓ/β возможно для $0{,}1\ \$ < \rho < \$$ с учетом применения модулируемого источника. Тот же метод также дает реактивность с помощью отношения мгновенных нейтронов к запаздывающим нейтронам для оптимальной частоты, причем на практике это происходит независимо от данных, относящихся к запаздывающим нейтронам, и от значения ℓ/β.

Статистика может быть улучшена для каждого метода в результате накопления большого количества циклов в многоканальном анализаторе. Если выход с генератора достаточно синусоидален, то чувствительность реактора может быть интегрирована для каждой четверти периода при условии, что цепь измерений управляется генератором; поэтому время измерения минимально. Зарегистрированные на перфорированной ленте наблюдения расшифровываются на цифровом вычислительном устройстве.

MEDICIONES EFECTUADAS EN REACTOR CON UNA FUENTE PULSADA Y MODULADA. Los laboratorios de investigación Philips han construido un generador neutrónico de flujo variable en función del tiempo. Con una serie de mediciones efectuadas en el reactor BRO2 en estado subcrítico, se ha demostrado su utililidad práctica en la esfera de la física de los reactores. El funcionamiento del generador es muy flexible debido a su alta estabilidad, a la posibilidad de variar bruscamente la intensidad neutrónica, y de pulsar el flujo o modularlo de manera sinusoidal. El generador permite determinar la reactividad ($\rho = \Delta k/\beta$) y la vida media de los neutrones (ℓ/β) según varios métodos independientes. Es posible proceder a una comparación exacta de esos métodos, dado que pueden aplicarse sin modificar las condiciones de medición.

El autor ha calculado los siguientes valores: a) ρ, sobre la base de los neutrones retardados, por reducción instantánea del flujo neutrónico; b) ρ, sobre la base de los neutrones inmediatos, por impulsos neutrónicos; c) ℓ/β, combinando 1) y 2), cuando 0,5 dólares $< \rho <$ 2 dólares, y d) ℓ/β, sobre la base de la función de transferencia del reactor para una fuente modulada.

En la memoria se examinan las funciones de transferencia correspondientes a un oscilador de reactividad y a una fuente de modulación sinusoidal. Se demuestra que es posible medir ℓ/β, cuando 0,1 dólar $< \rho <$ 10 dólares utilizando una fuente modulada. Por el mismo método se obtiene también la reactividad partiendo de la razón neutrones inmediatos/neutrones retardados para una frecuencia óptima que es prácticamente independiente de los datos relativos a los neutrones retardados y del cociente ℓ/β. La precisión estadística de cada método puede aumentarse acumulando un gran número de ciclos en el analizador multicanal. Como el flujo del generador es perfectamente sinusoidal, la respuesta del reactor puede integrarse en cada cuarto de período, puesto que el circuito de medición está gobernado por el generador; por consiguiente, el tiempo de medición es mínimo. Los datos registrados sobre cinta perforada se analizan con ayuda de una calculadora numérica.

1. INTRODUCTION

Le réacteur BR02 est le modèle nucléaire du réacteur à haut flux pour essai de matériaux BR2. En raison de sa conception, le réacteur BR2 pré-

sente une grande souplesse d'adaptation aux exigences du programme des irradiations : la disposition des éléments combustibles et des barres de contrôle peut être modifiée suivant les spécifications imposées [1].

L'exploitation du réacteur BR02 est justifiée par le souci de pouvoir valoriser cette souplesse sans immobiliser BR2 lui-même; la recherche des configurations successives et la détermination de leurs caractéristiques opérationnelles y sont effectuées.

Dans cette optique, il est nécessaire de disposer d'une méthode de calibration des barres de contrôle bien adaptée aux conditions de mesure : elle doit couvrir une large gamme d'antiréactivité avec une précision satisfaisante, sans nécessiter des temps de mesure trop longs. D'autre part, pour chacune des configurations, la connaissance des caractéristiques dynamiques, tel le temps de vie des neutrons, est souhaitable.

Cet objectif peut être atteint par l'utilisation d'une source de neutrons dont le débit peut être pulsé et modulé. Une telle source doit répondre à différents impératifs, notamment : intensité suffisante et variable d'une manière reproductible, pilotage synchronisé avec la chaîne de mesure, durée de vie aussi élevée que possible, dimensions et poids permettant l'introduction aisée dans les canaux de la matrice du réacteur.

Une étude comparative des différentes solutions et des caractéristiques des générateurs de neutrons disponibles sur le marché a montré l'intérêt d'utiliser un tube scellé [2, 3]. Des échanges de vues avec le Laboratoire de recherches PHILIPS ont conduit à la mise au point par ce laboratoire d'un appareillage de commande de la source permettant de faire varier le débit de celle-ci suivant une fonction arbitrairement choisie. Les résultats de ce développement sont décrits dans le document présenté par ELENGA et REIFENSCHWEILER à ce symposium [4].

A cette occasion, nous nous permettons de les remercier vivement, ainsi que les techniciens de leur groupe, de l'accueil qu'ils nous ont réservé et de l'attention qu'ils ont apportée à la solution de nos problèmes.

2. RELATIONS GÉNÉRALES

2.1. La réponse d'un réacteur sous-critique à une courte bouffée de neutrons provenant d'une source extérieure est une impulsion dont la partie décroissante [5] est caractérisée par la constante de décroissance α

$$\alpha = \frac{1}{l}\,[1 - (1 - \beta)k] \qquad (1)$$

$$= \alpha_0 (1 + \rho)$$

où

$$\alpha_0 = \frac{\beta k}{l},$$

$\rho = -\dfrac{k-1}{\beta k}$ (>0) antiréactivité en dollars (\$),

l	temps de vie des neutrons prompts,
β	fraction «effective» des neutrons retardés*,
k	facteur de multiplication effectif.

Lorsque ρ tend vers zéro, k tendant vers l'unité, α devient égal à $\alpha_c = \beta/l$. Les techniques conventionnelles utilisent cette valeur de α_c et l'identifient à α_0 pour déterminer une antiréactivité quelconque ρ à partir de la mesure correspondante de α.

2.2. Avant d'envisager la réponse d'un réacteur à une source neutronique extérieure variant sinusoïdalement, rappelons brièvement les relations décrivant la variation de la densité neutronique lors d'une oscillation sinusoïdale du facteur de multiplication k, telles qu'elles sont utilisées pour la mesure de β/l au moyen d'un oscillateur. Les équations de la cinétique s'écrivent

$$\frac{dn}{dt} = \frac{k_{ex}}{l} n - \frac{k\beta}{l} n + \sum_i \lambda_i C_i + S, \tag{2}$$

$$\frac{dC_i}{dt} = \frac{k\beta_i}{l} n - \lambda_i C_i \qquad (i = 1 \ldots\ldots m),$$

où $k_{ex} = k - 1$,
n = densité neutronique,
β_i, λ_i = caractéristiques des neutrons retardés du groupe i,
C_i = concentration des émetteurs des neutrons retardés du groupe i,
S = intensité de la source extérieure.
A une variation sinusoïdale d'amplitude Δk autour de k_0

$$k = k_0 + \Delta k \cdot \exp(j\omega t)$$

correspond une variation de la densité neutronique dans le réacteur

$$n = n_0 + \Delta n \cdot \exp(j\omega t)$$

dont l'amplitude et la phase, pour la distribution fondamentale, sont calculables à partir de la fonction de transfert

$$\frac{\Delta n/n_0}{\Delta k} = \frac{1 - j\omega \sum_i \frac{\beta_i}{j\omega + \lambda_i}}{j\omega \left(l + k_0 \sum_i \frac{\beta_i}{j\omega + \lambda_i} \right) - (k_0 - 1)}. \tag{3}$$

* Pour les calculs développés ci-après, les caractéristiques des neutrons retardés sont tirées de la référence [6]; celles des photoneutrons, mesurées dans BR02, sont données à la référence [7]. La fraction totale β est prise égale à $0,74 \cdot 10^{-2}$.

Cette relation est applicable à des oscillations de faible amplitude uniquement, car elle implique que le système soit linéaire.

La figure 1a représente l'amplitude relative $A(\omega)$ de la réponse du réacteur, par unité de Δk, en fonction de ω.

2.3. La réponse du réacteur à une source extérieure variant sinusoïdalement

$$S = S_0 + \Delta S \cdot \exp(j\omega t)$$

est donnée par

$$\frac{\Delta n}{\Delta S} = \frac{1}{j\omega\left(1 + k_0 \sum_i \frac{\beta_i}{j\omega + \lambda_i}\right) - (k_0 - 1)} \cdot \tag{4}$$

Dans ce cas, le comportement du système est toujours linéaire et la validité de l'expression précédente n'est pas limitée à de petites valeurs de ΔS (une variation $\Delta S/S_0 = 1$ reste admissible).

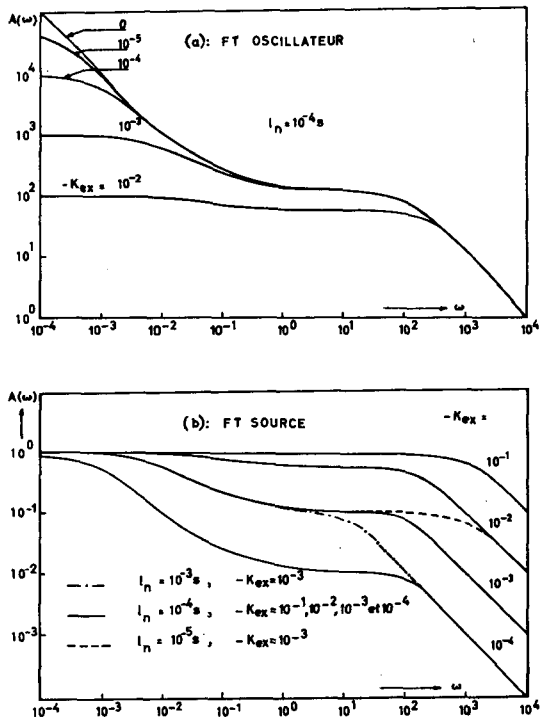


Figure 1

Fonction de transfert d'un réacteur pour une variation de la réactivité (oscillateur) et pour une source de neutrons modulée.

Une source constante d'intensité S_0 crée, dans le réacteur sous-critique ($k_0 < 1$), un état d'équilibre ($dn/dt = 0$, $dC_i/dt = 0$) caractérisé par

$$n_0 = -\frac{S_0 \cdot l}{k_0 - 1}. \tag{5}$$

Utilisant cette relation (5) ainsi que

$$\rho = -\frac{k_0 - 1}{k_0 \beta} = -\frac{k_{ex}}{k_0 \beta}, \tag{6}$$

la fonction de transfert peut s'écrire

$$\frac{\Delta n/n_0}{\Delta S/S_0} = \frac{\rho}{\rho + j\omega\left(\frac{1}{k_0\beta} + \frac{1}{\beta}\sum_i \frac{\beta_i}{\lambda_i + j\omega}\right)}. \tag{7}$$

Par séparation des termes réel et imaginaire, on obtient l'amplitude relative (ou le gain) A définie par

$$\left[\frac{\Delta n/n_0}{\Delta S/S_0}\right]^2 = A^2 = \frac{\rho^2}{\left(\rho + \frac{\omega^2}{\beta}\sum_i \frac{\beta_i}{\lambda_i^2 + \omega^2}\right)^2 + \omega^2\left(\frac{1}{k_0\beta} + \frac{1}{\beta}\sum_i \frac{\lambda_i \beta_i}{\lambda_i^2 + \omega^2}\right)^2} \tag{8}$$

et le déphasage entre le signal extérieur et la réponse du réacteur caractérisé par l'angle de phase φ.

$$\operatorname{tg}\varphi = \frac{\left[\frac{1}{k_0\beta} + \frac{1}{\beta}\sum_i \frac{\lambda_i \beta_i}{\lambda_i^2 + \omega^2}\right] \cdot \omega}{\rho + \frac{\omega^2}{\beta}\sum_i \frac{\beta_i}{\lambda_i^2 + \omega^2}}. \tag{9}$$

Des courbes $A(\omega)$ pour quelques valeurs de l'antiréactivité ($-k_{ex}$) sont représentées à la figure 1b.

2.4. La comparaison des deux fonctions de transfert (fig. 1a et 1b) montre que la succession des courbes suivant des valeurs de k_{ex} croissantes, pour une valeur déterminée de ω, est inversée et que les asymptotes communes aux fréquences élevées correspondent à une valeur déterminée de β/l dans un cas et de k_{ex}/l dans l'autre cas.

D'autre part, l'étalement des courbes diffère fortement d'un cas à l'autre; cet étalement, important surtout dans le cas du signal source aux fréquences utilisables en pratique ($\omega > 10^{-1}$), permet de mesurer aisément l'antiréactivité dans la gamme $-k_{ex} = 10^{-1}$ à 10^{-4}.

2.5. La fonction de transfert dans les cas de la source modulée, est déterminée aux fréquences élevées et petites, respectivement par le temps de vie des neutrons prompts et par les neutrons retardés. Entre ces deux régions

il existe une gamme de fréquence dans laquelle l'influence de ces deux facteurs est faible :

$$\frac{\omega^2}{\beta}\sum_i \frac{\beta_i}{\lambda_i^2+\omega^2} \approx 1,$$

$$\left[\frac{\omega l}{k_0\beta}+\frac{\omega}{\beta}\sum_i \frac{\lambda_i\beta_i}{\lambda_i^2+\omega^2}\right] \ll 1 .$$

Cette gamme est d'autant plus large que le temps de vie des neutrons prompts est court.

Il existe en plus dans cette gamme une fréquence optimale $\hat{\omega}$ définie par

$$\left(1-\frac{\hat{\omega}^2}{\beta}\sum_i \frac{\beta_i}{\lambda_i^2+\hat{\omega}^2}\right)^2 - 2(\rho+1)\left(1-\frac{\hat{\omega}^2}{\beta}\sum_i \frac{\beta_i}{\lambda_1^2+\hat{\omega}^2}\right)$$

$$+\left(\frac{\hat{\omega} l}{k\beta}+\frac{\hat{\omega}}{\beta}\sum_i \frac{\lambda_i\beta_i}{\lambda_i^2+\hat{\omega}^2}\right)^2 = 0$$

et pour laquelle l'équation (8) se réduit à

$$A = \frac{\rho}{1+\rho} . \qquad (10)$$

La valeur $\hat{\omega}$ est fonction de ρ, mais pour $l \lesssim 10^{-4}$ s l'équation (10) peut être utilisée en pratique dans un domaine (ρ, ω) assez étendu.

Au tableau I, quelques valeurs de A tirées de (10) sont comparées aux valeurs de A fournies par la fonction de transfert complète (8), pour une valeur unique $\omega = 10$ et différentes valeurs de $-k_{ex}$: l'écart relatif $\Delta A/A$ a été calculé pour $l = 10^{-4}$ s et 10^{-5} s. Cet écart reste inférieur à 1%, quoique

TABLE I

ÉCART RELATIF ENTRE LA VALEUR EXACTE DE A ET LA VALEUR CALCULÉE SUIVANT LA FORMULE SIMPLE

$A = \frac{\rho}{1+\rho}$, POUR $\omega = 10\ s^{-1}$

$-k_{ex}$	ρ (\$)	$A = \frac{\rho}{1+\rho}$	$\frac{\Delta A}{A}$ (%)	
			$l = 10^{-4}$ s	$l = 10^{-5}$ s
10^{-5}	$1,35 \cdot 10^{-3}$	$1,34955 \cdot 10^{-3}$	-0,98	+0,38
10^{-4}	$1,35 \cdot 10^{-2}$	$1,33346 \cdot 10^{-2}$	-0,95	+0,37
10^{-3}	0,135	$1,19152 \cdot 10^{-1}$	-0,71	+0,35
10^{-2}	1,365	0,57717	-0,06	+0,19
10^{-1}	15,02	0,93756	+0,03	+0,05

la valeur optimale $\tilde{\omega}(\rho)$ varie de 7 à 22 pour $l = 10^{-4}$ s et de 22 à 70 pour $l = 10^{-5}$ s.

2.6. Dans le cas d'une modulation d'amplitude maximum $\frac{\Delta S}{S_0} = 1$, on a

$$\frac{\Delta n}{n_0} = \frac{\rho}{1+\rho}$$

ou

$$\rho = \frac{\Delta n}{n_0 - \Delta n} .$$

En multipliant le numérateur et le dénominateur par la période T, on peut montrer que ρ est égal au rapport des surfaces hachurées à la figure 2 (en bas à droite) et que ce rapport vaut

$$\frac{\int_T n_{\text{prompts}}\, dt}{\int_T n_{\text{retardés}}\, dt} \qquad T = \frac{2\pi}{\hat{\omega}} = \text{période.} \tag{11}$$

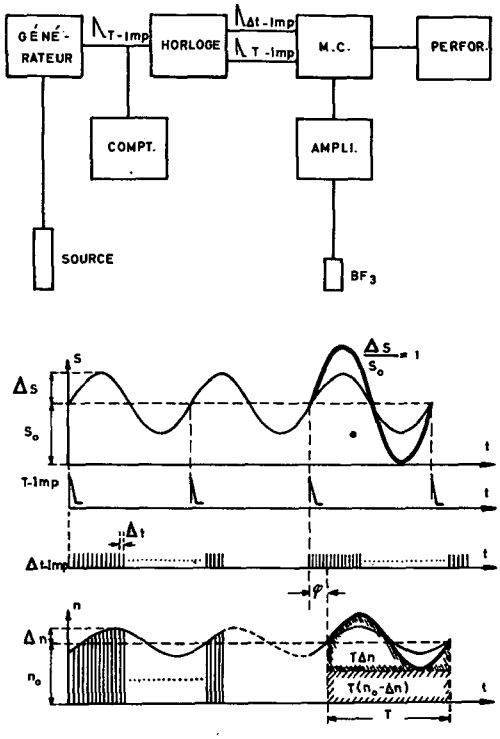


Figure 2

Principe d'utilisation de l'installation en régime sinusoïdal.

Cette relation peut être appliquée à d'autres fonctions périodiques, et cela d'une manière plus ou moins valable, lorsque la fondamentale de fréquence $\hat{\omega}/2\pi$ est prédominante.

SJÖSTRAND [8] a vérifié cette relation (11) au cours d'expériences avec neutrons pulsés (impulsions rectangulaires de durée T/2) : pour les périodes adoptées de T = 1 s et T = 0, 5 s ($\omega \approx \hat{\omega}$), la formule simplifiée (10) est précisément valable lorsqu'on l'applique à la composante fondamentale.

2.7. Aux fréquences élevées, le temps de vie des neutrons joue un rôle de plus en plus important dans la réponse du réacteur au signal sinusoïdal. La fonction de transfert (8) se simplifie lorsque $\omega^2 \gg \hat{\omega}^2$; on obtient alors

$$A^2 = \frac{\rho^2}{(1+\rho)^2 + \left(\frac{\omega \cdot l}{k \cdot \beta}\right)^2} \tag{12}$$

En utilisant l'expression de ρ donnée par la relation (1), on peut écrire

$$A^2 = \frac{(\alpha/\alpha_0 - 1)^2}{(\alpha/\alpha_0)^2 + (\omega/\alpha_0)^2} \tag{13}$$

ou, plus généralement, en tenant compte de l'influence des neutrons retardés,

$$A^2 = \frac{(\alpha/\alpha_0 - 1)^2}{(\alpha/\alpha_0 - 1 + p)^2 + (\omega/\alpha_0 + q)^2} \tag{14}$$

avec

$$p = \frac{\omega^2}{\beta} \sum_i \frac{\beta_i}{\lambda_i^2 + \omega^2}$$

et

$$q = \frac{\omega}{\beta} \sum_i \frac{\lambda_i \beta_i}{\lambda_i^2 + \omega^2} .$$

En mesurant A au moyen de la source modulée et α au moyen de la source pulsée, la valeur de α_0 peut être déterminée pour chaque fréquence.

3. TECHNIQUES DE MESURE

3.1. Les figures 3 et 4 représentent respectivement la disposition de l'appareillage de mesure et une vue en coupe du réacteur BR02 au niveau du plan médian horizontal montrant la localisation des éléments combustibles, des barres de contrôle et de la source*.

* Les pièces mécaniques pour l'installation et la protection de la source ont été conçues par M.J. Sevrin.

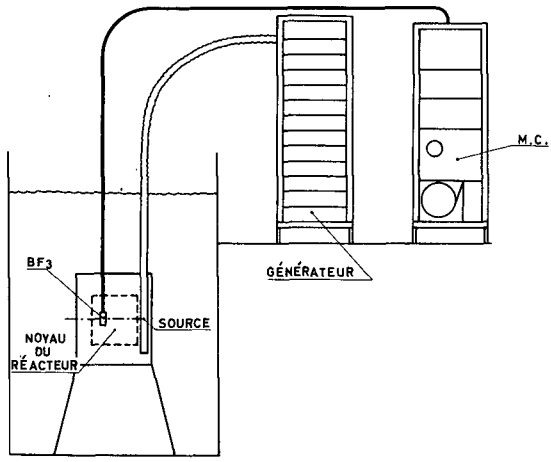


Figure 3

Représentation schématique de l'installation.

3.2. Le bloc-diagramme de l'installation de mesure est représenté à la figure 2; cet ensemble est utilisable lors du fonctionnement de la source en régime pulsé ou en régime sinusoïdal.

Le fonctionnement est illustré pour le fonctionnement en régime sinusoïdal. Le générateur commande la modulation sinusoïdale de l'émission de la source. A chaque début de période T, il délivre une impulsion à l'horloge d'un analyseur multicanal et fait commencer les comptages effectués au moyen de 100, 200 ou 400 canaux. Les impulsions fournies par l'amplificateur associé au détecteur BF_3 sont accumulées successivement dans chaque canal pendant un temps Δt. Après une série de comptages sur l'ensemble des canaux, l'impulsion du générateur fait commencer une nouvelle série.

La réponse du réacteur, au cours d'une période, est donc analysée d'une manière détaillée et l'accumulation se poursuit jusqu'à obtention d'une bonne précision statistique pour chaque point de mesure. Le contenu de chaque canal, C_j, est ensuite enregistré sur bande perforée; l'analyse est effectuée au moyen d'un calculateur digital Mercury suivant un développement de Fourier, de manière à déterminer la valeur de $\Delta n/n_0$ pour la fondamentale**. La fréquence d'oscillation est, d'autre part, mesurée sur un grand nombre de cycles, par comptage au moyen d'une échelle des impulsions fournies par le générateur.

3.3. Pour les mesures en régime pulsé, la méthode classique a été appliquée : les valeurs des C_j, obtenues après un délai de 2 à 4 ms succédant au signal de la source et corrigées pour le temps mort, sont analysées par moindres carrés au moyen d'une fonction $Y = a \exp(-\alpha tj) + C$. Un contrôle de l'influence des harmoniques est réalisé en calculant pour chaque point de mesure la déviation $(C_j - Y_j)/\sqrt{Y_j}$.

** Les programmes des différentes analyses utilisées dans ce rapport ont été établis par Mlle H. Depuydt, MM. R. Blyau et L. Kesselaers.

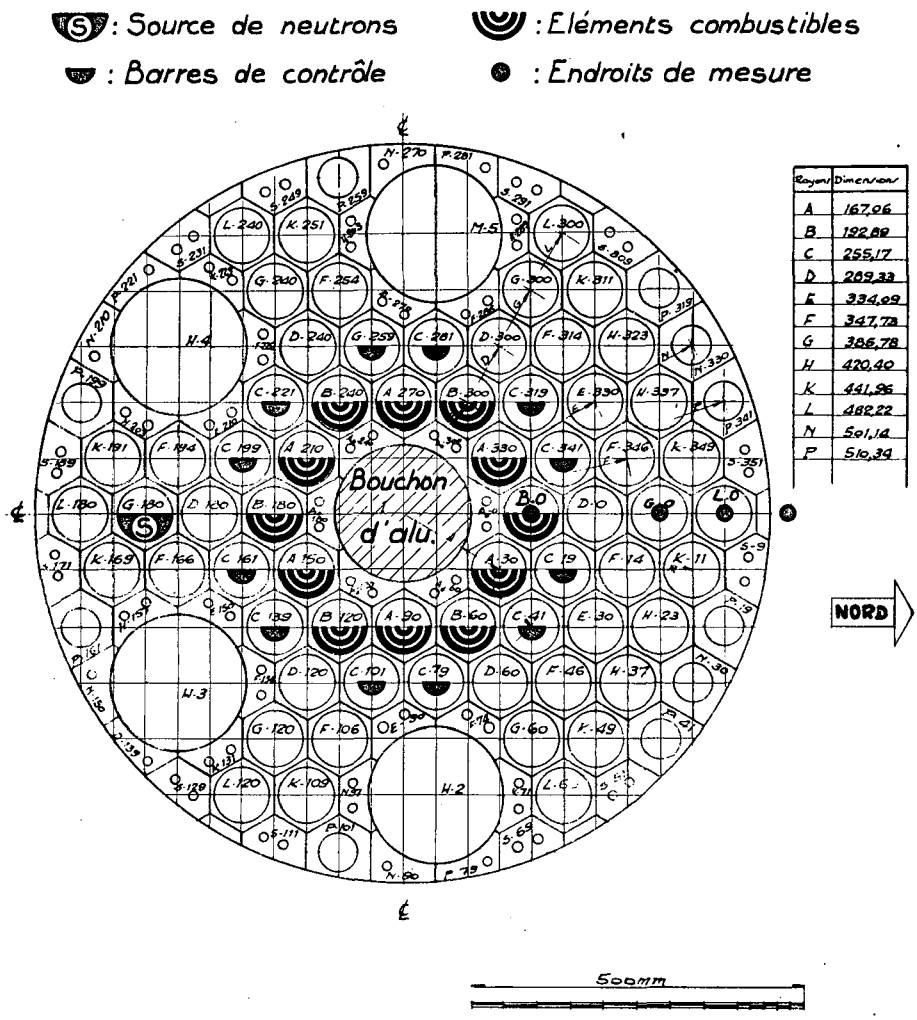


Figure 4

Coupe schématique du BR02 suivant le plan médian.

3.4. Une méthode bien connue de calibration des barres de contrôle consiste à mesurer la décroissance de la densité neutronique après éjection d'une source placée pendant quelque temps dans le réacteur sous-critique. Le rapport de la densité intégrale, mesurée pendant une durée déterminée après l'éjection, à la densité correspondant au niveau stable créé avant l'éjection, est une fonction de l'antiréactivité. Le calcul de cette fonction nécessite la connaissance des paramètres des neutrons retardés. L'éjection d'une source à grande vitesse peut être remplacée avantageusement par la réduction quasi instantanée du débit des neutrons fournis par le tube; cette

réduction est effectuée en 10 μs et l'analyseur multicanal est mis en marche par une impulsion simultanée.

3.5. En régime modulé, la technique exposée au paragraphe 3.2. peut être simplifiée en raison du caractère bien sinusoïdal du débit neutronique de la source: une analyse n'étant donc pas nécessaire, on peut intégrer la réponse sur des quarts de période [9]. Cette intégration est réalisable en utilisant seulement quatre canaux et quatre impulsions de mise en marche des comptages au cours d'une période. Si le contenu d'un canal est C_j (j = 1, 2, 3, 4), on peut établir que

$$\left(\frac{\Delta n}{n_0}\right)^2 = \frac{(C_1 - C_3)^2 + (C_2 - C_4)^2}{(C_1 + C_2 + C_3 + C_4)^2} \cdot \frac{\pi^2}{2}$$

et

$$\operatorname{tg}\varphi = \frac{(C_1 - C_3) - (C_2 - C_4)}{(C_1 - C_3) + (C_2 - C_4)} .$$

Les résultats des mesures rapportés ci-après ont été obtenus par analyse complète de la réponse du réacteur et non par application de la technique simplifiée.

4. RÉSULTATS DE MESURES

Les techniques décrites ci-dessus ont été appliquées à la calibration du faisceau des barres de contrôle, dans la configuration de géométrie simple constituée par 12 éléments combustibles. Ces premières mesures constituent un test de l'appareillage et des méthodes précitées.

4.1. Avant de procéder aux mesures dans le réacteur, la calibration de la source fonctionnant en régime sinusoïdal a été effectuée de manière à définir notamment $\Delta S/S$ (étalonnage des potentiomètres de réglage). A cette fin, la source est placée dans la piscine du réacteur.

Dans ce milieu diffusant non multiplicateur, l'amplitude de la modulation de la densité neutronique en un point est atténuée suivant la loi [10]

$$\frac{\Delta n/n_0}{\Delta S/S_0} = \frac{\exp(-\gamma \cdot r)}{\exp(-x \cdot r)} = \exp - r(\gamma - x) \qquad (15)$$

où r = distance source-détecteur,

$\frac{1}{x} = L$ = longueur de diffusion ($x^2 = \Sigma_a/D$),

$\frac{1}{\gamma}$ = longueur de diffusion complexe ($\gamma^2 = x^2 + j\frac{\omega}{Dv}$) .

Le module de la longueur de diffusion complexe est donné par

$$|\gamma| \approx x\left(1 + \frac{\omega^2 \cdot l^2}{4}\right)^{\frac{1}{2}} . \qquad (16)$$

Aux basses fréquences ($\omega^2 \cdot l^2 \ll 1$, $\gamma - x \approx 0$ et $\Delta n/n_0$ = constante), l'atténuation de l'amplitude de l'onde neutronique Δn est égale à l'atténuation de la valeur moyenne n_0. Dans l'eau, pour $r \gtrapprox 25$ cm, il en est ainsi à mieux d'un pour cent aux fréquences telles que $\omega < 500\ s^{-1}$; dans un milieu où le temps de vie l serait égal à 10^{-3} s, ω serait limité à $100\ s^{-1}$. En conclusion, pour les basses fréquences, la réponse $\Delta n/n_0$ d'un détecteur, dans une position adéquate, est égale à $\Delta S/S_0$. En plaçant le détecteur à 10 cm de la source, la grandeur $\Delta n/n_0$ a été mesurée en fonction de la fréquence, suivant la technique décrite en 3.2. La courbe a de la figure 5 a ainsi été obtenue; elle implique que pour la mesure effectuée avec $\omega \approx 7$, on a rigoureusement

$$\frac{\Delta n}{n_0} = \frac{\Delta S}{S_0}$$

4.2. La fonction de transfert a été mesurée dans le réacteur à différents degrés de sous-criticalité obtenus par enfoncement des 12 barres de contrôle alignées à une même cote. La position des barres de contrôle est définie par les cotes 960 mm (barres extraites), 480 mm (extrémité inférieure des parties absorbantes au niveau du plan médian) et 0 mm (barres totalement enfoncées). La cote critique est, dans le cas présent, 860 mm : l'excès de réactivité d'un tel chargement est faible (environ 0, 3 $). La source était introduite dans le canal G-180, la cible étant au niveau du plan médian; le détecteur BF_3 se trouvait généralement, au niveau du plan médian également, dans le tube-support central de l'élément combustible du canal B-0 (les éléments sont formés de tubes concentriques entourant un tube-support en aluminium). Pour les mesures de petites antiréactivités (0, 45 et 1, 1 $), le détecteur a été placé en G-0 ou en L-0 en raison des niveaux de flux élevés.

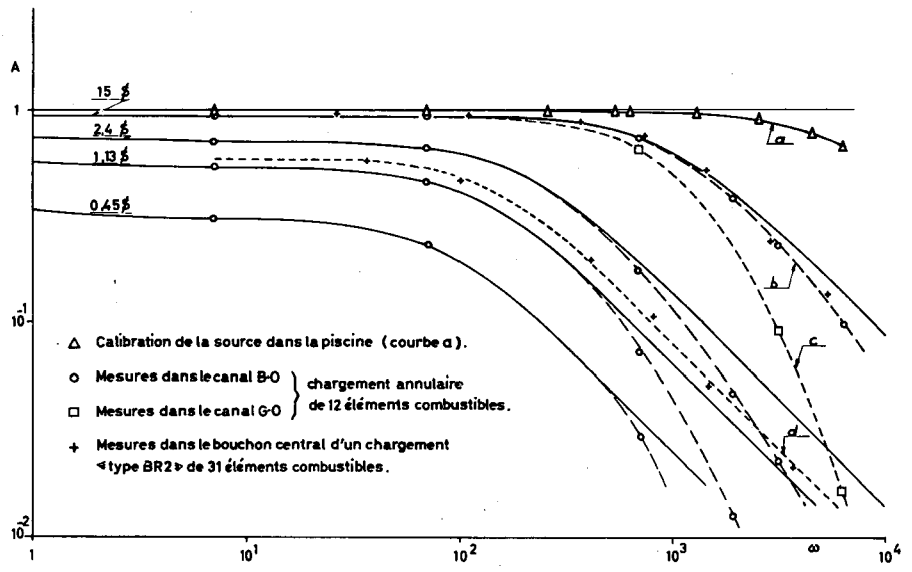


Figure 5

Calibration de la source dans la piscine et fonctions de transfert dans BR02.

La figure 5 montre la fonction de transfert mesurée à différents degrés de sous-criticalité.

4.3. Dans les mêmes conditions, on a mesuré

a) l'antiréactivité par réduction instantanée du débit neutronique de la source (voir 3.5.),

b) l'antiréactivité par modulation du débit pour $\omega \approx \hat{\omega}$ (voir 2.5.), et

c) la valeur de la constante de décroissance α par la méthode des neutrons pulsés (voir 2.1.).

Le tableau II et la figure 6 montrent les résultats de ces mesures. Puisque α constitue un paramètre caractéristique de l'état du réacteur, les valeurs de ρ mesurées par modulation (~) et par «step» (⌐¬) ont été portées en graphique en fonction de α (fig. 7).

5. DISCUSSION DES RESULTATS

5.1. La configuration de chargement du réacteur BR02, réalisée au moment des mesures rapportées au paragraphe précédent, a été conçue dans le cadre d'un programme expérimental particulier. En raison de l'existence de nombreux résultats expérimentaux relatifs à cette configuration, obtenus par d'autres techniques, il s'est avéré intéressant de lui appliquer les méthodes de pulsation et de modulation.

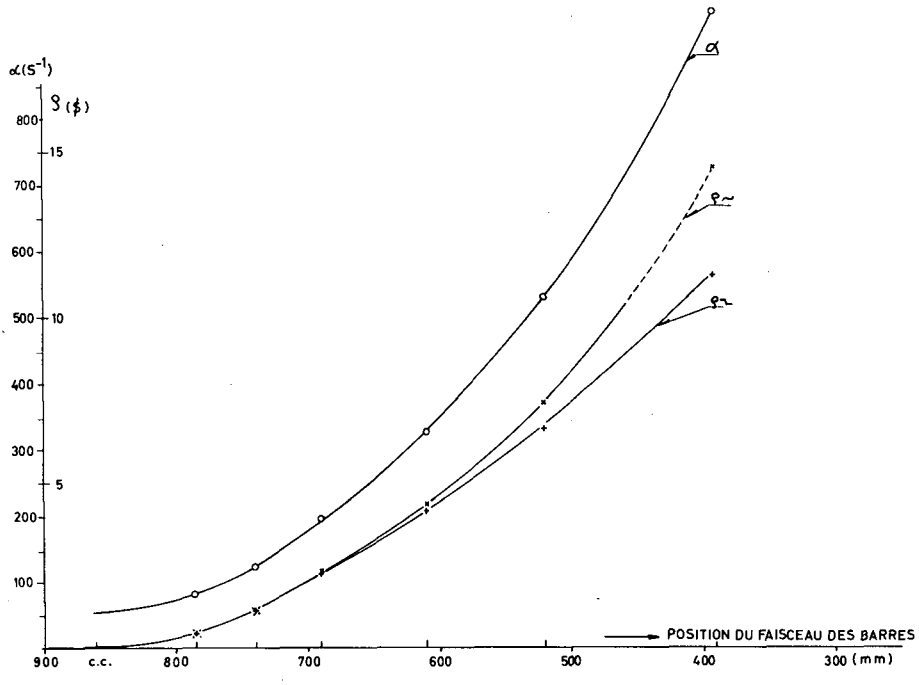


Figure 6

Mesure de l'effet des barres de contrôle suivant divers modes de fonctionnement de la source.

TABLEAU II

RÉSULTATS DE MESURES DANS LE RÉACTEUR BR02; CHARGEMENT ANNULAIRE

Position des barres (mm)	Localisation du détecteur			$\rho_{\lrcorner}$ ($)	$\rho_{\sim}$ ($)	α (s^{-1})	ω (s^{-1})	α_0 (s^{-1})	$10^4 \cdot l$ (s)
	canal	hauteur par rapport au plan médian (mm)							
785	L-0	+360	réflecteur	0,45	0,441	80,9	7,13	56,04	1,32
		+100	piscine N0	0,455	0,446	80,3	7,17		
	L-0	+360	réflecteur	1,13					
740	L-0	± 0	réflecteur		1,127	122,3	7,00	57,4	1,29
		+100	piscine N0	1,125	1,15		7,08		
690	B-0	± 0	noyau	2,28	2,37	196,44	7,31	58,3	1,25
	G-0	+700	piscine	2,44	2,53	196,5	7,09		
	B-180	± 0	noyau	2,89	3,14		7,04		
610	B-0	± 0	noyau	4,15	4,35	326	7,14	60,8	1,18
520	B-0	± 0	noyau	6,62	7,35	530,1	7,13	63,5	1,10
390	B-0	± 0	noyau	11,3	14,5	961	7,13	62,0	1,07

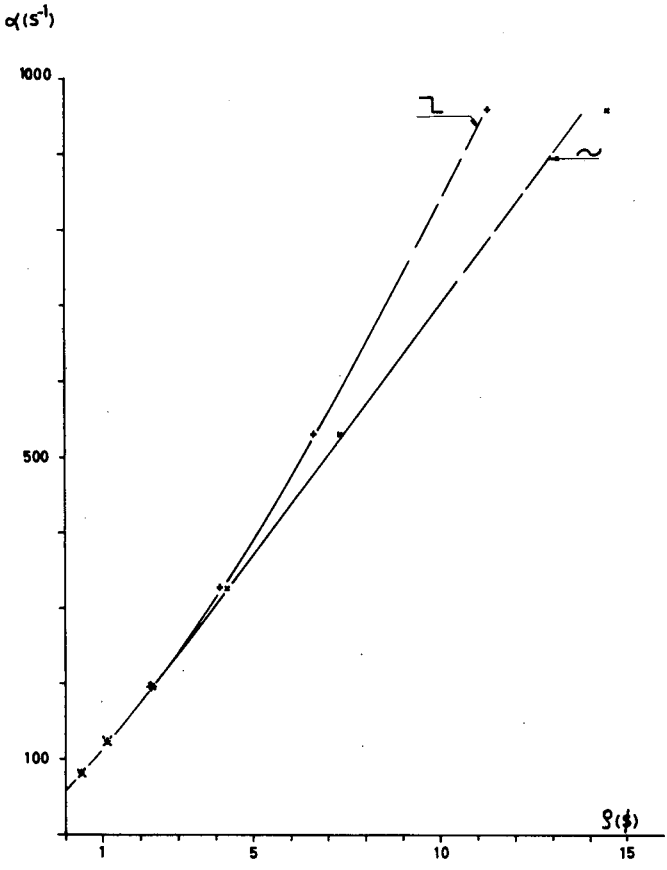


Figure 7

Comparaison des valeurs de réactivité ρ mesurées par variation brusque et par modulation de l'intensité de la source.

En raison de la géométrie particulière du chargement, les conditions de mesure sont difficiles et constituent un test sévère des méthodes utilisées; en effet, tous les éléments combustibles sont voisins des deux régions intérieure et extérieure et chaque élément est directement affecté par les barres de contrôle.

5.2. Tous les éléments étant «périphériques», la fonction de transfert est fortement influencée par le réflecteur. Les courbes de la figure 5 présentent toutes la même caractéristique : aux fréquences élevées, ω étant supérieur à 200 environ, la variation de l'atténuation A des ondes neutroniques est plus importante que la variation escomptée. L'influence des harmoniques ayant un effet opposé, ce résultat ne peut être expliqué que par la présence du réflecteur.

Trois mesures confirment cette hypothèse :

a) Lorsque le détecteur est situé dans l'ombre des barres de contrôle (au-dessus du niveau de leur extrémité inférieure), l'écart constaté est plus faible. La courbe b de la figure 5 représente la fonction de transfert mesurée lorsque les barres sont à la cote 390 mm; l'influence du réflecteur extérieur au point de mesure (canal B-0- plan médian) a été réduite par l'effet des absorbants.

b) La fonction de transfert, pour le même état du réacteur, mesurée dans le canal G-0 du réflecteur montre au contraire un écart plus accusé : courbe c de la figure 5.

c) Une mesure antérieure effectuée dans une configuration de chargement plus importante, entourant également le trou central occupé par un bouchon de béryllium, a donné la courbe d et les résultats indiqués par les signes + voisins de la courbe b; le détecteur était placé dans ce bouchon mais le signal utilisé était du type « square waves»; l'écart est, dans ce cas, assez faible.

Dans le combustible, en B-0, on mesure donc l'effet combiné des réponses du chargement et du réflecteur.

Pour les mesures du temps de vie des neutrons et de l'antiréactivité, cela exclut l'utilisation des fréquences telles que $\omega > 100$. Par contre, cet effet peut être mis à profit pour déterminer l'influence du réflecteur.

5.3. Un détecteur localisé au-dessus de la matrice de béryllium (cote supérieure à 450 mm) est sensible à deux sources modulées : le réacteur et la source elle-même. La modulation $\Delta n/n_0$ est alors la résultante pondérée de deux signaux sinusoïdaux. La mesure de la densité neutronique ne peut être effectuée qu'aux endroits où la contribution directe de la source est faible (tableau II : comparer les résultats, les barres étant placées à 690 mm).

5.4. La présence de la source dans le réacteur sous-critique perturbe la distribution du flux. L'importance des perturbations ou harmoniques d'espace qu'elle induit sont fonction de la fréquence; le temps de décroissance des harmoniques supérieures étant plus court que celui de la fondamentale, le contenu en harmonique est plus important aux fréquences élevées. Aux basses fréquences, ce sont les neutrons retardés qui déterminent principalement le comportement temporel du réacteur.

A la fréquence optimale $\hat{\omega}$, fréquence caractérisée par l'indépendance de $\Delta n/n_0$ vis-à-vis du temps de vie des neutrons prompts et des caractéristiques des neutrons retardés, on peut supposer que la valeur $\Delta n/n_0$ mesurée est assez voisine de la valeur correspondant à la distribution fondamentale.

5.5. Cette hypothèse doit être confirmée. Une vérification expérimentale peut être faite dans une configuration de chargement compacte, en effectuant des mesures en plusieurs endroits caractérisés par des contenus en harmoniques différents. En supposant que le rapport $\Delta n/n_0$, mesuré pour $\omega = \hat{\omega}$, représente bien la modulation de la fondamentale, l'écart entre les valeurs

de ρ mesurées par «step» ou par modulation doit mettre en évidence l'influence des harmoniques dans la technique de mesure par éjection d'une source.

5.6. Les antiréactivités ρ, mesurées à la fréquence optimale $\hat{\omega}$, peuvent être utilisées pour calculer $\alpha_0(\rho)$ au moyen de l'équation (1). En supposant que β reste constant et égal à $7,4 \cdot 10^{-3}$ (ce qui peut impliquer une erreur systématique de quelques pour cent), on peut également calculer le temps de vie $l(\rho)$. Les résultats sont portés en graphique à la figure 8 en fonction de la hauteur des barres de contrôle.

Ni α_0 ni l ne restent constants, comme cela est supposé généralement pour déterminer ρ à partir de valeurs mesurées α, en utilisant une valeur $\alpha_c = \beta/l$ mesurée à la criticalité.

5.7. Les courbes $\alpha_0(\rho)$ et $l(\rho)$, entre 8 et 15 \$ (ou pour les positions des barres inférieures à 500 mm) ne sont définies que par le seul point de mesure à la position 390 mm, assez peu précis : il faut en effet noter que la technique de modulation, pour $\omega = \hat{\omega}$, perd en sensibilité pour les grandes antiréactivités (voir fig. 5); l'erreur totale sur A, quoique inférieure à 0,7%, entraîne une incertitude de 10% sur la valeur de α_0 et l, pour $\rho = 15$ \$.

Les petites antiréactivités sont définies avec la même précision que A lui-même. La distribution statistique des points de mesure permettant de définir A limite inférieurement, en pratique, la gamme de mesure à 0,05 \$.

Une mesure de la réponse modulée à la criticalité n'est pas possible. La valeur de $\alpha_0 = \alpha_c = \beta/l$ à la criticalité a donc été déterminée par extrapolation de la courbe $\alpha_0(\rho)$ jusqu'à $\rho = 0$. La valeur trouvée est $\alpha_0 = 55,8 \pm 0,5\ s^{-1}$.

D'autre part, l'extrapolation de $\alpha(\rho)$ a donné $54,5 \pm 1,5\ s^{-1}$. Pour $\rho < 2,5$ \$, la pente $d\alpha/d\rho$, qui doit être égale à α_c au voisinage de la criticalité, vaut $59,7 \pm 1\ s^{-1}$.

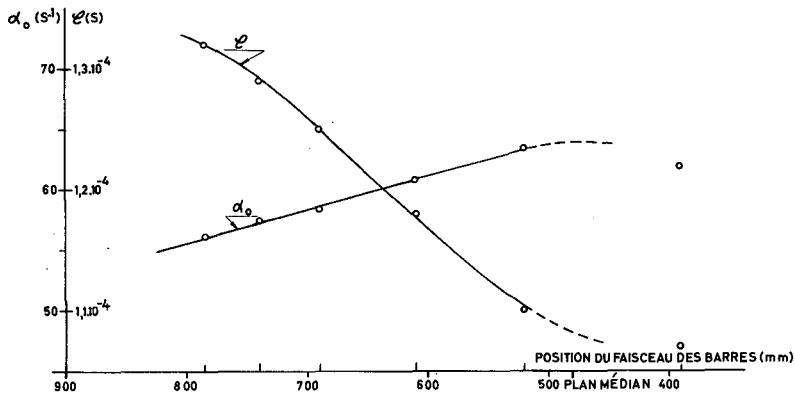


Figure 8

Variation de α_0 et du temps de vie de neutrons prompts l en fonction de la position des barres de contrôle dans BR02 (chargement annulaire).

REMERCIEMENTS

Qu'il me soit permis de remercier ici :

- MM. G. Stiennon et F. Motte de la possibilité qui m'a été donnée de développer la technique d'utilisation d'une source modulée et de l'intérêt qu'ils ont accordé à ce travail;
- MM. J. Debrue et H. Lenders pour les discussions en cours de travail;
- l'équipe d'exploitation du réacteur BR02, le service Réception et le Laboratoire des moyennes activités de BR2 pour leur collaboration sans laquelle la réalisation du programme dans un court délai n'aurait pas été possible.

RÉFÉRENCES

[1] Rapport CEN/SCK-MOL, BLG-59 (1961).

[2] REIFENSCHWEILER, O. et van DORSTEN, A.C., Phys. Verh., Mosbach 8 (1957) 163.

[3] REIFENSCHWEILER, O., Philips Research Reports 16 (1961) 401-18.

[4] ELENGA, C.W. et REIFENSCHWEILER, O., "The generation of neutron pulses and modulated neutron fluxes with sealed-off neutron tubes", ces comptes rendus.

[5] SIMMONS, R.E. et KING, J.S., Nucl. Sci. and Engng 3 (1958) 595-608.

[6] KEEPIN, G.R., WIMETT, T.F. et ZIEGLER, R.K., Phys. Rev. 107 (1957) 1044.

[7] ROTTER, W., Nukleonik 5 (1963) 227-36.

[8] SJÖSTRAND, N.G., "Measurements on a Subcritical Reactor with a Pulsed Neutron Source", Actes 2e Conf. Genève 5 (1956) 52-54.

[9] RAIEVSKI, V. et HOROWITZ, I., Onde élect. 35 (1955) 821-32.

[10] UHRIG, R.E., TID-7619 (1961).

DISCUSSION

(on the foregoing three papers)

R. UHRIG: Figure 1 of Mr. Rotter's paper (SM-62/38) shows the source transfer function and the linearized reactivity transfer function to be different. I would like to point out that this difference is due to his definition of the source transfer function, i.e. both neutron-source variation and neutron-density variation are normalized. If the source transfer function is defined as the ratio of ΔN to ΔS, it is substantially the same as the linearized reactivity transfer function. Furthermore the normalization process used by Mr. Rotter only changes the amplitude and not the frequency dependence. This is very important in slightly subcritical systems where variations of both source and reactivity contribute to the variations of the neutron density.

M. KÜCHLE: How do you intend to overcome the difficulties arising from the higher harmonic modes when using the modulation technique (paper SM-62/87)?

P. GOVAERTS: On theoretical grounds I don't think that these higher harmonic modes should give us much trouble. As for the experimental problem involved, perhaps Mr. Rotter would care to comment? The experiments he has performed are exactly the type we propose as the second version of the area method.

W. ROTTER: There are stationary harmonics in Δn as well as n_0. By always measuring the ratios $\Delta n/n_0$, one eliminates the higher harmonics. This is the advantage of using the normalized transfer function.

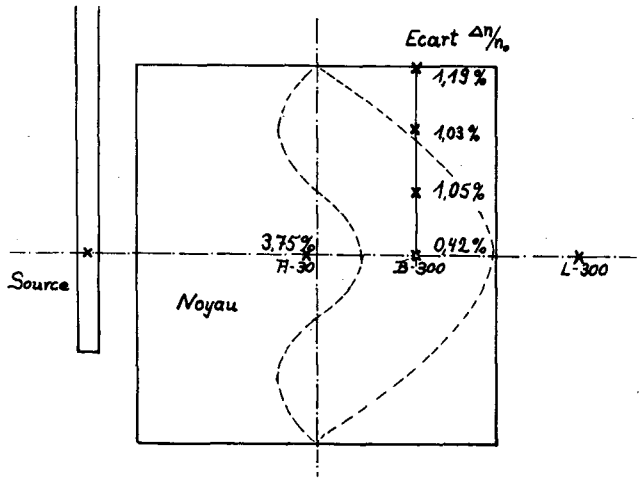
The prompt and the delayed neutron harmonics cannot exhibit different temporal behaviours because the measurements are made at $\omega \approx \Omega$. The only harmonics effect which remains is hidden in the k_{eff}. Since they have a different k, the harmonics are liable to distort the value of "ρ" (anti-reactivity). This effect must not be too big.

An experimental study – involving a symmetrical core configuration with 26 fuel elements – has shown the harmonics effect to be very small. The following diagram gives the variation in $\Delta n/n_0$ at different measured points. Although n_0 exhibits a considerable divergence (~9%) in comparison with the distribution of the neutron flux at criticality, the value of $\Delta n/n_0$ measured in the core (at B-300) at a different height varies no more than 0.8% as compared with the values measured at L-300 (reflector).

The direct contribution of the source can be seen, however, if the distance between the detector and the source is reduced.

F. STORRER (Chairman): I should like to add that the measurement of reactivity by the modulated technique is based on the determination of the ratio of the responses to two neighbouring frequencies: a zero frequency and a frequency of a few cycles per second. Thus practically the same space and energy eigenfunctions are excited by the two frequencies. Actually a modulation of a few cycles per second corresponds to a static experiment for prompt neutrons.

M. KÜCHLE: In connection with paper SM-62/26 I should like to point out that the rough agreement between the stationary and pulsed reactivity determinations in SUAK indicates that the β_{eff} cannot be as bad as it would



Variation in $\Delta n/n_0$ at different measured points

have to be in order to account for the discrepancies mentioned by Mr. Weale. As Mr. Weale has pointed out, another source of error is probably involved.

E. GARELIS: In connection with this same paper, it seems to me that the extrapolation of the α/reactivity curve is meaningful. Part of the difficulty is the method used to compute the reactivity. The reactivity is not a unique function and hence I do not believe that it is valid to make this extrapolation, which strongly depends upon the values of the reactivity in the higher subcritical range. Would you care to comment?

J.W. WEALE: Within the range from delayed critical to 1% or 2% subcritical, we achieve subcriticality by moving out one or two fuel elements at the edge of the core. These elements are used as control elements, calibrated by measuring the reactor asymptotic period for various settings. There may be some doubt about the reactivity scale for the very subcritical systems where a number of fuel elements have been removed from the core altogether. However, we consider that, at least down to 2% subcritical, the reactivity scale established by removing a few per cent of the fuel from the core-edge region is a well-defined one. The extrapolation intercepts are accurately fixed by the results obtained in the reactivity range between critical and -2%.

W. MANSFIELD: I was interested to hear Dr. Weale's comments on the time dependence of the neutron spectrum in VERA. Experiments we have performed on far subcritical assemblies of water and uranium have shown that several hundred microseconds are required before a constant cadmium ratio is obtained. This imposes limitations on the techniques for these far subcritical systems.

O. REIFENSCHWEILER: It would be useful to know what particular frequency range is of maximum interest to the reactor-modulating experts. My own particular field is modulated neutron output generation and this question is obviously of some importance for my work. As was pointed out in our paper (SM-62/9), we have developed a neutron generator with a sealed-

off neutron tube, which can generate sinusoidally-modulated neutron yields in the frequency range 1 - 1000 Hz. The tube can however also generate higher frequencies – I think at least up to 10^5 Hz. It is only a question of making a suitable electronic regulating system for higher frequencies. Of course different amplifiers can be used for different frequency ranges, and frequencies lower than 1 Hz are possible.

R. UHRIG: We have operated our Texas Nuclear Neutron Source at frequencies up to 1450 Hz. The limitation in frequency is due to the use of a 5000-Hz carrier frequency to transmit the sinusoidal input signal to the head (high-voltage) end of the accelerator. We have some evidence that frequencies as high as 10 000 Hz, perhaps even higher, might be useful in light-water-moderated systems.

P. GOVAERTS: Frequencies of interest for fast systems are in the range $\omega = 10^4$ to 10^7 rad/s, depending on the system. A modulated electrostatic accelerator is envisaged as the modulation source (see paper SM-62/85). If necessary the fast-source reactor harmonic could be used as an amplifier (lifetime: 2×10^{-8} s).

W. BARNES: I have a general question on the design of sealed-off neutron sources. Given the basic configuration of a sealed neutron source, it is possible to produce a source in which cables emerge from both ends; alternatively, by increasing the overall diameter, one can make all cables and feeders emerge from one end. Which configuration is the most useful – a long slim source with double-ended connections or a shorter source of larger diameter with single-ended connections?

W. ROTTER: The design of the neutron tube is a matter of secondary importance as far as we are concerned. All we need is a tube that fits into the reactor and works properly. We use our source (Philips) in two reactors possessing channels with diameters of ~84 and 81 mm. We are satisfied if the source and the feed cables are thin enough to fit into the shielding (stainless-steel tube, external diameter of 80 mm).

PULSED SOURCE AND NOISE MEASUREMENTS ON THE STARK REACTOR AT KARLSRUHE*

M. EDELMANN, G. KUSSMAUL, H. MEISTER,
D. STEGEMANN AND W. VÄTH
KERNFORSCHUNGSZENTRUM KARLSRUHE,
FEDERAL REPUBLIC OF GERMANY

Abstract — Résumé — Аннотация — Resumen

PULSED SOURCE AND NOISE MEASUREMENTS ON THE STARK REACTOR AT KARLSRUHE. The STARK reactor is a modified Argonaut-type reactor in which the inner graphite reflector is replaced by a fast core zone. The fast zone, however, is filled with natural uranium for these investigations. The main purpose of this paper is to compare the results for neutron lifetime and reactivity worth of control plates obtained by different techniques under the same loading conditions. Pulsed neutron experiments have been performed in the reactivity range from delayed critical to -8 $ subcritical. The neutron lifetime has been derived from measurements at delayed critical. Reactivity worths of control plates were obtained by two different evaluation methods: (1) comparison of the fundamental mode decay constant α with the value α_c at delayed critical; (2) evaluation of the ratio of the time integrals of prompt and delayed neutron fractions. Comparison of both methods shows that space-dependent effects caused by the outer graphite reflector have to be taken into consideration. Neutron lifetime and reactivity values from delayed critical to about -2 $ have also been determined by three types of statistical methods: the analysis of the power spectral density, the Rossi-α technique, and the measurement of variance over mean. Reactivity worths of the control plates were also obtained from conventional rod drop experiments, and from a digital method based on the analysis of the flux variation with time caused by the continuous withdrawal of a plate from the critical reactor. The results of the different methods are compared. The specific features as well as the advantages and disadvantages of these methods are discussed.

MESURES EFFECTUÉES AU MOYEN DE LA SOURCE DE NEUTRONS PULSÉS ET DU BRUIT, DANS LE RÉACTEUR STARK A KARLSRUHE. Le réacteur STARK est un réacteur du type Argonaute modifié dans lequel le réflecteur intérieur en graphite a été remplacé par une zone à neutrons rapides. Toutefois, pour ces recherches, cette zone est remplie d'uranium naturel. Le mémoire a essentiellement pour objet de comparer les résultats obtenus pour la durée de vie des neutrons et l'antiréactivité des plaques de commande à l'aide de différentes techniques dans le mêmes conditions de charge. Les expériences au moyen des neutrons pulsés ont été effectuées sur les réactivités de milieux critiques retardés et sous-critiques jusqu'à -8 dollars. La durée de vie des neutrons a été déduite de mesures effectuées sur un milieu critique retardé. Deux méthodes différentes ont été utilisées pour évaluer l'antiréactivité des plaques de commande: a) comparaison entre la constante de décroissance pour le mode fondamental α et la valeur α_c pour le milieu critique retardé; 2) évaluation du rapport entre les intégrales en temps des fractions de neutrons instantanés et retardés. La comparaison entre ces deux méthodes montre qu'il faut tenir compte des effets, variables dans l'espace, dus au réflecteur extérieur en graphite. Les valeurs de la durée de vie des neutrons et de la réactivité pour des milieux critiques retardés et sous-critiques jusqu'à -2 dollars environ, ont également été déterminées au moyen de méthodes statistiques de trois types: analyse de la densité spectrale, technique α de Rossi et mesure de la variance. On a également calculé l'antiréactivité des plaques de commande au moyen d'expériences classiques de chute des barres et d'une méthode numérique fondée sur l'analyse de la variation du flux en fonction du temps lorsqu'on retire progressivement une plaque du réacteur critique. Les auteurs comparent les résultats de ces différentes méthodes et discutent leurs particularités ainsi que leurs avantages et leurs inconvénients.

ИЗМЕРЕНИЕ С ПОМОЩЬЮ ИМПУЛЬСНОГО ИСТОЧНИКА И "ШУМОВ" НА РЕАКТОРЕ "ШТАРК" В КАРЛСРУЭ. Реактор "Штарк" является модифицированным типом реактора "Аргонавт", где внутренний графитовый отражатель заменен активной зоной на быстрых нейтронах. Зона на быстрых нейтронах, однако, использует природный уран для данных исследований. Основная цель настоящего доклада состоит в сравнении результатов измерения

* The work was performed within the scope of the Fast Breeder Project-Association, Karlsruhe-Euratom.

времени жизни нейтронов и компенсирующей способности регулирующих пластин, полученных различными методами в одинаковых условиях загрузки. Эксперименты с импульсными нейтронами проводили в интервале реактивности от критической на запаздывающих нейтронах до подкритической 8 долларов. Время жизни нейтронов было получено в результате измерений, проводившихся при запаздывающей критической реактивности. Реактивные способности регулирующих пластин получались двумя различными методами оценки: 1) сравнением постоянной распада α основного состояния с величиной α_c при критичности на запаздывающих нейтронах; 2) оценка соотношения временных интегралов доли мгновенных и запаздывающих нейтронов. Сравнение обоих методов показывает, что эффекты пространственной зависимости благодаря внешнему графитовому отражателю должны приниматься во внимание. Время жизни нейтронов и величины реактивности, полученные в интервале от критичности на запаздывающих нейтронах до подкритичности 2 доллара, также определялись тремя различными статистическими методами: анализом спектра энерговыделения, методом Росси-α и измерением отклонения от среднего значения. Реактивные способности регулирующих пластин получались также из обычных экспериментов с падением стержней, а также при помощи цифрового метода, основанного на анализе изменения потока со временем благодаря непрерывному поднятию пластины из критического реактора. Сравниваются результаты различных методов. Обсуждаются специфические особенности, а также преимущества и недостатки этих методов.

EXPERIMENTOS CON FUENTES PULSADAS Y MEDICIONES DEL RUIDO DEL REACTOR STARK DE KARLSRUHE. El reactor Stark es un Argonaut que se ha modificado sustituyendo el reflector interior de grafito por una zona central de neutrones rápidos. Esta zona se llena de uranio natural para las investigaciones descritas en la presente memoria en la que se comparan los resultados relativos a la vida media de los neutrones y a los valores de reactividad de las placas de control, obtenidos con técnicas diferentes en las mismas condiciones de carga. Los experimentos con neutrones pulsados se han efectuado en una gama de valores de reactividad comprendida entre la crítica por neutrones retardados y la subcrítica (-8 dólares). La vida media de los neutrones se ha deducido de valores medidos en estado crítico por neutrones retardados. Los valores de reactividad de las placas de control se obtuvieron por dos métodos de evaluación: a) comparando la constante de decrecimiento del modo fundamental α con el valor α_c en estado crítico por neutrones retardados; b) evaluando la razón de las integrales de tiempo de la fracción de neutrones inmediatos a la de neutrones retardados. La comparación de ambos métodos pone de manifiesto que hay que tomar en consideración los efectos de dependencia espacial debidos al reflector exterior de grafito. Igualmente, los autores han determinado la vida media de los neutrones y los valores de reactividad, desde la crítica por neutrones retardados y -2 dólares aproximadamente, utilizando tres métodos estadísticos: el análisis de la distribución espectral de la potencia específica, la técnica de Rossi-α y la medición de la variancia con respecto al término medio. Asimismo, obtuvieron los valores de la reactividad de las placas de control mediante el experimento tradicional de descenso de las barras y con un método numérico basado en el análisis de las variaciones temporales del flujo, obtenidas al retirar de modo continuo una placa en un reactor crítico. Los autores comparan los resultados logrados con los distintos métodos, examinando sus características y sus ventajas e inconvenientes.

1. INTRODUCTION

For the determination of kinetic reactor physics parameters, such as the prompt neutron decay constant α, the neutron generation time and related quantities, different experimental methods can be applied. The pulsed neutron source technique and the analysis of statistical phenomena caused by branching processes in neutron chains within the reactor are the most powerful tools for these investigations. It was therefore decided early to look into both possibilities, to have the best approach for the determination of reactor parameters, particularly in the Fast Zero Power Assembly SNEAK and the Fast Thermal Argonaut Reactor STARK. The main purpose of the experiments reported in this paper was to obtain a comparison of results which were measured under exactly the same loading and reactivity conditions in STARK, first by the pulsed neutron source technique and then by three dif-

ferent statistical methods, i.e. the Rossi-α experiment, the analysis of counting statistics and the frequency analysis of noise. Although the results are specific for this particular reactor system, the comparison should give some insight into the general problems and limitations of the different techniques.

2. DESCRIPTION OF THE SYSTEM

The STARK reactor was designed as a coupled fast-thermal zero-power reactor. A detailed description of the assembly and a discussion of its safety features have been given previously [1].

Basically, the reactor consists of a cylindrical fast core (37-cm average diameter, 61-cm height) which is surrounded by an annular Argonaut-type thermal driver zone and a large graphite reflector. As shown in Fig. 1, the fast core is an array of 37 vertical stainless steel matrix tubes filled with the core materials to be investigated. The fast core is enclosed in a natural uranium buffer zone of 5 cm average thickness to absorb thermal neutrons incident from the outside.

The present investigations were carried out on the first loading of STARK in which the central zone was filled with natural uranium metal. The thermal zone contained 364 Argonaut fuel plates (U^{235}-content = 7.58 kg) arranged in 24 groups with a plate spacing of 6.2 mm. The moderator was light water at 79°C.

According to fission chamber traverses, only about 1% of the reactor power is produced by fast fissions in the natural uranium zone so that the reactor can be considered essentially as a thermal system. Actually, the central zone causes a strong decoupling of opposite portions of the annular thermal core.

The control system of the reactor consists of 12 cadmium-plate control units of equal size, evenly distributed around the thermal core. Three of them (R_1, R_2, and R_3) are normally used as fine control plates, the others as safety plates (Fig. 1). For these experiments, however, the plate S_3^3 was used to adjust criticality with all other plates fully withdrawn. Hence, various subcritical states (Fig. 1) were obtained by inserting groups of control plates while S_3^3 was kept in its original position.

The location of the neutron detectors (BF_3 counters, boron chambers, and a U^{235} fission chamber) used for the various experiments is also shown in Fig. 1. Since the flux distribution in the annular core was known to be very sensitive to small loading changes, the detectors were always kept in their positions and no changes were made from one experiment to the other.

3. PULSED SOURCE EXPERIMENTS

3.1. Methods

Three different evaluation techniques have been described in the literature to determine reactivity ρ and prompt-neutron generation time Λ of a multiplying system from a pulsed source experiment. All of them are based on the observation of the neutron density n(t) as a function of time resulting

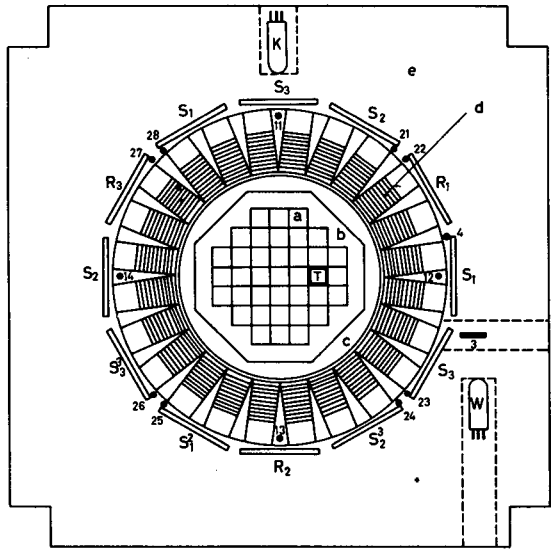


Fig. 1

Schematic cross-section of STARK with detector positions

a - fast core, b - natural uranium casing, c - graphite region
d - thermal Argonaut core, e - graphite reflector
R – fine control plates, S - safety plates, T - safety rod of fast core ● and ▬ BF_3-proportional counters, ⊛ U^{235}-fission chamber ⊂≡ B^{10}-γ-compensated ionization chamber

Description of reactor configurations investigated

Conf. No.	Position of control and safety plates	Conf. No.	Position of control and safety plates
I	delayed critical [1]	VI	R_3 in [1]
II	R_2 on 35 cm [1]	VII	S_1^2, R_2, and S_2^3 in [1]
III	R_2 on 20 cm [1]	VIII	R_1, R_2, and R_3 in [1]
IV	R_2 in [1]	IX	all S_1 and S_2 in [1]
V	R_1 in [1]	X	all plates in

Plate positions go from 0 (in) to 47 cm (out).
[1] All other plates out except S_3^3 which is in critical pos. 30.7 cm.

from the injection of a periodic sequence of neutron bursts. As is well known, n(t) is composed of an exponential decay of the prompt eigenfunction, $n_p(t)$, followed by a slowly varying delayed neutron part $n_d(t)$ which is usually assumed to be time-independent, $n_d(t) \approx n_d(0)$ within a cycle $(0 < t < T)$. Thus, for the fundamental mode one has

$$n(t) = n_p(t) + n_d(t) = A\, e^{-\alpha t} + n_d(t) \quad . \qquad (3.1)$$

(1) The first method [2] makes use of the prompt part only, $n_p(t)$, from which the prompt-neutron decay constant

$$\alpha = \frac{\beta}{\Lambda}\left(1 - \frac{\rho}{\beta}\right) \tag{3.2}$$

is derived. Hence, the reactivity ρ/β can be determined, either using calculated values of Λ and β, or the decay constant $\alpha_c = \beta/\Lambda_c$ measured at delayed critical and assuming Λ to be independent of ρ

$$-\rho/\beta = \alpha/\alpha_c - 1 \tag{3.3}$$

(2) SJÖSTRAND [3] and GOZANI [4] have shown that for an unreflected system

$$-\rho/\beta = \bar{n}_p/\bar{n}_d \tag{3.4}$$

where $\bar{n}_p$, $\bar{n}_d$ are the time-averaged quantities $n_p(t)$ and $n_d(t)$. Combining Eqs. (3.2) and (3.4) one finds

$$\beta/\Lambda = \frac{\alpha}{1 + \bar{n}_p/\bar{n}_d} \tag{3.5}$$

from which the generation time Λ can be derived.

(3) The third method developed by GARELIS and RUSSELL [5-7] allows one to determine $\gamma = \beta/\Lambda$ from $n_p(t)$ and $n_d(t)$ using the equation

$$\int_0^T n_p(t)\left[e^{\gamma t} - 1\right] dt = \int_0^T n_d(t)\, dt \tag{3.6}$$

(T = cycle length) which has been derived from a one-group model for an unreflected system. Equation (3.6) is also valid for mixtures of eigenfunctions if Λ is independent of ρ.

Method (3) was originally derived for a constant delayed-neutron density, $n_d(t) = \text{const}$. For measurements on thermal systems close to delayed critical, however, the variation of $n_d(t)$, which is caused by the build-up of precursors during the decay of $n_p(t)$, becomes important and the question arises how to split $n(t)$ into prompt and delayed parts. We define $n_p(t)$ and $n_d(t)$ in accordance with the usual space-independent kinetic equations [8] by

$$\begin{aligned}
&\frac{\rho-\beta}{\Lambda} n_p + q\,\delta(t) = \frac{dn_p}{dt} \\
&\frac{\rho-\beta}{\Lambda} n_d + \sum_{i=1}^{6} \lambda_i C_i = \frac{dn_d}{dt} \\
&\frac{\beta_i}{\Lambda}(n_p + n_d) - \lambda_i C_i = \frac{dC_i}{dt} \qquad (i = 1, \ldots 6)\,.
\end{aligned} \tag{3.7}$$

Equation (3.4) is valid only with this definition of n_p and n_d. This can be shown by integrating Eq. (3.7) over a cycle ($0 < t < T$). Also Eq. (3.6) holds as a consequence of Eqs. (3.2) and (3.4).

For the evaluation of the experimental decay curves, with $\rho < 0$, an approximate expression for $n_d(t)$ has been derived by an iteration process. By starting with $n(t) = n_p(0)\, e^{-\alpha t} + b$ as a first guess and using

$$C_i(t) = \frac{\beta_i}{\Lambda} \int_{-\infty}^{t} n(t')\, e^{-\lambda_i (t-t')}\, dt' , \qquad (3.8)$$

and

$$n_d(t) = \sum_{i=1}^{6} \lambda_i \int_{-\infty}^{t} C_i(t')\, e^{-\alpha (t-t')}\, dt' \qquad (3.8)$$

which follows from Eq. (3.7), we finally arrive at

$$n_d(t) = n_d(o) + n_p(o)\, \frac{\alpha_c \bar{\lambda}}{\alpha^2} \left[\left(1 - \frac{t}{T}\right) - (1 + \alpha t)\, e^{-\alpha t} \right] \qquad (3.9)$$

and

$$\bar{n}_d = n_d(o) \left[1 - \frac{1}{2} \frac{\rho}{\beta - \rho} \bar{\lambda} \cdot T \right], \qquad \bar{\lambda} = \sum_{i=1}^{6} \beta_i \lambda_i / \beta . \qquad (3.10)$$

These are valid for $\lambda_i \ll \alpha$ and $\lambda_i T \ll 1$. These equations allow the calculation of $n_d(t)$ and $\bar{n}_d$ from the value $n_d(T) = n_d(0)$, which is measured by the background channel of the time analyser.

3.2. Experiments

A number of systems with different control plate configurations (Fig. 1), ranging in reactivity from delayed critical down to -8$ subcritical, have been investigated by the pulsed source technique using the three different evaluation techniques outlined in section 3.1.

A compact 100-keV deuteron accelerator with duoplasmatron ion-source [9] was used as a pulsed neutron generator. The unit was fed through the central hole of the top shield of the reactor so that the tritium target was located on top of the natural uranium zone. BF_3 counters as neutron detectors were placed in three different radial positions (Fig. 1): in the graphite wedge between the fuel plates of the thermal core (Pos. 12), in the graphite reflector (Pos. 3), and in the air gap between core and reflector (Pos. 24).

The decay of the neutron intensity n(t) following each neutron burst (pulse width 10 or 20 μs) was measured with a 256-channel analyser (TMC, Model CN-110) with pulsed neutron input unit. The pulsed source was synchronized with the analyser in such a way that the first channel opened at the time when the neutron burst was injected. The repetition rate $f = 1/T$ of the source

was chosen low enough that the contribution of prompt neutrons to the background data, which were taken at the very end of each cycle, was negligibly small.

All measurements on subcritical systems were done under stationary-state conditions. To saturate the delayed neutron density $n_d(t)$, the pulsed source was kept in operation at constant intensity for 5 to 10 min before actual data were taken. The background data contained, in addition to the delayed neutrons, the effect of the spontaneous fission sources in the natural uranium. This effect was determined in a separate run without pulsed source and subtracted.

For an evaluation of the prompt-neutron decay $n_p(t)$, the slowly varying delayed part $n_d(t)$ was subtracted from the data. As a first approximation $n_d(t)$ was assumed to be a time-independent background given by the neutron intensity at the end of the cycle, $n_d(t) = n(T)$. This treatment was adequate for all subcritical measurements below -0.5\$. For the measurements closer to delayed critical the delayed neutron build-up during the decay of the prompt part given by Eq. (3.9) was taken into account

$$n_p(t) = \frac{n(t) - n_d(o)}{1 + F(\alpha, t)} \quad , \quad F(\alpha,T) = \frac{\alpha_c \bar{\lambda}}{\alpha^2} \left[\left(1 - \frac{t}{T}\right) e^{\alpha t} - (1+\alpha t) \right] \tag{3.11}$$

Figure 2 shows the effect of this second-order correction on the prompt-neutron decay curve at delayed critical. The decay constant was obtained by fitting an exponential function $e^{-\alpha t}$ to the later part of the curve $n_p(t)$, where contributions of higher modes are negligible. The α-values found in the three detector positions are listed in Table I.

The ratio of the average prompt and delayed neutron intensities, $\bar{n}_p/\bar{n}_d$, was also derived from the decay curves. The quantity $\bar{n}_p$ was found by extrapolating the fundamental mode decay back to $t = 0$, assuming zero slowing-down time. From the extrapolated value $n_0 = n_p(t = 0)$ one finds $\bar{n}_p = n_0/\alpha T$. The delayed neutron part $\bar{n}_d$ was obtained from the neutron intensity at the end of the cycle, $n(T) = n_d(T)$, using Eq. (3.10). Contributions of higher modes to $\bar{n}_d$, which are expected to be small near delayed critical, cannot be eliminated with this technique.

Finally, the quantity $\gamma = \beta/\Lambda$ was determined by the method of Garelis and Russell, Eq. (3.6). A Fortran code was written to evaluate the integral of the left-hand side in Eq. (3.6) as a function of γ from the experimental data $n_p(t)$ and $n_d(t)$, and the quantity $\gamma = \beta/\Lambda$ was sought for which Eq. (3.6) is fulfilled.

For measurements of the prompt-neutron decay at delayed critical, the following procedure was adopted to keep the delayed neutron background at a reasonably low level ($\approx 0.3 \times n_p(0)$): Starting from a reactor power of $\approx$ 1 mW a sequence of only 150 source pulses was injected ($f = 2$ to 5 s^{-1}) during which the delayed neutron intensity rose in a stepwise manner. Afterwards, the reactor power was brought down again to 1 mW by inserting a control plate, and the procedure was repeated several times to get a good statistical accuracy.

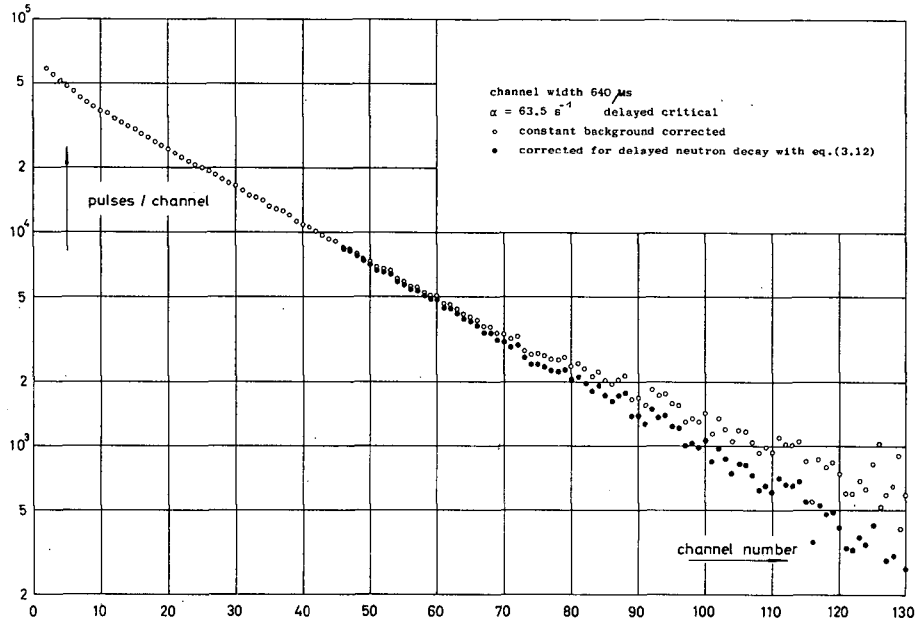


Fig. 2

Decay curve for configuration I, Position 12

channel width 640 μs

α = 63.5 s^{-1}, delayed critical
○ = constant background corrected
● = corrected for delayed neutron decay with Eq. (3.12).

Corrections for the delayed neutron build-up were made on the basis of Eq. (3.11) but using a somewhat different correction factor for the non-stationary case (cf. Fig. 2):

$$F(\alpha, T) = \frac{\bar{\lambda}}{\alpha_c} \left[(1 + b \cdot t)\, e^{\alpha t} - (1 + \alpha t) \right] . \qquad (3.12)$$

For most cases the constant b, which is a function of cycle length T, number of bursts injected and the strength of internal sources, was found by a fit to the background data to be zero, within experimental error.

3.3. Results

Table I gives the experimental results for the decay constant α and the ratio $\bar{n}_p/\bar{n}_d$. The quantity $\gamma = \beta/\Lambda$ as obtained from Eq. (3.6) by the method of Garelis and Russell for the various control plate configurations is given in Table II.

The α-values found with the three detector positions are in good agreement, showing that the effects of higher modes have been properly eliminated.

TABLE I

EXPERIMENTAL RESULTS FOR DECAY CONSTANT α, REACTIVITY $(\rho/\beta)_s$, AND THE RATIO $\bar{n}_p/\bar{n}_d$

	α	α	α	$\alpha_{av.}$	$\alpha/\alpha_c - 1$	$-(\rho/\beta)_s$	$\bar{n}_p/\bar{n}_d$	$\bar{n}_p/\bar{n}_d$	$\bar{n}_p/\bar{n}_d$
Detector position (cf. fig.1)	(12)	(24)	(3)				(12)	(24)	(3)
Control plate configuration (cf.fig.1)	$[sec^{-1}]$	$[sec^{-1}]$	$[sec^{-1}]$	$[sec^{-1}]$	[%]	[%]	[%]	[%]	[%]
Delayed critical I	63.5		62.3	62.9±1.5					
R_2 : 35.0 cm II	69.0		69.5	69.2±1.5	0.100	0.085	0.093		0.100
R_2 : 20.0 cm III	85.4		85.2	85.3±1.5	0.356	0.332	0.336		0.361
R_2 in IV	100.8		101.3	101.0±1.5	0.61	0.64	0.60		0.66
R_1 in V	100.8		101.0	100.9±1.5	0.60	0.63	0.54		0.61
R_3 in VI	102.1		102.1	102.1±1.5	0.62	0.63	0.57		0.65
S_1^2, R_2, S_2^3 in VII	136.4	137.6	134.9	136.3±2	1.17		1.16	1.16	1.31
R_1, R_2, R_3 in VIII	192	194	195	194 +3	2.08	2.50	1.59	1.82	2.08
S_1, S_2 in IX	357	367	360	360 ±8	4.72	5.2	3.26	3.74	4.87
S_1, S_2, S_3, R in X	569	591	577	576 ±15	8.16	12	4.46	6.12	10.1

TABLE II

EXPERIMENTAL RESULTS FOR β/Λ FOUND FROM EQ. (3.5) AND (3.6)

	β/Λ from eq.(3.5)			$\beta/\Lambda = \gamma$ from eq.(3.6)		
Detector position (cf.fig.1)	(12)	(24)	(3)	(12)	(24)	(3)
Control plate configuration (cf.fig.1)	$[\mathrm{sec}^{-1}]$	$[\mathrm{sec}^{-1}]$	$[\mathrm{sec}^{-1}]$	$[\mathrm{sec}^{-1}]$	$[\mathrm{sec}^{-1}]$	$[\mathrm{sec}^{-1}]$
R_2 : 35.0 cm II	60.0		59.9	61.1		61.1
R_2 : 20.0 cm III	63.0		62.2	62.3		61.7
R_2 in IV	63.0		61.2	62.3		60.1
R_1 in V	65.2		62.7	64.5		62.2
R_3 in VI	65.2		61.8	64.2		62.0
S_1^2, R_2, S_2^3 in VII	65.2	62.4	59.9	61.7	60.6	57.4
R_1, R_2, R_3 in VIII	74.1	68.8	63.4	72.2	66.6	61.0
S_1, S_2 in IX	83.6	77.5	61.4	79.5	78.2	58.3
S_1, S_2, S_3, R in X	106.4	83.1	52.0	91.3	77.8	50.4

From the decay constant $\alpha_c = \beta/\Lambda_c = 62.9 \pm 1.5\ s^{-1}$ and the calculated value $\beta = 0.00749$, a generation time $\Lambda_c = 1.19 \times 10^{-4}$ s was found at delayed critical.

The reactivity ρ/β of the various configurations was derived from α on the basis of Eq. (3.2) assuming a generation time $\Lambda = \Lambda_c$ independent of ρ. Table I compares this value $-\rho/\beta = \alpha/\alpha_c - 1$ with the reactivity $-(\rho/\beta)_s$ found by "rod-drop" and "continuous-run" techniques [10] where the variation of neutron intensity n(t) resulting from a stepwise or continuous insertion of control plates into the critical reactor was measured with a boron chamber and analysed by a digital code which calculates ρ/β as a function of time, i.e. of control plate position. The change in neutron flux observed in these methods is relatively slow, so that $(\rho/\beta)_s$ is expected to be close to the static reactivity. Except for the far subcritical systems ($\rho/\beta \lesssim -2$ \$) where effects of local control plate shadowing may be present, the $(\rho/\beta)_s$ values were expected to be very reliable. The pulsed source values $-\rho/\beta = \alpha/\alpha_c - 1$ are found to be somewhat lower than $-(\rho/\beta)_s$, even near delayed critical, which might indicate that Λ increases slightly with $-\rho/\beta$ rather than being a constant.

A comparison was also made for $\bar{n}_p/\bar{n}_d$, the ratio of prompt and delayed neutron intensities which would equal $-\rho/\beta$, according to Eq. (3.4), if the point reactor model were applicable. As a matter of fact, $\bar{n}_p/\bar{n}_d$ turned out to be strongly dependent on the detector position. That is, for each configuration the ratio $\bar{n}_p/\bar{n}_d$ increases as one proceeds with the detector from the core to the reflector.

This space-dependence of $\bar{n}_p/\bar{n}_d$ is a direct consequence of the different shapes of the static and the dynamic eigenfunctions, i.e. the non-separability of time and space variables, and shows the breakdown of the space-independent model for systems with large reflectors.

A similar behaviour is found for the quantity $\beta/\Lambda = \alpha\,(1+\bar{n}_p/\bar{n}_d)^{-1}$ which was derived from the experimental values α and $\bar{n}_p/\bar{n}_d$. Table II gives a comparison of this quantity with the value $\gamma = \beta/\Lambda$ found by the method of Garelis and Russell, Eq. (3.6). Except for minor deviations from the (positive) contribution of higher modes to $\bar{n}_d$, both methods give the same dependence of β/Λ on the detector position. For $\rho/\beta \to 0$ the β/Λ-values approach $\alpha_c = \beta/\Lambda_c$ as expected (Fig. 3).

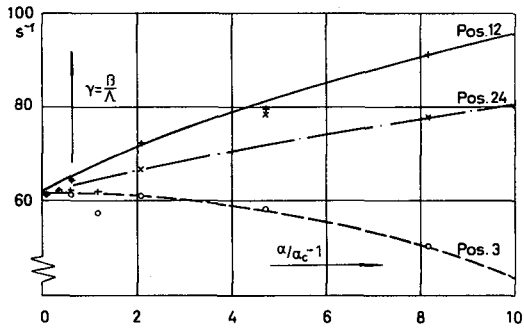


Fig. 3

γ versus $\alpha/\alpha_c - 1$ for different detector positions

The quantity $\alpha/\gamma - 1$, which would be equal to $-\rho/\beta$ for the point reactor model, is shown in Fig. 4 as a function of $\alpha/\alpha_c - 1$. Deviations in $\alpha/\gamma - 1$ for the various detector positions are increasing with $\alpha/\alpha_c - 1$ up to values as high as 50% at -8 $.

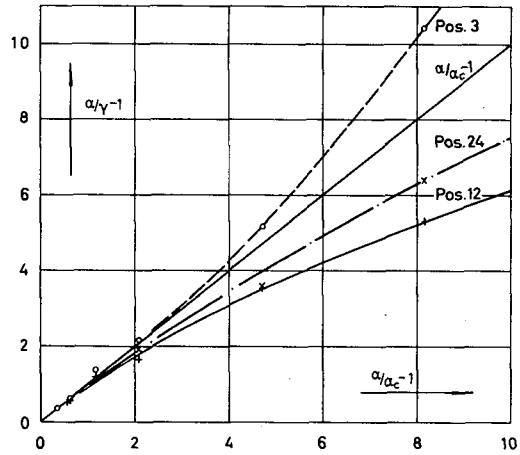


Fig. 4

$\alpha/\gamma - 1$ versus $\alpha/\alpha_c - 1$ for different detector positions

The question arises whether detector and source positions can be found in a reflected system such that the kinetic behaviour of n(t) corresponds to that of a point reactor. This question can only be answered, a priori, by detailed calculations of the static and dynamic eigenfunctions for a particular system. However, it can be shown from reactor theory that Eq. (3.4) remains valid for reflected systems for a detector distribution proportional to $\nu\Sigma_f\, n_s^+$, where n_s^+ is the adjoint density of the static problem.

These investigations have shown that the methods based on the point-reactor model to determine ρ/β from the prompt and delayed neutron intensities are of little use for systems like STARK with a small core and a large graphite reflector. On the other hand, no serious problems were encountered in measuring the prompt-neutron decay in such systems by the pulsed neutron technique.

The results found from the pulsed source experiments are compared to those of the other methods in Table VI.

4. STATISTICAL EXPERIMENTS

Information on reactor parameters which describe the neutronic behaviour of a zero-power reactor can be gained from a detailed analysis of the statistical fluctuations in detector signals. The common basis of all these experiments is the observation of correlated reaction processes caused by branching

events occurring in neutron chain reacting systems. A number of papers have been published [11-22] in which different theoretical models and techniques of analysing the fluctuating signals are discussed. Recently a common theoretical basis has been developed for neutronic noise analysis experiments [23] from which the fundamental equations for the experiments described in the following sections have been derived.

4.1. Rossi-α experiment

In this experiment correlated detector events caused by neutrons from the same chains are directly observed in a stationary reactor.

In the point reactor model approximation the fundamental equation to calculate the correlation function for a Rossi-α experiment performed with two absorption detectors is given by

$$c(\tau)\,\Delta\tau = \left[A\, e^{-\alpha\tau} + B_2\right]\Delta\tau \qquad (4.1.1)$$

with $\alpha = \dfrac{1 - k_p}{l} = \dfrac{1 - k\,(1 - \beta)}{l}$ = prompt neutron decay constant

$$A = W_2 \frac{\chi_2}{2} \frac{k^2}{\alpha\, l^2} \approx W_2 \frac{\chi_2}{2\beta^2} \frac{\alpha_c^2}{\alpha}$$

B_2 = W_2F = counting rate in detector channel 2 (4.1.2)

$c(\tau)\Delta\tau$ = expected number of counts from detector channel 2 in a time interval $\Delta\tau$ around a time τ following a trigger pulse from detector channel 1 at $\tau = 0$ (cross-correlation experiment)

F = fission rate in the whole system

k = effective multiplication constant

k_p = prompt neutron multiplication constant

l = prompt neutron lifetime

W_2 = detector efficiency in detector channel 2 (in counts per fission)

$\chi_2 = \dfrac{\overline{\nu\,(\nu-1)}_p}{\bar{\nu}^2} \approx 0.8$ (ν = number of neutrons per fission).

Equation (4.1.1) holds correspondingly also for an auto-correlation experiment in which only one detector channel is used, such that the first incoming pulse at $\tau = 0$ and the following pulses, which are to be time-analysed, come from the same detector. In both versions of the experiment this equation holds exactly only if an experimental setup is used which determines the correlation function by delayed coincidences as in the instrumentation used by ORNDOFF [11]. In the experiment described here a different electronic system was necessary to apply because it had to be used for measurements of much slower decay constants. The block diagram is shown in Fig. 5.

The time analyser is a TMC Model CN-110 with Pulsed Neutron Logic Unit 212 which has been slightly modified. The time analysis cycle is started in the cross-correlation experiment by a trigger pulse from detector channel 1. All pulses from channel 1 arriving during the cycle time are rejected. After

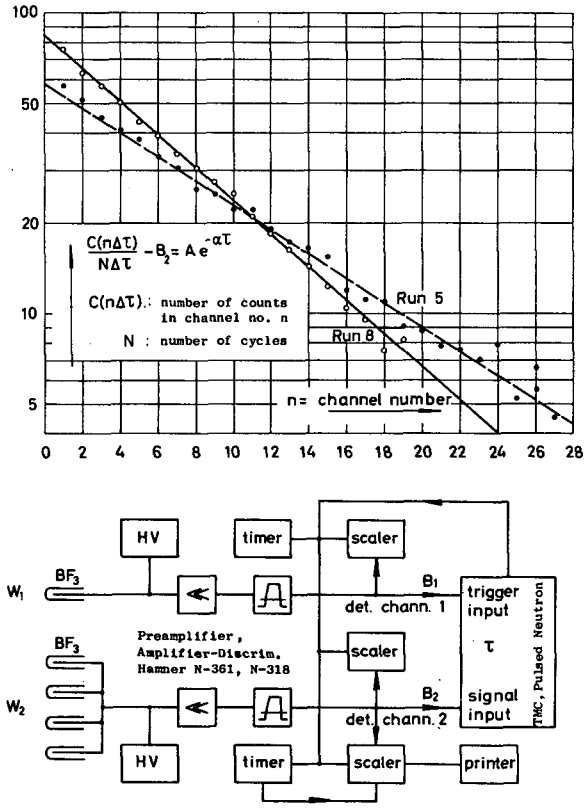


Fig. 5

Two Rossi-α runs on STARK with block diagram of apparatus

a cycle has been started, all pulses from detector channel 2 are sorted into the time channels of the analyser according to their time of arrival. Because of this the system analyses only correlations between single trigger pulses separated by at least one cycle time and signal pulses from detector channel 2 within the cycle time. This leads to a dependency of A and in a less degree also of α on the efficiency W_1 of detector channel 1.

Only the first term $A\, e^{-\alpha\tau}$ of Eq. (4.1.1) results from correlated events. The second term B_2 is the contribution from uncorrelated events. B_2 can be considered to be background in this experiment.

The fission rate F can be calculated from the ratio B_2/A,

$$F = \frac{B_2}{A} \cdot \frac{\chi_2}{2\beta^2} \cdot \frac{\alpha_c^2}{\alpha} \,. \qquad (4.1.3)$$

The efficiency can then be found from Eq. (4.1.2). Reactivity values have been calculated using Eq. (3.3) with $\alpha_c = 62.9\ s^{-1}$ from Table VI and the neutron source S_0 (mainly due to spontaneous fissions in U^{238}) from

$$S_o = F\,(1 - k_p - \beta)\,\nu \,. \qquad (4.1.4)$$

Various experimental runs have been made under the same loading and reactivity conditions specified for the other experiments. The channel width chosen was 640 μs for all runs with the channel numbers ranging from 32 to 128. The results are given in Table III. In the first four columns are listed: run number, control plate settings, detector positions (cf. Fig. 1), and efficiencies estimated from the neutron flux at that position and the reactor power and the boron content in the counting tube. The second part of the table contains measured results for α, A, and B_2 from which the quantities in the last part of the table have been calculated according to Eqs. (3.3), (4.1.3), (4.1.2), and (4.1.4).

The signal-to-background ratio, A/B_2, is inversely proportional to the fission rate and the neutron lifetime in the system. Because of spontaneous fissions in the fairly large amount of U^{238} in the central zone, the fission rate was unfavourably high for the experiments. In addition the neutron lifetime was long. For these reasons it was difficult to perform Rossi-α experiments near the delayed critical state of this loading of STARK. The results of runs 1-3 are therefore of poor quality and have been put into brackets. The fact that only one trigger pulse is accepted during one cycle may result in some pre-selection of trigger counts, particularly if the trigger channel has a highly efficient detector. From a comparison of run 4 with runs 5 and 6 one finds a noticeable influence of the detector efficiency on the signal-to-background ratio, so that the derived quantities F and S_0 are too large and W_2 is too small in run 4. From run 7 and 8 it may be concluded that not only is the signal-to-background ratio affected, but also α, which turns out to be too small in run 7 because of the high efficiency used in the run. Using this type of analysing equipment and applying Eq. (4.1.1) to the evaluation of the measured data, the restriction has to be considered which limits the efficiency, in other words counting rate, of the trigger channel to values low enough to eliminate these effects. The results of the Rossi-α experiment are compared to those of the other methods in Table VI.

4.2. Analysis of counting statistics

A new experimental technique has been applied to the measurement of the distribution of probabilities $p_n(T)$ for n detector counts in a specified time interval of length T. Correlated detector counts in chain reacting systems are responsible for the dependence of the variance of the distribution on reactor-physics parameters, i.e. on the multiplication constant k and the prompt neutron decay constant α, as well as on the detector sensitivity W. In other words, the main purpose of this technique is to determine the deviation of the counting statistics from Poisson's law.

An experimental setup was built for the direct measurement of the probabilities $p_n(T)$, where n can range from 0 to 127. This probability distribution analyser [24] is schematically shown in Fig. 6. The operating principle is as follows: Pulses from one or more detectors are fed into the input A of a fast acting electronic step switch, which proceeds by one step for each incoming pulse. Pulses from a time marker terminating the length T of the time interval are fed into input B. According to the position of the electronic switch, a gate is opened for the time pulse which gives a signal to the scaler

TABLE III

RESULTS OF THE ROSSI-α EXPERIMENTS

Run No.	Control plate configuration (cf.fig.1)	Detector positions (cf.fig.1)	Detector efficiency (W_1) (W_2)	Measured results α [sec^{-1}] Auto-corr.	Measured results α [sec^{-1}] Cross-corr.	Measured results A [sec^{-1}]	Measured results B_2 [sec^{-1}]	Calculated results ρ/β [β]	Calculated results F [sec^{-1}]	Calculated results W_2 [counts/fiss.]	Calculated results S_o [sec^{-1}]
1	R_2 = 20 cm III	22 21,23,25,27	$1.4\cdot10^{-4}$ $7.7\cdot10^{-4}$	-	(47)	(37)	2700	-	-	-	-
2	R_2 in IV	22 21,23,25,27	$1.4\cdot10^{-4}$ $7.7\cdot10^{-4}$	-	(79)	(47)	1500	-	-	-	-
3	R_2 in IV	21 11,12,13,14	$1.9\cdot10^{-4}$ $7.9\cdot10^{-4}$	-	(92)	(59)	1800	-	-	-	-
4	S_1^2, S_2^3, R_2 in VII	22,24,26,28 21,23,25,27	$5.6\cdot10^{-4}$ $7.7\cdot10^{-4}$	-	138	32	573	1.19	$(3.6\cdot10^{6})$	$(1.6\cdot10^{-4})$	$(8.3\cdot10^{4})$
5	S_1^2, S_2^3, R_2 in VII	22 21,23,25,27	$1.4\cdot10^{-4}$ $7.7\cdot10^{-4}$	-	139	58	573	1.20	$(2.0\cdot10^{6})$	$(2.9\cdot10^{-4})$	$(4.6\cdot10^{4})$
6	S_1^2, S_2^3, R_2 in VII	22 21,23,25,27	$1.4\cdot10^{-4}$ $7.7\cdot10^{-4}$	-	142	56	573	1.25	$(2.0\cdot10^{6})$	$(2.8\cdot10^{-4})$	$(4.9\cdot10^{4})$
7	R_1, R_2, R_3 in VIII	- 21,23,25,27	- $7.7\cdot10^{-4}$	(179)	-	(33)	394	(1.84)	$(2.7\cdot10^{6})$	$(1.5\cdot10^{-4})$	$(9.5\cdot10^{4})$
8	R_1, R_2, R_3 in VIII	22 21,23,25,27	$1.4\cdot10^{-4}$ $7.7\cdot10^{-4}$	-	196	83	394	2.11	$6.8\cdot10^{5}$	$5.8\cdot10^{-4}$	$2.7\cdot10^{4}$

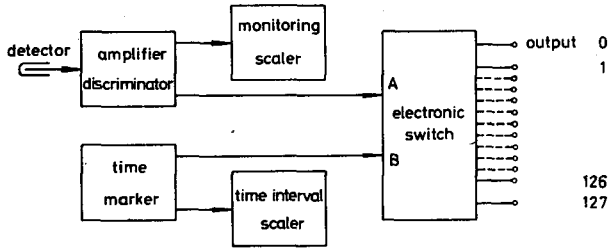


Fig. 6

Schematic diagram of the probability distribution analyser

connected to this output. If, for instance, 4 counts came in during the interval, output 4 of the switch opens gate 4 so that the pulse from the time marker delivers a signal into scaler 4. Thus 4 counts have been registered during this time interval. The step switch is reset and the probability distribution analyser is opened for a new cycle. After a sufficiently long time the run for one T-value is finished and the probabilities $p_n(T)$ are obtained directly by dividing the number of counts in scaler n, C_n, by the number of counts in the time interval scaler, C_T, giving

$$p_n = \frac{C_n}{C_T} . \tag{4.2.1}$$

The performance of the analyser is checked by the monitor scaler, because the relation

$$C_M = \sum_{n=1}^{127} n \cdot C_n \tag{4.2.2}$$

must be satisfied for the number of counts in the monitor scaler, C_M. An additional check is given by

$$C_T = \sum_{n=0}^{127} C_n . \tag{4.2.3}$$

From this distribution of probabilities $p_n(T)$ the following mean values may be computed:

$$\bar{n}(T) = \sum_{n=1}^{\infty} p_n(T) \cdot n \tag{4.2.4}$$

$$\overline{n^2}(T) = \sum_{n=1}^{\infty} p_n(T) \cdot n^2 \tag{4.2.5}$$

$$\overline{n(n-1)}(T) - \bar{n}^2(T) = \sum_{n=2}^{\infty} p_n(T) \cdot n(n-1) - \left[\sum_{n=1}^{\infty} p_n(T) \cdot n \right]^2 . \tag{4.2.6}$$

As has been shown earlier [14, 15, 23] in the point reactor model approximation, the equation to calculate the reactor physics parameters is given by

$$\frac{\overline{n^2}(T) - \bar{n}^2(T) - \bar{n}(T)}{T^2} = \frac{\bar{n}(T)}{T} \cdot \frac{W \cdot \chi_2 \cdot k^2}{\alpha l^2} \cdot \frac{e^{-\alpha T} - 1 + \alpha T}{(\alpha T)^2} \cdot \quad (4.2.7a)$$

with the symbols defined as in section 4.1.

The numerator on the left-hand side contains the difference between the measured variance ($\overline{n^2} - \bar{n}^2$) and the variance of a Poisson distribution, which is equal to $\bar{n}$. A rearrangement of this equation leads to an equivalent formulation

$$Y(T) = \frac{\overline{n(n-1)}(T) - \bar{n}^2(T)}{\bar{n}(T)} = W \cdot \chi_2 \cdot \frac{k^2}{(1-k_p)^2} \left[1 - \frac{1 - e^{-\alpha T}}{\alpha T} \right] \quad (4.2.7b)$$

which has been used for the evaluation of the experimental results.

This expression consists of two distinct terms. The second one within the brackets approaches unity for $T \to \infty$. From the first one, which near the delayed critical state is also given by

$$Y_\infty = W \cdot \chi_2 \cdot \frac{k^2}{(1-k_p)^2} = W \cdot \chi_2 \cdot \frac{1}{\beta^2} \cdot \left[\frac{\alpha_c}{\alpha} \right]^2$$

the efficiency W can be calculated if α_c, α, and β are known. The absolute fission rate follows from

$$F = \frac{C}{W}$$

where C is the counting rate in the experiment. The neutron source strength S_0 can directly be determined using Eq. (4.1.4).

The experiments were performed under the same loading and reactivity conditions as with the other methods described in this paper. The various experimental runs are listed in Table IV. For each run different time intervals were chosen so that several probability distributions were measured, from which Y(T) could be calculated. To assure good statistical accuracy at least 10^5 counts have been analysed for each distribution. The Y(T)-curves for three runs listed in Table IV are shown in Fig. 7. The quantities α and Y_∞ were computed from these curves by a least squares fit. These results, as well as the calculated efficiency W, fission rate F and source strength S_0, are given in the table.

Measurements could not be made at delayed critical because of small reactivity and power changes with time caused by the temperature coefficient

TABLE IV

RESULTS OF THE ANALYSIS OF COUNTING STATISTICS

Run No.	Control plate configuration (cf.fig.1)	Detector position (cf.fig.1)	$\alpha\,[\mathrm{sec}^{-1}]$	Y_∞	$\frac{\rho}{\beta}\,[\$]$	$W\,[\mathrm{counts/fiss.}]$	$C\,[\mathrm{sec}^{-1}]$	$F\left[\frac{\mathrm{fissions}}{\mathrm{sec}}\right]$	$S_o\left[\frac{\mathrm{neutrons}}{\mathrm{sec}}\right]$
1	R_2: 35 cm II	24	69.5	0.234	-0.10	$2.02\cdot10^{-5}$	245	$1.21\cdot10^{7}$	$2.27\cdot10^{4}$
2	R_2: 20 cm III	22	82.3	0.818	-0.31	$9.8\cdot10^{-5}$	370	$3.78\cdot10^{6}$	$2.19\cdot10^{4}$
3	R_2 in IV	22	111.5	1.03	-0.77	$2.28\cdot10^{-4}$	391	$1.72\cdot10^{6}$	$2.48\cdot10^{4}$
4	$S_1{}^2$ $S_2{}^3$ R_2 in VII	22	161	0.563	-1.56	$2.58\cdot10^{-4}$	183	$7.09\cdot10^{5}$	$2.06\cdot10^{4}$
5	$S_1{}^2$ $S_2{}^3$ R_2 in VII	21,23,25,27	138	1.73	-1.19	$5.84\cdot10^{-4}$	575	$9.85\cdot10^{5}$	$2.20\cdot10^{4}$
6	R_1 R_2 R_3 in VIII	21,23,25,27	216	0.929	-2.43	$7.68\cdot10^{-4}$	395	$5.14\cdot10^{5}$	$2.34\cdot10^{4}$
7	R_1 R_2 R_3 in VIII	21,23,25,27	212	1.027	-2.37	$8.18\cdot10^{-4}$	395	$4.83\cdot10^{5}$	$2.14\cdot10^{4}$

Remarks: Detectors listed in one row were connected in parallel.
To calculate the reactivity, $\alpha_c = 62.9\ \mathrm{sec}^{-1}$ has been taken from table VI.
$\beta = 7.5\cdot10^{-3}$ (calculated); $\bar{\nu} = 2.5$.

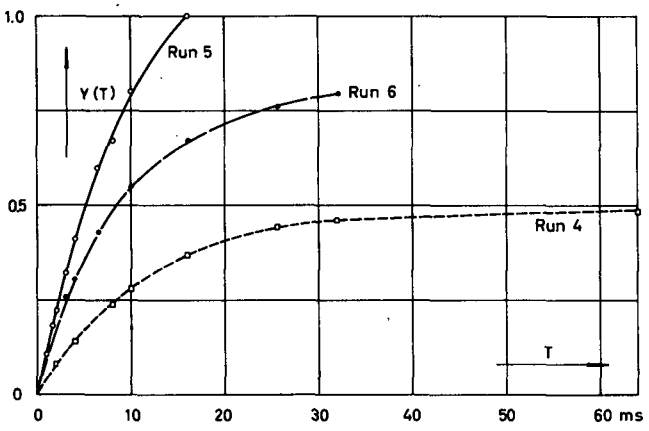


Fig. 7

Y(T)-curves from the analysis of counting statistics

in the heated thermal core section. The results obtained for the fission rates are in good agreement with the foil activation measurements which were used to calibrate the reactor instrumentation. The values found for the source strength S_0, which should be a constant for all runs, agree within ± 10%. A comparison with the results of the other techniques is given in Table VI.

4.3. Frequency analysis of reactor noise

In this experiment the observation of correlated events is performed in the frequency domain by analysing the fluctuations of ion-chamber currents. This can be done by a single-detector experiment (auto-correlation) or by the more flexible two-detector experiment (cross-correlation). The block diagram is shown in Fig. 8. The fundamental equations, derived from the

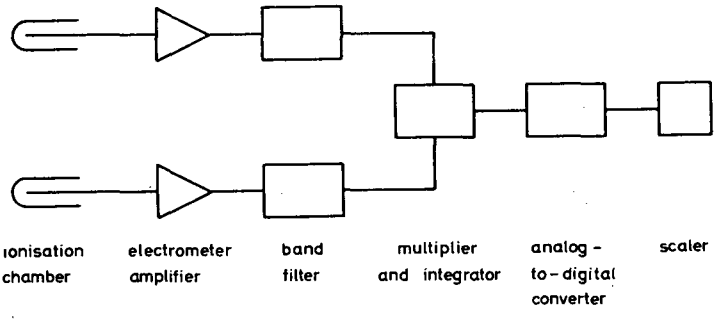


Fig. 8

Block diagram for measurement of cross power spectral density

common theoretical basis [23], are given in the point reactor and high frequency approximation (no delayed neutrons) by

$$\text{APSD} = \frac{\overline{r^2}(\omega,\Delta\omega)}{\Gamma(\omega,\Delta\omega)} = W \cdot F \cdot \bar{q}^2 \left[R + \frac{W \cdot \chi_2 k^2}{l^2(\alpha^2+\omega^2)} \right] \qquad (4.3.1)$$

for the auto-correlation experiment and by

$$\text{CPSD} = \frac{\overline{r_1 \cdot r_2}(\omega,\Delta\omega)}{\Gamma(\omega,\Delta\omega)} = \bar{q}_1 \cdot \bar{q}_2 \cdot F \cdot \frac{W_1 \cdot W_2 \cdot \chi_2 k^2}{l^2(\alpha^2+\omega^2)} \qquad (4.3.2)$$

for the cross-correlation experiment. The symbols W, F, χ_2, k, l and α were already defined in section 4.1. The others are

APSD = auto-power-spectral-density
CPSD = cross-power-spectral-density
r_n = chamber current (chamber n)
$\Gamma(\omega,\Delta\omega)$ = band width of filters = $\mathrm{Re} \int_0^\infty \frac{d\omega'}{\pi} B_1(\omega') B_2(-\omega')$
$B_n(\omega)$ = frequency characteristic of filter n
ω = $2\pi f$ = angular frequency
$\Delta\omega$ = frequency interval
$\bar{q}_n$ = average charge per detected neutron
R = $\frac{\overline{q^2}}{\bar{q}^2}$

From a comparison of Eqs. (4.3.1) and (4.3.2) it can be seen that the contribution from uncorrelated noise (first term on the right-hand side of Eq. (4.3.1)) is not present in the cross-correlation experiment. This is a specific feature of the two-detector experiment and is particularly important in all cases where the uncorrelated contribution is relatively large. The expression for the fission rate F is particularly simple if the experiment is performed in the low frequency range ($\omega \ll \alpha$). In this case

$$F = \frac{\chi_2}{\beta^2} \left[\frac{\alpha_c}{\alpha} \right]^2 \frac{\bar{i}_1 \cdot \bar{i}_2 \cdot \Gamma(\omega,\Delta\omega)}{\overline{r_1 \cdot r_2}(\omega,\Delta\omega)} \qquad (4.3.3)$$

where

$$\bar{i}_n = \bar{q}_n \cdot W_n \cdot F \qquad n = 1, 2 \qquad (4.3.4)$$

is the mean current of the ion chamber n. If F has been calculated, $\bar{q}_n \overline{W}_n$ is easily found from Eq. (4.3.4).

The block diagram of the experimental setup used for the cross- and auto-correlation measurements is shown in Fig. 8. The current fluctuations of the ion chambers (Type RC 6) are amplified in electrometer amplifiers

(Keithley 603) and fed into band-pass-filters (Krohn Hite 330 M). The filter output signals are multiplied (in a two-detector experiment) or squared (in a single-detector experiment) and integrated for a specified time T with analogue computing equipment (Pace TR 10) to give the mean value. The integrated voltage was converted into a digital form by use of an analogue-to-digital converter (Dymec 2210) and a normal pulse scaler.

Several experimental runs have been made under the specified loading condition (cf. section 2) in the auto-correlation and cross-correlation version of the method. The results of characteristic examples are listed in Table V. The positions of the two ion chambers used are indicated in Fig. 1. The prompt neutron decay constant α was determined by a least squares fit from the measured power spectral density versus frequency curves. Two examples, one for an auto-correlation (upper curve) and one for a cross-correlation measurement (lower curve), are shown in Fig. 9. The advantage of the two-detector experiment is clearly seen from the curves. The absolute fission rate F was calculated using Eq. (4.3.3). The comparison to the results found by foil activation, with which the reactor instrumentation was calibrated, shows that somewhat larger values were obtained by the frequency analysis technique. The values for $W_1\overline{q}_1$ and $W_2\overline{q}_2$ are also listed for comparison. Measurements more subcritical than indicated in the table could not be performed because of interfering effects in the electronic system. The results obtained by this technique are compared with the other results in Table VI.

5. COMPARISON OF RESULTS AND CONCLUSIONS

The comparable results of the different methods are listed in Table VI. The α-values have been averaged if more than one run has been made under the same conditions or if no differences were found for various detector positions. The individual numbers are found in Tables I-V. For the calculation of reactivity from α and α_c the pulsed neutron results have been taken for simplicity to compare reactivity values with the rod drop- or continuous run-data.

The comparison of measured prompt neutron decay constants in Table VI shows good agreement between the four methods in general. From the delayed critical state (I) to the control plate configuration III the results agree well within the error limits of about ± 3%. For configuration IV and particularly for VII with detector position 22 the discrepancy between the pulsed source and counting statistics data amounts up to 18%. This might be a result of the inclusion of higher harmonics contributions in the data of the counting statistics analysis if only one detector position (22) is used in this system. This explanation is supported by the fact that the agreement with the pulsed source data is within 2% if several detectors – distributed properly in the system – were used. The reason for the appearance of such discrepancies lies in the fact that in the pulsed neutron source technique contributions of higher harmonics are eliminated by excluding the first part of the n(t)-curve when α is determined from the exponential slope. In the analysis of counting statistics, on the other hand, all higher harmonics effects are included in the Y(T) curve from which the prompt neutron decay constant is derived.

TABLE V

RESULTS OF FREQUENCY ANALYSIS MEASUREMENTS

Run No.	Control plate configuration (cf.fig.1)	Method	Detector position (cf.fig.1)	α [sec^{-1}]	$W_1 \bar{q}_1$ [10^{-18} amp sec/fiss.]	$W_2 \bar{q}_2$ [10^{-18} amp sec/fiss.]	Reactor power instrum. (foil act.)	Reactor power frequency analysis
1	del. critical	auto	K	65	2.0	-	10 W	12 W
2	del. critical	cross	K, W	61.7	2.1	1.2	10 W	11.7 W
3	del. critical	cross	K, W	65	2.4	1.3	0.1 W	0.11 W
4	R_2 : 35.0 cm	cross	K, W	67	-	-	400 μ W	400 μ W
5	R_2 : 20.0 cm	cross	K, W	85	-	-	100 μ W	120 μ W

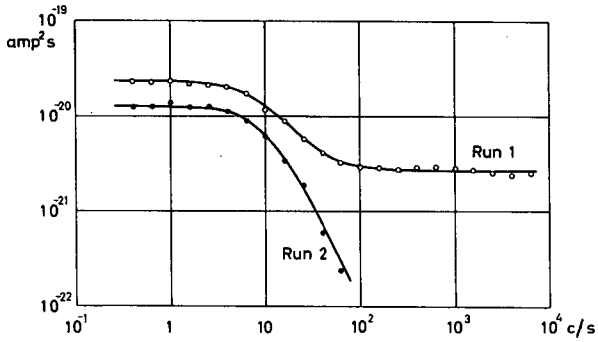


Fig. 9

Power spectral density for single-detector (upper curve) and two-detector experiment (lower curve)

From the comparison of the results the prompt neutron decay constant seems to be the least affected by detector position in a multiregion reactor system with special geometry like STARK. The comparison with the other quantities derived from the pulsed source technique showed a much stronger dependency in this regard, indicating, as expected, that space-independent models cannot be applied to systems with large reflectors.

A few remarks may be added to the applicability of the different techniques to determine the prompt neutron decay constant from the results obtained with loading 1 of STARK. From delayed critical to about -0.5 $ subdelayed critical, in the pulsed neutron technique exact corrections for the time-dependent background from delayed neutrons and eventually a spontaneous fission source are important for the evaluation of the data. In this reactivity range the Rossi-α technique is difficult to apply in thermal systems with strong sources because of the small signal-to-background ratio caused by the long lifetime and the relatively large fission rate. No difficulties exist for the analysis of counting statistics near and at delayed critical if the power is sufficiently stable. Such is not the case in STARK at delayed critical and at low power level (necessary for moderate counting rates) because of temperature effects. Very reliable results in this range can be obtained from the frequency analysis of noise without any corrections. Difficulties arose, however, below -0.5 $ with this technique, which are not of fundamental nature and could be overcome by use of other equipment. All other methods worked well below -0.5 $ to about -3 $. In the more subcritical states the effects of higher harmonics have to be taken into consideration, particularly in the case of the pulsed source n(t) curves.

ACKNOWLEDGEMENTS

The authors appreciate the help and co-operation given by Dr. W. Eyrich in constructing and operating the pulsed neutron source. They also wish to thank Mr. H. Borgwaldt for stimulating discussions and help in writing

TABLE VI

COMPARISON OF RESULTS

Control plate configuration (cf. fig.1)	Pulsed source		Rossi-α		Count. statistics		Frequency analysis		Pulsed source	Static Meas.
	Detector position	$\alpha\,[sec^{-1}]$	Detector position	$\alpha\,[sec^{-1}]$	Detector position	$\alpha\,[sec^{-1}]$	Detector position	$\alpha\,[sec^{-1}]$	$-\frac{\rho}{\beta}=\frac{\alpha}{\alpha_c}-1\,[\$]$	$-(\frac{\rho}{\beta})_s\,[\$]$
Delayed critical I	12, 3	62.9	-	-	-	-	K,W(cross) K (auto)	63.4	-	-
R_2: 35.0 cm II	12, 3	69.2	-	-	24	69.5	K,W(cross)	67	0.100	0.085
R_2: 20.0 cm III	12, 3	85.3	-	-	22	82.3	K,W(cross)	85	0.356	0.332
R_2 in IV.	12, 3	101.0	-	-	22	111.5	-	-	0.61	0.64
S_1^2, R_2, S_2^3 in VII	12,24,3	136.3	21-28	138	21,23,25,27	138	-	-	1.17	-
S_1^2, R_2, S_2^3 in VII	-	-	21,22,23,25,27	140.5	22	161	-	-	-	-
R_1, R_2, R_3 in VIII	12,24,3	194	21,22,23,25,27	196	21,23,25,27	214	-	-	2.08	2.50
S_1, S_2 in IX	12,24,3	360	-	-	-	-	-	-	4.72	5.2
S_1, S_2, S_3, R in X	12,24,3	576	-	-	-	-	-	-	8.16	12

auxiliary computer codes. The authors also acknowledge the support given by the operating staff of the STARK reactor, in particular Mr. C. Brückner.

REFERENCES

[1] MEISTER, H., BECKURTS, K. H., HÄFELE, W., KÖHLER, W. H. and OTT, K., KFK-Rpt No. 217 (1964).
[2] SIMMONS, B. E. and KING, J. S., Nucl. Sci. Engng 3 (1958) 595-608.
[3] SJÖSTRAND, N. G., Ark. Fys. 11 (1956) 233-46.
[4] GOZANI, T., Nukleonik 4 (1962) 348-49.
[5] GARELIS, E. and RUSSELL, J. L. Jr., Nucl. Sci. Engng 16 (1963) 263-70.
[6] GARELIS, E., Nucl. Sci. Engng 18 (1964) 242-45.
[7] GARELIS, E., Nucl. Sci. Engng 19 (1964) 131-33.
[8] LEWINS, J., Nucl. Sci. Engng 7 (1960) 122-26.
[9] EYRICH, W. and SCHMIDT, A., "Two compact, high-intensity pulsed neutron sources", these Proceedings II.
[10] CARPENTER, S. G., Rpt AI-8549, V (1963).
[11] ORNDOFF, J. D., Nucl. Sci. Engng 2 (1957) 450.
[12] BRUNSON, G. S. et al., Nucleonics 15 11 (1957) 132.
[13] BORGWALDT, H. and SANITZ, D., Nukleonik 5 (1963) 239.
[14] BENGSTON, I., Proc. 2nd UN Int. Conf. PUAE 12 (1958) 63.
[15] ALBRECHT, R. W., Nucl. Sci. Engng 14 (1962) 153.
[16] ZOLOTUKHIN, V. G. and MOGILNER, A. I., Atomnaja Energija 15 (1963) 11.
[17] MOORE, M. N., Nucl. Sci. Engng 6 (1959) 448.
[18] COHN, C. E., Nucl. Sci. Engng 7 (1960) 472.
[19] BENNETT, E. F., Nucl. Sci. Engng 8 (1960) 53.
[20] GRIFFIN, C. W. and RANDALL, R. L., Nucl. Sci. Engng 15 (1963) 131.
[21] SCHRÖDER, R., Nukleonik 4 (1962) 227.
[22] SCHULTZ, M. A., Symp. on Noise Analysis in Nucl. Systems, Rpt. TID 7679 (1964) 135.
[23] BORGWALDT, H. and STEGEMANN, D., Nukleonik, in press.
[24] STEGEMANN, D., to be published.

PULSED NEUTRON SOURCE AND REACTOR NOISE STUDIES OF PLUTONIUM SYSTEMS

S.R. BIERMAN AND E.D. CLAYTON
BATTELLE MEMORIAL INSTITUTE
PACIFIC NORTHWEST LABORATORIES, RICHLAND, WASH.,
UNITED STATES OF AMERICA

Abstract — Résumé — Аннотация — Resumen

PULSED NEUTRON SOURCE AND REACTOR NOISE STUDIES OF PLUTONIUM SYSTEMS. The results of pulsed neutron source experiments and reactor noise measurements performed on small plutonium systems are presented, and comparisons are given between the two methods of measurement. The measurements were made during approach-to-critical experiments performed in the Critical Mass Laboratory at Hanford and cover both thermal and intermediate systems of ideal geometry. The primary parameter experimentally determined in each measurement was the prompt neutron decay constant, α.

It can be shown that a dynamical relationship exists between the impulse response employed in pulsed neutron studies and the inherent randomness of the nuclear events taking place in the reactor. Specifically, the prompt neutron density decays as $e^{-\alpha t}$ following a burst of neutrons and the inherent fluctuations of the reactor cause a statistical fluctuation in the neutron density whose power spectral density varies as $1/(\alpha^2+\omega^2)$, where ω is the frequency of the statistical fluctuations. These phenomena provide two independent methods for analysing the dynamic behaviour of a system. From a consideration of the reactivity of the system, the speed and efficiency of the detector used and the magnitude of the inherent neutron source, it is possible to make a comparison between the two techniques and to determine which method provides the more reliable data. For example, in a relatively thermal plutonium system (near optimum moderation) of average size, the pulsed neutron method is expected to provide the better data for subcritical systems. Near delayed-critical, either method should be equally satisfactory and at delayed-critical reactor noise measurements are expected to be the more reliable. A reactor noise measurement at delayed-critical can be used to verify subcritical pulsed neutron source measurements. The converse is also true.

For all plutonium critical assemblies studied, excellent agreement was obtained between pulsed neutron source and reactor noise determinations of the prompt neutron decay constant.

ÉTUDES EFFECTUÉES SUR DES SYSTÈMES AU PLUTONIUM AU MOYEN DES MÉTHODES DE LA SOURCE DE NEUTRONS PULSÉS ET DU BRUIT DU RÉACTEUR. Les auteurs présentent les résultats d'expériences au moyen d'une source de neutrons pulsés et de mesures par l'intermédiaire du bruit du réacteur, effectuées sur de petits systèmes au plutonium; ils établissent des comparaisons entre les deux méthodes de mesure. Les mesures ont été faites au Critical Mass Laboratory de Hanford au cours d'expériences d'approche de la criticité; elles portaient à la fois sur des systèmes à neutrons thermiques et à neutrons intermédiaires ayant une géométrie idéale. Le paramètre primaire déterminé expérimentalement par chaque méthode de mesure est la constante de décroissance pour des neutrons instantanés.

On peut montrer qu'il existe une relation dynamique entre la réponse obtenue avec la méthode des neutrons pulsés et le caractère aléatoire inhérent aux événements nucléaires qui se produisent dans le réacteur. Spécifiquement, le nombre volumique des neutrons instantanés décroît selon la loi exponentielle $e^{-\alpha t}$ à la suite d'une bouffée de neutrons et les fluctuations inhérentes de la puissance du réacteur provoquent des fluctuations statistiques dont la densité spectrale varie comme $1/(\alpha^2+\omega^2)$ dans laquelle ω est la fréquence des fluctuations statistiques. Ces phénomènes permettent d'utiliser deux méthodes indépendantes pour analyser le comportement dynamique d'un système. En considérant la réactivité du système, la vitesse et l'efficacité du détecteur employé et la grandeur de la source de neutrons inhérente, il est possible d'établir une comparaison entre les deux méthodes et de déterminer laquelle donne les meilleurs résultats. Dans un système au plutonium à neutrons relativement thermiques (proche du ralentissement optimum) de taille moyenne, par exemple, on peut s'attendre que la méthode des neutrons pulsés donne les meilleurs résultats pour les systèmes sous-critiques. Dans un système presque critique retardé, les deux méthodes paraissent être également satisfaisantes et dans un milieu critique retardé, on peut s'attendre que les mesures par l'intermédiaire du bruit du réacteur soient les plus

sûres. On peut appliquer cette deuxième méthode à un système critique retardé pour vérifier les mesures effectuées au moyen de la source de neutrons pulsés sur un système sous-critique. L'inverse est également vrai.

Pour tous les assemblages critiques au plutonium étudiés, les auteurs ont trouvé que les valeurs de la constante de décroissance pour les neutrons instantanés obtenues au moyen de la source de neutrons pulsés et au moyen du bruit du réacteur étaient en très bon accord.

ИЗУЧЕНИЕ ИСТОЧНИКОВ ПУЛЬСИРУЮЩИХ НЕЙТРОНОВ И РЕАКТОРНЫХ "ШУМОВ" В РАБОТАЮЩИХ НА ПЛУТОНИИ СИСТЕМАХ. Излагаются результаты экспериментов с источником пульсирующих нейтронов и измерений реакторных "шумов", которые были проведены на небольших плутониевых системах. Сопоставляются эти два метода измерений. Измерения производились во время экспериментов с приближением к критическому состоянию в Лаборатории по критическим массам в Хенфорде: они распространяются на устройства с идеальной геометрией как на тепловых, так и на промежуточных нейтронах. Основным параметром, который определялся экспериментально при каждом измерении, была постоянная α распада мгновенных нейтронов.

Можно доказать, что между импульсным режимом, используемым при исследованиях на импульсных нейтронах, и происходящими в реакторе беспорядочными ядерными событиями существует динамическая связь. В частности, вслед за вспышкой нейтронов плотность мгновенных нейтронов распадается по виду $e^{-\alpha t}$, а присущие реактору флуктуации вызывают статистические флуктуации в плотности нейтронов, удельная мощность спектральной плотности которых изменяется по виду $1/(\alpha^2 + \omega^2)$, где ω является частотой статистических флуктуаций. Эти явления обеспечивают два независимых друг от друга метода анализа динамического поведения системы. На основании соображений относительно реактивности системы, скорости счета и эффективности применяемого детектора и величины имеющегося источника нейтронов представляется возможным сравнить эти два метода и определить, какой из них дает более надежные результаты. Так, например, в работающей на плутонии системе среднего размера, приближающейся к тепловому режиму (почти оптимальное замедление) с помощью метода импульсных нейтронов можно ожидать лучших результатов для подкритических устройств. При приближении к замедленному критическому режиму любой из этих двух методов должен быть в равной мере удовлетворительным, а при замедленном критическом режиме можно ожидать, что измерения реакторных "шумов" могут дать более надежные результаты. Измерения реакторных "шумов" при замедленном критическом режиме могут быть использованы для проверки измерений источника импульсных нейтронов при подкритическом режиме. Справедливо также и противоположное утверждение.

Для всех изученных работающих на плутонии критических сборок была достигнута великолепная согласованность между определениями постоянной распада мгновенных нейтронов как по методу пульсирующего нейтронного источника, так и по методу определения реакторных "шумов".

ESTUDIOS DE SISTEMAS DE PLUTONIO MEDIANTE UNA FUENTE DE NEUTRONES PULSADOS Y LOS RUIDOS DEL REACTOR. Los autores presentan los resultados de los experimentos y las mediciones efectuados en sistemas de plutonio de reducidas dimensiones con ayuda de una fuente de neutrones pulsados y de los ruidos del reactor; comparan ambos métodos de medición. Las mediciones se llevaron a cabo en el Critical Mass Laboratory de Hanford en el curso de experimentos próximos al estado crítico; se refieren a los sistemas de neutrones térmicos y de neutrones intermedios, de geometría ideal. El parámetro primario determinado experimentalmente en cada medición fue α, esto es, la constante de decrecimiento de los neutrones inmediatos.

Puede demostrarse la existencia de una relación dinámica entre la respuesta obtenida con el método de los neutrones pulsados y el carácter inherentemente aleatorio de los sucesos nucleares que tienen lugar en el reactor. Específicamente, la densidad de neutrones instantáneos decrece como $e^{-\alpha t}$ después de un impulso neutrónico; las fluctuaciones inherentes al reactor provocan fluctuaciones estadísticas cuya densidad espectral varía según la fórmula $1/(\alpha^2 + \omega^2)$, en la que ω es la frecuencia de las fluctuaciones estadísticas. Estos fenómenos constituyen la base de dos métodos independientes para analizar el comportamiento dinámico de un sistema. Considerando la reactividad del sistema, la velocidad y el rendimiento del detector utilizado así como la magnitud de la fuente neutrónica, es posible comparar ambos métodos y determinar cuál de los dos facilita los resultados más fidedignos. Por ejemplo, en un sistema de plutonio relativamente térmico (próximo a la moderación óptima) y de dimensiones medias, se considera que el método de los neutrones pulsados da mejores resultados para los sistemas subcríticos. En la proximidad del estado crítico por neutrones retardados, los dos métodos parecen sur igualmente satisfactorios, mientras que en el estado crítico por neutrones retardados, las

medidas efectuadas por medio de los ruidos del reactor parecen ser las más precisas. Para todos los conjuntos críticos de plutonio estudiados, se ha obtenido una excelente concordancia entre la constante de decrecimiento de los neutrones instantáneos, determinada con ayuda de la fuente de neutrones pulsados y la establecida mediante los ruidos del reactor.

INTRODUCTION

Pulsed neutron source and reactor noise measurements are concurrently being made with most of the criticality experiments performed in the Critical Mass Laboratory of Battelle Northwest Laboratories, Richland, Washington. The purposes of the measurements are to obtain fundamental kinetic information on the critical assemblies, and to determine material worth, prompt criticality and the worth of each assembly's control and safety systems. The measurements are also oriented toward developing an on-line reactor noise monitor reliable enough to be used for actuating safety shutdown systems, and to develop a pulsed neutron source technique whereby reactivity determinations can be made on subcritical in-plant systems.

The pulsed neutron source measurements presented in this paper were made with the system shown in Fig. 1. The neutron generator is a Kaman Nuclear Model A-810. It consists of a control unit and an accelerating head which produces an isotropic burst of 10^7, 14-MeV neutrons per pulse. The burst is approximately 5 μs in duration and consists of neutrons produced by the $H^3(d,n)He^4$ reaction.

The detection component of the system is a lead-shielded, boron-10 loaded, organic liquid scintillator for thermal neutron detection, and an RCA-6810 photomultiplier tube. The pulse produced by the photo tube is amplified in a wide band linear pulse amplifier and then fed to the pulse analyser system.

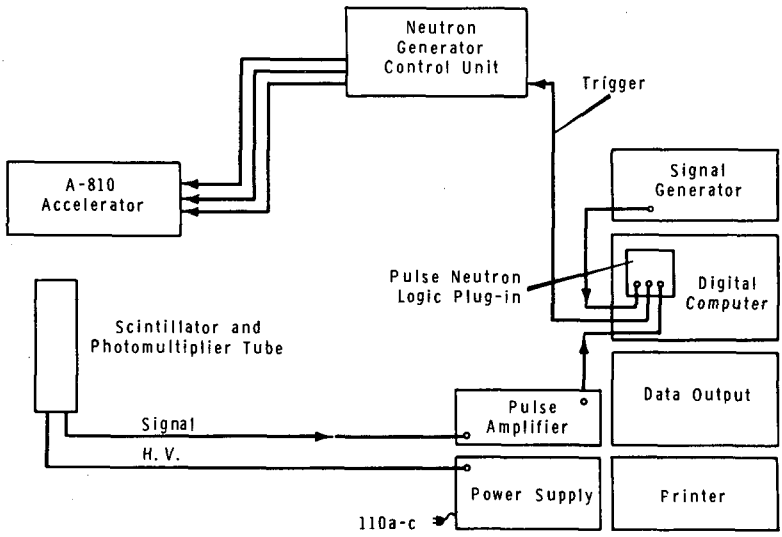


Fig. 1

Pulsed neutron source and data acquisition system Critical Mass Laboratory

The pulse analyser is a Technical Measurement Corporation Model CN-110 and consists of a digital computer unit with a 256 channel magnetic core memory and a data output unit. The data output unit supplies a digital printer with the channel number and the counts in that channel for print-out. A visual pre-presentation is also provided by an oscilloscope display on the front of the digital computer unit. Associated with the digital computer unit is a pulsed neutron logic plug-in which enables the CN-110 to measure the pulse rate from the detector as a function of time. The logic unit has provision for triggering the neutron generator. There are adjustments on the logic unit to set the desired analysis time for the 256 channels and to set the delay between the triggering pulse and the start of analysis time. A discriminator is also provided for low level pulses and noise.

The pulse analysis component is triggered by an external pulse generator which sets the repetition rate of the system. The pulse analysis component then triggers the pulsed neutron component as indicated by the arrows in the block diagram.

During the course of these experiments, the method of reactor noise data acquisition and analysis has undergone an evolutionary process to improve the quality of the data and the ease of analysis. The system that has evolved and is in current use in the Critical Mass Laboratory is shown in Fig. 2. Normally the same scintillator and photomultiplier tube is used in making the reactor noise measurements as is used in making the pulsed neu-

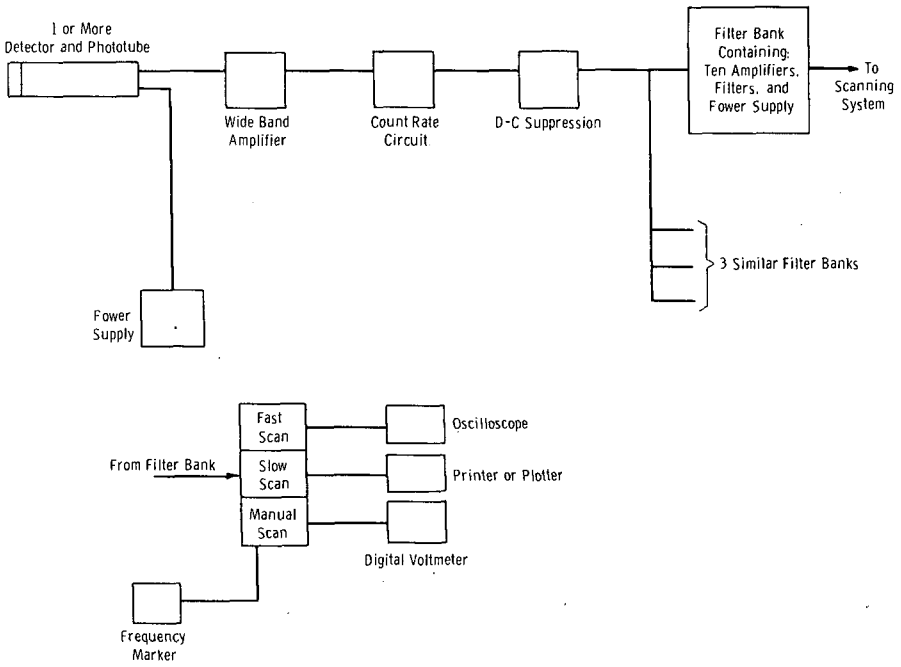


Fig. 2

Reactor noise analysis system Critical Mass Laboratory

tron source measurements. However, it is occasionally necessary to use a second scintillator located some distance from the reactor to avoid saturating the system.

The pulses from the photomultiplier tube are fed to a wideband linear amplifier which has a discriminator setting for unwanted noise or low level pulses. The amplifier is coupled to a high speed, specially built, count rate circuit, the voltage output of which is proportional (up to 500 000 c/s) to the rate at which pulses are received. The count rate circuit output signal is then passed through a DC voltage suppression network and then into four filter banks of ten frequency channels each. The input circuit to each bank is a bandpass filter to restrict the frequency of the signal to the frequencies of interest in that bank. For all frequencies below 400 c/s twin-T bandpass filters are used in the feedback circuit of the operational amplifiers. Above 400 c/s LC filters are used. The filter banks are arranged such that each filter has a 1/3 octave bandwidth and overlaps the adjacent filters at the -3 db point. The output of each filter is converted to its absolute value by a full wave rectifier. A low-pass filter circuit is used to average the resulting output over time and this signal is displayed on slow decibel meters and coupled to the scanning system.

The scanning system includes three separate scanning modes: fast, slow, and manual scan. The fast scan is for use in conjunction with an oscilloscope to give a continuous visual presentation of the spectrum, thus showing immediately any change in reactivity in the system or any malfunction of a component of the analyser. The fast scan and oscilloscope can also be used for calibration of the system. Either a "white" noise generator or a neutron source is used to provide an input spectrum of equal amplitude at all frequencies for calibration. The oscilloscope can also be used for maintenance to monitor the signal in the analyser at any desired point.

When the system reaches a steady state condition, the slow scan is used to read the spectrum and plot it on an X-Y recorder or to print out the magnitude on a digital printer. A manual scan is also included to aid in trouble shooting and calibrating the analyser. A digital voltmeter, which can measure the output of any channel, is also used as a transition device between the noise analyser and the digital printer.

A frequency marker is incorporated into the scan system so that a marker for each decade of frequency can be displayed on the oscilloscope or plotter. Commercially available components are used in all forty channels of the analyser system. Plug-in components in the bandpass filter section provide a maximum of flexibility in that the frequency range of the noise analyser can be lowered or raised to accomodate the change in frequency spectra of different assemblies and to extend the frequency range of the analyser to other frequencies which may become important in future applications. The present range of the analyser is from a centre frequency of 0.316 c/s to one of 3160 c/s. (Selection of these mid-frequencies and their associated bandwidths is covered in Ref. [1].)

The experimental data presented in this paper cover systems ranging in hydrogen to plutonium atomic ratios of from 15 to 1020 and in corresponding plutonium concentrations of from 1105 g/l to 25.4 g/l. Data from both bare and reflected assemblies are presented. However, interpretation

of the data from the reflected systems is not complete because of a lack of adequate theoretical models describing such systems. Critical assemblies having low H/Pu atomic ratios of 15, 35, and 39 were obtained by constructing solid assemblies to critical in stages using solid 2-in cubes of PuO_2-polystyrene [2]. One of these assemblies, loaded on the Critical Mass Laboratory's Remote Split-Table Machine, is shown in Fig. 3. At the time this picture was taken, the assembly was only five cubes high.

Critical assemblies having H/Pu atomic ratios of 88.5 and 1020 were obtained by filling to critical, in incremental steps, spheres with $PuNO_3$ solution [2]. A picture of such a solution system is shown in Fig. 4, with a sphere in place and the reflector tank filled with water.

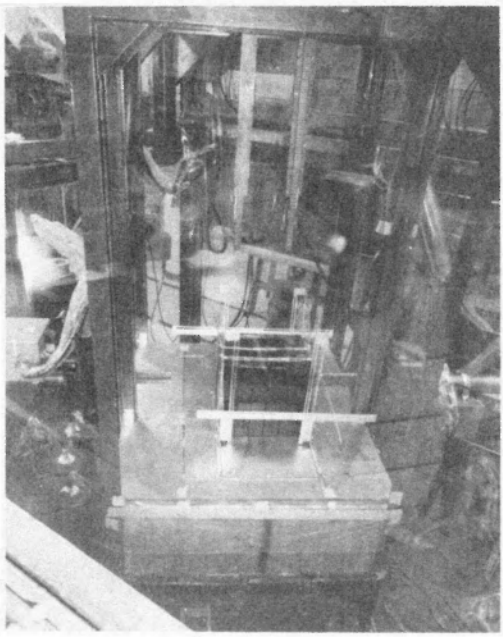


Fig. 3

Typical solids assembly

PULSED NEUTRON SOURCE AND REACTOR NOISE MEASUREMENTS

Detailed theoretical treatment of pulsed neutron source and reactor noise measurements can be found in Refs. [3-6]. These are referred to frequently in the analysis of the experimental data, but no attempt is made in this paper to derive the various theoretical models in detail.

The analysis of most of the data covered is based on the assumption that the reactor systems can be described by the usual reactor kinetic equations:

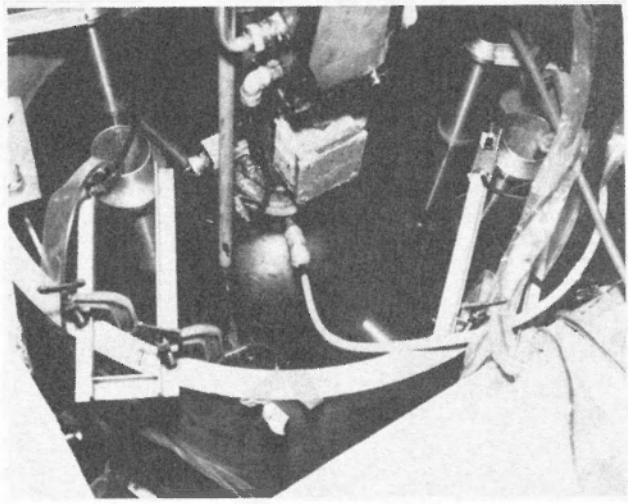


Fig. 4

Typical water reflected solution assembly

$$\frac{dn}{dt} = \frac{k(1-\beta)-1}{\ell} n + \sum_{i=1}^{m} \lambda_i C_i + S \qquad (1)$$

$$\frac{dC_i}{dt} = -\lambda_i C_i + \frac{k\beta_i}{\ell} n. \qquad (2)$$

Since only the dynamic behaviour of the prompt neutrons is examined in these measurements, the delayed neutrons can be assumed to be delayed an infinite amount of time, and Eq. (2) can be simplified to:

$$\frac{dC_i}{dt} = 0$$

$$C_i = C_{i0} \qquad (3)$$

$$C_i = \frac{k\beta_i}{\lambda_i \ell} n_0 .$$

If the assumption in Eq. (1) is used, a simplified description of the system as a first order, linear, differential equation with constant coefficients can be made:

$$\frac{dn}{dt} + \alpha n = \frac{k\beta}{\ell} n_0 + S = f(t) \qquad (4)$$

where

$$\alpha = \frac{1-k(1-\beta)}{\ell} \tag{5}$$

and the inhomogeneous terms are lumped together as a forcing function, f(t).

Some experimental data are presented from measurements made on a reflected system in which a spatial dependence was observed. Although they cannot be adequately defined by Eq.(4), the experimental data are presented and some tentative analyses are made.

COMPLEMENTARY FEATURE OF PULSED NEUTRON SOURCE AND REACTOR NOISE MEASUREMENTS

It has been shown [4] that a dynamical relationship exists between the impulse response employed in pulsed neutron source measurements and the inherent randomness of the nuclear events taking place in the reactor. In pulsed neutron source measurements the neutron density decays as $e^{\alpha t}$ following a burst of neutrons. In reactor noise measurements, the inherent fluctuations of the reactor cause a statistical fluctuation in the neutron density whose power spectral density varies as $1/(\alpha^2 + \omega^2)$. ω is the frequency of the statistical fluctuations and, in both cases, α is the prompt neutron decay constant as given by Eq.(5).

In systems that can be described by Eq.(4), the transient behaviour of the neutron density is observed to have a fundamental mode of decay which can be defined by:

$$n(t) = B_p e^{-\alpha t} + A_p \tag{6}$$

$\alpha = \frac{1-k(1-\beta)}{\ell}$, the prompt neutron decay constant.

A_p = A constant, the magnitude of which depends on the residual background of the system and the delayed neutron contribution to the pulse.

B_p = A constant, the magnitude of which depends on the size of the neutron pulse and the reactivity of the system.

The spectral density function for such systems is observed to have the following form over the frequency range dominated by the prompt neutrons:

$$\Psi(\omega) = A_n + \frac{B_n}{\alpha^2 + \omega^2} . \tag{7}$$

ω = centre frequency of filter network having a bandwidth $\Delta\omega$.

$\alpha = \frac{1-k(1-\beta)}{\ell}$

A_n = A constant, the magnitude of which depends on the background power spectrum caused by neutrons which have not participated in the fission process and instrumentation noise.

B_n = A constant, the relative magnitude of which depends on the reactivity of the system, the neutron lifetime in the reactor and the efficiency of the detection system.

The fact that these two experimental methods measure the identical parameter α can be very useful in studying the dynamic behaviour of a reactor system. They can be used to extend the range of reactivity over which measurements can be made and to obtain independent values and, thus, experimental verification of the same parameter.

Although both techniques measure the same parameter, it is not always feasible or possible to use either or both on the same reactor system. Considerations, such as the reactivity of the system, the magnitude of the neutron source inherent to the system, the size and cost of pulsed neutron generators, the efficiency and speed of neutron detectors, and the cost of reactor noise analysis equipment, enter the picture. In pulsed neutron source experiments in a multiplying medium, the residual neutron level caused by neutron sources may present a problem which can only be overcome by an increase in pulse intensity. In reactor noise experiments, the background power spectrum arising from the detection of neutrons which have not participated in the fission process may be so high as to blank out any correlated noise present.

By considering the constant coefficients in Eqs. (6) and (7) an insight can be obtained as to which method should provide the better data and when either method is applicable. In pulsed neutron source experiments (Eq. 6) the ratio $B_p/(A_p + B_p)$ approaches one for a large neutron pulse in a reactor having a small residual neutron density. In reactor noise experiments (Eq. 7) the ratio $B_n/(A_n + B_n)$ approaches one for a large fast sensitive detector in a nearly critical reactor. The magnitude of these ratios for any particular experiment depends upon the instrumentation available for the experiments as well as the configuration and reactor parametrics which are characteristic of the multiplying system under study.

In epithermal plutonium systems, a relatively large mass of plutonium is present. Since Pu^{240} is present and is a spontaneous fission source, the inherent, and unavoidable, neutron source is fairly large, and the residual neutron density becomes quite large as the reactor approaches critical. The large value for A_p near delayed critical tends to mask the pulses which may be introduced into the system by a moderately sized pulsed neutron generator. Because of the presence of the source, A_p approaches infinity as the reactor approaches critical. As a consequence the ratio $B_p/(A_p + B_p)$ approaches zero and pulsed neutron source measurements become impossible. On the other hand, as the reactor approaches critical, B_n becomes larger and the ratio $B_n/(A_n + B_n)$ increases, making it possible to obtain reactor noise information that is suitable for analysis on a standard spectrum analyser.

The experimental data shown in Figs. 5 through 9 illustrate these features of pulsed neutron source and reactor noise measurements in epithermal plutonium systems. The data were obtained from measurements made on a reactor assembly consisting only of 5.17 cm plutonium-polystyrene cubes having a 0.028-cm protective coating of rubber, a hydrogen to plutonium atomic ratio of 15, a plutonium concentration of 1.12 g/cm^3, and a Pu^{240} content of 2.2 wt.%. Its base dimensions were 31.01 cm on each side and its critical height of 32.56 cm made it almost cubical. The system was quite

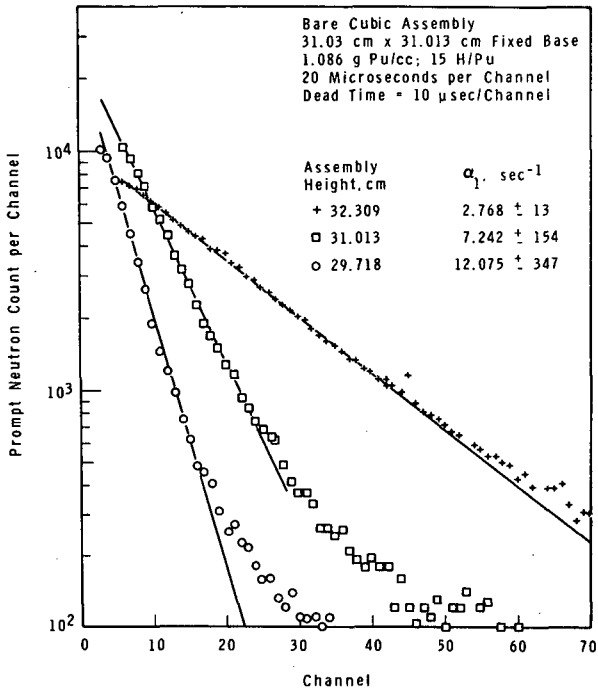


Fig. 5

Prompt neutron decay as a function of assembly height

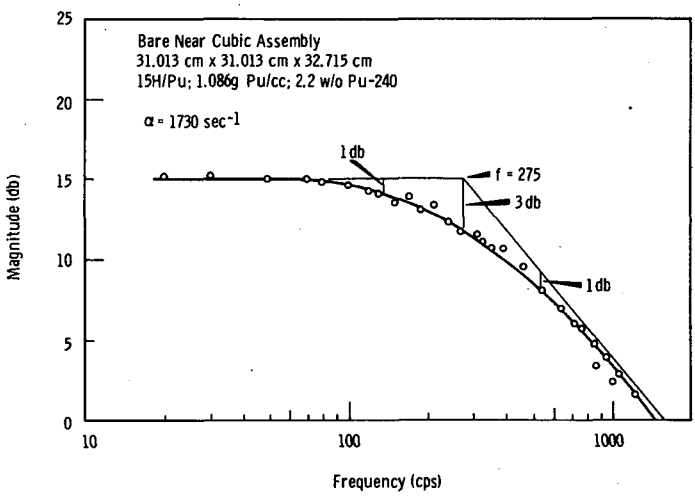


Fig. 6

Power spectrum of a bare cubic assembly

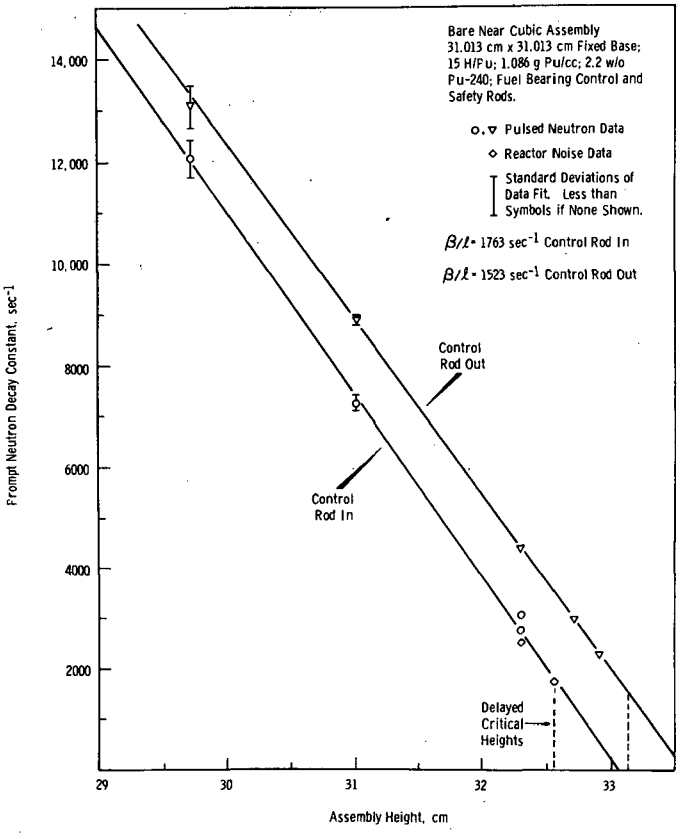


Fig. 7

Decay constant as a function of assembly height

epithermal, having a gold-cadmium ratio of approximately 1.02 and a prompt neutron lifetime of 1.2 μs. The pulsed neutron source measurements were close to marginal near critical, as can be seen from the raw data shown in Fig. 5, and completely unreliable at critical. The raw data shown in Fig. 5 has had the constant delayed neutron and background term A_p subtracted out. Thus, only the prompt neutron variation with time following a burst of neutrons is shown.

Figure 5 illustrates another limitation of pulsed neutron source measurements in epithermal multiplying systems. The decay rate of the prompt neutrons will increase as the energy spectrum of the system shifts upward and the measurements eventually become limited by the speed of the electronics available, as well as limitations on the duration of the pulse. As can be seen in Fig. 5, the decay of the prompt neutron flux following a pulse was relatively fast. Even with approximately 90% of the critical mass on the table (29.72 cm high assembly) the prompt neutron decay constant of (12 075 ± 347) s^{-1} was determined by observing the flux for only 200 μs. As

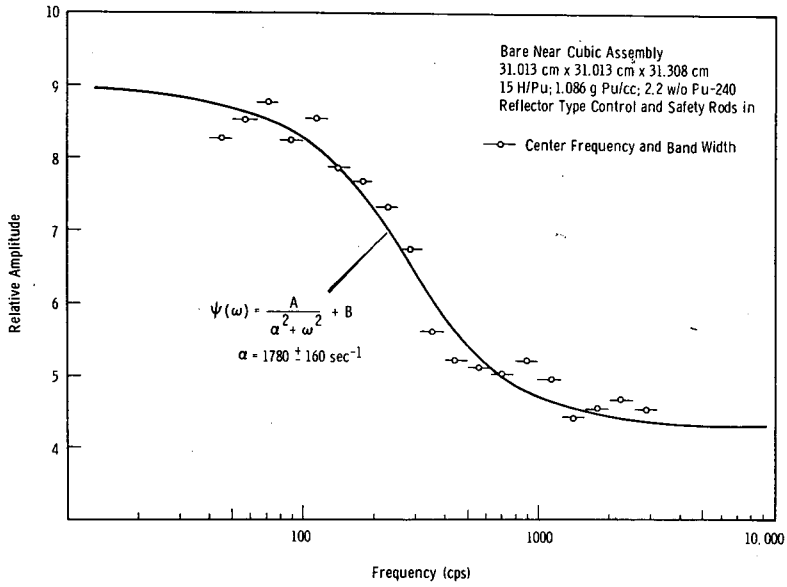


Fig. 8

Spectral density of a bare cubic assembly

the reactor system is made further subcritical, analysis of the pulse data must be based on shorter and shorter observation times, i.e. fewer and fewer data points over which to determine the decay rate of the fundamental mode.

Based on the data shown in Fig. 5 alone, it would be difficult to determine, reliably, values for the decay constant of the fundamental mode of decay for each of these measurements because of the large value of A_p and the fast decay. However, reactor noise measurements performed near criticality and at delayed criticality were easy to perform, and, as will be seen later, confirm the validity of the decay constants shown in Fig. 5.

The observed power spectral density in decibels versus frequency is shown in Fig. 6 for this same reactor system at delayed critical. Because of limitations in data acquisition, noise information was not obtained on frequencies above 1250 c/s. Consequently, it was not possible to determine the relative amplitude of the white noise A_n in the system. Thus fitting Eq.(7) to the experimental data is not appropriate, unless, of course, A_n is assumed to be zero. In such cases, however, the break-frequency α can be predicted by a technique analogous to that used in predicting the gain characteristics of control systems [7]. The theoretical spectral density in the prompt neutron region is given by

$$\Psi(\omega) = \frac{B_n}{\alpha^2 + \omega^2}, \tag{8}$$

which is the same as Eq.(7) except that there is no extraneous noise present.

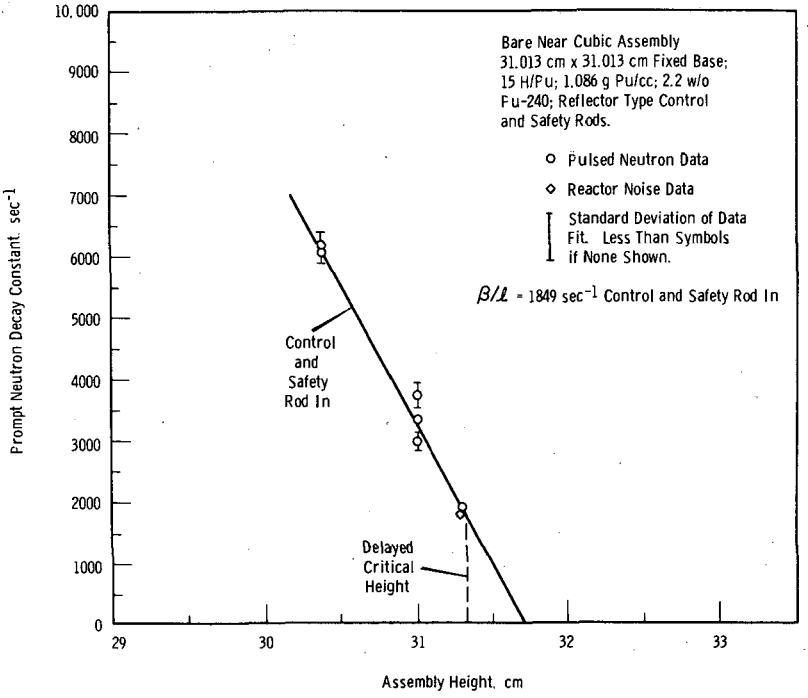


Fig. 9

Decay constant as a function of assembly height

Under these conditions, the spectral density goes to zero as the frequency increases. The rate at which $\Psi(\omega)$ goes to zero can be calculated by taking the partial derivative of Eq.(8) with respect to ω. This can be simplified if the spectral density is expressed in decibels. Thus Eq.(8) becomes:

$$10 \log_{10} \Psi(\omega) = 10 \log_{10} \frac{B_n}{\alpha^2 + \omega^2} .$$

In the high frequency region where ω is much larger than α, the slope of the spectral density is theoretically -20 decibels per decade, whereas in the lower frequency region where ω is much less than α, the spectral density curve becomes flat. Thus, the spectral density of the reactor noise over the prompt neutron frequency range can be theoretically described as two asymptotes. These two asymptotes will, of course, intercept at the break-frequency ($\omega = \alpha$). The difference between the asymptotic curves and the actual spectral density curve should be a maximum at the break-frequency and should be geometrically symmetrical about the break-frequency.

This method was employed to determine the break-frequency of the experimental data shown in Fig. 6. Since the actual spectral density curve is 3 db down from the asymptotic curves at the break-frequency, the white noise amplitude must be essentially zero. Had the amplitude been relatively high,

the difference would have been less than 3 db and the actual spectral density curve would have crossed the high frequency asymptote.

The prompt neutron decay constants obtained from both the pulsed neutron source and the reactor noise measurements on this reactor system are shown in Fig. 7 as a function of the assembly's height. Since extrapolation of the subcritical pulsed neutron source measurements to delayed criticality predicts, within the accuracy of the measurements, the break-frequency of the spectral density at delayed criticality, the respective decay modes shown in Fig. 5 are the fundamental modes of decay for the indicated assembly heights. A least squares fit of both the pulse and noise data predicts a value of 1763 s^{-1} for the decay constant of the reactor system at delayed criticality. This is with the fuel bearing control and safety rods full in; that is, a clean near cubic geometry. Subcritical pulsed neutron source data with the fuel bearing control rod full out are also shown in Fig. 7, and parallel those made with the control rod in. Their consistency provides further credence to the validity of the pulse data shown in Fig. 5.

Experimental data are shown in Figs. 8 and 9, in which sufficient high frequency noise information was obtained to permit determining the break-frequency of the reactor systems spectral density at delayed criticality from Eq. (7). The reactor was identical to the preceding one, except that the control rod and the safety rod were external to the system and were made of Lucite. The curve shown in Fig. 8 is a least squares fit of Eq. (7) to the experimental noise data. As can be seen in Fig. 9, the pulsed neutron source and reactor noise data are again in agreement.

Systems with an even smaller H/Pu atomic ratio than 15 should still be within the capabilities of a modest noise measuring system; however, pulsed neutron measurements would rapidly become impractical. In systems with a higher H/Pu ratio, either method should provide satisfactory results near delayed criticality. However, pulsed neutron source measurements should provide the better data on subcritical systems.

In plutonium systems having optimum moderation, a minimum mass of plutonium is present. Consequently, the residual neutron density from inherent neutron sources is a minimum and the relative magnitude of A_p in Eq. (7) would be modest, even near delayed critical. It should therefore be feasible to obtain satisfactory pulse data on such systems up to delayed criticality. Reactor noise measurements should also be satisfactory for these systems, since detector efficiency can be made relatively high for a moderately sized system. Therefore, near critical both the pulse ratio $B_p/(A_p + B_p)$ and the noise ratio $B_n/(A_n + B_n)$ should be acceptably large. However, B_n decreases rapidly in subcritical systems; therefore, pulsed neutron source measurements should yield the better data in the subcritical systems.

The experimental data shown in Figs. 10 and 11 were obtained from a reactor system having a H/Pu atomic ratio of 35. Although this was not close to optimum moderation (H/Pu ~800) the system was considerably more thermal than the previous one. The prompt neutron lifetime in this system was 7.7 μs as compared to the 1.2 μs in the 15 H/Pu system. The reactor consisted of 5.17 cm plutonium-polystyrene cubes and 5.17 cm Lucite cubes arranged in a three dimensional checkerboard array having a fixed base of 36.18 cm on each side. The Pu^{240} content was 2.2 wt.% as in the previous system.

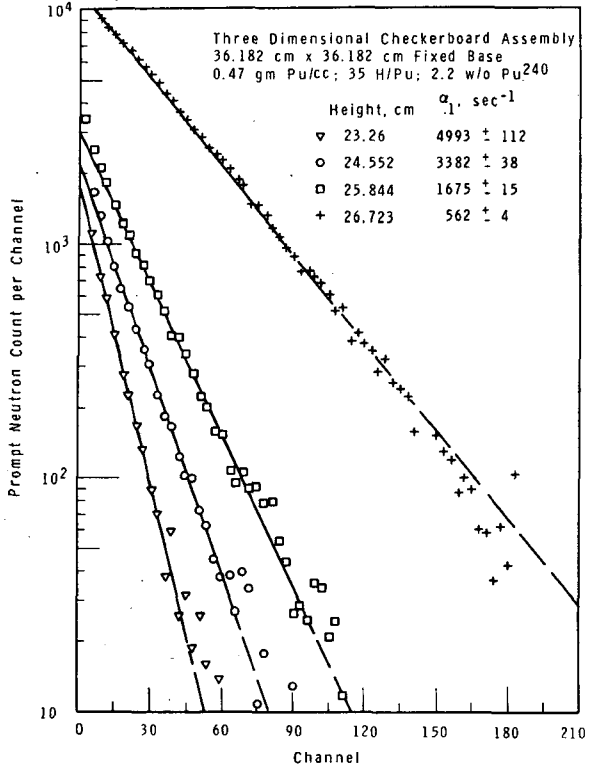


Fig. 10

Prompt neutron decay as a function of assembly height

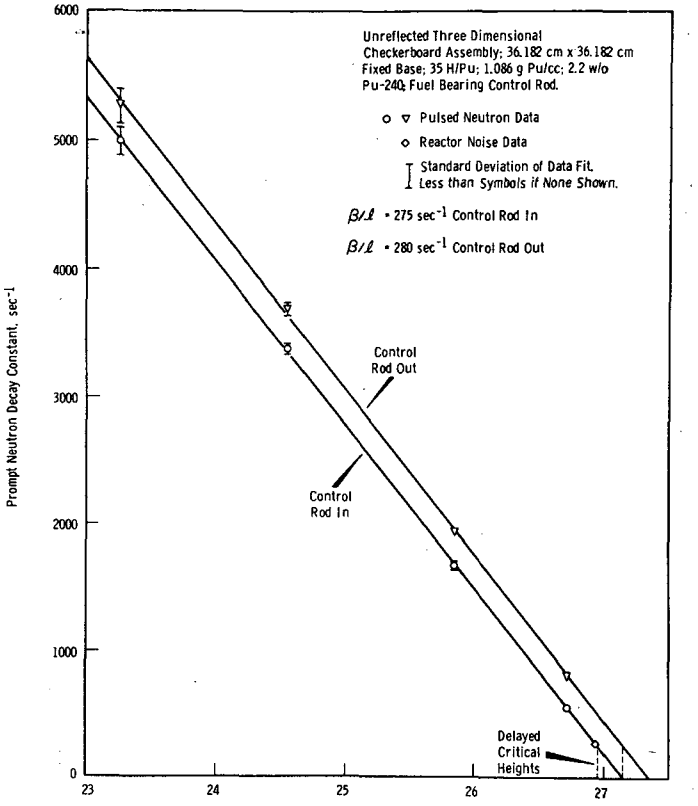


Fig. 11

Decay constant as a function of assembly height

Pulsed neutron source measurements of the decay constant were obtained during approach-to-critical. These data appear in Fig. 10. From these data, it is quite evident that the fundamental decay mode was established for each of the four measurements shown. A reactor noise measurement was made at delayed critical, and the value of α obtained is again in excellent agreement with the extrapolated subcritical pulsed neutron source data, as evidenced by the α versus assembly height data shown in Fig. 11. In Fig. 11 a least squares fit of the experimental data predicts a β/ℓ of 275 s^{-1} for the reactor system with the fuel bearing control rod in and 280 s^{-1} with it out.

EFFECTS OF MODERATION AND Pu^{240} CONTENT ON PROMPT NEUTRON DECAY

That a considerable amount of quantitative information concerning a particular fuel-moderator system can be obtained from pulse decay experiments is evident from the data presented in Fig. 12 where the dependence of the parameter α on the geometric buckling is shown. The effect of the H/Pu ratio and the presence of Pu^{240} on this dependence is also shown. These data were obtained from measurements on four different reactor systems. Two of these, those containing 2.2 wt.% Pu^{240}, have been described previously (see Figs. 7 and 11). The other two reactor systems were similarly constructed using plutonium-polystyrene cubes having a hydrogen-to-plutonium atomic ratio of 15 and a plutonium concentration of 1.038 g/cm^3 containing 8.08 wt.% Pu^{240}. The 39 H/Pu assembly was obtained by constructing a three dimensional checkerboard array using these cubes, encased in 0.020-in aluminium cans, and Lucite cubes alternatively.

Although the fuel in the three dimensional checkerboard assemblies (35 and 39 H/Pu) was not distributed homogeneously throughout the assemblies, the variation of α with the geometric buckling was observed to be of the form given by diffusion theory as

$$\alpha = \overline{\Sigma_a v} + D_0 B_g^2 - v\Sigma_f [\nu_p \overline{P}(B_g^2) - 1 - \Sigma_c/\Sigma_f], \quad (9)$$

where Σ_a v refers to the absorption rate in the moderator, Σ_f is the macroscopic thermal fission cross-section of the mixture, ν_p is the average number of prompt neutrons emitted per fission, Σ_c/Σ_f is the thermal capture-to-fission ratio of the fissile material, and $\overline{P}(B_g^2)$ denotes the probability that a fission neutron will slow down to thermal energies in an assembly of buckling B_g^2 [8]. A calculated curve of α for a pure moderator is also shown in Fig. 12 to illustrate the physical meaning of some of the terms in Eq. (9), and to indicate the capability of pulsed neutron measurements for testing reactor models and detailed computational methods. It is evident from the data shown in Fig. 12 that pulse measurements provide a measured parameter α which can be used to check the energy group constants of a computational method, not only at the delayed critical condition but over a wide range of subcritical conditions. It has been suggested [8] that measured prompt decay constants for subcritical systems (whether slow or fast) should

provide a more sensitive test of the lower energy group constants than is obtained from equivalent comparisons at the delayed critical condition.

For the fast 15 H/Pu assemblies, diffusion theory is not applicable and Monte Carlo or multigroup transport calculations must be used for interpreting the measured decay constants. A Monte Carlo calculation on the 2.2 wt.% Pu^{240} system is shown in Fig. 12. Computed variations of α with buckling for these assemblies are shown in Fig. 12 as a broken line. The decay constants were obtained by normalizing eighteen-group transport theory calculations using computer code DTF [9]. The computed variation of α with buckling is seen to be slightly greater than the experimentally observed variation. Both are observed to be extremely sensitive to any variation in geometric buckling in the fast H/Pu systems.

Values for the observed decay constants shown in Fig. 12 are tabulated in Tables I and II of the Appendix. Extrapolated values based on least squares fits of the measured values are also included in Tables I and II.

β/ℓ for the two checkerboard assemblies having approximately the same H/Pu (35 and 39) atomic ratio was observed to decrease by a factor of 1.67 (275 to 165 s^{-1}, respectively) as the Pu^{240} content was increased from 2.2 to 8.08 wt.%. If a value of 0.0021 is assumed for β, the neutron lifetime in these delayed critical assemblies is seen to increase from 7.7 to 12.7 μs as the Pu^{240} content is increased. Similar observations were made on the two reactor systems having H/Pu atomic ratios of 15. β/ℓ for these systems was observed to decrease from 1763 s^{-1} to 1357 s^{-1} as the Pu^{240} content is increased from 2.2 to 8.08 wt.%. If β is again assumed to be 0.0021, the neutron lifetime is seen to increase from 1.2 to 1.6 μs as the Pu^{240} is increased. Although Pu^{240} is a neutron poison, its inclusion in a constant H/Pu system displaces Pu^{239}. Based on Monte Carlo calculations [10] about 93% of the absorptions take place in the Pu^{239}. Consequently, an increase in the neutron lifetime is to be expected as the Pu^{240} content is only increased *from 2.2 to 8.08 wt.% in these reactor systems.*

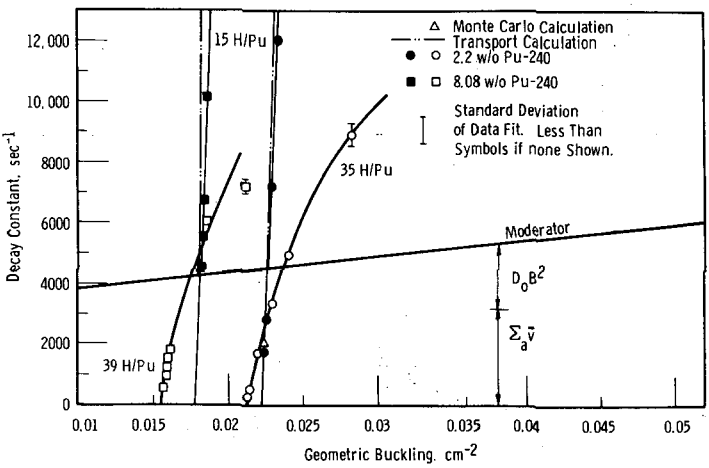


Fig. 12

Variation of prompt neutron decay constant with buckling of bare intermediate plutonium systems

TABLE I

DECAY CONSTANTS

Assembly description	Assembly height (cm)	Pulsed neutron source decay constant (s^{-1}) Control rod position		Reactor noise decay constant (s^{-1}) Control rod position
		IN	OUT	IN
Bare three-dimensional checkerboard assembly; 36.18 cm × 36.18 cm fixed base; 35 H/Pu; 0.47 g Pu/cm^3; 2.2 wt.% Pu^{240}; fuel bearing control and safety rods	19.38	8941 ± 390		
	23.26	4993 ± 112	5264 ± 137	
	24.55	3382 ± 38	3684 ± 46	
	25.84	1675 ± 15	1939 ± 24	
	26.72 [b]	562 ± 4	806 ± 8	
	26.945	275[a]	534[a]	275
	27.141	-	280[a]	
	27.162[a]	0	-	
	27.359[a]	-	0	
Bare near cubic assembly 31.01 cm × 31.01 cm fixed base; 15 H/Pu; 1,086 g Pu/cm^3; 2.2 wt.% Pu^{240}; fuel bearing control and safety rods	29.72	12075 ± 347	13079 ± 420	
	31.01	7242 ± 154	8866 ± 81	
	32.31	2768 ± 13	4388 ± 25	2515
	32.31	3056 ± 21	4383 ± 39	
	32.563	1910[a]	3494[a]	1730
	32.72[b]	-	2995 ± 20	
	32.72[b]	-	2971 ± 80	
	32.90[b]	-	2289 ± 64	
	33.049[c]	0	-	
	33.132	-	1523[a]	
	33.572[a]	-	0	

[a] Extrapolated from a least squares fit of the last few points.
[b] Flux weighted partial layers.

TABLE II

DECAY CONSTANTS

Assembly description	Assembly height (cm)	Pulsed neutron source decay constant (s^{-1}) Control rod and safety rod	
		IN	OUT
Bare three-dimensional	26.91	-	7192 ± 227
checkerboard assembly	32.29	5261 ± 100	5992 ± 121
36.58 cm×36.58 cm fixed	40.36[b]	1330 ± 18	1851 ± 38
base; 39 H/Pu; 0.476 g Pu/cm^3;	41.03	1005 ± 10	1599 ± 27
8.08 wt.% Pu^{240}; reflector	41.70[b]	713 ± 10	1279 ± 16
(Lucite) type control and	42.38	408 ± 4	991 ± 8
safety rods	43.05	-	683 ± 6
	44.196	-	165[a]
	42.813	207[a]	789[a]
	43.269[a]	0	-
	44.561[a]	-	0
Bare near cubic assembly	32.73	-	10415 ± 282
36.30 cm×36.15 cm fixed	33.37	-	6798 ± 110
base; 15 H/Pu; 1.038 g Pu/cm^3;	33.37	-	7046 ± 103
8.08 wt.% Pu^{240}; reflector	33.68[b]	-	5925 ± 124
(Lucite) type control and	33.68[b]	-	5526 ± 105
safety rods	34.012	-	4320 ± 75
	34.012	-	4556 ± 62
	34.808	-	1357[a]
	35.156[a]	-	0

[a] Extrapolated from a least squares fit of the last few points.
[b] Flux weighted partial layers.

EXPERIMENTAL OBSERVATIONS IN REFLECTED SYSTEMS

COHN [11] has shown that, for a reflected monoenergetic system spatially independent in each region, the kinetic behaviour of experimental interest corresponds to that of a bare reactor with the same 1/v lifetime. In their model, RANDALL and GRIFFITH [12] have shown that for a detector located in the reflector, the spectral density of the reactor noise should actually have three break-frequencies, α_1, α_2, α_3, according to:

$$\Psi(\omega) = A + \frac{B(\omega^2 + \alpha_4^2)(\omega^2 + \alpha_5^2)}{(\omega^2+\alpha_1^2)(\omega^2 + \alpha_2^2)(\omega^2 + \alpha_3^2)} \tag{10}$$

where

$$\alpha_1 = \beta/[\ell^* + \ell_r \beta (1-\beta_7)]$$
$$\alpha_2 = 1/\ell_r$$
$$\alpha_3 = \frac{\beta + \beta_7 - \beta\beta_7}{\ell_c} + \frac{1}{\ell_r} - \alpha_1 .$$

Experimental spectral density data are shown in Fig. 13 from a noise measurement made on a water reflected, 12.95-l sphere, partially filled with plutonium nitrate solution. The detector, a liquid organic filled, B^{10}-enriched scintillator, was located in the reflector. For a water reflector, α_2 is about 5000 s^{-1} and since α_3 is greater than α_2, it would appear that only the single break-frequency, α_1, lies within the frequency range covered by the data shown in Fig. 13. Therefore, a single break-frequency fit was

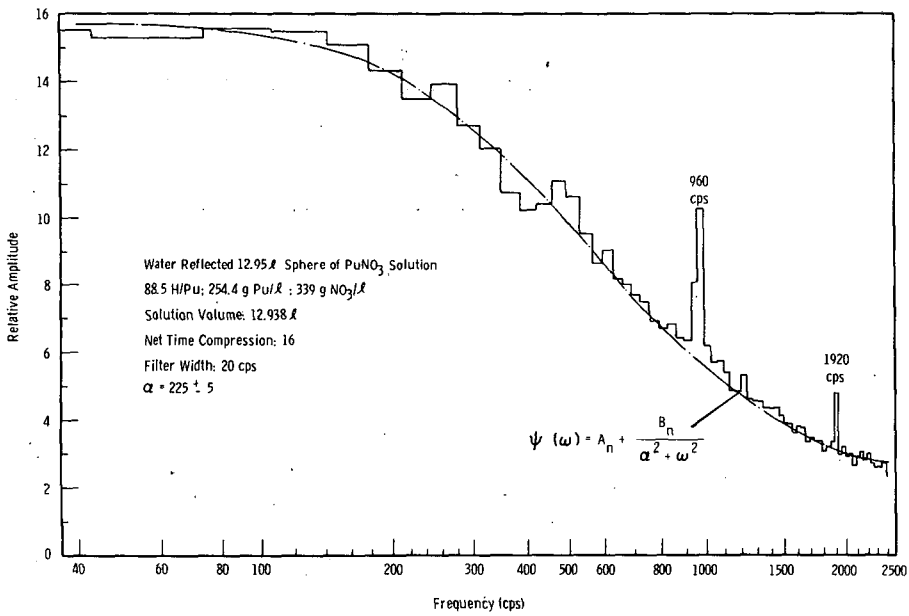


Fig. 13

Spectral density of a reflected sphere

made of these data to obtain a decay constant of $(225 \pm 5)s^{-1}$. However, pulsed neutron source measurements on this system indicate a decay constant of $(207 \pm 3)s^{-1}$. Either a second decay mode went unobserved in the pulse measurement and/or higher break-frequencies in the noise spectrum are contributing sufficiently to explain the discrepancy between the two measurements. An effort is currently being made to resolve this apparent discrepancy between noise and pulse measurements in reflected systems and also to investigate the effects of detector location.

That the prompt neutron decay constants are spatially-dependent in reflected systems has been experimentally observed. Measurements made on a reflected 30.2-l sphere of plutonium nitrate solution resulted in the data shown in Fig. 14. The transient flux following a burst of neutrons was observed with a small BF_3 tube positioned tangentially to the sphere 2 in out in the reflector and with an identical BF_3 tube positioned symmetrically in the centre of the core. The decay constants observed by these two detectors, as solution was added to the sphere, are shown in Fig. 14. At delayed criticality, the decay constant observed in the reflector (55 s^{-1}) was about 20% larger than that observed in the core (45 s^{-1}). This tends to strengthen the concept of an additional delayed neutron group caused by

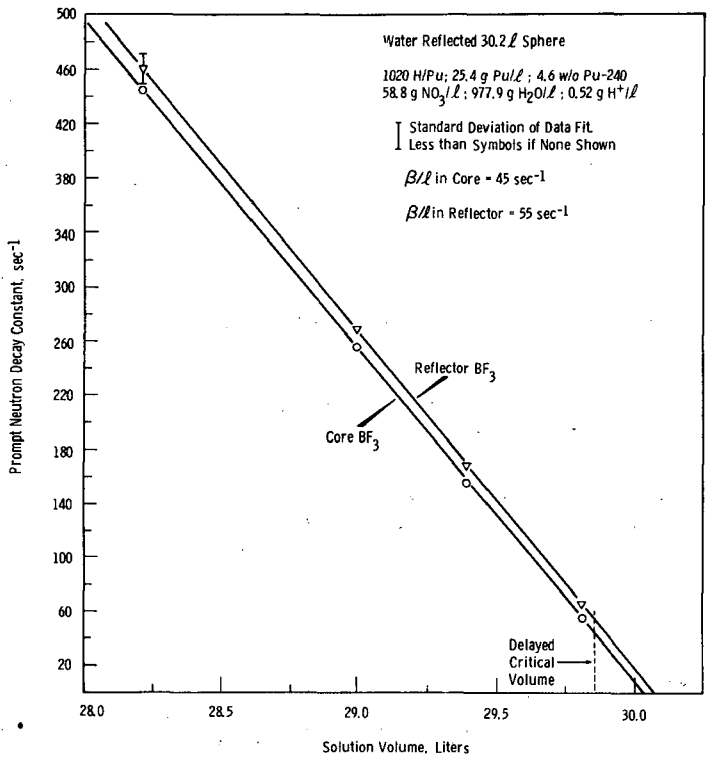


Fig. 14

Decay constant as a function of sphere volume and detector position

the neutrons "delayed" in the reflector. That is, if the 45 s^{-1} in the core is related to β/ℓ, the 55 s^{-1} in the reflector would seem to be related to K/ℓ, where K is some constant greater than β but less than 1. Raw pulse data from measurements made when the sphere contained 29.81 litres of solution are shown in Fig. 15.

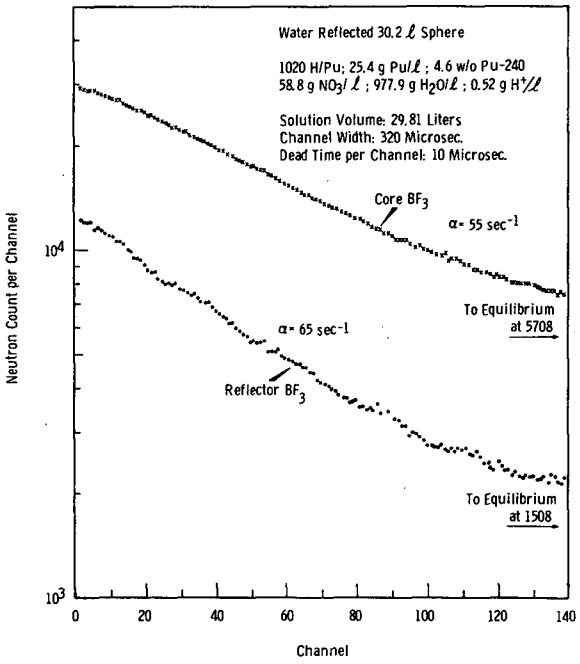


Fig. 15

Neutron decay as a function of detector location

To obtain a better understanding of reflected reactor kinetics, an effort is currently being made better to define these systems theoretically and to obtain supporting experimental data. It is hoped that, with the combined information available from reactor noise and pulsed neutron measurements, a theoretical model can be developed which will accurately describe the neutron parameters in a reflected system.

SUMMARY

Good agreement has been obtained between reactor noise and pulsed neutron source measurements for a number of plutonium systems. The complementary nature of these two experimental methods has been used to check the consistency of the measurements and to extend the reactivity range over which the decay constants could be measured. Measurements have also been made on systems containing different concentrations of Pu^{240}. Measure-

ments performed on a reflected assembly show that the flux decay observed in the reflector differs from that of the core region. The value of α at delayed criticality was observed to be 55 s^{-1} in the reflector and 45 s^{-1} in the core. These results tend to strengthen the concept of an additional delayed neutron group caused by the neutrons delayed in the reflector. Work is currently being performed at the Critical Mass Laboratory to gain an improved understanding of the neutron kinetics in reflected systems and to obtain measured decay constants over a wider range of H/Pu atomic ratios and geometric bucklings. Further results on reflected assemblies are particularly needed for the correct interpretation and analysis of the pulse and noise measurements.

ACKNOWLEDGEMENTS

The authors wish to express appreciation to Drs. R. W. Albrecht and K. L. Garlid of the Department of Nuclear Engineering of the University of Washington for their critical review of this paper and their assistance as consultants to Battelle-Northwest Laboratories in the accumulation and analysis of the data contained herein. Appreciation is also expressed to J. R. Clark for his success in keeping all of the electronic gear functioning properly.

APPENDIX

LIST OF SYMBOLS

C_i concentration of the i-th delayed precursor
$f(t)$ forcing function
k effective neutron multiplication constant
ℓ_c time neutrons spend in core
ℓ_r time neutrons spend in reflector
ℓ neutron lifetime
ℓ^* $\ell_c + \ell_r \beta_\gamma$
n neutron density
n_0 neutron density at time zero
s neutron contributions from a source
α prompt neutron decay constant
β $\sum_{i=1}^{m} \beta_i$, the effective average delayed neutron fraction
β_γ fraction of neutrons appearing in the core which came from the reflector
λ_i decay constant of the i-th delayed neutron group
$\Psi(\omega)$ power spectral density function
ω frequency

REFERENCES

[1] CLARK, J.R. and ALBRECHT, R.W., Preliminary proposal – noise analysis Critical Mass Laboratory, Rpt. HW-81081 (2 March 1964).

[2] CLAYTON, E.D., Progress in plutonium critical mass physics, Rpt. HW-83603, (Oct. 1964).

[3] BIERMAN, S.R., GARLID, K.L. and ALBRECHT, R.W., Rpt. HWSA 3700 (1964); (Submitted for publication in Nucl. Sci. Engng).

[4] THIE, J.A., Reactor Noise, Rowman and Littlefield, Inc., N.Y. (1963).

[5] UHRIG, R.E., Coordinator, Noise Analysis in Nuclear System (USAEC Symposium Series 4) Off. Techn. Services, US Dept. of Comm., Wash. DC (1964).

[6] LANING, J.H. and BATTIN, R.H., Random Processes in Automatic Control, McGraw-Hill Book Company, Inc., N.Y. (1956).

[7] TRUXAL, J.G., Control System Synthesis, McGraw-Hill Book Company, Inc., N.Y. (1956) 344-53.

[8] KEEPIN, G.R., Atom. Energy Rev. 2 2 (1965) 75-93.

[9] CARLSON, B.G. et al., DTF Users Manual I & II, United Nuclear Corporation, White Plains, N.Y. (1963).

[10] CARTER, L.L., personal communication.

[11] COHN, C.E., Nucl. Sci. Engng 13 (1962) 12-17.

[12] RANDALL, R.L. and GRIFFITH, C.W., in Noise Analysis in Nuclear Systems (USAEC Symposium Series 4) Off. Techn. Services, US Dept. of Comm., Wash. DC (1964) 107-33.

A SIMPLE CROSS-CORRELATION METHOD FOR THE STUDY OF THE NEUTRON PULSE TRANSFER FUNCTION IN MEDIA USING A STATISTICALLY PULSED NEUTRON SOURCE

R. HAAS, W. MATTHES AND B. WECKERMANN
EURATOM
CENTRO COMUNE DI RICERCHE, ISPRA, ITALY

Abstract — Résumé — Аннотация — Resumen

A SIMPLE CROSS-CORRELATION METHOD FOR THE STUDY OF THE NEUTRON PULSE TRANSFER FUNCTION IN MEDIA USING A STATISTICALLY PULSED NEUTRON SOURCE. The cross-correlation between the fission process in a fission neutron source and a neutron detector yields the pulse transfer function of the medium between source and detector position.

Because of the low background obtainable, the asymptotic behaviour and the short time behaviour of the decay curve, which results from space and energy transients, can be measured even with rather weak sources. The reported measurements are considered as a survey to determine the experimental possibilities of this method. The time constant for thermalization (the neutron energy decay) in paraffin is measured as $(5 \pm 1)\,\mu s$. Some fundamental aspects of the application of this correlation method to multiplying media are discussed.

MÉTHODE SIMPLE DE CORRÉLATION POUR L'ÉTUDE DE LA FONCTION DE TRANSFERT DE BOUFFÉES DE NEUTRONS DANS DES SYSTÈMES AU MOYEN D'UNE SOURCE DONT LES BOUFFÉES SONT STOCHASTIQUES. La corrélation entre le processus de fission dans une source de neutrons de fission et dans un détecteur de neutrons donne la fonction de transfert de bouffées du milieu compris entre la source et le détecteur.

Etant donné le faible bruit de fond qu'il est possible d'obtenir, on peut mesurer, même avec des sources assez peu intenses, le comportement asymptotique et le comportement à court terme de la courbe de décroissance, qui résulte des états transitoires variables dans l'espace et selon l'énergie. Les mesures dont les résultats sont présentés sont considérées comme une étude visant à déterminer les possibilités expérimentales de cette méthode. La mesure de la constante de temps pour la thermalisation (décroissance de l'énergie des neutrons) dans la paraffine a été de $5 \pm 1\,\mu s$. Les auteurs étudient certains aspects fondamentaux de l'application de cette méthode de corrélation dans des milieux multiplicateurs.

ПРОСТОЙ МЕТОД ПЕРЕКРЕСТНОЙ КОРРЕЛЯЦИИ ДЛЯ ИЗУЧЕНИЯ ПЕРЕДАТОЧНОЙ ФУНКЦИИ НЕЙТРОННЫХ ИМПУЛЬСОВ В СРЕДЕ С ПОМОЩЬЮ СТАТИСТИЧЕСКИ ПУЛЬСИРУЮЩЕГО ИСТОЧНИКА НЕЙТРОНОВ. Функция перекрестной корреляции между процессами деления в источнике нейтронного деления и в детекторе нейтронов дает функцию пульсирующего перехода среды между источником и положением детектора.

Согласно полученному низкому фону, асимтотическое поведение и кратковременное кривой рапада, которая получается из пространства с переходного процесса энергии, можно измерить даже с помощью очень слабых источников. Измерения, о которых идет речь, рассматриваются как обзор с целью определения экспериментальных возможностей этого метода. Постоянная времени для термализации (распад энергии нейтрона) в парафине измеряется как 5 ± мксек.

Обсуждаются некоторые основные аспекты применения этого метода корреляции к множественной среде.

METODO SENCILLO DE CORRELACION PARA ESTUDIAR LA FUNCION DE TRANSFERENCIA DE LOS IMPULSOS NEUTRONICOS MEDIANTE UNA FUENTE ESTADISTICAMENTE PULSADA. La correlación entre el proceso de fisión en una fuente de neutrones de fisión y un detector neutrónico permite conocer la función de transferencia de los impulsos neutrónicos en el medio de que se trate, entre la fuente y el lugar ocupado por el detector.

Debido a la baja actividad de fondo, resulta posible medir, incluso empleando fuentes relativamente débiles, el comportamiento asintótico y el comportamiento durante un tiempo breve de la curva de decreci-

miento, resultante de los fenómenos espaciales y energéticos de carácter transitorio. Las mediciones que los autores dan a conocer se consideran como un estudio general encaminado a determinar las posibilidades experimentales de este método. La medición de la constante de tiempo de termalización (decrecimiento de la energía neutrónica) en la parafina dio un valor de $5 \pm 1\,\mu s$. Los autores estudian diversos aspectos fundamentales de la aplicación de este método de correlación a las mediciones en medios multiplicadores.

1. INTRODUCTION

For the investigation of the time-dependent behaviour of the neutron population in systems, cross-correlation methods are widely used [1]. If discrete neutron bursts are injected into the medium M (see Fig. 1), the correlation function between the input x and the output y is given by:

$$K_{xy}(\tau) = \int_{-\infty}^{+\infty} K_{xx}(t-\tau)\, g(t)\, dt,$$

where g(t) is the desired pulse transfer function and $K_{xx}(t)$, the input self-correlation, can be expressed as:

$$K_{xx}(t) = \bar{x}\,\delta(t) + \bar{x}^2 + T_{xx}(t),$$

the three terms being the correlation of the input pulse with itself, the square of the mean input rate and $T_{xx}(t)$ being the input pulse to pulse correlation. In the absence of this last term, for instance for a white noise input, the cross-correlation reduces to

$$K_{xy}(\tau) = \bar{\bar{x}}\,[\bar{y} + g(\tau)]$$

so that we obtain directly the pulse transfer function on a constant background, which is equal to the mean detector count rate. The transfer function g(t) is the product of the detector sensitivity ϵ, the mean prompt neutron yield per burst $\bar{\nu}_s$ and the Green's function, relating source position $\vec{r}_s$, energy and time t_s, to the detector position $\vec{r}_D$, energy E and time t_D. With $t_D - t_s = \tau$,

$$g(\tau) = \bar{\nu}_s \int G^F(\vec{r}_s\,;\, \vec{r}_D,\, E,\, \tau)\,\epsilon(E)\, dE$$

All interpretations of the transfer function depend on the models introduced into G^F.

In our experiments the white noise input is verified by the use of a radioactive fission neutron source, where the input x is represented by the output of the fission detector.

2. AIM OF THE EXPERIMENT

Since there are at the time being no multiplying assemblies accessible for our experiments in Ispra, we decided to choose moderators for our test

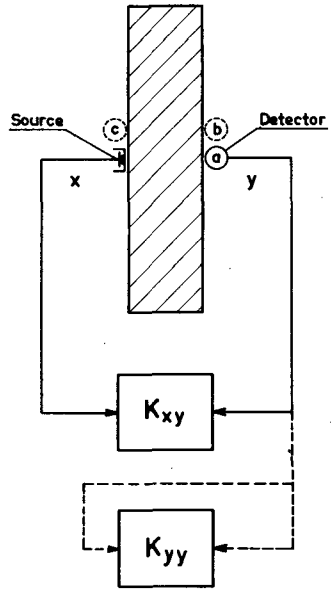


Fig. 1

Schematic arrangement of the correlation experiment for the determination of K_{xy} and K_{yy}

experiments. Since we have an experimental programme for the development of moderators for the pulsed fast reactor, we chose our programme so as to complement the results which will be obtained by experiments done at the Van de Graaff in Ispra, by the study of the short time behaviour of the moderating materials.

The advantageous characteristics of this method are the good time resolution which is 0.2 μs with standard electronics. This accuracy for the definition of the time zero point could, of course, be improved. Furthermore the input spectrum is a fission spectrum.

The disadvantage is the low neutron number per burst. Therefore the neutron spectrum can, at the output, only be determined in an integral way, along the line of a determination of the mean neutron temperature.

3. EXPERIMENTAL SETUP

A spontaneous fission source of Cf^{252} is used. The neutron emission is monitored through the detection of the fission products in approximately 2π geometry by a solid state detector. The mean prompt neutron yield per fission is $\overline{\nu}_s = 3.7$ [2]. The monitored fission rates were 16 fissions per second for one source and finally 60 fissions per second for a somewhat stronger one. As neutron detectors BF_3 and He^3 counters of equal dimensions were used, 2.5 cm diameter and 15 cm effective length.

A practically infinite slab geometry was used (see Fig. 1). Source and detector are located opposite to each other at the large surfaces of the medi-

um (50 cm × 50 cm). The thickness of the slab was varied between 2.2 and 13 cm. For convenience paraffin was chosen as moderator material. Positions b and c were also occupied by detectors in some experiments.

Because of the low source intensities the correlation function could be directly obtained with a standard time-of-flight analyser. The measuring times for one decay curve varied between 2 and 5 d. If, however, high source intensities would be available, up to 10^4 fissions per second would be useful; the trigger input dead-time of the time-of-flight analyser could be reduced easily with a shift register accompanied by an intermediate memory.

Of course, instead of spontaneous fission also induced fission can be used as a source by placing a fission chamber in a thermal neutron beam [3]. The fast neutron background in the beam and in the reactor hall however, presented a background problem and shieldings ruined the clean geometry, which was necessary for the present experiments.

In all plots the measured function g(t) divided by the width of the time channel Δt (μs) is shown. The background $\bar{y}$ is subtracted according to the readings of the last recorded channels or according to the first channels in the cases where a delay was introduced into the output line y.

4. EXPERIMENTS ON THE ASYMPTOTIC DECAY CURVES

The asymptotic decay constant λ was measured for slab thicknesses from 2.2 to 13 cm. Figure 2 shows some of the curves. It is at once apparent that very large measuring times were necessary for thicknesses larger than 10 cm. The asymptotic decay did not start before times of the order of one and a half decay times.

Figure 3 shows a plot of the asymptotic decay constants λ versus buckling B^2. The full line is obtained from the diffusion parameters measured with the pulsed source technique [4] with

$$\lambda = \lambda_a + D_0 B^2 - C B^4$$

Our values are, within the errors of the measurement ($\Delta\lambda$ results from the counting statistics and ΔB^2 from homogeneity and thickness variations of the stapled paraffin plates), consistent with the values given in literature.

The asymptotic time constant for epicadmium neutrons (measured with a 1/v counter covered by 0.5-mm cadmium) was obtained with $(2.2 \pm 0.2)\mu$s inside a paraffin slab 10-cm thick [3]. On the surface of a 2.2-cm-thick slab this time constant reduced to $(0.76 \pm 0.1)\mu$s. At the time being, no conclusions can be drawn from these data, concerning leakage properties for epithermal neutrons, because, as shown in section 5, these neutrons do not establish a fundamental space mode even in a very thin slab of moderator, however the decay curves follow, for times larger than 4 μs, an exponential decay within the accuracy of the experiment.

In any case flight-time corrections for the counters should be be small, because at times larger than 4 μs no significant change of the mean neutron velocity for the remaining neutron fraction above the cadmium cut-off is expected any more. If we assume that the mean energy of the neutrons is

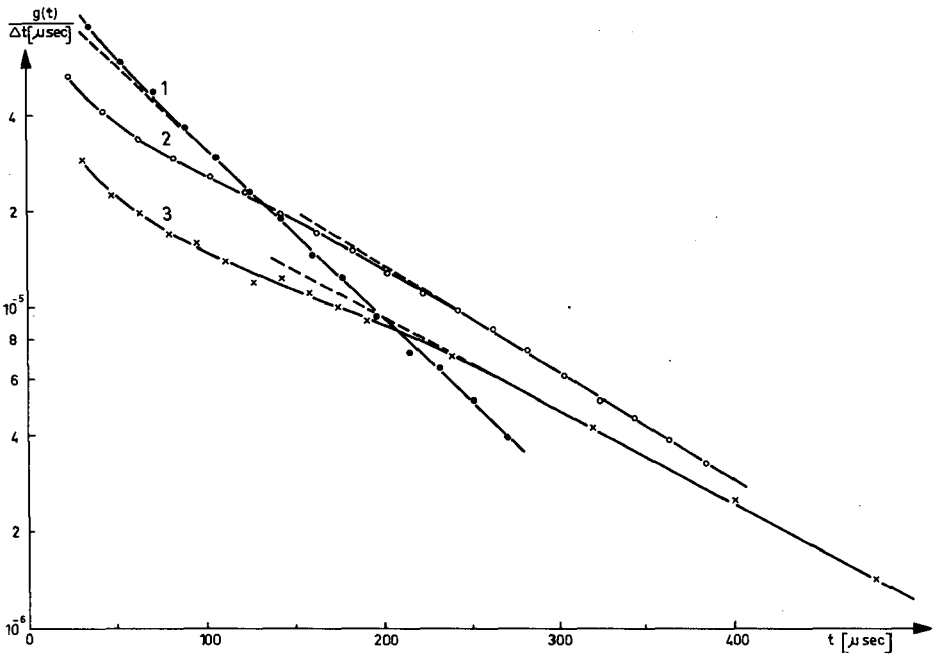


Fig. 2

Decay curve for paraffin slabs

Curve 1: thickness d = 6.6 cm, asymptotic time constant λ^{-1} = 82 μs
Curve 2: d = 11 cm, λ^{-1} = 128 μs
Curve 3: d = 13.2 cm, λ^{-1} = 146 μs

close to 0.3 eV, the decay time constant of 2.2 μs is consistent with the value obtained for water [5], 2.7 μs for 0.2 eV. The effect of the 10% larger hydrogen density in paraffin is within the error of the measurements.

5. EXPERIMENT ON SPATIAL TRANSIENTS

Figure 4 shows a set of four decay curves obtained from a 2.2-cm-thick slab, with the detector in three different positions. For curves 2, 3 and 4 the paraffin slab was covered with 0.5-mm cadmium leaving only a window of 2 cm × 13 cm. In this way thermal neutrons from outside the window could not contribute to the count rate and also the effective detector volume was kept constant.

Curves 1 and 2 are measured with the detector in the normal position opposite to the source (see Fig. 1, detector position a), for curve 4 the detector is displaced 5 cm to the side (position b), and curve 3 is taken with the detector in a reflecting position 5 cm from the source (position c).

All four curves show the same asymptotic time constant for $t > 35$ μs ($\lambda^{-1} = (25 \pm 1)$ μs). The time constant of curves 2, 3, 4 for $t < 10$ μs is about 2.5 μs. This decay originates mainly from the epithermal neutrons. These

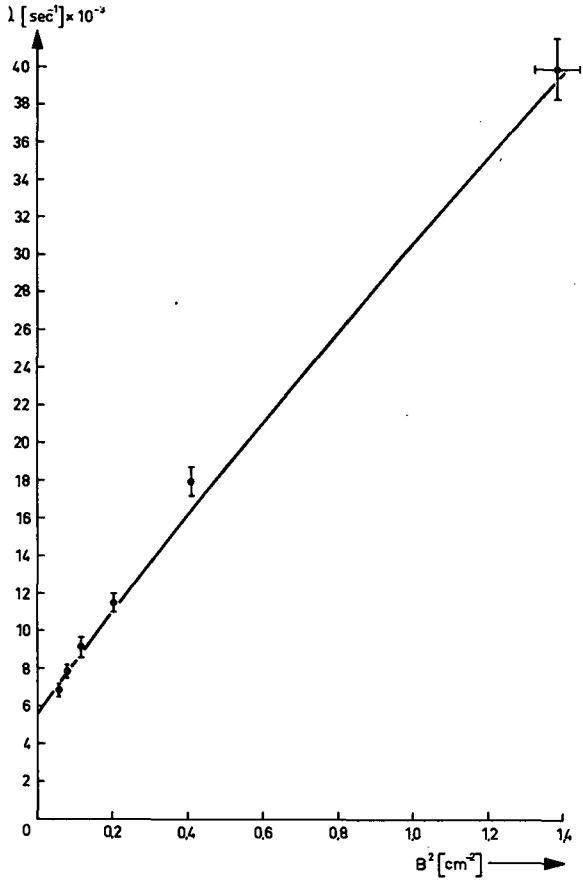


Fig. 3

Plot of asymptotic decay constants $\lambda(s^{-1})$ versus buckling $B^2(cm^{-2})$
The full line corresponds to $\lambda_a = 5620\ s^{-1}$,
$D_0 = 2700\ cm^2/s$ and $C = 2000\ cm^4/s$ [5].

epicadmium neutrons, however, do not establish a pure fundamental mode, as can be seen from the decay of curve 4, which is different from curves 2 and 3 for $10 < t < 35\ \mu s$. Whereas the latter ones show a decay time of $4.5\ \mu s$, curve 4 shows a dip. This transient behaviour must be attributed to the propagation of the neutron cloud, perpendicular to the slab (from position c to b), and parallel to the slab (from position a to b). The range of time at which this effect occurs is consistent with a propagation velocity $v_p = v_{th}/\sqrt{3} \approx 1300\ m/s$ for thermal neutrons.

Curve 1 was measured at detector position a (as curve 2), but without a cadmium screen. It shows the contribution to the count rate from the whole surface of the slab. This contribution increases with time.

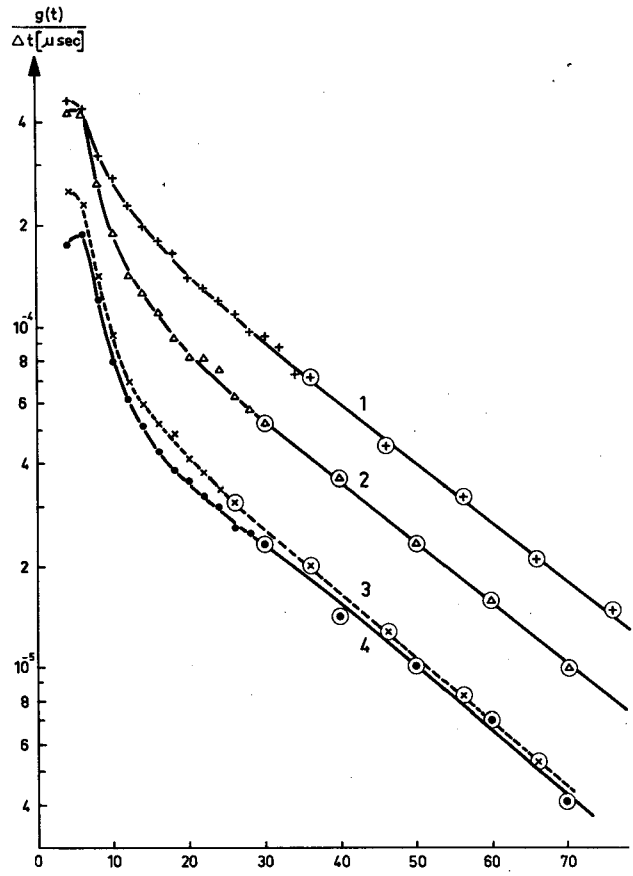


Fig. 4

Decay curves for a 2.2-cm-thick slab (for detector positions see Fig. 1)

Curve 1: detector position a, no cadmium window
Curve 2: detector position a, with cadmium window
Curve 3: detector position c, with cadmium window
Curve 4: detector position b, with cadmium window

6. EXPERIMENTS ON THE ENERGY TRANSIENT

Information about the decay of the mean energy of the neutrons can be obtained by the use of the two detector method [6]. In two identical experiments g(t) is measured with two different counters, which show different sensitivities (ϵ_1, ϵ_2) versus energy. Since the counters are always placed outside the medium, the neutron flux inside the medium is not influenced by the counters, so that the leakage spectrum is certainly independent of the counters. Two counters with 2.5 cm diameter were chosen, one filled with He^3 (4 atm) and the other filled with $B^{10}F_3$ (0.9 atm). The effective length

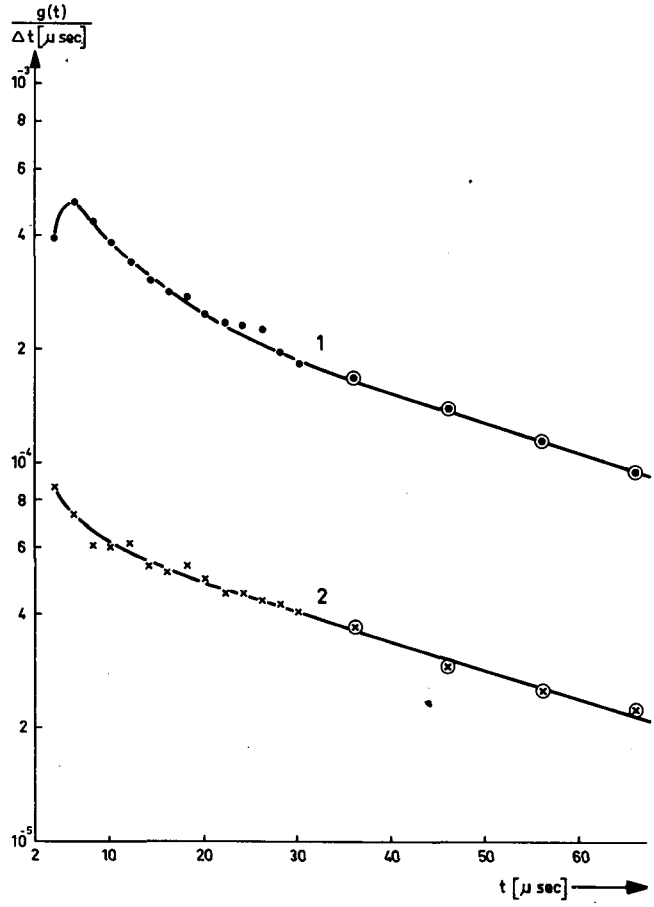


Fig. 5

Decay curves for thermalization measurement: slab thickness 4.4 cm

Curve 1: He^3 (4 atm) detector
Curve 2: $B^{10}F_3$ (0.9 atm) detector

was approximately 15 cm. Figure 5 shows such a pair of decay curves for a 4.5-cm-thick slab.

A different behaviour of g(t) at short times can only be caused by a change of the mean neutron energy with time. The ratio of the two curves can, in the model of an energy mode decay [7] be expressed as [6]:

$$R = \frac{\langle \epsilon_1 \phi_0 \rangle}{\langle \epsilon_2 \phi_0 \rangle} \left[1 + \frac{A_1}{A_0} \left(\frac{\langle \epsilon_1 \phi_1 \rangle}{\langle \epsilon_1 \phi_0 \rangle} - \frac{\langle \epsilon_2 \phi_1 \rangle}{\langle \epsilon_2 \phi_0 \rangle} \right) e^{-\alpha t} + \dots \right.$$

$$R = R_{t \to \infty} + \Delta R e^{-\alpha t},$$

where ϕ_0 and ϕ_1 are the asymptotic and the first energy mode, A_0 and A_1 are their intensities and ΔR is a constant. However, this simple represen-

tation implies that the neutron spectrum is very close to the fundamental mode and that the decay constant of the first mode is well isolated. The decay constant is then given as the difference between the first and the fundamental energy mode [6]:

$$\alpha = \lambda_1 - \lambda_0 = \lambda_{th} + 0.72\, D_0 B^2 + 2\, C B^4$$

For a thermalization constant which is of the order of $\lambda_{th} = 2 \times 10^5\ s^{-1}$, the contribution of the buckling-dependent parts is not considered to be appreciable (about 10% for $B^2 = 1$).

The ratio of two decay curves was finally corrected with the detector sensitivities as calculated from the counter data and the asymptotic energy was assumed to be 25 MeV. Figure 6 shows the time-dependent part of the energy on a semi-logarithmic scale. (The values for the ratio of the two curves are taken from the smoothed curves.) The thermalization time appears to be 5.5 μs. This measurement, which was done without a cadmium window in front of the counter, was repeated on a 6.6-cm slab with a cadmium window, to reduce flight-time effects from more distant parts of the slab surface. The thermalization time which resulted in this case was 5 μs.

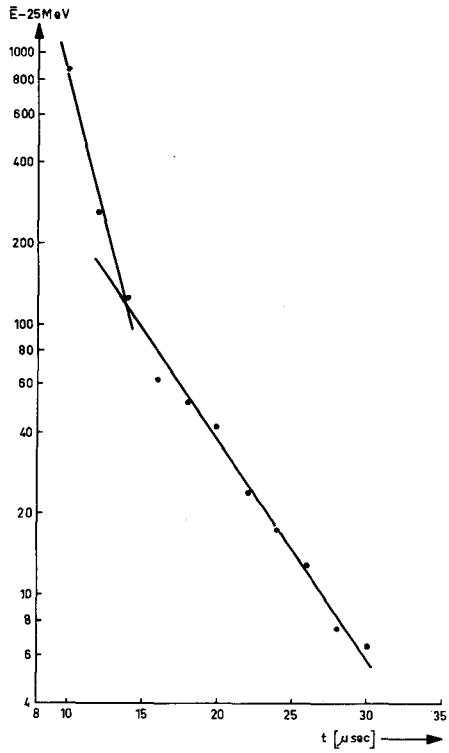


Fig. 6

Mean energy decay

The mean neutron energy minus the asymptotic energy (as derived from Fig. 5) versus time

There are, of course, uncertainties in this measurement. Possible flight-time effects in the counters distort the neutron spectrum in the counters. However, by comparison of the two measurements with and without a cadmium window, this effect is estimated to be negligible, because it was seen in Fig. 4, that despite the large contribution of the surface outside the cadmium window to the count-rate, the effect on the thermalization time is small (10%). The counter correction was only calculated ($\epsilon_1/\epsilon_2 = f(E)$); but it was found that the time dependence of the energy decay curve was very intensive to variations of the correction function f(E). Finally the leakage spectrum has a higher mean energy than the neutron spectrum inside the moderator. However, for the chosen slab thicknesses the difference should be small (which is also indicated by the small diffusion cooling constant [4]: 2000 cm^4/s), and the time dependence of both spectra should be the same. Also the counting statistics are still rather poor. Altogether we consider the value of the energy decay time constant to be $(5.0 \pm 1.0)\mu s$.

7. APPLICATION TO MULTIPLYING MEDIA

The above-discussed measurements showed that this correlation method yields practical intensities in systems where the distance detector-source is not large.

In the following it is briefly summarized how this cross-correlation complements the information obtained from the well-known Rossi-α experiment, which makes use of the output self-correlation of the system [8]. The fact that a one-point model is chosen for simplicity does not limit the general results to media to which this concept is applicable.

We denote the cross-correlation and the self-correlation as follows:

$$K_{xy} = x[y + g(\tau)]$$

$$K_{yy} = \bar{y}[\bar{y} + h(\tau)],$$

where $h(\tau)$ is the output pulse to pulse correlation. Both time-dependent functions show of course the same time behaviour

$$g(t),\ h(t) \sim \exp(\alpha t)$$

with

$$\alpha = \frac{\rho - \beta}{\Lambda} = \frac{k_p - 1}{\ell}$$

where ρ, β, Λ denote the reactivity, delayed neutron fraction and generation time, respectively and k_p and ℓ the prompt multiplication factor and neutron life-time respectively.

While the α with the self-correlation method is measured near criticality of the system, the cross-correlation can be obtained in the subcritical

region. From the above relation it follows that the ratio of signal-to-background in the time channel τ is

$$\frac{g(\tau)}{\bar{y}} = \frac{|\rho|}{\Lambda\bar{x}} \frac{g(\tau)}{g(0)}$$

The full exploitation of the self-correlation measurement would have to make use of the amplitude factor also.

If we take the ratio of the amplitudes of $g(\tau)$ and $h(\tau)$ or the ratio of the total correlation effects in the asymptotic range we find

$$\frac{g(\tau)}{h(\tau)} = \left(\frac{\overline{\nu_0(\nu_0 - 1)}}{2\bar{\nu}_0^2}\right)^{-1} \frac{\bar{\nu}_s}{\bar{\nu}} \left|\frac{k_p - 1}{k_p}\right| = C\,|\rho_p|$$

where ν_s is the prompt neutron yield per fission in the source and ν_0 is the same of the medium ($\nu = \nu_0(1+\beta)$). The result is the prompt reactivity of the system multiplied by a known constant C.

For the above evaluation it was assumed that the prompt decay constant of the system is large, compared to those of the delayed emitters, thus making the amplitude factor of $g(\tau)$ equal to 1, and that the multiplication factor of the system is large enough, so that the correction of the amplitude of $h(\tau)$ due to the input correlation (ν_s neutrons are emitted simultaneously from the source) can be neglected. This correction however can be easily applied. The neutron lifetime of the system follows directly from ρ_p and α.

ACKNOWLEDGEMENTS

The authors are indebted to Dr. G. Herrmann, University of Mainz, for giving them the Cf^{252} source on loan, and to Dr. H. Meister, EURATOM, Ispra, for some valuable suggestions on the experimental techniques.

REFERENCES

[1] UHRIG, R.E., Symp. on Noise Analysis in Nuclear Systems, Univ. of Florida, Nov. 1963.
[2] FIELDS, P.R. and DIAMOND, H., Neutron Dosimetry II IAEA, Vienna (1963) 581-94.
[3] HAAS, R. and WECKERMANN, B., Rpt EUR 1643 (1964) 131.
[4] KÜCHLE, M., Nukleonik 2 (1960) 131.
[5] MÖLLER, E. and SJÖSTRAND, N.G., Ark. Fys. 27 (1964) 501.
[6] STARR, E. and VILLIER, J.W.L., Rpt BNL 719 (1962).
[7] PUROHIT, S.N., Nucl. Sci. Engng 9 (1961) 157.
[8] MATTHES, W., Measurement of transfer function with statistical methods, to be published in Nukleonik.

DISCUSSION

(on the foregoing three papers)

M. N. MOORE: I should like to suggest a further development of Dr. Stegemann's results. The effectiveness of the method of two detectors depends upon the validity of the point-model assumption. If the point-model assumption is valid, the spectrum obtained by subtraction of the asymptotic single-detector spectrum from the single-detector system itself is a corrected spectrum identical to the two-detector spectrum. The discrepancy between the two-detector spectrum and the corrected single-detector spectrum is a measure of the inadequacy of the point-model assumption. In other words you should be able to see the effect of possible space dependence on your experiment.

D. STEGEMANN: Before commenting on your suggestion, I should like to point out that in the case investigated there was good agreement between the curve from the two-detector experiment and the single-detector curve after correction. As for your suggestion, the two detector experiment was actually planned for this type of experiment which makes it possible to study spatial effects. What we intend to do is, for instance, to place both detectors in the thermal zone, as has already been done, or both detectors at different spots within the fast section, or one detector in the thermal section and one in the fast section. We shall then look at the results to obtain information on spatial effects.

K. SUMITA: Dr. Bierman, I notice that you obtained a different prompt-neutron-decay value from the detector in the core and in the reflector, for the same core. It seems to me that there might be a fairly strong dependence of spatial harmonics on detector position in your results. How do you eliminate these harmonics and determine the neutron-decay constant of the fundamental mode?

S. BIERMAN: We performed our experiment with a view to finding out whether a consistent discrete decay mode could be observed in the reflector which differed from a corresponding, and observable, mode in the core. This is not necessarily the fundamental. In fact we don't believe it is, since in all cases the prompt decay approached a constant value for the core and the reflector after a time interval. This is probably the fundamental mode. It was precisely in order to answer questions such as these that we made the measurements. However, the assembly on which these measurements were made is not particularly suited to our objectives since the neutron lifetime does not differ very much in the core and the reflector media – they are both thermal media. As I mentioned, we plan to make measurements where 1c and 1r are not so close together in the hope that we will be able to develop a theory which will make it possible to take into account the effects, if any, of detector position.

S. CHWASZCZEWSKI: I should like to take this opportunity of mentioning a method we have been using in our laboratory in Poland to measure the attenuation constants of prompt neutrons. As everyone knows, the Rossi-alpha technique cannot be used in reactors in which the prompt-neutron lifetime is of the order of ~1 ms or longer. In the method we have been trying

out, use is made of the fluctuations of the reactor when it is close to critical. A time analyser is triggered by the fluctuation increase of the neutron density in the reactor. The starting pulse is produced by a circuit containing counting-rate meters. After being triggered the analyser measures the time-dependence of the decay in the density of the neutrons, which are measured with a very sensitive BF_3 detector.

Our measurements are in complete agreement with data obtained by means of a pulsed neutron source. Using this method we can make measurements in a graphite-water reactor at reactivity values as large as 2$ subcritical. Measurements have also been made of the time-dependence of the increase in neutron density after a negative fluctuation. Here the situation is more complicated than with positive fluctuations but the characteristic times are the same.

THEORY OF PULSED NEUTRON EXPERIMENTS IN HIGHLY HETEROGENEOUS MULTIPLYING MEDIA

S. E. CORNO
INSTITUTO DI FISICA "A. VOLTA"
UNVERSITY OF PAVIA, PAVIA,
AND
SNAM, MILAN, ITALY

Abstract — Résumé — Аннотация — Resumen

THEORY OF PULSED NEUTRON EXPERIMENTS IN HIGHLY HETEROGENEOUS MULTIPLYING MEDIA. In this work we investigate the time and space dependence of the neutron flux within a highly heterogeneous assembly, in which pulsed or sinusoidally modulated neutrons are injected. We consider, for the sake of simplicity, a device consisting of a cylindrical block of heavy moderator, along the axis of which a line-shaped region of fissionable material is located. The driving neutron source is assumed to be located on one of the end faces of the cylinder. The extent of the fissionable region allows us to deal with it as with an absorbing and multiplying singularity of the neutron field. As our attention is mostly concentrated on space and time variation of the neutron flux, rather crude approximations are assumed as far as the energy dependence of the neutron population is concerned. Within the limits of the age-diffusion theory, the response of the device to any neutron excitation may be found in closed form.

For a sinusoidally modulated source of given frequency, it may easily be shown that, if the axial singularity were a purely absorbing one, the neutron waves being propagated along the device would possess a phase shift, a wavelength and an attenuation constant depending on the absorbing properties of the singularity. This picture becomes more and more complicated when neutron multiplication occurs. For this general case the solution derived in our paper obviously turns out to be dependent on both absorption and multiplication properties of the singularity. This circumstance suggests, among others, the idea of using a device of the type described above for testing fuel elements of heterogeneous reactors.

THÉORIE DES EXPÉRIENCES AU MOYEN DES NEUTRONS PULSÉS, DANS LES MILIEUX MULTIPLICATEURS TRÈS HÉTÉROGÈNES. L'auteur étudie les variations du flux de neutrons en fonction du temps et du lieu dans un assemblage très hétérogène où l'on injecte des neutrons pulsés ou modulés sinusoïdalement. Il envisage, pour des raisons de simplicité, un dispositif constitué par un ralentisseur lourd en forme de bloc cylindrique sur l'axe duquel est placée une zone de matière fissile ayant une forme linéaire. La source de neutrons pulsés est supposée être placée sur l'une des bases du cylindre. L'étendue de la zone de matière fissile permet à l'auteur de la traiter comme s'il s'agissait d'une zone singulière d'absorption et de multiplication dans le champ de neutrons. Comme il concentre son attention principalement sur les variations du flux de neutrons en fonction du lieu et du temps, il adopte des approximations assez grossières pour ce qui est des variations de la population de neutrons en fonction de l'énergie. Dans les limites de la théorie diffusion-âge, il se peut que la réponse du dispositif à une excitation neutronique quelconque soit obtenue sous forme fermée.

Avec une source modulée sinusoïdalement de fréquence donnée, on peut aisément montrer que, si la zone axiale singulière est purement absorbante, le déphasage, la longueur d'onde et la constante d'atténuation des ondes neutroniques propagées le long du cylindre dépendent des propriétés absorbantes de cette zone. Cet état de choses se complique de plus en plus lorsqu'une multiplication des neutrons se produit. Dans ce cas général, la solution à laquelle l'auteur aboutit se révèle évidemment être dépendante des propriétés d'absorption et de multiplication de la zone singulière, ce qui peut donner, entre autres, l'idée d'utiliser un dispositif du modèle décrit ci-dessus pour soumettre à des essais les éléments de combustible des réacteurs hétérogènes.

О ТЕОРИИ ЭКСПЕРИМЕНТОВ С ИМПУЛЬСНЫМИ НЕЙТРОНАМИ В ГЕТЕРОГЕННЫХ РАЗМНОЖАЮЩИХ СРЕДАХ. Исследовались временная и пространственная зависимости нейтронного потока на высоко гетерогенной сборке, куда инжектируются импульсные или синусоидно модулированные нейтроны.

Для простоты рассматривается устройство, состоящее из цилиндрического блока замедлителя тяжелых нейтронов, по оси которого находится вытянутая область расщепляющегося материала. Предполагается, что усиляющий источник нейтронов размещается на одной из сторон цилиндра. Размер расщепляющейся области позволяет рассматривать ее как абсорбирующую и размножающую сингулярную составляющую нейтронного поля.

Поскольку внимание концентрировалось главным образом на пространственном и временном изменении нейтронного потока, то сделаны довольно грубые приближения относительно энергетической зависимости определенной популяции нейтронов.

В рамках возрастно-диффузионной теории реакция прибора на любое возбуждение нейтронов может иметь закрытую форму.

Для синусоидально модулированного источника данной частоты можно легко показать, что если осиальная сингулярная составляющая является чисто абсорбирующей, то нейтронные волны, проходящие через прибор, будут обладать фазой, длиной волны и постоянной ослабления, которые зависят от абсорбирующих свойств сингулярной составляющей.

Эта картина все более усложняется, когда происходит размножение нейтронов. Для данного общего случая решение, которое приводится в нашем докладе, очевидно, является зависимым как от абсорбирующих, так и от размножающих свойств сингулярной составляющей. Это обстоятельство предполагает, помимо прочего, возможность использования прибора вышеуказанного типа для испытания топливных элементов гетерогенных реакторов.

ASPECTOS TEORICOS DE LOS EXPERIMENTOS CON NEUTRONES PULSADOS EN MEDIOS MULTIPLICADORES MUY HETEROGENEOS. El autor ha investigado la variación del flujo neutrónico en función del tiempo y del espacio en un conjunto muy heterogéneo en el que se inyectan neutrones pulsados o de modulación sinusoidal. Para mayor sencillez se opera con una instalación formada por un bloque cilíndrico de moderador pesado, en cuyo eje se encuentra una región lineal de material fisionable. La fuente neutrónica se supone situada en una de las caras del cilindro. Gracias a sus dimensiones, la región fisionable puede considerarse como punto singular absorbente y multiplicador del campo neutrónico. Como el autor estudia sobre todo la variación espacial y temporal del flujo neutrónico, utiliza valores relativamente poco precisos por lo que respecta a la variación de la población neutrónica en función de la energía. Dentro de los límites de validez de la teoría de la edad de difusión, la instalación responde en forma analítica a una excitación provocada por los neutrones.

Cuando se trata de una fuente de modulación sinusoidal de frecuencia determinada, puede demostrarse fácilmente que si el punto singular axial fuese puramente absorbente, las ondas neutrónicas que se propagaran a lo largo de la instalación poseerían una fase, una longitud de onda y una constante de atenuación dependiente de las propiedades absorbentes del punto singular. Esto se complica en caso de multiplicación neutrónica. Para este caso general, la solución presentada en la memoria depende, desde luego, de las propiedades absorbentes y multiplicadoras del punto singular. Esta circunstancia, entre otras, ha inducido a utilizar una instalación como la que se acaba de describir para ensayar los elementos combustibles de los reactores heterogéneos.

INTRODUCTION

The interaction of time-dependent neutron sources with highly heterogeneous multiplying assemblies seems to be interesting from many points of view. As early as 1958 the opportunity of a systematic investigation by means of pulsed neutrons on "mockups of idealized, easily calculated geometries ... with the deliberate aim of testing theoretical techniques" had been suggested [1]. The purpose could be, for instance, the study of the thermalization of fission neutrons in a moderator at different temperatures, the space- and time-dependent slowing-down around a given fission source, etc.

In all cases a lump of fissionable material embedded in a large moderating block provides, when excited by a time-dependent neutron source, an easy means of creating experimentally the space- and time-dependent Green's functions for the slowing-down and thermalization equations.

If, on the other hand, the device under consideration possessed a privileged direction (let us mention, to be specific, a long thermal column,

including some multiplying material along the axis, and irradiated on one of its bases) we could consider it more or less as a "regenerative neutron conductor", and we should be faced with problems somehow similar to those arising in the theory of wave-guides for electromagnetic radiation. Furthermore, if the multiplying portion of the column were constituted by one or a few fuel elements of a heterogeneous reactor, it would be possible to relate the neutron absorption and multiplication properties of the fuel elements themselves with some generalized concepts of wavelength, attenuation distance and phase shift, which characterize the neutron signal being propagated along the column.

In this work we investigate theoretically the time- and space-dependent behaviour of the neutron population inside a heterogeneous device, which probably represents the simplest one that can be imagined. It consists of a long, bare cylinder of heavy moderator, within which an infinitely thin cylindrical shell of fissionable material has been embedded, parallel to the axis. Obviously, for vanishingly small values of the shell radius, we shall have to deal with a line-shaped singularity of the neutron field, which can well be used to simulate a reactor fuel element.

The injection of source neutrons is assumed to take place on one of the end faces of the moderating cylinder: this fact causes some of the peculiar features of the exponential pile to manifest themselves in our device, together with all the relevant characteristics of time-dependent phenomena. As a consequence many interesting conclusions can be derived. The same line of thought which allowed the understanding of "some of the most fundamental aspects of reactor theory" [2], through the investigation of the stationary exponential experiments and their relationship with the critical ones, may now be followed and generalized to the investigation of the problem at hand.

Because of the difficulties associated with space and time dependence, we restrict ourselves to the use of age-diffusion theory. It is felt, however, that even this rather crude approach, first, leads to an appreciable physical insight of the problem and secondly, represents a good starting point for the application of more sophisticated theories.

1. DERIVATION OF THE INTEGRO-DIFFERENTIAL EQUATION

1.1. Neutron balance in the moderator

As our attention is concentrated mostly on space and time variation of the neutron population, we restrict ourselves to the age-diffusion approach when dealing with energy dependence. Furthermore, we assume, for all fission neutrons born inside the device the same slowing-down time $\hat{t}$, defined as follows:

$$\hat{t} \equiv \int_0^{\infty} \chi(u) \left[\int_u^{u_{th}} \frac{du'}{\bar{\xi} \cdot \Sigma_s(u') \cdot v(u')} \right] du \tag{1}$$

The function $\chi(u)$ is the normalized fission spectrum, and u the lethargy. As far as the spatial distribution of the slowing-down neutrons is concerned,

we assume it to be described by the stationary kernel of the age theory. For a discussion of the conceptual difficulties associated with the above assumptions see Refs. [3, 4].

The migration of thermal neutrons is treated according to the simple scheme of one-group diffusion theory; severe criticisms could be raised against this assumption. It is felt, however, that the use of the telegrapher's approach, for instance, (see [5]) to which our theory could be immediately generalized, would only unduly complicate the formalism without essentially improving our physical understanding of the problem. On the other hand, it seems impossible to improve further the description of the physical situation without going definitively out of the diffusion scheme and losing, at the same time, the possibility of finding a closed-form solution.

Before stating the general neutron balance equation for our problem, we give the explicit form of the slowing-down kernels, as required in our geometry. The column is henceforth assumed to be infinitely extended in the axial direction.

We call $Q_\tau(r' \to r,\ z' \to z)$ the slowing-down density past age τ, at the point (r, z), caused by a ring-shaped fission source of unit strength, having radius r', and located on a plane perpendicular to the axis of the device, at height z'. Within the age-diffusion scheme this density can be derived, for example, from formulas given in Ref. [6] and reads

$$Q_\tau(r' \to r, z' \to z) = f_\tau(|z'-z|) \cdot q_\tau(r' \to r) \quad , \tag{2}$$

where

$$f_\tau(|z'-z|) \equiv \frac{e^{-\frac{|z-z'|^2}{4\tau}}}{\sqrt{4\pi\tau}} \quad ; \tag{3a}$$

and

$$q_\tau(r' \to r) \equiv \frac{1}{\pi R^2} \sum_1^\infty{}_j \frac{e^{-\frac{\alpha_j^2}{R^2}\tau} \cdot J_0\left(\frac{\alpha_j}{R} r'\right) \cdot J_0\left(\frac{\alpha_j}{R} r\right)}{J_1^2(\alpha_j)} \quad , \tag{3b}$$

the α's being the successive roots of $J_0(x) = 0$, and R the extrapolated radius of the column, which is assumed to be independent of neutron energy.

It can be verified easily from Eqs. (2) and (7) that the following "initial condition" is satisfied:

$$\lim_{\tau \to 0} Q_\tau(r' \to r, z' \to z) = \delta(z-z') \cdot \frac{\delta(r-r')}{2\pi r'} \quad ,$$

in agreement with our normalization requirements. (Equation (3b) represents the slowing-down density at a distance r from the axis of a shell-shaped, uniform source of fission neutrons, having radius r' and emitting one neutron per unit height and unit time.)

The actual multiplying shell of radius a, embedded in our moderating column, is taken as a surface singularity of the neutron field. Furthermore it is assumed to be transparent to epithermal neutrons and unable to destroy the continuity of the thermal flux across itself. According to the principles of the heterogeneous reactor theory [7, 8] we shall characterize the shell by means of two parameters, γ and η, which are to be taken as intrinsic properties of the shell itself; γ gives the current of thermal neutrons entering the unit surface of the shell per unit asymptotic thermal flux at $r = a$ and η is the number of fast neutrons emitted, per unit thermal absorbtion.

For the sake of clarity we ignore the epithermal absorptions. A detailed analysis of this problem, at least for stationary experiments, is given in [9(a)].

We assume that the external source is completely thermalized and located on the plane $z = 0$ of our device. This is not a restrictive hypothesis, because [4] a concentrated source of fast neutrons is completely equivalent to a distributed source of thermal neutrons.

We write our fundamental integro-differential equation for the unknown thermal flux $\Phi(r, z, t)$, under the additional assumptions that the multiplying shell is homogeneous, infinitely extended in the axial direction z, and that a burst of thermal neutrons is injected at $t = 0$ on the plane $z = 0$ with a radial distribution $S(r)$.

$$\left(\nabla_R^2 + \frac{\partial^2}{\partial z^2} - \varkappa^2\right)\Phi(r,z,t) + \frac{S(r)\cdot\delta(z)\cdot\delta(t-0^+)}{D}$$

$$+ \frac{\gamma}{D}\left[\eta\int_{-\infty}^{+\infty}\Phi(a,z',t-\hat{t})\cdot\mathcal{Q}_z(a\to r, z'\to z)\,dz' - \frac{\delta(r-a)}{2\pi a}\Phi(r,z,t)\right]$$

$$= \frac{1}{vD}\frac{\partial\Phi(r,z,t)}{\partial t} \quad . \tag{4}$$

Here ∇_R^2 is the radial Laplacian operator in cylindrical symmetry; κ, the inverse diffusion length, and D the diffusion coefficient with reference to the pure moderator. The term $\delta(r-a)/2\pi a$ takes into account the localized absorption of thermal neutrons.

For solving this equation we use a technique of combined Fourier and Laplace transforms acting on the variables z and t, respectively. To deal with the dependence on the r-variable we must apply, in addition, a finite Hankel transformation.

1.2. An auxiliary problem

To make our procedure more clear, we solve at once the simplest problem in our geometry, i.e. the evaluation of the time-independent neutron flux within an axially infinite column, which is acted on by a z-independent neutron source and whose radial distribution S(r) is the same as in Eq. (4).

This preliminary investigation will be used as the basis, in the next sections, for the discussion of the radial dependence for the more general problem stated above.

In the present simplified situation the balance equation for thermal neutrons is

$$\left(\nabla_R^2 - \varkappa^2\right)\Phi(r) + \frac{\gamma\eta}{D}\Phi(a)\cdot q_\tau(a\to r) - \frac{\gamma}{D}\Phi(a)\frac{\delta(r-a)}{2\pi a} + \frac{S(r)}{D} = 0 \quad . \tag{5}$$

Let the differential operator $\mathcal{R}$ be defined by the formula

$$\mathcal{R} \equiv \nabla_R^2 - \varkappa^2 = \frac{d^2}{dr^2} + \frac{1}{r}\frac{d}{dr} - \frac{1}{L^2} \quad , \tag{6}$$

and the Dirac δ-function be given its formal expansion, in terms of the finite Hankel transform [11]

$$\frac{\delta(r-a)}{a} \equiv \frac{\delta(r-a)}{r} = \frac{2}{R^2}\sum_{1\,j}^{\infty}\frac{J_0\left(\frac{\alpha_j}{R}a\right)\cdot J_0\left(\frac{\alpha_j}{R}r\right)}{J_1^2(\alpha_j)} \tag{7}$$

The source also can be represented in a similar way:

$$S(r) = \frac{2}{R^2}\sum_{1\,j}^{\infty}\frac{S_j}{J_1^2(\alpha_j)}\cdot J_0\left(\frac{\alpha_j}{R}r\right) \quad , \tag{8a}$$

where the S_j's defined by

$$S_j \equiv \int_0^R S(r)\cdot J_0\left(\frac{\alpha_j}{R}r\right) r\,dr \tag{8b}$$

are known constants.

If the above definitions, as well as Eq. (3b) are taken into account, Eq. (5) can be put in the equivalent form

$$\mathcal{R}\{\Phi(r)\} = -\frac{1}{\pi R^2 D}\sum_{1\,j}^{\infty}\left\{\gamma\Phi(a)\left[\eta e^{-\frac{\alpha_j^2}{R^2}\tau} - 1\right]J_0\left(\frac{\alpha_j}{R}a\right) + 2\pi S_j\right\}\frac{J_0\left(\frac{\alpha_j}{R}r\right)}{J_1^2(\alpha_j)} \tag{9}$$

Due to the fact that $J_0\left(\frac{\alpha_j}{R} r\right)$ happens to be an eigenfunction of the operator $\mathcal{A}$, belonging to the eigenvalue $-\left(\frac{\alpha_j^2}{R^2} + \varkappa^2\right)$, we can easily derive from Eq. (9) (under the assumption that $\Phi(a)$ is, at least for the moment, a known constant)

$$\mathcal{A}^{-1}\{\mathcal{A}\{\phi(r)\}\} \equiv \Phi(r) = \frac{1}{\pi R^2 D} \sum_{1}^{\infty}{}_j \left\{ \gamma \Phi(a) \left[\eta e^{-\frac{\alpha_j^2}{R^2}\tau} - 1\right] J_0\left(\frac{\alpha_j}{R} a\right) + 2\pi S_j \right\} \frac{J_0\left(\frac{\alpha_j}{R} r\right)}{\left(\frac{\alpha_j^2}{R^2} + \varkappa^2\right) \cdot J_1^2(\alpha_j)} \tag{10}$$

We introduce now three functions, F, G and φ^s in the following way:

$$F(r' \to r; \tau, \varkappa^2) \equiv \frac{1}{\pi R^2 D} \sum_{1}^{\infty}{}_j \frac{e^{-\frac{\alpha_j^2}{R^2}\tau} J_0\left(\frac{\alpha_j}{R} r'\right) \cdot J_0\left(\frac{\alpha_j}{R} r\right)}{\left(\frac{\alpha_j^2}{R^2} + \varkappa^2\right) J_1^2(\alpha_j)} \tag{11}$$

is the thermal flux at r due to the presence of a unit source of fast neutrons located on a cylindrical shell of radius r' in an axially infinite column of moderator, whose slowing-down area-to-thermal energy is τ and whose inverse square diffusion length is κ^2.

$$G(r' \to r; \varkappa) \equiv \frac{1}{\pi R^2 D} \sum_{1}^{\infty}{}_j \frac{J_0\left(\frac{\alpha_j}{R} r'\right) \cdot J_0\left(\frac{\alpha_j}{R} r\right)}{\left(\frac{\alpha_j^2}{R^2} + \varkappa^2\right) J_1^2(\alpha_j)} \equiv F(r' \to r; 0, \varkappa^2) \tag{12}$$

is the thermal flux at r, due to a unit thermal source located on the shell of radius r' within a medium in which the diffusion length is κ^{-1}.

For real as well as for purely imaginary values of κ the function G can be represented in closed form by means of zero-order Bessel functions. Its explicit expression is given, for instance, in [9].

$$\varphi^s(r) \equiv \frac{2}{R^2 D} \sum_{1}^{\infty}{}_j \frac{S_j \cdot J_0\left(\frac{\alpha_j}{R} r\right)}{\left(\frac{\alpha_j^2}{R^2} + \varkappa^2\right) \cdot J_1^2(\alpha_j)} \tag{13}$$

represents the thermal flux sustained in the column by the source, if the shell were absent.

If the definitions of Eqs. (11) to (13) are used, Eq. (10) can be written as follows

$$\Phi(r) = \gamma \Phi(a) \left[\eta F(a \to r; \tau, \varkappa^2) - G(a \to r; \varkappa)\right] + \varphi^s(r) \qquad (14)$$

As Eq. (14) has to be valid for all values of r, including r = a, we can derive immediately that

$$\Phi(a) = \frac{\varphi^s(a)}{1 - \gamma \cdot \left[\eta F(a \to a; \tau, \varkappa^2) - G(a \to a; \varkappa)\right]} \equiv \frac{\varphi^s(a)}{\Psi(\gamma, \eta)} \qquad (15)$$

and, as a consequence, instead of Eq. (14), it will be possible to write

$$\Phi(r) = \gamma \frac{\varphi^s(a)}{\Psi(\gamma, \eta)} \left[\eta F(a \to r; \tau, \varkappa^2) - G(a \to r; \varkappa)\right] + \varphi^s(r) \qquad (14')$$

This is the complete solution of our auxiliary problem. The denominator $\Psi(\gamma, \eta)$ on the right side of Eq. (15), when equated to zero, gives the critical equation of our column. In effect, it would be possible, for vanishingly small values of $\varphi^s(r)$, to sustain a persisting neutron population inside the device, provided that the condition $\Psi(\gamma, \eta) = 0$ be satisfied. This fact will soon appear of essential importance for the physical understanding of our general problem.

1.3. Fourier and Laplace transform of the time-dependent balance equation

We can operate now on Eq. (4) with the final aim of finding its solution in closed form. Simplifications of the solution itself are discussed a posteriori, so that physical insight of the problem will allow us to deduce, for instance, the asymptotic behaviour of the general integral with respect to both the axial and temporal variables.

As our procedure implies the use of direct and inverse Fourier and Laplace transformations, we define at once the nomenclature used. Let ψ be an arbitrary function, depending on several parameters, which we simply designate by α or β, and on one of the variables z or t or both. The definitions henceforth adopted for Fourier and Laplace transforms are as follows:

$$\mathcal{F}_{z \to \xi}\{\psi(\alpha; z)\} \equiv \frac{1}{\sqrt{2\pi}} \int_{-\infty}^{+\infty} \psi(\alpha; z) e^{i\xi z} dz \equiv \psi_{\mathcal{F}}(\alpha; \xi) \,, \qquad (16a)$$

$$\mathcal{F}^{-1}_{\xi \to z}\{\psi_{\mathcal{F}}(\alpha; \xi)\} \equiv \frac{1}{\sqrt{2\pi}} \int_{-\infty}^{+\infty} \psi_{\mathcal{F}}(\alpha; \xi) e^{-i\xi z} d\xi = \psi(\alpha; z) \,; \qquad (16b)$$

$$\begin{cases} \mathcal{L}_{t\to p}\{\psi(\beta;t)\} \equiv \int_0^\infty \psi(\beta;t)\, e^{-pt}\, dt \equiv \psi_{\mathcal{L}}(\beta;p)\ ; & (17a) \\ \mathcal{L}^{-1}_{p\to t}\{\psi_{\mathcal{L}}(\beta;p)\} \equiv \frac{1}{2\pi i}\int_{c-i\infty}^{c+i\infty} \psi_{\mathcal{L}}(\beta;p)\, e^{pt}\, dp = \psi(\beta;t), & (17b) \end{cases}$$

c being a real number, not smaller than the abscissa of convergence for the direct transform Eq. (17a). Fourier and Laplace transformations may obviously be applied one after the other.

The only assumption we need at the moment, before taking the Fourier transform of Eq. (4) is that once the dimensions of the device and the parameters γ and η have been assigned, the column remains in a subcritical state, even when it is considered as infinitely extended in the axial direction. As a consequence, the Fourier transform of Eq. (4) (attention being paid to the convolution theorem [10]) will be

$$\left[\nabla_R^2 - (\varkappa^2+\xi^2)\right]\Phi_{\mathcal{F}}(r,\xi,t) + \frac{S(r)\cdot\delta(t-0^+)}{\sqrt{2\pi}\,D} + \frac{\gamma}{D}\left[\eta e^{-\xi^2\tau}\cdot\Phi_{\mathcal{F}}(a,\xi,t-\hat{t})\cdot q_\tau(a\to r) - \frac{\delta(r-a)}{2\pi a}\cdot\Phi_{\mathcal{F}}(a,\xi,t)\right] = \frac{1}{\nu D}\frac{\partial\Phi_{\mathcal{F}}(r,\xi,t)}{\partial t}. \qquad (18)$$

Next we take the Laplace transform of Eq. (18), on the assumption that $\Phi(r, z, t \le 0) \equiv 0$. If we define

$$\Omega^2(\xi,p) \equiv \varkappa^2+\xi^2+\frac{p}{\nu D} \qquad (19)$$

the Laplace-Fourier transform of Eq. (4) reads

$$\left[\nabla_R^2 - \Omega^2(\xi,p)\right]\Phi_{\mathcal{F}\mathcal{L}}(r,\xi,p) = -\frac{\gamma}{D}\Phi_{\mathcal{F}\mathcal{L}}(a,\xi,p)\left[\eta e^{-(\xi^2\tau+\hat{t}p)}\cdot q_\tau(a\to r) - \frac{\delta(r-a)}{2\pi a}\right] - \frac{S(r)}{\sqrt{2\pi}D} \qquad (20)$$

The formal analogy between Eqs. (5) and (20) is now apparent. It is important to remark that, in the present case, an equation similar to (15) will play the role of a "self-consistency condition", to be satisfied by the unknown flux at r = a for all values of t and z. A procedure parallel to that used when passing from Eq. (5) to (14') leads to

$$\Phi_{\mathcal{J}\mathcal{L}}(r,\xi,p) = \gamma \frac{\varphi^{S}_{\mathcal{J}\mathcal{L}}(a,\xi,p)}{\Psi(\gamma,\eta;\xi,p)} \left[\eta\, e^{-(\xi^2\tau+\hat{t}p)} \cdot F(a\to r;\tau,\Omega^2) - G(a\to r;\Omega)\right] + \\ + \varphi^{S}_{\mathcal{J}\mathcal{L}}(r,\xi,p) \quad , \tag{21}$$

where the meaning of the symbols, apart from Eqs. (11) and (12), is as follows:

$$\varphi^{S}_{\mathcal{J}\mathcal{L}}(r,\xi,p) \equiv \frac{1}{R^2_D}\sqrt{\frac{2}{\pi}} \cdot \sum_{1}^{\infty}{}_{j} \frac{S_j\, J_o\left(\frac{\alpha_j}{R} r\right)}{\left[\frac{\alpha_j^2}{R^2} + \Omega^2(\xi,p)\right] \cdot J_1^2(\alpha_j)} \equiv \varphi^{S}_{\mathcal{J}\mathcal{L}}(a;\Omega) \tag{22}$$

$$\Psi(\gamma,\eta;\xi,p) \equiv 1 - \gamma\left[\eta\, e^{-(\xi^2\tau+p\hat{t})} \cdot F(a\to a;\tau,\Omega^2) - G(a\to a;\Omega)\right]. \tag{23}$$

1.4. Absorption and multiplication contributions to $\Phi_{\mathcal{J}\mathcal{L}}(r,\xi,p)$

The most suitable way of exploiting the Laplace-Fourier-transformed flux, as given by Eq. (21), is to separate the absorption and multiplication effects from each other, which are caused by the reaction of the shell-shaped singularity.

By adding to and subtracting from Eq. (21) a formula similar to Eq. (21) itself, in which η has been made identically zero, we obtain

$$\Phi_{\mathcal{J}\mathcal{L}}(r,\xi,p) = \Phi^{Abs}_{\mathcal{J}\mathcal{L}}(r,\xi,p) + \Phi^{Mult}_{\mathcal{J}\mathcal{L}}(r,\xi,p) \tag{24}$$

where, by definition,

$$\Phi^{Abs}_{\mathcal{J}\mathcal{L}}(r,\xi,p) \equiv -\gamma \frac{\varphi^{S}_{\mathcal{J}\mathcal{L}}(a,\xi,p)}{1+\gamma\, G(a\to a;\Omega)} G(a\to r;\Omega) + \varphi^{S}_{\mathcal{J}\mathcal{L}}(r,\xi,p) \quad ; \tag{25}$$

$$\Phi^{Mult}_{\gamma\zeta}(t,\xi,p) \equiv \gamma\eta \frac{\varphi^{s}_{\gamma\zeta}(a,\xi,p)}{\psi(\gamma,\eta;\xi,p)} e^{-(\xi^2\tau+p\hat{t})} \cdot \left[F(a\to\tau;\tau,\Omega^2)\right.$$

$$\left. -\gamma \frac{F(a\to a;\tau,\Omega^2)}{1+\gamma G(a\to a;\Omega)} G(a\to\tau;\Omega)\right] . \qquad (26)$$

The function $\Phi^{Abs}_{\gamma\zeta}$ is the Laplace-Fourier transform of the flux which we could find in the column if the multiplication were absent. The function $\Phi^{Mult}_{\gamma\zeta}$, on the other hand, takes into account the contribution to the transformed flux from multiplication effects. The first term in the square bracket accounts for thermal neutrons coming directly from the fission source, while the second one is, to some extent, a corrective term resulting from the fact that also those neutrons which have been multiplied can be absorbed by the shell as soon as they become thermalized.

The right side of Eq. (26) and, consequently, the flux which one can deduce by inverting it, seems to vanish for $\eta \to 0$. However, this assertion, which seems to be a straightforward one, is discussed more specifically in the following paragraphs. Some unsuspectable features of Eq. (26) then become self-evident.

Before attempting the general inversion of Eq. (24), let us discuss the inverse transformation for the much simpler case of Eq. (25); in other words, we look for the response of the column to a given excitation, under the assumption that the singularity is a purely absorbing one.

Let us carry out first the $\mathcal{L}^{-1}_{p\to t}$- transformation, taking ξ as a parameter.

$$\mathcal{L}^{-1}_{p\to t}\left\{\Phi^{Abs}_{\gamma\zeta}\right\} = \varphi^{s}_{\gamma}(r,\xi,t) + \frac{i}{2\pi}\gamma \int_{c-i\infty}^{c+i\infty} \frac{\varphi^{s}_{\gamma\zeta}(a,\xi,p)}{1+\gamma G(a\to a;\Omega)} G(a\to r;\Omega) e^{pt}\, dp$$

$$\equiv \Phi^{Abs}_{\gamma}(r,\xi,t) . \qquad (27)$$

We have been defining φ^{s}_{γ} as follows:

$$\varphi^{s}_{\gamma}(r,\xi,t) = \frac{v}{R^2}\sqrt{\frac{2}{\pi}} \sum_{1}^{\infty}{}_{j} \frac{S_j\, J_0\left(\frac{\alpha_j}{R} r\right)}{J_1^2(\alpha_j)} \cdot e^{-vD\left(\frac{\alpha_j^2}{R^2}+\varkappa^2+\xi^2\right)t} \qquad (28)$$

The integral in Eq. (27) can be evaluated by means of the standard technique of Chaucy's residue theorem on the complex plane of the variable p; there are in the integrand two numerable sequences of singularities. One of them is associated with the simple poles of $\varphi^{S}_{\mathcal{J}\mathcal{L}}(a,\xi,p)$, and the sum of the residues series associated with it is equal to Eq. (28) and opposite in sign.

The other sequence of first order poles, all lying on the negative $Re\{p\}$ axis, comes from the zeros of $1+\gamma G(a\to a;\Omega)$. It can be shown easily that this denominator, taken as a function of Ω^2 can only vanish for negative values of Ω^2. So we call $i\Omega_\nu (\nu = 1, 2, \ldots \infty)$ its roots, as a function of Ω and, taking into account Eq. (19), we have, on the p-plane, the zeros we are looking for located at the points $p = p_\nu(\xi)$ defined below

$$p_\nu(\xi) = -\nu D\left(\Omega_\nu^2 + x^2 + \xi^2\right) . \tag{29}$$

All the p's are negative, real numbers for real values of ξ. As a final result, we derive from Eq. (27)), using Eq. (22),

$$\Phi^{Abs}_{\mathcal{J}}(r,\xi,t) = -\nu D \sum_{1}^{\infty}{}_{\nu} \frac{\varphi^{S}_{\mathcal{J}\mathcal{L}}(a;i\Omega_\nu)}{\left.\frac{\partial G(a\to a;\Omega)}{\partial \Omega^2}\right|_{\Omega = i\Omega_\nu}} G(a\to r;i\Omega_\nu)\, e^{p_\nu(\xi)t} \tag{30}$$

The $\mathcal{J}^{-1}_{\xi\to z}$-transform of Eq. (30) becomes now a trivial matter

$$\mathcal{J}^{-1}_{\xi\to z}\left\{\Phi^{Abs}_{\mathcal{J}}(r,\xi,t)\right\} = \Phi^{Abs}(r,z,t)$$

$$= -\sqrt{\frac{\nu D}{2t}} \sum_{1}^{\infty}{}_{\nu} \frac{\varphi^{S}_{\mathcal{J}\mathcal{L}}(a;i\Omega_\nu)}{\left.\frac{\partial G(a\to a;\Omega)}{\partial \Omega^2}\right|_{\Omega = i\Omega_\nu}} G(a\to r;i\Omega_\nu)\, e^{-\frac{z^2}{4\nu D t} - \nu D(\Omega_\nu^2 + x^2)t} \tag{31}$$

Equation (31) can obviously be stated in precisely the same form, if the order of the inverse transformations is changed. Its important feature lies in the fact that it represents the thermal flux, diffusing within the column, as a superposition of infinitely many radial "eigenfunctions", i.e. the $G(a\to r; i\Omega_\nu)$'s, whose shape is only dependent on the absorbing properties of the shell.

As a matter of fact, the value of the Ω_ν's, for a given geometry, is only dependent on γ through the equation

$$1 + \gamma\, G(a\to a;\Omega) = 0 . \tag{32}$$

It is worth mentioning that the position of the roots $i\Omega_\nu$ of Eq. (32) can be specified quite easily. If we call L_j^{-2} the sum $(\alpha_j^2/R^2+\kappa^2)$, there is one and only one root $i\Omega_\nu$ such that $-(\Omega_\nu^2+\kappa^2) \equiv -\bar{\Omega}_\nu^2$ lies between $(-L_j^{-2})$ and $(-L_{j+1}^{-2})$, $j = 1, 2, \ldots \infty$.

If we had considered, instead of the actual situation, the time-independent problem for a column containing a purely absorbing shell and irradiated by a stationary source $S(r)\cdot\delta(z)$, we would have found that the $\bar{\Omega}_\nu^{-1}$'s are nothing but the axial relaxation lengths for the radial eigenfunctions $G(a\to r; i\Omega_\nu)$, in terms of which the stationary flux still happens to be represented.

On the other hand, the $L_j \equiv (\alpha_j^2/R^2+\kappa^2)^{-1/2}$ are the relaxation lengths of the "cylindrical harmonics" $J_0[(\alpha_j/R)r]$'s along the same column containing pure moderator only. It is perfectly understandable on physical grounds that the absorbing power of the shell changes; first, the harmonics $J_0[(\alpha_i/R)r]$'s are propagated along the homogeneous column into the $G(a\to r; i\Omega_\nu)$'s, and secondly, the axial relaxation length $\bar{\Omega}_j^{-1}$ for the j^{th} of these G's has to be shorter than L_j. In all cases, however, the column appears to offer an "impedance" for axial transmission of neutrons, which becomes increasingly higher with the increase of the order of the eigenfunction being propagated. As a consequence the column exerts the well-known filtering action on the radial eigenfunctions.

2. EXPLICIT CALCULATION OF THE SPACE- AND TIME-DEPENDENT FLUX

2.1. Preliminary remarks on the stationary problem for $\eta \neq 0$

When the time-independent problem discussed above is extended to the case $\eta \neq 0$, one can easily find for the $\mathcal{F}_{z\to\zeta}$ transform of the flux $\Phi(r, z)$ the following expression:

$$\Phi_{\mathcal{F}}(r,\zeta) = \gamma \frac{\varphi_{\mathcal{F}}^{S}(a,\zeta)}{\Psi_{Stat}(\gamma,\eta;\zeta)} \left[\eta e^{-\zeta^2\tau} \Gamma(a\to r;\tau, x^2+\zeta^2) - G(a\to r;\sqrt{x^2+\zeta^2})\right] + \varphi_{\mathcal{F}}^{S}(r,\zeta), \tag{33}$$

in which $\varphi_{\mathcal{F}}^{S}(r,\zeta)$ may be simply derived from the Eq. (22) of $\varphi_{\mathcal{F}\mathcal{L}}^{S}$, by putting $p \equiv 0$:

$$\varphi_{\mathcal{F}}^{S}(r,\zeta) \equiv \varphi_{\mathcal{F}\mathcal{L}}^{S}(r,\zeta,0) \tag{34}$$

Similarly, Ψ_{Stat} can be derived from Eq. (23) and reads

$$\Psi_{Stat}(\gamma,\eta;\zeta) \equiv \Psi(\gamma,\eta;\zeta,0) = 1-\gamma\left[\eta e^{-\zeta^2\tau}\Gamma(a\to a;\tau, x^2+\zeta^2) - G(a\to a;\sqrt{x^2+\zeta^2})\right] \tag{35}$$

It has been proved that the inversion of Eq. (33) can be made by means of a contour integral [9(b)] and that the final form of the radial flux is a superposition of "eigenfunctions"

$$f_h(r) \equiv \eta \cdot e^{-\zeta_h^2 \tau} \cdot F\left(a \to r; \tau, x^2 + \zeta_h^2\right) - G\left(a \to r; \sqrt{x^2 + \zeta_h^2}\right) \tag{36}$$

whose shape, for a given geometry, is determined by both γ and η, because, in the present case, the ζ_h's are the roots of

$$\Psi_{Stat}(\gamma, \eta; \zeta) = 0 \tag{37}$$

lying on the complex plane ζ. As opposed to Eq. (32), Eq. (37), considered as a function of ζ^2, possesses infinitely many sequences of roots, each one of them containing a numerable infinity of terms, which belong to the whole half plane $Re\{\zeta^2\} < 0$, not only to the negative portion of the real ζ^2-axis.

This complicated behaviour of the function $\Phi_{\gamma}(r, \zeta)$ on the complex ζ^2-plane is due to two reasons. Its $\mathcal{F}^{-1}_{\zeta \to x}$-transform accounts for both (i) the spectrum transients due to the presence of an external source [2] acting on a multiplying medium and (ii) the radial non-homogeneity of the experimental device, which gives rise, in its turn, to strong spectrum transients along the radial co-ordinate no matter how far away we go from the external source.

The $f_h(r)$'s given by Eq. (36) propagate along the axial direction either by vanishing exponentially, if the corresponding ζ_h^2 is real, or by doing damped oscillations, if ζ_h^2 is a complex quantity. Obviously the fundamental radial eigenfunction $f_1(r)$ propagates with a purely exponential decay.

It is also possible to state that all the roots of Eq. (37), belonging to the negative side of the real ζ^2-axis, lead, for sufficiently high values of η, to axial relaxation lengths for the associated $f_h(r)$'s which are larger than the corresponding L_h, defined in section 1.4. But when for fixed γ, η is passing continuously from its actual value to zero, the afore-mentioned relaxation lengths move from their initial values, larger than L_h, down to the $\bar{\Omega}_h^{-1}$ belonging to the column including a pure absorber. At the same time the complex relaxation lengths, whose presence is a peculiar consequence of multiplication, move to infinity.

This result will be extremely useful for the understanding of the general problem.

2.2. *Inverse transform of* $\Phi^{Mult}_{\gamma\zeta}$.

Starting from the definition in Eq. (26), we have to calculate, first of all, the inverse Laplace transform of $\Phi^{Mult}_{\gamma\zeta}$. Due to the factor $\exp\{\hat{\eta} t\}$ in front

of it, there is no doubt that we are dealing with a delayed contribution to the flux, which vanishes identically for $t < \hat{t}$. The $\mathcal{L}^{-1}_{p\to t}$-transformation will be carried out by taking ξ as a parameter.

$$\Phi^{Mult}_{\gamma}(\tau,\xi,t) \equiv \mathcal{L}^{-1}_{p\to t}\left\{\Phi^{Mult}_{\gamma\eta}(\tau,\xi,p)\right\}$$

$$= \gamma\eta\,\frac{e^{-\xi^2\tau}}{2\pi i}\int_{c-i\infty}^{c+i\infty} e^{-p\hat{t}}\,\frac{\varphi^{S}_{\gamma\eta}(a,\xi,p)}{\Psi(\gamma,\eta;\xi,p)}\left[F(a\to t;\tau,\Omega^2) - \gamma\,\frac{F(a\to a;\tau,\Omega^2)}{1+\gamma G(a\to a;\Omega)}\,G(a\to\tau;\Omega)\right]\cdot e^{pt}\,dp \qquad (38)$$

Our hypothesis on the subcriticality of the column allows us to take, for instance, $c = 0$.

We want to calculate the integral in Eq. (38) by means of a contour integration. The integrand for fixed, real values of ξ has the following properties on the p-plane:

(i) It is a regular function of p at all points

$$p_j = -\nu D\left(\frac{\alpha_j^2}{R^2} + \varkappa^2 + \xi^2\right) ;$$

(ii) It has an infinite sequence of first order poles, associated with the zeros of $1+\gamma G(a\to a;\Omega)$. The corresponding series of residues will bring to $\Phi^{Mult}_{\gamma}(\tau,\xi,t)$ a contribution exactly equal to $\Phi^{Abs}_{\gamma}(\tau,\xi,t)$, as given by Eq. (30), but opposite in sign.

(iii) As far as the singularities associated with the simple zeros of $\Psi(\gamma,\eta;\xi,p)$ are concerned, after restricting ourselves to those devices, for which the following inequality holds;

$$\log\eta - \frac{\alpha_1^2}{R^2}(\tau - \nu D\hat{t}) + \nu D\hat{t}\,\varkappa^2 < 0 \quad ,$$

we can extend the considerations outlined above for the time-independent case. Let us consider a system, in which the following changes have been made:

$$\eta \Rightarrow \eta e^{-\xi^2\tau} \equiv \eta(\xi) \quad ;$$
$$x^2 \Rightarrow x^2 + \xi^2 \equiv x^2(\xi) \quad . \tag{39}$$

This amounts, under our restrictive hypothesis of ξ^2 real and positive, to the assumption of a reduced multiplication efficiency for the fissionable material, together with an increased absorption cross-section for the moderator.

Let us write down explicitly the critical equation $\Psi = 0$, which has to be satisfied on the p-plane, for a given ξ, i.e.

$$\psi(\gamma,\eta;\xi,p) = 1 - \gamma\left[\eta(\xi)\cdot e^{-vD\hat{t}\cdot\frac{p}{vD}} \cdot F\left(a\to a;\tau,x^2(\xi)+\frac{p}{vD}\right)\right.$$
$$\left. - G\left(a\to a;\sqrt{x^2(\xi)+\frac{p}{vD}}\right)\right] = 0. \tag{40}$$

and compare it with Eq. (35). It becomes evident, by permitting p/vD of Eq. (40) to play the same role as ξ^2 in Eq. (35), that Eq. (40) will possess the same distribution of zeros in the p-plane as an equation of type (35) does on the ξ^2-plane, referred to a system characterized by the parameters of Eq. (39) and non-isotropic from the standpoint of neutron slowing-down. In effect such a system is required to possess two different slowing-down lengths: one in the radial direction, $\tau_R \equiv \tau$, and the other in the axial direction, $\tau_z \equiv vD\hat{t}$.

It happens, for all situations of practical interest, that τ_z, as defined above, is much smaller than τ. An important consequence of this fact is that on the p-plane, all roots of Eq. (40), and particularly the complex ones, are displaced to the left with respect to the position they would occupy if τ_z were coincident with τ: actually, for $\tau_z < \tau_R = \tau$ the importance of multiplication is apparently reduced. This behaviour can be derived from the considerations made at the end of the above paragraph.

Equation(40) allows us to evaluate the position of its infinitely many roots on the p-plane, for the particular case $\xi^2 \equiv 0$. Let us call them $p_k(0)$. Furthermore we can derive, by using, for instance, a steepest descent technique, the curves $p_k = p_k(\xi)$, which describe the motion of these roots as ξ^2 increases. It is important to stress that if a given root $p_1(0)$ falls on the negative portion of the real p-axis for $\xi = 0$, then the whole curve $p_1(\xi)$, describing its motion for positive values of ξ^2, will lie on the real axis itself, from $p_1(0) < 0$ to $-\infty$.

To summarize the above results, let us write first

$$\Psi\left(\gamma,\eta;\xi,p_k(\xi)\right) = 0 \tag{41}$$

as an implicit equation for the $p_k(\xi)$'s, and then define, instead of Eq. (19), infinitely many Ω_k's, as functions of the single variable

$$\Omega_K^2(\xi) \equiv \varkappa^2 + \xi^2 + \nu_K(\xi)/\nu D \equiv \Omega^2\left(\xi, \nu_K(\xi)\right) . \tag{42}$$

We possess now the complete information required for writing down the flux $\Phi(r, z, t)$, which constitutes the general solution of our problem. Taking into account the fact that, from $\Psi = 0$, it follows irrespective of the value of ξ, $1 + \gamma G(a \to a; \Omega_k) = \eta e^{-(\xi^2 \tau + p_k \hat{t})} \cdot F(a \to a; \tau, \Omega_k)$, we have

$$\Phi(r,z,t) = \left[\mathbb{1}(t) - \mathbb{1}(t-\hat{t})\right] \cdot \Phi^{Abs}(r,z,t)$$

$$+ \mathbb{1}(t-\hat{t}) \sqrt{\frac{2}{\pi}} \sum_1^\infty{}_K \gamma \int_0^\infty \frac{\varphi^S_{3D}(a; \Omega_\kappa(\xi))}{\left.\frac{\partial \Psi(\gamma, \eta; \xi, \nu)}{\partial \nu}\right|_{\nu = \nu_K(\xi)}} \left\{ \eta e^{-\left(\xi^2 \tau + \nu_K(\xi)\hat{t}\right)} \cdot F\left(a \to r; \tau, \Omega_K^2(\xi)\right) \right.$$

$$\left. - G\left(a \to r; \Omega_K(\xi)\right) \right\} e^{\nu_K(\xi) t} \cdot \cos(\xi z)\, d\xi \tag{43}$$

The symbol $\mathbb{1}(t)$ represents the unit step function, which jumps to the value 1 at $t = 0$. $\Phi^{Abs}(r, z, t)$ is reported in Eq. (31) and the summation over k extends in principle to all roots of Eq. (40).

$$Re\left\{\nu_K(\xi)\right\} < 0 \quad , \; K = 1, 2, \ldots \infty \; , \; for \; \xi^2 > 0 .$$

It can be shown also that the derivative of Ψ, occurring in the denominator of the integrand (43), may be computed in closed form at all real negative roots $p_1(\xi)$ of Ψ; furthermore, due to the fact that the afore-mentioned derivative can be calculated along the real axis, $\partial\Psi/\partial p$ can be expressed in terms of the usual Bessel functions

$$\left.\frac{\partial \Psi(\gamma, \eta; \xi, \nu)}{\partial \nu}\right|_{\nu = \nu_\ell(\xi)} = \left[1 + \gamma G\left(a \to a; \Omega_\ell(\xi)\right)\right] \cdot \left[\hat{t} - \frac{1 - e^{\Omega_\ell^2(\xi) \cdot \tau}}{\nu D \Omega_\ell^2(\xi)}\right]$$

$$+ \gamma \left.\frac{\partial}{\partial \nu} G\left(a \to a; \Omega\right)\right|_{\nu = \nu_\ell(\xi)} \cdot \left[1 - \eta(\xi) \cdot e^{-\nu_\ell(\xi)\hat{t} + \Omega_\ell^2(\xi)\cdot\tau}\right] \tag{44}$$

Equation (44) allows us to take the limit, for $\eta \to 0$, of Eq. (43) and to show that, in the limit, Eq. (44) reduces to Eq. (31), as required. So the inversion of Φ^{Mult}_{3D} does not lead to a contribution simply proportional to η as one at first sight would be inclined to think.

The solution of Eq. (43) deserves more attention as far as its asymptotic behaviour for large values of $|z|$ is concerned. Let us investigate in some more detail the radial shape of the functions

$$\eta e^{-\left(\xi^2\tau + \mu_k(\xi)t\right)} F\left(a \to t; \tau, \Omega_k^2(\xi)\right) - G\left(a \to t; \Omega_k(\xi)\right) , \tag{45}$$

which are integrated with respect to ξ (after multiplication by a suitable weighting function) to give, for fixed z and t, the general representation of the flux. Let us concentrate our attention, for instance, on the term k = 1. We notice that $\Omega_1^2(\xi)$ has a bounded variation for ξ ranging from 0 to ∞: in effect, it starts from the point (see Eq. (42))

$$\Omega_1^2(0) = \varkappa^2 + \mu_1(0)/\nu D < 0$$

and reaches $-\Omega_1^2$, the square of the first root of Eq. (32), referring to a purely absorbing shell. For all values of $\Omega_1^2(\xi)$ in this range, Eq. (45) is positive over the entire interval $0 \leq r < R$.

We designate now by K = 2 the next real negative root of Eq. (40). In this case also $\Omega_2^2(\xi)$ has a bounded variation: but for all of the values it can take, Eq. (45) has one zero in the interval $0 \leq r < R$.

One deduces intuitively, after the above considerations, how the column is going to maintain some kind of "filtering power" for spatial harmonics, even under time-dependent excitation. For large values of $|z|$ we shall only find in the column a flux whose space and time behaviour is that of the first term of the summations appearing in Eq. (44) as well as in Eq. (31).

To evaluate the asymptotic flux, for large $|z|$, one has to solve Eq. (41) only once, for deriving $p_1(\xi)$. Furthermore, due to the possibility of calculating the first (k = 1) integral of Eq. (43) for large values of $|z|$ by means of a method such as that named after Filon [10], the amount of computational work does not appear prohibitive.

In our opinion the above considerations, referring to the particular kind of filtering effects of non-homogeneous columns during time-dependent phenomena, can be extended and apply also when more sophisticated theories for slowing-down and thermalization are used. This fact throws some light on the possibility of using devices of the type illustrated here for studying space- and time-dependent thermalization of fission neutrons.

The response of a column containing a pure absorber to a sinusoidally modulated source is now a trivial matter. Beginning with Eq. (31) one can easily establish the relationship between Ω_ν's, or equivalently γ, and the wavelength, attenuation distance and phase shift of the waves being propagated. When multiplication occurs, one has to start from Eq. (43), as the time-dependent Green's function, for finding the response to an oscillating source.

For large values of z, we simply designate by

$$\frac{1}{\gamma}\sqrt{\frac{\pi}{2}}\,\varphi_1(\tau,\xi) \equiv \frac{\varphi^{S}_{\mathcal{L}}(a;\Omega_1)}{\left.\frac{\partial \mathcal{F}}{\partial p}\right|_{p=p_1(\xi)}} \left\{ \eta e^{-(\xi^2\tau + p_1(\xi)\hat{t})} \right.$$

$$\left. F[a\to\tau;\,\tau,\Omega_1(\xi)] - G[a\to\tau;\Omega_1(\xi)] \right\}$$

the factor which appears in the integrand of the first term in the summation of Eq. (43). We can write, as a general asymptotic response to a modulated source of frequency ω,

$$\Phi_{Asym}(r,z,t) = Re\left\{ \int_0^{\infty} \varphi_1(r,\xi)\cos\xi z \left[\int_{-\infty}^{t-\hat{t}} e^{-p_1(\xi)(t-\theta)+i\omega\theta}\, d\theta \right] d\xi \right.$$

$$\left. + \int_{t-\hat{t}}^{t} \Phi^{Abs}(r,z,t-\theta)\, e^{i\omega\theta}\, d\theta \right\} \qquad (46)$$

From Eq. (46) the "generalized wave length, phase shift and attenuation distance", as well as a "generalized dispersion law" for the neutron waves being propagated can be derived.

It would seem at first sight that the analytical effort made for solving a problem of this kind is not fully justified. On the contrary, in our opinion all this effort and even more is essential if one wants to pay due attention also to the thermalization problem and be able to solve it, for instance, with some finite difference techniques.

REFERENCES

[1] KEEPIN, G. R., Pulsed neutron techniques, Rpt. LAMS-2215 (1958).

[2] WEINBERG, A. M. and WIGNER, E. P., The Physical Theory of Neutron Chain Reactors, Univ. Chic. Press (1958) Ch. XIII.

[3] BECKURTS, K. M. and WIRTZ, K., Neutron Physics, Springer-Verlag, Berlin (1964) Ch. 9.

[4] KRIEGER, J. T. and ZWEIFEL, P. F., Nucl. Sci. Engng 5 (1959) 21-27.

[5] WEINBERG, A. M. and NODERER, L. C., USAEC Rpt. CF-51-5-98, Theory of neutron chain reactions, Oak Ridge (1951) Ch. II.

[6] CORNO, S. E., Nuovo Cim. X, 17 (1960) 580-598.

[7] FEINBERG, S. M., Proc. UN Int. Conf. PUAE 5 (1956) 484.

[8] VITTOZ, B., MANDRIN, C. and GAVIN, P.: J. math. et de Phys. appl. (ZAMP) XIII, 3 (1962) 201-223.

[9] CORNO, S. E., "Interpretazione teorica della esperienze di moltiplicazione neutronica su un solo elemento di combustibile", (Theoretical approach to the neutron multiplication experiments involving a single fuel element) (a) Energia nucl. 10 11 (1963) 598-614; (b) Energia nucl. 10 12 (1963) 653-670; (c) Energia nucl. 11 2 (1964) 75-91.
[10] SNEDDON, I. N., Fourier Transform, MacGraw Hill, N. Y. (1951).

BIBLIOGRAPHY

PEREZ, R. B. and UHRIG, R. E., Nucl. Sci. Engng 17 (1963) 90-100.
DAVISON, B., Neutron Transport Theory, Oxford Univ. Press, Oxford and New York (1957).

DISCUSSION

R. PEREZ: At the University of Florida we are performing experiments on the propagation of waves and pulses throughout heterogeneous systems. Unfortunately we have been unable to obtain the flux as a closed expression, and this has forced us to use very cumbersome expressions whose computation has exhausted the memory of our IBM-709 computer. I should like to congratulate Dr. Corno on his remarkable analytical treatment of this problem.

S. CORNO: Thank you. Unfortunately the analytical closed-form solution I reported in the paper is not so easy to handle as might appear at first sight. However, its asymptotic expression – for large values of z – can at least be calculated without too much trouble.

B. VITTOZ: I know that this is a complicated problem but it might be interesting to take the delayed neutrons into account.

S. CORNO: One could describe the delayed neutrons exactly in our formalism by adding a set of equations for the precursors. Unfortunately this would make the algorism even more cumbersome. One could try a practical method and run the pulsed or oscillated column for a while before starting the measurements. The delayed-neutron emitters would then give rise to a constant background, whose spatial distribution could be evaluated.

M. N. MOORE: I was very interested to note the emergence of a propagating diffraction pattern in these investigations. Each interference fringe should penetrate the medium to a different extent measured by $\bar{z} = \int z\, A(z)\, dz$, where A(z) is the amplitude of the fringe as a function of z, the axial distance. It would be interesting to see if one could separate an asymptotic fringe.

S. CORNO: Our approach enables us to isolate a contribution which is in all respects analogous to the fundamental harmonic in the exponential experiments. Furthermore, one can estimate the intensity of the disturbance due to the higher-order harmonics. It is then possible to calculate the dispersion associated with the wave propagation belonging to each radial mode.

SUMMARY

(Session VIII)

SUMMARY OF THE SYMPOSIUM ON PULSED NEUTRON RESEARCH

M. NELKIN
CORNELL UNIVERSITY,
ITHACA, N.Y., UNITED STATES OF AMERICA

INTRODUCTION

It is a difficult but very interesting assignment to attempt a summary of this Symposium. I cannot, of course, summarize all the papers that we have heard in the least five days, but I will try to outline the main trends of the Symposium as I see them. I am sure that other people will see them differently, and I hope that we will hear some other opinions in the discussion period following this talk.

Before dealing with the detailed subject matter of the Symposium, I would like to discuss briefly some of the qualitative features of our deliberations during the past five days. The most striking thing to me has been the impression that we are dealing with a mature and sophisticated subject. The things that we have been talking about are remarkably abstracted from the operational techniques employed in our day-to-day work. Despite this, or perhaps because of it, we accept to a great extent the work of our contemporaries who are working along similar lines. This is best exemplified by the things that have not been discussed at the Symposium. For example, the theoretical work is very heavily computer-oriented, yet the numerical methods used for solving the transport equation have hardly been discussed at all. There are two reasons for this. The primary reason is that these techniques are rather well understood, and there is good reason for confidence in the results of one's co-workers. A secondary and less encouraging reason is the difficulty of having a meaningful discussion of calculational techniques in a large symposium such as this one.

As a theorist it was even more surprising to hear so little discussion of experimental methods, and to see such good agreement among various experimenters. This was particularly true with regard to the sessions on thermal systems. To a great extent this lack of discussion reflects the complexity of the techniques involved, and the difficulty of discussing them at a large symposium, but, in part, it reflects a real confidence that we know how to perform the measurements. Many of the experiments require extremely complicated corrections before the data can be presented in a meaningful way. There seems to be an amazing degree of agreement among various experimenters that these corrections are being made correctly. (I suspect that some of my "experimental" friends will disagree with this point, but this was certainly the impression the audience received during the presentation and discussion of the papers.)

With regard to the scientific aspect, I think that two basic trends are clear from the material which has been presented at this Symposium. The first is the general degree of success which we have had in understanding

thermal systems, particularly with respect to the thermalization problem. This has been a rather massive effort of a high degree of competence, and one gets the feeling from this Symposium that it has been a very successful effort. Thermalization is by no means a completed subject, but it is by now a relatively well-understood subject. It is clear from the excitement displayed at the excellent session on fast neutron systems (session V) that the area of greatest interest is shifting towards such systems.

The second basic trend apparent at the Symposium deals with the theoretical aspect, and concerns the great progress of the last few years in understanding the mathematical structure of the transport equation. The linear neutron transport equation is an exact basis for the understanding of essentially every experiment that has been discussed at this Symposium. We now have at least a moderately good understanding of the mathematical properties of this equation. The very important idea of a fundamental mode decay constant and the associated persistent distribution has been critically analysed, and is now quite well understood. We have seen, however, that there are systems which have no discrete decay constant eigenvalues, but are experimentally almost indistinguishable from systems with a proper fundamental mode. In these systems, there is a "quasi-fundamental mode" behaviour (determined by the continuum eigenvalues) which dominates the physical problem under study. We still are far from an adequate physical understanding of this phenomenon, and its study will form the focus of much theoretical effort in the near future. This is particularly true now that we see that the phenomenon is more varied and more practically important than was first realized. We have heard of its occurrence in a variety of fast multiplying systems, as well as in the small samples of crystalline moderator, where it was first predicted and has now been observed.

NON-MULTIPLYING SYSTEMS - EXPERIMENT

I turn now to a more specific discussion of the subjects that were covered in the various sessions. Consider first the measurement of the asymptotic exponential decay as a function of buckling for thermal non-multiplying systems. We heard an excellent review of these measurements by Professor Beckurts, as well as several new results presented in session I. For sufficiently large samples (i.e. sufficiently small bucklings) a fundamental mode decay constant as a function of buckling can be unambiguously measured. Furthermore this α versus B^2 curve can be analysed to give unambiguous values for the diffusion coefficient and diffusion cooling coefficient of the principal moderators. My interpretation of Professor Beckurts' paper is that this can be done for crystalline moderators as well as for water. If we recall that the diffusion cooling coefficient is defined in terms of an expansion of α in powers of B^2, it is clear that one wants to interpret the α versus B^2 curve over the smallest range of B^2 which gives statistically reliable values for the coefficients of the expansion. On this basis, for example, the value of C of $(25-30)\times10^5$ cm^4/s for graphite seems well established.

For larger bucklings (smaller samples) there are several types of problems. The first, which I have just mentioned is in the expansion of α in

powers of B^2. It is difficult to know how many terms to keep in this expansion, or even to know if the expansion is convergent. This is not a very fundamental problem, but it is present if one wants a useful physical parameterization of the data. The second problem, which is more interesting, is that we have difficulty knowing what buckling to assign to a given sample. This is particularly troublesome in water since the extrapolation distance depends on how we average the transport mean free path over energy. The work at Birmingham, (paper No. 42) which directly measures the neutron density as a function of space and time, largely resolves this problem in agreement with theory and allows a reasonable definition of buckling for water systems. Again an unambiguous determination of the diffusion coefficient and diffusion cooling coefficient is possible. There remain, however, unresolved discrepancies for small water systems, particularly as to unexplained effects of sample shape.

The third and most fundamental problem concerns the existence of a fundamental mode. We have known for some time that many of the observed decay constants for small crystalline assemblies were larger than the theoretically allowed maximum value. In the Rensselaer Polytechnic Institute (RPI) data shown by Professor Beckurts for small beryllium assemblies, we saw explicitly that the decay curve broke away at long times to a slower decay. It is not known, either from experiment or from theory, whether this slower decay at long times is purely exponential. I would like to emphasize that this point cannot be resolved experimentally. Whatever time range is measured, the theorist can always assert that the time behaviour at longer times, when there are even less neutrons remaining, will be different. The RPI experiment on beryllium was difficult even with a very high intensity linear accelerator. It is my opinion, which I will discuss further in connection with the theory, that our present theoretical understanding of thermal neutron die-away in small systems is not quantitative enough to encourage more measurements of this type. I agree with Professor Beckurts that the measurement of decay constants on homogeneous samples of pure moderator is not an attractive area for continued intensive experimental investigation.

Having proposed a rule, I propose an immediate exception: the Friedmann experiment in which the decay constant is measured as a function of the concentration of a non-1/v absorber. This is a particularly simple experiment to analyse theoretically. Given the degree of confirmation of our thermalization models from other experiments, it seems extremely unlikely that the large disagreement in this case between theory and experiment can be the fault of the theory. Further experimentation in this area seems desirable better to understand the possible difficulties in pulsed neutron measurements.

NON-MULTIPLYING SYSTEMS - THEORY

With regard to the theory of these experiments, we know quite well how to calculate decay constants as a function of buckling from an essentially straightforward numerical approach. As long as we can make the assumption of asymptotic reactor theory, i.e. the equivalence to an infinite medium with an exp(i Bx) spatial distribution, we can calculate the decay constants

associated with any given thermalization model to good accuracy. This is best illustrated by Honeck's paper for the 1962 Thermalization Conference at Brookhaven in which he calculated the equivalent diffusion length problem in the B_3 approximation to transport theory. Actually we were able to compute the decay constants accurately in this case before we understood the mathematical structure of the problem, but no calculations were done for large enough values of B^2 that the mathematical singularities should occur.

For finite-bounded geometry, the situation is just the opposite. Thanks to the work of Albertoni and Montagnini and of Bednarz, presented at this Symposium, we now understand the spectrum of decay-constant eigenvalues in bounded media rather well. This adds greatly to the understanding of the infinite medium problem which was so nicely summarized in this Symposium by Dr. Corngold. These three papers were one of the high points of the Symposium since they give a sound theoretical basis to much past and future numerical work.

In contrast to the infinite medium case, we have not yet done a very good job of calculating decay-constant eigenvalues for finite-bounded geometry. This is essentially a computational problem, and the next generation of computers should make its solution feasible. It should then be possible to make quantitatively reliable predictions of decay constants for various shapes and sizes of small water assemblies. At that point a new round of more accurate experiments will be useful as a check on our ability to solve the transport equation.

To summarize the above considerations, let us examine what we do and do not know about the time decay of the neutron flux in small crystalline assemblies. First, we know that no assembly can have a fundamental mode decay constant larger than λ^*, where λ^* is the collision rate for neutrons of zero speed. Any decay more rapid than this which is measured cannot represent a truly stationary space and energy distribution, and is not the true asymptotic behaviour for that particular assembly. Secondly, we know that a sufficiently small assembly has no fundamental mode. In the work presented here, this has not been proven for a finite assembly in the presence of elastic Bragg scattering, but it appears that the proofs can be extended to this case. Thus the decay at long times for a sufficiently small sample is not exponential, and the neutron energy spectrum never becomes stationary. We do not know whether the particular phenomena which have been observed in small beryllium and graphite assemblies correspond to this disappearance of the fundamental mode, or merely to a very slow approach to a fundamental mode. We suspect the former, but have not yet shown it convincingly. As I mentioned previously, this is a point which must be settled by theory and not by experiment. It is remarkable that the same behaviour of the fundamental mode decay constant reaching its maximum value and then no longer existing occurs in the infinite medium $\exp(i Bx)$ theory and in the finite-bounded medium. We do not know, however, whether the infinite medium theory is quantitatively applicable to the disappearance of the fundamental mode in beryllium and graphite. It probably is applicable since the basic phenomenon seems to be a breakdown of time-energy separability rather than a breakdown of space-energy separability, but we are not sure.

Before leaving this topic, I want to emphasize that the idea of a fundamental mode eigenvalue associated with a stationary persisting distribution at long times is of fundamental physical importance, and is not just of mathematical interest. As emphasized by Dr. Storrer the very long time behaviour that we calculate will be affected by certain idealizations made in decoupling our system from its environment. These idealizations are, however, usually soundly based, and the asymptotic behaviour of the idealized problem is of physical interest. If this asymptotic behaviour is determined by a fundamental mode (i.e. isolated discrete decay constant eigenvalue), then the decay constant α and the associated stationary neutron distribution are properties of the system. They can be calculated as the lowest eigenvalue and the associated positive eigenfunction of a rigorously defined steady state problem. No restriction to spatially uniform systems or assumption of space-energy separability is required. If, on the other hand, there is no discrete fundamental mode, then the asymptotic time behaviour is not strictly exponential, and the energy and space distribution never becomes independent of time. There is no equivalent steady state problem to any aspect of the time-dependent measurement. Our analysis must include the source energy spectrum, the detector position and energy sensitivity, and must be explicitly time dependent. The result is no longer a property only of the system, but also of what we do to the system. We can still use our physical intuition to get sensible simplifications, but the warning flag is up; the problem is of a different type. On the other hand, we should be able to attach some physical significance to an almost exponential decay and an almost stationary distribution. As has been emphasized to me by Professor Kazarnovsky, we must do this in order to have a satisfactory physical understanding of the phenomenon. We have not yet had much success along this line. I will return to this subject later in connection with analogous phenomena in fast multiplying systems.

NEUTRON THERMALIZATION AND SPECTRA

Another subject which has been actively considered at this Symposium is neutron thermalization. We have heard many interesting papers on this subject, and the overall impression has been that this is now a reasonably well understood subject. In fact it is one of the best understood subjects in reactor physics, and perhaps the best understood subject that has been studied with pulsed neutrons. This does not mean, of course, that there are no interesting problems remaining in this area. There are, in fact, quantitative discrepancies between theory and experiment in almost all cases. The overall impression, however, is that of a massive, highly competent effort which has almost succeeded in doing itself out of a job. Fortunately both the accelerators and the people working in this area are very flexible, and can readily turn to the solution of less well-understood problems. This will undoubtedly happen over the course of the next several years.

We can divide the thermalization work presented at this Symposium into four categories: (1) scattering law, (2) steady state spectra measured by the Poole technique, (3) the integral measurement of time-dependent

reaction rates and (4) the measurement of time-dependent spectra. I will discuss the scattering law first since it underlies all the rest. This is not the subject of this Symposium, but its relevancy is such that a few words are in order.

Our knowledge of thermal neutron inelastic scattering from moderators is very incomplete. The experimental study of this subject is increasing, but the motivation for this increase is primarily to obtain a better understanding of the dynamics of atomic motion in condensed matter. A by-product of this will certainly be improved scattering laws for reactor physics, but I do not believe that one should consider reactor physics requirements as a primary justification for these experiments. They are sufficiently important in their own right not to require this justification.

Our incomplete knowledge of the scattering law is not, at present, the limiting factor in our understanding of neutron thermalization or of the physics of thermal neutron reactors. There are by now fairly realistic models for most moderators which appear to be adequate in the light of the relatively insensitive dependence of thermal neutron spectra on the scattering law. For example we have a model for water by Haywood, based largely on scattering law measurements, which includes the effects of molecular diffusion and hindered rotation in a reasonable way. This model gives substantially better agreement with measured spectra, as has been shown in Dr. Poole's paper. (I hope that we can stop talking about the rather crude model for water, which usually has my name attached to it, but which does not have much to do with water.) In the actual application of the Haywood model one must combine the neutron scattering information on the low frequency modes with the optical information on the molecular vibrations in an intelligent way. This has been done and we have a quite adequate description. As a second example, which employs a somewhat different approach, consider the case of beryllium. Here one starts with neutron measurements of the phonon dispersion relations for a single crystal. Young and Koppel then construct a phonon spectrum and a scattering law through the intermediate step of a set of force constants fitted to the dispersion law using the Born-Von Karman theory of lattice vibrations. This is a complicated procedure, but it has been carried out, and we have an adequate scattering law. For graphite there is not so much information from neutron scattering, but a procedure similar to that used for beryllium was possible, depending rather heavily, however, on specific heat data as the experimental indicator of the phonon spectrum. For all these moderators, as well as for heavy water and zirconium hydride which I have not discussed, the measurement of steady state neutron spectra by the Poole technique has been very valuable in confirming the adequacy of our scattering models. This has been well illustrated by the results that Dr. Poole and Dr. Russell have presented at this Symposium.

With regard to time-dependent experiments in neutron thermalization, consider first the measurements of thermalization time constants through the time dependence of reaction rates. This type of experiment is quite useful in understanding the thermalization process, but we have come to realize that a rather sophisticated analysis is necessary to obtain really useful information from the measured reaction rates. Our early naïve ideas (which I helped to promulgate) about discrete eigenvalues completely describing

the approach-to-equilibrium were wrong. We now know that both discrete and continuous eigenvalues play a role. In fact for some moderators, such as graphite, there are no discrete eigenvalues describing the transient behaviour of the neutron spectrum. This is an interesting and important point, but it is much less fundamental than the non-existence of a fundamental mode in a small assembly. All that happens is that the average neutron speed does not approach its asymptotic value exponentially. There is a perfectly normal approach-to-equilibrium, but it is just not exponential at long times. This means that there is no unambiguous definition possible for a thermalization time constant in certain moderators. A thermalization time constant measured with one particular non-1/v absorber in graphite should be different from one measured with another non-1/v absorber. Even in water, where a time constant does exist, it is very difficult to isolate this mode experimentally. Thus an analysis of the time-dependent reaction rate experiment requires a calculation of the time-dependent flux spectrum $\phi(E, t)$ followed by an integration over energy using the appropriate energy dependence of the activation cross-section. Such an analysis for water has been presented at this Symposium by Dr. Purohit.

Perhaps the most direct method for studying the process of neutron thermalization is the direct measurement of the time-dependent neutron energy spectrum. This is done by using a chopper synchronized with a pulsed accelerator. There have been very impressive data from RPI, from Harwell and from the USSR, using this method, reported at this Symposium. I do not know how well these data agree quantitatively, but it seems that we have here, with some refinements, the tool to pin down our quantitative understanding of the thermalization process. The RPI and USSR results on small beryllium assemblies were particularly interesting. At moderate times the measured spectrum was a usual diffusion-cooled spectrum, and appeared almost stationary. After most of the neutrons had leaked out, the very slow neutrons trapped in the Bragg peak stayed behind. At long times the spectrum changed character drastically, in agreement with our expectation from the die-away experiment discussed earlier. It was very nice to see a further experimental confirmation that the decay at intermediate times, which is faster than λ^*, cannot be associated with a stationary spectrum.

THERMAL MULTIPLYING SYSTEMS

A large number of papers on the pulsing of thermal multiplying systems was presented in session IV. I will say relatively little about these since I know relatively little about this subject. From the number of papers on this subject and the general success of the measurements, it is observed that the use of pulsed neutrons as a reactivity measuring technique is well established. In this case the existence of a prompt neutron fundamental decay mode is almost never in doubt, and the basic measurement is usually the prompt neutron decay constant α for this mode. In considering the response of a reactor to a pulsed source, our point of view varies considerably, depending whether we are near-to-critical or far subcritical.

When near-to-critical, it is generally agreed that reactivity is a useful concept, and that a knowledge of the reactivity of our system is desirable.

A reactivity scale can be defined, using perturbation theory, such that small reactivity effects are additive. In this situation we want a good method to determine reactivity from a pulsed neutron measurement. The most straightforward procedure is to measure the prompt neutron decay constant α_c at delayed critical. The reactivity is then given by $1-\alpha/\alpha_c$. As emphasized in the paper by Garelis, however, we would like to be able to determine the reactivity of a subcritical reactor without having to first reach a critical condition. To do this we need information from the subcritical reactor about both the prompt and delayed neutron response. We have heard about the method of Garelis and Russell and that of Gozani for obtaining such information, and we have heard several papers which indicate that these methods are quite successful, despite some doubt as to the generality of their theoretical basis.

By contrast, far-below-critical reactivity is not a quantitatively useful concept. It seems largely a question of taste whether one wants to define a reactivity scale, and it is probably not very important how it is defined as long as there is some internal consistency. What is really desired is to use the response of the reactor to a pulsed source as a test of our model for caculating the reactor. The important question is to decide what is an adequate test of our model. The simplest test is still in terms of the prompt neutron fundamental mode decay constant. This is relatively easy to measure far-below-critical. It can be calculated as a well-defined eigenvalue associated with the amount of uniform 1/v poison that must be removed from the reactor to obtain a prompt critical system. Thus an unambiguous comparison of calculation with experiment is possible. As emphasized by Dr. Preskitt, this is not always the information about the reactor which is of greatest interest. An extreme example is a heavily poisoned core with a large reflector. The fundamental mode decay constant is largely a property of the reflector, and is certainly not a sufficient check on a calculational model for the reactor. If one is going to measure the prompt neutron response to a pulsed source during the initial loading of a reactor, as Dr. Preskitt has discussed, then one really needs rather complete calculations of the space and time dependence of the thermal neutron flux to compare with experiment. Then one certainly has an adequate test of the calculational model. At the present time, I would rather suspect that one has too good a test. I do not think that we can yet calculate the full space-time response with any great degree of confidence. It will be interesting and important to improve our abilities in this direction. Both clean experiments and improved theory, particularly for reflected systems, offer attractive possibilities for pulsed neutron research in the next several years.

FAST NEUTRON SYSTEMS

One of the highlights of the Symposium was the session on fast neutron systems (session V). It is not yet clear how important a role pulsed neutron techniques will play in this field, but there are a wide range of interesting experimental results, and still only a fragmentary understanding. The measurements on fast non-multiplying systems with a mono-energetic source and a biassed detector were very interesting. In an idealized situation, in

which the detector is biassed to exclude all neutrons except those very close to the source energy, these experiments can be analysed in one-speed transport theory. This is a very highly developed theory which has almost no direct applications to experiment, so that it is very gratifying to a theorist to have an opportunity to use it honestly. The potential of the method was very nicely illustrated in terms of the classic problem of the fundamental mode of a thin slab by Dr. Beghian. This method can be used either to test cross-sections or to test methods of solving the transport equation, depending on the material and the geometry used. Chiefly by analogy with the thermal case, I expect that the main use will be in checking transport theory. As mentioned in Dr. Beckurts' review paper, by the time the method is sufficiently refined to allow measurements of cross-sections, it is likely that the direct differential measurements of the cross-sections will be equally reliable. By selecting materials where the cross-sections are well known, one can use the method as a check on our ability to solve the transport equation in space and time without the additional complication of energy dependence. It seems to me that we are still far enough away from obtaining accurate solutions for the complete problem that removal of the energy variable will be helpful in improving comparisons of theory with experiment for some time to come.

For fast multiplying systems we learned from Dr. Storrer's excellent review paper that there is not always a discrete fundamental mode, but that we again must deal with continuum eigenvalues. The analogy to the problem of thermal neutrons in small samples of crystalline moderators is quite close, but the fast multiplying system is more interesting for two reasons. It is of much greater practical interest and the phenomenon occurs over a much less restricted range of circumstances. We can have a true fundamental mode, or a quasi-fundamental mode in which the decay is almost exponential, or we can have a situation whereby the decay is not even approximately exponential. All three of these situations have been explicitly observed. Furthermore all three can occur even for an unreflected system. When a reflector is included there will presumably be an even greater richness of phenomena, the understanding of which will keep us busy for many years to come.

Just below prompt criticality there certainly is a fundamental mode, but it may happen that this mode disappears into the continuum for a system which is not very far subcritical. The reason for this is that the natural decay rate of the system becomes faster than the collision rate for the slowest neutrons. If one uses a fast source and a fast detector, as any sensible person would use with a fast reactor, this "trapping" of the slow neutrons will not play an important role. One measures a decay which is very nearly exponential except at very long times, and this quasi-exponential decay is certainly a physically meaningful behaviour. Several different approaches have been suggested, none of them completely successful, for unravelling the physics of this particular problem. This is a natural area for continued intensive study.

The first approach, mentioned by Dr. Storrer, is to truncate the problem by removing the lower energy neutron groups. This makes the minimum collision rate larger, and, so to speak, moves the continuum out of the way. The truncated problem will have a true fundamental mode which

looks very much like the quasi-fundamental mode of the full problem. This is a reasonable approach when we are sure, from physical considerations, that these slow neutrons are not important. For broad spectrum systems, however, these slow neutrons (typically around 50 eV) may be important as witnessed by the observed decays which are not even approximately exponential. To include these situations we need a more general method of analysis.

Two methods of accomplishing this have been discussed at this Symposium. The first, discussed by Dr. Storrer, is to examine all the eigenfunctions and eigenvalues in a multigroup calculation. We can identify as the quasi-fundamental mode that eigenfunction which has the strongest amplitude in the particular initial value problem that we are studying. Usually one can do this by inspection of the energy spectra associated with each of the eigenfunctions. If no one eigenfunction is dominant then there is no quasi-fundamental mode and no approximate exponential decay will be observed. This calculation has many features in common with the multigroup calculation of thermal neutrons in crystalline moderators. In particular one has the phenomenon that the dominant amplitude and physically interesting energy spectrum crosses from one eigenvalue to another as the buckling is increased beyond the critical value for the existence of a true fundamental mode.

The second method was discussed by Dr. Cadilhac, and is concerned with obtaining an analytic description in the continuous energy representation. This is the first serious attempt to obtain a physical understanding of the quasi-discrete eigenvalues in terms of a description which allows the continuum to be a continuum. The initial results are very interesting and this promises to be an important area for further work.

PULSED REACTORS AND NEUTRON SOURCES

Some impressive developments in new pulsed neutron sources were discussed in session VI. These included some very clever small pulsed neutron sources as well as the larger devices. A particularly interesting idea is that of combining a pulsed fast reactor with an accelerator. This seems to be a very promising direction for the next generation of high intensity neutron sources, both for applied and fundamental neutron physics investigations. Dr. Wimett discussed the change which the basic techniques of cross-section measurement may have to undergo because of the very high intensity of these devices. It is also quite clear that all the sophistication that we have developed in analysing pulsed source experiments will be absolutely necessary for the engineering of these devices.

RELATED TECHNIQUES

Finally, I want to say a few words on the technique of using modulated neutron sources. We do not yet seem to be at quite as sophisticated a level of understanding in this area as we are with pulsed sources. This is undoubtedly because of our smaller total amount of experience in this area.

We know that the modulated source technique gives very similar information, but we do not yet seem to clearly understand under what circumstances it is preferable to a pulsed source. I strongly suspect that there are such circumstances. The study of neutron thermalization with this technique, as reported by Dr. Perez, is a good way to develop this understanding. I think that at first we will learn more about the subtleties of the technique than about thermalization, but this phase should pass quickly. The modulated source technique will probably become increasingly important as a probe of the kinetic behaviour of neutron systems.

CONCLUSION

It is one thing to summarize the Symposium, but now I have the almost impossible job of summarizing the summary. Since I have to stop somewhere, let me try. We have learned a great deal in the last week about the space, time and energy distribution of neutrons in macroscopic media. Pulsed neutron experiments have been the major source for continually improving our understanding in this important area of applied physics. With a certain shift of emphasis from thermal neutron systems to fast neutron systems this work should continue profitably for many years.

Let me add, however, one note of caution about the meaningful exchange of scientific information in this area. As our final results become further and further abstracted from what we actually do, it is becoming increasingly difficult at a brief meeting to determine whether our colleagues are right or wrong. We all agree that we have already achieved a quite sophisticated understanding of the subject. We must think more about meaningful ways of communicating this knowledge to each other. Given another few years, another set of complex corrections, and another round of computer data processing before anybody sees it, and I am not sure what we will be able to communicate at a symposium. Partly inspite of, and partly because of this abstraction from the directly measured data, we learned a great deal at this Symposium. But one of the reasons we did not have more of the strong disagreements which are so important to a scientific meeting is that we were not quite sure what the other person did. We were fairly sure that it was all right, because he is intelligent and has been working at this subject for a long time, but we accepted much without fully understanding it. If we allow this condition to become worse, we could lose much of the integrity of our scientific communication.

Setting the above remark aside, where perhaps it belongs, we have spent a very enjoyable and informative week at an extremely well-organized symposium. It has been both a challenge and a pleasure to attempt this summary.

DISCUSSION

N. CORNGOLD: There is one parameter whose role in thermalization has not received our full attention at this Symposium, namely the temperature, It may be possible for us to extract further information about the decay in

small crystalline samples by working at low temperatures, rather than by employing neutron sources of higher intensity.

P. SCHOFIELD: I would like to raise two problems which are of a more mundane nature than many of those discussed in the papers presented at this meeting and in Dr. Nelkin's summary.

First, in connection with the scattering law, I feel that the effects of anisotropic scattering have been neglected in thermalization problems. I would remind you that one of the original motivations for studying thermalization phenomena was to be able to predict moderator-temperature coefficients for thermal reactors. We have now accumulated enough evidence to show that in some circumstances these may be "model-sensitive" but there has been little discussion of anisotropic scattering.

Secondly, an interesting feature of many of the measured thermal spectra, both time-dependent and space-dependent, is that they are semi-quantitatively and certainly qualitatively Maxwellian. It is a challenge to the theoretician to explain this phenomenon on a more sophisticated basis rather than in terms of the early "relaxation-time" theory of Dardel and Sjöstrand, which we now know to be inadequate in view of the absence of discrete modes.

A. HENRY: I believe we should now begin to analyse pulsed-neutron experiments in multiplying thermal systems by computing directly the die-away constant α rather than the reactivity. It is difficult, and for large degrees of subcriticality almost impossible, to infer reactivity values directly from experiments and to compute them exactly one must generally determine the eigenfunction associated with α and hence α itself. We should, I believe, stop there.

S.N. PUROHIT: I agree with Dr. Nelkin that we can compute the spectra in detail with the help of computing machines, but unfortunately we are not in a position to discuss these spectra in detail. The reaction rate and other integral parameter studies may be of some help in discussing these details in the form of parameters.

N.G. SJÖSTRAND: I agree with Dr. Purohit on this point. I would also like to point out that when we carry out experiments we always try to vary the experimental conditions – neutron-source energy, source and detector positions, etc. We do not rely on the results until we understand them completely. It would be very useful if this experimental approach were more in evidence among the people who do the computations.

Coming as I do from a small university laboratory with limited facilities, I have been glad to see that there is still plenty of work for the small laboratory to do, for example measurements of exponential or non-exponential decay curves for very small systems, investigations of the Friedmann method in cases where there are discrepancies, or studies in the very interesting field of wave propagation. In other words, we have not yet been forced out of business by the big linear accelerators!

M. KAZARNOVSKY: I fully agree with Dr. Nelkin that one of the most interesting problems facing us in the theoretical field is that of the discrete and quasi-discrete eigenvalues of the Boltzmann equation. Judging by the papers we have heard at this Symposium, I think it can be said that experimental techniques have now reached the stage where an experimental solution to this problem has also become possible.

N. CORNGOLD: On the subject of pulsed-neutron measurements of reactivity, it is important, I think, never to lose sight of the fact that the different schemes used are different "thermometers" which measure different reactivities.

E. SILVER: It should be pointed out that even in such well-understood fields as the decay of thermalized-neutron populations in non-multiplying media there are still a number of problems that remain to be solved, at least in the area of experiment analysis. I have in mind the fact that there is still no real agreement on the subject of extrapolation distances for small water systems and this in turn gives rise to problems in the evaluation of D_0 and C.

M. POOLE: There has been considerable speculation on whether thermalization studies are completely finished or not and on whether there is still room for work to be done in this connection in the smaller establishments or in the universities which cannot afford big Linacs. Fears have been expressed that institutes with the big Linacs might monopolize the field and leave nothing for their poorer cousins. Personally, I think these fears are unjustified. I feel convinced that the examination of the discrete or indiscrete eigenvalues of the Boltzmann equation will exercise the imaginations of mathematicians and their research students for perhaps a generation to come.

On the experimental side, I would like to make one point which I think is significant. At this Symposium a "Neutronenblitzröhre" was described. This is a small cheap neutron tube with an output some 20 times that of the Linac on which I did the first spectrum measurements and it can be used to perform almost all the thermalization measurements still required, with the possible exception of the time-dependent measurements. This has brought thermalization work effectively within the reach of everybody. Moreover, the very fact that this field is perhaps no longer quite so exciting as it was will tend, I think, to induce the people with big Linacs to look for new and more exciting areas of activity. There is always a tendency, or a temptation, to do half a job and then leave the details until later. The big Linacs, I am sure, will now be used for work in the field of fast spectra and fast measurements – I am referring now, of course, only to reactor physics and not nuclear measurements – for which fast and very intense pulses are essential and which can hardly be dealt with adequately by a weaker source. This leaves an immense amount of work to be done, namely the highly important job of clearing up and deciding on the best methods of dealing with neutron thermalization, and this work is certainly within the reach of even the smallest laboratory.

Note added in proof by the Scientific Secretaries

We wish to comment briefly on the problem of different reactivity scales which has been referred to by several participants during this Symposium. In the neutron balance equation, the reproduction factor k can be defined either by normalizing to neutron production or by normalizing to neutron losses (leakage plus absorption), thus giving two different reactivity scales. Other reactivity- or k-scales can be defined in terms of the number of

neutrons which must be added or removed at various energies to make the system critical. Thus, for example, when reactivity is defined by changing v until $k = 1$, this is equivalent to adding neutrons with the fission energy distribution, whereas when reactivity is defined by changing the amount of $1/v$ absorber to bring the system to critical, this is equivalent to adding or removing neutrons with a $1/v$ energy distribution. Clearly the number of neutrons required to produce the same change in neutron reproduction factor is not the same in these two cases. Back in the "good old days" when reactor calculations were primarily for very large, nearly-homogeneous systems, approximate methods (one- or two-group diffusion theories, four-factor formulas, etc.) were quite adequate. In these large systems it was relatively immaterial which reactivity scale one used; on the other hand, in modern heterogeneous systems, where detailed space, energy and time-dependence becomes important, there can arise large discrepancies between different reactivity scales.

In view of such difficulties with any point-model or system-averaged definition of reactivity (particularly in highly subcritical systems) several participants at this Symposium have suggested that in pulsed-neutron experiments we shift the emphasis to direct comparison of measured and computed α values. We support this general approach, as applied both to multiplying as well as non-multiplying (moderator) media. In the latter case, this also means one should not rely too much on modal analyses and multi-parameter fits which may be of questionable physical significance.

SYMPOSIUM ON PULSED NEUTRON RESEARCH

HELD AT KARLSRUHE, 10-14 MAY 1965

CHAIRMEN OF SESSIONS

Session I	N.G. SJÖSTRAND	Chalmer University of Technology, Göteborg
Session II	P. SCHOFIELD	Atomic Energy Research Establishment, Harwell
Session III	M. KAZARNOVSKY	P. N. Lebedev Institute of Physics, Moscow
Session IIIA	P. ZWEIFEL	Middle East Technical University, Ankara
Session IV	A. HENRY	Westinghouse Electric Corporation, Pennsylvania
Session V	V. RAIEVSKI	EURATOM, Ispra
Session VI	D. BRETON	Centre d'études nucléaires de Saclay
Session VII	F. STORRER	EURATOM, Brussels
Session VIII	K. WIRTZ	Kernforschungszentrum Karlsruhe

SECRETARIAT OF THE SYMPOSIUM

Scientific Secretaries:	G.R. KEEPIN	Division of Research and Laboratories
	D.W. MAGNUSON	Division of Research and Laboratories
Administrative Secretary:	H.H. STORHAUG	Division of Scientific and Technical Information
Editors:	D. NASTASIA-SCOTTI	Division of Scientific and Technical Information

	M.M. BROWN	Division of Scientific and Technical Information
Records Officer:	T.J. JONES	Division of Languages

LIST OF PARTICIPANTS

Name	Institution	Nominating State or Organization
Abbott, D.	Central Electricy Generating Board, Berkeley Nuclear Labs.	United Kingdom
Andres, R.	AEG Kernenergieversuchsanlage, Grosswelzheim	Federal Republic of Germany
Arai, E.	Kernforschungszentrum Karlsruhe	Federal Republic of Germany
Bader, M.	Kernforschungsanlage Jülich	Federal Republic of Germany
Barnes, W.	Atomic Weapons Research Establishment, Aldermaston, Berks.	United Kingdom
Beaugé, R.	Organisation for Economic Co-operation and Development, Paris	OECD
Beckurts, K.H.	Kernforschungszentrum Karlsruhe	Federal Republic of Germany
Bednarz, R.	Institute of Nuclear Research, Swierk	Poland
Beghian, L.	Massachusetts Institute of Technology, Cambridge, Mass.	United States of America
Benesch, F.	Atominstitut, Vienna	Austria
Benezech, G.	Centre d'Etudes nucléaires de Cadarache, Saint-Paul-lez-Durance (B. du R.)	France
Berthet, P.	Lab. de Génie Atomique de l'Ecole Polytechnique de l'Université de Lausanne	Switzerland
Bierman, S.	Pacific Northwest Labs., Battelle Memorial Inst., Richland, Wash.	United States of America
Bod, L.	Central Research Institute for Physics, Budapest	Hungary
Booth, R.	Nuclear Engineering Test Facility, Air Force Inst. of Technology, Ohio	United States of America
Borgwaldt, H.	Kernforschungszentrum Karlsruhe	Federal Republic of Germany

LIST OF PARTICIPANTS

Name	Institution	Nominating State or Organization
Bormann, H.J.	Kernforschungsanlage Jülich	Federal Republic of Germany
Bounden, J.	Ministry of Defence, Services Electronics Research Lab., Baldock, Herts.	United Kingdom
Bourion, R.	Cie Générale de télégraphe sans fil, Levallois-Perret (Seine)	France
Breton, D.	Commissariat à l'énergie atomique, Paris	France
Breunlich, W.	Institut für Radiumforschung und Kerntechnik der Österreichischen Akademie der Wissenschaften, Vienna	Austria
Briggs, A.J.	Atomic Energy Establishment, Dorchester, Dorset	United Kingdom
Bronner, G.	Siemens-Schuckertwerke AG, Garching, Munich	Federal Republic of Germany
Brunfelter, B.	Research Institute of National Defence, Stockholm	Sweden
Buchet, J.	Commissariat à l'energie atomique, Paris	France
Bünemann, D.	Gesellschaft für Kernenergieverwertung in Schiffbau und Schiffahrt mbH, Institut für Reaktorphysik, Tesperhude	Federal Republic of Germany
Cadilhac, M.	Centre d'études nucléaires de Saclay, Gif-sur-Yvette (Seine et Oise)	France
Christensen, P.S.	Danish Atomic Energy Commission, Risø, Roskilde	Denmark
Chwaszczewski, S.	Institute of Nuclear Research, Swierk	Poland
Comte, R.	Commissariat à l'énergie atomique, Paris	France
Constantine, G.	Atomic Energy Research Establishment, Harwell, Didcot, Berks.	United Kingdom
Čopić, M.	Nuclear Institute "Josef Stefan", Ljubljana	Yugoslavia
Corngold, N.	Brookhaven National Laboratory, Upton, N.Y.	United States of America

Name	Institution	Nominating State or Organization
Como, S.	Università di Pavia, Istituto di Fisica, Pavia	Italy
Cortellessa, G.	Istituto Superiore di Sanità, Rome	Italy
Daitch, P.	Rensselaer Polytechnic Institute, Troy, N.Y.	United States of America
De Juren, J.	Atomics International (NAA), Canoga Park, Calif.	United States of America
Demarmels, P.	Eidgenössisches Institut für Reaktorforschung, Würenlingen	Switzerland
Deniz, V.	Commissariat à l'énergie atomique, Paris	France
De Stefano, P.	Istituto di Fisica, Università di Pavia, Pavia	Italy
Devooght, J.	Université de Bruxelles, Brussels	Belgium
Dio, W.H.	Siemens-Schuckertwerke AG, Garching, Munich	Federal Republic of Germany
Döllgast, T.	Eidgenössisches Institut für Reaktorforschung, Würenlingen	Switzerland
Dragt, J.B.	Reactor Centrum Nederland, Petten	Netherlands
Drechsel, W.	Brown Boveri/Krupp Reaktorbau GmbH, Versuchs-Abteilung, Kernforschungsanlage Jülich	Federal Republic of Germany
Durrani, S.A.	Atomic Energy Centre, Lahore	Pakistan
Eastlake, R.	Elliott Bros. (London) Ltd., Radiation and Detector Group, EET, Borehamwood, Herts.	United Kingdom
Edelmann, M.	Kernforschungszentrum Karlsruhe	Federal Republic of Germany
Elenga, C.	Philips Research Laboratories, Eindhoven	Netherlands
Engler, H.D.	Siemens-Schuckertwerke AG, Garching, Munich	Federal Republic of Germany

Name	Institution	Nominating State or Organization
Eyrich, W.	Kernforschungszentrum Karlsruhe	Federal Republic of Germany
Falla, L.	Université d'Elisabethville, Elisabethville	Democratic Republic of Congo
Finnemann, H.	Siemens-Schuckert, Erlangen	Federal Republic of Germany
Fleck, C.M.	Atominstitut der Österr. Hochschulen, Vienna	Austria
Fournol, J.	SODERN, Paris	France
Fraude, A.	Gemeenschappelijke Kernenergie-centrale Nederland, Arnhem	EURATOM
Fuster, S.	Centre d'études nucléaires de Saclay, Gif-sur-Yvette (Seine et Oise)	France
Gaerttner, E.	Rensselaer Polytechnic Institute, Troy, N.Y.	United States of America
García-Castañer, B.	Junta de Energía Nuclear, Madrid	Spain
Garelis, E.	General Electric Company Vallecitos Atomic Laboratory, Pleasanton, Calif.	United States of America
Gavin, P.	Lab. de Génie Atomique de l'Ecole Polytechnique de l'Université de Lausanne	Switzerland
Gaythor, D.	Atomic Energy Research Establishment, Harwell, Didcot, Berks.	United Kingdom
Gerbier, R.	Centre d'études nucléaire de Grenoble, (Isère)	France
Govaerts, P.	Association EURATOM – CEA, Centre d'énergie nucléaires de Cadarache, Saint-Paul-lez-Durance (B. du R.)	France
Grosshög, G.	Chalmers University of Technology, Göteborg	Sweden
Haas, R.	Centro Comune di Ricerche, Ispra (Varese), Italy	EURATOM

Name	Institution	Nominating State or Organization
Hammer, P.	Centre d'études nucléaires de Cadarache, Saint-Paul-lez-Durance (B. du R.)	France
Hantke, H.J.	BBC/Krupp-Reaktorbau GmbH, Jülich, Laborbau	Federal Republic of Germany
Harder, H.	Gutehoffnungshütte AG,, Sterkrade	Federal Republic of Germany
Harding, J.M.	Scientific and Technical Unit, CINCUSNAVEUR, Frankfurt am Main	United States of America
Harris, M.	Dept. of Nuclear Engineering, University of Manchester	United Kingdom
Heckmann, P.H.	Kernforschungsanlage Jülich, Institut für Reaktorentwicklung, Jülich	Federal Republic of Germany
Heemskerk, F.	NV Philips, Nucl. Tubes Dept., Eindhoven	Netherlands
Hemmig, P.	United States Atomic Energy Commission, Wash.,D.C.	United States of America
Hennies, H.H.	INTERATOM, Internationale Atomreaktorbau GmbH., Bensberg	Federal Republic of Germany
Henry, A.	Westinghouse Electric Corp., Bettis Atomic Power Lab., West Mifflen, Pa.	United States of America
Hewitt, J.	Dept. of Physics, University of Birmingham	United Kingdom
v.d. Heyden, A.W.	Reaktor Instituut, Delft	Netherlands
Hollnagel, R.	Physikalisch-Technische Bundesanstalt, Braunschweig	Federal Republic of Germany
Honeck, H.	Brookhaven National Laboratory, Upton, N.Y.	United States of America
Houelle, M.	Commissariat à l'énergie atomique, Paris	France
Humbach, W.	Technische Hochschule, Darmstadt	Federal Republic of Germany

Name	Institution	Nominating State or Organization
Hurst, D.G.	Division of Nuclear Power and Reactors, Department of Technical Operations, Vienna	International Atomic Energy Agency
Jansson, R.	Research Institute of National Defence, Stockholm	Sweden
Jentzsch, U.	Gesellschaft für Strahlenforschung mbH, Neuherberg, Munich	Federal Republic of Germany
Joest, K.H.	INTERATOM, Reaktorbau GmbH, Bensberg	Federal Republic of Germany
Jonsson, E.	AB Atomenergi, Stockholm	Sweden
Joshi, B.V.	Atomic Energy Establishment Trombay, Bombay	India
Kalin, T.	Nuclear Institute Josef Stefan, Ljubljana	Yugoslavia
Kallfelz, J.	Institut für Angewandte Kernphysik, Kernforschungszentrum Karlsruhe	Federal Republic of Germany
Kaneko, Y.	Japan Atomic Energy Research Institute, Tokai-mura, Ibaraki-ken	Japan
Kato, W.	Argonne National Laboratory, Argonne, Ill.	United States of America
Kazarnovski, M.	Lebedev Physical Institute, Moscow	Union of Soviet Socialist Republics
Kemeny, L.G.	Nuclear Engineering Dept., Queen Mary College, University of London	United Kingdom
Kim, J.M.	Nuclear Energy Dept., Queen Mary College, University of London	United Kingdom
Kladnik, R.	Nuclear Institute Josef Stefan, Ljubljana	Yugoslavia
Kley, W.	Centro Comune di Ricerche, Ispra (Varese), Italy	EURATOM
Kockum, J.	Research Institute of National Defence, Stockholm	Sweden

Name	Institution	Nominating State or Organization
Kofink, W.	Institut für Struktur der Materie, Technische Hochschule, Karlsruhe	Federal Republic of Germany
Kohler, H.	Deutsche Babcock & Wilcox-Dampfkessel-Werke AG, Oberhausen, Rhld.	Federal Republic of Germany
Krebs, K.	Centro Comune di Ricerche, Ispra (Varese), Italy	EURATOM
Kressner, W.	BOEING International Corp., Munich	United States of America
Krug, H.	Institut für Mess- und Regelungstechnik, Munich	Federal Republic of Germany
Küchle, M.	Kernforschungszentrum Karlsruhe	Federal Republic of Germany
Kürsten, H.	Institut für Reaktorphysik Kernenergie, Hamburg	Federal Republic of Germany
Kuščer, I.	Institute of Physics, University of Ljubljana	Yugoslavia
Kussmaul, G.	Kernforschungszentrum Karlsruhe	Federal Republic of Germany
Lalande, J.	Centre d'études nucléaires de Grenoble (Isère)	France
Launois, M.	Commissariat à l'énergie atomique, Paris	France
Longo, G.	CNEN, Bologne	Italy
Louwrier, P. W. F.	Instituut voor Kernphysisch Onderzoek, Amsterdam	Netherlands
Lumb, R.	Western New York Nuclear Research Center, Power Drive, Buffalo, N. Y.	United States of America
Mangialajo, M.	CISE, Milan	Italy
Mansfield, W.	Nuclear Engineering Dept., Queen Mary College, University of London	United Kingdom
Marseguerra, M.	CNEN, Bologne	Italy

Name	Institution	Nominating State or Organization
Mascheretti, P.	Istituto di Fisica, Università di Pavia, Pavia	Italy
Matthes, W.	Centro Comune di Ricerche, Ispra (Varese), Italy	EURATOM
Meister, G.	Kernforschungsanlage Jülich	Federal Republic of Germany
Meister, H.	Kernforschungszentrum Karlsruhe	Federal Republic of Germany
Meister, H.	Centro Comune di Ricerche, Ispra (Varese), Italy	EURATOM
Meyer, P.	General Electric, Vallecitos Atomic Laboratory, Pleasanton, Calif.	United States of America
Miessner, H.	Institut für Angewandte Kernphysik, Kernforschungszentrum Karlsruhe,	Federal Republic of Germany
Mika, J.	Institute of Nuclear Research, Swierk	Poland
Mills, W.	Socony Mobil Oil Co., Inc., Field Research Lab., Dallas, Tex.	United States of America
Mitchell, E. W. J.	University of Reading, Whiteknights Park, Reading, Berks.	United Kingdom
Mockel, A.	Université Libre de Bruxelles, Brussels	Belgium
Möller, E.	AB Atomenergi, Studsvik, Nykoping	Sweden
Montagnini, B.	SNAM, Div. L.R.S.R., Milan	Italy
Moore, M. N.	Centre d'énergie nucléaires de Cadarache, Saint-Paul-lez-Durance (B. du R.)	France
Morton, J.	Lawrence Radiation Lab., Livermore, Calif.	United States of America
Mouraille, H.	Centre d'études nucléaires de Grenoble (Isère)	France
Mudtir, P.	Ministère des Terres, Mines et Energie, Léopoldeville	Democratic Republic of Congo

Name	Institution	Nominating State or Organization
Müller, H.	Reaktorinstitut Technische Hochschule, Graz	Austria
Müller, K. H.	Centro Comune di Ricerche, Ispra (Varese), Italy	EURATOM
Nagel, W.	Instituut vor Kernphysisch Onderzoek, Amsterdam	Netherlands
Nelkin, M.	Nuclear Reactor Lab., Cornell University, Ithaca, N. Y.	United States of America
Nicolaenko, B.	Centre d'études nucléaires de Cadarache, Saint-Paul-lez-Durance (B. du R.)	France
Noll, I. P.	Institut für Reaktortechnik, Technische Hochschule, Darmstadt	Federal Republic of Germany
O'Brien, P.	Sandia Corporation, Albuquerque, N. Mex.	United States of America
Oei, T. D.	Reactor Centrum Nederland, Petten	Netherlands
D'Oultremont, P.	Belgonucléaire, Brussels	Belgium
Pacilio, N.	Lab. Fisica e Calcolo Reattori, Comitato Nazionale Energia Nucleare, Rome	Italy
Page, R.	University of Southampton, Southampton, Hants.	United Kingdom
Palazzi, F.	CISE, Milan	Italy
Paterson, W. J.	Atomic Weapons Research Establishment, Aldermaston, Berks.	United Kingdom
Pérez, R.	University of Florida, Dept. of Nuclear Engineering, Gainesville, Fla.	United States of America
Petrovič, M.	Boris Kidrič Institute of Nuclear Sciences, Belgrade	Yugoslavia
Pregl, G.	Nuclear Institute Josef Stefan, Ljubljana	Yugoslavia
Preskitt, Ch. A.	Oak Ridge National Laboratory, Oak Ridge, Tenn.	United States of America

Name	Institution	Nominating State or Organization
Preus, G.	Bundesministerium für Wissenschaftliche Forschung, Bad Godesberg	Federal Republic of Germany
Pierpaoli, V.	Lab. Riuniti Studi Ricerche, SNAM, Milan	Italy
Pollak, H.	Centre Atomique Trico, Léopoldeville	Democratic Republic of Congo
Poole, M.	Atomic Energy Research Establishment, Harwell, Didcot, Berks.	United Kingdom
Popov, Y.	Joint Institute of Nuclear Research, Dubna, Moscow	Union of Soviet Socialist Republics
Pucker, N.	University of Graz	Austria
Purohit, S. N.	AB Atomenergi, Studsvik, Nyköping	Sweden
Purica, I.	Institut de Physique Atomique de l'Académie de la République Populaire Roumaine, Bucarest	Romania
Raievski, V.	Centro Comune di Ricerche, Ispra (Varese), Italy	EURATOM
Ramšak, V.	Nuclear Institute Josef Stefan, Ljubljana	Yugoslavia
Reichardt, W.	Kernforschungszentrum Karlsruhe,	Federal Republic of Germany
Reifenschweiler, O.	Philips Research Laboratories, Eindhoven	Netherlands
Ritchie, I.	Australian Atomic Energy Commission, Sutherland, New South Wales	Australia
Robert, P.	Lab. de Génie Atomique de l'Ecole Polytechnique de l'Université de Lausanne	Switzerland
Roche, M.	Commissariat à l'énergie atomique, Paris	France
Rodríguez-Mayquez, E.	Junta de Energía Nuclear, Madrid	Spain
Rossberg, D.	Johann Wolfgang Goethe-Universität, Frankfurt am Main	Federal Republic of Germany
Rotter, W.	Centre d'études nucléaires, Mol-Donk, Belgium	EURATOM

Name	Institution	Nominating State or Organization
Russell, J.	General Atomic, San Diego, Calif.	United States of America
Rutgers, E.	Lab. de Génie Atomique de l'Ecole Polytechnique de l'Université de Lausanne	Switzerland
Rzeszot, T.	Institute of Nuclear Research, Swierk	Poland
Sadikov, I.	Institute of Atomic Energy of Kurchatov, Moscow	Union of Soviet Socialist Republics
Sagot, M.	Centre d'études nucléaires de Cadarache Saint-Paul-lez-Durance (B. du R.)	France
Sanatani, S.	Division of Nuclear Power and Reactors, Department of Technical Operations, Vienna	International Atomic Energy Agency
Sancho, L.	Junta de Energía Nuclear, Madrid	Spain
Schett, A.	Institut für theoretische Physik, Universität Innsbruck	Austria
Schlosser, G.	Siemens-Schuckert AG, Erlangen	Federal Republic of Germany
Schmidt, A.	Kernforschungszentrum Karlsruhe	Federal Republic of Germany
Schofield, P.	Theoretical Physics Div., Atomic Energy Research Establishment, Harwell, Didcot, Berks.	United Kingdom
Schulze, E.	Institut für Reaktortechnik, Technische Hochschule, Darmstadt	Federal Republic of Germany
Scott, S.	TECHNION, Israel Institute of Technology, Haifa	Israel
Segal, Y.	TECHNION, Israel Institute of Technology, Haifa	Israel
Sherwin, J.	Windscale Works, Sellafield, Cumberland	United Kingdom
Silver, E.	Oak Ridge National Lab., Oak Ridge, Tenn.	United States of America
Sinclair, R.N.	Atomic Energy Research Establishment, Harwell, Didcot, Berks.	United Kingdom

Name	Institution	Nominating State or Organization
Sjöstrand, N.G.	Chalmers University of Technology, Göteborg	Sweden
Smith, D.	UK Atomic Energy Authority, Winfrith, Dorchester, Dorset	United Kingdom
Sumita, K.	Osaka University, Osaka-City	Japan
Stegemann, D.	Kernforschungszentrum Karlsruhe	Federal Republic of Germany
Steinberg, R.	Lewis Research Center, Cleveland, Ohio	United States of America
Stiévenart, M.	Belgonucléaire, Brussels	Belgium
Storrer, F.	Association EURATOM-CEA, Centre d'études nucléaires de Cadarache, Saint-Paul-lez-Durance (B. du R.)	France
Tagesen, S.	Institut für Radiumforschung und Kerntechnik der Österr. Akademie der Wissenschaften, Vienna	Austria
Tchernilin, Y.	Division of Nuclear Power and Reactors, Department of Technical Operations, Vienna	International Atomic Energy Agency
Tellier, H.	Commissariat à l'énergie atomique, Centre d'études nucléaires de Saclay, Gif-sur-Yvette, (Seine et Oise)	France
Thielheim, K.	Institut für Reine und Angewandte Kemphysik, Universität Kiel	Federal Republic of Germany
Uhrig, R.	Dept. of Nuclear Engineering, University of Florida, Gainesville, Fla.	United States of America
Unger, H.	Institut für Kernenergetik der Technischen Hochschule, Stuttgart	Federal Republic of Germany
Utzinger, E.	Eidgenössisches Institut für Reaktorforschung, Würenlingen	Switzerland
Väth, W.	Kernforschungszentrum Karlsruhe	Federal Republic of Germany
Verrière, P.	Centre d'études nucléaires de Cadarache, Saint-Paul-lez-Durance (B. du R.)	France

Name	Institution	Nominating State or Organization
Vittoz, B.	Lab. de Génie Atomique de l'Ecole Polytechnique de l'Université de Lausanne	Switzerland
Waltner, A.	North Carolina State University, Raleigh, N.C.	United States of America
Wattecapms, E.	EURATOM, Kernforschungszentrum Karlsruhe	Federal Republic of Germany
Weale, J.W.	Atomic Weapons Research Establishment, Aldermaston, Berks.	United Kingdom
Weber, G.	Institut für Reine und Angewandte Kernphysik, Kiel	Federal Republic of Germany
White, G.	Atomic Energy Research Establishment, Harwell, Didcot, Berks.	United Kingdom
Wiesner, S.	INTERATOM GmbH, Bensberg	Federal Republic of Germany
Williams, M.	University of Birmingham, Edgbaston, Birmingham	United Kingdom
Wimett, T.F.	Los Alamos Scientific Lab., University of California, Los Alamos, N. Mex.	United States of America
Wirtz, K.	Kernforschungszentrum Karlsruhe	Federal Republic of Germany
Wood, J.	Physics Dept., University of Birmingham, Edgbaston, Birmingham	United Kingdom
Wydler, P.	Eidgenössisches Institut für Reaktorforschung, Würenlingen	Switzerland
Young, J.	General Atomic, San Diego, Calif.	United States of America
Zweifel, P.	Middle East Technical University, Ankara, Turkey	Turkey

AUTHOR INDEX

Arabic numerals underlined refer to the first page of a paper by the author concerned.
Further Arabic numerals denote comments and questions in discussions.
Literature references are not indexed.

Adamantiades, A.: I 123
Albertoni, S.: I 239
Arai, E.: II 525, 526
Asaoka, T.: II 553
Bach, D.R.: I 517
Barnes, W.J.: II 623, 797
Beckurts, K.H.: I 3, 33, 34, 88, 103, 153, 190, 217, 307, 533, 669, 693; II 336, 459
Bednarz, R.: I 259, 271; II 525
Beghian, L.E.: II 335, 508, 509, 511, 525, 526
Bergman, A.A.: I 671
Bergström, A.: II 357
Beyster, J.R.: I 407, 567; II 445
Bierman, S.R.: II 825, 861
Bod, L.: I 165
Booth, R.S.: II 526, 701, 727
Borgwaldt, H.: II 399
Bounden, J.E.: II 608, 622, 623
Bourion, M.: II 653
Breton, D.: II 573, 587, 653
Bronner, G.: II 137, 179, 180
Brown, J.B.C.: I 49
Brown, J.R.: II 445
Bruna, J.G.: II 157
Brunet, J.P.: II 157
Brunfelter, B.: II 357
Buchet, J.: II 157
Cadilhac, M.: I 423; II 479, 491, 729
Calame, G.P.: I 465
Cerbone, R.J.: I 517
Chernyshov, A.A.: I 623, 643
Chwaszczewski, S.: II 47, 76, 287, 607, 652, 861
Clayton, E.D.: II 825
Comte, R.: II 337, 355, 356
Čopić, M.: I 337; II 727
Corngold, N.: I 199, 217, 271, 272, 381, 463, 533, 566; II 335, 491, 697, 895, 897
Corno, S.E.: II 863, 882
Crosbie, K.L.: II 373, 445
Cuny, G.: I 89
Daitch, P.B.: I 103, 483, 533; II 336, 727
Daughtry, J.W.: I 65
Debrue, J.: II 181
Deconninck, G.: II 493
De Juren, J.A.: I 323
Delrue, R.: II 181
Demarmels, P.: II 49
Deniz, V.: I 89
Dievoet, van J.: II 553
Dio, W.-H.: II 137
Duquesne, M.: II 635
Dybowski, K.: II 287
Edelmann, M.: II 799
Einfeld, K.: II 299
Elenga, C.W.: II 609
Eyrich, W.: II 589
Fossoul, E.: II 181
Fullwood, R.R.: I 465, 483, 501, 517
Fuster, S.: II 261
Gaerttner, E.R.: I 465, 483, 501, 517, 533, 534
García-Castañer, B.: I 185
Garelis, E.: II 3, 47, 48, 179, 796
Gavin, P.H.: II 219
Gayther, D.B.: II 435, 443, 459
Gerbier, R.: II 608, 635, 652
Giegerich, K.: II 553
Gläser, W.: I 423; II 570
Goode, P.O.: II 435
Goodfellow, H.: II 759
Govaerts, P.: II 479, 729, 795, 797
Gozani, T.: II 49
Graffstein, A.: I 191
Haas, R.: II 553, 849
Hammer, P.: II 479, 729
Heer, W.: II 119
Hennies, H.: II 299, 313

Henry, A.: I 88, 321; II 239, 313, 314, 510, 896
Hildebrand, H.: II 553
Honeck, H.C.: I 309, 320, 321, 696
Houelle, M.: II 157
Isakov, A.I.: I 671
Ishmaev, S.N.: I 623, 643
Jonsson, E.: I 695
Joshi, B.V.: II 231, 240
Kallfelz, J.: I 545
Kaneko, Y.: I 139, 153; II 241, 313
Kato, W.: I 463; II 355, 373, 397 433, 459
Kazarnovsky, M.: I 272, 321, 371, 381, 423, 671; II 726, 896
Keepin, G.R.: II 179, 314, 572
Kemeny, L.G.: I 87, 184, 320; II 698
Kenzhebaev, Sh.: I 371
Kley, W.: II 552, 553
Kockum, J.: II 357
Koppel, J.U.: I 123, 385
Kryster, R.C.: I 465
Küchle, M.: I 103, 153; II 399, 415, 459, 795
Kussmaul, G.: II 799
Lalande, J.: I 89
Larrimore, J.: II 553
Lee, R.R.: I 483
Le Ho, J.G.: I 89
Leng, J.H.: II 97
Lomer, R.D.: II 623
Lumb, R.F.: II 575, 587
Lutz, H.R.: II 119
Lyon, F.: II 635
MacPhee, J.: II 575
Main, G.W.: II 373
Maiorov, L.V.: I 657
Mansfield, W.: II 796
Massieux, J.: II 337
Matthes, W.: II 849
McCormick, W.B.: II 417
McTaggart, M.H.: II 759
Meister, H.H.: II 373, 799
Memert, G.: II 299
Menzel, J.H.: I 501
Meyer, P.: II 25, 47, 48, 313
Miegroet, van J.: II 553
Mika, J.: I 271
Misenta, R.: II 553
Mitzel, F.: II 399
Möller, E.: I 155
Montagnini, B.: I 239, 271
Moore, M.N.: I 34, 320
Morton, J.R.: II 193
Mostovoi, V.I.: I 623, 643, 657
Motte, F.: II 181
Mowry, W.R.: I 407
Nagel, W.: II 607, 608
Nargundkar, V.R.: II 231
Neill, J.M.: I 407, 567
Nelkin, M.: I 33, 88, 271, 272, 423, 463, 566; II 335, 525, 885
Nephew, E.A.: II 77
Nicolaenko, B.: II 479, 729
Nozik, V.Z.: I 623
Ogrzewalski, Z.: I 191
d'Oultremont, P.: II 493, 508, 509, 510, 725
Pál, L.: I 165
Paterson, W.J.: II 417, 433, 759
Pérez, R.B.: II 47, 701, 725, 726, 727, 882
Petrović, M.: II 281, 622
Pollak, H.: I 606, 621; II 571
Poole, M.J.: I 425, 463, 534, 535; II 397, 459, 552, 572, 897
Popov, Y.P.: I 671, 693; II 552, 571, 572, 573
Preskitt, C.A.: I 463, 696; II 47, 77, 179, 239, 240, 314
Profio, A.E.: I 123; II 445
Purohit, S.N.: I 34, 217, 273, 289, 307, 423, 463, 544; II 896
Quiquemelle, B.C.: I 309
Raievski, V.: II 460, 553, 570, 571, 572, 573
Randles, J.: II 553
Reichardt, W.: I 87, 217, 423, 566
Reifenschweiler, O.: II 609, 622, 796
Riccobono, G.: II 553
Rief, H.: II 553
Roche, M.: II 337
Rossberg, D.: I 597, 606
Rotter, W.: II 775, 795, 797

Russell, J.L.: I 579; II 76, 313, 373, 397, 415, 445, 459, 552, 573, 588
Rzeszot, T.: I 191, 545
Sadikov, I.P.: I 423, 533, 544, 623, 643, 669
Safin, Y.A.: I 657
Sagot, M.: I 89, 103, 104
Sancho, L.: I 185, 190
Schofield, P.: I 238, 271, 272, 307, 337, 381, 463, 579, 620; II 896
Schlosser, G.: II 137
Schmidt, A.: II 589, 607, 608
Schmitt, A.: II 635
Schwarz, H.R.: II 553
Sciuto, F.: II 553
Scott, S.A.: I 87, 184; II 63, 76, 180, 240
Shapiro, F.L.: I 671
Sherwin, J.: I 621; II 48, 97, 179 239, 443, 622
Silver, E.G.: I 35, 87, 88, 184, 321, 669; II 313, 526, 897
Sinclair, R.N.: I 581
Sjöstrand, N.G.: I 289, 533; I 47, 896
Slovacek, R.E.: I 483, 517
Springer, T.: I 579
Stegemann, D.: II 355, 396, 799, 861
Stepanov, A.V.: I 339, 355
Stiévenart, M.: II 181, 239, 240, 313, 461, 493, 572
Storrer, F.: II 317, 335, 336, 397, 459, 479, 729, 795
Subbarao, K.: II 231
Sumita, K.: I 139; II 241, 607, 861
Szatmáry, Z.: I 165
Tarabella, A.: II 261
Tavernier, G.: II 181, 553
Tellier, H.: II 157, 261
Toth, G.P.: I 501
Trimble, G.D.: I 567; II 445
Trukhanov, S.Y.: I 657
Uhrig, R.E.: II 657, 697, 698
Ullrich, W.: II 299, 795, 797
Utzinger, E.: II 119
Väth, W.: II 799
Verdaguer, F.: I 185
Vittoz, B.: II 882
Walker, J.: I 49
Waltner, A.W.: I 65, 87
Warda, E.: I 191
Wattecamps, E.: II 399
Weale, J.W.: II 417, 587, 759, 796
Weckermann, B.: II 849
Wilensky, S.: II 511
Williams, M.M.R.: I 607, 621
Williams, P.J.: I 581
Wimet, T.F.: II 529, 552, 571
Winkler, H.: II 49
Wood, J.D.: I 49, 87, 219, 238; II 623
Wundt, H.: II 553
Wydler, P.: I 535, 544
Young, J.A.: I 385, 407, 423, 463, 567
Yudkevich, M.S.: I 623
Zweifel, P.: I 217, 381, 669, 693, 695

IAEA SALES AGENTS

Orders for Agency publications can be placed with your bookseller or any of our sales agents listed below:

ARGENTINA
Comisión Nacional de
Energía Atómica
Avenida del Libertador
General San Martin 8250
Buenos Aires - Suc. 29

AUSTRALIA
Hunter Publications,
23 McKillop Street
Melbourne, C.1

AUSTRIA
Georg Fromme & Co.
Spengergasse 39
Vienna V

BELGIUM
Office international de librairie
30, avenue Marnix
Brussels 5

BRAZIL
Livraria Kosmos Editora
Rua do Rosario, 135-137
Rio de Janeiro

Agencia Expoente Oscar M. Silva
Rua Xavier de Toledo, 140-1° Andar
(Caixa Postal No. 5.614)
São Paulo

BYELORUSSIAN SOVIET SOCIALIST REPUBLIC
See under USSR

CANADA
The Queen's Printer
Ottawa, Ontario

CHINA (Taiwan)
Books and Scientific Supplies
Service, Ltd.,
P.O. Box 83
Taipei

DENMARK
Ejnar Munjsgaard Ltd.
6 Nörregade
Copenhagen K

FINLAND
Akateeminen Kirjakauppa
Keskuskatu 2
Helsinki

FRANCE
Office international de
documentation et librairie
48, rue Gay-Lussac
Paris 5e

GERMANY, Federal Republic of
R. Oldenbourg
Rosenheimer Strasse 145
8 Munich 8

ISRAEL
Heiliger and Co.
3 Nathan Strauss Street
Jerusalem

ITALY
Agenzia Editoriale Internazionale
Organizzazioni Universali (A.E.I.O.U.)
Via Meravigli 16
Milan

JAPAN
Maruzen Company Ltd.
6, Tori Nichome
Nihonbashi
(P.O. Box 605)
Tokyo Central

MEXICO
Librería Internacional
Av. Sonora 206
Mexico 11, D.F.

NETHERLANDS
N.V. Martinus Nijhoff
Lange Voorhout 9
The Hague

NEW ZEALAND
Whitcombe & Tombs, Ltd.
G.P.O. Box 1894
Wellington, C.1

NORWAY
Johan Grundt Tanum
Karl Johans gate 43
Oslo

PAKISTAN
Karachi Education Society
Haroon Chambers
South Napier Road
(P.O. Box No. 4866)
Karachi 2

INTERNATIONAL
ATOMIC ENERGY AGENCY
VIENNA, 1965

PRICE: USA and Canada: US $18.00
Austria and elsewhere: S 378,-
(£5.8.0; F.Fr. 72,-; DM 63,-)